Leonardo Dagdug
Jason Peña
Ivan Pompa-García

Diffusion Under Confinement

A Journey Through Counterintuition

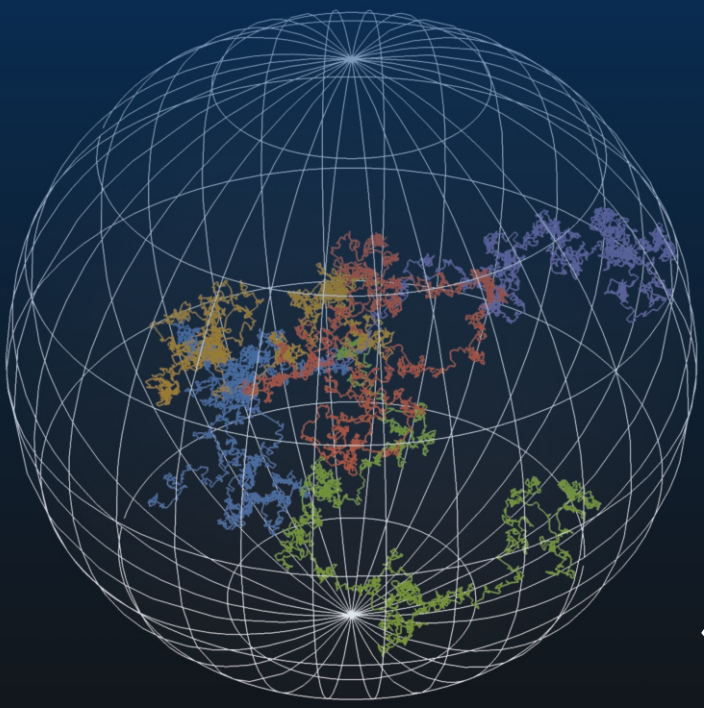

Springer

Diffusion Under Confinement

Leonardo Dagdug • Jason Peña •
Ivan Pompa-García

Diffusion Under Confinement

A Journey Through Counterintuition

Springer

Leonardo Dagdug
Universidad Autónoma Metropolitana
Mexico City, Mexico

Jason Peña
Universidad Autónoma Metropolitana
Mexico City, Mexico

Ivan Pompa-García
Universidad Autónoma Metropolitana
Mexico City, Mexico

ISBN 978-3-031-46474-4 ISBN 978-3-031-46475-1 (eBook)
https://doi.org/10.1007/978-3-031-46475-1

This Springer imprint is published by the registered company Springer Nature Switzerland AG
The registered company address is: Gewerbestrasse 11, 6330 Cham, Switzerland

Paper in this product is recyclable.

Preface

Diffusion is a universal phenomenon that controls a wide range of physical, chemical, and biological processes. The transport of spatially constrained molecules and small particles is ubiquitous in nature and technology, and plays an essential role in different processes. Understanding the physics of diffusion under conditions of confinement is essential for a number of biological phenomena and potential technological applications in micro- and nanofluidics, among others. Examples include diffusion of ions and macromolecular solutes through biological membrane channels, transport in zeolites, catalytic reactions, nanostructures of complex geometry, artificially produced pores in thin solid films, and protein and solid-state nanopores as single-molecule biosensors for detection and structural analysis of individual molecules. Also, geometrical constraints can induce novel dynamical scenarios, such as separation techniques of size-dispersed particles.

Aside from the development of experimental procedures, the problem of particle transport through confined quasi-one-dimensional structures has led to recent theoretical efforts to study the diffusion dynamics appearing in those geometries. In principle, the traditional method of solving the Smoluchowski equation with the necessary boundary conditions can be used to examine this confinement. While this approach has been effective when the system's boundaries have fairly regular shapes, it is exceedingly challenging to address the boundary value problem when the boundaries are uneven or periodic. To overcome this problem, we can simplify the description by reducing the system's dimensionality, therefore preserving only the main direction of transport and accounting for the irregularity of these borders by means of an entropic potential. Early studies by M.H. Jacobs and R. Zwanzig gave way to renewed research on this subject.

Studies on diffusion under confinement are typically difficult to understand for young scientists and students because of the extensive background on diffusion processes, physics, and mathematics that is required. All of this information is provided in this book, which is essentially self-contained as a result of our efforts to make it accessible to an audience of students from a variety of different backgrounds. We also provide the necessary mathematical details, so students can follow the technical process required to solve each problem. Readers will

also find detailed explanations of the main results based on the last 30 years of research devoted to studying diffusion under confinement. Lastly, because the approximations used when developing theoretical results are strongly dependent on the hypotheses, we also provide a detailed discussion on how to perform Brownian dynamics simulations to evaluate the range of applicability of the obtained results. We also explain how to apply the finite-difference method for numerically solving the diffusion equation. Readers will also find a code to numerically inverse the Laplace transform in Laplace's space, which is used to obtain many results.

This textbook is intended for young scientists, graduate students, and advanced undergraduates in physics, physical chemistry, biology, chemistry, chemical engineering, biochemistry, bioengineering, and polymer and material sciences.

This textbook is organized so as to facilitate the development of a two-semester course. We begin with a brief historical review of diffusion in Chap. 1. In Chap. 2, we introduce the physical and mathematical concepts that are used throughout the rest of the book to study and describe diffusion, such as diffusivity, flux, backward equation, mean first-passage time, and splitting probability, among others. In Chap. 3, we use different mathematical techniques to solve the diffusion equation in free space. We discuss the implications of the Central Limit Theorem and introduce Green's function method. Chapters 4–9 are devoted to studying the boundary value problem in one dimension and its main physical properties. In these chapters, we discuss problems related to semi-infinite systems, diffusion between two targets, diffusion in the presence of a force field, and diffusion with stochastic resetting. We end Part III of the book with the analysis of the Langevin equation and Brownian dynamics in Chap. 10, and the numerical solution of the diffusion equation by means of the finite-difference method in Chap. 11.

In Part IV of the book, which includes Chaps. 12 and 13, we focus on the two-dimensional diffusion equation and boundary conditions, and we discuss the main physical properties and their solutions. We also introduce the reaction-diffusion process in two dimensions by means of the Turing mechanism.

In Chap. 14, we first solve the diffusion equation in three dimensions with angular symmetry and given boundary conditions, such as a perfectly absorbent sphere, and a system consisting of two concentric spheres. Then, we study the diffusion particle trapping problem when there is an absorbent circular disk, or an arbitrary absorbing site, in a hard wall. Finally, we solve the problem of diffusion in a hyperboloidal cone.

Part VI of the book is devoted to the boundary homogenization approach. With this technique, we can study the problem of diffusing particles in the presence of heterogeneous boundaries. Part VII includes Chaps. 17–25, and is devoted to the study of the one-dimensional reduction of quasi-one-dimensional systems, as from the early study by R. Zwanzig to the representation of channels and tubes as a tubular manifold. We also include the work done by M. Rubi and D. Reguera, and the classical treatment of the problem by P. Kalinay and J. Percus. Some applications of the latter approach, such as asymmetric channels, periodic systems, and active Brownian particles, are also reviewed.

All Fortran codes can be downloaded from https://ixtlan.izt.uam.mx/leo/diffusionbookcodes/.

The contents of this book have been influenced by discussions or collaborations with Alexander M. Berezhkovskii, Sergey M. Bezrukov, George Weiss, Pavol Kalinay, Inti Pineda, Ralf Metzler, David Reguera, Miguel Rubi, Paolo Malgaretti, Denis Boyer, Arnab Pal, Jose Alvarez-Ramirez, Eduardo Rodriguez, Manuel Aguilar-Cornejo, Pavel Castro, Vladimir Y. Zitserman, Alexei T. Skvortsov, Ulrich F. Keyser, Stefano Pagliara, Attila Szabo, Marco V. Vazquez, Guillermo Chacón, Roberto Verdel, Mario Sandoval, F. J. Valdes-Parada, Victor Chernomordik, Amir H. Gandjbakhche, Yoshua Chávez, Pedro Julián, Adriana Pérez-Espinosa, Juan Daniel Rivera, and Juan Pablo Grajales.

We extend our gratitude to Claudia Reynaud for her constructive and illuminating comments on the manuscript. Without her invaluable assistance, this book would not have been possible.

Finally, and most importantly, we thank our families for their love and unending support throughout the process of writing this book.

Mexico City, Mexico — Leonardo Dagdug
Mexico City, Mexico — Jason Peña
Mexico City, Mexico — Ivan Pompa-García

Contents

Chapter 1
History of Brownian Motion in a Nutshell

Robert Brown was one of the greatest botanists of his time and is renowned for both his discovery of plant cell nuclei and his work on Brownian motion (see Fig. 1.1). Since he published his observations[1] on how amyloplasts (starch organelles) and spherosomes (lipid organelles), ejected from the pollen grains, floating on the water continuously move around jerkily in all directions, this tricky motion has captivated a great many scientists. After systematic and meticulous work, Brown was able to pinpoint two of the main characteristics of this phenomenon: (a) the motion of the pollen grains never stopped, not even after the grains had been kept for a long time in a sealed container, and (b) lifeless particles exhibit exactly the same behavior. Therefore, Brown categorically concluded that the phenomenon had nothing to do with life, but rather with the particle itself.

Although Robert Brown was not the first to observe this phenomenon,[2] he was the first one to study it thoroughly. The motion of particles due to the thermal agitation of the fluids in which they are immersed is known as Brownian motion, and the particles are called Brownian particles (see Fig. 1.2). In terms of this language, we say that Brownian motion is due to the collision of the fluid's atoms or molecules with the Brownian particles.

In the 30 years following the publication of Brown's leaflet, interest in this phenomenon was almost completely lost. It was not until 1858 that this discussion came back to life when Jules Regnault (1797–1863) suggested from his experiments

[1] His results were reported in a leaflet for personal distribution entitled "A brief account of microscopical observations made in the months of June, July and August, 1827 on the particles contained in the pollen of plants; and on the general existence of active molecules in organic and inorganic bodies." It is important to clarify that, in this title, the word molecule refers to the smallest constituent of a living organism.

[2] The first to report the observation of Brownian motion was Jan Ingen-Housz (1730–1799) in a small article published in 1784 called "Remarks on the use of the microscope," where he described his observations of the erratic movement of small pieces of charcoal in a drop of alcohol, as seen under a microscope.

L. Dagdug et al., *Diffusion Under Confinement*,
https://doi.org/10.1007/978-3-031-46475-1_1

Fig. 1.1 Robert Brown, botanist (1773–1858). Lithograph made by the Austrian Rudolph Hoffmann. Published in 1860 2 years after Brown passed away

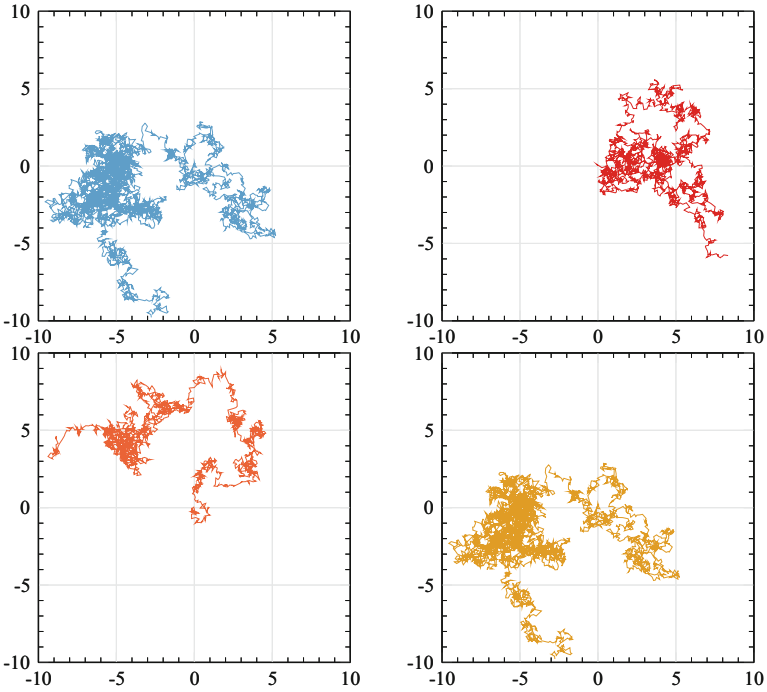

Fig. 1.2 Robert Brown noticed the random jiggling of pollen particles suspended in solution, even for systems in equilibrium. Paths of individual Brownian particles in two dimensions obtained by performing a Brownian dynamics simulation are shown. All paths start at the origin. When running simulations, we consider an overdamped point-like Brownian particle; the diffusivity is $D = 1$. The overdamped dynamics of the particle is modeled by the Langevin equation

that the cause of Brownian motion was the effect of incident light on the fluid. As he explained it, the heat from the incident light caused the fluid to evaporate, and such evaporation caused the motion of Brownian particles.

In the decade of 1860, several investigators proposed that Brownian motion was caused by continuous collisions between pollen grains and water molecules agitated by their thermal movement. More specifically, Giovanni Cantoni (1818–1897) demonstrated that the phenomenon was not caused by differences in temperature between different points in the fluid, given that the phenomenon was also present when the fluid had uniform temperature. He also observed the same phenomenon when his experiments were conducted in large containers, thus voiding the hypothesis that it was due to capillary forces.

In 1863, Christian Wiener (1826–1896) provided strong arguments to show that the movement of Brownian particles was not due to external causes, but rather had to be associated with internal movements in the fluid. In contrast, during the 1870s, Karl Nägeli (1871–1891) and William Ramsay (1852–1916), among others, provided arguments against these ideas. Their reasoning focused on the fact that Brownian particles have a vastly larger mass than the fluid's molecules, and consequently, the latter would not be able to cause appreciable displacement on the former. On the other hand, it is paramount to point out that in the late nineteenth century, a great number of illustrious scientists, such as Ernst Mach (1838–1916) and Wilhelm Ostwald (1853–1932), among others, did not agree with the hypothesis of the atomic constitution of matter.

Between the years of 1905 and 1908, Albert Einstein published five articles on Brownian motion, aiming to test the atomic hypothesis by looking at the fluctuations of small particles in a solution (see Fig. 1.3). His first paper includes all the foundations of this theory, while in the fourth one, published in 1907, he explains the difficulties of experimentally measuring Brownian velocities and why the existence of such quantities is a conflicting point.[3] The articles published in 1905 and 1906

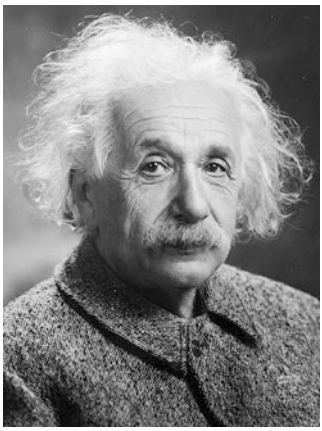

Fig. 1.3 Albert Einstein (1879–1955) in 1947. Photograph by Orren Jack Turner, Princeton, N.J. Modified with Photoshop by PM Poon and by Dantadd

[3] Entitled "On the motion of particles suspended in a resting fluid demanded by the molecular theory of heat" (1905) and "Theoretical Remarks on the Brownian Movement" (1907).

are particularly important, as in these articles, Einstein explained,[4] for the first time ever and without any room for doubt, the causes and properties of Brownian motion. Back in 1905, his primary motivation was to make macroscopic observable predictions considering the thermal molecular movement of the fluid. In fact, the article starts by saying: "This Article will show that, according to the molecular kinetic theory of heat, bodies of sizes which are able to be seen microscopically, which are suspended in a liquid, carry out movements due to the molecular thermal movements and of such magnitude that can be seen under the microscope. It is possible that the movements that will be here discussed are identical to the so called Brownian molecular movement." In this paper, Einstein modeled the movement of Brownian particles as a stochastic process.[5] His great success was to come up with the solution for random motion as a problem of probabilities, i.e., to write the problem's solution as the probability of finding a Brownian particle in a certain place at a certain time, putting aside the dogma of making deterministic descriptions of the particle's position. In his work, Einstein concluded that the averaged squared distance traveled Δ^2 by the Brownian particle divided by the time τ that it takes it to travel such distance is a constant.

Since Einstein's derivation of the diffusion equation and the relation between the diffusion coefficient and the fluid's viscosity are a turning point in the history of Brownian motion and a cornerstone of the modern theory of stochastic processes, let us follow Einstein in his demonstration published in 1905.[6] Assuming we have n particles suspended in a liquid, Einstein starts by considering only the one-dimensional case, where, in an interval of time τ, its position will increase by exactly Δ. The time interval τ is small compared to the duration of the observation, but large enough for the motions made by a particle to be observed during two consecutive intervals of time, which are to be considered as independent events. The number $\mathrm{d}n$ of particles with a displacement between Δ and $\Delta + \mathrm{d}\Delta$ is given by $\mathrm{d}n = n\ \phi(\Delta)\ \mathrm{d}\Delta$, where $\phi(\Delta)$ is the probability distribution to move along a distance Δ. In obtaining the evolution of the concentration, there are two essential assumptions to be made: The first is the symmetry in the jump probabilities, namely,

$$\phi(\Delta) = \phi(-\Delta). \tag{1.1}$$

In other words, the probability of being displaced a certain distance Δ is the same regardless of whether such displacement is to the right or to the left, i.e., there is no bias at either direction. The second feature of the distribution $\phi(\Delta)$ is the normalization property,

[4] The 1906 paper reads "On the theory of Brownian motion" where Einstein addresses the rotational Brownian motion of spherical particles.

[5] The theory of stochastic processes is centered in the study and modeling of systems that evolve along time, or space, according to some non-deterministic laws, i.e., laws of random character.

[6] In 1905, Albert Einstein published four papers that changed the history of science. These works encompass the photo-electric effect, his first two papers on special relativity theory, and his first paper on Brownian motion submitted on May 11, 1905.

$$\int_{-\infty}^{\infty} \phi(\Delta)\, \mathrm{d}\Delta = 1. \tag{1.2}$$

Then, the evolution of the distribution of particles between $x + \Delta$ and x from t to τ is given by

$$f(x, t + \tau) = \int_{-\infty}^{+\infty} f(x + \Delta, t)\, \phi(\Delta)\, \mathrm{d}\Delta. \tag{1.3}$$

This equation tells us that in order to find a particle at position x at a time $t + \tau$, we need to sum over all of the possible ways that the particle could have gotten to $x + \Delta$ and then jump to position x during the step time τ. Making a Taylor expansion in both sides of Eq. (1.3), we get

$$f(x, t + \tau) \approx f(x, t) + \frac{\partial f}{\partial t}\tau \tag{1.4}$$

and

$$f(x + \Delta, t) \approx f(x, t) + \frac{\partial f}{\partial x}\Delta + \frac{1}{2}\frac{\partial^2 f}{\partial x^2}\Delta^2, \tag{1.5}$$

respectively. Substituting these results into Eq. (1.3), we can write

$$\begin{aligned} f(x, t) + \frac{\partial f}{\partial t}\tau \approx f(x, t) \int_{-\infty}^{\infty} \phi(\Delta)\, \mathrm{d}\Delta + \frac{\partial f}{\partial x} \int_{-\infty}^{+\infty} \mathrm{d}\phi(\Delta)\, \mathrm{d}\Delta \\ + \frac{1}{2}\frac{\partial^2 f}{\partial x^2} \int_{-\infty}^{+\infty} \Delta^2\, \phi(\Delta)\, \mathrm{d}\Delta. \end{aligned} \tag{1.6}$$

The integral in the first term on the right side is 1 because of the normalization property. As a consequence, $f(x, t)$ is canceled out on both sides of the equation. Additionally, the second term of the right-hand side is concluded to be zero, since it represents the integration of an odd function over a symmetric domain. Then, Einstein defined the integral in the last term as

$$D \equiv \frac{1}{2\Delta t} \int_{-\infty}^{+\infty} \Delta^2\, \phi(\Delta)\, \mathrm{d}\Delta, \tag{1.7}$$

where $\tau \to \Delta t$. It is worth noting that Eq. (1.7) is the average of the quadratic variation produced by thermal agitation during the time Δt. Substituting it into Eq. (1.6), he finally arrived to Fick's second law of diffusion,

$$\frac{\partial f}{\partial t} = D\frac{\partial^2 f}{\partial x^2}. \tag{1.8}$$

Einstein demonstrated that the process of Brownian motion can be described by the diffusion equation.[7] Moreover, he showed that the trajectories of a Brownian particle can be regarded as memory-less and non-differentiable.

The solution of Eq. (1.8) is given by[8]

$$f(x,t) = \frac{n}{\sqrt{4\pi Dt}} \exp\left(-\frac{x^2}{4Dt}\right), \tag{1.9}$$

for which Einstein computed the second moment of distribution, i.e., the mean of squared displacements, as

$$\lambda_x^2 = \left\langle x^2 \right\rangle = 2Dt. \tag{1.10}$$

In addition, when considering Stokes' law, which describes the force of friction opposing to a sphere of radius a moving at constant velocity $\mathbf{v}$ in a fluid with viscosity η, and the crucial notion of osmotic pressure (pressure increase) Π, Einstein understood and proved that both arguments were equally valid in the description for Brownian particles. Therefore, he considered the equilibrium of these two force densities, that is, the gradient of the osmotic pressure and the external (friction) force density, leading to

$$nF - \frac{\partial \Pi}{\partial x} = 0, \tag{1.11}$$

where

$$\mathbf{F} = -6\pi\mu a\mathbf{v} \quad \text{and} \quad \Pi = \frac{nRT}{N_A}. \tag{1.12}$$

In the latter equations, μ is the friction coefficient, R the ideal gas constant, T the absolute temperature, and N_A the Avogadro-Loschmidt number, while n is the number of solute particles per unit volume or particle density. Substituting Eqs. (1.12) into Eq. (1.11) results in

$$nF = \frac{RT}{N_A} \nabla n(x,y,z). \tag{1.13}$$

The dynamics of moving in a liquid under force F brings the particle to a limit velocity, given by $V = F/\mu$, which allows us to write the number of particles crossing a unit surface as

[7] The diffusion equation is a parabolic partial differential equation. It was obtained for the first time with heuristic arguments by Adolf Fick (1829–1901) in 1855, as a continuity of the well-recorded math of heat and electricity conduction.

[8] See Chap. 3 for the complete derivation.

$$\Phi_F = nV = \frac{nF}{\mu}. \tag{1.14}$$

Later on, Einstein acknowledged that particle density, $n = n(x, y, z)$, satisfies the diffusion equation, Eq. (1.8). Therefore, n is directly connected to the flux due to diffusion,

$$\Phi_D = -D\,\nabla n(x, y, z). \tag{1.15}$$

By introducing both equations for the flux into the equilibrium condition, one finds

$$\frac{nF}{\mu} = D\,\nabla n(x, y, z). \tag{1.16}$$

And a comparison between Eqs. (1.13) and (1.16) leads to

$$D = \frac{RT}{N_A \mu}. \tag{1.17}$$

Then, by using the coefficient friction of a sphere $\mu = 6\pi\eta a$, Einstein found the following result:

$$D = \frac{RT}{N_A}\frac{1}{6\pi\eta a}. \tag{1.18}$$

This equation in known as the Stokes-Einstein-Smoluchowski relation and was later generalized by H. B. Callen and T. A. Welton in terms of the fluctuation-dissipation theorem and in terms of the linear response theory by Ryogo Kubo (1920–1995).

Finally, Einstein combined Eqs. (1.10) and (1.18) to obtain

$$\lambda_x = \sqrt{\frac{RT}{N_A}\frac{1}{3\pi\eta a}}\sqrt{t}. \tag{1.19}$$

Furthermore, Einstein presented Eq. (1.19) as a measurable quantity and calculated $\lambda_x = 0.8_{\mu\mathrm{m}}$ using typical values for Brownian motion experiments. The crucial consequence of Einstein's theory is that the diffusion constant coefficient can be measured by estimating the distance traveled rather than the velocity, thus making it possible to estimate the much debated Avogadro-Loschmidt number, N_A, something that inspired the study of the role of fluctuations through a series of experiments by Perrin and his students between the years 1908 and 1911. The publication of Einstein's papers provided strong evidence for the atomistic hypothesis of matter, a subject of physical investigation in the development of the foundations of thermodynamics and the dynamical interpretation of statistical mechanics.

Fig. 1.4 Marian Ritter von Smolan Smoluchowski (1872–1917) during his years at the University of Lviv. International Aerosol Research Assembly

At the end of the nineteenth century, the explanation of Brownian motion based on collisions between the molecules or atoms of the fluid and the Brownian particles seemed totally absurd to some investigators, and there apparently seemed to be no way to explain the occurrence. The first scientist to successfully use the kinetic theory[9] to study Brownian motion was Marian Ritter von Smolan Smoluchowski (see Fig. 1.4). He was able to qualitatively and quantitatively explain the phenomenon, obtaining results comparable to those of the experimental data. Smoluchowski used the results acquired by Ludwig Boltzmann and James Clerk Maxwell[10] to model and explain the causes of Brownian motion. On the one hand, Maxwell and Boltzmann had demonstrated that the particles in a fluid do not move at the same speed, but rather, it is a distribution of speeds in all directions. On the other hand, the number of collisions that a Brownian particle experiences is of the order of 10^{20} collisions per second. Because of these two reasons, the net effect of the Brownian particle's movement is appreciable.

Even though Smoluchowski started working on Brownian motion in the year 1900, focusing on the molecular kinetic approach, it was not until 1906 that he published his results. Smoluchowski's intention was to wait for more experimental data to support his theory, which he constructed so as to include these observations. However, he was driven to publish them early, largely as a result of Einstein's work being published in 1905. Einstein's and Smoluchowski's work is very different in approach, mainly in that Einstein was looking for a mathematical test of the kinetic

[9] The kinetic theory of gases, mainly developed by Ludwig Eduard Boltzmann (1844–1906) and James Clerk Maxwell (1831–1879) during the nineteenth century, explains the behavior and macroscopic properties of gases from the statistical description of microscopic molecular processes. This theory considers that gases are composed of atoms and molecules in random movement, particles that undergo random collisions between them and the container's walls.

[10] It is interesting to point out that neither Maxwell nor Boltzmann published on the topic, even though both of them were extremely knowledgeable of statistical mechanics and kinetic theory.

theory of gases and was not quite sure that the problem he was dealing with was really the so-called Brownian motion.[11]

Smoluchowski also calculated the second moment of the displacement, for which he obtained the following equation, using his own notation

$$\sqrt{\langle \Lambda_n \rangle^2} = \frac{8}{9}\sqrt{\frac{m'v'^2}{\pi \mu a}}\sqrt{t}, \tag{1.20}$$

where m' and v' are the mass and velocity of the medium particles. Equation (1.20) is comparable with Eq. (1.19) when using the equipartition of energy and writing $m'v'^2$ in terms of $k_B T$, leading to

$$\left\langle x^2 \right\rangle = \sqrt{\frac{64}{27}}\sqrt{\frac{k_B T}{3\pi \mu a}}\sqrt{t}, \tag{1.21}$$

which differs by a factor of $\sqrt{64/27}$ from Einstein's result, Eq. (1.19). This is a reasonable dissimilarity considering all the approximations made in the Smoluchowski procedure. Ultimately, Smoluchowski obtained the diffusion coefficient through qualitative reasoning of the mean free path and his latest works, namely,

$$D = \frac{16}{253}\frac{m'v'^2}{\mu \pi a}, \tag{1.22}$$

which again differs by a factor of 64/27 from Einstein's result, Eq. (1.18).

Between 1913 and 1915, Smoluchowski provided another great contribution to the Brownian motion theory by finding the equation that currently bears his name and describes the phenomenon in the presence of an external force, Eq. (1.23). In Smoluchowski's equation, $f(x,t)$ represents the concentration (the number of particles per volume unit), and D is a constant diffusion coefficient. The potential is given by $U(x)$, while $\beta = 1/(k_B T)$, with k_B being the Boltzmann constant and T the absolute temperature.

$$\frac{\partial f(x,t)}{\partial t} = D\,\frac{\partial}{\partial x}\left\{ \mathrm{e}^{-\beta U(x)}\frac{\partial}{\partial x}\left[\mathrm{e}^{\beta U(x)} f(x,t)\right]\right\}. \tag{1.23}$$

Smoluchowski also played an important role in designing some experiments. His work focused on measuring the spatial distribution of the Brownian particles,

[11] If he could prove that the kinetic theory of gases was true, then the random motion of particles under the microscope would be an immediate result. Nevertheless, such behavior was forbidden by classic thermodynamics, which required equilibrium. Thus, the mean of the squared displacements was defined by Einstein as a parameter that would be agreeable to either of both theories.

confirming that the theory developed by both him and Einstein truly corresponded to the experimentally observed Brownian motion.[12]

It is important to note that even though Smoluchowski and Einstein essentially obtained the same results, Einstein's results were derived using a language that was more accessible to individuals interested in the topic and summarized in three stages. Firstly, he related the diffusion coefficient to the properties of the medium; secondly, he derived the diffusion equation; and finally, he combined these two results. For that reason, Einstein's articles had a greater impact in the scientific community. In contrast, Smoluchowski used known arguments and approximations for all of those who were familiar with the kinetic theory, in topics like combinatorial analysis and concepts such as the mean free path.

It has been recently shown that the Scottish-born Australian theoretical physicist, William Sutherland, was the first to inform the scientific community of the existence of the Stokes-Einstein-Smoluchowski relation in a paper published back in 1904,[13] which he presented at the Dunedin tenth meeting of the Australasian Association for the Advancement of Science (see Fig. 1.5).

In his paper, Sutherland established a dynamical relation between the velocity of diffusion of a substance and the size of its molecule in order to measure the molecular mass of substances. This task is proposed to be accomplished through the application of Nernst's theory of diffusion in an electrolyte. Beyond that, the treatment of diffusion through a liquid as a parallel phenomenon to the transpiration of gasses through porous partitions is mentioned, in other words, that the square of

Fig. 1.5 Theoretical physicist William Sutherland (1859–1911) at the age of 20, 1879, in Australia. Work of public domain

[12] In fact, Smoluchowski exchanged correspondence with Theodor Svedberg (1884–1971) a Swedish chemist who worked on Brownian motion experiments. In their letters, Smoluchowski suggested modifications and improvements to Svedberg's method. Svedberg was awarded the Nobel Prize for Chemistry in 1926 for his work on disperse systems.

[13] With the title "A dynamical theory of diffusion for non-electrolytes and the molecular mass of albumin," 1904.

the velocity of diffusion of a substance through a given medium, when multiplied by the molecular mass of the substance, is a constant, (i.e., the kinetic energy of diffusion is constant for all molecules under like conditions). He assumed the existence of atoms to study the measurement of large molecular masses. His relation between diffusivity and viscosity is given by

$$D = \frac{RT}{N_A} \frac{1}{6\pi\eta a} \frac{1 + 3\eta/\beta a}{1 + 2\eta/\beta a}, \tag{1.24}$$

where β is the coefficient of sliding friction, in case of slippage between the spreading molecule and the solution. It is important to emphasize that Sutherland used exactly the same derivation as Einstein to obtain Eq. (1.24). If there is no slippage at the boundary, β goes to infinity and Eq. (1.24) becomes

$$D = \frac{RT}{N_A} \frac{1}{6\pi\eta a}, \tag{1.25}$$

which is the Stokes-Einstein-Smoluchowski relation, Eq. (1.18). Using the latter equation, Sutherland obtained the molar volume of albumin and estimated its atomic mass at 32,814 Da.

In 1908, Paul Langevin (see Fig. 1.6) published his one and only article on the study of a macroscopic description of Brownian motion, where he showed a beautiful derivation of the quantities we have already talked about. Nonetheless, because of the simplicity and power of his methods, these are worth discussing. Langevin wrote Newton's second law for Brownian particles and assumed that, when introduced into a fluid, they are affected by two forces: the first one due to the great number of collisions with the fluid's molecules and the second one due to the viscosity of the fluid. He modeled the forces due to collisions as those being stochastic in nature, while the viscosity effect was applied using its well-known

Fig. 1.6 Paul Langevin (1872–1946). Photograph by Henri Manuel. Wellcome Collection. Public Domain Mark

structure, opposite and proportional to its speed. The viscous force will describe the mean effect of resistance or friction, whereas the stochastic force X stands for the fluctuations around the average value, while maintaining the particle's motion, which would otherwise eventually stop. Mathematically, the Langevin equation reads as follows:

$$m\frac{\mathrm{d}^2x}{\mathrm{d}t^2} = -6\pi\mu a\frac{\mathrm{d}x}{\mathrm{d}t} + X. \tag{1.26}$$

This expression cannot be solved directly, because of stochastic noise, so by multiplying by x and using the chain rule, it transforms into

$$\frac{m}{2}\frac{\mathrm{d}^2x^2}{\mathrm{d}t^2} - m\left(\frac{\mathrm{d}x}{\mathrm{d}t}\right)^2 = -3\pi\mu a\frac{\mathrm{d}x^2}{\mathrm{d}t} + xX. \tag{1.27}$$

Thereafter, Langevin considered a large number of identical particles and took the average of Eq. (1.27), neglecting the mean value of xX because of the randomness of the collisions. Subsequently, he used the equipartition of energy to write $m\langle(\mathrm{d}x/\mathrm{d}t)^2\rangle = RT/N_A$ and introduced the new variable $z = \mathrm{d}\langle x^2\rangle/\mathrm{d}t$ to find

$$\frac{m}{2}\frac{\mathrm{d}z}{\mathrm{d}t} + 3\pi\mu a z = \frac{RT}{N_A}. \tag{1.28}$$

The solution of the latter differential equation is computed straightforward, namely,

$$z(t) = \frac{RT}{N_A}\frac{1}{3\pi\mu a} + C\exp\left(-\frac{6\pi\mu a}{m}t\right). \tag{1.29}$$

The second term of the solution decreases exponentially for $t > m/6\pi\mu a$, which is approximately 10^{-8}s. Given that this value is much smaller than the measurable time steps in experiments, the second term in Eq. (1.29) can always be neglected.[14] Therefore, by substituting z and integrating, Langevin arrives at Eqs. (1.18) and (1.25).

The French physicist was able to reproduce the theoretical results obtained by Einstein and Smoluchowski. Additionally, just as Smoluchowski did, Langevin wrote in his article that his method was "better" than Einstein's. Probably the greatest merit of Langevin was to write the first example of an equation with a random term, the solution of which is a stochastic function.

From 1908 to 1911, Jean Baptiste Perrin (see Fig. 1.7) worked experimentally to show that the average of the square of the distance traveled by a Brownian particle divided by time is a constant, a prediction that had been made by Thomas Graham (1805–1869), Percival Spencer Umfreville Pickering (1858–1920), William

[14] For times smaller than $m/6\pi\mu a$, there will be an extra exponential term in the $\langle x^2\rangle$ relation.

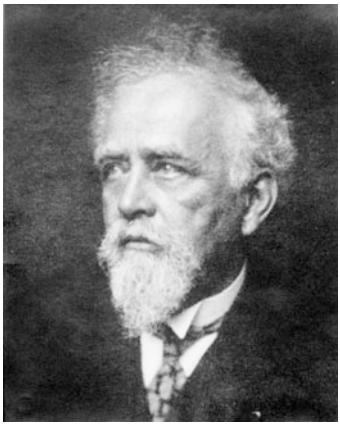

Fig. 1.7 Jean Baptiste Perrin (1870–1942). Perrin was awarded the Nobel Prize for Physics for his experimental studies on Brownian motion. AIP Emilio Segrè Visual Archives

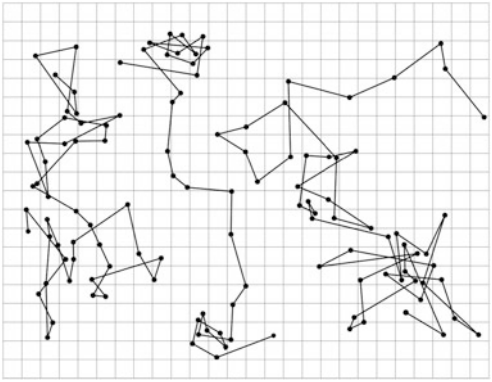

Fig. 1.8 Three tracings of moving colloidal particles of 0.53 μm in radius, as seen under the microscope. Successive positions determined every 30 seconds are joined by straight line segments (the mesh size is 3.2 μm). J. B. Perrin, *"Mouvement brownien et réalité moléculaire,"* Ann. de Chimie et de Physique (VIII) 18, 5–114 (1909). SVG drawing by Mirai Warren

Sutherland, Marian Smoluchowski, and Albert Einstein. For such purpose, Perrin and his team took photographs every 30 seconds of particles performing a Brownian motion (see Fig. 1.8). When plotting the square of the distance traveled by the particle against time, they obtained a straight line. Furthermore, since he knew the temperature and viscosity of the media, as well as the particles' dimensions, he calculated the Avogadro-Loschmidt number, obtaining $N_A = 6.4 \times 10^{23}\text{mol}^{-1}$, an extremely close approximation to the most accurate value that has been computed as of this day.[15]

A vast amount of experimental work is also attributed to Victor Henry (1872–1940) and Joseph Ulysses Chaudesaigues. Equation (1.19) was successfully tested, thanks to their contributions. As the reader may appreciate, this highlights how science is more of a community effort, rather than an individual endeavor.

[15] In 2017, the mole was redefined by the *Bureau International des Poids et Mesures* (BIPM) as being the amount of substance containing exactly $N_A = 6.02214076 \times 10^{23}\text{mol}^{-1}$ elementary entities.

The Brownian motion problem has played a key role in the development and evolution of the study and research of thermodynamics, statistical physics, and diffusion.[16] Among scientists who have branched out on this topic, there are some who have focused on calculating fluctuation-dissipation relations. As such, Callen and Welton, mentioned earlier in this chapter, generalized the relations derived by Einstein and Smoluchowski. Later on, an extension of the theory by Harry Nyquist (1889–1976) and John B. Johnson (1887–1970) for voltage fluctuations arrived in the form of the quantum version of the fluctuation-dissipation theorem. Other advances worth mentioning include the so-called Green-Kubo relations, where the corresponding fluctuations theorem provides extremely valuable information on the role of non-equilibrium fluctuations.

The debate on the true origin of the irregularity that causes the randomness of Brownian particles continues this day. It is thought to be either a chaotic microscopic dynamic effect or related to the extreme high dimensionality of the phase space that, in reduction, causes the agitated movement of the molecules under the microscope. Answering this question is even more difficult if quantum effects are to be considered, because of quantum fluctuations in stationary non-equilibrium systems or microscopic quantum chaos. Nevertheless, the Brownian theory of motion unquestionably has a significant impact in physics, particularly in statistical and quantum mechanics.

Researchers are still very active in this field of physics. Interesting things are yet to be discovered in the years to come, with applications in physics, chemistry, chemical kinetics, biology, and engineering, all stemming from the simple, random movement of a small particle.

So far, the very basics of diffusion theory have been developed, i.e., the diffusion equation: a result that has led scientists to review the improvements and contributions of Brownian motion, starting with the observations of a botanist all the way up to how it relates to quantum theory. In the next chapter, we will discuss the random elevator game, a version of a gambling issue that led to the creation of the mathematical theory of probability.

Further Reading and References

A. Einstein, Über die von der molekularkinetischen Theorie der Wärme geforderte Bewegung von in ruhenden Flüssigkeiten suspendierten Teilchen. Annalen der Physik **17**, 4 (1905). [Translated in english in Investigations on the Theory of the Brownian Movement (Dover Publications, Inc., New-York, 1956), pp. 1–18]

[16] The quest for the mathematical description of Brownian trajectories led to a new class of differential equations, called stochastic differential equations. The implicit theoretical complexity of these equations was analyzed and then clarified more than 40 years later by Kiyosi Itô (1915–2008), the inventor of the concept of the stochastic integral and the stochastic differential equation itself, a formalism that is widely referred to as Itô calculus.

A. Einstein, Zur Theorie der Brownschen Bewegung. Annalen der Physik **17**, 371–381 (1906). [Translated in english in Investigations on the Theory of the Brownian Movement (Dover Publications, Inc., New-York, 1956), pp. 19–35]

A. Fick, Ueber Diffusion, Annalen der Physik **94** (1855). [Translated in english by Tad W. Patzek in Advances in Historical Studies **3**, 207–220 (2014)]. https://www.scirp.org/pdf/AHS_2014093011510952.pdf

P. Langevin, Sur la théorie du mouvement Brownien.Comptes rendus de l'académie des sciences de Paris **14**, 6 (1908). [Translated in english in Am. J. Phys. **65**, 1079 (1997)]. https://doi.org/10.1119/1.18725

J.B. Perrin, Mouvement brownien et réalité moléculaire, in *Annales de Chimie et de Physique*, 8^{me} Series, September (1909). [Translated in english by Taylor & Francis, 1910]

M. Smoluchowski, Essai d'une théorie cinétique du mouvement Brownien et des milieux troubles, in *Bulletin International de l'académie des sciences de Cracovie* (1906). [Translated in english in *Marian Smoluchowski. Selected Scientific Works* (Wydawnictwa Uniwersytetu Warszawskiego, Warsaw, 2017), pp. 77–86]

M. Smoluchowski, Drei Vortage uber Diffusion, Brownsche Bewegun und Koagulation von Kolloideilchen. Physik **17** (1916). [Translated in english in *Marian Smoluchowski. Selected Scientific Works* (Wydawnictwa Uniwersytetu Warszawskiego, Warsaw, 2017), pp. 125–174]

W. Sutherland, The measurement of Large Molecular Masses, in *Report of the Meeting of the Australian Association for the Advancement of Science Held at Dunedin* (1904), pp. 117–121

W. Sutherland, A dynamical theory of diffusion for non-electrolytes and the molecular mass of albumin. The London, Edinburgh, and Dublin Philosophical Magazine and Journal of Science **9**, 54 (1905). https://doi.org/10.1080/14786440509463331

Part I
Brownian Motion and the Random Elevator Game

Brownian motion and gambling problems provide a simple way to derive the diffusion equation, as well as to understand concepts such as survival probability, mean first-passage time, and splitting probability.

"Everything existing in the universe is the fruit of chance and necessity."

—Democritus

Chapter 2
The Random Elevator Game

2.1 Introduction

This chapter aims to provide the reader with the basic physical and mathematical concepts that are used in the study and description of diffusion. To such end, we are introducing a new board game: *the random elevator*. This game is quite similar to *chutes and ladders*, but simpler. Unlike the game many of us played in our childhood, we removed the chutes and ladders, and instead of starting at square number 1, players can start at any square. The board is shown in Fig. 2.1, and the squares on the board represent the floors of the Empire State Building.

Let's pretend that you work at an office located in the Empire State Building and that there is nothing more relaxing than going up to the Observatory at the end of your work day to take in the breathtaking view. But on a certain day, the elevator breaks down and is working erratically, so it randomly goes up or down one floor at a time only, when pressing any button. Then, the movement of the elevator to its next stop (i.e., either up or down) has the same probability of getting heads or tails when tossing a coin. You are now trapped in a pretty annoying game that we call *the random elevator*. The object of the game is to get to the *Observatory* or the *Lobby*. If you reach the Observatory, you win, and if you reach the Lobby, you lose, and the game is over.

The random elevator game is similar to the gambler's ruin problem, which is a classical concept in probability theory, first discussed by French mathematicians Blaise Pascal and Pierre de Fermat, who formulated this problem in mathematical terms. These well-known personalities were motivated by compensation received from the Chevalier de Méré to calculate, and presumably optimize, the odds of winning in a variety of simple games of chance. Furthermore, Christiaan Huygens, one of Leibniz's teachers, published the first book on probability entitled *De Ratiociniis in Ludo Aleae*, a treatise on gambling-related problems. As a result, probability theory became popular, and the subject matter developed rapidly during the eighteenth century. Nevertheless, it was not until 1812, when Pierre-Simon de

L. Dagdug et al., *Diffusion Under Confinement*,
https://doi.org/10.1007/978-3-031-46475-1_2

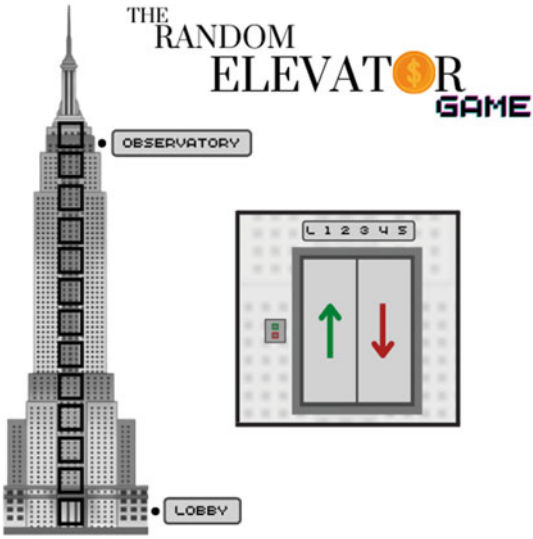

Fig. 2.1 Schematic representation of the random elevator gameboard. The elevator can move either up or down randomly, as when tossing a coin

Laplace introduced new ideas and mathematical techniques in his work *Théorie Analytique des probabilités*, that probabilistic ideas were applied to many scientific and practical problems.

In games of chance, such as the random elevator game, players are usually interested in finding the answer to two questions: what are the chances of winning, and how long can the game be expected to last. Both of these questions can only be answered within a probabilistic framework. As we will see, the answers will depend on the initial position of the player, i.e., whether the contestant is closer to the Observatory or the Lobby. The study and solution to these two questions provide a good illustration of some general ideas and physical properties to be used in analyzing different aspects of diffusion.

2.2 Mathematical Model of the Game: Discrete Version

The first step in formulating the game in mathematical terms is to define the *state space*. In the random elevator game, the states of the game are characterized in terms of the player's position j. To such end, let's set the Lobby at $j = 0$ and the Observatory at $j = L$, considering a diagram consisting of $L + 1$ squares outlined along the vertical length of the building (see Fig. 2.2). The complete possible set of states that may arise in the course of the game consists of integers $\{0, 1, 2, \ldots, L\}$.

Let $A(n)$ be the position of player A after n tosses of the coin. Let us assume that at the beginning of the game, $A(0) = j_0$, which is the floor where the office is located. Then, after the first toss of the coin, $A(1) = j_0 - 1$ if the coin lands on heads; otherwise, $A(1) = j_0 + 1$. A's position after one or more tosses is a random

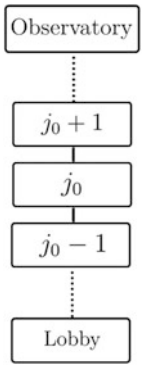

Fig. 2.2 Schematic representation of the random elevator gameboard. The player starts at floor j_0 and can move either up or down on every toss of the coin

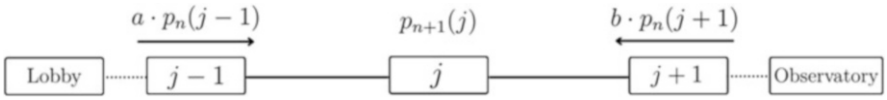

Fig. 2.3 Schematic representation of the state space and the probability of reaching j after $n+1$ steps. To reach j, the player had to be at $j-1$ or $j+1$ at step n and move to j with a probability of $a = b = 1/2$

variable that depends on the specific sequence of heads or tails. We assume that the outcome of every toss of the coin is statistically independent of each other. Then, A's position after $n+1$ tosses, i.e., $A(n+1)$, certainly depends on its location at the n-th toss, $A(n)$.

The random elevator game provides the simplest definition of a *random walk*: a random process that describes a path consisting of a succession of random steps on the integer number line $\mathbb{Z}$, which starts at 0. Each step moves $+1$ or -1 with equal probability. It is worth mentioning that if the process depends only on the previous outcome, then it is known as a *Markov process*.

Now, let's assume that the game ends at the m'th step. This means that at step $m-1$, A's position must have been equal to either $j = 1$, with A being one step from the Lobby, or $j = L-1$, with A preparing to get into the Observatory at the next coin toss with a probability of $1/2$. If $A(m) = 0$, A is already in the Lobby, while if $A(m) = L$, then the player has reached the Observatory. The coordinates $j = 0$ and $j = L$ will be referred to as *absorbing points*, or *traps*, given that the game is over when either one is reached. The specific number of steps m at which the game is over is known as the *first-passage time*.

Let us start by calculating the probability of reaching j after $n+1$ steps or tosses of a coin. This implies that the player had to be at $j-1$ or $j+1$ after n steps (see Fig. 2.3). Let $p_{n+1}(j)$ be the probability that A's position after $n+1$ steps is equal to j (i.e., $A(n+1) = j$). A mathematical equivalent of the rules of the game, i.e., the probability of being at j after $n+1$ steps, is given by the following *master equation*:

$$p_{n+1}(j) = \frac{1}{2}\left[p_n(j-1) + p_n(j+1)\right], \quad \text{where} \quad n = 0, 1, 2, \ldots \tag{2.1}$$

where $2 \leq j \leq L-2$. This equation must be modified at $j = 1$ and $j = L-1$. In the first case, we can only reach $j = 1$ from $j = 2$, and in the second one, we can get to $j = L-1$ from $j = L-2$, since there are no contributions from $j = 0$ or $j = L$. The master equation is essentially a differential equation of the first order in time for the probability density of a Markov stochastic variable. Therefore, when $A(j = 1)$ or $A(j = L-1)$,

$$p_{n+1}(1) = \frac{1}{2} p_n(2), \quad \text{and} \quad p_{n+1}(L-1) = \frac{1}{2} p_n(L-2). \tag{2.2}$$

The latter equations have the same form as Eq. (2.1), provided that we adopt the following conventions:

$$p_n(0) = 0, \quad \text{and} \quad p_n(L) = 0. \tag{2.3}$$

These last relations are a simple example of a boundary condition (BC) and define a *perfect absorbing boundary*. This boundary indicates that the game is over and the player is removed from the board when A's position reaches one of the values, either $j = 0$ or $j = L$. Equation (2.1) must be solved as well, subject to the following *initial conditions*:

$$p_0(j) = \begin{cases} 1, & j = j_0 \\ 0, & j \neq j_0 \end{cases}, \tag{2.4}$$

which is a formal statement of the condition that player A is at j_0 initially. Equations (2.1)–(2.4) translate the random elevator game into a mathematical description. In the remainder of this chapter, we will show that Eqs. (2.1)–(2.4) can be regarded as a discrete form of the diffusion equation. In other words, we will prove that a continuous version of the random elevator game leads to the system of a particle diffusing along a line bounded by two absorbing boundaries. Moreover, the previously presented mathematical formulation is used to answer the two questions posed in the "Introduction."

2.3 Continuous Version of the Game

A continuous version of the random elevator game problem can be formulated by assuming that successive coin tosses occur at very short intervals of time Δt and, similarly, that the step size, i.e., floor spacing, is also a small quantity given by Δx. This is equivalent to measuring an arbitrary time as an integer number of small-time units and, similarly, measuring an arbitrary displacement as an integer number of a small number of stops. Under this scenario, the game is sped up, but the positions and times remain as finite quantities. It will be seen that by letting both Δx and Δt tend to 0, the continuous analog of Eq. (2.1) becomes the diffusion equation.

Let's go a little further in generalizing Eq. (2.1) in the sense that probabilities of the player moving either up or down are not set to $1/2$, but as a and b, where by conservation of probability, $a + b = 1$. This would happen if we used a biased coin over the course of the game. Let's assume that the probability by unit time of going to j from $j + 1$ is given by a and that the probability by unit time of going from $j - 1$ to j is given by b (see Fig. 2.3). After all, we can always return to our original problem by setting $a = b = 1/2$. Then, the probability of being at j after $n + 1$ steps is

$$p_{n+1}(j) = a\, p_n(j+1) + b\, p_n(j-1). \tag{2.5}$$

In order to get to the continuous approach, we must rewrite Eq. (2.5) by changing $j \to x$, $j \pm 1 \to x \pm \Delta x$, $n \to t$, and $n + 1 \to t + \Delta t$. The time $t \in [0, \infty)$ and the spatial position $x \in \Omega$. The spatial domain Ω may be either a bounded or an infinite subset of $\mathbb{R}$, $\mathbb{R}^2$, or $\mathbb{R}^3$ or a manifold. In the cases we are considering here, the domain is restricted to subsets of $\mathbb{R}$. Thus, the latter equation translates into

$$p(x, t + \Delta t) = a\, p(x + \Delta x, t) + b\, p(x - \Delta x, t). \tag{2.6}$$

Expanding this last equation in a Taylor series around Δx and Δt yields

$$\begin{aligned} &p(x,t) + \Delta t \frac{\partial p(x,t)}{\partial t} + \cdots \\ &\quad = a\left[p(x,t) + \Delta x \frac{\partial p(x,t)}{\partial x} + \frac{(\Delta x)^2}{2}\frac{\partial^2 p(x,t)}{\partial x^2} + \cdots\right] \\ &\qquad + b\left[p(x,t) - \Delta x \frac{\partial p(x,t)}{\partial x} + \frac{(\Delta x)^2}{2}\frac{\partial^2 p(x,t)}{\partial x^2} + \cdots\right]. \end{aligned} \tag{2.7}$$

For instance, two identical terms in this last equation are canceled out, and by equating the lowest-order terms in both sides, we obtain

$$\begin{aligned} \Delta t \frac{\partial p(x,t)}{\partial t} &= a\left[\Delta x \frac{\partial p(x,t)}{\partial x} + \frac{(\Delta x)^2}{2}\frac{\partial^2 p(x,t)}{\partial x^2}\right] \\ &\quad + b\left[-\Delta x \frac{\partial p(x,t)}{\partial x} + \frac{(\Delta x)^2}{2}\frac{\partial^2 p(x,t)}{\partial x^2}\right]. \end{aligned} \tag{2.8}$$

When simplifying factors and terms, we find that

$$\frac{\partial p(x,t)}{\partial t} = (a-b)\frac{\Delta x}{\Delta t}\frac{\partial p(x,t)}{\partial x} + \frac{(\Delta x)^2}{2\Delta t}\frac{\partial^2 p(x,t)}{\partial x^2}. \tag{2.9}$$

Then, we define the *drag velocity* as

$$v \equiv -\lim_{\substack{\Delta x \to 0 \\ \Delta t \to 0}} (a-b)\frac{\Delta x}{\Delta t}, \tag{2.10}$$

in such a way that Δx and Δt must decrease as v remains finite. Likewise, we define the *diffusion coefficient* or *diffusivity* as

$$D \equiv \lim_{\substack{\Delta x \to 0 \\ \Delta t \to 0}} \frac{(\Delta x)^2}{2\Delta t}. \tag{2.11}$$

Inserting these last two definitions into (2.9), we get the *Fokker-Planck* or *convection-diffusion equation* in one dimension, namely,

$$\frac{\partial p(x,t)}{\partial t} = D\frac{\partial^2 p(x,t)}{\partial x^2} - v\frac{\partial p(x,t)}{\partial x}. \tag{2.12}$$

The latter equation describes the temporal evolution of the probability density $p(x,t)$. Furthermore, if we set $a = b$, the term involving the drag velocity vanishes, which is equivalent to zero-drift, finding that

$$\frac{\partial p(x,t)}{\partial t} = D\frac{\partial^2 p(x,t)}{\partial x^2}, \tag{2.13}$$

in other words, the well-known *diffusion equation*. The diffusion equation is first order in time and second order in space. It is classified as a parabolic partial differential equation.

It is important to note that after one passes the diffusion limit, $p(x,t)$ is no longer a probability, but rather a probability density. The distinction between these two is that now $p(x,t)\ dx$ is the probability of the diffusion particle being within the interval $x, x+dx$ at time t. Since probabilities are dimensionless and x has units of length, $p(x,t)$ has the dimension of L^{-1}. Furthermore, the continuous analog of the initial condition in Eq. (2.4) is

$$p(x,0) = \delta(x - x_0), \tag{2.14}$$

where x_0 is equal to A's initial position and δ is the Dirac delta function. The perfect absorbing boundary conditions in Eq. (2.3) are then translated into

$$p(0,t) = p(L,t) = 0. \tag{2.15}$$

These last three equations are the continuous analog of the discrete version of the game given by Eqs. (2.1), (2.3), and (2.4).

The diffusion equation can be written in terms of the density number or concentration. Since $c(x,t) = Np(x,t)$, then the classic diffusion equation is given by

$$\frac{\partial c(x,t)}{\partial t} = D\frac{\partial^2 c(x,t)}{\partial x^2}, \tag{2.16}$$

a relation that is also known as Fick's second law of diffusion. Therefore, we will use $c(x,t)$ and $p(x,t)$ interchangeably. The diffusive N particles are called *Brownian particles* or *diffusing particles*. The extrapolation of the diffusion equation to higher dimensions is straightforward using the Laplace operator:

$$\frac{\partial c(\boldsymbol{r},t)}{\partial t} = D\nabla^2 c(\boldsymbol{r},t). \tag{2.17}$$

The diffusion coefficient has dimensions of $L^2\ T^{-1}$, and it is defined according to the dimension of the problem, differing by a factor of $1/2$ for each extra space dimension. Therefore, to obtain the corresponding diffusion constant for a three-dimensional system, we need to remember that $\Delta r^2 = \Delta x^2 + \Delta y^2 + \Delta z^2$, which by dividing by $2\Delta t$, gives

$$\frac{\Delta r^2}{2\Delta t} = \frac{\Delta x^2}{2\Delta t} + \frac{\Delta y^2}{2\Delta t} + \frac{\Delta z^2}{2\Delta t}. \tag{2.18}$$

If the diffusion coefficient for any direction is equal to D, i.e., $D_x = D_y = D_z = D$, referring to an isotropic fluid, then the diffusivity in three dimensions is

$$D \equiv \lim_{\substack{\Delta\mathbf{r}\to 0\\ \Delta t\to 0}} \frac{\Delta\mathbf{r}^2}{6\Delta t}. \tag{2.19}$$

When the diffusion takes place into an anisotropic medium, the diffusivity is given by a tensor.

The diffusion coefficient depends on molecule size and other properties of the diffusing substance, as well as on temperature and pressure. Diffusion coefficients of one substance into the other are commonly determined experimentally. A typical diffusion coefficient for a molecule in the gas phase is in the range of 10^{-6} to 10^{-5} m^2/s. In contrast, diffusion for molecules dissolved in liquids is far slower, with the typical diffusion coefficient being in the range of 10^{-10} to 10^{-9} m^2/s. Therefore, diffusion in liquids is very slow over everyday length scales and is almost always dominated by convection.

For molecules diffusing within the cell, the time it takes them to travel a certain distance can be estimated using Eq. (2.11). For a monomeric protein with a 5-nm diameter, the diffusion constant in cytoplasm is around 10 $\mu m^2/s$. The time scale for such a typical protein to diffuse a distance equivalent to the length of an *E. coli* bacterium (i.e., 1 μm) is approximately 1 $\mu m^2/[6\ (10\ \mu m^2/s)] \approx 1.6 \times 10^{-2}$s. In contrast, the time required for diffusion to transport the same protein from one end of a neuronal cell axon to the other (i.e., a distance of around 1 cm) is approximately 1.6×10^6 s or nearly 20 days! Nature's solution to this dilemma is to use active

transport mechanisms where motor molecules use ATP to transport the cargo to its destination.

At this point, we are almost ready to answer the questions posed in the "Introduction." To such end, we will solve the diffusion equation in the next section, subject to the initial and boundary conditions given in Eqs. (2.14) and (2.15).

2.3.1 Solution to the Continuous Model

To find the solution of the diffusion equation within the interval $(0, L)$, we assume that $p(x, t)$ is sufficiently well-behaved so it can be expanded into a Fourier series (see Appendix A, Sect. A.6.2), namely,

$$p(x,t) = \sum_{n=1}^{\infty} \left[a_n(t) \ \sin\left(\frac{n\pi x}{L}\right) + b_n(t) \ \cos\left(\frac{n\pi x}{L}\right) \right]. \tag{2.20}$$

The BC $p(0, t) = 0$ implies that the $b_n(t)$ are all equal to zero, while the remaining term satisfies the boundary conditions (BCs) given in Eqs. (2.15). Then, if we substitute the remaining first term into the diffusion equation, Eq. (2.13), this leads to

$$\frac{\partial}{\partial t}\left[\sum_{n=1}^{\infty} a_n(t) \sin\left(\frac{n\pi x}{L}\right)\right] = D\frac{\partial^2}{\partial x^2}\left[\sum_{n=1}^{\infty} a_n(t) \sin\left(\frac{n\pi x}{L}\right)\right]. \tag{2.21}$$

Due to the linear independence of the sine functions, the latter equation is finally expressed as

$$\frac{\mathrm{d}a_n(t)}{\mathrm{d}t} = -\frac{\pi^2 n^2 D}{L^2} a_n(t), \tag{2.22}$$

which is directly integrable and has solution

$$a_n(t) = \mathcal{A}_n \ \exp\left(-\frac{\pi^2 n^2 D t}{L^2}\right). \tag{2.23}$$

The $\mathcal{A}_n$'s are constants to be determined by the initial conditions. Thus, we have the representation of $p(x, t)$ as

$$p(x,t) = \sum_{n=1}^{\infty} \mathcal{A}_n \ \exp\left(-\frac{\pi^2 n^2 D t}{L^2}\right) \sin\left(\frac{n\pi x}{L}\right). \tag{2.24}$$

To determine the $\mathcal{A}_n$'s constants, we set $t = 0$ and make use of the initial condition (2.14). This requires that

$$\sum_{n=1}^{\infty} \mathcal{A}_n \sin\left(\frac{n\pi x}{L}\right) = \delta(x - x_0). \tag{2.25}$$

Since the delta function can be represented as the Fourier series, namely,

$$\delta(x - x_0) = \frac{2}{L} \sum_{n=1}^{\infty} \sin\left(\frac{n\pi x_0}{L}\right) \sin\left(\frac{n\pi x}{L}\right), \tag{2.26}$$

and again by linear independence of the sine functions, the solution to Eq. (2.25) is therefore

$$\mathcal{A}_n = \frac{2}{L} \sin\left(\frac{n\pi x_0}{L}\right). \tag{2.27}$$

Finally, the probability density $p(x, t|x_0)$ is given by

$$p(x, t|x_0) = \frac{2}{L} \sum_{n=1}^{\infty} \exp\left(-\frac{n^2\pi^2 Dt}{L^2}\right) \sin\left(\frac{n\pi x_0}{L}\right) \sin\left(\frac{n\pi x}{L}\right). \tag{2.28}$$

The probability density decays in time characterized by the diffusion time L^2/D. The temporal evolution of the probability density (2.28) is depicted in Fig. 2.4. This timeline shows, in terms of Brownian particles, how they are captured by the absorbing traps when times goes by until they all finally leave the system.

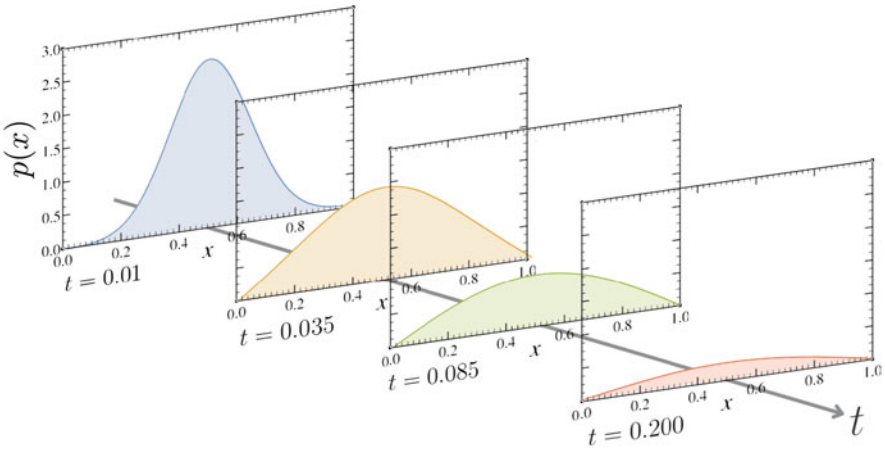

Fig. 2.4 Temporal evolution of the probability density $p(x, t|x_0)$ predicted by Eq. (2.28) is shown. The initial position of Brownian particles, system length, and diffusivity are $x_0 = 0.5$, $L = 1$, and $D = 1$, respectively. Whereas x_0 and L have units of length, D has units of length^2/time, and $p(x, t)$ of length^{-1}. The absorbing BCs are $p(x = 0, t) = p(x = L, t) = 0$

The probability density $p(x, t|x_0)$ will also be referred to as the *propagator*, as it describes the propagation of the particle from its initial position to its position at time t. Using (2.28), we will be able to find a solution to the two questions posed earlier: what is the mean first-passage time, and what is the probability that player A will reach the Observatory or the Lobby.

2.4 Duration of the Game

2.4.1 Survival Probability and First-Passage Time

As we are interested in determining the time it will take to finish the game, we have to determine the probability density for the duration of the game. Counter to our intuition, we start by calculating the probability that the game has not ended by time t. This can be written directly in terms of the propagator $p(x, t|x_0)$. This probability will be referred to as the *survival probability* and will be denoted by $S(t|x_0)$.

Let us return for a moment to the discrete version of the game and ask what is the probability of the game not having ended by the n'th toss, i.e., the probability of A's position being equal to $\{1, 2, \ldots, L-1\}$ at the n'th toss. This probability is

$$S_n(j_0) = \sum_{j=1}^{L-1} p_n(j|j_0) = \sum_{j=0}^{L} p_n(j|j_0). \tag{2.29}$$

Note that in the last equality, we have extended the summation interval to $[0, L]$, since there is no contribution to the survival probability due to $p_n(j = 0|j_0) = p_n(j = L|j_0) = 0$. If we pass to the continuum limit, the sum over j in Eq. (2.29) needs to be replaced by an integral with respect to x over the entire interval, in our case, from 0 to L. Meanwhile, the probability $p_n(j|j_0)$ is replaced by $p(x, t|x_0)\ \mathrm{d}x$, which is the probability of being between x and $x + dx$ at time t. Thus, $S(t|x_0)$ can be written as

$$S(t|x_0) = \int_0^L p(x, t|x_0)\ \mathrm{d}x. \tag{2.30}$$

Equation (2.30) gives the probability that the game has not ended by time t once the game has started at x_0. Since $p(x, t|x_0)$ is integrated with respect to x, $S(t|x_0)$ is dimensionless. This relation can be used to find the probability density for the duration of the game, i.e., the probability density of the first-passage time, which will be denoted by $\varphi(t|x_0)$. From this definition, we have that the probability of ending the game within the interval τ, $\tau + \mathrm{d}\tau$ is given by $\varphi(\tau|x_0)\ \mathrm{d}\tau$. This means that the integral of $\varphi(\tau|x_0)\ \mathrm{d}\tau$ from 0 to t is the probability of finishing the game at time t and this is equal to not surviving at time t, in other words, $1 - S(t|x_0)$. Hence,

$$\int_0^t \varphi(\tau|x_0)\,\mathrm{d}\tau = 1 - S(t|x_0). \tag{2.31}$$

Then, the probability of not having finished the game at time t is given by the integral of $\varphi(\tau|x_0)$ from $\tau = t$ to $\tau \to \infty$, which is the same as the survival probability. Consequently, the two functions are related by

$$\int_t^\infty \varphi(\tau|x_0)\,\mathrm{d}\tau = S(t|x_0). \tag{2.32}$$

Taking the derivative of both sides of this equation with respect to t

$$\frac{\mathrm{d}}{\mathrm{d}t}\int_t^\infty \varphi(\tau|x_0)\,\mathrm{d}\tau = \lim_{\zeta\to\infty}\varphi(\tau|x_0)\Big|_{\tau=t}^{\tau=\zeta} = \frac{\mathrm{d}S(t|x_0)}{\mathrm{d}t}, \tag{2.33}$$

and evaluating the upper limit since $\varphi(\tau \to \infty|x_0) = 0$, we get

$$\varphi(t|x_0) = -\frac{\mathrm{d}S(t|x_0)}{\mathrm{d}t}. \tag{2.34}$$

This last equation is a practical formula to calculate the probability density of the mean first-passage time, which is one of the fundamental properties of diffusion, and its dimension is T^{-1}.

Back to our game, the survival probability for the random elevator player is calculated if $p(x, t|x_0)$ in Eq. (2.28) is substituted into (2.30). As such,

$$S(t|x_0) = \int_0^L \frac{2}{L}\sum_{n=1}^\infty \exp\left(-\frac{n^2\pi^2 Dt}{L^2}\right)\sin\left(\frac{n\pi x_0}{L}\right)\sin\left(\frac{n\pi x}{L}\right)\mathrm{d}x. \tag{2.35}$$

Integrating gives

$$S(t|x_0) = -\frac{2}{L}\sum_{n=1}^\infty \exp\left(-\frac{n^2\pi^2 Dt}{L^2}\right)\sin\left(\frac{n\pi x_0}{L}\right)\left(\frac{L}{n\pi}\right)\cos\left(\frac{n\pi x}{L}\right)\Bigg|_0^L, \tag{2.36}$$

and after evaluating,

$$S(t|x_0) = -\frac{2}{\pi}\sum_{n=1}^\infty \exp\left(-\frac{n^2\pi^2 Dt}{L^2}\right)\sin\left(\frac{n\pi x_0}{L}\right)\left(\frac{1}{n}\right)[\cos(n\pi) - 1]. \tag{2.37}$$

Since in $\cos(n\pi) = (-1)^n$ only odd terms contribute to the sum, we finally have

$$S(t|x_0) = \frac{4}{\pi}\sum_{n=0}^\infty \exp\left[-\frac{(2n+1)^2\pi^2}{L^2}Dt\right]\frac{\sin\left[\frac{(2n+1)}{L}\pi x_0\right]}{2n+1}. \tag{2.38}$$

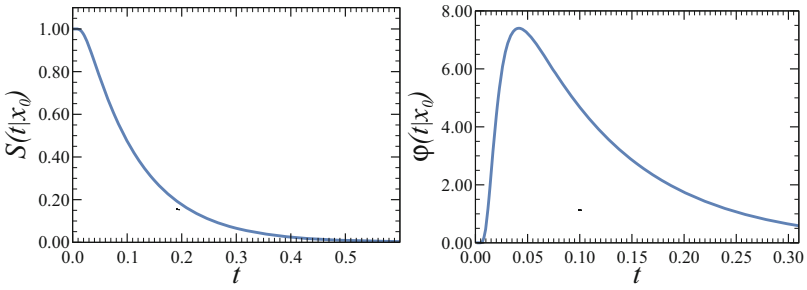

Fig. 2.5 Survival probability predicted by Eq. (2.38) and the probability density of first-passage time given by Eq. (2.39), as a function of time t. The relation between them is given by Eq. (2.34). The initial position, system length, and diffusivity are $x_0 = 0.5$, $L = 1$, and $D = 1$, respectively

Now, by introducing this survival probability into (2.34), we find the explicit expression of the probability density $\varphi(t|x_0)$ for the random elevator game:

$$\begin{aligned}\varphi(t|x_0) &= -\frac{\mathrm{d}}{\mathrm{d}t}\left\{\frac{4}{\pi}\sum_{n=0}^{\infty}\exp\left[-\frac{(2n+1)^2\pi^2}{L^2}Dt\right]\frac{\sin\left[\frac{(2n+1)}{L}\pi x_0\right]}{2n+1}\right\}\\ &= \frac{4D\pi}{L^2}\sum_{n=0}^{\infty}(2n+1)\exp\left[-\frac{(2n+1)^2\pi^2}{L^2}Dt\right]\sin\left[\frac{(2n+1)}{L}\pi x_0\right].\end{aligned} \tag{2.39}$$

Figure 2.5 shows the survival probability predicted by Eq. (2.38) and the probability density of the first-passage time given by Eq. (2.39), as a function of time t. As we can see, at the beginning of the process, the probability of Brownian particles surviving is equal to one, and as time passes, the probability begins to decrease until it reaches zero. On the other hand, at the beginning, $\varphi(t|x_0)$ starts at zero because it takes a while for the particles to become trapped. As time passes, it increases until it reaches a maximum, within which the most probable first-passage time is found. Finally, it tends toward zero, which means that very few Brownian particles will spend very long periods of time without being absorbed by the boundaries, something that is highly unlikely.

2.5 Moments of the Mean First-Passage Time

A fundamental definition in probability theory is given by the *moments* μ_n of a probability distribution $f(x)$, where $n = 0, 1, 2, 3, \ldots$, namely,

$$\mu_n \equiv \int_{-\infty}^{\infty} x^n f(x)\, \mathrm{d}x. \tag{2.40}$$

With this definition in hand, we can now answer the question of how long the game can be expected to last. The average duration $\langle t(x_0)\rangle$ of the random elevator game or *mean first-passage time* (MFPT), which is the probability of a random walk or a diffusing particle hitting the absorbing boundary for the first time, is given by the first moment of $\varphi(t|x_0)$, subsequently

$$\langle t(x_0)\rangle = \int_0^{\infty} t\ \varphi(t|x_0)\, \mathrm{d}t. \tag{2.41}$$

Introducing (2.34) into the last equation, we find a fundamental and practical relation between the MFPT and the survival probability, namely,

$$\langle t(x_0)\rangle = -\int_0^{\infty} t\ \frac{\mathrm{d}S(t|x_0)}{\mathrm{d}t}\, \mathrm{d}t. \tag{2.42}$$

Integrating it by parts leads to

$$\begin{aligned} \langle t(x_0)\rangle &= -\left[t \int \frac{\mathrm{d}S(t|x_0)}{\mathrm{d}t}\, \mathrm{d}t\right]_0^{\infty} + \int_0^{\infty} S(t|x_0)\mathrm{d}t \\ &= -\left[t\ S(t|x_0)\right]|_0^{\infty} + \int_0^{\infty} S(t|x_0)\, \mathrm{d}t. \end{aligned} \tag{2.43}$$

Considering that the survival probability is one at $t = 0$ and null after a very long time, meaning that the particle will definitely be absorbed, and because $S(t|x_0)$ goes to zero faster than the power law as t goes to infinity, then the latter equation is simplified to

$$\langle t(x_0)\rangle = \int_0^{\infty} S(t|x_0)\, \mathrm{d}t. \tag{2.44}$$

This relation is very useful for carrying out computations.

Back to our game, using the explicit equation for $S(t|x_0)$ given by Eq. (2.38), we get the MFPT in terms of a sum

$$\begin{aligned} \langle t(x_0)\rangle &= \frac{4}{\pi}\sum_{n=0}^{\infty} \frac{\sin\left[\frac{(2n+1)}{L}\pi x_0\right]}{2n+1} \int_0^{\infty} \exp\left[-\frac{(2n+1)^2\pi^2}{L^2} Dt\right] \mathrm{d}t \\ &= \frac{4}{\pi}\sum_{n=0}^{\infty} \frac{\sin\left[\frac{(2n+1)}{L}\pi x_0\right]}{2n+1} \left[-\frac{L^2}{(2n+1)^2 D\pi^2}\right] \exp\left[-\frac{(2n+1)^2\pi^2}{L^2} Dt\right]\Bigg|_0^{\infty}, \end{aligned} \tag{2.45}$$

leading to

$$\langle t(x_0)\rangle = \frac{4L^2}{D\pi^3}\sum_{n=0}^{\infty}\frac{\sin\left[\frac{(2n+1)}{L}\pi x_0\right]}{(2n+1)^3}. \tag{2.46}$$

It is possible to find a simpler expression than (2.46) by differentiating $\langle t(x_0)\rangle$ twice with respect to x_0, namely,

$$\frac{\mathrm{d}^2\langle t(x_0)\rangle}{\mathrm{d}x_0^2} = -\frac{4}{D\pi}\sum_{n=0}^{\infty}\frac{\sin\left[\frac{(2n+1)}{L}\pi x_0\right]}{2n+1} = -\frac{4}{D\pi}\sum_{n=1}^{\infty}\frac{\sin\left[\frac{(2n-1)}{L}\pi x_0\right]}{2n-1}, \tag{2.47}$$

and after computing the sum, given in Eq. (A.32), we have

$$\frac{\mathrm{d}^2\langle t(x_0)\rangle}{\mathrm{d}x_0^2} = -\frac{4}{D\pi}\left[\frac{\pi}{4}\,\mathrm{sgn}\left(\frac{\pi x_0}{L}\right)\right] = -\frac{1}{D}. \tag{2.48}$$

Integrating the latter equation twice gives

$$\langle t(x_0)\rangle = -\frac{1}{2D}x_0^2 + \mathcal{B}x_0 + \mathcal{A}. \tag{2.49}$$

The two constants $\mathcal{A}$ and $\mathcal{B}$ can be obtained by demanding that $\langle t(x_0)\rangle$ satisfies the BCs where $\langle t(0)\rangle = \langle t(L)\rangle = 0$, and the reader can immediately see that $\mathcal{A} = 0$ and $\mathcal{B} = L/(2D)$, leading to the solution:

$$\langle t(x_0)\rangle = \frac{x_0(L-x_0)}{2D}. \tag{2.50}$$

This mathematical expression is equal to 0 at the absorbing endpoints and reaches its maximum, $L^2/8D$, when the player starts at the middle point (see Fig. 2.6 for $n = 1$).

The nth moment of the first-passage time can be similarly derived using the same process above, simply by integrating the definition

$$\begin{aligned}\langle t^n(x_0)\rangle &= \int_0^{\infty} t^n\varphi(t|x_0)\,\mathrm{d}t = -\int_0^{\infty} t^n\frac{\mathrm{d}S(t|x_0)}{\mathrm{d}t}\,\mathrm{d}t, \qquad n = 1, 2, 3, \ldots \\ &= \left[-t^n\ S(t|x_0)\right]\Big|_0^{\infty} + n\int_0^{\infty} t^{n-1}S(t|x_0)\,\mathrm{d}t,\end{aligned} \tag{2.51}$$

which gives

$$\langle t^n(x_0)\rangle = n\int_0^\infty t^{n-1}S(t|x_0)\,\mathrm{d}t. \tag{2.52}$$

Talking about our game, and using the explicit equation for $S(t|x_0)$ given by Eq. (2.38) into (2.52), we can compute the n'th moment of the first-passage time, namely,

$$\begin{aligned}\langle t^n(x_0)\rangle &= n\int_0^\infty t^{n-1}\left\{\frac{4}{\pi}\sum_{m=0}^{\infty}\exp\left[-\frac{(2m+1)^2\pi^2}{L^2}Dt\right]\frac{\sin\left[\frac{(2m+1)}{L}\pi x_0\right]}{2m+1}\right\}\mathrm{d}t\\ &= \frac{4n}{\pi}\sum_{m=0}^{\infty}\frac{\sin\left[\frac{(2m+1)}{L}\pi x_0\right]}{2m+1}\int_0^\infty t^{n-1}\exp\left[-\frac{(2m+1)^2\pi^2}{L^2}Dt\right]\mathrm{d}t\\ &= \frac{4n}{\pi}\sum_{m=0}^{\infty}\frac{\sin\left[\frac{(2m+1)}{L}\pi x_0\right]}{2m+1}(n-1)!\left[\frac{(2m+1)^2\pi^2}{L^2}Dt\right]^{-(n-1)-1},\end{aligned} \tag{2.53}$$

using Eq. (A.10) to perform the integration. Finally, by collecting terms, we have

$$\langle t^n(x_0)\rangle = \frac{4}{\pi}\left(\frac{L^2}{D\pi^2}\right)^n n!\sum_{m=0}^{\infty}\frac{\sin\left[\frac{(2m+1)}{L}\pi x_0\right]}{(2m+1)^{2n+1}}. \tag{2.54}$$

Figure 2.6 depicts the first two moments of the MFPT.

In the next section, we will show that the calculation of $\langle t(x_0)\rangle$ can be done easily by solving an ordinary differential equation (ODE). This formalism also allows us to find expressions in closed form for the moments of higher order.

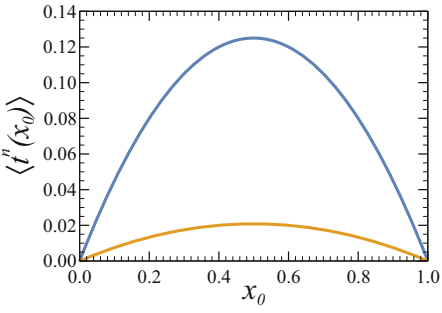

Fig. 2.6 First two moments of the MFPT predicted by Eq. (2.54), setting $n = 1$ (blue line) and $n = 2$ (yellow line). The first moment is reduced to Eq. (2.50). The system length and diffusivity are set to $L = 1$ and $D = 1$, respectively

2.6 The Backward Equation

If we take a close look at Eq. (2.28), it is easy to see that $p(x, t|x_0)$ is symmetric in the variables x and x_0, i.e.,

$$p(x, t|x_0) = p(x_0, t|x). \tag{2.55}$$

Then, the diffusion equation could also be written using the latter symmetry statement as

$$\frac{\partial p(x_0, t|x)}{\partial t} = D\frac{\partial^2 p(x_0, t|x)}{\partial x_0^2}. \tag{2.56}$$

Because of this last result, it is convenient to rename the diffusion equation, Eq. (2.13), as the *forward equation* and Eq. (2.56), in which the spatial derivatives are taken with respect to x_0, as the *backward equation*.

As we will see below, the importance of the backward equations is that it allows us to find the differential equations that govern both the survival probability and the MFPT. To such end, let us integrate both sides of (2.56) with respect to x and use (2.55). For the left-hand term, we have

$$\int_0^L \frac{\partial p(x, t|x_0)}{\partial t}\, \mathrm{d}x = \frac{\partial}{\partial t}\int_0^L p(x, t|x_0)\, \mathrm{d}x = \frac{\partial S(t|x_0)}{\partial t}, \tag{2.57}$$

and for the right-hand term, we have

$$D\int_0^L \frac{\partial^2 p(x, t|x_0)}{\partial x_0^2}\, \mathrm{d}x = D\frac{\partial^2}{\partial x_0^2}\int_0^L p(x, t|x_0)\, \mathrm{d}x = D\frac{\partial^2 S(t|x_0)}{\partial x_0^2}. \tag{2.58}$$

Therefore, equating these two last relations, we observe that $S(t|x_0)$ satisfies the following differential equation:

$$\frac{\partial S(t|x_0)}{\partial t} = D\frac{\partial^2 S(t|x_0)}{\partial x_0^2}. \tag{2.59}$$

Equation (2.59) provides a simpler way to calculate the survival probability without the integration of the propagator $p(x, t|x_0)$. It is worth noting that the boundary conditions in the presence of two absorbing boundaries at $x_0 = 0$ and $x_0 = L$ are given by $S(t|0) = S(t|L) = 0$ and the initial condition is $S(0|x_0) = 1$ for $x_0 \notin \{0, L\}$. Now, we are one step further to finding a similar relation to the MFPT. Accordingly, when multiplying Eq. (2.59) by nt^{n-1}, then

$$\frac{\partial S(t|x_0)}{\partial t} nt^{n-1} = D\frac{\partial^2 S(t|x_0)}{\partial x_0^2} nt^{n-1}, \tag{2.60}$$

and integrating with respect to t, while considering Eq. (2.52), leads to

$$\int_0^\infty \frac{\partial S(t|x_0)}{\partial t} n t^{n-1}\, \mathrm{d}t = \int_0^\infty D \frac{\partial^2 S(t|x_0)}{\partial x_0^2} n t^{n-1}\, \mathrm{d}t. \tag{2.61}$$

By performing the integrals, we finally find that $\langle t^n(x_0)\rangle$ must satisfy

$$-n\langle t^{n-1}(x_0)\rangle = D\frac{\mathrm{d}^2\langle t^n(x_0)\rangle}{\mathrm{d}x_0^2}. \tag{2.62}$$

The generalization to higher dimensions is given by

$$\nabla^2\langle t^n(\mathbf{r_0})\rangle = -\frac{n}{D}\langle t^{n-1}(\mathbf{r_0})\rangle. \tag{2.63}$$

If we were to look for the first moment, the MFPT, from Eq. (2.62), the reader could easily verify that it should satisfy

$$D\frac{\mathrm{d}^2\langle t(x_0)\rangle}{\mathrm{d}x_0^2} = -1, \tag{2.64}$$

due to the identity $\langle t^0(x_0)\rangle = 1$. This last equation gives a straightforward way to compute the MFPT and is one of the fingerprints of diffusion. The BCs in the presence of two absorbing boundaries at $x_0 = 0$ and $x_0 = L$ are given by $\langle t(0)\rangle = \langle t(L)\rangle = 0$, which correspond to the exit time being equal to zero if the particle starts at the boundary, and the initial condition is $\langle t(x_0)\rangle = 1$ for x_0.

The second moment of the MFPT for the random elevator game can be calculated from the first moment. By using (2.62), we have

$$D\frac{\mathrm{d}^2\langle t^2(x_0)\rangle}{\mathrm{d}x_0^2} = -2\langle t(x_0)\rangle = -\frac{x_0(L-x_0)}{D}, \tag{2.65}$$

where we have used the first moment given by Eq. (2.50). After solving (2.65), one finds that

$$\langle t^2(x_0)\rangle = -\frac{Lx_0^3}{6D^2} + \frac{x_0^4}{12D^2} + Ax_0 + B. \tag{2.66}$$

Now, subject to the BCs $\langle t^2(0)\rangle = \langle t^2(L)\rangle = 0$, we find that $B = 0$ and $A = L^3/12D^2$. Finally, the second moment is given by

$$\langle t^2(x_0)\rangle = \frac{1}{12D^2}\left(x_0^4 - 2Lx_0^3 + L^3x_0\right), \tag{2.67}$$

which finally leads to the result

$$\langle t^2(x_0)\rangle = \frac{x_0(L-x_0)\left(L^2+Lx_0-x_0^2\right)}{12D^2}. \tag{2.68}$$

Expressions for higher moments can be computed via a recurrence relation as well. Figure 2.6 shows the first two moments of the MFPT.

2.7 Going to the Observatory or the Lobby

The *splitting probability* is defined as the probability of player A reaching one of the endpoints, the Observatory or the Lobby. To find this probability, we need to calculate the probability of the player, who is initially at x_0 between the two absorbing points, becoming trapped at either $x = 0$ or $x = L$. This probability will be denoted by $\theta_0(x_0)$ and $\theta_L(x_0)$, respectively. To such end, we will limit ourselves to the continuous model and use a new quantity to be defined: the *probability flux*.

2.7.1 Probability Flux

Joseph Fourier made a significant contribution to the study of heat transfer phenomena by introducing the concept of *flux*. In his influential work, *Théorie analytique de la chaleur (The Analytical Theory of Heat)*, he defines fluxion as a fundamental measure and then proceeds to derive equations for flux based on temperature differentials. The same definition was later extended by Fick in terms of concentration.

In one dimension, diffusing particles can go to one side or the other, and the flux between two adjacent points is computed by counting the net number of particles crossing a unit length per unit of time. Now, in order to think in terms of fluxes, we need to recall that the probability density is analogous to the concentration of Brownian particles. This similarity will help us to define the *probability flux*, denoted by $J(x,t)$, with dimension of T^{-1}. Then, we note that the probability of being between x and $x+\Delta x$ within an interval of time Δt is equal to the difference between the fluxes in and out of the interval. This leads to

$$\frac{\partial p(x,t)}{\partial t}\Delta x = J(x,t) - J(x+\Delta x,t). \tag{2.69}$$

The Taylor series expression of the latter equation is given as follows:

$$\frac{\partial p(x,t)}{\partial t}\Delta x = J(x,t) - \left[J(x,t) + \Delta x \frac{\partial J(x,t)}{\partial x} + \frac{(\Delta x)^2}{2}\frac{\partial^2 J(x,t)}{\partial x^2} + \cdots \right]. \tag{2.70}$$

Retaining only the linear terms in Δx, we find that

$$\frac{\partial p(x,t)}{\partial t} = -\frac{\partial J(x,t)}{\partial x}, \tag{2.71}$$

which can be regarded as the *conservation equation* for the probability or *continuity equation*. The generalization to higher dimensions is straightforward, namely,

$$\frac{\partial p(\mathbf{r},t)}{\partial t} + \nabla \cdot \mathbf{J} = 0. \tag{2.72}$$

A direct comparison of Eq. (2.71) with the diffusion equation, Eq. (2.13), shows that

$$\mathbf{J}(x,t) = -D\frac{\partial p(x,t|x_0)}{\partial x}\,\hat{\mathbf{e}}_i, \tag{2.73}$$

which is widely known as Fick's first law of diffusion. It postulates that the flux goes from regions of high concentration to regions of low concentration, with a magnitude that is proportional to the concentration gradient. A diffusion process that obeys Fick's laws is called normal or Fickian diffusion.

The vectorial properties of the flux are manifested explicitly when the spatial derivative in Eq. (2.73) is replaced by the gradient ∇. Then, the generalization is

$$\mathbf{J}(\mathbf{r},t) = -D\nabla p(\mathbf{r},t). \tag{2.74}$$

In a three-dimensional Cartesian coordinate system, with a Euclidean metric, the gradient ∇ (see Appendix B) is given by

$$\nabla = \frac{\partial}{\partial x}\hat{\mathbf{e}}_i + \frac{\partial}{\partial y}\hat{\mathbf{e}}_j + \frac{\partial}{\partial z}\hat{\mathbf{e}}_k. \tag{2.75}$$

2.7.2 Probability Flux at the Observatory and the Lobby

Now, using Fick's first law, Eq. (2.74), we can calculate the fluxes for the random elevator game problem based on the propagator expressed in Eq. (2.28), which must be differentiated as follows:

$$-D\frac{\partial p(x,t|x_0)}{\partial x} = -\frac{2D\pi}{L^2}\sum_{n=1}^{\infty} n\,\exp\left(-\frac{n^2\pi^2 Dt}{L^2}\right)\sin\left(\frac{n\pi x_0}{L}\right)\cos\left(\frac{n\pi x}{L}\right). \tag{2.76}$$

In Fig. (2.7), we show the time evolution of the latter equation.

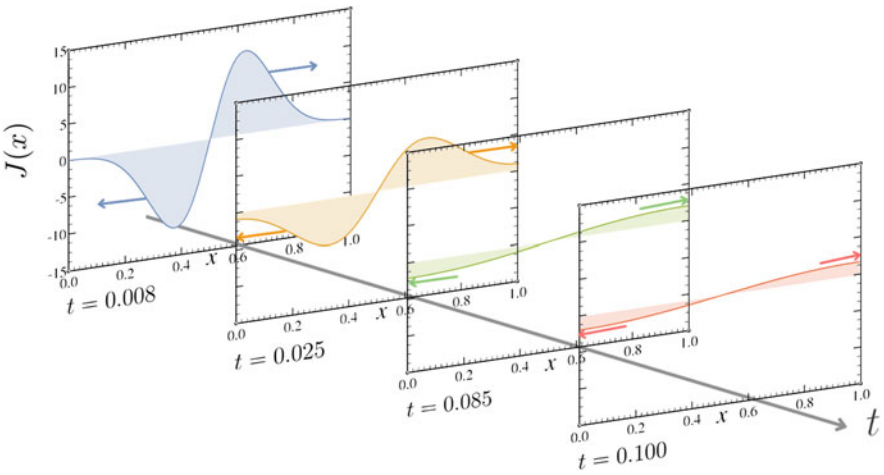

Fig. 2.7 Time evolution of the flux $J(x,t)$. The initial position of the Brownian particles, the system length, and the diffusivity are $x_0 = 0.5$, $L = 1$, and $D = 1$, respectively. Whereas x_0 and L have units of length, D has units of length^2/time, and $p(x,t)$ of length^{-1}. The absorbing BCs are $p(x=0,t) = p(x=L,t) = 0$

Once we have the general expression for the probability flux, Eq. (2.76), there are two points where measuring is relevant, namely, the absorbing points. It is worth noting that even though Eq. (2.76) gives the magnitude of the flux, the net flux of particles crossing a wall is given by $\mathbf{J}\cdot\hat{\mathbf{n}}$, where $\hat{\mathbf{n}}$ is the unit normal vector to the surface. Then, at $x = L$, we have

$$\begin{aligned} J(L,t) &= -D\frac{\partial p(x,t|x_0)}{\partial x}\bigg|_{x=L}\hat{\mathbf{e}}_i\cdot\hat{\mathbf{n}} \\ &= -\frac{2D\pi}{L^2}\sum_{n=1}^{\infty} n\ \exp\left(-\frac{\pi^2 n^2 Dt}{L^2}\right)\sin\left(\frac{n\pi x_0}{L}\right)\cos(n\pi)\,\hat{\mathbf{e}}_i\cdot\hat{\mathbf{e}}_i\,, \end{aligned} \tag{2.77}$$

where the factor $\cos(n\pi)$ yields 1 when n is an even number and -1 when n is an odd number. This leads to

$$J(L,t) = -\frac{2D\pi}{L^2}\sum_{n=1}^{\infty}(-1)^n\ n\ \exp\left(-\frac{\pi^2 n^2 Dt}{L^2}\right)\sin\left(\frac{n\pi x_0}{L}\right). \tag{2.78}$$

An analogous computation for the Lobby placed at $x = 0$ is carried out. Because the flux in this case is westward, it yields

$$J(0,t) = -\,D\frac{\partial p(x,t|x_0)}{\partial x}\bigg|_{x=0}\hat{\mathbf{e}}_i\cdot(-\hat{\mathbf{e}}_i)$$

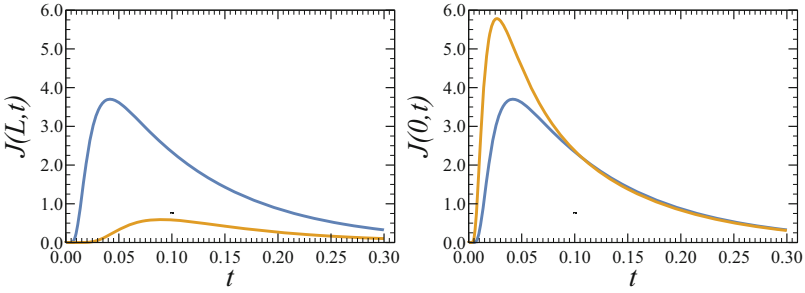

Fig. 2.8 Flux at L and 0 as a function of time, given by Eqs. (2.78) and (2.79), respectively. The initial position is $x_0 = 0.5$ (blue line) and $x_0 = 0.1$ (yellow line), along with $L = 1$ and $D = 1$ for both absorbing points

$$= \frac{2D\pi}{L^2} \sum_{n=1}^{\infty} n \, \exp\left(-\frac{\pi^2 n^2 Dt}{L^2}\right) \sin\left(\frac{n\pi x_0}{L}\right). \tag{2.79}$$

Both fluxes as a function of time and the initial position can be compared in Fig. 2.8. In order to analyze the curves obtained, it is simpler to think in terms of Brownian particles. These plots, as a function of time, show that they start with null flux, and as time goes by, they reach a maximum, followed by a decrease toward null flux, once there are no more particles in the system. As a function of the initial position, we can see that being closer to each of the absorbing boundaries speeds up how particles leave the system, reaching the maximum flux sooner. In contrast, being farther from the absorbing coordinate slows down how particles leave the system, and the maximum is reached later.

2.8 Moments of Mean First-Passage Time: Revisited

Our first task in this section will be to find the relationship between the density flux, the MFPT, and its probability density $\varphi(t|x_0)$. To such end, integrating both sides of the continuity equation with respect to x over the interval from 0 to L gives

$$\int_0^L \frac{\partial p(x,t)}{\partial t} \, \mathrm{d}x = -\int_0^L \nabla \cdot \mathbf{J} \, \mathrm{d}x = -\int_0^L \frac{\partial}{\partial x} \hat{\mathbf{e}}_i \cdot \mathbf{J}(x,t) \, \mathrm{d}x. \tag{2.80}$$

Then, by substituting Eqs. (2.30) and (2.34) into (2.80) for the left-hand side, we have

$$\frac{\partial}{\partial t} \int_0^L p(x,t) \, \mathrm{d}x = \frac{\partial S(t|x_0)}{\partial t} = -\varphi(t|x_0), \tag{2.81}$$

and for the right-hand side, we have

$$-\int_0^L \frac{\partial}{\partial x}\hat{\mathbf{e}}_i \cdot \mathbf{J}(x,t)\,\mathrm{d}x = -\hat{\mathbf{e}}_i \cdot [J(L,t)\hat{\mathbf{e}}_i - J(0,t)(-\hat{\mathbf{e}}_i)]. \tag{2.82}$$

Equating these two last results, we have

$$\varphi(x_0|t) = J(L,t) + J(0,t). \tag{2.83}$$

By substituting Eq. (2.83) into Eq. (2.41), we find the MFPT in terms of flux, namely,

$$\langle t(x_0)\rangle = \int_0^\infty t\,[J(L,t) + J(0,t)]\,\mathrm{d}t. \tag{2.84}$$

Equations (2.83) and (2.84) are a useful relation that will be used extensively throughout the text.

Our second task will be to show how the moments of the mean first-passage time in the time domain could be related to the Laplace transform of the survival probability $S(t|x_0)$, as well as to the Laplace transform of $\varphi(t|x_0)$. These relations are very useful if we know the integral transforms in closed form.

To find the first relation, let us transform the survival probability[1]

$$S(s|x_0) = \int_0^\infty S(t|x_0)\,\mathrm{e}^{-st}\,\mathrm{d}t. \tag{2.85}$$

Taking the $(n-1)$'th derivative with respect to s, we have

$$\frac{\partial^{n-1}S(s|x_0)}{\partial s^{n-1}} = \int_0^\infty S(t|x_0)\frac{\partial^{n-1}\,\mathrm{e}^{-st}}{\partial s^{n-1}}\,\mathrm{d}t = (-1)^{n-1}\int_0^\infty t^{n-1}S(t|x_0)\,\mathrm{e}^{-st}\,\mathrm{d}t, \tag{2.86}$$

and then, taking the limit when $s \to 0$, we have

$$\left.\frac{\partial^{n-1}S(s|x_0)}{\partial s^{n-1}}\right|_{s=0} = (-1)^{n-1}\int_0^\infty t^{n-1}S(t|x_0)\,\mathrm{d}t. \tag{2.87}$$

Substituting these derivatives into Eq. (2.52), the moments of MFPT are

$$\langle t^n(x_0)\rangle = n(-1)^{-(n-1)}\left.\frac{\partial^{n-1}S(s|x_0)}{\partial s^{n-1}}\right|_{s=0}, \tag{2.88}$$

[1] For further details of the Laplace transform, see Appendix A, Sect. A.8.

or, equivalently,[2]

$$\langle t^n(x_0)\rangle = (-1)^{n+1} n \left.\frac{\partial^{n-1} S(s|x_0)}{\partial s^{n-1}}\right|_{s=0} \qquad n = 1, 2, 3, \cdots \tag{2.90}$$

Now, we need to find a similar relation for $\varphi(t|x_0)$. To such end, we perform the Laplace transform of the probability density of first-passage time, which is

$$\varphi(s|x_0) = \int_0^\infty \varphi(t|x_0)\, \mathrm{e}^{-st}\, \mathrm{d}t. \tag{2.91}$$

Taking the nth derivative with respect to s, we have

$$\frac{\partial^n \varphi(s|x_0)}{\partial s^n} = \int_0^\infty \varphi(t|x_0) \frac{\partial^n\, \mathrm{e}^{-st}}{\partial s^n}\, \mathrm{d}t = (-1)^n \int_0^\infty t^n \varphi(t|x_0)\, \mathrm{e}^{-st}\, \mathrm{d}t. \tag{2.92}$$

After evaluating at $s = 0$, we arrive at the following relation:

$$\left.\frac{\partial^n \varphi(s|x_0)}{\partial s^n}\right|_{s=0} = (-1)^n \int_0^\infty t^n \varphi(t|x_0)\, \mathrm{d}t. \tag{2.93}$$

Thus, when using Eq. (2.52), moments of MFPT can be written as

$$\langle t^n(x_0)\rangle = (-1)^n \left.\frac{\partial^n \varphi(s|x_0)}{\partial s^n}\right|_{s=0}. \tag{2.94}$$

The importance of Eqs. (2.90) and (2.94) becomes clear when the solution of a problem is obtained in Laplace's space and finding the inverse Laplace transform is not easy.

2.9 Splitting Probability

The *splitting probability* is the probability of a player reaching the Observatory or the Lobby. In terms of Brownian particles, it is the fraction of particles that eventually reach any of the absorbing points. If the probability flux at the absorbing boundaries gives us the fraction of particles that reach such boundaries by unit time,

[2] Considering that

$$\frac{1}{(-1)^{n-1}} = (-1)^{n+1} \tag{2.89}$$

the integral from 0 to infinity will take into account the total fraction of particles that reach them. Therefore, the splitting probability at L is given by

$$\theta_L(x_0) = \int_0^\infty J(L,t|x_0)\,\mathrm{d}t = -D\frac{\partial}{\partial x}\int_0^\infty p(x,t|x_0)\,\mathrm{d}t\bigg|_{x=L}. \tag{2.95}$$

Explicitly for the random elevator game, by substituting Eq. (2.28) into (2.95), we have

$$\theta_L(x_0) = -D\frac{\partial}{\partial x}\int_0^\infty \frac{2}{L}\sum_{n=1}^{\infty}\exp\left(-\frac{\pi^2 n^2 Dt}{L^2}\right)\sin\left(\frac{n\pi x_0}{L}\right)\sin\left(\frac{n\pi x}{L}\right)\mathrm{d}t\bigg|_{x=L}. \tag{2.96}$$

By computing the integral and the derivative, we obtain

$$\theta_L(x_0) = -\frac{2D}{L}\sum_{n=1}^{\infty}\left(\frac{L^2}{\pi^2 n^2 D}\right)\left(\frac{n\pi}{L}\right)\cos\left(\frac{n\pi x}{L}\right)\sin\left(\frac{n\pi x_0}{L}\right)\bigg|_{x=L}. \tag{2.97}$$

Evaluating the sum at $x = L$, we have

$$\theta_L(x_0) = \frac{2}{\pi}\sum_{n=1}^{\infty}\frac{(-1)^{n-1}}{n}\sin\left(\frac{n\pi x_0}{L}\right). \tag{2.98}$$

Computing the sum into this last equation, given in Eq. (A.33), yields

$$\theta_L(x_0) = \frac{x_0}{L}. \tag{2.99}$$

This results shows that the probability of reaching L is the ratio of the distance from x_0 to L. It is proportional to the initial position, and the closer we are to L, the greater the possibility of reaching it.

Now, let us compute $\theta_0(x_0)$. This computation is easy because the only difference is given by the evaluation of $\cos(n\pi x/L)$ in Eq. (2.97). Hence, considering that $\theta_{x'}(x_0)$ is

$$\theta_{x'}(x_0) = -\frac{2}{\pi}\sum_{n=1}^{\infty}\frac{1}{n}\cos\left(\frac{n\pi x}{L}\right)\sin\left(\frac{n\pi x_0}{L}\right)\bigg|_{x=x'}, \tag{2.100}$$

consequently, taking into account the westward direction of the flux, when $x' = 0$, we have

$$\theta_0(x_0) = \frac{2}{\pi}\sum_{n=1}^{\infty}\frac{1}{n}\sin\left(\frac{n\pi x_0}{L}\right), \tag{2.101}$$

leading to the result anticipated by the conservation of probability,

$$\theta_0(x_0) = 1 - \frac{x_0}{L}. \tag{2.102}$$

This results shows that the probability of reaching 0 is a proportional ratio between the difference $L - x_0$ and L. It depends on the initial position, and the closer we are to 0, the greater the possibility of reaching it.

Now, we will explore a simpler way to obtain the splitting probability by means of a differential equation. To such end, we start from the backward equation in Eq. (2.56) and then differentiate with respect to the variable x_0. Making use of the relation in Eq. (2.73), we find that the flux must satisfy

$$\frac{\partial J(x,t|x_0)}{\partial t} = D\frac{\partial^2 J(x,t|x_0)}{\partial x_0^2}. \tag{2.103}$$

Setting $x = L$ and integrating both sides with respect to time, we find

$$\int_0^\infty \frac{\partial J(L,t|x_0)}{\partial t}\mathrm{d}t = D\frac{\partial^2}{\partial x_0^2}\int_0^\infty J(L,t|x_0)\,\mathrm{d}t, \tag{2.104}$$

and therefore,

$$J(L,t\to\infty|x_0) - J(L,t=0|x_0) = D\frac{\partial^2\theta}{\partial x_0^2}. \tag{2.105}$$

The left side of the latter equation is zero because, at $t \to \infty$, the game is guaranteed to have ended and, at $t = 0$, the status of the game does not have any contributions when $x_0 = L$. These arguments take us to the following ODE:

$$\frac{\mathrm{d}^2\theta_L(x_0)}{\mathrm{d}x_0^2} = 0. \tag{2.106}$$

This is another fingerprint of diffusion. The two BCs to be satisfied for the random elevator game are $\theta_L(0) = 0$ and $\theta_L(L) = 1$, i.e., whether A is already at the Observatory or the Lobby. Thus, the linear function in Eq. (2.99) is the solution of Eq. (2.106).

2.10 Concluding Remarks

In this chapter, we have computed and derived the fundamental physical properties of diffusion, as well as its mathematical representation. For the reader's convenience, listed below are the most important equations to depict and define diffusion that we have obtained so far, which will be frequently used throughout this book.

$$\frac{\partial p(\mathbf{r},t)}{\partial t} = D\nabla^2 p(\mathbf{r},t) \qquad \text{(Diffusion equation)}$$

$$\frac{\partial p(\mathbf{r},t)}{\partial t} = D\nabla^2 p(\mathbf{r},t) - \mathbf{v}\cdot\boldsymbol{\nabla} p(\mathbf{r},t) \qquad \text{(Fokker-Planck equation)}$$

$$\frac{\partial p(\mathbf{r},t|\mathbf{r_0})}{\partial t} = D\nabla^2 p(\mathbf{r},t|\mathbf{r_0}) \qquad \text{(Backward diffusion equation)}$$

$$\mathbf{J}(\mathbf{r},t) = -D\boldsymbol{\nabla} p(\mathbf{r},t) \qquad \text{(Probability flux)}$$

$$\frac{\partial p(\mathbf{r},t)}{\partial t} = -\boldsymbol{\nabla}\cdot\mathbf{J}(\mathbf{r},t) \qquad \text{(Continuity equation)}$$

$$\frac{\partial S(t|\mathbf{r_0})}{\partial t} = D\nabla^2 S(t|\mathbf{r_0}) \qquad \text{(Survival probability)}$$

$$\nabla^2\langle t^n(\mathbf{r_0})\rangle = -\frac{n}{D}\langle t^{n-1}(\mathbf{r_0})\rangle \qquad \text{(Moments of MFPT)}$$

$$\nabla^2\theta_{\mathbf{r}'}(\mathbf{r_0}) = 0. \qquad \text{(Splitting probability)}$$

All required representations of special differential operators, $\boldsymbol{\nabla}$, $\boldsymbol{\nabla}\cdot\nabla^2$, can be found in Appendix B.

Further Reading and References

J. Crank, *The Mathematics of Diffusion*, 2nd edn. (Clarendon Press, Oxford, 1975)
J. Klafter, I.M. Sokolov, *First Steps in Random Walks: From Tools to Applications* (Oxford University Press, Oxford, 2016)
L.E. Maistrov, *Probability Theory, A Historical Perspective* (Academic Press, Cambridge, 1974)
S. Redner, *A Guide to First-Passage Processes* (Cambridge University Press, Cambridge, 2001)
G.H. Weiss, *Aspects and Applications of the Random Walk* (North-Holland, Amsterdam, 1994)

Part II
Diffusion: Free Particle

On the diffusion equation and the techniques of its general solution in the one-dimensional unconfined space.

"All the effects of Nature are only the mathematical consequences of a small number of immutable laws"

—Pierre-Simon Laplace

Chapter 3
Solution of the Diffusion Equation in Free Space

In this chapter, we will focus on solving the diffusion equation under no spatial constraints, i.e., in free space, to find a unique solution that will satisfy both the partial differential equation and the initial condition. We will review the most widely used methods, the Fourier and Laplace transforms and Green's function formalism, presenting the complete step-by-step process for each. In later chapters, we will show how these solutions are to be modified when space boundaries are present. We also discuss the implications and consequences of the central limit theorem, which is a mainstay of statistics and probability.

3.1 Fourier Transform

One of the most useful methods to solve the diffusion equation consists in using the Fourier transform. The major advantage of this method is that it allows the original differential equation to become an ordinary differential equation (ODE), which is usually easier to solve. Once we have solved the ODE in Fourier's space, we then need to find the inverse Fourier transform of such solution in order to return to the original space. Unfortunately, most of the time, this process is not an easy task.

In this section, we solve the diffusion equation in a free space with the initial condition $p(x, t = 0) = \delta(x - x_0)$ by means of the Fourier transform.

The Fourier transform of a function $f(x)$ is given by[1]

$$\mathcal{F}\{f(x,t)\} = f(k,t) = \int_{-\infty}^{\infty} f(x)\, \mathrm{e}^{ikx}\, \mathrm{d}x. \tag{A.46}$$

[1] See Sect. A.7 for further details of the Fourier transform.

L. Dagdug et al., *Diffusion Under Confinement*,
https://doi.org/10.1007/978-3-031-46475-1_3

By applying the Fourier transform to the diffusion equation, i.e., Eq. (2.13), we have that

$$\mathcal{F}\left\{\frac{\partial p(x,t)}{\partial t}\right\} = \mathcal{F}\left\{D\frac{\partial^2 p(x,t)}{\partial x^2}\right\}. \tag{3.1}$$

To perform the transformation, we need to multiply both sides of the diffusion equation by e^{ikx} and integrate them with respect to x. Thereafter, we find for the left-hand side of Eq. (2.13) that

$$\mathcal{F}\left\{\frac{\partial p(x,t)}{\partial t}\right\} = \int_{-\infty}^{\infty} \frac{\partial p(x,t)}{\partial t}\,\mathrm{e}^{ikx}\,\mathrm{d}x = \frac{\partial}{\partial t}\int_{-\infty}^{\infty} p(x,t)\,\mathrm{e}^{ikx}\,\mathrm{d}x = \frac{\partial p(k,t)}{\partial t} \tag{3.2}$$

and for the right-hand side that

$$\mathcal{F}\left\{D\frac{\partial^2 p(x,t)}{\partial x^2}\right\} = D\int_{-\infty}^{\infty} \frac{\partial^2 p(x,t)}{\partial x^2}\,\mathrm{e}^{ikx}\,\mathrm{d}x. \tag{3.3}$$

To solve this last integral, we have to integrate it twice by parts. The first integration reads

$$\begin{aligned} &D\int_{-\infty}^{\infty} \frac{\partial^2 p(x,t)}{\partial x^2}\,\mathrm{e}^{ikx}\,\mathrm{d}x \\ &= D\left[\lim_{\zeta\to\infty} \mathrm{e}^{ikx}\,\frac{\partial p(x,t)}{\partial x}\bigg|_{x=-\zeta}^{x=+\zeta} - ik\int_{-\infty}^{\infty} \frac{\partial p(x,t)}{\partial x}\,e^{ikx}\,\mathrm{d}x\right]. \end{aligned} \tag{3.4}$$

Based on the physical requirement that the probability of finding a particle at infinity at time t is null, its derivative, i.e., the flux, also vanishes, as shown by

$$\lim_{\zeta\to\infty} \mathrm{e}^{ikx}\,\frac{\partial p(x,t)}{\partial x}\bigg|_{x=-\zeta}^{x=+\zeta} = 0. \tag{3.5}$$

Then, incorporating this consideration into Eq. (3.4), we have

$$\mathcal{F}\left\{D\frac{\partial^2 p(x,t)}{\partial x^2}\right\} = -ikD\int_{-\infty}^{\infty} \frac{\partial p(x,t)}{\partial x}\,\mathrm{e}^{ikx}\,\mathrm{d}x, \tag{3.6}$$

which we integrate by parts again, yielding

$$\mathcal{F}\left\{D\frac{\partial^2 p(x,t)}{\partial x^2}\right\} = -ikD\left[\lim_{\Delta\zeta\to\infty} \mathrm{e}^{ikx}\; p(x,t)\Big|_{x=-\zeta}^{x=+\zeta} - ik\int_{-\infty}^{\infty} p(x,t)\;\mathrm{e}^{ikx}\;\mathrm{d}x\right]$$
$$= D(ik)^2\int_{-\infty}^{\infty} p(x,t)\;\mathrm{e}^{ikx}\;\mathrm{d}x. \tag{3.7}$$

Using the definition of the Fourier transform, Eq. (A.46), the right-hand side transforms into

$$\mathcal{F}\left\{D\frac{\partial^2 p(x,t)}{\partial x^2}\right\} = -D\;k^2\;p(k,t). \tag{3.8}$$

Substituting Eqs. (3.2) and (3.8) into (3.1) yields

$$\frac{\partial p(k,t)}{\partial t} = -D\;k^2\;p(k,t). \tag{3.9}$$

Now, we transform the original partial differential equation (PDE) into an ODE. The solution of this ODE is given by

$$p(k,t) = p_0\;\mathrm{e}^{-Dk^2t}. \tag{3.10}$$

The explicit value of p_0 must be chosen in such a way that the general solution satisfies the initial conditions. To such end, we have to Fourier-transform the initial condition, which in this case turns out to be

$$p(k,t=0) = \int_{-\infty}^{\infty}\delta(x-x_0)\;e^{ikx}\;\mathrm{d}x = e^{ikx_0}. \tag{3.11}$$

Evaluating (3.10) at $t=0$ and equating to (3.11) lead to

$$p(k,t=0) = p_0 = e^{ikx_0}. \tag{3.12}$$

Thereafter, Eq. (3.10) is written as

$$p(k,t|x_0) = \exp\Big(-Dk^2t + ikx_0\Big). \tag{3.13}$$

In order to obtain the result as a function of space and time, we must make use of the inverse Fourier transform, defined as

$$f(t) = \frac{1}{2\pi}\int_{-\infty}^{\infty} f(k)\;\mathrm{e}^{-ikx}\;\mathrm{d}k. \tag{A.48}$$

When Eq. (3.13) is substituted into Eq. (A.48), one finds

$$p(x,t|x_0) = \frac{1}{2\pi}\int_{-\infty}^{\infty}\exp\Big[-(ikx - ikx_0) - Dk^2t)\Big]\,\mathrm{d}k. \tag{3.14}$$

It is helpful to perform this integration in the complex plane. Therefore, we rewrite the argument inside the exponential function by completing the square, namely,

$$-[ik(x-x_0)+Dk^2t] = -Dt\left\{k^2+2k\left[\frac{i}{2Dt}(x-x_0)\right] + \left[\frac{i}{2Dt}(x-x_0)\right]^2 - \left[\frac{i}{2Dt}(x-x_0)\right]^2\right\}. \tag{3.15}$$

Then, after some algebraic manipulations, we get to

$$\left[k+\frac{i}{2Dt}(x-x_0)\right]^2 = k^2+\frac{ik(x-x_0)}{Dt}+\left[\frac{i}{2Dt}(x-x_0)\right]^2. \tag{3.16}$$

Thus, the argument of the exponential becomes

$$-[ik(x-x_0)+Dk^2t] = -Dt\left\{\left[k+\frac{i}{2Dt}(x-x_0)\right]^2-\left[\frac{i}{2Dt}(x-x_0)\right]^2\right\}. \tag{3.17}$$

Then, Eq. (3.14) turns into

$$p(x,t|x_0) = \frac{1}{2\pi}\exp\left[-\frac{(x-x_0)^2}{4Dt}\right]\int_{-\infty}^{\infty}\exp\left[-Dt\left(k+\frac{i(x-x_0)}{2Dt}\right)^2\right]\mathrm{d}k. \tag{3.18}$$

When we introduce the change of variables

$$z \equiv k+\frac{i}{2Dt}(x-x_0), \tag{3.19}$$

into Eq. (3.18), we find that

$$p(x,t|x_0) = \frac{1}{2\pi}\exp\left[-\frac{(x-x_0)^2}{4Dt}\right]\int_{-\infty+i(x-x_0)/(2Dt)}^{\infty+i(x-x_0)/(2Dt)} \mathrm{e}^{-Dtz^2}\,\mathrm{d}z. \tag{3.20}$$

To solve the remaining integral, we make use of the Cauchy-Goursat theorem[2] by introducing the following change of variables:

[2] The Cauchy-Goursat theorem states that if there is a function $f(z) = u(x,y) + iv(x,y)$, and if $f(z)$ is analytic in a simply connected domain Ω, then for every closed curve C in Ω, the contour integral of $f(z)$ over C is zero, namely,

$$\oint_C f(z)\,\mathrm{d}z = 0. \tag{3.21}$$

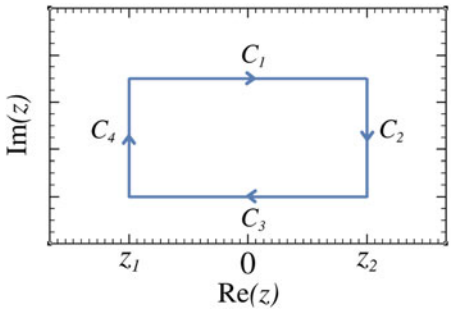

Fig. 3.1 Complex plane of integration. The path of the integral in Eq. (3.23) is represented with blue lines and goes in clockwise direction

$$z_1 = a + \frac{i(x - x_0)}{2Dt} \qquad \text{and} \qquad z_2 = b + \frac{i(x - x_0)}{2Dt}, \tag{3.22}$$

where a tends to minus infinity and b to plus infinity. In such a case, the auxiliary integral to solve is

$$\oint_C f(z)\,\mathrm{d}z = \int_{C_1} f(z)\,\mathrm{d}z + \int_{C_2} f(z)\,\mathrm{d}z + \int_{C_3} f(z)\,\mathrm{d}z + \int_{C_4} f(z)\,\mathrm{d}z = 0. \tag{3.23}$$

A graphic representation in the complex plane of the integration path is depicted in Fig. 3.1.

The function $f(z) = \mathrm{e}^{-Dtz^2}$ decays exponentially at a and b; therefore,

$$\int_{C_2} f(z)\,\mathrm{d}z = -\int_{C_4} f(z)\,\mathrm{d}z \tag{3.24}$$

as well as

$$\int_{C_1} f(z)\,\mathrm{d}z = -\int_{C_3} f(z)\,\mathrm{d}z. \tag{3.25}$$

Following the path integration in clockwise direction, or equivalently using (3.22) at the limit where a and b diverge, we have

$$\int_{C_1} f(z)\,\mathrm{d}z = \int_{z_1}^{z_2} \mathrm{e}^{-Dtz^2}\,\mathrm{d}z \qquad \text{and} \qquad \int_{C_3} f(z)\,\mathrm{d}z = \int_{z_2}^{z_1} \mathrm{e}^{-Dtz^2}\,\mathrm{d}z. \tag{3.26}$$

Including the latter result into the original integral, Eq. (3.14), we find

$$p(x, t|x_0) = \frac{1}{2\pi}\exp\left[-\frac{(x - x_0)^2}{4Dt}\right]\int_{-\infty}^{\infty} \mathrm{e}^{-Dtz^2}\,\mathrm{d}z. \tag{3.27}$$

This last integral can be solved considering Eq. (A.16), given by

$$\int_{-\infty}^{\infty} x^n \, \mathrm{e}^{-\lambda x^2} \, \mathrm{d}x = \frac{1+(-1)^n}{2} \, \lambda^{-\frac{1+n}{2}} \, \Gamma\left(\frac{1+n}{2}\right). \tag{A.16}$$

Then,

$$\int_{-\infty}^{\infty} \mathrm{e}^{-Dtz^2} \, \mathrm{d}z = \sqrt{\frac{\pi}{Dt}}. \tag{3.28}$$

Finally, the solution to the diffusion equation that satisfies the imposed initial conditions is

$$p(x,t|x_0) = \frac{1}{\sqrt{4\pi\, Dt}} \exp\left[-\frac{(x-x_0)^2}{4Dt}\right]. \tag{3.29}$$

This propagator is a Gaussian with a peak that becomes broader over time and is centered at the initial position x_0 and with its maximum decreases as $(4\pi\, Dt)^{-1/2}$. The time evolution of the propagator is given in Fig. 3.2.

When the particle initiates its trajectory at $x_0 = 0$, the later equation becomes

$$p(x,t|0) = \frac{1}{\sqrt{4\pi\, Dt}} \exp\left(-\frac{x^2}{4Dt}\right). \tag{3.30}$$

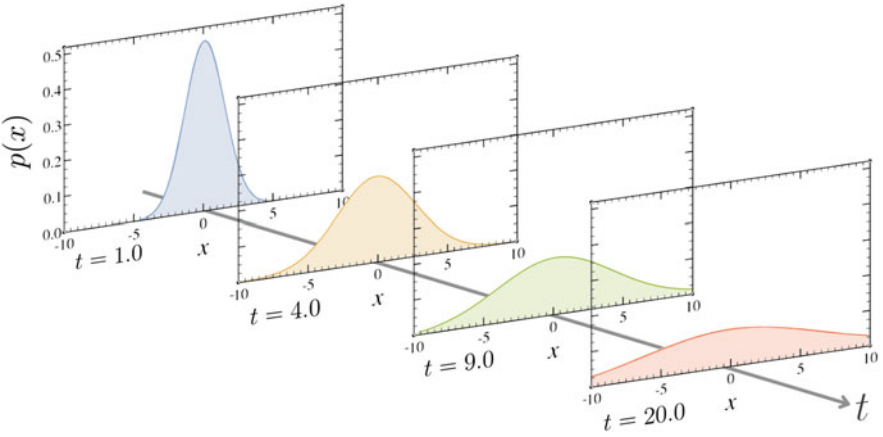

Fig. 3.2 Time evolution of the probability density for free Brownian particles given by Eq. (3.29) at different times, i.e., $t = 1.0$, $t = 4.0$, $t = 9.0$, and $t = 20.0$. The peak of the function is centered at the initial position, which is $x_0 = 0$, its height decreases as the square root of time t, and it becomes broader over time

3.2 Laplace Transform

The Laplace transform method applied to obtain the solution of a PDE is, in some way, similar to that of the Fourier transform: the original differential equation becomes an ODE that is usually easier to solve. After solving the ODE in Laplace's space, one obtains the original temporal space solution by performing the inverse Laplace transform. In this section, we will solve the diffusion equation in free space with the initial condition $p(x, t = 0) = \delta(x - x_0)$ through the Laplace transform.

The Laplace transform of a function $f(x, t)$ is defined as follows:[3]

$$\mathcal{L}\{f(x,t)\} = f(x,s) = \int_0^\infty f(x,t)\, \mathrm{e}^{-st}\, \mathrm{d}t. \tag{A.53}$$

Then, applying this definition to the diffusion equation, Eq. (2.13), we have

$$\mathcal{L}\left\{\frac{\partial p(x,t)}{\partial t}\right\} = \mathcal{L}\left\{D\frac{\partial^2 p(x,t)}{\partial x^2}\right\}. \tag{3.31}$$

To perform the transformation, we need to multiply both sides of the diffusion equation by e^{-st} and integrate with respect to t. Thereafter, the right-hand side yields

$$\mathcal{L}\left\{D\frac{\partial^2 p(x,t)}{\partial x^2}\right\} = D\int_0^\infty \frac{\partial^2 p(x,t)}{\partial x^2}\, \mathrm{e}^{-st}\, \mathrm{d}t = D\frac{\partial^2 p(x,s)}{\partial x^2}. \tag{3.32}$$

On the left-hand side, we have to integrate by parts, namely,

$$\int_0^\infty \frac{\partial p(x,t)}{\partial t}\, \mathrm{e}^{-st}\, \mathrm{d}t = \lim_{\zeta\to\infty} p(x,t)\, \mathrm{e}^{-st}\Big|_{t=0}^{t=\zeta} + s\int_0^\infty p(x,t)\, \mathrm{e}^{-st}\, \mathrm{d}t. \tag{3.33}$$

To evaluate the limit in this last equation, we consider that

$$\lim_{\zeta\to\infty} p(x,t)\, \mathrm{e}^{-st}\Big|_{t=0}^{t=\zeta} = 0. \tag{3.34}$$

Thus, by using the initial condition $p(x, t = 0) = \delta(x - x_0)$, Eq. (3.33) becomes

$$\int_0^\infty \frac{\partial p(x,t)}{\partial t}\, \mathrm{e}^{-st}\, \mathrm{d}t = s\ p(x,s) - \delta(x - x_0). \tag{3.35}$$

[3] See Sect. A.8 for further details of the Laplace transform.

Consequently, the Laplace transform of the diffusion equation is given by

$$s\ p(x,s|x_0) - \delta(x-x_0) = D\frac{\partial^2 p(x,s|x_0)}{\partial x^2}. \tag{3.36}$$

The latter ODE is referred to as the subsidiary diffusion equation or simply the *subsidiary equation*.[4] This last equation depends on the Dirac delta function $\delta(x - x_0)$ and on the difference $x - x_0$ or displacement. In the region where $x < x_0$ and $x > x_0$, the delta function is zero, and the solution is either a hyperbolic or real exponential function.

Let us propose a linear combination of real exponential functions as a solution of Eq. (3.36) given by

$$p(x,s|x_0) = \mathcal{A}\ \exp\left[\sqrt{\frac{s}{D}}(x-x_0)\right] + \mathcal{B}\ \exp\left[-\sqrt{\frac{s}{D}}(x-x_0)\right], \tag{3.37}$$

where $\mathcal{A}$ and $\mathcal{B}$ are constants fixed by the boundary conditions (BCs) of our problem. At the limit when $x \to -\infty$, the propagator, Eq. (3.37), should vanish, meaning that for such region, $\mathcal{B} = 0$. In contrast, when $x \to \infty$, we see that $\mathcal{A}$ should be zero so that $p(x,s|x_0)$ remains convergent. Therefore, to satisfy both physical arguments, it is convenient to write the propagator in two separate parts, i.e.,

$$p(x,s|x_0) = \begin{cases} \mathcal{A}\ \exp\left[\sqrt{\frac{s}{D}}(x-x_0)\right] & \text{for} \quad x < x_0 \\ \mathcal{B}\ \exp\left[-\sqrt{\frac{s}{D}}(x-x_0)\right] & \text{for} \quad x > x_0. \end{cases} \tag{3.38}$$

The constants $\mathcal{A}$ and $\mathcal{B}$ are obtained from the *joining conditions*. The first of these relations is found by observing that the solution must be continuous at the starting position $x = x_0$, the so-called conservation or continuity condition, namely,

$$p(x,s|x_0)|_{x_0^+} = p(x,s|x_0)|_{x_0^-}\,. \tag{3.39}$$

We denote as x_0^+ when we're approaching x_0 from the right and x_0^- when we are approaching from the left, respectively. Then, equating the solutions given by Eq. (3.38) in each region when $x = x_0$ yields

$$\mathcal{A} = \mathcal{B}. \tag{3.40}$$

[4] The subsidiary equation is the equation in terms of s, obtained by taking the transforms of all the terms in a linear differential equation.

To find the remaining constant $\mathcal{A}$, we impose the so-called discontinuity condition (for more details, see Sect. 3.5). To such end, we integrate the subsidiary diffusion equation, Eq. (3.36), over an infinitesimal interval from $x_0 - \epsilon$ to $x_0 + \epsilon$, namely,

$$\int_{x_0-\epsilon}^{x_0+\epsilon} s\ p(x,s|x_0)\ \mathrm{d}x - \int_{x_0-\epsilon}^{x_0+\epsilon} \delta(x-x_0)\ \mathrm{d}x = D\int_{x_0-\epsilon}^{x_0+\epsilon} \frac{\partial^2 p(x,s|x_0)}{\partial x^2}\ \mathrm{d}x. \tag{3.41}$$

Now, taking the limit when $\epsilon \to 0$, the first term of the latter equation is zero at the limit $\epsilon \to 0$, and the integral of $\delta(x - x_0)$ is 1 (see Subsection A.10.3), leading to

$$-\frac{1}{D} = \left.\frac{\partial p(x,s|x_0)}{\partial x}\right|_{x_0^+} - \left.\frac{\partial p(x,s|x_0)}{\partial x}\right|_{x_0^-}. \tag{3.42}$$

Introducing the propagator given by Eq. (3.38) into (3.42), we are led to the result

$$\mathcal{A} = \frac{1}{\sqrt{4Ds}}, \tag{3.43}$$

yielding a unique solution for the entire domain, i.e.,

$$p(x,s) = \frac{1}{\sqrt{4Ds}}\ \exp\left[-\sqrt{\frac{s}{D}}|x-x_0|\right]. \tag{3.44}$$

The last thing we need to do is transform Eq. (3.44) back to our initial temporal coordinate t. In order to accomplish this task, one usually works with the inversion theorem of the Laplace transformation through the Bromwich integral,

$$f(t) = \mathcal{L}^{-1}\{f(s)\} = \frac{1}{2\pi i}\ \lim_{T\to\infty} \int_{\gamma-iT}^{\gamma+iT} \mathrm{e}^{st}\ f(s)\ \mathrm{d}s, \tag{A.54}$$

by looking for the singularities (or poles) of function $f(s)$ and by choosing the right path in the complex plane to integrate Eq. (3.44) using Eq. (A.54). Due to the complications involved in solving this integral, let us find the inverse transform of Eq. (3.44) through a simpler method.

Consider two functions $g(r,s)$ and $q(r,s)$ defined as follows:

$$g(r,s) \equiv \frac{1}{\sqrt{s}}\mathrm{e}^{-k\sqrt{s}} \quad \text{and} \quad q(r,s) \equiv \mathrm{e}^{-k\sqrt{s}}, \tag{3.45}$$

with $k \equiv |x - x_0|/\sqrt{D}$, meaning that $p(x,s|x_0)$ is actually

$$p(x,s|x_0) = \frac{1}{\sqrt{4D}}g(r,s). \tag{3.46}$$

We can see that $g(r,s)$ and $q(r,s)$ are intrinsically linked through their derivatives with respect to s by noting that

$$\frac{\partial\sqrt{s}\;g(r,s)}{\partial s} = -\frac{k\;\mathrm{e}^{-k\sqrt{s}}}{2\sqrt{s}} \quad \text{and} \quad \frac{\partial q(r,s)}{\partial s} = -\frac{k\;\mathrm{e}^{-k\sqrt{s}}}{2\sqrt{s}}. \tag{3.47}$$

A combination of the last two equations leads us to the ordinary differential equations

$$2s\frac{\partial\;g(r,s)}{\partial s} + g(r,s) + k\;q(r,s) = 0 \quad \text{and} \quad 2\frac{\partial q(r,s)}{\partial s} + kg(r,s) = 0. \tag{3.48}$$

Additionally, the derivatives of Laplace transforms can be computed using the following formula:

$$\frac{\partial^n f(s)}{\partial s^n} = \int_0^\infty \mathrm{e}^{-st}(-t)^n f(t)\;\mathrm{d}t = \mathcal{L}\big\{(-t)^n f(t)\big\}, \tag{A.57}$$

which takes us to the general result

$$\mathcal{L}^{-1}\left\{\frac{\partial^n f(s)}{\partial s^n}\right\} = (-t)^n f(t), \tag{3.49}$$

and by taking the m'th derivative with respect to t, we find that

$$\frac{\partial^m(-t)^n f(t)}{\partial t^m} = \frac{1}{2\pi i}\lim_{T\to\infty}\int_{\gamma-iT}^{\gamma+iT}\mathrm{e}^{st}\;(s)^m\frac{\partial^n f(s)}{\partial s^n}\;\mathrm{d}s = \mathcal{L}^{-1}\left\{(s)^m\frac{\partial^n f(s)}{\partial s^n}\right\}. \tag{3.50}$$

Therefore, by inverse Laplace transforming both relations in Eq. (3.48), we arrive at[5]

[5] Using

$$g(r,t) = \mathcal{L}^{-1}\big\{g(r,s)\big\} = \frac{1}{2\pi i}\lim_{T\to\infty}\int_{\gamma-iT}^{\gamma+iT}\mathrm{e}^{st}\;g(r,s)\;\mathrm{d}s \tag{3.51}$$

and

$$q(r,t) = \mathcal{L}^{-1}\big\{q(r,s)\big\} = \frac{1}{2\pi i}\lim_{T\to\infty}\int_{\gamma-iT}^{\gamma+iT}\mathrm{e}^{st}\;q(r,s)\;\mathrm{d}s \tag{3.52}$$

$$\begin{aligned}\mathcal{L}^{-1}\left\{2s\frac{\partial g(r,s)}{\partial s}\right\} + \mathcal{L}^{-1}\{g(r,s)\} + \mathcal{L}^{-1}\{k\,q(r,s)\} \\ = -2\frac{\partial t\; g(r,t)}{\partial t} + g(r,t) + kq(r,t) \\ = -2t\frac{\partial g(r,t)}{\partial t} - g(r,t) + kq(r,t) = 0\end{aligned} \tag{3.53}$$

and

$$\mathcal{L}^{-1}\left\{2\frac{\partial q(r,s)}{\partial s}\right\} + \mathcal{L}^{-1}\{kg(r,s)\} = -2\,tq(r,t) + kg(r,t) = 0. \tag{3.54}$$

Using Eqs. (3.53) and (3.54), we obtain an ODE for $g(r,s)$, namely,

$$\frac{\partial g(r,t)}{\partial t} = \left(\frac{k^2}{4t^2} - \frac{1}{2t}\right) g(r,t), \tag{3.55}$$

which solution is given by

$$\begin{aligned}g(r,t) &= \mathcal{C}\exp\left(-\frac{k^2}{4t}\right)\exp\left(\frac{\ln t}{2}\right) \\ &= \frac{\mathcal{C}}{\sqrt{t}}\exp\left(-\frac{k^2}{4t}\right).\end{aligned} \tag{3.56}$$

In order to find the constant $\mathcal{C}$, we evaluate the definition of $g(r,s)$, i.e., Eq. (3.45), at $k = 0$, yielding

$$g(r,s)|_{k=0} = \frac{1}{\sqrt{s}}. \tag{3.57}$$

The inverse transform of the last equation is well-known and is given by $1/\sqrt{\pi t}$ (see Eq. (A.66)); then $\mathcal{C} = 1/\sqrt{\pi}$, leading to

$$g(r,t) = \frac{1}{\sqrt{\pi t}}\exp\left(-\frac{k^2}{4t}\right). \tag{3.58}$$

Finally, the inverse Laplace transform of Eq. (3.44) is now computed straightforward by adding the factor $1/\sqrt{4D}$ and replacing k for $|x - x_0|/\sqrt{D}$. Therefore,

$$p(x,t) = \frac{1}{\sqrt{4\pi Dt}}\;\exp\left[-\frac{(x-x_0)^2}{4Dt}\right], \tag{3.59}$$

which is the same as in Eq. (3.29), as expected.

3.3 Mean and Standard Deviation of Gaussian Distribution

In statistics, the standard deviation is a measure of the amount of variation or dispersion within a set of values. A low standard deviation indicates that the values tend to be close to the set's mean, while a high standard deviation indicates that the values expand over a wider range.

The expected value, average, mean, or first moment μ (also represented as $\mathbb{E}[x]$) and the standard deviation σ of a random variable x with probability distribution $f(x)$ are computed as

$$\mu = \int_{-\infty}^{\infty} x f(x)\, \mathrm{d}x \tag{3.60}$$

and

$$\sigma = \sqrt{\int_{-\infty}^{\infty} (x-\mu)^2\, f(x)\, \mathrm{d}x}, \tag{3.61}$$

respectively.

From the propagator for a free Brownian particle, Eq. (3.29), we can compute μ and σ for the Gaussian probability density. Starting with the expectation value of the position coordinate, we have

$$\mu = \langle x \rangle = \int_{-\infty}^{\infty} \frac{x}{\sqrt{4\pi D t}} \exp\left[-\frac{(x-x_0)^2}{4Dt} \right] \mathrm{d}x. \tag{3.62}$$

When imposing the change of variable $z = x - x_0$, the latter expression becomes[6]

$$\langle x \rangle = \frac{1}{\sqrt{4\pi D t}} \left\{ \int_{-\infty}^{\infty} z \exp\left(-\frac{z^2}{4Dt} \right) \mathrm{d}z + x_0 \int_{-\infty}^{\infty} \exp\left(-\frac{z^2}{4Dt} \right) \mathrm{d}z \right\}. \tag{3.63}$$

To evaluate the integral, we use (A.16), and after some algebraic manipulations, the latter equation reduces to

$$\mu = x_0. \tag{3.64}$$

Then, the mean for a Gaussian probability density is equal to x_0.

Additionally, we can find σ by substituting Eq. (3.64) into Eq. (3.61) and then expanding all terms, i.e.,

[6] The change of variables preserves the integral's limits.

$$\sigma = \sqrt{\frac{1}{\sqrt{4\pi\, Dt}} \int_{-\infty}^{\infty} (x^2 - 2xx_0 + x_0^2) \exp\left[-\frac{(x - x_0)^2}{4Dt}\right] \mathrm{d}x}. \tag{3.65}$$

Now, it is helpful to treat each integral individually and use the same change of variable, namely, $z = x - x_0$. As such, the first integral becomes

$$\int_{-\infty}^{\infty} x^2 \exp\left[-\frac{(x - x_0)^2}{4Dt}\right] \mathrm{d}x = \int_{-\infty}^{\infty} (z + x_0)^2 \exp\left(-\frac{z^2}{4Dt}\right) \mathrm{d}z. \tag{3.66}$$

Expanding terms, we find that

$$\begin{aligned} \int_{-\infty}^{\infty} x^2 \exp\left[-\frac{(x - x_0)^2}{4Dt}\right] \mathrm{d}x = &\int_{-\infty}^{\infty} z^2 \exp\left(-\frac{z^2}{4Dt}\right) \mathrm{d}z \\ &+ 2x_0 \int_{-\infty}^{\infty} z \exp\left(-\frac{z^2}{4Dt}\right) \mathrm{d}z \\ &+ x_0^2 \int_{-\infty}^{\infty} \exp\left(-\frac{z^2}{4Dt}\right) \mathrm{d}z \\ = &\, 2\sqrt{\pi\, Dt}\, \left(2Dt + x_0^2\right). \end{aligned} \tag{3.67}$$

Each term in the latter equation was calculated, again, using Eq. (A.16). The second integral inside Eq. (3.65) is computed similarly, namely,

$$\begin{aligned} 2x_0 \int_{-\infty}^{\infty} x \exp\left[-\frac{(x - x_0)^2}{4Dt}\right] \mathrm{d}x = &\, 2x_0 \left\{ \int_{-\infty}^{\infty} z \exp\left(-\frac{z^2}{4Dt}\right) \mathrm{d}z \right. \\ &\left. + x_0 \int_{-\infty}^{\infty} \exp\left(-\frac{z^2}{4Dt}\right) \mathrm{d}z \right\} \\ = &\, 4x_0^2 \sqrt{\pi\, Dt}. \end{aligned} \tag{3.68}$$

For the third integral, we have

$$x_0^2 \int_{-\infty}^{\infty} \exp\left[-\frac{(x - x_0)^2}{4Dt}\right] \mathrm{d}x = 2x_0^2 \sqrt{\pi\, Dt}. \tag{3.69}$$

Including all three latter results into Eq. (3.65) yields

$$\sigma = \sqrt{\frac{1}{\sqrt{4\pi\, Dt}} \left[2\sqrt{\pi\, Dt}\, \left(2Dt + x_0^2\right) - 4x_0^2 \sqrt{\pi\, Dt} + 2x_0^2 \sqrt{\pi\, Dt}\right]}, \tag{3.70}$$

which simplifies to

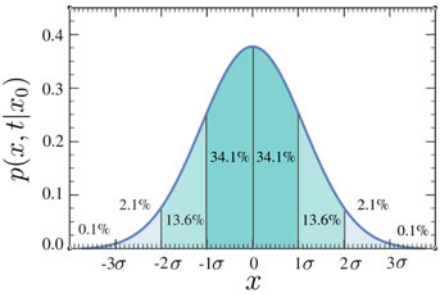

Fig. 3.3 Representative plot of normal distribution centered at $x_0 = 0$. For Eq. (3.73), all values less than one, two, and three standard deviations away from the mean account for 68.2%, 95.4%, and 99.6% of the set, respectively. It is worth noticing that inflection points occur where $x = \mu \pm \sigma$; consequently, the inflection points are located one standard deviation above the mean and one standard deviation below the mean

$$\sigma = \sqrt{2Dt}. \tag{3.71}$$

Considering that the variance is the standard deviation squared, we have

$$\sigma^2 = 2Dt. \tag{3.72}$$

Finally, by using Eq. (3.64), together with Eqs. (3.71) and (3.72), Eq. (3.29) given by a Gaussian or normal distribution (see Fig. 3.3) can be written as

$$p(x,t|x_0) = \frac{1}{\sqrt{2\pi}\sigma} \exp\left[-\frac{1}{2}\left(\frac{x-\mu}{\sigma}\right)^2\right]. \tag{3.73}$$

So far, we have learned that particles undergoing free diffusion in infinite space have zero mean displacement, Eq. (3.64). On the other hand, diffusing particles follow different trajectories, i.e., they travel different distances from their initial position at time t. The distribution of the distances traveled is predicted by a Gaussian distribution. From Eq. (3.73), it is inferred that for a fixed time t, 68.2% of the particles are traveling a distance x within -1σ and 1σ, while 95.4% are traveling within -2σ and 2σ, and so on (see Fig. 3.3). In order to obtain one of the latter values, we must integrate Eq. (3.73) from $-n\sigma$ to $n\sigma$, where n stands for the range of interest. The Gaussian distribution also predicts that the peak decreases as $\sqrt{2\pi}\sigma$ and becomes broader over time proportionally to σ, meaning that, as time passes, the particles move away from the origin to distribute uniformly.

A wide range of continuous random variables follow a Gaussian probability distribution. This distribution is ubiquitous throughout probability theory for various reasons, one of the most important ones being the central limit theorem, which we will discuss in detail in the next section.

3.4 The Central Limit Theorem and Moments of Displacement

Let $\{X_1, \ldots, X_N, \ldots\}$ be a sequence of random variables independently and identically distributed with mean μ and variance $\sigma^2 < \infty$. *The central limit theorem* (CLT) states that as N approaches infinity, their distribution probability converges into a normal distribution with zero mean μ and variance σ^2. The larger the number of samples, the closer to a Gaussian distribution it becomes. Note that if the variables do not have a zero mean, we can always normalize them by subtracting the expectation value from it.

It is worth noting that Laplace discovered the essentials of this fundamental theorem in 1810. Nowadays, the term CLT is related to a multitude of statements dealing with the convergence of probability distributions of functions of an increasing number of random elements to a normal distribution.

Now, we will provide proof of the theorem. Consider a one-dimensional random walker. The total displacement X after N steps is given by the sum of individual displacements on every step X, namely,

$$X = \sum_{i=1}^{N} X_i . \tag{3.74}$$

To obtain the displacement X, a coordinate X'must exist one step away from X after $N - 1$ steps. This can be viewed as a statement of the continuity of paths along the random walk, and it is known as the Chapman-Kolmogorov equation,[7] namely,

$$P_N(X) = \int_{-\infty}^{\infty} P_{N-1}(X')\ P\big(X - X'\big)\ \mathrm{d}X' \tag{3.75}$$

where $P_N(X)$ is the probability of the random walker being at position X after N steps. Then, $P_{N-1}(X')$ is the probability of the random walker being at position X' after $N - 1$ steps and $P(X - X')$ is the probability of the random walker taking the final step from X' to X. By Fourier transforming Eq. (3.75), we see that it is the definition of a convolution (see Eqs. (A.73) and (A.74)). Then, a recurrence relation on the probability distributions can be found in the Fourier domain,

$$P_N(k) = P_{N-1}(k)\ P(k). \tag{3.76}$$

The same procedure can be applied to $P_{N-1}(X)$, leading to

[7] The master equation is the Chapman-Kolmogorov equation expressed as a first-order differential equation in time for the probability density function of a Markovian stochastic variable.

$$P_{N-1}(X) = \int_{-\infty}^{\infty} P_{N-2}(X')\ P\big(X - X'\big)\ \mathrm{d}X', \tag{3.77}$$

where $P_{N-2}(X')$ is the probability of the random walker being at position X' after $N-2$ steps, and $P(X-X')$ is the probability of the random walker taking the final step from X' to X. Using the property of the convolution under a Fourier transform again, we have

$$P_{N-1}(k) = P_{N-2}(k)\ P(k). \tag{3.78}$$

Substituting (3.78) into (3.76) leads to

$$P_N(k) = P_{N-2}(k)\ P(k)^2. \tag{3.79}$$

Then, after N iterations, we arrive at

$$P_N(k) = P_0(k)\ \big[P(k)\big]^N. \tag{3.80}$$

Because we know that the initial condition is $P_0(x) = \delta(x - x_0)$ and that its Fourier transform is one, we obtain

$$P_N(k) = \big[P(k)\big]^N. \tag{3.81}$$

Performing the inverse Fourier transform of this last relation leads to

$$P_N(X) = \frac{1}{2\pi} \int_{-\infty}^{\infty} [P(k)]^N\ \mathrm{e}^{-ikX}\ \mathrm{d}k. \tag{3.82}$$

Now, we only have to express $P(k)$ in terms of $P(X)$. From the definition of a Fourier transform, we have

$$P(k) = \int_{-\infty}^{\infty} P(X)\ \mathrm{e}^{-ikX}\ \mathrm{d}k. \tag{3.83}$$

Because the first two moments are finite, we can Taylor expand the exponential function; therefore,

$$\begin{aligned} P(k) &= \int_{-\infty}^{\infty} P(X)[1 + ikX - \frac{1}{2}k^2X^2 + \cdots]\ \mathrm{d}X, \\ &= \int_{-\infty}^{\infty} [P(X) + ikXP(X) - \frac{1}{2}k^2X^2P(X) + \cdots]\ \mathrm{d}X, \\ &= \left[1 + ik\langle X\rangle - \frac{1}{2}k^2\langle X^2\rangle + \cdots\right]. \end{aligned} \tag{3.84}$$

For a random walker, we have proved that $\langle X \rangle = 0$. Keeping terms up to the second order in the latter equation, then

$$P(k) = \left[1 - \frac{1}{2}k^2\langle X^2 \rangle\right]. \tag{3.85}$$

Introducing Eq. (3.85) into Eq. (3.82), we obtain

$$P_N(X) = \frac{1}{2\pi}\int_{-\infty}^{\infty}\left[1 - \frac{1}{2}k^2\langle X^2 \rangle\right]^N \mathrm{e}^{-ikX}\,\mathrm{d}X. \tag{3.86}$$

At the limit of large N and small k, small k corresponding to large X in the Fourier domain, we can approximate the expression inside the brackets as an exponential function, so asymptotically, Eq. (3.86) goes to

$$P_N(X) \simeq \frac{1}{2\pi}\int_{-\infty}^{\infty}\mathrm{e}^{-\frac{1}{2}Nk^2\langle X^2 \rangle - ikX}\,\mathrm{d}X. \tag{3.87}$$

Given that the Fourier transform of a Gaussian function is a Gaussian function itself, by Fourier transforming Eq. (3.87), we arrive at the expected result:

$$P_N(X) = \frac{1}{\sqrt{2\pi N\langle X^2 \rangle}}\exp\left(\frac{-X^2}{2N\langle X^2 \rangle}\right). \tag{3.88}$$

This is the central limit theorem for the case of a symmetrical random walk. This universality does not only apply to a random walk but also accounts for innumerable phenomena in nature, as well as applications in physics, chemistry, and biology. Among them, we find the ideal long chain of a polymer and the measurement of errors, which can be regarded to be an accumulation of independent errors. In physics, when we have variables of a macroscopic or mesoscopic system, such as energy, volume, pressure, or number of particles, the deviations of the variables from their averages are statistically independent. Then, the deviations have a Gaussian distribution. The importance of the CLT stems from the fact that in a number of real-life applications, a random variable is the sum of a large number of independent random variables.

To demonstrate the central limit theorem, there is a toy designed as a probability machine introduced in 1894 by Francis Galton, otherwise known as the *Galton board*. Have you ever played with a Galton board or quincunx? A Galton board is a triangular or rectangular array of pegs. Balls are dropped, one at a time, onto the top peg, and they bounce all the way down to the bottom, where they are collected in bins. Each time a ball hits one of the pegs, it bounces either left or right with the same probability[8], executing a random walk as it moves from row to

[8] To fulfill this requirement, the device must be level and properly built.

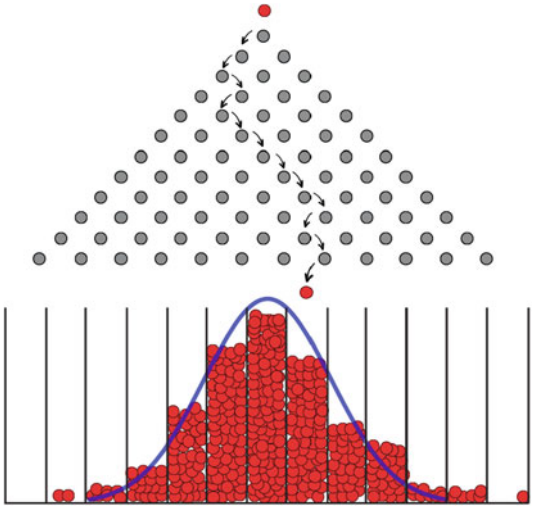

Fig. 3.4 Schematic representation of a Galton board consisting of a triangular array of pegs. Individual balls (represented as red points) are dropped at the top of the board. As these balls bounce down, they have an equal probability of going to either the left or the right of the peg. At the bottom of the board, the balls are collected into specific bins. The probability that a ball ends up in one of the bins depends on the number of trajectories it takes to reach it. The distribution of the balls in the bins forms a visual representation of the binomial distribution tending to a Gaussian distribution (blue solid curve) as the number of balls released increases

row. Interestingly, the balls collected in the bins follow a normal distribution (see Fig. 3.4).

We provide a *Mathematica* code, which requires the number of pegs and balls in the system to simulate a Galton board. The execution of this code results in the simulation of the random walk of the balls, together with the creation of a histogram depicting the final position distribution within the bins.

Additionally, a modified Galton board can help us visualize the splitting probability time and the first-passage time (Figs. 3.5 and 3.6). By using a square Galton board, where balls are dropped from above a fixed initial peg and collected in two bins once they reach either of the two end columns, we can reproduce the splitting probability process once the initial peg, above which the balls are dropped, is fixed. In this board, rows represent positions, and columns represent time steps. Furthermore, if the balls are collected in bins placed on both sides of every exit row, we obtain the probability distribution of the first-passage time, which is then used to calculate the mean first-passage time. It is worth noting that balls perform a random walk into the Galton board when moving between pegs.

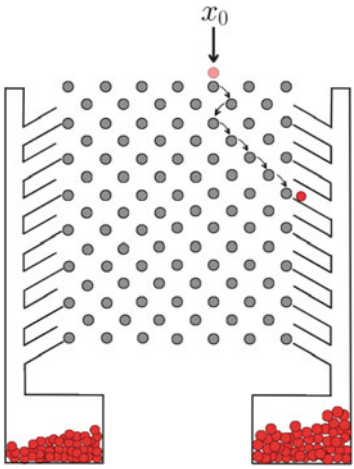

Fig. 3.5 Schematic representation of a modified Galton board consisting of a rectangular array of pegs. Individual balls are dropped at the top from a certain peg, labeling their initial position as x_0. Balls are collected in two bins once they reach any of the two ends. With this board, we are able to reproduce the splitting process. The codes simulating this modification of a Galton board can be downloaded from https://ixtlan.izt.uam.mx/leo/diffusionbookcodes/

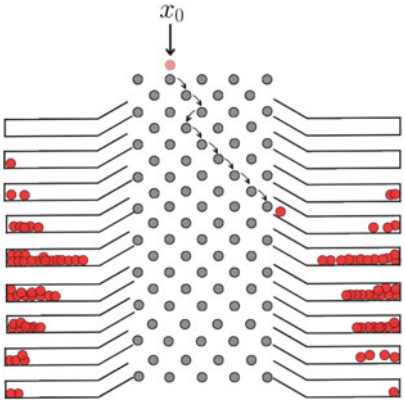

Fig. 3.6 Schematic representation of a modified Galton board consisting of a rectangular array of pegs. Individual balls are dropped at the top from a certain peg, labeling their initial position as x_0. Using this configuration of a Galton board, we obtain the probability distribution of the first-passage time, from which is then used to compute the mean first-passage time. The codes simulating this modified Galton board can be downloaded from https://ixtlan.izt.uam.mx/leo/diffusionbookcodes/

3.5 Green's Function Method

The Green functions, or Green's functions, are auxiliary functions used to find the solution of an ODE or PDE. Green's function is named after the British mathematician George Green (1793–1841). In 1828, Green published a privately printed booklet introducing the derivation of Green's theorem and the application of Green's functions to electrostatic problems. His work was ignored until William Thomson (Lord Kelvin) discovered and recognized its great value.

To begin our analysis, let us consider the following differential equation:

$$a_n(x)\frac{\mathrm{d}^n y(x)}{\mathrm{d}x^n} + \cdots + a_1(x)\frac{\mathrm{d}y(x)}{\mathrm{d}x} + a_0(x)y(x) = f(x), \tag{3.89}$$

where the $a_n(x)$'s, and its derivatives, are continuous functions on $[a, b]$. It is also required that the forcing term $f(x)$ is bounded within $[a, b]$. Using a simplified notation, we can write Eq. (3.89) as

$$\sum_{m=0}^{n} a_m(x)\frac{\mathrm{d}^m y(x)}{\mathrm{d}x^m} = f(x), \tag{3.90}$$

and for the sake of brevity, we denote the left-hand side with $\mathrm{L} = \mathrm{L}(x)$, which is a linear differential operator acting on $y(x)$, namely,

$$\mathrm{L} = \sum_{m=0}^{n} a_m(x)\frac{\mathrm{d}^m}{\mathrm{d}x^m}\ . \tag{3.91}$$

Consequently, Eq. (3.89) now reads

$$\mathrm{L}\, y(x) = f(x). \tag{3.92}$$

We now define *Green's function* $G(x|\xi)$ of $\mathrm{L}(x)$ to be the unique solution to the problem

$$\mathrm{L}\, G(x, |\xi) = \delta(x - \xi), \tag{3.93}$$

which satisfies the homogeneous boundary conditions $G(a|\xi) = G(b|\xi) = 0$, where ξ is an arbitrary point of excitation. In Eq. (3.93), the delta function $\delta(x - x_0)$ is acting as a source forcing function. The initial conditions show the importance of having homogeneous boundary conditions in the original differential equation, such as $y(a) = y(b) = 0$ or $y(a) = dy(b)/dx = 0$[9]. If such conditions apply to $G(t|\tau)$, then a solution that superimposes $G(t|\tau)$ for different values of τ will still satisfy the boundary conditions.

Green's function, $G(x|\xi)$, may be viewed physically as the response of a system to a unit impulse at $x = \xi$. Depending on the differential equation under consideration, the source $f(x)$ can be interpreted to be a load, a concentration flux, a charge density, and so on. The dimensions of a one-dimensional Green's function is $[G(x, x_0)] = [x^2][\delta(x)] = [x]$; then, in d dimensions, it becomes $[G(x, x_0)] = [x]^{2-d}$.

[9] If the boundaries are not homogeneous, for example, $y(a) = y(b) = c$, the problem would have to be manipulated into one for which the boundary conditions are homogeneous. In this explicit case, we have to write a differential equation for z with the substitution $z = y - c$.

Formally, a Green's function is the inverse of an arbitrary linear differential operator L that may depend on space and time. This tells us that Green's function is the solution to the differential equation with a forcing term given by a point source. Generally speaking, a Green's function inverts the operator L; thus, it is referred to as its *integral kernel*. In fact, the solution to Eq. (3.92) is the convolution $(G \star f)(x)$, as we will show below. To prove the latter statement, we multiply Eq. (3.93) by $f(\xi)$ and integrate along ξ, leading to

$$\int \mathrm{L}\left[G(x|\xi)\right] f(\xi)\, \mathrm{d}\xi = \int \delta(x-\xi) f(\xi)\, \mathrm{d}\xi = f(x). \tag{3.94}$$

The left-hand side of this last equation can be expressed as

$$\int \mathrm{L}\left[G(x|\xi)\right] f(\xi)\, \mathrm{d}\xi = \mathrm{L}\left[\int G(x|\xi) f(\xi)\, \mathrm{d}\xi\right]. \tag{3.95}$$

Now, due to transitivity,

$$\mathrm{L}\left[\int G(x|\xi) f(\xi)\, \mathrm{d}\xi\right] = f(x). \tag{3.96}$$

When comparing Eqs. (3.92) and (3.96), we see that $y(x)$ is given by

$$y(x) = \int G(x|\xi) f(\xi)\, \mathrm{d}\xi, \tag{3.97}$$

which is an integral representation of the solution.

In addition to Eq. (3.93), we must impose two further sets of restrictions on $G(x|\xi)$. The first is that the general solution $y(x)$ in Eq. (3.97) must satisfy the boundary conditions (BCs). This is simply arranged by demanding that $G(x|\xi)$ itself stratifies the BCs.

The second set of restrictions concerns the continuity or discontinuity of $G(x|\xi)$ and its derivatives at $x = \xi$. Such constraints are found by integrating Eq. (3.93) with respect to x over the small interval $[\xi - \epsilon, \xi + \epsilon]$ and then taking the limit as $\epsilon \to 0$. To such end, let us write Eq. (3.93) in the following form:

$$\frac{\mathrm{d}}{\mathrm{d}x}\left(a_n(x)\frac{\mathrm{d}^{n-1}G(x|\xi)}{\mathrm{d}x^{n-1}}\right) - \frac{\mathrm{d}^{n-1}G(x|\xi)}{\mathrm{d}x^{n-1}}\frac{\mathrm{d}a_n(x)}{\mathrm{d}x} + \cdots + a_1(x)\frac{\mathrm{d}G(x|\xi)}{\mathrm{d}x} + a_0(x)G(x|\xi) = \delta(x-\xi). \tag{3.98}$$

By integrating from $[\xi - \epsilon, \xi + \epsilon]$, we have

$$a_n(x)\frac{\mathrm{d}^{n-1}G(x|\xi)}{\mathrm{d}x}\bigg|_{\xi-\epsilon}^{\xi+\epsilon} - \int_{\xi-\epsilon}^{\xi+\epsilon}\frac{\mathrm{d}a_n(x)}{\mathrm{d}x}\frac{\mathrm{d}^{n-1}G(x|\xi)}{\mathrm{d}x^{n-1}}\mathrm{d}x + \cdots$$
$$+\int_{\xi-\epsilon}^{\xi+\epsilon} a_1(x)\frac{\mathrm{d}G(x|\xi)}{\mathrm{d}x}\mathrm{d}x + \int_{\xi-\epsilon}^{\xi+\epsilon} a_0(x)G(x|\xi)\mathrm{d}x = \int_{\xi-\epsilon}^{\xi+\epsilon}\delta(x-\xi)\mathrm{d}x. \tag{3.99}$$

Now, by taking the limit when $\epsilon \to 0$, all the terms except the first one vanish, because at ξ, the $a_n(x)$'s and their derivatives are continuous, yielding

$$\frac{\mathrm{d}^{n-1}}{\mathrm{d}x^{n-1}}G(x|\xi)\bigg|_{\xi_+} - \frac{\mathrm{d}^{n-1}}{\mathrm{d}x^{n-1}}G(x|\xi)\bigg|_{\xi_-} = \frac{1}{a_n(\xi)}. \tag{3.100}$$

In other words, the latter equation is telling us that the derivatives of $G(x|\xi)$ with respect to x up to order $n-2$ are continuous at $x=\xi$, but the $(n-1)$th-order derivative has a discontinuity of $1/a_n(\xi)$ at this point. This is the so-called jump condition or discontinuity. Finally, besides this condition, we have the *continuity condition*, namely,

$$\lim_{\epsilon\to 0}\left[G(x|\xi+\epsilon) - G(x|\xi-\epsilon)\right] = 0. \tag{3.101}$$

Summarizing, the jump condition (3.100), the continuity condition (3.101), and the boundary conditions give the 2n equations needed to complete the construction of Green's function.

3.5.1 An Application of Green's Function: The Forced Undamped Harmonic Oscillator

The primary use of Green's functions in mathematics and physics is to solve non-homogeneous boundary value problems. As an introduction to Green's function technique, we will solve the equation of motion of the *driven harmonic oscillator* by an applied external force $F(t)$. A simple harmonic oscillator consists of a mass m attached to a spring which, when displaced from its equilibrium position, experiences a restoring force $-kx$ proportional to the displacement x, which pulls the mass in the direction of the origin, $x=0$, and is characterized by a natural frequency $\omega_0 = \sqrt{k/m}$. The equation of motion of a harmonic oscillator in the presence of an external force $F(t)$ is given by

$$\frac{\mathrm{d}^2x}{\mathrm{d}t^2} + \omega^2 x = \frac{F(t)}{m} = f(t). \tag{3.102}$$

To solve Eq. (3.102) by Green's method, let us assume that instead of the oscillator experiencing a force $f(t)$, it receives a whole sequence of impulses $f(\tau)$ from 0 to t, in such a way that

$$f(t) = \int_0^\infty f(\tau)\delta(t-\tau)\,\mathrm{d}\tau. \tag{3.103}$$

Accordingly, we have to solve Eq. (3.102) with $f(t)$ replaced by $\delta(t-\tau)$, that is, we find the response of the system to a unit impulse at τ. When the system receives the impulse at $t = \tau$, the oscillator emits a response $G(t, \tau)$, and from Eq. (3.93),

$$\frac{\mathrm{d}^2 G(t|\tau)}{\mathrm{d}t^2} + \omega^2 G(t,\tau) = \delta(t-\tau), \tag{3.104}$$

where the linear operator L(t) is given by

$$\mathrm{L}(t) = \frac{\mathrm{d}^2}{\mathrm{d}t^2} + \omega^2. \tag{3.105}$$

On the other hand, we have from Eq. (3.97) that the solution to Eq. (3.102) is computed through

$$x(t) = \int_0^\infty G(t|\tau)\ f(\tau)\,\mathrm{d}\tau. \tag{3.106}$$

Now, solving Eq. (3.104) subject to the initial conditions $G(t|\tau) = 0$ and $\mathrm{d}G(t|\tau)/\mathrm{d}t = 0$, both at τ, we obtain Green's function of the problem

$$G(t|\tau) = \begin{cases} 0, & 0 < t < \tau, \\ \frac{1}{\omega}\sin\left[\omega(t-\tau)\right], & 0 < \tau < t. \end{cases} \tag{3.107}$$

Figure 3.7 shows the time evolution of $G(t|\tau)$.

Recalling that τ is an arbitrary reference time and that the value of Green's function is null for $\tau > t$, then, by substituting Eq. (3.107) into Eq. (3.106), we finally find that the solution of the driven harmonic oscillator is

$$x(t) = \int_0^t \frac{1}{\omega}\sin\left[\omega(t-\tau)\right]\ f(\tau)\,\mathrm{d}\tau, \tag{3.108}$$

where we add up all the single impulses $f(\tau)$ from 0 to t in order to reproduce the effect of $f(t)$ over the harmonic oscillator.

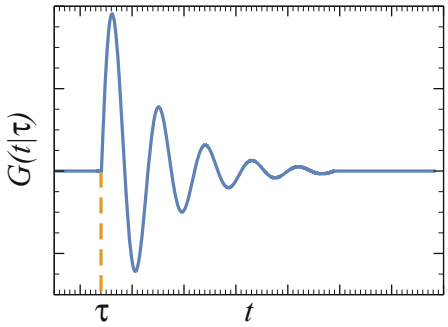

Fig. 3.7 Time evolution of Green's function for an undamped harmonic oscillator. $G(t, |tau)$ represents the system's response to an impulse from the source $f(t)$. When $t = 0$, the mass is elongated from its equilibrium position and then released without any impulse. Subsequently, at time τ, the external force starts to act on the system. When $0 < t < \tau$, the object will oscillate with its own frequency ω_0, and no response is produced, $G(t|\tau)$=0. In between $0 < \tau < t$, a new frequency ω resulting from $f(t)$ is obtained, leading to a sinusoidal response. Afterward, the external force is removed, meaning that the oscillator goes back to oscillating at ω_0

3.5.2 *The Inhomogeneous Diffusion Equation and Green's Function*

In Chap. 2, we derived the homogeneous diffusion equation in terms of the concentration $c(x, t)$, Eq. (2.16). In contrast, when a source is present in the system, the diffusion equation becomes inhomogeneous:

$$\frac{\partial c(x,t)}{\partial t} - D\frac{\partial^2 c(x,t)}{\partial x^2} = \rho(x,t), \tag{3.109}$$

where $\rho(x, t)$ is the concentration of Brownian particles per unit of time delivered into the system. In order to use Green's function method to solve the latter equation, we must write the complete source $\rho(x, t)$ as a sequence of infinitesimal components, namely,

$$\rho(x,t) = \int_0^\infty \int_{-\infty}^\infty \rho(\xi,\tau)\delta(x-\xi)\delta(t-\tau)\,\mathrm{d}\xi\,\mathrm{d}\tau. \tag{3.110}$$

Then, we look for the solution of Eq. (3.109) with a unit pulse of concentration located at $x = \xi$ when $t = \tau$, i.e., $\delta(x - \xi)\delta(t - \tau)$, to find the system's response to such perturbation, $G(x, t)$. This translates into solving

$$\frac{\partial G(x,t)}{\partial t} - D\frac{\partial^2 G(x,t)}{\partial x^2} = \delta(x-\xi)\delta(t-\tau), \tag{3.111}$$

which is subject to[10]

$$G(x,0)=0 \quad \text{and} \quad G(|x|\to\infty,t)=0. \tag{3.112}$$

Although we already solved the homogeneous problem using different methods, let us solve Eq. (3.111) using a combination of the Fourier and Laplace transforms in order to consider *causality*.[11] First, we take the Laplace transform of Eq. (3.111), which is

$$\int_0^\infty \left[\frac{\partial G(x,t)}{\partial x}-D\frac{\partial^2 G(x,t)}{\partial x^2}\right] \mathrm{e}^{-st}\,\mathrm{d}t=\int_0^\infty \delta(x-\xi)\delta(t-\tau)\mathrm{e}^{-st}\,\mathrm{d}t. \tag{3.113}$$

Now, the left-hand side of the transform has already been computed and can be found through Eq. (3.33) when considering that $G(x,t)\mathrm{e}^{-st}\big|_{t\to\infty}=0$ and $G(x,0)=0$. For the right-hand side, we use one of the main properties of the Dirac delta function, Eq. (A.92). These arguments, along with $\mathcal{L}\{G(x,t)\}=G(x,s)$, lead to

$$sG(x,s|\xi,\tau)-D\frac{\partial^2 G(x,s|\xi,\tau)}{\partial x^2}=\delta(x-\xi)\mathrm{e}^{-s\tau}. \tag{3.114}$$

Then, by taking the Fourier transform of the latter equation, we obtain

$$\int_{-\infty}^\infty \left[sG(x,s|\xi,\tau)-D\frac{\partial^2 G(x,s|\xi,\tau)}{\partial x^2}\right]\mathrm{e}^{ikx}\,\mathrm{d}x=\int_{-\infty}^\infty \delta(x-\xi)\mathrm{e}^{-s\tau}\mathrm{e}^{ikx}\,\mathrm{d}x, \tag{3.115}$$

leading to

$$sG(k,s|\xi,\tau)+Dk^2G(k,s|\xi,\tau)=\mathrm{e}^{-s\tau}\mathrm{e}^{ik\xi}, \tag{3.116}$$

where we used Eq. (3.8) for the transform of the second spatial derivative with respect to x. Moreover, by defining $\alpha^2\equiv s/D$, the last expression is reduced to

$$G(k,s|\xi,\tau)=\frac{\mathrm{e}^{ik\xi-s\tau}}{(\alpha^2+k^2)D}. \tag{3.117}$$

[10] The BC for Green's function arises from the fact that Eq. (3.111) is subject to the homogeneous version of the BC associated with Eq. (3.109). For instance, if the solution of Eq. (3.109) is required to satisfy an inhomogeneous Neumann BC, then Eq. (3.111) is to be solved together with the corresponding homogeneous Neumann BC.

[11] Causality refers to the fact that an event cannot occur before its cause is produced. This means that the solutions to be considered must be treated carefully, since the diffusion equation itself can distinguish past from future.

To find $G(x,t|\xi,\tau)$, we start by making the inverse Fourier transform of Eq. (3.117), that is,

$$G(x,s|\xi,\tau) = \frac{\mathrm{e}^{-s\tau}}{2\pi D}\int_{-\infty}^{\infty}\frac{\mathrm{e}^{-ik(x-\xi)}}{\alpha^2+k^2}\,\mathrm{d}k. \tag{3.118}$$

If we think about the inverse Fourier transform as a line integral along the real axis in the complex plane, the computation becomes easier. For such purpose, we rewrite the latter equation as

$$G(x,s|\xi,\tau) = \frac{\mathrm{e}^{-s\tau}}{2\pi D}\oint_C\frac{\mathrm{e}^{-ik(x-\xi)}}{\alpha^2+k^2}\,\mathrm{d}k - \frac{\mathrm{e}^{-s\tau}}{2\pi D}\int_{C_R}\frac{\mathrm{e}^{-ik(x-\xi)}}{\alpha^2+k^2}\,\mathrm{d}k, \tag{3.119}$$

in which the subscript C indicates the integration along a closed path laying on the real axis and the subscript C_R indicates the integration along a semicircular path joining the contour at point $k = 0$. In accordance with Jordan's lemma, we can neglect the second term,[12] yielding

$$G(x,s|\xi,\tau) = \frac{\mathrm{e}^{-s\tau}}{2\pi D}\oint_C\frac{\mathrm{e}^{-ik(x-\xi)}}{\alpha^2+k^2}\,\mathrm{d}k, \tag{3.122}$$

and by applying Cauchy's residue theorem,[13] we find that

[12] Jordan's lemma states that if having a circular arc C_R with radius R at the center of the origin and a function $f(z)$ such as $f(z) \to 0$ uniformly as $R \to \infty$, then

$$\lim_{R\to\infty}\int_{C_R} f(z)\mathrm{e}^{imz}\,\mathrm{d}z = 0, \qquad (m>0), \tag{3.120}$$

if C_R lies in the first and/or second quadrants, and

$$\lim_{R\to\infty}\int_{C_R} f(z)\mathrm{e}^{-imz}\,\mathrm{d}z = 0, \qquad (m>0), \tag{3.121}$$

if C_R lies in the third and/or fourth quadrants. Such requirements perfectly suit Green's function of the inhomogeneous diffusion equation. For instance, in Eq. (3.120), $m = x_0 - x > 0$ when we are to the left of x_0, and in Eq. (3.121), $m = x - x_0 > 0$ when we are to the right of x_0.

[13] Cauchy's residue theorem states that if C is a simple-closed contour, described in the positive sense, and if a function $f(z)$ is analytic inside and on C except for a finite number of singular points z_k inside C, then

$$\oint_C f(z)\,\mathrm{d}x = 2\pi i\sum_{k=1}^{N}\mathrm{Res}[f(z)]. \tag{3.123}$$

$$G(x,s|\xi,\tau) = \frac{\mathrm{e}^{-s\tau}}{2\pi D}\left\{2\pi i \sum_{n=1}^{N} \mathrm{Res}\left[\frac{\mathrm{e}^{-ik(x-\xi)}}{\alpha^2+k^2}\right]\right\}$$
$$= \frac{i\mathrm{e}^{-s\tau}}{D}\sum_{n=1}^{N} \mathrm{Res}\left[\frac{\mathrm{e}^{-ik(x-\xi)}}{\alpha^2+k^2}\right]. \tag{3.124}$$

To find the residues, we make a Taylor series of the argument around the singular points (or poles), $i\alpha$ and $-i\alpha$. Writing the first term only is enough to identify the residue, namely,

$$\frac{\mathrm{e}^{-ik(x-\xi)}}{\alpha^2+k^2} = -\frac{i\mathrm{e}^{(x-\xi)\alpha}}{2\alpha(k-i\alpha)} + \cdots \qquad \text{(around } i\alpha\text{)}, \tag{3.125}$$

$$\frac{\mathrm{e}^{-ik(x-\xi)}}{\alpha^2+k^2} = \frac{i\mathrm{e}^{-(x-\xi)\alpha}}{2\alpha(k+i\alpha)} + \cdots \qquad \text{(around } -i\alpha\text{)}. \tag{3.126}$$

Thus,

$$G(x,s|\xi,\tau) = \frac{i\ \mathrm{e}^{-s\tau}}{D}\left[-\frac{i\mathrm{e}^{(x-\xi)\alpha}}{2\alpha}\right] = \frac{\mathrm{e}^{(x-\xi)\alpha-s\tau}}{2D\alpha} \quad \text{for} \quad i\alpha, \tag{3.127}$$

and, given that for $-i\alpha$ the integration is in clockwise direction, for the second pole, we have that

$$G(x,s|\xi,\tau) = \frac{-i\ \mathrm{e}^{-s\tau}}{D}\left[\frac{i\mathrm{e}^{-(x-\xi)\alpha}}{2\alpha}\right] = \frac{\mathrm{e}^{-(x-\xi)\alpha-s\tau}}{2D\alpha} \quad \text{for} \quad -i\alpha. \tag{3.128}$$

Intending to express the solution in a single function, we use the absolute value of the difference $x-\xi$, yielding

$$G(x,s|\xi,\tau) = \frac{\mathrm{e}^{-|x-\xi|\alpha-s\tau}}{2D\alpha}, \tag{3.129}$$

and by substituting α, we find that

$$G(x,s|\xi,\tau) = \frac{\mathrm{e}^{-|x-\xi|\sqrt{s/D}-s\tau}}{\sqrt{4sD}}. \tag{3.130}$$

The Fourier inverse transform is now done. Then, by inverse Laplace transforming Eq. (3.130),

$$G(x,t|\xi,\tau)=\mathcal{L}^{-1}\left\{\frac{\mathrm{e}^{-|x-\xi|\sqrt{s/D}-s\tau}}{\sqrt{4sD}}\right\}, \tag{3.131}$$

and using the fact that $\mathcal{L}\{f(t-b)H(t-b)\}=\mathrm{e}^{-bs}F(s)$, where $F(s)$ is the Laplace transform of $f(t)$, $H(t)$ the step function, and b a real positive constant, together with the inverse Laplace transform of $\exp\left[-\sqrt{\frac{s}{D}}(x-\xi)\right]/\sqrt{4Ds}$, Eq. (3.59), we finally obtain Green's function of the inhomogeneous diffusion equation,

$$G(x,t|\xi,\tau)=\frac{H(t-\tau)}{\sqrt{4\pi D(t-\tau)}}\exp\left[-\frac{(x-\xi)^2}{4D(t-\tau)}\right]. \tag{3.132}$$

The Heaviside step function indicates that there is no response until the source is placed at time τ. In previous chapters, this time has been taken to be $\tau=0$. Since we start studying the diffusion process once the concentration source is placed in the system, say at $\xi=x_0$, such consideration simplifies Eq. (3.132) as follows:

$$G(x,t|\xi=x_0,\tau=0)=G(x,t|x_0)=\frac{1}{\sqrt{4\pi Dt}}\exp\left[-\frac{(x-x_0)^2}{4Dt}\right], \tag{3.133}$$

which is actually Eq. (3.30). This allows us to conclude that Green's function of the inhomogeneous diffusion equation is identical to the solution of the diffusion equation in free space. Lastly, we find that the solution of the inhomogeneous diffusion equation is given by

$$c(x,t)=\int_0^t\int_0^x\frac{H(t-\tau)}{\sqrt{4\pi D(t-\tau)}}\exp\left[-\frac{(x-\xi)^2}{4D(t-\tau)}\right]\rho(x_0,\tau)\,\mathrm{d}\tau\,\mathrm{d}\xi. \tag{3.134}$$

3.6 Free Diffusion on d-Dimensional Space

The propagator for a diffusing particle in a d-dimensional free space, subject to the initial condition $p(\mathbf{r},t=0)=\mathbf{r}_0$, can be found based on the fact that motion in different directions is independent from each other. Then, the d-dimensional diffusion equation can be written as

$$\frac{\partial p(\mathbf{r},t)}{\partial t}=D\left(\frac{\partial^2 p(\mathbf{r},t)}{\partial x_1^2}+\frac{\partial^2 p(\mathbf{r},t)}{\partial x_2^2}+\cdots+\frac{\partial^2 p(\mathbf{r},t)}{\partial x_d^2}\right). \tag{3.135}$$

Since the partial spatial derivatives are with respect to a single variable, we can use the superposition principle and propose a general solution as the product of the solutions for each dimension, namely,

$$p(\mathbf{r}, t|\mathbf{r_0}) = \prod_{i=1}^{d} p_i(x_i, t|x_{0_i}), \tag{3.136}$$

where $i = 1, 2, 3, \ldots, d$. Substituting (3.136) into (3.135), we find that $p_i(x_i, t|x_{0_i})$ must satisfy the following equation:

$$\frac{\partial p_i(x_i, t|x_{0_i})}{\partial t} = D\frac{\partial^2 p_i(x_i, t|x_{0_i})}{\partial x_i^2}. \tag{3.137}$$

Equation (3.137) must be solved subject to the initial conditions $p_i(x_i, t|x_{0_i}) = \delta(x_i - x_{0_i})$ for all i. The solution to the one-dimensional diffusion equation has been found using different methods in this chapter, and now we know that it is given by (3.29). When this solution is substituted into (3.136), we finally arrive at

$$p(\mathbf{r}, t|0) = \frac{1}{(4\pi Dt)^{d/2}} \exp\left(-\frac{(\mathbf{r} - \mathbf{r_0})^2}{4Dt}\right). \tag{3.138}$$

The propagator is a Gaussian with a peak centered at $\mathbf{r_0}$. When d is set equal to 1, Eq. (3.29) is recovered. Now, as times goes by, the peak's decrease depends on the dimension, as well as on how it broadens (see Fig. 3.8).

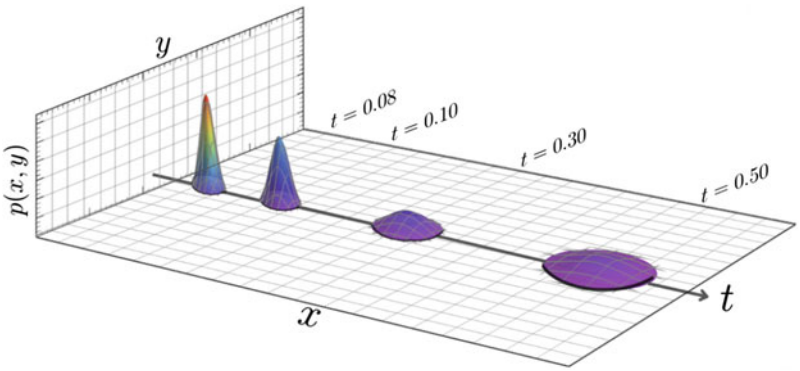

Fig. 3.8 Representative plot of the time evolution of the probability density for free Brownian particles in two dimensions, given by Eq. (3.138) and setting $d = 2$ at different times, i.e., $t = 0.08$, $t = 0.10$, $t = 0.30$, and $t = 0.50$. The peak of the function is centered at the initial position $\mathbf{r_0}$ and becomes broader over time

3.7 Concluding Remarks

In this chapter, we solved the diffusion equation in free space, i.e., we found a unique solution that satisfies both the PDE and the initial conditions. To solve the free-space diffusion problem, we reviewed the most commonly used methods: the Fourier and Laplace transforms and Green's function formalism. We also proved the central limit theorem and discussed its important implications, i.e., if the first two moments of a sequence of independent and identically distributed random variables are finite, their distribution probability converges to a normal distribution.

For the reader's convenience, listed below are the most important equations we have obtained in this chapter.

$$p(x,t|x_0) = \frac{1}{\sqrt{2\pi}\sigma}\exp\left[-\frac{1}{2}\left(\frac{x-\mu}{\sigma}\right)^2\right] \qquad \text{(Gaussian or normal distribution)}$$

$$\frac{\partial c(x,t)}{\partial t} - D\frac{\partial^2 c(x,t)}{\partial x^2} = \rho(x,t) \qquad \text{(Inhomogeneous diffusion equation)}$$

$$G(x,t|\xi,\tau) = \frac{H(t-\tau)}{\sqrt{4\pi D(t-\tau)}}\exp\left[-\frac{(x-\xi)^2}{4D(t-\tau)}\right]$$
(Green's function for the diffusion equation)

$$p(\mathbf{r},t|0) = \frac{1}{(4\pi Dt)^{d/2}}\exp\left(-\frac{(\mathbf{r}-\mathbf{r_0})^2}{4Dt}\right)$$
(Propagator in a d-dimensional free space)

3.A Galton Board Simulation

This appendix presents Listing 3.1, in which we provide a *Mathematica* code to simulate the random walk of balls within a Galton board. The execution of function *Galtonboard*, which requires the number of pegs and balls in the system, generates a histogram from a list of the final positions of the balls. For instance, by running the function `Galtonboard[100, 10000]`, we obtain the distribution of 10,000 balls within the bins after interacting with 100 pegs (see Fig. 3.9).

Listing 3.1 [Galtonboard.nb]: Mathematica code to simulate a Galton board and provide an histogram of final positions

```
(*Definition of the Galton board simulation*)

Galtonboard[(*number of pegs*)pegs_, (*number of balls*)
    balls_] :=
   Module[(*Definition of local variables*)

    {position, list, motionofparticle},

    (*We create a table containing all balls' final
    position*)

    list = Table[

      (*Initial position of each ball*)
      (*we drop each ball at the center of the board*)
    position = IntegerPart[pegs/2];

      (*Calculation of the position after bouncing off all
     pegs*)
    Do[
     (*equal probability of moving to the left of the
    right*)

     motionofparticle = RandomChoice[{-1, 1}];

     (*new position computation*)

     position = position + motionofparticle;

     , pegs (*random motion after each bounce*)];
    position, {balls}];

    (*Finally, we make an histogram using the list of
    balls' final positions*)

    Histogram[list, {1}, Frame -> True]
    ]

```

Listing continued on next page

Listing continued from last page

```
(*As an example, we show the distribution of 10,000 balls
    in the bins after interacting with 100 pegs*)

Galtonboard[(*number of pegs*)100,(*number of balls*)
    10000]
```

Listing ended

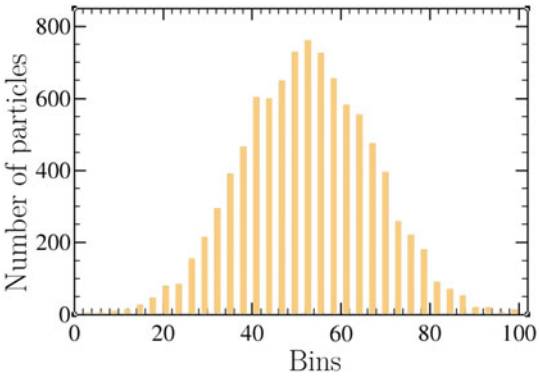

Fig. 3.9 The bar chart represents the number of paths leading to each slot obtained from the code in Listing 3.1 by means of the function `Galtonboard[100, 10000]`

Further Reading and References

C. Constanda, *Solution Techniques for Elementary Partial Differential Equations* (Chapman & Hall/CRC, Boca Raton, 2010)

Part III
One-Dimensional Diffusion and Boundary Conditions

The randomness of being trapped and reflected in one dimension.

"*In physics, you don't have to go around making trouble for yourself - nature does it for you.*"

—Frank Wilczek

Chapter 4
One-Dimensional Semi-infinite Systems Solutions

When a Brownian particle hits a boundary, its fate is determined by the physical properties of this boundary. For example, if the particle hits a *perfectly reflecting* boundary, it bounces off, and if it hits a *perfectly absorbing* wall, it is removed from the system. The latter occurs, for example, when the particle either crosses through a different container that it cannot go back to or reacts with the wall by binding to it or turning into another substance. A third possibility is that the boundary wall may be neither perfectly reflecting nor perfectly absorbing, and instead, both effects occur with a certain probability. In this case, the boundary is referred to as a *partially absorbent* or *radiation boundary*. It turns out that the solution to the diffusion equation is dependent on the boundary conditions (BCs) imposed.

In the previous chapter, we focused on solving the diffusion equation under no spatial constrains and with one initial condition. In this chapter, we will impose a boundary condition (BC) from those described in the previous paragraph, as well as an initial condition, to solve the diffusion equation in a semi-infinite system. These BCs can be described mathematically by the Dirichlet and Neumann BCs. With Dirichlet BCs, we can define the perfectly absorbing boundary, while Neumann BCs are used to describe perfectly reflecting and radiation boundaries. As we will see, the properties of the propagator $p(x,t)$ and its flux $\partial p(x,t)/\partial x$ at the boundary become essential when defining BCs.

Solving the diffusion equation with BCs can be carried out using different approaches. Since all of them are important and useful, in this chapter, we will solve each problem using different mathematical methods and tools. Even though it might seem unnecessary, when facing new problems related with diffusion under confinement, knowing the different ways in which these problems can be solved can prove to be extremely helpful. Usually, one method will turn out to be easier or more useful than others depending on the characteristics of the system under study, making it worthwhile.

L. Dagdug et al., *Diffusion Under Confinement*,
https://doi.org/10.1007/978-3-031-46475-1_4

4.1 Boundary Conditions

This section is intended to provide a brief introduction to the concept of BCs. The conditions we impose on the boundary $\partial\Omega$ of the domain Ω are called *boundary conditions*. The BCs are the constraints that need to be satisfied by the solution of a *boundary value problem* : a differential equation together with a set of additional constraints that make its solution unique. For instance, in one dimension, the only choice for a domain Ω is an interval. In a finite spatial domain $[a, b]$, it is necessary to specify two constraints, one at $x = a$ and the other at $x = b$, in addition to the time constraints, that typically is the initial condition at $t = 0$.

There are five types of BCs: Dirichlet, Neumann, Robin, mixed, and Cauchy BCs. The Dirichlet, Neumann, and Robin BCs are also called the first-, second-, and third-type BCs, respectively. It is worth remembering that a BC is homogeneous if its value is set to be zero; otherwise, it is called inhomogeneous.

Dirichlet BCs specify the value of the function on $\partial\Omega$. For example, we could specify Dirichlet BCs for the interval domain $[a, b]$, such as in a one-dimensional (1D) constrained diffusion problem where both ends of the system are maintained with constant concentration, namely, $c(x = a) = c_a$ and $c(x = b) = c_b$. When these constants are set to be zero, each boundary describes a perfectly absorbing point, namely, $c(x = a) = c(x = b) = 0$. In general, the boundary value could also be dependent on time, for example, $c(x = a, t) = f(x = a, t)$.

Neumann BCs specify the value of the normal derivative of the function on $\partial\Omega$. Accordingly, the derivative of the dependent variable is known for the entire boundary. For example, in our 1D diffusion example, we could be interested in specifying the flux at the two endpoints, i.e., $\partial c_x(x = a)\partial x = f(x = a)$ and $\partial c(x = b)\partial x = f(x = b)$. When $f(x)$ is equal to zero, this boundary describes a perfectly reflecting point, namely, $\partial c_x(x = a)\partial x = \partial c_x(x = b)\partial x = 0$. On the other hand, when the flux is proportional to the concentration, a partially absorbing point is described, namely, $\partial c_x(x = a)\partial x = \kappa c_x(x = a)$. If the proportionally constant κ tends to infinity, we recover the perfectly absorbing BC, and if it is set equal to zero, a perfectly reflecting BC is described. As in the Dirichlet case, the boundary constraint could also depend on time.

The Robin BCs, when imposed on an ordinary or a partial differential equation, are a weighted combination of the Dirichlet and Neumann BCs at $\partial\Omega$. When dealing with diffusion in 1D, such constraints can be written as follows: $\alpha_1 c(x = a) + \alpha_2 \partial c_x(x = a)\partial x = f(x = a, t)$ and $\alpha_1 c(x = b) + \alpha_2 \partial c_x(x = b)\partial x = f(x = b, t)$, where α_i $(i = 1, 2)$ are constants representing the weights.

The Cauchy BCs correspond to imposing Dirichlet and Neumann BCs simultaneously. For example, if a diffusion process takes place in 1D interval domain $[a, b]$, this corresponds to the condition where concentration is specified at one end of the domain, $c(x = a) = c_a$, while the flux is known at the other end of the domain, i.e., $\partial c(x = b)\partial x = f(x = b)$.

The mixed BCs are commonly used in second-order differential equations, in which one may specify the value of the function $c(x, t)$ and its derivative.

Consequently, the Dirichlet and Neumann BCs, regarding the bounded 1D diffusion problem, can be written as $c(x = a) = c_a$ and $\partial c(x = a)\partial x = f(x = a)$.

The selection of any of the mentioned BCs depends on the geometrical and physical properties of the domain, as we will see in the following sections.

4.2 Derivation of Boundary Conditions

In order to present a derivation of the BCs, we will assume a discrete one-dimensional random walk on $x \geq 0$, with the probability of the particle being at site j at the nth time step given by $p_n(j)$, in the presence of either: a reflecting, absorbing, or partially absorbing boundary at the origin, $j = 0$. We will start deriving the partially absorbing boundary, because once we have it in the continuous limit, the perfectly absorbing and reflecting boundaries can be derived as special cases. Let us start with the definition of probability flux in the x direction from j to $j + 1$ at the n'th step:

$$J_n(j) = -[b\, p_n(j + 1) - a\, p_n(j)], \tag{4.1}$$

where a and b are the probability of hopping to the right and to the left, respectively. It is convenient to write this equation with a minus sign, given that the diffusive flux is proportional but opposite in sign to the concentration gradient. In terms of Brownian particles, the relationship inside the square brackets is obtained by counting the particles that enter at j from $j + 1$, minus those that leave j to reach $j + 1$, at the nth step.

In a random walk, the partially absorbing boundary is defined in terms of the probability β of a particle becoming trapped or else being reflected when reaching the boundary, with a probability of $1 - \beta$. If the boundary is placed at the origin, $j = 0$, by definition, when a particle is reflected, the flux is zero,[1] and in our case, this occurs with a probability of $(1 - \beta)$. Then, from Eq. (4.1), we have

$$J_n(0) = 0 = a\, p_n(0) - (1 - \beta)\, b\, p_n(1). \tag{4.2}$$

Consequently, the master equation for site 1 is given by

$$p_n(1) = \frac{a}{b(1 - \beta)}\, p_n(0). \tag{4.3}$$

This relation in the continuous limit is

[1] In classical mechanics, a particle colliding with a reflecting or impenetrable wall instantaneously changes the sign of the component of its velocity perpendicular to this surface. Consequently, the net flux of particles crossing the wall is equal to zero.

$$p(x + \Delta x, t) = \frac{a}{b(1-\beta)}\, p(x, t). \tag{4.4}$$

By Taylor expanding this last equation to the lowest order, we arrive at

$$p(x, t) + \Delta x \frac{\partial p(x, t)}{\partial x} = \frac{a}{b(1-\beta)}\, p(x, t). \tag{4.5}$$

Then, for isotropic diffusion, namely, $a = b = 1/2$, we have

$$\frac{\partial p(x, t)}{\partial x} = \frac{1}{\Delta x}\left(\frac{\beta}{1-\beta}\right) p(x, t). \tag{4.6}$$

This flux is proportional to the ratio of the probability of being trapped and the probability of being reflected. Now, defining

$$k \equiv \frac{1}{\Delta x}\left(\frac{\beta}{1-\beta}\right), \tag{4.7}$$

we finally find that the continuum version of the partially absorbing or radiation boundary is

$$\left.\frac{\partial p(x, t)}{\partial x}\right|_{x=x_b} = k\, p(x_b, t), \tag{4.8}$$

where $p(x, t)$ and its derivative are evaluated at the boundary x_b. The units of k are inverse of length. Setting $\beta = 0$ and consequently $k = 0$, we recover a reflecting BC, namely,

$$\left.\frac{\partial p(x, t)}{\partial x}\right|_{x=x_b} = 0. \tag{4.9}$$

By setting $\beta = 1$ and therefore $k \to \infty$, a perfectly absorbing BC is recovered, i.e.,

$$p(x_b, t) = 0. \tag{4.10}$$

If we wish to express Eq. (4.8) in terms of the probability flux, we have to multiply it by D. Then, by defining the $\kappa \equiv Dk$, the so-called trapping rate coefficient, we arrive at

$$D\left.\frac{\partial p(x, t)}{\partial x}\right|_{x=x_b} = \kappa\, p(x_b, t). \tag{4.11}$$

Observing that κ and $p(x_b, t)$ are positive-definite quantities, regardless of the direction of the outward flow crossing the boundary, we can write a more affordable

equation for a partially absorbing BC in one dimension, specifically

$$\mathbf{J}(x_b, t) \cdot \hat{\mathbf{e}}_i = \kappa\, p(x_b, t), \tag{4.12}$$

where $\hat{\mathbf{e}}_i$ is the unit outward-facing normal vector to the boundary x_b. It is worth noting that the trapping rate coefficient, κ, has units of length per time, consequently units of velocity, and it characterizes the trapping efficiency. The analog equation associated with the concentration of particles can be found in a straightforward manner if we recall that $c(\mathbf{r}, t) = Np(\mathbf{r}, t)$, where N is the number of diffusing particles. Therefore, in one dimension, the flux of the concentration has units of number of particles per time.

The partially absorbing BC is generalized in higher dimensions as follows:

$$\mathbf{J}(\mathbf{r}_b, t) \cdot \hat{\mathbf{n}} = \kappa\, p(\mathbf{r}_b, t). \tag{4.13}$$

For the sake of clarity, some examples of the most useful formulas for the trapping rate coefficients are provided in the next section. Later on, in the following chapters, these formulas will be deduced.

4.2.1 Useful Formulas for Trapping Rate Coefficients and Rate Constants

Trapping of diffusing particles by perfectly absorbing, reflecting, and partially absorbing regions on the otherwise reflecting surface plays an important role in many physical, chemical, technological, and biophysical processes, such as electric current through an array of microelectrodes, reactions on supported catalysis, transport passing through porous membranes, and ligand binding to cell surface receptors. These trapping problems are extremely complicated for analytical treatment, but one can take advantage of simple formulas for the trapping rate coefficients.

4.2.2 Perfectly Absorbing Sphere

Consider trapping of diffusing particles in a perfectly absorbing sphere of radius R centered at the origin, where as soon as a particle reaches the surface of the sphere, it is removed from the system. In a steady state, $\mathrm{d}c(r)/\mathrm{d}t = 0$, where $c(r)$ is the particle concentration and r is the distance from the origin. Consequently, the diffusion equation, Eq. (2.17), in spherical coordinates simplifies to

$$\frac{D}{r^2}\frac{\mathrm{d}}{\mathrm{d}r}\left(r^2\frac{\mathrm{d}c(r)}{\mathrm{d}r}\right) = 0, \qquad r > R, \tag{4.14}$$

which is to be solved subject to the following boundary conditions: perfectly absorbing on the surface of the sphere, $c(R) = 0$ ($\kappa \to \infty$), and uniform concentration at infinity, $c(r)|_{r\to\infty} = c_\infty$. Integrating Eq. (4.14), we find that the solution of this boundary value problem is given by

$$c(r) = \left(1 - \frac{R}{r}\right) c_\infty. \tag{4.15}$$

Once we know the concentration, and keeping in mind that the flux goes inward toward the center of the sphere, we can calculate it using the following expression in spherical coordinates:

$$J = D\frac{\mathrm{d}c(r)}{\mathrm{d}r} = \frac{DRc_\infty}{r^2}. \tag{4.16}$$

We can then use this result to find the *diffusion current*, or *total flux*, which is the number of particles trapped by the sphere per unit time:

$$I = 4\pi R^2 D \left.\frac{\mathrm{d}c(r)}{\mathrm{d}r}\right|_{r=R} = 4\pi RDc_\infty. \tag{4.17}$$

The ratio of the diffusion current to the particle concentration at infinity, I/c_∞, is the *diffusion-controlled rate constant*, or *rate constant*, for a perfectly absorbing sphere,

$$\mathrm{k}_S = 4\pi RD, \tag{4.18}$$

which has units of volume per time. This formula is known as the Smoluchowski rate constant.

4.2.3 Partially Absorbing Sphere

Considering diffusing particles in the presence of a partially absorbing sphere of radius R centered at the origin, the corresponding boundary condition, on this surface takes the following form:

$$D \left.\frac{\mathrm{d}c(r)}{\mathrm{d}r}\right|_{r=R} = \kappa c_\infty, \tag{4.19}$$

where κ is the trapping rate constant that characterizes the trapping efficiency. When $\kappa \to \infty$ or $\kappa = 0$, the boundary condition corresponds to a perfectly absorbing or reflecting surface, respectively. The association of the effective rate constant in this case, also known as the Collins-Kimball rate constant, is given by

$$\mathrm{k}_{CK} = \frac{\mathrm{k}_S \, \kappa A}{\mathrm{k}_S + \kappa A} = \frac{4\pi R^2 D\kappa}{D + R\kappa}, \tag{4.20}$$

where $A = 4\pi R^2$ is the surface area of the sphere. The physical interpretation of this expression seems to be quite simple: It describes the decrease of the Smoluchowski rate constant by the factor

$$\frac{\kappa A}{\mathrm{k}_S + \kappa A}, \tag{4.21}$$

which is the trapping probability of a particle that starts diffusing from the surface of the sphere. The details of the derivations of Eq. (4.20) are given in Sect. 15.1.2.

4.2.4 Perfectly Absorbing Circular Disk

If a three-dimensional diffusion process takes place in the presence of a perfectly absorbing circular disk of radius a located on a flat reflecting surface, the diffusion current, or total flux, at steady state is given by $I = 4Dac_\infty$. Consequently, the rate constant is given by

$$\mathrm{k}_{HBP} = 4Da. \tag{4.22}$$

This formula is also known as the Hill-Berg-Purcell rate constant. The units of this constant are volume per unit time. The details of the derivations of Eq. (4.22) are given in Sect. 14.4.

4.2.5 Boundary Homogenization

The main idea behind the so-called boundary homogenization is to replace a heterogeneous boundary condition on a surface with a homogeneous one that has a properly chosen effective trapping rate (or rate constant), so that the steady-state flux remains unchanged. Such a replacement is possible because the memory of a local configuration of the absorbing patch decays with distance from the surface. Sufficiently far away from a patchy surface, the steady-state fields of the particle, i.e., fluxes and concentrations, are indistinguishable from the corresponding fields in the case of a uniform partially absorbing surface with a properly chosen κ. Even though boundary homogenization focuses on the steady-state flux, the approach can also be used to find the moments of the particle's mean first-passage time (MFPT), the probability density of the MFPT, and the particle's survival probability.

4.2.5.1 Patchy Surface

Consider trapping of diffusing particles by $\mathtt{N}$ small perfectly absorbing circular disks of radius a randomly distributed over the surface of a perfectly reflecting sphere of radius R, where $a \ll R$. In such a system, we want to replace this inhomogeneity by an effective rate constant. To such end, we introduce the rate coefficient for a perfectly absorbing disk, given by Eq. (4.22), into the Collins-Kimball formula, Eq. (4.20), leading to

$$\mathtt{k}_{BP} = \frac{4\pi DRa\mathtt{N}}{\pi R + a\mathtt{N}}. \tag{4.23}$$

This formula was first obtained by Berg and Purcell in a classical paper on chemotaxis using an analogy to an electrical case, that although it is a clever method, it only applies in the steady-state problem. The details of the derivations of Eq. (4.23) are given in Sect. 15.2.

4.2.5.2 Cylindrical Capillary: One-Dimensional Reduction

The boundary homogenization also is useful to reduce the dimension of a problem. For example, the diffusion into a cylinder of length L with two perfectly absorbing ends at $x = 0$ and $x = L$ can be replaced with diffusion along a line by choosing the correct κ. In such a case, the radiation boundary conditions at either the end or the beginning of the line of length L involve flux densities, which replace the capillary, given by

$$\left.\frac{\partial p(x,t|x_0)}{\partial x}\right|_{x=0} = \kappa_0\ p(0,t|x_0), \tag{4.24}$$

$$\left.\frac{\partial p(x,t|x_0)}{\partial x}\right|_{x=L} = \kappa_L\ p(L,t|x_0), \tag{4.25}$$

where $p(x,t|x_0)$ is the propagator for a particle initially at x_0. The rate constant κ_i is obtained by dividing the Hill-Berg-Purcell rate constant, Eq. (4.22), by the area of the circular plane surface ends of the cylinder, which gives

$$\kappa_i = \frac{4D}{\pi a}, \qquad i = 0, L. \tag{4.26}$$

The units of this effective rate constant are length per unit time, as expected. The details of the derivations of Eq. (4.26) are given in Sect. 16.2.

All these examples give us an incentive motivation to solve the diffusion equation in one dimension subject to boundary conditions. In Chap. 16, we will take an in-depth look at boundary homogenization and consider some of its applications.

4.3 Semi-infinite: Perfectly Absorbing Endpoint

4.3.1 The Fourier Transform Solution

Consider a Brownian particle diffusing along a one-dimensional semi-infinite domain in the presence of a perfectly absorbing point at $x = 0$ (see Fig. 4.1). The mathematical description of the absorbing boundary is given by Eq. (4.10); consequently,

$$p(0, t) = 0, \tag{4.27}$$

which is a Dirichlet BC.

To solve the diffusion equation under this BC, it is required that $x_0 > 0$. In previous chapters, we defined the Fourier transform using the kernel e^{ikx} (see Eq. (A.46)). But we can take either the real or imaginary parts of this exponential, namely, $\cos kx$ or $\sin kx$, to compute the transform. We can take advantage of this flexibility by choosing the proper kernel that satisfies the BC.

When the Brownian particle has an initial position $x_0 > 0$, it never leaves the positive domain and $p(0, t) = 0$. Thus, in this case, it is helpful to define the Fourier transform as

$$p(k, t) = \int_0^\infty p(x, t)\ \sin(kx)\ \mathrm{d}x, \tag{4.28}$$

with the inverse of the latter equation given by

$$p(x, t|x_0) = \frac{1}{\pi} \int_0^\infty p(k, t)\ \sin(kx)\ \mathrm{d}k. \tag{4.29}$$

It is worth noting that the BC given in (4.27) is satisfied by this last equation once we choose the sine function to define the Fourier transform, Eq. (4.28). Since the propagator must satisfy the diffusion equation, its Fourier transform is given by Eq. (3.13), which, excluding the imaginary part, reduces to

$$p(k, t) = p(k, 0) \exp\left(-Dk^2 t\right). \tag{4.30}$$

The transform of the initial condition, $p(0, t) = \delta(x - x_0)$, in the Fourier domain using Eq. (4.28), is $p(k, 0) = \sin(kx_0)$. Then, using this initial condition in

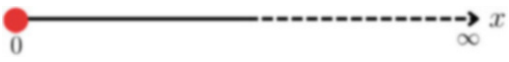

Fig. 4.1 Schematic representation of a one-dimensional semi-infinite domain with an absorbing end at $x = 0$ (red circle)

Eq. (4.30), the propagator given in (4.29) can be represented as

$$p(x,t|x_0) = \frac{2}{\pi}\int_0^\infty \exp\left(-Dtk^2\right)\sin(kx_0)\sin(kx)\,\mathrm{d}k.$$
$$= \frac{1}{\pi}\int_0^\infty \exp\left(-Dtk^2\right)\{\cos[(k-x_0)] - \cos[(k+x_0)]\}\mathrm{d}k.$$

Using Eq. (A.12) to solve the integrals yields

$$p(x,t|x_0) = \frac{1}{\sqrt{4\pi Dt}}\left\{\exp\left[-\frac{(x-x_0)^2}{4Dt}\right] - \exp\left[-\frac{(x+x_0)^2}{4Dt}\right]\right\}. \tag{4.31}$$

We see that the concentration has a linear dependence on x near the origin and a Gaussian large-distance tail, as illustrated in Fig. 4.2.

4.3.2 The Laplace Transform Solution

The solution to our current problem can also be found by means of a Laplace transform. As you may recall from Sect. 3.2, the Laplace transform of the diffusion equation subject to the initial condition $p(x, t = 0) = \delta(x - x_0)$ is given by

$$s\ p(x,s|x_0) - \delta(x-x_0) = D\frac{\partial^2 p(x,s|x_0)}{\partial x^2}. \tag{3.36}$$

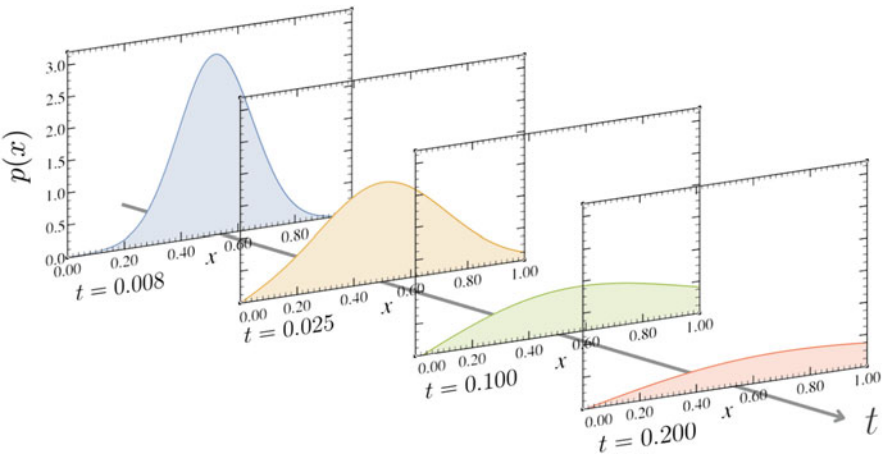

Fig. 4.2 Time evolution of the probability density $p(x, t|x_0)$ in Eq. (4.31) as a function of x evaluated at different times. The starting position of the particles is set at $x_0 = 0.5$, and the diffusion coefficient is $D = 1$

Since the particle is diffusing in a one-dimensional semi-infinite domain, where a perfectly absorbing point is set at $x = 0$, the solution must be canceled at the origin and decrease when x tends to infinity. Therefore, the solution in each region should be a linear combination of exponentials or hyperbolic functions. The most appropriate functions are those that meet the BCs at the origin and when x tends to infinity. Consequently, let us propose that

$$p(x, s|x_0) = \begin{cases} \mathcal{A}\ \sinh\left(\sqrt{\frac{s}{D}}\, x\right), & x < x_0 \\ \mathcal{B}\ \exp\left(-\sqrt{\frac{s}{D}}\, x\right), & x > x_0. \end{cases} \tag{4.32}$$

By imposing the continuity condition, given by Eq. (3.39), to the propagator $p(x, t, |x_0)$, we find that

$$\mathcal{A}\ \sinh\left(\sqrt{\frac{s}{D}}\, x_0\right) = \mathcal{B}\ \exp\left(-\sqrt{\frac{s}{D}}\, x_0\right), \tag{4.33}$$

and substituting (4.32) into the discontinuity condition, Eq. (3.42), we obtain

$$\mathcal{B}\ \exp\left(-\sqrt{\frac{s}{D}}\, x_0\right) - \mathcal{A}\ \cosh\left(\sqrt{\frac{s}{D}}\, x_0\right) = \frac{-1}{\sqrt{sD}}. \tag{4.34}$$

Solving the system of equations given by (4.33) and (4.34), and writing the hyperbolic sine function in terms of real exponentials, we find that

$$\mathcal{A} = \frac{1}{\sqrt{sD}} \exp\left(-\sqrt{\frac{s}{D}}\, x_0\right) \tag{4.35}$$

and consequently

$$\begin{aligned} \mathcal{B} &= \frac{1}{\sqrt{sD}} \sinh\left(\sqrt{\frac{s}{D}}\, x_0\right) \\ &= \frac{1}{2\sqrt{sD}} \left[\exp\left(\sqrt{\frac{s}{D}}\, x_0\right) - \exp\left(-\sqrt{\frac{s}{D}}\, x_0\right)\right]. \end{aligned} \tag{4.36}$$

Then, substituting the constants into (4.32) yields

$$p(x, s|x_0) = \begin{cases} \frac{1}{2\sqrt{sD}} \left\{\exp\left[\sqrt{\frac{s}{D}}(x - x_0)\right] - \exp\left[-\sqrt{\frac{s}{D}}(x + x_0)\right]\right\}, & x < x_0 \\ \frac{1}{2\sqrt{sD}} \left\{\exp\left[\sqrt{\frac{s}{D}}\ (x_0 - x)\right] - \exp\left[-\sqrt{\frac{s}{D}}\ (x + x_0)\right]\right\}, & x > x_0. \end{cases} \tag{4.37}$$

The latter equation can be rewritten in a compact form, namely,

$$p(x,s|x_0) = \frac{1}{2\sqrt{sD}}\left[\exp\left(\sqrt{\frac{s}{D}}|x-x_0|\right) - \exp\left(-\sqrt{\frac{s}{D}}|x+x_0|\right)\right]. \tag{4.38}$$

Finally, by using Eq. (A.70) to invert Laplace (4.38), we find that

$$p(x,t|x_0) = \frac{1}{\sqrt{4\pi Dt}}\left\{\exp\left[-\frac{(x-x_0)^2}{4Dt}\right] - \exp\left[-\frac{(x+x_0)^2}{4Dt}\right]\right\}, \tag{4.39}$$

which is Eq. (4.31), as the reader may have anticipated.

4.3.3 *From the Propagator of Two Absorbing Endpoints*

Alternatively, the solution obtained by the Fourier and Laplace transforms can be derived from the propagator for a free particle diffusing between two absorbing endpoints at $x = 0$ and $x = L$, by taking the limit when $L \to \infty$. Therefore, our starting point is Eq. (2.28), namely,

$$p(x,t|x_0) = \frac{2}{L}\sum_{n=0}^{\infty}\exp\left(-\frac{n^2\pi^2 Dt}{L^2}\right)\sin\left(\frac{n\pi x_0}{L}\right)\sin\left(\frac{n\pi x}{L}\right). \tag{2.28}$$

Note that we have extended the summation limits from $n = 0$ instead of 1, since $p(x,t|x_0) = 0$. The convenience of doing this will become clear later. To find the solution that describes a single absorbing point at the origin, let $L \to \infty$ in Eq. (2.28). The result is obtained using the definition of the Riemann integral, which is

$$\lim_{\Delta z\to 0}\Delta z\sum_{n=0}^{\infty} f(n\Delta z) = \int_0^{\infty} f(z)\mathrm{d}z. \tag{4.40}$$

Setting $\Delta z = 1/L$ and taking the limit when $L \to \infty$, Eq. (2.28) becomes

$$\begin{aligned} p(x,t|x_0) &= 2\int_0^{\infty}\exp\left(-\pi^2 Dtz^2\right)\sin(\pi x_0 z)\sin(\pi x z)\,\mathrm{d}z, \\ &= \int_0^{\infty}\exp\left(-\pi^2 Dtz^2\right)\{\cos[\pi(x-x_0)z] - \cos[\pi(x+x_0)z]\}\mathrm{d}z. \end{aligned}$$

Using (A.12) to solve the integrals, we ultimately arrive at

$$p(x,t|x_0) = \frac{1}{\sqrt{4\pi Dt}}\left\{\exp\left[-\frac{(x-x_0)^2}{4Dt}\right] - \exp\left[-\frac{(x+x_0)^2}{4Dt}\right]\right\}. \tag{4.41}$$

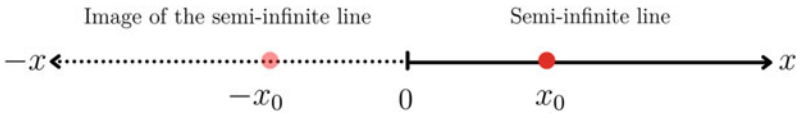

Fig. 4.3 Schematic representation of the method of images applied to the semi-infinite one-dimensional system. On the right-hand side, we have the real space where diffusion will take place. On the left-hand side, we have the image, with its own domain and mirror particle

4.3.4 Method of Images

A solution to our problem can be also found by the method of images, a mathematical tool for solving differential equations, commonly used in electrostatics. The main idea behind this method is to find a solution as a linear combination of the free-space propagator when describing two particles: the real particle and the image particle (see Fig. 4.3). To such end, let the propagator in free space, given by Eq. (3.29), be denoted by $p_F(x, t|x_0)$. Thus, considering that the initial position of the real particle is x_0 and the initial position of the image particle is $-x_0$,

$$p_F(x, t|x_0) = \frac{1}{\sqrt{4\pi Dt}} \exp\left[-\frac{(x - x_0)^2}{4Dt}\right] \tag{4.42}$$

is the solution for the real particle, and

$$-p_F(x, t| - x_0) = -\frac{1}{\sqrt{4\pi Dt}} \exp\left[-\frac{(x + x_0)^2}{4Dt}\right] \tag{4.43}$$

is the solution for the image particle. This last solution is obtained by making two transformations. First, we set p_F to $-p_F$, which takes the probability distribution to negative values, and then, we set x_0 to $-x_0$, leading to an anti-Gaussian. We see that if both contributions are added, they are ultimately canceled out at the origin, which is the solution to the corresponding boundary-value problem (see Fig. 4.4). Finally, the solution to the diffusion equation in the presence of an absorbing boundary is given by

$$p(x, t|x_0) = p_F(x, t|x_0) - p_F(x, t| - x_0), \tag{4.44}$$

which is again, Eq. (4.31),

$$p(x, t|x_0) = \frac{1}{\sqrt{4\pi Dt}} \left\{\exp\left[-\frac{(x - x_0)^2}{4Dt}\right] - \exp\left[-\frac{(x + x_0)^2}{4Dt}\right]\right\}. \tag{4.45}$$

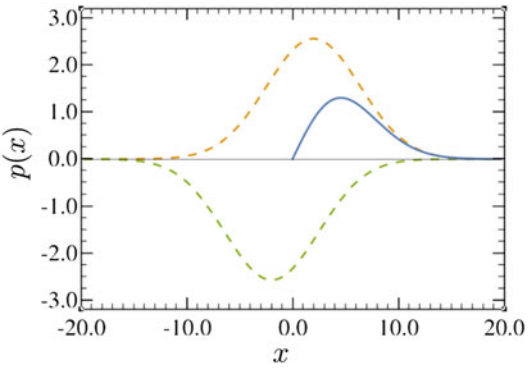

Fig. 4.4 Graphic interpretation of the method of images applied to the semi-infinite system with a perfectly absorbing endpoint: The orange dashed curve represents the propagator describing a real particle, i.e., $p_F(x, t = 10, x_0 = 2)$, while the green dashed curve stands for the propagator of the image particle, i.e.,$-p_F(x, t = 10, x_0 = -2)$. The superposition of the dashed curves produces the solid blue line, which is the solution of the boundary-value problem. It is worth pointing out that the domain of the solution in Eq. (4.45) is $[0, \infty)$

4.3.5 Survival Probability and First-Passage Time

Once we have found the propagator $p(x, t|x_0)$, we now can obtain the survival probability

$$S(t|x_0) = \int_0^\infty p(x, t|x_0)\, \mathrm{d}x, \tag{4.46}$$

which, following substitution of the propagator, becomes

$$S(t|x_0) = \int_0^\infty \frac{1}{\sqrt{4\pi Dt}} \left\{ \exp\left[-\frac{(x - x_0)^2}{4Dt} \right] - \exp\left[-\frac{(x + x_0)^2}{4Dt} \right] \right\} \mathrm{d}x. \tag{4.47}$$

To solve the integrals, it is helpful to calculate them separately by defining

$$I_1 \equiv \int_0^\infty \frac{1}{\sqrt{4\pi Dt}} \exp\left[-\frac{(x - x_0)^2}{4Dt} \right] \mathrm{d}x \tag{4.48}$$

and

$$I_2 \equiv \int_0^\infty \frac{1}{\sqrt{4\pi Dt}} \exp\left[-\frac{(x + x_0)^2}{4Dt} \right] \mathrm{d}x. \tag{4.49}$$

Setting

$$y \equiv \frac{x - x_0}{\sqrt{4Dt}}, \tag{4.50}$$

then

$$\mathrm{d}y = \frac{\mathrm{d}x}{\sqrt{4Dt}}, \tag{4.51}$$

and consequently, the integration limits change to $y \in [-x_0/\sqrt{4Dt}, \infty)$. We can write I_1 as follows:

$$I_1 = \frac{1}{\sqrt{\pi}} \int_{-x_0/\sqrt{4Dt}}^{\infty} \mathrm{e}^{-y^2} \mathrm{d}y = \frac{1}{\sqrt{\pi}} \int_{-x_0/\sqrt{4Dt}}^{0} \mathrm{e}^{-y^2} \mathrm{d}y + \frac{1}{\sqrt{\pi}} \int_{0}^{\infty} \mathrm{e}^{-y^2} \mathrm{d}y. \tag{4.52}$$

Using the error and complementary error function, given by Eqs. (A.81) and (A.82), respectively, we obtain

$$I_1 = \frac{1}{\sqrt{\pi}} \int_{-x_0/\sqrt{4Dt}}^{0} \mathrm{e}^{-y^2} \mathrm{d}y + \frac{1}{2}[1 - \mathrm{erf}(0)] = \frac{1}{\sqrt{\pi}} \int_{-x_0/\sqrt{4Dt}}^{0} \mathrm{e}^{-y^2} \mathrm{d}y + \frac{1}{2}. \tag{4.53}$$

Following the same steps to integrate I_2, we find that

$$I_2 = -\frac{1}{\sqrt{\pi}} \int_{0}^{x_0/\sqrt{4Dt}} \mathrm{e}^{-y^2} \mathrm{d}y + \frac{1}{2}. \tag{4.54}$$

Thereafter, the survival probability is given by

$$S(t|x_0) = I_1 - I_2 = \frac{1}{\sqrt{\pi}} \int_{-x_0/\sqrt{4Dt}}^{0} \mathrm{e}^{-y^2} \mathrm{d}y + \frac{1}{\sqrt{\pi}} \int_{0}^{x_0/\sqrt{4Dt}} \mathrm{e}^{-y^2} \mathrm{d}y. \tag{4.55}$$

To reduce the latter expression, we use the error function again. Consequently, we can write

$$S(t|x_0) = -\frac{1}{2}\mathrm{erf}\left(-\frac{x_0}{\sqrt{4Dt}}\right) + \frac{1}{2}\mathrm{erf}\left(\frac{x_0}{\sqrt{4Dt}}\right), \tag{4.56}$$

which takes the final following form:

$$S(t|x_0) = \mathrm{erf}\left(\frac{x_0}{\sqrt{4Dt}}\right). \tag{4.57}$$

From this last equation, we see that its value is practically constant until we reach the diffusion length $\sqrt{Dt}$. The survival probability vanishes when $t \to \infty$, meaning it is certain that the Brownian particles become trapped. Therefore, the probability

of becoming trapped is 1. The long-time behavior, $t \gg x_0^2/D$, is obtained when the first term of the Taylor series in Eq. (4.57) is kept, namely,

$$S(t|x_0) \approx \frac{x_0}{\sqrt{\pi\, Dt}}. \tag{4.58}$$

A curve of Eq. (4.57) is shown in Fig. 4.5.

Aiming to compute the probability density of first-passage time, we introduce (4.57) into Eq. (2.34), yielding

$$\varphi(t|x_0) = -\frac{\mathrm{d}S(t|x_0)}{\mathrm{d}t} = -\frac{\mathrm{d}}{\mathrm{d}t}\left[\mathrm{erf}\left(\frac{x_0}{\sqrt{4Dt}}\right)\right]. \tag{4.59}$$

Using the result of the derivative in Eq. (A.86) together with the chain rule, we arrive at its simplified version, namely,

$$\varphi(t|x_0) = \frac{x_0 t^{-3/2}}{\sqrt{4\pi\, D}} \exp\left(-\frac{x_0^2}{4Dt}\right). \tag{4.60}$$

This last equation starts at zero, then reaches a maximum, and then goes to zero again (see Fig. 4.5).

After substituting the probability density for the survival probability given by Eq. (4.57) into the moments of the mean first-passage time (MFPT) given in (2.52), we find that

$$\langle t^n(x_0)\rangle = n\int_0^\infty t^{n-1} S(t|x_0)\,\mathrm{d}t = n\int_0^\infty t^{n-1}\mathrm{erf}\left(\frac{x_0}{\sqrt{4Dt}}\right)\mathrm{d}t, \tag{4.61}$$

which by integrating by parts yields

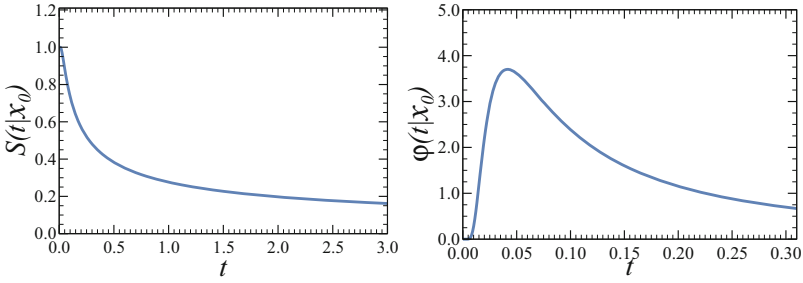

Fig. 4.5 The survival probability given in Eq. (4.57) is depicted in the left-hand panel. On the right-hand panel, the probability density of first-passage time $\varphi(t|x_0)$ is depicted, given by Eq. (14.15). The starting position of the particle is set at $x_0 = 0.5$, and the diffusion coefficient is $D = 1$

$$\langle t^n(x_0)\rangle = n\left\{\frac{t^n}{n}\operatorname{erf}\left(\frac{x_0}{\sqrt{4Dt}}\right)\Big|_0^\infty + \int_0^\infty \frac{x_0 t^{n-3/2}}{n\sqrt{4\pi D}}\exp\left(\frac{x_0^2}{\sqrt{4Dt}}\right)\mathrm{d}t\right\}. \tag{4.62}$$

It is worth noting that the latter expression diverges, meaning that every moment of MFPT is infinite. Interestingly, even though the probability of hitting the absorbing target is 1, the MFPT is infinite. The latter is due to the fact that a Brownian particle may arbitrarily move across a long trajectory before becoming trapped. Counterintuition begins to unfold.

4.3.6 *Survival Probability: Revisited*

In this section, we will find the survival probability by solving its partial differential equation (PDE) for the system we have been studying: a particle diffusing in a one-dimensional semi-infinite domain in the presence of a perfectly absorbing point at $x = 0$. Hence, now we must solve the following equation:

$$\frac{\partial S(t|x_0)}{\partial t} = D\frac{\partial^2 S(t|x_0)}{\partial x_0^2}, \tag{2.59}$$

with the initial and BCs given by $S(0|x_0) = 1$ and $S(t|x_0 = 0) = 0$, respectively. To such end, we use the Laplace transform given by

$$S(s|x_0) = \int_0^\infty S(t|x_0)\,\mathrm{e}^{-st}\,\mathrm{d}t. \tag{4.63}$$

Then, applying the Laplace transform to Eq. (2.59), we have

$$\mathcal{L}\left\{\frac{\partial S(t|x_0)}{\partial t}\right\} = \mathcal{L}\left\{D\frac{\partial^2 S(t|x_0)}{\partial x_0^2}\right\}. \tag{4.64}$$

By following the same procedure used in Sect. 3.2, we have that the subsidiary equation for the transformed survival probability is

$$s\;S(s|x_0) - 1 = D\frac{\mathrm{d}^2 S(s|x_0)}{\mathrm{d}x_0^2}. \tag{4.65}$$

It is worth noting that we have replaced the partial derivative in Eq. (4.63) with an ordinary derivative. The general solution to Eq. (4.65) is the sum of the solution to the homogeneous problem plus the solution to the inhomogeneous equation, namely,

$$S(s|x_0) = \mathcal{A}\ \exp\left(x_0\sqrt{\frac{s}{D}}\right) + \mathcal{B}\ \exp\left(-x_0\sqrt{\frac{s}{D}}\right) + \frac{1}{s}. \tag{4.66}$$

The constants $\mathcal{A}$ and $\mathcal{B}$ must be chosen so that $S(s|x_0)$ satisfies the Laplace transform of the BCs. Since $S(s|x_0)$ has to remain finite when $x_0 \to \infty$, we assert that $\mathcal{A} = 0$. Since $S(s|x_0 = 0) = 0$, then $\mathcal{B} = -1/s$. Consequently, the solution is

$$S(s|x_0) = \frac{1}{s}\left[1 - \ \exp\left(-x_0\sqrt{\frac{s}{D}}\right)\right]. \tag{4.67}$$

Since the inverse Laplace transform of $e^{-k\sqrt{s}}/s$ is $\text{erfc}(k/\sqrt{4t})$, the real-space solution of $S(s|x_0)$ is

$$S(t|x_0) = \text{erf}\left(\frac{x_0}{\sqrt{4Dt}}\right), \tag{4.57}$$

as expected.

4.4 Perfectly Reflecting Endpoint

4.4.1 The Fourier Transform Solution

In this section, we assume that a Brownian particle diffuses in a one-dimensional semi-infinite domain in the presence of a perfectly reflecting point at $x = 0$ (see Fig. 4.6). In mathematical terms, we define a reflecting boundary by requiring that the flux at the reflecting point is equal to zero, which corresponds to a Neumann BC, Eq. (4.9). The physical motivation to perfectly reflecting boundary comes from mechanics: When a particle collides with a perfectly reflecting wall, its velocity component that is perpendicular to the wall instantaneously changes directions (i.e., changes signs). Consequently, the net flux of particles crossing the wall is equal to zero. Therefore, a reflecting boundary is one for which

$$\mathbf{J} \cdot \hat{\mathbf{n}} = 0, \tag{4.68}$$

where $\hat{\mathbf{n}}$ is the unit normal vector to the reflecting boundary. Then, when the reflecting point is at $x = 0$, the reflecting BC is given by

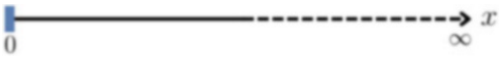

Fig. 4.6 Schematic representation of a one-dimensional semi-infinite domain with a reflecting end at $x = 0$ (blue bar)

$$\begin{aligned}\mathbf{J}(x,t|x_0)\cdot\hat{\mathbf{n}}\big|_{x=0} &= -D\frac{\partial p(x,t|x_0)}{\partial x}\,\hat{\mathbf{e}}_x\cdot\,(-\hat{\mathbf{e}}_x)\Big|_{x=0}\\ &= D\frac{\partial p(x,t|x_0)}{\partial x}\Big|_{x=0} = 0.\end{aligned} \tag{4.69}$$

In this case, $\hat{\mathbf{n}} = -\hat{\mathbf{e}}_x$, since the unit normal vector to the reflecting boundary points eastward.

Because the particle has an initial position greater than zero, it never leaves the positive domain. Therefore, it is useful to define the Fourier transform as

$$p(k,t) = \int_0^\infty p(x,t)\,\cos(kx)\,\mathrm{d}x, \tag{4.70}$$

with the inverse given by

$$p(x,t|x_0) = \frac{1}{\pi}\int_0^\infty p(k,t)\,\cos(kx)\,\mathrm{d}k. \tag{4.71}$$

The BC given in Eq. (4.69) is satisfied by this last equation. The equivalent initial condition, $p(0,t) = \delta(x-x_0)$, in the Fourier domain, using Eq. (4.70), is $\tilde{p}(k,0) = \cos(kx_0)$. Then, using this initial condition in Eq. (4.30), the propagator given in (4.71) is

$$p(x,t|x_0) = \frac{1}{\pi}\int_0^\infty \exp\left(-Dtk^2\right)\{\cos[(k-x_0)] + \cos[(k+x_0)]\}\mathrm{d}k.$$

Finally, using (A.12) to solve the integrals, we find that the propagator is given by

$$p(x,t|x_0) = \frac{1}{\sqrt{4\pi\,Dt}}\left\{\exp\left[-\frac{(x-x_0)^2}{4Dt}\right] + \exp\left[-\frac{(x+x_0)^2}{4Dt}\right]\right\}. \tag{4.72}$$

Equation (4.72) is depicted in Fig. 4.7.

4.4.2 The Laplace Transform Solution

The solution to our current problem can also be found by means of a Laplace transform. Starting from Eq. (3.36),

$$s\;p(x,s|x_0) - \delta(x-x_0) = D\frac{\partial^2 p(x,s|x_0)}{\partial x^2}, \tag{3.36}$$

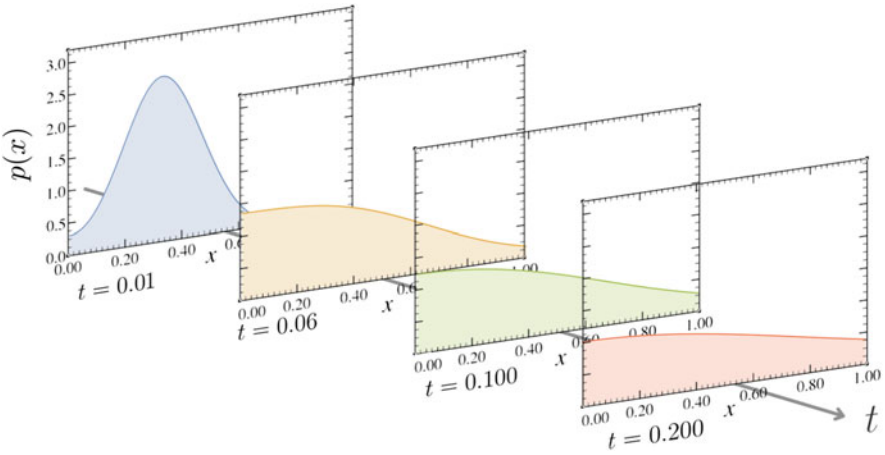

Fig. 4.7 Time evolution of the probability density given by Eq. (4.72). The starting position of the particles is set at $x_0 = 0.3$, and the diffusion coefficient is $D = 1$

we require a solution such that its derivative vanishes both at $x = 0$ and when x tends to infinity. Since we already have known from the latter section that the general solution of (3.36) must be a linear combination of real exponential or hyperbolic functions, the most appropriate functions are those that meet the BCs at the origin and when x tends to infinity. Consequently, let us propose the following solution:

$$p(x,t|x_0) = \begin{cases} \mathcal{A}\cosh\left(\sqrt{\frac{s}{D}}\,x\right), & x < x_0 \\ \mathcal{B}\exp\left(-\sqrt{\frac{s}{D}}\,x\right), & x > x_0. \end{cases} \tag{4.73}$$

In addition, we must apply the continuity condition, given by Eq. (3.39), so that the propagator is well-behaved across the entire domain. Then, equating the solutions in each region when $x = x_0$ yields

$$\mathcal{A}\cosh\left(\sqrt{\frac{s}{D}}\,x_0\right) = \mathcal{B}\exp\left(-\sqrt{\frac{s}{D}}\,x_0\right). \tag{4.74}$$

Substituting Eq. (4.73) into the discontinuity condition, Eq. (3.42), we obtain

$$\mathcal{B}\exp\left(-\sqrt{\frac{s}{D}}\,x_0\right) - \mathcal{A}\sinh\left(\sqrt{\frac{s}{D}}\,x_0\right) = \frac{-1}{\sqrt{sD}}. \tag{4.75}$$

Solving the system of equations given by Eqs. (4.74) and (4.75), we can find the constants $\mathcal{A}$ and $\mathcal{B}$. Consequently,

$$\mathcal{A} = \frac{1}{\sqrt{sD}} \exp\left(-\sqrt{\frac{s}{D}}\, x_0\right) \tag{4.76}$$

and

$$\begin{aligned} \mathcal{B} &= \sqrt{\frac{s}{D}} \cosh\left(\sqrt{\frac{s}{D}}\, x_0\right) \\ &= \frac{1}{2\sqrt{sD}} \left[\exp\left(\sqrt{\frac{s}{D}}\, x_0\right) + \exp\left(-\sqrt{\frac{s}{D}}\, x_0\right)\right]. \end{aligned} \tag{4.77}$$

Substituting the two latter equations in the solution, we find that the propagator is

$$p(x, s|x_0) = \begin{cases} \frac{1}{2\sqrt{sD}} \left\{\exp\left[\sqrt{\frac{s}{D}}\,(x + x_0)\right] + \exp\left[-\sqrt{\frac{s}{D}}\,(x - x_0)\right]\right\}, & x < x_0 \\ \frac{1}{2\sqrt{sD}} \left\{\exp\left[-\sqrt{\frac{s}{D}}\,(x + x_0)\right] + \exp\left[\sqrt{\frac{s}{D}}\,(x - x_0)\right]\right\}, & x > x_0 \end{cases} \tag{4.78}$$

an expression that can be written as follows:

$$p(x, s|x_0) = \frac{1}{2\sqrt{sD}} \left\{\exp\left[\sqrt{\frac{s}{D}}\,|x + x_0|\right] + \exp\left[\sqrt{\frac{s}{D}}\,|x - x_0|\right]\right\}. \tag{4.79}$$

Finally, taking the inverse transform using Eq. (A.70) yields

$$p(x, t|x_0) = \frac{1}{\sqrt{4\pi Dt}} \left\{\exp\left[-\frac{(x - x_0)^2}{4Dt}\right] + \exp\left[-\frac{(x + x_0)^2}{4Dt}\right]\right\}, \tag{4.80}$$

which is Eq. (4.72).

4.4.3 *Method of Images*

Using the method of images, the propagator for diffusion with a reflecting boundary at the origin is given by

$$p(x, t|x_0) = p_F(x, t|x_0) + p_F(x, t| - x_0), \tag{4.81}$$

given that the derivative of $p_F(x, t|x_0)$ is an odd function, namely,

$$\left.\frac{\partial p_F(x, t| - x_0)}{\partial x}\right|_{x=0} = -\left.\frac{\partial p_F(x, t|x_0)}{\partial x}\right|_{x=0}. \tag{4.82}$$

As a result, the flux is zero in the reflecting point, and the BC in Eq. (4.69) is satisfied. Consequently, Eq. (4.81) is the solution to the semi-infinite line, and substituting the expressions for $p_F(x,t|x_0)$ and $p_F(x,t|-x_0)$ yields

$$p(x,t|x_0) = \frac{1}{\sqrt{4\pi Dt}}\left\{\exp\left[-\frac{(x-x_0)^2}{4Dt}\right] + \exp\left[-\frac{(x+x_0)^2}{4Dt}\right]\right\}. \tag{4.83}$$

4.4.4 Survival Probability and First-Passage Time

In this system, the survival probability must evidently be 1, which is easy to demonstrate, as shown below.

The survival probability is computed using Eq. (2.30) with $L \to \infty$ and Eq. (4.72), namely,

$$S(t|x_0) = \int_0^\infty \frac{1}{\sqrt{4\pi Dt}}\left\{\exp\left[-\frac{(x-x_0)^2}{4Dt}\right] + \exp\left[-\frac{(x+x_0)^2}{4Dt}\right]\right\} \mathrm{d}x. \tag{4.84}$$

In order to reduce the latter expression, we use the definition of the integrals I_1 and I_2 computed in the last section. Therefore, $S(t|x_0)$ can be written as follows:

$$\begin{aligned} S(t|x_0) = I_1 + I_2 &= \frac{1}{\sqrt{\pi}}\left[-\frac{\sqrt{\pi}}{2}\mathrm{erf}\left(-\frac{x_0}{\sqrt{4Dt}}\right)\right] - \frac{1}{\sqrt{\pi}}\left[\frac{\sqrt{\pi}}{2}\mathrm{erf}\left(\frac{x_0}{\sqrt{4Dt}}\right)\right] + 1 \\ &= 1, \end{aligned} \tag{4.85}$$

as expected.

Accordingly, the probability density of first-passage time is computed straightforward, resulting in

$$\varphi(t|x_0) = -\frac{\partial S(t|x_0)}{\partial t} = 0. \tag{4.86}$$

4.5 Partially Absorbing Endpoint

Consider a Brownian particle diffusing along a one-dimensional semi-infinite domain in the presence of a partially absorbing endpoint at the origin, $x = 0$ (see Fig. 4.8). Mathematically, this property can be expressed using a *trapping rate* κ in the BC. Appealing to Eq. (4.13), we have

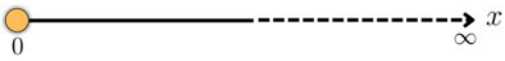

Fig. 4.8 Schematic representation of a one-dimensional semi-infinite domain with a partially absorbing end at $x = 0$ (yellow circle)

$$\begin{aligned}\mathbf{J}(0,t|x_0)\cdot\hat{\mathbf{n}} &= -D\frac{\partial p(x,t|x_0)}{\partial x}\,\hat{\mathbf{e}}_x\cdot(-\hat{\mathbf{e}}_x)\bigg|_{x=0}\\ &= D\frac{\partial p(x,t|x_0)}{\partial x}\bigg|_{x=0} = \kappa p(0,t|x_0),\end{aligned} \tag{4.87}$$

which is a Neumann BC and where $\hat{\mathbf{n}} = -\hat{\mathbf{e}}_x$, since the unit normal vector to the partially absorbing boundary points westward. This is also called a radiation BC because its application is to be found in Newton's law of cooling. If we think of Eq. (4.87) in terms of concentration expressed in particles/L, then κ gives the fraction of particles absorbed out of all those that reach the boundary per unit of time, whereas the right-hand side gives the fraction of particles absorbed out of the total particles that hit the boundary per unit of time.

To solve the diffusion equation under this BC, it is useful to define an auxiliary function, which is actually a Robin BC given by

$$q(x,t|x_0) \equiv D\frac{\partial p(x,t|x_0)}{\partial x} - \kappa p(x,t|x_0). \tag{4.88}$$

Our first task will be to show that $q(x,t|x_0)$ also satisfies the diffusion equation. To such end, we derive Eq. (4.88) twice with respect to x, yielding

$$\begin{aligned}D\frac{\partial^2 q(x,t|x_0)}{\partial x^2} &= D\frac{\partial^2 p(x,t|x_0)}{\partial x^2} - \kappa D\frac{\partial^2 p(x,t|x_0)}{\partial x^2}\\ &= \frac{\partial}{\partial t}\left[D\,p(x,t|x_0) - \kappa p(x,t|x_0)\right],\end{aligned}$$

an expression that reduces properly to the diffusion equation,

$$D\frac{\partial^2 q(x,t|x_0)}{\partial x^2} = \frac{\partial q(x,t|x_0)}{\partial t}. \tag{4.89}$$

The advantage of solving the problem by means of the auxiliary equation $q(x,t|x_0)$ is revealed when we find that the BC at the origin translates into

$$q(0,t|x_0) = D\frac{\partial p(x,t|x_0)}{\partial x}\bigg|_{x=0} - \kappa p(0,t|x_0), \tag{4.90}$$

which is actually

$$q(0, t|x_0) = 0. \tag{4.91}$$

Comparing Eqs. (4.27) and (4.91), we can notice that the diffusion equation in terms of $q(0, t|x_0)$ becomes a problem with a perfectly absorbing boundary at the origin, which we have already solved. Its solution is given by Eq. (4.81); consequently,

$$q(x, t|x_0) = q_F(x, t|x_0) - q_F(x, t| - x_0). \tag{4.92}$$

The next step is to find the solution of the propagator $p(x, t|x_0)$ in terms of $q(x, t|x_0)$. To such end, we need to solve Eq. (4.88). This can be solved using the integrating factor method,[2] resulting in

$$p(x, t|x_0) = \mathcal{C}\mathrm{e}^{-\mu x} + \frac{1}{D}\mathrm{e}^{\kappa x/D} \int \mathrm{e}^{-\kappa y/D} q(y, t|x_0)\, \mathrm{d}y. \tag{4.93}$$

Since $p(x, t|x_0)$ is the probability of finding the particle at position x at time t, the limits of the integral must go from x to ∞ or, conversely, from ∞ to x. Both directions are allowed in our mathematical problem. Additionally, the probability of finding the Brownian particle at infinity is null, which translates into

$$p(x \to \infty, t|x_0) = 0. \tag{4.94}$$

Taking the abovementioned arguments into account, and considering both possibilities in the sign, the propagator becomes

$$p(x, t|x_0)_{\pm} = \mathcal{C}\mathrm{e}^{\kappa x/D} \pm \frac{1}{D}\mathrm{e}^{\kappa x/D} \int_x^{\infty} \mathrm{e}^{-\kappa y/D} q(y, t|x_0)\, \mathrm{d}y. \tag{4.95}$$

Furthermore, from the BC at infinity, we have that

$$p(x \to \infty, t|x_0)_{\pm} = \mathcal{C}\mathrm{e}^{\kappa x \to \infty/D} \pm \frac{1}{D}\mathrm{e}^{\kappa x \to \infty/D} \int_{\infty}^{\infty} \mathrm{e}^{-\kappa y/D} q(y, t|x_0)\, \mathrm{d}y; \tag{4.96}$$

consequently, $\mathcal{C} = 0$. Then,

$$p(x, t|x_0)_{\pm} = \pm\frac{1}{D}\mathrm{e}^{\kappa x/D} \int_x^{\infty} \mathrm{e}^{-\kappa y/D} q(y, t|x_0)\, \mathrm{d}y. \tag{4.97}$$

[2] The integrating method is commonly used in ordinary differential equations in which, by multiplying by a special factor, we transform an inexact differential into an exact differential, making the integral a simple process. Section A.4.1 of Appendix 4.A shows the steps leading to Eq. (4.93).

Substituting the latter result into $q(x,t|x_0)$'s definition, Eq. (4.88) will tell us which sign we should keep in order to get the correct solution. As it turns out, the minus sign is the proper choice (see Sect. A.4.2). Therefore,

$$p(x,t|x_0) = -\frac{1}{D}\mathrm{e}^{\kappa x/D}\int_x^\infty \mathrm{e}^{-\kappa y/D} q(y,t|x_0)\,\mathrm{d}y. \tag{4.98}$$

From Eq. (4.98), we see that the function $q(x,t|x_0)$ must be found in terms of $p(x,t|x_0)$ to give a closed solution of the propagator. To such end, we need to write Eq. (4.92) in a much simpler way. Let us start by writing $q(x,t|x_0)$ using the Chapman-Kolmogorov equation (see Sect. 3.4), namely,

$$q(x,t|x') = \int_{-\infty}^{\infty} q(x,t-\tau|x')\,q(x',\tau|x')\,\mathrm{d}x'. \tag{4.99}$$

Setting $\tau = 0$ and because the system under study is semi-infinite, we have that

$$q(x,t|x') = \int_0^{\infty} q(x,t|x')\,q(x',0|x')\,\mathrm{d}x'. \tag{4.100}$$

Introducing Eq. (4.92) into this integral yields

$$q(x,t|x') = \int_0^{\infty} [q_F(x,t|x_0) - q_F(x,t|-x_0)]\,q(x',0|x')\,\mathrm{d}x'. \tag{4.101}$$

This integral can be calculated by evaluating the initial condition of $q(x,t|x_0)$ and then relating such result to the initial distribution, i.e., a Dirac delta function. Accordingly,

$$q(x,0|x_0) = D\frac{\partial}{\partial x}p(x,0|x_0) - \kappa\ p(x,0|x_0) = D\frac{\partial\delta(x-x_0)}{\partial x} - \kappa\ \delta(x-x_0), \tag{4.102}$$

which can be written as

$$q(x,0|x_0) = \left(D\frac{\partial}{\partial x} - \kappa\right)\delta(x-x_0). \tag{4.103}$$

Thereafter, including the solution in Eq. (4.44), which is the free-space propagator in the presence of a perfectly absorbing point at $x = 0$, and Eq. (4.103) into (4.99), we find that[3]

[3] Section A.4.3 shows the steps leading to Eq. (4.104).

$$q(x,t|x_0) = D\frac{\partial}{\partial x}\left[p_F(x,t|-x_0)+p_F(x,t|x_0)\right]+\kappa\left[p_F(x,t|-x_0)-p_F(x,t|x_0)\right]. \tag{4.104}$$

Substituting this last expression into Eq. (4.98), we find that

$$\begin{aligned} p(x,t|x_0) = -\frac{1}{D}\mathrm{e}^{\kappa x/D}\int_x^\infty \mathrm{e}^{-\kappa y/D}\left\{D\,\frac{\partial}{\partial y}\left[p_F(y,t|-x_0)+p_F(y,t|x_0)\right]\right. \\ \left. +\kappa\left[p_F(y,t|-x_0)-p_F(y,t|x_0)\right]\right\}\mathrm{d}y \\ = -\mathrm{e}^{\kappa x/D}\int_x^\infty \mathrm{e}^{-\kappa y/D}\,\frac{\partial p_F(y,t|-x_0)}{\partial y}\,\mathrm{d}y \\ -\mathrm{e}^{\kappa x/D}\int_x^\infty \mathrm{e}^{-\kappa y/D}\,\frac{\partial p_F(y,t|x_0)}{\partial y}\,\mathrm{d}y \\ -\frac{1}{D}\kappa\mathrm{e}^{\kappa x/D}\int_x^\infty \mathrm{e}^{-\kappa y/D}p_F(y,t|-x_0)\,\mathrm{d}y \\ +\frac{1}{D}\kappa\mathrm{e}^{\kappa x/D}\int_x^\infty \mathrm{e}^{-\kappa y/D}p_F(y,t|x_0)\,\mathrm{d}y. \end{aligned} \tag{4.105}$$

In order to give an exact solution to the latter equation, it is helpful to define the following relations:

$$I_3^{\pm} \equiv \int_x^\infty \mathrm{e}^{-\kappa y/D}\,\frac{\partial p_F(y,t|\pm x_0)}{\partial y}\,\mathrm{d}y \quad \text{and} \quad I_4^{\pm} \equiv \int_x^\infty \mathrm{e}^{-\kappa y/D}\,p_F(y,t|\pm x_0)\,\mathrm{d}y, \tag{4.106}$$

from where we can write Eq. (4.105) as follows:[4]

$$\begin{aligned} p(x,t|x_0) &= -\mathrm{e}^{\kappa x/D}\,I_3^- - \mathrm{e}^{\kappa x/D}\,I_3^+ + \frac{1}{D}\kappa\mathrm{e}^{\kappa x/D}\left(I_4^+ - I_4^-\right) \\ &= -\mathrm{e}^{\kappa x/D}\left[-\mathrm{e}^{-\kappa x/D}\,p_F(x,t|-x_0)+\frac{1}{D}\kappa\,I_4^+\right] \\ &\quad -\mathrm{e}^{\kappa x/D}\left[-\mathrm{e}^{-\kappa x/D}\,p_F(x,t|x_0)+\frac{1}{D}\kappa\,I_4^-\right]+\frac{1}{D}\kappa\,\mathrm{e}^{\kappa x/D}\left(I_4^+ - I_4^-\right) \\ &= p_F(x,t|x_0)+p_F(x,t|-x_0) \\ &\quad -\frac{2}{D}\,\kappa\,\mathrm{e}^{\kappa x/D}\left\{\frac{1}{2}\exp\left[-\frac{x_0^2-(2\kappa t+x_0)^2}{4Dt}\right]\mathrm{erfc}\left[\frac{x+(2\kappa t+x_0)}{\sqrt{4Dt}}\right]\right\}. \end{aligned} \tag{4.107}$$

[4] Section A.4.4 shows the steps leading to Eq. (4.107).

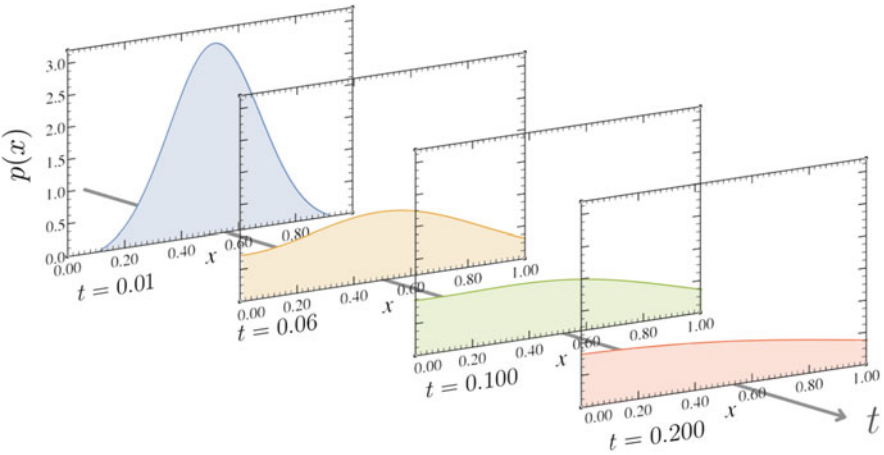

Fig. 4.9 Time evolution of the probability density given by Eq. (4.108). The starting position of the particles is set at $x_0 = 0.5$, and the diffusion coefficient is $D = 1$

Finally, the propagator for a partially absorbing target is

$$p(x,t|x_0) = p_F(x,t|x_0) + p_F(x,t|-x_0) - \frac{2}{D}\,\kappa\,\mathrm{e}^{\kappa x/D}\left\{\frac{1}{2}\exp\left[-\frac{x_0^2-(2\kappa t+x_0)^2}{4Dt}\right]\mathrm{erfc}\left[\frac{x+(2\kappa t+x_0)}{\sqrt{4Dt}}\right]\right\}. \tag{4.108}$$

Equation (4.108) is depicted in Fig. 4.9. The effect of selectivity through the trapping rate κ is present in the last term of the last equation. The reader can easily verify that, if κ is equal to zero, then the propagator is the solution of a semi-infinite system with a perfectly reflecting point at the origin, i.e., Eq. (4.81).

4.5.1 Survival Probability and First-Passage Time

The survival probability $S(t|x_0)$, given by Eq. (2.30), will be computed using Eq. (4.98), yielding

$$\begin{aligned} S(t|x_0) &= -\int_0^\infty \frac{1}{D}\mathrm{e}^{\kappa x/D}\int_x^\infty \mathrm{e}^{-\kappa y/D}\,q(y,t|x_0)\,\mathrm{d}y\,\mathrm{d}x \\ &= -\left\{\left[\int_x^\infty \mathrm{e}^{-\kappa y/D}\,q(y,t|x_0)\,\mathrm{d}y\int\frac{1}{D}\mathrm{e}^{\kappa x/D}\,dx\right]_0^\infty \right. \\ &\quad \left. -\int_0^\infty\left(\int\frac{\mathrm{e}^{\kappa x/D}}{D}dx\right)\frac{\partial}{\partial x}\left[\int_x^\infty \mathrm{e}^{-\kappa y/D}\,q(y,t|x_0)\,\mathrm{d}y\right]\partial x\right\} \end{aligned}$$

$$= -\left\{\left[\frac{1}{\kappa}\int_x^\infty \mathrm{e}^{-\kappa y/D}\, q(y,t|x_0)\,\mathrm{d}y\,\mathrm{e}^{\kappa x/D}\right]_0^\infty - \int_0^\infty \frac{1}{\kappa}\mathrm{e}^{\kappa x/D}\left[-\mathrm{e}^{-\kappa x/D}\, q(x,t|x_0)\right]\mathrm{d}x\right\}, \tag{4.109}$$

where the evaluation of the first term leads to

$$S(t|x_0) = -\left[-\frac{1}{\kappa}\int_0^\infty \mathrm{e}^{-\kappa y/D}\, q(y,t|x_0)\mathrm{d}y + \frac{1}{\kappa}\int_0^\infty q(x,t|x_0)\,\mathrm{d}x\right]. \tag{4.110}$$

Simplifying, we eventually find

$$S(t|x_0) = -\frac{1}{\kappa}\int_0^\infty \left(1-\mathrm{e}^{-\kappa x/D}\right)\, q(x,t|x_0)\,\mathrm{d}x. \tag{4.111}$$

If we introduce this last expression $q(x,t|x_0)$, given by Eq. (4.104), we arrive at

$$\begin{aligned} S(t|x_0) &= -\frac{1}{\kappa}\int_0^\infty \left(1-\mathrm{e}^{-\kappa x/D}\right)\left\{D\frac{\partial}{\partial x}\left[p_F(x,t|-x_0)+p_F(x,t|x_0)\right]\right. \\ &\quad \left.+\kappa\left[p_F(x,t|-x_0)-p_F(x,t|x_0)\right]\right\}\mathrm{d}x \\ &= -\frac{1}{\kappa}\int_0^\infty \left\{D\frac{\partial}{\partial x}\left[p_F(x,t|-x_0)+p_F(x,t|x_0)\right]\right. \\ &\quad \left.+\kappa\left[p_F(x,t|-x_0)-p_F(x,t|x_0)\right]\right\}\mathrm{d}x \\ &\quad +\frac{1}{\kappa}\int_0^\infty \mathrm{e}^{-\kappa x/D}\left\{D\frac{\partial}{\partial x}\left[p_F(x,t|-x_0)+p_F(x,t|x_0)\right]\right. \\ &\quad \left.+\kappa\left[p_F(x,t|-x_0)-p_F(x,t|x_0)\right]\right\}\mathrm{d}x. \end{aligned} \tag{4.112}$$

Every term of the last equation has already been computed (see Eqs. (4.48)–(4.49), (4.53), and (4.54)). Moreover, the integral of $\kappa\,[p_F(x,t|-x_0)-p_F(x,t|x_0)]$ with respect to x is minus κ times the survival probability of a Brownian particle in the presence of a perfectly absorbing boundary (see Eqs. (4.47) and (4.57)). The integral of the derivative of the free diffusion propagator is simply the evaluation of such function at the limits ∞ and 0, although there is a unique detail the reader should keep in mind: Since we are considering that the probability of finding a particle in space converges to a finite value, more specifically, to zero when x tends to infinity, the only contribution comes from evaluating the equation at $x = 0$. Therefore, Eq. (4.112) becomes

$$S(t|x_0) = \frac{1}{\kappa} D\left[p_F(0,t|x_0) + p_F(0,t|-x_0)\right] + \operatorname{erf}\left(\frac{x_0}{\sqrt{4Dt}}\right) + \frac{1}{\kappa}\int_0^\infty \mathrm{e}^{-\kappa x/D}\left\{D\frac{\partial}{\partial x}[p_F(x,t|-x_0) + p_F(x,t|x_0)] + \kappa[p_F(x,t|-x_0) - p_F(x,t|x_0)]\right\}\mathrm{d}x. \tag{4.113}$$

To calculate the remaining integrals, let us first differentiate

$$\frac{\mathrm{d}}{\mathrm{d}x}\left[\frac{D\mathrm{e}^{-\kappa x/D}}{\kappa}\, p_F(x,t|\pm x_0)\right] = \frac{D\mathrm{e}^{-\kappa x/D}}{\kappa}\,\frac{\partial}{\partial x} p_F(x,t|\pm x_0) - \mathrm{e}^{-\kappa x/D}\, p_F(x,t|\pm x_0) \tag{4.114}$$

and then integrate between 0 and ∞

$$\int_0^\infty \frac{\mathrm{d}}{\mathrm{d}x}\left[\frac{D\mathrm{e}^{-\kappa x/D}}{\kappa}\, p_F(x,t|\pm x_0)\right]\mathrm{d}x = \int_0^\infty \frac{D\mathrm{e}^{-\kappa x/D}}{\kappa}\,\frac{\partial}{\partial x} p_F(x,t|\pm x_0)\,\mathrm{d}x - \int_0^\infty \mathrm{e}^{-\kappa x/D}\, p_F(x,t|\pm x_0)\,\mathrm{d}x. \tag{4.115}$$

Afterward, we can write that

$$\int_0^\infty \frac{D\mathrm{e}^{-\kappa x/D}}{\kappa}\frac{\partial}{\partial x} p_F(x,t|\pm x_0)\,\mathrm{d}x = -\frac{1}{\kappa} D\; p_F(0,t|\pm x_0) + \int_0^\infty \mathrm{e}^{-\kappa x/D}\, p_F(x,t|\pm x_0)\,\mathrm{d}x. \tag{4.116}$$

Thus, Eq. (4.113) reduces to

$$S(t|x_0) = \frac{1}{\kappa} D\left[p_F(0,t|x_0) + p_F(0,t|-x_0)\right] + \operatorname{erf}\left(\frac{x_0}{\sqrt{4Dt}}\right) - \frac{1}{\kappa} D\; p_F(0,t|-x_0) + \int_0^\infty \mathrm{e}^{-\kappa x/D}\, p_F(x,t|-x_0)\,\mathrm{d}x - \frac{1}{\kappa} D\; p_F(0,t|x_0) + \int_0^\infty \mathrm{e}^{-\kappa x/D}\, p_F(x,t|x_0)\,\mathrm{d}x + \int_0^\infty \mathrm{e}^{-\kappa x/D}\, p_F(x,t|-x_0)\,\mathrm{d}x - \int_0^\infty \mathrm{e}^{-\kappa x/D}\, p_F(x,t|x_0)\,\mathrm{d}x, \tag{4.117}$$

leading to

$$S(t|x_0) = \operatorname{erf}\left(\frac{x_0}{\sqrt{4Dt}}\right) + 2\int_0^\infty \mathrm{e}^{-\kappa x/D}\; p_F(x, t| - x_0)\; \mathrm{d}x. \tag{4.118}$$

Calculating the last integral, which is actually I_4^-, given in Eq. (4.146), and evaluated at $x = 0$, we finally arrive at

$$S(t|x_0) = \operatorname{erf}\left(\frac{x_0}{\sqrt{4Dt}}\right) + \exp\left[-\frac{x_0^2 - (2\kappa t + x_0)^2}{4Dt}\right]\operatorname{erfc}\left(\frac{2\kappa t + x_0}{\sqrt{4Dt}}\right). \tag{4.119}$$

Figure 4.10 shows the time evolution of Eq. (4.119). There are two special cases in which Eq. (4.119) is reduced to Eqs. (4.57) and (4.85), i.e., when $\kappa = 0$ or approaches infinity, respectively. Apart from this, other probabilistic features are interesting to analyze. For instance, the reader can verify that for long times, the second term of the latter equation vanishes, while the first is Eq. (4.58). Therefore, all moments of the MFPT $\langle t^n(x_0)\rangle$ approach infinity.

Once we have computed $S(t|x_0)$, we can find the probability density of first-passage time with Eq. (2.34), namely,

$$\varphi(t|x_0) = -\frac{\mathrm{d}}{\mathrm{d}t}\operatorname{erf}\left(\frac{x_0}{\sqrt{4Dt}}\right) - \frac{\mathrm{d}}{\mathrm{d}t}\left\{\exp\left[-\frac{x_0^2 - (2\kappa t + x_0)^2}{4Dt}\right]\operatorname{erfc}\left(\frac{2\kappa t + x_0}{\sqrt{4Dt}}\right)\right\}. \tag{4.120}$$

The first term of $\varphi(t|x_0)$ is the probability density of first-passage time for the absorbing point, given by Eq. (4.60). Therefore, by using the chain rule together with the error function properties for derivatives, we have that

$$\begin{aligned}\varphi(t|x_0) = {} & \frac{x_0 t^{-3/2}}{\sqrt{4\pi D}}\exp\left(-\frac{x_0^2}{4Dt}\right) - \left\{-\exp\left[-\frac{x_0^2 - (2\kappa t + x_0)^2}{4Dt}\right]\right. \\ & \times \frac{\mathrm{d}}{\mathrm{d}t}\operatorname{erf}\left(\frac{2\kappa t + x_0}{\sqrt{4Dt}}\right) + \frac{1}{D}\kappa^2\exp\left[-\frac{x_0^2 - (2\kappa t + x_0)^2}{4Dt}\right] \\ & \left.\times \operatorname{erfc}\left(\frac{2\kappa t + x_0}{\sqrt{4Dt}}\right)\right\}.\end{aligned} \tag{4.121}$$

The derivative of the error function is computed as follows:

$$\begin{aligned}\frac{\mathrm{d}}{\mathrm{d}t}\operatorname{erf}\left(\frac{2\kappa t + x_0}{\sqrt{4Dt}}\right) &= \frac{2}{\sqrt{\pi}}\exp\left[-\frac{(2\kappa t + x_0)^2}{4Dt}\right]\frac{\mathrm{d}}{\mathrm{d}t}\left(\frac{2\kappa t + x_0}{\sqrt{4Dt}}\right) \\ &= \frac{1}{\sqrt{4\pi D}}\exp\left[-\frac{(2\kappa t + x_0)^2}{4Dt}\right]\left(2\kappa t^{-1/2} - x_0 t^{-3/2}\right).\end{aligned} \tag{4.122}$$

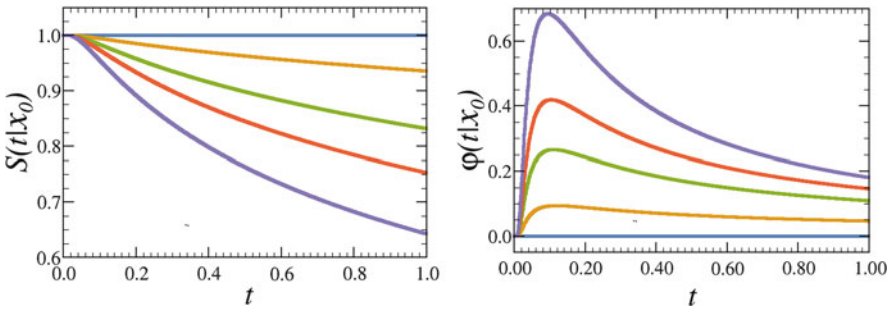

Fig. 4.10 Schematic representation of survival probability, Eq. (4.119), and the probability density of first-passage time, Eq. (4.124), for different values of the trapping rate: $\kappa = 0$ (blue line), $\kappa = 0.1$ (yellow line), $\kappa = 0.3$ (green line), $\kappa = 0.5$ (orange line), and $k = 0.9$ (purple line). The starting position of the particles is set at $x_0 = 0.5$, and the diffusion coefficient is $D = 1$

Then,

$$\varphi(t|x_0) = \frac{x_0 t^{-3/2}}{\sqrt{4\pi D}} \exp\left(-\frac{x_0^2}{4Dt}\right) - \left\{-\frac{1}{\sqrt{4\pi D}} \exp\left(-\frac{x_0^2}{4Dt}\right) \times (2\kappa t^{-1/2} - x_0 t^{-3/2}) + \frac{1}{D}\kappa^2 \exp\left[-\frac{x_0^2 - (2\kappa t + x_0)^2}{4Dt}\right] \times \operatorname{erfc}\left(\frac{2\kappa t + x_0}{\sqrt{4Dt}}\right)\right\}. \tag{4.123}$$

Factoring and rearranging common terms, the latter equation yields

$$\varphi(t|x_0) = \frac{1}{\sqrt{4\pi D}} \exp\left(-\frac{x_0^2}{4Dt}\right) \left\{2\kappa t^{-1/2} - \sqrt{\frac{4\pi k^4}{D}} \exp\left[\frac{(2\kappa t + x_0)^2}{4Dt}\right] \operatorname{erfc}\left(\frac{2\kappa t + x_0}{\sqrt{4Dt}}\right)\right\}. \tag{4.124}$$

Figure 4.10 shows the time evolution of Eq. (4.124).

4.6 Concluding Remarks

The most important result found in this chapter is that for a semi-infinite system, even though the survival probability is finite, the moments of the MFPT are not.

The latter property is due to the fact that a Brownian particle may arbitrarily move across a long trajectory before becoming trapped, leading to an infinite MFPT.

Finally, the most important equations that were obtained in this chapter are listed below.

Boundary Conditions

Boundary conditions for a function y, where c_0 and c_1 are constants and f and g are scalar functions

$$y = f. \qquad \text{(Dirichlet BC)}$$

$$\tfrac{\partial y}{\partial n} = f. \qquad \text{(Neumann BC)}$$

$$c_0 y + c_1 \tfrac{\partial y}{\partial n} = f. \qquad \text{(Robin BC)}$$

$$\text{Both } \; y = f \quad \text{and} \quad c_0 \tfrac{\partial y}{\partial n} = g. \qquad \text{(Cauchy BC)}$$

$$\text{Both } \; y = f \quad \text{and} \quad c_0 y + c_1 \tfrac{\partial y}{\partial n} = f. \qquad \text{(Mixed BC)}$$

Semi-infinite Propagators

Perfectly absorbing endpoint:

$$p(x,t|x_0) = \frac{1}{\sqrt{4\pi\, Dt}} \left\{ \exp\left[-\frac{(x-x_0)^2}{4Dt} \right] - \exp\left[-\frac{(x+x_0)^2}{4Dt} \right] \right\}.$$

Perfectly reflecting endpoint:

$$p(x,t|x_0) = \frac{1}{\sqrt{4\pi\, Dt}} \left\{ \exp\left[-\frac{(x-x_0)^2}{4Dt} \right] + \exp\left[-\frac{(x+x_0)^2}{4Dt} \right] \right\}.$$

Partially absorbing endpoint:

$$p(x,t|x_0) = p_F(x,t|x_0) + p_F(x,t|-x_0) - \frac{2}{D}\,\kappa\, \mathrm{e}^{\kappa x/D} \left\{ \frac{1}{2} \exp\left[-\frac{x_0^2 - (2\kappa t + x_0)^2}{4Dt} \right] \mathrm{erfc}\left[\frac{x + (2\kappa t + x_0)}{\sqrt{4Dt}} \right] \right\}.$$

4.A Mathematical Computations

Additional and intermediate mathematical computations are provided in this appendix.

4.A.1 Derivation of Eq. (4.88)

In order to solve to Eq. (4.88), let us simplify the problem by rearranging this equation as

$$\frac{\partial p(x,t|x_0)}{\partial x} - \frac{1}{D}\,\kappa p(x,t|x_0) = \frac{1}{D}\,q(x,t|x_0). \tag{4.125}$$

By defining the following variables as

$$\mu \equiv -\frac{1}{D}\,\kappa \quad \text{and} \quad g(x) \equiv \frac{1}{D}\,q(x,t|x_0), \tag{4.126}$$

we find that

$$\frac{\partial p(x,t|x_0)}{\partial x} + \mu\ p(x,t|x_0) = g(x). \tag{4.127}$$

Multiplying both sides of the latter equation by an arbitrary function $u(x)$ leads to

$$u(x)\frac{\partial p(x,t|x_0)}{\partial x} + \mu\ u(x)p(x,t|x_0) = u(x)g(x). \tag{4.128}$$

The left-hand side of the last equation can be written alternatively as

$$u(x)\frac{\partial p(x,t|x_0)}{\partial x} + \mu\ u(x)\ p(x,t|x_0) = \frac{\mathrm{d}}{\mathrm{d}x}\left[u(x)\ p(x,t|x_0)\right], \tag{4.129}$$

as long as

$$\frac{\mathrm{d}u(x)}{\mathrm{d}x} = \mu\ u(x) \qquad \text{or} \qquad u(x) = \mathrm{e}^{\mu x}. \tag{4.130}$$

Thus,

$$\mathrm{d}\left[u(x)p(x,t|x_0)\right] = u(x)g(x)\ \mathrm{d}x. \tag{4.131}$$

By integrating, we have that

$$u(x)\ p(x,t|x_0) = \int u(x)g(x)\ \mathrm{d}x + \mathcal{C}. \tag{4.132}$$

Solving for $p(x,t|x_0)$ gives

$$p(x,t|x_0) = \frac{1}{u(x)} \int u(x)g(x)\ \mathrm{d}x + \frac{\mathcal{C}}{u(x)}, \tag{4.133}$$

which can be simplified by substituting $u(x)$ given by Eq. (4.130), together with Eq. (4.126), leading to Eq. (4.93), namely,

$$p(x,t|x_0) = \mathcal{C}\mathrm{e}^{-\mu x} + \frac{1}{D}\mathrm{e}^{\kappa x/D} \int \mathrm{e}^{-\kappa y/D} q(y,t|x_0)\ \mathrm{d}y. \tag{4.93}$$

4.A.2 *Derivation of Eq. (4.98)*

By substituting Eq. (4.97) into Eq. (4.125), we have that

$$\begin{aligned} q(x,t|x_0) =& D\frac{\mathrm{d}}{\mathrm{d}x}\left[\pm\frac{1}{D}\mathrm{e}^{\kappa x/D}\int_x^\infty \mathrm{e}^{-\kappa y/D} q(y,t|x_0)\ \mathrm{d}y\right] \\ & \mp \frac{1}{D}\kappa \mathrm{e}^{\kappa/D}\int_x^\infty \mathrm{e}^{-\kappa y/D} q(y,t|x_0)\ \mathrm{d}y. \end{aligned} \tag{4.134}$$

Then, using the product rule for derivatives, we have

$$\begin{aligned} q(x,t|x_0) =& D\left[\pm\frac{\mathrm{d}}{\mathrm{d}x}\left(\frac{1}{D}\mathrm{e}^{\kappa x/D}\right)\int_x^\infty \mathrm{e}^{-\kappa y/D} q(y,t|x_0)\ \mathrm{d}y \right. \\ & \left. \pm\frac{1}{D}\mathrm{e}^{\kappa x/D}\ \frac{\mathrm{d}}{\mathrm{d}x}\int_x^\infty \mathrm{e}^{-\kappa y/D} q(y,t|x_0)\ dy\right] \\ & \mp \frac{\kappa \mathrm{e}^{\kappa x/D}}{D}\int_x^\infty \mathrm{e}^{-\kappa y/D} q(y,t|x_0)\mathrm{d}y, \end{aligned} \tag{4.135}$$

and applying the Leibniz rule for the derivative of the integral, we find that

$$\begin{aligned} q(x,t|x_0) =& \pm\frac{2}{D}\kappa \mathrm{e}^{\kappa x/D}\int_x^\infty \mathrm{e}^{-\kappa y/D} q(y,t|x_0)\ \mathrm{d}y \mp \mathrm{e}^{\kappa x/D}\ \mathrm{e}^{-\kappa x/D} q(x,t|x_0) \\ & \mp \frac{1}{D}\kappa \mathrm{e}^{\kappa x/D}\int_x^\infty \mathrm{e}^{-\kappa y/D} q(y,t|x_0)\ \mathrm{d}y, \end{aligned} \tag{4.136}$$

leading to

$$q(x,t|x_0) = \mp q(x,t|x_0), \tag{4.137}$$

where

$$\frac{\mathrm{d}}{\mathrm{d}x}\int_x^\infty \mathrm{e}^{-\kappa y/D} q(y,t|x_0)\,\mathrm{d}y = 0 - \mathrm{e}^{\kappa x/D} q(x,t|x_0). \tag{4.138}$$

Since Eq. (4.137) requires the positive sign, the correct solution of Eq. (4.97) is

$$p(x,t|x_0) = -\frac{1}{D}\mathrm{e}^{\kappa x/D}\int_x^\infty \mathrm{e}^{-\kappa y/D} q(y,t|x_0)\,\mathrm{d}y. \tag{4.98}$$

4.A.3 *Derivation of Eq. (4.104)*

When substituting the free-space propagator given by Eq. (4.44) and Eq. (4.103) into (4.99), we have

$$\begin{aligned}
q(x,t|x_0) &= \int_0^\infty [p_F(x,t|y) - p_F(x,t|-y)]\; q(y,0|x_0)\,\mathrm{d}y \\
&= \int_0^\infty [p_F(x,t|y) - p_F(x,t|-y)]\left(D\frac{\partial}{\partial y} - \kappa\right)\delta(y-x_0)\,\mathrm{d}y \\
&= \int_0^\infty p_F(x,t|y) D\frac{\partial}{\partial y}\delta(y-x_0)\,\mathrm{d}y \\
&\quad - \int_0^\infty p_F(x,t|-y) D\frac{\partial}{\partial y}\delta(y-x_0)\,\mathrm{d}y \\
&\quad - \int_0^\infty p_F(x,t|y)\kappa\delta(y-x_0)\,\mathrm{d}y + \int_0^\infty p_F(x,t|-y)\kappa\delta(y-x_0)\,\mathrm{d}y.
\end{aligned}$$

Then, using Eqs. (A.92), (A.97), and (A.102), the integration process leads to

$$\begin{aligned}
q(x,t|x_0) &= -\int_0^\infty \delta(y-x_0) D\frac{\partial p_F(x,t|y)}{\partial y}\,\mathrm{d}y \\
&\quad + \int_0^\infty \delta(y-x_0) D\frac{\partial p_F(x,y|-y)}{\partial y}\,\mathrm{d}y \\
&\quad - \kappa\; p_F(x,t|x_0)\; H(x_0) + \kappa\; p_F(x,t|-x_0)\; H(x_0) \\
&= DH(x_0)\left[\frac{\partial p_F(x,t|-x_0)}{\partial x_0} - \frac{\partial p_F(x,t|x_0)}{\partial x_0}\right] \\
&\quad + \kappa\; H(x_0)\,[p_F(x,t|-x_0) - p_F(x,t|x_0)],
\end{aligned}$$

from where

$$\begin{aligned} q(x,t|x_0) =& D\ H(x_0)\frac{\partial}{\partial x_0}\left[p_F(x,t|-x_0) - p_F(x,t|x_0)\right] \\ &+ \kappa\ H(x_0)\left[p_F(x,t|-x_0) - p_F(x,t|x_0)\right]. \end{aligned} \tag{4.139}$$

One of the conditions of the semi-infinite system is that $x_0 > 0$, i.e., the particles have an initial position on the real side of the domain. For that reason, the Heaviside function evaluated in the initial position is 1. On the one hand, $q(x,t|x_0)$ is given by

$$q(x,t|x_0) = \left(D\frac{\partial}{\partial x_0} + \kappa\right)\left[p_F(x,t|-x_0) - p_F(x,t|x_0)\right]. \tag{4.140}$$

On the other hand, we know that for the free diffusion propagator

$$\frac{\partial p_F(x,t|x_0)}{\partial x_0} = -\frac{\partial p_F(x,t|x_0)}{\partial x}, \qquad \frac{\partial p_F(x,t|-x_0)}{\partial x_0} = -\frac{\partial p_F(x,t|-x_0)}{\partial x}. \tag{4.141}$$

Therefore, Eq. (4.139) leads to

$$q(x,t|x_0) = D\frac{\partial}{\partial x}\left[p_F(x,t|-x_0) + p_F(x,t|x_0)\right] + \kappa\left[p_F(x,t|-x_0) - p_F(x,t|x_0)\right]. \tag{4.104}$$

4.A.4 Derivation of Eq. (4.107)

The first and second integrals of Eq. (4.105) have a similar structure, so we can integrate both signs by parts at the same time using the first relation of the definitions in Eq. (4.106), namely,

$$\begin{aligned} I_3^{\pm} &\equiv \int_x^{\infty} \mathrm{e}^{-\kappa y/D}\ \frac{\partial p_F(y,t|\pm x_0)}{\partial y}\,\mathrm{d}y \\ &= \left[\mathrm{e}^{-\kappa/D}\int \frac{\partial p_F(y,t|\pm x_0)}{\partial y}\,\mathrm{d}y\right]_{y=x}^{y=\infty} \\ &\quad + \frac{1}{D}\kappa\int_x^{\infty}\mathrm{e}^{-\kappa y/D}\left[\int \frac{\partial p_F(y,t|\pm x_0)}{\partial y}\,\mathrm{d}y\right]\mathrm{d}y, \end{aligned} \tag{4.142}$$

which through Eq. (4.94) becomes

$$I_3^{\pm} = -\mathrm{e}^{-\kappa x/D}\ p_F(x,t|\pm x_0) + \frac{1}{D}\kappa\int_x^{\infty}\mathrm{e}^{-\kappa y/D}\ p_F(y,t|\pm x_0)\,\mathrm{d}y. \tag{4.143}$$

The remaining integral in Eq. (4.143) is the same integral of the third and fourth terms in Eq. (4.142). Thus, it is useful to solve it separately including both signs through the second definition in Eq. (4.106), namely,

$$I_4^{\pm} \equiv \int_x^{\infty} \mathrm{e}^{-\kappa y/D}\; p_F(y,t|\pm x_0)\,\mathrm{d}y. \tag{4.144}$$

Introducing into this last integral the expression for the propagator of a free diffusing particle, we find that

$$\begin{aligned} I_4^{\pm} &= \int_x^{\infty} \frac{\mathrm{e}^{-\kappa y/D}}{\sqrt{4\pi\, Dt}} \exp\left[-\frac{(y\mp x_0)^2}{4Dt}\right]\mathrm{d}y \\ &= \frac{1}{\sqrt{4\pi\, Dt}} \int_x^{\infty} \exp\left[-\frac{\kappa y}{D} - \frac{y^2 \mp 2yx_0 + x_0^2}{4Dt}\right]\mathrm{d}y \\ &= \frac{1}{\sqrt{4\pi\, Dt}} \int_x^{\infty} \exp\left[-\frac{4\kappa yt + y^2 \mp 2yx_0 + x_0^2}{4Dt}\right]\mathrm{d}y \\ &= \frac{1}{\sqrt{4\pi\, Dt}} \int_x^{\infty} \exp\left[-\frac{y^2 + 2y(2\kappa t \mp x_0) + x_0^2}{4Dt}\right]\mathrm{d}y. \end{aligned}$$

Completing the perfect square in the argument of the exponential, we arrive at

$$\begin{aligned} I_4^{\pm} &= \frac{1}{\sqrt{4\pi\, Dt}} \int_x^{\infty} \exp\left[-\frac{[y+(2\kappa t \mp x_0)]^2 + x_0^2 - (2\kappa t \mp x_0)^2}{4Dt}\right]\mathrm{d}y \\ &= \frac{1}{\sqrt{4\pi\, Dt}} \exp\left[-\frac{x_0^2 - (2\kappa t \mp x_0)^2}{4Dt}\right] \int_x^{\infty} \exp\left[-\left(\frac{y+(2\kappa t \mp x_0)}{\sqrt{4Dt}}\right)^2\right]\mathrm{d}y. \end{aligned}$$

By making the change $z = [y + (2\kappa t \mp x_0)]/\sqrt{4Dt}$, we have

$$I_4^{\pm} = \frac{\sqrt{4Dt}}{\sqrt{4\pi\, Dt}} \exp\left[-\frac{x_0^2 - (2\kappa t \mp x_0)^2}{4Dt}\right] \int_{[x+(2\kappa t \mp x_0)]/\sqrt{4Dt}}^{\infty} \mathrm{e}^{-z^2}\,\mathrm{d}z, \tag{4.145}$$

where the definition of the complementary error function, Eq. (A.81), is used to obtain the following solution:

$$I_4^{\pm} = \frac{1}{2} \exp\left[-\frac{x_0^2 - (2\kappa t \mp x_0)^2}{4Dt}\right] \operatorname{erfc}\left[\frac{x + (2\kappa t \mp x_0)}{\sqrt{4Dt}}\right], \tag{4.146}$$

a result that allows us to write Eq. (4.143) as follows:

$$I_3^{\pm} = -\mathrm{e}^{-\kappa x/D}\ p_F(x,t|\pm x_0) + \frac{1}{D}\kappa\ I_4^{\mp}. \tag{4.147}$$

Then,

$$\begin{aligned} I_3^{\pm} &= -\mathrm{e}^{-\kappa x/D}\ p_F(x,t|\pm x_0) \\ &\quad + \frac{1}{2D}\kappa \exp\left[-\frac{x_0^2-(2\kappa t \mp x_0)^2}{4Dt}\right]\mathrm{erfc}\left[\frac{x+(2\kappa t \mp x_0)}{\sqrt{4Dt}}\right]. \end{aligned} \tag{4.148}$$

Thus, Eq. (4.105) is

$$\begin{aligned} p(x,t|x_0) &= -\mathrm{e}^{\kappa x/D}\ I_3^- - \mathrm{e}^{\kappa x/D}\ I_3^+ + \frac{1}{D}\kappa \mathrm{e}^{\kappa x/D}\left(I_4^+ - I_4^-\right) \\ &= -\mathrm{e}^{\kappa x/D}\left[-\mathrm{e}^{-\kappa x/D}\ p_F(x,t|-x_0) + \frac{1}{D}\kappa\ I_4^+\right] \\ &\quad - \mathrm{e}^{\kappa x/D}\left[-\mathrm{e}^{-\kappa x/D}\ p_F(x,t|x_0) + \frac{1}{D}\kappa\ I_4^-\right] + \frac{1}{D}\kappa\ \mathrm{e}^{\kappa x/D}\left(I_4^+ - I_4^-\right) \\ &= p_F(x,t|x_0) + p_F(x,t|-x_0) \\ &\quad - \frac{2}{D}\ \kappa\ \mathrm{e}^{\kappa x/D}\left\{\frac{1}{2}\exp\left[-\frac{x_0^2-(2\kappa t + x_0)^2}{4Dt}\right]\mathrm{erfc}\left[\frac{x+(2\kappa t + x_0)}{\sqrt{4Dt}}\right]\right\}. \end{aligned} \tag{4.107}$$

Further Reading and References

A.M. Berezhkovskii, L. Dagdug, V.A. Lizunov, J. Zimmerberg, S.M. Bezrukov, Trapping by clusters of channels, receptors, and transporters: quantitative description. Biophys. J. **106**, 500–509 (2014). 10.1016/j.bpj.2013.12.015

H.C. Berg, E.M. Purcell, Physics of chemoreception. Biophys. J. **20**, 193–219 (1977). 10.1016/S0006-3495(77)85544-6

F.C. Collins, G. Kimball, Diffusion-controlled reaction rates. J. Colloid Sci. **4**, 425–437 (1949). 10.1063/1.1763137

C. Constanda, *Solution Techniques for Elementary Partial Differential Equations* (Chapman & Hall/CRC, Boca Raton, 2010)

O.K. Dudko, A.M. Berezhkovskii, G.H. Weiss, Rateconstant for diffusion-influenced ligand binding to receptors of arbitrary shape on a cell surface. J. Chem. Phys. **121**, 1562–1565 (2004). 10.1016/0095-8522(49)90023-9

T.L. Hill, Effect of rotation on the diffusion-controlled rate of ligand-protein association. Proc. Natl. Acad. Sci. USA **72**, 4918–4922 (1975). 10.1073/pnas.72.12.4918

D. Shoup, A. Szabo, Role of diffusion in ligand binding to macromolecules and cell-bound receptors. Biophys. J. **40**, 33–39 (1982). 10.1016/S0006-3495(82)84455-X

R. Zwanzig, A. Szabo, Time-dependent rate of diffusioninfluenced ligand binding to receptors on cell surfaces. Biophys. J. **60**, 671–678 (1991). 10.1016S0006-3495(91)82096-3

Chapter 5
Diffusion Between Two Targets

In this chapter, we will solve a set of diffusion problems within a finite one-dimensional interval, by means of the separation of variables method (where possible) and the Laplace transform. In the separation of variables method, one assumes that the solution of the propagator is given by the product of two independent functions. When using the Laplace transform, we will write $p(x, s)$ as a linear combination of real exponential or hyperbolic functions, which depend explicitly on a phase. This phase is determined in such a way that the solution satisfies the subsidiary diffusion equation with the imposed boundary conditions, i.e., the boundary-value problem. Our main goal is to characterize the system with physical parameters such as propagator, flux, survival probability, mean first-passage time, and splitting probability.

5.1 Separation of Variables

Separation of variables is a method of solving ordinary and partial differential equations, and it is useful in solving equations arising in mathematical physics, such as the diffusion equation, Laplace's equation, the Helmholtz differential equation, and the Schrödinger equation, among others. The method of separation of variables relies upon the assumption that if the product of functions of independent variables is a constant, each function must separately be a constant. It was first used by L'Hospital in 1750. This method reduces an ordinary or partial differential equation to two ordinary differential equations, thus simplifying the original problem. In order to use the method of separation of variables, we must be working with a linear homogeneous partial differential equation with linear homogeneous boundary conditions.

L. Dagdug et al., *Diffusion Under Confinement*,
https://doi.org/10.1007/978-3-031-46475-1_5

Now, let's apply the method to solve the diffusion equation. Consider a Brownian particle diffusing along a one-dimensional domain Ω, and let the propagator $p(x,t)$ be a product of two independent functions, one dependent on the position x, $\chi(x)$, and the other dependent on time t, $T(t)$, where $x \in \Omega$ and $t \in [0,\infty)$. This initial assumption allows us to write the following solution:

$$p(x,t) = \chi(x)\ T(t). \tag{5.1}$$

When substituting Eq. (5.1) into the diffusion equation, i.e., Eq. (2.13), we immediately notice that

$$\frac{D}{\chi(x)}\frac{\partial^2\chi(x)}{\partial x^2} = \frac{1}{T(t)}\frac{\partial T(t)}{\partial t}. \tag{5.2}$$

Since the right-hand side depends only on x and the left-hand side only on t, both factors must be equal to a constant, which, for the sake of convenience, can be defined as $-\lambda^2 D$. Consequently, two ordinary differential equations (ODE) arise, namely,

$$\frac{\mathrm{d}^2\chi(x)}{\mathrm{d}x^2} + \lambda^2\chi(x) = 0 \qquad \text{and} \qquad \frac{\mathrm{d}T(t)}{\mathrm{d}t} + \lambda^2 D\ T(t) = 0. \tag{5.3}$$

The analytic solutions of Eqs. (5.3) are given by

$$\chi(x) = \mathcal{A}\sin(\lambda x) + \mathcal{B}\cos(\lambda x) \qquad \text{and} \qquad T(t) = k\mathrm{e}^{-\lambda^2 Dt}, \tag{5.4}$$

respectively, where $\mathcal{A}$, $\mathcal{B}$, and k are integration constants. The general solution, as an eigenfunction expansion or spectral representation, is a superposition of these functions, namely,

$$p(x,t) = \sum_{n=0}^{\infty}\left[\mathcal{A}_n\ \sin(\lambda_n x) + \mathcal{B}_n\ \cos(\lambda_n x)\right]\ \mathrm{e}^{-\lambda^2 Dt}. \tag{5.5}$$

Constants $\mathcal{A}_n$ and $\mathcal{B}_n$, together with the eigenvalues λ_n, are determined by the boundary and initial conditions of the problem. Considering only the spatial dependence of Eq. (5.5), we define the eigenfunctions of variable x as follows:

$$\phi_n(x) = \mathcal{A}_n\ \sin(\lambda_n x) + \mathcal{B}_n\ \cos(\lambda_n x). \tag{5.6}$$

The results obtained so far will be of great use throughout the rest of the chapter when solving the diffusion equation under different boundary conditions.

5.2 Reflecting-Reflecting

Consider a Brownian particle diffusing along a one-dimensional system into the interval $[0, L]$ in the presence of two reflecting points, one at $x = 0$ and the other at $x = L$ (see Fig. 5.1). The boundary conditions (BCs) are zero flux at the endpoints, i.e., Neumann BCs, given by

$$\mathbf{J}(x, t|x_0) \cdot \hat{\mathbf{n}}\big|_{x=0,L} = \pm \frac{\partial p(x, t|x_0)}{\partial x}\bigg|_{x=0,L} = 0, \tag{5.7}$$

where $\hat{\mathbf{n}}$ is the unit normal vector to the reflecting boundary equal to $\hat{\mathbf{e}}_i$ at $x = 0$ and $-\hat{\mathbf{e}}_i$ at $x = L$ (see Eq. (4.68)).

We will use two different methods to solve the diffusion equation under these BCs, the boundary-value problem: the separation of variables method and the Laplace transform.

5.2.1 The Separation of Variables Method

In Sect. 5.1, we found that the eigenfunctions of variable x are given by Eq. (5.6). The first derivative of this equation is

$$\frac{\partial \phi_n(x)}{\partial x} = \mathcal{A}_n \lambda_n \ \cos(\lambda_n x) - \mathcal{B}_n \lambda_n \ \sin(\lambda_n x). \tag{5.8}$$

Since the propagator is a product of independent functions of time and space, the BCs in space are directly translated in terms of $\phi_n(x)$. Therefore,

$$\frac{\partial \phi_n(x)}{\partial x}\bigg|_{x=0,L} = 0. \tag{5.9}$$

Substituting Eq. (5.6) into the last equation and evaluating at $x = 0$ allow us to conclude that $\mathcal{A}_n = 0$. Additionally, the evaluation of the derivative of $\phi_n(x)$ at $x = L$ yields

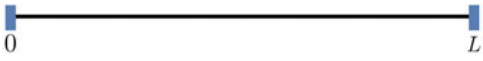

Fig. 5.1 Schematic representation of a one-dimensional domain $[0, L]$ with two reflecting points at $x = 0$ and $x = L$ (blue bars)

$$\left.\frac{\partial \phi_n(x)}{\partial x}\right|_{x=L} = -\mathcal{B}_n \lambda_n \ \sin(\lambda_n L) = 0, \tag{5.10}$$

meaning that $\lambda_n = n\pi/L$. Substituting the latter two relations into Eq. (5.6) leads to

$$\phi_n = \mathcal{B}_n \ \cos\left(\frac{n\pi x}{L}\right). \tag{5.11}$$

Thus, the propagator for the reflecting-reflecting system, given by Eq. (5.5), becomes

$$p(x,t) = \sum_{n=0}^{\infty} \mathcal{B}_n \ \cos\left(\frac{n\pi x}{L}\right) \ \exp\left(-\frac{n^2\pi^2 Dt}{L^2}\right). \tag{5.12}$$

Using the initial condition, $p(x,0|x_0) = \delta(x - x_0)$, in the last expression, the propagator transforms into

$$p(x,0|x_0) = \sum_{n=0}^{\infty} \mathcal{B}_n \ \cos\left(\frac{n\pi x}{L}\right) = \delta(x - x_0). \tag{5.13}$$

Now, to determine $\mathcal{B}_n$, we need to multiply the left-hand side of Eq. (5.13) by $\cos\left(\frac{m\pi x}{L}\right)$ and integrate the result over the interval $[0, L]$, resulting in

$$\sum_{n=0}^{\infty} \mathcal{B}_n \int_0^L \cos\left(\frac{n\pi x}{L}\right) \cos\left(\frac{m\pi x}{L}\right) \ \mathrm{d}x = \int_0^L \cos\left(\frac{m\pi x}{L}\right) \ \delta(x - x_0) \ \mathrm{d}x. \tag{5.14}$$

Thereafter,[1]

$$\sum_{n=0}^{\infty} \mathcal{B}_n \int_0^L \cos\left(\frac{n\pi x}{L}\right) \cos\left(\frac{m\pi x}{L}\right) \ \mathrm{d}x = \cos\left(\frac{m\pi x_0}{L}\right). \tag{5.17}$$

From Eq. (5.17), we find that the family of solutions depends on the values of n and m. If $n = m = 0$, $\mathcal{B}_n$ is given by

[1] Contributions are null in the regions outside the domain $[0, L]$, which gives

$$\int_{-\infty}^{0} \cos\left(\frac{m\pi x}{L}\right) \delta(x - x_0) \ \mathrm{d}x = 0 \quad \text{and} \quad \int_{L}^{\infty} \cos\left(\frac{m\pi x}{L}\right) \delta(x - x_0) \ \mathrm{d}x = 0, \tag{5.15}$$

leading to

$$\int_0^L \cos\left(\frac{m\pi x}{L}\right) \delta(x - x_0) \ \mathrm{d}x = \int_{-\infty}^{\infty} \cos\left(\frac{m\pi x}{L}\right) \delta(x - x_0) \ \mathrm{d}x = \cos\left(\frac{m\pi x_0}{L}\right). \tag{5.16}$$

$$\mathcal{B}_0 = \frac{1}{L}. \tag{5.18}$$

In contrast, when $n = m \neq 0$, we find that

$$\sum_{n=1}^{\infty} \mathcal{B}_n \int_0^L \cos\left(\frac{n\pi x}{L}\right)^2 \mathrm{d}x = \sum_{n=1}^{\infty} \mathcal{B}_n \frac{L}{2} \delta_{m,n} = \mathcal{B}_m \frac{L}{2}, \tag{5.19}$$

which means that for non-zero integers n and m, the coefficient $\mathcal{B}_n$ becomes

$$\mathcal{B}_n = \frac{2}{L} \cos\left(\frac{n\pi x_0}{L}\right). \tag{5.20}$$

Finally, in the case where $n \neq m$, the coefficient turns out to be null. In order to find the solution to our present problem, we include both non-zero solutions, namely,

$$p(x, t|x_0) = \frac{1}{L} + \frac{2}{L} \sum_{n=1}^{\infty} \exp\left(-\frac{n^2\pi^2 Dt}{L^2}\right) \cos\left(\frac{n\pi x_0}{L}\right) \cos\left(\frac{n\pi x}{L}\right). \tag{5.21}$$

The asymptotic value of the propagator in the limit where t tends to infinity is $1/L$. In other words, the entire concentration will be distributed uniformly along the interval $[0, L]$. Representative plots of the propagator $p(x, t|x_0)$ are depicted in Fig. 5.2.

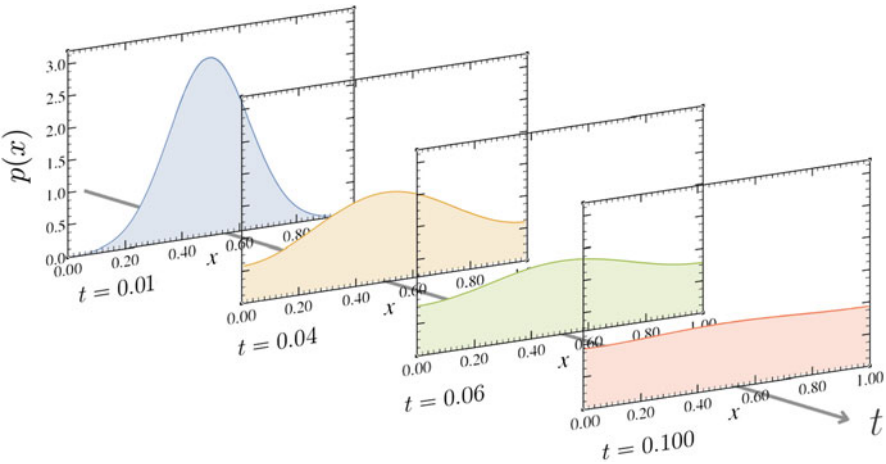

Fig. 5.2 Temporal evolution of the propagator $p(x, t|x_0)$, Eq. (5.21). The initial position of Brownian particles, system length, and diffusivity are $x_0 = 0.5$, $L = 1$, and $D = 1$, respectively

5.2.2 The Laplace Transformation Solution

Alternatively, we can use the Laplace transform to find the solution to the reflecting-reflecting system. It is generally more practical to use the Laplace transform rather than the Fourier transform, given that the propagator may be expressed as a single function rather than an infinite series.

The Laplace transform of the diffusion equation has the following subsidiary equation:

$$s\ p(x,s|x_0) - \delta(x-x_0) = D\frac{\partial^2 p(x,s|x_0)}{\partial x^2}. \tag{3.36}$$

In order to solve this last equation in the Laplace domain, we must Laplace transform the BCs to be applied to the proposed solution of Eq. (3.36). Given that the Laplace transform integrates in time and leaves the space coordinate unchanged, the BCs for the subsidiary equation have the same structure as in real space. Therefore, the Laplace transforms of the BCs for our system are

$$\mathbf{J}(x,t|x_0)\cdot\hat{\mathbf{n}}\big|_{x=0,L} = \pm D\left.\frac{\partial p(x,s|x_0)}{\partial x}\right|_{x=0,L} = 0. \tag{5.22}$$

Physically, they represent zero flux at $x=0$ and $x=L$, respectively. The function that satisfies such conditions is a hyperbolic cosine function with a modification on its argument. Consequently, let's propose the following solution:

$$p(x,s|x_0) = \begin{cases} \mathcal{A}\cosh\left[\sqrt{\frac{s}{D}}\,(x-x_\varphi)\right] & \text{for} \quad x < x_0, \\ \mathcal{B}\cosh\left[\sqrt{\frac{s}{D}}\,(x-x_\theta)\right] & \text{for} \quad x > x_0, \end{cases} \tag{5.23}$$

where x_θ and x_φ are phases, which must be determined by the BCs. Then, x_φ is found by applying the BC at $x=0$, namely,

$$\left.\frac{\partial p(x,s|x_0)}{\partial x}\right|_{x=0} = -\mathcal{A}\sqrt{\frac{s}{D}}\sinh\left(\sqrt{\frac{s}{D}}\,x_\varphi\right) = 0. \tag{5.24}$$

From this last equation, we can assert that

$$x_\varphi = 0. \tag{5.25}$$

Now, the BC at $x=L$ is used to find x_θ, which leads to

$$\left.\frac{\partial p(x,s|x_0)}{\partial x}\right|_{x=L} = \mathcal{B}\sqrt{\frac{s}{D}}\sinh\left[\sqrt{\frac{s}{D}}\,(L-x_\theta)\right] = 0, \tag{5.26}$$

and consequently,

$$x_\theta = L. \tag{5.27}$$

The remaining constants in Eq. (5.23) can be found by imposing the continuity condition on the propagator and its derivative at x_0, the joining conditions. From requiring continuity at x_0, given by Eq. (3.39), we have

$$\mathcal{A}\cosh\left[\sqrt{\frac{s}{D}}\,x_0\right] = \mathcal{B}\cosh\left[\sqrt{\frac{s}{D}}\,(x_0 - L)\right]. \tag{5.28}$$

Now, by imposing the discontinuity condition, given by Eq. (3.42), on the propagator in Eq. (5.23), we find another relation, namely,

$$\sqrt{\frac{s}{D}}\left\{\mathcal{B}\sinh\left(\sqrt{\frac{s}{D}}\,(x_0 - L)\right) - \mathcal{A}\sinh\left(\sqrt{\frac{s}{D}}\,x_0\right)\right\} = -\frac{1}{D}. \tag{5.29}$$

This system of equations is used to determine $\mathcal{A}$ and $\mathcal{B}$, and they are given by

$$\mathcal{A} = \frac{\cosh\left[\sqrt{\frac{s}{D}}(x_0 - L)\right]}{\sqrt{sD}\sinh\left(\sqrt{\frac{s}{D}}\,L\right)} \quad \text{and} \quad \mathcal{B} = \frac{\cosh\left[\sqrt{\frac{s}{D}}\,x_0\right]}{\sqrt{sD}\sinh\left(\sqrt{\frac{s}{D}}\,L\right)}. \tag{5.30}$$

As a result, the complete solution in Laplace's space for the reflecting-reflecting system is

$$p(x, s|x_0) = \begin{cases} \dfrac{\cosh\left[\sqrt{\frac{s}{D}}\,(x_0 - L)\right]\cosh\left(\sqrt{\frac{s}{D}}\,x\right)}{\sqrt{sD}\sinh\left(\sqrt{\frac{s}{D}}\,L\right)} & \text{for} \quad x < x_0, \\ \dfrac{\cosh\left[\sqrt{\frac{s}{D}}\,(x - L)\right]\cosh\left(\sqrt{\frac{s}{D}}\,x_0\right)}{\sqrt{sD}\sinh\left(\sqrt{\frac{s}{D}}\,L\right)} & \text{for} \quad x > x_0. \end{cases} \tag{5.31}$$

Plots in real space of the latter equation are identical to those depicted in Fig. 5.2.[2]

[2] It is often impossible to find the inverse Laplace transform function analytically. For such reason, numerical methods that provide an approximate solution to the problem have been developed. In Appendix 5.A, the reader will find a discussion on the Gaver-Stehfest numerical method, as well as the *Mathematica* code, to perform the inversion numerically.

5.3 Final Value Theorem

The *final value theorem* is used to relate the Laplace domain expression to the time domain solution as time approaches infinity. In this section, we will provide proof of the theorem and use it to find the behavior of the propagator in Eq. (5.31) for long times.

Let us suppose that a function $f(t)$ and its derivative $f'(t) = \partial f(t)/\partial t$ have Laplace transforms for all $s > 0$. Thus, from Eq. (A.55),

$$\mathcal{L}\left\{\frac{\mathrm{d}f(t)}{\mathrm{d}t}\right\} = \int_0^\infty \mathrm{e}^{-st}\,\frac{\mathrm{d}f(t)}{\mathrm{d}t}\,\mathrm{d}t = s\,\mathcal{L}\{f(t)\} - f(0). \tag{A.55}$$

Now, taking the limit as $s \to 0$, we have

$$\begin{aligned}\lim_{s\to 0}\left[\int_0^\infty \frac{\mathrm{d}f(t)}{\mathrm{d}t}\mathrm{e}^{-st}\,\mathrm{d}t\right] &= \int_0^\infty \frac{\mathrm{d}f(t)}{\mathrm{d}t}\lim_{s\to 0}\left(\mathrm{e}^{-st}\right)\,\mathrm{d}t \\ &= \lim_{s\to 0}\left[s\,\mathcal{L}\{f(t)\} - f(0)\right]\end{aligned} \tag{5.32}$$

which, by substituting $\lim_{s\to 0}\mathrm{e}^{-st} = 1$ and using the fundamental theorem of calculus, turns into

$$f(t)|_0^\infty = \lim_{s\to 0} s\mathcal{L}\{f(t)\} - f(0). \tag{5.33}$$

After the evaluation, we arrive at

$$\lim_{t\to\infty} f(t) = \lim_{s\to 0} sf(s). \tag{5.34}$$

This is *the final value theorem*, which enables us to find the final value of a function $f(t)$ when $t \to \infty$ from its Laplace transform $f(s)$ without needing to find the inverse Laplace transform.

Now, let us make use of the theorem to calculate the values of the propagator in Eq. (5.31) when $t \to \infty$. To take the limit when s goes to 0, we first obtain the Taylor series of the product $s\ p(x, s|x_0)|_{x_0^-}$ around $s = 0$, namely,

$$\begin{aligned}\lim_{t\to\infty} p(x,t|x_0) &= \lim_{s\to 0} s\,p(x,s|x_0)\Big|_{x_0^-} \\ &= \lim_{s\to 0}\left[\frac{1}{L} + \frac{2L^2 + 3x^2 - 6Lx_0 + 3x_0^2}{6DL}s + \cdots\right],\end{aligned} \tag{5.35}$$

from where we can conclude that

$$\lim_{t\to\infty} p(x,t|x_0) = \frac{1}{L}, \tag{5.36}$$

as expected. The reader can verify that the same value is found when using the solution for the right-hand side of the domain in Eq. (5.31).

Finally, it is worth mentioning that the *initial value theorem* of the Laplace transform enables us to calculate the initial value of a function $f(t)$ from its Laplace transform $f(s)$ without needing to find the inverse Laplace transform of $f(s)$, and it is given by

$$\lim_{t\to 0^+} f(t) = \lim_{s\to\infty} sf(s). \tag{5.37}$$

Together, the initial value theorem and the final value theorem are known as the *limiting theorems*.

5.4 Absorbing-Absorbing: Revisited

The absorbing-absorbing finite system is presented as follows: Consider a system in the interval $[0, L]$, and place two absorbing targets at $x = 0$ and $x = L$. Accordingly, $p(0,t) = p(L,t) = 0$ (see Fig. 5.3). Between the two absorbing walls, at x_0, a Brownian particle starts to diffuse and is removed from the system when hitting one of the two endpoints. The setting just described is the same as the one depicted in the random elevator game, Chap. 2.

As in the previous section, to solve the boundary-value problem, we will use two different methods: the separation of variables and the Laplace transform.

5.4.1 The Separation of Variables Method

The utility of the separation of variables method formalism will be illustrated again. The general solution to the diffusion equation using this method is given by Eq. (5.5), and when applying the absorbing boundary conditions at the endpoints, i.e., $p(0,t|x_0) = p(L,t|x_0) = 0$, it transforms into

Fig. 5.3 Schematic representation of a one-dimensional domain $[0, L]$ with two absorbing points at $x = 0$ and $x = L$ (red circles)

$$p(x,t) = \sum_{n=1}^{\infty} \mathcal{A}_n \sin(\lambda_n\, x) \mathrm{e}^{\lambda^2 Dt}, \tag{5.38}$$

with $\lambda_n = n\pi/L$. Additionally, the initial condition translates into the following relation:

$$p(x,0|x_0) = \sum_{n=1}^{\infty} \mathcal{A}_n \sin\left(\frac{n\pi x}{L}\right) = \delta(x - x_0). \tag{5.39}$$

To obtain $\mathcal{A}_n$, we simply to follow the same steps we used from Eqs. (2.25) to (2.28), and then, Eq. (5.38) becomes

$$p(x,t|x_0) = \frac{2}{L} \sum_{n=1}^{\infty} \exp\left(-\frac{\pi^2 n^2 Dt}{L^2}\right) \sin\left(\frac{n\pi x_0}{L}\right) \sin\left(\frac{n\pi x}{L}\right). \tag{5.40}$$

The reader should recognize the difference between the procedure to find the propagator written in Eq. (2.28) and the process to solve the diffusion equation by means of the separation of variables method. Even though both of them properly represent the evolution of the propagator, the solution derived in Chap. 2 comes from the assumption of $p(x,t)$ being a well-behaved function and was solved through Fourier analysis, while the separation of variables method provides us with a glimpse of the advantage of knowing the spectral decomposition of the propagator. Characteristic plots of Eq. (5.40) are depicted in Fig. 2.4. Every other probability feature, such as the survival probability or moments of mean first-passage time, is computed in the same way as in Chap. 2.

5.4.2 *The Laplace Transform Solution*

In this subsection, we will solve our current problem using the Laplace transform. We start by invoking the subsidiary equation, namely,

$$s\ p(x,s|x_0) - \delta(x - x_0) = D \frac{\partial^2 p(x,s|x_0)}{\partial x^2}. \tag{3.36}$$

The Laplace transforms of the BCs associated with the absorbing targets are

$$p(0,s|x_0) = p(L,s|x_0) = 0. \tag{5.41}$$

Now, let us propose the following solution:

$$p(x,s|x_0) = \begin{cases} \mathcal{A}\sinh\left[\sqrt{\frac{s}{D}}\,(x - x_\varphi)\right] & \text{for} \quad x < x_0 \\ \mathcal{B}\sinh\left[\sqrt{\frac{s}{D}}\,(x - x_\theta)\right] & \text{for} \quad x > x_0. \end{cases} \tag{5.42}$$

We find the explicit form of x_φ by evaluating the left-hand side solution at $x = 0$ and equating such result to zero, yielding

$$\mathcal{A}\sinh\left(\sqrt{\frac{s}{D}}\,x_\varphi\right) = 0, \tag{5.43}$$

which leads to

$$x_\varphi = 0. \tag{5.44}$$

Now, evaluating the propagator for $x > x_0$ at $x = L$ results in

$$\mathcal{B}\sinh\left[\sqrt{\frac{s}{D}}\,(L - x_\theta)\right] = 0, \tag{5.45}$$

from where we find that

$$x_\theta = L. \tag{5.46}$$

Therefore,

$$p(x,s|x_0) = \begin{cases} \mathcal{A}\sinh\left(\sqrt{\frac{s}{D}}\,x\right) & \text{for} \quad x < x_0 \\ \mathcal{B}\sinh\left[\sqrt{\frac{s}{D}}\,(x - L)\right] & \text{for} \quad x > x_0. \end{cases} \tag{5.47}$$

The continuity condition of the propagator, given by Eq. (3.39), and its derivatives, Eq. (3.42), applied to Eqs. (5.47), results in two other relations:

$$\mathcal{A}\sinh\left(\sqrt{\frac{s}{D}}\,x_0\right) = \mathcal{B}\sinh\left[\sqrt{\frac{s}{D}}(x_0 - L)\right], \qquad \text{and} \tag{5.48}$$

$$\sqrt{\frac{s}{D}}\left\{\mathcal{B}\cosh\left[\sqrt{\frac{s}{D}}(x_0 - L)\right] - \mathcal{A}\cosh\left(\sqrt{\frac{s}{D}}\,x_0\right)\right\} = -\frac{1}{D}. \tag{5.49}$$

Solving this system of equations for $\mathcal{A}$ and $\mathcal{B}$, we find that

$$\mathcal{A} = -\frac{\sinh\left[\sqrt{\frac{s}{D}}(x_0 - L)\right]}{\sqrt{sD}\sinh\left(\sqrt{\frac{s}{D}}\,L\right)} \quad \text{and} \quad \mathcal{B} = -\frac{\sinh\left(\sqrt{\frac{s}{D}}\,x_0\right)}{\sqrt{sD}\sinh\left(\sqrt{\frac{s}{D}}\,L\right)}. \tag{5.50}$$

Finally, substituting these last relations into Eq. (5.48), we find that the solution in the Laplace space of the propagator is given by

$$p(x,s|x_0) = \begin{cases} -\dfrac{\sinh\left(\sqrt{\frac{s}{D}}\,x\right)\sinh\left[\sqrt{\frac{s}{D}}(x_0-L)\right]}{\sqrt{sD}\sinh\left(\sqrt{\frac{s}{D}}\,L\right)} & \text{for} \quad x < x_0, \\ -\dfrac{\sinh\left(\sqrt{\frac{s}{D}}\,x_0\right)\sinh\left[\sqrt{\frac{s}{D}}(x-L)\right]}{\sqrt{sD}\sinh\left(\sqrt{\frac{s}{D}}\,L\right)} & \text{for} \quad x > x_0. \end{cases} \tag{5.51}$$

Real-space plots of the latter equation are identical to those depicted in Fig. 2.4.

5.4.3 *Survival Probability and Moments of MFPT: Revisited*

As we already know, we can find the survival probability in Laplace's space when integrating the propagator $p(x,s|x_0)$ with respect to x along the entire domain, namely,

$$\begin{aligned} S(t|x_0) &= \int_0^L p(x,s|x_0)\,\mathrm{d}x \\ &= \lim_{\epsilon\to 0}\int_0^{x_0-\epsilon} p(x<x_0,s|x_0)\,\mathrm{d}x + \lim_{\epsilon\to 0}\int_{\epsilon+x_0}^{L} p(x>x_0,s|x_0)\,\mathrm{d}x \\ &= \int_0^{x_0^-} p(x<x_0,s|x_0)\,\mathrm{d}x + \int_{x_0^+}^{L} p(x>x_0,s|x_0)\,\mathrm{d}x, \end{aligned} \tag{5.52}$$

where we define

$$x_0^- \equiv \lim_{\epsilon\to 0} x_0 - \epsilon \quad \text{and} \quad x_0^+ \equiv \lim_{\epsilon\to 0} x_0 + \epsilon. \tag{5.53}$$

Performing the integration of Eq. (5.52) results in

$$\begin{aligned} S(s|x_0) = \frac{1}{s\sinh\left(\sqrt{\frac{s}{D}}\,L\right)}\Bigg\{ &\cosh\left(\sqrt{\frac{s}{D}}\,x\right)\sinh\left[\sqrt{\frac{s}{D}}(L-x_0)\right]\Bigg|_0^{x_0^-} \\ &-\cosh\left[\sqrt{\frac{s}{D}}(L-x)\right]\sinh\left(\sqrt{\frac{s}{D}}\,x_0\right)\Bigg|_{x_0^+}^{L}\Bigg\}. \end{aligned} \tag{5.54}$$

After evaluating, we find that

$$S(s|x_0) = \frac{1}{s \sinh\left(\sqrt{\frac{s}{D}}\, L\right)} \Bigg\{ \left[\cosh\left(\sqrt{\frac{s}{D}}\, x_0\right) - 1\right] \sinh\left[\sqrt{\frac{s}{D}}(L - x_0)\right] + \left\{\cosh\left[\sqrt{\frac{s}{D}}(L - x_0)\right] - 1\right\} \sinh\left(\sqrt{\frac{s}{D}}\, x_0\right) \Bigg\}, \tag{5.55}$$

leading to

$$S(s|x_0) = \frac{1 - \cosh\left[\sqrt{\frac{s}{D}}\, \left(\frac{L-2x_0}{2}\right)\right] \operatorname{sech}\left(\sqrt{\frac{s}{D}}\, \frac{L}{2}\right)}{s}. \tag{5.56}$$

If we Taylor-expand the latter equation around $s = 0$ using Eq. (A.17), the survival probability $S(s|x_0)$ becomes

$$S(s|x_0) = \frac{x_0(L - x_0)}{2D} + \frac{s(-x_0^4 + 2Lx_0^3 - L^3 x_0)}{24D^2} + \cdots \tag{5.57}$$

Now we can use Eq. (2.90), i.e.,

$$\langle t^n(x_0)\rangle = (-1)^{n+1} n \left.\frac{\partial^{n-1} S(s|x_0)}{\partial s^{n-1}}\right|_{s=0} \qquad n = 1, 2, 3, \cdots, \tag{2.90}$$

to compute the moments of MFPT. For instance, the first moment is

$$\langle t(x_0)\rangle = (-1)^2 S(s|x_0)\Big|_{s=0} = \frac{x_0(L - x_0)}{2D}, \tag{5.58}$$

and the second moment is

$$\langle t^2(x_0)\rangle = (-1)^3(2)\, s \left.\frac{\partial S(s|x_0)}{\partial s}\right|_{s=0} = \frac{x_0(L - x_0)\left(L^2 + Lx_0 - x_0^2\right)}{12D^2}, \tag{5.59}$$

which are Eqs. (2.50) and (2.68), respectively.

5.4.4 *Splitting Probability: Revisited*

Furthermore, we can calculate the probability density of mean first-passage time in Laplace's space using the propagator given in Eq. (5.51). To such end, we compute the flux at each endpoint using the Laplace transform of Eq. (2.73), namely,

$$\mathbf{J}(x, s) = -D \frac{\partial p(x, s|x_0)}{\partial x}\, \hat{\mathbf{e}}_x, \tag{5.60}$$

from which we find that

$$\begin{aligned} J(0,s|x_0) &= -D\,\frac{\partial p(x,s|x_0)}{\partial x}\,\hat{\mathbf{e}}_x\cdot(-\hat{\mathbf{e}}_x)\bigg|_{x=0} \\ &= \operatorname{csch}\left(\sqrt{\frac{s}{D}}\,L\right)\sinh\left[\sqrt{\frac{s}{D}}(L-x_0)\right], \\ J(L,s|x_0) &= -D\,\frac{\partial p(x,s|x_0)}{\partial x}\,\hat{\mathbf{e}}_x\cdot\hat{\mathbf{e}}_x\bigg|_{x=L} = \operatorname{csch}\left(\sqrt{\frac{s}{D}}\,L\right)\sinh\left[\sqrt{\frac{s}{D}}x_0\right]. \end{aligned} \tag{5.61}$$

On the other hand, the Laplace transform of the first-passage time probability density, given by Eq. (2.83), is

$$\int_0^\infty \varphi(x_0|t)\,\mathrm{e}^{-st}\,\mathrm{d}t = \int_0^\infty [J(L,t)+J(0,t)]\,\mathrm{e}^{-st}\,\mathrm{d}t \tag{5.62}$$

or, equivalently,

$$\varphi(s|x_0) = J(L,s|x_0)+J(0,s|x_0). \tag{5.63}$$

Now, substituting the closed expression of Eq. (5.61) into Eq. (5.63), we find that

$$\varphi(s|x_0) = \operatorname{csch}\left(\sqrt{\frac{s}{D}}L\right)\left\{\sinh\left[\sqrt{\frac{s}{D}}(L-x_0)\right]+\sinh\left(\sqrt{\frac{s}{D}}\,x_0\right)\right\}, \tag{5.64}$$

an expression that we can use to obtain the first two moments of MFPT, i.e., Eqs. (2.50) and (2.68).

Since the Laplace transform of the flux reduces to the sum of probabilities between $t\in[0,\infty)$ when s tends to zero, i.e.,[3]

$$\begin{aligned} \lim_{s\to 0} J(x',s|x_0) &= \pm\lim_{s\to 0}\,\frac{\partial p(x,s|x_0)}{\partial x}\bigg|_{x=x'} \\ &= \pm\int_0^\infty \lim_{s\to 0}\left(\mathrm{e}^{-st}\right)\,\frac{\partial p(x,t|x_0)}{\partial x}\,\mathrm{d}t\bigg|_{x=x'} \\ &= \int_0^\infty J(x',t|x_0)\,\mathrm{d}t = \theta_{x'}(x_0), \end{aligned} \tag{5.65}$$

[3] The plus-minus sign $\pm$ indicates the direction of the flux at $x'=0$ and $x'=L$. For eastward flux, we use a minus sign, and for westward flux, we use a plus sign, which is the same convention we used to write Eq. (5.61).

the flux in Laplace space at $x' = 0$ and $x' = L$ becomes the splitting probability at the endpoints (see Eq. (2.95)), namely,

$$\begin{aligned}\theta_{x'}(x_0) &= \lim_{s\to 0} J(x', s|x_0) \\ &= J(x', s \to 0|x_0)\end{aligned} \tag{5.66}$$

Therefore, when Taylor-expanding the flux of the absorbing-absorbing system around $s = 0$, given by Eqs. (5.61), and considering just the first order term, then $\theta_{0,L}(x_0)$ are given by

$$\theta_0(x_0) = J(0, s \to 0|x_0) = 1 - \frac{x_0}{L} \quad \text{and} \quad \theta_L(x_0) = J(L, s \to 0|x_0) = \frac{x_0}{L}, \tag{5.67}$$

as expected.

5.5 Absorbing-Absorbing: Uniformly Distributed Initial Position

It may be the case that the Brownian particles are initially uniformly distributed throughout the domain, rather than positioned in a single point. Consequently, in order to obtain the new propagator, we need to integrate Eq. (2.28) over x_0 from 0 to L, divided by the integral of $\mathrm{d}x_0$ over the entire interval, that is,

$$p(x, t|x_0) = \frac{2}{L}\sum_{n=1}^{\infty} \exp\left(-\frac{\pi^2 n^2 Dt}{L^2}\right) \sin\left(\frac{n\pi x}{L}\right) \frac{\int_0^L \sin\left(\frac{n\pi x_0}{L}\right) \mathrm{d}x_0}{\int_0^L \mathrm{d}x_0}. \tag{5.68}$$

Performing the integral, we have that the propagator with a uniformly distributed initial position in the presence of two absorbing boundaries is

$$p(x, t) = \frac{4}{\pi L}\sum_{n=1}^{\infty} \exp\left[-\frac{(2n-1)^2\pi^2 Dt}{L^2}\right] \frac{\sin\left[\frac{(2n-1)\pi x}{L}\right]}{2n-1}. \tag{5.69}$$

Representative plots of the probability distribution $p(x, t)$, Eq. (5.69), are depicted in Fig. 5.4.

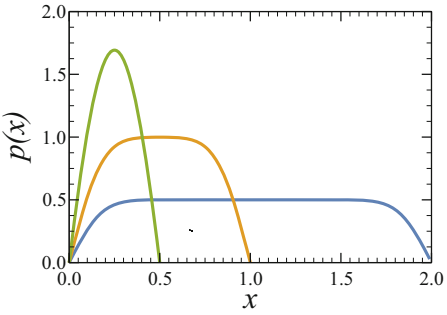

Fig. 5.4 Schematic representation of the probability distribution $p(x,t)$ in Eq. (5.69) for different channel lengths: $L = 2$ (blue line), $L = 1$ (yellow line), and $L = 0.5$ (green line) at time $t = 0.01$. The starting position of the particle is uniformly distributed, and the diffusion coefficient is $D = 1$

5.5.1 Survival Probability and Mean First-Passage Time

When integrating the propagator in the space coordinate over the domain, we find the survival probability, namely,

$$S(t) = \frac{4}{\pi L}\sum_{n=1}^{\infty}\frac{1}{2n-1}\exp\left[-\frac{(2n-1)^2\pi^2 Dt}{L^2}\right]\int_0^L \sin\left[\frac{(2n-1)\pi x}{L}\right]\mathrm{d}x. \tag{5.70}$$

After performing the integral, we find

$$S(t) = \frac{8}{\pi^2}\sum_{n=1}^{\infty}\frac{1}{(2n-1)^2}\exp\left[-\frac{(2n-1)^2\pi^2 Dt}{L^2}\right]. \tag{5.71}$$

From this last equation, we can conclude that the longest decay time is when $n = 1$, given by $L^2/\pi^2 D$, as well as when the particles start from a single point. Given that the probability density of first-passage time is just minus the derivative in time of Eq. (5.71), we have

$$\varphi(t) = \frac{8D}{L^2}\sum_{n=1}^{\infty}\exp\left[-\frac{(2n-1)^2\pi^2 Dt}{L^2}\right]. \tag{5.72}$$

Representative plots of the survival probability, Eq. (5.71), and the probability density of first-passage time, Eq. (5.72), are depicted in Fig. 5.5.

5.5.2 Moments of MFPT and Splitting Probability

For the moments of MFPT, we have the following integral:

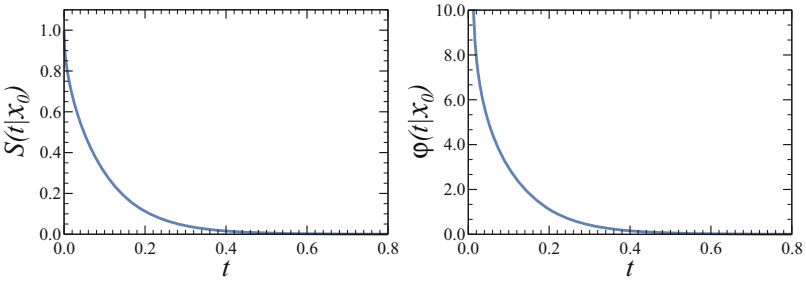

Fig. 5.5 Schematic representation of survival probability, Eq. (5.71), and the probability density of first-passage time, Eq. (5.72). The starting position of the particles is set at $x_0 = 0.5$, and the diffusion coefficient is $D = 1$

$$\langle t_u^n \rangle = \frac{8n}{\pi^2} \sum_{m=1}^{\infty} \frac{1}{(2m-1)^2} \int_0^{\infty} t^{n-1} \exp\left[-\frac{(2m-1)^2 \pi^2 D t}{L^2} \right] \mathrm{d}t. \tag{5.73}$$

Using Eq. (A.10), we arrive at

$$\begin{aligned} \langle t_u^n \rangle &= \frac{8n}{\pi^2} \sum_{m=1}^{\infty} \frac{1}{(2m-1)^2} (n-1)! \left[\frac{(2m-1)^2 D \pi^2}{L^2} \right]^{-(n-1)-1} \\ &= \frac{8}{\pi^2} \left(\frac{L^2}{D\pi^2} \right)^n n! \sum_{m=1}^{\infty} \frac{1}{(2m-1)^{2(n+1)}}. \end{aligned} \tag{5.74}$$

Using Eq. (A.37) for the sum, the latter equation becomes

$$\langle t_u^n \rangle = \frac{8n!}{\pi^2} \left(\frac{L^2}{D\pi^2} \right)^n \left\{ \left[1 - 2^{-2(n+1)} \right] \zeta[2(n+1)] \right\}, \tag{5.75}$$

where $\zeta(x)$ is the Riemann zeta function of variable x (see Sect. A.10.5). For the first moment, we set $n = 1$, leading to

$$\langle t_u \rangle = \frac{L^2}{12D}. \tag{5.76}$$

When comparing this solution to the case when the particles start from a predetermined x_0, given by Eqs. (2.50), we can see that

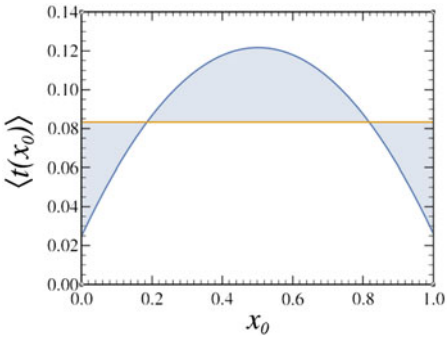

Fig. 5.6 MFPT as a function of x_0 predicted by Eq. (2.50) (blue line) and Eq. (5.76) (yellow line). The different domains predicted by Eq. (5.78) are shown by shadows. The initial system length and diffusivity are set to $L = 1$ and $D = 1$, respectively

$$\langle t \rangle = \frac{6(L - x_0)}{L^2} \langle t_u \rangle. \tag{5.77}$$

From this last relation, we can determine the domain for which the particles leave the system faster for a predetermined x_0 as compared to the case where they are uniformly distributed by setting $6(L-x_0)/L^2 > 1$. This inequality has the following solution:

$$\frac{L}{2} - \frac{L}{2\sqrt{3}} < x_0 < \frac{L}{2} + \frac{L}{2\sqrt{3}}. \tag{5.78}$$

When x_0 is equal to these values, both initial position arrangements will have the same MFPT time. Representative plots of the inequality (5.78), as well as the MFPT given by Eqs. (2.50) and (5.76), are depicted in Fig. 5.6.

The splitting probability is computed through Eq. (2.95), namely,

$$\theta_{x'} = -D \frac{\partial}{\partial x} \int_0^\infty \frac{4}{\pi L} \sum_{n=1}^{\infty} \exp\left[-\frac{(2n-1)^2 \pi^2 D t}{L^2} \right] \frac{\sin\left[\frac{(2n-1)\pi x}{L} \right]}{2n-1} \, \mathrm{d}t \Bigg|_{x=x'}. \tag{5.79}$$

After integrating and taking the derivative, we have

$$\begin{aligned} \theta_{x'} &= -\frac{4D}{\pi L} \left(\frac{L^2}{\pi^2 D} \right) \frac{\partial}{\partial x} \sum_{n=1}^{\infty} \frac{\sin\left[\frac{(2n-1)\pi x}{L} \right]}{(2n-1)^3} \Bigg|_{x=x'} \\ &= -\frac{4}{\pi^2} \sum_{n=1}^{\infty} \frac{\cos\left[\frac{(2n-1)\pi x}{L} \right]}{(2n-1)^2} \Bigg|_{x=x'}. \end{aligned} \tag{5.80}$$

Making use of the general result of the sum, Eq. (A.38), the $\theta_{x'}$ evaluated at $x' = L$ yields

$$\theta_L = \frac{1}{2}. \tag{5.81}$$

Then, by using the normalization property, $\theta_0 = 1 - \theta_L$, we have

$$\theta_0 = \frac{1}{2}. \tag{5.82}$$

5.6 Absorbing-Reflecting

The absorbing-reflecting finite system is depicted as follows: In an interval $[0, L]$, we place an absorbing boundary at $x = 0$ and a reflecting boundary at $x = L$ (see Fig. 5.7). Consequently, in this problem, we have to consider mixed boundary conditions. In the domain, at x_0, a Brownian particle starts to diffuse and is removed from the system as soon as it hits the absorbing target. As in the previous section, we will solve this boundary-value problem by using the separation of variables method and the Laplace transform.

It is worth mentioning that when we consider the limit when $L \to \infty$, a semi-infinite interval boundary-value problem is recovered.

5.6.1 The Separation of Variables Method

The reflecting and absorbing boundary conditions are described by Eqs. (4.27) and (4.69), respectively. Therefore, in the separation of variables method, the BCs are given by

$$\phi_n(0) = 0 \quad \text{and} \quad \left.\frac{\partial \phi_n(x)}{\partial x}\right|_{x=L} = 0. \tag{5.83}$$

Fig. 5.7 Schematic representation of a one-dimensional domain with an absorbing point at $x = 0$ (red circle) and a reflecting target at $x = L$ (blue bar)

From the absorbing boundary condition, we find that $\mathcal{B}_n = 0$ in Eq. (5.6). From the reflecting boundary condition, we determine that the eigenvalue is $\lambda_n = (2n + 1)\pi/2L$, since

$$\left.\frac{\partial \phi_n(x)}{\partial x}\right|_{x=L} = \mathcal{A}_n \lambda_n \cos(\lambda_n L) = 0. \tag{5.84}$$

This leads to the following solution:

$$p(x,t) = \sum_{n=0}^{\infty} A_n \ \exp\left[-\frac{(2n+1)^2\pi^2 Dt}{4L^2}\right] \ \sin\left[\frac{(2n+1)\pi x}{2L}\right]. \tag{5.85}$$

To obtain $\mathcal{A}$ as previously performed, the Dirac delta function as the initial condition translates into

$$p(x,0|x_0) = \frac{2}{L}\sum_{n=0}^{\infty} \mathcal{A}_n \sin\left[\frac{(2n+1)\pi x}{2L}\right] = \delta(x - x_0), \tag{5.86}$$

where

$$\delta(x - x_0) = \sum_{n=0}^{\infty} \sin\left[\frac{(2n+1)\pi x_0}{2L}\right] \sin\left[\frac{(2n+1)\pi x}{2L}\right].$$

Thus, the solution to the propagator of the absorbing-reflecting system is

$$p(x,t|x_0) = \frac{2}{L}\sum_{n=0}^{\infty} \exp\left[-\frac{(2n+1)^2\pi^2 Dt}{4L^2}\right] \ \sin\left[\frac{(2n+1)\pi x_0}{2L}\right] \ \sin\left[\frac{(2n+1)\pi x}{2L}\right]. \tag{5.87}$$

At this point, the reader should be aware of the similarity between Eqs. (5.87) and (2.28).

5.6.2 *Survival Probability and First-Passage Time*

Using Eqs. (5.52) and (5.87), we find that the survival probability is given by

$$
\begin{aligned}
S(t|x_0) &= \frac{2}{L}\sum_{n=0}^{\infty}\exp\left[-\frac{(2n+1)^2\pi^2 Dt}{4L^2}\right]\sin\left[\frac{(2n+1)\pi x_0}{2L}\right] \\
&\quad\times\int_0^L \sin\left[\frac{(2n+1)\pi x}{2L}\right]\mathrm{d}x \\
&= -\frac{2}{L}\sum_{n=0}^{\infty}\left\{\exp\left[-\frac{(2n+1)^2\pi^2 Dt}{4L^2}\right]\sin\left[\frac{(2n+1)\pi x_0}{2L}\right]\left[\frac{2L}{(2n+1)\pi}\right]\right. \\
&\qquad\left.\times\cos\left[\frac{(2n+1)\pi x}{2L}\right]_0^L\right\}.
\end{aligned}
\tag{5.88}
$$

If we simplify the above expression, we get

$$
S(t|x_0) = \frac{4}{\pi}\sum_{n=0}^{\infty}\frac{\sin\left[\frac{(2n+1)\pi x_0}{2L}\right]}{2n+1}\exp\left[-\frac{(2n+1)^2\pi^2 Dt}{4L^2}\right]. \tag{5.89}
$$

The probability density of the first-passage time is computed through Eq. (2.34), leading to

$$
\varphi(t|x_0) = -\frac{\mathrm{d}}{\mathrm{d}t}\left\{\frac{4}{\pi}\sum_{n=0}^{\infty}\exp\left[-\frac{(2n+1)^2\pi^2 Dt}{4L^2}\right]\frac{\sin\left[\frac{(2n+1)\pi x_0}{2L}\right]}{(2n+1)}\right\}. \tag{5.90}
$$

Finally, we arrive at

$$
\varphi(t|x_0) = \frac{D\pi}{L^2}\sum_{n=0}^{\infty}(2n+1)\exp\left[-\frac{(2n+1)^2\pi^2 Dt}{4L^2}\right]\sin\left[\frac{(2n+1)\pi x_0}{2L}\right]. \tag{5.91}
$$

This last equation will be used in the next section to calculate the moments of MFPT.

5.6.3 *Moments of MFPT*

The first moment of mean first-passage time is found by using Eq. (2.44) and applying the techniques outlined in Sect. 2.5, namely,

$$\begin{aligned}\langle t(x_0)\rangle &= \frac{4}{\pi}\sum_{n=0}^{\infty}(-1)^n\frac{\sin\left[\frac{(2n+1)\pi x_0}{2L}\right]}{2n+1}\int_0^{\infty}\exp\left[-\frac{(2n+1)^2\pi^2 Dt}{4L^2}\right]\mathrm{d}t \\ &= \frac{4}{\pi}\sum_{n=0}^{\infty}(-1)^n\frac{\sin\left[\frac{(2n+1)\pi x_0}{2L}\right]}{2n+1}\left[-\frac{4L^2}{(2n+1)^2 D\pi^2}\right] \\ &\quad\times\exp\left[-\frac{(2n+1)^2\pi^2 Dt}{4L^2}\right]\Bigg|_0^{\infty},\end{aligned} \tag{5.92}$$

leading to

$$\langle t(x_0)\rangle = \frac{16L^2}{D\pi^3}\sum_{n=0}^{\infty}\frac{\sin\left[\frac{(2n+1)\pi x_0}{2L}\right]}{(2n+1)^3}. \tag{5.93}$$

The simplest way to calculate the moments of MFPT is by solving its differential equation. For instance, if we want to obtain the first moment, we have to solve

$$D\frac{\mathrm{d}^2\langle t(x_0)\rangle}{\mathrm{d}x_0^2} = -1, \tag{2.64}$$

which has a general solution given by

$$\langle t(x_0)\rangle = A + Bx_0 - \frac{x_0^2}{2D}, \tag{2.49}$$

subject to the following boundary conditions:

$$\langle t(0)\rangle = 0 \quad \text{and} \quad \left.\frac{\mathrm{d}\langle t(x_0)\rangle}{\mathrm{d}x_0}\right|_{x_0=L} = 0, \tag{5.94}$$

from which we find that $A = 0$ and $B = L/D$, yielding

$$\langle t(x_0)\rangle = \frac{x_0(2L - x_0)}{2D}. \tag{5.95}$$

This equation predicts that $\langle t(0)\rangle = 0$ and has a maximum equal to $L^2/2D$ at L. Finally, it is worth noting that the MFPT for the absorbing-reflecting system could be obtained the absorbing-absorbing system. The relation between both systems is shown in Fig. 5.8, where we can see that in order to map the absorbing-reflecting system to the absorbing-absorbing system, we have to set a domain from 0 to $2L$ in the latter. Actually, we can obtain Eq. (5.93) from Eq. (2.46) by substituting L for $2L$. Nevertheless, we could just make this substitution into Eqs. (2.50) and (2.68) to find the first two moments of mean first-passage time, namely,

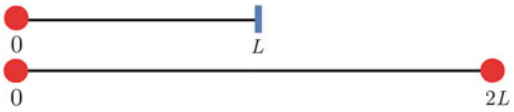

Fig. 5.8 Comparison of one-dimensional domain systems. The absorbing-reflecting and the absorbing-absorbing systems are shown. From this schematic representation, we can see that the absorbing-reflecting system of length L is equivalent to the absorbing-absorbing system of length $2L$

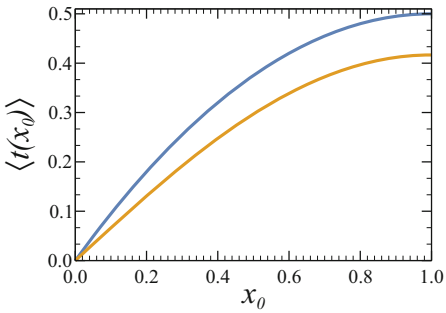

Fig. 5.9 Characteristic plots of MFPT, Eq. (5.96), i.e., $\langle t(x_0) \rangle$ (blue line) and $\langle t^2(x_0) \rangle$ (yellow line), as a function of x_0. The initial system length and diffusivity are set to $L = 1$ and $D = 1$, respectively

$$\langle t(x_0) \rangle = \frac{x_0(2L - x_0)}{2D}, \qquad \langle t^2(x_0) \rangle = \frac{x_0(2L - x_0)(4L^2 + 2Lx_0 - x_0^2)}{12D^2}. \tag{5.96}$$

Characteristic plots of Eqs. (5.96) are shown in Fig. 5.9.

5.6.4 *The Laplace Transform Solution*

To solve the absorbing-reflecting system by means of the Laplace transform, we start from the subsidiary equation of the diffusion equation, i.e.,

$$s\ p(x, s|x_0) - \delta(x - x_0) = D\frac{\partial^2 p(x, s|x_0)}{\partial x^2}, \tag{3.36}$$

subject to the Laplace transformed BCs in Eq. (5.83), namely,

$$p(0, s|x_0) = 0 \quad \text{and} \quad \left.\frac{\partial p(x, s|x_0)}{\partial x}\right|_{x=L} = 0. \tag{5.97}$$

The main properties that the propagator has to satisfy for this boundary-value problem are: For the left-hand side, it has to be zero when evaluated at $x = 0$, while for the right-hand side, its derivative must vanish at $x = L$, so

there is no flux at such boundary. As previously discussed, the algebra to find the propagator can be simplified considerably by choosing the appropriate linear combination of hyperbolic function solutions that satisfy the boundary conditions. These considerations lead to

$$p(x,s|x_0) = \begin{cases} \mathcal{A}\sinh\left[\sqrt{\frac{s}{D}}\,(x-x_\varphi)\right] & \text{for} \quad x < x_0, \\ \mathcal{B}\cosh\left[\sqrt{\frac{s}{D}}\,(x-x_\theta)\right] & \text{for} \quad x > x_0. \end{cases} \tag{5.98}$$

Substituting the absorbing BC at $x = 0$ in the propagator leads to the relation

$$-\mathcal{A}\sinh\left[\sqrt{\frac{s}{D}}\,x_\varphi\right] = 0, \tag{5.99}$$

from which we can assert that

$$x_\varphi = 0. \tag{5.100}$$

On the other hand, by substituting the reflecting BC, we arrive at

$$\left.\frac{\partial p(x,s|x_0)}{\partial x}\right|_{x=L} = \mathcal{B}\sqrt{\frac{s}{D}}\sinh\left[\sqrt{\frac{s}{D}}\,(L-x_\theta)\right] = 0, \tag{5.101}$$

leading to

$$x_\theta = L. \tag{5.102}$$

The joining condition for the propagator and its derivative, given by Eqs. (3.39) and (3.42), respectively, yields the following system of equations:

$$\mathcal{A}\sinh\left(\sqrt{\frac{s}{D}}\,x_0\right) = \mathcal{B}\cosh\left[\sqrt{\frac{s}{D}}\,(x_0-L)\right] \quad \text{and} \tag{5.103}$$

$$\sqrt{\frac{s}{D}}\left\{\mathcal{B}\sinh\left[\sqrt{\frac{s}{D}}\,(x_0-L)\right] - \mathcal{A}\cosh\left(\sqrt{\frac{s}{D}}\,x_0\right)\right\} = -\frac{1}{D}, \tag{5.104}$$

from which we arrive at

$$\mathcal{A} = \frac{\cosh\left[\sqrt{\frac{s}{D}}\,(x_0-L)\right]}{\sqrt{sD}\cosh\left(\sqrt{\frac{s}{D}}L\right)} \quad \text{and} \quad \mathcal{B} = \frac{\sinh\left(\sqrt{\frac{s}{D}}\,x_0\right)}{\sqrt{sD}\cosh\left(\sqrt{\frac{s}{D}}\,L\right)}. \tag{5.105}$$

Therefore, as expected, the correct solution is

$$p(x,s|x_0)=\begin{cases}\dfrac{\sinh\left(\sqrt{\frac{s}{D}}\,x\right)\cosh\left[\sqrt{\frac{s}{D}}\,(x_0-L)\right]}{\sqrt{sD}\cosh\left(\sqrt{\frac{s}{D}}L\right)} & \text{for} \quad x<x_0,\\ \dfrac{\sinh\left(\sqrt{\frac{s}{D}}\,x_0\right)\cosh\left[\sqrt{\frac{s}{D}}\,(x-L)\right]}{\sqrt{sD}\cosh\left(\sqrt{\frac{s}{D}}\,L\right)} & \text{for} \quad x>x_0.\end{cases} \tag{5.106}$$

5.6.5 *Survival Probability and Moments of MFPT: Revisited*

Substituting Eq. (5.106) into Eq. (5.52), we compute $S(s|x_0)$ for the current problem, namely,

$$\begin{aligned}S(s|x_0)&=\int_0^L p(x,s|x_0)\,\mathrm{d}x\\&=\frac{1}{\sqrt{sD}\cosh\left(\sqrt{\frac{s}{D}}\,L\right)}\left\{\int_0^{x_0^-}\sinh\left(\sqrt{\frac{s}{D}}\,x\right)\cosh\left[\sqrt{\frac{s}{D}}\,(x_0-L)\right]\mathrm{d}x\right.\\&\qquad\left.+\int_{x_0^+}^{L}\sinh\left(\sqrt{\frac{s}{D}}\,x_0\right)\cosh\left[\sqrt{\frac{s}{D}}\,(x-L)\right]\mathrm{d}x\right\}.\end{aligned} \tag{5.107}$$

Performing the integration, we have

$$\begin{aligned}S(s|x_0)=\frac{1}{s\cosh\left(\sqrt{\frac{s}{D}}\,L\right)}&\left\{\cosh\left(\sqrt{\frac{s}{D}}\,x\right)\cosh\left[\sqrt{\frac{s}{D}}\,(x_0-L)\right]\Big|_0^{x_0^-}\right.\\&\left.+\sinh\left(\sqrt{\frac{s}{D}}\,x_0\right)\sinh\left[\sqrt{\frac{s}{D}}\,(x-L)\right]\Big|_{x_0^+}^{L}\right\}.\end{aligned} \tag{5.108}$$

Substituting the limits, we obtain

$$\begin{aligned}S(s|x_0)=\frac{1}{s\cosh\left(\sqrt{\frac{s}{D}}\,L\right)}&\left\{\left[\cosh\left(\sqrt{\frac{s}{D}}\,x_0\right)-1\right]\cosh\left[\sqrt{\frac{s}{D}}\,(x_0-L)\right]\right.\\&\left.-\sinh\left(\sqrt{\frac{s}{D}}\,x_0\right)\sinh\left[\sqrt{\frac{s}{D}}\,(x_0-L)\right]\right\}.\end{aligned} \tag{5.109}$$

After some simplifications, we arrive at

$$S(s|x_0)=\frac{1}{s}-\frac{\cosh\left[\sqrt{\frac{s}{D}}\,(x_0-L)\right]\operatorname{sech}\left(\sqrt{\frac{s}{D}}\,L\right)}{s}. \tag{5.110}$$

It is worth noting that by using the final limit theorem, from this last expression, we obtain that $S(x_0)$ goes to zero at long times.

Moments of MFPT are computed using Eq. (2.90) after Taylor-expanding Eq. (5.110), namely,

$$S(s|x_0) = \frac{x_0(2L - x_0)}{2D} + \frac{s\, x_0(x_0 - 2L)(4L^2 + 2Lx_0 - x_0^2)}{24D^2} + \cdots \tag{5.111}$$

When evaluating the latter equation and its derivative at $s = 0$, we find the first and second moments of mean first-passage time, i.e.,

$$\langle t(x_0)\rangle = \frac{x_0(2L - x_0)}{2D} \quad \text{and} \quad \langle t^2(x_0)\rangle = \frac{x_0(2L - x_0)(4L^2 + 2Lx_0 - x_0^2)}{12D^2}, \tag{5.112}$$

respectively, which are the expressions we obtained in Sect. 5.6.3, namely, Eq. (5.96).

5.6.6 *First-Passage Time and Splitting Probability: Revisited*

To find the probability density of first-passage time in Laplace's space, we first have to calculate the flux at each boundary. By applying the Laplace transform of the continuity equation, Eq. (5.60), to the solution in Eq. (5.106), we obtain

$$J(0, s|x_0) = \frac{\cosh\left[\sqrt{\frac{s}{D}}\,(x_0 - L)\right]}{\cosh\left(\sqrt{\frac{s}{D}}\,L\right)} \quad \text{and} \quad J(L, s|x_0) = 0. \tag{5.113}$$

Substituting the last results into Eq. (5.63) leads to

$$\varphi(s|x_0) = \frac{\cosh\left[\sqrt{\frac{s}{D}}\,(x_0 - L)\right]}{\cosh\left(\sqrt{\frac{s}{D}}\,L\right)}. \tag{5.114}$$

Finally, the splitting probability is computed as indicated in Eq. (5.66), i.e.,

$$\theta_0(x_0) = 1 \quad \text{and} \quad \theta_L(x_0) = 0, \tag{5.115}$$

which simply corroborates the consistency of the results obtained.

5.7 Partially Absorbing-Reflecting

The description of diffusion between a partially absorbing boundary and a reflecting target in the interval $[0, L]$ requires a combination of the Neumann BC to describe the reflecting point, Eq. (4.69), and the Robin-like BC for the single, partially absorbing target, Eq. (4.87) (see Fig. 5.10). Thus, the diffusion equation, Eq. (2.13), has to be solved within the following constraints:

$$-D\frac{\partial}{\partial x}p(x,t|x_0)\bigg|_{x=0} = \kappa p(0,t|x_0) \quad \text{and} \quad \frac{\partial p(x,t|x_0)}{\partial x}\bigg|_{x=L} = 0, \tag{5.116}$$

defining this boundary-value problem.

It is worth remembering that the partially absorbing boundary or radiation boundary condition may be viewed as a Brownian particle visiting the boundary a certain number of times before it is finally absorbed. On the other hand, as we already know, in the limits when κ goes to infinity and 0, we recover the perfectly absorbing and reflecting boundaries, respectively.

5.7.1 The Separation of Variables Method

Just as in later systems presented in this chapter, the partially absorbing-reflecting system can be solved by means of the spectral representation of the propagator, Eq. (5.5), working first in terms of the eigenfunctions by using Eq. (5.6), i.e.,

$$\phi_n(x) = \mathcal{A}_n \ \sin(\lambda_n x) + \mathcal{B}_n \ \cos(\lambda_n x). \tag{5.6}$$

Invoking the first constraint of Eq. (5.116), i.e., the partially absorbing boundary condition yields

$$\mathcal{B}_n \kappa = \mathcal{A}_n D \lambda_n, \tag{5.117}$$

while the second BC gives

$$\mathcal{A}_n = \mathcal{B}_n \tan(L\lambda_n). \tag{5.118}$$

Fig. 5.10 Schematic representation of a one-dimensional domain with a partially absorbing point at $x = 0$ (yellow circle) and a reflecting target at $x = L$ (blue bar)

By combining the two latter relations, we find

$$\frac{\kappa}{D\lambda_n} = \tan(L\lambda_n), \tag{5.119}$$

which is the main equation to find the correct eigenvalue for our problem.

The dimensionless version of Eq. (5.119) is constructed by defining[4]

$$\lambda_n \equiv \frac{\xi_n}{L}. \tag{5.120}$$

Thus, a new equation arises to find the characteristic values, namely,

$$\frac{\kappa L}{D} = \xi_n \tan(\xi_n) \quad \text{for} \quad n = 1, 2, 3, \ldots \tag{5.121}$$

There are two limits in which approximate solutions of the latter equation can be found: (a) The first is when $\kappa \to \infty$, this makes the right side of Eq. (5.121) tend to infinity and corresponds to the case in which the target is not partially but perfectly absorbent (see Fig. 5.11). In such system, ξ_n is determined as $\xi_n = (2n+1)\pi/2L$. In contrast, (b) the second limit to find an approximate solution is when $\kappa \to 0$, which means that the particle has only a slight change of being absorbed. For the ideal case, where $\kappa = 0$, we should be describing the reflecting-reflecting system with $\xi_n = n\pi/L$. Following this reasoning, the eigenvalues of our present problem must be within the eigenvalues associated with the reflecting-reflecting system and the eigenvalues for the absorbing-reflecting system. Additionally, the eigenvalue we are looking for is close to zero since κ is close to being null as well. Therefore, the first eigenvalue κ and ξ_1 are small, i.e., $\tan\ x \approx x$; then, Eq. (5.121) becomes

$$\xi_1^2 = \frac{\kappa L}{D} \tag{5.122}$$

meaning that Eq. (5.120) is now

$$\lambda_1 = \sqrt{\frac{\kappa}{LD}}. \tag{5.123}$$

For higher eigenvalues, (5.121) should be small, and since ξ_n may not always be a small number for $n \geq 2$, then $\tan(\xi n)$ must be, so to contra rest this effect. By knowing that $\tan(\xi_n)$ is zero in any integer multiple of π, then ξ_n must be

[4] To understand which possible values of ξ_n are available when changing variables, we appeal to Eq. (5.85), meaning that for the absorbing-reflecting system, $\xi_n = (2n+1)\pi$.

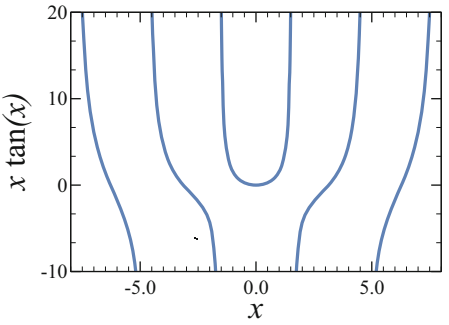

Fig. 5.11 Representative plots of Eq. (5.121) for the behavior of the curve $x\tan(x)$, which tends to infinity on every $\pm(2n+1)/2$ with n being an integer

slightly different from that value, and such perturbation will be denoted by γ_n. This statement leads to the following proposal:[5]

$$\xi_n = (n-1)\pi + \gamma_n, \quad \text{for} \quad n = 2, 3, 4, \ldots \tag{5.124}$$

Substituting the latter equation into Eq. (5.121), we obtain

$$[(n-1)\pi + \gamma_n]\tan[(n-1)\pi + \gamma_n] = \frac{\kappa L}{D}, \tag{5.125}$$

a relation that can be approximated as[6]

$$(n-1)\pi\gamma_n \approx \frac{\kappa L}{D}. \tag{5.127}$$

Solving for γ_n yields

$$\gamma_n = \frac{\kappa L}{(n-1)\pi D}, \tag{5.128}$$

which is indeed small for $n \geq 2$. Consequently, the higher eigenvalues are approximated as

$$\lambda_n = \frac{\xi_n}{L} \approx \frac{(n-1)\pi}{L}. \tag{5.129}$$

[5] Notice that in this case, n starts at $n = 2$ instead of $n = 1$, because the solution of the very first eigenvalue is small enough to be determined with Eq. (5.123).

[6] Unlike the fundamental period of functions sine and cosine, the tangent and the cotangent functions have fundamental period of π, meaning that for any integer n,

$$\tan x = \tan(x + n\pi). \tag{5.126}$$

To find the eigenfunctions ϕ_n, instead of a linear combination of trigonometric functions, we propose a cosine function,

$$\phi_n(x) = \mathcal{A}_n \cos(\lambda_n x - \alpha_n) = \mathcal{A}_n \cos\left[\frac{(n-1)\pi x}{L} - \alpha_n\right] \tag{5.130}$$

According to (5.119), α_n can be computed using the tangent and the eigenvalues just found. Thus,

$$\tan\alpha_1 \approx \sqrt{\frac{\kappa L}{D}} \quad \text{and} \quad \tan\alpha_n \approx \frac{\kappa L}{(n-1)\pi D} \quad \text{for} \quad n = 2, 3, 4, \ldots \tag{5.131}$$

Since $\kappa L/D$ is small, the angle α_n can be neglected for all n.

$$\begin{aligned}\phi_1(x) &= \mathcal{A}_1 \cos\left(\sqrt{\frac{\kappa}{LD}}x\right) \approx \mathcal{A}_1,\\ \phi_n(x) &= \mathcal{A}_n \cos\left[\frac{(n-1)\pi x}{L}\right] \quad \text{for} \quad n = 2, 3, 4, \ldots\end{aligned} \tag{5.132}$$

Therefore, the propagator of the partially absorbent-reflecting system, using Eq. (5.5) together with Eqs. (5.123) and (5.129), reads

$$\begin{aligned}p(x,t|x_0) &\approx \mathcal{A}_1 \exp\left(-\lambda_1^2 Dt\right) + \sum_{n=2}^{\infty} \mathcal{A}_n \cos\left[\frac{(n-1)\pi x}{L}\right] \exp\left(-\lambda_n^2 Dt\right)\\ &= \mathcal{A}_1 \exp\left(-\frac{\kappa}{L}t\right) + \sum_{n=2}^{\infty} \mathcal{A}_n \cos\left[\frac{(n-1)\pi x}{L}\right] \exp\left[-\frac{(n-1)^2\pi^2}{L^2} Dt\right].\end{aligned} \tag{5.133}$$

The second term of the latter equation is very similar to Eq. (5.21), so the aftermath of the initial condition being $\delta(x - x_0)$ is computed straightforward, leading to

$$\begin{aligned}p(x,t|x_0) \approx \frac{\exp\left(-\frac{\kappa}{L}t\right)}{L} + \frac{2}{L}\sum_{n=2}^{\infty} \exp\left[-\frac{(n-1)^2\pi^2}{L^2} Dt\right] \cos\left[\frac{(n-1)\pi x_0}{L}\right]\\ \times \cos\left[\frac{(n-1)\pi x}{L}\right].\end{aligned} \tag{5.134}$$

Representative plots of the time evolution of the propagator in Eq. (5.134), using a permeability of $\kappa = 0.2$, are depicted in Fig. 5.12. We can see that the propagator's behavior is similar to the solution of the absorbing-absorbing system, as we expected, since replacing an absorbing endpoint by a reflecting target is equivalent

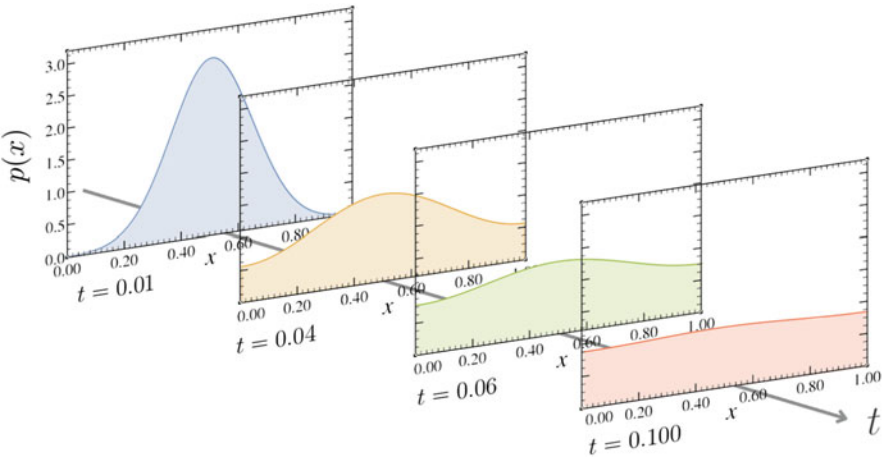

Fig. 5.12 Time evolution of the probability distribution, Eq. (5.134), with a trapping rate $\kappa = 0.2$. The starting position of the particle is set at $x_0 = 0.5$, the length is $L = 1$, and the diffusion coefficient is $D = 1$

to increase the space domain when dealing with the diffusion between two absorbing walls, as the reader will see in the following sections.

5.7.2 *Survival Probability and First-Passage Time*

The survival probability $S(t|x_0)$ is calculated by integrating Eq. (5.134) along $[0, L]$, i.e.,

$$S(t|x_0) \approx \int_0^L \frac{\exp\left(-\frac{\kappa}{L}t\right)}{L}\,\mathrm{d}x + \frac{2}{L}\sum_{n=2}^{\infty}\exp\left[-\frac{(n-1)^2\pi^2}{L^2}Dt\right]\cos\left[\frac{(n-1)\pi x_0}{L}\right] \times \int_0^L \cos\left[\frac{(n-1)\pi x}{L}\right]\mathrm{d}x. \tag{5.135}$$

The second integral is identically zero, making the first term the only contribution, which leads to

$$S(t|x_0) \approx \exp\left(-\frac{\kappa t}{L}\right). \tag{5.136}$$

If we set $\kappa = 0$ in the latter equation, the survival probability for the reflecting-reflecting system is recovered, i.e., $S(t|x_0) = 1$. If we identify $1/L = p_{eq}(0)$, consequently,

$$S(t|x_0) \approx e^{-\kappa\, p_{eq}(0) t}. \tag{5.137}$$

Then, the decay rate is determined by the equilibrium density at the partially absorbing end target. It is worthwhile to mention that the argument of the exponential is the flux at steady state at the absorbing end.

On the other hand, the probability density of first-passage time is

$$\varphi(t|x_0) = -\frac{\mathrm{d}S(t|x_0)}{\mathrm{d}t} \approx \frac{\kappa}{L}\exp\left(-\frac{\kappa t}{L}\right), \tag{5.138}$$

which reduces to Eq. (4.86) when $\kappa = 0$. Plots of Eqs. (5.136) and (5.138) for different values of the constant κ are presented in Fig. 5.14.

5.7.3 Moments of MFPT and Splitting Probability

Moments for mean first-passage time can be computed either with Eq. (2.41) or with Eq. (2.52). Using the survival probability for the first moment, we have that

$$\langle t(x_0)\rangle \approx \int_0^\infty \exp\left(-\frac{kt}{L}\right)\mathrm{d}t = -\frac{L}{\kappa}\exp\left(-\frac{\kappa t}{L}\right)\Big|_0^\infty, \tag{5.139}$$

$$\langle t(x_0)\rangle \approx \frac{L}{\kappa}. \tag{5.140}$$

The second moment is

$$\langle t^2(x_0)\rangle \approx 2\int_0^\infty t\exp\left(-\frac{\kappa t}{L}\right)\mathrm{d}t, \tag{5.141}$$

which is integrated by parts, i.e.,

$$\begin{aligned}\langle t^2(x_0)\rangle &\approx 2\left[-\frac{Lt}{\kappa}\exp\left(-\frac{\kappa t}{L}\right)\Big|_0^\infty + \frac{L}{\kappa}\int_0^\infty \exp\left(-\frac{\kappa t}{L}\right)\mathrm{d}t\right] \\ &\approx \frac{2L^2}{\kappa^2}.\end{aligned} \tag{5.142}$$

The splitting probability is found through Eq. (2.95).

$$\theta_{x'}(x_0) = -D\,\frac{\partial}{\partial x}\int_0^\infty p(x,t|x_0)\,\mathrm{d}t\Big|_{x=x'}. \tag{2.95}$$

Just by looking at such expression, knowing that we can interchange the order of the differential operators,[7] we can conclude that

$$\theta_0(x_0) = 0 \quad \text{and} \quad \theta_L(x_0) = 0. \tag{5.143}$$

The reader may notice that $S(t|x_0)$ and $\varphi(t|x_0)$, together with all moments $\langle t^n(x_0)\rangle$, are independent of the initial position x_0! Evidently, the preceding method is not accurate physically speaking, why? The mathematical requirement of having a small value for the eigenvalue, which is a recurrent feature in our approximations, translates into the property of having a small absorbing rate in the system, characterizing the diffusion process with a much greater relaxation time that the commonly L^2/D. This solution works perfectly for a partially absorbing target that has low interaction with Brownian particles, i.e., we are dealing more with a reflecting target rather than with a partially absorbing endpoint.

In the following section, we will approach the same problem using Laplace transforms to show the great advantage of this method.

If a particle hits the wall at $x = 0$, there's only a slight change of being absorbed.

5.7.4 The Laplace Transform Solution

Since the results for the moments of mean first-passage time and splitting probability, Eqs. (5.140), (5.142), and (5.143), are physically inaccurate, we intend to obtain a better answer through the Laplace transforms.

To solve this problem by means of the Laplace transform technique, we use the subsidiary equation, Eq. (3.36), which needs to be solved considering the Laplace transform of the BCs, Eq. (5.116), as follows:

$$D\left.\frac{\partial p(x,s|x_0)}{\partial x}\right|_{x=0} = \kappa\ p(0,s|x_0) \quad \text{and} \quad \left.\frac{\partial p(x,s|x_0)}{\partial x}\right|_{x=L} = 0. \tag{5.144}$$

Since the propagator must describe the trapping rate on the left-hand side, $x < x_0$, and the zero flux property for the right-hand side, $x > x_0$, let us work with the following general solution:[8]

[7] In this case, we take the derivative with respect to x and then the integral in time t.

[8] In Eq. (5.145), we added a phase L to the solution for the right-hand side of the domain. This modification was helpful to obtain Eqs. (5.23) and (5.27), when imposing hyperbolic functions in the description of a reflecting point at $x = L$.

$$p(x,s|x_0) = \begin{cases} \mathcal{A}\sinh\left[\sqrt{\frac{s}{D}}\,(x-x_\theta)\right] & \text{for} \quad x < x_0, \\ \mathcal{B}\cosh\left[\sqrt{\frac{s}{D}}\,(x-L)\right] & \text{for} \quad x > x_0, \end{cases} \tag{5.145}$$

By applying the BC for the partially absorbing endpoint to the left-hand side solution, we find an equation for phase x_θ, which is

$$\mathcal{A}\sqrt{Ds}\cosh\left(\sqrt{\frac{s}{D}}\,x_\theta\right) = -\kappa\mathcal{A}\sinh\left(\sqrt{\frac{s}{D}}\,x_\theta\right) \tag{5.146}$$

yielding

$$x_\theta = -\sqrt{\frac{D}{s}}\,\operatorname{arctanh}\left(\frac{\sqrt{sD}}{k}\right). \tag{5.147}$$

From this last equation, we can verify that if $\kappa \to \infty$, then $x_\theta = 0$. Consequently, we obtain the solution for the absorbing-reflecting system for $x < x_0$, i.e., $\mathcal{A}\sinh\left(\sqrt{\frac{s}{D}}\,x\right)$.

By applying the continuity condition, given by Eq. (3.39), as well as the discontinuity condition in Eq. (3.42), to Eq. (5.145), we find a system of equations that may be used to determine constants $\mathcal{A}$ and $\mathcal{B}$, given by

$$\mathcal{A}\sinh\left[\sqrt{\frac{s}{D}}\,(x_0-x_\theta)\right] = \mathcal{B}\cosh\left[\sqrt{\frac{s}{D}}\,(x_0-L)\right] \quad \text{and} \tag{5.148}$$

$$\sqrt{\frac{s}{D}}\left\{\mathcal{B}\sinh\left[\sqrt{\frac{s}{D}}\,(x_0-L)\right] - \mathcal{A}\cosh\left[\sqrt{\frac{s}{D}}\,(x_0-x_\theta)\right]\right\} = -\frac{1}{D}. \tag{5.149}$$

Solving this system of equations, we have

$$\mathcal{A} = \frac{\cosh\left[\sqrt{\frac{s}{D}}\,(x_0-L)\right]}{\sqrt{sD}\cosh\left[\sqrt{\frac{s}{D}}\,(x_\theta-L)\right]} \quad \text{and} \quad \mathcal{B} = \frac{\sinh\left[\sqrt{\frac{s}{D}}\,(x_0-x_\theta)\right]}{\sqrt{sD}\cosh\left[\sqrt{\frac{s}{D}}\,(x_\theta-L)\right]}. \tag{5.150}$$

Thus, the solution of the propagator in the Laplace space is

$$p(x,s|x_0) = \begin{cases} \dfrac{\cosh\left[\sqrt{\frac{s}{D}}\,(x_0-L)\right]\sinh\left[\sqrt{\frac{s}{D}}\,(x-x_\theta)\right]}{\sqrt{sD}\cosh\left[\sqrt{\frac{s}{D}}\,(x_\theta-L)\right]} & \text{for} \quad x < x_0 \\ \dfrac{\cosh\left[\sqrt{\frac{s}{D}}\,(x-L)\right]\sinh\left[\sqrt{\frac{s}{D}}\,(x_0-x_\theta)\right]}{\sqrt{sD}\cosh\left[\sqrt{\frac{s}{D}}\,(x_\theta-L)\right]} & \text{for} \quad x > x_0. \end{cases} \tag{5.151}$$

Representative plots of the propagator in real space are shown in Fig. 5.13.

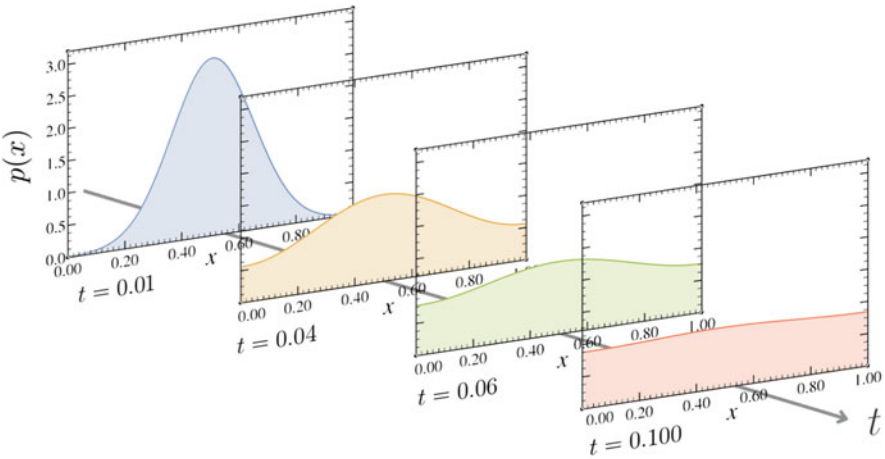

Fig. 5.13 Time evolution of the probability distribution, Eq. (5.151), with a trapping rate $\kappa = 0.2$. The starting position of the particle is set at $x_0 = 0.5$, the length is $L = 1$, and the diffusion coefficient is $D = 1$

5.7.5 *Survival Probability and Moments of MFPT*

To calculate the survival probability in the Laplace space, we substitute the propagator given by Eq. (5.151) into Eq. (5.52), leading to

$$\begin{aligned} S(s|x_0) &= \int_0^L p(x, s|x_0)\, \mathrm{d}x \\ &= \frac{1}{\sqrt{sD}\cosh\left[\sqrt{\frac{s}{D}}\,(x_\theta - L)\right]} \\ &\quad \times \left\{ \int_0^{x_0^-} \cosh\left[\sqrt{\frac{s}{D}}\,(x_0 - L)\right] \sinh\left[\sqrt{\frac{s}{D}}\,(x - x_\theta)\right] \mathrm{d}x \right. \\ &\quad \left. + \int_{x_0^+}^L \cosh\left[\sqrt{\frac{s}{D}}\,(x - L)\right] \sinh\left[\sqrt{\frac{s}{D}}\,(x_0 - x_\theta)\right] \mathrm{d}x \right\}. \end{aligned} \tag{5.152}$$

After integration and evaluation, we obtain

$$S(s|x_0) = \frac{1}{s} - \frac{\cosh\left[\sqrt{\frac{s}{D}}\,(L + x_\theta - x_0)\right] + \cosh\left[\sqrt{\frac{s}{D}}\,(x_0 + x_\theta - L)\right]}{2s\cosh\left[\sqrt{\frac{s}{D}}\,(x_\theta - L)\right]}. \tag{5.153}$$

Now, if we substitute the explicit expression for x_θ given by Eq. (5.147), we arrive at the following result:

$$S(s|x_0) = \frac{1}{s} - \frac{\kappa \cosh\left[\sqrt{\frac{s}{D}}\,(L - x_0)\right]}{s\left[\kappa \cosh\left(\sqrt{\frac{s}{D}}\,L\right) + \sqrt{sD}\sinh\left(\sqrt{\frac{s}{D}}\,L\right)\right]}. \tag{5.154}$$

The survival probability in real space is obtained numerically by means of the Gaver-Stehfest method. The result is depicted in Fig. 5.14.[9]

Moments of mean first-passage time are computed using Eq. (2.90). First, we Taylor-expand the survival probability $S(s|x_0)$, leading to

$$S(s|x_0) = \frac{L}{\kappa} + \frac{x_0(2L - x_0)}{2D} - \left[\frac{L^2}{\kappa^2} + \frac{L(2L^2 + 6Lx_0 - 3x_0^2)}{6D\kappa} + \frac{8L^3x_0 - 4Lx_0^3 + x_0^4}{24D^2}\right]s + \cdots \tag{5.155}$$

Thus, when evaluating the last expression at $s = 0$, we obtain the first moment of MFPT, namely,

$$\langle t(x_0)\rangle = \frac{x_0(2L - x_0)}{2D} + \frac{L}{\kappa}. \tag{5.156}$$

Using this equation, we can recover the result obtained for MFPT for the absorbing-reflecting system by setting $\kappa \to \infty$.

It is worth noting that when $x_0 = 0$, the MFPT reduces to

$$\langle t(x_0 = 0)\rangle = \frac{L}{\kappa}. \tag{5.157}$$

This result tells us that once the particle reaches the partially absorbing boundary for the first time, it has to keep visiting it a mean time L/κ before being trapped. Now, with this interpretation in hand, a quick glance of Eq. (5.156) shows that the MFPT for the partially absorbing-reflecting system is given by the sum of two terms with a clear interpretation. From the first term, we have the mean time that it takes the particle to reach the partially absorbing boundary for the first time. Then, we have the mean time that the particle spends repeatedly returning to this boundary, until it becomes trapped. It is important to note that Eq. (5.156) predicts that when $\kappa \to \infty$, the particle is absorbed on the first attempt.

The second moment of MFPT is computed by taking the second derivative of the survival probability, i.e.,

$$\langle t^2(x_0)\rangle = \frac{24D^2L^2 + 4DL\kappa(2L^2 + 6Lx_0 - 3x_0^2) + x_0\kappa^2(8L^3 - 4Lx_0^2 + x_0^3)}{12D^2\kappa^2}. \tag{5.158}$$

[9] See Appendix 5.A for further details on the numerical Laplace inversion.

This expression reduces to the well-known result corresponding to the absorbing-reflecting system when setting the limit $\kappa \to \infty$.

5.7.6 *Density of Mean First-Passage Time and Splitting Probability*

Now, we compute the flux at x_0 by substituting the propagator given by Eq. (5.151) into Eq. (5.60), finding that

$$J(0, s|x_0) = \frac{\cosh\left[\sqrt{\frac{s}{D}}\,(x_0 - L)\right]\cosh\left[\sqrt{\frac{s}{D}}\,x_\theta\right]}{\cosh\left[\sqrt{\frac{s}{D}}\,(x_\theta - L)\right]}. \tag{5.159}$$

Using the last results in Eq. (5.63) to obtain the probability density of first-passage time, we obtain

$$\phi(s|x_0) = \frac{\cosh\left[\sqrt{\frac{s}{D}}\,(x_0 - L)\right]\cosh\left[\sqrt{\frac{s}{D}}\,x_\theta\right]}{\cosh\left[\sqrt{\frac{s}{D}}\,(x_\theta - L)\right]}. \tag{5.160}$$

Representative plots of $\varphi(t|x_0)$ are obtained numerically and shown in Fig. 5.14.[10]

The splitting probability is found through Eq. (5.66). Consequently, expanding the flux in Eq. (5.159) in power series in s, and setting $s = 0$ lead to

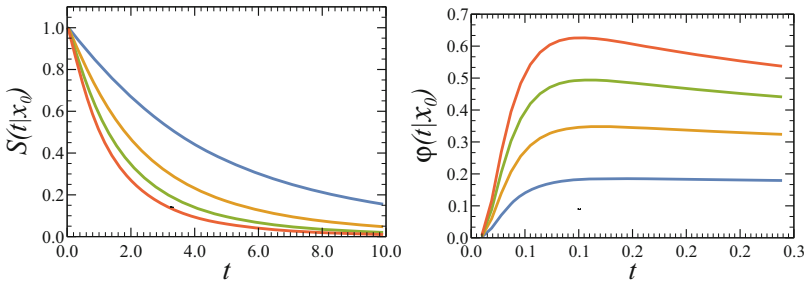

Fig. 5.14 Schematic representation of survival probability, Eq. (5.154), and the probability density of first-passage time, Eq. (5.160), for different values of the trapping rate κ: $\kappa = 0.2$ (blue line), $\kappa = 0.4$ (yellow line), $\kappa = 0.6$ (green line), and $\kappa = 0.8$ (orange line). The starting position of the particles is set at $x_0 = 0.5$, the length is $L = 1$, and the diffusion coefficient is $D = 1$

[10] See Appendix 5.A for further details on the numerical Laplace inversion.

$$\theta_0(x_0) = 1 \quad \text{and} \quad \theta_L(x_0) = 0. \tag{5.161}$$

These results are obtained for the sole purpose of showing consistency between our results.

5.8 Absorbing-Partially Absorbing

Consider a Brownian particle diffusing along a finite domain in the presence of a perfectly absorbing end at $x = 0$ and a partially absorbing one at $x = L$, as shown in Fig. 5.15. The mathematical BCs for this system are a combination of a Dirichlet BC and a Neumann BC, Eqs. (4.27) for $x = 0$ and (4.87) for $x = L$. Consequently,

$$p(0, t|x_0) = 0 \quad \text{and} \quad -D\frac{\partial p(x, t|x_0)}{\partial x}\bigg|_{x=L} = \kappa\ p(L, t|x_0). \tag{5.162}$$

In this case, $\hat{\mathbf{n}} = -\hat{\mathbf{e}}_i$ at $x = L$, since the unit normal vector to the partially absorbing boundary points westward.

5.8.1 The Laplace Transform Solution

This system will be solved using the Laplace method, as done for all other systems mentioned earlier in this chapter. Then, we invoke again the subsidiary equation for the diffusion equation, i.e.,

$$s\ p(x, s|x_0) - \delta(x - x_0) = D\frac{\partial^2 p(x, s|x_0)}{\partial x^2}, \tag{3.36}$$

subject to the transformed BCs, namely,

$$p(0, s|x_0) = 0, \quad \text{and} \quad -D\frac{\partial p(x, s|x_0)}{\partial x}\bigg|_{x=L} = \kappa p(L, s|x_0). \tag{5.163}$$

Because the propagator has to be identical to zero at $x = 0$, and based on the experience we have accumulated so far in proposing solutions in this chapter, let's propose the following solution in the Laplace space:

Fig. 5.15 Schematic representation of a one-dimensional domain with a perfectly absorbing point at $x = 0$ (red circle) and a partially absorbing end at $x = L$ (yellow circle)

$$p(x,s|x_0) = \begin{cases} \mathcal{A}\sinh\left(\sqrt{\frac{s}{D}}\,x\right), & \text{for} \quad x < x_0 \\ \mathcal{B}\sinh\left[\sqrt{\frac{s}{D}}\,(x-x_\theta)\right], & \text{for} \quad x > x_0. \end{cases} \tag{5.164}$$

We can obtain x_θ by imposing the BC on the solution for the region $x > x_0$. In this process, we find that

$$-\mathcal{B}\sqrt{Ds}\cosh\left[\sqrt{\frac{s}{D}}\,(L-x_\theta)\right] = \kappa\mathcal{B}\sinh\left[\sqrt{\frac{s}{D}}\,(L-x_\theta)\right], \tag{5.165}$$

leading to

$$x_\theta = L + \sqrt{\frac{D}{s}}\,\text{arctanh}\left(\frac{\sqrt{sD}}{\kappa}\right). \tag{5.166}$$

Note that if κ tends to infinity, $x_\theta = L$, and the solution in Eq. (5.164) reduces to the solution of the absorbing-absorbing system in the Laplace space, Eq. (5.47).

Now, imposing the continuity condition, given by Eq. (3.39), translates into

$$\mathcal{A}\sinh\left(\sqrt{\frac{s}{D}}\,x_0\right) = \mathcal{B}\sinh\left[\sqrt{\frac{s}{D}}\,(x_0-x_\theta)\right], \tag{5.167}$$

and imposing the discontinuity condition at $x = x_0$, given by Eq. (3.42), yields

$$\sqrt{\frac{s}{D}}\left\{\mathcal{B}\cosh\left[\sqrt{\frac{s}{D}}\,(x_0-x_\theta)\right] - \mathcal{A}\cosh\left(\sqrt{\frac{s}{D}}\,x_0\right)\right\} = -\frac{1}{D}. \tag{5.168}$$

Using the last two equations, we can calculate constants $\mathcal{A}$ and $\mathcal{B}$, finding the following solutions:

$$\mathcal{A} = -\frac{\sinh\left[\sqrt{\frac{s}{D}}\,(x_0-x_\theta)\right]}{\sqrt{sD}\sinh\left(\sqrt{\frac{s}{D}}\,x_\theta\right)} \quad \text{and} \quad \mathcal{B} = -\frac{\sinh\left(\sqrt{\frac{s}{D}}\,x_0\right)}{\sqrt{sD}\sinh\left(\sqrt{\frac{s}{D}}\,x_\theta\right)}. \tag{5.169}$$

Therefore, the propagator is

$$p(x,s|x_0) = \begin{cases} -\frac{\sinh\left(\sqrt{\frac{s}{D}}\,x\right)\sinh\left[\sqrt{\frac{s}{D}}\,(x_0-x_\theta)\right]}{\sqrt{sD}\sinh\left(\sqrt{\frac{s}{D}}\,x_\theta\right)} & \text{for} \quad x < x_0, \\ -\frac{\sinh\left(\sqrt{\frac{s}{D}}\,x_0\right)\sinh\left[\sqrt{\frac{s}{D}}\,(x-x_\theta)\right]}{\sqrt{sD}\sinh\left(\sqrt{\frac{s}{D}}\,x_\theta\right)} & \text{for} \quad x > x_0. \end{cases} \tag{5.170}$$

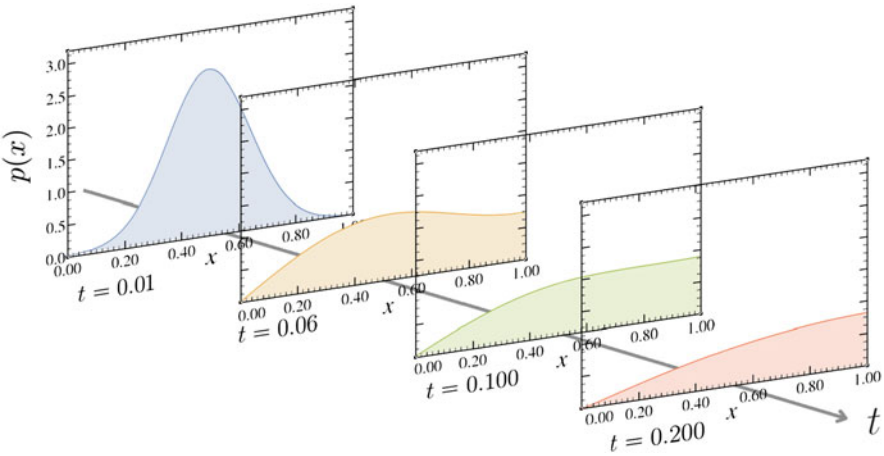

Fig. 5.16 Time evolution of the propagator $p(x, t|x_0)$ of the absorbing-partially absorbing system, obtained by the numerical inversion of Eq. (5.170) at different times. The initial position, system length, diffusivity, and trapping rate are $x_0 = 0.5$, $L = 1$, $D = 1$, and $\kappa = 0.5$, respectively

The reader can directly verify that the latter solution obeys the subsidiary equation, Eq. (3.36), which is the Laplace transform of the diffusion equation, in both regions. Since computing the inverse Laplace transform of Eq. (5.170) is quite complicated, we invert Laplace transform $p(x, s|x_0)$ numerically.[11] In Fig. 5.16, we show the time evolution of the propagator in real space.

5.8.2 *Survival Probability and Moments of First-Passage Time*

To calculate the survival probability in the Laplace space, we introduce Eq. (5.170) into Eq. (5.52), which gives

$$\begin{aligned} S(s|x_0) &= \int_0^L p(x, s|x_0)\, \mathrm{d}x \\ &= -\frac{1}{\sqrt{sD}\sinh\left(\sqrt{\frac{s}{D}}\, x_\theta\right)} \left\{ \int_0^{x_0^-} \sinh\left(\sqrt{\frac{s}{D}}\, x\right) \sinh\left[\sqrt{\frac{s}{D}}\, (x_0 - x_\theta)\right] \mathrm{d}x \right. \\ &\qquad \left. + \int_{x_0^+}^L \sinh\left(\sqrt{\frac{s}{D}}\, x_0\right) \sinh\left[\sqrt{\frac{s}{D}}\, (x - x_\theta)\right] \mathrm{d}x \right\}. \end{aligned} \tag{5.171}$$

[11] See Appendix 5.A for further details on the numerical Laplace inversion.

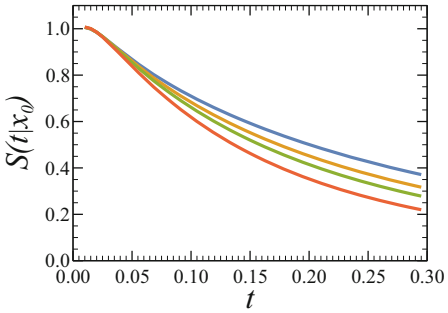

Fig. 5.17 Survival probability $S(t|x_0)$ of the absorbing-partially absorbing system as a function of time, Eq. (5.172), for different values of the trapping rate: $\kappa = 0.2$ (blue), $\kappa = 0.6$ (yellow), $\kappa = 1.0$ (green), and $\kappa = 2.0$ (orange). The initial position, system length, and diffusivity are $x_0 = 0.5$, $L = 1$, and $D = 1$, respectively

After integration and evaluation, we have that

$$S(s|x_0) = \frac{1}{s} + \frac{\sinh\left[\sqrt{\frac{s}{D}}\,(x_0 - x_\theta)\right] - \cosh\left[\sqrt{\frac{s}{D}}\,(L - x_\theta)\right]\sinh\left(\sqrt{\frac{s}{D}}\,x_0\right)}{\sinh\left(\sqrt{\frac{s}{D}}\,x_\theta\right)\,s}. \tag{5.172}$$

The survival probability in real space as a function of time is depicted in Fig. 5.17.

To calculate the moments of MFPT, we have to expand $S(s|x_0)$ in a Taylor series, yielding

$$\begin{aligned} S(s|x_0) &= \frac{x_0\left[\kappa L^2 - x_0(D+\kappa L) + 2DL\right]}{2D(D+\kappa L)} \\ &\quad - \frac{s x_0\left(8D^2L^3 + 5DL^4\kappa + L^5\kappa^2 - 4D^2Lx_0^2 - 6DL^2x_0^2\kappa - 2L^3x_0^2\kappa^2 + D^2x_0^3\right)}{24D^2(D+\kappa L)^2} \\ &\quad - \frac{s x_0\left(2DLx_0^3\kappa + L^2x_0^3\kappa^2\right)}{24D^2(D+\kappa L)^2} + \cdots \end{aligned} \tag{5.173}$$

Introducing Eq. (5.173) into Eq. (2.90), we find that the first and second moments of MFPT are given by

$$\langle t(x_0)\rangle = \frac{x_0\left[\kappa L^2 - x_0(D+\kappa L) + 2DL\right]}{2D(D+\kappa L)} \quad \text{and} \tag{5.174}$$

$$\langle t^2(x_0)\rangle = \frac{L^3 x_0\left(8D^2+5DL\kappa+L^2\kappa^2\right)-2Lx_0^3(D+L\kappa)(2D+L\kappa)+x_0^4(D+L\kappa)^2}{12D^2(D+L\kappa)^2}. \tag{5.175}$$

These results reduce correctly to the first and second moments of mean first-passage time for (a) the absorbing-absorbing system when $\kappa \to \infty$ and (b) the absorbing-reflecting system when $\kappa = 0$.

5.8.3 *Probability Density and Splitting Probability*

To calculate the probability density and the splitting probability, we need to know the flux at the boundaries. From Eqs. (5.60) and (5.170), we have that the fluxes in the Laplace space at the endpoints are

$$J(0,s|x_0) = -\frac{\sinh\left[\sqrt{\frac{s}{D}}\,(x_0-x_\theta)\right]}{\sinh\left(\sqrt{\frac{s}{D}}\,x_\theta\right)} \quad \text{and} \tag{5.176}$$

$$J(L,s|x_0) = \frac{\cosh\left[\sqrt{\frac{s}{D}}\,(L-x_\theta)\right]\sinh\left(\sqrt{\frac{s}{D}}\,x_0\right)}{\sinh\left(\sqrt{\frac{s}{D}}\,x_\theta\right)}. \tag{5.177}$$

If Eq. (5.63) is used to find the probability density of first-passage time in Laplace's space, we find

$$\varphi(s|x_0) = \frac{\cosh\left[\sqrt{\frac{s}{D}}\,(L-x_\theta)\right]\sinh\left(\sqrt{\frac{s}{D}}\,x_0\right)-\sinh\left[\sqrt{\frac{s}{D}}\,(x_0-x_\theta)\right]}{\sinh\left(\sqrt{\frac{s}{D}}\,x_\theta\right)}. \tag{5.178}$$

The schematic representation of Eq. (5.178) is shown in Fig. 5.18.

Finally, the splitting probability of the system is computed through Eq. (5.66). By expanding the corresponding flux in Taylor series, we have

$$J(0,s|x_0) = \left(1-\frac{\kappa x_0}{D+L\kappa}\right) + \frac{sx_0\left[3(D+L\kappa)^2-2L\left(3D^2+3DL\kappa+L^2\kappa^2\right)-x_0^2\kappa(D+L\kappa)\right]}{6D(D+L\kappa)^2}+\cdots \tag{5.179}$$

and

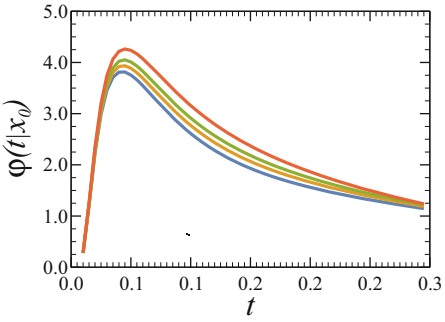

Fig. 5.18 Schematic representation of the probability density of mean first-passage time, Eq. (5.178), for different values of the trapping rate κ: $\kappa = 0.2$ (blue), $\kappa = 0.4$ (yellow), $\kappa = 0.6$ (green), and $\kappa = 1.0$ (orange). The initial position, system length, and diffusivity are $x_0 = 0.5$, $L = 1$, and $D = 1$, respectively

$$J(L, s|x_0) = \frac{\kappa x_0}{D + L\kappa} + \frac{s\left[x_0^3\kappa(D + L\kappa) - L^2\kappa(3D + L\kappa)\right]}{6D(D + L\kappa)^2}, \tag{5.180}$$

and after evaluating these expressions at $s = 0$, we find that

$$\theta_0(x_0) = 1 - \frac{x_0\kappa}{D + L\kappa} \quad \text{and} \quad \theta_L(x_0) = \frac{x_0\kappa}{D + L\kappa}. \tag{5.181}$$

Representative plots of Eq. (5.181) are shown in Fig. 5.19.

5.9 Partially Absorbing-Partially Absorbing

In this section, we describe a diffusing particle in a partially absorbing-partially absorbing system. The technique outlined here is the same one we used in the last two sections. The reader will be able to appreciate the advantage of using the Laplace phase method.

Consider a particle diffusing along the domain $\Omega \in [0, L]$ in the presence of two partially absorbing endpoints, one at $x = -L$ and another one at $x = L$, as shown in Fig. 5.20. The BCs of this system are Neumann BCs, given by

$$\mathbf{J}(x, t|x_0) \cdot \hat{\mathbf{n}}_L\big|_{x=-L} = D\frac{\partial p(x, t|x_0)}{\partial x}\bigg|_{x=-L} = \kappa_L\ p(-L, t|x_0) \quad \text{and}$$

$$\mathbf{J}(L, t|x_0) \cdot \hat{\mathbf{n}}_R\big|_{x=L} = -D\frac{\partial p(x, t|x_0)}{\partial x}\bigg|_{x=L} = \kappa_R\ p(L, t|x_0), \tag{5.182}$$

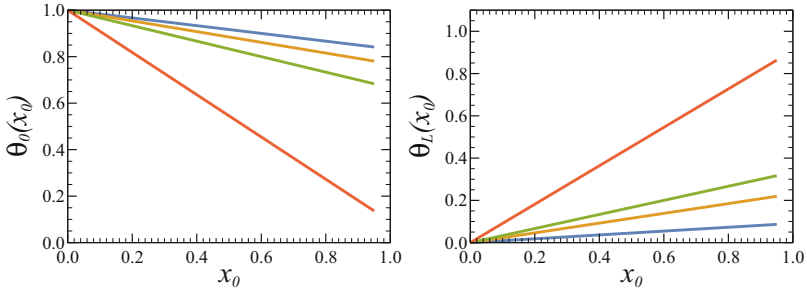

Fig. 5.19 Representative plots of the splitting probability of the absorbing-partially absorbing system, Eq. (5.181), for different values of the trapping rate κ: $\kappa = 0.1$ (blue line), $\kappa = 0.3$ (yellow line), $\kappa = 0.5$ (green line), and $\kappa = 10.0$ (orange line). The system length is $L = 1$, and the diffusion coefficient is $D = 1$

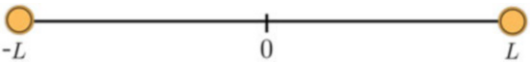

Fig. 5.20 Schematic representation of a one-dimensional domain with two partially absorbing endpoints (yellow circles), one at $x = -L$ and the other at $x = L$

where κ_L and κ_R are the trapping rates associated with the partially absorbing target at $x = -L$ and $x = L$, respectively, and $\hat{\mathbf{n}}_L = -\hat{\mathbf{e}}_i$ and $\hat{\mathbf{n}}_R = \hat{\mathbf{e}}_i$, which represent the unit normal vectors to their respective boundaries.

5.9.1 The Laplace Transform Solution

Again, we approach this problem starting with the subsidiary equation for the diffusion equation, namely,

$$s\ p(x,s|x_0) - \delta(x-x_0) = D\frac{\partial^2 p(x,s|x_0)}{\partial x^2}, \tag{3.36}$$

and the Laplace transform of the BCs in Eq. (5.182), which are given by

$$\begin{aligned} D\frac{\partial p(x,s|x_0)}{\partial x}\bigg|_{x=-L} &= \kappa_L\ p(-L,s|x_0) \quad \text{and} \\ -D\frac{\partial p(x,s|x_0)}{\partial x}\bigg|_{x=L} &= \kappa_R\ p(L,s|x_0). \end{aligned} \tag{5.183}$$

Since we already found the solution for the right-hand side of the absorbing-partially absorbing system, Eq. (5.164), let us assume that the propagator is given by

$$p(x,s|x_0) = \begin{cases} \mathcal{A}\sinh\left[\sqrt{\frac{s}{D}}\,(x-x_\alpha)\right], & \text{for} \quad x < x_0 \\ \mathcal{B}\sinh\left[\sqrt{\frac{s}{D}}\,(x-x_\theta)\right], & \text{for} \quad x > x_0. \end{cases} \tag{5.184}$$

We compute the closed form of x_α and x_θ with the BCs for each of the endpoints the same way we did to find Eqs. (5.147) and (5.166), using the BCs, yielding

$$x_\alpha = -\left[L + \sqrt{\frac{D}{s}}\,\text{arctanh}\left(\frac{\sqrt{sD}}{\kappa_L}\right)\right] \quad \text{and} \quad x_\theta = L + \sqrt{\frac{D}{s}}\,\text{arctanh}\left(\frac{\sqrt{sD}}{\kappa_R}\right). \tag{5.185}$$

On the other hand, constants $\mathcal{A}$ and $\mathcal{B}$ are found using the continuity and discontinuity equations, i.e., Eqs. (3.39) and (3.42), leading to

$$\mathcal{A} = \frac{\sinh\left[\sqrt{\frac{s}{D}}\,(x_0-x_\theta)\right]}{\sqrt{sD}\sinh\left[\sqrt{\frac{s}{D}}\,(x_\alpha-x_\theta)\right]} \quad \text{and} \quad \mathcal{B} = \frac{\sinh\left[\sqrt{\frac{s}{D}}\,(x_0-x_\alpha)\right]}{\sqrt{sD}\sinh\left[\sqrt{\frac{s}{D}}\,(x_\alpha-x_\theta)\right]} \tag{5.186}$$

Therefore, the solution of the propagator in Laplace's space is

$$p(x,s|x_0) = \begin{cases} \frac{\sinh\left[\sqrt{\frac{s}{D}}\,(x_0-x_\theta)\right]}{\sqrt{sD}\sinh\left[\sqrt{\frac{s}{D}}\,(x_\alpha-x_\theta)\right]}\sinh\left[\sqrt{\frac{s}{D}}\,(x-x_\alpha)\right], & \text{for} \quad x < x_0 \\ \frac{\sinh\left[\sqrt{\frac{s}{D}}\,(x_0-x_\alpha)\right]}{\sqrt{sD}\sinh\left[\sqrt{\frac{s}{D}}\,(x_\alpha-x_\theta)\right]}\sinh\left[\sqrt{\frac{s}{D}}\,(x-x_\theta)\right] & \text{for} \quad x > x_0. \end{cases} \tag{5.187}$$

The time evolution of the propagator in real space $p(x,t|x_0)$ is shown in Fig. 5.21.

5.9.2 *Survival Probability and Moments of First-Passage Time*

The survival probability in the Laplace space is obtained by integrating Eq. (5.187) along the entire domain. Then, the survival probability reads

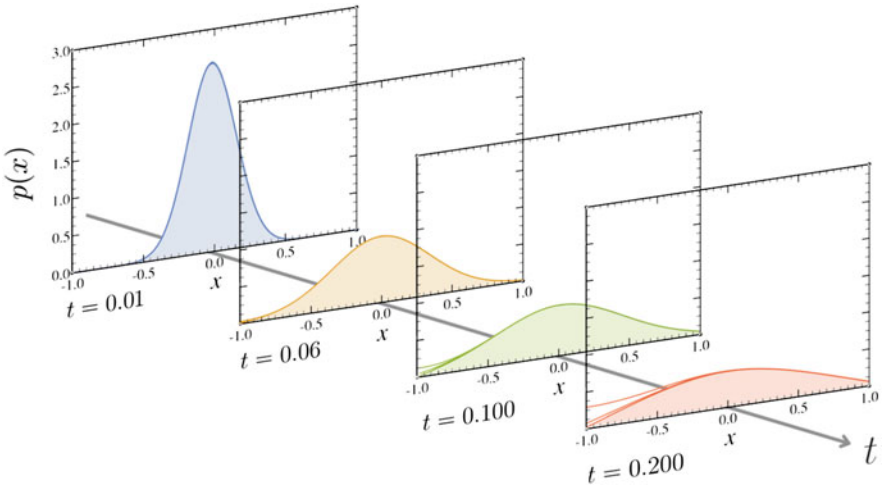

Fig. 5.21 Temporal evolution of the propagator $p(x, t|x_0)$, Eq. (5.187). The trapping rates are $\kappa_L = 0.1,\ 10,\ 100$ and $\kappa_R = 10$. The initial position of Brownian particles, system length, and diffusivity are $x_0 = 0.0$, $L = 1$, and $D = 1$, respectively

$$S(s|x_0) = \int_{-L}^{L} p(x, s|x_0)\ \mathrm{d}x$$

$$= \frac{\sinh\left[\sqrt{\frac{s}{D}}\ (x_0 + L - x_\alpha - x_\theta)\right] + 2\sinh\left[\sqrt{\frac{s}{D}}\ (x_\alpha - x_\theta)\right]}{2s\sinh\left[\sqrt{\frac{s}{D}}\ (x_\alpha - x_\theta)\right]}$$

$$- \frac{\sinh\left[\sqrt{\frac{s}{D}}\ (x_0 + L + x_\alpha - x_\theta)\right] - \sinh\left[\sqrt{\frac{s}{D}}\ (L - x_0 + x_\alpha + x_\theta)\right]}{2s\sinh\left[\sqrt{\frac{s}{D}}\ (x_\alpha - x_\theta)\right]}. \tag{5.188}$$

The first-passage time is calculated first by expanding the latter equation in a Taylor series around $s = 0$ and then setting $s = 0$. This process yields

$$\langle t(x_0)\rangle = \frac{4D^2L + 2L\kappa_L\kappa_R(L^2 - x_0^2) + D\kappa_L(3L - x_0)(L + x_0) + D\kappa_R(L - x_0)(3L + x_0)}{2D\left[D(\kappa_L + \kappa_R) + 2L\,\kappa_L\kappa_R\right]}. \tag{5.189}$$

Representative plots of $S(s|x_0)$ and $\langle t(x_0)\rangle$ in real space are depicted in Fig. 5.22.

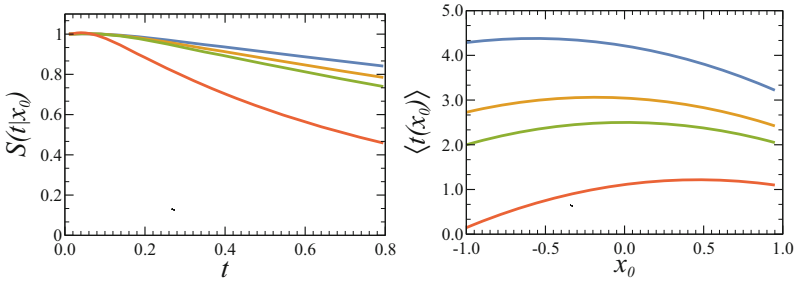

Fig. 5.22 Schematic representation of survival probability, Eq. (5.188), and the first-passage time, Eq. (5.189), for different values of the trapping rate κ_L: $\kappa_L = 0.1$ (blue line), $\kappa_L = 0.3$ (yellow line), $\kappa_L = 0.5$ (green line), $\kappa_L = 10.0$ (orange line), and fixed $\kappa_R = 0.5$. The starting position of the particles is set at $x_0 = 0.0$, the length is $L = 1$, and the diffusion coefficient is $D = 1$

5.9.3 *Probability Density of MFPT and Splitting Probability*

To find the probability density of MFPT, we need to compute the flux at each of the endpoints. By using the Laplace transform of Eq. (5.60), we see that

$$J(-L,s|x_0) = \frac{\cosh\left[\sqrt{\frac{s}{D}}\,(L+x_\alpha)\right]\sinh\left[\sqrt{\frac{s}{D}}\,(x_0-x_\theta)\right]}{\sinh\left[\sqrt{\frac{s}{D}}\,(x_\alpha-x_\theta)\right]} \quad \text{and} \tag{5.190}$$

$$J(L,s|x_0) = \frac{\cosh\left[\sqrt{\frac{s}{D}}\,(L-x_\theta)\right]\sinh\left[\sqrt{\frac{s}{D}}\,(x_0-x_\alpha)\right]}{\sinh\left[\sqrt{\frac{s}{D}}\,(x_\theta-x_\alpha)\right]}. \tag{5.191}$$

Then, using Eq. (5.63), we obtain the probability density of MFPT in Laplace's space, namely,

$$\varphi(s|x_0) = \frac{\cosh\left[\sqrt{\frac{s}{D}}\,(L+x_\alpha)\right]\sinh\left[\sqrt{\frac{s}{D}}\,(x_0-x_\theta)\right]-\cosh\left[\sqrt{\frac{s}{D}}\,(L-x_\theta)\right]\sinh\left[\sqrt{\frac{s}{D}}\,(x_0-x_\alpha)\right]}{\sinh\left[\sqrt{\frac{s}{D}}\,(x_\alpha-x_\theta)\right]}. \tag{5.192}$$

The schematic representation of Eq. (5.192) is shown in Fig. 5.23.

Finally, the splitting probability of the system is obtained by expanding the corresponding flux in a Taylor series, namely,

$$J(L,s|x_0) = \frac{\kappa_L\left[D+\kappa_R(L-x_0)\right]}{D(\kappa_L+\kappa_R+2L\kappa_L\kappa_R)} + \cdots, \tag{5.193}$$

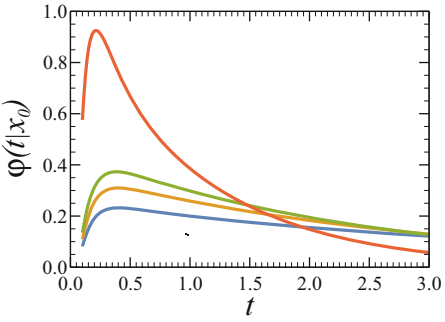

Fig. 5.23 Schematic representation of the probability density of mean first-passage time, Eq. (5.192), for different values of the trapping rate κ_L: $\kappa_L = 0.1$ (blue), $\kappa_L = 0.3$ (yellow), $\kappa_L = 0.5$ (green), and $\kappa_L = 10.0$ (orange) and fixed $\kappa_R = 0.5$. The initial position, system length, and diffusivity are $x_0 = 0.0$, $L = 1$, and $D = 1$, respectively

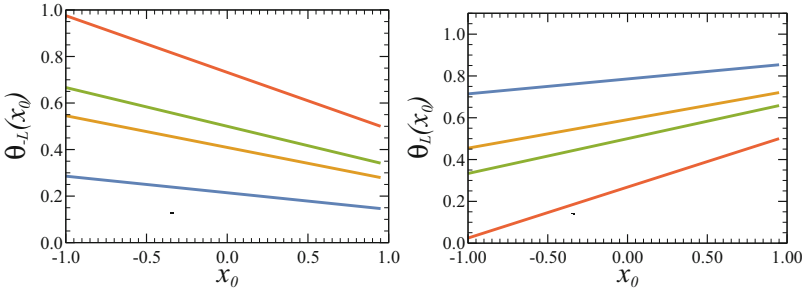

Fig. 5.24 Characteristic plots of the splitting probability, Eqs. (5.195), for different values of the trapping rate κ_L: $\kappa_L = 0.1$ (blue line), $\kappa_L = 0.3$ (yellow line), $\kappa_L = 0.5$ (green line), $\kappa_L = 10.0$ (orange line), and fixed $\kappa_R = 0.5$. The system length is $L = 1$, and the diffusion coefficient is $D = 1$

and

$$J(-L, s|x_0) = \frac{\kappa_R\,[D + \kappa_L(L + x_0)]}{D(\kappa_L + \kappa_R) + 2L\kappa_L\kappa_R} + \cdots . \tag{5.194}$$

Therefore, the splitting probability is

$$\theta_{-L}(x_0) = \frac{\kappa_L\,[D + \kappa_R(L - x_0)]}{D(\kappa_L + \kappa_R + 2L\kappa_L\kappa_R)} \quad \text{and} \quad \theta_L = \frac{\kappa_R\,[D + \kappa_L(L + x_0)]}{D(\kappa_L + \kappa_R) + 2L\kappa_L\kappa_R}. \tag{5.195}$$

If we want to recover the physical results of simpler systems, we need to study the limit cases of one or both of the trapping rates κ_L and κ_R after making the transformation $x_0 \to (L - x_0)$ and $L \to L/2$. For instance, we could recover the splitting probability for the absorbing-partially absorbing system by making $\kappa_L \to \infty$ in Eqs. (5.195). Characteristic plots of θ_{-L} and θ_L are shown in Fig. 5.24.

5.10 Concluding Remarks

In this chapter, we extensively solved the diffusion equation in one dimension, when diffusion takes place in a finite domain, by means of the separation of variables method and the Laplace transform technique. One of the things we learned is that it is generally more practical to use the Laplace transform rather than the Fourier transform, because the propagator may be expressed as a single function instead of an infinite series. On the other hand, the huge advantage of using the separation of variables method is that the propagator is obtained in the time domain. In contrast, it is rarely possible to invert an equation from Laplace's space to time. Nevertheless, we can use numerical methods to make this inversion, such as the Gaver-Stehfest method.

Although we solved all the possible boundary condition combinations, in order to extensively discuss each of their physical properties, we can ultimately summarize all our solutions in the one obtained in Sect. 5.9 for the partially absorbing-partially absorbing system.

5.A Numerical Laplace Inversion: Gaver-Stehfest Method

As the reader may already know, and from our experience in Chap. 5, the Laplace transform plays a significant role in mathematical applications and physics. Moreover, it is a powerful tool for solving and analyzing linear differential equations. Unfortunately, it is oftentimes impossible to analytically find the inverse Laplace transform function, thereby necessitating a numerical approach. There are several numerical algorithms in the literature, and each individual method has its own applications and is suitable for particular types of functions. In this book, we use a very robust approximation, the so-called Gaver-Stehfest method.

In order to accomplish a numerical Laplace inversion, we define a new complex variable $z \equiv st$ and rewrite the Bromwich integral, i.e.,

$$f(t) = \mathcal{L}^{-1}\{\hat{f}(s)\} = \frac{1}{2\pi i} \lim_{T\to\infty} \int_{\gamma-iT}^{\gamma+iT} \mathrm{e}^{st}\ \hat{f}(s)\ \mathrm{d}s, \tag{A.54}$$

as follows:

$$f(t) = \frac{1}{2\pi i t} \lim_{T\to\infty} \int_{\gamma-iT}^{\gamma+iT} \hat{f}\left(\frac{z}{t}\right) \mathrm{e}^{z}\ \mathrm{d}z. \tag{5.196}$$

Now, we approximate the exponential as a rational function

$$\mathrm{e}^{z} \approx \sum_{k=0}^{n} \frac{w_k}{\alpha_k - z}, \tag{5.197}$$

where w_k and α_k are complex numbers, called weights and nodes, respectively. Substituting this approximation into Eq. (5.197), and applying the Cauchy integral formula given by Eq. (3.123), yields

$$f(t) \approx \frac{1}{t} \sum_{k=0}^{n} w_k \, \hat{f}\left(\frac{\alpha_k}{t}\right). \tag{5.198}$$

This last equation approximates the inverse Laplace transform by a linear combination of transform values.

The Gaver-Stehfest approximation is based on a probabilistic derivation and considers the case where $f(t)$ is real-valued and weights and nodes are real. Finally, this algorithm approximates the time domain solution given by Eq. (5.198), using the following equation:

$$f(t) = \frac{\ln(2)}{t} \sum_{k=1}^{n} w_k \, \hat{f}\left(\frac{\alpha_k}{t}\right), \tag{5.199}$$

with $\alpha_k = k \ln(2)$, and

$$w_k = (-1)^{k+\frac{n}{2}} \sum_{j=\lfloor \frac{k+1}{2} \rfloor}^{min\left(k, \frac{n}{2}\right)} \frac{j^{\frac{n}{2}} (2j)!}{\left(\frac{n}{2} - j\right)! \, j! \, (j-1)! \, (k-j)! \, (2j-k)!}, \tag{5.200}$$

where n is the number of terms used and $\lfloor x \rfloor$ is the floor function, which gives the greatest integer less than or equal to x. The precision of this method depends on the parameter n and must be an even integer between 4 and 20, which should be chosen by trial and error. If n rises, the accuracy of results will initially increase, but will later decline due to round-off errors. It is worth noting that this method is easy to implement and very accurate when exponential functions are involved. This method may fail for functions with oscillatory behavior in the time domain. Listing 5.1 shows the method implemented in *Mathematica*.

Listing 5.1 [`Gaver-Stehfest.nb`]: *Mathematica's* implementation of the Gaver-Stehfest method to find numerically the inverse Laplace transform, where f is the function to invert, t is the time to be evaluated, and n is the number of terms used. The number n should be an even integer between 4 and 20

```
csteh[n_, k_] = (-1)^(k + n) Sum[
  j^(n/2) (2j)! / (
    (n/2 - j)! j! (j-1)! (k-j)! (2j-k)!
  ),
```

Listing continued on next page

Listing continued from last page

```
  {j, Floor[(k+1) / 2], Min[k, n/2]}
];

NLInvSteh[f_, s_, t_, n_] := Log[2] / t Sum[
  csteh[n, k] f /. s -> k Log[2] / t,
  {k, 1, n}
] // N
```

Listing ended

When using a numerical method, it is always a good idea to compare your results with well-known results. To such end, we compared the numerical values obtained by applying the Gaver-Stehfest method to equation

$$f(s) = \frac{1}{\sqrt{s} + \sqrt{s+1}}, \tag{5.201}$$

with its analytical inverse Laplace transform, given by

$$f(t) = \frac{1 - e^{-t}}{\sqrt{2\pi t^3}}. \tag{5.202}$$

Figure 5.25 illustrates how the numerical and exact solutions compare, while Listing 5.2 shows the *Mathematica* code needed to generate a table of inverted values. The tests performed show an excellent agreement between the numerical method and the exact analytical solution, with an error of less than 0.5% along the entire range.

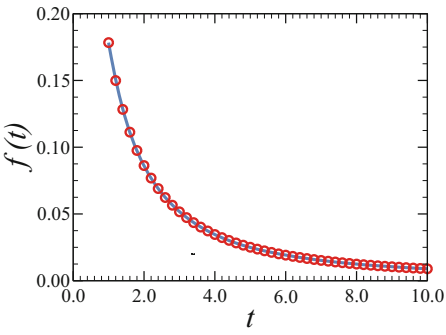

Fig. 5.25 The numerical solution of Eq. (5.201) obtained by using the Gaver-Stehfest method (red circles) is compared to the exact solution (blue line) given by Eq. (5.201)

Listing 5.2 [`Gaver-Stehfest-Example.nb`]: *Mathematica's* code to generate the table of numerical values obtained by the inverse Laplace transform applying the Gaver-Stehfest method to Eq. (5.200) (red hollow dots in Fig. 5.25). The table is calculated from $t = 0$ to 10, with steps equal to 0.2

```
Table[
  {
    t,
    NLInvSteh[1 / ( Sqrt[s] + Sqrt[s + 1] ), s, t
, 20]
  },
  {t, 1, 10, 0.20}
]
```

Further Reading and References

C. Constanda, *Solution Techniques for Elementary Partial Differential Equations* (Chapman & Hall/CRC, New York, 2010)

Chapter 6
Diffusion in the Presence of a Force Field

In this chapter, we derive the diffusion equation for the case when an external or internal force on each of the diffusing particles is applied. This equation is referred to in the literature as the *Smoluchowski*. equation, which is fundamental in the study of stochastic dynamics, as it can be applied to a number of problems related to physics and chemistry. Moreover, it plays a key role in biology because the most ubiquitous mode of transport into the cell is diffusion subject to external forces. These forces, among others, might be due to an electric field or a centrifugal force, or even result of two-body interactions, once they are derivable from a potential.

It is worth remembering that the symmetric property in x and x_0 of the propagator $p(x, t|x_0)$ in the standard diffusion equation has an important consequence: the forward and backward diffusion equations are identical. Although this condition in the presence of a force is no longer true, the backward Smoluchowski equation can be found in terms of the forward Smoluchowski equation. Moreover, the backward operator, $\mathcal{L}^{\dagger}(x_0)$, will be shown to be the *adjoint* operator of the forward operator, $\mathcal{L}(x)$.

6.1 The Smoluchowski Equation

To generalize the diffusion equation incorporating a force $F(x, t)$, let us break down the total flux into the sum of two terms:

$$J(x, t) = J_{\text{diffusion}}(x, t) + J_{\text{drift}}(x, t). \tag{6.1}$$

On the one hand, the flux due to diffusion is given by Fick's first law, Eq. (2.73). On the other hand, recalling the flux definition in fluid dynamics, we know that this quantity is proportional to concentration and net drift velocity, in turn due to the analogy between probability density and concentration. This reasoning leads to

L. Dagdug et al., *Diffusion Under Confinement*,
https://doi.org/10.1007/978-3-031-46475-1_6

$$J_{\text{drift}}(x,t) = v(x,t)\ p(x,t). \tag{6.2}$$

From experimental evidence, we know that net drift velocity and force are directly proportional, where the proportionality constant is mobility μ. Thus, $v(x,t) = \mu F(x,t)$. This relation can be derived in terms of the conservation of the particle's momentum: the frictional force balanced with the external force. Then, the momentum $F(x)\ \Delta t$ gained by the particle from the external force at time Δt should be equal to the momentum lost through the frictional force given by $-\zeta\ v(x,t)\Delta t$, where ζ is the friction coefficient. Because mobility is defined as the inverse of the friction coefficient, we recover Eq. (6.2). Rewriting the total flux given by Eq. (6.1), using Eq. (6.2), and Fick's first law, leads to

$$J(x,t) = -D\frac{\partial p(x,t)}{\partial x} + \mu F(x)\ p(x,t). \tag{6.3}$$

If the force is derivable from a time-independent potential, $U(x)$, which is only dependent on position, then the last equation can be written as

$$J(x,t) = -D\left[\frac{\partial p(x,t)}{\partial x} + \frac{\mu}{D}\frac{\mathrm{d}U(x)}{\mathrm{d}x}\,p(x,t)\right]. \tag{6.4}$$

For such a potential, there is an equilibrium probability density $p_{eq}(x) \propto e^{-\beta U(x)}$, where $\beta = 1/k_\beta T$, k_β is Boltzmann's constant, and T is the absolute temperature. When time goes to infinity, $p(x,t)$ tends to $p_{eq}(x)$, and the flux must vanish. Then from Eq. (6.4), by taking the derivative with respect to x of the equilibrium probability density, we find

$$\frac{\mathrm{d}U(x)}{\mathrm{d}x}\,\beta\, e^{-\beta U(x)} = \frac{\mu}{D}\frac{\mathrm{d}U(x)}{\mathrm{d}x}\,e^{-\beta U(x)}, \tag{6.5}$$

and consequently,

$$\mu = \beta D = \frac{1}{\zeta}. \tag{6.6}$$

This last relation is referred to as the *Smoluchowski-Einstein* relation. The physical properties and consequences of this important result will be discussed in depth later, in Sect. 6.4.

Introducing the Smoluchowski-Einstein relation, Eq. (6.6), into Eq. (6.4) leads us to the result

$$J(x,t) = -D\left[\frac{\partial p(x,t)}{\partial x} + \beta\,\frac{\mathrm{d}U(x)}{\mathrm{d}x}\,p(x,t)\right]. \tag{6.7}$$

Now, let us represent the flux in this last relation in a more compact way. To such end, we rewrite this last equation as follows:

$$J(x,t) = -D\,\mathrm{e}^{-\beta U(x)}\left[\frac{\partial p(x,t)}{\partial x}\,\mathrm{e}^{\beta U(x)} + \beta\,\frac{\mathrm{d}U(x)}{\mathrm{d}x}\,p(x,t)\,\mathrm{e}^{\beta U(x)}\right]. \tag{6.8}$$

Now, using the chain rule for derivatives, the second term of the right-hand side can be written as

$$\beta\,\frac{\mathrm{d}U(x)}{\mathrm{d}x}\,p(x,t)\,e^{\beta U(x)} = p(x,t)\,\frac{\mathrm{d}e^{\beta U(x)}}{\mathrm{d}x}. \tag{6.9}$$

By taking these relations into account, we find

$$J(x,t) = -D(x)\,e^{-\beta U(x)}\,\frac{\partial}{\partial x}\left[e^{\beta U(x)}\,p(x,t)\right]. \tag{6.10}$$

It is worth noticing that we wrote the flux in a very general way, namely, we are assuming the possibility of a position-dependent diffusivity. Its usefulness will become clear later on.

If we substitute Eq. (6.10) into the continuity equation, Eq. (2.71), we ultimately find the relation between the evolution of probability density and force by means of its potential, referred to as the Smoluchowski equation, namely,

$$\frac{\partial p(x,t)}{\partial t} = \frac{\partial}{\partial x}\left\{D(x)\,e^{-\beta U(x)}\,\frac{\partial}{\partial x}\left[e^{\beta U(x)}\,p(x,t)\right]\right\}. \tag{6.11}$$

In the absence of external or internal forces, the diffusion equation is recovered.

Now, the *Smoluchowski operator* is defined as follows:

$$\mathcal{L}(x) \equiv \frac{\partial}{\partial x}D(x)\;e^{-\beta U(x)}\,\frac{\partial}{\partial x}e^{\beta U(x)}. \tag{6.12}$$

Accordingly, the Smoluchowski equation can be written as

$$\frac{\partial p(x,t)}{\partial t} = \mathcal{L}(x)\;p(x,t). \tag{6.13}$$

The extrapolation of the Smoluchowski equation to higher dimensions is a straight-forward process accomplished by using the nabla operator, namely,

$$\mathcal{L}(\boldsymbol{r}) \equiv \nabla\cdot\boldsymbol{D}(\boldsymbol{r})\cdot\mathrm{e}^{-\beta U(\boldsymbol{r})}\,\nabla\mathrm{e}^{\beta U(\boldsymbol{r})}, \tag{6.14}$$

where now $\boldsymbol{D}(\boldsymbol{r})$ is a tensor.

Before finishing the section, it is worth noting that the generalization to higher dimension of the flux is given by

$$\mathbf{J}(\mathbf{r},t) = -D\left[\nabla p(\mathbf{r},t) + \beta p(\mathbf{r},t)\nabla U(\mathbf{r})\right]. \tag{6.15}$$

In fact, substituting this flux into conservation equation, Eq. (2.72), leads us to a useful form of the Smoluchowski equation, namely,

$$\frac{\partial p(\mathbf{r},t)}{\partial t} = D\nabla\cdot\left[\nabla p(\mathbf{r},t) + \beta p(\mathbf{r},t)\nabla U(\mathbf{r})\right]. \tag{6.16}$$

In the next section, we will derive the form of the backward Smoluchowski operator and its corresponding equation.

6.2 The Backward Smoluchowski Equation

In this section, we derive the backward Smoluchowski equation. To such end, the first step is to deduce the *detailed balance condition*, which can be found by means of *Bayes' theorem*.

Bayes' theorem can be obtained from the definition of conditional probability $P(A|B)$: the probability of event A occurring, given that event B has already occurred, namely,

$$P(A|B) = \frac{P(A\cap B)}{P(B)}, \tag{6.17}$$

where $P(A\cap B)$ is the probability of both A and B occurring. Similarly,

$$P(B|A) = \frac{P(A\cap B)}{P(A)}. \tag{6.18}$$

Solving for $P(A\cap B)$ and substituting the result into Eq. (6.17), we arrive at Bayes' theorem:

$$P(A|B) = \frac{P(B|A)\ P(A)}{P(B)}. \tag{6.19}$$

Therefore, Bayes' theorem for the conditional propagator reads

$$p(x,t|x_0)\ dt = \frac{p(x_0,t|x)\ dt\ \ p(x)\ dt}{p(x_0)\ dt} \tag{6.20}$$

or

$$p(x,t|x_0)\ p(x_0) = p(x_0,t|x)\ p(x). \tag{6.21}$$

Introducing the equilibrium probability density, $p_{eq}(x) \propto e^{-\beta U(x)}$, in this last equation, we obtain the detailed balance condition, i.e.,

$$p(x,t|x_0)\,\mathrm{e}^{-\beta U(x_0)} = p(x_0,t|x)\,\mathrm{e}^{-\beta U(x)}. \tag{6.22}$$

Physically, the detailed balance is obtained when the equilibrium is imposed, i.e., when the flux is equal to zero. Consequently, from Eq. (6.10), we have

$$e^{\beta U(x_0)}\,p(x_0,t|x) = e^{\beta U(x)}\,p(x,t|x_0). \tag{6.23}$$

This relation guarantees that, at equilibrium, there are no net fluxes between the arbitrary chosen points x and x_0. In other words, the probability flux from x to x_0 is exactly balanced by the probability flux from x_0 to x. Moreover, the detailed balance is a consequence of time reversibility of diffusion trajectories contributing to the propagator. What the principle of detailed balance states is that, in equilibrium, there is balance between any two pairs of states.[1] The result is very powerful, because it applies not only to individual states but also to any grouping of them. It is worth noticing that if there are no external or internal forces, $p(x,t|x_0)$ is symmetric in the variables x and x_0, the same condition that we used in Sect. 2.6 to derive the backward diffusion equation.

In order to obtain the backward Smoluchowski equation, let us rewrite Eq. (6.22) as

$$p(x_0,t|x) = p(x,t|x_0)\,\mathrm{e}^{-\beta[U(x_0)-U(x)]}. \tag{6.24}$$

We already know that the propagator satisfies the forward Smoluchowski equation, namely,

$$\frac{\partial p(x_0,t|x)}{\partial t} = \mathcal{L}(x_0)\;p(x_0,t|x). \tag{6.25}$$

Now, applying the detailed balance condition to both sides of this last equation yields

$$\frac{\partial}{\partial t}\left\{p(x,t|x_0)\;\mathrm{e}^{\beta U(x)}\;\mathrm{e}^{-\beta U(x_0)}\right\} = \mathcal{L}(x_0)\left\{p(x,t|x_0)\;\mathrm{e}^{\beta U(x)}\;\mathrm{e}^{-\beta U(x_0)}\right\}, \tag{6.26}$$

which is reduced to

$$\frac{\partial p(x,t|x_0)}{\partial t} = \mathrm{e}^{\beta U(x_0)}\,\mathcal{L}(x_0)\left\{\mathrm{e}^{-\beta U(x_0)}\;p(x,t|x_0)\right\}. \tag{6.27}$$

From Eq. (6.27), we can define the backward Smoluchowski operator as

[1] Detailed balance as a consequence of the reversibility of collisions, where at equilibrium each collision is equilibrated by the reverse collision, was introduced in 1872 by Ludwig Eduard Boltzmann. He used it in the proof of the H-theorem.

$$\mathcal{L}^{\dagger}(x_0) \equiv \mathrm{e}^{\beta U(x_0)}\, \mathcal{L}(x_0)\, \mathrm{e}^{-\beta U(x_0)}, \tag{6.28}$$

which can be finally written as follows:

$$\mathcal{L}^{\dagger}(x_0) = e^{\beta U(x_0)}\, \frac{\partial}{\partial x_0} D(x_0)\, e^{-\beta U(x_0)} \frac{\partial}{\partial x_0}. \tag{6.29}$$

Consequently,

$$\frac{\partial p(x,t|x_0)}{\partial t} = \mathcal{L}^{\dagger}(x_0)\; p(x,t|x_0). \tag{6.30}$$

It is worth noticing that Eq. (6.29) is the adjoint operator of (6.12) evaluated at $x = x_0$.[2] Lastly, we find that the Smoluchowski backward equation with position-dependent diffusivity is given by

$$\frac{\partial p(x,t|x_0)}{\partial t} = e^{\beta U(x_0)}\, \frac{\partial}{\partial x_0} \left[D(x_0)\, e^{-\beta U(x_0)} \frac{\partial}{\partial x_0} p(x,t|x_0) \right]. \tag{6.31}$$

Comparing Eqs. (6.12) and (6.29), the reader can verify that if $U(x)$ is constant, both operators coincide. A simple example that we can study is when the force is constant in space and time, F, namely, $U(x) = -Fx$. If the velocity is proportional to this force by means of mobility, then $U(x) = -v\; x/(\beta D)$. Thus, the backward and forward operators become

$$\mathcal{L}(x) = D \frac{\partial^2}{\partial x^2} - v\, \frac{\partial}{\partial x} \tag{6.32}$$

and

$$\mathcal{L}^{\dagger}(x_0) = D \frac{\partial^2}{\partial x_0^2} + v\, \frac{\partial}{\partial x_0}, \tag{6.33}$$

respectively. The former recovers the Fokker-Planck equation, Eq. (2.12), which will be solved in detail in the following sections. For purposes of simplicity, in this example, we set diffusivity as a quantity that is independent of position.

[2] See Appendix 6.A for further details on the adjoint operator of the Smoluchowski operator.

6.3 Survival Probability and the Moments of MFPT in the Presence of a Force Field

To obtain the evolution equation for the survival probability and moments of mean first-passage time (MFPT), in the presence of a force field, we will follow the techniques outlined in Sect. 2.6. Nevertheless, in this case, we start by integrating Eq. (6.30) with respect to x over the domain $[0, L]$; considering two absorbing endpoints placed at $x = 0$ and $x = L$, we find that the evolution equation for survival probability is given by

$$\frac{\partial S(t|x_0)}{\partial t} = \mathcal{L}^{\dagger}(x_0)\ S(t|x_0). \tag{6.34}$$

To obtain the relation with the MFPT, we multiply this last equation by nt^{n-1} and integrate with respect to t, namely,

$$\int_0^{\infty} nt^{n-1}\,\frac{\partial S(t|x_0)}{\partial t}\,\mathrm{d}t = \int_0^{\infty} nt^{n-1}\,\mathcal{L}^{\dagger}(x_0)\ S(t|x_0)\mathrm{d}t. \tag{6.35}$$

By performing the integrals, we finally find that $\langle t^n(x_0)\rangle$ must satisfy

$$\mathcal{L}^{\dagger}(x_0)\langle t^n(x_0)\rangle = -n\langle t^{n-1}(x_0)\rangle. \tag{6.36}$$

The equations can be solved sequentially starting from the first moment, $n = 1$, for which the equation reads

$$\mathcal{L}^{\dagger}(x_0)\langle t(x_0)\rangle = -1. \tag{6.37}$$

Substituting the definition for the Smoluchowski backward operator, given by Eq. (6.33), leads to

$$\frac{\partial}{\partial x_0}\left[D(x_0)\,\mathrm{e}^{-\beta U(x_0)}\,\frac{\partial}{\partial x_0}\langle t(x_0)\rangle\right] = -\mathrm{e}^{-\beta U(x_0)}. \tag{6.38}$$

In the absence of bias, and setting the diffusivity to a constant, we recover Eq. (2.64). The reader can easily extend this equation to higher dimensions using the nabla operator.

6.4 Fluctuation-Dissipation Theorem

The *fluctuation-dissipation theorem* states that the linear response of a given system to an external perturbation is expressed in terms of fluctuation properties of the system in thermal equilibrium. This theorem is a powerful tool in statistical physics

and is used to predict the behavior of systems that obey detailed balance conditions. In particular, for Brownian motion, we find that

$$D = \frac{1}{\zeta} k_B T, \tag{6.6}$$

where k_B is the Boltzmann constant and T the absolute temperature. From this relation, we have that random impacts with surrounding molecules generally cause two types of effects: a) they act as a random driving force on the Brownian particle, and b) they produce frictional force for imposed motion. This means that the frictional and the random forces must be related, because both have the same origin. This relationship between the systematic and the random parts of microscopic forces is one example of the fluctuation-dissipation theorem. One property worthy of notice is that friction dissipates energy, i.e., it converts mechanical work into thermal energy.

The Smoluchowski-Einstein relation also provides a useful formula to estimate the diffusion coefficient of microscopic particles moving through a fluid, which has important theoretical implications.

Using the Stokes formula, $\zeta = 6\pi\eta R$ (derivation of this relation is given in Appendix 23.A) for a spherical particle of radius R in a fluid of viscosity η, Eq. (6.6) becomes the *Stokes-Einstein-Sutherland relation*,[3] namely,

$$D = \frac{k_B T}{6\pi\eta R}. \tag{6.39}$$

After substituting this relation into the diffusivity definition for an isotropic fluid in three dimensions, given by Eq. (2.18), we arrive at

$$\langle \Delta \mathbf{r}^2(t) \rangle = \frac{k_B T}{3\pi\eta R} t. \tag{6.40}$$

In 1909, using this relation, J. B. Perrin estimated the Boltzmann constant and the radius of a molecule suspended in water. It should be mentioned that this relation served as a verification of the existence of atoms and molecules, which was still not fully accepted at that time.

To illustrate the utility of Eqs. (6.39) and (6.40), we use them to calculate the diffusivity and the mean square displacement for the protein myoglobin in water at room temperature, $T = 300\text{K}$. The Boltzmann constant is 1.381×10^{-16} cm^2 g s^{-2} K^{-1}, therefore (300 K) $k_B = 4.143 \times 10^{-14}$ cm^2 g s^{-2}. The values of the radius of myoglobin and the viscosity of water at room temperature are 1×10^{-2} g cm^{-1} s^{-2} and 20×10^{-8} cm, respectively. Substituting all of these

[3] The reader interested in the derivation of this formula can consult the book of Landau and Lifshitz *Fluid Mechanics* 1975.

values into Eqs. (6.39) and (6.40), we obtain $D = 1.098 \times 10^{-6}$ cm^2 s^{-1} and $\langle \Delta \mathbf{r}^2(t) \rangle = 2.198 \times 10^{-6}$ cm s^{-1}.

The densities for different proteins are practically the same because they are comprised of the same amino acids, which are comprised of similar chemical groups. Then, for spherical proteins, the relation between their ratio and molecular weight (M) is $R \propto \sqrt[3]{M}$. Thus, their diffusivity is inversely dependent on the cube root of molecular weight.

Regarding friction forces, we have that the friction force is larger for non-spherical molecules than for a spherical molecule with the same M. For prolate spheroid shapes (like an American football) and oblate ellipsoidal shapes (disk-like), characterized by a long-axis length a and a short-axis length b, their values are only moderately sensitive compared to spherical shapes up to $a/b \approx 6$. The increased friction when $a/b > 6$ seems counterintuitive, as one would think that the motion along the direction of the long axis would be facilitated. While this is true, the direction of motion is random, and the molecules also move in the direction of the short axis and in every other direction as well. Ultimately, the observed friction accounts for average motion over all directions.

6.5 Diffusion in a Linear Potential: Constant Drift

In this section, we will solve the Smoluchowski equation with constant drift given by the uniform force, $F = v/(\beta D)$, by means of different mathematical techniques. First, we will solve it using a reduction method, first reducing the Smoluchowski equation to a diffusion-like equation by defining two auxiliary functions, and then using the Fourier and Laplace transforms.

As shown in Sect. 6.1, the diffusion equation in the presence of an external force is given by Eq. (6.11). Then, by substituting the potential $U(x) = -Fx = -vx/(\beta D)$ into Eq. (6.11), and setting diffusivity as a constant, we find

$$\frac{\partial p(x,t)}{\partial t} = D \frac{\partial}{\partial x} \left\{ \exp\left(\frac{vx}{D}\right) \frac{\partial}{\partial x} \left[\exp\left(-\frac{vx}{D}\right) p(x,t) \right] \right\}. \tag{6.41}$$

The solution to this last equation can be written in terms of the propagator in the absence of an external force. In order to accomplish this task, we have to apply two reductions. Firstly, we rewrite the propagator as

$$p(x,t|x_0) = \exp\left(\frac{vx}{2D}\right) \psi(x,t|x_0), \tag{6.42}$$

which makes it possible to rewrite Eq. (6.41) as a Fokker-Planck-like equation, namely,

$$\frac{\partial \psi(x,t|x_0)}{\partial t} = D\frac{\partial^2 \psi(x,t|x_0)}{\partial x^2} - \frac{v^2}{4D}\,\psi(x,t|x_0). \tag{6.43}$$

The second step is defining the function

$$q(x,t|x_0) \equiv \exp\left(\frac{v^2 t}{4D}\right)\psi(x,t|x_0), \tag{6.44}$$

which allows us to write Eq. (6.43) as a diffusion-like equation, namely,

$$\frac{\partial q(x,t|x_0)}{\partial t} = D\,\frac{\partial^2 q(x,t|x_0)}{\partial x^2}. \tag{6.45}$$

Now, we have to solve this diffusion equation subject to an appropriate initial condition. Since $p(x,0|x_0) = \delta(x - x_0)$, using Eqs. (6.42) and (6.44), the initial condition on $q(x,t|x_0)$ is

$$\delta(x - x_0) = \exp\left(-\frac{v^2 t}{4D} + \frac{vx}{2D}\right)\,q(x,0|x_0). \tag{6.46}$$

Following the method outlined in Sect. 3.1, we solve Eq. (6.45) subject to the initial conditions given in (6.46), by means of the Fourier transform, leading to

$$q(x,t|x_0) = \frac{1}{\sqrt{4\pi\,Dt}}\exp\left[-\frac{(x - x_0)^2 + 2x_0\,v\,t}{4Dt}\right]. \tag{6.47}$$

Substituting this last equation into Eq. (6.42) and the resulting expression into Eq. (6.44), the final result is

$$p(x,t|x_0) = \frac{1}{\sqrt{4\pi\,Dt}}\exp\left[-\frac{(x - x_0 - vt)^2}{4Dt}\right]. \tag{6.48}$$

The variance generated by this propagator is $2Dt$, the same as in free diffusion. Meanwhile, the mean, $\langle x_0(t)\rangle = x_0 + vt$, is modified by the force as a drift with constant velocity. This equation reduces to Eq. (3.29) when $v = 0$. The evolution of this propagator in space and time is depicted in Fig. 6.1.

6.5.1 *Diffusion with Constant Drift Revisited: Integral Transforms*

Integral transforms offer an alternative approach when solving problems of diffusion in the presence of a force field. In this subsection, we provide the solution to the Smoluchowski equation with a constant drift using Fourier and Laplace transforms.

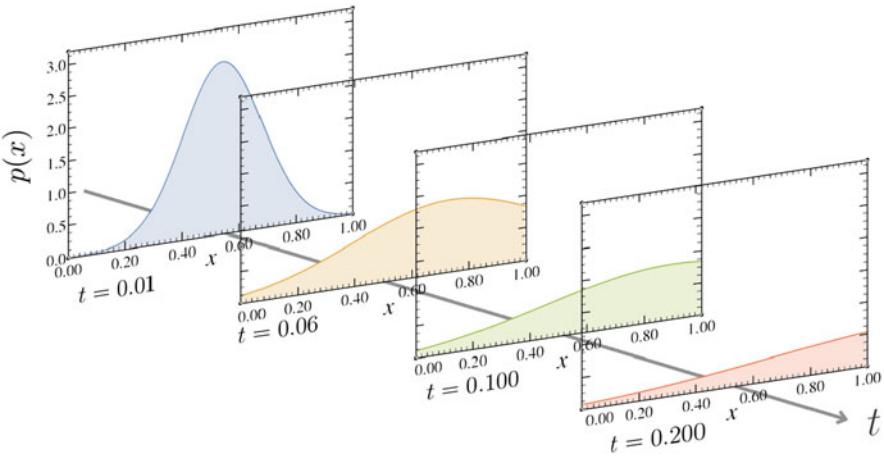

Fig. 6.1 Time evolution of the propagator $p(x, t|x_0)$ in the presence of a constant drift, Eq. (6.48), at different times. The initial position, system length, and diffusivity are $x_0 = 0.5$, $L = 1$, and $D = 1$, respectively. The velocity drag is set at $v = 4$, which is giving the *tail effect* at the end of the domain

6.5.1.1 Fourier Transform

Equation (6.41) is the result of implementing the potential $U(x) = -vx/(\beta D)$ into Eq. (6.12). By differentiating with respect to x, as indicated in the general expression, we ultimately find the following relation:

$$\frac{\partial p(x,t|x_0)}{\partial t} = D\,\frac{\partial^2 p(x,t|x_0)}{\partial x^2} - v\frac{\partial p(x,t|x_0)}{\partial x}, \tag{6.49}$$

which is the classical diffusion equation with drift: the Fokker-Planck equation. The extrapolation of this last equation to higher dimensions is accomplished by means of the del[4] (∇) and Laplace ($\nabla^2 \equiv \nabla \cdot \nabla$) operators, namely,

$$\frac{\partial p(\mathbf{r},t|\mathbf{r}_0)}{\partial t} = D\,\nabla^2 p(\mathbf{r},t|\mathbf{r}_0) - \mathbf{v}\cdot\nabla p(\mathbf{r},t|\mathbf{r}_0), \tag{6.50}$$

where $\mathbf{r}$ is the position vector, $\mathbf{r}_0$ the initial position of the particle, and $\mathbf{v}$ the drag velocity vector. Considering the three-dimensional problem, we refer to Chap. 2 to conclude that

$$D \equiv \lim_{\substack{\Delta\mathbf{r}\to 0\\ \Delta t\to 0}} \frac{(\Delta\mathbf{r})^2}{6\Delta t} \tag{2.19}$$

[4] Sometimes called nabla.

together with

$$\mathbf{v} \equiv - \lim_{\substack{\Delta \mathbf{r} \to 0 \\ \Delta t \to 0}} (a - b) \frac{\Delta \mathbf{r}}{3 \Delta t}, \tag{6.51}$$

referring to an isotropic fluid.

Now, by Fourier transforming Eq. (6.49), using Eqs. (A.52), we arrive at

$$\begin{aligned} \frac{\partial p(x, t|x_0)}{\partial t} &= -D k^2 p(k, t|x_0) + ikv\, p(k, t|x_0) \\ &= (-D k^2 + ikv)\, p(k, t|x_0). \end{aligned} \tag{6.52}$$

The solution of the resulting ordinary differential equation (ODE) is computed, i.e.,

$$p(k, t|x_0) = p_0 \exp\left[\left(-D k^2 + ikv\right) t\right]. \tag{6.53}$$

Then, we need to apply the initial condition, namely,

$$p(k, t = 0|x_0) = \int_{-\infty}^{\infty} \delta(x - x_0)\, \mathrm{e}^{ikx}\, \mathrm{d}x = \mathrm{e}^{ikx_0}. \tag{6.54}$$

Thus, $p_0 = \mathrm{e}^{ikx_0}$, meaning that

$$p(k, t|x_0) = \exp\left\{\left[-D k^2 + ik(x_0 + v)\right] t\right\}. \tag{6.55}$$

By comparing Eqs. (3.13) and (6.55), we notice that we can reproduce Eq. (6.55) simply by making $x_0 \to x_0 + vt$. Thus, the process to inverse transform the last equation is basically the same as the one outlined in Sect. 3.1. Therefore, we can find the solution to our present problem by making $x_0 \to x_0 + vt$ in Eq. (3.29), namely,

$$p(x, t|x_0) = \frac{1}{\sqrt{4\pi D t}} \exp\left[-\frac{(x - x_0 - vt)^2}{4Dt}\right]. \tag{6.56}$$

6.5.1.2 Laplace Transform

When using Laplace transforms, we need to apply the definition in (A.53) to Eq. (6.49). This process transforms the Fokker-Planck equation, Eq. (6.49), into the following:

$$s\, p(x, s|x_0) - \delta(x - x_0) = D\, \frac{\partial^2 p(x, s|x_0)}{\partial x^2} - v\, \frac{\partial p(x, s|x_0)}{\partial x} \tag{6.57}$$

or, equivalently,

$$D\, \frac{\partial^2 p(x, s|x_0)}{\partial x^2} - v\, \frac{\partial p(x, s|x_0)}{\partial x} - s\, p(x, s|x_0) = 0. \tag{6.58}$$

Let us propose the following solution:

$$p(x, s|x_0) = \mathcal{A}\, \mathrm{e}^{r(x - x_0)}. \tag{6.59}$$

By substituting the propagator into the differential equation, we find the characteristic equation associated with the problem, which is

$$D\, r^2 - v r - s = 0. \tag{6.60}$$

The solutions to this second-order equation are

$$r_1 = \frac{v + \sqrt{v^2 + 4Ds}}{2D} \quad \text{and} \quad r_2 = \frac{v - \sqrt{v^2 + 4Ds}}{2D}. \tag{6.61}$$

It is important to note that $v^2 + 4Ds$ is always greater than zero, which means that the correct solution is[5]

$$p(x, s|x_0) = \begin{cases} \mathcal{A}\, \mathrm{e}^{r_1 (x - x_0)} & \text{for} \quad x < x_0, \\ \\ \mathcal{B}\, \mathrm{e}^{r_2 (x - x_0)} & \text{for} \quad x > x_0. \end{cases} \tag{6.62}$$

We have to be careful when calculating the integration constants. The continuity condition in the starting position remains the same, i.e.,

$$p(x, s|x_0)\Big|_{x_0^+} = p(x, s|x_0)\Big|_{x_0^-}. \tag{3.39}$$

Nevertheless, to find the joining condition, we need to integrate Eq. (6.58) from $x_0 - \epsilon$ and $x_0 + \epsilon$, which lead us to

[5] The reader should be aware of the relation between v and the $\sqrt{v^2 + 4Ds}$ terms. Since D and s are always positive, we can assure that $v < \sqrt{v^2 + 4Ds}$. This implies that the solution for $x > x_0$, i.e., $\mathcal{B}\, \mathrm{e}^{r_2 (x - x_0)}$, converges correctly at the limit $x \to \infty$.

$$\int_{x_0-\epsilon}^{x_0+\epsilon} s\, p(x,s|x_0)\, \mathrm{d}x - \int_{x_0-\epsilon}^{x_0+\epsilon} \delta(x-x_0)\, \mathrm{d}x = D\int_{x_0-\epsilon}^{x_0+\epsilon} \frac{\partial^2 p(x,s|x_0)}{\partial x^2}\, \mathrm{d}x - v\int_{x_0-\epsilon}^{x_0+\epsilon} \frac{\partial p(x,s|x_0)}{\partial x}\, \mathrm{d}x. \tag{6.63}$$

Then, taking the limit when $\epsilon \to 0$, and considering the properties of the Dirac delta function, we arrive at

$$-\frac{1}{D} = \frac{\partial p(x,s|x_0)}{\partial x}\bigg|_{x_0^-}^{x_0^+} - v\, p(x,s|x_0)\bigg|_{x_0^-}^{x_0^+}. \tag{6.64}$$

By applying the continuity equation on the propagator, we find that $\mathcal{A} = \mathcal{B}$. Moreover, the discontinuity condition in Eq. (6.64) is reduced to[6]

$$-\frac{1}{D} = \frac{\partial p(x,s|x_0)}{\partial x}\bigg|_{x_0^+} - \frac{\partial p(x,s|x_0)}{\partial x}\bigg|_{x_0^-}, \tag{3.42}$$

leading us to

$$\mathcal{A} = \frac{1}{\sqrt{v^2+4Ds}}. \tag{6.65}$$

Thus, we can write a unique solution as

$$p(x,s|x_0) = \frac{\mathrm{e}^{r_2|x-x_0|}}{\sqrt{v^2+4Ds}} = \frac{\exp\left[\dfrac{\left(v-\sqrt{v^2+4Ds}\right)|x-x_0|}{2D}\right]}{\sqrt{v^2+4Ds}} \tag{6.66}$$

In order to make the inverse Laplace transform of $p(x,s|x_0)$, let us make

$$s' = \frac{v^2}{4D} + s. \tag{6.67}$$

Therefore, the inverse Laplace transform of the propagator, in terms of s', is

[6] When combining the continuity and discontinuity equations, Eqs. (3.39) and (6.64), we see that the term $-v\, p(x,s|x_0)\Big|_{x_0^-}^{x_0^+}$ is identically zero, since we are already requiring that the propagators at the left and at the right are the same when evaluated at $x = x_0$ from the first condition.

$$
\begin{aligned}
p(x,t|x_0) &= \frac{1}{2\pi i}\lim_{T\to\infty}\int_{\gamma-iT}^{\gamma+iT} \mathrm{e}^{s't}\; p(x,s'|x_0)\;\mathrm{d}s' \\
&= \frac{1}{2\pi i}\lim_{T\to\infty}\int_{\gamma-iT}^{\gamma+iT} \exp\left(s't-\frac{v^2t}{4D}\right)\; p(x,s'|x_0)\;\mathrm{d}s' \\
&= \exp\left(-\frac{v^2t}{4D}+\frac{v|x-x_0|}{2D}\right)\frac{1}{2\pi i}\lim_{T\to\infty}\int_{\gamma-iT}^{\gamma+iT} \mathrm{e}^{s't}\,\frac{\exp\left(-\sqrt{\frac{s'}{D}}|x-x_0|\right)}{\sqrt{4Ds'}}\;\mathrm{d}s' \\
&= \exp\left(-\frac{v^2t}{4D}+\frac{v|x-x_0|}{2D}\right)\;\mathcal{L}^{-1}\left\{\frac{1}{\sqrt{4Ds'}}\exp\left(-\sqrt{\frac{s'}{D}}|x-x_0|\right)\right\}
\end{aligned}
\tag{6.68}
$$

In fact, we already computed the inverse transform in the latter equation (see Eq. (3.44)), and the result is given by Eq. (3.59). Thus, $p(x,t|x_0)$ is

$$
p(x,t|x_0) = \exp\left(-\frac{v^2t}{4D}+\frac{v|x-x_0|}{2D}\right)\;\frac{1}{\sqrt{4\pi Dt}}\exp\left[-\frac{(x-x_0)^2}{4Dt}\right]. \tag{6.69}
$$

Finally, after rearranging the argument of the exponential, we arrive at

$$
p(x,t|x_0) = \frac{1}{\sqrt{4\pi Dt}}\exp\left[-\frac{(x-x_0-vt)^2}{4Dt}\right], \tag{6.70}
$$

as we expected.

6.6 Diffusion in a Harmonic Potential

In this section, we solve the Smoluchowski equation in the presence of a harmonic potential, given by

$$
U(x) = \frac{K}{2}\,x^2, \tag{6.71}
$$

where K is the *force* or *spring constant*, subject to the initial condition $p(x,0|x_0) = \delta(x-x_0)$. The forward Smoluchowski equation, Eq. (6.11), describing diffusion on such a potential is

$$\frac{\partial p(x,t|x_0)}{\partial t} = D\left[\frac{\partial^2 p(x,t|x_0)}{\partial x^2} + \beta K\, x\, \frac{\partial p(x,t|x_0)}{\partial x} + \beta K\; p(x,t|x_0)\right]. \tag{6.72}$$

By following the same technique as in the previous section, we reduce this equation to a Fokker-Planck-like equation. In order to accomplish this task, we introduce the following dimensionless variables, $\tau = D\beta K t$ and $\xi = (\beta K)^{\frac{1}{2}} x$, which transform Eq. (6.72) into

$$\frac{\partial p(\xi,\tau)}{\partial \tau} = \frac{\partial^2 p(\xi,\tau)}{\partial \xi^2} + \xi \frac{\partial p(\xi,\tau)}{\partial \xi} + p(\xi,\tau), \tag{6.73}$$

subject to the initial condition $p(\xi,0) = \delta(\xi - \xi_0)$, where $\xi_0 = (\beta K)^{\frac{1}{2}} x_0$.

We will solve this equation by the Fourier transform technique. Note that the two last terms of the right-hand side in (6.73) can be written as

$$\xi \frac{\partial p(\xi,\tau)}{\partial \xi} + p(\xi,\tau) = \frac{\partial}{\partial \xi}\left[\xi\; p(\xi,\tau)\right], \tag{6.74}$$

which Fourier transform is calculated as follows:

$$\begin{aligned}\mathcal{F}\left\{\frac{\partial}{\partial \xi}\left[\xi\; p(\xi,\tau)\right]\right\} &= \int_{-\infty}^{\infty} \frac{\partial}{\partial \xi}\left[\xi\; p(\xi,\tau)\right]\, \mathrm{e}^{ik\xi}\, \mathrm{d}\xi \\ &= \int_{-\infty}^{\infty} \left\{\frac{\partial}{\partial \xi}\left[\xi\; p(\xi,\tau)\, \mathrm{e}^{ik\xi}\right] - ik\xi\; p(\xi,\tau)\, \mathrm{e}^{ik\xi}\right\} \mathrm{d}\xi.\end{aligned} \tag{6.75}$$

Now, the first integral can be solved by observing that $p(\xi \to \pm\infty) = 0$, namely,

$$\int_{-\infty}^{\infty} \frac{\partial}{\partial \xi}\left[\xi\; p(\xi,\tau)\, \mathrm{e}^{ik\xi}\right] \mathrm{d}\xi = \xi\; p(\xi,\tau)\, \mathrm{e}^{ik\xi}\Big|_{\xi\to-\infty}^{\xi\to+\infty} = 0. \tag{6.76}$$

From (6.75), we identify the second integral of the last equality as

$$-ik\int_{-\infty}^{\infty} \xi\; p(\xi,\tau)\, \mathrm{e}^{ik\xi}\, \mathrm{d}\xi = -ik\, \mathcal{F}\{\xi\; p(\xi,\tau)\} = -ik\left[-i\; \frac{\partial p(k,\tau)}{\partial k}\right], \tag{6.77}$$

which was obtained using the relation (A.50). By using (A.52) and substituting (6.77) into Eq. (6.73), we find that its Fourier transform is given by

$$\frac{\partial p(k,\tau)}{\partial \tau} = -\,k\; \frac{\partial p(k,\tau)}{\partial k} - k^2\; p(k,\tau) \tag{6.78}$$

or, equivalently,

$$\frac{\partial p(k,\tau)}{\partial \tau} = -\, k\, e^{-\frac{k^2}{2}}\, \frac{\partial}{\partial k}\left[e^{\frac{k^2}{2}}\, p(k,\tau)\right]. \tag{6.79}$$

This equation can be reduced in terms of a new auxiliary function defined as $\psi(k,\tau) \equiv e^{\frac{1}{2}k^2}\, p(k,\tau)$. By multiplying both sides of Eq. (6.79) by $e^{\frac{1}{2}k^2}$, we find that $\psi(k,\tau)$ satisfies

$$\frac{\partial \psi(k,\tau)}{\partial \tau} = -\, k\, \frac{\partial \psi(k,\tau)}{\partial k}. \tag{6.80}$$

This last equation can be solved by the method of characteristics.[7] To such end, we need to compare it with

$$a(k,\tau)\, \frac{\partial \psi(k,\tau)}{\partial k} + b(k,\tau)\, \frac{\partial \psi(k,\tau)}{\partial \tau} = 0, \tag{6.81}$$

from which we identify that $a(k,\tau) = k$ and $b(k,\tau) = 1$. Then, the derivatives of the parameterized characteristics, using η as the independent parameter, are

$$k'(\eta) = a(k(\eta),\tau(\eta)) = k(\eta) \qquad \text{and} \qquad \tau'(\eta) = b(k(\eta),\tau(\eta)) = 1. \tag{6.82}$$

Solving these last differential equations, we find that

$$k(\eta) = c_1\, \mathrm{e}^{\eta} \qquad \text{and} \qquad \tau(\eta) = \eta + c_2, \tag{6.83}$$

where c_1 and c_2 are integration constants. The parameter η can be removed equating these last expressions, namely,

$$k = c_3\, \mathrm{e}^{\tau}, \tag{6.84}$$

where $c_3 = c_1 e^{-c_2}$. Then,

$$k\, \mathrm{e}^{-\tau} = c_3 \tag{6.85}$$

defines a level curve, also called a characteristic, which allows us to write the general solution for Eq. (6.80) in terms of an arbitrary function f, namely,

[7] The method of characteristics is a technique for solving partial differential equations. The method consists of reducing a partial differential equation (PDE) to a family of ordinary differential equations, their solution which can be integrated from certain initial conditions given on a suitable hyper-surface, rather than solving the original PDE.

$$\psi(k,\tau) = f(ke^{-\tau}). \tag{6.86}$$

Using the definition of ψ, the Fourier transform of the propagator takes the form

$$p(k,\tau) = f(ke^{-\tau})\, e^{-\frac{1}{2}k^2}. \tag{6.87}$$

This $f(ke^{-\tau})$ function can be found imposing the initial conditions into the Fourier transform of $p(\xi,\tau)$. Consequently,

$$p(k,\tau=0|\xi_0) = e^{-\frac{k^2}{2}}\, f(k) = \int_{-\infty}^{\infty} \delta(\xi-\xi_0)\, e^{ik\xi}\, \mathrm{d}\xi = e^{ik\xi_0}, \tag{6.88}$$

or

$$f(k) = e^{ik\xi_0+\frac{k^2}{2}}. \tag{6.89}$$

Substituting this last equation into Eq. (6.87), and evaluating it at $k\mathrm{e}^{-\tau}$, we obtain that the propagator's Fourier transform takes on the following form:

$$p(k,\tau) = \exp\left[-\frac{k^2}{2}(1-e^{-2\tau}) + ik\xi_0\, e^{-\tau}\right]. \tag{6.90}$$

Using the definition of the inverse Fourier transform given by Eq. (A.48), we find

$$p(\xi,\tau|\xi_0) = \frac{1}{2\pi}\int_{-\infty}^{\infty} \exp\left[-\frac{k^2}{2}(1-e^{-2\tau}) + ik\xi_0\, e^{-\tau}\right] \mathrm{e}^{-ik\tau}\, \mathrm{d}k. \tag{6.91}$$

Inverting this transform using Eq. (A.51) yields

$$p(\xi,\tau|\xi_0) = \frac{1}{\sqrt{2\pi(1-e^{-2\tau})}} \exp\left[-\frac{(\xi-\xi_0 e^{-\tau})^2}{2(1-e^{-2\tau})}\right]. \tag{6.92}$$

To finish the derivation, we return to the original variables, x and t, and as a result, the propagator is given by

$$p(x,t|x_0) = \sqrt{\frac{\beta K}{2\pi(1-e^{-2\beta DKt})}} \exp\left[-\frac{\beta K(x-x_0 e^{-\beta DKt})^2}{2(1-e^{-2\beta DKt})}\right]. \tag{6.93}$$

The evolution of this propagator in time and space is depicted in Fig. 6.2. Comparing this last equation with Eq. (3.73), we see that the expectation value of the position for this propagator approaches the Boltzmann distribution and is given by

$$\langle x(t)\rangle = x_0 \mathrm{e}^{-\beta DKt}. \tag{6.94}$$

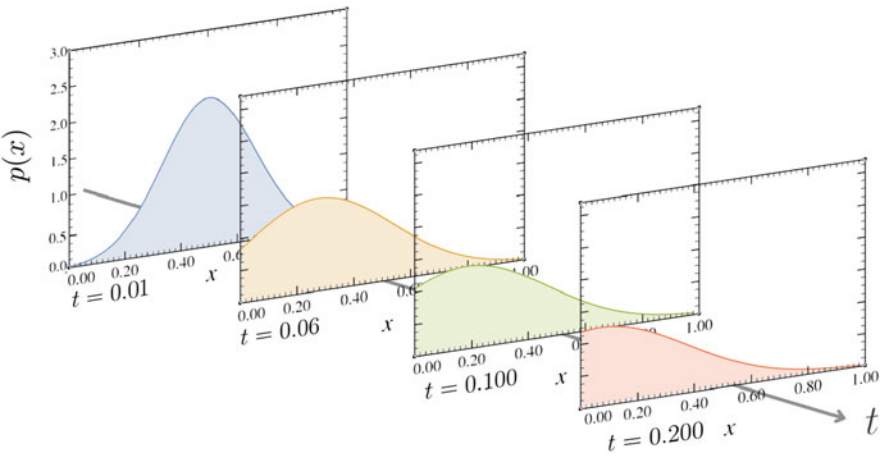

Fig. 6.2 Time evolution of the propagator $p(x, t|x_0)$ in the presence of a harmonic potential, Eq. (6.93), at different times. The initial position, system length, and diffusivity are $x_0 = 0.5$, $L = 1$, and $D = 1$, respectively. Meanwhile, $\beta = 1$, and the *characteristic factor* K is set at $K = 15$

It is worth noticing that the expression for the mean and mean-squared displacement, when t goes to infinity, are given by $\langle x \rangle = 0$ and $\langle x^2 \rangle = k_B\ T/K$, respectively. This latter expression is consistent with the results of the equipartition theorem, i.e.,

$$\frac{1}{2} K \langle x^2 \rangle = \frac{k_B T}{2}. \tag{6.95}$$

Contrarily, the mean displacement for short times, $t \ll 1/\sqrt{K\beta}$, is given by x_0, which otherwise decreases exponentially to zero regardless of the starting position.

On the other hand, the variance is given by $[1 - \exp(-2\beta DKt)]/\beta K$. This variance increases linearly as $DK\beta t$ when $t < 1/\sqrt{K\beta}$, and then it reaches a plateau value equal to $k_B T/K$. Consequently, for long times, we conclude that Eq. (6.93) tends to a standard normal distribution.[8]

6.7 Ionic Diffusion Through Membrane: The Nernst Potential

Both the identities and quantities of the different ion species within cells are involved in signaling, energy storage, protein function, and other processes. Con-

[8] A standard normal distribution, or z-distribution, is a normal distribution with zero mean ($\mu = 0$) and unit standard deviation ($\sigma = 1$). Any normal distribution can be standardized.

sequently, one of the essential functions of the cell is regulated ion concentrations. These ionic placements within cells has to be controlled both spatially and temporally. To such end, there are whole families of proteins whose job is to either open or close pores in the membrane, allowing ions to enter or exit the cell.

There are different classes of driving forces that can induce ion channels to change their open probability. This driving force can be the voltage applied across the membrane, mechanical effects by applying membrane tension, or concentration of ligands. Some ion channels open in response to specific ligands binding to the channels, for example, and consequently, the driving force is the concentration of ligands.

Now, let us assume that the concentration of K^+ ions is high inside (i) the cell and low outside (o) the cell and that the cell membrane contains some open K^+ channels. Then, the concentration gradient provides a driving force for the translocation of K^+ ions from inside the cell to the outside through these channels. The translocation of these ions generates a voltage across the cell membrane, with the inside of the cell at negative electrical potential with respect to the outside. The cell membrane is said to be *polarized*. The flow of ions will stop when the drive to move outward, due to the concentration gradient, is balanced by the opposition generated by the voltage difference, $(V_o - V_i)ze$, where z is the ion valence and e the unit electric charge ($e = 1.6 \times 10^{-19}$C). The membrane potential at steady state is called the *rest potential*.

To calculate the rest potential, we need to know the concentration at both ends of the channel. To such end, we simplify the ion channel's shape by considering it as a cylinder. Then, the transport of ions through the channel can be approximated as a one-dimensional system. Recalling that the detailed balance applies in the steady state, the calculations are quite simplified. Therefore, multiplying Eq. (6.24) by the number of ions at both ends of the channel leads to (see Eq. (2.16))

$$c(x_i) = c(x_o)\, \mathrm{e}^{-\beta[U(x_i)-U(x_o))]}. \tag{6.96}$$

From this last equation, we have that the potential difference across the membrane, the so-called Nernst potential, is given by

$$\Delta U = k_B T \ \ln\left(\frac{c(x_i)}{c(x_o)}\right), \tag{6.97}$$

where $\Delta U = [U(x_o) - U(x_i))]$, T is the temperature, and k_B is the Boltzmann constant. The value of the Boltzmann constant in joules per kelvin is $1.380\,649 \times 10^{-23}\mathrm{m}^2\ \mathrm{kg}\ \mathrm{s}^{-2}\ \mathrm{K}^{-1}$. Equation (6.97) is an important consequence of the detailed balance, which indicates that a difference in concentration generates the rest potential. Equating Eq. (6.97) with $(V_o - V_i)e$ and setting the temperature at 37 ∘C (310.15 K) lead to $k_B T/e \approx 27$mV. Then, we can say that the difference in concentration scale corresponds to a 27 mV voltage potential difference. For a typical mammalian, skeletal muscle cells are at 37 °C, and the extracellular and intracellular concentrations of sodium (Na^+) and potassium (K^+) ions are 145 and

12 mM and 4 and 155 mM, respectively. Consequently, the rest potentials for Na^+ and K^+ are 67 and -98 mV, respectively.

Lastly, it is worth emphasizing that according to Nernst equations, positive ions tend to move away from regions of positive potential and toward regions of negative potential. Negative charges move the opposite way.

6.8 Concluding Remarks

In this chapter, we have computed and derived the fundamental physical properties of diffusion in the presence of an external potential, which is independent of time. An important result is that the backward Smoluchowski operator is the adjoint operator of the forward Smoluchowski operator. We also found that for particles diffusing in a potential, detailed balance guarantees the absence of net fluxes at equilibrium. It is important to emphasize that the fluctuation-dissipation theorem states that the linear response of a given system to an external perturbation is expressed in terms of fluctuation properties of the system in thermal equilibrium.

For the reader's convenience, listed below are the most important equations to depict and define diffusion in the presence of a force field.

$$\frac{\partial p(x,t)}{\partial t} = \frac{\partial}{\partial x}\left\{ D(x)\ \mathrm{e}^{-\beta U(x)} \frac{\partial}{\partial x}\left[\mathrm{e}^{\beta U(x)}\ p(x,t)\right]\right\}.$$

(Smoluchowski forward equation)

$$\frac{\partial p(x_0,t)}{\partial t} = \mathrm{e}^{\beta U(x_0)} \frac{\partial}{\partial x_0}\left\{ D(x_0)\ \mathrm{e}^{-\beta U(x_0)}\ \frac{\partial}{\partial x_0} p(x_0,t)\right\}.$$

(Smoluchowski backward equation)

$$\mathcal{L}(x) = \frac{\partial}{\partial x} D(x)\ \mathrm{e}^{-\beta U(x)} \frac{\partial}{\partial x} \mathrm{e}^{\beta U(x)}.$$

(Smoluchowski forward operator)

$$\mathcal{L}^{\dagger}(x_0) = \mathrm{e}^{\beta U(x_0)} \frac{\partial}{\partial x_0} D(x_0)\ \mathrm{e}^{-\beta U(x_0)}\ \frac{\partial}{\partial x_0}.$$

(Smoluchowski backward operator)

$$\frac{\partial S(t|x_0)}{\partial t} = \mathcal{L}^{+}(x_0)\ S(t|x_0).$$

(Survival probability)

$$\mathcal{L}^{+}(x_0)\langle t^n(x_0)\rangle = -n\langle t^{n-1}(x_0)\rangle.$$

(Moments of the MFPT)

6.A The Adjoint Operator of the Smoluchowski Operator

In order to determine the explicit form of the adjoint operator of the Smoluchowski operator, we first need to recall the formalisms of *functional analysis*.

Consider a Hilbert space $\mathcal{H}$ over a field $\mathbb{F} \in \{\mathbb{R}, \mathbb{C}\}$. If T is a bounded linear operator on $\mathcal{H}$, there is a unique operator $T^\dagger \in \mathcal{H}$, such that

$$\langle Tf, g\rangle = \langle f, T^\dagger g\rangle \qquad \forall\ f, g \in \mathcal{H}. \tag{6.98}$$

The operator $T^\dagger$ is called the adjoint operator of T. It is important to note that the angle notation in Eq. (6.98) represents the finite scalar product between Tf and g on the left-hand side and between f and $T^\dagger g$ on the right-hand side.

To find $\mathcal{L}^\dagger(x)$, we require two arbitrary functions (propagators): $p(x, t|x_0)$ and $q(x, t|x_0)$. The space domain in this case is $\Omega := (-\infty, \infty)$.[9] Therefore, the scalar product of $\mathcal{L}(x)p(x, t|x_0)$ and $q(x, t|x_0)$ is

$$\langle \mathcal{L}(x)p(x, t|x_0), q(x, t|x_0)\rangle = \int_{-\infty}^{\infty} \mathcal{L}(x)p(x, t|x_0)\overline{q(x, t|x_0)}\,\mathrm{d}x, \tag{6.99}$$

where the bar on $\overline{q(x, t|x_0)}$ is denoting a complex conjugate. Substituting the Smoluchowski operator as shown in Eq. (6.12) into the latter equation leads to

$$\begin{aligned}&\langle \mathcal{L}(x)p(x, t|x_0), q(x, t|x_0)\rangle \\ &\quad = \int_{-\infty}^{\infty} \frac{\partial}{\partial x}\left\{D(x)\mathrm{e}^{-\beta U(x)}\frac{\partial}{\partial x}\left[\mathrm{e}^{\beta U(x)}p(x, t|x_0)\right]\right\}\overline{q(x, t|x_0)}\,\mathrm{d}x.\end{aligned} \tag{6.100}$$

Integrating by parts yields

$$\begin{aligned}\langle \mathcal{L}(x)p(x, t|x_0), q(x, t|x_0)\rangle &= \overline{q(x, t|x_0)}D(x)\mathrm{e}^{-\beta U(x)}\frac{\partial}{\partial x}\left[\mathrm{e}^{-\beta U(x)}p(x, t|x_0)\right]\Big|_{-\infty}^{\infty} \\ &\quad - \int_{-\infty}^{\infty} D(x)\mathrm{e}^{-\beta U(x)}\frac{\partial}{\partial x}\left[\mathrm{e}^{\beta U(x)}p(x, t|x_0)\right]\left[\frac{\partial}{\partial x}\overline{q(x, t|x_0)}\right]\mathrm{d}x.\end{aligned} \tag{6.101}$$

Based on the same physical requirements we used in Chap. 3, we set the probability of finding the particle at infinity at any finite time t as null. Thus, both propagators, $p(x, t|x_0)$ and $q(x, t|x_0)$, together with their derivatives vanish at such limit, meaning that

[9] The reader must recognize the difference between Hilbert space $\mathcal{H}$ and the space domain Ω.

$$\langle \mathcal{L}(x)p(x,t|x_0), q(x,t|x_0)\rangle$$
$$= -\int_{-\infty}^{\infty} D(x)\mathrm{e}^{-\beta U(x)}\frac{\partial}{\partial x}\left[\mathrm{e}^{\beta U(x)}p(x,t|x_0)\right]\left[\frac{\partial}{\partial x}\overline{q(x,t|x_0)}\right]\,\mathrm{d}x. \tag{6.102}$$

Now, by using the chain rule, we find that

$$\frac{\partial}{\partial x}\left[\mathrm{e}^{\beta U(x)}p(x,t|x_0)\right] = p(x,t|x_0)\frac{\partial}{\partial x}(\mathrm{e}^{\beta U(x)}) + \mathrm{e}^{\beta U(x)}\frac{\partial}{\partial x}p(x,t|x_0), \tag{6.103}$$

a simple result that allows us to write the following equation:

$$\begin{aligned}\langle \mathcal{L}(x)p(x,t|x_0), q(x,t|x_0)\rangle &= -\int_{-\infty}^{\infty} D(x)p(x,t|x_0)\frac{\partial}{\partial x}\left(\mathrm{e}^{\beta U(x)}\right)\mathrm{e}^{-\beta U(x)}\frac{\partial}{\partial x}\overline{q(x,t|x_0)}\,\mathrm{d}x \\ &\quad -\int_{-\infty}^{\infty} D(x)\mathrm{e}^{\beta U(x)}\frac{\partial}{\partial x}p(x,t|x_0)\,\mathrm{e}^{-\beta U(x)}\frac{\partial}{\partial x}\overline{q(x,t|x_0)}\,\mathrm{d}x.\end{aligned} \tag{6.104}$$

It is helpful to calculate each of the integrals individually by defining

$$I_5 \equiv -\int_{-\infty}^{\infty} D(x)p(x,t|x_0)\frac{\partial}{\partial x}\left(\mathrm{e}^{\beta U(x)}\right)\mathrm{e}^{-\beta U(x)}\frac{\partial}{\partial x}\overline{q(x,t|x_0)}\,\mathrm{d}x \tag{6.105}$$

and

$$I_6 \equiv -\int_{-\infty}^{\infty} D(x)\mathrm{e}^{\beta U(x)}\frac{\partial}{\partial x}p(x,t|x_0)\,\mathrm{e}^{-\beta U(x)}\frac{\partial}{\partial x}\overline{q(x,t|x_0)}\,\mathrm{d}x. \tag{6.106}$$

The integral I_5, when integrating by parts, becomes

$$\begin{aligned}I_5 = &-\left\{\left[p(x,t|x_0)\mathrm{e}^{\beta U(x)} - \int \mathrm{e}^{\beta U(x)}\frac{\partial}{\partial x}p(x,t|x_0)\,\mathrm{d}x\right]D(x)\mathrm{e}^{-\beta U(x)}\frac{\partial}{\partial x}\overline{q(x,t|x_0)}\right\}_{-\infty}^{\infty} \\ &+\int_{-\infty}^{\infty}\left[p(x,t|x_0)\mathrm{e}^{\beta U(x)} - \int \mathrm{e}^{\beta U(x)}\frac{\partial}{\partial x}p(x,t|x_0)\,\mathrm{d}x\right] \\ &\quad \frac{\partial}{\partial x}\left[D(x)\mathrm{e}^{-\beta U(x)}\frac{\partial}{\partial x}\overline{q(x,t|x_0)}\right]\,\mathrm{d}x\end{aligned} \tag{6.107}$$

The first term of the latter equation is zero because of the behavior of the propagator and its derivatives at $\pm\infty$. Therefore,

$$I_5 = \int_{-\infty}^{\infty} \left[p(x,t|x_0)\mathrm{e}^{\beta U(x)} - \int \mathrm{e}^{\beta U(x)} \frac{\partial}{\partial x} p(x,t|x_0)\, \mathrm{d}x \right] \frac{\partial}{\partial x} \left[D(x)\mathrm{e}^{-\beta U(x)} \frac{\partial}{\partial x} \overline{q(x,t|x_0)} \right] \mathrm{d}x. \tag{6.108}$$

Furthermore, the integral I_6 is computed in the same way, i.e.,

$$I_6 = -\int_{-\infty}^{\infty} \mathrm{e}^{\beta U(x)} \frac{\partial}{\partial x} p(x,t|x_0) \left[D(x)\mathrm{e}^{-\beta U(x)} \frac{\partial}{\partial x} \overline{q(x,t|x_0)} \right] \mathrm{d}x. \tag{6.109}$$

After integrating by parts, we have

$$I_6 = -\left[D(x)\mathrm{e}^{\beta U(x)} \frac{\partial}{\partial x} \overline{q(x,t|x_0)} \int \mathrm{e}^{\beta U(x)} \frac{\partial}{\partial x} p(x,t|x_0)\, \mathrm{d}x \right]_{-\infty}^{\infty} + \int_{-\infty}^{\infty} \left[\int \mathrm{e}^{\beta U(x)} \frac{\partial}{\partial x} p(x,t|x_0)\, \mathrm{d}x \right] \frac{\partial}{\partial x} \left[D(x)\mathrm{e}^{-\beta U(x)} \frac{\partial}{\partial x} \overline{q(x,t|x_0)} \right] \mathrm{d}x, \tag{6.110}$$

which, similarly, reduces to

$$I_6 = \int_{-\infty}^{\infty} \left[\int \mathrm{e}^{\beta U(x)} \frac{\partial}{\partial x} p(x,t|x_0)\, \mathrm{d}x \right] \frac{\partial}{\partial x} \left[D(x)\mathrm{e}^{-\beta U(x)} \frac{\partial}{\partial x} \overline{q(x,t|x_0)} \right] \mathrm{d}x. \tag{6.111}$$

Substituting Eqs. (6.108) and (6.111) into Eq. (6.104) yields

$$\begin{aligned} &\langle \mathcal{L}(x)\, p(x,t|x_0), q(x,t|x_0) \rangle \\ &\quad = I_5 + I_6 \int_{-\infty}^{\infty} p(x,t|x_0)\mathrm{e}^{\beta U(x)} \frac{\partial}{\partial x} \left[D(x)\mathrm{e}^{-\beta U(x)} \frac{\partial}{\partial x} \overline{q(x,t|x_0)} \right] \mathrm{d}x \\ &\quad - \int_{-\infty}^{\infty} \left[\int \mathrm{e}^{\beta U(x)} \frac{\partial}{\partial x} p(x,t|x_0)\, \mathrm{d}x \right] \frac{\partial}{\partial x} \left[D(x)\mathrm{e}^{-\beta U(x)} \frac{\partial}{\partial x} \overline{q(x,t|x_0)} \right] \mathrm{d}x \\ &\quad + \int_{-\infty}^{\infty} \left[\int \mathrm{e}^{\beta U(x)} \frac{\partial}{\partial x} p(x,t|x_0)\, \mathrm{d}x \right] \frac{\partial}{\partial x} \left[D(x)\mathrm{e}^{-\beta U(x)} \frac{\partial}{\partial x} \overline{q(x,t|x_0)} \right] \mathrm{d}x. \end{aligned} \tag{6.112}$$

Rearranging the last equation, we obtain

$$\langle \mathcal{L}(x)\, p(x,t|x_0), q(x,t|x_0)\rangle = \int_{-\infty}^{\infty} \overline{\overline{p(x,t|x_0)}\, \mathrm{e}^{\beta U(x)} \frac{\partial}{\partial x}\left[D(x)\mathrm{e}^{-\beta U(x)} \frac{\partial}{\partial x} q(x,t|x_0)\right]}\, \mathrm{d}x. \tag{6.113}$$

With the use of Eq. (6.98), we finally arrive, at[10]

$$\begin{aligned}\langle \mathcal{L}(x)\, p(x,t|x_0), q(x,t|x_0)\rangle &= \int_{-\infty}^{\infty} \overline{\overline{p(x,t|x_0)}\, \mathrm{e}^{\beta U(x)} \frac{\partial}{\partial x}\left[D(x)\mathrm{e}^{-\beta U(x)} \frac{\partial}{\partial x} q(x,t|x_0)\right]}\, \mathrm{d}x \\ &= \langle p(x,t|x_0), \mathcal{L}^{\dagger}(x) q(x,t|x_0)\rangle\end{aligned}$$

from which we can conclude that

$$\mathcal{L}^{\dagger}(x) = \mathrm{e}^{\beta U(x)} \frac{\partial}{\partial x} D(x) \mathrm{e}^{-\beta U(x)} \frac{\partial}{\partial x}, \tag{6.114}$$

as stated in Eq. (6.29).

Further Reading and References

B. Cichocki (ed.), *Marian Smoluchowski. Selected Scientific Works* (Wydawnictwa Uniwersytetu Warszawskiego, Warsaw, 2017)
L.D. Landau, E.M. Lifshitz, *Fluid Mechanics* (Pergamon Press, Oxford, 1975)
G.H. Weiss, *Aspects and Applications of the Random Walk* (North-Holland, Amsterdam, 1994)

[10] The complex conjugate of the whole function inside the integral that multiplies $p(x,t|x_0)$, together with the propagator $q(x,t|x_0)$, is real. This is why, only in this specific case, we can ignore the complex conjugate operation.

Chapter 7
Trapping Particles Influenced by External Forces

In the preceding chapter, we introduced fundamental physical properties of diffusion in the presence of an external potential by means of the Smoluchowski equation, Eq. (6.11), and worked out two examples of diffusion in the presence of a force field, specifically, the linear and harmonic potentials. In this chapter, we will study diffusion in the presence of an external field in semi-infinite, finite, and periodic systems. This extension has a significant number of applications, including studying the conduction pathway for selected ions to trasverse the membrane through ion channels in the presence of an external force, which is a critical and ubiquitous process in cells. Other examples are chromatography and electrophoresis, where the separation of molecular species is based on their size and electrical charge in the presence of a uniform electrical field. Moreover, an important approach for measuring the rate of motion of molecules is to create a continuous force that drives the motion in one direction in a centrifuge, which is used to measure the sedimentation coefficient that in turn allows us to measure the viscosity coefficient.

7.1 Semi-infinite: Perfectly Absorbing Endpoint, $U(x) = -Fx$

In the present section, we assume that a constant force F acts on a diffusing particle in a semi-infinite one-dimensional domain Ω with an absorbing wall at $x = 0$. As we already know, this is equivalent to saying that the particle moves in the presence of a scalar potential $U(x) = -Fx$, where a perfect absorbing point is placed at $x = 0$. The description of the diffusion process in this case requires solving the Smoluchowski equation subject to the boundary condition (BC) $p(0, t|x_0) = 0$, for which purpose we use the method of images. The main idea behind this method is to find a solution in terms of a linear combination of propagator in free space in the

L. Dagdug et al., *Diffusion Under Confinement*,
https://doi.org/10.1007/978-3-031-46475-1_7

presence of a constant drift, Eq. (6.48), in such a way that the solution is canceled out at the origin.

We start by writing the solution of the diffusion system with constant drift, given by Eq. (6.48), as follows:

$$p(x,t|x_0) = \frac{1}{\sqrt{4\pi Dt}} \exp\left[-\frac{(x-x_0)^2}{4Dt}\right] \exp\left[-\frac{v^2 t}{4D} + \frac{v(x-x_0)}{2D}\right]. \tag{6.48}$$

The factor inside the brace brackets is actually the solution to the free-field and free-space diffusing particle, which we obtained in Chap. 3 and renamed in Sect. 4.3.4 as $p_F(x,t|x_0)$, namely,

$$p_F(x,t|x_0) = \frac{1}{\sqrt{4\pi Dt}} \exp\left[-\frac{(x-x_0)^2}{4Dt}\right]. \tag{3.29}$$

Thus, the solution to the free-space diffusion with constant drift problem can be written as

$$p(x,t|x_0) = \exp\left[-\frac{v^2 t}{4D} + \frac{v(x-x_0)}{2D}\right] p_F(x,t|x_0). \tag{7.1}$$

Now, we make the two transformations mentioned in Sect. 4.3.4 for the propagator to describe the image particle, i.e., we take the free-field propagator to negative values and move its starting position to $-x_0$, yielding $-p_F(x,t|-x_0)$. This process leads us to the propagator for the image particle subject to a constant drift, that is,

$$p(x,t|x_0) = -\exp\left[-\frac{v^2 t}{4D} + \frac{v(x-x_0)}{2D}\right] p_F(x,t|-x_0). \tag{7.2}$$

Therefore, aiming to depict the semi-infinite system with a perfect absorbing endpoint at the origin, we add both contributions, Eqs. (7.1) and (7.2), yielding

$$p(x,t|x_0) = \exp\left[-\frac{v^2 t}{4D} + \frac{v(x-x_0)}{2D}\right] \left[p_F(x,t|x_0) - p_F(x,t|-x_0)\right], \tag{7.3}$$

a solution that satisfies the absorbing BC. By writing the last equation explicitly, and recalling that $v = \mu F = \beta D F$, we finally find

$$p(x,t|x_0) = \frac{1}{\sqrt{4\pi Dt}} \left\{ \exp\left[-\frac{(x-x_0-\mu Ft)^2}{4Dt}\right] - \mathrm{e}^{-\beta F x_0} \exp\left[-\frac{(x+x_0-\mu Ft)^2}{4Dt}\right] \right\}. \tag{7.4}$$

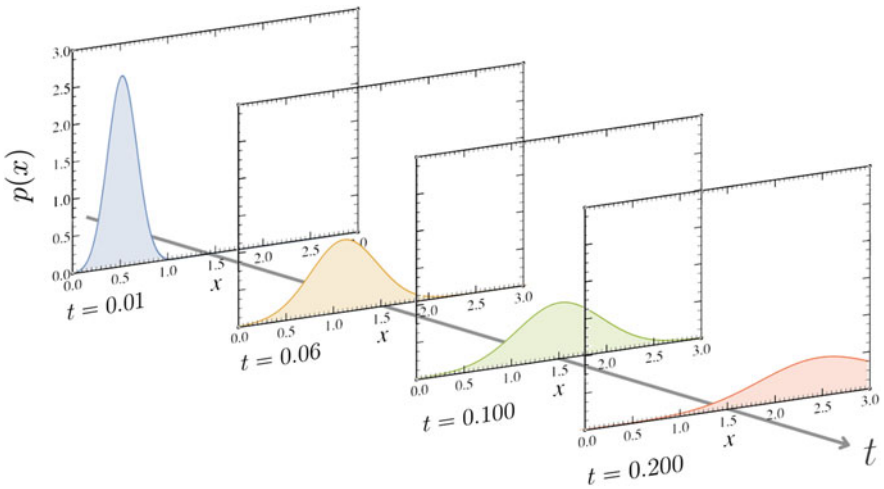

Fig. 7.1 Time evolution of the propagator $p(x, t|x_0)$ of the semi-infinite system in the presence of a linear potential and an absorbing point at $x = 0$, Eq. (7.4), at different times. The initial position, system length, and diffusivity are $x_0 = 0.5$, $L = 1$, and $D = 1$, respectively. Additionally, the force F and parameters μ and β are set to $F = 10$ and $\mu = \beta = 1$

It is worth noting that when $F = 0$, this propagator reproduces Eq. (4.31), as expected. The temporal evolution of Eq. (7.4) is depicted in Fig. 7.1.

7.1.1 Survival Probability and First-Passage Time

From the definition given in Eq. (2.30), the survival probability, $S(t|x_0)$, is calculated by integrating Eq. (7.4) over the entire domain Ω, i.e., $x > 0$, namely,

$$S(t|x_0) = \frac{1}{\sqrt{4\pi Dt}} \int_0^\infty \left\{ \exp\left[-\frac{(x - x_0 - \mu F t)^2}{4Dt} \right] - \mathrm{e}^{-\beta F x_0} \exp\left[-\frac{(x + x_0 - \mu F t)^2}{4Dt} \right] \right\} \mathrm{d}x. \tag{7.5}$$

To perform the integration, we use Eq. (A.85), leading to

$$S(t|x_0) = \frac{1}{2} \left[\mathrm{erfc}\left(-\frac{x_0 + \mu F t}{\sqrt{4Dt}} \right) - \mathrm{e}^{-\beta F x_0} \mathrm{erfc}\left(\frac{x_0 - \mu F t}{\sqrt{4Dt}} \right) \right]. \tag{7.6}$$

The survival probability, predicted by Eq. (7.6), is illustrated on the left-hand side of Fig. 7.2. In the case where $F = 0$, Eq. (7.6) reduces to Eq. (4.57), namely,

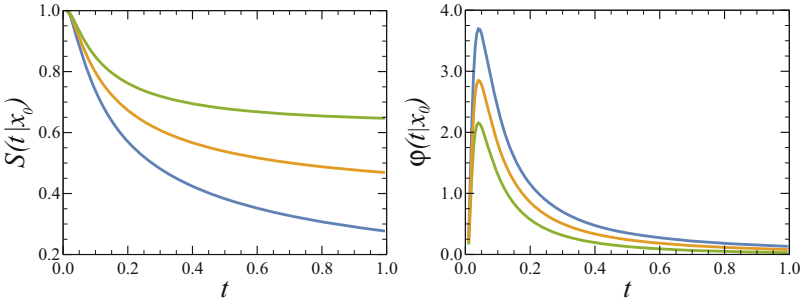

Fig. 7.2 Survival probability predicted by Eq. (7.6) and probability density of mean first-passage time, Eq. (7.7), for different values of the external force: $F = 0$ (blue line), $F = 1$ (yellow line), $F = 2$ (green line). In all cases, the starting position is set at $x_0 = 0.5$ and the constant coefficients are set equal to 1, i.e., $D = \beta = \mu = 1$

$$S(t|x_0) = \operatorname{erf}\left(\frac{x_0}{\sqrt{4Dt}}\right). \tag{4.57}$$

This result follows from the properties of the error function. Explicitly, we use the identity (A.82) to obtain that $\operatorname{erfc}(-x) - \operatorname{erfc}(x) = 2\operatorname{erf}(x)$.

The probability density of mean first-passage time is computed using Eq. (2.34), namely,

$$\varphi(t|x_0) = -\frac{\mathrm{d}S(t|x_0)}{\mathrm{d}t}. \tag{2.34}$$

Therefore, using Eq. (A.86) for the derivative of $S(t|x_0)$ with respect to t, we have

$$\varphi(t|x_0) = \frac{x_0}{\sqrt{4\pi Dt^3}} \exp\left[-\frac{(x_0 + DF\beta t)^2}{4Dt}\right]. \tag{7.7}$$

Representative plots of the probability density of mean first-passage time are shown on the right-hand side of Fig. 7.2.

The first moment of mean first-passage time is calculated according to Eq. (2.41). Nonetheless, we have to be careful when integrating. It is appropriate to separate the computation into two cases, i.e., when $F < 0$ and $F > 0$. For positive forces, the process is straightforward:

$$\begin{aligned}\langle t_{F>0}(x_0)\rangle &= \int_0^\infty t \left\{\frac{x_0}{\sqrt{4\pi Dt^3}} \exp\left[-\frac{(x_0 + DF\beta t)^2}{4Dt}\right]\right\} \mathrm{d}t \\ &= \int_0^\infty \frac{x_0}{\sqrt{4\pi Dt}} \exp\left[-\left(\frac{x_0 + DF\beta t}{\sqrt{4Dt}}\right)^2\right] \mathrm{d}t.\end{aligned} \tag{7.8}$$

Using the change of variables $u = \sqrt{4Dt}$, we are able to write it as

$$\langle t_{F>0}(x_0)\rangle = \frac{x_0}{2D\sqrt{\pi}} \int_0^\infty \exp\left[-\left(\frac{x_0 + \frac{F\beta u^2}{4}}{u} \right)^2 \right] \mathrm{d}u. \tag{7.9}$$

Then, by making a series of the binomial factor inside the exponential and keeping terms up to the second order in u, we arrive at

$$\langle t_{F>0}(x_0)\rangle = \frac{x_0}{2D\sqrt{\pi}} \mathrm{e}^{-F\beta x_0/2} \int_0^\infty \exp\left(-\frac{x_0^2}{u^2} - \frac{F^2\beta^2 u^2}{16} \right) \mathrm{d}u. \tag{7.10}$$

Using Eq. (A.13) to solve the integral, we arrive at

$$\langle t_{F>0}(x_0)\rangle = \frac{\mathrm{e}^{-F\beta x_0}}{DF\beta} x_0. \tag{7.11}$$

Similarly, we obtain the first moment of mean first-passage time for negative forces. In this case, the integral that we have to compute is the following:

$$\langle t_{F<0}(x_0)\rangle = \int_0^\infty \frac{x_0}{\sqrt{4\pi Dt}} \exp\left[-\left(\frac{x_0 - D|F|\beta t}{\sqrt{4Dt}} \right)^2 \right] \mathrm{d}t, \tag{7.12}$$

and through the same process, we find that

$$\begin{aligned} \langle t_{F<0}(x_0)\rangle &= \frac{\mathrm{e}^{|F|\beta x_0}}{2D\sqrt{\pi}} x_0 \left[\frac{1}{2}\sqrt{\frac{\pi}{F^2\beta^2}} \exp\left(-2\sqrt{\frac{F^2\beta^2 x_0^2}{16}} \right) \right] \\ &= \frac{x_0}{D|F|\beta}. \end{aligned} \tag{7.13}$$

To analyze the long time behavior of the survival probability given by Eq. (7.6), we need to use the following properties of the complementary error function:

$$\lim_{x\to\infty} \operatorname{erfc}(x) = 0, \tag{7.14}$$

and

$$\lim_{x\to\infty} \operatorname{erfc}(-x) = 2. \tag{7.15}$$

Since the force defines the sign of the argument of the complementary error function in Eq. (7.6), once again, we divide the problem into two cases: when $F < 0$ and $F > 0$. The latter drives the particle away from the absorbing target and Eq. (7.6) reduces to

$$\lim_{t\to\infty} S(t|x_0) = 1 - e^{-\beta F x_0}. \tag{7.16}$$

It is worth noting that in this case, the survival probability approaches a constant other than zero and reaches a plateau value equal to 1 as Fx_0 increases. This means that there is a finite probability that a particle will never reach the absorbing endpoint.

On the contrary, when $F < 0$, the force drives the diffusing particle toward the absorbing endpoint, and from Eq. (7.6), we find that the survival probability tends to zero. In this case, all the particles reach the absorbing target. To obtain an asymptotic expression for this case, we substitute the asymptotic relation for a long x, $\text{erfc}(x) \approx e^{-x^2}/x\sqrt{\pi}$, into Eq. (7.6), finding that

$$S(t|x_0) \approx \frac{e^{-\mu\beta F^2 t/4}}{\sqrt{\pi\,\mu\beta\, t\,|F|}}. \tag{7.17}$$

When the force drives the particle toward the absorbing endpoint, the survival probability tends to zero more rapidly than when $F = 0$. We can see this more clearly from the result obtained in Sect. 4.3.5, given by Eq. (4.57), namely,

$$S(t|x_0) \approx \frac{x_0}{\sqrt{\pi\, Dt}}. \tag{4.57}$$

Representative plots of Eqs. (7.17) and (4.57) are shown in Fig. 7.3.

The probability of a diffusion particle hitting the absorbing boundary for the first time when the force drives it toward the absorbing endpoint, the mean first-passage time (MFPT), is calculated by integrating Eq. (7.17) over the entire time period, leading to

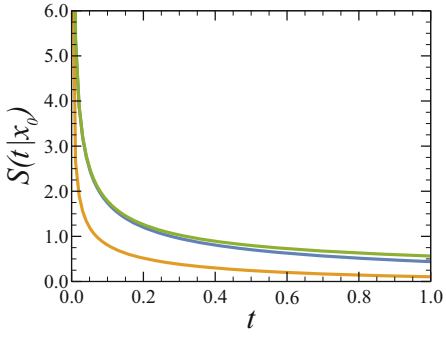

Fig. 7.3 Survival probability distribution predicted by Eqs. (7.17) and (4.57) for different values of the external force: $F = -1$ (blue line), $F = -2$ (yellow line), $F = 0$. (green line). In Eq. (4.57), the starting position of the particle is set at $x_0 = 1$. In all cases, the coefficient are set equal to 1, $D = \mu = \beta = 1$

$$\langle t(x_0)\rangle = \int_0^\infty \frac{e^{-\mu\beta F^2 t/4}}{\sqrt{\pi\mu\beta\, t\,|F|}}\,\mathrm{d}t = \frac{2}{\beta\mu\, F^2}, \tag{7.18}$$

which decreases inversely proportional to the square of F.

7.2 Drift and Diffusion into Partially Absorbing and Absorbing Endpoints, $U(x) = -Fx$

The general approach to solve Brownian particle finite-length diffusing systems in the presence of special targets, *e.g.*, reflecting, absorbing, and partially absorbing endpoints, was introduced in Chap. 5 as the Laplace transform method, where we were interested in finding the proper phase to include into the anzats' argument, mainly hyperbolic functions (sinh or cosh), so to satisfy both the diffusion equation and the boundary conditions (BCs). This technique is quite powerful, since it allows us to obtain analytically physical quantities, such as moments of MFPT $\langle t^n(x_0)\rangle$ and splitting probabilities $\theta_{x'}(x_0)$ simply by imposing the BCs together with the continuity and discontinuity conditions. Nevertheless, its drawback is that most of the solutions are found in Laplace's space. As we have pinpointed before, finding the inverse Laplace transform of a function $f(s)$ can be extremely difficult, reason why we appeal to numerical methods (see Appendix 5.A).

In this section and the next one, we will solve a set of diffusion problems within a finite domain Ω in the presence of a constant drift by means of Laplace transform, firsty by making certain considerations in order to simplify the problem and secondly by approaching its most general version.

Consider a Brownian particle diffusing along the interval $[0, L]$ in the presence of a partially absorbing endpoint at $x = 0$ and a perfect absorbing target at $x = L$, as depicted in Fig. 7.4. Our goal is to solve the Smoluchowski equation, Eq. (6.11), within the BCs associated with the problem and $U(x) = -Fx$. We have used these mathematical requirements before (as an example, see Sects. 5.7–5.9 and 6.5). In this case, we have

$$p(x, t = 0|x_0) = \delta(x - x_0), \tag{7.19}$$

as the initial condition, and

Fig. 7.4 Schematic representation of a one-dimensional domain with a partially absorbing end at $x = 0$ (yellow circle) and a perfectly absorbing point at $x = L$ (red circle)

$$D\frac{\partial p(x,t|x_0)}{\partial x}\bigg|_{x=0} - D\beta F p(0,t|x_0) = \kappa p(0,t|x_0) \quad \text{together with} \quad p(L,t|x_0) = 0, \tag{7.20}$$

as the BCs.

In order to simplify the problem, we set the particle's trajectory to $x_0 = 0$ and make $p(x,t|0) = p(x,t)$. The primary consideration is to write the propagator as follows:

$$p(x,t) = \mathrm{e}^{\beta F x/2} g(x,t). \tag{7.21}$$

Now, following a process similar to the one used to go from Eq. (6.42) to Eq. (6.43), we find that the Smoluchowski equation, when implementing Eq. (7.21), would be giving as

$$\frac{\partial g(x,t)}{\partial t} = \frac{\partial^2 g(x,t)}{\partial x^2} - \left(\frac{\beta F}{2}\right)^2 g(x,t). \tag{7.22}$$

In this new boundary value problem, all boundary and initial conditions are transformed to provide the same structure as Eqs. (7.19) and (7.20), except for the partially absorbent boundary condition, in which case it modifies to

$$D\frac{\partial g(x,t)}{\partial t}\bigg|_{x=0} - \frac{D\beta F}{2} g(0,t) = \kappa g(0,t). \tag{7.23}$$

Then, we have to Laplace transform Eq. (7.22). Using Eq. (A.55), this yields

$$sg(x,s) - \delta(x) = D\left[\frac{\partial^2 g(x,s)}{\partial s^2} - \left(\frac{F\beta F}{2}\right)^2 g(x,s)\right], \tag{7.24}$$

and, when rearranging, we find that

$$\frac{\partial^2 g(x,s)}{\partial s} = q^2 g(x,s) - \frac{\delta(x)}{D}, \tag{7.25}$$

with

$$q \equiv \sqrt{\frac{s}{D} + \left(\frac{\beta F}{2}\right)^2}, \tag{7.26}$$

is the differential equation to be solved. The ansatz will be a hyperbolic function. Here, it is convenient to choose the hyperbolic sine function. Since we have gained experience from Chap. 5 on computing the proper phase so as to satisfy the system, let us propose[1]

$$g(x,s) = A\sinh\left[q(L-x)\right]. \tag{7.27}$$

To find the constant A, we substitute the latter equation into Eq. (7.23), obtaining

$$A = \frac{1}{D\left[q\cosh(Lq) + \left(\frac{\beta F}{2} + \frac{\kappa}{D}\right)\sinh(Lq)\right]}. \tag{7.28}$$

The complete solution is then

$$p(x,s) = A\sinh[q(L-x)]\mathrm{e}^{\beta F x/2}. \tag{7.29}$$

Representative plots of the propagator in real space are shown in Fig. 7.5.[2]

The survival probability in Laplace and first moment of MFPT are computed as indicated in Chap. 2, Eqs. (2.30) and (2.90), namely,

$$S(s) = \int_0^L p(x,s)\,\mathrm{d}x = \frac{2A\left[\beta F\sinh(qL) + 2q\cosh(qL) - 2\mathrm{e}^{\beta FL/2}\right]}{4q^2 - \beta^2F^2}, \tag{7.30}$$

and, by making a Taylor series of $S(s)$ around $s = 0$, we obtain

$$\langle t\rangle = S(s)\Big|_{s=0} = \frac{1 + \mathrm{e}^{\beta FL}(\beta FL - 1)}{\beta F\left[\mathrm{e}^{\beta FL}(D\beta F + \kappa) - \kappa\right]}. \tag{7.31}$$

The plot of the survival probability, Eq. (7.30), as a function of time, is shown on the left-hand side of Fig. 7.6.

[1] Note that we have skipped the split solution and therefore the continuity condition. This is because the system is composed by Brownian particles that start their trajectory at $x_0 = 0$, so the solution we are looking for is the right-hand side solution, which turns to comprise the whole diffusing domain.

[2] It is often impossible to find the inverse Laplace transform function analytically. For such reason, numerical methods that provide an approximate solution to the problem have been developed. In Appendix 5.A, the reader will find a discussion on the Gaver-Stehfest numerical method, as well as the *Mathematica* code, to perform the inversion numerically.

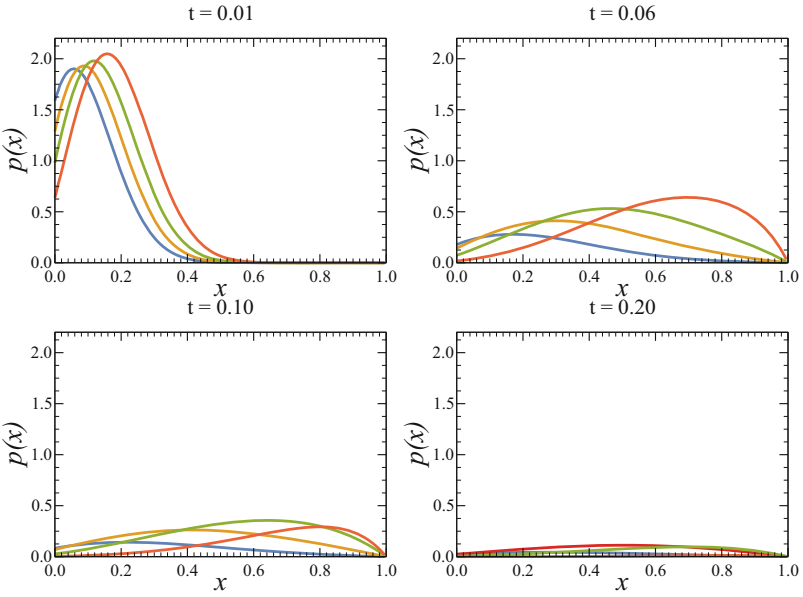

Fig. 7.5 Frames of the temporal evolution of the propagator $p(x,t)$, Eq. (7.29), for different values of the drag force F: $F = -3$ (blue line), $F = 1$ (yellow line), $F = 5$ (green line), $F = 10$ (orange line). The trapping rate is $\kappa = 10$. The initial position of Brownian particles, system length, and diffusivity are $x_0 = 0.0$, $L = 1$, and $D = 1$, respectively

7.2.1 Flux and Splitting Probability

The flux in Laplace space can be found directly through the propagator $p(x,s)$ (see Eq. (5.60)). As such

$$J(L,s) = -D\frac{\partial p(x,s)}{\partial x}\hat{\mathbf{e}}_x \cdot \hat{\mathbf{e}}_x = \frac{q\mathrm{e}^{\beta FL/2}}{q\cosh(qL) + (\frac{\beta F}{2} + \frac{\kappa}{D})\sinh(qL)}. \tag{7.32}$$

Furthermore, the splitting probability for the right-hand side endpoint is computed using Eq. (5.66) when making a series of $J(L,s)$ around $s = 0$, i.e.,

$$\theta_L = J(L,s)\Big|_{s=0} = \frac{D\beta F\mathrm{e}^{\beta FL}}{\mathrm{e}^{\beta FL}(D\beta F + \kappa) - \kappa}. \tag{7.33}$$

As an illustration, let us calculate the conditional probability density of MFPT at the right-hand side, $\varphi_L(s)$, a physical property that we will explore in detail in Chap. (8). In accordance with Eq. (8.6), we have

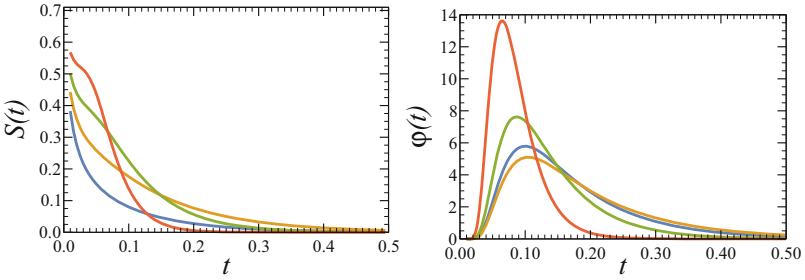

Fig. 7.6 Schematic representation of survival probability, Eq. (7.30), and the conditional probability density of first-passage time, Eq. (7.34), for different values of the force F: $F = -3$ (blue line), $F = 1$ (yellow line), $F = 5$ (green line), $F = 10$ (orange line). The starting position of the particles is set at $x_0 = 0.0$, the length is $L = 1$, the trapping rate is $\kappa = 10$, and the diffusion coefficient is $D = 1$

$$\varphi_L(s) = \frac{J(L,s)}{\theta_L} = \frac{\mathrm{e}^{-\beta FL/2}\left[\mathrm{e}^{\beta FL} q(D\beta F + \kappa) - q\kappa\right]}{\beta F\left[Dq\cosh(qL) + \left(\frac{D\beta F}{2} + \kappa\right)\sinh(qL)\right]}. \tag{7.34}$$

Characteristic plots of φ_L in real space are shown on the right-hand side of Fig. 7.6.

It is worth mentioning that two systems are contained within the partially absorbing-absorbing diffusion system with drift: the absorbing-absorbing and the reflecting-absorbing settings, meaning that the physical quantities, i.e., $\langle t\rangle$, θ_L, and $\varphi_L(s)$ can be obtained as a special cases of Eqs. (7.31), (7.33), and (7.34), respectively.

7.2.2 *Reflecting-Absorbing and Absorbing-Absorbing*

As stated in Sect. 4.2, special cases of the partially absorbing-absorbing system can be derived by using the limit values of κ, namely, $\kappa \to 0$, for the reflecting-absorbing system, and $\kappa \to \infty$, for the absorbing-absorbing system, resulting in

$$\varphi_L^{\kappa\to 0}(s) = \frac{\mathrm{e}^{\beta FL/2} q}{q\cosh(qL) + \frac{\beta F}{2}\sinh(qL)}, \tag{7.35}$$

$$\langle t\rangle_{\kappa\to 0} = \frac{\mathrm{e}^{-\beta FL}\left[1 + \mathrm{e}^{\beta FL}(\beta FL - 1)\right]}{D\beta^2 F^2}, \tag{7.36}$$

together with

$$\theta_L^{\kappa\to 0} = 1, \tag{7.37}$$

for the reflecting-absorbing system, and

$$\varphi_L^{\kappa\to\infty}(s) = \frac{\mathrm{e}^{-\beta FL/2} q(\mathrm{e}^{\beta FL} - 1)}{\beta F \sinh(qL)}, \tag{7.38}$$

$$\langle t \rangle_{\kappa\to\infty} = 0, \tag{7.39}$$

together with

$$\theta_L^{\kappa\to\infty} = 0, \tag{7.40}$$

for the absorbing-absorbing system.

7.3 Drift and Diffusion into Two Partially Absorbing Points, $U(x) = -Fx$

The general problem of particles diffusing in a one-dimensional interval $[0, L]$, with an arbitrary starting position x_0 in the presence of a constant force (see Fig. 7.7), can be solved analytically by means of the Laplace transform. The process is quite alike to the one we showed in Sect. 5.9. The boundary conditions subject to the Smoluchowski equation with $U = -Fx$ are

$$D\frac{\partial p(x,t|x_0)}{\partial x}\bigg|_{x=0} = \kappa_1 p(0,t|x_0) \quad \text{and} \quad -D\frac{\partial p(x,t|x_0)}{\partial x}\bigg|_{x=L} = \kappa_2 p(L,t|x_0) \tag{7.41}$$

Additionally, the suggested solution for the Smoluchowski equation in Laplace space is the following:

$$p(x_<, s|x_0) = A\mathrm{e}^{r_1 x} + B\mathrm{e}^{r_2 x} \quad \text{for the left-hand side of } x_0 \tag{7.42}$$

and

$$p(x_>, s|x_0) = E\mathrm{e}^{r_1 x} + G\mathrm{e}^{r_2 x} \quad \text{for the right-hand side of } x_0 \tag{7.43}$$

Fig. 7.7 Schematic representation of a one-dimensional domain with two partially absorbing endpoints (yellow circles), one at $x = 0$ and the other at $x = L$

where $r_1 = \frac{v+\sqrt{v^2+4Ds}}{D}$, $r_2 = \frac{v-\sqrt{v^2+4Ds}}{D}$, and $A, B, E, and G$ are constants. Using the BCs, combined with the continuity and discontinuity conditions, Eqs. (3.39) and (3.42), is possible to find the solution in Laplace space for the propagator, flux, survival probability, and, therefore, first-passage time and splitting probability. These last two are written below:

$$\begin{aligned}\langle t(x_0)\rangle = &\frac{D\left[\mathrm{e}^{F(L+x_0)\mu/D}\kappa_1 + \mathrm{e}^{Fx_0\mu/D}\kappa_2 - \mathrm{e}^{FL\mu/D}(\kappa_1+\kappa_2)\right]}{\mathrm{e}^{F\mu x_0/D}F\mu\left[\mathrm{e}^{F\mu L/D}\kappa_1(\kappa_2+F\mu) + F\mu\kappa_2 - \kappa_1\kappa_2\right]}\\ &+\frac{\mathrm{e}^{Fx_0\mu/D}\kappa_2 x_0(\kappa_1 - F\mu) + \mathrm{e}^{F(L+x_0)\mu/D}\kappa_1(L-x_0)(\kappa_2+F\mu)}{\mathrm{e}^{F\mu x_0/D}F\mu\left[\mathrm{e}^{F\mu L/D}\kappa_1(\kappa_2+F\mu) + F\mu\kappa_2 - \kappa_1\kappa_2\right]}\\ &+\frac{\mathrm{e}^{F\mu L/D}(-\kappa_1+F\mu)(\kappa_2+F\mu)}{\mathrm{e}^{F\mu x_0/D}F\mu\left[\mathrm{e}^{F\mu L/D}\kappa_1(\kappa_2+F\mu) + F\mu\kappa_2 - \kappa_1\kappa_2\right]},\end{aligned} \tag{7.44}$$

$$\theta_0(x_0) = \frac{\mathrm{e}^{F(L-x_0)\mu/D}\kappa_1(\kappa_2+F\mu) - \kappa_1\kappa_2}{\mathrm{e}^{FL\mu/D}\kappa_1(\kappa_2+F\mu) + F\kappa_2\mu - \kappa_1\kappa_2}, \tag{7.45}$$

and

$$\theta_L(x_0) = \frac{\mathrm{e}^{F(L-2x_0)\mu/2D}\kappa_2\left[F\mu + \kappa_1\left(\mathrm{e}^{Fx_0\mu/D}-1\right)\right]}{F(\kappa_1+\kappa_2)\mu\cosh\left(\frac{FL\mu}{2D}\right) + [2\kappa_1\kappa_2 + F(\kappa_1-\kappa_2)\mu]\sinh\left(\frac{FL\mu}{2D}\right)}. \tag{7.46}$$

In the rest of the chapter, we will explore the Smoluchowski equation within harmonic and periodic potentials.

7.4 Perfectly Absorbent Target: Harmonic Potential

In this section, we consider a particle diffusing in a harmonic potential with a single absorbing endpoint placed at the origin, subject to the initial condition $p(x,0) = \delta(x)$. We are interested in calculating its survival probability and the MFPT to the absorbent target. In this problem, it is possible to find a solution in closed form when the absorbing point lies at the minimum of the harmonic potential, which is given by

$$U(x) = \frac{K}{2}x^2, \tag{6.71}$$

where K is the force constant. To accomplish this, we invoke the method of images. As we know from the last section, we need two contributions, one for the real

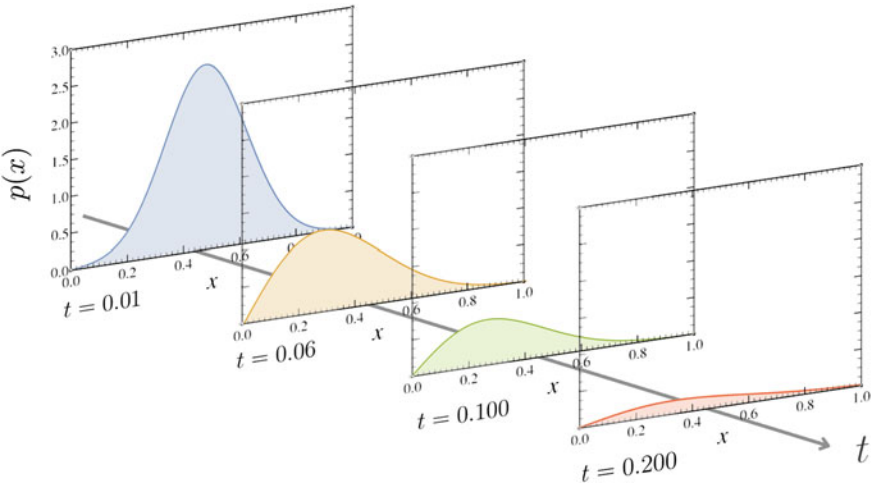

Fig. 7.8 Time evolution of the propagator $p(x, t|x_0)$ in the presence of a harmonic oscillator, Eq. (7.47), at different times. The initial position, system length, and diffusivity are $x_0 = 0.5$, $L = 1$, and $D = 1$, respectively. Also, $\beta = 1$ and the characteristic factor K is set at $K = 15$

particle and another one for the image particle that, when subtracted, they cancel out at the origin, i.e., $x = 0$. As shown in Sect. 6.6, the propagator in free space is given by

$$p_F(x, t|x_0) = \sqrt{\frac{\beta K}{2\pi(1 - \mathrm{e}^{-2\beta DKt})}} \exp\left[-\frac{\beta K(x - x_0 e^{-\beta DKt})^2}{2(1 - \mathrm{e}^{-2\beta DKt})}\right]. \tag{6.93}$$

Therefore, the solution proposed by the image method is given by $p(x, t|x_0) = p_F(x, t|x_0) - p_F(x, t| - x_0)$. Consequently

$$p(x, t|x_0) = \sqrt{\frac{\beta K}{2\pi(1 - e^{-2\beta DKt})}} \left\{ \exp\left[-\frac{\beta K(x - x_0\, e^{-\beta DKt})^2}{2(1 - e^{-2\beta DKt})}\right] - \exp\left[-\frac{\beta K(x + x_0\, e^{-\beta DKt})^2}{2(1 - e^{-2\beta DKt})}\right]\right\}. \tag{7.47}$$

The temporal evolution of the propagator (7.47) is depicted in Fig. 7.8.

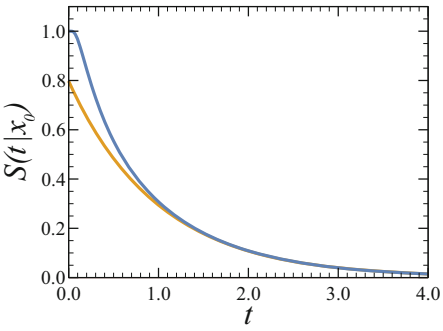

Fig. 7.9 Survival probability distribution predicted by Eqs. (7.48) (blue line) and (7.49) (yellow line), respectively. The starting position of the particle is set at $x_0 = 1$; the diffusion coefficient, the force constant, and β are set equal to one

7.4.1 Survival Probability and First-Passage Time

From the definition given in Eq. (2.30), the survival probability, $S(t|x_0)$, is calculated by integrating this last equation over all $x > 0$, which gives

$$S(t|x_0) = \text{erf}\left(\sqrt{\frac{\beta K}{2(eK^{2D\beta Kt} - 1)}}x_0\right). \tag{7.48}$$

Expanding this last equation in a Taylor series around x_0 for long times (using Eq. (A.22)) up to the first order yields

$$S(t|x_0) \approx \frac{2}{\sqrt{\pi}}x_0\, e^{2D\beta Kt}. \tag{7.49}$$

This expression tends to zero exponentially in time, which means that absorption is a certain event. In Fig. 7.9, the survival probability given by Eq. (7.48) is compared with Eq. (7.49).

The probability of the diffusing particle hitting the absorbing boundary for the first time, or MFPT, is calculated by integrating the survival probability over the entire time period. The solution of this integration cannot be obtained in closed form from Eq. (7.48) but, rather, by means of numerical integration. The result is shown in Fig. 7.10. On the other hand, for a small x_0, integrating Eq. (7.49) yields

$$\langle t(x_0)\rangle = \int_0^\infty \frac{2}{\sqrt{\pi}}x_0\, e^{2D\beta kt}\, \mathrm{d}t = \frac{2}{\sqrt{\pi}}x_0. \tag{7.50}$$

Figure 7.10 depicts the MFPT predicted by Eq. (7.50). From this figure, we can see that this approximation works reasonably well for small $x_0$when compared to the exact result obtained numerically.

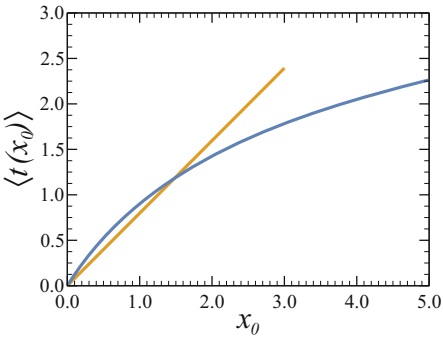

Fig. 7.10 Mean first-passage time predicted by numerical integration of Eq. (7.48) (blue line) and Eq. (7.50) (yellow line), respectively. The starting position of the particle is set at $x_0 = 1$; the diffusion coefficient, the force constant, and β are set equal to one

7.5 Drift and Diffusion for the Periodic Potential $U(x) = V(x) - Fx$

Consider a one-dimensional diffusion in the presence of a periodic potential $U(x) = V(x) - Fx$, where $V(x) = V(x+L)$ is periodic of period L and $F \geq 0$ is a uniform force. Here, we are interested in calculating splitting probability, the probability of the particle begin trapped at the left (L) and right (R) endpoints. The propagator considered as a function of x_0 satisfies the backward Smoluchowski equation given by Eq. (6.31), where $D(x) = D(x + L)$ is also a periodic function. The initial condition is given by $p(x, 0|x_0) = \delta(x - x_0)$. Because of periodicity, we set the boundaries as perfectly absorbing at the ends x_L and x_R. The splitting probability is found following an analogous procedure to the one shown in Sect. 2.9.

First, we take the x-derivative of the backward Smoluchowski equation, expression (6.31), noting that everything but the propagator depends on x. Now, we obtain the flux as stated in Fick's first law, Eq. (2.73), calculated at the endpoints, namely,

$$\frac{\partial}{\partial t}\frac{\partial p(x_0,t|x)}{\partial x}\bigg|_{x=x_L,x_R} = \mathrm{e}^{\beta U(x_0)}\frac{\partial}{\partial x_0}\left\{D(x_0)\,\mathrm{e}^{-\beta U(x_0)}\frac{\partial}{\partial x_0}\frac{\partial p(x_0,t|x)}{\partial x}\bigg|_{x=x_L,x_R}\right\}. \tag{7.51}$$

The latter expression actually represents two equations, one for each endpoint. The next step is to multiply the entire equation by the diffusivity evaluated at the corresponding endpoint, resulting in

$$\frac{\partial}{\partial t}D(x_{L,R})\frac{\partial p(x_0,t|x)}{\partial x}\bigg|_{x=x_L,x_R} = \mathrm{e}^{\beta U(x_0)}\frac{\partial}{\partial x_0}\left\{D(x_0)\,\mathrm{e}^{-\beta U(x_0)}\frac{\partial}{\partial x_0}D(x_{L,R})\frac{\partial p(x_0,t|x)}{\partial x}\bigg|_{x=x_L,x_R}\right\}, \tag{7.52}$$

which, integrating with respect to time and applying the definition of splitting probability, Eq. (2.95), yields

$$J(x_{L,R}, t \to \infty) - J(x_{L,R}, t = 0) = \mathrm{e}^{\beta U(x_0)} \frac{\partial}{\partial x_0} \left\{ D(x_0)\, \mathrm{e}^{-\beta U(x_0)} \frac{\partial}{\partial x_0} \theta_{L,R}(x_0) \right\}. \tag{7.53}$$

The left-hand side of this last equation is zero because of the boundary conditions (see Eq. (2.106)). Then, the ordinary differential equation (ODE) for the splitting probability reads

$$\frac{\mathrm{d}}{\mathrm{d}x_0} \left[D(x_0)\, e^{-\beta U(x_0)} \frac{\mathrm{d}\theta_{L,R}(x_0)}{\mathrm{d}x_0} \right] = 0, \tag{7.54}$$

where $\theta_L(x_0)$ and $\theta_L(x_0)$ are the probabilities of the particle being trapped at the left and the right endpoints, respectively, and the boundary conditions given by $\theta_L(x_L) = \theta_R(x_R) = 1$.
Integrating Eq. (7.54) with respect to x_0 gives

$$D(x_0)\, e^{-\beta U(x_0)} \frac{\mathrm{d}\theta_{L,R}(x_0)}{\mathrm{d}x_0} = C_1, \tag{7.55}$$

with C_1 being an integration constant. Now, the general solution can be written in terms of an integral, namely,

$$\theta_{L,R}(x_0) = C_1 \int \frac{\mathrm{e}^{\beta U(z)}}{D(z)}\, \mathrm{d}z. \tag{7.56}$$

The integration limits are established to fulfill the boundary conditions $\theta_L(x_R) = \theta_R(x_L) = 0$, that is,

$$\theta_L(x_0) = C_L \int_{x_0}^{x_R} \frac{\mathrm{e}^{\beta U(z)}}{D(z)}\, \mathrm{d}z, \qquad \theta_R(x_0) = C_R \int_{x_0}^{x_L} \frac{\mathrm{e}^{\beta U(z)}}{D(z)}\, \mathrm{d}z, \tag{7.57}$$

and the integration constants are renamed to avoid ambiguity. These constants can be found by means of boundary conditions $\theta_L(x_L) = \theta_R(x_R) = 1$, yielding

$$\frac{1}{C_L} = \int_{x_L}^{x_R} \frac{\mathrm{e}^{\beta U(z)}}{D(z)}\, \mathrm{d}z, \qquad \frac{1}{C_R} = \int_{x_R}^{x_L} \frac{\mathrm{e}^{\beta U(z)}}{D(z)}\, \mathrm{d}z. \tag{7.58}$$

Direct substitution of Eq. (7.58) into Eq. (7.57) gives

$$\theta_L(x_0) = \int_{x_0}^{x_R} \frac{e^{\beta U(z)}}{D(z)} \mathrm{d}z \Bigg/ \int_{x_L}^{x_R} \frac{e^{\beta U(z)}}{D(z)} \mathrm{d}z, \quad \text{and}$$
$$\theta_R(x_0) = \int_{x_L}^{x_0} \frac{e^{\beta U(z)}}{D(z)} \mathrm{d}z \Bigg/ \int_{x_L}^{x_R} \frac{e^{\beta U(z)}}{D(z)} \mathrm{d}z. \tag{7.59}$$

Taking $z \to z + L$, we have

$$\int_{x_0-L}^{x_0} \frac{e^{\beta U(z)}}{D(z)} \, \mathrm{d}z = \int_{(x_0+L)-L}^{x_0+L} \frac{e^{\beta U(z+L)}}{D(z+L)} \, \mathrm{d}(z+L) = \int_{x_0}^{x_0+L} \frac{e^{\beta U(z+L)}}{D(z)} \, \mathrm{d}z, \tag{7.60}$$

where we used the periodicity property of $D(z)$. Noticing that $V(x + L) = V(x)$, then

$$U(z+L) = V(z+L) - (z+L)F = V(z) - Fz - FL = U(z) - FL, \tag{7.61}$$

which allows us to write Eq. (7.60) as follows:

$$\int_{x_0-L}^{x_0} \frac{e^{\beta U(z)}}{D(z)} \, \mathrm{d}z = \mathrm{e}^{-\beta FL} \int_{x_0}^{x_0+L} \frac{e^{\beta U(z)}}{D(z)} \, \mathrm{d}z \tag{7.62}$$

Lastly, setting $x_L = x_0 - L$ and $x_R = x_0 + L$ in Eq. (7.59) and using the latter relation, we explicitly find that the splitting probabilities are given by

$$\theta_R(x_0) = \frac{1}{1 + e^{-\beta FL}}, \qquad \text{and} \qquad \theta_L(x_0) = \frac{e^{-\beta FL}}{1 + e^{-\beta FL}}. \tag{7.63}$$

Counterintuitively, these results are independent of the presence of the periodic potential.

7.6 Concluding Remarks

Throughout this chapter, we analyzed, computed, and derived the most important physical properties of semi-infinite, finite, and periodic systems when particles diffuse in the presence of different potentials. Once again, we demonstrated the importance of the various methods on solving diffusion problems, namely, the method of images and integral transforms. It is important to emphasize that we can summarize the solutions of $\langle t(x_0) \rangle$ and $\theta_{x'}(x_0)$ for all possible boundary condition combinations in finite-length systems in Eqs. (7.44) and (7.46) of Sect. 7.3, by studying the limit values of κ. Probably, the most interesting yet counterintuitive

result arises when deriving the splitting probability for the periodic potential, which turns out to be independent of any periodicity feature.

In the following chapter, we will dive into the mathematical description of conditional processes.

Further Reading and References

B. Cichocki (ed.), *Marian Smoluchowski. Selected Scientific Works* (Wydawnictwa Uniwersytetu Warszawskiego, Warsaw, 2017)

G.H. Weiss, *Aspects and Applications of the Random Walk* (North-Holland, Amsterdam, 1994)

Chapter 8
Splitting and Breaking Brownian Pathways: Conditional Processes

The importance of conditional probabilities arises in the analysis of models where there may be more than one pathway that can be taken by a Brownian particle. In such a case, the properties that characterize the system depend on the particular pathway taken. For example, the ion channels provide a conduction pathway for specific ions to translocate the cell membranes. Ionic transport through the cell membrane is an essential process occurring ubiquitously in cells. Even though the structure of an ion channel is very complex, we can think about the transport of an ion as a one-dimensional diffusion process between two absorbent boundaries, of crossing the free energy barriers as a result of the concentration gradient, structure, and interactions. Evidently, if an ion enters the channel, two pathways can be followed: a) return to the entry side or b) translocate to the opposite side. Then, we can ask: What is the probability that the particle will come out of the selected side without visiting the other side? What is the average time it will take to do it? And, what is the survival probability? Conditional probability plays a key role in answering these questions.

8.1 Conditional Propagators: A First Glance

Let us consider a system in the interval $[0, L]$ and place two absorbing targets at $x = 0$ and $x = L$, and let's suppose that we are interested in finding the conditional propagator, $p_0(x, t|x_0)$, for the subset of particles which are ultimately trapped at the origin (see Fig. 5.3). In such a case, we would need to exclude the particles that would have been absorbed in $x = L$. In other words, we are interested in the diffusing particles with trajectories starting at x_0 that are trapped at $x = 0$ and that never cross $x = L$. Consequently, we can replace the trapping boundary at $x = L$ by a perfect reflecting boundary at L. This conditional propagator is governed by the following diffusion equation:

L. Dagdug et al., *Diffusion Under Confinement*,
https://doi.org/10.1007/978-3-031-46475-1_8

$$\frac{\partial p_0(x,t|x_0)}{\partial t} = D\frac{\partial^2 p_0(x,t|x_0)}{\partial x^2}, \tag{8.1}$$

subject to the following boundary conditions:

$$p_0(0,t|x_0) = 0 \quad \text{and} \quad -D\frac{\partial p_0(x,t|x_0)}{\partial x}\bigg|_{x=L} = 0. \tag{8.2}$$

The solution to this boundary problem is the absorbing-reflecting propagator obtained in Chap. 5, given by Eq. (5.87), namely,

$$p(x,t|x_0) = \frac{2}{L}\sum_{n=0}^{\infty}\exp\left[-\frac{(2n+1)^2\pi^2}{4L^2}Dt\right]\sin\left[\frac{(2n+1)}{2L}\pi x_0\right]\sin\left[\frac{(2n+1)}{2L}\pi x\right]. \tag{5.87}$$

Its means properties are discussed in Sect. 5.4.

8.2 Conditional Probability Fluxes and Densities of the First-Passage Time

Two of the main physical properties that characterize diffusion when taking place into a domain bounded by absorbing ends are the conditional probability fluxes and densities of the first-passage time or, in other words, these properties at each absorbing boundary. Using Fick's first law, Eq. (2.74), we can calculate the conditional fluxes at the desired absorbing end. The flux, evaluated at $x = 0$ and $x = L$, is

$$J(0,t) = D\frac{\partial p(x,t|x_0)}{\partial x}\bigg|_{x=0}, \tag{8.3}$$

$$J(L,t) = -D\frac{\partial p(x,t|x_0)}{\partial x}\bigg|_{x=L}, \tag{8.4}$$

Now, considering these last two equations together with Eq. (2.83), we are able to find the expressions for the conditional probability density of first-passage time, yielding

$$\varphi_0(x_0|t) = \frac{J(0,t)}{\int_0^\infty J(0,t)\,\mathrm{d}t} = \frac{J(0,t)}{\theta_0(x_0)}, \tag{8.5}$$

and

$$\varphi_L(x_0|t) = \frac{J(L,t)}{\int_0^\infty J(L,t)\,\mathrm{d}t} = \frac{J(L,t)}{\theta_L(x_0)}, \tag{8.6}$$

where the denominators are the splitting probabilities, $\theta_0(x_0)$ and $\theta_L(x_0)$, which normalize those probability densities. It is worth noting that $\varphi(x_0|t)$ given by Eq. (2.83) is normalized, but once we *split* the trajectories into their final fate, they are not normalized. In the rest of the chapter, we will use these results to calculate the mean conditional times.

8.3 Conditional Mean First-Passage Time

The *conditional mean first-passage* time is the mean time it takes a particle reach one of the boundaries without hitting the opposite boundary first. These conditional times are calcuated from their definition, using Eqs. (8.5) and (8.6). Consequently, when Brownian particles reach the absorbing boundary at $x = 0$ or $x = L$, these conditional times are given by

$$\langle t_0(x_0)\rangle = \frac{\int_0^\infty t\ J(0,t)\,\mathrm{d}t}{\int_0^\infty J(0,t)\,\mathrm{d}t} = \frac{\int_0^\infty t\ J(0,t)\,\mathrm{d}t}{\theta_0(x_0)}, \tag{8.7}$$

and

$$\langle t_L(x_0)\rangle = \frac{\int_0^\infty t\ J(L,t)\,\mathrm{d}t}{\int_0^\infty J(L,t)\,\mathrm{d}t} = \frac{\int_0^\infty t\ J(L,t)\,\mathrm{d}t}{\theta_L(x_0)}. \tag{8.8}$$

From these last two equations and the relation of the mean first-passage time (MFPT) with the total flux, Eq. (8.8), we arrive at

$$\langle t(x_0)\rangle = \theta_0(x_0)\langle t_0(x_0)\rangle + \theta_L(x_0)\langle t_L(x_0)\rangle. \tag{8.9}$$

To obtain the closed form of the conditional mean first-passage times given by Eqs. (8.7) and (8.8), we need the fluxes and the splitting probabilities. These properties were calculated for this system in Sects. 2.7.2 and 2.9 and are given by Eqs. (2.78) and (2.79) and by Eqs. (2.99) and (2.102), respectively. Then, for $\langle t_0(x_0)\rangle$, we have

$$\langle t_0(x_0)\rangle = \frac{L}{L-x_0}\int_0^\infty t\left[D\frac{2\pi}{L^2}\sum_{n=1}^{\infty} n\ \exp\left(-\frac{\pi^2 n^2 Dt}{L^2}\right)\sin\left(\frac{n\pi x_0}{L}\right)\right]\mathrm{d}t$$

$$= \frac{2\pi D}{(L-x_0)L}\sum_{n=1}^{\infty} n\sin\left(\frac{n\pi x_0}{L}\right)\int_0^\infty t\ \exp\left(-\frac{\pi^2 n^2 Dt}{L^2}\right)\mathrm{d}t. \tag{8.10}$$

Applying Eq. (A.10) to the remaining integral, we obtain

$$\langle t_0(x_0)\rangle = \frac{2L^3}{\pi^3 D}\frac{1}{(L-x_0)}\sum_{n=1}^{\infty}\frac{\sin\left(\frac{n\pi x_0}{L}\right)}{n^3}. \tag{8.11}$$

By substituting the result of the series, Eq. (A.35), into the latter equation, we arrive at

$$\langle t_0(x_0)\rangle = \frac{x_0(2L-x_0)}{6D}. \tag{8.12}$$

Now, for $\langle t_L(x_0)\rangle$, we have the following expression:

$$\langle t_L(x_0)\rangle = \frac{L}{x_0}\int_0^\infty t\left[-D\frac{2\pi}{L^2}\sum_{n=1}^{\infty}(-1)^n\ n\ \exp\left(-\frac{\pi^2 n^2 Dt}{L^2}\right)\sin\left(\frac{n\pi x_0}{L}\right)\right]\mathrm{d}t. \tag{8.13}$$

By using Eq. (A.10), we obtain

$$\langle t_L(x_0)\rangle = -\frac{2L^3}{Dx_0\pi^3}\sum_{n=1}^{\infty}\frac{(-1)^n}{n^3}\sin\left(\frac{n\pi x_0}{L}\right). \tag{8.14}$$

To complete the computation, we make use of the fundamental theorem of calculus to give a closed solution to the sum, namely,

$$\langle t_L(x_0)\rangle = -\frac{2L^3}{Dx_0\pi^3}\sum_{n=1}^{\infty}\frac{(-1)^n}{n^3}\int\left\{\frac{\partial}{\partial x_0}\left[\sin\left(\frac{n\pi x_0}{L}\right)\right]\right\}\mathrm{d}x_0$$

$$= \frac{2L^2}{Dx_0\pi^2}\int\left[\sum_{n=1}^{\infty}\frac{(-1)^{n-1}}{n^2}\cos\left(\frac{n\pi x_0}{L}\right)\right]\mathrm{d}x_0, \tag{8.15}$$

an expression that allows us to use the result obtained from Eq. (A.36) for the series, yielding

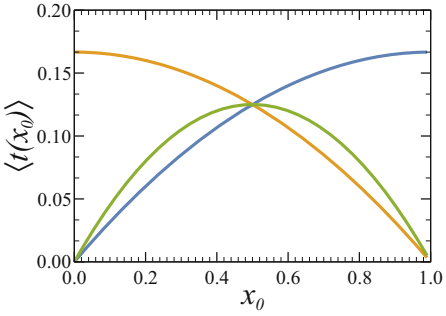

Fig. 8.1 Representative plots of conditional and unconditional first moment of mean first-passage time, i.e., $\langle t_0(x_0)\rangle$ Eq. (8.12) (blue line), $\langle t_L(x_0)\rangle$ in Eq. (8.17) (yellow line) and $\langle t(x_0)\rangle$ in Eq. (2.50) (green line). System length and diffusivity are set to $L = 1$ and $D = 1$, respectively

$$\langle t_L(x_0)\rangle = \frac{2L}{x_0 D}\int\left(\frac{1}{12} - \frac{x_0^2}{4L^2}\right)\mathrm{d}x_0. \tag{8.16}$$

Then, after performing the integral in this last equation, we find that

$$\langle t_L(x_0)\rangle = \frac{L^2 - x_0^2}{6D}. \tag{8.17}$$

Figure 8.1 depicts the conditional and unconditional first moments of MFPT.

If we set $x_0 = 0$ in Eq. (8.17), we obtain the *translocation time*, also known as *direct transit time*: the trajectory drawn by the particle that trascolates, i.e., leaves the starting point and goes to the other end without returning to the starting point. Then, the direct-transit time is given by

$$\langle t_{dt}\rangle = \frac{L^2}{6D}. \tag{8.18}$$

In the next section, we will relate this quantity with the MFPT and discuss its implications.

8.3.1 Direct-Transit Time and Looping Time

In the previous section, we focused on studying Brownian diffusion between one absorbing and one reflecting boundary. Now, we will focus on the diffusing particles that start at the reflecting boundary and end their trajectory as soon as the absorbing boundary is reached for the first time. To gain new insights into the escape dynamics, we analyze the *"fine structure"* of these trajectories. Specifically, we divide trajectories into two segments: the transition path segment and the looping segment. The transition path segment, also referred to as the direct-transit segment, is the final part of the trajectory that leaves the starting point for the last time and goes to the opposite end without returning to the starting point. The remaining part

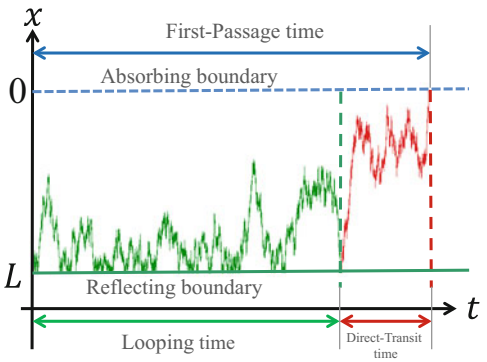

Fig. 8.2 Position dependence on time of a Brownian particle in a one-dimensional domain, obtained by Brownian dynamics simulations. The Brownian particle's trajectory starts at the reflecting boundary at $x = L$ (continous green line) and ends when it reaches the perfect absorbing boundary at $x = 0$ (dashed blue line). The trajectory is divided into two parts: the looping and the transition path segments. The duration of these two segments is separated by dashed lines. The total duration of the trajectory is given by the first-passage time. The looping segment (show in green) starts and ends at the starting point without touching the absorbing boundary. The transition path segment (shown in red) is the final part of the trajectory that leaves the initial position for the last time and goes directly to the absorbing boundary

of the trajectory is the looping segment, where a number of loops that start and end at the same starting point are completed. When both path segments are put together, the complete scenario is recovered (see Fig 8.2). Consequently, the MFPT is related to the mean looping time and mean direct-transit time by

$$\langle t_{fp} \rangle = \langle t_l \rangle + \langle t_{dt} \rangle. \tag{8.19}$$

In Sect. 8.2, we found that the mean time for the transition path segment is given by Eq. (8.18). In Sect. 5.6.3, we found that the MFPT for a segment with an absorbing boundary at $x = 0$ and a reflecting end at $x = L$ is given by Eq. (5.96), namely,

$$\langle t(x_0) \rangle = \frac{x_0(2L - x_0)}{2D}. \tag{5.96}$$

Now, if the particle's initial position is at the reflecting boundary, i.e., $x_0 = L$, we find that

$$\langle t_{fp} \rangle = \frac{L^2}{2D} \tag{8.20}$$

Consequently, the mean loping time is given by

$$\langle t_l \rangle = \frac{L^2}{3D}. \tag{8.21}$$

In conclusion, the particle spends 2/3 of the MFPT looping and 1/3 of the MFTP translocating. This *"fine structure"* has wide applications in experiments with single biological nanopores, pulling proteins and nucleic acid folding studies, and single-molecule fluorescence spectroscopy.

8.4 Conditional Survival Probabilities

Let us consider a system in the interval $[0, L]$ with two absorbing targets, one at $x = 0$ and the other at $x = L$. In this instance, we are interested in finding the conditional survival probability, $S_0(t|x_0)$, for the subset of particles that are ultimately trapped at the origin. The crucial point in calculating this quantity is that at very long times, this probability does not go to zero. This is because all the particles that are trapped in $x = L$ would be survivors of becoming trapped in $x = 0$ and vice versa. In fact, the fraction of particles trapped in $x = L$ is the splitting probability $\theta_L(x_0)$. Consequently

$$\lim_{t\to\infty} S_0(t|x_0) = \theta_L(x_0). \tag{8.22}$$

To find $S_0(t|x_0)$, let's assume that we know the survival probability when the absorbing boundary at $x = L$ is replaced by a reflecting boundary, $S(t|x_0)$. Because we are interested in the particles that reach $x = 0$, we have to subtract from this quantity, $\theta_L(x_0)$. Then, from the definition of conditional probability, Eq. (6.17),[1] we have

$$S_0(t|x_0) = \frac{S(t|x_0) - \lim_{t\to\infty} S_0(t|x_0)}{\theta_0(x_0)} = \frac{S(t|x_0) - \theta_L(x_0)}{1 - \theta_L(x_0)}, \tag{8.23}$$

where $\theta_0(x_0)$ is the fraction of particles that leave the system through the absorbing boundary at $x = 0$.
With this definition in hand, we are able to define the nth moment of the conditional time to be trapped in terms of the conditional survival probability (see Eq. (2.52)). In other words

$$\langle t_0^n(x_0)\rangle = n\int_0^\infty t^{n-1} S_0(t|x_0)\, \mathrm{d}t, \qquad \text{where } n = 1, 2, 3, .. \tag{8.24}$$

[1] Conditional probability $P(A|B)$ is the probability of an event A occurring given that event B has already occurred. This quantity is given by $P(A|B) = P(A \cap B)/P(B)$, where $P(A \cap B)$ is the probability of both A and B occurring. In our case, the conditional probability is the probability of the particle surviving until time t ($P(A)$) and eventually being trapped at $x = 0$ ($P(B)$), which is equal to $S(t|x_0) - \lim_{t\to\infty} S_0(t|x_0)$, with $P(B)$ representing the probability of being trapped at the origin, i.e., $\theta_0(x_0) = 1 - \theta_L(x_0)$.

Subsequently, we will provide the steps to find the differential equation that governs the nth moment of the conditional time $\langle t_0^n(x_0)\rangle$. The first step is to recall that, because of the detailed balance, $S_0(t|x_0)$ satisfies the backward Smoluchowski equation, namely,

$$\frac{\partial S_0(t|x_0)}{\partial t} = \mathcal{L}^\dagger(x_0)\ S_0(t|x_0), \tag{8.25}$$

where $\mathcal{L}^\dagger(x_0)$, in the more general form, is given by (6.29), namely,

$$\mathcal{L}^\dagger(x_0) = e^{\beta U(x_0)}\frac{\partial}{\partial x_0}D(x_0)e^{-\beta U(x_0)}\frac{\partial}{\partial x_0}. \tag{6.29}$$

The second step is to multiply both sides of Eq. (8.23) by $\theta_0(x_0)$ and operate on the resulting equation by $\mathcal{L}^\dagger(x_0)$, yielding

$$\mathcal{L}^\dagger(x_0)\theta_0(x_0)S_0(t|x_0) = \mathcal{L}^\dagger(x_0)\Big\{S(t|x_0) - \theta_L(x_0)\Big\} = \mathcal{L}^\dagger(x_0)S(t|x_0). \tag{8.26}$$

To find that $\mathcal{L}^\dagger(x_0)\theta_L(x_0) = 0$, we have to take the limit when t goes to infinity in Eq. (8.25) and make use of Eq. (8.22). Equation (8.26) gives the differential equation that governs the evolution of the splitting probability. Direct substitution of Eq. (8.25) into Eq. (8.26) results in

$$\mathcal{L}^\dagger(x_0)\theta_0(x_0)S_0(t|x_0) = \frac{\partial S(t|x_0)}{\partial t}. \tag{8.27}$$

Lastly, by multiplying this last equation by $n\,t^{n-1}$ and integrating over time from 0 to infinity, we find that $\langle t^n(x_0)\rangle$ must satisfy

$$\mathcal{L}^\dagger(x_0)\Big\{\theta_0(x_0)\langle t_0^n(x_0)\rangle\Big\} = -n\theta_0(x_0)\langle t^{n-1}(x_0)\rangle. \tag{8.28}$$

The left-hand side is obtained by observing that

$$\lim_{t\to\infty} S(t|x_0) - S(0|x_0) = \lim_{t\to\infty} S(t|x_0) = -\theta_0(x_0), \tag{8.29}$$

because of the boundary conditions. It is worth noting that the splitting probability satisfies the following differential equation:

$$\mathcal{L}^\dagger(x_0)\theta_0(x_0) = 0. \tag{8.30}$$

From Eq. (8.28), it follows that the conditional first moment of the MFPT is given by

$$\mathcal{L}^\dagger(x_0)\{\theta_0(x_0)\langle t_0(x_0)\rangle\} = -\theta_0(x_0). \tag{8.31}$$

Finally, let's calculate the conditional mean first-passage time for a free particle using Eq. (8.31). For such purpose, we substitute $U(x_0) = 0$, $D(x_0) = D$, and $\theta_0(x_0) = (x_0 - L)/L$, given by Eq. (2.102), into Eq. (8.31). This leads to the relation

$$D\frac{\mathrm{d}^2}{\mathrm{d}x_0^2}\left[\left(\frac{x_0 - L}{L}\right)\langle t(x_0)\rangle\right] = -\frac{x_0 - L}{L}, \tag{8.32}$$

After integrating this last equation twice with respect to x_0, we find

$$\left(\frac{x_0 - L}{L}\right)\langle t(x_0)\rangle = -\frac{x_0^3 - 3Lx_0^2}{6D} + Ax_0 + B. \tag{8.33}$$

Constants A and B are obtained by the boundary conditions, i.e.,

$$\langle t_0(0)\rangle = 0 \quad \text{and} \quad \left.\frac{\partial\langle t_0(x_0)\rangle}{\partial x_0}\right|_{x_0=L} = 0, \tag{8.34}$$

leading to $A = L^2/3D$ and $B = 0$. Substituting these two values into Eq. (8.33), we find

$$\langle t_0(x_0)\rangle = \frac{x_0(2L - x_0)}{6D}, \tag{8.35}$$

as expected.

8.4.1 *Direct-Transit Time and Looping Time in the Presence of a Constant External Force*

In this section, we will study direct-transit time and looping time in the presence of an constant external force, when diffusion takes place into a domain of length L, bounded by one reflecting and by one absorbing boundary, placed at $x = 0$ and $x = L$, respectively (see Sect. 7.2.2). For such purpose, we will focus on the densities of their respective first-passage times. As we know, these probability densities can be obtained through the flux. When replacing the reflecting boundary for an absorbing endpoint, we obtain the properties of the direct-transit path. As calculated in Sect. 7.2.2, the first-passage direct-transit probability density in Laplace space is given by (see Eq. (7.38))

$$\varphi_{dt}^{F}(s) = \frac{q\sinh\left(\tilde{F}/2\right)}{(\tilde{F}/2L)\sinh(Lq)}, \tag{8.36}$$

where $\tilde{F} = \beta F L$ is the dimensionless biasing force and $q = \sqrt{s/D + (\tilde{F}/2)^2}$. The mean direct-transit time, $\langle t_{dt} \rangle$, is defined as

$$\langle t_{dt}^F \rangle = \int_0^\infty t\, \varphi_{dt}^F(t)\, \mathrm{d}t \tag{8.37}$$

and can be found by making a series around small-s of the Laplace transform in Eq. (8.36), namely,

$$\varphi_{dt}^F(s) = 1 + \frac{L^2 \left[2 - \tilde{F} \coth\left(\frac{\tilde{F}}{2}\right)\right]}{D\tilde{F}^2} s + \cdots \tag{8.38}$$

By using Eq. (2.94), the result is

$$\langle t_{dt}^F \rangle = \frac{L^2}{2D} \frac{(\tilde{F}/2)\coth(\tilde{F}/2) - 1}{(\tilde{F}/2)^2}, \tag{8.39}$$

where $\langle t_{dt} \rangle = L^2/2D$. It is worth mentioning that the first factor is the MFPT from the reflecting boundary along the interval of length L to its absorbing boundary in the absence of bias, given by Eq. (8.20). The F-dependence of $\langle t_{dt}(x_0) \rangle$ shows that the mean direct-transit time is a symmetric function of F that monotonically decreases as the absolute value of the biasing force increases. Its maximum value at $F = 0$ is $L^2/6D$, and its asymptotic behavior as $|F|$ goes to infinity is given by $L/(D\beta|F|)$ (see Fig. 8.3).

To find the distribution of the looping time, we make use of the fact that the total duration of the escape trajectory, which is the first-passage time from the reflecting to the absorbing boundary, $\langle t_{fp}(x_0) \rangle$, is the sum of the duration of its looping and direct-transit segments, $\langle t_{fp}^F \rangle = \langle t_l^F \rangle + \langle t_{dt}^F \rangle$ (see Eq. (8.19)). Then, the probability density of the first-passage time is the convolution of the probability densities and of the direct-transit and looping times, namely,

$$\varphi_{fp}^F(t) = \int_0^\infty \varphi_{dt}^F(t - t')\varphi_l^F(t')\, \mathrm{d}t'. \tag{8.40}$$

The Laplace transform of this relation is $\varphi_{fp}^F(s) = \varphi_{dt}^F(s)\varphi_l^F(s)$, and hence, we have

$$\varphi_l^F(s) = \frac{\varphi_{fp}^F(s)}{\varphi_{dt}^F(s)}. \tag{8.41}$$

From Eq. (7.35), we know that, in simplified notation

$$\varphi_{fp}^F(s) = \frac{q e^{\tilde{F}/2}}{q\cosh(Lq) + (\tilde{F}/2L)\sinh(Lq)}. \tag{8.42}$$

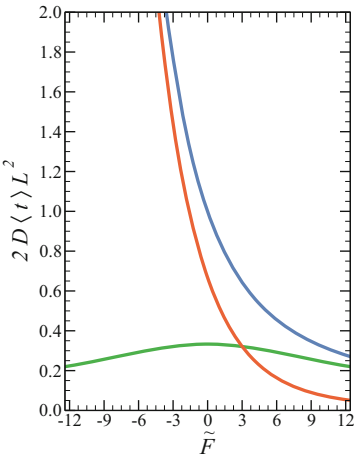

Fig. 8.3 The dimensionless $2D\langle t_{dt}^F\rangle/L^2$ (green line), $2D\langle t_l^F\rangle/L^2$ (red line), and $2D\langle t_{fp}^F\rangle/L^2$ (blue line), given by Eqs. (8.39), (8.45), and (8.44), respectively, are shown. The values used are $D = \beta = 1$

Substituting this last equation, together with Eq. (8.36), into Eq. (8.41), we arrive at

$$\varphi_l^F(s) = \frac{2\mathrm{e}^{\tilde{F}}\,\tilde{F}}{L(\mathrm{e}^{\tilde{F}}-1)\left[\frac{\tilde{F}}{L}+2q\coth(Lq)\right]} \tag{8.43}$$

Additionally, Eq. (7.36) can be written as follows:

$$\langle t_{fp}^F\rangle = \frac{L^2}{D}\frac{\tilde{F}-1+e^{-\tilde{F}}}{\tilde{F}^2}. \tag{8.44}$$

From this last equation, we observe that the MFPT is determined by the mean looping time when $F \to -\infty$, while, when $F \to \infty$, it is determined by the mean direct-transit time. This behavior is depicted in Fig. 8.3.

The force dependence of the MFPT is the sum of the mean looping and direct-transit times, and therefore

$$\langle t_l^F\rangle = \langle t_{fp}^F\rangle - \langle t_{dt}^F\rangle = \frac{L^2}{D}\frac{1+e^{-\tilde{F}}+\tilde{F}(1-\coth(\tilde{F}/2))}{\tilde{F}^2}. \tag{8.45}$$

This equation shows that the mean looping time monotonically decreases with F (see Fig. 8.3). In the absence of bias, this mean time is $L^2/(3D)$, as expected (see Eq. (8.21)). Its asymptotic behavior as F goes to infinity is given by $2/[D(\beta F)^2]$ and, when F goes to minus infinity, is given by $2e^{\tilde{F}}/[D(\beta F)^2]$. The exponential increase of the mean looping time is a consequence of the fact that the particle diffuses in a deep potential well, and to escape, it has to overcome a high energy barrier.

8.5 Concluding Remarks

In this chapter, we have calculated the fundamental physical properties of conditional probabilities when particular pathways are taken by Brownian particles as well as their mathematical representation. To gain new insights into the escape dynamics, we analyze the *"fine structure"* of these trajectories. Specifically, we divide trajectories into two segments: a looping segment, when a particle unsuccessfully tries to escape returning to the trap bottom again and again, and a direct-transit segment, when it finally escapes moving without touching the bottom. Analytical expressions are derived for the Laplace transforms of the probability densities of the duration of the two segments.

In the presence of bias, the mean looping time monotonically increases as F decreases, approaching exponential F-dependence at large negative forces pushing the particle toward the trap at $x = 0$. In contrast to this intuitively appealing behavior, the mean direct-transit time shows rather *counterintuitive* behavior: it decreases as the force magnitude, $|F|$, increases, independently of whether the force pushes the particles to the trap at $x = 0$ or to the exit from the trap, having a maximum at $F = 0$.

For the reader's convenience, listed below are the most important equations to depict and define diffusion that we have obtained so far, which will be frequently used throughout this book:

$$\nabla^2 \theta_i(\mathbf{r_0}) \langle t_i^n(\mathbf{r_0}) \rangle = -\frac{n}{D} \langle t_i^{n-1}(\mathbf{r_0}) \rangle \theta_i(\mathbf{r_0}) \qquad \text{(Conditional Moments of MFPT)}$$

Further Reading and References

A.M. Berezhkovskii, L. Dagdug, S.M. Bezrukov, A new insight into diffusional escape from a biased cylindrical trap. J. Chem. Phys. **147**, 104103 (2017). https://doi.org/10.1063/1.5002127

A.M. Berezhkovskii, L. Dagdug, S.M. Bezrukov, Mean direct-transit and looping times as functions of the potential shape. J. Phys. Chem. B **121**, 21, 5455–5460 (2017). 10.1021/acs.jpcb.7b04037

A.M. Berezhkovskii, L. Dagdug, S.M. Bezrukov, Exact solutions for distributions of first-passage, direct-transit, and looping times in symmetric cusp potential barriers and wells. J. Phys. Chem. B **123**, 17, 3786–3796 (2019). 10.1021/acs.jpcb.9b01616

A.M. Berezhkovskii, L. Dagdug, S.M. Bezrukov, Peculiarities of the mean transition path time dependence on the barrier height in entropy potentials. J. Phys. Chem. B **124**, 12, 2305–2310 (2020). 10.1021/acs.jpcb.9b09595

A. Pérez-Espinosa, M. Aguilar-Cornejo, L. Dagdug, First-passage, transition path, and looping times in conical varying-width channels: Comparison of analytical and numerical results. AIP Adv. **10**, 055201 (2020). 10.1063/5.0004026

Chapter 9
Diffusion with Stochastic Resetting

9.1 Introduction

The *stochastic resetting* processes, whereby the position of the particle is reset to a fixed location at a random sequence of times, are frequently observed in phenomena related to physics, chemistry, biophysics, and scientific computation. In the latter, it has been applied as a useful strategy to optimize search algorithms in hard combinatorial problems. In particular, it has been used to show that resetting can significantly reduce the first arrival time of a diffusive particle to a target by mitigating large fluctuations that can occur when resetting is absent. Such strategies have been shown to be favorable in a variety of contexts such as animal foraging, a flexible polymer translocating through a narrow pore, and the target search of proteins on DNA molecules. Other interesting observations include a whole family of properties associated with optimal processes under resetting, as well as the existence of a universal strategy for effective resetting.

A common example of a diffusive process with resetting is depicted in the act of searching for a lost object. Normally, the search starts where the object is most likely to be. Later on, we randomly walk around the place. If we do not find it after a reasonable amount of time and if we are far away enough that the chances of finding the object are slim, we usually give up, and we will most likely return to the place of origin, to start the search again. Another example in which we use a search strategy similar to the previous one is when we are asked to find an object that is different from others, like in the *Where's Willy* books (see Fig. 9.1). We can also observe the stochastic resetting process in the animal kingdom. For example, bears and other burrowing mammals go out in search of food only to eventually return to their burrow after a successful or unsuccessful search. One additional example is presented in the mass extinction processes.

L. Dagdug et al., *Diffusion Under Confinement*,
https://doi.org/10.1007/978-3-031-46475-1_9

Fig. 9.1 The goal for this puzzle is to find the single Mayan zero (mih) that is different from all the others. Sometimes, the search strategy is to start at the first icon and move randomly, and if we don't find the target after a while, return to the starting point to continue the search. The Mayan numeral system was the system to represent numbers and calendar dates in the Mayan civilization. It was a vigesimal (base-20) positional numeral system. The dash-and-dot number system, which formed the basis of Mayan numeration, was in use in Mesoamerica as from 1000 B.C. The numbers had different representations. In head-style notation, each of the numbers is expressed by a distinctive type of head, and each has its own essential characteristic that distinguished it from all the others

9.2 Diffusion Equation with Stochastic Resetting

In this section, we will demonstrate how to obtain an equation describing the evolution of the propagator for a diffusive particle, taking the stochastic resetting into account. To such end, we will write the master equation for the processes taking place in a discrete one-dimensional lattice. Let's start by calculating the probability of reaching j after $n+1$ steps. This implies that the Brownian particle had to be at $j-1$ or $j+1$ after n steps. But for now, let's allow this particle at $j-1$ and $j+1$ to make a jump to the resetting position j_r, with rate r and probability $r\Delta t$ (see Fig. 9.2). The dimension of r is T^{-1}. Now, in order to calculate the probability of being at j after $n+1$ steps, we have to subtract all trajectories that end at j_r. Therefore, when stochastic resetting is added to diffusion, the processes are governed by the following master equation:

$$\begin{aligned} p_{n+1}(j) - \frac{r\Delta t}{2}\, p_{n+1}(j_r) - \frac{r\Delta t}{2}\, p_{n+1}(j_r) \\ = \frac{1-r\Delta t}{2}\, p_n(j+1) + \frac{1-r\Delta t}{2}\, p_n(j-1). \end{aligned} \tag{9.1}$$

For the purpose of obtaining the continuous approach, we must rewrite Eq. (9.1) in terms of $j \to x$, $j \pm 1 \to x \pm \Delta x$, $n \to t$, and $n+1 \to t+\Delta t$, yielding

$$\begin{aligned} p(x, t+\Delta t) = \frac{1-r\Delta t}{2}\, p(x+\Delta x, t) + \frac{1-r\Delta t}{2}\, p(x-\Delta x, t) \\ + r\Delta t\, p(x_r, t+\Delta t). \end{aligned} \tag{9.2}$$

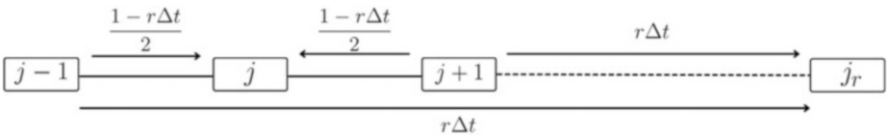

Fig. 9.2 Schematic representation of the one-dimensional lattice of a random walk under stochastic resetting

After Taylor expanding this last equation around $\Delta x = 0$ and $\Delta t = 0$ and keeping terms up to linear order on the left-hand side, we have

$$\begin{aligned} & p(x,t) + \Delta t \frac{\partial p(x,t)}{\partial t} \\ & = \frac{1-r\Delta t}{2}\left[p(x,t) + \Delta x \frac{\partial p(x,t)}{\partial x} + \frac{(\Delta x)^2}{2}\frac{\partial^2 p(x,t)}{\partial x} + \cdots\right] \\ & \quad + \frac{1-r\Delta t}{2}\left[p(x,t) - \Delta x \frac{\partial p(x,t)}{\partial x} + \frac{(\Delta x)^2}{2}\frac{\partial^2 p(x,t)}{\partial x^2} + \cdots\right] \\ & \quad + r\Delta t\left[p(x_r,t) + \Delta t \frac{\partial p(x_r,t)}{\partial t} + \cdots\right]. \end{aligned} \tag{9.3}$$

By simplifying the above expression and keeping terms up to second order in Δx, it takes the form of

$$\frac{\partial p(x,t)}{\partial t} \approx \left[(1-r\Delta t)\frac{(\Delta x)^2}{2\Delta t}\frac{\partial^2 p(x,t)}{\partial x^2}\right] - r\, p(x,t) + r\, p(x_r,t) + r\Delta t \frac{\partial p(x_r,t)}{\partial t}. \tag{9.4}$$

Taking the limit when Δx and Δt go to zero from this last equation, we can conclude that the diffusion coefficient is naturally defined as

$$D \equiv \lim_{\substack{\Delta x \to 0 \\ \Delta t \to 0}} (1 - r\Delta t)\frac{(\Delta x)^2}{2\Delta t} = \lim_{\substack{\Delta x \to 0 \\ \Delta t \to 0}} \frac{(\Delta x)^2}{2\Delta t}. \tag{9.5}$$

Finally, we find that the differential equation which governing the diffusion under a stochastic resetting is given by

$$\frac{\partial p(x,t)}{\partial t} = D\frac{\partial^2 p(x,t)}{\partial x^2} - r\, p(x,t) + r\, p(x_r,t). \tag{9.6}$$

The first term on the right-hand side of Eq. (9.6) refers to diffusion, the second term stands for the Brownian particles that are at position x at time t with rate r and finally reach x_r, and the third term considers the gain of particles arriving

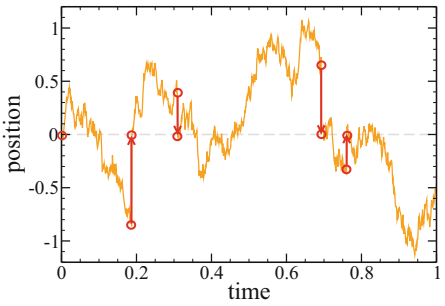

Fig. 9.3 Typical position dependence on time (solid yellow line) obtained by performing a one-dimensional Brownian dynamics simulation. This trajectory was taken at random from the 25,000 that were simulated. Particles start at $x_0 = 0$ and reset stochastically to its initial position $x_r = x_0 = 0$ at rate $r = 0.6$. The resetting times are marked by red circles, while the trajectory from the former position to x_r is depicted by a red arrow. When running simulations, we considered an overdamped point-like Brownian particle, diffusivity as $D = 1$ and $\Delta t = 1 \times 10^{-6}$, so that $\sqrt{2D\Delta t} \ll 1$. The overdamped dynamics of the particle is modeled by the Langevin equation

at the resetting point x_r at time t. The schematic space-time trajectory of a one-dimensional Brownian motion under resetting is shown in Fig. 9.3.

To have a deeper understanding of the physics of a reset, we will focus only on the resetting processes. For such purpose, we only keep the second term of Eq. (9.6), namely,

$$\frac{\partial p_r(x,t)}{\partial t} = -r\, p_r(x,t), \tag{9.7}$$

where $p_r(x,t)$ is the probability density of leaving position x at time t to reach x_r. The solution of this last equation, since $p(t=0) = 1$, is given by

$$p_r(t) = \mathrm{e}^{-rt}. \tag{9.8}$$

On one hand, this distribution returns a random time exponential distributed with mean $1/r$. On the other hand, the exponential distribution is the probability distribution of the time between events in a Poisson process.[1] This means that the interval of time between two consecutive resetting times is given by

[1] The master equation for a Poisson process is a particular case of the random walk in which a=0 (see Eq. (2.5)). If position j, or one event, increases randomly by unit at an average rate of $b = \lambda$, then

$$p_{n+1}(j) = \lambda\, p_n(j-1). \tag{9.9}$$

$$p(k) = \frac{\mathrm{e}^{-rt}(rt)^k}{k!}, \tag{9.10}$$

where k is the number of occurrences of the event ($k = 1, 2, 3, ...$). This distribution is applied to rare events that have a very small probability of occurring. In our problem, Eq. (9.10) gives the probability of having k resetting events within an interval time from 0 to t. For example, if $r = 4$ resettings per second and we want to calculate the probability of having 5 resettings in 10 seconds, then $k = 5$ and $rt = 4\ \mathrm{s}^{-1} \times 10\ \mathrm{s} = 40$.

In the next section, we will solve the diffusion equation under stochastic resetting in the steady state.

9.3 Steady-State Solution

As we anticipated, we will solve the diffusion equation with stochastic resetting, Eq. (9.6), in the steady state, which is attained as $t \to \infty$. In other words, we intend to solve

$$D\frac{\partial^2 p(x,t)}{\partial x^2} - r\,p(x,t) + r\,p(x_r,t) = 0, \tag{9.11}$$

subject to the following initial condition: $p(x, t = 0) = \delta(x - x_0)$. For the sake of simplicity and having in mind that we will solve this differential equation in the Laplace space, by following the same steps as depicted in Sect. 3.2, it is useful to describe the particles' arrival to x_r as a Dirac delta function and set $x_r = x_0$. Therefore, Eq. (9.11) is modified to

$$D\frac{\partial^2 p(x,t|x_0)}{\partial x^2} - r\,p(x,t|x_0) = -r\,\delta(x - x_0). \tag{9.12}$$

For $x \neq x_0$, the Dirac delta function is zero, and we recover the homogeneous equation which general solutions are given by $\mathrm{e}^{\pm\alpha_0 x}$, where

$$\alpha_0 \equiv \sqrt{\frac{r}{D}}. \tag{9.13}$$

The solution to Eq. (9.12) is constructed from a linear combination of the real exponential functions that satisfy the following boundary conditions (BCs): $p(x,t) \to 0$ as $x \to \pm\infty$, and $p(x,t)$ is continuous at $x = x_0$. By imposing these conditions, we find that

$$p(x|x_0) = A\mathrm{e}^{-\alpha_0|x-x_0|}. \tag{9.14}$$

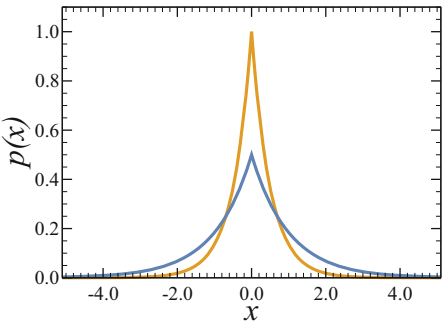

Fig. 9.4 The stationary probability densities $p(x)$ given by Eq. (9.15) for $\alpha_0 = 1$ (blue line) and $\alpha_0 = 2$ (yellow line), $x_r = x_0 = 0$, and $D = 1$

Constant A is fixed by using the discontinuity equation associated to the problem, which is obtained in the exact same way we obtained Eq. (3.42). Therefore, $A = \alpha_0/2$, so that

$$p(x|x_0) = \frac{\alpha_0}{2} \mathrm{e}^{-\alpha_0|x-x_0|}. \tag{9.15}$$

Note that Eq. (9.15) is a nonequilibrium stationary state. This means that there is circulation of probability even in the one-dimensional geometry. At all points, there is always a diffusive flux of probability in the direction away from x_0 and a nonlocal resetting flux in the opposite direction from all points $x \neq x_0$ to x_0 (see Fig. 9.4).

9.4 Mean First-Passage Time Under Resetting: Semi-Infinite Line

Let us assume that a diffusive process with resetting take places in a one-dimensional system in the presence of a perfect absorbing target at the origin, $x = 0$. The mean first-passage time (MFPT) can be calculated from the survival probability density under resetting, i.e., $S_r(t|x_0, x_r)$, or, in compact notation, $S_r(t|x_0)$, namely,

$$\langle T_r(x_0) \rangle = -\int_0^\infty t \frac{\partial S_r(t|x_0)}{\partial t} \, \mathrm{d}t = \int_0^\infty S_r(t|x_0) \, \mathrm{d}t, \tag{9.16}$$

Following the same steps as we did in Sect. 2.6 to obtain the differential equation that governs $S_r(x_0, t|x_r)$, namely, integrating Eq. (9.6), using the analog of the backward equation for resetting, from 0 to infinity with respect to x, we have

$$\frac{\partial S_r(t|x_0)}{\partial t} = D \frac{\partial^2 S_r(t|x_0)}{\partial x^2} - r S_r(t|x_0) + r S_r(t|x_r). \tag{9.17}$$

By making $r = 0$ in the previous expression, the equation describing the function in the absence of resetting is recovered (see Eq. (2.59)). Now, to obtain the expression for the MFPT, we substitute Eq. (9.17) into (9.16) and integrate it over time, leading to

$$\int_0^\infty \frac{\partial S_r(t|x_0)}{\partial t}\,\mathrm{d}t = D\frac{\partial^2}{\partial x_0^2}\int_0^\infty S_r(t|x_0)\,\mathrm{d}t - r\int_0^\infty S_r(t|x_0)\,\mathrm{d}t + r\int_0^\infty S_r(t|x_r)\,\mathrm{d}t. \tag{9.18}$$

Since $S_r(t \to \infty|x_0) = 0$, $S_r(t = 0|x_0) = 1$, and given that the differential and integral operators either commute or are reduced because of the fundamental theorem of calculus, we finally obtain

$$D\frac{\partial^2\langle T_r(x_0)\rangle}{\partial x_0^2} - r\langle T_r(x_0)\rangle + r\langle T_r(x_r)\rangle = -1. \tag{9.19}$$

Once again, if $r = 0$, Eq. (9.19) turns into the equation for the MFPT in free diffusion, Eq. (2.48). This equation is a nonhomogeneous ordinary differential equation (ODE), and its solution is given by

$$\langle T_r(x_0)\rangle = A\mathrm{e}^{\alpha_0 x_0} + B\mathrm{e}^{-\alpha_0 x_0} + \frac{1 + r\langle T_r(x_r)\rangle}{r}. \tag{9.20}$$

The boundary condition which states that $T(x_0)$ is finite as $x_0 \to \infty$ implies $A = 0$, and the boundary condition $T(x_0 = 0) = 0$ fixes B. Thus

$$\langle T_r(x_0)\rangle = \frac{1 + r\langle T_r(x_r)\rangle}{r}\left[1 - \mathrm{e}^{-\alpha_0 x_0}\right]. \tag{9.21}$$

Setting $x_r = x_0$, we ultimately arrive at

$$\langle T_r(x_0)\rangle = \frac{1}{r}\left[\mathrm{e}^{\alpha_0 x_0} - 1\right], \tag{9.22}$$

where $\alpha_0 \equiv \sqrt{r/D}$.

It is worth noting that for fixed x_0, the MFPT is finite for $0 < r < \infty$, and it diverges when $r \to 0$ as $1/r$, as expected, and $x_0\sqrt{r/D} \to \infty$ when r goes to infinity. The latter conclusion is drawn from the fact that, as the particle is continuously restarting, it stays close to x_r and is unlikely to hit the absorbing target (see Fig. 9.5). Additionally, we can see that the MFPT times r is the total average resetting per particle before being trapped. Then, from Eq. (9.22), we have that this important physical parameter is given by $\mathrm{e}^{\alpha_0 x_0} - 1$.

Since the MFPT diverges as r goes to zero and infinity, there must be a minimum with respect to r, denoted by r^*. This r^* is an optimal rate to which the minimum value of the MFPT is observed. This critical phenomenon occurs if

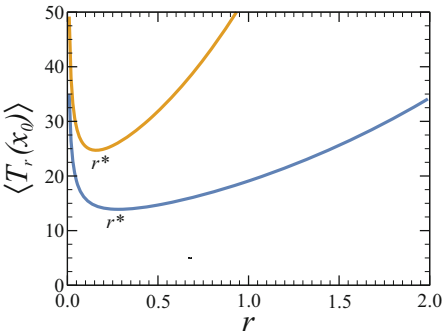

Fig. 9.5 The mean first-passage time, given by Eq. (9.22), is plotted as a function of r for fixed $x_r = x_0 = 3$ (blue line), $x_r = x_0 = 4$ (yellow line), and $D = 1$. In both cases, a minimum is shown at $r^* \simeq 0.28218\ s^{-1}$ and $r^* \simeq 0.158726\ s^{-1}$, respectively. The MFPT diverges as r goes to zero and infinity

the first derivative of Eq. (9.22) with respect to r is zero, yielding

$$e^{-\gamma} - 1 = -\frac{\gamma}{2}, \tag{9.23}$$

where $\gamma \equiv \alpha_0 x_0$. The solution of Eq. (9.23) is given by $\gamma_0^* = 2 + W(-2e^{-2}) \approx 1.59362$, where $W(z)$ is the Lambert function, with $z > -e^{-1}$, then $r^* = D\gamma_0^{*2}/x_0^2$. Optimal resetting is inversely proportional to the square of the initial position. This last result is quite significant as it allows us to establish rates to perform optimal search processes, surely one of the most important features of diffusion with resetting.

9.5 Renewal Equation Approach for Poissonian Resetting

In this section, we will see that, once we calculate the survival probability density for a diffusive particle that follows the initial conditions and BCs, we can write their distribution when stochastic resetting is added. In other words, we can write $S_r(x_0, t|x_r)$ in terms of $S(t|x_0)$. Also, we can show that the MFPT is related to the unconstrained problem by means of the *renewal equation approach*, namely,

$$S_r(t|x_0) = e^{-rt}\ S_0(t|x_0) + r\int_0^t S_r(t-\tau|x_0)\ e^{-r\tau}\ S_0(\tau|x_r)\ d\tau, \tag{9.24}$$

where we introduced the notation for the survival probability density in the absence of resetting $S(t|x_0)$ as $S_0(t|x_0)$. The benefits are clearly demonstrated below. To understand each term in this equation, we need to think of the different possible trajectories followed by survival particles at time t. Additionally, it is important to remember that the probability of no resetting event having occurred up to time t is e^{-rt} (see Eq. (9.8)). This holds for Poissonian resetting with a constant rate r.

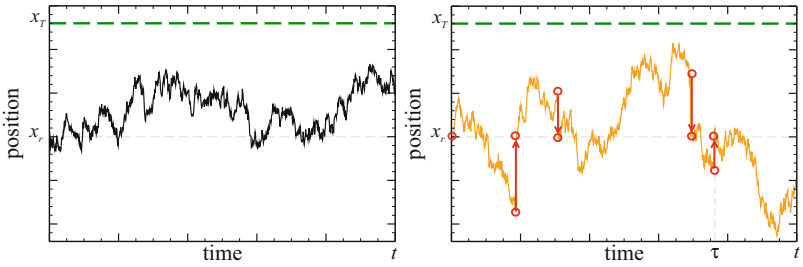

Fig. 9.6 Time-dependent trajectories obtained by performing a one-dimensional Brownian dynamics simulation are shown. The simulated system consists of a semi-infinite line in which the diffusive particles experience stochastic resetting with rate r at time intervals given by a Poisson distribution. As soon as the particle reaches the absorbing target x_T (dashed green line), it is removed from the system, and the time at which this occurs defines the MFPT. The two possible trajectories of the particles that have not reached x_T at time t are shown in the panels. The particle's initial position is placed at the same position to which it is reset, i.e., $x_r = x_0$ (dashed gray line). The left panel shows the trajectory of a particle that diffuses without having experienced any reset until time t (black solid line). The right panel shows the trajectory of a particle whose last reset was at time τ (solid yellow line), i.e., from time τ to t this particle has not experienced any other reset. From this panel, we can see that τ can take values from 0 to t, imposing the limits for the integral in Eq. (9.24). When running simulations, the parameters are the same as in Fig. 9.3

The first term on the right-hand side stands for trajectories starting at x_0 where there has been no resetting up to time t, depicted by a solid black line on the left-side panel of Fig. 9.6. Furthermore, we have that the first factor inside the integral stands for all trajectories starting at x_0 for which the last reset was at time τ, depicted on the right-side panel of Fig. 9.6 by the solid yellow line starting from the origin up to τ. Then, the particles continue their journey with a trajectory now starting at x_r with no reset from τ to t. This last part of the trajectory is represented by the last two factors inside the integral and is depicted in Fig. 9.6 by the yellow solid line going from τ up to t, starting for the last time at x_r.

Now, to write $S_r(t|x_0)$ in terms of $S_0(t|x_0)$, let us redefine the Laplace transform, using the variable r instead of s, as follows:

$$S_r(s|x_0) \equiv \int_0^\infty \mathrm{e}^{-rt}\, S_r(t|x_0)\, \mathrm{d}t. \tag{9.25}$$

Laplace transforming the renewal equation, Eq. (9.24), yields

$$S_r(s|x_0) = S_0(r+s, x_0) + r\, S_0(r+s|x_r)\, S_r(s|x_0). \tag{9.26}$$

Then, solving for $S_r(s|x_0)$, we finally have

$$S_r(s|x_0) = \frac{S_0(r+s|x_0)}{1 - r\,\tilde{S}_0(r+s|x_r)}. \tag{9.27}$$

This is a very general and useful result for Poissonian resetting, relating the Laplace transform of the survival probability when $r = 0$ to that in the presence of resetting.

Once we know $S_r(s|x_0)$, we can relate the MFPT with $S_0(r + s|x_0)$ using the definition given in Eq. (9.16), namely,

$$\langle T_r(x_0)\rangle = \int_0^\infty S_r(t|x)\,\mathrm{d}t = S_r(s = 0|x_r). \tag{9.28}$$

This last expression is very useful and allow us to calculate the MFPT with resetting from the survival probability setting $r = 0$ in Laplace's space. As an example, let's find the MFPT for a Brownian particle diffusing in a one-dimensional system with an absorbing target at $x_T = 0$ and with $x_r = x_0 > 0$. The survival probability density when $r = 0$ is given by Eq. (4.57). Laplace transforming it, using Eq. (A.72), we find that

$$S_r(s, x_0) = \frac{1 - \mathrm{e}^{-\alpha_{rs}x_0}}{s + r(1 - \mathrm{e}^{-\alpha_{rs}x_0})}, \tag{9.29}$$

with $\alpha_{rs} = \sqrt{s/D}$. By introducing this result into Eq. (9.28) and setting $s = 0$, Eq. (9.22) is obtained when $x_0 = 0$, as expected.

9.6 Mean First-Passage Time Under Resetting: Absorbing-Absorbing

In this section, we consider a Brownian particle initially located at x_0, diffusing between two perfect absorbing boundaries in the one-dimensional interval $[0, L]$. In addition, the particle stochastically resets to the initial position $x_r = x_0$ at a constant rate r (see Fig. 9.7). For such a system, we are interested in the first-passage properties as well as the survival probability density. Aiming to compute these physical quantities, we will solve Eq. (9.17) with the corresponding boundary conditions, $S_r(t|x_0 = 0) = S_r(t|x_0 = L) = 0$, and substitute the result into Eq. (9.28) to calculate the MFPT.

Laplace transforming Eq. (9.17), which manifestly satisfies the boundary conditions $S_r(0|x_0) = 1$, leads to

$$D\frac{\partial^2 \tilde{S}_r(s|x_0)}{\partial x_0^2} - (s + r)S_r(s|x_0) = -1 - r\tilde{S}_r(s|x_r). \tag{9.30}$$

Equation (9.30) is a nonhomogeneous ordinary differential equation, and its general solution is given by

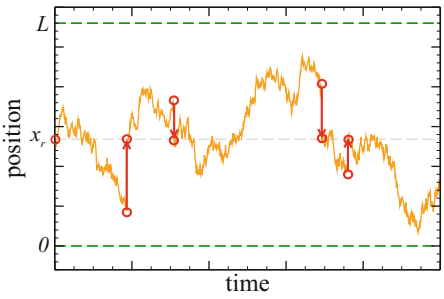

Fig. 9.7 Time-dependent trajectories are shown. These are obtained by performing a one-dimensional Brownian dynamics simulation, using the same parameters as in Fig. 9.3. The simulated system consists of a line segment from 0 to L, where the diffusive particles experience stochastic resetting at rate r and at time intervals given by a Poisson distribution. As soon as the particle hits any of the two absorbing ends at 0 or L (dashed green lines), it is removed from the system. This event defines the MFPT when several realizations are made

$$S_r(s|x_0) = A\cosh(\alpha_s x_0) + B\sinh(\alpha_s x_0) + \frac{1 + r\tilde{S}_0(s|x_r)}{r+s}, \tag{9.31}$$

where $\alpha_s \equiv \sqrt{(r+s)/D}$. Constants A and B can be obtained from the initial conditions, $S_r(s|x_0 = 0) = S_r(s|x_0 = L) = 0$, namely,

$$\begin{aligned} A &= -\frac{1 + r\tilde{S}_0(t|x_r)}{s+r}, \\ B &= \left[\frac{\cosh(\alpha_s L) - 1}{\sinh(\alpha_s L)}\right]\frac{1 + r\tilde{S}_0(t|x_r)}{s+r}. \end{aligned} \tag{9.32}$$

Inserting these two last equations into Eq. (9.31) and setting $x_r = x_0$, we finally find that

$$S_r(s|x_0) = \frac{1 - g_r(s, x_0)}{s + r g_r(s, x_0)}, \tag{9.33}$$

where

$$g_r(x_0, s) = \frac{\sinh[\alpha_s(L - x_0)] + \sinh(\alpha_s x_0)}{\sinh(\alpha_s L)}. \tag{9.34}$$

Introducing this result into (9.28) leads to

$$\langle T_r(x_0)\rangle = \frac{1 - g_r(x_0, 0)}{r g_r(x_0, 0)}. \tag{9.35}$$

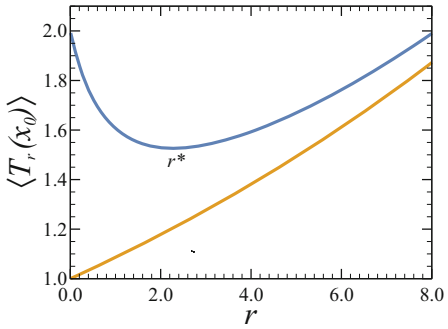

Fig. 9.8 The mean first-passage time given by Eq. (9.36) is plotted as a function of r for fixed $L = 5$ (blue line) and $L = 3$ (yellow line), when $x_0 = 1$ and $D = 1$. In the former case, a minimum is shown at $r^* \simeq 2.275402$, while in the latter, it does not exist. The MFPT does not diverge as r goes to zero, and it does diverge when r goes to infinity

Further simplifications lead us to the following expression:

$$\langle T_r(x_0)\rangle = \frac{1}{r}\left[\frac{\sinh(L\alpha_0)}{\sinh[(L-x_0)\alpha_0] + \sinh(x_0\alpha_0)} - 1\right]. \tag{9.36}$$

The MFPT as a function of r is depicted in Fig. 9.8. Its main characteristic is that there are values for which r^* exists, while in other cases, it does not. In such a case, the presence of resetting increases the MFPT and the minimum value is when $r = 0$. This shows important diversity in the output.

In the next section, we will focus on describing a mathematical formalism to obtain r^* and its value.

9.7 Optimal Restart Rate

From the theory of first-passage time under resetting, it is well known that restarting minimizes the MFPT if $CV > 1$, where CV stands for the ratio between the standard deviation $\sigma(\langle T(x_0)\rangle)$ and the mean first-passage time $\langle T(x_0)\rangle$ in the absence of restart, namely,

$$CV \equiv \frac{\sigma(\langle T(x_0)\rangle)}{\langle T(x_0)\rangle} > 1. \tag{9.37}$$

Applying this criterion, we can find the domain that the Brownian particle with resetting, in the presence of two absorbing boundaries, minimizes the MFPT, i.e., the domain where r^* exists. To such end, we first calculate $\sigma^2(T(x_0))$, which is given by

$$\sigma^2(T(x_0)) = \langle T(x_0)^2 \rangle - \langle T_0(x_0) \rangle^2, \tag{9.38}$$

where the first and the second moments are given by (2.50) and (2.68), namely,

$$\langle T(x_0) \rangle = \frac{x_0(L - x_0)}{2D}, \tag{2.50}$$

and

$$\langle T^2(x_0) \rangle = \frac{x_0(L - x_0)\left(L^2 + Lx_0 - x_0^2\right)}{12D^2}. \tag{2.68}$$

Substituting these equations into Eq. (9.38) and then the obtained expression into (9.37), we find

$$CV = \sqrt{\frac{L^2 - 2x_0(L - x_0)}{3x_0(L - x_0)}}. \tag{9.39}$$

This last expression is greater than one when

$$5u^2 - 5u + 1 > 0, \tag{9.40}$$

where the dimensionless quantity u is given by $u = x_0/L$. This inequality determines the domain where a restart expedites the completion of the underlying process. The solution of Eq. (9.40) is given by

$$\mathfrak{D} = [(0, u_-) \cup (u_+, 1)], \tag{9.41}$$

where

$$u_\pm = \frac{5 \pm \sqrt{5}}{10}. \tag{9.42}$$

Then, r^* exists if u belongs to the domain $\mathfrak{D}$.

Now, we will describe the procedure leading to an explicit expression to calculate r^*. To such end, Eq. (9.36) must be rescaled in terms of u and a new dimensionless variable β given by

$$\beta \equiv \frac{L}{2}\alpha_0, \tag{9.43}$$

leading to

$$\langle T_r(x_0)\rangle = \frac{L^2}{4D\beta^2}\left[\frac{\sinh 2\beta}{\sinh(2\beta - x_0\alpha_0) + \sinh(x_0\alpha_0)} - 1\right]. \tag{9.44}$$

Then, after some algebraic work, this last equation can be rewritten as

$$\langle T_r\rangle = \frac{L^2}{4D}\mathcal{G}(\beta, u), \tag{9.45}$$

where

$$\mathcal{G}(\beta, u) = \frac{1}{\beta^2}\left[\frac{\cosh(\beta)}{\cosh[(1-2u)\beta]} - 1\right]. \tag{9.46}$$

To find the optimal restart rate, r^*, one sets

$$\left.\frac{\partial \mathcal{G}(\beta, u)}{\partial \beta}\right|_{\beta=\beta^*} = 0, \tag{9.47}$$

leading to the following transcendental equation:

$$2+\text{sech}(\beta-2u\beta)\{\beta\sinh\beta + \cosh\beta[(2u-1)\tanh(\beta-2u) - 2]\} = 0. \tag{9.48}$$

This means that, once we set u, we can find β^*. Then, from the definitions of u and β, we find that

$$r^* = \frac{4\beta^{*2}}{L^2}D. \tag{9.49}$$

In summary, once x_0 and L have been set, we have to check if u belongs to $\mathfrak{D}$; if so, then r^* exists. To find its numerical value, we first have to calculate β^* using Eq. (9.48) and finally substitute it into Eq. (9.49).

We will end this section with a practical example where we will use the same numerical values as in Fig. 9.8: firstly, let us set $L = 3$, $x_r = x_0 = 1$, and $D = 1$. Then, $u = x_0/L = 1/3$, which is not an element of $\mathfrak{D}$; therefore, there is no r^*. Let's remember that $\mathfrak{D}$ is approximately $[(0, 0.276393) \cup (0.723607, 1)]$. In the second case, we set $L = 5$, $x_r = x_0 = 1$, and $D = 1$. Then $u = 1/5 = 0.2 \in \mathfrak{D}$, and consequently, r^* exists. Thirdly, by numerically solving Eq. (9.48), we find that $\beta^* = 3.771109$. Therefore, using Eq. (9.49) we arrive to $r^* \simeq 2.27540$. All of these results are in perfect agreement with those shown in Fig. 9.8.

9.8 Semi-Infinite Revisited: $x_0 = x_r \cup x_0 \neq x_r$

Consider a Brownian particle with initial position x_0 diffusing in a semi-infinite one-dimensional system with a perfect absorbing point x_T at the origin. In addition, the particle is stochastically reset to x_r with a constant rate r, which could now be different from x_0. For such a system, we are interested in the first-passage properties as a function of x_0 and x_r. In this section, we will generalize the results obtained in Sect. 9.4.

The most general expression for the MFPT is given in Eq. (9.21), and from Eq. (9.22), we know that the MFPT with an initial position x_r reads

$$\langle T_r(x_r)\rangle = \frac{1}{r}\left[\mathrm{e}^{\alpha_0 x_r} - 1\right]. \tag{9.50}$$

Substituting this last expression into Eq. (9.21), the generalization of the MFPT is obtained, namely,

$$\langle T_r(x_0, x_r)\rangle = \frac{\mathrm{e}^{\alpha_0 x_r}\left[1 - \mathrm{e}^{-\alpha_0 x_0}\right]}{r}. \tag{9.51}$$

As we already know, there has to be a minimum for the MFPT in r, i.e., r^*. Once again, r^* is the optimal rate to which the minimum value of the MFPT is observed, as shown in Fig. 9.9.

The optimal rate r^* is calculated by setting the first derivative of Eq. (9.51) with respect to r equal to zero. This yields

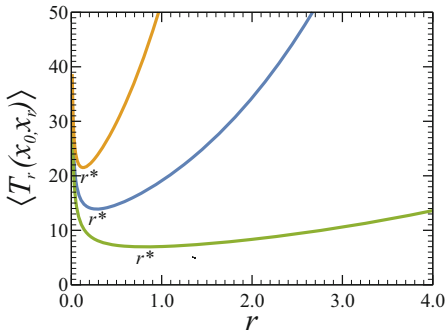

Fig. 9.9 The mean first-passage time given by Eq. (9.51) is plotted as a function of r for fixed $x_0 = 3$ and $x_r = 2$ (solid green line), $x_r = 3$ (solid blue line), and $x_r = 4$ (solid yellow line). The diffusivity is $D = 1$. In all cases, a minimum is shown at $r^* \simeq 0.816199$, $r^* \simeq 0.282182$, and $r^* \simeq 0.130708$, respectively. The MFPT diverges as r goes to zero and infinity

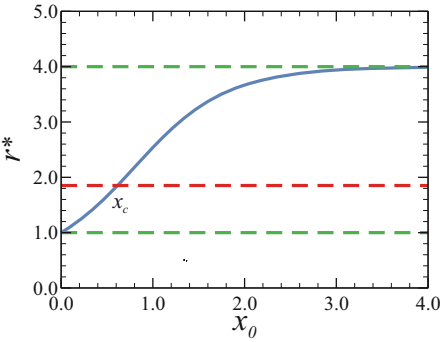

Fig. 9.10 The optimal rate r^*, calculated from Eq. (9.53), is plotted as a function of x_0 setting $x_r = 1$ (solid blue line). The domain given by Eq. (9.55) for $x_r = 1$ and $D = 1$ is $1 \leq r^* \leq 4$ (dashed green line). The crossing point is given by $x_c = 0.615068$ and $r_u^* = 1.85172$ (dashed red line)

$$\sqrt{\frac{r^*}{D}}x_r \mathrm{e}^{\sqrt{\frac{r^*}{D}}x_r} - 2\mathrm{e}^{\sqrt{\frac{r^*}{D}}x_r} - \sqrt{\frac{r^*}{D}}\,(x_r - x_0)\,\mathrm{e}^{\sqrt{\frac{r^*}{D}}(x_r - x_0)} + 2\mathrm{e}^{\sqrt{\frac{r^*}{D}}(x_r - x_0)} = 0. \tag{9.52}$$

As the reader may see, this equation is transcendental, and we can only solve it numerically. However, we can obtain the domain of the solutions by taking the limits when x_0 goes to zero and infinity. In the latter case, Eq. (9.52) reduces to

$$\mathrm{e}^{\sqrt{\frac{r}{D}}x_r}\left(\sqrt{\frac{r}{D}}x_r - 2\right) = 0. \tag{9.53}$$

Then, $r^* = 4D/x_r^2$. When x_0 goes to zero, we proceed as follows: we make a Taylor series of Eq. (9.52), keeping terms up to linear order and then take the limit when x_0 approaches to

$$\alpha_0^2 \frac{x_0 x_r}{2} = \alpha_0\,(x_0 - x_r) + 1, \tag{9.54}$$

therefore, $r^* = D/x_r^2$. We conclude that the domain in which restart expedites the completion of the underlying process is given by

$$\frac{D}{x_r^2} \leq r^* \leq \frac{4D}{x_r^2}. \tag{9.55}$$

In Fig. 9.10, we can see the behavior predicted by our analysis.

Finally, we want to answer the following question: what is more efficient, to start all Brownian particles at a single point or to distribute them between the absorbing and resetting points? In order to answer this question, when placing the absorbing target at the origin, we have to integrate Eq. (9.51) from 0 to x_r, namely,

$$\langle T_r(x_r)\rangle = \frac{1}{x_r}\int_0^{x_r} \frac{\mathrm{e}^{\alpha_0 x_r}\left[1 - \mathrm{e}^{-\alpha_0 x_0}\right]}{r}\,\mathrm{d}x_0 = \frac{1 + \mathrm{e}^{\alpha_0 x_r}\,(\,\alpha_0 x_r - 1)}{x_r\, r^{3/2}}. \tag{9.56}$$

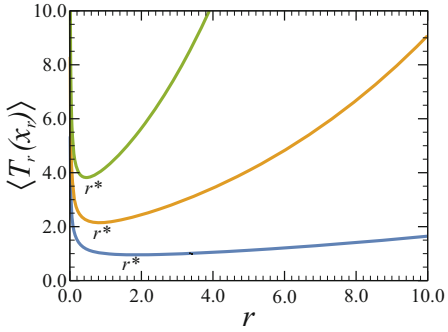

Fig. 9.11 The mean first-passage time given by Eq. (9.56) is plotted as a function of r for $x_r = 1$ (solid blue line), $x_r = 1.5$ (solid yellow line), and $x_r = 2$ (solid green line). The diffusivity is $D = 1$. The minimums are shown at $r^* = 1.85172$, $r^* = 0.82298$, and $r^* = 0.4629$, respectively. The MFPT diverges as r goes to zero and infinity

The optimal rate r^* at which the minimum value of the MFPT is observed occurs when the first derivative of Eq. (9.56) with respect to r is zero. This yields

$$\frac{1}{2}\gamma_r^{2*} - \frac{3}{2}\gamma_r^* - \frac{3}{2}\mathrm{e}^{-\gamma_r^*} + \frac{3}{2} = 0, \tag{9.57}$$

where $\gamma_r^* = \sqrt{r/D}x_r$. This last equation has a unique solution given by $\gamma_r^* = 1.36078$, and then, $r^* = 1.85172D/x_r^2$. Finally, it is worth noting that the existence of a crossing point between the uniformly distributed initial positions and a single initial position given by $x_c = 0.615068\,x_r$ can be found numerically. Below this point, it is more efficient to place all the random walkers at x_0; otherwise, it is more efficient to distribute them uniformly (see Fig. 9.11).

9.9 Concluding Remarks

Throughout this chapter, we have shown that when a one-dimensional diffusion process takes place in the presence of an absorbing target with resetting, the MFPT is finite, contrary to the case where resetting is not present. Additionally, we showed that the survival probability density and the MFPT under resetting have a simple connection with the survival probability density without resetting in a Laplace domain. Finally, we provided the condition that must be fulfilled for the existence of the optimal restart rate r^*, namely, $CV > 1$.

The most important equations that were obtained in this chapter are listed below:

$$\frac{\partial p(x,t)}{\partial t} = D\frac{\partial^2 p(x,t)}{\partial x^2} - r\, p(x,t) + r\, p(x_r,t)$$

(Diffusion equation with resetting)

$$\frac{\partial S_r(x_0,t|x_r)}{\partial t} = D\frac{\partial^2}{\partial x_0^2} S_r(x_0,t|x_r) - r\, S_r(x_0,t|x_r) + r\, S_r(x_r,t|x_r)$$

(Survival probability with resetting)

$$\frac{\partial^2 \langle T_r(x_0)\rangle}{\partial x_0^2} - r\langle T_r(x_0)\rangle + r\langle T_r(x_r)\rangle = -1$$

(Mean First-Passage time with resetting)

$$S_r(s|x_0) = \frac{S_0(x_r)}{1 - r\, S_0(x_r)}$$

(Survival probability with resetting)

$$\langle T_r(x_0)\rangle = \frac{S_0(x_r)}{1 - r\, S_0(x_r)}$$

(Mean First-Passage time with resetting)

Further Reading and References

M.R. Evans, S.N. Majumdar, Diffusion with stochastic resetting. Phys. Rev. Lett. **106**, 160601 (2011). https://doi.org/0.1103/PhysRevLett.106.160601.

M.R. Evans, S.N. Majumdar, G. Schehr, Stochastic resetting and applications. J. Phys. A: Math. Theor **53**(19), 193001 (2020). https://doi.org/0.1103/PhysRevLett.106.160601

S. Jain, D. Boyer, A. Pal, L. Dagdug, Fick–Jacobs description and first passage dynamics for diffusion in a channel under stochastic resetting. J. Chem. Phys. **158**, 054113 (2023). https://doi.org/10.1063/5.0135249

A. Pal, V.V. Prasad, First passage under stochastic resetting in an interval. Phys. Rev. E **99**, 032123 (2019). https://doi.org/10.1103/PhysRevE.99.032123

S. Reuveni, Optimal stochastic restart renders fluctuations in first passage times universal. Phys. Rev. Lett. **116**, 170601 (2016). https://doi.org/0.1103/PhysRevLett.106.160601

Chapter 10
Langevin Equation and Brownian Dynamics Simulations

The objective underlying the intention to simulate Brownian motion on a computer is to accurately replicate the empirical observations obtained from an experiment in a laboratory. For example, we might want to replicate the trajectories of the pollen grains in water, which are moving stochastically, as observed by Robert Brown, or perhaps, we might like to describe the colloidal particles seen under the microscope by J. B. Perrin (see Fig. 1.8). To such end, computationally speaking, we have to discretize the diffusion processes in order to calculate the position of the Brownian particles for every time interval Δt. Each new position is generated as a random number with a Gaussian distribution as the one given by Eq. (3.73), which captures the physical essence of the process. Then, the continuous Brownian motion is generated by the cumulative summation of a sequence of normally distributed random displacements.

Numerous processes at the macromolecular scale occur in the mesoscopic regime,[1] where thermal motion drives diffusion and kinetics. Within this context, *Brownian dynamics simulations* (BDSs) offer a computer method ideally suited for such a regime, wherein explicit solvent molecules are replaced instead by a stochastic force. The technique takes advantage of the large separation in timescales between the rapid motion of solvent molecules and the more slower motion of diffusing particles. Additionally, the ability to coarse-grain out these fast modes of the solvent allows us to simulate considerably larger timescales than in a molecular dynamics simulation (MDS).

Further elaborating on the framework of computational tools, a key component of BDSs involves the integration of a stochastic differential equation to generate trajectories of diffusing particles. The method naturally incorporates time, enabling the study of the temporal dynamics and evolution of complex fluids. For instance, in colloidal or particle suspension systems, the motion of particles influences the

[1] The mesoscopic regime is an intermediate scale between the microscopic and macroscopic ranges, i.e., between the atomic or molecular scale and human observable scale.

L. Dagdug et al., *Diffusion Under Confinement*,
https://doi.org/10.1007/978-3-031-46475-1_10

solvent, leading to alterations in the velocity field. Consequently, these changes in velocity induce modifications to the viscous drag force exerted on neighboring particles. This interplay, mediated by the solvent, is known as hydrodynamic interaction. These interactions, together with external forces, such as magnetic or electric fields, can be included in BDSs through the use of an interaction tensor contained in the diffusion tensor.

Brownian dynamics simulations have been used to study the physics of different kinds of macromolecules and soft matter and allow us to model several different spatiotemporal processes, such as the rheological behavior of polymers, the dynamics of proteins and DNA, the flow behavior of colloids, the structural dynamics of liquid crystals, the dynamics of carbon nanotubes, models of intracellular calcium dynamics, and signal transduction in *Escherichia coli* chemotaxis. They can also be used to compute biomolecular association rate constants, dock molecules to predict the structure, and investigate the effects of macromolecular crowding on molecular association and biomolecular recognition processes accounting for hydrodynamic interactions, among others.

In this chapter, we aim to elucidate the details behind writing computational codes and running a BDS. Given that the generation of random numbers serves as a crucial component in BDSs, we will start by providing a comprehensive overview of all essential elements pertaining to this topic. Then, the derivation and analysis of the Langevin equation are presented. Lastly, with these theoretical foundations on hand, we will show the main steps in the process of writing code and performing BDSs.

10.1 Discrete Equations of Brownian Dynamics

As previously established, our computational experiments must be carried out by means of the Langevin equation while taking into account all the relevant physical considerations. To such end, we present the equipartition theorem to then derive and analyze the Langevin equation.

10.1.1 Equipartition Theorem

The *equipartition theorem* was first formulated by James Clerk Maxwell in the mid-1900s. The modern and most general formulation uses the Hamiltonian, which is a way of expressing the theorem in terms of the Hamiltonian of a system. Here, we are going to present a heuristic derivation of it.

A couple of ubiquitous forms of energy exhibited in physical systems are kinetic and potential energies. Both of these energies are occasionally written as a quadratic formula depending on their respective coordinates. Some of kinetic energy include translational, rotational, or vibrational energies. Conversely, only some potential

energies can be written in this quadratic representation, e.g., the harmonic potential. Moreover, every degree of freedom will make a contribution to the total energy, meaning that if we only have translational motion in two dimensions, then there will be two contributions. Nevertheless, it is worth noting that, in its most general form, the theorem states that non-quadratic forms also contribute proportionally to the final outcome.

Consider a system in thermal equilibrium such that the probability of such system being in a certain state i, with energy ε_i, is given by the Boltzmann factor, namely,

$$p(x) \propto \mathrm{e}^{-\beta\,\varepsilon_i}, \tag{10.1}$$

where $p(x)$ is a probability distribution function (PDF), and it is not normalized. Normalization can be achieved by integrating across the entire domain, specifically

$$p(x) = \frac{\mathrm{e}^{-\beta\varepsilon_i}}{\displaystyle\int_{-\infty}^{\infty} \mathrm{e}^{-\beta\varepsilon_i}\,\mathrm{d}x}. \tag{10.2}$$

Additionally, the average energy can be computed as the expected value of the distribution, namely,

$$\langle E\rangle = \int_{-\infty}^{\infty} E\; p(x)\,\mathrm{d}x. \tag{10.3}$$

A particular form for the system's energy is now needed, so we will assume that it is built from contributions of quadratic forms, as stated earlier, leading to

$$E = \sum_{i=1}^{n} \alpha_i\, x_i^2. \tag{10.4}$$

It is worth noting that, since x_i are system variables, we calculate the average energy by performing an n-dimensional integral. Consequently

$$\langle E\rangle = \int_{-\infty}^{\infty}\cdots\int_{-\infty}^{\infty} \frac{\displaystyle\sum_{i=1}^{n}\left[\alpha_i\, x_i^2\right]\exp\left[-\beta\sum_{j=1}^{n}\alpha_j\, x_j^2\right]}{\displaystyle\int_{-\infty}^{\infty}\cdots\int_{-\infty}^{\infty}\exp\left[-\beta\sum_{k=1}^{n}\alpha_i\, x_k^2\right]\mathrm{d}x_1\cdots\mathrm{d}x_n}\,\mathrm{d}x_1\cdots\mathrm{d}x_n. \tag{10.5}$$

As the denominator is a definite integral, it becomes a constant in terms of the outer integrals' integration variables and can be taken out of all of them. Furthermore, the external sum can be factorized out of the integrals, that is,

$$\langle E\rangle = \sum_{i=1}^{n} \frac{\displaystyle\int_{-\infty}^{\infty}\cdots\int_{-\infty}^{\infty} \alpha_i\, x_i^2\, \exp\left[-\beta \sum_{j=1}^{n} \alpha_j\, x_j^2\right] \mathrm{d}x_1 \cdots \mathrm{d}x_n}{\displaystyle\int_{-\infty}^{\infty}\cdots\int_{-\infty}^{\infty} \exp\left[-\beta \sum_{k=1}^{n} \alpha_i\, x_k^2\right] \mathrm{d}x_1 \cdots \mathrm{d}x_n}. \tag{10.6}$$

Moreover, the denominator can be rewritten as the product of n-independent integrals of exponentials, namely,

$$\begin{aligned}&\int_{-\infty}^{\infty}\cdots\int_{-\infty}^{\infty} \exp\left[-\beta \sum_{k=1}^{n} \alpha_i\, x_k^2\right] \mathrm{d}x_1 \cdots \mathrm{d}x_n \\ &\quad = \int_{-\infty}^{\infty} \mathrm{e}^{-\beta\,\alpha_1\, x_1^2}\, \mathrm{d}x_1 \int_{-\infty}^{\infty} \mathrm{e}^{-\beta\,\alpha_2\, x_2^2}\, \mathrm{d}x_2 \cdots \int_{-\infty}^{\infty} \mathrm{e}^{-\beta\,\alpha_n\, x_n^2}\, \mathrm{d}x_n. \end{aligned} \tag{10.7}$$

Regarding the numerator, we must consider that every exponential can be factored out to become the integrand of a variable integral, which will be identical to one in the denominator. The only term that will be different is the i-term of the sum, i.e.,

$$\begin{aligned}&\int_{-\infty}^{\infty}\cdots\int_{-\infty}^{\infty} \alpha_i\, x_i^2\, \exp\left[-\beta \sum_{j=1}^{n} \alpha_j\, x_j^2\right] \mathrm{d}x_1 \cdots \mathrm{d}x_n \\ &\quad = \int_{-\infty}^{\infty} \mathrm{e}^{-\beta\,\alpha_1\, x_1^2}\, \mathrm{d}x_1 \cdots \int_{-\infty}^{\infty} \alpha_i\, x_i^2\, \mathrm{e}^{-\beta\,\alpha_i\, x_i^2}\, \mathrm{d}x_i \cdots \int_{-\infty}^{\infty} \mathrm{e}^{-\beta\,\alpha_n\, x_n^2}\, \mathrm{d}x_n. \end{aligned} \tag{10.8}$$

From Eqs. (10.7) and (10.8), we can identify $n-1$ common factors that are simplified, reducing to

$$\langle E\rangle = \sum_{i=1}^{n} \frac{\displaystyle\int_{-\infty}^{\infty} \alpha_i\, x_i^2\, \mathrm{e}^{-\beta\,\alpha_i\, x_i^2}\, \mathrm{d}x_i}{\displaystyle\int_{-\infty}^{\infty} \mathrm{e}^{-\beta\,\alpha_i\, x_i^2}\, \mathrm{d}x_i}. \tag{10.9}$$

Finally, using the Gaussian integrals given in Appendix A.5, we obtain

$$\langle E\rangle = \sum_{i=1}^{n} \frac{\alpha \dfrac{1}{2}\sqrt{\dfrac{\pi}{\alpha^3\,\beta^3}}}{\sqrt{\dfrac{\pi}{\alpha\,\beta}}} = \sum_{i=1}^{n} \frac{1}{2\beta}, \tag{10.10}$$

resulting in

$$\langle E \rangle = n \frac{1}{2} k_B T. \tag{10.11}$$

This is an outstanding result that, together with the initial considerations, can be expressed as: *If any degree of freedom of a system can be expressed as a quadratic form, then every one of them contributes equally to the average energy of the system that is in contact with a thermal bath at temperature T, and the contribution of each is $k_B T/2$.*

10.1.2 Langevin Equation

To obtain the Langevin equation, let us start with one-dimensional Newton's second law:

$$F(t) = m \frac{\mathrm{d}v(t)}{\mathrm{d}t}, \tag{10.12}$$

where $F(t)$ is the force generated by the medium (solute) components and is exerted over a particle of mass m. For a Brownian particle, there is a velocity-dependent friction force, which is given by

$$f_f(t) = \zeta \, v(t), \tag{10.13}$$

with ζ being the friction coefficient with the dimensions of MT^{-1}. In 1851, Stokes showed ζ to be

$$\zeta = 6\pi \eta a \tag{10.14}$$

for a spherical particle, a formula that is derived in Appendix 23.A, where η is the viscosity and a is the particle's radius. Moreover, the Einstein-Smoluchowski equation for mobility is the inverse of the drag coefficient and reads as

$$\mu \equiv \frac{v(x,t)}{F(x)} = \frac{v(x,t)}{-\dfrac{\mathrm{d}U(x)}{\mathrm{d}x}} = \frac{1}{\zeta} = \beta D. \tag{10.15}$$

Then, the *Netwonian* equation of motion for the Brownian particle is

$$m \frac{\mathrm{d}v(t)}{\mathrm{d}t} = -\zeta \, v(t), \tag{10.16}$$

where the minus sign of the drag force tells us that its action is opposite to the particle's motion. The steps to solve the equation are written out in detail in Sect. 10.1.2.1, and its solution is

$$v(t) = v_0 \exp\left[-\frac{\zeta}{m}t\right], \tag{10.17}$$

where a long time after reaching thermal equilibrium, the velocity predicted by Eq. (10.17) is zero. Nevertheless, we know from the equipartition theorem that a particle under those assumptions should have a mean square velocity of

$$\langle v(t)^2 \rangle_{\text{eq}} = \frac{1}{m} k_B T, \tag{10.18}$$

and so, another force must be involved in the physical process. The missing component is attributed to a purely random force present in the system. This stochastic force is denoted by $\xi(t)$ and arises from the collisions between the medium particles and the Brownian particle, also called random walker. Upon closer examination, it is important to note that the force should change very quickly following collisions with the surrounding media particles, that is, in an infinitesimal amount of time, but this is not necessarily true. To capture the essence of the phenomenon, we can choose to state its statistical properties, which can provide a more accurate description of the physical reality. The first of them would be the average stochastic force, which does not have any particular preference for magnitude or direction, so the average over different collisions (realizations) must be null; hence

$$\langle \xi(t) \rangle = 0. \tag{10.19}$$

Also, there is no relation between the force at different times. Every value of the force for a certain time t is independent of the force exerted at any other time t'. Then, the Dirac delta function helps us provide an accurate description through the property stated in Eq. (A.91) of Appendix A.10.3, leading to

$$\langle \xi(t)\, \xi(t') \rangle = \mathcal{C}\, \delta(t - t'), \tag{10.20}$$

where factor $\mathcal{C}$ is the strength of the fluctuating force and will be determined later. Furthermore, Eq. (10.20) is named an *autocorrelation function*, which means that the Brownian motion is a Markovian process, i.e., without memory. Consequently

$$F(t) = -\zeta\, v(t) + \xi(t), \tag{10.21}$$

and the Langevin equation reads

$$m\frac{\mathrm{d}v(t)}{\mathrm{d}t} = -\zeta\, v(t) + \xi(t). \tag{10.22}$$

Moreover, since

$$v(t) = \frac{\mathrm{d}x(t)}{\mathrm{d}t}, \tag{10.23}$$

we are able to write Eq. (10.22) as two ordinary differential equations (ODEs), a form commonly presented in the literature as

$$\frac{\mathrm{d}x(t)}{\mathrm{d}t} = v(t) \quad \text{and} \quad m\frac{\mathrm{d}v(t)}{\mathrm{d}t} = -\zeta\, v(t) + \xi(t), \tag{10.24}$$

which can be written as follows:

$$m\frac{\mathrm{d}^2x(t)}{\mathrm{d}t^2} = -\zeta\, v(t) + \xi(t). \tag{10.25}$$

In the case of systems subjected to external forces, an extra term can be added to obtain a generalized version of the Langevin equation, namely,

$$m\frac{\mathrm{d}^2x(t)}{\mathrm{d}t^2} = -\zeta\, v(t) + \xi(t) + F_{ext}(t). \tag{10.26}$$

10.1.2.1 Analysis of Velocity

Equation (10.24) is an inhomogeneous linear differential equation that can be solved by the integrating factor technique, namely,

$$v(t) = v_h(t) + v_p(t), \tag{10.27}$$

which is the solution to the homogeneous equation, $v_t(t)$, plus a particular solution to the inhomogeneous case, $v_p(t)$. First, let us write the Langevin equation in its standard form, namely,

$$\frac{\mathrm{d}v(t)}{\mathrm{d}t} + \frac{\zeta}{m}\, v(t) = \frac{1}{m}\xi(t). \tag{10.28}$$

The solution $v_h(t)$ is found through the simplification of the latter equation, i.e.,

$$\frac{1}{v(t)}\frac{\mathrm{d}v(t)}{\mathrm{d}t} = -\frac{\zeta}{m}. \tag{10.29}$$

By integrating this last equation in time, we obtain

$$\ln v(t) = -\frac{\zeta}{m} + \mathcal{A}, \tag{10.30}$$

where $\mathcal{A}$ is the integration constant. Taking the exponential in both sides of the last expression and reducing the constants, the solution of the homogeneous equation becomes

$$v_h(t) = \mathcal{B} \exp\left(-\frac{\zeta}{m}t\right). \tag{10.31}$$

If at some specific time $t = 0$, the value of the velocity is known and well defined, e.g.,

$$v(0) = v_0, \tag{10.32}$$

constant $\mathcal{B}$ can be determined, leading to

$$v_h(t) = v_0 \exp\left(-\frac{\zeta}{m}t\right). \tag{10.33}$$

To complete the process, a particular solution to the inhomogeneous equation must be computed. As a first step, the integrating factor should be identified as

$$\exp\left(\int \frac{\zeta}{m}\,\mathrm{d}t\right) = \exp\left(\frac{\zeta}{m}t\right), \tag{10.34}$$

which multiplied by Eq. (10.28) leads to

$$\frac{\mathrm{d}v_p(t)}{\mathrm{d}t} \exp\left(\frac{\zeta}{m}t\right) + \frac{\zeta}{m} v_p(t) \exp\left(\frac{\zeta}{m}t\right) = \frac{1}{m}\xi(t) \exp\left(\frac{\zeta}{m}t\right). \tag{10.35}$$

This last equation can be written by using the chain rule, i.e.,

$$\frac{\mathrm{d}}{\mathrm{d}t}\left[v_p(t) \exp\left(\frac{\zeta}{m}t\right)\right] = \frac{1}{m}\xi(t) \exp\left(\frac{\zeta}{m}t\right). \tag{10.36}$$

The integration yields

$$\int_0^t \frac{\mathrm{d}}{\mathrm{d}t'}\left[v_p(t') \exp\left(\frac{\zeta}{m}t'\right)\right]\mathrm{d}t' = \frac{1}{m}\int_0^t \xi(t') \exp\left(\frac{\zeta}{m}t'\right)\mathrm{d}t', \tag{10.37}$$

where t' is a dummy variable. In addition, we must impose the initial condition which satisfies Eq. (10.32) since we have Eqs. (10.27) and (10.33), namely

$$v_p(0) = 0. \tag{10.38}$$

Note that this initial condition is different from that of the homogeneous solution. Thus, the particular solution of the inhomogeneous equation is

$$v_p(t) = \frac{1}{m}\int_0^t \xi(t')\,\exp\left[-\frac{\zeta}{m}(t-t')\right]\,\mathrm{d}t'. \tag{10.39}$$

Finally, we can write the complete solution for the velocity, Eq. (10.27), which is

$$v(t) = v_0\,\exp\left(-\frac{\zeta}{m}t\right) + \frac{1}{m}\int_0^t \xi(t')\,\exp\left[-\frac{\zeta}{m}(t-t')\right]\,\mathrm{d}t'. \tag{10.40}$$

The usefulness of Eq. (10.40) does not stem from the equation itself, but rather from its mean value. Since $\xi(t)$ is a random Gaussian process, the integral in the last equation cannot be solved in terms of the usual integration techniques. The reason for this is that, because $\xi(t)$ does not have a certain or deterministic value for a fixed t, it will change for every realization of the walk, making it impossible to perform the integration.

To obtain actual information about the system, Eqs. (10.19) and (10.20) should be invoked as they are written, that is, as averages or mean values. Then, the average of the velocity can be obtained, namely,

$$\langle v(t)\rangle = v_0\,\exp\left(-\frac{\zeta}{m}t\right) + \frac{1}{m}\int_0^t \langle\xi(t')\rangle\,\exp\left[-\frac{\zeta}{m}(t-t')\right]\,\mathrm{d}t'. \tag{10.41}$$

It is worth remembering that the average is taken over different realizations (particles), and not over time, allowing us to calculate the mean value inside the time-dependent integral. Recalling Eq. (10.19), the average velocity for a Brownian particle is

$$\langle v(t)\rangle = v_0\,\exp\left(-\frac{\zeta}{m}t\right), \tag{10.42}$$

where the relaxation time of the system can be defined as

$$\tau_r \equiv \frac{m}{\zeta}. \tag{10.43}$$

10.1.2.2 Correlation of Velocities and the Diffusion Coefficient

The correlation between velocities is calculated as follows: Let us take the product of Eq. (10.40) for two different times and then calculate the average, leading to

$$\langle v(t_1)\,v(t_2)\rangle = v_0^2\,\exp\left[-\frac{\zeta}{m}\,(t_1+t_2)\right]$$

$$+\frac{1}{m^2}\int_0^{t_2}\int_0^{t_1}\langle\xi(t_1')\,\xi(t_2')\rangle\,\exp\left[-\frac{\zeta}{m}\left(t_1-t_1'+t_2-t_2'\right)\right]\mathrm{d}t_1'\,\mathrm{d}t_2', \tag{10.44}$$

where using the correlation function in Eq. (10.20) yields

$$\langle v(t_1)\,v(t_2)\rangle = v_0^2\,\exp\left[-\frac{\zeta}{m}\,(t_1+t_2)\right]+\frac{\mathcal{C}}{m^2}\,\exp\left[-\frac{\zeta}{m}\,(t_1+t_2)\right] \times\int_0^{t_2}\int_0^{t_1}\delta(t_1'-t_2')\,\exp\left[+\frac{\zeta}{m}\left(t_1'+t_2'\right)\right]\mathrm{d}t_1'\,\mathrm{d}t_2'. \tag{10.45}$$

Using the property in Eq. (A.92) of Dirac's delta function, this last equation is transformed into

$$\langle v(t_1)\,v(t_2)\rangle = v_0^2\,\exp\left[-\frac{\zeta}{m}\,(t_1+t_2)\right]+\frac{\mathcal{C}}{m^2}\,\exp\left[-\frac{\zeta}{m}\,(t_1+t_2)\right] \times\int_0^{t_2}\exp\left[2\frac{\zeta}{m}t_2'\right]\mathrm{d}t_2'. \tag{10.46}$$

The remaining integral is solved to obtain

$$\langle v(t_1)\,v(t_2)\rangle = v_0^2\,\exp\left[-\frac{\zeta}{m}\,(t_1+t_2)\right]+\frac{\mathcal{C}}{m^2}\,\exp\left[-\frac{\zeta}{m}\,(t_1+t_2)\right] \times\frac{m}{2\zeta}\left\{\exp\left[2\frac{\zeta}{m}t_2\right]-1\right\}, \tag{10.47}$$

which simplifies to

$$\langle v(t_1)\,v(t_2)\rangle = v_0^2\,\exp\left[-\frac{\zeta}{m}\,(t_1+t_2)\right] +\frac{\mathcal{C}}{2m\zeta}\left\{\exp\left[-\frac{\zeta}{m}\,(t_1-t_2)\right]-\exp\left[-\frac{\zeta}{m}\,(t_1+t_2)\right]\right\}. \tag{10.48}$$

This is the correlation equation for the velocities of the Langevin equation.

10.1.2.3 Long Time Limit

Once the system has evolved for a sufficiently long period of time, we will assume that it has reached a *steady state*. Consequently, the exponential terms where the times t_1 and t_2 are summed will tend to zero, namely,

$$\langle v(t_1)\, v(t_2)\rangle_{\text{eq}} = \frac{\mathcal{C}}{2m\zeta}\, \exp\left[-\frac{\zeta}{m}\,(t_1 - t_2)\right], \tag{10.49}$$

where, after taking $t_1 = t_2 = t$, it becomes

$$\langle v(t)^2\rangle_{\text{eq}} = \frac{\mathcal{C}}{2m\zeta}. \tag{10.50}$$

Using the consideration of an equilibrium state, the energy equipartition can be applied to the system, so then

$$\langle E\rangle = \frac{1}{2} k_B\, T, \tag{10.51}$$

which is considering one degree of freedom. Since the kinetic energy is

$$\langle E\rangle = \frac{1}{2} m \langle v(t)^2\rangle_{\text{eq}}, \tag{10.52}$$

then, by solving for $k_B\, T$, it leads to

$$k_B T = m\langle v(t)^2\rangle_{\text{eq}}. \tag{10.53}$$

Equating this last expression with Eq. (10.50), we find

$$\mathcal{C} = 2k_B T\, \zeta. \tag{10.54}$$

This result is an example of the fluctuation-dissipation theorem, which was discussed in Sect. 6.4. Furthermore, it fixes the amplitude of the fluctuations shown in Eq. (10.20). Hence, the stochastic force autocorrelation function becomes

$$\langle \xi(t')\, \xi(t'')\rangle = 2k_B T\, \zeta\, \delta(t' - t''). \tag{10.55}$$

10.1.2.4 Analysis of Position

Upon obtaining an expression for the velocity of a Brownian particle, we can use it to obtain an equation describing its position by integrating Eq. (10.40) with respect to time, namely,

$$\int_0^t \frac{\mathrm{d}x(t'')}{\mathrm{d}t''}\,\mathrm{d}t'' = v_0 \int_0^t \exp\left(-\frac{\zeta}{m}t''\right)\mathrm{d}t'' + \frac{1}{m}\int_0^t \int_0^{t''} \xi(t')\, \exp\left[-\frac{\zeta}{m}(t'' - t')\right]\mathrm{d}t'\,\mathrm{d}t'', \tag{10.56}$$

where the integration order can be inverted as both integration regions go from 0 to t using its own dummy variable, leading to

$$x(t) - x(0) = -v_0 \frac{m}{\zeta}\left[\exp\left(-\frac{\zeta}{m}t\right) - 1\right] + \frac{1}{m}\int_0^t \xi(t') \exp\left[\frac{\zeta}{m}t'\right]\int_0^t \exp\left[-\frac{\zeta}{m}t''\right] \mathrm{d}t'' \,\mathrm{d}t'. \tag{10.57}$$

Given that the initial condition for position is

$$x(0) = x_0, \tag{10.58}$$

then, the particle's position is given by

$$x(t) = x_0 + v_0 \frac{m}{\zeta}\left[1 - \exp\left(-\frac{\zeta}{m}t\right)\right] + \frac{1}{\zeta}\int_0^t \xi(t') \left\{1 - \exp\left[-\frac{\zeta}{m}(t - t')\right]\right\} \mathrm{d}t'. \tag{10.59}$$

Once again, the integral cannot be performed by the usual methods because of the stochastic force $\xi(t)$, but its mean value can be calculated using the property given in Eq. (10.19), which establishes that mean Gaussian noise is null, so then

$$\langle x(t)\rangle = x_0 + v_0 \frac{m}{\zeta}\left[1 - \exp\left(-\frac{\zeta}{m}t\right)\right], \tag{10.60}$$

where, again, the relaxation time is

$$\tau_r = \frac{m}{\zeta}. \tag{10.61}$$

For the case where $t \gg \tau_r$, the exponential term vanishes, so that

$$\langle x(t)\rangle = x_0 + v_0 \frac{m}{\zeta}, \qquad t \gg \tau_r. \tag{10.62}$$

This result is valid for a long time range.

10.1.2.5 Displacement Variance

The variance of a random variable Y is defined as

$$\sigma_Y^2 \equiv \left\langle (Y - \langle Y\rangle)^2 \right\rangle = \langle Y^2\rangle - \langle Y\rangle^2. \tag{10.63}$$

If the one-dimensional displacement of the diffusive particle is $x(t) - x_0$, then its variance is given by

$$\sigma_x^2 = \left\langle \{[x(t) - x_0] - \langle x(t) - x_0 \rangle\}^2 \right\rangle = \left\langle [x(t) - x_0 - \langle x(t) \rangle + x_0]^2 \right\rangle. \tag{10.64}$$

From this last equation, we see that the variance of the displacement is the same as the variance of the position. Using Eq. (10.63), the latter equation results in

$$\sigma_x^2 = \langle x(t)^2 \rangle - \langle x(t) \rangle^2. \tag{10.65}$$

Now, we substitute Eqs. (10.59) and (10.60) into Eq. (10.65). For the sake of clarity, let us calculate each term separately. First, we square position $x(t)$ and take the average, namely,

$$\begin{aligned} \langle x(t)^2 \rangle = x_0^2 + 2x_0 v_0 \frac{m}{\zeta} \left[1 - \exp\left(-\frac{\zeta}{m} t \right) \right] + v_0^2 \frac{m^2}{\zeta^2} \left[1 - \exp\left(-\frac{\zeta}{m} t \right) \right]^2 \\ + \frac{1}{\zeta^2} \int_0^t \int_0^t \langle \xi(t'') \, \xi(t') \rangle \\ \times \left\{ 1 - \exp\left[-\frac{\zeta}{m} (t - t') \right] \right\} \left\{ 1 - \exp\left[-\frac{\zeta}{m} (t - t'') \right] \right\} \mathrm{d}t'' \, \mathrm{d}t'. \end{aligned} \tag{10.66}$$

Integrating this last equation and using Eq. (10.20) while considering that the mean stochastic force is zero, $\langle \xi(t) \rangle = 0$, we arrive at the following relation:

$$\begin{aligned} \langle x(t)^2 \rangle = x_0^2 + 2\, x_0\, v_0 \frac{m}{\zeta} \left[1 - \exp\left(-\frac{\zeta}{m} t \right) \right] + v_0^2 \frac{m^2}{\zeta^2} \left[1 - \exp\left(-\frac{\zeta}{m} t \right) \right]^2 \\ + \frac{\mathcal{C}}{\zeta^2} \int_0^t \left\{ 1 - \exp\left[-\frac{\zeta}{m} (t - t') \right] \right\}^2 \mathrm{d}t'. \end{aligned} \tag{10.67}$$

Now, the second term on the right-hand side of Eq. (10.65) is

$$\langle x(t) \rangle^2 = x_0^2 + 2\, x_0\, v_0 \frac{m}{\zeta} \left[1 - \exp\left(-\frac{\zeta}{m} t \right) \right] + v_0^2 \frac{m^2}{\zeta^2} \left[1 - \exp\left(-\frac{\zeta}{m} t \right) \right]^2. \tag{10.68}$$

Substituting these last two expressions into Eq. (10.65) and after some manipulation, we find

$$\sigma_x^2 = \frac{\mathcal{C}}{\zeta^2} \int_0^t \left\{ 1 - \exp\left[-\frac{\zeta}{m} (t - t') \right]^2 \right\} \mathrm{d}t'. \tag{10.69}$$

By performing the integration, we obtain

$$\sigma_x^2 = \frac{\mathcal{C}}{\zeta^2}\left\{t - \frac{2m}{\zeta}\left[1 - \exp\left(-\frac{\zeta}{m}t\right)\right] + \frac{m}{2\zeta}\left[1 - \exp\left(-\frac{2\zeta}{m}t\right)\right]\right\}. \tag{10.70}$$

Using Eq. (10.54), this last expression results in

$$\sigma_x^2 = \frac{2k_BT}{\zeta}\left\{t - \frac{2m}{\zeta}\left[1 - \exp\left(-\frac{\zeta}{m}t\right)\right] + \frac{m}{2\zeta}\left[1 - \exp\left(-\frac{2\zeta}{m}t\right)\right]\right\}. \tag{10.71}$$

From Eq. (6.6), we can identify that the common factor in this last equation is the diffusion coefficient. As a result, the variance can be written as follows:

$$\sigma_x^2 = 2D\left\{t - \frac{2m}{\zeta}\left[1 - \exp\left(-\frac{\zeta}{m}t\right)\right] + \frac{m}{2\zeta}\left[1 - \exp\left(-\frac{2\zeta}{m}t\right)\right]\right\}. \tag{10.72}$$

10.1.2.6 Overdamped Langevin Equation

An important limiting study case is where the acceleration term in the Lagenvin equation can be dropped due to high friction between the medium and the diffusing particles, making the inertia term irrelevant. Mathematically, we can describe this assumption as follows:

$$|\zeta v(t)| = \left|\zeta \frac{\mathrm{d}x(t)}{\mathrm{d}t}\right| \gg \left|m\frac{\mathrm{d}^2x(t)}{\mathrm{d}t^2}\right|. \tag{10.73}$$

Introducing this relation into the Langevin equation, Eq. (10.25), results in

$$\frac{\mathrm{d}x(t)}{\mathrm{d}t} = \frac{1}{\zeta}\xi(t). \tag{10.74}$$

Integrating this equation with respect to time yields

$$\int_0^t \frac{\mathrm{d}x(t')}{\mathrm{d}t'}\,\mathrm{d}t' = \frac{1}{\zeta}\int_0^t \xi(t')\,\mathrm{d}t'. \tag{10.75}$$

Using the initial condition given in Eq. (10.58), we arrive at

$$x(t) - x_0 = \frac{1}{\zeta}\int_0^t \xi(t')\,\mathrm{d}t'. \tag{10.76}$$

From this equation, we have that the mean position is given by

$$\langle x(t)\rangle = x_0 + \frac{1}{\zeta}\int_0^t \langle \xi(t')\rangle \, \mathrm{d}t' = x_0. \tag{10.77}$$

Using the property that the average random force is null and setting $x_0 = 0$, we find

$$\langle x(t)\rangle = 0. \tag{10.78}$$

Furthermore, the variance in displacement for the overdamped Langevin equation, or for a Brownian particle, is

$$\sigma_x^2 = \Big\langle [x(t) - \langle x(t)\rangle]^2 \Big\rangle = \langle x(t)^2\rangle, \tag{10.79}$$

or

$$\sigma_x^2 = \frac{1}{\zeta^2}\int_0^t \int_0^t \langle \xi(t'')\, \xi(t')\rangle \, \mathrm{d}t'' \, \mathrm{d}t' = \frac{1}{\zeta^2}\int_0^t \mathcal{C}\, \delta(t' - t'') \, \mathrm{d}t'' \mathrm{d}t' = \frac{\mathcal{C}}{\zeta^2}\int_0^t \mathrm{d}t, \tag{10.80}$$

which together with the Eq. (10.54), yields

$$\sigma_x^2 = \frac{2k_B T}{\zeta}\, t = 2Dt, \tag{10.81}$$

and consequently

$$D = \frac{\sigma_x^2}{2t} = \frac{\big\langle [x(t) - \langle x(t)\rangle]^2 \big\rangle}{2t}. \tag{10.82}$$

Remarkably, this is the same result obtained by Einstein, i.e., Eq. (1.10). Also, it was derived as the variance of Gaussian distribution without any physical consideration, i.e., Eq. (3.72). Furthermore, Eq. (10.82) will play a key role calculating the diffusion coefficient in diffusive system simulations. Nontheless, readers should note that the square of the quantities involved can result in the phenomenon known as *catastrophic cancellation* due to floating point arithmetics used in computer systems and alternative methods to calculate the variance will need to be considered.

10.1.3 Brownian Dynamics Simulations

Brownian dynamics simulation focuses on a particle's motion that obeys the overdamped Langevin equation, namely,

$$|\zeta\, v(t)| = \left|\zeta \frac{\mathrm{d}x(t)}{\mathrm{d}t}\right| \gg \left|m \frac{\mathrm{d}^2 x(t)}{\mathrm{d}t^2}\right|. \tag{10.73}$$

Under this consideration, the (overdamped) Langevin equation reads

$$\frac{\mathrm{d}x(t)}{\mathrm{d}t} = \frac{1}{\zeta}\xi(t) + \frac{1}{\zeta}F_{ext}(t), \tag{10.83}$$

where F_{ext} corresponds to the external forces.

The stochastic nature of $\xi(t)$ prevents us from obtaining a solution for the differential equation using the usual techniques. We must remember that our goal is to simulate the system, and given that a computer can only handle discrete values, the discretization of Eq. (10.83) must be done by writing it as a finite difference function. By setting $x_n \equiv x(t)$, the particle's position at time $t + \Delta t$ is given by

$$x_{n+1} = x(t_n + \Delta t). \tag{10.84}$$

Now, after making the Taylor series of the last expression, we obtain

$$x_{n+1} = x_n + \Delta t \frac{\mathrm{d}x}{\mathrm{d}t} + \ldots. \tag{10.85}$$

Then, truncating the series up to order $\mathcal{O}(\Delta t^2)$ allows us to write the derivative as follows:

$$\frac{\mathrm{d}x}{\mathrm{d}t} \to \frac{1}{\Delta t}(x_{n+1} - x_n). \tag{10.86}$$

Substituting this last relation into Eq. (10.83) gives

$$x_{n+1} = x_n + \frac{\Delta t}{\zeta}\xi(t) + \frac{\Delta t}{\zeta}F_{ext}(t). \tag{10.87}$$

Working with the external forces and using Eq. (10.15), we see that

$$\frac{\Delta t}{\zeta}F_{ext}(t) = \beta\, D\, \Delta t\, F_{ext}(t). \tag{10.88}$$

The stochastic term of Eq. (10.87) is truly a force with the corresponding dimensions, but it is convenient to split it into a deterministic factor, which will carry the dimensionality of the force, and an adimensional stochastic factor generated by a pseudorandom number generator.

We already deduced an important property of Brownian motion, namely, the standard deviation, or

$$\sigma = \sqrt{2D\Delta t}, \tag{10.89}$$

whose dimensions are

$$[\sigma] = L. \tag{10.90}$$

Now, a standard normal distribution $N(\mu = 0, \sigma = 1)$ can be transformed into another normal distribution with different parameters by

$$N(\mu, \sigma) = \mu + \sigma N(0, 1) = \sigma N(0, 1). \tag{10.91}$$

Due to the thermal bath, from Eq. (10.91), we can see that the displacement of particles is given by $\sigma\eta(t)$, where $\eta(t)$ is a random number, which can be described by the normal distribution in Eq. (10.91). Therefore,

$$\xi(t) = \sqrt{\frac{2\zeta}{\beta\Delta t}}\,\eta(t), \tag{10.92}$$

where the dimensions of the square root are

$$\left[\sqrt{\frac{2\zeta}{\beta\Delta t}}\right] = MLT^{-2}, \tag{10.93}$$

which is dimensionaly equivalent to a force. Then, $\eta(t)$ has no dimensions, and $\eta(t) \sim N(0, 1)$. Finally, using Eqs. (10.89), (10.92), and (10.87) yields

$$x_{n+1} = x_n + \sqrt{2D\Delta t}\,\eta(t) + \beta\, D\, \Delta t\, F_{ext}(t). \tag{10.94}$$

This is the cornerstone result that allows us to obtain the next step, x_{n+1}, of a random walker by means of the previous step, x_n. This equation gives us the trajectory of a diffusing particle through time.

10.2 Random and Pseudorandom Numbers

The measurement of *randomness* is a complicated process. However, statistics addresses this issue by quantifying certain properties, including correlation, periodicity, and dimensional distribution. Moreover, the generation of artificial randomness, and therefore of *random numbers*, is considerably difficult, and its production demands a distinctive combination of rigorous formal mathematics, creativity, and intuition. Primarily, the absence of *true random number generators* (TRNGs) lies in the attempt to obtain randomness through computational deterministic algorithms. In order to overcome this challenge, deterministic algorithms are used to generate *pseudorandom numbers* (PRNs). They are "random" in the sense that, on average, they pass statistical tests regarding their distribution and correlation and differ from true random numbers in that they are generated by an algorithm rather than a truly random process. Early developments in generating PRNs trace back thousands of

years, illustrating the persistent search for unpredictability throughout time. For a concise historical overview of PRNs, the reader is referred to a brief historical review[2] made by Pierre L'Ecuyer in 2017.

The use of *pseudorandom number generators* (PRNGs) is employed in a variety of applications including gambling, computer simulation, statistical sampling, encryption, and digital signature creation, as well as other areas where the ability to generate random numbers is critical.

10.2.1 Middle Square Method

In 1949, John von Neumann proposed the *middle square method* as a PRNG. Although this method is no longer viable due to the availability of far superior techniques, its historical significance as the pioneering effort in random number generation remains noteworthy.

The idea of this method is to use an n-digit starting value, or *seed*, to generate n-digit PRNs with an arithmetic procedure. The algorithm is shown below:

1. Set an n-digit as the seed number, and let it be the first number in the PRN sequence.
2. Square the last number in the PRN sequence, which will probably result in a $2n$-digit number.
3. If the result is not a $2n$-digit number, then left-pad with zeros.
4. Take the middle n-digits as the next PRN in the sequence.
5. Repeat from the step 2.

Let us give a couple of examples where (a) we choose a seed that generates several PRNs without apparent repetition and (b) we show the limited applicability of the method. In the first example, we start with 4321 as the seed and we proceed to execute the above steps as follows:

- 4321 is the seed and the first number in the PRN sequence.
- Square the last number in the sequence: $4321^2 = 18671041$.
- As 18671041 has 8 digits (twice the number of digits of 4321), there is no need to left-pad with zeros.
- Take the middle four digits of 18671041, which are 6710, and make them part of the PRN sequence.
- Square the last number in the sequence: $6710^2 = 45024100$.
- As 45024100 has 8 digits, there is no need to left-pad with zeros.
- Take the middle four digits of 45024100, which are 0241, and make it part of the PRN sequence.
- Square the last number in the sequence: $241^2 = 58081$.

[2] *History of Uniform Random Number Generation*, P. L'Ecuyer, Proceedings of the 2017 Winter Simulation Conference (2017), Art. 13. DOI: 10.5555/3242181.3242195.

- As 58081 does not have 8 digits, we need to left-pad with zeros to obtain 00058081.
- Take the middle four digits of 00058081, which are 0580, and make them part of the PRN sequence.
- PRN sequence: 4321, 6710, 241, 580.
- Square the last number in the sequence: $580^2 = 336400$.
- As 336400 does not have 8 digits, we need to left-pad with zeros to obtain 00336400.
- Take the middle four digits of 00336400, which are 3364, and make them part of the PRN sequence.
- Square the last number in the sequence: $3364^2 = 11316496$.
- As 11316496 has 8 digits, there is no need to left-pad with zeros.
- Take the middle four digits of 11316496, which are 3164, and make them part of the PRN sequence.
- PRN sequence: 4321, 6710, 241, 580, 3364, 3164.
- *And so on...*[3]

The next illustrative example will show the weakness of the method when setting 24 as the seed:

- 24 is the seed and the first number in the PRN sequence.
- Square the last number in the sequence: $24^2 = 576$.
- As 576 does not have 4 digits (twice the number of digits of 24), we need to left-pad with zeros to obtain: 0576.
- Take the middle two digits of 0576, which are 57, and make them part of the PRN sequence.
- Square the last number in the sequence: $57^2 = 3249$.
- As 3249 has 4 digits, there is no need to left-pad with zeros.
- Take the middle four digits of 3249, which are 24, and make them part of the PRN sequence.
- PRN sequence: 24, 57, 24.

From the last example, we see that only two different numbers (including the seed), 24, 57, can be obtained from the middle square method by using 24 as the seed.

10.2.2 Linear Congruential Generator

Since von Neumann's proposal, several attempts were made to generate random numbers, and the analysis of their properties and failures was studied in depth. In 1951, Derrick Lehmer published a new method for a PRNG consisting of generating

[3] The 71th number in the PRN sequence is 8100, causing the method to enter a loop: 8100, 6100, 2100, 4100, 8100.

a large number of PRNs before the sequence repeats. The new approach to generate PRNs was named *Lehmer random number generator*, sometimes found as *Park-Miller random number generator*, and became the first in a new kind of algorithms, otherwise known as *linear congruential generators* (LCGs). Its main attribute is that the period can be long and known under certain circumstances. The method is based on the following equation:

$$x_{k+1} = a + b\, x_k \bmod m, \tag{10.95}$$

where mod is the modulo function.[4] For example, the expression 5 mod 2 would evaluate to 1, because 5 divided by 2 has a quotient of 2 and a remainder of 1. The term a is an element of high multiplicative order[5] modulo m, and the seed x_0 is coprime[6] to m. The maximum number for 32 bits unsigned integers is $2^{32} - 1$, while $2^{31} - 1$ is the largest for signed integers. The seed, x_0, is the first number in the sequence of the PRNs and must be fixed at start.

Since Eq. (10.95) contains the modulus operation, the sequence will repeat after m iterations, at the most. This is the period of the generator. Certainly, this period can be shorter and directly depends on the chosen values of a, b, and m. In practice, the generated numbers are normalized, that is, they are mapped to the interval (0, 1) by calculating the ratio of the generated number with m.

When using the LGCs, the choice of constants is fundamental to getting a long period (i.e., a large set of non-repeating sequences) and uniformly distributed pseudorandom numbers into the interval. As a naive approach to the "quality" of the numbers, let us consider the number line, where we place the generated numbers that must not have any preference for a particular location or set of locations on the line, and visually, there will be no clusters of numbers. If we only generate a few numbers, we will not be able to appreciate their distribution and will thus be perceived as random.

By extrapolating this idea to a three-dimensional box, we can draw a point for each triplet of generated numbers. The behavior of the points will be different for "bad" and "good" choices of constants for the LGC, as shown in Figs. 10.1 and 10.2. On the left-side panels of the mentioned figures, the numbers generated from "bad" alternatives of constants are depicted, from which we can see how the points in space are aligned into planes. Meanwhile, on the right-side panels of the plots, we draw the numbers coming from a "good" choice of the constants; those points look intuitively random.

[4] In computing, the modulo function, mod, takes as arguments two real numbers and returns the remainder from the division of the integer part of the first argument (the dividend) by the integer part of the second argument (the divisor). For example, mod(10,3) = 1.

[5] The multiplicative order of a modulo n is the smallest positive integer k such that $a^k 1 \bmod n$.

[6] In number theory, two integers a and b are coprime if the only positive integer that is a divisor of both is 1.

10.2.2.1 An Implementation of an LCG

All the codes presented in this book are written in FORTRAN. Old versions of the language used to rely on a so-called congruential PRNG, known for giving bad quality random numbers, so it is best to avoid it. The GNU Compiler Collection (GCC) contains a FORTRAN compiler best known as GFortran, which in early versions implemented the old FORTRAN 77 standard *rand()* function, as of version 4.2.4 (2008), it came out with a new-brand *random_number()* subroutine that implements the George Marsaglia's infamous KISS (Keep It Simple Stupid) algorithm. Starting from GCC 7.5.0 (late 2019), GFortran is equipped with the *xorshift1024** algorithm to generate uniformly distributed PRNs, which can be used even in multithreaded programs, a valuable feature these days. In contrast, the Intel© FORTRAN compiler implements L'Ecuyer's portable combination of two congruential methods, offering a bit less flexibility and reliability. Despite the above, because of the scope of this book, any of the available PRNGs are suitable to do the job.

Let us build a working example of an LCG by taking some values from popular implementations. It is worth noting that some of them, like *glibc*, Java implementations, and POSIX standards, truncate the output of the algorithm to obtain statistically better values. In our implementation, we do not use such truncation for purposes of simplicity and practicality.

In order to understand the difference between "good" and "bad" PRNGs, we list the code of the *c++11* standard implementation of the function called *minstd_rand*. We will show that when setting $a = 0$, $b = 48271$, and $m = 2^{31} - 1 = 2147483647$, "good" PRNs are generated, whereas when setting $a = 1$, $b = 1,229$, and $m = 2^{32}$, "bad" PRNs are generated.[7] The Fortran implementation is shown in Listing 10.1.

Listing 10.1 [lcg-cpp11.f90]: Fortran 90 implementation of C++11 standard minstd_rand function, an LCG-type generator.

```
1 ! ****************************************************** !
2 ! ****************** lcg-cpp11.f90 ******************* !
3 ! ****************************************************** !
4 !
5 !    Leonardo Dagdug, Ivan Pompa-García, Jason Peña
6 !
7 ! From the book:
8 ! ****************************************************** !
```

Listing continued on next page

[7] In 1999, L'Ecuyer provided a table with "good" values of a, b, and m. For further details, see *Tables of linear congruential generators of different sizes and good lattice structure*, P. L'Ecuyer, Math. Comp. **68** (1999), 249–260. DOI: 10.1090/S0025-5718-99-00996-5.

Listing continued from last page

```
!      Diffusion Under Confinement:
!               A Journey Through Counterintuition
! ************************************************** !

! ************************************************** !
! This file contains the source code that implements
! the minstd function specified in the cpp11
! standard. It generates 10,000 numbers and compares
! the result with the one stated in the standard.
! ************************************************** !

! ************************************************** !
! To compile with GFortran, you must include the
! helpers.f90 module.
!         gfortran helpers.f90 lcg_cpp11.f90
! Then you can run the program:
!         ./a.out
!
! After running, a file called «minstd_numbers.dat»
! is generated, and can be plotted with any software
! of your choice. To do this using gnuplot, execute:
!         gnuplot -p -e 'plot "minstd_numbers.dat"'
! -p means that the plot must persist until the
!    user closes it explicitly.
! -e is used to specify the instructions
!    for using  gnuplot directly in the commandline.
! ************************************************** !

program lcg_cpp11

! Load the helpers module, which contains functions,
! constants, and more...
use helpers

! Every data type must be explicitly stated.
implicit none

! Declare and initialize our LCG parameters
! as constants.
integer(kind=i32), parameter :: a = 0
```

Listing continued on next page

Listing continued from last page

```
integer(kind=i32), parameter :: b = 48271
! We must write the result. If we try to calculate it,
! the compiler drops an error because 2^31 overflows the
! capacity of an integer, even if 2^31 - 1 fits.
integer(kind=i32), parameter :: m = 2147483647

! How many numbers will be generated.
integer(kind=i32), parameter :: n = 10000
! According to c++11 standard, the 10,000th generated
! number must be 399268537 when the initial seed is 1.
integer(kind=i64), parameter :: xstd = 399268537

! A unit number for the file where the numbers
! will be saved. Fortran >= 2003 will
! assign this automatically in the open call.
integer(kind=i32) :: FUNIT

! Number in the sequence. Initially this must be
! the seed.
integer(kind=i64) :: x = 1

! A counter
integer :: i

! Open a file to write the normalized numbers
open(newunit=FUNIT, file='minstd_numbers.dat')

do i=1, n
  x = a + mod(b * x, m)

  ! You must not forget that «x», and «m» are integers
  ! and Fortran will be perform integer arithmetic.
  ! You must multiply one of the operands by a real
  ! factor.
  write(FUNIT,*) 1.0_dp * x / m
end do

! Close the file
close(unit=FUNIT)

```

Listing continued on next page

Listing continued from last page

```
if(x == xstd) then
  print *, 'The 10000 number from seed 1 is correct: ' &
    // nstr(x)
else
  print *, &
    'Something goes wrong, the last number should be ' &
    // nstr(xstd) // ' and not ' // nstr(x)
end if

end program lcg_cpp11
```

Listing ended

Compiling and Running of Listing 10.1

```
        # Compile
        gfortran helpers.f90 lcg-cpp11.f90

        # Run
        ./a.out

        # Sample output
          The 10000 number from seed 1 is correct:
    399268537

        # Plot
        gnuplot -p -e 'plot "minstd_numbers.dat"'
```

10.2.3 Inverse Transform Sampling

Now, we will provide all the mathematical tools needed to obtain a generator of Gaussian or normal random numbers. Based on the assumption that we can generate uniformly distributed PRNs of good enough quality, we are able to transform them into normally distributed PRNs by means of *pseudorandom number sampling*. This method consists of generating sample numbers at random from any probability distribution that follows a certain distribution. For continuous distributions, there are

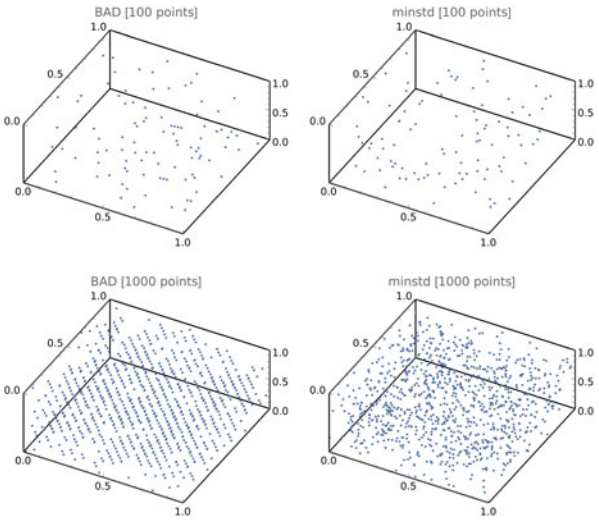

Fig. 10.1 Comparison between two LGC implementations in a three-dimensional box. On the left-hand side, we show the points corresponding to a "bad" choice of constants $[a = 1, b = 1,229, m = 2^{32}]$. In contrast, on the right, we depict the points generated with a "good" choice of constants (minstd $[a = 0, b = 48,271, m = 2^{31} - 1]$). When there are very few points, the *randomness* is apparent for both sets, but as soon as more points are added, the not-so-random distribution of the points for a "bad" choice of the LGC constants is apparent

different methods, such as the ratio of uniforms, slice sampling, rejection sampling, the convolution generator, and inverse transform sampling, among others.

For our purposes, we will use the inverse transform sampling method. Let us define U as a uniformly distributed random variable within the interval $(0, 1)$ and consider a continuous distribution function of the form

$$F_X(x) = P\{X \leq x\} = P\left\{F^{-1}(U) \leq x\right\}, \tag{10.96}$$

where the random variable $X = F^{-1}(U)$ and the uniformly distributed random numbers U within the interval $(0, 1)$, Unif$(0, 1)$. From probability theory, we know that if F is a *cumulative density function* (CDF), then it is a monotonic increasing function, so if we have $x_1 \leq x_2$ inside its domain, then $F(x_1) \leq F(x_2)$; hence

$$F_X(x) = P\left\{F\left(F^{-1}(U)\right) \leq F(x)\right\} = P\{U \leq F(x)\} = F(x). \tag{10.97}$$

The last equality holds by the knowledge that U is uniformly distributed. This procedure allows us to generate a random variable X, which will be distributed as F by means of a uniformly distributed random number U, and then applying the transformation $X = F^{-1}(U)$. Consequently, we have a method for generating random numbers from any probability distribution by using its inverse cumulative

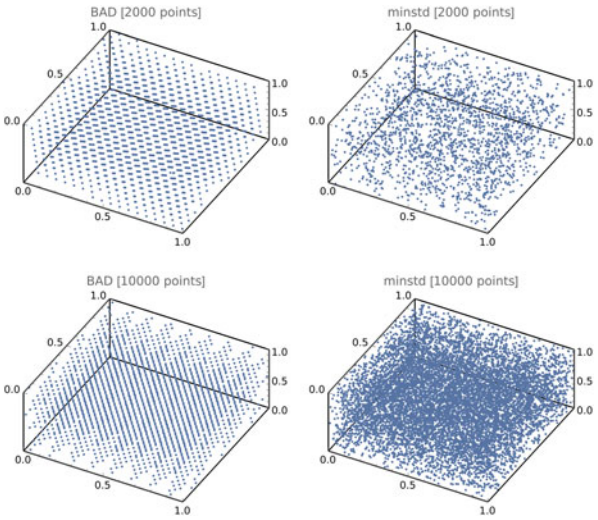

Fig. 10.2 Comparison between two LGC implementations in a three-dimensional box. On the left-hand side, we show the points corresponding to a *bad* choice of constants [$a = 1, b = 1,229, m = 2^{32}$]. In contrast, on the right-hand side, we depict the points generated with a *good* choice of constants (minstd [$a = 0, b = 48,271, m = 2^{31} - 1$]). When there are very few points, the *randomness* is apparent for both sets, but as soon as more points are added, the not-so-random distribution of the points for a bad choice of the LGC constants is apparent

distribution, or in other words, we can generate X from $F^{-1}(U)$. Hereafter, we assume that our computer can generate independent realizations of a random variable U uniformly distributed in (0, 1), on demand.

Let us exemplify the method. Assume X is an exponential random variable with probability density $\lambda \mathrm{e}^{-\lambda y}$, for $y > 0$. Our goal is to generate random numbers with such a distribution. To such end, first, we compute the CDF, namely,

$$F(x) = \int_0^x \lambda \mathrm{e}^{-\lambda y} \, \mathrm{d}y = 1 - \mathrm{e}^{-\lambda x}. \tag{10.98}$$

Solving for the inverse (solving for x), where

$$x = F\left(F^{-1}(y)\right), \tag{10.99}$$

yields

$$x = F\left(F^{-1}(y)\right) = 1 - \exp\left(-\lambda F^{-1}(y)\right). \tag{10.100}$$

From this last equation, we have that

$$X = F^{-1}(y) = -\frac{1}{\lambda}\ln(1-y)\,. \tag{10.101}$$

In practice, we first generate $U \sim \text{Unif}(0, 1)$, and then set

$$X_i = -\frac{1}{\lambda}\ln(1-U_i)\,. \tag{10.102}$$

Finally, we have to evaluate this function according to the amount of random numbers desired, using one U_i in each step.

10.2.4 Box-Müller Method

A popular transformation that transforms uniformly distributed numbers into normally distributed ones is the Box-Müller algorithm. This algorithm, named after George E. P. Box and Mervin E. Müller, is made of square roots and logarithmic calculations and is capable of generating pairs of independent standard normal random variables. It is worth noting that if a large amount of PRNs is needed, this transformation becomes slower than others, such as Kinderman and Monahan's *ratio method* or the *Ziggurat* transformation by Marsaglia and Tsang.

If we wish to apply the inverse transform sampling to obtain a normally distributed numbers,[8] a closed form of a Gaussian probability distribution function (PDF) cannot be obtained in terms of elementary functions. Furthermore, its CDF is given by

$$I = \frac{1}{\sqrt{2\pi}}\int_{-\infty}^{\infty} \mathrm{e}^{-\frac{1}{2}x^2}\,\mathrm{d}x. \tag{10.103}$$

Despite this limitation, we can take the integral squared

$$I^2 = \frac{1}{\sqrt{2\pi}}\int_{-\infty}^{\infty} \mathrm{e}^{-\frac{1}{2}x^2}\,\mathrm{d}x\,\frac{1}{\sqrt{2\pi}}\int_{-\infty}^{\infty} \mathrm{e}^{-\frac{1}{2}y^2}\,\mathrm{d}y, \tag{10.104}$$

which under a transformation to polar coordinates becomes

$$I^2 = \frac{1}{2\pi}\int_0^{2\pi} \mathrm{d}\theta \int_0^{\infty} r\,\mathrm{e}^{-\frac{1}{2}r^2}\,\mathrm{d}r. \tag{10.105}$$

Solving the integral for θ and using the variable change $\tau = r^2/2$, and $\mathrm{d}\tau = r\,\mathrm{d}r$, we have

[8] *A Note on the Generation of Random Normal Deviates*, G. E. P. Box and Mervin E. Müller, Ann. Math. Statist. **29** (2): 610–611. DOI: 10.1214/aoms/1177706645.

$$I^2 = \int_0^\infty \mathrm{e}^{-\tau}\,\mathrm{d}\tau = 1. \tag{10.106}$$

The same technique used to solve the I integral, also known as a Gaussian integral, can be used to obtain the inverse transform sampling for normally distributed numbers. We start by writting a PDF for a two-dimensional Gaussian distribution, namely,

$$f(x, y) = \frac{1}{\sqrt{2\pi}}\mathrm{e}^{-\frac{1}{2}x^2}\,\frac{1}{\sqrt{2\pi}}\mathrm{e}^{-\frac{1}{2}y^2} = \frac{1}{2\pi}\mathrm{e}^{-\frac{1}{2}(x+y)^2}, \tag{10.107}$$

which can be written in polar coordinates as

$$f(r, \theta) = \frac{1}{2\pi}\mathrm{e}^{-\frac{1}{2}r^2}. \tag{10.108}$$

Originally, x and y were uniformly distributed in the $[0, 1]$ interval, so the new variable θ must be uniformly distributed along its own domain, $[0, 2\pi]$, and this can be written in terms of $U_1 \sim \mathrm{Unif}(0, 1)$, yielding

$$\theta = 2\pi U_1, \tag{10.109}$$

which can be understood as a scale transformation. Now, we need to obtain the CDF, which is

$$F(r, \theta) = \frac{1}{2\pi}\int_0^{2\pi}\int_0^r r'\,\mathrm{e}^{-\frac{1}{2}r'^2}\,\mathrm{d}r'\,\mathrm{d}\theta = 1 - \mathrm{e}^{-\frac{1}{2}r^2}. \tag{10.110}$$

Then, we can apply the inversion, but we must not forget that our CDF only depends on r, which must be uniformly distributed, so

$$r = F\left(F^{-1}(r)\right) = 1 - \mathrm{e}^{-\frac{1}{2}F^{-1}(r)^2} \tag{10.111}$$

since $\ln(1 - r) = -F^{-1}(r)^2/2$, then

$$-\frac{1}{2}\left[F^{-1}(r)\right]^2 = \ln(1 - r), \tag{10.112}$$

leading to

$$F^{-1}(r) = \sqrt{-2\ln(1 - r)}. \tag{10.113}$$

As $r \sim \mathrm{Unif}(0, 1)$, then $U_2 \equiv 1 - r \sim \mathrm{Unif}(0, 1)$. Now, for practical purposes, we simply change the variables, i.e.,

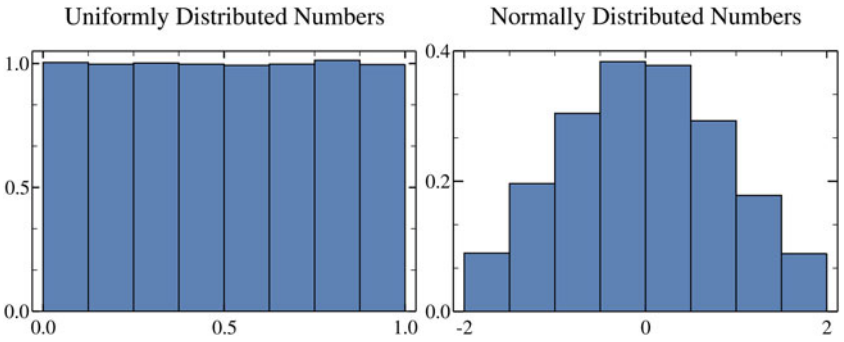

Fig. 10.3 Distribution of the PRNs generated with the Fortran code in Listing (10.2). The histogram on the left-hand side shows U generated with the *random_number()* Fortran procedure, which yields uniformly distributed numbers. The histogram on the right-hand side shows the normally distributed numbers obtained after applying the Box-Müller inversion method sampling on U

$$r = F^{-1}(U_2) = \sqrt{-2\ln(U_2)}. \tag{10.114}$$

Equations (10.109) and (10.114) are the transformations that allow us to obtain the normally distributed PRNs. All we need to do is invert the coordinate transformation, that is,

$$x = r\cos(\theta), \qquad y = r\sin(\theta). \tag{10.115}$$

Consequently

$$x = \sqrt{-2\ln(U_2)}\,\cos(2\pi U_1), \qquad y = \sqrt{-2\ln(U_2)}\,\sin(2\pi U_1). \tag{10.116}$$

These last two equations give us a pair of independent and normally distributed PRNs using two uniformly distributed numbers, and it is called the Box-Müller method.[9]

The Fortran implementation is shown in Listing (10.2), while the histograms for the generated numbers are shown in Fig. 10.3.

[9] Despite the method's name, it was first reported in *Fourier Transforms in the Complex Domain*, R. C. Paley and N. Wiener, Colloquium Publications, American Mathematical Society, **19** (1934), [pages 146–147].

Listing 10.2 [box-muller.f90]: Fortran 90 implementation of the Box-Müller method using the Fortran default PRNG to obtain the uniformly distributed numbers.

```
! ****************************************************** !
! ***************** box-muller.f90 ******************* !
! ****************************************************** !
!
!    Leonardo Dagdug, Ivan Pompa-García, Jason Peña
!
! From the book:
! ****************************************************** !
!      Diffusion Under Confinement:
!               A Journey Through Counterintuition
! ****************************************************** !

! ****************************************************** !
! This file contains the source code for performing
! a Box-Müller transformation over uniformly
! distributed numbers to make them follow a Gaussian
! distribution.
! ****************************************************** !

! ****************************************************** !
! To compile with GFortran, you must include the
! helpers.f90 module.
!         gfortran helpers.f90 box_muller.f90
! Then you can run the program:
!         ./a.out
!
! After running, a couple of files are generated:
!  - «random_uniform.dat», uniformly distributed numbers
!  - «random_normal.dat», normally distributed numbers
! Their histograms can be plotted with any software
! of your choice. To do this using gnuplot, execute:
!         gnuplot -p -e 'width=0.125 ; bin(x, width) = \
!          width*floor(x/width) ; plot \
!          "random_uniform.dat" u (bin($1,width)):(1.0)\
!          smooth freq with boxes notitle'
! and
!         gnuplot -p -e 'width=0.5 ; bin(x, width) = \
!          width*floor(x/width) ; plot \
```

Listing continued on next page

Listing continued from last page

```
!          "random_normal.dat" u (bin($1,width)):(1.0)\
!          smooth freq with boxes notitle'
!
! -p means that the plot must persist until the
!    user closes it explicitly.
! -e is used to specify the instructions
!    for using  gnuplot directly in the commandline.
! ************************************************ !

program box_muller

! Load the helpers module, which contains functions,
! constants, ...
use helpers

! Every data type must be explicitly stated.
implicit none

! How many numbers will be generated.
integer(kind=i32), parameter :: n = 10000

! A unit number for the file where the
! uniformly distributed numbers will be saved.
! Fortran >= 2003 will
! assign this automatically in the open call.
integer(kind=i32) :: UNIF_UNIT
! A unit number for the file where the
! normally distributed numbers will be saved.
! Fortran >= 2003 will
! assign this automatically in the open call.
integer(kind=i32) :: NORMAL_UNIT

! Normally distributed numbers
real(kind=dp) :: x = 1.0_dp
real(kind=dp) :: y = 1.0_dp

! Variables to hold the uniformly distributed numbers
real(kind=dp) :: u1, u2

! A counter
```

Listing continued on next page

Listing continued from last page

```
  integer :: i

  ! Open a file to write the uniformly distributed numbers
  open(newunit=UNIF_UNIT, file='random_uniform.dat')
  ! Open a file to write the normally distributed numbers
  open(newunit=NORMAL_UNIT, file='random_normal.dat')

  ! The cycle is executed only n/2 times because in every
  ! loop, two numbers of each kind are obtained. You must
  ! make sure that «n» is an even number  to get the
  ! desired quantity of numbers.
  do i=1, n/2
    ! Get the two uniformly distributed numbers
    call random_number(u1)
    call random_number(u2)

    ! Apply the Box-Müller method
    x = sqrt( -2.0_dp * log(u2) ) * cos(2.0_dp * PI * u1)
    y = sqrt( -2.0_dp * log(u2) ) * sin(2.0_dp * PI * u1)

    ! Write the uniformly distributed numbers to the files
    write(UNIF_UNIT,  *) u1
    write(UNIF_UNIT,  *) u2

    ! Write the normally distributed numbers to the files
    write(NORMAL_UNIT,  *) x
    write(NORMAL_UNIT,  *) y
  end do

  ! Close the files
  close(UNIF_UNIT)
  close(NORMAL_UNIT)

  print *, nstr(n) // ' uniformly distributed numbers, ' &
        // 'and ' // nstr(n) // ' normally distributed' &
        // ' numbers were generated!'

  end program box_muller
```

Listing ended

Compiling and Running of Listing 10.2

```
# Compile
gfortran helpers.f90 box-muller.f90

# Run
./a.out

# Sample output
  10000 uniformly distributed numbers, and 10000
normally distributed numbers were generated!

# Plot
gnuplot -p -e 'set multiplot layout 1,2 ;
  bin(x, width) = width*floor(x/width) ;
  width=0.125 ;
  set title "Uniform distributed numbers" ;
  plot "random_uniform.dat" u
    (bin($1,width)):(1.0) smooth freq
    with boxes notitle ;
  width=0.5 ;
  set title "Normally distributed numbers" ;
  plot "random_normal.dat" u
    (bin($1,width)):(1.0) smooth freq
    with boxes notitle'
```

10.3 Simulation Helpers and Programs

The process of making the computational experiments involves certain other details related to the tools we are using, e.g., the programming language or compilers. As Fortran will be used, a companion helper library is provided featuring functions/subroutines that cover certain aspects of the code that are not within the scope of this book. To this end, the `helpers.f90` file is included and presented in Appendix 10.A. Note the comments included that provide a comprehensive guide for the code, which also allows interested readers to make their own adjustments.

In addition to the helpers file, the provided source code for each computational experiment can be copied directly from the PDF and pasted into your preferred editor.

10.4 Computational Experiments

10.4.1 Absorbing-Absorbing

In Sect. 2.5, we derived the expression for mean first-passage time (MFPT) for particles diffusing into a one-dimensional channel of length L, in the presence of absorbing points at $x = 0$ and $x = L$, namely,

$$\langle t(x_0) \rangle = \frac{x_0(L - x_0)}{2D}. \tag{2.50}$$

With the aim of comparing the results obtained from BDSs and Eq. (2.50), let us assume that the Brownian particles start at $x_0 = 1/3$ and the absorbing boundaries are placed at $x = 0$ and $L = 1$, respectively. In the code presented in Listing 10.3, the repetitions of the experiment are set to $NRW = 2500$, namely, the number of particles or random walkers.

The first-passage time is measured for each particle and printed out when it is removed from the system (when particles reach one of the absorbing boundaries for the first time), together with the theoretical value and their relative error as a percentage. At the end of running the program, the mean first-passage time is obtained.

Listing 10.3 [abs-abs.f90]: Fortran 90 program to simulate a one-dimensional channel of length $L = 1$ with absorbing points at positions $x = 0$ and $x = L$. Every particle starts at $x_0 = 1/3$.

```
1  ! ******************************************************* !
2  ! ****************** abs-abs.f90 ********************** !
3  ! ******************************************************* !
4  !
5  !    Leonardo Dagdug, Ivan Pompa-García, Jason Peña
6  !
7  ! From the book:
8  ! ******************************************************* !
9  !      Diffusion Under Confinement:
10 !               A Journey Through Counterintuition
11 ! ******************************************************* !
12
13 ! ******************************************************* !
14 ! This file contains the source code for the simulation
15 ! of a 1D channel of length L.
16 ! It has two absorbent points at x=0, and x=L.
```

Listing continued on next page

Listing continued from last page

```
!
! The Brownian walkers start their path at x=x0, and
! the simulation for each of them ends when an
! absorbent point is reached. Then, the Mean First
! Passage Time (MFPT or <tau>) is obtained.
!
! The theoretical value is used to calculate the
! relative error of the simulation. D0 is the bulk
! diffusion constant, usually set to 1.
!
! tau = x0 * (L-x0) / (2.0 * D0)
! ************************************************** !

! ************************************************** !
! To compile with GFortran, you must include the
! helpers.f90 module.
!         gfortran helpers.f90 abs-abs.f90
! Then you can run the program:
!         ./a.out
! ************************************************** !

program absabs

! Load the helpers module, which contains functions,
! constants, and more...
use helpers

! Mandatory declaration of data type variables
! and constants.
implicit none

! ************************************************** !
!              Declaration of constants
! ************************************************** !

!!! Simulation parameters
! Seed of the PRNG
integer, parameter :: RSEED = 0
! Number of random walkers (particles)
integer, parameter :: NRW = 2500
```

Listing continued on next page

Listing continued from last page

```
! Channel length
real(kind=dp), parameter :: L = 1.0_dp
! Initial position of the particles is fixed
real(kind=dp), parameter :: x0 = 1 / 3.0_dp
! Temporal step size
real(kind=dp), parameter :: DT = 1.0e-6_dp

!!! Physical parameters of the system
! Diffusion constant (bulk)
real(kind=dp), parameter :: D0 = 1.0_dp
! Thermal energy inverse (1/k_b T)
real(kind=dp), parameter :: BETA = 1.0_dp
! Standard deviation for Brownian motion
real(kind=dp), parameter :: SIGMA &
                            = dsqrt(2.0_dp * D0 * DT)
! Mean distribution for Brownian motion
real(kind=dp), parameter :: MU = 0.0_dp

! Theoretical value
real(kind=dp), parameter :: THEOV &
                          = x0 * (L-x0) / (2.0_dp * D0)


! ************************************************** !
!               Declaration of variables
! ************************************************** !

! General counter
integer :: i
! Current position of the particle
real(kind=dp) :: x
! Current particle passage time
real(kind=dp) :: tau
! Sum of passage times
real(kind=dp) :: ttau = 0.0_dp
! MFPT (<tau>)
real(kind=dp) :: mfpt


! ************************************************** !
```

Listing continued on next page

Listing continued from last page

```
!           Main simulation program
! ************************************************** !

! Set the seed of the PRNG to achieve repeatable results
call setseed(RSEED)

! The loop iterates over each (i) particle.
do i=1, NRW
  !!! Initializing the needed variables
  ! The passage time is set to zero
  tau = 0.0_dp
  ! The particle current position is set to x0 (initial)
  x = x0

  !!! The random walk starts. Follow the particle until
  !!! it is removed by an absorbent point (x=0,x=L).
  do
    ! Make a step in space
    x = x + nrand(MU, SIGMA)
    ! Make a step in time
    tau = tau + DT

    ! Check for the removal of the particle
    if(x <= 0.0 .or. x >= L) then
      ! If it was removed from the channel, stop the
      ! simulation.
      exit
    end if
  end do ! End of i-particle's random walk.

  ! We need to add the passage time of the i-particle to
  ! the total time.
  ttau = ttau + tau

  ! You can print out the MFPT up to this point.
  print *, &
          '[' // nstr(i) // ' particles simulated | ' &
          // nstr(NRW-i) // ' to go]: ' &
          // TNL // TAB &
          // '<tau-sim> = ' // nstr(ttau / i) &
```

Listing continued on next page

Listing continued from last page

```
            // TNL // TAB &
            // '<tau-theo> = ' // nstr(THEOV) &
            // TNL // TAB &
            // 'Error = ' &
            // nstr( abs( (ttau/i) - THEOV ) / THEOV &
                    * 100, 1) &
            // '%'
end do ! End of the particle's loop.

! At this point, every particle's simulation is done.
! Obtain the <tau>
mfpt = ttau / NRW

! Now we print out the MFPT, and show the theoretical
    value.
print *
print *, '=== Final result of simulation ==='
print *, TAB // '<tau-sim> = ' // nstr(mfpt)
print *, TAB // '<tau-theo> = ' // nstr(THEOV)
! Calculates and prints the percentage error.
print *, TAB // 'Error = ' &
            // nstr( abs( mfpt - THEOV ) &
                    / THEOV * 100, 1) &
            // '%'
! As a reminder, print out the number of walkers.
print *, TAB // 'NRW = ' // nstr(NRW)
! The time step.
print *, TAB // 'dt = ' // nstr(DT, 6)
! And the PRNG seed.
print *, TAB // 'PRNG seed = ' // nstr(RSEED)

end program absabs
```

Listing ended

Compiling and Running of Listing 10.3

```
    # Compile
    gfortran helpers.f90 abs-abs.f90
```

Listing continued on next page

Listing continued from last page

```
# Run
./a.out

# Sample output
⋮
[14 particles simulated | 2486 to go]:
    <tau-sim> = 0.084245
    <tau-theo> = 0.111111
    Error = 24.2%
⋮
[2500 particles simulated | 0 to go]:
    <tau-sim> = 0.111107
    <tau-theo> = 0.111111
    Error = 0.0%

=== Final result of simulation ===
    <tau-sim> = 0.111107
    <tau-theo> = 0.111111
    Error = 0.0%
    NRW = 2500
    dt = 0.000001
```

End of Compile and Run

10.4.2 Absorbing-Absorbing: Initial Position Uniformly Distributed

The analytical result for an absoring-absorbing one-dimensional channel, when the particles start by being uniformly distributed along the entire channel, is given by

$$\langle t_u \rangle = \frac{L^2}{12D}, \tag{5.76}$$

which was obtained in Sect. 5.5.2. We set up our system such that the absorbing boundaries are at $x = 0$ and $L = 1$, respectively.

The source code contained in Listing 10.4 sets the number of random walkers to $NRW = 2500$, and their first-passage time is measured and printed out after

each particle is absorbed. The percentage error and the theoretical value are also presented. After every particle completes its trajectory, the mean first-passage time is provided.

Listing 10.4 [abs-abs-unif.f90]: Fortran 90 program to simulate a one-dimensional channel of length $L = 1$ with absorbing points at positions $x = 0$ and $X = L$. The particles start their travel with uniform distribution along the entire channel length.

```
! ****************************************************** !
! *************** abs-abs-unif.f90 ******************** !
! ****************************************************** !
!
!    Leonardo Dagdug, Ivan Pompa-García, Jason Peña
!
! From the book:
! ****************************************************** !
!      Diffusion Under Confinement:
!               A Journey Through Counterintuition
! ****************************************************** !

! ****************************************************** !
! This file contains the source code for the simulation
! of a 1D channel of length L.
! It has two absorbent points at x=0, and x=L.
!
! The Brownian walkers start their path with uniform
! distribution along the entire channel lenght.
! x0=U(0,L), and the simulation for each of Brownian
! walker ends when an absorbent point is reached. Then,
! the Mean First Passage Time (MFPT or <tau>) is
! obtained.
!
! The theoretical value is used to calculate the
! relative error of the simulation. D0 is the bulk
! diffusion constant usually set to 1.
!
! <tau> = L**2 / (12.0 * D0)
! ****************************************************** !

! ****************************************************** !
! To compile with GFortran, you must include the
```

Listing continued on next page

Listing continued from last page

```
! helpers.f90 module.
!         gfortran helpers.f90 abs-abs-unif.f90
! Then you can run the program:
!         ./a.out
! ************************************************** !

program absabsunif

! Load the helpers module, which contains functions,
! constants, and more...
use helpers

! Mandatory declaration of data type variables
! and constants.
implicit none

! ************************************************** !
!               Declaration of constants
! ************************************************** !

!!! Simulation parameters
! Seed of the PRNG
integer, parameter :: RSEED = 0
! Number of random walkers (particles)
integer, parameter :: NRW = 2500
! Channel length
real(kind=dp), parameter :: L = 1.0_dp
! Temporal step size
real(kind=dp), parameter :: DT = 1.0e-6_dp

!!! Physical parameters of the system
! Diffusion constant (bulk)
real(kind=dp), parameter :: D0 = 1.0_dp
! Thermal energy inverse (1/k_b T)
real(kind=dp), parameter :: BETA = 1.0_dp
! Standard deviation for Brownian motion
real(kind=dp), parameter :: SIGMA &
                              = dsqrt(2.0_dp * D0 * DT)
! Mean distribution for Brownian motion
real(kind=dp), parameter :: MU = 0.0_dp
```

Listing continued on next page

Listing continued from last page

```
74
75  ! Theoretical value
76  real(kind=dp), parameter :: THEOV &
77                                  = L**2 / (12.0_dp * D0)
78
79
80  ! ************************************************** !
81  !              Declaration of variables
82  ! ************************************************** !
83
84  ! General counter
85  integer :: i
86  ! Current position of the particle
87  real(kind=dp) :: x
88  ! Current particle passage time
89  real(kind=dp) :: tau
90  ! Sum of passage times
91  real(kind=dp) :: ttau = 0.0_dp
92  ! MFPT (<tau>)
93  real(kind=dp) :: mfpt
94
95
96  ! ************************************************** !
97  !           Main simulation program
98  ! ************************************************** !
99
100 ! Set the seed of the PRNG to achieve repeatable results
101 call setseed(RSEED)
102
103 ! The loop iterates over each (i) particle.
104 do i=1, NRW
105   !!! Initializing the needed variables
106   ! The passage time is set to zero
107   tau = 0.0_dp
108   ! The particle's current position is set to a
109   ! randomized initial value uniformly distributed
110   ! along the entire channel.
111   x = urand(0.0_dp, L)
112
113   !!! The random walk starts. Follow the particle until
```

Listing continued on next page

Listing continued from last page

```
   !!! it is removed by an absorbent point (x=0,x=L).
   do
     ! Make a step in space
     x = x + nrand(MU, SIGMA)
     ! Make a step in time
     tau = tau + DT

     ! Check for the removal of the particle
     if(x <= 0.0 .or. x >= L) then
       ! If it was removed from the channel, stop
       ! its simulation.
       exit
     end if
   end do ! End of i-particle's random walk.

   ! We need to add the passage time of the i-particle to
   ! the total time.
   ttau = ttau + tau

   ! You can print out the MFPT up to this point.
   print *, &
            '[' // nstr(i) // ' particles simulated | ' &
            // nstr(NRW-i) // ' to go]: ' &
            // TNL // TAB &
            // '<tau-sim> = ' // nstr(ttau / i) &
            // TNL // TAB &
            // '<tau-theo> = ' // nstr(THEOV) &
            // TNL // TAB &
            // 'Error = ' &
            // nstr( abs( (ttau/i) - THEOV ) / THEOV &
                     * 100, 1) &
            // '%'
end do ! End of the particle's loop.

! At this point, every particle's simulation is done.
! Obtain the <tau>
mfpt = ttau / NRW

! Now we print out the MFPT, and show the theoretical
    value.
```

Listing continued on next page

Listing continued from last page

```
153 print *
154 print *, '=== Final result of simulation ==='
155 print *, TAB // '<tau-sim> = ' // nstr(mfpt)
156 print *, TAB // '<tau-theo> = ' // nstr(THEOV)
157 ! Calculates and prints the percentage error.
158 print *, TAB // 'Error = ' &
159           // nstr( abs( mfpt - THEOV ) &
160                   / THEOV * 100, 1) &
161           // '%'
162 ! As a reminder, print out the number of walkers.
163 print *, TAB // 'NRW = ' // nstr(NRW)
164 ! The time step.
165 print *, TAB // 'dt = ' // nstr(DT, 6)
166 ! And the PRNG seed.
167 print *, TAB // 'PRNG seed = ' // nstr(RSEED)
168
169 end program absabsunif
```

Listing ended

Compiling and Running of Listing 10.4

```
1  # Compile
2  gfortran helpers.f90 abs-abs-unif.f90
3
4  # Run
5  ./a.out
6
7  # Sample output
8  ⋮
9  [71 particles simulated | 2429 to go]:
10     <tau-sim> = 0.078130
11     <tau-theo> = 0.083333
12     Error = 6.2%
13 ⋮
14 [2500 particles simulated | 0 to go]:
15     <tau-sim> = 0.085229
16     <tau-theo> = 0.083333
```

Listing continued on next page

Listing continued from last page

```
        Error = 2.3%

    === Final result of simulation ===
        <tau-sim> = 0.085229
        <tau-theo> = 0.083333
        Error = 2.3%
        NRW = 2500
        dt = 0.000001
```

End of Compile and Run

10.5 Concluding Remarks

In this chapter, we established the basic notions of computational physics and the importance of pseudorandom number (PRN) generation, along with some of their properties and transformations. Additionally, the first computational experiments with PRNs were shown. Subsequently, the equipartition theorem was deduced from the basic concepts of statistical mechanics. This led to the analysis of the Langevin equation, starting from its heuristic derivation to the examination of its properties, such as the mean-squared displacement. Furthermore, the assumption of an overdamped regime and the discretization of the Langevin equation, Eq. (10.94), are the fundamental expressions that allow us to simulate the diffusing Brownian particles using a computer system.

Finally, two computational experiments were presented to solve a couple of problems tackled analytically in Chap. 5. These were two one-dimensional systems with absorbing boundaries at their start and end points, one with all the particles starting at a fixed position and another in which the particles' starting position was uniformly distributed along the entire channel.

For the reader's convenience, a list of the most relevant expressions used in this Chapter is provided below:

$$\langle E \rangle = n\,\frac{1}{2}k_B T. \qquad \text{(Energy According to the Equipartition Theorem)}$$

$$m\frac{\mathrm{d}^2 x(t)}{\mathrm{d}t^2} = -\zeta\, v(t) + \xi(t) + F_{ext}(t).$$

(Langevin Equation with External Forces)

$$\langle \xi(t')\,\xi(t'')\rangle = 2k_B T\,\zeta\,\delta(t'-t'').$$

(Autocorrelation Function of the Stochastic Force)

$$D = \frac{\sigma_x^2}{2t} = \frac{\left\langle [x(t) - \langle x(t)\rangle]^2 \right\rangle}{2t}. \qquad \text{(Diffusion Coefficient for a Brownian Particle)}$$

$$x_{n+1} = x_n + \sqrt{2D\Delta t}\,\eta(t) + \beta\,D\,\Delta t\,F_{ext}(t). \qquad \text{(Discretized Position Equation of Brownian Dynamics)}$$

10.A `helpers.f90` Companion File

This Appendix includes the source code for the file used in the programs included in this book. It contains constants, functions, and subroutines written to be helpers in order to simplify some common tasks in the computer codification of diffusion-like problems. Many comments have been inserted in an attempt to provide a clear and instructive explanation of the intention of the intention of each line, but readers are also invited to customize them according to their own specific needs.

Listing 10.5 [`helpers.f90`]: Fortran 90 library `helpers.f90`.

```
! ****************************************************** !
! ****************** helpers.f90 ********************** !
! ****************************************************** !
!
!    Leonardo Dagdug, Ivan Pompa-García, Jason Peña
!
! From the book:
! ****************************************************** !
!      Diffusion Under Confinement:
!               A Journey Through Counterintuition
! ****************************************************** !

! ****************************************************** !
! This file is used to define a general module
! that stores definitions, constants, functions,
! and procedures that may be helpful in the study
! of diffusion.
```

Listing continued on next page

Listing continued from last page

```
18 ! ************************************************** !
19
20 module helpers
21
22 ! From the intrinsics of Fortran, we import certain
23 ! constants to make our data types portable between
24 ! systems.
25 ! The «iso_fortran_env» intrinsic is available for
26 ! Fortran >= 2003, but the needed data type constants
27 ! were introduced in Fortran >= 2008
28 !
29 !   sp -> Single Precision
30 !   dp -> Double Precision
31 !   qp -> Quadruple Precision
32 !
33 ! There are many more functions, procedures, and
34 ! definitions inside «iso_fortran_env». Using the
35 ! «only» keyword, we only import the ones we need.
36 use, intrinsic :: iso_fortran_env, &
37       only: sp => real32, dp => real64, qp => real128, &
38           i8 => int8, i16 => int16, i32 => int32, &
39           i64 => int64
40
41 ! Mandatory declaration of data type variables
42 ! and constants.
43 implicit none
44
45 ! Define a generic name for the number to string
46 ! converting functions. This is how we avoid having to
47 ! select the specific function; the compiler will do it
48 ! for us.
49 interface nstr
50   module procedure i8str, i16str, i32str, i64str, &
51                    spstr, dpstr, qpstr
52 end interface
53
54 ! ************************************************** !
55 !               Declaration of constants
56 ! ************************************************** !
57
```

Listing continued on next page

Listing continued from last page

```
! pi/4
real(kind=dp), parameter :: PI4 = atan(1.0_dp)
! pi/2
real(kind=dp), parameter :: PI2 = 2.0_dp * PI4
! pi
real(kind=dp), parameter :: PI = 4.0_dp * PI4

! Tabulator
character, parameter :: TAB = char(9)
! New line
character, parameter :: TNL = new_line('l')

! Default decimal digits when converting to char
integer, parameter :: DDECN = 6


! ************************************************** !
!               Functions and Subroutines
! ************************************************** !
contains

! To make «repeatable» simulations, we need to set a
! seed before generating our PRNs. Fortran requires
! an array of length «n», which length depends
! directly on the system and the compiler. But setting
! the seed helps us to make sure that we can obtain
! repeatable results, at least in a machine with the
! same version of the compiler.
! This function sets a seed in a very basic manner
! by fixing all the numbers in the seed array to
! the same integer.
subroutine setseed(nseed)
  implicit none

  ! Input parameter
  integer, intent(in) :: nseed
  ! Variable to hold the size of the needed array
  integer :: n
  ! Array to set the seed
  integer, allocatable :: seed(:)
```

Listing continued on next page

Listing continued from last page

```
98
99    ! Read the size of the needed array
100   call random_seed(size=n)
101
102   ! Allocate the array
103   allocate( seed(n) )
104   ! Set all the elements in the array to «nseed»
105   seed = nseed
106
107   ! Set the seed
108   call random_seed(put=seed)
109 end subroutine setseed
110
111 ! Fortran contains random_number procedure to
112 ! generate uniformly distributed pseudorandom numbers
113 ! within the interval 0 <= x < 1. Occasionally it is
114 ! also advisable to use it as a function instead.
115 ! Also, returning 1.0_dp - x gives us the possibility
116 ! to obtain 1.0 as a value, and the uniform distribution
117 ! will hold. This is the interval 0 < x <= 1.
118 function usrand() result(fn_res)
119   implicit none
120
121   ! Output value
122   real(kind=dp) :: fn_res
123
124   ! This gives us: 0 <= x < 1
125   call random_number(fn_res)
126
127   ! Now, the interval is: 0 < x <= 1
128   fn_res = 1.0_dp - fn_res
129 end function usrand
130
131 ! Sometimes we will need to get a pseudorandom number
132 ! within an interval (a,b] other than (0,1]. So, we made
133 ! a simple transformation.
134 ! We are asumming that a < b.
135 function urand(a, b) result(fn_res)
136   implicit none
137
```

Listing continued on next page

Listing continued from last page

```
138   ! Input parameters
139   real(kind=dp), intent(in) :: a, b
140   ! Output value
141   real(kind=dp) :: fn_res
142
143   fn_res = a + usrand() * (b - a)
144 end function urand
145
146 ! For the specific case of Brownian motion, the steps
147 ! are normally distributed with parameters
148 !   mu = 0 (mean)
149 !   sigma = \sqrt{2 D dt} (standard deviation)
150 ! By default we want to generate normally distributed
151 ! pseudorandom numbers with
152 !   mu = 0 (mean)
153 !   sigma = 1 (standard deviation)
154 !
155 ! The transformation from U~(0,1) to N(0,1) is made via
156 ! the Box-Müller transformation.
157 !
158 ! Original Box & Müller paper:
159 !       https://doi.org/10.1214%2Faoms%2F1177706645
160 !
161 function nrand(imu, isigma) result (fn_res)
162   implicit none
163
164   ! Input parameters
165   real(kind=dp), intent(in), optional :: imu, isigma
166   ! Output value
167   real(kind=dp) :: fn_res
168   ! Parameters for calculation
169   real(kind=dp) :: mu, sigma
170   ! Variables to hold normally distributed PRNs
171   real(kind=dp) :: u1, u2
172
173   ! Variable to save the non-used PRN
174   real(kind=dp), save :: saved_val
175   ! Flag to mark if we have a previously
176   ! calculated value
177   logical, save :: saved = .false.
```

Listing continued on next page

Listing continued from last page

```
178
179     ! If there is a previously generated value ready
180     ! to be used...
181     if(saved) then
182       ! Set the return variable to the saved value
183       fn_res = saved_val
184       ! We must rememeber that the value was used. Then
185       ! in the next function call, all calculations
186       ! must be performed again.
187       saved  = .false.
188
189       ! Exit from this function, no calculation needed.
190       return
191     end if
192
193     ! Check for parameter values. If some of them
194     ! are missing, then the default values will be used.
195     if( present(imu) ) then
196       mu = imu
197     else
198       mu = 0.0_dp
199     end if
200
201     if( present(isigma) ) then
202       sigma = isigma
203     else
204       sigma = 1.0_dp
205     end if
206
207     ! Generates two numbers uniformly distributed within
208     ! the interval (0,1), required by the
209     ! Box-Müller transformation.
210     u1 = usrand()
211     u2 = usrand()
212
213     ! The Box-Müller transformation.
214     ! Both numbers, u1 and u2 are used. If we change the
215     ! cosine <-> sine, we can generate another normally
216     ! distributed number independent from the first one.
217     ! The election of one of the trigonometric functions
```

Listing continued on next page

Listing continued from last page

```
    ! to return one PRN is completely arbitrary.
    ! The second generated value is held and used
    ! in the next function call to avoid a new
    ! calculation.

    ! One of the generated numbers is saved to be used
    ! in the next function call without calculations.
    saved_val = sigma * sqrt( -2.0_dp * log(u1) ) &
                            * sin( 2.0_dp * PI * u2 ) + mu
    ! Flag to inform that one value is saved.
    saved = .true.

    ! The number to be returned in this function call.
    fn_res = sigma * sqrt( -2.0_dp * log(u1) ) &
                            * cos( 2.0_dp * PI * u2 ) + mu
  end function nrand

  ! This family of functions i*str(num) makes it possible
  ! to print out an integer concatenated with a string,
  ! avoiding the odd space characters introduced by
  ! Fortran.
  function i8str(num) result(fn_res)
      implicit none

      ! Input integer value
      integer(kind=i8), intent(in) :: num
      ! Temporary string of 'sufficient' length
      character(len=256) :: stmp
      ! Dynamic length variable to hold the final string
      character(len=:), allocatable :: fn_res

      ! Copy the integer into the temporary character
      ! variable.
      ! This copies the «num» integer value into the
      ! «stmp» character variable using the I0 format,
      ! which means that there will be no leading or
      ! padding zeros. This is their most compact form.
      write(stmp, '(I0)') num
      ! Move the string to the left
      stmp = adjustl(stmp)
```

Listing continued on next page

Listing continued from last page

```
258
259       ! Cut the moved string from the start to the
260       ! spaces at the right of it.
261       fn_res = stmp( 1:len_trim(stmp) )
262   end function i8str
263
264   function i16str(num) result(fn_res)
265     implicit none
266
267     ! Input integer value
268     integer(kind=i16), intent(in) :: num
269     ! Temporary string of 'sufficient' length
270     character(len=256) :: stmp
271     ! Dynamic length variable to hold the final string
272     character(len=:), allocatable :: fn_res
273
274     ! Copy the integer into the temporary character
275     ! variable
276     write(stmp, '(I0)') num
277     ! Move the string to the left
278     stmp = adjustl(stmp)
279
280     ! Cut the moved string from the start to the
281     ! spaces at the right of it.
282     fn_res = stmp( 1:len_trim(stmp) )
283   end function i16str
284
285   function i32str(num) result(fn_res)
286     implicit none
287
288     ! Input integer value
289     integer(kind=i32), intent(in) :: num
290     ! Temporary string of 'sufficient' length
291     character(len=256) :: stmp
292     ! Dynamic length variable to hold the final string
293     character(len=:), allocatable :: fn_res
294
295     ! Copy the integer into the temporary character
296     ! variable
297     write(stmp, '(I0)') num
```

Listing continued on next page

Listing continued from last page

```
  ! Move the string to the left
  stmp = adjustl(stmp)

  ! Cut the moved string from the start to the
  ! spaces at the right of it.
  fn_res = stmp( 1:len_trim(stmp) )
end function i32str

function i64str(num) result(fn_res)
  implicit none

  ! Input integer value
  integer(kind=i64), intent(in) :: num
  ! Temporary string of 'sufficient' length
  character(len=256) :: stmp
  ! Dynamic length variable to hold the final string
  character(len=:), allocatable :: fn_res

  ! Copy the integer into the temporary character
  ! variable
  write(stmp, '(I0)') num
  ! Move the string to the left
  stmp = adjustl(stmp)

  ! Cut the moved string from the start to the
  ! spaces at the right of it.
  fn_res = stmp( 1:len_trim(stmp) )
end function i64str

! This family of functions *pstr(num) makes it possible
! to print out a real number concatenated with a string,
! avoiding the odd space characters introduced by
! Fortran.
function spstr(num, idigits) result(fn_res)
  implicit none

  ! Input real single-precision value
  real(kind=sp), intent(in) :: num
  ! Digits after decimal point to be printed
  integer, intent(in), optional :: idigits
```

Listing continued on next page

Listing continued from last page

```
338    ! The actual value used
339    integer :: digits
340    ! Temporary string of 'sufficient' length
341    character(len=256) :: stmp
342    ! Dynamic length variable to hold the final string
343    character(len=:), allocatable :: fn_res
344
345    ! Check for parameter values. If some of them
346    ! are missing, then the default values will be used.
347    if( present(idigits) ) then
348      digits = idigits
349    else
350      digits = DDECN
351    end if
352
353    ! Copy the real_sp into the temporary character
354    ! variable
355    write(stmp, '(F100.' // nstr(digits) // ')') num
356    ! Move the string to the left
357    stmp = adjustl(stmp)
358
359    ! Cut the moved string from the start to the
360    ! spaces to the right of it.
361    fn_res = stmp( 1:len_trim(stmp) )
362  end function spstr
363
364  function dpstr(num, idigits) result(fn_res)
365    implicit none
366
367    ! Input real double-precision value
368    real(kind=dp), intent(in) :: num
369    ! Digits after decimal point to be printed
370    integer, intent(in), optional :: idigits
371    ! The actual used value
372    integer :: digits
373    ! Temporary string of 'sufficient' length
374    character(len=256) :: stmp
375    ! Dynamic length variable to hold the final string
376    character(len=:), allocatable :: fn_res
377
```

Listing continued on next page

Listing continued from last page

```
   ! Check for parameter values. If some of them
   ! are missing, then the default values will be used.
   if( present(idigits) ) then
     digits = idigits
   else
     digits = DDECN
   end if

   ! Copy the real_sp into the temporary character
   ! variable
   write(stmp, '(F100.' // nstr(digits) // ')') num
   ! Move the string to the left
   stmp = adjustl(stmp)

   ! Cut the moved string from the start to the
   ! spaces at the right of it.
   fn_res = stmp( 1:len_trim(stmp) )
end function dpstr

function qpstr(num, idigits) result(fn_res)
   implicit none

   ! Input real quadruple-precision value
   real(kind=qp), intent(in) :: num
   ! Digits after decimal point to be printed
   integer, intent(in), optional :: idigits
   ! The actual value used
   integer :: digits
   ! Temporary string of 'sufficient' length
   character(len=256) :: stmp
   ! Dynamic length variable to hold the final string
   character(len=:), allocatable :: fn_res

   ! Check for parameter values. If some of them
   ! are missing, then the default values will be used.
   if( present(idigits) ) then
     digits = idigits
   else
     digits = DDECN
   end if
```

Listing continued on next page

Listing continued from last page

```
418
419     ! Copy the real_sp into the temporary character
420     ! variable
421     write(stmp, '(F100.' // nstr(digits) // ')') num
422     ! Move the string to the left
423     stmp = adjustl(stmp)
424
425     ! Cut the moved string from the start to the
426     ! spaces at the right of it.
427     fn_res = stmp( 1:len_trim(stmp) )
428   end function qpstr
429
430   end module helpers
```

Listing ended

Compiling and Running of Listing 10.5

```
1       # As an auxiliar library, helpers.f90
2       # cannot be run directly. It is only a companion
3       # for the other codes.
```

Further Reading and References

N. Pottier, *Nonequilibrium Statistical Physics: Linear Irreversible Processes* (Oxford University, Oxford, 2009)

H. Risken, *The Fokker-Planck Equation: Methods of Solution and Applications* (Springer, Berlin, 1996). https://doi.org/10.1007/978-3-642-61544-3

S.M. Ross, *Simulation* (Academic Press, New York, 2023). https://doi.org/10.1016/C2020-0-00043-5

N.G. Van Kampen, *Stochastic Processes in Physics and Chemistry* (North-Holland, Amsterdam, 2007)

Chapter 11
Numerical Solutions of the Diffusion Equation

The diffusion equation can be solved analytically for a limited number of systems and conditions; for all other cases, a numerical approximation is required. The procedure to be studied in this chapter consists of replacing the partial derivatives in a partial differential equation (PDE) by finite-difference expressions. Additionally, the boundary conditions (BCs), initial conditions, and available spatial domain must be properly defined in order to obtain a satisfactory approximation of the solution. These numerical techniques are referred to as *finite-difference methods* (FDMs). This method is applied when solving linear, nonlinear, time-independent, and time-dependent problems. Some applications of FDMs include structural analysis of buildings and bridges, heat transfer analysis, predicting deformation and stress fields within solid bodies subjected to external forces, fluid flow analysis in pipes, and electromagnetic potential analysis, among others.

The finite-difference methods for solving the diffusion equation with constant coefficients are useful in the study of various physical phenomena, ranging from hydraulic and transportation applications to heat diffusion in solid bodies. In this chapter, we will present an introductory overview for solving the diffusion equation in one dimension. It is well beyond the scope of this book to attempt to provide even a general introduction to this subject matter. The reader who is interested in learning more about these methods is referred to the references provided at the end of the chapter.

11.1 Differences Construction

As previously mentioned, an FDM is based on the approximation of the partial derivatives in a PDE to be solved. In order to establish meaningful correlations between partial derivatives and finite-difference expressions, we start by considering a continuous and infinitely derivable function $f(x)$, which is expanded in a Taylor

L. Dagdug et al., *Diffusion Under Confinement*,
https://doi.org/10.1007/978-3-031-46475-1_11

series around $x = x_0$, namely,

$$f(x) = f(x_0) + f'(x_0)(x - x_0) + \frac{1}{2} f''(x_0)(x - x_0)^2 + \mathcal{O}(x^3). \tag{11.1}$$

By defining $\Delta x \equiv x - x_0 > 0$, then $x = x_0 + \Delta x$, and Eq. (11.1) results in

$$f(x_0 + \Delta x) = f(x_0) + f'(x_0)(x_0 + \Delta x - x_0) + \frac{1}{2} f''(x_0)(x_0 + \Delta x - x_0)^2 + \mathcal{O}\left([x_0 + \Delta x]^3\right). \tag{11.2}$$

This last equation simplifies to

$$f(x_0 + \Delta x) = f(x_0) + f'(x_0)\,\Delta x + \frac{1}{2} f''(x_0)\,\Delta x^2 + \mathcal{O}\left(\Delta x^3\right). \tag{11.3}$$

Now, by truncating the series up to the first order on Δx, we arrive at

$$f'(x_0) \approx \frac{f(x_0 + \Delta x) - f(x_0)}{\Delta x}, \tag{11.4}$$

which is known as *forward difference* because the $+\Delta x$ step is taken away from x_0. Notice that the approximation in Eq. (11.4) is very similar to the derivative definition.

Furthermore, another two basic differences can be calculated. The *backward difference* is obtained by taking $x - \Delta x$ as the argument of function f, i.e.,

$$f(x_0 - \Delta x) = f(x_0) - f'(x_0)\,\Delta x + \frac{1}{2} f''(x_0)\,\Delta x^2 + \mathcal{O}\left(\Delta x^3\right). \tag{11.5}$$

In this equation, the signs of each term are provided by the power and the sign of the increment itself. Subsequently, after truncating and rearranging, we obtain

$$f'(x_0) \approx \frac{f(x_0) - f(x_0 - \Delta x)}{\Delta x}. \tag{11.6}$$

Now, let us calculate the difference between Eqs. (11.5) and (11.3), which results in

$$f(x_0 + \Delta x) - f(x_0 - \Delta x) = 2 f'(x_0)\,\Delta x + \mathcal{O}\left(\Delta x^3\right). \tag{11.7}$$

After truncating and rearranging terms, it follows that

$$f'(x_0) \approx \frac{f(x_0 + \Delta x) - f(x_0 - \Delta x)}{2\Delta x}, \tag{11.8}$$

known as a *centered difference* or *central difference*. Moreover, we may also take the sum of Eqs. (11.5) and (11.3), namely,

$$f(x_0 + \Delta x) + f(x_0 - \Delta x) = 2f(x_0) + f''(x_0)\,\Delta x^2 + \mathcal{O}\left(\Delta x^3\right). \tag{11.9}$$

When solving for $f''(x_0)$, we find that

$$f''(x_0) \approx \frac{f(x_0 + \Delta x) - 2f(x_0) + f(x_0 - \Delta x)}{\Delta x^2}, \tag{11.10}$$

which is the central difference, but for the second derivative of $f(x)$.

Up to this point, we have examined three distinct finite-difference schemes, and now, we need to designate one of them for the discretization of the equation. The chosen selection will determine the fixed solution scheme along with its associated properties, such as stability and convergence, which will be addressed in subsequent sections of this chapter.

11.1.1 Discretization and Mesh

In the previous section, we showed how to write finite differences that enable the discretization of the PDEs by replacing the partial derivatives with either Eq. (11.6), (11.8), and (11.10). Now, some associations between continuous and discrete variables must be made. If we have two variables, x and t, and their interval domain is given by

$$x \in [x_i, x_f], \qquad t \in [t_i, t_f], \tag{11.11}$$

then the discrete associations are set to

$$x \to j, \qquad t \to n, \qquad \pm\Delta x \to \pm 1, \qquad \pm\Delta t \to \pm 1. \tag{11.12}$$

For the sake of clarity, the temporal variables are written as superscripts, and the spatial variables are expressed as subscripts. Some examples of discretization notation are

$$\begin{aligned} c(x,t) &\to c_j^n, & c(x + \Delta x, t) &\to c_{j+1}^n, \\ c(x, t - \Delta t) &\to c_j^{n-1}, & c(x - \Delta x, t + \Delta t) &\to c_{j-1}^{n+1}. \end{aligned} \tag{11.13}$$

As the continuous variables are now linked to discrete quantities, it is necessary to map the space in which these variables reside onto a discrete structure. The new discrete space is called a *mesh*, or sometimes a *grid*, and it is obtained by splitting the intervals from where the variables take their values. For a one-dimensional

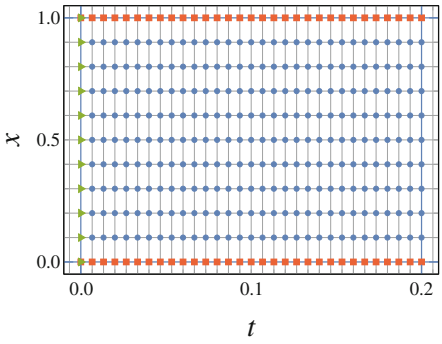

Fig. 11.1 Schematic representation of a mesh for variables x and t, representing the boundary conditions (orange dots), the initial conditions (green dots), and the points at which the mesh is divided (blue dots). The parameters are $N_x = 10$, $N_t = 30$, $t \in [0, 0.2]$, and $x \in [0, 1.0]$

equation with a spatial-temporal dependence, i.e., (x, t), we can visualize the grid after defining N_x and N_t, which are the number of parts into which the intervals of x and t will be split, respectively. A schematic representation of a mesh is shown in Fig. 11.1.
The parameters N_x and N_y are fundamental to defining the increments appearing in the difference equations, since

$$\Delta x = \frac{x_f - x_i}{N_x} \quad \text{and} \quad \Delta t = \frac{t_f - t_i}{N_t}, \tag{11.14}$$

where subscripts in the independent variables x and t denote the start and end values of the variables' domains, as defined through Eq. (11.11).

11.2 Forward Time-Centered Space Method

The initial approach that we will employ to solve the diffusion equation is Euler's *forward time-centered space (FTCS) method*. Firstly, we invoke the one-dimensional diffusion equation in terms of concentration, namely,

$$\frac{\partial c(x,t)}{\partial t} = D \frac{\partial^2 c(x,t)}{\partial^2 x}. \tag{2.13}$$

Following the method's name, we associate the left-hand side of the latter equation with a forward in time difference, Eq. (11.4), leading to

$$\frac{\partial c(x,t)}{\partial t} \iff \frac{c_j^{n+1} - c_j^n}{\Delta t}. \tag{11.15}$$

Then, the right-hand side of Eq. (2.13) will be related to a central difference for the second derivative, Eq. (11.10), which indicates

$$\frac{\partial^2 c(x,t)}{\partial x^2} \iff \frac{c_{j+1}^n - 2c_j^n + c_{j-1}^n}{\Delta x^2}. \tag{11.16}$$

Furthermore, the discretization of Eq. (2.13) as an FTCS is

$$\frac{c_j^{n+1} - c_j^n}{\Delta t} = D\frac{c_{j+1}^n - 2c_j^n + c_{j-1}^n}{\Delta x^2}, \tag{11.17}$$

which can be written as

$$c_j^{n+1} = c_j^n + D\frac{\Delta t}{\Delta x^2}\left(c_{j+1}^n - 2c_j^n + c_{j-1}^n\right). \tag{11.18}$$

This equation gives us the dynamic evolution of concentration c_j^n in time. The FTCS is an *explicit method*, meaning that it uses only current time values to evaluate the next iteration, in contrast with *implicit methods*, which also need to use later time values to obtain the solution. Those will be studied in the next section. This one-step iterative relation in time is particularly useful, since we do not need to store the values of c_j^n for all j in the computer.

11.2.1 Numerical Implementation

In this section, we will describe the main steps to implement the FTCS method to solve the one-dimensional diffusion equation, Eq. (2.13). To such end, we will consider a concentration gradient of diffusing particles with initial position $x_0 = 1/2$ in a system of length L with diffusion constant D, in the presence of perfectly reflecting walls at $x = 0$ and $x = L$. The analytical solution for such a system can be found in Sect. 5.2. The BCs to solve this equation are Neumann BCs, Eq. (5.7), which, for our specific problem, becomes

$$\left.\frac{\partial c(x,t|x_0)}{\partial x}\right|_{x=0,L} = 0 \tag{11.19}$$

and, after discretizing with a central difference, results in

$$\left.\frac{c_{j+1}^n - c_{j-1}^n}{2\Delta x}\right|_{j=0,N_x} = 0. \tag{11.20}$$

From this last equation, we have that

$$\left.c_{j+1}^n\right|_{j=0,N_x} = \left.c_{j-1}^n\right|_{j=0,N_x}. \tag{11.21}$$

As a result of the imposed boundary conditions, the particles are restricted from moving to the left of $j = 0$ or to the right of $j = N$. Nevertheless, Eq. (11.21) can be used in Eq. (11.18) to obtain modified equations that work within the boundaries and obey the desired conditions. In the first case, the equation for $j = 0$ is obtained by changing the term with $j - 1$ to j in Eq. (11.18), yielding

$$c_j^{n+1} = c_j^n + 2D\frac{\Delta t}{\Delta x^2}\left(c_{j+1}^n - c_j^n\right), \qquad \text{for } j = 0. \tag{11.22}$$

The same reasoning is used at $j = L$. Then, the point $j + 1$ must be replaced by j, resulting in

$$c_j^{n+1} = c_j^n + 2D\frac{\Delta t}{\Delta x^2}\left(c_{j-1}^n - c_j^n\right), \qquad \text{for } j = N_x. \tag{11.23}$$

Equations (11.22) and (11.23) dictate the behavior of the system at positions $j = 0$ and $j = N_x$, respectively, and they are the discrete equivalence of the BCs in Eq. (11.19).

Now, the initial conditions for the continuous case are given by

$$c(x, t = 0) = \delta(x - x_0). \tag{11.24}$$

On the one hand, the discretization of this initial condition then reads

$$\delta(x - x_0) \iff \frac{1}{\Delta x}\delta_{j,j'}, \tag{11.25}$$

where $\delta_{j,j'}$ is Kronecker's delta defined as in Eq. (C.5). If $\Delta x \to 0$, then the infinity value of Dirac's delta is correctly recovered. On the other hand, the initial position, Eq. (11.24), is discretized as follows:

$$c_j^{n=0} = \frac{1}{\Delta x}\delta_{j,j'}. \tag{11.26}$$

For example, if we set $x_0 = 1/2$, and our grid has $N_x = 10$ parts for $x \in [0, 1]$, then

$$x_0 = \frac{1}{2} \qquad \to \qquad j = \frac{x_0}{\Delta x} = x_0\frac{N_x}{x_f - x_i} = 5, \tag{11.27}$$

and the initial position in the discretized system is placed at $j = 5$ and $x_0 = 1/2 \to j' = 5$.

The initial conditions are usually placed within the boundary, which does not have any inconveniences. However, the fixed number of points in the mesh may ocassionally cause the initial condition position to not have a corresponding point on the grid. This can be solved by interpolating values between near points, but this approach can create additional errors in the method. As a solution, extra positions

can be added to the mesh to include the initial conditions, or we can pick different numbers of points to build the grid in order. Even though this type of issue is not present in our specific case, it should be noted that it is worth being mindful of this when tackling other specific problems.

At this point, we have all the relevant equations needed to numerically solve the diffusion equation by means of the FTCS FDM scheme. Let us summarize it as follows:

$$\text{FTCS} \rightarrow \begin{cases} c_j^{n+1} = c_j^n + D\frac{\Delta t}{\Delta x^2}\left(c_{j+1}^n - 2c_j^n + c_{j-1}^n\right) & \text{for } 0 < j < N_x, \\ c_j^{n+1} = c_j^n + 2D\frac{\Delta t}{\Delta x^2}\left(c_{j+1}^n - c_j^n\right) & \text{for } j = 0, \\ c_j^{n+1} = c_j^n + 2D\frac{\Delta t}{\Delta x^2}\left(c_{j-1}^n - c_j^n\right) & \text{for } j = N_x, \\ c_j^{n=0} = \frac{1}{\Delta x}\delta_{j,j'}. \end{cases} \tag{11.28}$$

Upon careful examination of the preceding equations, one can appreciate that an effective way to computationally incorporate the method alongside the parameters associated with the physical system is not readily apparent. Therefore, here is a step-by-step guide summarizing the process:

- Set the number of steps that can be taken within the mesh in any direction, that is, N_x, and N_t.
- Determine the increments as

$$\Delta x = \frac{x_f - x_i}{N_x} \quad \text{and} \quad \Delta t = \frac{t_f - t_i}{N_t}. \tag{11.29}$$

- Define the data structure to store $c(x)$ at a certaint timepoint. This usually can be done using an array or list, and the length is determined by $N_x + 1$.
- On working with the solution at $t = 0$, apply the initial conditions to the corresponding points in the mesh.
- Set the BCs on all grid positions, as needed.
- Start a loop for every timepoint. This loop will consist of N_t iterations.
  - Start a loop for every spatial position on the grid. There will be $N_x + 1$ iterations.
    - Calculate $c(x)$ at time t, by means of the corresponding equation depending on the point, which could be a general point in the mesh or a boundary point in it.
  - Finish the loop for the positions. The time is incremented. Repeat until every time step is done.
- All times are finished. The computation is done.

Algorithm 1 Forward time-centered space method pseudocode for the one-dimensional diffusion equation with two reflecting targets

procedure FTCS
  $N_x \leftarrow$ Number of slices of the spatial interval
  $N_t \leftarrow$ Number of slices of the temporal interval
  $\Delta x \leftarrow (x_f - x_i)/N_x$ ▷ Spatial increment
  $\Delta t \leftarrow (t_f - t_i)/N_t$ ▷ Temporal increment
  $c_j^0 \leftarrow 1/\Delta x$ ▷ Initial conditions are set
  for $1 \leq n \leq N_t$ **do**
    $c_0^n = c_0^{n-1} + 2r\left(c_1^{n-1} - c_0^{n-1}\right)$ ▷ BC on the left
    for $j \leq N_x$ **do**
      $c_j^n \leftarrow c_j^{n-1} + r\left(c_{j+1}^{n-1} - 2\,c_j^{n-1} + c_{j-1}^{n-1}\right)$
    end for ▷ Spatial loop finished
    $c_{N_x}^n = c_{N_x}^{n-1} + 2r\left(c_{N_x-1}^{n-1} - c_{N_x}^{n-1}\right)$ ▷ BC on the right
  end for ▷ Time loop ended
end procedure

The coding steps are shown as a *pseudocode* that can be translated into any programming language, although our implementation is in FORTRAN. The pseudocode is presented in Algorithm 1. To such end, we consider the one-dimensional diffusion equation within the intervals $x \in [0, 1]$ and $t \in [0, 0.2]$, with $N_x = 10$ and $N_t = 30$, with the initial position of concentration at 0.5.

The implementation to Fortran is shown in Listing 11.1 and the results are presented in Fig. 11.2. These results can be contrasted with the plots in Fig. 5.2 containing the graphical representation of the analytical solution for this system, which was solved in Sect. 5.2.

Listing 11.1 [`ftcs-ref-ref.f90`]: Fortran 90 implementation of the FTCS FDM method to solve the 1D diffusion equation with two completely reflecting boundaries

```
1  ! ******************************************************** !
2  ! ****************** ftcs-ref-ref.f90 ****************** !
3  ! ******************************************************** !
4  !
5  !    Leonardo Dagdug, Ivan Pompa-García, Jason Peña
6  !
7  ! From the book:
8  ! ******************************************************** !
9  !      Diffusion Under Confinement:
10 !               A Journey Through Counterintuition
11 ! ******************************************************** !
```

Listing continued on next page

Listing continued from last page

```
12
13  ! ************************************************** !
14  ! This file contains the source code to numerically
15  ! solve the 1D diffusion equation for a channel
16  ! of length L.
17  ! It has two reflecting points at x=0 and x=L.
18  !
19  ! The initial condition is such that
20  !                 p(x,t=0) = \delta(x-x0),
21  ! where x0 is the initial position (default = 1/2).
22  !
23  ! The solver uses the Forward Time-Centered Space
24  ! (FTCS) Finite Difference Method (FDM).
25  !
26  ! As the FTCS is stable only with:
27  !         D \Delta t / \Delta x^2 <= 1/2,
28  ! those parameters must be chosen carefully.
29  !
30  ! ************************************************** !
31
32  ! ************************************************** !
33  ! To compile with GFortran, you must include the
34  ! helpers.f90 module.
35  !         gfortran helpers.f90 ftcs_ref_ref.f90
36  ! Then you can run the program:
37  !         ./a.out
38  !
39  ! After running the program, a file is generated:
40  !   - «ftcs-aa.dat», a file with time, position,
41  !                    and concentration
42  ! It can be plotted with any software
43  ! of your choice. To do this using gnuplot, execute:
44  !  gnuplot -p -e '
45  !     set title "FTCS FDM for the Diffusion Equation";
46  !     set xlabel "x (position)" ;
47  !     set ylabel "c(x,t) (concentration)" ;
48  !times = system("awk '"'"'{print $1}'"'"' ftcs-aa.dat |
        sort -u");
49  !     plot for [t in times] "<awk '"'"'$1==".t."'"'"' ftcs
        -aa.dat"
```

Listing continued on next page

Listing continued from last page

```
!       u 2:3 with linespoints title "t=".sprintf("%.3f",
    t*1.0)'
!
! -p means that the plot must persist until the
!    user closes it explicitly.
! -e is used to specify the instructions
!    for using  gnuplot directly in the commandline.
! ************************************************** !

program ftcsrefref

! Load the helpers module which contains functions,
! constants, and more...
use helpers

! Mandatory declaration of data type variables
! and constants.
implicit none

! ************************************************** !
!               Declaration of constants
! ************************************************** !

!!! FDM parameters
! Number of pieces in the partition of «x»
integer, parameter :: NX = 10
! Number of pieces in the partition of «t»
integer, parameter :: NT = 30
! Total system evolution time
! (assuming that it starts at t=0)
real(kind=dp), parameter :: TF = 0.1_dp
! Start of channel
real(kind=dp), parameter :: XI = 0.0_dp
! End of channel
real(kind=dp), parameter :: XF = 1.0_dp
! Initial Condition continous position
real(kind=dp), parameter :: X0 = 0.5_dp
! Temporal step size
real(kind=dp), parameter :: DT = TF / NT
! Spatial step size
```

Listing continued on next page

Listing continued from last page

```
real(kind=dp), parameter :: DX = (XF - XI) / NX
! Diffusion constant (bulk)
real(kind=dp), parameter :: D0 = 1.0_dp
! «r» factor
real(kind=dp), parameter :: R = D0 * DT / DX**2
! Discrete initial condition position
! Substract 1 from the index because our array
! will be defined to start at 0.
integer, parameter :: J0 = int(X0 / DX + 1)


! ************************************************** !
!                 Declaration of variables
! ************************************************** !

! General counter
integer :: i
! Time counter
integer :: n
! Spatial counter
integer :: j
! Current continous position
real(kind=dp) :: x
! Current continous time
real(kind=dp) :: t
! Array to hold the current time concentrations «c»
real(kind=dp) :: c(NX+1) = 0.0_dp
! Array to hold the previous time concentrations «c»
real(kind=dp) :: c0(NX+1) = 0.0_dp

! A unit number for the file where
! time, position, and concentration data
! will be saved.
! Fortran >= 2003 will
! assign this automatically in the open call.
integer(kind=i32) :: FUNIT



! ************************************************** !
```

Listing continued on next page

Listing continued from last page

```
!              Main calculation program
! ************************************************** !

! Open a file to write the data
open(newunit=FUNIT, file='ftcs-aa.dat')

! Show a warning if R > 1/2
if(R > 0.5) then
  print *, 'r > 0.5. Under this condition the method ' &
           // 'is not stable! Try to choose ' &
           // ' different values of DX and DT.'
end if

! Set the discretized Initial Condition
c(J0) = 1.0_dp / DX

! Print the values for the time zero
do j=1, NX+1
  write(FUNIT,  *) 0.0_dp, (j-1) * DX, c(j)
end do

! The loop iterates over each time step until NT is
! reached.
! In other words, it walks along every point on the mesh
! for the respective amount of time.
! Keeping the notation of the book, the current time
! step is held in «n».
do n=1, NT
  ! Obtain the current continous time
  t = n * DT

  ! Save the previous time concentration before
  ! calculating the next one.
  c0 = c

  ! The first element of «c» is calculated separately
  ! because it is a boundary and uses another equation.
  c(1) = c0(1) + 2.0_dp * R * ( c0(2) - c0(1) )

  ! Write out the time, space position, and
```

Listing continued on next page

Listing continued from last page

```
169     ! concentration
170     write(FUNIT,  *) t, x, c(j)
171
172     ! Now we go through every point on the mesh for the
173     ! spatial axis, holding the time «n» constant.
174     ! The final point in j=Nx is a boundary and it is
175     ! excluded.
176     do j=2, NX
177       ! The continous position is calculated
178       x = (j-1) * DX
179
180       ! Obtain the «c»
181       c(j) = c0(j) &
182               + R * ( c0(j+1) - 2.0_dp * c0(j) + c0(j-1) )
183
184       ! Write out the time, space position, and «c»
185       write(FUNIT,  *) t, x, c(j)
186     end do ! End of the spatial loop for time «n»
187
188     x = (j-1) * DX
189
190     ! The last element (a boundary) is calculated outside
191     ! the loop for the inner points of the mesh, because
192     ! it obeys a different equation.
193     c(j) = c0(j) + 2.0_dp * R * ( c0(j-1) - c0(j) )
194
195     ! Write out the time, space position, and «c»
196     write(FUNIT,  *) t, x, c(j)
197   end do ! Ends the loop for all timepoints.
198
199   ! Close the file.
200   close(FUNIT)
201
202   !!! At this point, the calculation is done.
203   ! As a reminder, print out some numbers:
204   print *
205   print *, TAB // '=== FTCS FDM finished with params ==='
206   ! ! The number of slides for space
207   print *, TAB // 'Nx = ' // nstr(NX)
208   ! ! The spatial step
```

Listing continued on next page

Listing continued from last page

```
print *, TAB // 'dx = ' // nstr(DX, 3)
! ! The number of slides for time
print *, TAB // 'Nt = ' // nstr(NT)
! ! The time step, too
print *, TAB // 'dt = ' // nstr(DT, 3)
! ! r factor
print *, TAB // 'r = ' // nstr(R, 2)

end program ftcsrefref
```

Listing ended

Compiling and Running of Listing 11.1

```
    # Compile
    gfortran helpers.f90 ftcs-ref-ref.f90

    # Run
    ./a.out

    # Sample output

    # Plot
    gnuplot -p -e '
      set title "FTCS FDM for the Diffusion Equation";
      set xlabel "x (position)" ;
      set ylabel "c(x,t) (concentration)" ;

times = system("awk '"'"'{print $1}'"'"' ftcs-aa.dat |
    sort -u");

      plot for [t in times] "<awk '"'"'$1==".t."'"'"' ftcs
    -aa.dat"
         u 2:3 with linespoints title "t=".sprintf("%.3f",
    t*1.0)'
```

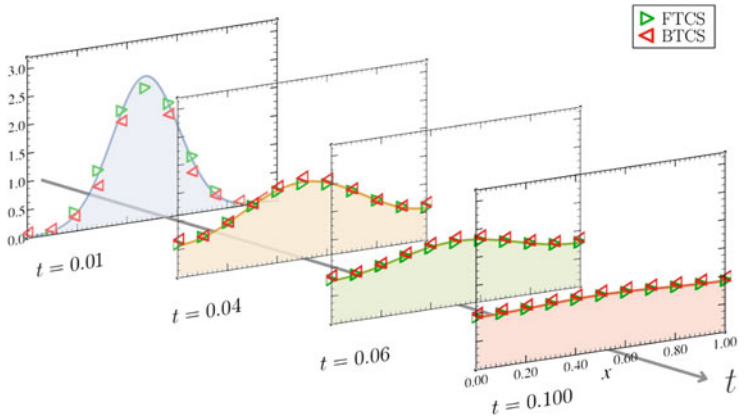

Fig. 11.2 Numerical solution using the FTCS and BTCS FDM schemes and analytical solution given by Eq. (5.21). The parameters are $N_x = 10$, $N_t = 30$, $t \in [0, 0.2]$, and $x \in [0, 1.0]$

11.3 Backward Time-Centered Space Method

An alternative scheme that can be employed for the numerical solution of our diffusion equation is the *backward time-centered space* (BTCS) *method*. The first association to make is between the left-hand side of the diffusion equation with a backward difference, Eq. (11.6), and an index change $n \rightarrow n + 1$, namely,

$$\frac{\partial c(x,t)}{\partial t} \iff \frac{c_j^{n+1} - c_j^n}{\Delta t}. \tag{11.30}$$

The second derivative of the diffusion equation, Eq. (2.13), has to be written as a central difference, Eq. (11.10), with the same index change as in the previous discretization, resulting in

$$\frac{\partial^2 c(x,t)}{\partial x^2} \iff \frac{c_{j+1}^{n+1} - 2c_j^{n+1} + c_{j-1}^{n+1}}{\Delta x^2}. \tag{11.31}$$

The BTCS discretization of Eq. (2.13) is

$$\frac{c_j^{n+1} - c_j^n}{\Delta t} = D\frac{c_{j+1}^{n+1} - 2c_j^{n+1} + c_{j-1}^{n+1}}{\Delta x^2}, \tag{11.32}$$

and it is customary to write it with c_j^n on the left-hand side, namely,

$$c_j^n = c_j^{n+1} - D\frac{\Delta t}{\Delta x^2}\left(c_{j+1}^{n+1} - 2c_j^{n+1} + c_{j-1}^{n+1}\right). \tag{11.33}$$

It is worth noting that further times values are needed to calculate the values for the current time, meaning that the BTCS is an *implicit method*, and linear algebra techniques are required to solve the resulting system of equations. This will become clearer in the next section.

11.3.1 Numerical Implementation

Our objective is to determine the values at the current time step n at position j, namely, c_j^n. To such end, we need to have the previous values at $n+1$. The known values are those of the BCs, whose central discretization in space is the same as for FTCS, given by Eq. (11.21). By shifting $n \to n+1$, we arrive at

$$c_{j+1}^{n+1}\Big|_{j=0,N_x} = c_{j-1}^{n+1}\Big|_{j=0,N_x}. \tag{11.34}$$

This last equation needs to be substituted into Eq. (11.33). For $j=0$, the values of $j-1$ must be replaced, and then

$$c_j^n = c_j^{n+1} - 2D\frac{\Delta t}{\Delta x^2}\left(c_{j+1}^{n+1} - c_j^{n+1}\right), \qquad \text{for } j=0. \tag{11.35}$$

For $j=N_x$, $j+1$ should be substituted, leading to

$$c_j^n = c_j^{n+1} - 2D\frac{\Delta t}{\Delta x^2}\left(c_{j-1}^{n+1} - c_j^{n+1}\right), \qquad \text{for } j=N_x. \tag{11.36}$$

If we have a mesh with N_x+1 points, then the system of equations to be solved is

$$\begin{cases} c_0^n = (1+2r)\,c_0^{n+1} - 2r\,c_1^{n+1}, \\ \vdots \\ c_j^n = -r\,c_{j-1}^{n+1} + (1+2r)\,c_j^{n+1} - r\,c_{j+1}^{n+1}, \\ \vdots \\ c_{N_x}^n = -2r\,c_{N_x-1}^{n+1} + (1+2r)\,c_{N_x}^{n+1}. \end{cases} \tag{11.37}$$

This last expression, written in a matrix form, is reduced to

$$b = \begin{pmatrix} c_0^n \\ \vdots \\ c_j^n \\ \vdots \\ c_{N_x}^n \end{pmatrix}, \qquad c = \begin{pmatrix} c_0^{n+1} \\ \vdots \\ c_j^{n+1} \\ \vdots \\ c_{N_x}^{n+1} \end{pmatrix}, \tag{11.38}$$

where

$$A = \begin{pmatrix} (1+2r) & -2r & 0 & 0 & \cdots & \cdots & \cdots & 0 \\ 0 & \ddots & \vdots & \ddots & \ddots & \ddots & \ddots & \vdots \\ \vdots & \ddots & \ddots & \ddots & \ddots & \ddots & \ddots & \vdots \\ 0 & \cdots & 0 & -r & (1+2r) & -r & 0 \cdots & \vdots \\ \vdots & \ddots & \ddots & 0 & 0 & 0 & \ddots & \vdots \\ \vdots & \ddots & \ddots & \ddots & \ddots & \ddots & \ddots & \vdots \\ 0 & \cdots & \cdots & \cdots & \cdots & \cdots & -2r & (1+2r) \end{pmatrix}. \tag{11.39}$$

Notice that for the positions outside the boundaries, i.e., the rows in the matrix with indices other than 0 and N_x, the non-null coefficients are

$$A_{j,j-1} = -r, \qquad A_{j,j} = (1+2r), \qquad A_{j,j+1} = -r. \tag{11.40}$$

From Eqs. (11.39) and (11.40), we can observe that A is a constant matrix. Consequently, it does not need to be updated or recalculated. Then, the problem to be solved is given by

$$Ac = b. \tag{11.41}$$

Concentration values are calculated from this linear algebra problem, which needs to be solved N_t times, one for each timepoint in the mesh, which is computationally expensive, as compared to FTCS. The step-by-step summary is shown below:

- Set the number of steps that can be taken inside the mesh in any direction, that is, N_x, and N_t.
- Determine the increments as

$$\Delta x = \frac{x_f - x_i}{N_x} \quad \text{and} \quad \Delta t = \frac{t_f - t_i}{N_t}. \tag{11.42}$$

- Define the data structure to store vector c at a certain timepoint. The initialization is made by setting the initial conditions. This can generally be done using an array or list, and the length is determined by $N_x + 1$.
- Define a data structure to store matrix A. This is a constant matrix, so it will remain unchanged over time.
- Define a data structure to store column vector b for a certain time t.
- Now that we are working in $t = 0$, apply the initial conditions to the corresponding points in the mesh.

- Set the BCs on all the grid positions, as needed.
- Start a loop for every timepoint. This loop will consist of N_t iterations.
  - Set column vector b equal to vector c.
  - Solve the linear algebra problem $Ac = b$. The result is stored in vector c.
  - Apply the BCs as needed.
- All times are finished. The computation is done.

Generally, the linear problem is solved using libraries or packages that already implement appropiate routines for the task. In FORTRAN, a popular choice is *LAPACK* (Lxxinear Algebra PACKage), which, by the way, is also the back end for the famous *scipy* solver for Python language. As coding your own appropiate routines requires extra effort and adds a new layer of complexity to the final code, these are not implemented in this book. Instead, LAPACK will be used, as it only requires some auxiliary variables and just one extra line to call the subroutine which solves the linear system.
The pseudocode of the method is shown in the Algorithm 2.

Algorithm 2 Backward time-centered space method pseudocode for the 1D diffusion equation with two reflecting targets

procedure BTCS
  $N_x \leftarrow$ Number of slices of the spatial interval
  $N_t \leftarrow$ Number of slices of the temporal interval
  $\Delta x \leftarrow (x_f - x_i)/N_x$ ▷ Spatial increment
  $\Delta t \leftarrow (t_f - t_i)/N_t$ ▷ Temporal increment
  $A \leftarrow \mathbf{0}$ ▷ The matrix is initialized
  $A_{j,j-1} = A_{j,j+1} = -r$, $A_{j,j} = 1 + 2r$
  $A_{0,1} = A_{N_x+1,N_x} = -2r$ ▷ BCs are set
  $A_{0,0} = A_{N_x+1,N_x+1} = 1 + 2r$
  $c_j^0 \leftarrow 1/\Delta x$ ▷ Initial conditions are set
  for $1 \leq n \leq N_t$ **do**
    $b \leftarrow c$ ▷ The previous time c is saved to vector b
    dsgesv(...) ▷ $Ac = b$ is solved using LAPACK
    $c_0^n = c_1^n$, $c_{N_x+1}^n = c_{N_x}^n$ ▷ BCs are set
  end for ▷ Time loop ended
end procedure

The FORTRAN coding for this method is shown in Listing 11.2. The results are presented in Fig. 11.2, together with the FTCS method. These can be contrasted with the plots in Fig. 5.2, showing the analytical solution for this system, solved in Sect. 5.2.

Listing 11.2 [btcs-ref-ref.f90]: Fortran 90 implementation of the BTCS FDM method to solve the 1D diffusion equation with two completely reflecting boundaries

```
! ****************************************************** !
! ***************** btcs-ref-ref.f90 ***************** !
! ****************************************************** !
!
!    Leonardo Dagdug, Ivan Pompa-García, Jason Peña
!
! From the book:
! ****************************************************** !
!      Diffusion Under Confinement:
!               A Journey Through Counterintuition
! ****************************************************** !

! ****************************************************** !
! This file contains the source code to numerically
! solve the 1D diffusion equation for a channel
! of length L.
! It has two reflecting points at x=0 and x=L.
!
! The initial condition is such that
!                 p(x,t=0) = \delta(x-x0),
! where x0 is the initial position (default = 1/2).
!
! The solver uses the Backward Time-Centered Space
! (BTCS) Finite Difference Method (FDM).
!
! The BTCS is inconditionally stable, so the increment
! values do not need to be adapted to a
! specific rule as in FTCS.
!
! ****************************************************** !

! ****************************************************** !
! To compile with GFortran, you must include the
! helpers.f90 module, and also indicate that the
! program needs to be linked with LAPACK:
!         gfortran helpers.f90 btcs_ref_ref.f90 -llapack
!
```

Listing continued on next page

Listing continued from last page

```
! LAPACK must be installed in your operating system's
! standard location.
!
! Then you can run the program:
!         ./a.out
!
! After running the program, a file is generated:
!   - «btcs-aa.dat», a file with time, position,
!                    and concentration
! It can be plotted with any software
! of your choice. To do this using gnuplot, execute:
!  gnuplot -p -e '
!     set title "BTCS FDM for the Diffusion Equation";
!     set xlabel "x (position)" ;
!     set ylabel "c(x,t) (concentration)" ;
!times = system("awk '"'"'{print $1}'"'"' btcs-aa.dat |
    sort -u");
!     plot for [t in times] "<awk '"'"'$1==".t."'"'"' btcs
    -aa.dat"
!       u 2:3 with linespoints title "t=".sprintf("%.3f",
    t*1.0)'
!
! -p means that the plot must persist until the
!    user closes it explicitly.
! -e is used to specify the instructions
!    for using  gnuplot directly in the commandline.
! ************************************************** !

program btcsrefref

! Load the helpers module, which contains functions,
! constants, ...
use helpers

! Mandatory declaration of data type variables
! and constants.
implicit none

! ************************************************** !
!               Declaration of constants
```

Listing continued on next page

Listing continued from last page

```
! ****************************************************** !

!!! FDM parameters
! Number of pieces in the partition of «x»
integer, parameter :: NX = 10
! Number of pieces in the partition of «t»
integer, parameter :: NT = 30
! Total system evolution time
! (assuming that it starts at t=0)
real(kind=dp), parameter :: TF = 0.1_dp
! Start of channel
real(kind=dp), parameter :: XI = 0.0_dp
! End of channel
real(kind=dp), parameter :: XF = 1.0_dp
! Cintinuous initial condition position
real(kind=dp), parameter :: X0 = 0.5_dp
! Temporal step size
real(kind=dp), parameter :: DT = TF / NT
! Spatial step size
real(kind=dp), parameter :: DX = (XF - XI) / NX
! Diffusion constant (bulk)
real(kind=dp), parameter :: D0 = 1.0_dp
! «r» factor
real(kind=dp), parameter :: R = D0 * DT / DX**2
! Discrete initial condition position
! Substract 1 from the index because our array
! will be defined to start at 0.
integer, parameter :: J0 = int(X0 / DX + 1)


! ****************************************************** !
!               Declaration of variables
! ****************************************************** !

! General counter
integer :: i
! Time counter
integer :: n
! Spatial counter
integer :: j
```

Listing continued on next page

Listing continued from last page

```
! Current continous position
real(kind=dp) :: x
! Current continous time
real(kind=dp) :: t
! Array to hold the current time concentrations «c»
real(kind=dp) :: c(NX+1) = 0.0_dp
! Column vector «b»
real(kind=dp) :: b(NX+1) = 0.0_dp
! Matrix A
real(kind=dp) :: A(NX+1,NX+1) = 0.0_dp

! A unit number for the file where
! time, position, and concentration data
! will be saved.
! Fortran >= 2003 will
! assign this automatically in the open call.
integer(kind=i32) :: FUNIT

!!! Auxilliary variables for LAPACK
integer :: ipiv(NX+1) = 0
integer :: info = 0
integer :: iter = 0
real(kind=dp) :: work(NX+1) = 0.0_dp
real(kind=dp) :: swork((NX+1)*(NX+1+1)) = 0.0_dp


! ****************************************************** !
!              Main calculation program
! ****************************************************** !

! Open a file to write the data
open(newunit=FUNIT, file='btcs-aa.dat')

! Populate matrix «A» with the appropiate values.
do j=2, NX
  A(j,j-1) = -r
  A(j,j+1) = -r
  A(j,j) = 1 + 2*r
end do

```

Listing continued on next page

Listing continued from last page

```
155 ! Set the boundary conditions.
156 A(1,2) = -2*r
157 A(NX+1,NX) = -2*r
158 A(1,1) = 1 + 2*r
159 A(NX+1,NX+1) = 1 + 2*r
160
161 ! Set the discretized initial condition.
162 c(J0) = 1.0_dp / DX
163
164 ! Print out the values for time zero.
165 do j=1, NX+1
166   write(FUNIT,  *) 0.0_dp, (j-1) * DX, c(j)
167 end do
168
169 ! The loop iterates over each time step until NT is
170 ! reached.
171 ! In other words, it walks along every point on the mesh
172 ! for the respective amount of time.
173 ! Keeping the notation of the book, the current time
174 ! step is held in «n».
175 do n=1, NT
176   ! Obtain the current continous time
177   t = n * DT
178
179   ! Vector «b» must be set to the values of
180   ! «c» for the previous time step.
181   b = c
182
183   ! The equation «Ac=b» is solved using LAPACK.
184   ! The arguments are (in order):
185     ! Number of linear equations
186     ! Number of columns in «b»
187     ! «A»
188     ! Leading dimension of A
189     ! Pivot integer
190     ! «b», also the output if the operation was
191     ! successful.
192     ! Leading dimension of «b»: NX+1
193     ! The result: «c»
194     ! Leading dimension of the result: «NX+1»
```

Listing continued on next page

Listing continued from last page

```
    ! Residual hold vectors: «NX+1»
    ! To use a single precision matrix: «(NX+1)*(NX+1+1)»
    ! An indicator if iterative methods were used.
  call dsgesv(NX+1, 1, A, NX+1, ipiv, b, NX+1, &
                       c, NX+1, work, swork, iter, info)

  if(info /= 0) then
    print *, 'An error has ocurred solving the' &
             // ' problem Ac=b, verify!'

    call exit(info)
  end if

  ! Set the BCs
  c(1) = c(2)
  c(NX+1) = c(NX)

  ! Print out the whole «c» for this specific time step.
  do j=1, NX+1
    write(FUNIT,  *) t, (j-1) * DX, c(j)
  end do
end do ! Ends the loop for all timepoints.

! Close the file.
close(FUNIT)

!!! At this point, the calculation is done.
! As a reminder, print out some numbers:
print *
print *, TAB // '=== BTCS FDM finished with params ==='
! ! The number of slides for space
print *, TAB // 'Nx = ' // nstr(NX)
! ! The spatial step
print *, TAB // 'dx = ' // nstr(DX, 3)
! ! The number of slides for time
print *, TAB // 'Nt = ' // nstr(NT)
! ! The time step, too
print *, TAB // 'dt = ' // nstr(DT, 3)
! ! r factor
print *, TAB // 'r = ' // nstr(R, 2)
```

Listing continued on next page

Listing continued from last page

```
235
236
237 end program btcsrefref
```

Listing ended

Compiling and Running of Listing 11.2

```
1       # Compile
2       gfortran helpers.f90 btcs-ref-ref.f90 -llapack
3
4       # Run
5       ./a.out
6
7       # Sample output
8
9       # Plot
10      gnuplot -p -e '
11        set title "BTCS FDM for the Diffusion Equation";
12        set xlabel "x (position)" ;
13        set ylabel "c(x,t) (concentration)" ;
14
15  times = system("awk '"'"'{print $1}'"'"' btcs-aa.dat |
        sort -u");
16
17        plot for [t in times] "<awk '"'"'$1==".t."'"'"' btcs
        -aa.dat"
18            u 2:3 with linespoints title "t=".sprintf("%.3f",
        t*1.0)'
```

11.4 Stability Analysis

The numerical analysis always comes with two terms, *convergence* and *stability*, which are often mixed up and confused.

The numerical method's capability of providing an approximation of the analytical solution is known as convergence. This condition consists of increments of the method, i.e., Δx or Δt tend to zero. This is reasonable because FDMs are

constructed with expressions that are too similar with the derivatives. However, the limit does not appear in the formulae. Convergence will not be analyzed in this book. The inherent characteristics of numerical methods result in the propagation of errors that may increase with each successive step of the process Thus, it is essential to ensure that these errors do not escalate in further calculations, a property referred to as stability.

11.4.1 Stability of the FTCS FDM

Let us begin with the assumption that the unknown function of our PDE can be written as a term of a Fourier series, namely,

$$c_j^n = \xi^n \mathrm{e}^{ikj\,\Delta x}, \tag{11.43}$$

where ξ is known as the *amplification factor*. Additionally, a condition for the error to be bounded is given by

$$|\xi| \leq 1. \tag{11.44}$$

By defining $\gamma \equiv k\,\Delta x$, we have that

$$c_j^n = \xi^n\,\mathrm{e}^{ij\,\gamma}. \tag{11.45}$$

This last relation has to be introduced into a discretized equation, e.g., Eq. (11.18), leading to

$$\xi^{n+1}\,\mathrm{e}^{ij\,\gamma} = \xi^n\,\mathrm{e}^{ij\,\gamma} + r\left[\xi^n\,\mathrm{e}^{i(j+1)\,\gamma} - 2\xi^n\,\mathrm{e}^{ij\,\gamma} + \xi^n\,\mathrm{e}^{i(j-1)\,\gamma}\right], \tag{11.46}$$

where r has been defined as

$$r \equiv D\frac{\Delta t}{\Delta x^2}. \tag{11.47}$$

Now, the goal is to obtain a value for the amplification factor. If we divide Eq. (11.46) by $\xi^n\,\mathrm{e}^{ij\,\gamma}$, this yields

$$\xi = 1 + r\left(\mathrm{e}^{+i\,\gamma} - 2 + \mathrm{e}^{-i\,\gamma}\right), \tag{11.48}$$

where the term inside the parentheses can be rewritten. In fact, if

$$\sin\left(\frac{\gamma}{2}\right) = \frac{\mathrm{e}^{+i\,\gamma/2} - \mathrm{e}^{-i\,\gamma/2}}{2i}, \tag{11.49}$$

then

$$\sin^2\left(\frac{\gamma}{2}\right) = -\frac{e^{+i\gamma} + e^{-i\gamma} - 2}{4}, \tag{11.50}$$

which can be substituted into Eq. (11.46) to obtain

$$\xi = 1 - 4r\sin^2\left(\frac{\gamma}{2}\right). \tag{11.51}$$

The condition stated in Eq. (11.44) is imposed, leading to

$$\left|1 - 4r\sin^2\left(\frac{\gamma}{2}\right)\right| \leq 1 \tag{11.52}$$

that can be split into two inequalities, the first being

$$1 - 4r\sin^2\left(\frac{\gamma}{2}\right) \leq 1, \tag{11.53}$$

the solution of which is

$$r \geq 0. \tag{11.54}$$

The second inequality is

$$1 - 4r\sin^2\left(\frac{\gamma}{2}\right) \geq -1, \tag{11.55}$$

and its solution is given by

$$r \leq \frac{1}{2}. \tag{11.56}$$

Then, the criteria for the stability of the FTCS method for the diffusion equation reads

$$r = D\frac{\Delta t}{\Delta x^2} \leq \frac{1}{2}. \tag{11.57}$$

This means that the choice of spatial and temporal increments is essential for the stability of the scheme.

11.4.2 Stability of the BTCS FDM

The procedure in this case closely resembles that of the FTCS method in nearly every step. Now, the starting point is Eq. (11.33), which leads us to

$$\xi^n \, \mathrm{e}^{ij\gamma} = \xi^{n+1} \, \mathrm{e}^{ij\gamma} - r\left[\xi^{n+1} \, \mathrm{e}^{i(j+1)\gamma} - 2\xi^{n+1} \, \mathrm{e}^{ij\gamma} + \xi^{n+1} \, \mathrm{e}^{i(j-1)\gamma}\right]. \tag{11.58}$$

By dividing this last equation by $\xi^n \, \mathrm{e}^{ij\gamma}$, and rearranging it, we arrive at

$$\xi = \frac{1}{1 + 4r \sin^2\left(\dfrac{\gamma}{2}\right)}. \tag{11.59}$$

Then, applying the criteria for the amplification factor, we obtain

$$\frac{1}{\left|1 + 4r \sin^2\left(\dfrac{\gamma}{2}\right)\right|} \leq 1, \tag{11.60}$$

where the factor inside the absolute value is always positive, making the denominator equal to or greater than the unity.

The conclusion is that the BTCS is *inconditionally stable*. The trade-off for achieving stability in this implicit scheme is the computational workload associated with solving a system of equations, as elucidated in the method's derivation.

11.5 Concluding Remarks

In this chapter, we solved the diffusion equation numerically by means of finite-difference methods (FDMs). For such purpose, the basic relations of the FDM were derived, and the diffusion equation was discretized. Emphasis was placed on the correct discretization of the boundary and initial conditions, even if a Dirac delta is included. Dissimilarities between the FTCS and the BTCS were highlighted, showing that two very similar methods can ultimately lead to very different courses of action. Furthermore, the step-by-step process to computationally implement both schemes was summarized, and their pseudocodes were also presented. Finally, their stability analysis was developed for greater clarity.

For the reader's convenience, listed below are the most important equations we have obtained in this chapter:

$$f'(x_0) \approx \frac{f(x_0 + \Delta x) - f(x_0)}{\Delta x}. \qquad \text{(First-Order Forward Difference)}$$

$$f'(x_0) \approx \frac{f(x_0) - f(x_0 - \Delta x)}{\Delta x}. \qquad \text{(First-Order Backward Difference)}$$

$$f'(x_0) \approx \frac{f(x_0 + \Delta x) - f(x_0 - \Delta x)}{2\Delta x}. \qquad \text{(First-Order Central Difference)}$$

$$f''(x_0) \approx \frac{f(x_0 + \Delta x) - 2f(x_0) + f(x_0 - \Delta x)}{\Delta x^2}. \qquad \text{(First-Order Central Difference for the Second Derivative)}$$

Further Reading and References

K.N. Anagnostopoulos, *Computational Physics: A Practical Introduction to Computational Physics and Scientific Computing* (The Author & National Technical University of Athens, Athens, 2016). http://www.physics.ntua.gr/~konstant/ComputationalPhysics/index.html

J. Franklin, *Computational Methods for Physics* (Cambridge University Press, Cambridge, 2013)

H.P. Langtangen, S. Linge, *Finite Difference Computing with PDEs - A Modern Software Approach* (The Authors, Athens, 2016). https://hplgit.github.io/fdm-book/doc/web/index.html

R.J. LeVeque, *Finite Difference Methods for Ordinary and Partial Differential Equations: Steady-State and Time-Dependent Problems* (Society for Industrial and Applied Mathematics, Philadelphia, 2007). 10.1137/1.9780898717839

Part IV
Two-Dimensional Diffusion and Reaction-Diffusion Equations

The randomness of being trapped, reflected, and reacted in two dimensions.

"The future of science lies in the development of new mathematical methods for the analysis of complex systems."

—John von Neumann

Chapter 12
Two-Dimensional Systems

In previous chapters, we focused on solving the diffusion equation in one dimension under spatial constraints. In this chapter, we will solve a set of diffusion problems within a two-dimensional system with radial symmetry, such as diffusion into disklike surfaces. These solutions can also be applied to the problem of diffusion into a cylinder in the more general case, which is a problem of diffusion in three dimensions. If the cylinder is very long in comparison to its diameter, then, we consider the diffusion toward its ends to be negligible. Concentration does not depend on the axial position z, and the problem becomes one of diffusion in two dimensions instead of three, leading to a significant simplification of its mathematical treatment. Moreover, assuming radial symmetry, these cases can be reduced to a one-dimensional problem with a straightforward solution.

The problem of trapping of diffusing particles involving symmetrical diffusion into or out of a long cylinder or a disk arises in the analysis of various processes in physics, chemistry, and biology. Examples include electric current through arrays of microelectrodes, porous membrane transport, reactions on supported catalysts, water exchange in plants, ligand binding to cell surface receptors, and ligand accumulation in cell culture assays, among others.

12.1 Partially Absorbent Disk: Internal Problem

Consider a point particle diffusing within a circular disk of radius R with a partially absorbing boundary, which corresponds to a Neumann boundary condition, given by Eq. (5.182) and characterized by a trapping rate κ, as shown in Fig. 12.1. Initially, at $t = 0$, the initial position of the particles is uniformly distributed across the disk's surface area. Assuming angular independence and using Eq. (B.8), we see that the diffusion equation simplifies to

L. Dagdug et al., *Diffusion Under Confinement*,
https://doi.org/10.1007/978-3-031-46475-1_12

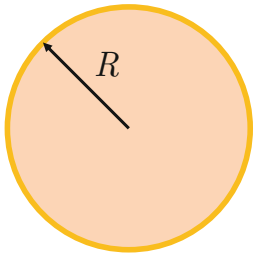

Fig. 12.1 Schematic representation of a disk with radius R and a partially absorbing perimeter (yellow)

$$\frac{\partial p(r,t)}{\partial t} = \frac{D}{r}\frac{\partial}{\partial r}\left(r\frac{\partial p(r,t)}{\partial r}\right) = D\left(\frac{\partial^2 p(r,t)}{\partial r^2} + \frac{1}{r}\frac{\partial p(r,t)}{\partial r}\right), \tag{12.1}$$

where r is the radial coordinate and $r \leq R$. In the present case, the initial condition is $p(r,0) = 1/\pi R^2$, and the boundary conditions (BCs) are given by

$$\left.\frac{\mathrm{d}p(r,t)}{\mathrm{d}r}\right|_{r=0} = 0 \quad \text{and} \quad \left.\mathbf{J}(r)\cdot\hat{\mathbf{n}}_R\right|_{r=R} = -D\left.\frac{\mathrm{d}p(r,t)}{\mathrm{d}r}\right|_{r=R} = \kappa\, p(R,t). \tag{12.2}$$

with D being the diffusivity and κ the trapping rate coefficient. The Laplace transform of Eq. (12.1) is given by

$$s\,p(r,s) - \frac{1}{\pi R^2} = D\left(\frac{\mathrm{d}^2 p(r,s)}{\mathrm{d}r^2} + \frac{1}{r}\frac{\mathrm{d}p(r,s)}{\mathrm{d}r}\right). \tag{12.3}$$

To simplify these equations, we use the following change of variable:

$$g(r,s) = p(r,s) - \frac{1}{s\pi R^2}, \tag{12.4}$$

then, Eq. (12.3) becomes

$$\frac{\mathrm{d}^2 g(r,s)}{\mathrm{d}r^2} + \frac{1}{r}\frac{\mathrm{d}g(r,s)}{\mathrm{d}r} - \frac{s}{D}\,g(r,s) = 0. \tag{12.5}$$

Multiplying this last equation by r^2, we arrive at the modified Bessel equation of zero order, namely,

$$r^2\frac{\mathrm{d}^2 g(r,s)}{\mathrm{d}r^2} + r\frac{\mathrm{d}g(r,s)}{\mathrm{d}r} - \frac{r^2 s}{D}\,g(r,s) = 0. \tag{12.6}$$

Let us solve the Bessel equation using the method that is usually found in the literature. Regardless of whether Eq. (12.6) is expressed using other terms, such as

extra coefficients or swapped signs, the main result can be used by making a variable change, which we will do later in this chapter.

Let us use a function $f = f(x)$ defined by means of an ordinary differential equation (ODE), namely,

$$x^2 \frac{\mathrm{d}^2 f(x)}{\mathrm{d}x^2} + x \frac{\mathrm{d} f(x)}{\mathrm{d}x} + (x^2 - \nu^2) f(x) = 0, \tag{12.7}$$

which is known as the Bessel equation and $\nu \geq 0$. Then, according to Fuchs' theorem,[1] at least one solution can be found using the Frobenius method, meaning that the solution can be built as a series, as shown below:

$$f(x) = \sum_{n=0}^{\infty} a_n \, x^{n+\sigma}, \tag{12.8}$$

and its derivatives are

$$\begin{aligned} f'(x) &= \sum_{n=0}^{\infty} (n+\sigma) \, a_n \, x^{n+\sigma-1}, \\ f''(x) &= \sum_{n=0}^{\infty} (n+\sigma) \, (n+\sigma-1) \, a_n \, x^{n+\sigma-2}, \end{aligned} \tag{12.9}$$

which are substituted back into the Bessel equation, to get

$$\begin{aligned} \sum_{n=0}^{\infty} (n+\sigma) \, (n+\sigma-1) \, a_n \, x^{n+\sigma} + \sum_{n=0}^{\infty} (n+\sigma) \, a_n \, x^{n+\sigma} \\ + \sum_{n=0}^{\infty} a_n \, x^{n+\sigma+2} - \sum_{n=0}^{\infty} \nu^2 \, a_n \, x^{n+\sigma} = 0, \end{aligned} \tag{12.10}$$

from where we can group terms, obtaining

$$\sum_{n=0}^{\infty} \Big[(n+\sigma)^2 - \nu^2 \Big] a_n \, x^{n+\sigma} + \sum_{n=0}^{\infty} a_n \, x^{n+\sigma+2} = 0. \tag{12.11}$$

From the first sum of the last equation, we change the index from $n \to n+2$, arriving at

[1] Fuchs' theorem states that at least one power solution of the ODE can be obtained by means of the Frobenius method if the expansion of the series is made around a singular, regular, or ordinary point, which is the case in the Bessel equation.

$$\sum_{n=0}^{\infty}\Big[(n+\sigma)^2-\nu^2\Big]a_n\,x^{n+\sigma}=\sum_{n=-2}^{\infty}\Big[(n+2+\sigma)^2-\nu^2\Big]a_{n+2}\,x^{n+2+\sigma},\tag{12.12}$$

and write the two first terms of the sum explicitly, that is,

$$\begin{aligned}\sum_{n=-2}^{\infty}\Big[(n+2+\sigma)^2-\nu^2\Big]a_{n+2}\,x^{n+2+\sigma}&\\ =\Big[\sigma^2-\nu^2\Big]a_0\,x^{\sigma}+\Big[(\sigma+1)^2-\nu^2\Big]a_1\,x^{\sigma+1}&\\ +\sum_{n=0}^{\infty}\Big[(n+2+\sigma)^2-\nu^2\Big]a_{n+2}\,x^{n+2+\sigma}.&\end{aligned}\tag{12.13}$$

This is substituted into Eq. (12.11), yielding

$$\begin{aligned}&\Big[\sigma^2-\nu^2\Big]a_0\,x^{\sigma}+\Big[(\sigma+1)^2-\nu^2\Big]a_1\,x^{\sigma+1}\\ &+\sum_{n=0}^{\infty}\Big[(n+2+\sigma)^2-\nu^2\Big]a_{n+2}\,x^{n+2+\sigma}+\sum_{n=0}^{\infty}a_n\,x^{n+\sigma+2}=0,\end{aligned}\tag{12.14}$$

where taking $x^{n+\sigma+2}$ as a common factor gives

$$\begin{aligned}&\Big[\sigma^2-\nu^2\Big]a_0\,x^{\sigma}+\Big[(\sigma+1)^2-\nu^2\Big]a_1\,x^{\sigma+1}\\ &+\sum_{n=0}^{\infty}\left\{\Big[(n+2+\sigma)^2-\nu^2\Big]a_{n+2}+a_n\right\}x^{n+\sigma+2}=0.\end{aligned}\tag{12.15}$$

As every power of x is linearly independent, then every coefficient must be null to hold the equality. This leads us to a set of three equations, namely,

$$\begin{aligned}\Big(\sigma^2-\nu^2\Big)a_0&=0,\\ \Big[(\sigma+1)^2-\nu^2\Big]a_1&=0,\\ \Big[(n+2+\sigma)^2-\nu^2\Big]a_{n+2}+a_n&=0,\end{aligned}\tag{12.16}$$

where the third expression can be manipulated, obtaining

$$\begin{aligned}\left(\sigma^2-\nu^2\right)a_0&=0,\\ \left[(\sigma+1)^2-\nu^2\right]a_1&=0,\\ a_{n+2}&=\frac{a_n}{\nu^2-(n+2+\sigma)^2}.\end{aligned}\tag{12.17}$$

Let us check the convergence of the series by using the ratio criteria, namely,

$$\lim_{k\to\infty}\left|\frac{a_{k+1}}{a_k}\right|=r<1,\tag{12.18}$$

that is, the ratio of two successive terms of the series. The inequality must hold to ensure convergence. Applied to our case, it yields

$$r=\lim_{n\to\infty}\left|\frac{1}{\nu^2-(n+2+\sigma)^2}\right|x^2=\lim_{n\to\infty}\frac{1}{n^2}x^2=0,\tag{12.19}$$

meaning that irrespective of the value of x we take, the convergence of the series is ensured, unlike the case of the Legendre equation, where the series has to be truncated to converge.

Now, going back to the third expression in (12.17) and assuming that $a_0\neq 0$, this yields

$$\sigma=\pm\nu,\tag{12.20}$$

which can be substituted into the second equation of (12.17) to give

$$(2\sigma+1)a_1=0,\tag{12.21}$$

resulting into two different options, which are

$$a_1=0,\qquad \sigma=-\frac{1}{2}.\tag{12.22}$$

Working with the case when $a_1=0$ and looking into the third equation of (12.17), we note that

$$a_1=a_3=a_5=\cdots=0,\tag{12.23}$$

allowing us to switch the index $n+2\to 2n$, obtaining

$$a_{2n}=\frac{a_{2n-2}}{\nu^2-(2n\pm\nu)^2},\qquad n=1,2,3,\ldots\tag{12.24}$$

or

$$a_{2n} = -\frac{a_{2n-2}}{2^2\, n(n \pm \nu)}, \qquad n = 1, 2, 3, \ldots \tag{12.25}$$

By explicitly writing out some coefficients, we get

$$\begin{aligned} a_2 &= -\frac{a_0}{2^2 \cdot 1(1 \pm \nu)}, \\ a_4 &= -\frac{a_2}{2^2 \cdot 2(2 \pm \nu)} = \frac{a_0}{2^4 \cdot 1 \cdot 2(1 \pm \nu)(2 \pm \nu)}, \\ a_6 &= -\frac{a_4}{2^2 \cdot 3(3 \pm \nu)} = -\frac{a_0}{2^6 \cdot 1 \cdot 2 \cdot 3(1 \pm \nu)(2 \pm \nu)(3 \pm \nu)}, \end{aligned} \tag{12.26}$$

which allow us to obtain a general structure, namely,

$$a_{2n} = \frac{(-1)^n\, a_0}{2^{2n}\, n!\, (1 \pm \nu)(2 \pm \nu) \cdots (n \pm \nu)}. \tag{12.27}$$

It is necessary to fix the value of a_0, so as a convention, we have

$$a_0 = \frac{1}{2^\nu\, \Gamma(1 \pm \nu)}. \tag{12.28}$$

This is convenient because of the properties of the Γ function, particularly the one stated in Eq. (A.77) in Appendix A.10.1. Furthermore, Eq. (12.27) can be casted into

$$a_{2n} = \frac{(-1)^n}{2^{2n+\nu}\, n!\, \Gamma(1 \pm \nu + n)}, \tag{12.29}$$

which is substituted into the power series in Eq. (12.8), yielding

$$f(x) = \sum_{n=0}^{\infty} \frac{(-1)^n}{n!\, \Gamma(1 \pm \nu + n)} \left(\frac{x}{2}\right)^{2n+\nu}. \tag{12.30}$$

These are the *Bessel functions of the first kind* of order $\pm\nu$:

$$J_{\pm\nu}(x) = \sum_{n=0}^{\infty} \frac{(-1)^n}{n!\, \Gamma(1 \pm \nu + n)} \left(\frac{x}{2}\right)^{2n+\nu}, \tag{12.31}$$

and it can be seen that if $\nu = 0$, then J_ν and $J_{-\nu}$ are the same, and we would need to look for another solution.

Assuming that the two solutions of the Bessel equation are $h(x) = J_\nu(x)$ and $g(x)$, then, substituting these into Eq. (12.7), we obtain

$$\begin{aligned} x^2\,h''(x) + x\,h'(x) + (x^2 - \nu^2)\,h(x) &= 0, \\ x^2\,g''(x) + x\,g'(x) + (x^2 - \nu^2)\,g(x) &= 0, \end{aligned} \tag{12.32}$$

where the first expression is multiplied by $g(x)$ and the second by $h(x)$, to get

$$\begin{aligned} g(x)\,x^2\,h''(x) + g(x)\,x\,h'(x) + g(x)\,(x^2 - \nu^2)\,h(x) &= 0, \\ h(x)\,x^2\,g''(x) + h(x)\,x\,g'(x) + h(x)\,(x^2 - \nu^2)\,g(x) &= 0, \end{aligned} \tag{12.33}$$

from where we subtract one equation from the other, yielding

$$x\left[g(x)\,h''(x) - h(x)\,g''(x)\right] + \left[g(x)\,h'(x) - h(x)\,g'(x)\right] = 0, \tag{12.34}$$

where this is identified as the derivative of a product, namely,

$$\begin{aligned} \frac{\mathrm{d}}{\mathrm{d}x}\left\{x\left[g(x)\,h'(x) - h(x)\,g'(x)\right]\right\} &= \left[g(x)\,h'(x) - h(x)\,g'(x)\right] \\ &+ x\left[g(x)\,h''(x) + h'(x)\,g'(x) - h(x)\,g''(x) - h'(x)\,g'(x)\right]. \end{aligned} \tag{12.35}$$

Then, Eq. (12.34) can be stated as

$$\frac{\mathrm{d}}{\mathrm{d}x}\left\{x\left[g(x)\,h''(x) - h(x)\,g'(x)\right]\right\} = 0, \tag{12.36}$$

meaning that

$$x\left[g(x)\,h'(x) - h(x)\,g'(x)\right] = \mathcal{A}_0, \tag{12.37}$$

with $\mathcal{A}_0$ being a constant. After a few calculations, we arrive at

$$\frac{g(x)\,h'(x) - h(x)\,g'(x)}{h(x)^2} = \frac{\mathcal{A}_0}{x\,h(x)^2}. \tag{12.38}$$

Furthermore, the left-hand side can be seen as the derivative of a ratio:

$$\frac{\mathrm{d}}{\mathrm{d}x}\left[\frac{g(x)}{h(x)}\right] = \frac{g(x)\,h'(x) - h(x)\,g'(x)}{h(x)^2}, \tag{12.39}$$

which, when substituted into (12.38), yields

$$\frac{\mathrm{d}}{\mathrm{d}x}\left[\frac{g(x)}{h(x)}\right] = \frac{\mathcal{A}_0}{x\,h(x)^2} \tag{12.40}$$

that needs to be integrated, obtaining

$$\frac{g(x)}{h(x)} = \mathcal{A}_0 \int \frac{\mathrm{d}x}{x\, h(x)^2} + \mathcal{A}_1, \tag{12.41}$$

or

$$g(x) = \mathcal{A}_0\, h(x) \int \frac{\mathrm{d}x}{x\, h(x)^2} + \mathcal{A}_1\, h(x). \tag{12.42}$$

As stated earlier, $h(x)$ is the solution that had already been found, so considering that $h(x) = J_\nu(x)$, then

$$g(x) = \mathcal{A}_0\, J_\nu(x) \int \frac{\mathrm{d}x}{x\, J_\nu(x)^2} + \mathcal{A}_1\, J_\nu(x), \tag{12.43}$$

where the first term on right-hand side can be written by defining a new function, namely,

$$Y_\nu(x) \equiv \mathcal{A}_0\, J_\nu(x) \int \frac{\mathrm{d}x}{x\, J_\nu(x)^2}, \tag{12.44}$$

which has a specific form known as *Neumman functions* or *Bessel functions of the second kind*. This is also commonly defined as

$$Y_\nu(x) = \frac{J_\nu(x)\, \cos(\nu\pi) - J_{-\nu}(x)}{\sin(\nu\pi)}. \tag{12.45}$$

Equations (12.31) and (12.45) are used to write the most general solution of the Bessel equation (12.7), which is

$$f(x) = \mathcal{A}\, J_\nu(x) + \mathcal{B}\, Y_\nu(x), \tag{12.46}$$

where $\mathcal{A}$ and $\mathcal{B}$ are, as usual, constants to be determined by the boundary conditions (BCs).

The solution presented in Eq. (12.46) solves Eq. (12.7), the Bessel equation. But, upon comparing the latter to our original equation to solve this, Eq. (12.6), we find some discrepancies. To tackle them, let us rewrite Eq. (12.6) in terms of an $f = f(x)$ function, namely,

$$x^2 \frac{\mathrm{d}^2 f(x)}{\mathrm{d}x^2} + x \frac{\mathrm{d}f(x)}{\mathrm{d}x} - \frac{s}{D} x^2 f(x) = 0, \tag{12.47}$$

meaning that $\nu = 0$. Moreover, a difference in sign can be seen in the last term. Also, a constant is joined with x^2, and this does not appear in the Bessel equation as we solved it earlier. Therefore, a variable change is needed, that is,

$$\xi \equiv i \sqrt{\frac{s}{D}} x, \tag{12.48}$$

making x^2 to be

$$x^2 = -\frac{s}{D}\xi^2, \tag{12.49}$$

and the chain rule is applied

$$\frac{\mathrm{d}f(\xi)}{\mathrm{d}x} = \frac{\mathrm{d}f(\xi)}{\mathrm{d}\xi}\frac{\mathrm{d}\xi}{\mathrm{d}x} = i\sqrt{\frac{s}{D}}\,f'(\xi), \tag{12.50}$$

where the second derivative is

$$\frac{\mathrm{d}^2 f(\xi)}{\mathrm{d}x^2} = \frac{\mathrm{d}}{\mathrm{d}x}\left[i\sqrt{\frac{s}{D}}\,f'(\xi)\right] = \frac{\mathrm{d}\xi}{\mathrm{d}x}\frac{\mathrm{d}}{\mathrm{d}\xi}\left[i\sqrt{\frac{s}{D}}\,f'(\xi)\right] = -\frac{s}{D}\,f''(\xi). \tag{12.51}$$

These two derivatives are substituted back into the Bessel equation, yielding

$$\xi^2\,f''(\xi) + \xi\,f'(\xi) + \xi^2\,f(\xi) = 0, \tag{12.52}$$

which is the Bessel equation in terms of the ξ variable and $\nu = 0$. This makes the solution, according to Eq. (12.46), to be

$$f(\xi) = \mathcal{A}\,J_0(\xi) + \mathcal{B}\,Y_0(\xi), \tag{12.53}$$

and, when going back to the original variable x, becomes

$$f(x) = \mathcal{A}\,J_0\left(i\sqrt{\frac{s}{D}}\,x\right) + \mathcal{B}\,Y_0\left(i\sqrt{\frac{s}{D}}\,x\right). \tag{12.54}$$

This last equation has complex arguments, a reason why, together with Eqs. (A.125) and (A.126), it lead us to the solution to the original ODE (12.6), proposed in the problem, which is given by Eq. (A.128), namely,

$$g(r,s) = \mathcal{A}\,I_0\left(\sqrt{\frac{s}{D}}r\right) + \mathcal{B}\,K_0\left(\sqrt{\frac{s}{D}}r\right), \tag{12.55}$$

where $\mathcal{A}$ and $\mathcal{B}$ are integration constants and $I_0(x)$ and $K_0(x)$ are the modified Bessel functions[2] or hyperbolic Bessel functions of the first and second kind,

[2] Diverse cylindrical symmetric problems in physics, such as the vibration modes of circular drumheads of a thin circular, tubular, or annular membrane, and the radial modes in optical fibers, lead to Bessel functions, among others. Bessel functions are a set of mathematical functions that were systematically derived around 1817 by the German astronomer Friedrich Wilhelm Bessel, which arise as a solution of Kepler's equations of planetary motion. The first one to propose the zero-order Bessel function was Daniel Bernoulli, which appeared when he was studying the

respectively. Now, we can substitute this result into Eq. (12.4) to obtain $p(r, s)$. By applying the boundary condition (BC) given in Eq. (12.2) at $r = 0$ and using the relations

$$\frac{\mathrm{d}I_0(x)}{\mathrm{d}x} = I_1(x) \quad \text{and} \quad \frac{\mathrm{d}K_0(x)}{\mathrm{d}x} = -K_1(x), \tag{12.56}$$

which are obtained from Eqs. (A.134) and (A.136), and the fact that $K_1(0)$ diverges, we find that $\mathcal{B} = 0$. Additionally, using the second BC in Eq. (12.3), at $r = R$, the constant that remains to be determined is found, namely,

$$\mathcal{A} = -\frac{\kappa}{\pi R^2 s \left[\kappa\, I_0\left(\sqrt{\frac{s}{D}}R\right) + \sqrt{sD}\, I_1\left(\sqrt{\frac{s}{D}}R\right)\right]}. \tag{12.57}$$

With this last result, the propagator becomes

$$p(r, s) = \frac{1}{\pi R^2 s}\left[1 - \frac{\kappa\, I_0\left(\sqrt{\frac{s}{D}}r\right)}{\kappa\, I_0\left(\sqrt{\frac{s}{D}}R\right) + \sqrt{sD}\, I_1\left(\sqrt{\frac{s}{D}}R\right)}\right]. \tag{12.58}$$

Figure 12.2 shows the time evolution of this propagator in space and time.

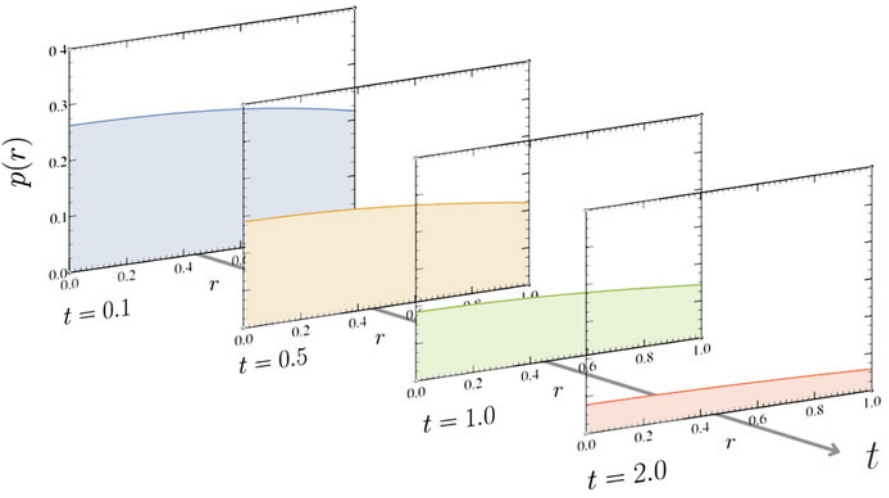

Fig. 12.2 Time evolution of the probability density $p(r, t)$ given by Eq. (12.58) at different times, i.e., $t = 0.1$, $t = 0.5$, $t = 1.0$, and $t = 2.0$. The radius of the disk and the diffusion coefficient are set to $D = R = 1$, while the trapping rate coefficient κ is set to 0.5

properties of heavy chains. Later, Leonhard Euler and Joseph Fourier deduced this function while working on the study of vibrations and heat transport, respectively.

On one hand, when the perimeter of the disk is perfectly reflecting, i.e., $\kappa = 0$, the propagator reduces to $(\pi R^2 s)^{-1}$. Moreover, since the inverse Laplace transformation of $1/s$ is the Heaviside step function,[3] the system always has the same distribution of particles for $t > 0$. On the other hand, if the perimeter is perfectly absorbing, then, $\kappa \to \infty$, and Eq. (12.58) reduces to

$$p(r,s) = \frac{1}{\pi R^2 s}\left[1 - \frac{I_0\left(\sqrt{\frac{s}{D}}r\right)}{I_0\left(\sqrt{\frac{s}{D}}R\right)}\right]. \tag{12.59}$$

Now, let us calculate the particle's probability density of mean first-passage time, also called lifetime probability $\varphi(s)$, which is related to the flux probability density, by means of Eq. (5.63). Consequently, all we have to do is take the derivative of Eq. (12.58) with respect to r and multiply it by $-2\pi DR$, which leads to

$$\varphi(s) = \frac{2\kappa\sqrt{D}\, I_1\left(\sqrt{\frac{s}{D}}R\right)}{R\sqrt{s}\left[\kappa\, I_0\left(\sqrt{\frac{s}{D}}R\right) + \sqrt{sD}\, I_1\left(\sqrt{\frac{s}{D}}R\right)\right]}. \tag{12.60}$$

The relation between the survival probability and the lifetime probability density is obtained from Eqs. (2.81) and (2.91):

$$\varphi(s|x_0) = \int_0^\infty \varphi(t|x_0)\, \mathrm{e}^{-st}\, \mathrm{d}t = -\int_0^\infty \frac{\partial S(t|x_0)}{\partial t}\, \mathrm{e}^{-st}\, \mathrm{d}t. \tag{12.61}$$

After integrating by parts the right hand-side, we obtain

$$\varphi(s|x_0) = -\left[\mathrm{e}^{-st}\, S(t|x_0)\Big|_0^\infty + s\int_0^\infty S(t|x_0)\, \mathrm{e}^{-st}\, \mathrm{d}t\right]. \tag{12.62}$$

The evaluation of the survival probability at infinity tends to zero, while the second term is actually the Laplace transform of the survival probability; therefore

$$\varphi(s|x_0) = -\left[-1 + sS(s|x_0)\right] = -s\, S(s|x_0) + 1. \tag{12.63}$$

By solving for $S(s|x_0)$, we finally arrive at

$$S(s|x_0) = \frac{1}{s}\left[1 - \varphi(s|x_0)\right]. \tag{12.64}$$

[3] Notice that in Eq. (A.64) we have written the inverse Laplace transform of 1/s as 1. The reason why we are using the Heaviside step function is because we want to correctly describe the time-ordered aspects of the system. In other words, we ensure a solution for $t \geq 0$.

As the reader may appreciate, this relationship is very useful: In Laplace space, once we have either the survival probability or the lifetime probability, we are able to compute the other.

Moving forward, we shall compute the evolution equation for the mean first-passage time (MFPT) given by Eq. (2.63). Assuming angular independence, such equation reduces to

$$\frac{\mathrm{d}}{\mathrm{d}r_0}\left(\frac{\mathrm{d}\langle t(\mathrm{d}r_0)\rangle}{r_0}\right) = -\frac{r_0}{D}, \tag{12.65}$$

where r_0 is the initial position and $r_0 \leq R$. The solution of Eq. (12.65) is subject to a null flux at $r_0 = 0$ and a radiation BC at $r_0 = R$, namely,

$$\left.\frac{\mathrm{d}\langle t(r_0)\rangle}{\mathrm{d}r}\right|_{r_0=0} = 0 \quad \text{and} \quad -D\left.\frac{\mathrm{d}\langle t(r_0)\rangle}{\mathrm{d}r}\right|_{r_0=R} = \kappa\,\langle t(r_0)\rangle, \tag{12.66}$$

respectively. A first integration of Eq. (12.65) leads to

$$\frac{\mathrm{d}\langle t^n(r_0)\rangle}{\mathrm{d}r_0} = -\frac{r_0}{2D} + \frac{\mathcal{A}}{r_0}. \tag{12.67}$$

Introducing the first BC, at $r = 0$, gives $\mathcal{A} = 0$. Integrating one more time yields

$$\langle t^n(r_0)\rangle = -\frac{r_0^2}{4D} + \mathcal{B}. \tag{12.68}$$

From the second BC, evaluating at $r_0 = R$, we find that

$$\mathcal{B} = \frac{R}{2}\left(\frac{1}{\kappa} + \frac{R}{2D}\right). \tag{12.69}$$

Finally, we obtain that the MFPT is given by

$$\langle t(r_0)\rangle = \frac{1}{4D}\left(R^2 - r_0^2\right) + \frac{R}{2\kappa}. \tag{12.70}$$

This last equation predicts that when $\kappa = 0$, the MFPT tends to infinity and that when $\kappa \to \infty$, the MFPT is

$$\langle t(r_0)\rangle = \frac{1}{4D}\left(R^2 - r_0^2\right). \tag{12.71}$$

If the initial position of diffusing particles is placed at the origin, this formula reduces to $R^2/4D$, as expected. It is worth remembering that, unlike the case for one dimension, in two dimensions, the factor is four instead of two (see Eq. (5.156)), and we need to use the transformation $x_0 \to L - x_0$).

To finish this section, we compute the MFPT if the particles are initially uniformly distributed. To such end, we have to perform the following integral:

$$\begin{aligned}\langle t_u(R)\rangle &= \frac{\int_0^R \int_0^{2\pi} \left[\frac{1}{4D}\left(R^2 - r_0^2\right) + \frac{R}{2\kappa}\right] r_0 \, \mathrm{d}\theta \, \mathrm{d}r_0}{\int_0^R \int_0^{2\pi} r_0 \, \mathrm{d}\theta \, \mathrm{d}r_0} \\ &= \frac{2}{R^2}\int_0^R \left[\frac{1}{4D}\left(R^2 - r_0^2\right) + \frac{R}{2\kappa}\right] r_0 \, \mathrm{d}r_0 = \frac{R^2}{8D} + \frac{R}{2\kappa}.\end{aligned} \tag{12.72}$$

This result, when $\kappa \to \infty$, reduces to $R^2/8D$, which stands for the MFPT when the perimeter boundary is perfectly absorbing.

12.2 Perfectly Absorbent Disk: External Problem

Consider a particle concentration $c(r, t)$ diffusing around a circular disk of radius R with a perfectly absorbing perimeter, $c(r = R, t) = 0$. Initially, at $t = 0$, the particles' initial position is uniformly distributed with a normalized concentration, $\varrho(r, t = 0) = 1$. Assuming angular independence, the diffusion equation is given by Eq. (12.1), namely,

$$\frac{\partial \varrho(r,t)}{\partial t} = D\left(\frac{\partial^2 \varrho(r,t)}{\partial r^2} + \frac{1}{r}\frac{\partial \varrho(r,t)}{\partial r}\right), \tag{12.1}$$

where D is the diffusivity and κ the trapping rate coefficient. The Laplace transform of this equation is

$$\frac{\partial^2 \varrho(r,s)}{\partial r^2} + \frac{1}{r}\frac{\partial \varrho(r,s)}{\partial r} = \frac{s}{D}\varrho(r,s) - \frac{1}{D}. \tag{12.73}$$

The reader can show that a particular solution of this differential equation is given by $\varrho(r, s) = 1/s$ by direct substitution. Furthermore, a solution to the homogeneous equation (without the second term on the right-hand side) may be written as Eq. (12.55). Since the solution must be finite and normalized far away from the disk, the integration constant multiplying the Bessel function $I_0(r, s)$ must be null. Consequently, a general solution is given by

$$\varrho(r,s) = \frac{1}{s} + \mathcal{A}K_0\left(\sqrt{\frac{s}{D}}r\right). \tag{12.74}$$

The integration constant $\mathcal{A}$ is computed by imposing the absorbing boundary condition at the disk perimeter, i.e.,

$$\varrho(R,s) = \frac{1}{s} + \mathcal{A} K_0\left(\sqrt{\frac{s}{D}} R\right) = 0, \tag{12.75}$$

then

$$\mathcal{A} = -\frac{1}{s\, K_0\left(\sqrt{\frac{s}{D}} R\right)}. \tag{12.76}$$

Substituting this constant into the solution yields

$$\varrho(r,s) = \frac{1}{s}\left[1 - \frac{K_0\left(\sqrt{\frac{s}{D}} r\right)}{K_0\left(\sqrt{\frac{s}{D}} R\right)}\right]. \tag{12.77}$$

Representative plots of the propagator in Eq. (12.77) are depicted in Fig. 12.3.

The flux, $\mathbf{j}(r,s)$, in Laplace space of the concentration $\varrho(r,s)$ can be calculated by means of Eq. (2.73), resulting in

$$\mathbf{j}(r,s) = -\sqrt{\frac{D}{s}} \frac{K_1\left(\sqrt{\frac{s}{D}} r\right)}{K_0\left(\sqrt{\frac{s}{D}} R\right)} \hat{\mathbf{e}}_r, \tag{12.78}$$

which can be inverted numerically.

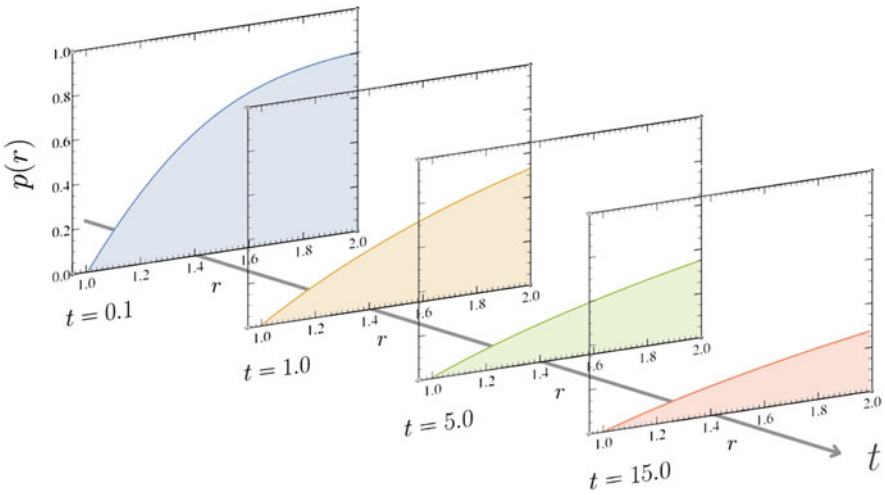

Fig. 12.3 Time evolution of the probability density $\varrho(r,t)$ given by Eq. (12.77) at different times, i.e., $t = 0.1$, $t = 1.0$, $t = 5.0$, and $t = 15.0$. The radius of the disk and the diffusion coefficient are set to $D = R = 1$. It should be noted that the solution holds for $r > R$, in this case, $r > 1$

12.3 Partially Absorbent Disk

Consider the same physical and geometrical arrangement as in the previous section but with a partially absorbing perimeter instead. Now, the integration constant $\mathcal{A}$, which appears in Eq. (12.74), should be determined by the following BC:

$$D\frac{\partial \varrho(r,s)}{\partial r}\bigg|_{r=R} = \kappa\ \varrho(r,s)\bigg|_{r=R}. \tag{12.79}$$

Using Eq. (12.74), this BC reads

$$-\mathcal{A}\sqrt{sD}K_1\left(\sqrt{\frac{s}{D}}R\right) = \kappa\ \left[\frac{1}{s} + \mathcal{A}K_0\left(\sqrt{\frac{s}{D}}R\right)\right]. \tag{12.80}$$

From this last relation, we find that

$$\mathcal{A} = -\frac{1}{s}\frac{\kappa}{\sqrt{sD}K_1\left(\sqrt{\frac{s}{D}}R\right) + \kappa K_0\left(\sqrt{\frac{s}{D}}R\right)}. \tag{12.81}$$

Substituting this constant into Eq. (12.74) leads to

$$\varrho(r,s) = \frac{1}{s}\left[1 - \frac{\kappa\ K_0\left(\sqrt{\frac{s}{D}}r\right)}{\sqrt{sD}K_1\left(\sqrt{\frac{s}{D}}R\right) + \kappa K_0\left(\sqrt{\frac{s}{D}}R\right)}\right]. \tag{12.82}$$

By setting $\kappa \to \infty$, we recover Eq. (12.77). The flux in Laplace space of the normalized concentration is given by

$$\mathbf{j}(r,s) = -\sqrt{\frac{D}{s}}\left[\frac{\kappa\ K_1\left(\sqrt{\frac{s}{D}}r\right)}{\sqrt{sD}K_1\left(\sqrt{\frac{s}{D}}R\right) + \kappa K_0\left(\sqrt{\frac{s}{D}}R\right)}\right]\hat{\mathbf{e}}_r. \tag{12.83}$$

12.4 Concentric Disks

12.4.1 Steady State: Effect of Dimensionality

In this section, we will study the *steady-state* solution of the diffusion equation in d dimensions, assuming angular independence, when diffusion takes place within two concentric spheres, long cylinders, or disks. Let us assume that the boundaries of the concentric d-dimensional system are placed at R_{in} and R_{out}, $R_{in} < R_{out}$.

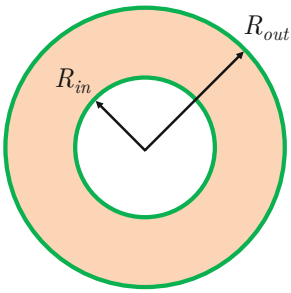

Fig. 12.4 Schematic representation of a concentric disk with radii R_{in} and R_{out}. The outer and inner perimeters (green) are kept at constant concentrations c_{in} and c_{out}, respectively

The two-dimensional cases are shown in Fig. 12.4. From Eqs. (2.16), (12.1), and (14.1), we are able to deduce that, in general, the diffusion equation in d dimension, with no angular dependence, can be written as follows:

$$\frac{\partial p(r,t)}{\partial t} = \frac{D}{r^{d-1}}\frac{\partial}{\partial r}\left(r^{d-1}\frac{\partial p(r,t)}{\partial r}\right) = D\left[\frac{\partial^2 p(r,t)}{\partial r^2} + \frac{d-1}{r}\frac{\partial p(r,t)}{\partial r}\right]. \tag{12.84}$$

By definition, a steady-state quantity yields to the same value as any latter measurement, as long as all external conditions remain constant in time. From such definition, and the use of the conservation or continuity equation, Eq. (2.72), we conclude that the flux is free of divergence and consequently Eq. (12.84) becomes

$$\frac{\partial}{\partial r}\left(r^{d-1}\frac{\partial p(r)}{\partial r}\right) = 0. \tag{12.85}$$

Thereafter, the probability flux is given by

$$\frac{\mathrm{d}}{\mathrm{d}r}\left(r^{d-1}J(r)\right) = 0. \tag{12.86}$$

By integrating Eq. (12.85) once, we obtain

$$\frac{\partial p(r)}{\partial r} = \frac{\mathcal{A}}{r^{d-1}}, \tag{12.87}$$

where $\mathcal{A}$ is a constant of integration. A second integration yields

$$p(r) = \begin{cases} \mathcal{A}\frac{r^{2-d}}{2-d} + \mathcal{B} & \text{for} \quad d \neq 2, \\ \mathcal{A}\ln(r) + \mathcal{B} & \text{for} \quad d = 2, \end{cases} \tag{12.88}$$

where $\mathcal{B}$ is also a constant of integration. As the reader may observe, at steady state, the concentration is independent of diffusivity. The probability flux is obtained

taking the derivative with respect to r of these last expressions, which is given in Eq. (12.87), and multiplying it by $-D$, namely,

$$J(r) = -D\frac{\mathcal{A}}{r^{d-1}}. \tag{12.89}$$

It is important to note that with the exception of a one-dimensional system, Eqs. (12.88) and (12.89) are singular at the origin, i.e., $r = 0$.

12.4.1.1 Constant Concentration

Our objective at this point is to apply the formulas obtained in the preceding section to a case of use: Diffusion of Brownian particles through a long hollow cylinder or concentric disks, considering that the surfaces at $r = R_{in}$ and at $r = R_{out}$ are kept at constant concentration, c_{in}, and c_{out}, respectively.[4] A schematic representation of the system in two dimensions is shown in Fig. 12.4. These systems are of practical interest since they have been frequently used to test diffusivities or thermal conductivities.

Let us start with the two-dimensional case. By imposing the BCs to Eq. (12.88) and setting $d = 2$, we find that the constants of integration are

$$\mathcal{B} = c_{in} - \mathcal{A}\ln(R_{in}), \tag{12.90}$$

and

$$\mathcal{A} = \frac{c_{out} - c_{in}}{\ln(R_{out}/R_{in})}, \tag{12.91}$$

respectively. Substituting these results into Eq. (12.88) results in

$$c(r) = \frac{c_{in}\ln\left(\frac{R_{out}}{r}\right) + c_{out}\ln\left(\frac{r}{R_{in}}\right)}{\ln\left(\frac{R_{out}}{R_{in}}\right)} \qquad \text{for} \quad d = 2. \tag{12.92}$$

The limit cases, when one of the surfaces is perfectly absorbing, are obtained by setting either c_{in} or c_{out} equal to zero. Figure 12.5 shows the steady-state concentration as a function of r predicted by Eq. (12.92).

For $d \neq 2$, by following the same procedure as in the latter case, we find

[4] It should be noted that although Eqs. (12.85) and (12.87) are written in terms of the propagator $p(r)$, we can obtain the corresponding relations for the concentration by remembering that $c(r) = Np(r)$. Therefore, the solution in Eq. (12.88) also holds for concentration.

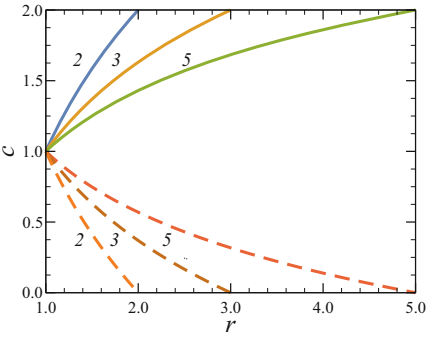

Fig. 12.5 Concentration as a function of r predicted by Eq. (12.92) for different values of R_{out}. In all cases, $R_{in} = c_{in} = 1$. The curves represented by solid lines are obtained setting $c_{out} = 2$. The curves represented by dashed lines are obtained when placing a perfectly absorbing perimeter at R_{out}; consequently, $c_{out} = 0$. The numbers on the curves indicate the values used for R_{out}

$$\mathcal{B} = c_{in} - \frac{\mathcal{A}}{2-d} R_{in}^{2-d}, \tag{12.93}$$

and

$$\mathcal{A} = \frac{(2-d)(c_{out} - c_{in})}{R_{out}^{2-d} - R_{in}^{2-d}}. \tag{12.94}$$

Inserting these equations into Eq. (12.88), we arrive at the following relation:

$$c(r) = \frac{c_{out}\left(r^{2-d} - R_{in}^{2-d}\right) + c_{in}\left(R_{out}^{2-d} - r^{2-d}\right)}{R_{out}^{2-d} - R_{in}^{2-d}} \qquad \text{for} \quad d \neq 2. \tag{12.95}$$

Once again, if one of the surfaces is perfectly absorbing, all we have to do is set either c_{in} or c_{out} equal to zero. When $d = 1$, we just have to set $2 - d = 1$. Furthermore, when $d = 3$, after some manipulation, we find that the concentration simplifies to

$$c(r) = \frac{c_{in} R_{in}(R_{out} - r) + c_{out} R_{out}(r - R_{in})}{r(R_{out} - R_{in})} \qquad \text{for} \quad d = 3. \tag{12.96}$$

Figure 12.6 shows the steady-state concentration as a function of r described by Eqs. (12.92) for $d = 2$, (12.95) when setting $d = 1$, and (12.96) for $d = 3$.

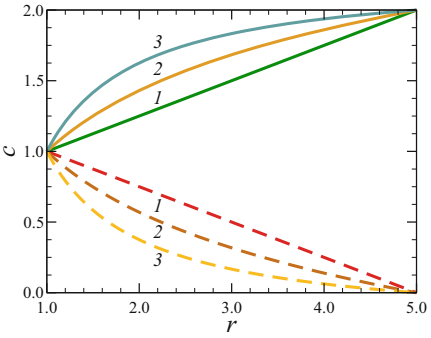

Fig. 12.6 Concentration as function of r, described by Eqs. (12.92) for $d = 2$, (12.95) when setting $d = 1$, and (12.96) for $d = 3$. In all cases, $R_{in} = c_{in} = 1$ and $R_{out} = 5$. The curves represented by continuous lines are obtained setting $c_{out} = 2$. The curves represented by dashed lines are obtained when placing a perfectly absorbent surface at $R_{out} = 5$; then, $c_{out} = 0$. The numbers on the curves are values of dimension, d

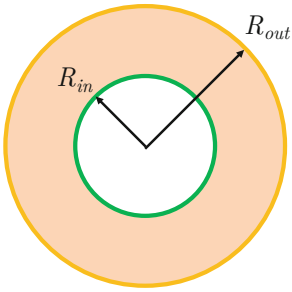

Fig. 12.7 Schematic representation of a concentric disk with radius R_{in} and R_{out}. The outer perimeter is partially absorbing (yellow), while the inner perimeter is kept at constant concentration (green)

12.4.1.2 Constant Concentration (Partially Absorbing)

A second steady-state problem leading to an interesting result is that of concentric systems whose surface at $r = R_{in}$ is kept at a constant concentration c_{in}, while at $r = R_{out}$, a partially absorbing at surface is imposed. The latter feature corresponds to a Neumann BC, given by Eq. (5.182). A schematic representation of the system in two dimensions is shown in Fig. 12.7. Now, the solution of Eq. (12.88) is subject to the following BCs:

$$c(r)\Big|_{r=R_{in}} = c(R_{in}) \quad \text{and} \quad \mathbf{J}(r)\cdot\hat{\mathbf{n}}_{R_{out}}\Big|_{r=R_{out}} = -D\frac{\partial c(r)}{\partial r}\Big|_{r=R_{out}} = \kappa\, c(R_{out}), \tag{12.97}$$

where κ is the trapping rate coefficient associated with the partially absorbing boundary at $r = R_{out}$.

Using the first boundary condition on the left-hand side of Eq. (12.88), we find that

$$\mathcal{B} = \begin{cases} c_{in} - \mathcal{A}\ln(R_{in}) & \text{for} \quad d \neq 2, \\ c_{in} - \frac{\mathcal{A}R_{in}^{2-d}}{2-d} & \text{for} \quad d = 2. \end{cases} \tag{12.98}$$

Now, imposing the second boundary condition into Eq. (12.87), we arrive at the following relations:

$$\mathcal{A} = \begin{cases} \dfrac{(2-d)\kappa c_{in} R_{in}^{d} R_{out}^{d}}{\kappa R_{in}^{2} R_{out}^{d} - R_{out} R_{in}^{d}\left[(2-d)D + \kappa R_{out}\right]} & \text{for} \quad d \neq 2, \\ \dfrac{\frac{\kappa}{D} R_{out} c_{in}}{\frac{\kappa}{D} R_{out} \ln\left(\frac{R_{in}}{R_{out}}\right) - 1} & \text{for} \quad d = 2. \end{cases} \tag{12.99}$$

By introducing these constants into Eq. (12.87), the concentration as a function of r is found, namely,

$$c(r) = \begin{cases} c_{in}\left\{\dfrac{r^{2-d} - R_{in}^{2-d}}{R_{out}^{1-d}\left[(d-2)\frac{D}{\kappa} - R_{out}\right] + R_{in}^{2-d}} + 1\right\} & \text{for} \quad d \neq 2, \\ \dfrac{c_{in}\left[1 + \frac{\kappa}{D} R_{out} \ln\left(\frac{R_{out}}{r}\right)\right]}{1 + \frac{\kappa}{D} R_{out} \ln\left(\frac{R_{out}}{R_{in}}\right)} & \text{for} \quad d = 2. \end{cases} \tag{12.100}$$

The latter equation for one and three dimensions reads

$$c(r) = \frac{c_{in}\left[\frac{\kappa}{D}\left(R_{out} - r\right) + 1\right]}{\frac{\kappa}{D}\left(R_{out} - R_{in}\right) + 1} \qquad \text{for} \quad d = 1, \tag{12.101}$$

and

$$c(r) = \frac{c_{in} R_{in}\left[r\left(D - \kappa R_{out}\right) + \kappa R_{out}^{2}\right]}{r\left[R_{in}\left(D - \kappa R_{out}\right) + \kappa R_{out}^{2}\right]} \qquad \text{for} \quad d = 3, \tag{12.102}$$

respectively. By setting $\kappa = 0$ into these formulas, we find that $c(r) = c_{in}$, as expected. Also, we can take the limit when $R_{in} = 0$ and reproduce the results for a disk.

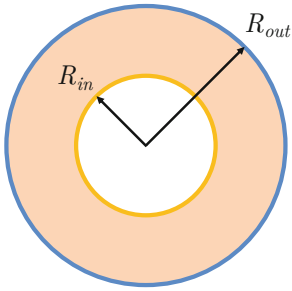

Fig. 12.8 Schematic representation of a system consisting of two concentric disks with radius R_{in} and R_{out}, respectively. The outer perimeter is perfectly reflecting (blue), while the inner perimeter is partially absorbing

12.4.2 Mean First-Passage Times in 2D: Perfectly Reflecting (Partially Absorbing)

Consider a point particle diffusing within the annulus bounded by two concentric circles of radii R_{in} and R_{out}, $R_{out} > R_{in}$. The outer circle of radius R_{out} is reflecting, while the inner circle with radius R_{in} has a uniform partially absorbing perimeter, characterized by a trapping rate κ (see Fig. 12.8). Then, the evolution equation for the mean first passage time, Eq. (12.65), is now subject to a reflecting BC at $r = R_{out}$ and a radiation BC at $r = R_{in}$, namely,

$$\left.\frac{\mathrm{d}\langle t(r_0)\rangle}{\mathrm{d}r_0}\right|_{r_0=R_{out}} = 0, \quad \text{and} \quad D\left.\frac{\mathrm{d}\langle t(r_0)\rangle}{\mathrm{d}r_0}\right|_{r_0=R_{in}} = \kappa\,\langle t(r_0)\rangle. \tag{12.103}$$

Using the first boundary condition in Eq. (12.67), we find that

$$\mathcal{A} = \frac{R_{out}^2}{2D}. \tag{12.104}$$

Consequently

$$\frac{\mathrm{d}\langle t(r_0)\rangle}{\mathrm{d}r_0} = -\frac{r_0}{2D} + \frac{R_{out}^2}{2D}\frac{1}{r_0}. \tag{12.105}$$

Integrating this last expression leads to

$$\frac{\mathrm{d}\langle t(r_0)\rangle}{\mathrm{d}r_0} = -\frac{r_0^2}{4D} + \frac{R_{out}^2}{2D}\ln r_0 + \mathcal{B}. \tag{12.106}$$

Applying the second BC, i.e., the partially absorbing boundary, to the latter equation, we are able to find $\mathcal{B}$, yielding

$$\mathcal{B} = \frac{R_{in}^2}{4D} - \frac{R_{out}^2}{2D}\ln(R_{in}) + \frac{R_{out}^2 - R_{in}^2}{2\kappa R_{in}}. \tag{12.107}$$

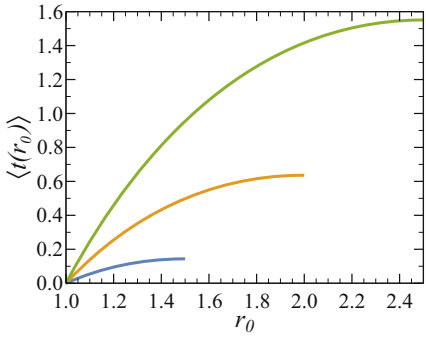

Fig. 12.9 Mean first-passage time as a function of the initial position r_0 predicted by Eq. (12.109), setting $D = R_{in} = 1$ for different values of the outer radius: $R_{out} = 1.5$ (blue line), $R_{out} = 2.0$ (yellow line), and $R_{out} = 2.5$ (green line)

By substituting this constant into Eq. (12.106), we obtain

$$\langle t(r_0)\rangle = \frac{1}{4D}\left[2R_{out}^2 \ln\left(\frac{r_0}{R_{in}}\right) - r_0^2 + R_{in}^2\right] + \frac{R_{out}^2 - R_{in}^2}{2\kappa R_{in}}. \tag{12.108}$$

Setting $\kappa \to \infty$, particles would diffuse between an inner disk with a perfectly absorbing boundary and a outer disk reflective perimeter. Then, the MFPT becomes

$$\langle t(r_0)\rangle = \frac{1}{4D}\left[2R_{out}^2 \ln\left(\frac{r_0}{R_{in}}\right) - r_0^2 + R_{in}^2\right]. \tag{12.109}$$

From Eq. (12.109), we see that Eq. (12.108) now has a clear interpretation: The first term represents the first encounter of the particle with the partially absorbing boundary when the particle starts at r_0, while the second term represents the trapping time when the particle starts at R_{out} and is later trapped. Theoretical predictions for the MFPT as a function of r_0 when $\kappa \to \infty$, given by Eq. (12.109), are shown in Fig. 12.9.

The problem of a concentric disk will be discussed in a very general way in Sect. 14.3. In this section, we will find the propagator, as well as the splitting probabilities, and we will discuss the effect of dimensionality. It is worth noting that the formulas obtained in this section identical if we switch R_{in} for R_{out}, and vice versa, leading to a reflecting inner disk and a partially absorbing outer disk.

12.5 Concluding Remarks

In this chapter, we were able to explicitly appreciate the effects of dimensionality in diffusive processes. For example, assuming angular independence, the diffusion equation becomes a Bessel function. We also introduced the concept of steady state, which is useful in many practical cases and significantly simplifies the solution of the diffusion equation.

Further Reading and References

L. Dagdug, A.M. Berezhkovskii, A.T. Skvortsov, Trapping of diffusing particles by striped cylindrical surfaces. Boundary homogenization approach. J. Chem. Phys. **142**, 234902 (2015). https://aip.scitation.org/doi/10.1063/1.4922444

L. Dagdug, A.M. Berezhkovskii, V.Yu. Zitserman, S.M. Bezrukov, Trapping of particles diffusing in two dimensions by a hidden binding site. Phys. Rev. E **103**, 012135 (2021). https://doi.org/10.1103/PhysRevE.103.012135

S. Redner, *A Guide to First-Passage Processes* (Cambridge University, Cambridge, 2001)

Chapter 13
Reaction-Diffusion Equations

Oftentimes, it is important to take into account the diffusion of components within a chemical system, people in an environment, or genes in a population, which leads to diffusion with an extra reaction term. Reaction-diffusion equations also arise naturally in systems consisting of many interacting components and are widely used to describe pattern-formation phenomena in a variety of biological, chemical, and physical systems. In this chapter, we will introduce the Turing bifurcations, a type of bifurcation arising in reaction-diffusion systems. They lead to nontrivial spatial patterns, which we will study both analytically and numerically. These patterns form instabilities in spatially extended dissipative systems driven away from equilibrium. Examples of these patterns are observed on the skin of a giant puffer fish, as well as on the formation of spots on the fur of animals. Additionally, Turing patterns have explained the shell structure and patterns observed in aquatic mollusks. This theoretical framework has become a basic model in theoretical biology.

13.1 Turing-Like Reaction-Diffusion Equations

Patterns in nature serve not only as aesthetic features, but are also necessary for locomotion, reproduction, protection, and alimentation. The periodic stripes on the skins of animals such as giraffes, zebras, or leopards, along with gradients of colors on the feathers of birds, serve various purposes such as signaling, recognition, and camouflage. Additionally, patterns are crucial for the growth and functionality of tissues including the skin, kidneys, and heart. In 1952, Alan Turing's[1] work on morphogenesis emphasized the importance of chemical gradients in generating

[1] Alan Turing, a British mathematician and computer scientist, is widely considered to be the father of computer science and artificial intelligence. He was born on June 23, 1912, in London, England, and died on June 7, 1954, in Wilmslow, Cheshire. During World War II, he worked for the

L. Dagdug et al., *Diffusion Under Confinement*,
https://doi.org/10.1007/978-3-031-46475-1_13

patterns and their determining effect on cell differentiation. In general, two-dimensional Turing patterns may spontaneously appear under completely different spatial configurations. Also, Turing structures have been exhaustively studied in different reaction-diffusion systems, such as the chlorite-dioxide-iodine-malonic acid reaction and the Belousov-Zhabotinsky reaction. In the remainder of the chapter, we will develop Turing's mechanism on reaction-diffusion systems and provide the necessary conditions for instability that lead to the formation of two-dimensional patterns.

13.1.1 Turing Mechanism

During 1952, Alan Turing published an article entitled *The Chemical Basis of Morphogenesis*, where he developed a mathematical model in which he established that, under certain conditions, two chemical substances can react and diffuse in such a way that a heterogeneous steady state is produced, leading to the emergence of spatial patterns of concentration of *morphogens*.[2] Intended to describe the mathematical structure of reaction-diffusion equations, consider a system wherein two substances, denoted as A and B, coexist and interact through a chemical reaction, meaning that A can transform into B and B into A while freely diffusing in space. Within this framework, we would expect that A and B molecules sustain a state of uniform mixture. Nevertheless, with the use of certain reaction kinetics, we may start with a homogeneous mixture of both substances and, after some time, due to small fluctuations, obtain well-defined regions of gradients of a particular chemical species.

Further exploring the model, let S be an arbitrary surface surrounding a volume V containing a certain concentration gradient of the mixture of A and B. The principle of mass conservation states that the rate of change in concentration of either substance A or B, represented in a single variable as $c_{\mathrm{A,B}}$, is equal to substance transfer across surface S, in addition to the amount of *reagents* created or destroyed inside V due to local reactions. Therefore, the number of particles per unit time present in the system must satisfy the following equation:

British government as a codebreaker and helped crack the German Enigma code. He made major contributions to mathematics, cryptanalysis, logic, philosophy, and mathematical biology.

[2] In the context of developmental biology, the term *morphogen* is associated with signaling molecules secreted in a limited region of a tissue that diffuse away from the source where they generate a concentration gradient. This molecule is produced by embryonic cells and is characterized by its ability to spread and act at a distance on other cells or tissues, besides being able to acquire positional information for spatial organization in the formation of complex structures, such as organs in embryonic development. Throughout the book, morphogens will be considered as Brownian point particles.

$$\frac{\partial}{\partial t}\int_V c_{\mathrm{A,B}}(\mathbf{r},t)\,\mathrm{d}v = -\int_S \mathbf{J}_{\mathrm{A,B}}\cdot\hat{\mathbf{n}}\,\mathrm{d}A + \int_V f_{\mathrm{A,B}}\,\mathrm{d}v, \tag{13.1}$$

where $\mathbf{J}_{\mathrm{A,B}}$ is the flux, $f_{\mathrm{A,B}}$ is a scalar function representing the rate of chemical creation and annihilation, while $\hat{\mathbf{n}}$ is the unit normal vector to the surface, and $\mathrm{d}A$ and $\mathrm{d}v$ are the infinitesimal area and volume elements, respectively. Assuming that the concentration is a continuous function, meaning a smooth and differentiable curve, we invoke the divergence theorem

$$\int_V \nabla\cdot\mathbf{F}\,\mathrm{d}v = \int_S \mathbf{F}\cdot\hat{\mathbf{n}}\,\mathrm{d}A, \tag{13.2}$$

with $\mathbf{F}$ being a continuously differentiable vector field in the neighborhood of S. By applying the latter equation to the first term of the right-hand side of Eq. (13.1), we arrive at

$$\int_V \left[\frac{\partial c_{\mathrm{A,B}}(\mathbf{r},t)}{\partial t} + \nabla\cdot\mathbf{J}_{\mathrm{A,B}} - f_{\mathrm{A,B}}\right] = 0. \tag{13.3}$$

For the last equation to hold true for any given volume V, the argument of the function must necessarily vanish, resulting in a new conservation equation for $c_{\mathrm{A,B}}$, namely,

$$\frac{\partial c_{\mathrm{A,B}}(\mathbf{r},t)}{\partial t} + \nabla\cdot\mathbf{J}_{\mathrm{A,B}} = f_{\mathrm{A,B}}(c_{\mathrm{A,B}},\mathbf{r},t), \tag{13.4}$$

where we have indicated that the function $f_{\mathrm{A,B}}$ may generally depend on concentration, position, and time, i.e., $f_{\mathrm{A,B}} = f_{\mathrm{A,B}}(c_{\mathrm{A,B}},\mathbf{r},t)$. By substituting the conservation equation, which is

$$\mathbf{J}(\mathbf{r},t) = -D\nabla c(\mathbf{r},t), \tag{2.74}$$

we obtain

$$\frac{\partial c_{\mathrm{A,B}}(\mathbf{r},t)}{\partial t} = f_{\mathrm{A,B}}(c_{\mathrm{A,B}},\mathbf{r},t) + \nabla\cdot\big(D\nabla c_{\mathrm{A,B}}(\mathbf{r},t)\big). \tag{13.5}$$

For the above equation, D is a 2×2 diagonal matrix of diffusion coefficients. In the generalization of Eq. (13.5), when considering m chemical species that interact with each other, there will be a column vector $c_i(\mathbf{r},t)$ (for $i = 1,2,3,\cdots,m$) that represents the concentration of every substance, each diffusing with a diffusion coefficient D_i and interacting according to $f_{1,2,3,\cdots,m}$. Furthermore, given the condition of a diagonal matrix with constant entries, we have that

$$\frac{\partial c_{\mathrm{A,B}}(\mathbf{r},t)}{\partial t} = D_{\mathrm{A,B}}\nabla^2 c_{\mathrm{A,B}}(\mathbf{r},t) + f_{\mathrm{A,B}}. \tag{13.6}$$

In the original case of a mixture of two chemical species A and B, Eq. (13.6) is decomposed to yield two equations[3]

$$\frac{\partial c_{\mathrm{A}}(\mathbf{r},t)}{\partial t} = f + D_{\mathrm{A}}\nabla^2 c_{\mathrm{A}}(\mathbf{r},t) \quad \text{and} \tag{13.7}$$

$$\frac{\partial c_{\mathrm{B}}(\mathbf{r},t)}{\partial t} = g + D_{\mathrm{B}}\nabla^2 c_{\mathrm{B}}(\mathbf{r},t), \tag{13.8}$$

that is, a system of reaction-diffusion equations. Our goal in this section will be to solve a system of partial differential equations (PDEs) for two chemical substances, satisfying Turing conditions that ultimately lead to spatial pattern formation.

In the absence of diffusion, i.e., $D_{\mathrm{A}} = D_{\mathrm{B}} = 0$, the system containing both species A and B tends to a stable linear steady state. The instability arises when the elements, diffusion, and reaction combine, specifically when $D_{\mathrm{A}} \neq D_{\mathrm{B}}$. Now, allow us to make additional assumptions: Let chemical species A be an *activating reagent* and species B an *inhibitory reagent*, where $D_{\mathrm{B}} >> D_{\mathrm{A}}$, and make the starting position of reagents $r_{\mathrm{A}0}$ and $r_{\mathrm{B}0}$. Under these circumstances, the inhibitory substance prevents the distribution of the activator; thus, the space available for the activator to react and diffuse is restricted to a finite domain that depends on the ratio $D_{\mathrm{B}}/D_{\mathrm{A}}$ and certain specific reaction parameters. On the contrary, if instead of having a single initial point of reagent concentration, we have several random starting positions, we would have a heterogeneous spatial distribution in the steady state, with well-defined activator and inhibitor regions. Moreover, if both species diffuse at the same rate, that is, $D_{\mathrm{A}} = D_{\mathrm{B}}$, the system cannot develop any kind of pattern.

This is the Turing mechanism, a simple system with impressive results. The emergence of instability is due to the combination of two individual models that are stable when isolated. Diffusion leads to instability in the interaction of two reagents. In the following sections, we derive Turing conditions, to later present a simple model that has all the aforementioned characteristics, leading to two-dimensional patterns.

13.2 Turing Conditions

Reaction-diffusion equations consisting of one or more chemical substances experience the so-called Turing instability when the system has a stable steady state that is invariant to small perturbations in the absence of diffusion and becomes unstable to those perturbations in its presence. Therefore, it is referred to as having *diffusion-*

[3] Notice that we have set $f_{\mathrm{A}} = f$ and $f_{\mathrm{B}} = g$. These functions will be describing the reaction kinetics of the system, indicating the way in which the substances are transformed into each other. It is an inherent characteristic that these functions are always nonlinear so to induce Turing instability.

driven instability.[4] Furthermore, all reaction-diffusion systems, such as Eqs. (13.7) and (13.8), have a dimensionless version that can be written in the following form:[5]

$$\frac{\partial u(\mathbf{r},t)}{\partial t} = \gamma f(u,v) + \nabla^2 u(\mathbf{r},t), \qquad \frac{\partial v(\mathbf{r},t)}{\partial t} = \gamma g(u,v) + d\,\nabla^2 v(\mathbf{r},t), \tag{13.9}$$

where now $u(\mathbf{r},t)$ takes the place of $c_{\mathrm{A}}(\mathbf{r},t)$ and $v(\mathbf{r},t)$ of $c_{\mathrm{B}}(\mathbf{r},t)$, whereas d is the diffusion coefficient ratio $D_{\mathrm{v}}/D_{\mathrm{u}}$ and γ can take one of the following interpretations:

- $\gamma^{1/2}$ is proportional to the linear size of the spatial domain in one dimension. When working with a two-dimensional system, γ is proportional to the surface area.
- γ represents the relative force between reagent terms. This may cause an increase in γ to produce an increase in a activity of some constraints in the step of the reaction sequence.
- an increase in γ could lead to the attenuation of the ratio d.

The formation of spatial patterns strongly depends on the choice of functions f and g, together with the specific values assigned to γ and d. Therefore, we must derive the necessary conditions so that the system shows stability in the absence of diffusion and instability when diffusion is included. For this purpose, we follow the traditional approach of deriving the so-called Turing conditions.

As in most problems involving an ordinary differential equation (ODE) or a partial differential equation (PDE), boundary and initial conditions are needed to give a unique solution to the problem. Considering given initial conditions and reflecting BCs, the latter are determined by[6]

$$\nabla \begin{pmatrix} u(\mathbf{r},t) \\ v(\mathbf{r},t) \end{pmatrix} \Bigg|_{\mathbf{r}=\partial\Omega} \cdot \hat{\mathbf{n}} = 0, \tag{13.10}$$

corresponding to a Neumann BC, where $\partial\Omega$ is the external boundary and $\hat{\mathbf{n}}$ is the unit normal vector to the surface. The relevant homogeneous steady state of Eq. (13.9) is given by the positive solution of

$$f(u,v) = 0, \qquad g(u,v) = 0. \tag{13.11}$$

[4] In an ecological context, such behavior becomes apparent as spatial disturbances give rise to oscillatory patterns in the population dynamics of the endemic species.

[5] When all the terms of an ordinary differential equation (ODE) or partial differential equation (PDE) describing a physical phenomenon are dimensionally homogeneous, we can define appropriate parameters in order to obtain a dimensionless version of the equation. For such purpose, we use the *Vaschy-Buckingham π theorem*. This type of simplification reduces the number of variables in the equation and uncovers the underlying relationships between them.

[6] By defining this type of BC, the study is restricted to self-organizing spatial patterns. The null flux BC implies that there are no external contributions to the system.

We are especially interested in the linear stability of the steady state when no spatial variations are occurring, i.e., the homogeneous linearly stable steady state. In the absence of diffusion, Eq. (13.9) is reduced to

$$\frac{\partial u(\mathbf{r},t)}{\partial t} = \gamma f(u,v), \qquad \frac{\partial v(\mathbf{r},t)}{\partial t} = \gamma g(u,v). \tag{13.12}$$

Intending to perform a local linearization around (u_0, v_0),[7] as shown in Appendices 13.A and 13.B, we define

$$\mathbf{c}_{u,v}(\mathbf{r},t) \equiv \begin{pmatrix} u(\mathbf{r},t) - u_0 \\ v(\mathbf{r},t) - v_0 \end{pmatrix}. \tag{13.13}$$

Thus, Eq. (13.12) is written as (see Eqs. (13.83) and (13.93))

$$\frac{\partial \mathbf{c}_{u,v}(\mathbf{r},t)}{\partial t} = \gamma \mathbb{A} \mathbf{c}_{u,v}(\mathbf{r},t), \tag{13.14}$$

where, according to Eq. (13.83),[8]

$$\mathbb{A} = \begin{pmatrix} f_u & f_v \\ g_u & g_v \end{pmatrix}_{u_0,v_0}. \tag{13.15}$$

Therefore, the eigenvalue problem of Eq. (13.14) is described as follows:

$$|\gamma \mathbb{A} - \lambda \mathbb{I}| = \begin{vmatrix} \gamma f_u - \lambda & \gamma f_v \\ \gamma g_u & \gamma g_v - \lambda \end{vmatrix} = 0, \tag{13.16}$$

After some algebraic manipulations, we obtain

$$\lambda^2 - \gamma(f_u + g_v)\lambda + \gamma^2(f_u g_v - f_v g_u) = 0, \tag{13.17}$$

and by solving for λ, we arrive at

[7] Corresponding to the points where the functions vanish, are undefined, or discontinuous.

[8] The subscripts u_0, v_0 in the stability matrix, denoting the evaluation of the matrix at critical points, will be omitted from now on. Furthermore, for the sake of simplifying notation, unless otherwise indicated, the derivatives of functions f and g with respect to either u and v will always be evaluated at critical points.

$$\begin{aligned}\lambda_{1,2} &= \frac{\gamma}{2}\left[(f_u + g_v) \pm \sqrt{(f_u + g_v)^2 - 4(f_u g_v - f_v g_u)}\right] \\ &= \frac{\gamma}{2}\left[\mathrm{Tr}(\mathbb{A}) \pm \sqrt{\mathrm{Tr}(\mathbb{A})^2 - 4\mathrm{Det}(\mathbb{A})}\right].\end{aligned} \tag{13.18}$$

A stable node is present for $\lambda_i < \lambda_j < 0$ $(i, j = 1, 2)$, as the trajectories asymptotically approach the critical point as t tends to infinity. We can verify that for Re $(\lambda) < 0$, all corresponding terms in the equation must be strictly negative, yielding

$$\mathrm{Tr}(\mathbb{A}) = f_u + g_v < 0, \qquad \mathrm{Det}(\mathbb{A}) = f_u g_v - f_v g_u > 0. \tag{13.19}$$

As the reader may note, the critical points strongly depend on the choice of kinetic reaction, and the inequalities in Eq. (13.19) impose constraints on the parameters that determine the eigenvalues.

Once we have established stability in the absence of diffusion, we return to the original reaction-diffusion equations to demand instability in the spatial coordinates. The reaction-diffusion equations, Eq. (13.9), can be written as a single expression, by using Eq. (13.13), as follows:

$$\frac{\partial \mathbf{c}_{u,v}(\mathbf{r}, t)}{\partial t} = \gamma \mathbb{A}\mathbf{c}_{u,v}(\mathbf{r}, t) + \mathbb{D}\nabla^2 \mathbf{c}_{u,v}(\mathbf{r}, t), \tag{13.20}$$

where $\mathbb{D}$ is a diagonal matrix of diffusion coefficients, given by

$$\mathbb{D} = \begin{pmatrix} 1 & 0 \\ 0 & d \end{pmatrix}. \tag{13.21}$$

Equation (13.20) will be linearized around[9] $\mathbf{c}_{u,v} = 0$ and solved together with the BCs in Eq. (13.10). Assuming a separable solution of the form $\mathbf{c}_{u,v}(\mathbf{r}, t) = T(t)\boldsymbol{\chi}_{u,v}(\mathbf{r})$ for the system of PDEs in Eq. (13.20), two ODEs arise, namely,[10]

$$\frac{1}{T(t)}\frac{\mathrm{d}T(t)}{\mathrm{d}t} = \lambda \quad \text{and} \quad \gamma \mathbb{A}\boldsymbol{\chi}_{u,v}(\mathbf{r}) + \mathbb{D}\nabla^2 \boldsymbol{\chi}_{u,v}(\mathbf{r}) = \lambda \mathbb{I}\boldsymbol{\chi}_{u,v}(\mathbf{r}), \tag{13.22}$$

where λ is the separation constant and $\mathbb{I}$ is the 2×2 identity matrix. On one hand, the solution to the ODE in time is given by

$$T(t) = \mathcal{E}e^{\lambda t}, \tag{13.23}$$

[9] See Appendix 13.B for further details on linearization around the origin.

[10] Notice that $T(t)$ is a usual ODE, while $\boldsymbol{\chi}(\mathbf{r})$ is a column matrix with two rows containing second-order ODEs.

with $\mathcal{E}$ being an integration constant. On the other hand, in the one-dimensional case where $\mathbf{r} \to x$, along the interval $x \in [0, L]$, the spatial functions in $\boldsymbol{\chi}(\mathbf{x})_{u,v}$ satisfy the following equation:

$$\frac{\mathrm{d}^2 \chi_{u,v}(x)}{\mathrm{d}x^2} + k_{ij}^2 \chi_{u,v}(x) = 0, \tag{13.24}$$

with $k_{ij}^2 = \mathbb{D}_{ij}^{-1}\left(\lambda - \gamma \mathbb{A}_{ij}\right)$, since

$$\boldsymbol{\chi}_{u,v}(x) = \begin{pmatrix} \chi_u(x) \\ \\ \chi_v(x) \end{pmatrix}. \tag{13.25}$$

The analytic solution of Eq. (13.24) for each of the substances u and v is given by a linear combination of trigonometric functions or, equivalently, an imaginary exponential, namely,

$$\boldsymbol{\chi}_{u,v}(x) = \mathcal{A}\cos\left(k_{ij}x\right) + \mathcal{B}\sin\left(k_{ij}x\right). \tag{13.26}$$

where $\mathcal{A}$ and $\mathcal{B}$ are integration constants. By using the BCs in Eq. (13.10), we conclude that[11]

$$\boldsymbol{\chi}_{u,v,n}(x) = \mathcal{A}_n \cos\left(\frac{n\pi x}{L}\right) \quad \text{with} \quad n = 1, 2, 3, \ldots \tag{13.27}$$

for $k = k_{11} = k_{22} = n\pi/L$. The general solution, as a spectral representation, is a superposition of the product of functions $\mathbf{T}(t)$ and $\boldsymbol{\chi}_{u,v,n}(x)$, i.e.,

$$\mathbf{c}_{u,v}(x,t) = \sum_n \mathcal{C}_n e^{\lambda t} \boldsymbol{\chi}_{u,v,n}(x). \tag{13.28}$$

All constants $\mathcal{C}_n$ are determined by Fourier expansion and the use of initial conditions. By substituting the latter solution into Eq. (13.28), we arrive at

$$\frac{\partial}{\partial t}\left(\mathcal{C}_n e^{\lambda t} \boldsymbol{\chi}_{u,v,n}(x)\right) = \gamma \mathbb{A} \mathcal{C}_n e^{\lambda t} \boldsymbol{\chi}_{u,v,n}(x) + \mathbb{D}\frac{\partial^2}{\partial x^2}\left(\mathcal{C}_n e^{\lambda t} \boldsymbol{\chi}_{u,v,n}(x)\right), \tag{13.29}$$

and after rearrangement, we find

$$\lambda \mathcal{C}_n e^{\lambda t} \boldsymbol{\chi}_{u,v,n}(x) = \gamma \mathbb{A} \mathcal{C}_n e^{\lambda t} \boldsymbol{\chi}_{u,v}(x) - \mathbb{D}\mathcal{C}_n e^{\lambda t} k^2 \boldsymbol{\chi}_n(x). \tag{13.30}$$

[11] See Sect. 5.2.1 for the solution of a diffusion one-dimensional problem with reflecting boundaries.

In the view of need for nontrivial solutions for $\mathbf{c}_{u,v}(x,t)$ in the implementation of λ, we state that

$$|\lambda\mathbb{I} - \gamma\mathbb{A} + \mathbb{D}k^2| = 0, \tag{13.31}$$

which, by explicitly using $\mathbb{D}$ and $\mathbb{A}$, results in

$$\left|\begin{pmatrix}\lambda & 0\\ 0 & \lambda\end{pmatrix} - \gamma\begin{pmatrix}f_u & f_v\\ g_u & g_v\end{pmatrix}_{u_0,v_0} + k^2\begin{pmatrix}1 & 0\\ 0 & d\end{pmatrix}\right| = \begin{vmatrix}\lambda - \gamma f_u + k^2 & -\gamma f_v\\ -\gamma g_u & \lambda - \gamma g_v + k^2 d\end{vmatrix} = 0. \tag{13.32}$$

Following a small computation, we obtain

$$\lambda^2 + \lambda\Big[k^2 + d\,k^2 - \gamma(f_u + g_v)\Big] + d\,k^4 - k^2\gamma(d\,f_u + g_v) + \gamma^2(f_u g_v - f_v g_u) = 0, \tag{13.33}$$

or

$$\lambda^2 + \lambda\Big[k^2(1+d) - \gamma\mathrm{Tr}(\mathbb{A})\Big] + k^2\Big[d\,k^2 - \gamma(d\,f_u + g_v)\Big] + \gamma^2\mathrm{Det}(\mathbb{A}) = 0. \tag{13.34}$$

Using the relations in Eq. (13.19), together with the definition of

$$h(k^2) \equiv k^2\Big[d\,k^2 - \gamma(d\,f_u + g_v)\Big] + \gamma^2\mathrm{Det}(\mathbb{A}), \tag{13.35}$$

yields

$$\lambda^2 + \lambda\Big[k^2(1+d) - \gamma(f_u + g_v)\Big] + h(k^2) = 0, \tag{13.36}$$

which is a simplified version of Eq. (13.33).

The steady state (u_0, v_0) is linearly stable if both solutions of Eq. (13.36) satisfy Re $\lambda < 0$. The analysis of constraints for the stable steady state in the absence of diffusion was previously considered, corresponding to $k^2 = 0$, in which case, the relations in Eq. (13.19) must be fulfilled simultaneously. Additionally, if we require the steady state to be unstable to small perturbations in coordinates, when both reaction and diffusion are studied, we need that Re $\lambda > 0$ for all values of k different from zero. Now, solving for λ in Eq. (13.36), we obtain

$$\lambda_{1,2} = \frac{1}{2}\left\{\gamma(f_u + g_v) - k^2(1+d) \pm \sqrt{\left[k^2(1+d) - \gamma(f_u + g_v)\right]^2 - 4\,h(k^2)}\right\}. \tag{13.37}$$

From Eq. (13.19), we know that $\mathrm{Tr}(\mathbb{A}) = (f_u + g_v) < 0$. Moreover, it is clear that $k^2(1+d) > 0$, then

$$k^2(1+d) - \gamma(f_u + g_v) > 0. \tag{13.38}$$

As the reader may note, the only way in which Re $\lambda(k^2) > 0$ is true is if $h(k^2) < 0$, which in turn holds if $(d\, f_u + g_v) > 0$! A potential contradiction seems to arise in this last statement, since already established that $(f_u + g_v) < 0$ in Eq. (13.19). However, the intersection of constraints requires that $d \neq 1$ together with a sign difference between derivatives f_u and g_v. Hence,

$$d\, f_u + g_v > 0, \quad \text{with} \quad d \neq 1. \tag{13.39}$$

In the case where $f_u > 0$ and $g_v < 0$, then $d > 1$, and it follows that v is the activator of u while u inhibits v.[12] The inequality in Eq. (13.39) is necessary but insufficient to ensure that Re $\lambda > 0$. Therefore, we must fully consider $h(k^2)$. Within this framework, the minimum with respect to k^2 of function $h(k^2)$ must be negative, leading to

$$\frac{\partial}{\partial k^2}\left[d\, k^4 - k^2\gamma(d\, f_u + g_v) + \gamma^2 \text{Det}(\mathbb{A})\right] = 0, \tag{13.40}$$

or

$$2d\, k^2 - \gamma(d\, f_u + g_v) = 0, \tag{13.41}$$

from which we find that

$$k^2_{min} = \frac{(d\, f_u + g_v)}{2d}\gamma, \tag{13.42}$$

where the subscript min indicates that the correct value of k^2 minimizes $h(k)$. By substituting this last relation in $h(k^2)$, we find

$$\begin{aligned} h_{min}(k^2_{min}) &= d\left[\frac{\gamma(d\, f_u + g_v)}{2d}\right]^2 - \left[\frac{\gamma(d\, f_u + g_v)}{2d}\right]\gamma(d\, f_u + g_v) + \gamma^2 \text{Det}(\mathbb{A}) \\ &= \gamma^2\left[\text{Det}(\mathbb{A}) - \frac{(d\, f_u + g_v)^2}{4d}\right]. \end{aligned} \tag{13.43}$$

For this last value to be negative, we have that

$$\frac{(d\, f_u + g_v)^2}{4d} > \text{Det}(\mathbb{A}). \tag{13.44}$$

In addition, we define the critical diffusion coefficient ratio d_c when

[12] It is important to note that in an activator-inhibitor mechanism, the inhibitor reagent must diffuse more rapidly than the activator reagent.

$$\frac{(d\, f_u + g_v)^2}{4d} = \text{Det}(\mathbb{A}). \tag{13.45}$$

from which we see that it is determined by

$$d_c^2 f_u^2 + 2d_c(2 f_v g_u - f_u g_v) + g_v^2 = 0. \tag{13.46}$$

Furthermore, by substituting d_c in Eq. (13.42) and using Eq. (13.44), we obtain the critical wave number, namely,

$$k_c^2 = \frac{(d_c f_u + g_v)}{2d_c}\gamma = \gamma \left[\frac{\text{Det}(\mathbb{A})}{d_c}\right]^{1/2}, \tag{13.47}$$

thus,

$$k_c^2 = \gamma \left[\frac{f_u g_v - f_v g_u}{d_c}\right]^{1/2}. \tag{13.48}$$

The domain of the unstable wave number is found through the roots of $h(k)$, specifically,

$$h(k^2) = dk^4 - k^2\gamma(df_u + g_v) + \gamma^2 \text{Det}(\mathbb{A}) = 0, \tag{13.49}$$

yielding

$$k_{1,2}^2 = \frac{\gamma}{2d}\left[(d\, f_u + g_v) \pm \sqrt{(d\, f_u + g_v)^2 - 4\, d \cdot \text{Det}(\mathbb{A})}\right]. \tag{13.50}$$

The dominant terms in the solution of Eq. (13.28) are those that meet the condition $\text{Re}\ \lambda(k^2) > 0$, since all other terms tend to zero exponentially. Moreover, the linearly unstable eigenfunctions, which grow exponentially in time, will eventually be bounded by the nonlinear terms in the reaction-diffusion equations, leading to a spatially inhomogeneous steady-state solution.

In this section, we obtained the conditions for the generation of spatial patterns using a system of reaction-diffusion equations, i.e., Eq. (13.9). A compact overview of such conditions, i.e., Turing conditions, is provided below

$$f_u + g_v < 0, \qquad f_u g_v - f_v g_u > 0, \tag{13.51}$$

$$df_u + g_v > 0, \quad \text{and} \quad (df_u + g_v)^2 - 4d(f_u g_v - f_v g_u) > 0. \tag{13.52}$$

According to our analysis, the derivatives f_u and g_v, when evaluated at the critical points, must have opposite signs, for instance, $f_u > 0$, $g_v < 0$, while $d > 1$. Therefore, there are two different possibilities for cross terms in $\mathbb{A}$. Since the only restriction is that $f_v g_u < 0$, we can set $f_v > 0$ and $g_u < 0$, or $f_v < 0$, $g_u > 0$,

which indicates two different kinds of reactions. In terms of the stability matrix, we have the following two cases:

$$\begin{pmatrix} f_u & f_v \\ g_u & g_v \end{pmatrix} \to \begin{pmatrix} + & - \\ + & - \end{pmatrix}, \tag{13.53}$$

and

$$\begin{pmatrix} f_u & f_v \\ g_u & g_v \end{pmatrix} \to \begin{pmatrix} + & + \\ - & - \end{pmatrix}. \tag{13.54}$$

In the first case, u is the activator reagent for both itself and v, whereas v serves as the inhibitor reagent for u. This configuration is known as a *pure activator-inhibitor system*. In contrast, in the second case, u activates its own production while inhibits the production of v, and v activates u while self-inhibiting. The latter configuration is referred to as a *cross activation and inhibition system*.

13.3 Gierer-Meinhardt Model

The *Gierer-Meinhardt model*, introduced in 1972 by Alfred Gierer and Hans Meinhardt in a paper titled *Theory of biological pattern formation*, is a mathematical model that describes the formation of patterns in biological systems by using two reaction-diffusion equations describing the concentration of two substances classified as activator and inhibitor: On the one hand, the activator is a short-range substance that promotes the formation of patterns, and on the other hand, the inhibitor is a long-range substance that inhibits the formation of patterns. The small initial variations, disturbances in concentration, and interactions between these reagents can create regions with different concentrations, resulting in the emergence of stripes, spots, or other types of patterns. The Gierer-Meinhardt model has been a turning point for its simplicity and success in explaining and reproducing a variety of biological patterns.

In the remainder of the chapter, we study a dimensionless version of the Gierer-Meinhardt model in one and two dimensions, find the Turing conditions for instability, and provide visual results on the formation of spatial patterns.

Gierer-Meinhardt

Consider two chemical substances whose concentrations at position x and time t are described by functions $u(x,t)$ and $v(x,t)$. A dimensionless version of the Gierer-Meinhardt model is written as follows:

$$\frac{\partial u(x,t)}{\partial t} = D_u \frac{\partial^2 u(x,t)}{\partial x^2} + \frac{u(x,t)^2}{v(x,t)} - b\,u(x,t), \tag{13.55}$$

$$\frac{\partial v(x,t)}{\partial t} = D_v \frac{\partial^2 v(x,t)}{\partial x^2} + u(x,t)^2 - v(x,t). \tag{13.56}$$

In this case, u is the activator reagent and v the inhibitor, while b represents a parameter linked to the degradation of the substance, solely acting on the activator, i.e., the reaction rate. First, we analyze the stability of the system in the absence of diffusion by following the exact same procedure as in Eq. (13.2). Under this consideration, the latter two equations are reduced to

$$\frac{\partial u(x,t)}{\partial t} = f(u,v) = \frac{u(x,t)^2}{v(x,t)} - b\,u(x,t), \tag{13.57}$$

$$\frac{\partial v(x,t)}{\partial t} = g(u,v) = u(x,t)^2 - v(x,t). \tag{13.58}$$

The critical points are computed by making $f(u^*, v^*)$ and $g(u^*, v^*)$ identically zero, from which we find that

$$(u^*, v^*) = \left(\frac{1}{b}, \frac{1}{b^2}\right). \tag{13.59}$$

The stability matrix of the system is then given by

$$\mathbb{A} = \begin{pmatrix} f_u & f_v \\ g_u & g_v \end{pmatrix} = \begin{pmatrix} b & -b^2 \\ 2/b & -1 \end{pmatrix}. \tag{13.60}$$

For this particular case, the stability conditions in Eq. (13.19) are

$$\mathrm{Tr}(\mathbb{A}) = b - 1 < 0, \quad \text{and} \quad \mathrm{Det}(\mathbb{A}) = b > 0. \tag{13.61}$$

The above conditions induce a restriction on the values that b can take, i.e., $b \in [0, 1]$. Now, we induce instability in the presence of diffusion. Intending to linearize around (u^*, v^*), we define

$$\mathbf{c}_{u,v}(x,t) \equiv \begin{pmatrix} u(x,t) - u^* \\ v(x,t) - v^* \end{pmatrix} \tag{13.62}$$

leading to a set of reaction-diffusion equations of the form

$$\frac{\partial \mathbf{c}_{u,v}(x,t)}{\partial t} = \left[\begin{pmatrix} D_u & 0 \\ 0 & D_v \end{pmatrix} \frac{\partial}{\partial x} + \begin{pmatrix} b & -b^2 \\ 2/b & -1 \end{pmatrix} \right] \mathbf{c}_{u,v}(x,t). \tag{13.63}$$

Since we have already dealt with the general problem in Sect. 13.27, we can assert that the solutions are

$$\mathbf{c}_{u,v}(x,t) = \begin{pmatrix} \mathcal{A} \\ \mathcal{B} \end{pmatrix} \cos(k\,x) e^{\lambda t}, \tag{13.64}$$

where the BCs are those of Eq. (13.10) and $\mathcal{A}$ together with $\mathcal{B}$ are integration constants. The eigenvalue problem yields to (see Eq. (13.31))

$$\lambda^2 + \lambda \left[1 - b + k^2 (D_u + D_v) \right] + h(k^2) = 0, \tag{13.65}$$

where

$$h(k^2) = k^4 D_u D_v + k^2 (D_u - b\, D_v) + b. \tag{13.66}$$

Equating the above equation to zero, we find that

$$k_{1,2}^2 = \frac{(b\, D_v - D_u) \pm \sqrt{(bD_v - D_u)^2 - 4 D_u D_v b}}{2 D_u D_v}. \tag{13.67}$$

Depending on the type of solution obtained from the previous equation, the two following cases may emerge:

$$b\, D_v - D_u > 2\sqrt{D_u D_v b}, \text{ for different and positive roots,}$$

$$b\, D_v - D_u = 2\sqrt{D_u D_v b}, \text{ for equal and positive roots.}$$

Then, by minimizing $h(k^2)$ with respect to k^2, we find that the minimum is at

$$k_{min}^2 = \frac{(bD_v - D_u)}{2 D_u D_v}, \tag{13.68}$$

and by using Eq. (13.46), we conclude that the diffusion coefficient ratio is given by

$$d_c = \frac{D_v}{D_u} = \frac{3 \pm 2\sqrt{2}}{b}. \tag{13.69}$$

13.3.1 Turing Domain

A *Turing domain* is a domain or region encompassing all possible values of the reaction parameters that lead to the formation of patterns. More specifically, given the inequalities of (13.51) and (13.52), or Eqs. (13.61) and (13.69) for the Gierer-Meinhardt model, we are able to determine a parameter space in which the system

is unstable to small perturbations in space.[13] Furthermore, as long as the Turing conditions are satisfied and k is within the interval of k_1 and k_2, according to Eq. (13.67), then the eigenfunctions of Eq. (13.64) will be linearly unstable.

In Sect. 13.2, we set Neumann BCs to avoid external interaction with the system. This condition can also be physically implemented by enforcing periodic BCs of the form

$$\begin{pmatrix} u(0,t) \\ \\ v(0,t) \end{pmatrix} = \begin{pmatrix} u(\mathbf{r},t) \\ \\ v(\mathbf{r},t) \end{pmatrix}_{\mathbf{r}=\partial\Omega} . \tag{13.71}$$

Thereafter, the solutions expressed in Eq. (13.28) are now represented using a cosine function, specifically,[14]

$$\mathbf{c}_{u,v}(x,t) = \sum_n \mathcal{C}_n e^{\lambda t} \cos(kx), \tag{13.72}$$

with

$$k = \frac{2n\pi}{L}, \tag{13.73}$$

which is the appropriate value to satisfy the BCs. We can see that the minimum admissible value of k is $2\pi/L$, with $n = 1$. Overall, the smallest value for L corresponds to the maximum value of k, that is,

$$k_{max}^2 = \frac{(b\,D_v - D_u) + \sqrt{(bD_v - D_u)^2 - 4D_u D_v b}}{2D_u D_v} = \frac{4\pi^2}{L_c^2}, \tag{13.74}$$

where L_c is the critical length of the system; below this value, patterns cannot arise.

In the following sections, we address the numerical solution to the reaction-diffusion equations and present characteristic plots of concentration patterns in both

[13] Notice that the inequalities in Eq. (13.52) simplify to

$$\frac{D_v}{D_u} b - 1 > 0, \quad \text{and} \quad D_u - 6D_v b + \frac{D_v^2 b^2}{D_u} > 0 \tag{13.70}$$

regarding the reaction-diffusion system in Eqs. (13.55) and (13.56). Both of the latter inequalities lead to the same threshold, which leads us to Eq. (13.69).

[14] It should be noted that Turing conditions are identical regardless of whether Neumann or periodic BCs are applied. This applies to most of the remaining parameters, including the critical diffusivity ratio d_c and the roots of k in Eq. (13.50). The unique difference arises in the quantization of k in Eq. (13.73) and the one used in Eq. (13.27). Such disagreement results in a different critical length for each type of BCs. Nonetheless, a suitable selection of these conditions allows for the observation of spatial pattern formation.

one and two-dimensional spatial domains. In both instances, we will use periodic BCs, as they contribute to optimizing computation time in numerical methods.

13.4 Pattern Formation: One-Dimensional Model

In the preceding section, we concluded that by satisfying the Turing conditions and selecting a value for k from the interval defined by k_1 and k_2, the reaction-diffusion system exhibits instability due to small spatial perturbations, also called *Turing instability*. When considering values outside the Turing domain, there are *bifurcation points*, i.e., critical points of the system in which stability transitions can occur, e.g., a transition from a stable to an unstable state, the emergence of new stable states, or the disappearance of existing ones. Moreover, there are parameter domains where Turing instability is completely absent, for instance, when the diffusion coefficient ratio is below d_c.

From the graphic representation of $h(k^2)$, Eq. (13.66), it is possible to select plausible values for d and b, yielding to the definition of the Turing domain for the dimensionless Gierer-Meinhardt model. By choosing $b = 0.35$ and $D_u = 1$, $D_v = 30$, so that $d = 30$, we may choose any value of k^2 that is bounded between its two positive roots, k_1 and k_2, satisfying $h(k^2) < 0$. In addition, the critical diffusion coefficient ratio and the critical length of the system are given by $d_c \approx 16.65$ and $L_c \approx 12.00$. See Fig. 13.1 for representative plots of $h(k^2)$ for different values of d.

Now, we proceed to numerically solve the reaction-diffusion equations, Eqs. (13.55) and (13.56), by means of a *Mathematica* code, which is presented in Appendix 13.C.1. In this Appendix, we define a function named *PDEsSolution1D*, which requires the system's length L, reaction rate b, diffusion coefficient ratio (diffusivity ratio) d, and computation time t_c. The execution of this function

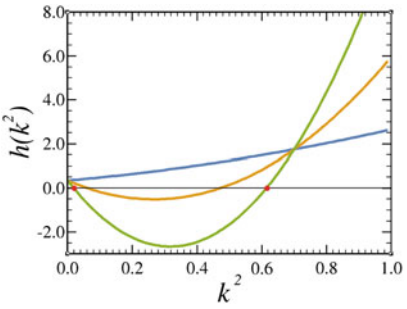

Fig. 13.1 Characteristic plots of function $h(k^2)$ in Eq. (13.65). The blue curve shows the function $h(k^2)$ when the diffusivity ratio is below the critical value, in this case $d_c > d = 1$. Additionally, the yellow curve shows the behavior when $d = d_c \approx 12.00$, whereas the green curve, for $d_c < d = 30$, shows two real and different roots (indicated along the x-axis with red dots) that generate the correct Turing domain as a one-dimensional interval

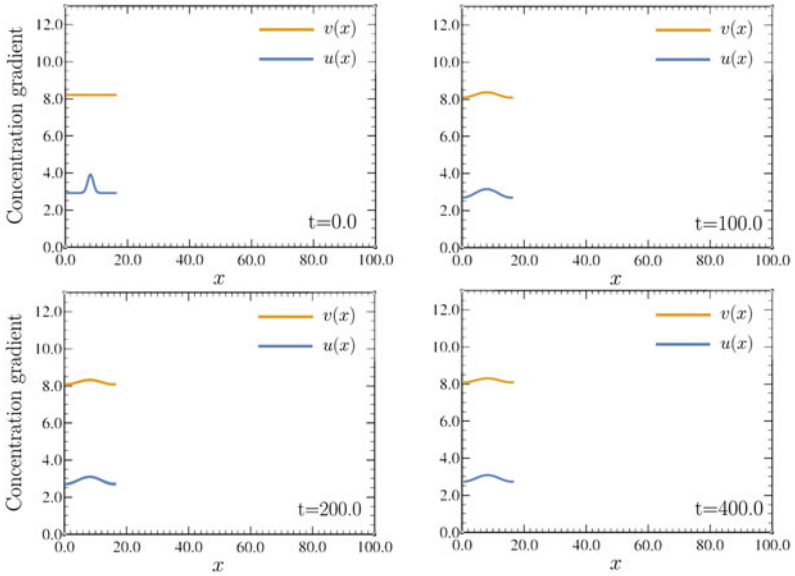

Fig. 13.2 Temporal evolution of the concentration gradients of species u and v described by the numerical solution of Eqs. (13.55) and (13.56) obtained from using the code in Appendix 13.C.1 as *PDEsSolution1D[12, 0.35, 30, 400]*, which indicates that $L = 12$, reaction rate $b = 0.35$, diffusivity ratio $d = 30$, and computation time $t_c = 400$

yields to the numerical solutions of the partial differential equations (PDEs) and simultaneously generates the density plot animation.

Figure 13.2 shows the graph of the concentration gradients of species u and v for $L = 12$, $b = 0.35$, and $d = 30$ at different times, from which we can verify that if the length of the system is equal to or smaller than the critical length L_c, no spatial patterns emerge even if there are small perturbations in concentration.

Furthermore, the temporal evolution of both reagents u and v is depicted in Fig. 13.3 when $L = 100$. As the reader may see, both concentration gradients undergo significant oscillations that vary with position. This pronounced variation implies that the system exhibits Turing instability.

In order to visualize the results more directly and to conclude the analysis of systems with varying lengths, in Fig. 13.4 we present a concentration density plot for species u for the two length settings, i.e., $L = 12$ and $L = 100$.

In the following section, we explore the Gierer-Meinhardt model in two dimensions.

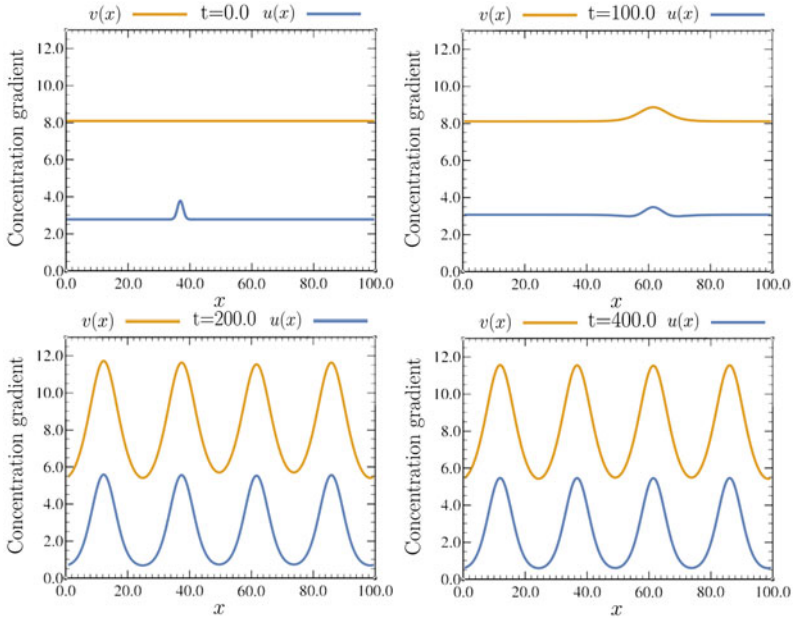

Fig. 13.3 Temporal evolution of the concentration gradients of species u and v described by the numerical solution of Eqs. (13.55) and (13.56) obtained from using the code in Appendix 13.C.1 as *PDEsSolution1D[100, 0.35, 30, 400]*, which indicates that $L = 100$, reaction rate $b = 0.35$, diffusivity ratio $d = 30$, and computation time $t_c = 400$

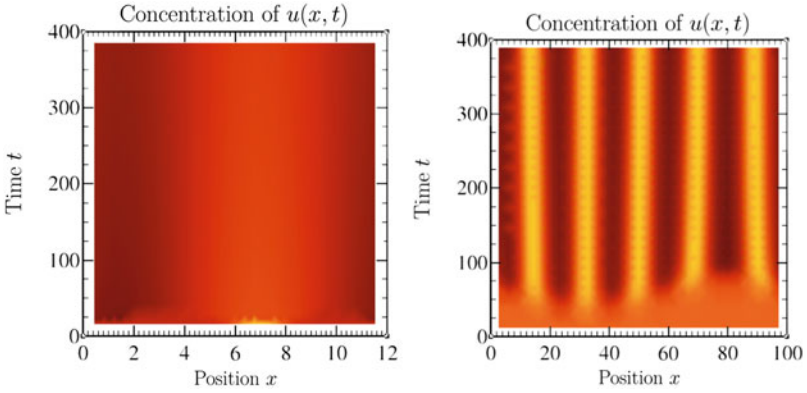

Fig. 13.4 Comparison of the density plot of substance $u(x, t)$ for different lengths, i.e., $L = 12$ (left-hand side) and $L = 100$ (right-hand side). In the left panel, the concentration of the reagent u (in orange) does not show significant modifications over time and remains uniform throughout the entire domain of the system. Conversely, in the right panel, there is a uniform concentration gradient for shorter times (up to $t \approx 90$), while a stable spatial pattern is observed for longer times. In both instances, the figures were obtained from the code in Appendix 13.C.1, using the values $b = 0$, $d = 30$, and $t_c = 400$

13.4.1 Pattern Formation: Two-Dimensional Model

The system of reaction-diffusion PDEs in Eqs. (13.55) and (13.56) can be readily extended to two dimensions, leading to

$$\frac{\partial u(x,t)}{\partial t} = D_u \left(\frac{\partial^2 u(x,t)}{\partial x^2} + \frac{\partial^2 u(x,t)}{\partial y^2} \right) + \frac{u(x,t)^2}{v(x,t)} - b\, u(x,t), \tag{13.75}$$

together with

$$\frac{\partial v(x,t)}{\partial t} = D_v \left(\frac{\partial^2 v(x,t)}{\partial x^2} + \frac{\partial^2 v(x,t)}{\partial y^2} \right) + u(x,t)^2 - v(x,t), \tag{13.76}$$

i.e., the two-dimensional model of Gierer-Meinhardt.

The Turing conditions remain valid for higher dimensions. Therefore, the mathematical formulation of k_c, d, and domain size hold. The only notable change is in the quantization of k, which, given that Eqs. (13.75) and (13.76) are separable, is given by

$$k_{n,m} = \frac{n^2\pi^2}{L_x^2} + \frac{m^2\pi^2}{L_y^2}, \tag{13.77}$$

where L_x and L_y represent the system's length in the x-direction and y-direction, respectively. Additionally, the integers n and m are associated with the eigenvalue problem along each direction, either x or y. For this two-dimensional system, we use the parameters $b = 45$, $d = 30$, and $t_c = 2000$.

We shall now undertake the numerical solution of the reaction-diffusion equations, namely, Eqs. (13.75) and (13.76), by using the Mathematica code introduced in Appendix 13.C.2. After running the code, specifically when using the function *PDEsSolution2D[80, 10, 0.45, 30, 2000]*, we find the numerical solution of the reaction-diffusion PDEs, together with its graphical representation. Such results are illustrated in Fig. 13.5 for a rectangular system with $L_x = 80$, $L_y = 10$, and the parameters established above.

It should be noted that the length of the system in the vertical direction, L_y, is smaller than the previously deduced critical length given in Eq. (13.74), meaning that the patterns will be formed along the horizontal domain only, while the concentration gradient remains uniform along the vertical coordinate.

Now, we want to see the domain's effect in the formation of more complex patterns. For such purpose, we analyze the solutions in a square system in which $L_x = L_y = 100$ and where the other parameters remain unchanged. The evolution of substance concentration, found through *PDEsSolution2D[80, 80, 0.45, 30, 2000]*, is represented in Fig. 13.5, where we can see six pattern development frames, this time generating spots.

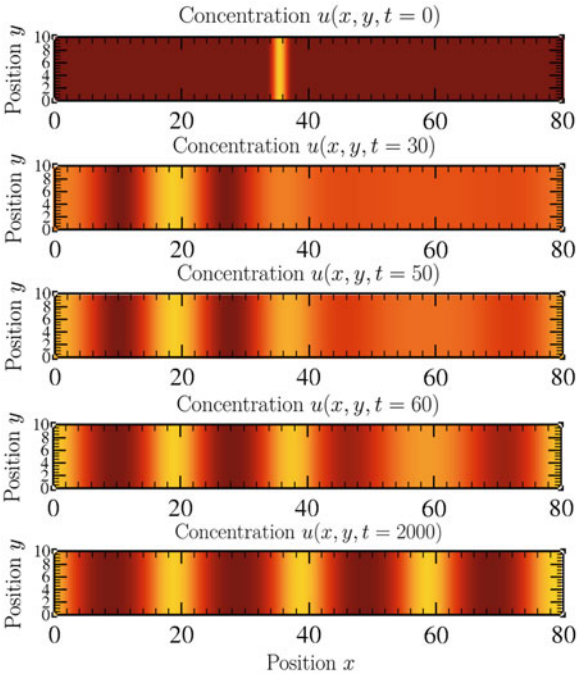

Fig. 13.5 Temporal evolution of the density plot of substance $u(x, y)$ obtained from the code in Appendix 13.C.2 as *PDEsSolution2D[80, 10, 0.45, 30, 2000]*, which indicates that $L_x = 80$, $L_y = 10$, $b = 45$, and $t_c = 2000$. At time $t = 0$, the concentration of u starts to diffuse at a certain position x_0 located somewhere along the x-direction within the interval $[0, L_x]$ while being uniformly distributed in the y-direction. As time progresses, substances u and v begin to interact according to Gierer-Meinhardt reaction kinetics (see Eqs. (13.75) and (13.76)) and spatial patterns emerge. In this particular case, stripes arise on the x-y plane

In the latter case, we see that the concentration gradient of species u starts to diffuse from position x_0 contained along the interval $[0, L_x]$ while being uniformly distributed along the vertical axis. As time progresses, strip patterns are formed, and then we have spots emerging on the x-y plane. This behavior verifies the postulates of Turing instability: The larger the spatial domain, the more complex concentration patterns are formed, as shown in Fig. 13.6.

In Fig. 13.7, we show a schematic representation of Turing patterns in nature, from which we can see that, in the progressive transition from narrow to wide (or bottom to top) regions, different patterns emerge. Initially (at the bottom), the region assumes a homogeneous coloration (a black or white solid color). Then, a notable transformation unfolds, leading to the formation of stripes. Finally, in the case of the left-hand panel, these stripes culminate in the creation of spots. This observation is in complete accordance with the concept of the Turing domain in pattern formation, as described by Eq. (13.74), and is consistent with the patterns obtained through the application of Gierer-Meinhardt kinetics (see Figs. 13.5 and 13.6).

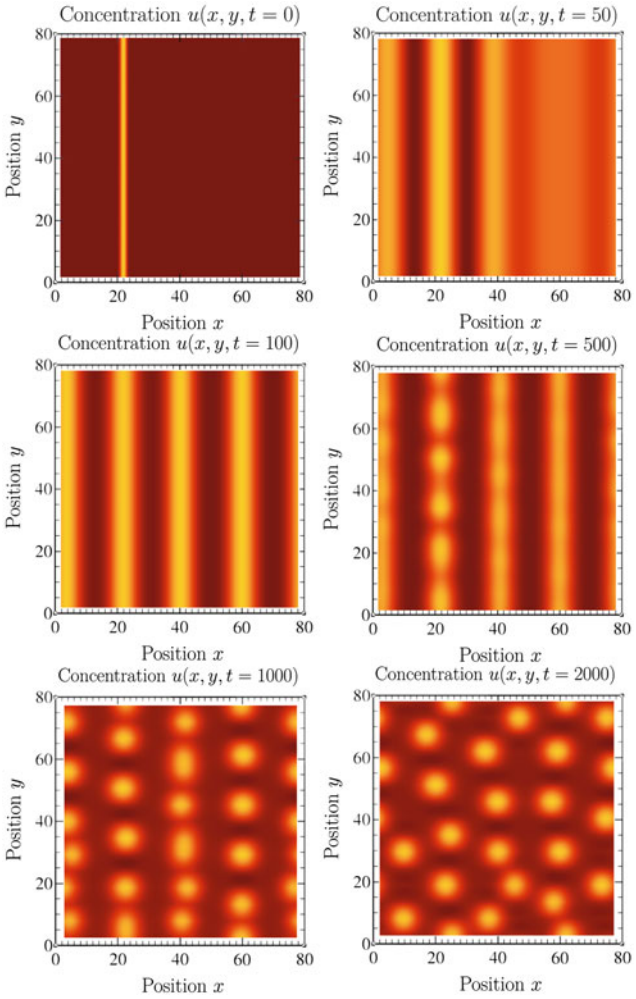

Fig. 13.6 Temporal evolution of the density plot of the substance $u(x, y)$ obtained from the code in Appendix 13.C.1 as *PDEsSolution2D[80, 80, 0.45, 30, 2000]*, which indicates that $L_x = L_y = 80$, $b = 45$, and $t_c = 2000$. At time $t = 0$, the concentration of u starts to diffuse at a certain position x_0 located somewhere along the x-direction within the interval $[0, L_x]$ while being uniformly distributed in the y-direction. As time progresses, substances u and v begin to interact according to Gierer-Meinhardt reaction kinetics (see Eqs. (13.75) and (13.76)), first forming stripes and then changing to spots

13.5 Concluding Remarks

Throughout this chapter, we have presented a brief yet comprehensive derivation of the reaction-diffusion equations for purposes of introducing the ideas behind the Turing mechanism of pattern formation. Subsequently, we deduced the Turing

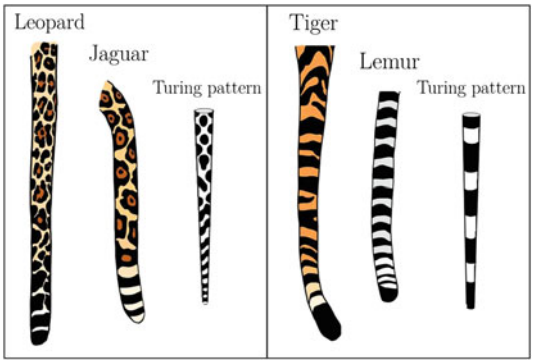

Fig. 13.7 In the left-hand panel, a schematic illustration showcases the distinctive tail patterns found in leopards and jaguars. Similarly, the right-hand panel exhibits a schematic depiction of the tail patterns observed in tigers and lemurs. Moreover, we show a monochromatic depiction of the concentration patterns generated by solving a system of reaction-diffusion equations. In the progressive transition from narrow to wide (bottom to top), different types of patterns emerge, e.g., in the leopard's tail, we can see the transition toward the formation of spots

conditions that make a system of reaction-diffusion equations stable in the absence of diffusion and unstable in its presence. Finally, we applied Turing's theory for spatial pattern formation to the dimensionless system of PDEs, as regards the Gierer-Meinhardt kinetics, in one and two dimensions. Within this model, we concluded that we can determine the Turing domain by appropriately the values of the reaction rate b and the relative diffusion coefficient d, which can be done more easily by relying on a graphical representation of the function $h(k^2)$, as we did in Fig. 13.1. We then solved the reaction-diffusion equations, in both one and two dimensions, using the Mathematica codes provided in Appendices 13.C.1 and 13.C.2. The results are astounding: The shape of the spatial patterns of concentration depend on the type of spatial domain that contains the reagents u and v. Moreover, the larger the domain, the more complex patterns can be formed, something that reproduces what happens in nature very well, for example, the patterns that are observed in the skins of different species, including cats, tapirs, fish, etc.

The success of this theory lies in its ability to explain patterns observed in nature, including various biological phenomena such as animal coat markings and plant pigmentation. Ultimately, Turing's instability theory has found broader applications in a number of fields, including materials science, neuronal networks, and, most recently, social science, offering insights into population dynamics and ecosystem stability.

13.A Stability Matrix and Principles of Linearization

This Appendix is devoted to reviewing of the stability matrix and principles of linearization. We initiate our study with the mathematical formulation of a system of first-order ordinary differential equations, namely,

$$\frac{\mathrm{d}x}{\mathrm{d}t} = f(x, y), \qquad \frac{\mathrm{d}y}{\mathrm{d}t} = g(x, y). \tag{13.78}$$

The relationship from which the *phase curves*, also called *phase trajectories*, of a dynamical system are obtained[15] has the form

$$\frac{\mathrm{d}x}{\mathrm{d}y} = \frac{f(x, y)}{g(x, y)}. \tag{13.79}$$

Once we have established the initial conditions, every point (x, y) is part of a unique curve in the phase space. This happens for all coordinates, except for *singular* or *critical points*,[16] denoted by (x_c, y_c), regarding which

$$f(x_c, y_c) = g(x_c, y_c) = 0. \tag{13.80}$$

Typically, trajectories either converge toward stable critical points or diverge from unstable critical points. Now, by making the transformation $x \to x - x_c$ and $y \to y - y_c$, then $(0, 0)$ is the new critical point of the phase space. Therefore, we can always set the critical coordinates at the origin. In other words,

$$f(0, 0) = g(0, 0) = 0. \tag{13.81}$$

If both functions f and g are continuous around $(0, 0)$, we are able to make a Taylor series for each of them. Through this process, and considering just the first order terms, we obtain

$$\frac{\mathrm{d}x}{\mathrm{d}y} = \frac{ax + by}{cx + dy}, \tag{13.82}$$

where a, b, c, and d are constants. We proceed with defining the stability matrix $\mathbb{A}$, specifically,

[15] In order to fully understand the role of a dynamical system in the stability matrix and principles of linearization, the concept of phase space must be roughly defined: A phase space is a multidimensional space where each dimension represents a state variable of the system. It is constructed by considering all the possible values of the state variables, leading to a full description of all possible states of a system. Furthermore, a phase curve or phase trajectory is a term used to describe a path that represents the sequence of states or phases of the system as time progresses. For example, in a simple pendulum, the commonly used coordinates to represent the phase space are the angle of the pendulum and its angular velocity. Together, they depict how the system goes through different states as the pendulum swings back and forth.

[16] A *singular point* refers to a point in the phase space where the rate of change of the system's state is undefined or discontinuous. In contrast, a *critical point* is a point in the phase space whose derivative is zero.

$$\mathbb{A} \equiv \begin{pmatrix} a & b \\ c & d \end{pmatrix} = \begin{pmatrix} f_x & f_y \\ g_x & g_y \end{pmatrix}_{x_c, y_c} . \tag{13.83}$$

where the subscript in the functions indicates partial differentiation with respect to x, for instance, $f_x = \partial f / \partial x$, and the matrix is evaluated at the critical points. The linear equivalence of Eq. (13.83) in the system yields to

$$\frac{\mathrm{d}x}{\mathrm{d}t} = ax + by, \qquad \frac{\mathrm{d}y}{\mathrm{d}t} = cx + dy. \tag{13.84}$$

On the condition that λ_1 and λ_2 are the eigenvalues of A, the eigenvalue problem is described as

$$|\mathbb{A} - \lambda \mathbb{I}| = \begin{vmatrix} a - \lambda & b \\ c & d - \lambda \end{vmatrix} = 0, \tag{13.85}$$

resulting in

$$\lambda_{1,2} = \frac{1}{2} \left[\mathrm{Tr}(\mathbb{A}) \pm \sqrt{\mathrm{Tr}(\mathbb{A})^2 - 4\,\mathrm{Det}(\mathbb{A})} \right], \tag{13.86}$$

where $\mathrm{Tr}(\mathbb{A})$ and $\mathrm{Det}(\mathbb{A})$ are the trace and determinant of the stability matrix, respectively. Using the eigenvalues approach to solve Eq. (13.84),[17] we arrive at

$$\begin{pmatrix} x \\ y \end{pmatrix} = c_1 \mathbf{v}_1 e^{\lambda_1 t} + c_2 \mathbf{v}_2 e^{\lambda_2 t}, \tag{13.87}$$

with c_1 and c_2 being arbitrary constants, whereas $\mathbf{v}_i$ is the eigenvector corresponding to the eigenvalue λ_i.

This process can be applied to assess the stability of various systems, including chemical reactions and biological systems dynamics. For instance, it can be used to analyze systems like the Lotka-Volterra equations, which serve as an illustrative model for predator-prey dynamics.

13.B Linearization

Consider a function with a multidimensional argument:

$$f = f(\mathbf{x}) = f(x^1, x^2, x^3, \cdots, x^n). \tag{13.88}$$

[17] It is widely known that the solution of an $n \times n$ system of ordinary differential equations is a linear combination of real exponential functions with a structure of $\mathrm{e}^{\lambda_i t}$.

Function f is linear only if, in its explicit formulation, it is a linear combination of coordinates $\mathbf{x} = (x^1, x^2, x^3, \cdots, x^n)$, which is a highly distinctive limitation. In a wide range of cases, f is a nonlinear function. The *linearization* process allows us to analyze the local stability of an equilibrium point for a nonlinear system of equations. Our objective is to find a simplified function that produces identical values to the original function when evaluated at specific coordinates $\mathbf{x}_0 = (x_0^1, x_0^2, x_0^3, \cdots, x_0^n)$ while also matching the values of its partial derivatives. Mathematically, this process is carried out through[18]

$$L(\mathbf{x}) = f(\mathbf{x}_0) + \nabla f(\mathbf{x})\Big|_{\mathbf{x}_0} \cdot (\mathbf{x} - \mathbf{x}_0). \tag{13.89}$$

Consequently, a local linearization of f, i.e., $L(\mathbf{x})$, is obtained in the vicinity of $\mathbf{x}_0$.

Here is an example: Consider a one-dimensional function $f(x)$. If $f(x)$ is locally linear at a point x_0, it means that the function can be well approximated by a straight line in a small neighborhood around that point. Therefore,

$$y(x) = f(x_0) + f_x(x_0)(x - x_0), \tag{13.90}$$

meaning that $y(x)$ is a linear approximation of $f(x)$ at x_0. Now, upon examination of a two-dimensional function $f(x, y)$, which is to be linearized around (x_0, y_0), Eq. (13.89) becomes

$$g(x, y) = f(x_0, y_0) + f_x(x_0, y_0)(x - x_0) + f_y(x_0, y_0)(y - y_0), \tag{13.91}$$

where we have used the tangent plane to f at (x_0, y_0) as an approximation.

As a final example, consider a first-order ODE, namely,

$$\frac{\mathrm{d}x}{\mathrm{d}t} = g(x). \tag{13.92}$$

Linearization of $\mathrm{d}x/\mathrm{d}t$ around x_0 is given by

$$h(x) = g(x_0) + g_x(x_0)(x - x_0). \tag{13.93}$$

Since x_0 is an equilibrium point of $\mathrm{d}x/\mathrm{d}t$, then $g(x_0) = 0$ and Eq. (13.93) reduces to

$$\frac{\mathrm{d}x}{\mathrm{d}t} \approx g_x(x_0)(x - x_0), \tag{13.94}$$

[18] The scalar product in the second term of Eq. (13.89) guarantees that functions f and L exhibit identical directional variation at the specified point. In other words, the partial derivatives of these functions share identical information.

which solution is found in a straightforward manner, yielding

$$x(t) = x_0 + c\, e^{g_x(x_0)}. \tag{13.95}$$

with c being an integration constant. The instability of the system can be classified into two categories: For $g_x(x_0) < 0$, the solution converges to the critical point at longer times exhibiting *asymptotic stability*. In contrast, if $g_x(x_0) > 0$, the solution diverges from x_0 and becomes unstable.

13.C Numerical Solution of Reaction-Diffusion Equations

13.C.1 One-Dimensional Gierer-Meinhardt Model

This Appendix discusses the numerical solution of the coupled partial differential equations (PDEs) in Eqs. (13.55) and (13.56), namely,

$$\frac{\partial u(x,t)}{\partial t} = D_u \frac{\partial u(x,t)}{\partial x} + \frac{u(x,t)^2}{v(x,t)} - b\, u(x,t), \tag{13.55}$$

together with

$$\frac{\partial v(x,t)}{\partial t} = D_v \frac{\partial^2 v(x,t)}{\partial x^2} + u(x,t)^2 - v(x,t), \tag{13.56}$$

and its graphical representation. We tackled this problem by employing the computational software *Mathematica*.

The following code, Listing 13.1, requires the values of system length L, reaction rate b, diffusion coefficient ratio d, and computation time t_c, in that specific order. Its output provides the numerical solution of $u(x,t)$ and $v(x,t)$, the concentration plot as a function of x, and a density plot of concentration $u(x)$. For example, if we want to see the results for a system with $L = 100$, $\beta = 0.35$, $d = 30$, and $t_c = 400$, we should write `PDEsSolution1D[100, 0.35, 30, 400]`.

Listing 13.1 [`GMmodel1D.nb`]: Mathematica code to numerically solve the one-dimensional Gierer-Meinhardt model.

```
1 (*Definition of the function PDEsSolution1D[L, b, d, tc]
    for the one-dimensional Gierer-Meinhardt reaction-
    diffusion model*)
2
```

Listing continued on next page

Listing continued from last page

```
PDEsSolution1D[L_ (*length of the system*), b_  (*reaction
     rate*), d_ (*diffusivity ratio*), tc_ (*computation
    time*)] :=

(*Specification of the variables used within the Module*)
 Module[{Dv = d, PDEs, initialconditions, x0, BCs, Eqs,
    Plotuv1D,    Densityplotuv},

     (* NUMERICAL SOLUTION OF THE REACTION-DIFFUSION
    SYSTEM *)

(*First, we define the system of PDEs according to Eqs.
    (13.55) and (13.56), namely,*)

PDEs = {(*Eq. (13.55)*)
   D[u[t,x],t] == Du D[u[t,x],{x,2}] + u[t,x]^2/v[t,x] - b
     u[t,x],
 (*Eq.(13.56)*)
 D[v[t,x],t] == Dv D[v[t,x],{x,2}] + u[t,x]^2 - v[t,x]};

(*The concentration gradients of the substances are
    represented as u[t,x] (activator) and v[t,x]
    (inhibitor). The variables inside the square brackets
    indicate the  dependence of both functions u and v on
    time and space, while command D[f[x1,x2, ...,xn],{xn,m
    }] gives the m-order partial derivative of function f
    with respect to xn. Thus, D[u[t,x],t] denotes the
    partial derivative of u[t,x] with respect to time.*)

(*For the sake of simplicity, we set Du=1*)

Du = 1;

(*Now, we set the initial and boundary conditions. On the
    one hand, a random value x0 is selected within the
    interval [0,L] to represent the initial position of
    species u, i.e.,*)

x0 = RandomReal[{0,L}];

```

Listing continued on next page

Listing continued from last page

```
(*This selection is based on a Gaussian-like distribution
    centered at x0. On the other hand, we choose a
    constant value for v[0,x]. Therefore, the initial
    conditions are given by*)

initialconditions = {u[0,x]==1/b + Exp[-(x-x0)^2], v[0,x
    ]==1/b^2};

(*When opting for periodic boundary conditions, we are led
     to write*)

BCs = {u[t,0] == u[t,L], v[t,0] == v[t,L]};

(*Moving forward, we associate the initial and boundary
    conditions to the PDEs by using the Join command in
    Mathematica, which is*)

Eqs = Join[PDEs,initialconditions,BCs];

(*Finally, we solve numerically the system of PDEs over
    the given range [0, tc] for t and [0, L] for x. The
    solution is obtained by means of the NDSolve command
    and we name the solution solution1D*)

solution1D = NDSolve[Eqs (*System of PDEs to solve*),
{u,v} (*variables we wish to solve*),
{t,0,tc} (*computation time*),
{x,0,L} (*spatial domain*)];

          (*VISUALIZATION OF RESULTS AND DENSITY PLOT*)

(*The rest of the code is intended to show the position-
    dependent plots of concentrations u(x) and v(x) in
    blue and orange, respectively, at different times. We
    incorporated controls to enable interactive time
    manipulation. Additionally, a density plot is
    displayed on the plane x-t.*)

(*Plot of concentration gradients ~~the variable time is a
     dummy variable~~*)
```

Listing continued on next page

Listing continued from last page

```
51
52  Plotuv1D =
53    (*We use the Animate command to animate the plot*)
54    Animate[
55    (*Evaluating functions u and v at the numerical
       solution solution1D and plotting its result*)
56    Plot[
57    Evaluate[{u[time, x], v[time, x]} /.solution1D],
58    (*Selecting the spatial domain of the plot*)
59    {x, 0, L},
60    (*Detailed specification of legends*)
61    PlotLegends -> {"u(x)","v(x)"},
62    (*Frame Labels*)
63    Frame -> True,
64    FrameLabel -> {"Position x","Concentration gradient"},
65    (*Fixing plot range*)
66    PlotRange -> {0,12}],
67    (*Time domain of the animation increasing in steps of
       tc/100*)
68    {time, 0, tc , tc/100},
69    (*Selecting manual reproduction of the animation*)
70    AnimationRunning -> False];
71
72  (*Density plot of concentration ~~the variable time is a
      dummy variable~~*)
73
74  Densityplotuv =
75     (*Making a density plot of function u evaluated at the
        numerical solution solution1D*)
76     DensityPlot[Evaluate[u[time, x] /. solution1D],
77     (*Selecting the spatial domain of the plot*)
78     {x, 0, L},
79     (*Time domain of the density plot*)
80     {time,0,tc},
81     (*Plot label*)
82     PlotLabel -> Style["Concentration u(x)"],
83     (*Detailed specification of frame labels*)
84     Frame -> True, FrameLabel -> {"Position x","Time t"},
85     (*Definition of a color style*)
86     ColorFunction -> "SolarColors",
```

Listing continued on next page

Listing continued from last page

```
    (*Using 100 initial sample points ~~Higher values give
     smoother plots~~*)
    PlotPoints -> 100,
    (*Size to display the plot*)
    ImageSize -> 300];

(*Finally, we show all previous results in the form of a
    list, specifically the numerical solution, the
    concentration plot, and the density plot:*)

{solution1D, Plotuv1D, Densityplotuv}]

(*Subsequently, we undertake the solution of the system
    with L=80, b=0.35,d=30, and tc=400, using the latter
    function as PDEsSolution1D[80, 0.35, 30, 400]*)

PDEsSolution1D[100, 0.35, 30, 400]

(*As we can see, the concentration gradient of both
    substances starts to oscillate along the x-axis and,
    after a certain time, both functions reach a steady
    state*)


(*The reader may change the values of any of the
    parameters to see the role of reaction rate b,
    critical length Lc, critical diffusion coefficient
    ratio dc, and time computation tc. For instance, by
    using Eq. (13.74), we can see that the critical length
     is about Lc= 12.0, meaning that below that value,
    concentration remains approximately constant and no
    patterns emerge in the density plot. Therefore, as the
     domain size increases, the substance concentration
    exhibits steeper transitions*)
```

Listing ended

13.C.2 Two-Dimensional Gierer-Meinhardt Model

This Appendix focuses on the numerical solution of the coupled partial differential equations (PDEs) outlined in Eqs. (13.75) and (13.76), namely,

$$\frac{\partial u(x,t)}{\partial t} = D_u \left(\frac{\partial^2 u(x,t)}{\partial x^2} + \frac{\partial^2 u(x,t)}{\partial y^2} \right) + \frac{u(x,t)^2}{v(x,t)} - b\, u(x,t), \tag{13.75}$$

and

$$\frac{\partial v(x,t)}{\partial t} = D_v \left(\frac{\partial^2 v(x,t)}{\partial x^2} + \frac{\partial^2 v(x,t)}{\partial y^2} \right) + u(x,t)^2 - v(x,t), \tag{13.76}$$

respectively. We address this problem using Mathematica. The following code, Listing 13.2, requires the values of system length L_x and L_y, reaction rate b, diffusion coefficient ratio d, and computation time t_c, in that specific order. Its output provides the numerical solution of $u(x, y, t)$ and $v(x, y, t)$, the concentration plot as a function of x and y, and a density plot of concentrations. For example, if we want to see the results for $L_x = 80$, $L_y = 10$, $b = 0.35$, $d = 30$, and $t_c = 1000$, we should write `PDEsSolution2D[80, 10, 0.35, 30, 1000]`.

Listing 13.2 [**GMmodel2D.nb**]: Mathematica code to numerically solve the two-dimensional Gierer-Meinhardt model.

```
(*Definition of the function PDEsSolution2D[Lx,Ly,b, d, tc
    ] for the two-dimensional Gierer-Meinhardt reaction-
    diffusion model*)

PDEsSolution2D[Lx_ (*length along the x-axis*),Ly_ (*
    length along the y-axis*),b_  (*reaction rate*),d_ (*
    diffusivity ratio*),tc_ (*computation time*)] :=

(*Specification of the variables used within the Module*)

Module[{Dv = d, PDEs, initialconditions, x0, BCs, Eqs,
    Densityplotuv},

     (* NUMERICAL SOLUTION OF THE REACTION-DIFFUSION
    SYSTEM *)

(*First, we define the system of (PDEs) according to Eqs.
    (13.73) and (13.74), namely,*)
```

Listing continued on next page

Listing continued from last page

```
12
13  PDEs = {(*Eq.(13.73)*)
14      D[u[t,x,y],t] == Du (D[u[t,x,y],{x,2}] + D[u[t,x,y],{y
        ,2}]) + u[t,x,y]^2/v[t,x,y] - b u[t,x,y],
15      (*Eq.(13.74)*)
16      D[v[t,x,y],t] == Dv (D[v[t,x,y],{x,2}] + D[v[t,x,y],{y
        ,2}]) + u[t,x,y]^2 - v[t,x,y]};
17
18  (*The concentration gradients of the substances are
        represented as u[t,x,y] (activator) and v[t,x,y] (
        inhibitor).The variables inside the square brackets
        indicate the dependence of both functions u and v on
        time and space, while command D[f[x1,x2,...,xn],{xn,m
        }] gives the m-order partial derivative of function f
        with respect to xn. Thus, D[u[t,x,y],t] denotes the
        partial derivative of u[t,x,y] with respect to time.*)
19
20  (*For the sake of simplicity, we set Du=1*)
21
22  Du = 1;
23
24  (*Now, we set the initial and boundary conditions. On the
        one hand, a random value for x0 is selected within the
         interval [0,Lx] to represent the initial position of
        species u, i.e.,*)
25
26  x0 = RandomReal[{0,Lx}];
27
28  (*This selection is based on a Gaussian-like distribution
        centered at (x0, y). On the other hand, we choose a
        constant value for v[0,x,y]. Therefore, the initial
        conditions are given by*)
29
30  initialconditions = {u[0,x,y] == 1/b + Exp[-(x-x0)^2],
31                       v[0,x,y] == 1/b^2};
32
33  (*When opting for periodic boundary conditions, we are led
         to write*)
34
```

Listing continued on next page

Listing continued from last page

```
BCs = {u[t, 0, y] == u[t, Lx, y], v[t, x, 0] == v[t, x, Ly
    ]};

(*Moving forward, we associate the PDEs to the initial and
     boundary conditions using the Join command in
    Mathematica, this is*)

Eqs = Join[PDEs, initialconditions, BCs];

(*Finally, we numerically solve the system of PDEs over
    the given range [0, tc] for t, [0, Lx] for x, and [0,
    Ly] for y. The solution is obtained by means of the
    NDSolve command and we name the solution solution2D*)

solution2D =
NDSolve[Eqs (*System of PDEs to solve*), {u, v},
{t,0,tc} (*computation time*),
{y,0,Ly} (*spatial domain along the y-axis*),
{x, 0, Lx} (*spatial domain along the x-axis*)];

          (*VISUALIZATION OF RESULTS AND DENSITY PLOT*)

(*The rest of the code is intended to show the density
    plots of concentrations u(x,y) and v(x,y) with
    incorporated controls to enable interactive time
    manipulation.*)

(*Density plot of concentration ~~the variable time is a
    dummy variable~~*)

Densityplotuv =
   (*We use the ListAnimate command to animate the results
     provided in the Table below*)
   ListAnimate[
   (*Generating a list of the DensityPlot  when time goes
    from 0 to tc*)
   Table[
   (*Making a density plot of function v evaluated at the
    numerical solution solution2D*)
   DensityPlot[Evaluate[v[time, x, y] /.solution2D],
```

Listing continued on next page

Listing continued from last page

```
    (*Selecting the spatial domain of the plot*)
    {x,0,Lx}, {y,0,Ly},
    (*Definition of a color style*)
    ColorFunction -> "SolarColors",
    (*Plot label*)
    PlotLabel -> Style["Concentración de u(x,t)"],
    (*Frame label*)
    FrameLabel -> {"Position x","Position y"},
    (*Using 100 initial sample points ~~Higher values give
     smoother plots~~*)
    PlotPoints -> 100,
    (*Automatic setup of plot's height-to-width ratio*)
    AspectRatio ->Automatic],
    (*Time domain of the animation increasing in steps of
     tc/100*)
    {time, 0, tc,tc/100}],
    (*Selecting manual reproduction of the animation*)
    AnimationRunning -> False];


(*Finally, we show previous results in the form of a list,
     specifically the numerical solution and the density
    plot*)

{solution2D,  Densityplotuv}]

(*Subsequently, we undertake solving the system with Lx
    =80, Ly=10, b=0.45, d=30, and tc=1000, using the
    latter function as PDEsSolution2D[80, 10, 0.45, 30,
    1000]*)

PDEsSolution2D[80  (*length along the x-axis*),
80  (*length along the y-axis*),
0.45 (*reaction rate*),
30 (*diffusivity ratio*),
2000 (*computation time*)]


(*The reader may change the values of any of the
    parameters to see the role of reaction rate b, domain
```

Listing continued on next page

Listing continued from last page

```
    size, critical diffusion coefficient ratio dc, and
    time computation tc. For instance, when using
    PDEsSolution2D[80, 10, 0.35, 30, 400], the resulting
    patterns show stripes, whereas upon employing a
    different configuration, say a square system with
    PDEsSolution2D[80, 80, 0.45, 30, 1000], dots are
    observed. As in the one-dimensional case, we conclude
    that the larger the diffusion reaction domain, the
    more complex the spatial patterns.*)
```

Listing ended

Further Reading and References

L.J.S. Allen, *An Introduction to Mathematical Biology* (Pearson, London, 2006)

A. Gierer, H. Meinhardt, A theory of biological pattern formation. Kybernetik **12**, 30–39 (1972). 10.1007/BF00289234

J.D. Murray, *Mathematical Biology I. An Introduction* (Springer, Berlin, 2002)

J.D. Murray, *Mathematical Biology II. Spatial Models and Biomedical Applications* (Springer, Berlin, 2003)

A.M. Turing, The chemical basis of morphogenesis. Phil. Trans. R. Soc. Lond. B **237**, 37 (1952). 10.1098/rstb.1952.0012

Part V
Three-Dimensional Diffusion

The randomness of being trapped and reflected in three dimensions.

"Without calculations, it is difficult to develop a quantitative sense of the phenomena."

—Richard Feynman

Chapter 14
Three-Dimensional Systems

As we know, for infinitely large regions in space, boundary conditions do not play an important role, but in a finite region of space, shape and dimension need to be taken into account by specifying the physical properties of the boundaries. This chapter is devoted to the study of diffusing particles in three dimensions in the presence of boundary conditions.

Much of the movement of molecules in cells is passive, occurs in random directions, and is an essential part of their function. Diffusion is a fundamental process at molecular scales. All molecular processes must either exploit diffusion or overcome it. Examples include ligand binding to receptors, ionic transport through cell membranes, and oxygen molecules diffusing into the cell, among others.

In engineering, there are many applications of diffusion in three dimensions, such as metal bonding in welding, brazing, soldering, galvanizing, oxidation of metals, doping of semiconductors, recrystallization, and surface treatment of steel to increase its hardness, like in carburization, where carbon is diffused into the steel surface enhancing its structural integrity. Diffusion is widely used in the manufacture of semiconductors. Dopants are introduced by diffusion into the semiconductor to create regions of different electrical properties. Diffusion is a key process in much of materials science, and it is responsible for mass transfer in chemical engineering.

In summary, diffusion in three dimensions is ubiquitous in nature and artificial environments, and it is always present at molecular length scales.

L. Dagdug et al., *Diffusion Under Confinement*,
https://doi.org/10.1007/978-3-031-46475-1_14

14.1 Perfectly Absorbent Sphere

14.1.1 Perfectly Absorbing Sphere: Internal Problem

Consider diffusing particles within a perfectly absorbing sphere of radius R with initial position at $\mathbf{r}_0$, $\mid \mathbf{r} \mid < R$. Particles are moved from the system as soon as they reach the sphere's surface, leading to the Dirichlet boundary condition $p(\mathbf{r} = R, t) = 0$. Assuming spherical symmetry and consequently angular independence, using Eq. (B.17), we can see that the diffusion equation simplifies to

$$\frac{\partial p(r,t)}{\partial t} = \frac{D}{r^2}\frac{\partial}{\partial r}\left(r^2 \frac{\partial p(r,t)}{\partial r}\right), \tag{14.1}$$

where $p(r,t)$ is the propagator of a diffusing particle at position r at time t and D is the diffusivity. To solve Eq. (14.1), we use the following change of variable: $u(r,t) = rp(r,t)$, then, Eq. (14.1) becomes

$$\frac{\partial u(r,t)}{\partial t} = D\frac{\partial^2 u(r,t)}{\partial r^2}. \tag{14.2}$$

Now, the boundary conditions are given by

$$u(r = 0, t) = u(r = R, t) = 0. \tag{14.3}$$

This problem is the same as diffusing particles in the presence of two absorbing points at $r = 0$ and $r = R$. This system was already solved previously in Sect. 5.4.1, and the solution is given in by Eq. (5.40), which, mapped to our propagator, becomes

$$p(r,t|r_0) = \frac{2}{Rr}\sum_{n=1}^{\infty} \exp\left(-\frac{\pi^2 n^2 Dt}{R^2}\right) \sin\left(\frac{n\pi r_0}{R}\right) \sin\left(\frac{n\pi r}{R}\right). \tag{5.40}$$

Moreover, if the initial particles are initially uniformly distributed, we have

$$p(r,t) = \frac{4}{\pi Rr}\sum_{n=1}^{\infty} \exp\left[-\frac{(2n-1)^2\pi^2 Dt}{R^2}\right] \frac{\sin\left[\frac{(2n-1)\pi r}{R}\right]}{2n-1}. \tag{5.69}$$

It is worth noting that all the solutions obtained in Sect. 5.4, namely, mean first-passage time, survival probability, and probability densities, are applicable to our present system.

14.1.2 Perfectly Absorbing Sphere: External Problem

Consider a particle that diffuses outside of a perfectly absorbing sphere of radius R with initial position at $\mathbf{r}_0$, $\mid \mathbf{r} \mid \geq R$. Because of angular independence, the diffusion equation for the spherically symmetric system is given by Eq. (14.1), namely,

$$\frac{\partial p(r,t)}{\partial t} = \frac{D}{r^2}\frac{\partial}{\partial r}\left(r^2 \frac{\partial p(r,t)}{\partial r}\right). \tag{14.1}$$

Applying the chain rule, this results in

$$\frac{\partial p(r,t)}{\partial t} = D\left[\frac{\partial^2 p(r,t)}{\partial r^2} + \frac{2}{r}\frac{\partial p(r,t)}{\partial r}\right], \tag{14.4}$$

which has to be solved subject to the boundary conditions $p(R,t) = 0$. The initial condition is given by

$$p(r,0,\mid r_0) = \frac{\delta(r-r_0)}{4\pi r^2} = \frac{\delta(r-r_0)}{4\pi r_0^2}. \tag{14.5}$$

There is a transformation that reduces the diffusion Eq. (14.4) to an equation in one dimension. This transformation is given by

$$p(r,t) = \frac{g(r,t)}{r}. \tag{14.6}$$

Using this last expression in Eq. (14.4), we arrive at

$$\frac{\partial g(r,t)}{\partial t} = D\frac{\partial^2 g(r,t)}{\partial r^2}, \tag{14.7}$$

which is the diffusion equation in one dimension. The boundary conditions transform to $g(R,t) = 0$, and initial condition is

$$q(r,0,\mid r_0) = \frac{\delta(r-r_0)}{4\pi r^2} = \frac{\delta(r-r_0)}{4\pi r_0^2}. \tag{14.8}$$

Also, we can set $\chi = r - R$ to place the absorbing point at the origin, $\chi = 0$, in these new coordinates. Now, we have mapped our problem to one dimension, with a perfectly absorbing point at the origin, which solution is given in Eq. (4.31) (see Sect. 4.3). This solution should be slightly modified so that it correctly reproduces the initial condition given in Eq. (14.8). Consequently,

$$g(\chi, t|\chi_0) = \frac{1}{4\pi r_0\sqrt{4\pi Dt}}\left\{\exp\left[-\frac{(\chi-\chi_0)^2}{4Dt}\right] - \exp\left[-\frac{(\chi+\chi_0)^2}{4Dt}\right]\right\}, \tag{14.9}$$

where $\chi_0 = r_0 - R$. Finally, the concentration in the original variables is given by

$$p(r, t|r_0) = \frac{1}{4\pi r_0\sqrt{4\pi Dt}}\left\{\exp\left[-\frac{(r-r_0)^2}{4Dt}\right] - \exp\left[-\frac{(r+r_0-2R)^2}{4Dt}\right]\right\}. \tag{14.10}$$

The solution of this problem at steady state can be found in Sect. 4.2.2.

To calculate the survival probability, we need to integrate from R to infinity, in spherical coordinates, Eq. (14.10), namely,

$$S(t|r_0) = \int_0^{\pi}\int_0^{2\pi}\int_R^{\infty} \frac{r^2}{4\pi r_0\sqrt{4\pi Dt}}\left\{\exp\left[-\frac{(r-r_0)^2}{4Dt}\right] - \exp\left[-\frac{(r+r_0-2R)^2}{4Dt}\right]\right\} \mathrm{d}r\ \mathrm{d}\theta\ \mathrm{d}\phi, \tag{14.11}$$

To solve this integral, we simply need to follow the steps described in Sect. (4.3.5), yielding

$$S(t|r_0) = 1 - \frac{R}{r_0}\,\mathrm{erfc}\left(\frac{r_0-R}{\sqrt{4Dt}}\right), \tag{14.12}$$

where $\mathrm{erfc}(x)$ is the complementary error function of argument x (see Sect. A.10.2 of Appendix A). This function has the following property: $\mathrm{erfc}(0) = 1$. Then, when $t \to \infty$,

$$S(\infty|r_0) = 1 - \frac{R}{r_0}. \tag{14.13}$$

It is worth noting that this probability is finite, different from 0. Consequently, there is the probability that the particle will never be absorbed as it can escape to infinity, in contrast to the one-dimensional case, where the diffusing particle is always absorbed.

To calculate the probability density of first-passage time, we introduce (14.12) into Eq. (2.34), yielding

$$\varphi(t|r_0) = -\frac{\mathrm{d}S(t|r_0)}{\mathrm{d}t} = -\frac{\mathrm{d}}{\mathrm{d}t}\left[1 - \frac{R}{r_0}\,\mathrm{erfc}\left(\frac{r_0-R}{\sqrt{4Dt}}\right)\right]. \tag{14.14}$$

Using the result of the derivative in Eq. (A.86), we finally obtain

$$\varphi(t|x_0) = \frac{r_0 - R}{\sqrt{4\pi D t^3}} \left(\frac{R}{r_0}\right) \exp\left\{-\frac{(r_0 - R)^2}{4Dt}\right\}. \tag{14.15}$$

14.2 Concentric Spheres

Consider diffusing particles between two concentric spheres with radii R_{in} and R_{out}, $R_{in} < R_{out}$, for the inner and outer spheres, respectively, schematically represented in Fig. 14.1. Particles start at distance r_0 from the origin, located at the center of both spheres, $R_{in} < r_0 < R_{out}$. In this section, we will study the main properties of this system for different properties of the spheres when they are absorbing or partially absorbing. In the next section, we will focus on the case where both spheres are perfectly absorbing.

14.2.1 Absorbing-Absorbing

Let us assume that now both concentric spheres are perfectly absorbing. Consider a particle with an initial position r_0, $R_{in} < r_0 < R_{out}$. As we already know, the propagator (Green's function) satisfies Eq. (14.1), subject to the initial conditions $p(r, t = 0) = \delta(r - r_0)/(4\pi r_0^2)$ and absorbing boundary conditions $p(r, t|r_0)\big|_{r=R_{in}} = p(r, t|r_0)\big|_{r=R_{out}} = 0$. Then, the Laplace transform of Eq. (14.1) is given by

$$s\, p(r, s|r_0) - \frac{1}{4\pi r_0^2}\, \delta(r - r_0) = \frac{D}{r^2} \frac{\mathrm{d}}{\mathrm{d}r} \left(r^2 \frac{\mathrm{d}}{\mathrm{d}r} p(r, s|r_0)\right). \tag{14.16}$$

Using the change of variable $f(r, s|r_0) = r p(r, s|r_0)$, this last equation becomes

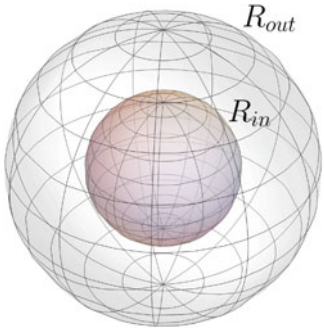

Fig. 14.1 Schematic representation of two concentric spheres with radii R_{in} and R_{out}, $R_{in} > R_{out}$

$$s\, f(r,s|r_0) - \frac{1}{4\pi r_0^2}\,\delta(r-r_0) = D\frac{\mathrm{d}^2}{\mathrm{d}r^2} f(r,s|r_0), \tag{14.17}$$

subject to the boundary conditions $f(r,s|r_0)\big|_{r=R_{in}} = f(r,s|r_0)\big|_{r=R_{out}} = 0$. This boundary problem is one-dimensional in the presence of two absorbing endpoints. Its solution can be obtained from Eq. (5.47) by dividing the delta function by $4\pi r_0$ and setting the argument of the hyperbolic functions in Eq. (5.47) to $r - R_{in}$ and $R_{out} - r$, which leads us to

$$p(x,s|x_0) = \begin{cases} \dfrac{\sinh\left[\sqrt{\frac{s}{D}}\,(R_{out}-r_0)\right]\sinh\left[\sqrt{\frac{s}{D}}(r-R_{in})\right]}{4\pi r_0\sqrt{sD}\sinh\left[\sqrt{\frac{s}{D}}\,(R_{out}-R_{in})\right]} & \text{for} \quad R_{in} \le r \le r_0, \\ \dfrac{\sinh\left[\sqrt{\frac{s}{D}}\,(r_0-R_{in})\right]\sinh\left[\sqrt{\frac{s}{D}}(R_{out}-r)\right]}{4\pi r_0\sqrt{sD}\sinh\left[\sqrt{\frac{s}{D}}\,(R_{out}-R_{in})\right]} & \text{for} \quad r_0 \le r \le R_{out}. \end{cases} \tag{14.18}$$

We can also calculate the respective probability fluxes for each sphere at time t, given by

$$\begin{aligned} J_{in}(s|r_0) &= 4\pi R_{in}^2 D\frac{\partial p(s|x_0)}{\partial r}\bigg|_{r=R_{in}} \\ &= 4\pi R_{in} D\frac{\partial f(s|x_0)}{\partial r}\bigg|_{r=R_{in}} \\ &= \frac{R_{in}\sinh\left[\sqrt{\frac{s}{D}}\,(R_{out}-r_0)\right]}{r_0\sinh\left[\sqrt{\frac{s}{D}}\,(R_{out}-R_{in})\right]}, \end{aligned} \tag{14.19}$$

and

$$\begin{aligned} J_{out}(s|r_0) &= -4\pi R_{out}^2 D\frac{\partial p(s|x_0)}{\partial r}\bigg|_{r=R_{out}} \\ &= -4\pi R_{out} D\frac{\partial f(s|x_0)}{\partial r}\bigg|_{r=R_{out}} \\ &= \frac{R_{out}\sinh\left[\sqrt{\frac{s}{D}}\,(r_0-R_{in})\right]}{r_0\sinh\left[\sqrt{\frac{s}{D}}\,(R_{out}-R_{in})\right]}. \end{aligned} \tag{14.20}$$

To calculate the conditional splitting probabilities, we have to integrate the fluxes over time from zero to infinity. Using Eq. (5.66), we have that they are the Laplace transforms at $s = 0$, so by setting $s = 0$ in Eqs. (14.19) and (14.20), we arrive at

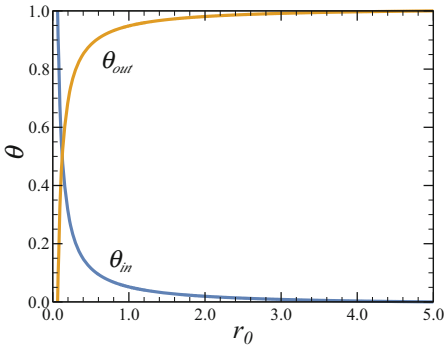

Fig. 14.2 Splitting probabilities as functions of the particle's starting point, given in by Eqs. (14.21) and (14.22), for the following set of parameters: $a = 0.1$, $R_{in} = 1$, and $R_{out} = 5$

$$\theta_{in} = \frac{R_{in}(R_{out} - r_0)}{(R_{out} - R_{in})r_0}, \tag{14.21}$$

and

$$\theta_{out} = \frac{R_{out}(r_0 - R_{in})}{(R_{out} - R_{in})r_0}. \tag{14.22}$$

From these last expressions, we observe that θ_{in} monotonically decreases from 1 to 0, while θ_{out} monotonically increases from 0 to 1, as r_0 increases from R_{in} to R_{out}. This behavior is shown in Fig. 14.2.

The conditional mean first-passage times (MFPTs) are calculated by introducing Eqs. (14.19)–(14.22), into Eqs. (8.7) and (8.8), yielding

$$\langle t(r_0)\rangle_{in} = \frac{\int_0^\infty t\ J(0,t)\ \mathrm{d}t}{\theta_0(x_0)} = \frac{1}{6D}(r_0 - R_{in})(2R_{out} - r_0 - R_{in}), \tag{14.23}$$

and

$$\langle t(r_0)\rangle_{out} = \frac{\int_0^\infty t\ J(L,t)\ \mathrm{d}t}{\theta_L(x_0)} = \frac{1}{6D}(R_{out} - r_0)(R_{out} + r_0 - 2R_{in}). \tag{14.24}$$

As r_0 increases from R_{in} to R_{out}, $\langle t_0(r_0)\rangle_{in}$ monotonically increases from 0 at $r_0 = R_{in}$ to $(R_{out} - R_{in})^2/(6D)$ at $r_0 = R_{out}$. On the other hand, $\langle t_L(r_0)\rangle_{out}$ monotonically decreases from the mean transition path time $(R_{out} - R_{in})^2/(6D)$ at $r_0 = R_{in}$ to 0 at $r_0 = R_{out}$, as shown in Fig. 14.3. As $R_{out} \to \infty$, the splitting probabilities reduce to $\langle t_0(r_0)\rangle_{in} = R/r_0$ and $\langle t_0(r_0)\rangle_{out} = 1 - R/r_0$, and both MFPTs diverge.

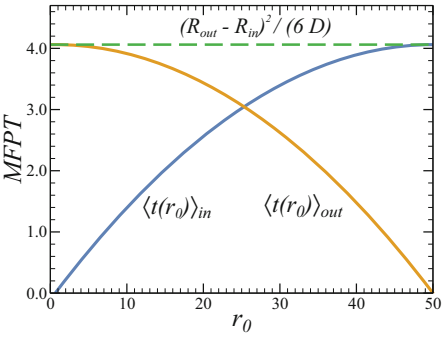

Fig. 14.3 Conditional MFPTs as functions of the particle's starting point, given in by Eqs. (14.23) and (14.24) for the following set of parameters: $a = 0.1$, $R_{in} = 1$, and $R_{out} = 5$

14.3 Concentric Spheres Propagator Revisited: The Effect of Dimensionality

In this section, we will study the solution to the diffusion equation in the Laplace space in d dimensions assuming angular independence when diffusion takes place into two concentric spheres, long cylinders, disks, or a line, where the boundaries of the d-dimensional spheres are given by R_{in} and R_{out}, $R_{in} < R_{out}$. In such a case, the diffusion equation reduces to one dimension, namely,

$$\frac{\partial p(r,t)}{\partial t} = \frac{D}{r^{d-1}}\frac{\partial}{\partial r}\left(r^{d-1}\frac{\partial p(r,t)}{\partial r}\right) = D\left[\frac{\partial^2 p(r,t)}{\partial r^2} + \frac{d-1}{r}\frac{\partial p(r,t)}{\partial r}\right]. \tag{12.84}$$

The Laplace transform of this diffusion equation in d dimensions is given by

$$s\,p(r,s) - \frac{\delta(r-r_0)}{\Omega_d\, r^{d-1}} = D\left[\frac{\partial^2 p(r,t)}{\partial r^2} + \frac{d-1}{r}\frac{\partial p(r,t)}{\partial r}\right], \tag{14.25}$$

where Ω_d is the solid angle subtended by the complete $(d-1)$-dimensional spherical surface of the unit sphere in a d-dimensional Euclidean space defined as

$$\Omega_d = \frac{2\pi^{\frac{d}{2}}}{\Gamma\left(\frac{d}{2}\right)} = \begin{cases} \dfrac{1}{\left(\frac{d}{2}-1\right)!}2\pi^{\frac{d}{2}} & \text{for} \quad d \quad \text{even}, \\ \dfrac{\left(\frac{1}{2}(d-1)\right)!}{(d-1)!}2^d\pi^{\frac{1}{2}(d-1)} & \text{for} \quad d \quad \text{odd}, \end{cases} \tag{14.26}$$

where Γ is the gamma function. Explicitly, $\Omega_1 = 2$, $\Omega_2 = 2\pi$, and $\Omega_3 = 4\pi$. In the case when $d = 1$, the factor of 2 appears because the origin-centered one-dimensional "sphere" is the interval $[-r, r]$.

To simplify Eq. (14.25), we use the following change of variable $x = r\sqrt{s/D}$, leading to

$$p(x,s) - \frac{s^{(d-2)/2}}{D^{d/2}} \frac{\delta(x-x_0)}{\Omega_d\, x_0^{d-1}} = \frac{\partial^2 p(r,s)}{\partial r^2} + \frac{d-1}{x}\frac{\partial p(r,s)}{\partial r}. \tag{14.27}$$

When performing the change of variable, it is essential that we take into account the factor arising from the change of variable of the delta function argument,[1] which is in fact $\sqrt{s/D}$. Multiplying Eq. (14.27) by x^2 becomes

$$x^2 \frac{\partial^2 p(x,s)}{\partial r^2} + (d-1)x\frac{\partial p(x,s)}{\partial r} - x^2\, p(x,s) = -x^2 \frac{s^{(d-2)/2}}{D^{d/2}} \frac{\delta(x-x_0)}{\Omega_d\, x_0^{d-1}}, \tag{14.31}$$

which is a modified Bessel equation. Its solution is a combination of $x^\nu I_\nu(r)$ and $x^\nu K_\nu(r)$, where $\nu = 1 - d/2$. $I_\nu(r)$ and $K_\nu(r)$ are the modified Bessel functions of first and second kind, respectively.

In the next two sections, we will apply the appropriate boundary conditions to this problem when both boundaries are perfectly reflecting and when one boundary is perfectly absorbing and the other one is perfectly reflecting.

14.3.1 Perfectly Absorbing-Perfectly Absorbing

The condition that the propagator has to be null at R_{in} and R_{out}, given by Eq. (5.41),

$$p(R_{in}, s|r_0) = p(R_{out}, s|r_0) = 0, \tag{5.41}$$

leads to the following solution:

[1] Consider the following definition of $\delta(x)$:

$$\delta(u) \equiv \lim_{b\to 0} \frac{1}{\mid b \mid \sqrt{\pi}}\, e^{-(u/b)^2}. \tag{14.28}$$

Now, applying to this definition the following two changes of variables, $u = \alpha x$ and αc, we obtain

$$\delta(\alpha x) = \frac{1}{\mid \alpha \mid} \lim_{c\to 0} \frac{1}{\mid c \mid \sqrt{\pi}}\, e^{-(x/c)^2} = \frac{1}{\mid \alpha \mid}\delta(x). \tag{14.29}$$

From the first and last term of this equation, we conclude that $\delta(x) = \mid \alpha \mid \delta(u)$. Finally, we have that

$$\delta(x - x_0) = \mid \alpha \mid \delta(u - u_0). \tag{14.30}$$

$$p(x,s) = \begin{cases} \mathcal{A}x^{\nu}\left[I_{\nu}(x)K_{\nu}(R_{in}) - I_{\nu}(R_{in})K_{\nu}(x)\right] & \text{for} \quad R_{in} \leq x < x_0, \\ \mathcal{B}x^{\nu}\left[I_{\nu}(x)K_{\nu}(R_{out}) - I_{\nu}(R_{out})K_{\nu}(x)\right] & \text{for} \quad x_0 < x \leq R_{out}. \end{cases} \tag{14.32}$$

Both solutions go to zero when $x_0 \to R_{in}, R_{out}$, respectively. In fact, when $d = 1$ or 3, the functional form of these solutions can be written in a reduced form, namely,

$$-\frac{\sinh(a-x)}{\sqrt{a}\,x^{(d-1)/2}}, \tag{14.33}$$

where $a = R_{in}$ or R_{out}, depending on the interval. This function goes to zero when $x \to a$. The inclusion of an auxiliary function defined as

$$Q^{(i)}_{\alpha,\beta}(w,z) \equiv I_{\alpha}(w)K_{\beta}(z) + (-1)^i I_{\beta}(z)K_{\alpha}(w), \tag{14.34}$$

can make operations more practical. Then, Eq. (14.32) simplifies to

$$p(x,s) = \begin{cases} \mathcal{A}x^{\nu}Q^{(1)}_{\nu,\nu}(x,R_{in}) & \text{for} \quad R_{in} \leq x < x_0, \\ \mathcal{B}x^{\nu}Q^{(1)}_{\nu,\nu}(x,R_{out}) & \text{for} \quad x_0 < x \leq R_{out}. \end{cases} \tag{14.35}$$

Now, to determine the constants in Eq. (14.32) subject to two perfectly absorbing boundaries, we are going to follow the steps described in Sect. 5.4.2. In this section, we find that the joint conditions given by Eq. (3.39) and Eq. (3.42) lead to two relations that will help us to find the constants to be determined. Using the first relation, which imposes that the solution must be continuous at the starting point x_0, we have that

$$p(x,s|x_0)\Big|_{x_0^+} = p(x,s|x_0)\Big|_{x_0^-}. \tag{3.39}$$

Substituting Eqs. (14.35) into this relation leads to

$$\mathcal{A}\,x^{\nu}Q^{(1)}_{\nu,\nu}(x,R_{in}) = \mathcal{B}\,x^{\nu}Q^{(1)}_{\nu,\nu}(x,R_{out}). \tag{14.36}$$

By using the second relation, the discontinuity condition, and the recurrence relation of $Q^{(i)}_{\alpha,\beta}(a,z)$ and its derivative, given in Eq. (A.138), we arrive at

$$-\frac{s^{(d-2)/2}}{D^{d/2}}\frac{1}{\Omega_d\,x_0^{d-1}} = \frac{\partial p(x,s|x_0)}{\partial x}\bigg|_{x_0^+} - \frac{\partial p(x,s|x_0)}{\partial x}\bigg|_{x_0^-}. \tag{14.37}$$

Substituting Eqs. (14.35) into this last relation results in

$$x_0^{\nu}\left[\mathcal{B}\,Q^{(2)}_{\nu,\nu-1}(R_{out},x_0)-\mathcal{A}\,Q^{(2)}_{\nu,\nu-1}(R_{in},x_0)\right]=-\frac{s^{(d-2)/2}}{D^{d/2}}\frac{1}{\Omega_d\,x_0^{d-1}}. \tag{14.38}$$

Solving the system given by Eqs. (14.36) and (14.38) leads to

$$\mathcal{A}=\frac{s^{(d-2)/2}}{D^{d/2}}\frac{1}{\Omega_d\,x_0^{d-1+\nu}}\frac{Q^{(1)}_{\nu,\nu}(R_{out},x_0)}{Q^{(1)}_{\nu,\nu}(R_{out},R_{in})Q^{(2)}_{\nu,\nu-1}(x_0,x_0)}, \tag{14.39}$$

and

$$\mathcal{B}=\frac{s^{(d-2)/2}}{D^{d/2}}\frac{1}{\Omega_d\,x_0^{d-1+\nu}}\frac{Q^{(1)}_{\nu,\nu}(R_{in},x_0)}{Q^{(1)}_{\nu,\nu}(R_{out},R_{in})Q^{(2)}_{\nu,\nu-1}(x_0,x_0)}, \tag{14.40}$$

respectively. Using these constants in Eqs. (14.35), we find that the propagator is given by

$$p(x,s)=\frac{s^{(d-2)/2}}{\Omega_d\,D^{d/2}}(xx_0)^{\nu}\begin{cases}\dfrac{Q^{(1)}_{\nu,\nu}(R_{out},x_0)Q^{(1)}_{\nu,\nu}(R_{in},x)}{Q^{(1)}_{\nu,\nu}(R_{in},R_{out})} & \text{for}\quad R_{in}\le x<x_0,\\[2ex] \dfrac{Q^{(1)}_{\nu,\nu}(R_{in},x_0)Q^{(1)}_{\nu,\nu}(R_{out},x)}{Q^{(1)}_{\nu,\nu}(R_{in},R_{out})} & \text{for}\quad x_0<x\le R_{out}.\end{cases} \tag{14.41}$$

All we need to do to calculate the first-passage properties is to obtain the flux, since we already know the lifetime probability density, $\varphi(s)$, is related with the flux probability density by means of Eq. (5.63). Moreover, the survival probability density is related in Laplace space with $\varphi(s)$ by means of Eq. (12.64). Then, taking the derivative of Eq. (14.41) with respect to x by means of the recurrence relation (A.138) yields

$$J(x,s)=\frac{s^{(d-2)/2}}{\Omega_d\,D^{\frac{d}{2}-1}}(xx_0)^{\nu}\begin{cases}\dfrac{Q^{(1)}_{\nu,\nu}(R_{out},x_0)Q^{(2)}_{\nu,\nu-1}(R_{in},x)}{Q^{(1)}_{\nu,\nu}(R_{in},R_{out})} & \text{for}\ R_{in}\le x<x_0,\\[2ex] \dfrac{Q^{(1)}_{\nu,\nu}(R_{in},x_0)Q^{(2)}_{\nu,\nu-1}(R_{out},x)}{Q^{(1)}_{\nu,\nu}(R_{in},R_{out})} & \text{for}\ x_0<x\le R_{out}.\end{cases} \tag{14.42}$$

It is worth noting that the flux is obtained by multiplying the flux evaluated at the desired boundary by the perimeter of the chosen boundary.

14.3.2 Perfectly Absorbing-Perfectly Reflecting

If the inner d-dimensional sphere is perfectly reflecting and the outer d-dimensional sphere is perfectly absorbing, the boundary conditions are given by Eq. (5.97), namely,

$$p(x,s)\Big|_{x=R_{in}} = \frac{\partial p(x,s)}{\partial x}\Big|_{x=R_{out}} = 0. \tag{14.43}$$

Then, we have to solve Eq. (14.27) subject to these boundaries. We can write the solution of this diffusion equation as a superposition of a Bessel function of the first and second kind, keeping the boundary conditions in mind. To this end, we have that

$$p(x,s) = \begin{cases} \mathcal{A}x^{\nu}\left[I_{\nu}(x)K_{\nu}(R_{in}) - I_{\nu}(R_{in})K_{\nu}(x)\right] & \text{for} \quad R_{in} \leq x < x_0, \\ x^{\nu}\left[\mathcal{B}I_{\nu}(x) + \mathcal{C}K_{\nu}(x)\right] & \text{for} \quad x_0 < x \leq R_{out}. \end{cases} \tag{14.44}$$

The upper term of the solutions should be the same as in Eq. (14.44), since both stand for a perfectly absorbing inner boundary. The lower term has two constants so as to allow us to fix one from the null flux and the other from the discontinuity condition. Then, applying the null flux condition at R_{out} to Eq. (14.44), we arrive at the following relation:

$$\frac{\partial p(x,s)}{\partial x}\Big|_{x=R_{out}} = R_{out}^{\nu}(BI_{\nu-1}(R_{out}) - CK_{\nu-1}(R_{out})) = 0, \tag{14.45}$$

which leads to

$$\mathcal{C} = \mathcal{B}\frac{I_{\nu-1}(R_{out})}{K_{\nu-1}(R_{out})}, \tag{14.46}$$

so that Eq. (14.44) becomes

$$p(x,s) = \begin{cases} \mathcal{A}x^{\nu}\left[I_{\nu}(x)K_{\nu}(R_{in}) - I_{\nu}(R_{in})K_{\nu}(x)\right] & \text{for} \quad R_{in} \leq x < x_0, \\ \mathcal{B}x^{\nu}\dfrac{I_{\nu}(x)K_{\nu-1}(R_{out}) + I_{\nu-1}(R_{out})K_{\nu}(x)}{K_{\nu-1}(R_{out})} & \text{for} \quad x_0 < x \leq R_{out}. \end{cases} \tag{14.47}$$

In terms of function $Q_{\alpha,\beta}^{(i)}(w,z)$, given by Eq. (14.34), this reduces to

$$p(x,s) = \begin{cases} \mathcal{A}\, x^{\nu}\, Q^{(1)}_{\nu,\nu}(x,\, R_{in}) & \text{for} \quad R_{in} \le x < x_0, \\ \mathcal{B}\, x^{\nu}\, \dfrac{Q^{(2)}_{\nu,\nu-1}(x,\, R_{out})}{K_{\nu-1}(R_{out})} & \text{for} \quad x_0 < x \le R_{out}. \end{cases} \tag{14.48}$$

Now, we will follow the same steps as in the preceding section to obtain the remaining constants using the joint conditions. From the continuity condition at the starting point, we see that

$$\mathcal{A}\, x_0^{\nu}\, Q^{(1)}_{\nu,\nu}(x_0,\, R_{in}) = \mathcal{B}\, x_0^{\nu}\, \frac{Q^{(2)}_{\nu,\nu-1}(x_0,\, R_{out})}{K_{\nu-1}(R_{out})}. \tag{14.49}$$

On the other hand, using the recurrence formula (A.140), the discontinuity condition given by Eq. (14.37) yields

$$x_0^{\nu}\left[-\mathcal{B}\, \frac{Q^{(1)}_{\nu-1,\nu-1}(R_{out},\, x_0)}{K_{\nu-1}(R_{out})} - \mathcal{A}\, Q^{(2)}_{\nu,\nu-1}(R_{in},\, x_0)\right] = -\frac{s^{(d-2)/2}}{D^{d/2}}\, \frac{1}{\Omega_d\, x_0^{d-1}}. \tag{14.50}$$

Solving the system of equations given by Eqs. (14.49) and (14.50) for $\mathcal{A}$ and $\mathcal{B}$ leads to

$$\mathcal{A} = \frac{s^{(d-2)/2}}{D^{d/2}}\, \frac{1}{\Omega_d\, x_0^{d-1+\nu}}\, \frac{Q^{(2)}_{\nu,\nu-1}(x_0,\, R_{out})}{Q_c}, \tag{14.51}$$

and

$$\mathcal{B} = \frac{s^{(d-2)/2}}{D^{d/2}}\, \frac{1}{\Omega_d\, x_0^{d-1+\nu}}\, \frac{K_{\nu-1}(R_{out})\, Q^{(2)}_{\nu,\nu-1}(x_0,\, R_{out})}{Q_c}, \tag{14.52}$$

respectively, where we define the denominator of these two constants as

$$Q_c = Q^{(1)}_{\nu,\nu}(x_0,\, R_{in})\, Q^{(1)}_{\nu-1,\nu-1}(R_{out},\, x_0) + Q^{(2)}_{\nu,\nu-1}(R_{in},\, x_0)\, Q^{(2)}_{\nu,\nu-1}(x_0,\, R_{out}). \tag{14.53}$$

Substituting the constants into Eq. (14.48), we arrive to

$$p(x,s) = \frac{s^{(d-2)/2}}{\Omega_d\, D^{d/2}}\, \frac{(x x_0)^{\nu}}{Q_c} \begin{cases} Q^{(2)}_{\nu,\nu-1}(x_0,\, R_{out})\, Q^{(1)}_{\nu,\nu}(x,\, R_{in}) & \text{for} \quad R_{in} \le x < x_0, \\ Q^{(2)}_{\nu,\nu-1}(x_0,\, R_{out})\, Q^{(2)}_{\nu,\nu-1}(x,\, R_{out}) & \text{for} \quad x_0 < x \le R_{out}. \end{cases} \tag{14.54}$$

By means of the flux, we can obtain all the first-passage properties for the inner boundary.

14.3.3 Splitting Probability Absorbing-Absorbing: The Effect of Dimensionality

An interesting problem is raised by generalizing the study of free diffusion in the presence of two concentric perfectly absorbing spheres in d dimensions. Then, assuming angular independence, the differential equation for the splitting probability, given by Eq. (2.106), in spherical coordinates and d dimensions, reads

$$\frac{\mathrm{d}}{\mathrm{d}r_0}\left(r_0^{d-1}\frac{\mathrm{d}\theta(r_0)}{\mathrm{d}r_0}\right)=0, \tag{14.55}$$

where r_0 is the initial position. Let us denominate θ_{in} and θ_{out} probability of hitting the inner and outer spheres. These probabilities are subject to the following boundary conditions:

$$\theta_{in}(R_{in})=1 \quad \text{and} \quad \theta_{in}(R_{out})=0 \tag{14.56}$$

and

$$\theta_{out}(R_{out})=1 \quad \text{and} \quad \theta_{out}(R_{in})=0. \tag{14.57}$$

Now, to solve Eq. (14.55), we will split the problem into two separate cases, when $d=2$ and when $d\neq 2$. Integrating Eq. (14.55) with respect to r_0 for $d=2$ leads to

$$\theta(r_0)=\mathcal{A}\ln(r_0)+\mathcal{B}. \tag{14.58}$$

To obtain θ_{out}, we have to find the integration constants by applying the boundary conditions given in Eqs. (14.57), from which we have that

$$\theta_{out}(r_0)=\frac{\ln(r_0/R_{in})}{\ln(R_{out}/R_{in})}. \tag{14.59}$$

θ_{in} can be obtained from this last result since $\theta_{in}+\theta_{out}=1$, or by applying the boundary conditions given in Eqs. (14.56) into Eq. (14.58), namely,

$$\theta_{in}(r_0)=\frac{\ln(R_{out}/r_0)}{\ln(R_{out}/R_{in})}. \tag{14.60}$$

Now, integrating Eq. (14.55) for $d\neq 2$, we obtain

$$\theta(r_0) = \frac{\mathcal{A}}{r_0^{d-2}} + \mathcal{B}. \tag{14.61}$$

Applying the boundary conditions given by Eqs. (14.57), we find that

$$\theta_{out}(r_0) = \frac{1 - \left(\frac{R_{in}}{r_0}\right)^{d-2}}{1 - \left(\frac{R_{in}}{R_{out}}\right)^{d-2}}, \tag{14.62}$$

and consequently

$$\theta_{in}(r_0) = \frac{1 - \left(\frac{R_{out}}{r_0}\right)^{d-2}}{1 - \left(\frac{R_{out}}{R_{in}}\right)^{d-2}}. \tag{14.63}$$

Summarizing

$$\theta_{out}(r_0) = \begin{cases} \frac{r_0 - R_{in}}{R_{out} - R_{in}} & \text{for} \quad d = 1, \\ \frac{\ln\left(\frac{r_0}{R_{in}}\right)}{\ln\left(\frac{R_{out}}{R_{in}}\right)} & \text{for} \quad d = 2, \\ \frac{1 - \left(\frac{R_{in}}{r_0}\right)^{d-2}}{1 - \left(\frac{R_{in}}{R_{out}}\right)^{d-2}} & \text{for} \quad d \geq 3. \end{cases} \tag{14.64}$$

Taking the limit when $R_{out} \to \infty$, we see that $\theta_{out}(r_0) = 0$ in one and two dimensions and

$$\theta_{out}(r_0) = 1 - \left(\frac{R_{in}}{r_0}\right)^{d-2} \tag{14.65}$$

in three and more dimensions. Consequently, in one and two dimensions, the diffusing particles cannot drift to infinity and are absorbed by the inner sphere with a probability equal to 1. In three or more dimensions, there is a probability that the particles will escape to infinity. When $d \to \infty$, in three dimensions, $\theta_{out}(r_0) = 1$. Then, in very high-number dimensions, there is so much space available for the diffusing particles that they will never hit the inner sphere. In contrast, when $R_{in} \to 0$, in one dimension $\theta_{out}(r_0) = r_0/R_{out}$, and $\theta_{out}(r_0) = 1$ for three and more dimensions (see Fig. 14.4).

Now, let us quantify the value for the initial position, $r_{1/2}$, at which the affinity of the diffusing particles to each boundary is the same. To such end, we set the splitting probability equal to one half. From Eqs. (14.59) and (14.62), one finds that

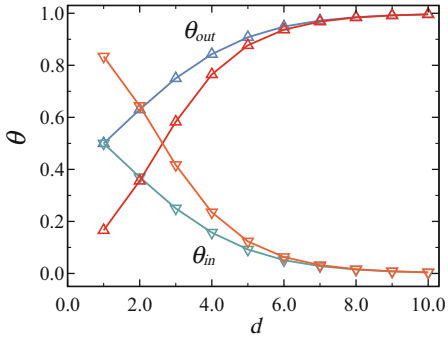

Fig. 14.4 Splitting probability θ_{out} (triangles up) and θ_{in} (triangles down) as a function of dimension d. θ_{out} is calculated using Eq. (14.64), since θ_{in} is calculated using the conservation of probability, $\theta_{in} = 1 - \theta_{out}$. The inner radius is set at $R_{in} = 1$ and $r_0 = 2$. Symbols in blue colors stand for $R_{out} = 3$, since symbols in red tones stand for $R_{out} = 7$. Lines are a guide to the eye that show the general trend of the data

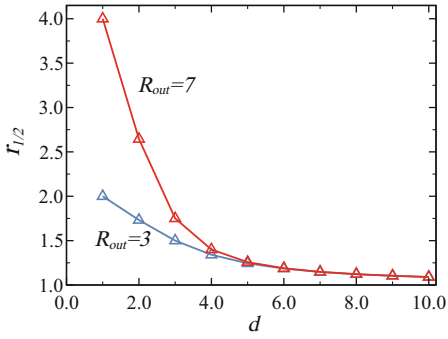

Fig. 14.5 Initial position $r_{1/2}$ as a function of d. The inner radius is set at $R_{in} = 1$ and $r_0 = 2$. Symbols in blue stand for $R_{out} = 3$, and symbols in red stand for $R_{out} = 7$. Lines are a guide to the eye that show the general trend of the data

$$r_{1/2} = \begin{cases} \frac{1}{2}\left(R_{in} + R_{out}\right) & \text{for} \quad d = 1, \\ \sqrt{R_{in} R_{out}} & \text{for} \quad d = 2, \\ \left[\frac{1}{2}\left(R_{in}^{2-d} + R_{out}^{2-d}\right)\right]^{\frac{1}{2-d}} & \text{for} \quad d \geq 3. \end{cases} \tag{14.66}$$

As d increases, $r_{1/2}$ tends to R_{in} (see Fig. 14.5). In the limiting case when $R_{out} \gg R_{in}$, in one dimension, we have that $\theta_{out}(r_{1/2}) = (1/2) R_{out}$ and

$$\left(\frac{1}{2}\right)^{\frac{1}{2-d}} R_{out} \tag{14.67}$$

for three dimensions.

14.3.4 Mean First-Passage Time: The Effect of Dimensionality

In this section we will study the mean first-passage time (MFPT) or mean hitting time to either boundary in d dimensions. To such end, we have to solve Eq. (2.63) in spherical coordinates, namely,

$$\frac{D}{r_0^{d-1}}\frac{\mathrm{d}}{\mathrm{d}r_0}\left(r_0^{d-1}\frac{\mathrm{d}\langle t(r_0)\rangle}{\mathrm{d}r_0}\right) = -1, \tag{14.68}$$

where r_0 is the initial position and D is the diffusivity, subject to the following boundary conditions:

$$\langle t(R_{in})\rangle = \langle t(R_{out})\rangle = 0. \tag{14.69}$$

First let us solve the problem in two dimensions. In such a case, Eq. (14.68) becomes

$$\frac{D}{r_0}\frac{\mathrm{d}}{\mathrm{d}r_0}\left(r_0\frac{\mathrm{d}\langle t(r_0)\rangle}{\mathrm{d}r_0}\right) = -1. \tag{14.70}$$

Integrating the latter equation twice gives

$$\langle t(r_0)\rangle = -\frac{r_0^2}{4D} + \mathcal{A}\ln(r_0) + \mathcal{B}. \tag{14.71}$$

Applying the boundary conditions given in Eq.(14.69), we arrive at

$$\langle t(r_0)\rangle = \frac{1}{4D}\left[\left(R_{out}^2 - R_{in}^2\right)\frac{\ln(r_0/R_{in})}{\ln(R_{out}/R_{in})} - \left(r_0^2 - R_{in}^2\right)\right]. \tag{14.72}$$

Now, solving Eq. (14.68) for $d \neq 2$, we integrate it once and have

$$\frac{\mathrm{d}\langle t(x_0)\rangle}{\mathrm{d}r_0} = -\frac{r_0}{dD} + \frac{\mathcal{A}}{r_0^{d-1}}. \tag{14.73}$$

Integrating this last expression again yields

$$\langle t(r_0)\rangle = -\frac{r_0^2}{2dD} + \mathcal{A}\frac{r_0^{2-d}}{2-d} + \mathcal{B}, \tag{14.74}$$

and imposing the boundary conditions given by Eq. (14.69) leads to

$$\langle t(r_0)\rangle = \frac{1}{2dD}\left[\frac{R_{out}^2 - R_{in}^2}{R_{out}^{2-d} - R_{in}^{2-d}}\left(r_0^{2-d} - R_{in}^{2-d}\right) - \left(r_0^2 - R_{in}^2\right)\right]. \tag{14.75}$$

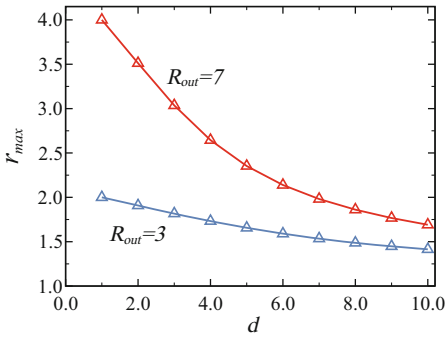

Fig. 14.6 Initial position r_{max} as a function of d. The inner radius is set at $R_{in} = 1$ and $r_0 = 2$. Symbols in blue stand for $R_{out} = 3$, and symbols in red stand for $R_{out} = 7$. Lines are a guide to the eye that show the general trend of the data

From Eqs. (14.72) and (14.75), we can calculate the initial position that maximizes the MFPT, r_{max}, and, consequently, maximize the survival probability as well. This initial position values is given by

$$r_{max} = \begin{cases} \frac{1}{2}\frac{R_{out}^2 - R_{in}^2}{R_{out} - R_{in}} & \text{for} \quad d = 1, \\ \left[\frac{1}{2}\frac{R_{out}^2 - R_{in}^2}{\ln(R_{out}/R_{in})}\right]^{\frac{1}{2}} & \text{for} \quad d = 2, \\ \left[\frac{2-d}{2}\frac{R_{out}^2 - R_{in}^2}{R_{out}^{2-d} - R_{in}^{2-d}}\right]^{\frac{1}{d}} & \text{for} \quad d \geq 3. \end{cases} \tag{14.76}$$

It is worth noting that r_{max} tends to R_{in} as d grows (see Fig. 14.6).

14.3.5 Partially Absorbing and Reflecting: MFPT

Consider a particle diffusing between two concentric spheres of radii R_{in} and R_{out}, $R_{in} < R_{out}$. The inner and outer spheres are partially absorbing and perfectly reflecting, respectively. The MFPT, which depends on the initial distance r_0 from the center of both spheres, denoted by $\langle t(x_0)\rangle$, satisfies Eq. (14.70) subject to the following boundary conditions:

$$D\left.\frac{\mathrm{d}\langle t(r_0)\rangle}{\mathrm{d}r_0}\right|_{r_0=R_{in}} = \kappa\,\langle t(R_{in})\rangle \quad \text{and} \quad \left.\frac{\mathrm{d}\langle t(r_0)\rangle}{\mathrm{d}r_0}\right|_{r_0=R_{out}} = 0, \tag{14.77}$$

where D is the diffusivity and κ is the trapping rate coefficient of the inner sphere surface. Introducing the boundary condition at $r_0 = R_{out}$ into Eq. (14.73) and setting $d = 3$, one finds that

$$\mathcal{A} = \frac{R_{out}^3}{3D}. \tag{14.78}$$

By substituting this constant into Eq. (14.74), it transforms into

$$\langle t(r_0)\rangle = -\frac{r_0}{2dD} - \frac{R_{out}^3}{3Dr_0} + \mathcal{B}. \tag{14.79}$$

Now, using the boundary condition at $r_0 = R_{in}$, the second constant is obtained:

$$\mathcal{B} = \frac{1}{\kappa}\left[\frac{R_{out}^3}{3R_{in}^2} - \frac{R_{in}}{3}\right] + \frac{R_{out}^3}{3DR_{in}} + \frac{R_{in}^2}{6D}. \tag{14.80}$$

Substituting this into the previous equation, we finally arrive at

$$\langle t(r_0)\rangle = \frac{1}{6D}\left(R_{in}^2 - r_0^2\right) - \frac{R_{out}^3}{3DR_{in}}\left(1 - \frac{R_{in}}{r_0}\right) + \frac{1}{3\kappa R_{in}^2}\left(R_{out}^3 - R_{in}^3\right). \tag{14.81}$$

This equation reduces to a relatively simple expression for the mean lifetime of a particle starting from the inner partially absorbing sphere, namely,

$$\langle t(R_{in})\rangle = \frac{R_{out}^3 - R_{in}^3}{3\kappa R_{in}^2}. \tag{14.82}$$

14.3.5.1 Circular Disk on a Reflecting Flat Surface: Absorbing Hemisphere Approximation

The study of the trapping of diffusing particles by a circular disk on a reflecting flat surface, which will also be addressed in Sect. 14.4 in a more rigorous way, is one of the interesting applications of the findings from the earlier section, among other uses. In fact, the exact solution to this problem is unknown. In this section, we discuss an approximate solution to the problem where an absorbing hemisphere with the right radius replaces the absorbing disk. A schematic representation of this approximation is given in Fig. 14.7.

With this replacement, the problem becomes effectively one-dimensional and angular-independent, allowing an approximate analytical treatment of the problem. To such end, we use the classical results by Smoluchowski, Hill, and Berg-Purcell for the rate constants that describe the trapping of diffusing particles by a perfectly absorbing sphere in free space and a perfectly absorbing disk on a reflecting flat surface, given by Eqs. (4.18) and (4.22), to establish a connection between the disk and hemisphere radii, denoted by a and R_{hs}, respectively. To find the hemisphere radius R_{hs} in terms of the disk radius a, it is necessary for the steady-state flux

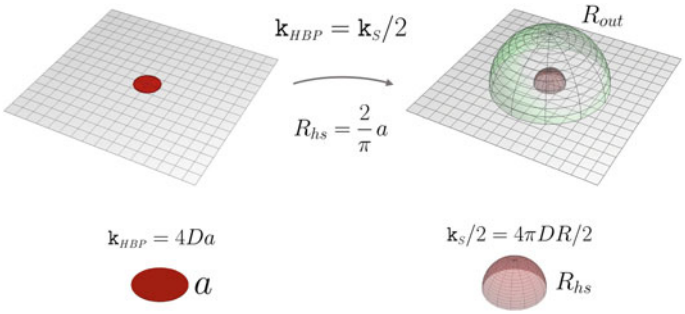

Fig. 14.7 Schematic representation of the absorbing hemisphere approximation. The absorbing hemisphere approximation consists of replacing the absorbing disk with an absorbing hemisphere of a properly chosen radius, in such a way that the absorbing hemisphere has the same flux of particles as the original disk. In other words, they have the same flux crossing their areas at the steady state

through the disk to be equal to the current flux through the hemisphere (half of a sphere). As we already know, this flux is proportional to the rate constant and the concentration at infinity, given by Eqs. (4.17) and (14.112). Then, equating these two last equations, and replacing $\mathtt{k}_S$ by $\mathtt{k}_S/2$, we have that $\mathtt{k}_{HBP} = \mathtt{k}_S/2$. This leads to the following relation between the hemisphere and disk radii:

$$R_{hs} = \frac{2}{\pi}a, \tag{14.83}$$

which is the assumption on which this approximation is based.

To check the accuracy of this angle-independent approach and establish the range of its applicability, one has to run three-dimensional Brownian dynamics simulations of the system with the absorbing disk on the reflecting flat surface and compare the obtained results with the corresponding theoretical predictions derived using the absorbing hemisphere approximation. This theoretical description from the splitting probability and the MFPT to the disk is obtained by replacing R_{in} by R_{hs} into Eqs. (14.21) and (14.23), leading to

$$\theta_{in} = \frac{2a(R_{out} - r_0)}{r_0(\pi R_{out} - 2a)}, \tag{14.84}$$

and

$$\langle t(r_0)\rangle_{in} = \frac{1}{6D}\left(r_0 - \frac{2a}{\pi}\right)\left(2R_{out} - r_0 - \frac{2a}{\pi}\right), \tag{14.85}$$

respectively.

In simulations, it is convenient to surround the absorbing disk of radius a with a large absorbing hemisphere to count from those particles which escape to infinity.

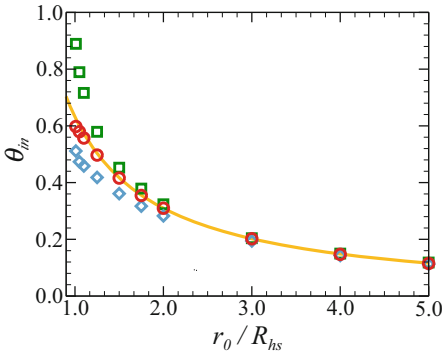

Fig. 14.8 Conditional splitting probability θ_{in}. The theoretical prediction given by Eq. (14.84) is compared to the results obtained by Brownian dynamics simulations (symbols) for three values of the azimuthal angle of the initial position: 0° (blue diamonds), 30° (red circles), and 90° (green squares)

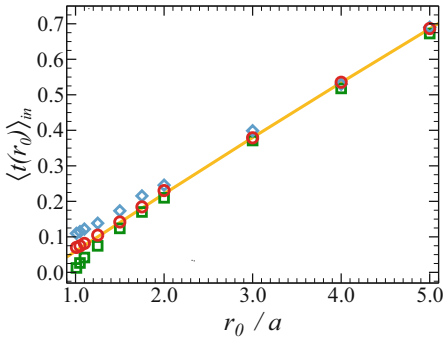

Fig. 14.9 Conditional MFPT $\langle t(r_0)\rangle_{in}$. The theoretical prediction given by Eq. (14.85) is compared to the results obtained by Brownian dynamics simulations (symbols) for three values of the azimuthal angle of the initial position: 0° (blue diamonds), 30° (red circles), and 90° (green squares)

From simulations shown in Figs. 14.8 and 14.9, it is observed that the angular dependencies of the splitting probabilities and the MFPT are really pronounced at small values of the initial position, $r_0 \leq 2a$. On the other hand, it shows excellent agreement between the theory and simulations for $r_0/a > 2$. Moreover, even when the initial distance is only two disk radii, the maximum relative error of the theoretical predictions is around 10%.

14.4 Diffusion to an Absorbent Circular Disk: Weber's Disk

Consider diffusing particles in a semi-infinite medium in the presence of a perfectly absorbing circular disk of radius a located on a flat reflecting surface. As soon as a particle reaches the surface of the absorbing disk, it is removed from the system, and consequently, the concentration at the disk is null. The concentration at infinity is uniform, $c(r, z, t)\big|_{z\to\infty} = c_\infty$. It is worth noting that the geometry of this problem is cylindrically symmetric. Then, assuming angular independence, the diffusion equation at steady state is given by

$$\nabla^2 c(r,z) = \frac{1}{r}\frac{\partial}{\partial r}\left(r\frac{\partial c(r,z)}{\partial r}\right) + \frac{\partial^2 c(r,z)}{\partial z^2} = 0. \tag{14.86}$$

Applying the chain rule results in

$$\frac{\partial^2 c(r,z)}{\partial r^2} + \frac{1}{r}\frac{\partial c(r,z)}{\partial r} + \frac{\partial^2 c(r,z)}{\partial z^2} = 0. \tag{14.87}$$

The boundary conditions on the surface are no concentration at the surface disk and no flux at the reflecting surface

$$c(r,z) = 0 \qquad z = 0, \qquad r \le a,$$

and

$$\frac{\partial c(r,z)}{\partial z} = 0, \qquad z = 0, \qquad r > a,$$

respectively. Let's solve Eq. (14.87) by applying the separation of variables method, assuming that

$$c(r,z) = R(r)G(z). \tag{14.88}$$

Substituting (14.88) into (14.87) results in

$$\frac{\partial^2 R}{\partial r^2}G(z) + \frac{1}{r}\frac{\partial R(r)}{\partial r}G(z) = -R(r)\frac{\partial^2 G(z)}{\partial z^2}. \tag{14.89}$$

Since the right-hand side depends only on x and the left-hand side only on t, both factors must be equal to a constant, which, for practical purposes can be defined as $-\lambda^2 D$. Consequently, two ordinary differential equations (ODE) arise:

$$\frac{1}{R(r)}\left(\frac{\partial^2 R(r)}{\partial r^2} + \frac{1}{r}\frac{\partial R(r)}{\partial r}\right) = -\frac{1}{G(z)}\frac{\partial^2 G(z)}{\partial z^2} = -\lambda^2. \tag{14.90}$$

As a result, we have two ODEs, namely,

$$\frac{\partial^2 R}{\partial r^2} + \frac{1}{R}\frac{\partial R}{\partial r} + \lambda^2 R = 0, \tag{14.91}$$

and

$$\frac{\partial^2 G}{\partial z^2} - \lambda^2 G = 0. \tag{14.92}$$

The general solution of this last equation is

$$G(z) = \mathcal{A}e^{\lambda z} + \mathcal{B}e^{-\lambda z}. \tag{14.93}$$

Because the concentration must meet the following condition, $c(r, z, t)\big|_{z\to\infty} = c_\infty$, $\mathcal{A} = 0$, and the solution is

$$G(z) = \mathcal{B}e^{-\lambda z}. \tag{14.94}$$

To solve Eq. (14.91), we first need to discuss certain properties of *Bessel functions*. The starting point corresponds to the following properties of the Bessel function of the first kind $J_n(x)$:

$$\frac{\mathrm{d}J_0(x)}{\mathrm{d}x} = -J_1(x), \tag{14.95}$$

and

$$\frac{\mathrm{d}[x^n J_n(x)]}{\mathrm{d}x} = x^n J_{n-1}(x). \tag{14.96}$$

Setting $n = 1$, we arrive at

$$\frac{d}{dx}[xJ_1(x)] = xJ_0(x). \tag{14.97}$$

Substituting (14.95) into (14.97), one finds that

$$\frac{\mathrm{d}}{\mathrm{d}x}\left[x\frac{\mathrm{d}J_0(x)}{\mathrm{d}x}\right] + xJ_0(x) = 0. \tag{14.98}$$

Applying the chain rule gives

$$x\frac{\mathrm{d}^2J_0}{\mathrm{d}x^2} + \frac{\mathrm{d}J_0}{\mathrm{d}x} + xJ_0(x) = 0. \tag{14.99}$$

Replacing x by λr, it reduces to Eq. (14.91) and, consequently,

$$R(r) = \mathcal{C}\,J_0(\lambda r). \tag{14.100}$$

By multiplying the right side of this equation by a function that depends on λ, it continues to be a solution, so that

$$R(r) = \mathcal{C}\,f(\lambda)J_0(\lambda r). \tag{14.101}$$

Substituting Eq. (14.94) and Eq. (14.101) into Eq. (14.88) yields

$$c(r, z) = \beta f(\lambda)e^{-\lambda z}J_0(\lambda r), \tag{14.102}$$

where $\beta = \mathcal{AC}$. By the principle of superposition, the sum of the eigenfunctions $c_\lambda = R(r)\,G(z)$ is also a solution, and in a continuous spectrum of λ, the most general solution is given by

$$c(r,z) = \beta \int_0^\infty f(\lambda) e^{-\lambda z} J_0(\lambda r) d\lambda + \alpha. \tag{14.103}$$

Setting $z \to \infty$, we find that $\alpha = c_\infty$.

Now, by choosing $f(\lambda) = \sin(\lambda a)/\lambda$, the boundary conditions are met when performing the integrals of the Bessel functions, since

$$\int_0^\infty \frac{\sin(\lambda a)}{\lambda} J_0(\lambda r)\,\mathrm{d}\lambda = \begin{cases} \arcsin\left(\frac{a}{r}\right), & r > a \\ \frac{\pi}{2}, & r < a. \end{cases} \tag{14.104}$$

For $r < a$, the concentration should be as follows:

$$c(r,z) = c_\infty - \frac{2c_\infty}{\pi} \int_0^\infty \frac{\sin(\lambda a)}{\lambda} e^{-\lambda z} J_0(\lambda r)\,\mathrm{d}\lambda. \tag{14.105}$$

The gradient of the concentration is found by taking the derivative with respect to z as follows:

$$\frac{\partial c}{\partial z} = \frac{\partial}{\partial z}\left[-\frac{2c_\infty}{\pi} \int_0^\infty \frac{\sin(\lambda a)}{\lambda} J_0(\lambda r) e^{-\lambda z}\,\mathrm{d}\lambda \right], \tag{14.106}$$

which satisfies $c(r,z,t)\big|_{z\to\infty} = c_\infty$. Now, the perpendicular flux, Eq. (2.74), to the flat reflecting surface is

$$J(r,z) = -D\,\frac{\partial c}{\partial z} = -D\,\frac{2c_\infty}{\pi} \int_0^\infty \sin(\lambda a)\, J_0(\lambda r) e^{-\lambda z}\,\mathrm{d}\lambda, \tag{14.107}$$

where D is the diffusivity. In fact, the flux through the absorbing circular disk is given by

$$J(r,z)\Big|_{z=0} = -D\,\frac{2c_\infty}{\pi} \int_0^\infty \sin(\lambda a) J_0(\lambda r)\,\mathrm{d}\lambda, \tag{14.108}$$

one of Weber's discontinuous integrals. The solution of this integral is

$$\int_0^\infty J_0(\lambda r)\sin(\lambda a) d\lambda = \begin{cases} \frac{1}{\sqrt{a^2 - r^2}}, & r < a, \\ 0, & r > a. \end{cases} \tag{14.109}$$

Then,

$$J(r,z)\Big|_{z=0} = \frac{2c_\infty}{\pi}\frac{1}{\sqrt{a^2-r^2}}. \tag{14.110}$$

Finally, we want to calculate the *diffusion current* or *total flux*, which is the number of particles trapped by the circular disk per unit time, and this is calculated by integrating over the entire disk, namely,

$$I = \int_0^{2\pi}\int_0^a \frac{2Dc_\infty}{\pi}\frac{r}{\sqrt{a^2-r^2}}\mathrm{d}r\mathrm{d}\phi. \tag{14.111}$$

Solving this integral, we find that the flux current through the circular disk is given by

$$I = 4ac_\infty D. \tag{14.112}$$

This flux current is proportional not to the area of the disk, as one would expect, but to its radius. The ratio of the diffusion current to the particle concentration, $\mathtt{k} = I(t)/c_\infty$, is the *rate constant*, and for a circular disk placed on a flat reflecting wall, it is given by the so-called Hill-Berg-Purcell formula:

$$\mathtt{k}_{HBP} = 4Da. \tag{14.113}$$

It is worth noting that the rate constant is in units of volume per time.

14.5 Absorbing Patches of Arbitrary Shape

In the preceding sections, we derived the rate constant for a perfectly absorbing circular disk and a perfectly absorbing ellipse on a flat reflecting wall. In this section, our goal is to extend this result to perfectly absorbing patches of any shape, given by the so-called Dudko-Berezhkovskii-Weiss (DBW) formula. To such end, we will need the rate constant for an elliptical patch attached to a reflecting wall.

Consider diffusing particles in a semi-infinite medium in the presence of a perfectly absorbing elliptical patch of width $2a_1$ and height $2a_2$, located on a flat reflecting surface. As soon as a particle reaches the surface of the absorbing ellipse, it is removed from the system, so then, the rate constant is

$$\mathtt{k}_{elipse} = \frac{2\pi Da_1}{k(\epsilon)}, \tag{14.114}$$

where $k(\epsilon)$ is the complete elliptic integral of the first kind

$$k(\epsilon) = \int_0^{\pi/2} \frac{d\theta}{\sqrt{1 - \epsilon^2 \sin^2 \theta}}. \tag{14.115}$$

Now, we are ready to continue deducing the formula for our original problem, the rate constant for an absorbing patch of any shape. The dimensional analysis is the starting point for constructing an approximate formula for the rate constant for perfectly absorbing patches of general shape. The unit of the rate constant is length cubed over time. Consequently, let us assume that it must be proportional to diffusivity D and length. Furthermore let us assume that this length is proportional to the area A and perimeter P as $A^\nu P^\xi$. Then, the resulting formula is

$$\mathtt{k}_{DBW} = \alpha\, A^\nu P^\xi\, D. \tag{14.116}$$

where α is a proportionality constant to be determined, as well as ν and ξ. As $A^\nu P^\xi$ is in units of length and $\xi = 1 - 2\nu$, so then $A^\nu P^\xi = A^\nu P^{1-2\nu}$. The constant α is obtained by requiring that $\mathtt{k}_{DBW}$ should reduce to $\mathtt{k}_{HBP} = 4Da$ for a circular receptor, where $A = \pi a^2$ and $P = 2\pi a$. This leads to $\alpha = (2^{1-2\nu})/(\pi^{1-\nu})$. Substituting these constants into Eq. (14.116) yields

$$\mathtt{k}_{DBW} = \frac{2^{1-2\nu}}{\pi^{1-\nu}} A^{1-2\nu} P^{1-2\nu}\, D. \tag{14.117}$$

Now, ν will be found by requiring that this last formula to reproduce $\mathtt{k}_{elipse}$, given by Eq. (14.114). To such end, we equate the expansion for small values of ϵ of Eqs. (14.117) and (14.114). As we will show later, keeping terms up to ϵ^4 is enough to obtain a highly accurate, approximate formula.

On the one hand, expanding the integral in the denominator of Eq. (14.117) in a Taylor series around ϵ up to fourth order yields

$$\begin{aligned} \int_0^{\pi/2} \frac{1}{\sqrt{1 - \epsilon^2 \sin^2 \theta}} &\approx \int_0^{\pi/2} \left[1 + \frac{\sin^2 \theta}{2} \epsilon^2 + \frac{3 \sin^4 \theta}{8} \epsilon^4 + \cdots \right] \\ &= \frac{\pi}{2} \left[1 + \frac{\epsilon^2}{4} + \frac{9}{64} \epsilon^4 + \cdots \right]. \end{aligned} \tag{14.118}$$

Consequently,

$$k(\epsilon) = \frac{4Da_1}{\left[1 + \frac{\epsilon^2}{4} + \frac{9}{64} \epsilon^4 + \cdots \right]}. \tag{14.119}$$

Expanding again the numerator of this last expression, we arrive at

$$\mathtt{k}_{elipse} = 4Da_1 \left[1 - \frac{\epsilon^2}{4} - \frac{5\epsilon^4}{64} + \cdots \right]. \tag{14.120}$$

On the other hand, substituting the area and perimeter of an ellipse, $A_\epsilon = \pi a_1 a_2$ and $P_\epsilon = 4a_1 E(\epsilon)$, respectively, into Eq. (14.117), yields

$$\mathtt{k}_{DBW} = \frac{2^{1-2\nu}}{\pi^{1-\nu}}[\pi a_1^2\sqrt{1-\epsilon^2}]^{\nu}[4a_1 E(\epsilon)]^{1-2\nu}, \tag{14.121}$$

where

$$E(\epsilon) = \int_0^{\pi/2} \sqrt{1-\epsilon^2 \sin^2\theta}\, d\theta. \tag{14.122}$$

Taylor expanding Eq. (14.121) up to fourth order, we have

$$\mathtt{k}_{DBW} = 4a_1 D\left[1 - \frac{\epsilon^2}{4} - \frac{3}{64}(1+2\nu)\epsilon^4 + \cdots\right] \tag{14.123}$$

Equating Eqs. (14.121) and (14.123), we obtain

$$5 = 3(1+2\nu), \tag{14.124}$$

and solving for ν, we find that

$$\nu = \frac{1}{3}. \tag{14.125}$$

Finally, the formula for the rate constant for a perfectly absorbing patch of arbitrary shape is given by

$$\mathtt{k}_{DBW} = \left(\frac{2^5 AP}{\pi^2}\right)^{1/3} D. \tag{14.126}$$

Using Brownian dynamics simulations, it has been shown that this formula works reasonably well for many different shapes, and its predictions have an error of less than 5% for moderately asymmetric patches with smooth (non-jagged) boundaries.

14.6 Hyperboloidal Cone

This specific 3D system is of great interest because it is one of the few exactly solvable cases in the study of diffusion. More specifically, both an effective diffusion coefficient and the flux can be found. These quantities will be calculated later in Sect. 18.4.

Finding the solution of the diffusion equation for the hyperboloidal cone in Cartesian coordinates is not an easy task, reason why we need to consider studying

in other curvilinear coordinates, specifically oblate spheroidal coordinates. First, let us write the gradient for a scalar function $f(q_1, q_2, q_3)$ in curvilinear coordinates (q_1, q_2, q_3), which is

$$\nabla f(q_1, q_2, q_3) = \frac{1}{h_1}\frac{\partial f}{\partial q_1}\,\hat{\mathbf{e}}_1 + \frac{1}{h_2}\frac{\partial f}{\partial q_2}\,\hat{\mathbf{e}}_2 + \frac{1}{h_3}\frac{\partial f}{\partial q_3}\,\hat{\mathbf{e}}, \tag{14.127}$$

and if we have a vector function

$$\mathbf{F}(q_1, q_2, q_3) = (F_1(q_1, q_2, q_3),\, F_2(q_1, q_2, q_3),\, F_3(q_1, q_2, q_3)), \tag{14.128}$$

its divergence is

$$\nabla \cdot \mathbf{F}(q_1, q_2, q_3) = \frac{1}{h_1 h_2 h_3}\left[\frac{\partial}{\partial q_1}(V_1 h_2 h_3) + \frac{\partial}{\partial q_2}(V_2 h_1 h_3) + \frac{\partial}{\partial q_3}(V_3 h_1 h_2)\right], \tag{14.129}$$

making the Laplacian look as

$$\begin{aligned}\nabla^2 f(q_1, q_2, q_3) &= \nabla \cdot \nabla f(q_1, q_2, q_3) \\ &= \frac{1}{h_1 h_2 h_3}\left[\frac{\partial}{\partial q_1}\left(\frac{h_2 h_3}{h_1}\frac{\partial f}{\partial q_1}\right) + \frac{\partial}{\partial q_2}\left(\frac{h_1 h_3}{h_2}\frac{\partial f}{\partial q_2}\right) + \frac{\partial}{\partial q_3}\left(\frac{h_1 h_2}{h_3}\frac{\partial f}{\partial q_3}\right)\right].\end{aligned} \tag{14.130}$$

And the scale factors for the oblate spheroidal coordinates are given by

$$h_\xi = a\sqrt{\frac{\xi^2 + \eta^2}{1 + \xi^2}}, \qquad h_\eta = a\sqrt{\frac{\xi^2 + \eta^2}{1 - \eta^2}}, \qquad h_\phi = a\sqrt{(1 + \xi^2)(1 - \eta^2)}. \tag{14.131}$$

Also, the coordinate transformation between oblate spheroidal and Cartesian coordinates is

$$x = a\sqrt{1 + \xi^2}\sqrt{1 - \eta^2}\cos(\phi), \quad y = a\sqrt{1 + \xi^2}\sqrt{1 - \eta^2}\sin(\phi), \quad z = a\xi\eta. \tag{14.132}$$

The domain of the coordinates is

$$-\infty < \xi < \infty, \qquad -1 < \eta < 1, \qquad 0 \le \phi < 2\pi. \tag{14.133}$$

To form the hyperboloidal cone, a fixed η must be chosen. In this case, it is $\eta = \eta_0$. Also, if we want to have only the upper or positive part of the cone, the ξ domain must be restricted to $0 < \xi < \infty$. Then, the diffusion will take place inside the region defined by

$$0 < \xi < \infty, \qquad \eta_0 < \eta < 1, \qquad 0 \leq \phi < 2\pi, \tag{14.134}$$

under the conditions

$$c(\xi = 0, \eta, \phi) = 0, \qquad c(\xi \to \infty, \eta, \phi) = c_0, \qquad \left.\frac{\partial c(\xi, \eta, \phi)}{\partial \eta}\right|_{\eta=\eta_0} = 0, \tag{14.135}$$

the first one of which tells us that the concentration is null at the origin of the coordinates. Also, very far from the origin, the concentration will be constant, and the third condition is no-flux, meaning that the hyperboloidal cone is a completely reflectant wall.

Now, we can write the Laplacian operator over a concentration $c(\xi, \eta, \phi)$ as

$$\nabla^2 c(\xi, \eta, \phi) = \frac{1}{a^2(\xi^2 + \eta^2)} \left\{ \frac{\partial}{\partial \xi} \left[(1 + \xi^2) \frac{\partial c(\xi, \eta, \phi)}{\partial \xi} \right] + \frac{\partial}{\partial \eta} \left[(1 - \eta^2) \frac{\partial c(\xi, \eta, \phi)}{\partial \eta} \right] + \frac{\xi^2 + \eta^2}{(1 + \xi^2)(1 - \eta^2)} \frac{\partial^2 c(\xi, \eta, \phi)}{\partial \phi^2} \right\}. \tag{14.136}$$

The diffusion equation in oblate spheroidal coordinates can be obtained from this last expression, namely,

$$\frac{\partial c(\xi, \eta, \phi)}{\partial t} = \nabla^2 c(\xi, \eta, \phi) = \frac{1}{a^2(\xi^2 + \eta^2)} \left\{ \frac{\partial}{\partial \xi} \left[(1 + \xi^2) \frac{\partial c(\xi, \eta, \phi)}{\partial \xi} \right] + \frac{\partial}{\partial \eta} \left[(1 - \eta^2) \frac{\partial c(\xi, \eta, \phi)}{\partial \eta} \right] + \frac{\xi^2 + \eta^2}{(1 + \xi^2)(1 - \eta^2)} \frac{\partial^2 c(\xi, \eta, \phi)}{\partial \phi^2} \right\}. \tag{14.137}$$

We are looking for a solution in the steady state, which is valid for long enough times, and this is equivalent to solving the Laplace equation as stated in Eq. (14.136) equated to zero. In this coordinate system, the Laplace equation is separable, which means that we can find the concentration by assuming that

$$c(\xi, \eta, \phi) = \Xi(\xi)\, H(\eta)\, \Phi(\phi), \tag{14.138}$$

which is substituted into Eq. (14.136), and dividing the entire expression by Eq. (14.138), yielding

$$0 = \frac{1}{\Xi(\xi)}\frac{\partial}{\partial\xi}\left[(1+\xi^2)\frac{\partial\Xi(\xi)}{\partial\xi}\right] + \frac{1}{H(\eta)}\frac{\partial}{\partial\eta}\left[(1-\eta^2)\frac{\partial H(\eta)}{\partial\eta}\right] + \frac{1}{\Phi(\phi)}\frac{\xi^2+\eta^2}{(1+\xi^2)(1-\eta^2)}\frac{\partial^2\Phi(\phi)}{\partial\phi^2}. \tag{14.139}$$

To separate the equation, we must use a constant m^2, allowing us to write

$$\frac{\mathrm{d}^2\Phi(\phi)}{\mathrm{d}\phi^2} + m^2\,\Phi(\phi) = 0, \tag{14.140}$$

and

$$m^2 = \frac{(1+\xi^2)(1-\eta^2)}{\xi^2+\eta^2}\left\{\frac{1}{\Xi(\xi)}\frac{\partial}{\partial\xi}\left[(1+\xi^2)\frac{\partial\Xi(\xi)}{\partial\xi}\right] + \frac{1}{H(\eta)}\frac{\partial}{\partial\eta}\left[(1-\eta^2)\frac{\partial H(\eta)}{\partial\eta}\right]\right\}. \tag{14.141}$$

This last equation can be also separated by means of another constant n, to obtain

$$\frac{\mathrm{d}}{\mathrm{d}\xi}\left[(1+\xi^2)\frac{\partial\Xi(\xi)}{\partial\xi}\right] + \frac{m^2}{1+\xi^2}\,\Xi(\xi) - n\,\Xi(\xi) = 0, \tag{14.142}$$

and

$$\frac{\mathrm{d}}{\mathrm{d}\eta}\left[(1-\eta^2)\frac{\mathrm{d}H(\eta)}{\mathrm{d}\eta}\right] - \frac{m^2}{1-\eta^2}\,H(\eta) - n\,H(\eta) = 0. \tag{14.143}$$

Joining together all three separate equations reads

$$\begin{aligned} &\frac{\mathrm{d}^2\Phi(\phi)}{\mathrm{d}\phi^2} + m^2\,\Phi(\phi) = 0,\\ &\frac{\mathrm{d}}{\mathrm{d}\xi}\left[(1+\xi^2)\frac{\partial\Xi(\xi)}{\partial\xi}\right] + \frac{m^2}{1+\xi^2}\,\Xi(\xi) - n\,\Xi(\xi) = 0,\\ &\frac{\mathrm{d}}{\mathrm{d}\eta}\left[(1-\eta^2)\frac{\mathrm{d}H(\eta)}{\mathrm{d}\eta}\right] - \frac{m^2}{1-\eta^2}\,H(\eta) - n\,H(\eta) = 0. \end{aligned} \tag{14.144}$$

The solutions[2] of the second and third equations are written as a linear combination of associated Legendre polynomials of the first kind, P_n^m, and of the second kind,

[2] P. M. Morse & H. Feshbach, *Methods of Theoretical Physics*, McGraw-Hill Book Company, 1953.

Q_n^m. The first equation is obtained by a linear combination of sine and cosine functions, which can always be replaced by a complex exponential.

Nevertheless, for the hyperboloidal cone, the solution of the diffusion equation is rather simple because of the symmetry of the figure, which makes Eq. (14.137) to void the derivative with respect to the ϕ variable. Then, remembering that the system is in a steady state, we can write

$$0 = \frac{\partial}{\partial \xi}\left[(1+\xi^2)\frac{\partial c(\xi,\eta,\phi)}{\partial \xi}\right] + \frac{\partial}{\partial \eta}\left[(1-\eta^2)\frac{\partial c(\xi,\eta,\phi)}{\partial \eta}\right], \tag{14.145}$$

from where we can immediately separate the equations by means of a constant α if we propose that $c(\xi,\eta) = \Xi(\xi)\,H(\eta)$, substitute into Eq. (14.145), and divide the whole equation by $\Xi(\xi)\,H(\eta)$, after which we can write it for η

$$\frac{\mathrm{d}}{\mathrm{d}\eta}\left[(1-\eta^2)\frac{\mathrm{d}H(\eta)}{\mathrm{d}\eta}\right] + \alpha H(\eta) = 0, \tag{14.146}$$

and for ξ

$$\frac{\mathrm{d}}{\mathrm{d}\xi}\left[(1+\xi^2)\frac{\mathrm{d}\Xi(\xi)}{\mathrm{d}\xi}\right] - \alpha\,\Xi(\xi) = 0. \tag{14.147}$$

As the reader may note, both equations are fairly similar. The equation for ξ can be manipulated (through a variable change that will be performed later) to take the form of the equation for η, which is known as the Legendre equation.

If a placeholder function $f = f(x)$ is used, we can find the solution for the generic equation, so then

$$\frac{\mathrm{d}}{\mathrm{d}x}\left[(1-x^2)\frac{\mathrm{d}f(x)}{\mathrm{d}x}\right] + \alpha f(x) = 0, \tag{14.148}$$

which can be written to be seen as the Legendre equation,

$$(1-x^2)\,f''(x) - 2x\,f'(x) + \alpha\,f(x) = 0, \tag{14.149}$$

which is going to be solved by the power series method, better known as the Frobenius method. The first step is to propose that the solution $f(x)$ is a power series of the form

$$f(x) = \sum_{n=0}^{\infty} a_n\,x^n, \tag{14.150}$$

where its derivatives are

$$f'(x) = \sum_{n=0}^{\infty} n\, a_n\, x^{n-1}, \qquad f''(x) = \sum_{n=0}^{\infty} n(n-1)\, a_n\, x^{n-2}. \tag{14.151}$$

As Eq. (14.150) is a solution of Eq. (14.149), Eqs. (14.151) can be replaced into it, and the equality will hold. This yields

$$0 = (1-x^2) \sum_{n=0}^{\infty} n(n-1)\, a_n\, x^{n-2} - 2x \sum_{n=0}^{\infty} n\, a_n\, x^{n-1} + \alpha \sum_{n=0}^{\infty} a_n\, x^n, \tag{14.152}$$

which may be simplified to

$$0 = \sum_{n=0}^{\infty} n(n-1)\, a_n\, x^{n-2} - \sum_{n=0}^{\infty} n(n-1)\, a_n\, x^n - \sum_{n=0}^{\infty} 2n\, a_n\, x^n + \sum_{n=0}^{\infty} \alpha\, a_n\, x^n. \tag{14.153}$$

The first sum may be rewritten by switching the index to $n \to n-2$, that is,

$$0 = \sum_{n=-2}^{\infty} (n+1)(n+2)\, a_{n+2}\, x^n - \sum_{n=0}^{\infty} n(n-1)\, a_n\, x^n - \sum_{n=0}^{\infty} 2n\, a_n\, x^n + \sum_{n=0}^{\infty} \alpha\, a_n\, x^n, \tag{14.154}$$

where the first two terms of the first sum are null because for $n = -2$, the factor $(n+2)$ is zero, and for $n = -1$, the factor $(n+1)$ is also zero. This allows us to group everything under one sum as

$$0 = \sum_{n=0}^{\infty} \{(n+1)(n+2)\, a_{n+2} - n(n-1)\, a_n - 2n\, a_n + \alpha\, a_n\}\, x^n. \tag{14.155}$$

As all the powers of x are linearly independent, we obtain

$$(n+1)(n+2)\, a_{n+2} - n(n-1)\, a_n - 2n\, a_n + \alpha\, a_n = 0, \tag{14.156}$$

or

$$(n+1)(n+2)\, a_{n+2} = +n(n-1)\, a_n + 2n\, a_n - \alpha\, a_n, \tag{14.157}$$

yielding

$$a_{n+2} = \frac{n(n+1) - \alpha}{(n+1)(n+2)}\, a_n. \tag{14.158}$$

This constitutes a recurrence relation for the coefficients of the power series (14.150), which can be quickly analyzed for convergence using the D'Alembert criterion, also known as the *ratio* test. This convergence criterion is

$$\lim_{k\to\infty}\left|\frac{a_{k+1}}{a_k}\right| = r < 1, \tag{14.159}$$

that is, the ratio of two successive terms of the series. If the inequality holds, then the series converges. Applying this to Eq. (14.150) with their corresponding coefficients from (14.158), it yields

$$r = \lim_{n\to\infty}\left|\frac{n(n+1)-\alpha}{(n+1)(n+2)}\right| x^2 = x^2. \tag{14.160}$$

Then, to ensure convergence, the relation $x^2 < 1$ must hold, or equivalently, $-1 < x < 1$. As $n \geq 0$, and it is an integer, two different solutions for the Legendre equation may be identified. The first one comes from choosing $a_0 \neq 0$, and $a_1 = 0$, which makes $a_1 = a_3 = a_5 = \cdots = 0$, then

$$\begin{aligned} f_{even}(x) &= a_0\, x^0 + a_2\, x^2 + a_4\, x^4 + \cdots \\ &= a_0 - \frac{1}{2}\alpha\, a_0\, x^2 + \frac{6-\alpha}{12} a_2\, x^4 \\ &= a_0 - \frac{\alpha}{2} a_0\, x^2 - \frac{(6-\alpha)\alpha}{12\cdot 2} a_0\, x^4 + \cdots, \end{aligned} \tag{14.161}$$

which can be written as

$$f_{even}(x) = a_0\left[1 - \frac{\alpha}{2}x^2 - \frac{(6-\alpha)\alpha}{24}x^4 + \cdots\right]. \tag{14.162}$$

But we can also take $a_0 = 0$ with $a_1 \neq 0$, yielding $a_0 = a_2 = a_4 = \cdots = 0$, to obtain

$$\begin{aligned} f_{odd}(x) &= a_1\, x^1 + a_3\, x^3 + a_5\, x^5 + \cdots \\ &= a_1\, x + \frac{2-\alpha}{6}\, a_1\, x^3 + \frac{12-\alpha}{20} a_3\, x^5 \\ &= a_1\, x + \frac{2-\alpha}{6}\, a_1\, x^3 + \frac{(12-\alpha)(+2-\alpha)}{20\cdot 6} a_1\, x^5 + \cdots, \end{aligned} \tag{14.163}$$

which becomes

$$f_{odd}(x) = a_1\left[x + \frac{2-\alpha}{6}x^3 + \frac{(12-\alpha)(2-\alpha)}{120}x^5 + \cdots\right]. \tag{14.164}$$

Equations (14.164) and (14.162) are linearly independent by means of the powers of x and lead us to a general solution for the Legendre equation, which is

$$f(x) = \mathcal{A}\, f_{even}(x) + \mathcal{B}\, f_{odd}(x), \tag{14.165}$$

where $\mathcal{A}$ and $\mathcal{B}$ are constants to be fixed by the boundary conditions (BCs).

Nevertheless, there is a loose end: choosing of value of the separation constant α. This should be done keeping in mind the convergence of the series. The first approach is to truncate the series to ensure it remains finite, and this can be achieved by fixing the value of α to $l(l+1)$, so the polynomial of the series only contains powers of x up to the l-th one. This transforms the recurrence relation, Eq. (14.158), into

$$a_{l+2} = \frac{l(l+1) - \alpha}{(l+1)(l+2)}\, a_l. \tag{14.166}$$

Using these coefficients, the solution for our differential equation (14.149) can be written as polynomials known as the Legendre polynomials, denoted by $P_l(x)$, where l is their order. The convention is to set

$$P_l(1) = 1, \tag{14.167}$$

which is also known as *normalization*. The form of the polynomial will be obtained from Eqs. (14.162) and (14.164) if l is even or odd, respectively. As the solutions depends on their coefficients, we start by calculating $a_0 \neq 0$, knowing that for $l = 0$, we have $\alpha = 0$, then

$$a_2 = 0, \tag{14.168}$$

and as a consequence, $a_2 = a_4 = a_6 = \cdots = 0$. This allows us to calculate $P_0(x)$ from Eq. (14.162), yielding

$$P_0(x) = a_0, \tag{14.169}$$

and from the normalization condition

$$P_0(x = 1) = a_0 = 1, \tag{14.170}$$

from which all a_l for an even l can be calculated using the recurrence relation. For odd values, we need to calculate a_1, so $a_1 \neq 0$. Knowing that for $l = 1$ we have $\alpha = 2$, then

$$a_3 = 0, \tag{14.171}$$

meaning that $a_3 = a_5 = a_7 = \cdots = 0$. Furthermore, from Eq. (14.164), we obtain

$$P_1(x) = a_1\, x, \tag{14.172}$$

and from the normalization condition, we arrive at

$$P_1(x = 1) = a_1 = 1, \tag{14.173}$$

then

$$P_1(x) = x. \tag{14.174}$$

Now that we have a_0 and a_1, every coefficient of the series can be obtained from the recurrence relation, keeping in mind that the series must remain finite, the value of α should be set accordingly.

Up to this point, we have obtained solutions for the Legendre equation, which are known as Legendre polynomials, but as mentioned earlier, there is a second approach based on the assumption that α takes a value that does not truncate the series. This means that solutions (14.162) and (14.164) keep it as an infinite series.

Allow us to calculate the case for $\alpha = 0$, starting by substituting back into Eq. (14.162) to obtain

$$f_{even}(x) = a_1 \left(x + \frac{1}{3}x^3 + \frac{1}{5}x^5 + \cdots \right), \tag{14.175}$$

where some structure can be identified from the denominators and the powers. Recalling series (A.20) and (A.21) of the Appendix A.6.1, we can write

$$\ln(1+x) - \ln(1-x) = \left(x - \frac{1}{2}x^2 + \frac{1}{3}x^3 - \cdots \right) - \left(-x - \frac{1}{2}x^2 - \frac{1}{3}x^3 - \cdots \right), \tag{14.176}$$

from where we can see that the even powers vanish, to obtain

$$\ln\left(\frac{1+x}{1-x}\right) = 2\left(x + \frac{1}{3}x^3 + \frac{1}{5}x^5 + \cdots \right), \tag{14.177}$$

where logarithmic properties were used, identifying that the last expression is twice the Eq. (14.175) without a_1. Then,

$$Q_0(x) \equiv f_{even}(x) = \frac{1}{2} \ln\left(\frac{1+x}{1-x}\right) a_1, \tag{14.178}$$

and the value of $a_1 = 1$ is obtained by normalization, yielding

$$Q_0(x) = \frac{1}{2} \ln\left(\frac{1+x}{1-x}\right). \tag{14.179}$$

This last equation is known as the *Legendre function of the second kind* and zero order. The general function is denoted by $Q_l(x)$, and they are also known as *second solutions* for the Legendre equation. As we can see, Eq. (14.179) diverges in $x = \pm 1$, a behavior that is avoided in the first solutions or Legendre polynomials.

Now, the most general solution for the Legendre equation can be stated, namely,

$$f(x) = \sum_{n=0}^{\infty} \left[\mathcal{A}_n \, P_n(x) + \mathcal{B}_n \, Q_n(x) \right], \tag{14.180}$$

where constants $\mathcal{A}_n$ and $\mathcal{B}_n$ are found from the BCs.

Going back to our original problem, the solution of Eq. (14.146) will be

$$H(\eta) = \sum_{n=0}^{\infty} \left[\mathcal{A}_{\eta,n} \, P_n(\eta) + \mathcal{B}_{\eta,n} \, Q_n(\eta) \right], \tag{14.181}$$

and the corresponding solution for Eq. (14.147) will be presented after a variable change is made. Let us first define a variable

$$\mu \equiv i \, \xi, \tag{14.182}$$

which yields

$$\mu^2 = -\xi^2, \tag{14.183}$$

and the chain rule must be applied, that is,

$$\frac{\mathrm{d}\Xi(\mu)}{\mathrm{d}\xi} = \frac{\mathrm{d}\Xi(\mu)}{\mathrm{d}\mu} \frac{\mathrm{d}\mu}{\mathrm{d}\xi} = i \, \Xi'(\mu). \tag{14.184}$$

The calculated derivative is substituted back into Eq. (14.147) to obtain

$$\frac{\mathrm{d}}{\mathrm{d}\mu} \left[(1 - \mu^2) \frac{\mathrm{d}\Xi(\mu)}{\mathrm{d}\mu} \right] + \alpha \, \Xi(\mu) = 0, \tag{14.185}$$

which is the Legendre equation in terms of $\Xi = \Xi(\mu)$, and its solution can be written using Eq. (14.180). Then

$$\Xi(\mu) = \sum_{n=0}^{\infty} \left[\mathcal{A}_{\mu,n} \, P_n(\mu) + \mathcal{B}_{\mu,n} \, Q_n(\mu) \right], \tag{14.186}$$

which is written back to the original variable ξ, yielding

$$\Xi(\xi) = \sum_{n=0}^{\infty} \left[\mathcal{A}_{\xi,n} \, P_n(i \, \xi) + \mathcal{B}_{\xi,n} \, Q_n(i \, \xi) \right], \tag{14.187}$$

which leads us to the solution of the steady-state diffusion equation in spheroidal oblate coordinates, namely,

$$c(\xi,\eta)=\Xi(\xi)\,H(\eta)=\sum_{n=0}^{\infty}\left[\mathcal{A}_{\xi,n}\,P_n(i\,\xi)+\mathcal{B}_{\xi,n}\,Q_n(i\,\xi)\right]\left[\mathcal{A}_{\eta,n}\,P_n(\eta)+\mathcal{B}_{\eta,n}\,Q_n(\eta)\right], \tag{14.188}$$

where the multiple constants are to be determined from BCs. For our hyperboloidal cone, we have a no-flux condition. This means that all the diffusive processes are taking place inside the cone, namely,

$$\left.\frac{\partial c(\xi,\eta)}{\partial\eta}\right|_{\eta=\eta_0}=0, \tag{14.189}$$

and the derivative of the concentration is

$$\frac{\partial c(\xi,\eta)}{\partial\eta}=\sum_{n=0}^{\infty}\left[\mathcal{A}_{\xi,n}\,P_n(i\,\xi)+\mathcal{B}_{\xi,n}\,Q_n(i\,\xi)\right]\left[\mathcal{A}_{\eta,n}\,P_n'(\eta)+\mathcal{B}_{\eta,n}\,Q_n'(\eta)\right], \tag{14.190}$$

which evaluating into $\eta=\eta_0$ yields

$$0=\sum_{n=0}^{\infty}\left[\mathcal{A}_{\xi,n}\,P_n(i\,\xi)+\mathcal{B}_{\xi,n}\,Q_n(i\,\xi)\right]\left[\mathcal{A}_{\eta,n}\,P_n'(\eta_0)+\mathcal{B}_{\eta,n}\,Q_n'(\eta_0)\right]. \tag{14.191}$$

We can note that now P_n' and Q_n' are being evaluated to a fixed argument η_0, but the ξ-dependent quantities are not. Moreover, the equality must hold for every ξ, so consequently

$$0=\mathcal{A}_{\eta,n}\,P_n'(\eta_0)+\mathcal{B}_{\eta,n}\,Q_n'(\eta_0). \tag{14.192}$$

As not all constants $\mathcal{A}_{\eta,n}$ and $\mathcal{B}_{\eta,n}$ can be zero to avoid the trivial solution, we need to observe that every $Q_n(\eta)$ has the term[3]

$$\ln\left(\frac{1+\eta}{1-\eta}\right), \tag{14.193}$$

the derivative of which is

$$\frac{1}{1-\eta^2}. \tag{14.194}$$

[3] D. Jackson, *Legendre Functions of the Second Kind and Related Functions*, Am. Math. Mon., **50** (5), 291, DOI: 10.2307/2302827.

This implies that $Q'_n(\eta_0)$ cannot be null for any arbitrary n, therefore $\mathcal{B}_{\eta,n} = 0$. The remaining equation is

$$0 = \mathcal{A}_{\eta,n}\, P'_n(\eta_0), \tag{14.195}$$

from where we deduce that $P'_n(\eta_0) = 0$. Furthermore, $P_n(\eta) = constant$, and the only adequate Legendre polynomial is $P_0(\eta) = 1$. This condition reduces Eq. (14.188) to

$$c(\xi) = \mathcal{A}_0\, P_0(i\,\xi) + \mathcal{B}_0\, Q_0(i\,\xi), \tag{14.196}$$

where the constants were reduced to $\mathcal{A}_0 = \mathcal{A}_{\eta,n}\, \mathcal{A}_{\xi,n}$, and $\mathcal{B}_0 = \mathcal{A}_{\eta,n}\, \mathcal{B}_{\xi,n}$. For our hyperboloidal cone, concentration at $\xi = 0$ must be null, then

$$c(0) = 0 = \mathcal{A}_0, \tag{14.197}$$

making Eq. (14.196) become

$$c(\xi) = \mathcal{B}_0\, Q_0(i\,\xi). \tag{14.198}$$

Also, far away from the origin of the coordinates, the concentration will be a constant concentration c_0, namely,

$$c(\xi \to \infty) = c_0. \tag{14.199}$$

Equation (14.198) with $Q_0(i\,\xi)$ explicitly written is

$$c(\xi) = \mathcal{B}_0\, \frac{1}{2} \ln\left(\frac{1 + i\,\xi}{1 - i\,\xi}\right), \tag{14.200}$$

and for large ξ values, it can be written as

$$c_0 = c(\xi \to \infty) = \mathcal{B}_0\, \frac{1}{2} \ln\left(\frac{i\,\xi}{-i\,\xi}\right) = \mathcal{B}_0\, \ln(-1), \tag{14.201}$$

where we are looking for the univaluated natural complex logarithm, then

$$x + i\, y \equiv \ln(-1), \tag{14.202}$$

with $x, y \in \mathbb{R}$, giving

$$\mathrm{e}^{x+i\,y} = -1 = \mathrm{e}^x\, [\cos(y) + i\, \sin(y)], \tag{14.203}$$

where the imaginary part must be zero, and if the function is univaluated, then $y = \pi$ and $x = 0$. Therefore,

$$\ln(-1) = i\,\pi. \tag{14.204}$$

This value is substituted into Eq. (14.201) to yield

$$\mathcal{B}_0 = -i\frac{2}{\pi}\,c_0. \tag{14.205}$$

As we already have the values for every constant for the solution of Eq. (14.145), we can write

$$c(\xi,\eta) = -i\frac{1}{\pi}\,c_0\,\ln\left(\frac{1+i\,\xi}{1-i\,\xi}\right). \tag{14.206}$$

We might consider the problem solved, but allow us to rephrase it in another way to avoid the imaginary quantities. Then, by working with the complex logarithm, we can assume that the result can be written as

$$2w\,i = \ln\left(\frac{1+i\,\xi}{1-i\,\xi}\right), \tag{14.207}$$

from where the exponential is calculated

$$\mathrm{e}^{2w\,i} = \frac{1+i\,\xi}{1-i\,\xi}, \tag{14.208}$$

and rearranging terms gives

$$i\,\xi = \frac{\mathrm{e}^{2w\,i}-1}{\mathrm{e}^{2w\,i}+1}, \tag{14.209}$$

and $\mathrm{e}^{-w\,i}$ is used to obtain

$$i\,\xi = \frac{\mathrm{e}^{w\,i}-\mathrm{e}^{-w\,i}}{\mathrm{e}^{w\,i}+\mathrm{e}^{-w\,i}}. \tag{14.210}$$

From last equation, we can identify the exponential forms of the sine and cosine functions as listed in Eqs. (A.2) and (A.3), respectively (see Appendix A.1), allowing us to write

$$i\,\xi = \frac{i\,\sin(w)}{\cos(w)}, \tag{14.211}$$

or

$$\xi = \tan(w). \tag{14.212}$$

Remembering that we are looking for the value of the logarithm in $c(\xi, \eta)$, which is $2w\,i$, we get

$$2w\,i = \ln\left(\frac{1+i\,\xi}{1-i\,\xi}\right) = 2\,i\,\arctan(\xi). \tag{14.213}$$

This last equation is replaced into Eq. (14.206), yielding

$$c(\xi) = \frac{2}{\pi}\,c_0\,\arctan(\xi). \tag{14.214}$$

Equation (14.214) is the concentration inside a steady-state diffusive system made by an hyperboloidal cone with a fixed $\eta = \eta_0$. As we have azimuthal (ϕ) symmetry, there is no dependence on the ϕ coordinate. Remarkably, the result does not depend on the η coordinate either.

14.7 Single Exponential Decay

In 1991, Zhou and Zwanzig found that when a particle escapes from a cavity through a small window, its survival probability in the cavity decays in time as a single exponential. In fact, there is a general property typical for all single-exponential rate processes: The escape is a rare event, meanly that its characteristic time is much greater than all other characteristic times of the problem. When this condition is fulfilled, the survival probability, $S(t)$, for $t = t_1 + t_2$ is a product of the survival probabilities $S(t_1)$ and $S(t_2)$. Consequently, $S(t)$ satisfies

$$S(t_1 + t_2) = S(t_1)S(t_2). \tag{14.215}$$

The solution of this equation is given by

$$S(t) = e^{-\kappa t}. \tag{14.216}$$

The fact that the survival probability decays exponentially means that it satisfies a simple rate equation:

$$\frac{\mathrm{d}S(t)}{\mathrm{d}t} = -\kappa\,S(t). \tag{14.217}$$

To identify k, let's use Eq. (5.137), namely,

$$S(t|x_0) \approx e^{-\mathrm{k}\,c_{eq}t}. \tag{5.137}$$

Consequently, in Eq. (14.217) $\kappa = \mathtt{k}\, c_{eq}$, where $\mathtt{k}$ is the rate constant. Now consider a large cavity of volume V containing a single particle. In such a case, the particle concentration is equal to $1/V$, then

$$\kappa = \mathtt{k}/V. \tag{14.218}$$

From Eq. (2.44) and using Eq. (14.216), the mean lifetime of the particle is

$$\langle t\,(x_0)\rangle = \int_0^\infty S(t|x_0)\ \mathrm{d}t = \int_0^\infty e^{-\frac{\mathtt{k}}{V}\mathtt{k}t}\ \mathrm{d}t = \frac{V}{\mathtt{k}}, \tag{14.219}$$

which is the fingerprint if a single-exponential decay.

As an example of the application of this last result, consider a perfectly absorbing disk of radius s located on an infinite reflecting wall (see Sect. 14.4). Let's assume that, at $t = 0$, particles are uniformly distributed in the semi-infinite space on one side of the wall and their concentration is at equilibrium and given by c_{eq}. We already know that the steady-state rate constant for this system is given by

$$\mathtt{k}_{HBP} = 4Ds. \tag{14.113}$$

Inserting this last result into Eq. (14.219), we have that the mean first-passage time of a particle diffusing into a volume V where a perfectly absorbing disk is placed is given by

$$\langle t\,(x_0)\rangle = \frac{V}{4s\,D}. \tag{14.220}$$

For a particle escaping through a hole, the escape is evidently a rare event when the hole is small enough. This is why the escape is single-exponential even in the absence of a potential barrier. The reason is that the rate process is controlled by an entropy barrier, rather than an energy barrier.

14.8 Computational Experiments: Perfectly Absorbent Sphere from the Inside

In Sect. 14.1.1, we presented the propagator, Eq. (5.40), for a perfectly absorbent sphere of radius R. Its mean first-passage time (MFPT) was not explicitly calculated there, but it can be directly obtained from Eq. (14.24), namely,

$$\langle t\,(r_0)\rangle_{out} = \frac{\int_0^\infty t\ J(L,t)\ \mathrm{d}t}{\theta_L(x_0)} = \frac{1}{6D}(R_{out} - r_0)(R_{out} + r_0 - 2R_{in}). \tag{14.24}$$

This is the equation for the problem of two perfectly absorbent and concentric spheres of radius R_{in} and R_{out}, for the inner and outer spheres, respectively, where r_0 is the starting point of the diffusing particles and $R_{in} < r_0 < R_{out}$.

As our problem states that we have only one absorbent sphere, we set $R_{in} = 0$ in Eq. (14.24), obtaining

$$\langle t(r_0)\rangle = \frac{1}{6D}\left(R^2 - r_0^2\right), \tag{14.221}$$

where the subindex *out* has been removed because we now only have one sphere. In the specific case of the simulation presented in Listing 14.1, $r_0 = 0$, causing Eq. (14.221) to become

$$\langle t(r_0)\rangle = \frac{1}{6D}R^2. \tag{14.222}$$

Listing 14.1 [abs-sphere.f90]: Fortran 90 program to simulate a perfectly absorbent sphere of radius $R = 1$. The particles start from a fixed point $\mathbf{r}_0$ inside the sphere.

```
! ******************************************************* !
! ***************** abs-sphere.f90 ******************** !
! ******************************************************* !
!
!    Leonardo Dagdug, Ivan Pompa-García, Jason Peña
!
! From the book:
! ******************************************************* !
!      Diffusion Under Confinement:
!               A Journey Through Counterintuition
! ******************************************************* !

! ******************************************************* !
! This file contains the source code for the simulation
! of a 2D (circular) / 3D (spherical) channel of
! radius R.
! The whole circumference is completely absorbent.
!
! The Brownian walkers start their path from the
! origin of the coordinates.
! The simulation for each of them ends when the
! absorbent shell is reached. Then, the Mean
```

Listing continued on next page

Listing continued from last page

```
! First-Passage Time (MFPT or <tau>) is obtained.
!
! The theoretical value is used to calculate the
! relative error of the simulation. D0 is the bulk
! diffusion constant, generally set to 1.
!
! tau = R**2 / (6 * D0)
! ************************************************** !

! ************************************************** !
! To compile with GFortran, you must include the
! helpers.f90 module.
!         gfortran helpers.f90 abs-sphere.f90
! Then you can run the program:
!         ./a.out
! ************************************************** !

program abssphere

! Load the helpers module, which contains functions,
! constants, and more...
use helpers

! Mandatory declaration of data type variables
! and constants.
implicit none

! ************************************************** !
!              Declaration of constants
! ************************************************** !

!!! Simulation parameters
! Seed of the PRNG
integer, parameter :: RSEED = 0
! Number of random walkers (particles)
integer, parameter :: NRW = 2500
! Circle / Sphere radius
real(kind=dp), parameter :: R = 1.0_dp
! Temporal step size
real(kind=dp), parameter :: DT = 1.0e-6_dp
```

Listing continued on next page

Listing continued from last page

```
63
64  !!! Physical parameters of the system
65  ! Diffusion constant (bulk)
66  real(kind=dp), parameter :: D0 = 1.0_dp
67  ! Thermal energy inverse (1/k_b T)
68  real(kind=dp), parameter :: BETA = 1.0_dp
69  ! Standard deviation for Brownian motion
70  real(kind=dp), parameter :: SIGMA &
71                                = dsqrt(2.0_dp * D0 * DT)
72  ! Mean distribution for Brownian motion
73  real(kind=dp), parameter :: MU = 0.0_dp
74
75  ! Theoretical value
76  real(kind=dp), parameter :: THEOV &
77                                   = R**2 / (6.0_dp * D0)
78
79
80  ! ******************************************************* !
81  !               Declaration of variables
82  ! ******************************************************* !
83
84  ! General counter
85  integer :: i
86  ! Initial position of the particle
87  real(kind=dp) :: x0, y0, z0
88  ! Current position of the particle
89  real(kind=dp) :: x, y, z
90  ! Current particle passage time
91  real(kind=dp) :: tau
92  ! Sum of passage times
93  real(kind=dp) :: ttau = 0.0_dp
94  ! MFPT (<tau>)
95  real(kind=dp) :: mfpt
96
97
98  ! ******************************************************* !
99  !               Main simulation program
100 ! ******************************************************* !
101
102 ! Set the seed of the PRNG to achieve repeatable results
```

Listing continued on next page

Listing continued from last page

```
103 call setseed(RSEED)
104
105 ! The loop iterates over each (i) particle.
106 do i=1, NRW
107   !!! Initializing the needed variables.
108   ! The passage time is set to zero
109   tau = 0.0_dp
110
111   ! Every particle starts at the origin
112   x0 = 0.0_dp
113   y0 = 0.0_dp
114   z0 = 0.0_dp
115
116   ! The particle's current position is set to the initial
      position.
117   x = x0
118   y = y0
119   z = z0
120
121   !!! The random walk starts. Follow the particle until
122   !!! it is removed by the shell at radius R.
123   do
124     ! Make a step in space
125     x = x + nrand(MU, SIGMA)
126     y = y + nrand(MU, SIGMA)
127     z = z + nrand(MU, SIGMA)
128     ! Make a step in time
129     tau = tau + DT
130
131     ! This code also works for a 2D problem (CIRCLE),
132     ! if you remove the «z» position so it is not taken
133     ! into account for the calculation of the distance.
134     ! If it's a 2D problem, just uncomment the next line
135     ! z = 0.0_dp
136
137     ! Check for removal of the particle.
138     ! As we are inside a sphere (or a circle), the
139     ! distance is calculated from the origin using
140     ! the Euclidean distance.
141     if( sqrt(x**2 + y**2 + z**2) >= R ) then
```

Listing continued on next page

Listing continued from last page

```
      ! If it was removed from the channel, stop the
      ! simulation for this particle.
      exit
    end if
  end do ! End of i-particle's random walk.

  ! We need to add the passage time of the i-particle to
  ! the total time.
  ttau = ttau + tau

  ! You can print  out the MFPT up to this point.
  print *, &
          '[' // nstr(i) // ' particles simulated | ' &
          // nstr(NRW-i) // ' to go]: ' &
          // TNL // TAB &
          // '<tau-sim> = ' // nstr(ttau / i) &
          // TNL // TAB &
          // '<tau-theo> = ' // nstr(THEOV) &
          // TNL // TAB &
          // 'Error = ' &
          // nstr( abs( (ttau/i) - THEOV ) / THEOV &
                  * 100, 1) &
          // '%'
end do ! End of the particle's loop.

! At this point, every particle's simulation is done.
! Obtain the <tau>
mfpt = ttau / NRW

! Now we print out the MFPT, and show the theoretical
! value.
print *
print *, '=== Final result of simulation ==='
print *, TAB // '<tau-sim> = ' // nstr(mfpt)
print *, TAB // '<tau-theo> = ' // nstr(THEOV)
! Calculates and prints the percentage error.
print *, TAB // 'Error = ' &
          // nstr( abs( mfpt - THEOV ) &
                  / THEOV * 100, 1) &
          // '%'
```

Listing continued on next page

Listing continued from last page

```
! As a reminder, print out the number of walkers.
print *, TAB // 'NRW = ' // nstr(NRW)
! The time step.
print *, TAB // 'dt = ' // nstr(DT, 6)
! And the PRNG seed.
print *, TAB // 'PRNG seed = ' // nstr(RSEED)

end program abssphere
```

Listing ended

Compiling and Running of Listing 14.1

```
    # Compile
    gfortran helpers.f90 abs-sphere.f90

    # Run
    ./a.out

    # Sample output
    ⋮
    [62 particles simulated | 2438 to go]:
      <tau-sim> = 0.156571
      <tau-theo> = 0.166667
      Error = 6.1%
    ⋮
    [2500 particles simulated | 0 to go]:
      <tau-sim> = 0.166057
      <tau-theo> = 0.166667
      Error = 0.4%

  === Final result of simulation ===
      <tau-sim> = 0.166057
      <tau-theo> = 0.166667
      Error = 0.4%
      NRW = 2500
      dt = 0.000001
```

14.9 Computational Experiments: Perfectly Absorbent Sphere from the Inside with Uniformly Distributed Particles

As in the past experiment, we start from Eq. (14.24), that is,

$$\langle t(r_0)\rangle_{out} = \frac{\int_0^\infty t\ J(L,t)\ \mathrm{d}t}{\theta_L(x_0)} = \frac{1}{6D}(R_{out} - r_0)(R_{out} + r_0 - 2R_{in}). \tag{14.24}$$

Also, we need to set $R_{in} = 0$, to keep only the external sphere, yielding

$$\langle t(r_0)\rangle = \frac{1}{6D}(R^2 - r_0^2), \tag{14.223}$$

where, again, the *out* subindex was removed because only one sphere is present. In this case, the random walkers should start by being uniformly distributed inside the sphere. To obtain the theoretical result to describe this system, we need to perform an integration over the whole sphere in order to consider the contribution of every possible starting position of the particles, and this result must be divided by the complete volume of interest, which is the sphere itself.

The MFPT for the sphere of radius R, and uniformly distributed particles at the start, will be given by

$$\langle t_u\rangle = \frac{\displaystyle\int_0^{2\pi}\int_0^{\pi}\int_0^{R} \langle t(r_0)\rangle\ r_0^2\ \sin\theta\ \mathrm{d}r_0\,\mathrm{d}\theta\,\mathrm{d}\phi}{\displaystyle\int_0^{2\pi}\int_0^{\pi}\int_0^{R} r_0^2\ \sin\theta\ \mathrm{d}r_0\,\mathrm{d}\theta\,\mathrm{d}\phi}, \tag{14.224}$$

or

$$\langle t_u\rangle = \frac{1}{6D}\,\frac{\displaystyle\int_0^{2\pi}\int_0^{\pi}\int_0^{R} (R^2 - r_0^2)\, r_0^2\ \sin\theta\ \mathrm{d}r_0\,\mathrm{d}\theta\,\mathrm{d}\phi}{\dfrac{4}{3}\pi R^3}, \tag{14.225}$$

which yields

$$\langle t_u\rangle = \frac{1}{6D}\cdot\frac{3}{4\pi R^3}\cdot 4\pi\int_0^R \left[R^2\, r_0^2 - r_0^4\right]\mathrm{d}r_0. \tag{14.226}$$

Then,

$$\langle t_u \rangle = \frac{1}{2D} \cdot \frac{1}{R^3} \left[\frac{1}{3} R^2 r_0^3 - \frac{1}{5} r_0^5 \right] \Bigg|_{r_0=0}^{r_0=R}, \tag{14.227}$$

that is reduced to

$$\langle t_u \rangle = \frac{1}{2D} \cdot \frac{1}{R^3} \left[\frac{1}{3} R^5 - \frac{1}{5} R^5 \right], \tag{14.228}$$

leading to

$$\langle t_u \rangle = \frac{1}{15D} R^2. \tag{14.229}$$

For comparative purposes, the simulation for $R = 1$ can be seen in Listing 14.2.

Listing 14.2 [abs-sphere-unif.f90]: Fortran 90 program to simulate a perfect absorbent sphere of radius $R = 1$. At the start, the particles are uniformly distributed inside the whole volume of the sphere.

```
! ******************************************************* !
! ************** abs-sphere-unif.f90 ******************** !
! ******************************************************* !
!
!    Leonardo Dagdug, Ivan Pompa-García, Jason Peña
!
! From the book:
! ******************************************************* !
!      Diffusion Under Confinement:
!               A Journey Through Counterintuition
! ******************************************************* !

! ******************************************************* !
! This file contains the source code for the simulation
! of a 2D (circular) / 3D (spherical) channel of
! radius R.
! The whole circumference is completely absorbent.
!
! The Brownian walkers start their path being uniformly
! distributed inside the sphere / circle.
! The simulation for each of them ends when the
! absorbent shell is reached. Then, the Mean
! First-Passage Time (MFPT or <tau>) is obtained.
```

Listing continued on next page

Listing continued from last page

```
!
! The theoretical value is used to calculate the
! relative error of the simulation. D0 is the bulk
! diffusion constant, generally set to 1.
!
! tau = 1 / (15 * D0) * R**2
! ************************************************** !

! ************************************************** !
! To compile with GFortran, you must include the
! helpers.f90 module.
!         gfortran helpers.f90 abs-sphere-unif.f90
! Then you can run the program:
!         ./a.out
! ************************************************** !

program absspherеunif

! Load the helpers module, which contains functions,
! constants, and more...
use helpers

! Mandatory declaration of data type variables
! and constants.
implicit none

! ************************************************** !
!              Declaration of constants
! ************************************************** !

!!! Simulation parameters
! Seed of the PRNG
integer, parameter :: RSEED = 0
! Number of random walkers (particles)
integer, parameter :: NRW = 2500
! Circle / Sphere radius
real(kind=dp), parameter :: R = 1.0_dp
! Temporal step size
real(kind=dp), parameter :: DT = 1.0e-6_dp

```

Listing continued on next page

Listing continued from last page

```
!!! Physical parameters of the system
! Diffusion constant (bulk)
real(kind=dp), parameter :: D0 = 1.0_dp
! Thermal energy inverse (1/k_b T)
real(kind=dp), parameter :: BETA = 1.0_dp
! Standard deviation for Brownian motion
real(kind=dp), parameter :: SIGMA &
                            = dsqrt(2.0_dp * D0 * DT)
! Mean distribution for Brownian motion
real(kind=dp), parameter :: MU = 0.0_dp

! Theoretical value
real(kind=dp), parameter :: THEOV &
                = (1.0_dp) / (15.0_dp * D0) * R**2


! ************************************************** !
!               Declaration of variables
! ************************************************** !

! General counter
integer :: i
! Initial position of the particle
real(kind=dp) :: x0, y0, z0
! Current position of the particle
real(kind=dp) :: x, y, z
! Current particle passage time
real(kind=dp) :: tau
! Sum of passage times
real(kind=dp) :: ttau = 0.0_dp
! MFPT (<tau>)
real(kind=dp) :: mfpt


! ************************************************** !
!               Main simulation program
! ************************************************** !

! Set the seed of the PRNG to achieve repeatable results
call setseed(RSEED)
```

Listing continued on next page

Listing continued from last page

```

! The loop iterates over each (i) particle.
do i=1, NRW
  !!! Initializing the needed variables.
  ! The passage time is set to zero
  tau = 0.0_dp

  ! Initially, the particles should be uniformly
  ! distributed inside the whole volume of the sphere.
  ! For a cube in cartesian coordinates, this would be
  ! straightforward, but for spherical coordinates
  ! the strategy needs to be modified, as otherwise the
  ! points will be inside a cube of edge R, and some
  ! points will remain outside the sphere.

  ! The calculation can be made using the sampling
  ! technique, which involves a cubic root and
  ! a transformation from spherical to cartesian
  ! coordinates.
  ! This can be computationally expensive and not
  ! readily understood, and some prefer to reject
  ! the points outside the sphere and get a new
  ! position until the point  remains inside. The latter
  ! is the approach we are taking here.
  do
    x0 = urand(-R, R)
    y0 = urand(-R, R)
    z0 = urand(-R, R)

    ! If the point lies inside the sphere of radius
    ! R, then we can continue.
    if( sqrt(x0**2 + y0**2 + z0**2) < R ) then
      exit
    end if
  end do

  ! The particle's current position is set to the
  ! initial position.
  x = x0
  y = y0
```

Listing continued on next page

Listing continued from last page

```
144   z = z0
145
146   !!! The random walk starts. Follow the particle until
147   !!! it is removed by the shell at radius R.
148   do
149     ! Make a step in space
150     x = x + nrand(MU, SIGMA)
151     y = y + nrand(MU, SIGMA)
152     z = z + nrand(MU, SIGMA)
153     ! Make a step in time
154     tau = tau + DT
155
156     ! This code also works for a 2D problem (CIRCLE),
157     ! if you remove the «z» position so it is not taken
158     ! into account for the calculation of the distance.
159     ! If it's a 2D problem, just uncomment the next line
160     ! z = 0.0_dp
161
162     ! Check for removal of the particle.
163     ! As we are inside a sphere (or a circle), the
164     ! distance is calculated from the origin using
165     ! the Euclidean distance.
166     if( sqrt(x**2 + y**2 + z**2) >= R ) then
167       ! If it was removed from the channel, stop its
168       ! simulation.
169       exit
170     end if
171   end do ! End of i-particle's random walk.
172
173   ! We need to add the passage time of the i-particle to
174   ! the total time.
175   ttau = ttau + tau
176
177   ! You can print  out the MFPT up to this point.
178   print *, &
179           '[' // nstr(i) // ' particles simulated | ' &
180           // nstr(NRW-i) // ' to go]: ' &
181           // TNL // TAB &
182           // '<tau-sim> = ' // nstr(ttau / i) &
183           // TNL // TAB &
```

Listing continued on next page

Listing continued from last page

```
            // '<tau-theo> = ' // nstr(THEOV) &
            // TNL // TAB &
            // 'Error = ' &
            // nstr( abs( (ttau/i) - THEOV ) / THEOV &
                    * 100, 1) &
            // '%'
end do ! End of the particle's loop.

! At this point, every particle's simulation is done.
! Obtain the <tau>
mfpt = ttau / NRW

! Now we print out the MFPT, and show the theoretical
! value.
print *
print *, '=== Final result of simulation ==='
print *, TAB // '<tau-sim> = ' // nstr(mfpt)
print *, TAB // '<tau-theo> = ' // nstr(THEOV)
! Calculates and prints the percentage error.
print *, TAB // 'Error = ' &
            // nstr( abs( mfpt - THEOV ) &
                    / THEOV * 100, 1) &
            // '%'
! As a reminder, print out the number of walkers.
print *, TAB // 'NRW = ' // nstr(NRW)
! The time step.
print *, TAB // 'dt = ' // nstr(DT, 6)
! And the PRNG seed.
print *, TAB // 'PRNG seed = ' // nstr(RSEED)

end program absspherеunif
```

Listing ended

Compiling and Running of Listing 14.2

```
    # Compile
    gfortran helpers.f90 abs-sphere-unif.f90

```

Listing continued on next page

Listing continued from last page

```
# Run
./a.out

# Sample output
⋮
[3 particles simulated | 2497 to go]:
  <tau-sim> = 0.017252
  <tau-theo> = 0.066667
  Error = 74.1%
⋮
[2500 particles simulated | 0 to go]:
  <tau-sim> = 0.066788
  <tau-theo> = 0.066667
  Error = 0.2%

=== Final result of simulation ===
  <tau-sim> = 0.066788
  <tau-theo> = 0.066667
  Error = 0.2%
  NRW = 2500
  dt = 0.000001
```

End of Compile and Run

14.10 Concluding Remarks

In this chapter, we introduce the interesting problem of concentric spheres in different dimensions and its main consequences related to mean first-passage times and splitting probabilities. For example, when the outer sphere goes to infinity, the splitting probability related to this boundary tends to zero for one and two dimensions while being finite for systems with three dimensions or more.

We also study the absorption of a disk over a flat reflecting wall. At steady state, we can find the rate constant for such a system. An important extension to any shape is given by the Dudko-Berezhkovskii-Weiss formula.

Finally, the most important equations that were obtained in this chapter are listed below:

$$\theta_{out}(r_0) = \begin{cases} \dfrac{\ln\left(\frac{r_0}{R_{in}}\right)}{\ln\left(\frac{R_{out}}{R_{in}}\right)} & \text{for} \quad d = 2, \\ \dfrac{1-\left(\frac{R_{in}}{r_0}\right)^{d-2}}{1-\left(\frac{R_{in}}{R_{out}}\right)^{d-2}} & \text{for} \quad d \neq 2. \end{cases}$$

(Splitting Probability Concentric Spheres)

$$\mathrm{k}_{elipse} = \frac{2\pi\, Da_1}{k(\epsilon)}. \qquad \text{(Ellipse)}$$

$$\mathrm{k}_{DBW} = \left(\frac{2^5 AP}{\pi^2}\right)^{1/3} D. \qquad \text{(Hill-Berg-Purcell formula)}$$

$$\mathrm{k}_{DBW} = \left(\frac{2^5 AP}{\pi^2}\right)^{1/3} D. \qquad \text{(Dudko-Berezhkovskii-Weiss formula)}$$

Further Reading and References

H.C. Berg, E.M. Purcell, Physics of chemoreception. Biophys. J. **20**, 193 (1977). 10.1016/S0006-3495(77)85544-6

H.S. Carslaw, J.C. Jaeger, *Conduction of Heat in Solids* (Oxford University Press, Oxford, 1959)

J. Crank, *The Mathematics of Diffusion*, 2nd edn. (Clarendon Press, Oxford, 1975)

O.K. Dudko, A.M. Berezhkovskii, G.H. Weiss, Boundary homogenization for a circle with periodic absorbing arcs. Exact expression for the effective trapping rate. J. Chem. Phys. **121**, 3, 1562 (2015). 10.1063/1.1763137

J. Koplik, S. Redner, E.J. Hinch, Tracer dispersion in planar multipole flows. Phys. Rev. E **50**, 4650 (1994). 10.1103/PhysRevE.50.4650

Part VI
Trapping Rate Coefficient and Boundary Homogenization

The randomness of being reacted.

"Truth is much too complicated to allow anything but approximations."

—John Von Neumann

Chapter 15
Trapping Rate Coefficient

The problem of entrapment of diffusing particles by heterogeneous boundaries with perfectly or partially absorbing regions on otherwise perfectly or partially reflecting surfaces plays an important role in the analysis of various processes in physics, chemistry, and biology. Examples include electric current through arrays of microelectrodes, porous membrane transport, reactions on supported catalysts, water exchange in plants, and ligand binding to cell surface receptors, to mention just a few. The boundary properties of these systems can be described by imposing mixed Dirichlet and Neumann boundary conditions. Evidently, this is an extremely complicated problem because it involves non-uniform boundary conditions. *Boundary homogenization* (BH) is an approximate method that significantly simplifies the solution of such problems by using an approximate effective medium-type approach. The main idea is to replace the non-uniform boundary conditions on a surface for a uniform boundary condition with an appropriately chosen effective *trapping rate coefficient* (see Fig. 15.1).

We can use BH as a useful approximation when, at sufficiently long distances, the steady-state particle fluxes and concentrations of the heterogeneous original system are indistinguishable from its effective counterpart. The trapping rate coefficient depends on the shape and size of the absorbing regions, as well as on their distribution on the surface, and is known only in a few special cases. Some of these cases are discussed in this chapter.

15.1 The Rate Coefficient

Smoluchowski's seminal work on chemical kinetics is based on the simplification that the many-body aspects of kinetics can be studied as the reactions of only two reactant molecules when the concentration of reactants is low enough. The events in a reaction process can be depicted qualitatively in the two-body picture, where

L. Dagdug et al., *Diffusion Under Confinement*,
https://doi.org/10.1007/978-3-031-46475-1_15

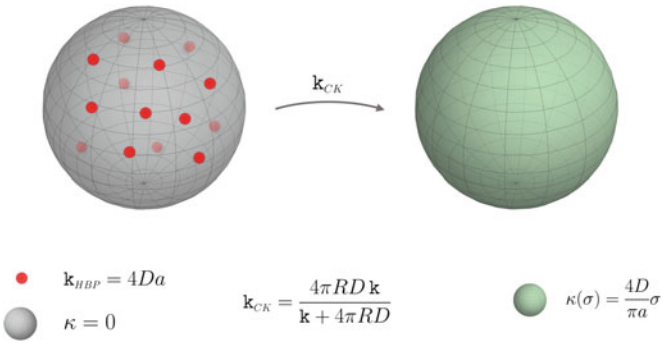

Fig. 15.1 Schematic representation of boundary homogenization. The mixed Dirichlet (red) and Neumann (gray) BCs of the original problem (left) are transformed into an effective Dirichlet(green) boundary condition (right). In other words, the problem of heterogeneous BCs is mapped to a homogeneous boundary condition by means of the Collins-Kimball formula, Eq. (15.61)

two molecules move within a solvent and occasionally come into contact with each other. A reaction may or may not occur upon such an encounter. Smoluchowski theory applies at a rate limited only by the speed at which the reactants can approach each other when they are close enough to react chemically almost instantaneously. In such case, the reaction is only limited by diffusion and is known as *diffusion-controlled reaction* or *diffusion-limited reaction*.

If the chemical reaction is not instantaneous, the observed rate of reaction may be influenced by both the rate of approach and the rate of subsequent chemical reaction. Taking into account these phenomena, Collins and Kimball extended Smoluchowski's theory. Indeed, while Smoluchowski's theory focuses on the trapping rate for a sphere with a perfectly absorbing surface, the Collins-Kimball approach is based on studying the trapping rate for a sphere with a partially absorbing surface. In this section, we will solve the diffusion equation imposing these two boundary conditions (BCs) in order to calculate the concentration, flux, and current of the diffusing particles, as well as the associated rate constants of the processes.

15.1.1 Smoluchowski Formula: Perfectly Absorbing Sphere

Consider a diffusing particle in the presence of a perfectly absorbing sphere of radius R, which particle is removed from the system as soon as it reaches the sphere's surface. The diffusion equation must be solved under the following BCs if the concentration at infinity is kept constant: (a) perfectly absorbing on the surface of the sphere, $c(R,t) = 0$, and (b) uniform concentration at infinity, $c(r,t)\big|_{r\to\infty} = c_\infty$. Before solving the boundary value problem, let us give some preliminary definitions related to the flux. Because of the symmetry of the system,

assuming angular independence, the flux in spherical coordinates is given by (see Sect. B.3 in Appendix B)

$$\mathbf{J}(r,t) = -D\frac{\partial c(r,t)}{\partial r}\hat{\mathbf{e}}_r. \tag{15.1}$$

From this last equation, we can find the *diffusion current* or *total flux*, $I(r,t)$, by integrating $\mathbf{J}(R,t)$ over a surface S, which is the number of particles trapped by the sphere per unit time

$$I(t) = \int_S \mathbf{J}(R,t)\cdot\hat{\mathbf{n}}\,\mathrm{d}A, \tag{15.2}$$

with $\mathrm{d}A$ being the differential element of area and $\hat{\mathbf{n}}$ the unit vector normal to the spherical surface.[1] Thus,

$$\begin{aligned} I(t) &= \int_0^{2\pi}\int_0^{\pi}\left(-D\frac{\partial c(r,t)}{\partial r}\bigg|_{r=R}\hat{\mathbf{e}}_r\right)\cdot(-\hat{\mathbf{e}}_r)\,R^2\sin\theta\;\mathrm{d}\theta\,\mathrm{d}\phi \\ &= 4\pi R^2 D\frac{\partial c(r,t)}{\partial r}\bigg|_{r=R}. \end{aligned} \tag{15.3}$$

The ratio of diffusion current to particle concentration, $\mathtt{k}(t) = I(t)/c_\infty$, is the *rate coefficient*, which has units of volume per unit time. It is worth mentioning that the *diffusion-controlled rate constant* or *rate constant*, $\mathtt{k}$, is defined in the long time limit $\mathtt{k}(t)_{t\to\infty}$, when the system reaches the steady state and the rate coefficient becomes independent of time. Now, let's define the normalized concentration as

$$\varrho(\mathbf{r},t) \equiv \frac{c(\mathbf{r},t)}{c_\infty}. \tag{15.4}$$

The main idea of this definition is that the rate constant is calculated from the flux current divided by the uniform concentration at infinity. Consequently, the rate coefficient in terms of the normalized concentration is given by

$$\mathtt{k}(t) = 4\pi R^2 D\frac{\partial\varrho(r,t)}{\partial r}\bigg|_{r=R}, \tag{15.5}$$

[1] In Sect. 2.7.2, we defined $\hat{\mathbf{n}}$ as the unit normal vector pointing in the *outward* direction of the boundary (either eastward, $-\hat{\mathbf{e}}_x$, or westward, $\hat{\mathbf{e}}_x$, depending on the case). For this system, we adopt a different convention, making the normal vector to the spherical surface point in the *inward* direction of the sphere. This ensures that the flux through the surface is positive if the vector field is flowing into the sphere and negative if is flowing outside the sphere.

which has units of volume per unit time. The primary intention of this section is to calculate such coefficient. For this purpose, we must first calculate $\varrho(r,t)$ from the diffusion equation.

In terms of the normalized concentration, $\varrho(r)$, the diffusion equation, when considering spherical symmetry, is given by

$$\frac{\partial \varrho(\boldsymbol{r},t)}{\partial t} = D\frac{1}{r^2}\frac{\partial}{\partial r}\left(r^2\frac{\partial \varrho(\boldsymbol{r},t)}{\partial r}\right). \tag{15.6}$$

Taking the Laplace transform of Eq. (15.6) and integrating the time derivative by parts gives

$$s\varrho(r,s) - \varrho(r,0) = \frac{D}{r}\frac{\partial^2 r\varrho(r,s)}{\partial r^2} = D\left(\frac{\partial^2 \varrho(r,s)}{\partial r^2} + \frac{2}{r}\frac{\partial \varrho(r,s)}{\partial r}\right). \tag{15.7}$$

Using the change of variable

$$z = r\left[\varrho(r,s) - \frac{\varrho(r,0)}{s}\right], \tag{15.8}$$

the latter equation becomes

$$\frac{\partial^2 z}{\partial r^2} - \frac{s}{D}z = 0. \tag{15.9}$$

The solution of this equation is

$$z = \mathcal{A}\exp\left(\sqrt{\frac{s}{D}}r\right) + \mathcal{B}\exp\left(-\sqrt{\frac{s}{D}}r\right), \tag{15.10}$$

where $\mathcal{A}$ and $\mathcal{B}$ are constants of integration. Reverting this solution to the original variable $\varrho(r,s)$ leads to

$$\varrho(r,s) = \frac{1}{s}\varrho(r,0) + \frac{\mathcal{A}}{r}\exp\left(\sqrt{\frac{s}{D}}r\right) + \frac{\mathcal{B}}{r}\exp\left(-\sqrt{\frac{s}{D}}r\right). \tag{15.11}$$

Once we have the general solution, we can now solve the boundary value problem. As we already mentioned, for the Smoluchowski approach, we have the following BCs:

$$\varrho(r,t)\Big|_{r\to\infty} = 1 \qquad t \geq 0, \tag{15.12}$$

and

$$\varrho(R,t)=0 \qquad t\geq 0. \tag{15.13}$$

Their corresponding Laplace transform are

$$\varrho(r,s)\Big|_{r\to\infty}=\frac{1}{s}, \tag{15.14}$$

and

$$\varrho(R,s)=0, \tag{15.15}$$

respectively.

By substituting Eq. (15.14) into Eq. (15.11), and taking the limit $r\to\infty$, we observe that the first term on the left-hand side of such equation goes to $1/s$, the third goes to zero, and the second goes to infinity, consequently, $\mathcal{A}=0$. Now, evaluating Eq. (15.11) at $r=R$ and using Eq. (15.15), leads to

$$0=\frac{1}{s}\varrho(R,0)+\frac{\mathcal{B}}{R}\exp\left(-\sqrt{\frac{s}{D}}R\right). \tag{15.16}$$

Solving for $\mathcal{B}$, we obtain

$$\mathcal{B}=-\frac{R}{s}\varrho(r,0)\exp\left(\sqrt{\frac{s}{D}}R\right). \tag{15.17}$$

Substituting this last relation into Eq. (15.11) and using that $\varrho(r,0)=1$ results in

$$\varrho(r,s)=\frac{1}{s}\left\{1-\frac{R}{r}\exp\left[\sqrt{\frac{s}{D}}(R-r)\right]\right\}. \tag{15.18}$$

The inverse Laplace transform of the latter expression can be found using the same technique outlined in Sect. 3.2, where we obtained the inverse Laplace transform of Eq. (3.44), i.e., Eq. (3.59). Taking this into consideration, let us first apply the inverse Laplace transform operator $\mathcal{L}^{-1}$ on both sides of Eq. (15.18),[2] namely,

[2] Commonly, the operator $\mathcal{L}^{-1}$ acting on a function $f(s)$ is defined as

$$f(t)=\mathcal{L}^{-1}\{f(s)\}=\frac{1}{2\pi i}\lim_{T\to\infty}\int_{\gamma-iT}^{\gamma+iT}\mathrm{e}^{st}f(s)\,\mathrm{d}s. \tag{15.19}$$

See Sect. A.8 for further details on the Laplace transform.

$$\varrho(r,t) = \mathcal{L}^{-1}\{\varrho(r,s)\} = \mathcal{L}^{-1}\left\{\frac{1}{s} - \frac{R}{sr}\exp\left[\sqrt{\frac{s}{D}}(R-r)\right]\right\} \\ = 1 - \frac{R}{r}\mathcal{L}^{-1}\left\{\frac{1}{s}\exp\left[\sqrt{\frac{s}{D}}(R-r)\right]\right\}, \tag{15.20}$$

where we used the linearity of $\mathcal{L}^{-1}$ together with Eq. (A.64). Now, by defining the following functions:

$$g(r,s) \equiv \frac{\mathrm{e}^{\sqrt{s}\alpha}}{s} \quad \text{and} \quad q(r,s) \equiv \frac{\mathrm{e}^{\sqrt{s}\alpha}}{\sqrt{s}}, \tag{15.21}$$

with $\alpha \equiv (R-r)/\sqrt{D}$, we can say state that $g(r,s)$ is actually a factor of the second term in Eq. (15.20), still to be inverse transformed. Additionally, both functions $g(r,s)$ and $q(r,s)$ are intrinsically related through their derivatives, that is,

$$\frac{\partial\sqrt{s}g(r,s)}{\partial s} = \frac{\partial q(r,s)}{\partial s} = \frac{\mathrm{e}^{\alpha\sqrt{s}}(\alpha\sqrt{s}-1)}{2s^{3/2}}. \tag{15.22}$$

Thus, we can establish a system of partial differential equations (PDEs), such as

$$2s\frac{\partial g(r,s)}{\partial s} + 2g(r,s) - \alpha q(r,s) = 0 \quad \text{and} \quad 2s\frac{\partial q(r,s)}{\partial s} - \alpha s g(r,s) + q(r,s) = 0. \tag{15.23}$$

Using Eq. (3.50), i.e.,

$$\frac{\partial^m(-t)^n f(t)}{\partial t^m} = \mathcal{L}^{-1}\left\{(s)^m\frac{\partial^n f(s)}{\partial s^n}\right\}, \tag{3.50}$$

the inverse Laplace transform of each of the PDEs in Eq. (15.23) is obtained, yielding

$$2t\frac{\partial g(r,t)}{\partial t} + \alpha q(r,t) = 0 \quad \text{and} \quad -2\frac{\partial\left[tq(r,t)\right]}{\partial t} - \alpha\frac{\partial g(r,t)}{\partial t} + q(r,t) = 0, \tag{15.24}$$

from where we can determine that

$$-(\alpha^2 - 6t)\frac{\partial g(r,t)}{\partial t} + 4t^2\frac{\partial^2 g(r,t)}{\partial t^2} = 0. \tag{15.25}$$

The solution of the latter equation reads

$$g(r,t) = \mathcal{A} - \frac{\sqrt{4\pi}\,\mathrm{erf}\left(\frac{\alpha}{\sqrt{4t}}\right)}{\alpha}\mathcal{B}. \tag{15.26}$$

In order to find the integration constants $\mathcal{A}$ and $\mathcal{B}$, we must compare $\mathcal{L}^{-1}\{g(r,s)\}$ and $\varrho(r,t)$, when the particles are infinitely close to the absorbing surface, i.e., in the limit where $\alpha \to 0$. More specifically, by making a Taylor series around $\alpha = 0$ of $g(r,s)$, keeping the first two terms and inverse transforming such result, we arrive at (see Eqs. (A.64) and (A.66))

$$\mathcal{L}^{-1}\{g(r,s)\}_{\alpha\to 0} = \mathcal{L}^{-1}\left\{\frac{1}{s} + \frac{\alpha}{s} + \cdots\right\} = 1 + \frac{\alpha}{\sqrt{\pi t}} + \cdots, \tag{15.27}$$

while the first two terms of the Taylor series of Eq. (15.26) are

$$\varrho(r,t)_{\alpha\to 0} = \mathcal{A} - \frac{2B}{\sqrt{t}} + \cdots, \tag{15.28}$$

meaning that $\mathcal{A} = 1$ and $\mathcal{B} = -\alpha/\sqrt{4\pi}$. Therefore, the complete solution, after substituting $\alpha = (R-r)/\sqrt{D}$, is

$$g(r,t) = 1 - \text{ erf}\left(\frac{r-R}{\sqrt{4Dt}}\right). \tag{15.29}$$

By introducing this result into Eq. (15.20), we finally arrive at

$$\varrho(r,t) = 1 - \frac{R}{r}\,\text{erfc}\left(\frac{r-R}{\sqrt{4Dt}}\right), \tag{15.30}$$

where, generally, $\text{erfc}(x)$ is the complementary error function of a complex variable x (see Sect. A.10.2 of Appendix A). This function has the following properties:

$$\text{erfc}(-x) = 2 - \text{erfc}(x), \qquad \text{erfc}(0) = 1, \qquad \text{erfc}(\infty) = 0. \tag{A.83}$$

Using these properties, we obtain the correct values at the boundary for the normalized concentration, Eq. (15.30), namely, $r \to \infty$, $\varrho(r,t) = 1$, and $r \to R$, $\varrho(R,t) = 0$. Furthermore, the normalized concentration at steady state, when $t \to \infty$, is

$$\varrho(r) = 1 - \frac{R}{r}. \tag{15.31}$$

This equation correctly predicts the behavior of normalized concentration for different values of r, for instance, when $r = R$, $\varrho(r) = 0$, and $r \gg R$, it tends to 1,

as expected. Finally, using Eq. (15.30) into Eq. (15.5)[3] to obtain the rate coefficient results in

$$\mathrm{k}_S(t) = 4\pi R^2 D \left.\frac{\mathrm{d}\varrho(r)}{\mathrm{d}r}\right|_{r=R} = \frac{4\pi D R^3}{r^2}\left[\operatorname{erfc}\left(\frac{r-R}{\sqrt{4Dt}}\right) + \frac{r\mathrm{e}^{-\frac{(r-R)^2}{4Dt}}}{\sqrt{\pi Dt}}\right]_{r=R}$$

$$= 4\pi R D\left[1 + \frac{R}{\sqrt{\pi Dt}}\right], \tag{15.33}$$

namely, the well-known Smoluwchoski rate coefficient. At the steady state, when $t \to \infty$, we obtain the Smoluchowski rate constant, namely,

$$\mathrm{k}_S = 4\pi R D, \tag{15.34}$$

which is Eq. (4.18), as expected. It is important to mention that the Smoluchowski constant can be obtained using a considerably more direct technique. According to the final value theorem, it follows that

$$\lim_{t\to\infty} f(t) = \lim_{s\to 0} sf(s). \tag{5.34}$$

Thus, we are able to obtain the steady-state propagator from Eq. (15.18) by taking the limit of the product $s\varrho(r, s)$, yielding to

$$\varrho(r, t \to \infty) = \lim_{s\to 0}(s\varrho(r, s)) = 1 - \frac{R}{r}, \tag{15.35}$$

which is Eq. (15.31). Afterward, the process consists of substituting the latter equation into Eq. (15.5) to ultimately arrive at Eq. (15.34).

15.1.2 Collins-Kimball Formula: Partially Absorbing Sphere

Collins and Kimball suggested that the rate at which the chemically activated process leads to the formation of products from the encounter pair is proportional to the probability of the encounter pair existing, which can be expressed by means of the flux current as follows:

[3] The derivative of the complementary function is

$$\frac{\mathrm{d}}{\mathrm{d}x}\operatorname{erfc}(x) = -\frac{2}{\sqrt{\pi}}\,\mathrm{e}^{-x^2}. \tag{15.32}$$

$$\mathrm{k}\,\varrho(R,t) = 4\pi R^2 D \left.\frac{\partial \varrho(r,t)}{\partial r}\right|_{r=R}. \tag{15.36}$$

Under this approximation, they generalized the Smoluchowski approach assuming that the surface of the sphere is partially absorbing. As we already know, taking limit $\mathrm{k} \to \infty$ corresponds to the case of a perfectly absorbing sphere, and consequently, the Smoluchowski approach is recovered. Now, it is interesting to explore how the rate coefficient is modified when this boundary condition (BC) is imposed on the spherical surface.

We start by taking the Laplace transform of the flux current, Eq. (15.36), yielding

$$\mathrm{k}\,\varrho(R,s) = 4\pi R^2 D \left.\frac{\partial \varrho(r,s)}{\partial r}\right|_{r=R}. \tag{15.37}$$

Then, the general solution of the diffusion equation in terms of the normalized concentration in Laplace space, given by Eq. (15.11), must be solved by imposing Eqs. (15.37) and (15.14), i.e., $\varrho(r \to \infty, s) = 1/s$. On the one hand, by applying the latter condition, we again find $\mathcal{A} = 0$. On the other hand, by imposing Eq. (15.37) and recalling that the initial condition is $\varrho(r,0) = 1$, we obtain

$$\begin{aligned} \mathrm{k}\left(\frac{1}{s} + \frac{\mathcal{B}}{R}\,\mathrm{e}^{-\sqrt{\frac{s}{D}}R}\right) &= -4\pi R^2 D\left[\frac{\mathcal{B}}{r^2}\left(1+\sqrt{\frac{s}{D}}r\right)\mathrm{e}^{-\sqrt{\frac{s}{D}}r}\right]_{r=R} \\ &= -4\pi D\,\mathcal{B}\left(1+\sqrt{\frac{s}{D}}R\right)\mathrm{e}^{-\sqrt{\frac{s}{D}}R}. \end{aligned} \tag{15.38}$$

Solving for $\mathcal{B}$ yields

$$\mathcal{B} = -\frac{R}{s}\,\mathrm{e}^{\sqrt{\frac{s}{D}}R}\,\frac{\mathrm{k}}{\mathrm{k} + 4\pi R D + 4\pi R^2\sqrt{sD}}. \tag{15.39}$$

By substituting this expression into Eq. (15.11), it becomes

$$\varrho(r,s) = \frac{1}{s}\left[1 - \frac{\mathrm{k}}{\mathrm{k} + 4\pi R D + 4\pi R^2\sqrt{sD}}\,\frac{R\,\mathrm{e}^{\sqrt{\frac{s}{D}}(R-r)}}{r}\right]. \tag{15.40}$$

Finding the inverse Laplace transform of the latter equation is the final step. For such purpose, let us write Eq. (15.40) as follows:

$$\varrho(r,s) = \frac{1}{s} - \frac{\mathrm{k}\,R}{r}\,\frac{\mathrm{e}^{-\sqrt{s}\,\alpha}}{s(\beta + A_{sph}\sqrt{sD})}, \tag{15.41}$$

where $\beta = \mathrm{k} + \mathrm{k}_S$, $\alpha = (r-R)/\sqrt{D}$, and $A_{sph} = 4\pi R^2$. By applying the inverse Laplace transform operator to $\varrho(s,r)$, we obtain

$$\begin{aligned}\varrho(r,t) &= \mathcal{L}^{-1}\left\{\frac{1}{s} - \frac{\mathrm{k}\,R}{r}\frac{\mathrm{e}^{-\sqrt{s}\,\alpha}}{s(\beta + A_{sph}\sqrt{s\,D})}\mathrm{e}^{-\sqrt{s}\,\alpha}\right\} \\ &= 1 - \frac{\mathrm{k}\,R}{r}\mathcal{L}^{-1}\left\{\frac{\mathrm{e}^{-\sqrt{s}\,\alpha}}{s(\beta + A_{sph}\sqrt{s\,D})}\right\}.\end{aligned} \tag{15.42}$$

The first term is obtain in a straightforward manner from Eq. (A.64). Thereafter, our attention is directed solely toward the second term, for which we define

$$g(r,z) \equiv \frac{\mathrm{e}^{-z\alpha}}{z^2(\beta + A_{sph}\sqrt{D}z)}, \tag{15.43}$$

i.e., a function in the Laplace space with the new Laplace variable given by $z \equiv \sqrt{s}$. The strategy we will implement involves finding the inverse Laplace transform of Eq. (15.43) to later connect it to $\varrho(r,t)$, which is in terms of our initial temporal coordinate, by means of

$$\begin{aligned}\varrho(r,t) &= 1 - \frac{\mathrm{k}R}{r}\int_0^\infty \mathcal{L}^{-1}\left\{\mathrm{e}^{-\sqrt{s}\tau}\right\} g(r,\tau)\,\mathrm{d}\tau \\ &= 1 - \frac{\mathrm{k}R}{r}\int_0^\infty \left(\frac{\tau\,\mathrm{e}^{-\tau^2/4t}}{2\sqrt{\pi t^3}}\right) g(r,\tau)\,\mathrm{d}\tau,\end{aligned} \tag{15.44}$$

where we used Eq. (A.69). To ensure a clear understanding of the origin of this last equation, see Sect. A.8, specifically Eq. (A.62), where the formulation of the latter equation is validated.

Now, resuming our original task, we see that

$$\frac{\partial[zg(r,z)]}{\partial z} = -\frac{A_{sph}z\sqrt{D}(2+z\alpha) + \beta + z\alpha\beta}{z^2(A_{sph}\sqrt{D}z + \beta)^2}\mathrm{e}^{-z\alpha}. \tag{15.45}$$

The expansion of the product results in the following equation:

$$\begin{aligned}&g(r,z) + z\frac{\partial g(r,z)}{\partial z} \\ &= -\left\{(2A_{sph}\sqrt{D} + \alpha\beta)\frac{\mathrm{e}^{-\alpha z}}{z(A_{sph}z\sqrt{D} + \beta)} + A_{sph}\alpha\sqrt{D}\frac{\mathrm{e}^{-\alpha z}}{A_{sph}z\sqrt{D} + \beta}\right. \\ &\quad \left. + \beta\frac{\mathrm{e}^{-\alpha z}}{z^2(A_{sph}z\sqrt{D} + \beta)}\right\}\frac{1}{A_{sph}z\sqrt{D} + \beta},\end{aligned} \tag{15.46}$$

which, by means of Eq. (15.43) and after a small rearrangement, enables us to write an equivalent equation solely in terms of $g(z)$, specifically,

$$A_{sph}\sqrt{D}z^2\frac{\partial g(r,z)}{\partial z}+\beta z\frac{\partial g(r,z)}{\partial z}+(3A_{sph}\sqrt{D}+\alpha\beta)zg(r,z)$$
$$+A_{sph}\alpha\sqrt{D}z^2g(r,z)+2\beta g(r,z)=0. \tag{15.47}$$

Using Eq. (3.50), it is now possible to find the inverse Laplace transform of the complete partial differential equation. This process leads us to

$$A_{sph}\sqrt{D}\frac{\partial^2}{\partial t^2}[(-t)g(r,t)]+\beta\frac{\partial}{\partial t}[(-t)g(r,t)]+(3A_{sph}\sqrt{D}+\alpha\beta)\frac{\partial g(r,t)}{\partial t}$$
$$+A_{sph}\alpha\sqrt{D}\frac{\partial^2 g(r,t)}{\partial t^2}+2\beta g(r,t)=0, \tag{15.48}$$

and eventually, we arrive at

$$A_{sph}\sqrt{D}(\alpha-t)\frac{\partial^2 g(r,t)}{\partial t^2}+\left[A_{sph}\sqrt{D}+\beta(\alpha-t)\right]\frac{\partial g(r,t)}{\partial t}+\beta g(r,t)=0. \tag{15.49}$$

The solution to the latter partial differential equation (PDE) is given by

$$g(r,t)=\left\{\mathcal{A}\exp\left[\frac{(\alpha-t)\beta}{A_{sph}\sqrt{D}}\right]-\frac{A_{sph}\sqrt{D}\left[A_{sph}\sqrt{D}+\beta(\alpha-t)\right]}{\beta^2}\mathcal{B}\right\}H(t-\alpha), \tag{15.50}$$

where $H(t-\alpha)$ is the Heaviside function of $t-\alpha$. Notice that the solution is different from zero when $t>\alpha$.[4] Then, we determine the integration constants $\mathcal{A}$ and $\mathcal{B}$ by comparing Eq. (15.50) and the inverse Laplace transform of (15.43) when $\alpha\to 0$. Thus, on the one hand,[5]

[4] See Appendix A, Sect. A.10.4 for further details on the Heaviside function.

[5] Every term in Eq. (15.51) can be computed by following the same technique described in Sects. 3.2, 15.1.1, and this present section. This process is excluded for the purpose of brevity, yet the results can be found in Eqs. (A.67) and (A.68).

$$\mathcal{L}_z^{-1}\{g(r,z)\}_{\alpha\to 0} = \mathcal{L}_z^{-1}\left\{\frac{1}{z^2(A_{sph}z\sqrt{D}+\beta)} - \frac{\alpha}{z(A_{sph}z\sqrt{D}+\beta)} + \cdots\right\}$$

$$= -\frac{A_{sph}\sqrt{D}}{\beta^2} + \frac{A_{sph}\sqrt{D}}{\beta^2}\exp\left(-\frac{t\beta}{A_{sph}\sqrt{D}}\right) + \frac{t}{\beta} - \frac{\alpha}{\beta} + \cdots \tag{15.51}$$

On the other hand, the first four terms of the Taylor series of Eq. (15.50) are[6]

$$g(r,t)_{\alpha\to\infty} = \mathcal{A}\exp\left(-\frac{t\beta}{A_{sph}\sqrt{D}}\right) - \frac{A_{sph}^2 D}{\beta}\mathcal{B} + \frac{A_{sph}\sqrt{D}t}{\beta}\mathcal{B} - \frac{A_{sph}\alpha\sqrt{D}}{\beta}\mathcal{B} + \cdots \tag{15.52}$$

from which we determine that

$$\mathcal{A} = \frac{A_{sph}\sqrt{D}}{\beta^2} \quad \text{and} \quad \mathcal{B} = \frac{1}{A_{sph}\sqrt{D}}. \tag{15.53}$$

For pragmatic reasons, although the integration constants have already been deduced, it is practical to express them as $\mathcal{A}$ and $\mathcal{B}$ instead of expressing them in their explicit form. Subsequently, by substituting $g(t)$, Eq. (15.50), inside the integral in Eq. (15.44), we obtain

$$\int_0^\infty \left(\frac{\tau\, \mathrm{e}^{-\tau^2/4t}}{2\sqrt{\pi t^3}}\right) g(r,\tau)\, \mathrm{d}\tau$$

$$\approx \frac{\mathcal{A}}{2\sqrt{\pi t^3}}\int_\alpha^\infty \tau\, \exp\left(-\frac{\tau^2}{4t}\right)\exp\left[\frac{(\alpha-\tau)\beta}{A_{sph}\sqrt{D}}\right]\mathrm{d}\tau$$

$$-\frac{\mathcal{B}}{2\sqrt{\pi t^3}}\int_\alpha^\infty \tau\, \exp\left(-\frac{\tau^2}{4t}\right)\frac{A_{sph}\sqrt{D}\left[A_{sph}\sqrt{D}+\beta(\alpha-\tau)\right]}{\beta^2}\,\mathrm{d}\tau. \tag{15.54}$$

The reader should be aware of the change of limits in the latter integral, i.e., a transition from $[0,\infty)$ to $[\alpha,\infty)$: the reason for this is that $g(t<\alpha)=0$. Upon performing the integrals, we obtain

[6] It is worth noting that each term in the Taylor series of $g(r,t)$ around $\alpha=0$ should be multiplied by a Heaviside function of the form $H(t)$. Nevertheless, we can guarantee that t is always greater than zero within the physical system, yielding to $H(t)=1$ (see Eq. (A.102)).

$$\int_0^\infty \left(\frac{\tau\, \mathrm{e}^{-\tau^2/4t}}{2\sqrt{\pi t^3}}\right) g(r,\tau)\, \mathrm{d}\tau$$

$$= \frac{\mathrm{e}^{-\alpha^2/4t}}{\sqrt{\pi t}}\mathcal{A} - \frac{A_{sph}^2 D\, \mathrm{e}^{-\alpha^2/4t}}{\sqrt{\pi t}\beta^2}\mathcal{B} + \frac{A_{sph}\sqrt{D}\,\mathrm{erfc}\left(\dfrac{\alpha}{\sqrt{4t}}\right)}{\beta}\mathcal{B} \tag{15.55}$$

$$- \frac{\beta\, \exp\left[\dfrac{\beta\left(A_{sph}\sqrt{D}\alpha + t\beta\right)}{A_{sph}^2 D}\right]\mathrm{erfc}\left(\dfrac{\alpha + \frac{2t\beta}{A_{sph}\sqrt{D}}}{\sqrt{4t}}\right)}{A_{sph}\sqrt{D}}\mathcal{A}.$$

Now, from the last mathematical solution, we must work only with the physically congruent part of it. Since for short times the function must be convergent, we must get rid of every term leading to an indeterminate result at $t \to 0$, yielding to

$$\int_0^\infty \left(\frac{\tau\, \mathrm{e}^{-\tau^2/4t}}{2\sqrt{\pi t^3}}\right) \mathrm{d}\tau = \frac{A_{sph}\sqrt{D}\,\mathrm{erfc}\left(\dfrac{\alpha}{\sqrt{4t}}\right)}{\beta}\mathcal{B}$$

$$- \frac{\beta\, \exp\left[\dfrac{\beta\left(A_{sph}\sqrt{D}\alpha + t\beta\right)}{A_{sph}^2 D}\right]\mathrm{erfc}\left(\dfrac{\alpha + \frac{2t\beta}{A_{sph}\sqrt{D}}}{\sqrt{4t}}\right)}{A_{sph}\sqrt{D}}\mathcal{A}. \tag{15.56}$$

Finally, by substituting the latter equation into Eq. (15.44), together with the definition of all constants, including $\mathcal{A}$ and $\mathcal{B}$ in Eq. (15.53), we arrive at

$$\varrho(r,t) = 1 - \frac{R}{r}\frac{\mathrm{k}}{\mathrm{k} + 4\pi RD}\left\{\mathrm{erfc}\left(\frac{r-R}{\sqrt{4Dt}}\right) - \exp\left[\frac{(4\pi RD + \mathrm{k})(r-R)}{4\pi R^2 D}\right]\times\right.$$

$$\left.\times \exp\left[\frac{(4\pi RD + \mathrm{k})^2 t}{(4\pi R^2)^2 D}\right]\mathrm{erfc}\left(\frac{r-R}{\sqrt{4Dt}} + \frac{4\pi RD + \mathrm{k}}{4\pi R^2\sqrt{D/t}}\right)\right\}. \tag{15.57}$$

This equation gives us the normal concentration as a function of time and position in the presence of an immobile partially absorbing sphere placed at the origin and reproduces the correct limiting case, $\varrho(r \to \infty, t) = 1$.

Finally, the Collins-Kimball rate coefficient is calculated by substituting $\varrho(r,t)$ into Eq. (15.5), which gives

$$\mathtt{k}_{CK}(t) = \mathtt{k}\varrho(R,t) = \frac{4\pi R D\,\mathtt{k}}{\mathtt{k}+4\pi R D}\left\{1+\frac{\mathtt{k}}{4\pi R D}\exp\left[\frac{Dt}{R^2}\left(1+\frac{\mathtt{k}}{4\pi R D}\right)^2\right]\times\right.$$
$$\left.\times\,\mathrm{erfc}\left[\frac{\sqrt{Dt}}{R}\left(1+\frac{\mathtt{k}}{4\pi R D}\right)\right]\right\}. \tag{15.58}$$

There are some interesting limits to analyze in this last equation, which in fact are easily obtained if we focus on Eq. (15.57) instead of Eq. (15.58). At large values of $\mathtt{k}$, i.e., $\mathtt{k}\to\infty$, Eq. (15.58) reduces to the density distribution predicted by Smoluchowski, Eq. (15.30). If $\mathtt{k}=0$, the diffusing particles and the sphere collide elastically. Additionally, the steady-state limit, taking $t\to\infty$, is given by

$$\varrho(r) = 1-\frac{\mathtt{k}}{\mathtt{k}+4\pi R D}\,\frac{R}{r}. \tag{15.59}$$

Consequently, substituting this density into Eq. (15.36), the Collins-Kimball rate constant results in[7]

$$\mathtt{k}_{CK} = \frac{4\pi R D\,\mathtt{k}}{\mathtt{k}+4\pi R D}. \tag{15.61}$$

For a perfectly absorbing sphere, $\mathtt{k}\to\infty$, $\mathtt{k}_S$ is recovered. Now, in terms of the Smoluchowski rate constant, Eq. (15.34), the latter formula can be rewritten as follows:

$$\mathtt{k}_{CK} = \frac{\mathtt{k}_S\,\mathtt{k}}{\mathtt{k}+\mathtt{k}_S}. \tag{15.62}$$

This formula has a simple physical interpretation: It describes the decrease of the Smoluchowski rate constant by the factor

$$\frac{\mathtt{k}}{\mathtt{k}+\mathtt{k}_S}, \tag{15.63}$$

[7] Note that the Collins-Kimball rate constant can be derived by using Eq. (5.34). Then,

$$\varrho(r,t\to\infty) = \lim_{s\to 0} s\varrho(r,s) = \lim_{s\to 0} s\left[\frac{1}{s}-\frac{\mathtt{k}R}{r}\,\frac{\mathrm{e}^{-\sqrt{s}\alpha}}{s(\beta+A\sqrt{sD})}\right]$$
$$= 1-\frac{\kappa R}{r\beta}, \tag{15.60}$$

where $\varrho(r,s)$ is substituted by Eq. (15.41). The latter equation is actually Eq. (15.59), which unambiguously leads us to Eq. (15.61).

which is the trapping probability of a particle that starts from the surface of the disk. In other words, if the Smoluchowski rate constant alone stands for the first encounter of a Brownian particle with a perfectly absorbing sphere, in the Collins-Kimball system, because the particle has a probability of not being trapped by the partially absorbing sphere in its first encounter, the latter factor stands for the trapping probability for a particle that starts from the surface of the sphere.

Finding the corresponding κ associated with $\mathtt{k}$ is an important task because the trapping rate constant provides the proportionality between flux and concentration. Multiplying the definition of the partially absorbing boundary, given in Eq. (4.11), by the area and equating it with Eq. (15.36), results in (see Eq. (15.5))

$$\mathtt{k} = A\,\kappa, \tag{15.64}$$

where A is the area of the partially absorbing surface, $\mathtt{k}$ its rate constant, and κ its trapping rate. Now, we can write Eq. (15.62) in terms of its trapping rate coefficient κ, using Eq. (15.64), namely, $\mathtt{k} = \kappa\, A_{sph}$, so that

$$\mathtt{k}_{CK} = \frac{\mathtt{k}_S\,\kappa\, A_{sph}}{\mathtt{k}_S + \kappa\, A_{sph}}, \tag{15.65}$$

where, again, A_{sph} is the area of the sphere.

In the following section, we will address the problem of diffusion through a reflective sphere with absorbent circular patches uniformly distributed on its surface by means of the Collins-Kimball rate constant. Some of the results obtained for this system, besides having a large number of applications, are surprisingly counterintuitive.

15.2 Berg-Purcell Formula: The Patchy Sphere

Berg and Purcell studied *chemotaxis*[8] and considered the trapping of diffusing particles by $\mathtt{N}$ small perfectly absorbing circular disks of radius a, which are randomly and uniformly distributed over the surface of a perfectly reflecting sphere of radius R, where $R \ll a$ (see Fig. 15.1). It is important to keep in mind that the Hill-Berg-Purcell constant rate is computed for an absorbing disk with radius a placed on a flat reflecting surface. To obtain the rate constant for $\mathtt{N}$ small perfectly absorbing circular disks on the surface of a reflecting sphere, we use the Collins-

[8] Chemotaxis is referred to as the biological phenomenon in which molecules or organisms, e.g., cells, bacteria, and fungi, move in response to the gradient of a chemical substance in their environment. For instance, during an immune response, white cells utilize chemotaxis to detect and eliminate invading pathogens.

Kimball formula, Eq. (15.61). In this formula, the trapping efficiency is regulated by $\mathtt{k}$.

On one hand, the trapping efficiency of Eq. (15.61) is regulated by $\mathtt{k}$. On the other hand, regarding the patchy sphere, the trapping efficiency would be given by the $\mathtt{N}$ absorbing disks. Then, substituting the Hill-Berg-Purcell rate constant for $\mathtt{N}$ perfectly absorbing circular disks of radius a, $\mathtt{N}\mathtt{k}_{HBP} = 4Da\mathtt{N}$, into the Collins-Kimball formula, leads to the Berg-Purcell (BP) formula

$$\begin{aligned} \mathtt{k}_{BP} &= \frac{\mathtt{N}\,\mathtt{k}_S\mathtt{k}_{HBP}}{\mathtt{N}\,\mathtt{k}_{HBP} + \mathtt{k}_S} \\ &= \frac{4\pi DRa\mathtt{N}}{\pi R + a\mathtt{N}}. \end{aligned} \tag{4.23}$$

According to this formula, when $\mathtt{N}$ is small, $a\mathtt{N} \ll R$, the rate constant is equal to the sum of the rate constant of $\mathtt{N}$ non-interacting perfectly absorbing disks, $4Da\mathtt{N} = \mathtt{k}_S\mathtt{N}$ (see Eq. (4.22)). In the opposite limiting case, $a\mathtt{N} \gg R$, diffusing particles are trapped by the patchy sphere as if it were perfectly absorbing, $4\pi RD = \mathtt{k}_S$.

Now, let's find a relation between $\mathtt{k}_{BP}$ and its related κ_{BP}. Using Eq. (15.64), this relation between the rate constant and its trapping rate coefficient is

$$\mathtt{k}_{BP} = A_{sph}\,\kappa_{BP}, \tag{15.66}$$

where A_{sph} is the area of the patchy sphere. Substituting Eq. (4.23) in this last formula and the area of the sphere $A_{sph} = 4\pi R^2$, it becomes

$$\frac{4\pi DRa\mathtt{N}}{\pi R + a\mathtt{N}} = 4\pi R^2\,\kappa_{BP}. \tag{15.67}$$

Solving Eq. (15.67) for κ under the approximation $a\mathtt{N} \ll R$ and using the definition of the fraction occupied by the disk results in

$$\sigma = \frac{a^2\mathtt{N}}{4R^2}. \tag{15.68}$$

Then, setting $\mathtt{N} = 1$, we obtain

$$\kappa_{BP}(\sigma) = \frac{4D}{\pi a}\sigma = \frac{2D}{\pi R}\sqrt{\sigma}. \tag{15.69}$$

This last expression is a simple approximate formula that works for a small disk compared to the size of the sphere. In fact, this expression gives only the leading term of the small-σ-expansion of the dependence of $\kappa(\sigma)$ over the entire range, i.e., $0 \le \sigma \le 1$. The formula can be expressed in a more general way in to make it applicable for a bigger disk or cap, namely,

$$\kappa(\sigma) = \frac{4D}{\pi a}\sigma f(\sigma) = \frac{2D}{\pi R}\sqrt{\sigma} f(\sigma). \tag{15.70}$$

Among other techniques, a *computer-assisted boundary homogenization approach* can be used to determine the function $f(\sigma)$. In Sect. 16.1, we will thoroughly examine this procedure.

15.3 Zwanzig-Szabo Formula: The Partially Absorbing Circular Disk and Diffusing Interference Between Binding Sites

A similar formula to the Collins-Kimball formula can be derived for a partially absorbing circular disk of radius a, with rate constant κ, on a reflecting flat surface. This formula is known as the *Zwanzig-Szabo rate constant* and is given by

$$\mathtt{k}_{ZS} = \frac{\kappa_{HBP}\kappa A_{disk}}{\kappa_{HBP} + \kappa A_{disk}} = \frac{4\pi a^2 D\kappa}{4D + a\pi\kappa}, \tag{15.71}$$

where $0 \leq \kappa \leq 1$ and $A_{disk} = \pi a^2$ is the area of the disk. Then, when $\kappa \to \infty$ the perfectly absorbing circular disk, κ_{HBP}, is recovered, Eq. (4.22). In the opposite case, when $\kappa \to 0$, the diffusing particles and the disk collide elastically and the system becomes a perfectly reflecting wall. In a similar way to the Collins-Kimball formula, the Zwanzig-Szabo formula, Eq. (15.71), has a simple physical interpretation: It describes the decrease of the Hill-Berg-Purcell rate constant by the factor

$$\frac{\pi a\kappa}{4D + a\kappa\pi}. \tag{15.72}$$

Unlike the Collins-Kimball formula, which is an exact result, Eq. (15.71) provides a very good approximation.[9] Additionally, we can compute the rate constant for $\mathtt{N}$ partially absorbing circular disks, each of radius a, on the surface of a perfectly reflecting sphere of radius R. This process is carried out by substituting $\mathtt{N}$ times Eq. (15.71) into Eq. (15.62), yielding to

[9] The Zwanzig-Szabo formula, Eq. (15.71), is originally derived as the first member of a series of successively more accurate approximations. Moreover, it is reasonably accurate for all values of κ with a maximum deviation of less than 4%.

$$\begin{aligned} \mathtt{k}_{\mathtt{ZSPA}} &= \frac{A_{disk}\kappa\, \mathtt{k}_{HBP}\mathtt{k}_S}{\mathtt{k}_{HBP}\mathtt{k}_S + A_{disk}\kappa(\mathtt{k}_S + \kappa \mathtt{N}\, \mathtt{k}_{HBP})} \\ &= \frac{4\pi DR\kappa a^2 \mathtt{N}}{4DR + a\kappa(a\mathtt{N} + \pi R)}. \end{aligned} \tag{15.73}$$

Naturally, the later expression reduces to Eq. (4.23) at the limit $\kappa \to \infty$ and becomes null when $\kappa = 0$.

Up to now, all presented formulas were derived on the assumption that there are no competitive effects between absorbing patches. For instance, the BP formula is obtained considering that the size of a single receptor is much smaller than the typical distance between neighboring sites. According to Brownian dynamics simulations, Eq. (4.23) predicts good results at low coverage; however, when approximately $1/4$ of the spherical surface is covered by receptors, simulations are about 5% higher than the results obtained with the BP formula. Based on these observations, we can impose an upper threshold to determine the appropriateness of using the BP formula.

In order to consider the effect of interference between perfectly absorbing sites embedded a spherical reflecting surface, Zwanzig proposed a modification to the Berg-Purcell formula by including a term depending on the factor $1 - \sigma$, which represents the total area of the sphere minus the area occupied by the patches, i.e., free reflecting surface (see Eq. (15.68)), leading to

$$\mathtt{k}_{Zint} = \mathtt{k}_S \frac{\mathtt{N}a}{\mathtt{N}a + \pi R(1-\sigma)}. \tag{15.74}$$

Later, Zwanzig's modification was used by Zwanzig and Szabo to consider partially, instead of perfectly, absorbing sites. With the intention of outlining a clear path toward determining such rate constant, below is a comprehensive examination of the original derivation by Zwanzig and Szabo.

The primary objective is to derive the rate coefficient, given generally by Eq. (15.5), for $\mathtt{N}$ partially absorbing disks experimenting the neighbor interference effect, embedded on the reflecting sphere. This task shall be accomplished by means of the Laplace transform and an *effective medium approximation*. Hence, for an observer who is far away from the reflecting sphere with $\mathtt{N}$ partially absorbing disks, such arrangement resembles a partially absorbing sphere, i.e., an *effective sphere*, labeled as a system $\mathtt{E}$ with rate coefficient $\mathtt{k}_{\mathtt{E}}(t)$.

In addition, the probability of locating a point that is on a reflecting region when randomly picking a place on the spherical surface is determined by $1 - \sigma$, given that Eq. (15.68) stands for the probability of locating a point that is in a partially absorbing disk. In the vicinity of the chosen point, we construct a disk-shaped region and assign it the corresponding BC depending on its location, i.e., either outside or inside a partially absorbing disk. The latter and former cases are labeled as system system $\mathtt{PA}$ with rate coefficient $\mathtt{k}_{\mathtt{PA}}(t)$ and probability of occurrence σ and system $\mathtt{R}$ with rate coefficient $\mathtt{k}_{\mathtt{R}}(t)$ and probability of occurrence $1 - \sigma$, respectively. We

can conclude that the BC for system R is given by $\partial \varrho_{\mathtt{R}}(r,t)/\partial r\big|_{r=R} = 0$, while system PA is to be solved together with the BC $D\partial \varrho_{\mathtt{PA}}(r,t)/\partial r\big|_{r=R} = \kappa \varrho_{\mathtt{PA}}(R,t)$. Moreover, since the distant observer calculates the rate coefficient as $\mathtt{k}_{\mathtt{E}}(t)$ when selecting any region, which also has Eq. (15.36) as a BC, then such solution can be written as an *average* of PA and R cases, yielding to the *effective medium condition*, namely,

$$\mathtt{k}_{\mathtt{E}}(t) = \sigma\, \mathtt{k}_{\mathtt{PA}}(t) + (1-\sigma)\, \mathtt{k}_{\mathtt{R}}(t). \tag{15.75}$$

Now, it is worth noting that the effective sphere, system E, corresponds exactly to the Collins-Kimball problem, presented in Sect. 15.1.2, whose rate coefficient is given by

$$\mathtt{k}_{\mathtt{E}}(t) = 4\pi R^2 D \frac{\partial \varrho_{\mathtt{E}}(r,t)}{\partial r}\bigg|_{r=R}, \tag{15.76}$$

or by Eq. (15.58), once we have substituted $\varrho_{\mathtt{E}}(r,t)$ as in Eq. (15.57). Furthermore, for system PA, the BC outside the disk is chosen to be the same as for system E, leading to

$$\frac{\partial \varrho_{\mathtt{PA}}(r,t)}{\partial r}\bigg|_{r=R} = \frac{\partial \varrho_{\mathtt{E}}(r,t)}{\partial r}\bigg|_{r=R} \quad \text{outside the disk,} \tag{15.77}$$

while the BC inside the disk reads

$$D\frac{\partial \varrho_{\mathtt{PA}}(r,t)}{\partial r}\bigg|_{r=R} = \kappa \varrho_{\mathtt{PA}}(R,t) \quad \text{inside the disk.} \tag{15.78}$$

Thus, we can formulate an expression for the rate coefficient of system PA as follows:

$$\mathtt{k}_{\mathtt{PA}}(t) = (4\pi R^2 - \pi a^2)\frac{\partial \varrho_{\mathtt{E}}(r,t)}{\partial r}\bigg|_{r=R} + \int_{\text{in}} \mathbf{J}_{\mathtt{PA}}(R,t)\cdot \hat{\mathbf{n}}\, \mathrm{d}A, \tag{15.79}$$

in which the first term stands for all contributions outside the disk-shaped region where the behavior of the effective sphere is dominant and the second term is to be integrated over the disk area. We can carry out the same process for system R, resulting in[10]

$$\mathtt{k}_{\mathtt{R}}(t) = (4\pi R^2 - \pi a^2)\frac{\partial \varrho_{\mathtt{E}}(r,t)}{\partial r}\bigg|_{r=R}. \tag{15.80}$$

[10] Note that Eq. (15.80) has one term only because the BC inside the disk requires null flux.

By substituting Eqs. (15.79) and (15.80) into Eq. (15.75), we find

$$\mathtt{k}_{\mathtt{E}}(t) = \mathtt{k}_{\mathtt{E}}(t) - \pi a^2 \frac{\partial \varrho_{\mathtt{E}}(r,t)}{\partial r}\bigg|_{r=R} + \sigma \int_{\text{in}} \mathbf{J}_{\mathtt{PA}}(R,t)\cdot\hat{\mathbf{n}}\,\mathrm{d}A, \tag{15.81}$$

meaning that

$$\pi a^2 \frac{\partial \varrho_{\mathtt{E}}(r,t)}{\partial r}\bigg|_{r=R} = \sigma \int_{\text{in}} \mathbf{J}_{\mathtt{PA}}(R,t)\cdot\hat{\mathbf{n}}\,\mathrm{d}A. \tag{15.82}$$

Furthermore, we require a fourth case in which a single partially absorbing disk is placed on a reflecting sphere, say a system $\mathtt{S}$ with rate coefficient $\mathtt{k}_{\mathtt{S}}$. At the end of the section, the reader will see that we only need to solve cases $\mathtt{E}$ and $\mathtt{S}$. In the case of a single receptor, system $\mathtt{S}$, the BCs are

$$\begin{aligned} D\frac{\partial \varrho_{\mathtt{S}}(r,t)}{\partial r}\bigg|_{r=R} &= \kappa \varrho_{\mathtt{S}}(R,t) \quad \text{inside the disk,} \\ \frac{\partial \varrho_{\mathtt{S}}(r,t)}{\partial t}\bigg|_{r=R} &= 0 \qquad\qquad \text{outside the disk,} \end{aligned} \tag{15.83}$$

as we would expect.

The next step is to find $J_{\mathtt{PA}}(R,t)$, which will then allow us to establish a relation between the flux of systems $\mathtt{E}$ and $\mathtt{S}$, i.e., $J_{\mathtt{E}}(r,s)$ and $J_{\mathtt{S}}(r,s)$, respectively. This process can be done more simply when using the Laplace transform. As we know, the Laplace transform of the diffusion equation is given by Eq. (15.7), which can be expressed as

$$s\varrho(r,s) - 1 = D\nabla^2 \varrho(r,s). \tag{15.84}$$

Therefore by using such equation, as well as the BC for the chosen system, the problem admits an exact solution. Additionally, given that the solution of every case, $\mathtt{E}$, $\mathtt{PA}$, $\mathtt{R}$, or $\mathtt{S}$, differs only in the BCs that they satisfy, this suggests a linear relation between solutions, namely,

$$\varrho_{\mathtt{PA}}(r,s) = \mu_{\mathtt{S}}\varrho_{\mathtt{S}}(r,s) + \mu_{\mathtt{E}}\varrho_{\mathtt{E}}(r,s) + \mu_{\mathtt{C}}, \tag{15.85}$$

where $\mu_{\mathtt{S}}$, $\mu_{\mathtt{E}}$, and $\mu_{\mathtt{C}}$ are constants to be determined. By replacing the latter equation into Eq. (15.84), we find

$$s\,\left(\mu_{\mathtt{S}}\varrho_{\mathtt{S}}(r,s) + \mu_{\mathtt{E}}\varrho_{\mathtt{E}}(r,s) + \mu_{\mathtt{C}}\right) - 1 = D\nabla^2\left(\mu_{\mathtt{S}}\varrho_{\mathtt{S}}(r,s) + \mu_{\mathtt{E}}\varrho_{\mathtt{E}}(r,s) + \mu_{\mathtt{C}}\right) \tag{15.86}$$

and after recursively using the linearity of Laplace's equation, we are led to

$$1 - s\mu_{\mathrm{C}} = \mu_{\mathrm{S}} + \mu_{\mathrm{E}}. \tag{15.87}$$

Moreover, Eq. (15.85) implies that[11]

$$J_{\mathrm{PA}}(r,s) = \mu_{\mathrm{S}} J_{\mathrm{S}}(r,s) + \mu_{\mathrm{E}} J_{\mathrm{E}}(r,s), \tag{15.89}$$

and since $J_{\mathrm{A}} = J_{\mathrm{E}}$ outside of the disk, and also given that $J_{\mathrm{S}} = 0$, we conclude that $\mu_{\mathrm{E}} = 1$. On the contrary, inside the disk, we require that

$$\begin{aligned} J_{\mathrm{PA}}(R,s) &= \kappa \varrho_{\mathrm{PA}}(R,s) \\ &= \kappa \left(\mu_{\mathrm{S}} \varrho_{\mathrm{S}}(R,s) + \mu_{\mathrm{E}} \varrho_{\mathrm{E}}(R,s) + \mu_{\mathrm{C}}\right), \end{aligned} \tag{15.90}$$

or

$$\mu_{\mathrm{S}} J_{\mathrm{S}}(R,s) + \mu_{\mathrm{E}} J_{\mathrm{E}}(R,s) = \kappa \mu_{\mathrm{S}} \varrho_{\mathrm{S}}(R,s) + \mu_{\mathrm{E}} J_{\mathrm{E}}(R,s). \tag{15.91}$$

By comparing these last two equations, we arrive at

$$\mu_{\mathrm{E}} J_{\mathrm{E}} = \kappa \left(\mu_{\mathrm{E}} \varrho_{\mathrm{E}}(R,s) + \mu_{\mathrm{C}}\right). \tag{15.92}$$

Thus, after performing various algebraic rearrangements, Eq. (15.85) can be formulated as follows:

$$\varrho_{\mathrm{PA}}(r,s) = \varrho_{\mathrm{E}}(r,s) + \left(\varrho_{\mathrm{E}}(R,s) - \frac{J_{\mathrm{E}}(R,s)}{\kappa}\right)\left(s\varrho_{\mathrm{S}}(r,s) - 1\right). \tag{15.93}$$

The flux for system PA can be obtained from the latter equation by taking the derivative with respect to r, yielding

$$J_{\mathrm{PA}}(r,s) = J_{\mathrm{E}}(r,s) + \left(\varrho_{\mathrm{E}}(R,s) - \frac{J_{\mathrm{E}}(R,s)}{\kappa}\right) s J_{\mathrm{S}}(r,s). \tag{15.94}$$

By substituting Eq. (15.94), following the evaluation at the boundary, into Eq. (15.82), we obtain[12]

[11] Be aware that

$$J_i(R,t) = D \left.\frac{\partial \varrho_i(r,t)}{\partial r}\right|_{r=R}. \tag{15.88}$$

The minus sign that usually appears in the computation of the probability flux, for example, in Eq. (15.1), becomes positive after making the scalar product with the unit normal vector $\hat{\mathbf{n}}$.

[12] Notice that Eq. (15.82) is originally written in real space, i.e., in terms of t. Nevertheless, after taking the Laplace transform of the entire equation, the result is an equation having the same mathematical structure.

$$\pi a^2 J_{\mathrm{E}}(R,s) = \sigma \int_{\mathrm{in}} \left[J_{\mathrm{E}}(R,s) + \left(\varrho_{\mathrm{E}}(R,s) - \frac{J_{\mathrm{E}}(R,s)}{k} \right) s J_{\mathrm{S}}(R,s) \right] \mathrm{d}A$$

$$= \sigma \int_{\mathrm{in}} J_{\mathrm{E}}(R,s)\,\mathrm{d}A + \sigma s \left(\varrho_{\mathrm{E}}(R,s) - \frac{J_{\mathrm{E}}(R,s)}{k} \right) \int_{\mathrm{in}} J_{\mathrm{S}}(R,s)\,\mathrm{d}A, \tag{15.95}$$

which, after integration over the area of a single receptor, simplifies to

$$\pi a^2 J_{\mathrm{E}}(R,s) = \pi a^2 \sigma J_{\mathrm{E}}(R,s) + \sigma s \left(\varrho_{\mathrm{E}}(R,s) - \frac{J_{\mathrm{E}}(R,s)}{\kappa} \right) \mathtt{k}_{\mathrm{S}}. \tag{15.96}$$

This leads to

$$(1-\sigma)\pi a^2 J_{\mathrm{E}}(R,s) = \sigma s \left(\varrho_{\mathrm{E}}(R,s) - \frac{J_{\mathrm{E}}(R,s)}{k} \right) \mathtt{k}_S. \tag{15.97}$$

Furthermore, the solution in Laplace space for the propagator regarding the Collins-Kimball problem in Sect. 15.1.2 can be expressed more generally in terms of the flux evaluated at the spherical surface, that is,

$$\varrho_E(r,s) = \frac{1}{s} + \frac{J_{\mathrm{E}}(R,s)R^2}{r(D + R\sqrt{sD})} \mathrm{e}^{\sqrt{\frac{s}{D}}(R-r)}, \tag{15.98}$$

in which we have redefined $\varrho(r,s)$ as $\varrho_{\mathrm{E}}(r,s)$, since system $\mathtt{E}$ corresponds to the Collins-Kimball system, i.e., a partially absorbing sphere. The last equation naturally yields to Eq. (15.40), and, when evaluated at $r = R$, it gives us a relation between $\varrho_{\mathrm{E}}(R,s)$ with $J_{\mathrm{E}}(R,s)$, namely,

$$\varrho_{\mathrm{E}}(R,s) = \frac{1}{s} + \frac{J_{\mathrm{E}}(R,s)R}{D + R\sqrt{sD}}. \tag{15.99}$$

Then, by substituting Eq. (15.99) into Eq. (15.97) and solving for $J_{\mathrm{E}}(R,s)$, we arrive at

$$J_{\mathrm{E}}(R,s) = \frac{\mathtt{k}_{\mathrm{S}}\sigma}{\pi a^2(1-\sigma) - \dfrac{\mathtt{k}_{\mathrm{S}} s\sigma}{\kappa} - \dfrac{\mathtt{k}_{\mathrm{S}} R s\sigma}{D + R\sqrt{sD}}}. \tag{15.100}$$

Thereafter, we substitute $\sigma = \mathtt{N}a^2/4R^2$ solely in the numerator and take the limit at $s \to 0$, intending to outline a large time description, and, for simplicity purposes, we write the result in reciprocal form, leading to[13]

[13] It is important to pinpoint that the trapping efficiency is now controlled by the $\mathtt{N}$ partially absorbing disks, meaning that $\mathtt{k}_{\mathrm{S}}$ is replaced by Eq. (15.71).

$$\frac{1}{\mathtt{k}_{\mathtt{ZS}}} = \frac{1}{4aD\mathtt{N}} + \frac{1}{\pi a^2 \kappa \mathtt{N}} - \frac{\sigma}{4DaN} - \frac{\sigma}{\pi a^2 \kappa \mathtt{N}}. \tag{15.101}$$

Ultimately, by means of Eqs. (15.61) and (15.68), we rewrite the last term of the latter equation, that is,

$$\frac{1}{\mathtt{k}_{\mathtt{ZS}}} = \frac{1}{4aD\mathtt{N}} + \frac{1}{\pi a^2 \kappa \mathtt{N}} - \frac{\sigma}{4DaN} + \frac{1}{4\pi DR} - \frac{1}{\mathtt{k}_{CK}}. \tag{15.102}$$

The solution must simplify to the Smoluchowski formula at the limit $\kappa \to \infty$. Therefore by neglecting the last term, we arrive at the Zwanzig-Szabo formula

$$\frac{1}{\mathtt{k}_{\mathtt{ZS}}} = \frac{1}{\mathtt{k}_S} + \frac{1-\sigma}{\mathtt{N}\,\mathtt{k}_{HBP}} + \frac{1}{\mathtt{N}\kappa A_{disk}}, \tag{15.103}$$

where we have used Eqs. (4.22), (15.34), and $A_{disk} = \pi a^2$.

Finally, it is worth noting that in the Berg-Purcell, Collins-Kimball, and Zwanzig-Szabo formulas, the absorbing circular disk can be replaced by an absorbing or partially absorbing shape (spot), by means of $\mathtt{k}_{DBW}$, given by

$$\mathtt{k}_{DBW} = \left(\frac{2^5 AP}{\pi^2}\right)^{1/3} D, \tag{14.126}$$

where A and P are the area and perimeter of the selected absorbing site.

In the following subsections, we will describe more systems for which these rate constants are known. Moreover, it should be noted that Eq. (15.103) is derived using a perturbative theory in σ. In Sect. 16.1, we shall demonstrate that utilizing $\sqrt{\sigma}$ yields to significantly more suitable results.

15.4 Chemoreceptors over a Spherical Cell

Cell intercommunication (CI), also known as *cell signaling*, can be triggered by several factors, including physical, chemical, and biological signals. In a vast number of CI processes, the key ingredient in starting a signaling cascade that ultimately affects cell behavior is a *ligand*, i.e., a small protein or ion that binds to a specific *chemoreceptor*, which is a specialized sensory receptor embedded in cell membranes, e.g., the membranes present in sensory neurons or immune system cells. More precisely, the ligand-receptor interactions allow cells to communicate with each other and respond to different environmental conditions, where chemoreceptors are essential for the detection and response to chemical stimuli and ligands are the primary input in the process.

The ligand-receptor interaction over a spherical cell can be roughly modeled using a reflecting sphere of radius R centered at the origin with $\mathtt{N}$ perfectly absorbing

circular patches, each of radius a, embedded on its surface. Within the framework of this model, the reflecting sphere, absorbing patches, and constant concentration of Brownian particles at infinity will take the place of the cell, the chemoreceptors, and the concentration gradient of ligands, respectively. This description is actually the Berg-Purcell patchy sphere, from which we have obtained the rate constant, namely,

$$\mathtt{k}_{BP} = \frac{4\pi D R a \mathtt{N}}{\pi R + a\mathtt{N}}. \tag{4.23}$$

As previously mentioned, the units of the rate constant are volume per unit time, meaning that, in this case, it would be describing the volume of ligands per unit time binding into chemoreceptors. Therefore, a large value of $\mathtt{k}$ indicates a remarkable trapping efficiency of ligands. Moreover, the more ligands that can be captured with the least possible absorbing area, the better the configuration of chemoreceptors regarding geometry and distribution. In preparation for further exploration of this topic, let us present a mental experiment to be able to understand the counterintuitive results behind Eq. (4.23).

15.4.1 A Counterintuitive Experiment: Circular and Elliptical Absorbing Patches

Suppose we have two spheres of the same radius. One of the spheres has one reflective and one absorbing hemisphere, meaning that 1/2 of its surface is capable of absorbing ligands. In contrast, the second sphere has tiny, uniformly distributed absorbing circular patches on its reflecting surface, so that, combined, they occupy minimal on the sphere, say four hundredths of it. This arrangement is represented in Fig. 15.2 and the related question is: Which configuration can absorb more ligands if they are immersed in a fluid with a specific concentration gradient? The answer

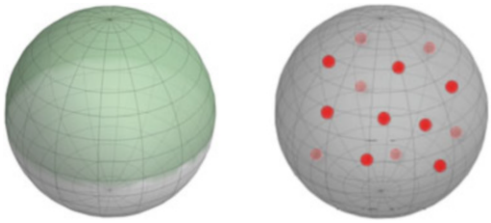

Fig. 15.2 Schematic representation of a sphere having one reflecting and one absorbing hemisphere (green cap) on the left-hand side and a reflecting sphere with $\mathtt{N}$ absorbing circular receptors (red spots) embedded on its surface on the right-hand side. Even though on $1/2$ of the sphere on the left is an effective absorbent area, which is much larger than the $1/400$ effective absorbing area associated with the sphere on the right, both configurations are able to bind the same amount of molecules in their environment

seems to be obvious, as the first sphere has a bigger absorbing surface than the second one. Nevertheless, upon close examination of this question, we come to a different conclusion: From Eqs. (4.23) and (15.34), we see that the rate constant of the Berg-Purcell patchy surface, $\mathtt{k}_{BP}$, is smaller than the Smoluchowski rate constant, $\mathtt{k}_S$, by a factor of $1 + \pi R/\mathtt{N}a$. Moreover, the number of circular patches needed to equalize the rate constant of an absorbing hemisphere, i.e., $\mathtt{k}_S/2$, is given by

$$\mathtt{N}_* = \frac{R}{a}\pi, \tag{15.104}$$

a number that depends on the ratio of the radius of the sphere to the radius of the chemoreceptors. Now, on determining who many circular patches we need, we must provide specific values to R and a: It is worth noting that the specific size of a chemoreceptor can vary among different organisms and specific receptor types. However, as an approximation and useful example, let us define $R = 1\,\mu\text{m}$ and $a = 2\,\text{nm}$. This cell size is very similar to that found in prokaryotic cells, e.g., *Escherichia coli* (*E.coli*), and in spherically shaped bacterium, e.g., *Staphylococcus aureus* (*S. aureus*), a useful member of the microbiota of the human body (and sometimes an opportunistic pathogen, which can cause infections). Regarding the chemoreceptors, these are modeled to be about 500 times smaller than the cell membrane. In order to have a clearer picture of the difference in size between these two components, we would have to increase the size of the cell to that of an average bowling ball (21.6 cm) to see chemoreceptors in the size of a grain of salt.

Using these values, we see that the number of patches needed to equalize the absorbing hemisphere is $\mathtt{N}_* \approx 1{,}570$ and the ratio of the total area of the chemoreceptors to the area of the sphere is $\sigma = a^2\mathtt{N}_*/4R^2 \approx 1.16 \times 10^{-3}$. Additionally, we are able to compute the distance between neighboring sites through $(4\pi R^2/\mathtt{N}_*)^{1/2} \approx 0.089\,\mu\text{m}$, which is about 45 times larger than the chemoreceptor radius, allowing us to neglect the interference or competitive effects between absorbing patches and consider the binding to a single receptor to be reaction-limited. Under these assumptions and scales, we find that the rate constant to $\mathtt{N}$ absorbing patches over a spherical cell can be described by Eq. (4.23), namely,

$$\mathtt{k}_{BP-DBW} = \frac{\mathtt{N}\,\mathtt{k}_S\mathtt{k}_{DBW}}{\mathtt{N}\,\mathtt{k}_{DBW} + \mathtt{k}_S}, \tag{15.105}$$

where we have replaced the Hill-Berg-Purcell rate constant, $\mathtt{k}_{HBP}$, with the more general rate constant derivation for an arbitrary-shaped absorbing patch with area A and perimeter P placed on a reflecting plane. There is an interesting feature of the latter result: The strong dependence on area and perimeter of Eq. (14.126) is passed on to Eq. (15.105). This means that if we restrict the area of a single chemoreceptor to that obtained for a circular patch, the best chemoreceptor would be the one with the largest perimeter. Let us compare the number of chemoreceptors needed to equalize half the Smoluchowski rate constant when using circular patches,

i.e., $\mathtt{N}_* \approx 1,570$, to what we obtain when using elliptical absorbing sites, each with semi-major axis a_1, semi-minor axis a_2, and eccentricity ϵ. For this purpose, we substitute Eq. (14.114), i.e.,

$$\mathtt{k}_{ellipse} = \frac{2\pi D a_1}{k(\epsilon)} \tag{14.114}$$

where $k(\epsilon)$ is given by

$$k(\epsilon) = \int_0^{\pi/2} \frac{d\theta}{\sqrt{1-\epsilon^2 \sin^2\theta}}, \tag{14.115}$$

into Eq. (4.23), resulting in

$$\mathtt{k}_{BPE} = \frac{4\pi D R \,\mathtt{N}\, a_1 \sqrt{1-\epsilon^2}}{\mathtt{N} a_1 \sqrt{1-\epsilon^2} + 2R\, k(\epsilon)}. \tag{15.106}$$

Thus, in the process of making $\mathtt{k}_{BDE} = \mathtt{k}_S/2$ and solving for $\mathtt{N}$, the value of $\mathtt{N}$ satisfying the absorbing hemisphere, we find

$$\mathtt{N}_{\epsilon *} = \frac{2k(\epsilon) R}{a_1 \sqrt{1-\epsilon^2}}, \tag{15.107}$$

which reduces to Eq. (15.104) at the limit $\epsilon \to 0$, since the first term in the Taylor series of $(1-\epsilon^2 \sin^2\theta)^{-1/2}$ is 1. Now, by imposing the area of a single elliptical receptor, $A_{ellipsoid} = \pi a_1^2 \sqrt{1-\epsilon^2}$, to be equal to that of a circular patch, $A_{disk} = \pi a^2$, we are led to $a_1 = a(1-\epsilon^2)^{-1/4}$. Consequently, using the same values for R and a defined above, we obtain $\mathtt{N}_{\epsilon *} \approx 1,348$, denoting that the use of elliptical chemoreceptors reduces the area occupied by patches on the spherical cell membrane by approximately 15%. Moreover, regarding the ratio of $\mathtt{N}_*$ to $\mathtt{N}_{\epsilon *}$, we find

$$\frac{\mathtt{N}_*}{\mathtt{N}_{\epsilon *}} = \frac{2k(\epsilon)}{\pi (1-\epsilon^2)^{1/4}}, \tag{15.108}$$

a number that is always smaller than 1.

Overall, a circular chemoreceptor distribution is as good as a perfectly absorbent hemisphere, and it can be even better if elliptical receptors are considered instead. Furthermore, the most effective geometry will be the one with the largest perimeter once the area of a single binding site has been restricted. In the following section, study the effective rate coefficient and mean first-passage time of a sphere with an absorbing cap.

15.5 Reaction Between Charged Particles: Debye-Smoluchowski Formula

In Sects. 15.1.1 and 15.1.2, a theory on diffusion-limited chemical reactions has been described for two situations: (a) where the encounter pair reacts much more quickly than it forms and (b) where these rates are of equivalent magnitude. Moreover, the fact that one of the reacting particles was stationary was a crucial simplification. In this section, we will show that an interaction potential between the diffusing reactant particles has an important effect on the flux current and the rate constant. As an example, we will quantify this effect for a Coulomb-type interaction. Furthermore, we will now study the case in which the two particles, or molecules, are diffusing.

15.5.1 Debye-Smoluchowski Equation

To analyze the evolution of the propagator of a reacting pair of particles, we need information on its relative motion. Let $\mathbf{r}_i$ and $\mathbf{r}_j$ denote the position of particles i and j at time t, with $\mathcal{C} = \mathcal{C}(\mathbf{r}_i, \mathbf{r}_j, t|\mathbf{r}_i(0), \mathbf{r}_j(0))$ being the propagator. This propagator is the joint probability density for finding particle i at $\mathbf{r}_i$ and particle j at $\mathbf{r}_j$ at time t. We will show that it is possible to decompose this concentration into two parts, only one of which describes the relative motion of the reactants. The evolution of $\mathcal{C}$ is governed by the Smoluchowski equation, Eq. (6.25), then

$$\frac{\partial \mathcal{C}}{\partial t} = \left[\mathcal{L}_i(\mathbf{r}_i|\mathbf{r}_j) + \mathcal{L}_j(\mathbf{r}_j|\mathbf{r}_i) \right] \mathcal{C}, \tag{15.109}$$

where

$$\mathcal{L}_i(\mathbf{r}_i|\mathbf{r}_j) \equiv D_i \nabla_{\mathbf{r}_i} \cdot \left[\mathrm{e}^{-\beta U(\mathbf{r}_j - \mathbf{r}_i)} \nabla_{\mathbf{r}_i} \mathrm{e}^{\beta U(\mathbf{r}_j - \mathbf{r}_i)} \right]. \tag{15.110}$$

$\beta = 1/k_\beta T$, where k_β is the Boltzmann's constant and T is the absolute temperature. The operator $\mathcal{L}_j$ is obtained interchanging i by j in this last definition, while D_i and D_j are the diffusivity of each reacting particle. Equation (15.109) is to be solved subject to

$$\mathcal{C}(\mathbf{r}_i, \mathbf{r}_j, t|\mathbf{r}_i(0), \mathbf{r}_j(0)) = \delta(\mathbf{r}_i - \mathbf{r}_i(0))\, \delta(\mathbf{r}_j - \mathbf{r}_j(0)). \tag{15.111}$$

To reduce the problem to one involving relative motion, the coordinate $(\mathbf{r}_i, \mathbf{r}_j)$ is replaced by $(\mathbf{r}, \mathbf{R})$ defined as follows:

$$\mathbf{r} \equiv \mathbf{r}_j - \mathbf{r}_i, \tag{15.112}$$

and

$$\mathbf{R} \equiv \frac{D_j \mathbf{r}_i + D_i \mathbf{r}_j}{D_i + D_j}, \tag{15.113}$$

respectively. The coordinate $\mathbf{R}$ is analogous to the center of mass but weighted by diffusion constants rather than by particles masses. Moreover, $\mathbf{r}$ is the coordinate that accounts for the relative motion of the two particles. In these variables, we observe that

$$\mathbf{r}_i - \mathbf{R} = -\frac{D_i}{D}\mathbf{r}, \tag{15.114}$$

and

$$\mathbf{r}_j - \mathbf{R} = \frac{D_j}{D}\mathbf{r}, \tag{15.115}$$

where $D = D_i + D_j$. By using the chain rule, the reader can verify the following relation between the corresponding operators:

$$\nabla_{\mathbf{r}_i} = \frac{D_j}{D}\nabla_{\mathbf{R}} - \nabla_{\mathbf{r}}, \tag{15.116}$$

and

$$\nabla_{\mathbf{r}_j} = \frac{D_i}{D}\nabla_{\mathbf{R}} + \nabla_{\mathbf{r}}. \tag{15.117}$$

By substituting Eqs. (15.116) and (15.117) into Eq. (15.109), after some manipulations, we obtain the Smoluchowski equation in terms of coordinates $(\mathbf{r}, \mathbf{R})$, which is given by

$$\frac{\partial \mathcal{C}}{\partial t} = \left[D_R \nabla^2_{\mathbf{R}} + \mathcal{L}(\mathbf{r}) \right] \mathcal{C}, \tag{15.118}$$

where

$$D_R = \frac{D_i D_j}{D_i + D_j}, \tag{15.119}$$

and $\mathcal{C} = \mathcal{C}(\mathbf{r}, \mathbf{R}, t|\mathbf{r}(0), \mathbf{R}(0))$. Since the first term on the right-hand side of this last equation stands for standard diffusion, the second operator describes the evolution of the relative motion in terms of the interactions of the two diffusing particles. The motion with respect to variables $\mathbf{r}$ and $\mathbf{R}$ is independent, and therefore, the propagator can be expressed by means of two functions, each depending on only one of these variables, namely,

$$\mathcal{C} = c(\mathbf{r}, t|\mathbf{r}_0)g(\mathbf{R}, t|\mathbf{R}_0). \tag{15.120}$$

Substituting this factorization into Eq. (15.118) leads to

$$\frac{\partial g(\mathbf{R}, t|\mathbf{R}_0)}{\partial t} - D_R \nabla^2_{\mathbf{R}} g(\mathbf{R}, t|\mathbf{R}_0) = \frac{\partial c(\mathbf{r}, t|\mathbf{r}_0)}{\partial t} - \mathcal{L}(\mathbf{r})c(\mathbf{r}, t|\mathbf{r}_0) = 0. \tag{15.121}$$

Now, we are interested in the evolution of the relative motion of the particles, given by the description of the propagator $c(\mathbf{r}, t|\mathbf{r}_0)$ and its differential equation,

$$\frac{\partial c(\mathbf{r}, t|\mathbf{r}_0)}{\partial t} = \mathcal{L}(\mathbf{r})c(\mathbf{r}, t|\mathbf{r}_0). \tag{15.122}$$

For the sake of simplicity, let us write the latter equation as Eq. (6.16), in terms of the normalized concentration, by means of Eq. (15.4), yielding

$$\frac{\partial \varrho(\boldsymbol{r}, t|\mathbf{r}_0)}{\partial t} = D\,\nabla \cdot [\nabla \varrho(\boldsymbol{r}, t|\mathbf{r}_0) + \varrho(\boldsymbol{r}, t|\mathbf{r}_0)\,\beta\,\nabla U(\boldsymbol{r})]\,, \tag{15.123}$$

the so-called Debye-Smoluchowski equation.

15.5.2 Steady-State Rate Constant

If we want to include the Coulomb interaction between the reactant particles, then the potential energy of particles placed at $\mathbf{r}_i$ and $\mathbf{r}_j$ having charges z_i and z_j, respectively, is given by

$$U(\mathbf{r}_i, \mathbf{r}_j) = \frac{z_i z_j e^2}{4\pi\epsilon_0\epsilon|\mathbf{r}_j - \mathbf{r}_i|} = \frac{\beta r_c}{4\pi\epsilon_0|\mathbf{r}|}, \tag{15.124}$$

where e is the absolute electron charge, ϵ_0 the permittivity of the free space, ϵ the relative permittivity of the solvent, and r_c the Onsager distance $z_i z_j e^2/\epsilon\beta$, i.e., the distance where the Coulomb energy is β. Over separations less than r_c, the Coulomb interactions dominate diffusion.

Substituting Eq. (15.124) into Eq. (15.123), assuming angular independence at steady stated, reads

$$\frac{1}{r^2}\frac{\partial}{\partial r} r^2 D \left[\frac{\mathrm{d}\varrho(r)}{\mathrm{d}r} - \varrho(r)\frac{r_c}{r^2}\right] = 0. \tag{15.125}$$

Integrating over r leads to

$$r^2 \left[\frac{\mathrm{d}\varrho(r)}{\mathrm{d}r} - \varrho(r)\frac{r_c}{r^2}\right] = \mathcal{A}. \tag{15.126}$$

To solve this canonical first-order linear differential equation, we will use the integrating factor method. To such end, let us write Eq. (15.126) as follows:

$$\frac{\mathrm{d}\varrho(r)}{\mathrm{d}r} + P(r)\varrho(r) = Q(r), \tag{15.127}$$

where

$$P(r) = -\frac{r_c}{r^2}, \tag{15.128}$$

and

$$Q(r) = \frac{\mathcal{A}}{r^2}. \tag{15.129}$$

By multiplying Eq. (15.127) by the integrating factor $e^{\int P(r)\mathrm{d}r}$, we find that its general solution is

$$\varrho(r) = e^{-\int P(r)\mathrm{d}r}\left(\int Q(r)e^{\int P(r)\mathrm{d}r}\,\mathrm{d}r\right) + \mathcal{B}\,e^{-\int P(r)\mathrm{d}r}. \tag{15.130}$$

By substituting Eqs. (15.128) and (15.129) in this last expression, performing the integrals over r, and after some manipulations, we find

$$\varrho(r) = \left[\mathcal{B} - \frac{\mathcal{A}}{r_c}\exp\left(\frac{r_c}{r}\right)\right]\exp\left(-\frac{r_c}{r}\right). \tag{15.131}$$

To set the boundary conditions, let us reduce our problem to one in which there is a reaction of a species i with a vast excess of j; then, it can be considered as one where the j species are statistically independent of each other. As the density $\varrho(r)$ at large distances of separation may be considered constant, then,

$$\varrho(r)\Big|_{r\to\infty} = 1. \tag{15.132}$$

When encounter particles i and j react much faster than they come together,

$$\varrho(R) = 0, \tag{15.133}$$

where R is the radius of particle i. Finally, when substituting Eqs. (15.132) and (15.133) into Eq. (15.131), this yields

$$\varrho(r) = \frac{1 - \exp\left(\frac{r_c}{R} - \frac{r_c}{r}\right)}{1 - \exp\left(\frac{r_c}{R}\right)}. \tag{15.134}$$

The flux can be calculated by means of Eq. (6.15), which in spherical coordinates reads

$$J = D\frac{\mathrm{d}\varrho(r)}{\mathrm{d}r} + \beta\,\varrho(r)\,\frac{\mathrm{d}U(r)}{\mathrm{d}r}. \tag{15.135}$$

From this last equation, we can obtain the current flux at R, which for the normalized concentration is the rate constant, namely,

$$\mathtt{k} = 4\pi R^2\,D\left[\frac{\mathrm{d}\varrho(r)}{\mathrm{d}r} + \beta\,\varrho(r)\,\frac{\mathrm{d}U(r)}{\mathrm{d}r}\right]_{r=R} = 4\pi r_c\,D\left[\exp\left(\frac{r_c}{R}\right) - 1\right]^{-1}. \tag{15.136}$$

It is worth noting that repulsive forces reduce the rate of reaction, while attractive forces conversely increase such rate of reaction above the Smoluchowski values. This theory is applicable to ionic reactions in solution.

15.6 Concluding Remarks

By means of boundary homogenization, one can replace non-uniform boundary conditions on a surface with an effective uniform partially absorbing boundary condition with the proper effective trapping rate. This approach reduces the initial two- or three-dimensional problem with non-uniform boundary conditions to an effective one-dimensional problem, significantly simplifying the study of the problem.

The replacement is based on the observation that at distances that are sufficiently far from the boundary, the fluxes are uniform and directed normal to it. The trapping rate entering the radiation boundary conditions on these surfaces should be chosen so that it correctly reproduces the steady-state fluxes far away from the surface. Numerical tests demonstrate good agreement between the rates predicted by the theory and obtained from Brownian dynamics simulations for different systems.

Further Reading and References

A.M. Berezhkovskii, M.I. Monine, C.B. Muratov, S.Y. Shvartsman, Homogenization of boundary conditions for surfaces with regular arrays of traps. J. Chem. Phys. **14**, 036103 (2006). 10.1063/1.2161196

H.C. Berg, E.M. Purcell, Physics of chemoreception. Biophys J. **20**, 193 (1977). 10.1016/S0006-3495(77)85544-6

H.S. Carslaw, J.C. Jaeger, *Conduction of Heat in Solids* (Oxford University, Oxford, 1959)

F.C. Collins, G. Kimball, Diffusion-controlled reaction rates. J. Colloid Sci. **4**, 425 (1949). 10.1016/0095-8522(49)90023-9

L. Dagdug, A.M. Berezhkovskii, S.M. Bezrukov, Particle lifetime in cylindrical cavity with absorbing spot on the wall: going beyond the narrow escape problem. J. Chem. Phys. **137**, 234108 (2012). 10.1063/1.4772183

L. Dagdug, A.M. Berezhkovskii, A.T. Skvortsov, Trapping of diffusing particles by striped cylindrical surfaces. Boundary homogenization approach. J. Chem. Phys. **142**, 234902 (2015). 10.1063/1.4922444

L. Dagdug, M.-V. Vázquez, A.M. Berezhkovskii, V.Y. Zitserman, Boundary homogenization for a sphere with an absorbing cap of arbitrary size. J. Chem. Phys. **145**, 214101 (2016). 10.1063/1.4968598

L. Dagdug, A.M. Berezhkovskii, V.Y. Zitserman, S.M. Bezrukov, Trapping of particles diffusing in two dimensions by a hidden binding site. Phys. Rev. E **103**, 012135 (2021). 10.1103/PhysRevE.103.012135

O.K. Dudko, A.M. Berezhkovskii, G.H. Weiss, Boundary homogenization for a circle with periodic absorbing arcs. Exact expression for the effective trapping rate. J. Chem. Phys. **121**(3), 1562 (2015). 10.1063/1.1763137

B.Y. Moizhes, Zh. Tech. Fiz. **25**, 167 (1955) (in Russian)

C.B. Muratov, S.Y. Shvartsman, Multiscale Model. Simul. **7**, 44 (2008). 10.1137/0706928

J. Peña, L. Dagdug, Elliptical chemoreceptors: the key to an effective absorption. AIP Conf. Proc. **2731**(1), 050008. 10.1063/5.0133058

D. Shoup, A. Szabo, Role of diffusion in ligand binding to macromolecules and cell-bound receptors. Biophys J. **40**, 33 (1982). 10.1016/S0006-3495(82)84455-X

A.T. Skvortsov, A.M. Berezhkovskii, L. Dagdug, Rate constant for diffusion-influenced ligand binding to receptors of arbitrary shape on a cell surface. J. Chem. Phys. **143**, 226101 (2015). 10.1063/1.4936866

M.V. Smoluchowski, Versuch Einer Mathematischen Theorie der Koagulationskinetik kolloider Losungen. Zeitschrift f. Physik. Chemie. XCII **92**, 129–168 (1917)

H.X. Zhou, R. Zwanzig, A rate process with an entropy barrier. J. Chem. Phys. **94**, 6147 (1991). 10.1063/1.460427

R. Zwanzig, A. Szabo, Time dependent rate of diffusion-influenced ligand binding to receptors on cell surfaces. Biophys. J. **60**, 671 (1991). 10.1016/S0006-3495(91)82096-3

R. Zwanzig, Diffusion-controlled ligand binding to spheres partially covered by receptors: an effective medium treatment. Proc. Natl. Acad. Sci. U S A. **87**, 5856 (1991). 10.1073/pnas.87.15.5856

Chapter 16
Boundary Homogenization

More examples of the boundary homogenization technique for two- and three-dimensional geometrical systems with complex heterogeneous boundaries and abrupt geometry changes will be provided in this chapter.

16.1 Sphere with an Absorbing Cap

Consider the trapping of diffusing particles by a sphere with an absorbing cap of arbitrary size on the otherwise reflecting surface, shown in Fig. 16.1. In this system, we will focus on describing the analysis to obtain the rate constant as a function of the ratio of the area occupied by the absorbing cap to the total spherical surface, i.e., σ, by means of the so-called computer-assisted boundary homogenization approach. This method consists of two primary steps: (a) First, express the trapping rate coefficient, κ, as the product of a dimensional factor, with units of length per unit time, and a dimensionless function of the surface ratio σ, $f(\sigma)$; (b) second, find a relatively simple expression for this function by approximating the numerically computed values of the trapping rate, $\kappa = \kappa(\sigma)$, for different values of σ. In this concluding step, it is desirable for the formula thus obtained to be capable of reproducing the behavior throughout the entire range of σ, namely, $0 \leq \sigma \leq 1$. Equation (15.70) is an example of such an expression for a sphere with N perfectly absorbing disks.

For a sphere with an absorbing cap, the theoretical formula is constructed starting from the asymptotic behavior for a small cap, for $\sigma \to 0$. At this limit, the cap can be approximated as a disk, and the theoretical expression should reduce to Eq. (15.69), namely,

$$\kappa(\sigma)_{BP} = \frac{2D}{\pi R}\sqrt{\sigma}. \tag{15.69}$$

L. Dagdug et al., *Diffusion Under Confinement*,
https://doi.org/10.1007/978-3-031-46475-1_16

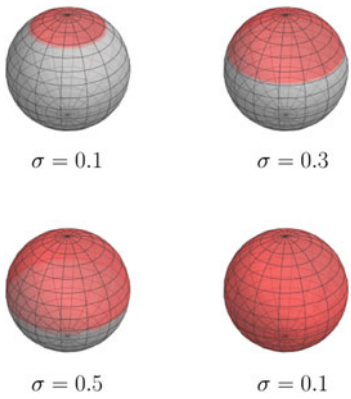

Fig. 16.1 Spheres with absorbing caps (red) with $\sigma = 0.1, 0.3, 0.5$, and 1. This last value represents a perfectly absorbing sphere. Conversely a perfectly reflecting sphere is obtained when $\sigma = 0$

As mentioned in Sect. 15.2, in order for $\kappa(\sigma)$ to be applicable over the entire range of σ, it need to be written as

$$\kappa(\sigma) = \frac{2D}{\pi R}\sqrt{\sigma}\, f(\sigma). \tag{15.70}$$

Now, on directing our attention at the limit when $\sigma \to 1$, we observe from simulations that $\kappa_{sim}(\sigma)\big|_{\sigma\to 1}$ diverges as $1/(1-\sigma)^{3/2}$. With these two asymptotic behaviors, we propose the following formula for the effective rate coefficient:

$$\kappa(\sigma) = \frac{2D}{\pi R}\sqrt{\sigma}\frac{1 + A\sqrt{\sigma} - B\sigma^2}{(1-\sigma)^{3/2}}, \tag{16.1}$$

where A and B are constants.

To find the mathematical expression for $\kappa(\sigma)$ using the computer-assisted boundary homogenization approach, we compute the mean first-passage time (MFPT) of a particle diffusing in a spherical layer between two concentric spheres by running Brownian dynamics simulations. The system is set as follows: Consider an outer perfectly reflecting sphere of radius R_{out} and an inner sphere of radius R_{in} ($R_{in} < R_{out}$) with an absorbing cap that occupies a fraction σ of the total spherical surface, which is otherwise perfectly reflecting. This configuration is shown in Fig. 16.2.

From Brownian dynamics simulations, the MFPT, $\langle t_{sim}(\sigma)\rangle$, was obtained by averaging the first-passage time over 1×10^6 particle trajectory realizations, where the initial position of the particle was uniformly distributed over the surface of the inner sphere. This MFPT from simulations is compared with its counterpart predicted by the theory obtained in Sect. 14.3.5 and given by Eq. (14.82), namely,

$$\langle t_{theory}(R_{in})\rangle = \frac{R_{out}^3 - R_{in}^3}{3\kappa R_{in}^2}. \tag{14.82}$$

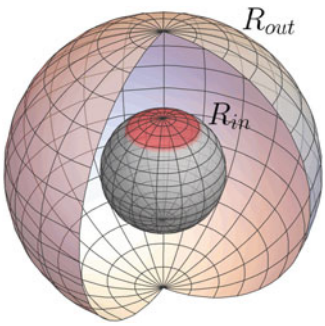

Fig. 16.2 Schematic representation of two concentric spheres with radii R_{in} and R_{out} ($R_{in} > R_{out}$). The inner reflecting sphere has a perfectly absorbing cap shown in red, while the outer sphere is perfectly reflecting

Table 16.1 Values of the MFPT $\langle t_{sim} \rangle$, obtained from Brownian dynamics simulations and the corresponding effective trapping rate κ_{sim}. All values of κ_{sim} are calculated by substituting $\langle t_{sim} \rangle$ into Eq. (16.2). The results are shown for three different values of σ, $\sigma = 0.25$, 0.5, and 0.75, as a function of R_{out}

	$\sigma = 0.25$		$\sigma = 0.50$		$\sigma = 0.75$	
R_{out}	$\langle t_{sim} \rangle$	κ_{sim}	$\langle t_{sim} \rangle$	κ_{sim}	$\langle t_{sim} \rangle$	κ_{sim}
0.5	1.5251679	0.519069	1.1968618	1.94954	0.18859636	4.19768
1.0	3.0101097	0.775166	1.1968618	1.94954	0.42745918	5.45861
2.0	9.1517757	0.946993	3.7009341	2.34175	1.4142088	6.12828
3.0	20.977742	1.00106	8.6014151	2.44146	3.3088036	6.3467
4.0	40.234302	1.02732	16.521454	2.5018	6.4869618	6.37176
5.0	70.223754	1.02055	28.247285	2.53712	11.194770	6.4018
6.0	110.16816	1.03478	44.893695	2.53933	17.696684	6.44188
7.0	165.39188	1.02988	66.699141	2.55376	26.580346	6.40824
8.0	233.68433	1.03844	94.623539	2.56455	37.505649	6.47014

Assuming that $\langle t_{sim}(\sigma) \rangle = \langle t_{theory}(r_0) \rangle$, and solving this last equation with respect to κ, yields

$$\kappa_{sim}(\sigma) = \frac{R_{out}^3 - R_0^3}{3\langle t_{sim}(\sigma) \rangle R_{in}^2}. \tag{16.2}$$

For values of R_{out} that are not too large, $\kappa(\sigma)$ is a function of R_{out} as stated in Eq. (16.2). Nevertheless, as R_{out} increases, $\kappa(\sigma)$ becomes independent of R_{out} approaching its plateau value, which gives us the effective trapping rate we are looking for. Table 16.1 displays the R_{out}-dependence of $\kappa(\sigma)$ for σ =0.25, 0.5, and 0.75. The values of $\kappa(\sigma)$ were calculated from Eq. (16.2). $\langle t_{sim}(\sigma) \rangle$ is obtained from Brownian dynamics simulations where diffusivity D and radius R_{in} are set equal to 1, and the time step is set to $\Delta t = 10^{-7}$.

Finally, using the plateau value from $\kappa_{sim}(\sigma)$, the best fit to Eq. (16.1), shown in Fig. 16.3, gives us that $A = 2.61$ and $B = 3.22$. Consequently,

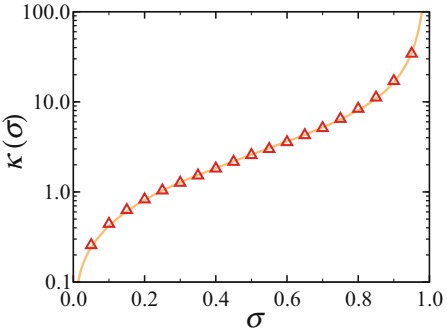

Fig. 16.3 Plot of trapping rate σ-dependencies when the starting positions of Brownian particles are uniformly distributed over the shell of the inner sphere. Up triangles in red are obtained by Brownian simulations. The best-fit formula was determined by fitting these simulation data to Eq. (16.3), with $A = 2.61$ and $B = 3.22$, which accurately described the observed behavior (solid line)

$$\kappa(\sigma)_{cap} = \frac{2D}{\pi R}\sqrt{\sigma}\frac{1 + 2.61\sqrt{\sigma} - 3.22\sigma^2}{(1-\sigma)^{3/2}}. \tag{16.3}$$

With exception of $\sigma < 0.05$, where the relative error is approximately 6%, this formula is accurate within 5% for all values of σ.

The effective trapping rate given by Eq. (16.3) can be used to determine the rate constant that characterizes the trapping of diffusing particles by a sphere with an absorbing cap of any size. Substituting Eq. (16.3) into the Collins-Kimball formula, Eq. (15.65), leads to

$$\mathrm{k}_{cap}(\sigma) = \frac{8\pi DR\sqrt{\sigma}(1 + 2.61\sqrt{\sigma} - 3.22\sigma^2)}{\pi\,(1-\sigma)^{3/2} + 2\sqrt{\sigma}(1 + 2.61\sqrt{\sigma} - 3.22\sigma^2)}. \tag{16.4}$$

When $\sigma = 1$, this rate constant reduces to the Smoluchowski rate constant, Eq. (15.34). Conversely, when $\sigma \to 0$, for a small disk of radius $a = 2R\sqrt{\sigma}$, it reduces to Eq. 15.69.

It is worth remarking that the computer-assisted boundary homogenization approach is a very powerful method for simplifying complicated problems, as we will see in the remaining sections of the chapter.

16.2 Absorbing Circular Spot at a Cylinder End Wall

Modern crystallography and electron microscopy studies have shown that ion and metabolite channels of cell and organelle membranes are not perfect cylinders or even cylinders with smoothly varying radii. Instead, they are characterized by abrupt

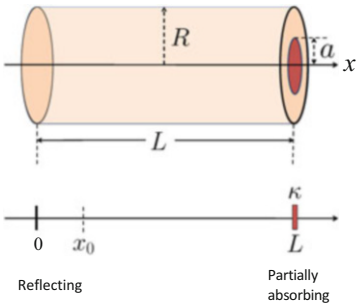

Fig. 16.4 Top panel: Schematic representation of a 3D cylindrical tube with radius R and length L, with a perfectly absorbing circular disk of radius a placed on the right circular wall. Bottom panel: A simplified boundary homogenization one-dimensional model is used to describe the particle dynamics in the system with a proper trapping rate coefficient κ

changes in the water-filled pore radii measured along their central axis. Diffusion in these systems can be studied using boundary homogenization. We will show how to solve some of these systems in the subsequent sections.

Consider a point particle diffusing in a cylindrical cavity of radius R and length L with a perfectly absorbing circular spot of radius a located in the center of the cavity end wall as shown in Fig. 16.4, where $0 < a \leq R$. Initially, at $t = 0$, particles are uniformly distributed over the cavity cross section at $x = x_0$, where the x-coordinate measures the particle position along the cavity axis and $0 \leq x_0 \leq L$. To study the MFPT of the diffusing particles, we apply the boundary homogenization approach to replace the non-uniform BCs on the cylinder end wall with an effective partially absorbing BC, by properly choosing an effective trapping rate (see bottom panel of Fig. 16.4).

Now, let's reduce the original problem to a one-dimensional system. The concentration of particles satisfies the diffusion equation, more specifically

$$\frac{\partial c(x,t)}{\partial t} = D\frac{\partial^2 c(x,t)}{\partial x^2}, \qquad 0 \leq x \leq L, \tag{2.16}$$

subject to the initial condition $c(x, t = 0|x_0) = \delta(x - x_0)$, as well as reflecting or partially absorbing BCs at $x = 0$ and $x = L$,

$$\left.\frac{\partial c(x,t)}{\partial x}\right|_{x=0} = 0, \tag{4.9}$$

and

$$D\left.\frac{\partial c(x,t)}{\partial x}\right|_{x=L} = \kappa\, c(L,t), \tag{4.11}$$

respectively. Now, we need to find a proper value of κ such that it replaces the non-uniform BCs on the surface for a uniform radiation-type boundary condition, Eq. (4.11) (see Fig. 16.4, bottom panel). We know that the leading terms of an expansion of κ are given by Eq. (15.64), namely,

$$\mathtt{k} = A\,\kappa. \tag{15.64}$$

For this system, $\mathtt{k}$ is the rate constant of a disk, $\mathtt{k}_{HBP} = 4Da$, and A is the area of the cylinder wall, πR^2, consequently, $\kappa = 4Da/\pi R^2$.

As we know, this formula can be written in a more general form as follows:

$$\kappa(\nu) = \frac{4D}{\pi a}\sigma f(\sigma) = \frac{4Da}{\pi R^2} f(\nu), \tag{16.5}$$

where $\sigma = \pi a^2/\pi R^2$, and the normalized variable $\ni$ is given by $\nu = a/R = \sqrt{\sigma}$, $0 < \nu \leqslant 1$. Berezhkovskii et al., by fitting the dependencies obtained numerically for κ, determined an approximate formula for the trapping rate coefficient by means of Eq. (16.5), namely,

$$\kappa_{BMMS}(\nu) = \frac{4Da}{\pi R^2}\left[\frac{1 + 1.37\nu - 0.37\nu^2}{(1-\nu^2)^4}\right], \tag{16.6}$$

meaning that

$$f(\nu) = \frac{1 + 1.37\nu - 0.37\nu^2}{(1-\nu^2)^4}. \tag{16.7}$$

The relative error of Eq. (16.6) is less than 1% over the range of $\nu < 0.9$. This formula monotonically increases from 1 at $\nu = 0$ to infinity as $\nu \to 1$. Consequently, κ_{BMMS} monotonically increases from $4Da/\pi R^2$ for small a to infinity as a approaches R.

As previously shown, the solution of our boundary value problem, posted by Eqs. (4.9) and (4.11), is given in Sect. 5.7. In particular, the MFPT is given by (see Eq. (5.156))[1]

$$\langle t(x_0)\rangle = \frac{L^2 - x_0^2}{2D} + \frac{L}{\kappa}. \tag{16.8}$$

Substituting $\kappa_{BMMS}(\nu)$, Eq. (16.6), into the latter equation, we arrive at

[1] It is worth noting that in Sect. 5.7, we solved the boundary value problem placing the partially absorbing boundary at the origin $x = 0$ and the reflecting boundary at $x = L$. In the present case, such boundaries are placed in the opposite way. Then, to express the correct solution, we apply the transformation $x_0 \to L - x_0$. Consequently, $x_0(2L - x_0)$ is mapped to $L^2 - x_0^2$.

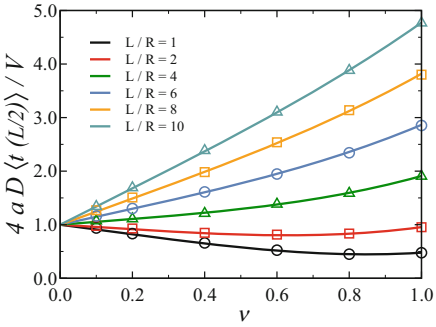

Fig. 16.5 The σ-dependencies of the mean particle lifetime given by Eq. (16.9) with $x_0 = L/2$ and $L/R = 1, 2, 4, 6, 8$, and 10 (solid curves) and obtained from Brownian dynamics simulations (symbols). The simulations were averaged over 50,000 trajectories setting the time step at $10^{-6}R^2/D$. The starting positions of the trajectories were evenly distributed over the cavity cross section at $x_0 = L/2$. D was set equal to 1

$$\langle t(x_0)\rangle = \frac{L^2 - x_0^2}{2D} + \frac{V}{4Daf(\nu)}, \tag{16.9}$$

where V is the volume of the cylinder.

To obtain the MFPT when particles are uniformly distributed over the cylinder, we have to average over the uniform distribution of the particles' starting point by means of

$$\langle t(x_u)\rangle = \frac{\displaystyle\int_0^L \langle t(x_0)\rangle \mathrm{d}x_0}{\displaystyle\int_0^L \mathrm{d}x_0}. \tag{16.10}$$

Then, substituting Eq. (16.9) into this last equation leads to

$$\langle t(x_u)\rangle = \frac{V}{4Da}\left[\frac{4\nu L}{3\pi R} + \frac{(1-\nu^2)^2}{1 + 1.37\nu - 0.37\nu^4}\right]. \tag{16.11}$$

The ν-dependence predicted by Eq. (16.9) is compared with the values of the ratio $4Da\langle t(x_0)\rangle/V$, which is obtained by from Brownian dynamics simulations at $x_0 = L/2$. In Fig. 16.5, we present a comparison between the theoretical and numerical results for different values of ratio L/R, specifically, 1, 2, 4, 8. As the reader can see, the numerical results are in excellent agreement with the theoretical predictions.

Finally, ν-dependency predicted by Eq. (16.11) is compared with the values $4Da\langle t(x_u)\rangle/V$ obtained from Brownian dynamics simulations for $L/R = 10$ in

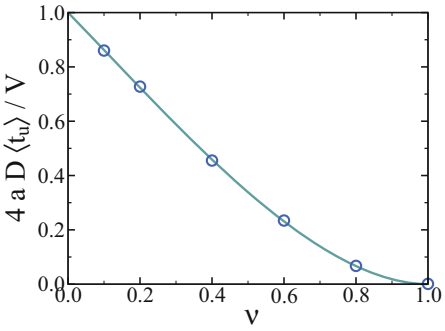

Fig. 16.6 The σ-dependencies of the mean particle lifetime given by Eq. (16.11) with $x_0 = L$ and $L/R = 10$ (solid curve) and obtained from Brownian dynamics simulations (symbols). The simulations were averaged over 50,000 trajectories, and a time step of $10^{-6}R^2/D$ was used. The starting positions of the trajectories were evenly distributed over the entire cylinder. D was set equal to 1

Fig. 16.6. Once again, we emphasize that the theoretical predictions are in perfect agreement with the numerical results.

16.3 Cylinder with Absorbing Stripes

In this section, we will study the trapping of diffusing particles by a cylindrical surface containing alternating absorbing and reflecting stripes. Figure 16.7 shows the unfolded surface area of the cylindrical wall. We use the boundary homogenization approach to replace the non-uniform boundary conditions on the tube wall with an effective partially absorbing boundary condition. Additionally, we noticed that the exact solution for the effective trapping rate, known for a flat striped surface, is still an excellent approximation when this surface is rolled into a cylindrical tube. This approximation is very accurate for both internal and external problems, where the particles diffuse inside and outside the striped tube.

There is a simple analytical expression for the effective trapping rate for such a system, which is valid for all values of the stripe surface ratio. If L and l are the period and the width of individual absorbing stripes, respectively, the stripe surface fraction, σ, is given by

$$\sigma = \frac{l}{L}, \tag{16.12}$$

and the effective trapping rate, as a function of σ and L, by

$$\mathrm{k}_{MMS}(\sigma) = \frac{\pi D}{L \ln\left[1/\sin\left(\frac{\pi\sigma}{2}\right)\right]}, \tag{16.13}$$

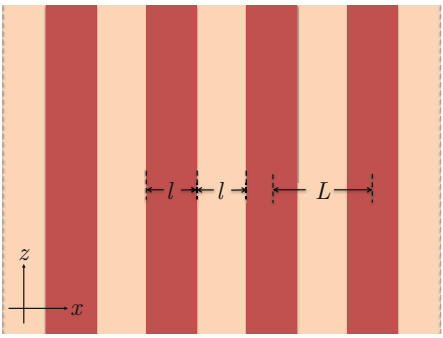

Fig. 16.7 Schematic representation of an infinite plane surface formed by equally spaced absorbing stripes of length l (red stripes), on an otherwise reflecting surface (orange stripes), with period L

which is the so-called Moizhes-Muratov-Shvartsman formula.

Once we know the effective trapping rate, we proceed as in the previous section. In fact, we will solve two different configurations: when the stripes are oriented (a) perpendicular and (b) parallel to the z-axis, as shown on the top panels of Figs. 16.8 and 16.12, respectively. For each orientation, we study the internal and external problems, schematically represented on the top panels of Figs. 16.10 and 16.15, respectively. For every configuration, we will calculate theoretical expressions for the MFPT using the homogenized boundary approach, and then, we will compare these times with the times obtained by Brownian dynamics simulations.

In our theoretical approach for calculating the MFPT, we make use of the fact that the trapping problem in a striped cylindrical tube becomes effectively a one-dimensional problem after boundary homogenization. Consequently, the internal problem is defined as follows: Consider a diffusing point particle in a circular disk of radius R bounded by a partially absorbing boundary characterized by a trapping rate κ at R, given by $\mathtt{k}_{MMS}(\sigma)$. The external problem is defined as follows: Consider a diffusing point particle in the annulus bounded by two concentric circles of radii R and R_{out}, $R_{out} > R$. The outer circle of radius R_{out} is a reflecting one, whereas the inner circle of radius R is a partially absorbing one, characterized by a trapping rate κ, given by $\mathtt{k}_{MMS}(\sigma)$. This last assertion states that once we roll on the striped plane surface to create the cylinder, the same rate constant is applicable. This is the main idea behind the application of boundary homogenization to these types of systems.

As we already proved in Sects. 12.1 and 12.4.2, the MFPTs for such systems are given by Eqs. (12.70) and (12.108), namely,

$$\langle t_{in}(r_0)\rangle = \frac{1}{4D}\left(R^2 - r_0^2\right) + \frac{R}{2\kappa}, \tag{12.70}$$

and

$$\langle t_{out}(r_0)\rangle = \frac{1}{4D}\left[2R_{out}^2 \ln\left(\frac{r_0}{R}\right) - r_0^2 + R^2\right] + \frac{R_{out}^2 - R^2}{2\kappa R}, \tag{12.108}$$

respectively, where r_0 is the initial position and D the diffusivity. In these formulas, we have to replace κ for $\mathtt{k}_{MMS}(\sigma)$. Explicitly, by substituting Eq. (16.13) into the preceding equations, we arrive at

$$\langle t_{in}(r_0)\rangle = \frac{1}{4D}\left(R^2 - r_0^2\right) + \frac{R\,L}{2\pi\,D}\,\ln\left[\frac{1}{\sin\left(\pi\sigma/2\right)}\right], \tag{16.14}$$

and

$$\langle t_{out}(r_0)\rangle = \frac{1}{4D}\left[2R_{out}^2\,\ln\left(\frac{r_0}{R}\right) - r_0^2 + R^2\right] + \frac{\left(R_{out}^2 - R^2\right)L}{2\pi\,D}\,\ln\left[\frac{1}{\sin\left(\pi\sigma/2\right)}\right]. \tag{16.15}$$

Moreover, assuming an initially uniform distribution of particles over the entire system, and averaging Eq. (16.14) over r_0, we find that

$$\langle t_{inu}\rangle = \frac{R^2}{8D} + \frac{R\,L}{2\pi\,D}\,\ln\left[\frac{1}{\sin\left(\pi\sigma/2\right)}\right]. \tag{16.16}$$

Finally, we have obtained all the information needed to determine the range of applicability of our hypothesis through the MFPT for both cases, i.e., when the stripes are oriented perpendicular and parallel to the z-axis, either for the internal or external problem.

16.3.1 Stripes Perpendicular to the Tube Axis

A tube with absorbing stripes perpendicular to the tube axis is obtained when the flat striped surface is rolled around the x-axis, as in Fig. 16.7. In this case, the system is defined by two dimensionless parameters (refer to Fig. 16.8): (a) the stripe surface

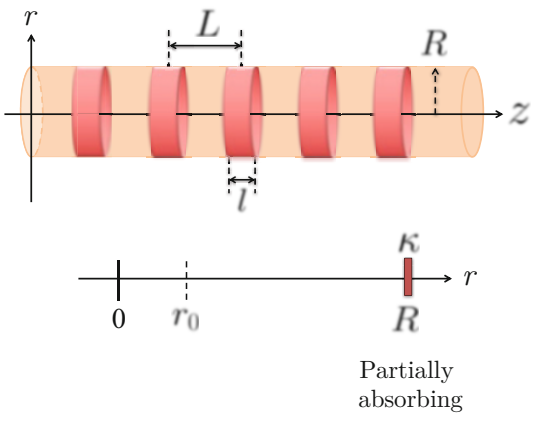

Fig. 16.8 Top panel: Schematic representation of a 3D cylindrical tube with radius R and length L, with absorbing stripes perpendicular to the tube axis. Bottom panel: A simplified boundary homogenization one-dimensional model is used to describe the particle dynamics in a system with $\kappa = \mathtt{k}_{MMS}(\sigma)$

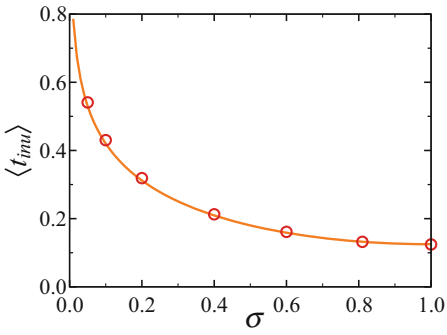

Fig. 16.9 The σ-dependencies of the mean particle lifetime given by Eq. (16.16) with r_0 uniformly distributed and $L = R = D = 1$ (solid curve) and the time obtained from Brownian dynamics simulations (symbols). The simulations were based on 50,000 trajectories and used a time step of 10^{-6}

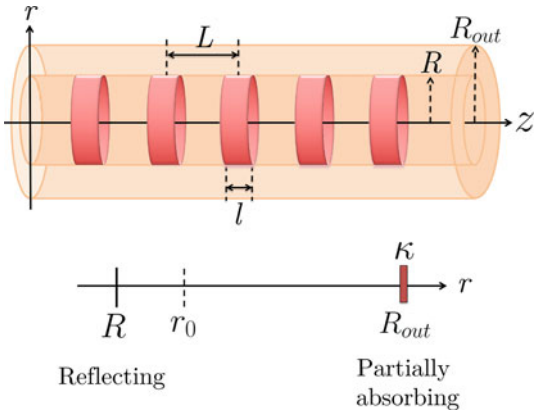

Fig. 16.10 Top panel: Schematic representation of a 3D cylindrical tube with radius R and length L, with absorbing stripes perpendicular to the tube axis. Bottom panel: A simplified boundary homogenization one-dimensional model is used to describe the particle dynamics in a system with $\kappa = \mathrm{k}_{MMS}(\sigma)$

fraction, $\sigma = l/L$, and (b) the ratio of the stripe period to the tube radius, namely, L/R.

Figure 16.9 shows a comparison between the Brownian dynamics simulations, when particles are uniformly distributed inside the cylinder, and Eq. (16.16). The relative error of the theoretical predictions compared with the result of the simulations does not exceed 3%.

To assess the accuracy for the external problem, we set $L = R = D = 1$ and $\sigma = 0.6$. The R_{out}-dependencies of the MFPT when $r_0 = 0$, uniformly distributed over L, are shown in Fig. 16.10. The error of the theoretical predictions given by Eq. (16.15) (setting $r_0 = 0$) depends on the difference between R and R_{out}. The error does not exceed 3% for $R_{out} \geq 1.4R$, as shown in Fig. 16.11. It is important to keep in mind that boundary homogenization is applicable when the distances between the boundaries are sufficiently large.

16.3.2 Stripes Parallel to the Tube Axis

A tube with absorbing stripes parallel to the tube axis is obtained when the flat striped surface is rolled around in the z direction, as in Fig. 16.7. The final

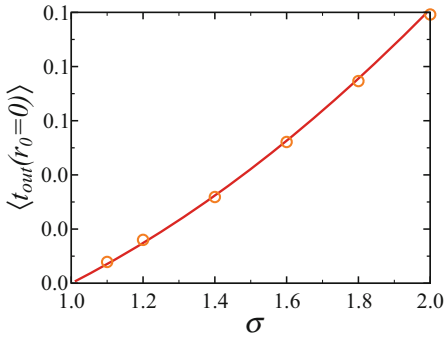

Fig. 16.11 Mean first-passage time against σ. Comparison of theoretical prediction, Eq. (16.15) (solid curve) with the values obtained from Brownian dynamics simulations (symbols). The simulations were averaged over 50,000 trajectories using a time step of 10^{-6}. The initial position was set at $r_0 = R$ and uniformly distributed along the z direction over L, when $L = R = D = 1$

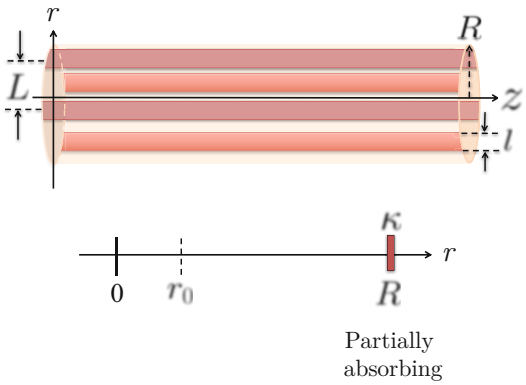

Fig. 16.12 Top panel: Schematic representation of a 3D cylindrical tube with radius R and length L, with stripes parallel to the tube axis. Bottom panel: A simplified boundary homogenization one-dimensional model is used to describe the particle dynamics in a system with a proper $\kappa_{MMS}(\sigma)$

configuration is shown on Fig. 16.12. In this case, the tube radius R cannot be arbitrary. The periodicity of a tube created from a periodically striped flat surface with a period L is only retained when the tube's radius R satisfies

$$R = \frac{nL}{2\pi}, \tag{16.17}$$

where n is the number of absorbing stripes, $n \geq 1$.

When the stripes are parallel to the tube axis, i.e., z-axis, the problem exhibits translational invariance in this direction. Consequently, the system is simplified to the plane orthogonal to the tube axis, as shown on the left panel of Fig. 16.13. Then, to assert the accuracy of the theory, simulations can be performed in two-dimensional disks. For the internal problem, the simulations were performed within a circular disk of radius R, with the inclusion of 1, 2, 3, and 4 identical and equally spaced absorbing arcs of length l. The line fraction occupied by the arcs, σ, is equivalent to the stripe surface fraction and can be expressed as

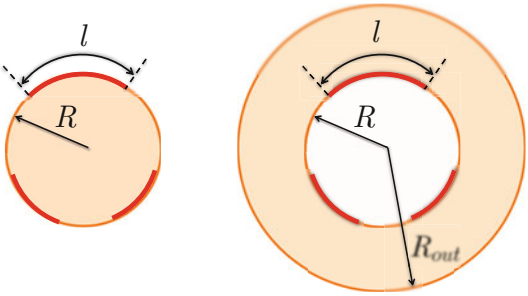

Fig. 16.13 The left panel depicts a schematic representation of a disk with radius R, while right panel illustrates an annulus enclosed by the inner and outer circles with radii of R and R_{out} (where $R_{out} > R$), respectively, and $n = 3$. In the left panel, the line ratio $\sigma = nl/L = 3l/(2\pi R)$ of the boundary of the disk is occupied by three identical and evenly spaced absorbing arcs of length l, while on the right panel, the same line ratio σ is occupied by these arcs in the inner circle

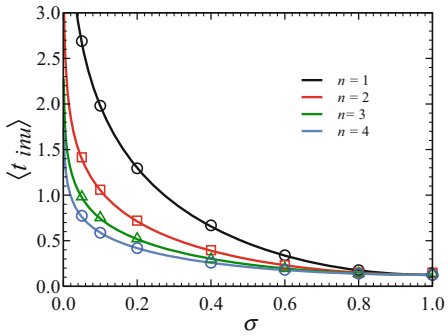

Fig. 16.14 The σ-dependencies of the mean particle lifetime given by Eq. (16.16) (solid lines) and Brownian dynamics simulations (symbols) for four values of n (1, 2, 3, and 4). The initial values of the Brownian dynamics particles were uniformly distributed over the entire disk. The simulations were based on 50,000 trajectories and used a time step of 10^{-6}. The radius and the diffusivity were set $R = D = 1$

$$\sigma = \frac{l}{L} = \frac{nl}{2\pi R}. \tag{16.18}$$

The values of the MFPT obtained for different n and σ are shown in Fig. 16.14, where the theoretical predictions (solid lines) are calculated from Eq. (16.16). The error of the theoretical predictions does not exceed 3% the value obtained by simulations (symbols). Finally, it is worth mentioning that in the case of only one absorbing stripe, Eq. (16.16) provides an exact solution. Even though the analysis within the boundary homogenization approach is advantageous in terms of its simplicity, it is limited by the requirement that the outer circle must be distant enough from the inner circle.

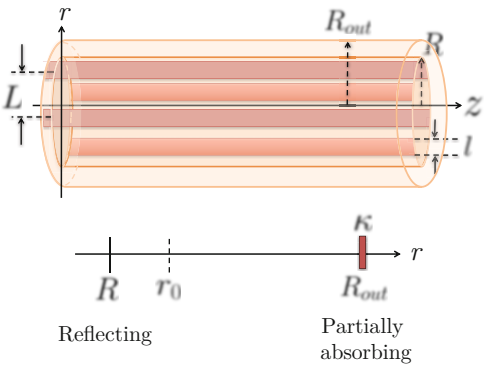

Fig. 16.15 Top panel: Schematic representation of a 3D cylindrical tube with radius R and length L, with parallel stripes to the tube axis. Bottom panel: A simplified boundary homogenization one-dimensional model is used to describe the particle dynamics in the system with a proper $\mathtt{k}_{MMS}$

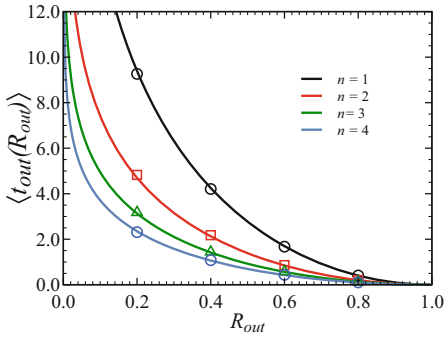

Fig. 16.16 The σ-dependencies of the first-passage times given by Eq. (16.15) for $R_{out} = 3$ (solid lines) and Brownian simulations (symbols) for $n = 1, 2, 3$, and 4. The initial values of the Brownian particles were uniformly distributed over the outside boundary, at R_{out}. The simulations were based on 50,000 trajectories and used a time step of 10^{-6}. The radius and the diffusivity were set at $R = D = 1$

The external problem of a concentric cylinder with an external perfectly reflecting boundary and a striped internal cylinder, as shown in Fig. 16.15, can be reduced to a two-dimensional annuli (see right panel of Fig. 16.13). In such a case, the external boundary is a perfectly reflecting circle, while the internal boundary is a circle having identical and evenly distributed absorbing arcs along its perimeter. To assess the accuracy of the theoretical predictions of the external problem, given by Eq. (16.15), we perform Brownian dynamics simulations in annuli that are enclosed by the inner circle with a radius R and outer circles of radii R_{out}.

In Fig. 16.16, we show some values for the σ-dependence of the MFPT by setting $R_{out} = 3$. The theoretical prediction given by Eq. (16.15) (solid lines) is compared to the results obtained by Brownian dynamics simulations (symbols). The theoretical predictions have a relative error of no more than 3% for values of R_{out} greater than or equal to three times the radius R, i.e., $R_{out} \geq 3R$. This inequality sets the criterion for when the boundary homogenization approach is valid for the

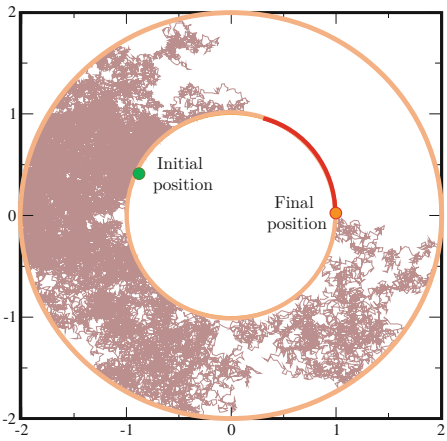

Fig. 16.17 Typical trajectory obtained by Brownian dynamics simulation. Particle starts from the inner circle and leaves the systems as soon as it touches the perfectly absorbing arc for the very first time. The absorbing arc is $0.2R$, which has been placed from 0 to 72 degrees, $R_{out} = 2$, $D = 1$, and the time step $\Delta t = 10^{-6}$, in such a way that $\sqrt{2D_0\Delta t} \ll 1$

external problem in the two-dimensional geometry depicted in Fig. 16.12. When the outer circle radius decreases and falls below $3R$, the relative error increases rapidly.

Finally, to gain further insight into the diffusion of a Brownian particle in the system, we show a typical realization in Fig. 16.17. When running simulations, we take diffusivity $D = 1$ and the time step $\Delta t = 10^{-6}$, so that $\sqrt{2D_0\Delta t} \ll 1$. The actual particle position $\mathbf{r}_n$ is given by $\mathbf{r}_n = \mathbf{r}_0 + \mathbf{r}_{ran}$, where $\mathbf{r}_0$ is the former position and $\mathbf{r}_{ran}$ is a vector of *pseudorandom numbers* generated with Gaussian distribution ($\mu = 0, \sigma = \sqrt{2D_0\Delta t}$). For more details related with Brownian dynamics simulations, see Chap. 10.

Boundary homogenization can be successfully used to find higher moments of the MFPT, as well as the particle survival probability, $S(t)$, and the lifetime probability density, $\varphi(t)$. In Sect. 12.1, we find the formulas for these last two values for a particle diffusing in a circular disk with a partially absorbing boundary. When the particle's starting point is uniformly distributed over the disk area, the lifetime probability density, in the Laplace space, is given by Eq. (12.60), namely,

$$\varphi(s) = \frac{2\kappa\sqrt{D}\, I_1\left(\sqrt{\frac{s}{D}}R\right)}{R\sqrt{s}\left[\kappa\, I_0\left(\sqrt{\frac{s}{D}}R\right) + \sqrt{sD}\, I_1\left(\sqrt{\frac{s}{D}}R\right)\right]}, \tag{12.60}$$

where $I_0(z)$ and $I_1(z)$ are the modified Bessel functions. Furthermore, the relation between the survival probability and the density of first-passage time, or lifetime probability density, is given by Eq. (12.64).

The survival probability and the density of first-passage time, obtained from the simulations of the internal problem in the cylindrical tube of radius $R = L/\pi$ with stripe line fraction $\sigma = l/L = 0.2$ (n = 2) and two different stripe orientations, perpendicular and parallel to the tube axis, are presented in Fig. 16.18. The particle's initial position inside the tube was uniformly distributed in all simulations. The

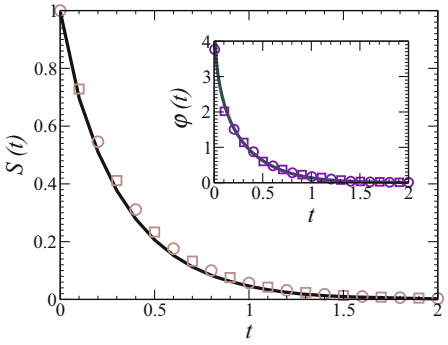

Fig. 16.18 Theoretical predictions using the boundary homogenization approach are compared with the survival probability $S(t)$ and its lifetime probability density $\varphi(t)$ (inset) obtained from simulations for the internal problem. The strip surface fraction, in both orientations, were set to $\sigma = l/L = 0.2$ ($n = 2$). The tube radius is given by $R = L/\pi$. The simulation results for perpendicular and parallel strip orientations with respect to the tube axis are represented by circles and squares, respectively, while the theoretical curves are given by numerically inverting the Laplace transforms of $S(t)$ and $\varphi(t)$ as given by Eqs. (12.64) and (12.60), shown as solid lines

solid curves in this figure represent the Laplace transforms of $S(t)$ and $\varphi(t)$, which were numerically inverted (the numerical method and the code used is described in Appendix 5.A). Again, we found an excellent agreement between theory and simulations independent of the stripe orientation.

Finally, it is worth noting that the boundary homogenization approach, used to describe trapping of diffusing particles in a striped cylinder, is not limited to the two specific stripe orientations discussed above; it can also be applied to cylinders with stripes oriented in an arbitrary direction.

16.4 Trapping of Particles Diffusing in a Two-Dimensional Rectangular Chamber by an Absorbing Strip

Consider diffusing particles within a two-dimensional rectangular chamber in the presence of an absorbing trap, as illustrated in Fig. 16.19. By using boundary homogenization, we can reduce the original problem to a one-dimensional system, as done in the previous section. Then, we have to solve the diffusion equation in one dimension, Eq. (2.16), subject to the BCs of one reflecting and one partially absorbing boundary, given by Eqs. (4.9) and (4.11), respectively. The problem reduces to finding κ, such that it replaces the non-uniform boundary conditions (see the bottom panel of Fig. 16.19). For our present problem, κ is known and given by the Moizhes-Muratov-Shvartsman formula, Eq. (16.13), where now $\sigma = w/W$ and $L = W$, namely,

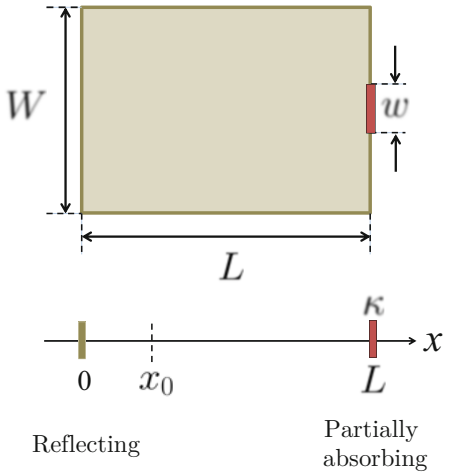

Fig. 16.19 Top panel: Schematic representation of a rectangular chamber characterized by length L and width W, which contains an absorbing strip of width $w \leq W$ positioned at the center of its right wall. Bottom panel: A simplified boundary homogenization one-dimensional model is used to describe the particle dynamics in the system with the use of a proper κ

$$\kappa_{MMS} = \frac{\pi D}{W \ln\left[1/\sin\left(\frac{\pi w}{2W}\right)\right]}. \tag{16.19}$$

As we know, the mean first-passage time of the simplified one-dimensional model is given by Eq. (5.156). By substituting Eq. (16.19) into (5.156), we have[2]

$$\langle t(x_0)\rangle = \frac{L^2 - x_0^2}{2D} + \frac{LW}{\pi D} \ln\left[1/\sin\left(\frac{\pi w}{2W}\right)\right]. \tag{16.20}$$

If we average $\langle t(x_0)\rangle$ across x_0, using Eq. (16.10), assuming that all initial particle positions within the chamber are equally likely, we arrive at

$$\langle t_u\rangle = \frac{L^2}{3D} + \frac{LW}{\pi D} \ln\left[1/\sin\left(\frac{\pi w}{2W}\right)\right]. \tag{16.21}$$

In order to verify the precision of these two equations and determine the applicable range of the boundary homogenization approach, we compare the value of $\langle t(L)\rangle$ predicted by the theory, given by Eq. (16.20), to that obtained through Brownian dynamics simulations. Table 16.2 displays the relative error associated with our theoretical predictions, which are evaluated for six different values of the chamber length, $L/W = 0.25$, 0.5, 0.75, 1.0, 2.0, and 3.0, and three values of the sleeve entrance width, $w/W = 0.25$, 0.5, and 0.75. When the length of the chamber is greater than half its width, $L \geq 0.5\,\mathrm{W}$, Eq. (16.20) can accurately predict $\langle t(x_0)\rangle$ with a relative error of less than 3%. However, it is expected to fail for shorter chambers, $L < 0.5\,\mathrm{W}$, since the derivation of Eq. (16.20) is based on the

[2] Note that in obtaining Eq. (16.20), we have made use of the transformation $x_0 \to L - x_0$.

Table 16.2 The relative error in percentages of our approximate analytical expression for the MFPT, $\langle t(L)\rangle$, from Brownian dynamics simulations. The Brownian simulations were run with $N = 200{,}000$ trajectories with starting points uniformly distributed over the chamber wall containing the absorbing strip

		L/W					
		0.25	0.50	0.75	1.0	2.0	3.0
w/W	0.25	8.7807	1.7507	1.9426	1.5900	1.5520	2.2699
	0.50	8.2737	2.2392	1.5170	1.2268	0.9686	0.5592
	0.75	5.7125	2.2721	2.2029	2.1300	1.9823	1.8323

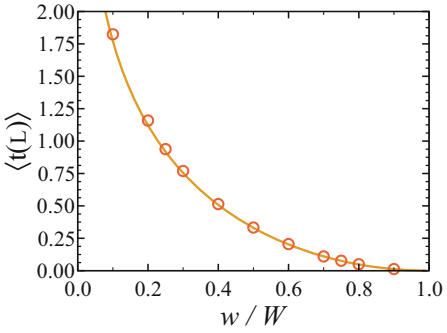

Fig. 16.20 The w/W-dependencies of the mean particle lifetime given by Eq. (16.20) with trajectory starting positions evenly distributed over the cylinder wall at $L = 3$ $x_0 = L = 3$ (solid curve) and the times obtained from Brownian dynamics simulations (symbols). The simulations were based on 200,000 trajectories and used a time step of 10^{-6}. D was set equal to 1

Moizhes-Muratov-Shvartsman formula for κ, Eq. (16.19), which was obtained for a semi-infinite system.

The comparison of the theoretical predictions given by Eq. (16.20), when $L = x_0 = 3$, with the simulation results is presented in Fig. 16.20. The chart shows an excellent correspondence between the theoretical and computational results.

16.5 Binding Site Hidden in a Tunnel

In this section, we solve an extension of the problem outlined in the previous section, i.e., the trapping of diffusing particles by a hidden binding site hidden in a tunnel, as shown in Fig. 16.21. The system consists of a rectangular chamber, $0 < x < L$, and a tunnel or sleeve, $L < x < L + l$. The boundary at $x = L$ separating these parts is partially absorbing and is characterized by the trapping rate κ and κ' from the chamber and sleeve sides, respectively. The boundary at $x = 0$ is reflecting, whereas the boundary at $x = L + l$ is perfectly absorbing.

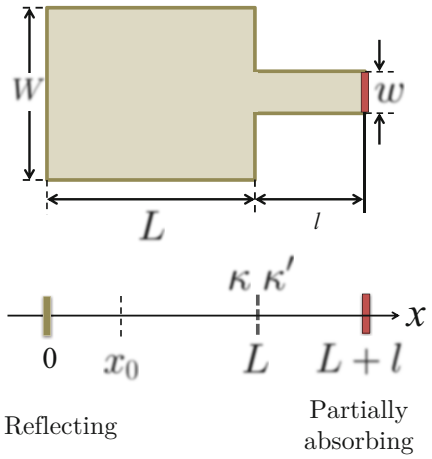

Fig. 16.21 Top panel: Schematic representation of a rectangular chamber characterized by a length L and a width W, with a sleeve of length l and width w, which contains an absorbing site of length $w \leq W$ at the end of its right wall. Bottom panel: A simplified boundary homogenization one-dimensional model is used to describe the particle dynamics in the system with a proper κ and κ'

In this case, a particle first has to find an entrance to the tunnel leading to the site. After entering the tunnel, the particle either diffuses to the binding site, where it is trapped, or escapes from the tunnel back to the bulk.

The first step is to establish κ', the trapping rate of the flux from the sleeve to the rectangular chamber. To such end, consider the case where the sleeve boundary at $x = L + l$ is reflecting rather than absorbing, which would be like having two chambers connected by a bottleneck. At equilibrium, the number of particles going into the rectangular chamber is $N_r = N(A_r/A_T)$, where $Ar = WL$ and $A_T = (WL + wl)$. In contrast, the number of particles going into the sleeve is $N_s = N(A_s/A_T)$, where $A_s = wl$ and N is the total number of particles diffusing in the system. Then, concentrations at equilibrium per unit length are $c_{req} = N_r/L = NW/(WL + wl)$ and $c_{seq} = N_s/l = Nw/(WL + wl))$, respectively. The identity of the two fluxes at $x = L$ allows us to establish a relation between the trapping rates, $j_{req} = c_{req}\kappa = NW\kappa/(WL + wl)$ and $j_{seq} = c_{seq}\kappa' = Nw\kappa'/(WL + wl))$ and consequently

$$W\kappa = w\kappa'. \tag{16.22}$$

Therefore, substituting Eq. (16.19) into this last expression, we arrive at

$$\kappa' = \frac{\pi D}{w \ln\left[1/\sin\left(\frac{\pi w}{2W}\right)\right]}. \tag{16.23}$$

Now, we will proceed to obtain the MFPT at the steady state for the complete system, specifically, the rectangular chamber and the sleeve with the perfectly absorbing strip. The one-dimensional model used in our derivation depends on the steady-state picture, which is maintained by a constant flux j injected at the particle starting point x_0, managing to compensate the flux of particles trapped by the hidden site. The one-dimensional system is shown in Fig. 16.22.

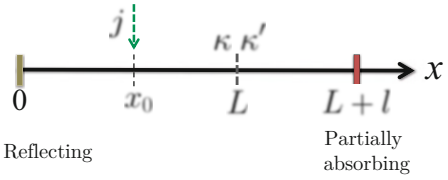

Fig. 16.22 The MFPT, or mean particle lifetime, is derived using a one-dimensional model that uses the steady-state picture. The steady state is maintained by applying a constant flux j at the particle's initial position x_0

The starting point is the relation between the MFPT, the steady-state one-dimensional concentration $c(x)$, and flux j, given by

$$\langle t(x_0)\rangle = \frac{N}{j} = \frac{\int_0^{L+l} c(x)\,\mathrm{d}x}{j}. \tag{16.24}$$

This equation can be deduced by remembering that the flux is the number of particles crossing the border per unit time. As a result, if we have a diffusing particle, it will cross the boundary in the average time given by the MFPT. The same reasoning follows for N particles.

From Eq. (16.24), the reader may see that, in order to find $\langle t(x_0)\rangle$, our main task is to find $c(x)$, the steady-state one-dimensional concentration of the system. For such purpose, let us calculate the concentration at each compartment, i.e., concentration into the chamber, $c_{ch}(x)$, and the sleeve, $c_s(x)$, so that $c(x) = c_{ch}(x) + c_s(x)$. Inside the sleeve, $c_s(x)$ satisfies the Fick's first law, Eq. (2.73), i.e.,

$$\mathbf{j}(x) = -D\frac{\mathrm{d}c_s(x,|x_0)}{\mathrm{d}x}\,\hat{\mathbf{e}}_i, \tag{2.73}$$

subject to the absorbing BC, $c_s(L+l) = 0$. The solution at the steady state is given by[3]

$$c_s(x) = -\frac{j}{D}x + \mathcal{A}, \tag{16.25}$$

where $\mathcal{A}$ is an integration constant. By applying the boundary conditions (BCs), we arrive at

$$c_s(x) = \frac{j}{D}(L + l - x) \qquad L < x \leq L + l. \tag{16.26}$$

[3] Note that when solving the ordinary differential equation (ODE), we have assumed that the flow of diffusing particles goes from left to right.

Now, to calculate the concentration inside the chamber, we apply that fact that, at the interface $x = L$, the concentration of the system $c(x)$ jumps from $c_{ch}(L-\epsilon)\big|_{\epsilon\to 0}$ to $c_s(L+\epsilon)\big|_{\epsilon\to 0} = jl/D$. The magnitude of the jump is determined by the need for preservation of the flux,

$$j = \kappa c_{ch}(L-\epsilon)\Big|_{\epsilon\to 0} - \kappa' c_s(L+\epsilon)\Big|_{\epsilon\to 0}. \tag{16.27}$$

From this last equation, together with Eqs. (16.26) and (16.22), we find

$$c_{ch}(L-\epsilon)\Big|_{\epsilon\to 0} = \frac{j}{\kappa} + \frac{\kappa'}{\kappa} c_s(L+\epsilon)\Big|_{\epsilon\to 0} = \frac{j}{D}\left(\frac{W}{w}l + \frac{D}{\kappa}\right). \tag{16.28}$$

Fick's first law should also remain valid in the chamber; therefore, by using such equation we can find the concentration as a function of x. In such a case, we have to find the solution for two intervals of the system, from 0 to x_0 and from x_0 to L. In this last interval, we have to impose the joining condition given by Eq. (16.25). Equating Eq. (16.25) evaluated at $x = L$ with Eq. (16.28) results in

$$c_{ch}(L) = \frac{j}{D}\left(\frac{W}{w}l + \frac{D}{\kappa}\right) = \frac{j}{D}L + \mathcal{A}. \tag{16.29}$$

On solving for $\mathcal{A}$, $c_{ch}(x)$ becomes

$$c_{ch}(L) = \frac{j}{D}\left(\frac{W}{w}l + \frac{D}{\kappa} + L - x\right) \qquad x_0 \le x \le L. \tag{16.30}$$

Furthermore, the latter equation defines the concentration at x_0, which in fact, at steady state, is constant on the interval from 0 to x_0, because the reflecting boundary is at the origin. Consequently,

$$c_{ch}(x) = \frac{j}{D}\left(\frac{W}{w}l + \frac{D}{\kappa} + L - x_0\right) \qquad 0 < x \le x_0. \tag{16.31}$$

Additionally, by means of the Heaviside step function, we write a single expression for the concentration inside the chamber along the whole interval, yielding

$$c_{ch}(x) = \frac{j}{D}\left(\frac{W}{w}l + \frac{D}{\kappa} + L - xH(x-x_0) - x_0 H(x_0 - x)\right) \qquad 0 < x \le L. \tag{16.32}$$

Once we have obtained the concentration in the system, we can calculate the MFPT using Eq. (16.24), which simply reduces to calculating the integral of the concentration over the interval from 0 to $L+l$, which is the total number of particles. Therefore

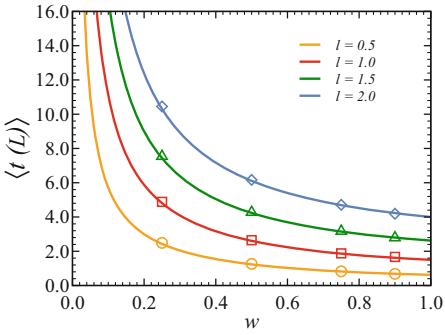

Fig. 16.23 Comparison of mean first-passage times predicted by Eq. (16.34) for $l = 0.5$, 1.0, 1.5, and2.0 (solid lines) to those obtained from Brownian dynamics simulations (symbols). A total of 5×10^4 initially uniformly distributed particles at $x_0 = L$ were used for each configuration, where we set $L = W = D = 1$

$$
\begin{aligned}
N &= \int_0^{L+l} c(x)\,\mathrm{d}x = \int_0^{L} c(x)_{ch}\,\mathrm{d}x + \int_L^{L+l} c(x)_s\,\mathrm{d}x \\
&= \frac{j}{D}\left[\int_0^{L}\left(\frac{W}{w}l + \frac{D}{\kappa} + L - xH(x-x_0) - x_0H(x_0-x)\right)\mathrm{d}x\right. \\
&\quad \left. + \int_L^{L+l}\left(\frac{W}{w}l + \frac{D}{\kappa} + L - x\right)\mathrm{d}x\right] \\
&= \frac{j}{D}\left\{\frac{L^2 - x_0^2}{2} + \frac{LW}{\pi}\ln\left[\frac{1}{\sin(\pi w/2W)}\right] + \frac{LlW}{w} - \frac{l^2}{2}\right\}.
\end{aligned}
\tag{16.33}
$$

Finally, dividing this expression by j, we arrive to the desired result:

$$
\langle t(x_0)\rangle = \frac{L^2 - x_0^2}{2D} + \frac{LW}{\pi D}\ln\left[\frac{1}{\sin(\pi w/2W)}\right] + \frac{Ll}{D}\frac{W}{w} + \frac{l^2}{2D}. \tag{16.34}
$$

If we set $l = 0$, in this last equation, it reduces to Eq. (16.20). In fact, Eq. (16.34) has a transparent physical interpretation: The first two terms give the mean time it takes for the particle to enter the sleeve from the chamber, while the last two terms give the average lifespan of a particle entering the chamber, that is, from the sleeve entrance.

A comparison between theoretical predictions, Eq. (16.34), and simulation results is given in Fig. 16.23 as function of w, where the curves correspond to four values of l. The particles' initial positions are uniformly distributed at $x_0 = L$. The symbols are the values obtained from Brownian dynamics simulations. One can observe an excellent agreement between the theoretical predictions and the simulation results, with a relative error of less than 2% when $l \geq 0.5$.

Finally, averaging over x_0, assuming that all initial particles positions within the chamber are equally likely, we arrive at Eq. (16.21) plus a couple of terms related to the sleeve, namely,

$$
\langle t_u\rangle = \frac{L^2}{3D} + \frac{LW}{\pi D}\ln\left[\frac{1}{\sin(\pi w/2W)}\right] + \frac{Ll}{D}\frac{W}{w} + \frac{l^2}{2D}. \tag{16.35}
$$

16.6 Table of Useful Trapping Rates

In this section, we sumarize in Table 16.3 the trapping rates obtained in this chapter.

Table 16.3 Useful trapping rate formulas

Trapping rate	System description
$\mathtt{k}_S = 4\pi RD$	Absorbing sphere
$\mathtt{k}_{HS} = 2\pi RD$	Absorbing hemisphere on a flat wall
$\mathtt{k}_{HBP} = 4Ds$	Absorbing disk on a cylinder wall
$\mathtt{k}_{DBW} = \left(\frac{2^5 AP}{\pi^2}\right)^{1/3} D$	Arbitrary absorbing spot on a flat wall
$\mathtt{k}_{MMS} = \frac{\pi D}{L \ln\left[1/\sin\left(\frac{\pi l}{2L}\right)\right]}$	Absorbing strips on a flat wall & absorbing stripes on a cylinder surface & absorbing arcs over a reflecting circle
$\kappa_{cap} = \frac{2D}{\pi R}\sqrt{\sigma}\frac{1+2.61\sqrt{\sigma}-3.22\sigma^2}{(1-\sigma)^{3/2}}$	Absorbing cap
$\mathtt{k}_{MMS} = \frac{\pi D}{W \log\left[1/\sin\left(\frac{\pi w}{2W}\right)\right]}$	Absorbing strip on a reflecting wall
$\mathtt{k}_{CK} = \frac{4\pi R^2 D\kappa}{D+R\kappa}$	Partially absorbing sphere
$\mathtt{k}_{BP} = \frac{4\pi DRa\mathtt{N}}{\pi R+a\mathtt{N}}$	Absorbing disks over a spherical reflecting sphere
$\mathtt{k}_{ZS} = \frac{4\pi a^2 D\kappa}{4D+a\pi\kappa}$	Partially absorbing disk on a reflecting flat surface

16.7 Concluding Remarks

Boundary homogenization is an approximate approach to replace heterogeneous boundary conditions on the surface with homogeneous BCs using a properly chosen effective trapping rate. This is possible because, at sufficiently large distances, the steady-state particle fluxes and concentrations are indistinguishable from their original problem, in the case of a uniform partially absorbing boundary with a properly chosen surface trapping rate. This trapping rate is the key value that one needs in order to be able to study trapping by a heterogeneous boundary in the framework of this approach. Boundary homogenization can also be used to find higher moments of the particle's lifetime, the lifetime probability density, and the particle survival probability.

There are a lot of other physical effects involved in Brownian particle binding by absorbing patches that have not been taken into account. These include, for example, rotational diffusion of Brownian particles, enhancement of trapping rate due to particle surface diffusion, buried patchy sites, and patch clustering.

It is worth noting that there is a relation between the capacitance $\mathtt{C}$[4] and the trapping rate diffusion κ, which can be used to go from a diffusive system to an electrical system, and vice versa, namely, $\kappa = 4\pi D\mathtt{C}$.

[4] Capacitance is the capability of a material object or device to store electric charge.

Further Reading and References

A.M. Berezhkovskii, M.I. Monine, C.B. Muratov, S.Y. Shvartsman, Homogenization of boundary conditions for surfaces with regular arrays of traps. J. Chem. Phys. **14**, 036103 (2006). https://doi.org/10.1063/1.2161196

H.C. Berg, E.M. Purcell, Physics of chemoreception. Biophys J. **20**, 193 (1977). 10.1016/S0006-3495(77)85544-6

H.S. Carslaw, J.C. Jaeger, *Conduction of Heat in Solids* (Oxford University, Oxford, 1959)

F.C. Collins, G. Kimball, Diffusion-controlled reaction rates. J. Colloid Sci. **4**, 425 (1949). 10.1016/0095-8522(49)90023-9

L. Dagdug, A.M. Berezhkovskii, S.M. Bezrukov, Particle lifetime in cylindrical cavity with absorbing spot on the wall: going beyond the narrow escape problem. J. Chem. Phys. **137**, 234108 (2012). https://doi.org/10.1063/1.4772183

L. Dagdug, A.M. Berezhkovskii, A.T. Skvortsov, Trapping of diffusing particles by striped cylindrical surfaces. Boundary homogenization approach. J. Chem. Phys. **142**, 234902 (2015). https://doi.org/10.1063/1.4922444

L. Dagdug, M.-V. Vázquez, A.M. Berezhkovskii, V.Y. Zitserman, Boundary homogenization for a sphere with an absorbing cap of arbitrary size. J. Chem. Phys. **145**, 214101 (2016). https://doi.org/10.1063/1.4968598

L. Dagdug, A.M. Berezhkovskii, V.Y. Zitserman, S.M. Bezrukov, Trapping of particles diffusing in two dimensions by a hidden binding site. Phys. Rev. E **103**, 012135 (2021). https://doi.org/10.1103/PhysRevE.103.012135

O.K. Dudko, A.M. Berezhkovskii, G.H. Weiss, Boundary homogenization for a circle with periodic absorbing arcs. Exact expression for the effective trapping rate. J. Chem. Phys. **121**(3), 1562 (2015). https://doi.org/10.1063/1.1763137

B.Y. Moizhes, Zh. Tech. Fiz. **25**, 167 (1955) (in Russian)

C.B. Muratov, S.Y. Shvartsman, Multiscale Model. Simul. **7**, 44 (2008). https://doi.org/10.1137/0706928

D. Shoup, A. Szabo, Role of diffusion in ligand binding to macromolecules and cell-bound receptors. Biophys J. **40**, 33 (1982). 10.1016/S0006-3495(82)84455-X

A.T. Skvortsov, A.M. Berezhkovskii, L. Dagdug, Rate constant for diffusion-influenced ligand binding to receptors of arbitrary shape on a cell surface. J. Chem. Phys. **143**, 226101 (2015). https://doi.org/10.1063/1.4936866

M.V. Smoluchowski, Versuch Einer Mathematischen Theorie der Koagulationskinetik kolloider Losungen. Zeitschrift f. Physik. Chemie. XCII **92**, 129–168 (1917)

H.X. Zhou, R. Zwanzig, A rate process with an entropy barrier. J. Chem. Phys. **94**, 6147 (1991). https://doi.org/10.1063/1.460427

R. Zwanzig, A. Szabo, Time dependent rate of diffusion-influenced ligand binding to receptors on cell surfaces. Biophys. J. **60**, 671 (1991). https://doi.org/10.1016/S0006-3495(91)82096-3

R. Zwanzig, Diffusion-controlled ligand binding to spheres partially covered by receptors: an effective medium treatment, Proc. Natl. Acad. Sci. U S A. **87**, 5856 (1991). https://doi.org/10.1073/pnas.87.15.5856

Part VII
Quasi-one-dimensional Diffusion: Channel/Tube

On the diffusion coefficient and the projection techniques in confined space.

"Make things as simple as possible, but not simpler."

—Albert Einstein

Chapter 17
Fick-Jacobs 1D Reduction

17.1 Introduction

The Brownian motion of particles, molecules, or even living microorganisms in confined geometries, such as pores and channels, plays a key role on various scales, in both nature and technology. Diffusion in such systems has been studied in-depth theoretically and experimentally given its ubiquitousness and due to the fact that they control the dynamics of many physical, chemical, and biochemical processes. Transport in confined geometries within quasi-one-dimensional systems exhibits a very rich and striking phenomenology. Examples include diffusion in artificially produced pores in thin solid films, proteins through a phase space funnel-like region, membrane channel, transport in zeolites, solid-state nanopores as single-molecule biosensors for the detection and structural analysis of individual molecules, and as a model of a chemical reaction where the kinetics are dominated by crossing through a bottleneck rather than passage over a potential barrier.

In this and the following chapters, we will present the theory developed to study diffusion under spatial confinement by means of one-dimensional reduction for quasi-one-dimensional systems. In this case, diffusion is controlled by both the fluctuation statistics of the jittering particles and the phase space available to their dynamics, by means of an entropic barrier. Earlier studies by Merkel H. Jacobs and Robert Zwanzig triggered renewed research on this subject. Their work focus on systems consisting of wide channels or tubes, where one can map the particle motion into an effective one-dimensional description. Assuming that the distribution of the solute in the cross section of the system is uniform at equilibrium, variations in the structural shape of a channel or tube along the direction of motion imply changes in the number of accessible particle states or, equivalently, lead to spatial variations of entropy.

L. Dagdug et al., *Diffusion Under Confinement*,
https://doi.org/10.1007/978-3-031-46475-1_17

17.2 The Fick-Jacobs Equation

The so-called Fick-Jacobs approach consists of reducing spatial coordinates, which means that even if diffusion takes place into a tube or channel, the concentration can be approximated as a function of the longitudinal spatial coordinate and time. This theoretical framework leads to a modification of Fick's equation, also known as *Fick-Jacobs equation*. This equation appeared for the first time in the original article published by Adolf Fick in 1855. In fact, it is the very first equation written in the manuscript. For this one-dimensional reduction to be applied, two conditions must be satisfied: a) The system boundaries, or walls, must be described by a well-behaved function, and b) the channel must be narrow, in such a way that the concentration equilibrates much faster in the direction perpendicular to the channel. Thus, the problem is reduced to studying the concentration along the channel. The latter condition is satisfied by assuming that the diffusion constant along the channel is very small compared to the diffusion constant corresponding to the transversal direction of the channel, i.e., $D_\perp \gg D_\parallel$, or if the channel is very narrow.

In order to derive the Fick-Jacobs equation (FJ), we will write the master equation for a random walker for whom the probability of moving from one site to another is now a function of position, and such functionality depends on the fraction of the channel's area or tube's volume that the particle will have to face in its next step (see Fig. 17.1). We will restrict the derivation to a symmetric channel in two dimensions, but its generalization to a three-dimensional tube is straightforward. To such end, we define the *effective one-dimensional concentration*, or *projected one-dimensional density*, as follows:

$$\rho(x,t) \equiv \int_0^{h(x)} p(x,y,t)\,\mathrm{d}y. \tag{17.1}$$

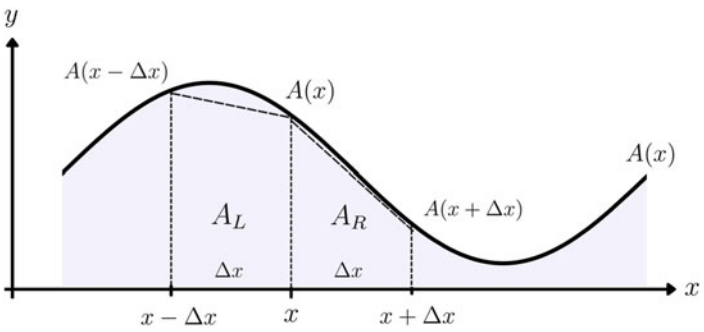

Fig. 17.1 Schematic diagram of the upper half of a symmetric channel confining the motion of Brownian particles. Because this has been restricted to symmetric channels, we only have to focus on the half-width of the channel. The channel's wall is represented by the channel half width $h(x)$

This reduction is applicable for a wide channel after long times, assuming fast equilibration in the y direction. Under this approximation, there is no change in the particle's concentration in the transversal direction, therefore, $p(x, y, t) \approx p(x, t)$, and from Eq. (17.1) we have that $p(x, t) = \rho/h(x)$. With these considerations, the master equation is given by

$$\rho(x, t + \Delta t) = a(x + \Delta x, t)\, \rho(x + \Delta x, t) + b(x - \Delta x, t)\, \rho(x - \Delta x, t), \tag{17.2}$$

where time $t \in [0, \infty)$ and spatial position $x \in \mathbb{R}$. Expanding both sides of Eq. (17.2) in a Taylor series around Δx and Δt yields

$$\begin{aligned} &\rho(x, t) + \Delta t \frac{\partial \rho(x, t)}{\partial t} + \cdots \\ &= \left[a(x)\rho(x, t) + \Delta x \frac{\partial a(x)\rho(x, t)}{\partial x} + \frac{(\Delta x)^2}{2} \frac{\partial^2 a(x)\rho(x, t)}{\partial x^2} + \cdots \right] \\ &+ \left[b(x)\rho(x, t) - \Delta x \frac{\partial b(x)\rho(x, t)}{\partial x} + \frac{(\Delta x)^2}{2} \frac{\partial^2 b(x)\rho(x, t)}{\partial x^2} + \cdots \right]. \end{aligned} \tag{17.3}$$

Keeping terms up to the first order on t and second order on x, and dividing both sides of the equation by Δt, we have[1]

$$\frac{\partial \rho(x, t)}{\partial t} = \left[\frac{(\Delta x)^2}{2\Delta t} \frac{\partial^2 \rho(x, t)}{\partial x^2} + \frac{\Delta x}{\Delta t} \frac{\partial [a(x) - b(x)]\rho(x, t)}{\partial x} \right]. \tag{17.4}$$

The product rule applied to the second term on the right-hand side yields

$$\begin{aligned} &\frac{\partial \rho(x, t)}{\partial t} \\ &= \left[\frac{(\Delta x)^2}{2\Delta t} \frac{\partial^2 \rho(x, t)}{\partial x^2} + \frac{\Delta x}{\Delta t} \rho(x, t) \frac{\partial [a(x) - b(x)]}{\partial x} + \frac{\Delta x}{\Delta t} [a(x) - b(x)] \frac{\partial \rho(x, t)}{\partial x} \right]. \end{aligned} \tag{17.5}$$

The last relation is completely general; thus $a(x)$ and $b(x)$ should be set depending on the problem. In this approximation, they are given by a fraction of area. From Fig. 17.1, we see that the areas enclosed from x to $x + \Delta x$ and $x - \Delta x$ can be approximated in terms of $h(x)$ by

$$A_R = \frac{\Delta x}{2} \left[h(x) + A(x + \Delta x) \right], \tag{17.6}$$

and

[1] Where we have used the conservation of probability, i.e., $a(x) + b(x) = 1$.

$$A_L = \frac{\Delta x}{2}\left[h(x) + A(x - \Delta x)\right], \tag{17.7}$$

respectively. Performing a Taylor expansion,

$$A_R = \frac{\Delta x}{2}\left[2h(x) + \Delta x \frac{\partial h(x)}{\partial x} + \frac{(\Delta x)^2}{2}\frac{\partial^2 h(x,t)}{\partial x^2} + \cdots\right], \tag{17.8}$$

$$A_L = \frac{\Delta x}{2}\left[2h(x) - \Delta x \frac{\partial h(x)}{\partial x} + \frac{(\Delta x)^2}{2}\frac{\partial^2 h(x,t)}{\partial x^2} + \cdots\right], \tag{17.9}$$

and keeping up to second order in x, we have

$$A_R = \frac{\Delta x}{2}\left[2h(x,t) + \Delta x \frac{\partial h(x)}{\partial x}\right], \tag{17.10}$$

and

$$A_L = \frac{\Delta x}{2}\left[2h(x,t) - \Delta x \frac{\partial h(x)}{\partial x}\right], \tag{17.11}$$

hence, the total area is given by

$$A_T = A_R + A_L = 2h(x)\Delta x. \tag{17.12}$$

With these relations for the areas, for the probabilities, we now have

$$a(x) = \frac{A_R}{A_T} = \frac{1}{2h(x)}\left[h(x) - \frac{1}{2}\Delta x h'(x)\right], \tag{17.13}$$

and

$$b(x) = \frac{A_R}{A_T} = \frac{1}{2h(x)}\left[h(x) + \frac{1}{2}\Delta x h'(x)\right], \tag{17.14}$$

where $h'(x)$ indicates derivation with respect to x. Introducing the last two equations into Eq. (17.5) leads to

$$\frac{\partial \rho(x,t)}{\partial t} = D_x \frac{\partial^2 \rho(x,t)}{\partial x^2} - \frac{\partial}{\partial x} D_x \frac{h'(x)}{h(x)}\rho(x,t), \tag{17.15}$$

where we define the diffusion coefficient

$$D_x \equiv \lim_{\substack{\Delta x \to 0 \\ \Delta t \to 0}} \frac{(\Delta x)^2}{2\Delta t}. \tag{17.16}$$

The relation between D_x and the bulk diffusivity, from now on D_0, can be obtained from Eq. (2.18), setting $\Delta z = 0$, namely,

$$\frac{\Delta r^2}{2\Delta t} = \frac{\Delta x^2}{2\Delta t} + \frac{\Delta y^2}{2\Delta t}. \tag{2.18}$$

The Fick-Jacobs approximation is obtained precisely for very narrow channels when setting $D_x = D_y$, so $\langle \Delta \mathbf{r}^2 \rangle = 4D_x\, \Delta t$, and accordingly,

$$D_x = D_0 \equiv \lim_{\substack{\Delta r \to 0 \\ \Delta t \to 0}} \frac{(\Delta \mathbf{r})^2}{4\Delta t}. \tag{17.17}$$

Finally, by substituting this last relation into Eq. (17.15), and after some algebraic manipulation, the Fick-Jacobs equation can be written in the following compact form:

$$\frac{\partial \rho(x,t)}{\partial t} = D_0 \frac{\partial}{\partial x}\left[h(x) \frac{\partial}{\partial x} \frac{\rho(x,t)}{h(x)} \right]. \tag{17.18}$$

In the literature, it is more common to find the FJ equation in terms of the width of the channel instead of its half width. For a symmetric channel, its width is $w(x) = 2h(x)$, and therefore, the FJ equation can be written as

$$\frac{\partial \rho(x,t)}{\partial t} = D_0 \frac{\partial}{\partial x}\left[w(x) \frac{\partial}{\partial x} \frac{\rho(x,t)}{w(x)} \right]. \tag{17.19}$$

An important feature of Eq. (17.19) is observed when diffusion takes place into a channel with parallel walls. In such a case, the channel width $w(x)$ is constant and Fick's equation is recovered, as expected.

One of the most important results under the Fick-Jacobs approach is that Eq. (17.19) is formally equivalent to the Smoluchowski equation, Eq. (6.11), namely,

$$\frac{\partial \rho(x,t)}{\partial t} = D_0 \frac{\partial}{\partial x}\left\{ e^{-\beta U(x)} \frac{\partial}{\partial x}\left[e^{\beta U(x)} \rho(x,t) \right] \right\}, \tag{17.20}$$

where the entropic potential is given by

$$-\beta U(x) = \ln\left[w(x)/w(x_m) \right], \tag{17.21}$$

$\beta = 1/(k_B T)$, k_B is the Boltzmann constant, T is the absolute temperature, and $U(x)$ at $x = x_m$ is taken to be zero. Then we can say that the FJ equation describes diffusion past an entropy barrier, where this barrier is associated solely with changes in entropy. This analogy shows that confinement in higher dimensions gives rise to

an effective entropic potential in reduced dimensions. It is reasonable to associate this potential with entropy since it is given only by area or width.

From the equation for flux in the presence of a potential, Eq. (6.10), and the definition of entropic potential, we have that the flux from a diffusive particle under geometrical constraint is given by

$$J(x,t) = -D_0\, w(x)\, \frac{\partial \rho(x,t)}{\partial x}. \tag{17.22}$$

The Fick-Jacobs equation in a symmetric three-dimensional tube is given by

$$\frac{\partial \rho(x,t)}{\partial t} = D_0\, \frac{\partial}{\partial x}\left[r^2(x)\, \frac{\partial}{\partial x} \frac{\rho(x,t)}{r^2(x)} \right], \tag{17.23}$$

where $r(x)$ is the tube radius and $\mathcal{A} = \pi r^2(x)$ is the tube cross-sectional area at a given value of x. Hence, the entropic potential is given by $-\beta U(x) = \ln[\mathcal{A}/\mathcal{A}_m]$. From the conservation equation, we have that

$$J(x,t) = -D_0\, \mathcal{A}(x)\, \frac{\partial}{\partial x} \frac{\rho(x,t)}{A(x)}. \tag{17.24}$$

Again, from this last relation, we can define the boundary conditions.

Finally, it is important to comment that another system of great relevance where the Fick-Jacobs approach can be applied, and for which there seems to be no connection, is to study the slowdown of unconstrained diffusion in the presence of obstacles. For such purpose, we need to visualize the spacing between obstacles as channels.

In the next section, we will solve a problem of diffusion into a vessel of variable cross section using the Fick-Jacobs approach.

17.3 Fick's Funnel

To illustrate the applicability of the Fick-Jacobs approach, this section discusses how the FJ equation can be applied to predict the concentration and the flux of a channel formed by a funnel, vessel of variable cross section in steady state, as shown in Fig. 17.2. This problem arose in the original paper by Fick. The experimental arrangement was used to assess the validity of his theoretical predictions. To reproduce the theoretical results obtained in Fick's paper, we have to define the problem in the following way: A constant concentration ρ_0 is maintained at the small end of the funnel, at distance h from the tip of the funnel, while a perfectly absorbing wall is placed at the other end. Once a steady state has been established, we want to find the concentration as a function of position, as well as the flux at the

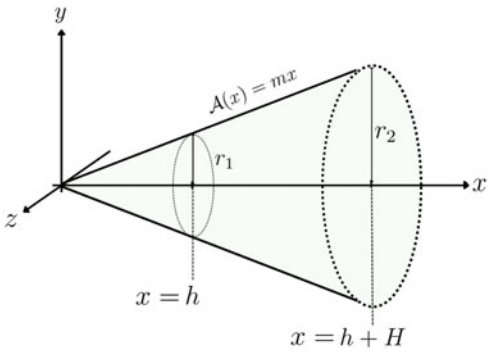

Fig. 17.2 Schematical representation of a funnel channel formed by a funnel of variable crossed section. The boundaries are given by function $\mathcal{A}(x) = mx$ while the smaller and larger radii are r_1 and r_2, respectively

end of the funnel. Let us call the smaller and larger radii of the funnel r_1 and r_2, respectively, and its length H (see Fig. 17.2).
To such end, let us write out the FJ equation in a third form, namely,

$$\frac{\partial \rho(x,t)}{\partial t} = D_0 \left[\frac{\partial^2 \rho(x,t)}{\partial x^2} + \frac{\mathcal{A}'(x)}{\mathcal{A}(x)} \rho(x,t) \right]. \tag{17.25}$$

The funnel radius is given by $r(x) = mx$, where m is the tangent of one half. Then, we have that the tube cross-sectional area is given by $\mathcal{A}(x) = \pi r^2(x) = \pi m^2 x^2$, and its derivative is $\mathcal{A}'(x) = \pi r^2(x) = 2\pi m^2 x$. Hence, at steady state, we have

$$\frac{\partial^2 \rho(x)}{\partial x^2} + \frac{2}{x} \rho(x) = 0. \tag{17.26}$$

The solution of Eq. (17.26) is given by

$$\rho(x) = C_2 - \frac{C_1}{x}. \tag{17.27}$$

Evaluating the constants in this equation from the boundary conditions, namely, $\rho(x = h, t) = \rho_0$ and $\rho(x = h + H, t) = 0$, the solution becomes

$$\rho(x) = \frac{h}{H} \left[\frac{h + H}{x} - 1 \right] \rho_0. \tag{17.28}$$

These results show that density is proportional to ρ_0 and inversely proportional to the length of the funnel H and does not depend on diffusivity because of the steady state.

Next, we will calculate the flow at $x = H$. To such end, we introduce $\mathcal{A}(x) = \pi m^2 x^2$ and Eq. (17.28) into Eq. (17.24), leading to

$$J = \frac{D_0 \pi m^2 h (h + H)}{H} \rho_0. \tag{17.29}$$

Recalling that $r_1 = mh$ and $r_2 = m(H + h)$, we can finally write the flux in a more useful form, as follows:

$$J = \frac{D_0 \, \pi \, r_1 \, r_2}{H} \rho_0. \tag{17.30}$$

It is worth mentioning that these equations predict that the flux is also proportional to ρ_0 and inversely proportional to H; it reaches its maximum when $r_1 = r_2$ and would be exactly the same if the large and small ends of the funnel were interchanged. This proportionality only depends on the geometrical parameters of the funnel.

It has been shown that the FJ approximation better reproduces the observed results when the diffusion coefficient has a spatial dependence. We will look at this in more detail in the following chapter.

17.4 Concluding Remarks

In this chapter, we show how Fick's equation is modified when diffusion takes place into a two-dimensional channel or a three-dimensional tube, to become the so-called Fick-Jacobs equation. The most important equations that were obtained in this chapter are listed below:

$$\frac{\partial \rho(x,t)}{\partial t} = D_0 \frac{\partial}{\partial x}\left[w(x) \frac{\partial}{\partial x} \frac{\rho(x,t)}{w(x)} \right] \qquad \text{(Fick-Jacobs equation for a channel)}$$

$$\frac{\partial \rho(x,t)}{\partial t} = D_0 \frac{\partial}{\partial x}\left[h(x) \frac{\partial}{\partial x} \frac{\rho(x,t)}{h(x)} \right] \qquad \text{(Fick-Jacobs equation for a tube)}$$

Further Reading and References

A. Fick, Ueber diffusion. Annalen der Physik **94** (1855). [Translated into English by Tad W. Patzek in *Advances in Historical Studies*, **3**, 207–220 (2014)]. https://www.scirp.org/pdf/AHS_2014093011510952.pdf

M.H. Jacobs, *Diffusion Processes* (Springer, New York, 1935)

R. Zwanzig, Diffusion past an entropy barrier. J. Phys. Chem. **96**, 10, 3926–3930 (1992). https://doi.org/10.1021/j100189a004

Chapter 18
Zwanzig 1D Reduction

A formal derivation of the Fick-Jacobs (FJ) equation was introduced in 1992 by Robert Zwanzig (Zw) taking into account small deviations from local equilibrium. The key point of his derivation is the assumption of equilibration in the transverse direction, or y-coordinate. Zwanzig demonstrated that the introduction of this approximation, which eventually falls into the category of a *position-dependent diffusion coefficient* $D(x)$, considerably improves the accuracy of the FJ equation extending its range of validity to more winding geometries. Moreover, Zw proposed the first expression for the position-dependent diffusion coefficient for channels of smoothly varying geometry in two and three dimensions. These coefficients depend on the position by means of the rate of change of the channel width, $w'(x)$. Zwanzig also showed that his *modified Fick-Jacobs equation* corresponds to the Smoluchowski equation, if the entropic potential is identified as $w(x)/w(0)$. This chapter is dedicated to reviewing Zwanzig's work.

18.1 Zwanzig's Derivation of the FJ Equation in 2D

In this section, we will describe the steps proposed by Zwanzig to give a more general and rigorous derivation of the Fick-Jacobs (FJ) equation. The method consists of performing a reduction of the two- or three-dimensional Smoluchowski equation to a one-dimensional description. For the sake of simplicity, let us focus on the reduction of the two-dimensional system, making the starting point a two-dimensional (2D) Smoluchowski equation for a diffusing concentration $c(x, y, t)$, taking place in the presence of a potential $U(x, y)$, *i.e.*,

L. Dagdug et al., *Diffusion Under Confinement*,
https://doi.org/10.1007/978-3-031-46475-1_18

$$\frac{\partial c(x,y,t)}{\partial t} = D_x \frac{\partial}{\partial x}\left\{ \mathrm{e}^{-\beta U(x,y)} \frac{\partial}{\partial x}\left[\mathrm{e}^{\beta U(x,y)}\, c(x,y,t)\right]\right\} + D_y \frac{\partial}{\partial y}\left\{ \mathrm{e}^{-\beta U(x,y)} \frac{\partial}{\partial y}\left[\mathrm{e}^{\beta U(x,y)}\, c(x,y,t)\right]\right\}, \tag{18.1}$$

where D_x and D_y are the longitudinal and transversal diffusion constants, respectively. $\beta = 1/(k_B T)$, with k_B and T denoting the Boltzmann constant and absolute temperature. Then, in order to perform the reduction, this last equation is integrated over the variable y, leading to

$$\int \frac{\partial c(x,y,t)}{\partial t}\,\mathrm{d}y = \int D_x \frac{\partial}{\partial x}\left\{ \mathrm{e}^{-\beta U(x,y)} \frac{\partial}{\partial x}\left[\mathrm{e}^{\beta U(x,y)}\, c(x,y,t)\right]\right\}\mathrm{d}y + \int D_y \frac{\partial}{\partial y}\left\{ \mathrm{e}^{-\beta U(x,y)} \frac{\partial}{\partial y}\left[\mathrm{e}^{\beta U(x,y)}\, c(x,y,t)\right]\right\}\mathrm{d}y. \tag{18.2}$$

Now, let us consider that the concentration is bounded by a symmetric system with upper and lower boundaries given by $h(x)$ and $-h(x)$, respectively. Integrating Eq. (18.2) term by term over $[-h(x), h(x)]$ and using the Leibniz integral rule, Eq. (A.9), the left-hand side yields

$$\begin{aligned}\int_{-h(x)}^{h(x)} \frac{\partial c(x,y,t)}{\partial t}\,\mathrm{d}y &= \frac{\partial}{\partial t}\int_{-h(x)}^{h(x)} c(x,y,t)\,\mathrm{d}y - c(x,y,t)\Big|^{y=h(x)} \cdot \frac{\mathrm{d}}{\mathrm{d}y}h(x) \\ &\quad + c(x,y,t)\Big|_{y=-h(x)} \cdot \frac{\mathrm{d}}{\mathrm{d}y}[-h(x)] \\ &= \frac{\partial \rho(x,t)}{\partial t},\end{aligned} \tag{18.3}$$

where

$$\rho(x,t) \equiv \int_{-h(x)}^{h(x)} c(x,y,t)\,\mathrm{d}y \tag{18.4}$$

is the *reduced* or *marginal concentration*.

Now, using the fundamental theorem of calculus on the first term on the right-hand side of Eq. (18.2), we have

$$\begin{aligned}&\int_{-h(x)}^{h(x)} D_y \frac{\partial}{\partial y}\mathrm{e}^{-\beta U(x,y)} \frac{\partial}{\partial y}\left[\mathrm{e}^{\beta U(x,y)}\, c(x,y,t)\right]\mathrm{d}y \\ &= D_y \frac{\partial}{\partial y}\int_{-h(x)}^{h(x)} \mathrm{e}^{-\beta U(x,y)} \frac{\partial}{\partial y}\left[\mathrm{e}^{\beta U(x,y)}\, c(x,y,t)\right]\mathrm{d}y = 0.\end{aligned} \tag{18.5}$$

This last integral is null because the antiderivative of the integral's argument will depend on x and t, so its derivative with respect to y vanishes.

Finally, if the Leibniz rule is applied to the second term on the right-hand side of Eq. (18.2), we arrive at

$$\begin{aligned}&\int_{-h(x)}^{h(x)} D_x \frac{\partial}{\partial x}\left\{\mathrm{e}^{-\beta U(x,y)} \frac{\partial}{\partial x}\left[\mathrm{e}^{\beta U(x,y)}\, c(x,y,t)\right]\right\} \mathrm{d}y \\ &\quad = D_x \frac{\partial}{\partial x}\int_{-h(x)}^{h(x)} \mathrm{e}^{-\beta U(x,y)} \frac{\partial}{\partial x}\left[\mathrm{e}^{\beta U(x,y)}\, c(x,y,t)\right] \mathrm{d}y.\end{aligned} \tag{18.6}$$

Substitution of Eqs. (18.3), (18.5), and (18.6) into Eq. (18.2) results in

$$\frac{\partial \rho(x,t)}{\partial t} = D_0 \frac{\partial}{\partial x}\int \mathrm{e}^{-\beta U(x,y)} \frac{\partial}{\partial x}\left[\mathrm{e}^{\beta U(x,y)}\, c(x,y,t)\right] \mathrm{d}y, \tag{18.7}$$

where we set $D_0 = D_x = D_y$.

Now, we have to make an assumption about $c(x, y, t)$ to express it in terms of $\rho(x, t)$. The key point is to assume equilibration in the transverse direction. In other words, equilibrium in the y-axis is almost instantly restored. Under this approximation, one can define an averaged x-dependent free energy $f(x)$ as follows:

$$\mathrm{e}^{-\beta f(x)} \equiv k \int \mathrm{e}^{-\beta U(x,y)}\, \mathrm{d}y, \tag{18.8}$$

where constant k is a result of the indefinite integration. From this equation, we can define a normalized conditional probability distribution: the local distribution of y, conditional on a given x, namely,

$$\vartheta(y|x) = \frac{\mathrm{e}^{-\beta U(x,y)}}{\int \mathrm{e}^{-\beta U(x,y)}\, \mathrm{d}y} = \frac{\mathrm{e}^{-\beta U(x,y)}}{k\mathrm{e}^{-\beta f(x)}}. \tag{18.9}$$

By definition, this probability distribution is normalized to unity in y:

$$\vartheta(y|x)\, \mathrm{e}^{\beta U(x,y)} = \frac{1}{k}\mathrm{e}^{\beta f(x)}. \tag{18.10}$$

Then, under the local equilibrium approximation, we can assume proportionality between the original concentration and the reduced density, that is, $c(x, y, t) \propto \rho(x, t)$, where proportionality is provided by the conditional probability distribution, and consequently,

$$c(x, y, t) \cong \rho(x, t)\, \vartheta(y|x). \tag{18.11}$$

Naively, Eq. (18.11) can be seen as a separation of variables. Direct substitution of Eq. (18.11) into Eq. (18.7) gives

$$\frac{\partial \rho(x,t)}{\partial t} = D_0 \frac{\partial}{\partial x} \int \mathrm{e}^{-\beta U(x,y)} \frac{\partial}{\partial x} \left[\mathrm{e}^{\beta U(x,y)} \rho(x,t) \vartheta(y|x) \right] \mathrm{d}y. \tag{18.12}$$

Now, to rewrite this equation in terms of $\rho(x,t)$, we calculate the derivative of Eq. (18.8) with respect to the transverse coordinate:

$$\frac{\partial}{\partial y} \mathrm{e}^{-\beta f(x)} = \frac{\partial}{\partial y} \int \mathrm{e}^{-\beta U(x,y)} \mathrm{d}y = \mathrm{e}^{-\beta U(x,y)}. \tag{18.13}$$

If we now use Eqs. (18.10) and (18.13) in Eq. (18.12), this results in

$$\begin{aligned} \frac{\partial \rho(x,t)}{\partial t} &= D_0 \frac{\partial}{\partial x} \int \frac{\partial}{\partial y} \left[\hbar \mathrm{e}^{-\beta f(x)} \right] \frac{\partial}{\partial x} \left[\frac{1}{\hbar} \mathrm{e}^{\beta f(x)} \rho(x,t) \right] \mathrm{d}y \\ &= D_0 \frac{\partial}{\partial x} \left\{ \mathrm{e}^{-\beta f(x)} \frac{\partial}{\partial x} \left[\mathrm{e}^{\beta f(x)} \rho(x,t) \right] \right\}. \end{aligned} \tag{18.14}$$

The simplification of constant $\hbar$ can be done by knowing that it provides the appropriate dimensions to the exponential of free energy. Therefore, this dimensionality should be carried out implicitly in further calculations. Then, Eq. (18.14) can be rewritten as

$$\frac{\partial \rho(x,t)}{\partial t} = D_0 \frac{\partial}{\partial x} \left\{ \mathrm{e}^{-\beta f(x)} \frac{\partial}{\partial x} \left[\mathrm{e}^{\beta f(x)} \rho(x,t) \right] \right\}. \tag{18.15}$$

This last expression is a generalization of the Fick-Jacobs equation with a constant diffusion coefficient D_0. The extension to three dimensions is obtained by replacing the integration over y for double integration over y and z.

Now, comparing Eq. (18.15) and the FJ equation, Eq. (17.19),

$$\frac{\partial \rho(x,t)}{\partial t} = D_0 \frac{\partial}{\partial x} \left[w(x) \frac{\partial}{\partial x} \frac{\rho(x,t)}{w(x)} \right]; \tag{17.19}$$

we see that

$$\mathrm{e}^{-\beta f(x)} = w(x). \tag{18.16}$$

This last expression states that the system's confinement by its boundaries, $\pm h(x)$, can be described by means of a potential, which is shown to be entropic, that is, temperature-independent. Now, Eq. (17.20) is formally proved.

As a relevant note, the equality in expression (18.16) is guaranteed by means of the dimensions provided by constant $\hbar$, as previously noted.

18.2 Effective Diffusion Coefficient

Zwanzig also proposed an improvement to the Fick-Jacobs equation. This enhancement is made by assuming that the diffusivity is not constant anymore, but rather, a longitudinal coordinate-dependent function, making the Fick-Jacobs equation take the following form:

$$\frac{\partial \rho(x,t)}{\partial t} = \frac{\partial}{\partial x}\left\{ D(x)\, \mathrm{e}^{-\beta f(x)} \frac{\partial}{\partial x}\left[\mathrm{e}^{\beta f(x)}\, \rho(x,t) \right] \right\}. \tag{18.17}$$

This new function, $D(x)$, is the so-called effective diffusion coefficient or effective diffusivity. Its calculation is a difficult task, but we will show you how to find it for systems where the boundaries interact with the diffusing particles by means of a harmonic potential and a box-like potential. The derivation presented here will be exposed for two- and three-dimensional (3D) diffusive systems.

The computation of the effective diffusion coefficient starts by integrating the 2D Smoluchowski equation calculated in the previous section, in the transversal (y) direction, namely,

$$\frac{\partial \rho(x,t)}{\partial t} = D_x \frac{\partial}{\partial x} \int \mathrm{e}^{-\beta U(x,y)} \frac{\partial}{\partial x}\left[\mathrm{e}^{\beta U(x,y)}\, c(x,y,t) \right] \mathrm{d}y. \tag{18.7}$$

Now, we consider the difference between concentration $c(x,y,t)$ and its approximation, Eq. (18.11), that is,

$$\delta c(x,y,t) = c(x,y,t) - \rho(x,t)\, \vartheta(y|x). \tag{18.18}$$

This equation can be substituted into (18.7), yielding

$$\begin{aligned} \frac{\partial \rho(x,t)}{\partial t} &= D_x \frac{\partial}{\partial x} \int \mathrm{e}^{-\beta U(x,y)} \frac{\partial}{\partial x}\left\{ \mathrm{e}^{\beta U(x,y)} \left[\delta c(x,y,t) + \rho(x,t)\, \vartheta(y|x) \right] \right\} \mathrm{d}y \\ &= D_x \frac{\partial}{\partial x} \int \mathrm{e}^{-\beta U(x,y)} \frac{\partial}{\partial x}\left[\mathrm{e}^{\beta U(x,y)} \delta c(x,y,t) \right] \mathrm{d}y \\ &\quad + D_x \frac{\partial}{\partial x} \int \mathrm{e}^{-\beta U(x,y)} \frac{\partial}{\partial x}\left[\mathrm{e}^{\beta U(x,y)} \rho(x,t)\, \vartheta(y|x) \right] \mathrm{d}y. \end{aligned} \tag{18.19}$$

The second term on the right-hand side of the previous equation can be written as

$$\begin{aligned} &\frac{\partial}{\partial x} \int \mathrm{e}^{-\beta U(x,y)} \frac{\partial}{\partial x}\left[\mathrm{e}^{\beta U(x,y)}\, \rho(x,t)\, \vartheta(y|x) \right] \mathrm{d}y \\ &\quad = \frac{\partial}{\partial x}\left\{ \mathrm{e}^{-\beta f(x)} \frac{\partial}{\partial x}\left[\mathrm{e}^{\beta f(x)}\, \rho(x,t) \right] \right\}, \end{aligned} \tag{18.20}$$

where Eq. (18.14) was used. Substituting the local equilibrium definition, Eq. (18.9), into the first term of Eq. (18.19), we arrive at

$$\frac{\partial}{\partial x}\int \mathrm{e}^{-\beta U(x,y)}\frac{\partial}{\partial x}\left[\mathrm{e}^{\beta U(x,y)}\,\delta c(x,y,t)\right]\mathrm{d}y$$
$$=\frac{\partial}{\partial x}\int \vartheta(y|x)\,\mathrm{e}^{-\beta f(x)}\,\frac{\partial}{\partial x}\left[\frac{1}{\vartheta(y|x)}\mathrm{e}^{\beta f(x)}\,\delta c(x,y,t)\right]\mathrm{d}y. \tag{18.21}$$

By inserting Eqs. (18.20) and (18.21) into Eq. (18.19), this yields

$$\frac{\partial \rho(x,t)}{\partial t}=D_x\,\frac{\partial}{\partial x}\left\{\mathrm{e}^{-\beta f(x)}\frac{\partial}{\partial x}\left[\mathrm{e}^{\beta f(x)}\,\rho(x,t)\right]\right\}$$
$$+D_x\,\frac{\partial}{\partial x}\int \vartheta(y|x)\,\mathrm{e}^{-\beta f(x)}\frac{\partial}{\partial x}\left[\frac{1}{\vartheta(y|x)}\mathrm{e}^{\beta f(x)}\,\delta c(x,y,t)\right]\mathrm{d}y. \tag{18.22}$$

Now, operating over the second right-hand side term of Eq. (18.19), one finds that

$$\frac{\partial}{\partial x}\int \vartheta(y|x)\,\mathrm{e}^{-\beta f(x)}\frac{\partial}{\partial x}\left[\frac{1}{\vartheta(y|x)}\mathrm{e}^{\beta f(x)}\,\delta c(x,y,t)\right]\mathrm{d}y$$
$$=\frac{\partial}{\partial x}\left\{\mathrm{e}^{-\beta f(x)}\int \vartheta(y|x)\frac{\partial}{\partial x}\left[\frac{1}{\vartheta(y|x)}\mathrm{e}^{\beta f(x)}\,\delta c(x,y,t)\right]\right\}\mathrm{d}y. \tag{18.23}$$

The expression inside the integral of this last equation can be modified using the chain rule for derivatives, that is,

$$\frac{\partial}{\partial x}\left[\vartheta(y|x)\frac{1}{\vartheta(y|x)}\mathrm{e}^{\beta f(x)}\,\delta c(x,y,t)\right]=\vartheta(y|x)\,\frac{\partial}{\partial x}\left[\frac{1}{\vartheta(y|x)}\mathrm{e}^{\beta f(x)}\,\delta c(x,y,t)\right]$$
$$+\frac{\partial}{\partial x}\left[\vartheta(y|x)\right]\frac{1}{\vartheta(y|x)}\mathrm{e}^{\beta f(x)}\,\delta c(x,y,t), \tag{18.24}$$

then

$$\int \vartheta(y|x)\frac{\partial}{\partial x}\left[\frac{1}{\vartheta(y|x)}\mathrm{e}^{\beta f(x)}\;\delta p(x,y,t)\right]\mathrm{d}y$$
$$=\frac{\partial}{\partial x}\int \vartheta(y|x)\frac{1}{\vartheta(y|x)}\mathrm{e}^{\beta f(x)}\,\delta c(x,y,t)\,\mathrm{d}y \tag{18.25}$$
$$-\int \frac{\partial}{\partial x}\left[\vartheta(y|x)\right]\frac{1}{\vartheta(y|x)}\mathrm{e}^{\beta f(x)}\,\delta c(x,y,t)\,\mathrm{d}y,$$

where the integral in the second term of the right-hand side will be calculated later (see Eq. (18.111)). Meanwhile, the first term on the right-hand side is

$$\frac{\partial}{\partial x}\int \vartheta(y|x)\frac{1}{\vartheta(y|x)}\mathrm{e}^{\beta f(x)}\,\delta c(x,y,t)\,\mathrm{d}y = \frac{\partial}{\partial x}\left\{\mathrm{e}^{\beta f(x)}\int \delta c(x,y,t)\,\mathrm{d}y\right\} = 0, \tag{18.26}$$

consequently,

$$\begin{aligned}&\frac{\partial}{\partial x}\int \vartheta(y|x)\,\mathrm{e}^{-\beta f(x)}\frac{\partial}{\partial x}\left\{\frac{1}{\vartheta(y|x)}\mathrm{e}^{\beta f(x)}\,\delta c(x,y,t)\right\}\,\mathrm{d}y\\ &\quad = -\frac{\partial}{\partial x}\left\{\mathrm{e}^{-\beta f(x)}\int\left[\frac{\partial}{\partial x}\vartheta(y|x)\right]\frac{\mathrm{e}^{\beta f(x)}}{\vartheta(y|x)}\delta c(x,y,t)\,\mathrm{d}y\right\},\end{aligned} \tag{18.27}$$

which can be substituted into Eq. (18.22) to obtain

$$\begin{aligned}\frac{\partial\rho(x,t)}{\partial t} &= D_x\,\frac{\partial}{\partial x}\left\{\mathrm{e}^{-\beta f(x)}\frac{\partial}{\partial x}\left[\mathrm{e}^{\beta f(x)}\,\rho(x,t)\right]\right\}\\ &\quad - D_x\,\frac{\partial}{\partial x}\left\{\mathrm{e}^{-\beta f(x)}\int\left[\frac{\partial}{\partial x}\vartheta(y|x)\right]\frac{\mathrm{e}^{\beta f(x)}}{\vartheta(y|x)}\delta c(x,y,t)\,\mathrm{d}y\right\}.\end{aligned} \tag{18.28}$$

Now we need to obtain a closed form for $\delta c(x,y,t)$. The procedure is shown in Appendix 18.A.1, and it yields

$$\delta c(x,y,t) = D_x\int_0^t \mathrm{e}^{t'\mathscr{P}}\left[\frac{\partial}{\partial x}\rho(y|x)\right]\mathrm{e}^{-\beta f(x)}\frac{\partial}{\partial x}\left[\mathrm{e}^{\beta f(x)}\,\rho(x,t-t')\right]\mathrm{d}t'. \tag{18.29}$$

Now, Eq. (18.29) is substituted into (18.28)

$$\begin{aligned}\frac{\partial\rho(x,t)}{\partial t} &= D_x\,\frac{\partial}{\partial x}\left\{\mathrm{e}^{-\beta f(x)}\frac{\partial}{\partial x}\left[\mathrm{e}^{\beta f(x)}\,\rho(x,t)\right]\right\}\\ &\quad - D_x\,\frac{\partial}{\partial x}\left\{\mathrm{e}^{-\beta f(x)}\int\left[\frac{\partial}{\partial x}\vartheta(y|x)\right]\frac{\mathrm{e}^{\beta f(x)}}{\vartheta(y|x)}\int_0^t \mathrm{e}^{t'\mathscr{P}}\left[\frac{\partial}{\partial x}\rho(y|x)\right]\right.\\ &\quad \left.\times\,\mathrm{e}^{-\beta f(x)}\frac{\partial}{\partial x}\mathrm{e}^{\beta f(x)}\rho(x,t-t')\,\mathrm{d}t'\,\mathrm{d}y\right\}\\ &= D_x\,\frac{\partial}{\partial x}\left\{\mathrm{e}^{-\beta f(x)}\frac{\partial}{\partial x}\left[\mathrm{e}^{\beta f(x)}\,\rho(x,t)\right]\right\}\\ &\quad - D_x\,\frac{\partial}{\partial x}\int\left[\frac{\partial}{\partial x}\vartheta(y|x)\right]\frac{1}{\vartheta(y|x)}\int_0^t \mathrm{e}^{t'\mathscr{P}}\left[\frac{\partial}{\partial x}\rho(y|x)\right]\\ &\quad \times\,\mathrm{e}^{-\beta f(x)}\frac{\partial}{\partial x}\left[\mathrm{e}^{\beta f(x)}\,\rho(x,t-t')\right]\mathrm{d}t'\,\mathrm{d}y.\end{aligned} \tag{18.30}$$

An additional important assumption is imposed: $\rho(x,t)$ smoothly changes with respect to x. As a consequence, in Eq. (18.102), the only term that is conserved is the one proportional to ∂_y, that is,

$$\mathscr{P}' = D_y \frac{\partial}{\partial y}\left\{ \mathrm{e}^{-\beta U(x,y)} \frac{\partial}{\partial y}\left[\mathrm{e}^{\beta U(x,y)} \right] \right\} = D_y \frac{\partial}{\partial y}\left\{ \vartheta(y|x) \frac{\partial}{\partial y}\left[\frac{1}{\vartheta(y|x)} \right] \right\}, \tag{18.31}$$

where Eq. (18.9) was used again. To simplify our results even more, we impose a Markovian approximation into Eq. (18.30). To such end, a new quantity is defined

$$\kappa(x) = D_x \int \int_0^\infty \left[\frac{\partial}{\partial x} \vartheta(y|x) \right] \frac{1}{\vartheta(y|x)} \mathrm{e}^{t\mathscr{P}'} \left[\frac{\partial}{\partial x} \vartheta(y|x) \right] \mathrm{d}t \, \mathrm{d}y, \tag{18.32}$$

consequently,

$$\begin{aligned} \frac{\partial \rho(x,t)}{\partial t} = {} & D_x \frac{\partial}{\partial x}\left\{ \mathrm{e}^{-\beta f(x)} \frac{\partial}{\partial x}\left[\mathrm{e}^{\beta f(x)} \, \rho(x,t) \right] \right\} \\ & - D_x \frac{\partial}{\partial x}\left\{ \mathrm{e}^{-\beta f(x)} \, \kappa(x) \frac{\partial}{\partial x}\left[\mathrm{e}^{\beta f(x)} \, \rho(x,t) \right] \right\}, \end{aligned} \tag{18.33}$$

from where we can finally arrive at

$$\frac{\partial \rho(x,t)}{\partial t} = D_x \frac{\partial}{\partial x}\left\{ \mathrm{e}^{-\beta f(x)} \, [1-\kappa(x)] \frac{\partial}{\partial x}\left[\mathrm{e}^{\beta f(x)} \, \rho(x,t) \right] \right\}. \tag{18.34}$$

Setting $D_x = D_0$, we have that

$$D(x) = D_0 \, [1-\kappa(x)]. \tag{18.35}$$

It is worth noting that this approximation is very poor, as will be shown in Sect. 18.4. Instead, it is much better to approximate $D(x)$ by

$$D(x) \approx \frac{D_0}{1+\kappa(x)}. \tag{18.36}$$

Substituting this last relation into Eq. (18.34), we arrive at the FJ equation with a position-dependent diffusivity, known as the *modified Fick-Jacobs equation*, or *Fick-Jacobs-Zwanzig equation*, namely,

$$\frac{\partial \rho(x,t)}{\partial t} = \frac{\partial}{\partial x}\left\{ \mathrm{e}^{-\beta f(x)} \, D(x) \, \frac{\partial}{\partial x}\left[\mathrm{e}^{\beta f(x)} \, \rho(x,t) \right] \right\}, \tag{18.37}$$

or

$$\frac{\partial \rho(x,t)}{\partial t} = \frac{\partial}{\partial x}\left\{ w(x)\, D(x)\, \frac{\partial}{\partial x}\, \frac{\rho(x,t)}{w(x)} \right\}, \tag{18.38}$$

which is the most important result of this chapter and a cornerstone in the study of diffusion under geometrical confinement.

At this point, let's propose that the term inside the square brackets in the last equation is actually an infinite series, which is why the last equality can be written. Now, the value of $\kappa(x)$ must be obtained in terms of the interaction potential between the boundaries and the diffusing particles. The procedure is presented in Appendix 18.A.2 and results in

$$\kappa(x) = \left[A'(x)\right]^2 \int z^2\, \mathrm{e}^{-\beta V(z)}\, \mathrm{d}z \Big/ \int \mathrm{e}^{-\beta V(z)}\, \mathrm{d}z. \tag{18.39}$$

Substituting this equation into the effective diffusivity, Eq. (18.35), it takes the following form:

$$D(x) = \frac{D_0}{1+\kappa(x)} = \frac{D_0}{1 + [A'(x)]^2 \int z^2\, \mathrm{e}^{-\beta V(z)}\, \mathrm{d}z \,/\, \int \mathrm{e}^{-\beta V(z)}\, \mathrm{d}z}. \tag{18.40}$$

Up to now, we have not taken account of the fact that there is no normal flux at the channel walls. This physical property can be taken into account in the potential. In the next two sections, we will use Eq. (18.40) to obtain $D(x)$ for two different potentials.

18.2.1 Harmonic Potential

Let's start by modeling the interactions between the diffusing particles and the boundaries by a harmonic potential, which is given by

$$V(z) = \frac{z^2}{2}, \qquad 0 \le z < \infty. \tag{18.41}$$

To obtain the effective diffusion coefficient for this potential, we need to calculate the integrals in the denominator of Eq. (18.40). We can solve the first integral using Eq. (A.15), then

$$\int_0^\infty z^2\, \mathrm{e}^{-\beta z^2/2} \mathrm{d}z = \int_0^\infty z^2\, \mathrm{e}^{-\alpha z^2} \mathrm{d}z = \frac{1}{4}\sqrt{\frac{\pi}{\alpha^3}} = \frac{1}{4}\sqrt{\frac{8\pi}{\beta^3}}. \tag{18.42}$$

On the other hand, the solution for the second integral is given in Eq. (A.14), yielding

$$\int_0^\infty \mathrm{e}^{-\beta z^2/2}\mathrm{d}z = \int_0^\infty \mathrm{e}^{-\alpha z^2}\mathrm{d}z = \frac{1}{2}\sqrt{\frac{\pi}{\alpha}} = \frac{1}{2}\sqrt{\frac{2\pi}{\beta}}. \tag{18.43}$$

Then, the ratio of the last two integrals is

$$\int_0^\infty z^2\mathrm{e}^{-\beta z^2/2}\mathrm{d}z \Big/ \int_0^\infty \mathrm{e}^{-\beta z^2/2}\mathrm{d}z = \frac{1}{2}\sqrt{\frac{8\pi\beta}{2\pi\beta^3}} = \frac{1}{\beta}, \tag{18.44}$$

and consequently

$$\kappa(x) = \left[A'(x)\right]^2 \frac{1}{\beta} = \left[A'(x)\right]^2 k_B T. \tag{18.45}$$

Finally, the effective diffusivity for a harmonic potential is

$$D(x) = \frac{D}{1+\kappa(x)} = \frac{D}{1+\left[A'(x)\right]^2 k_B T}. \tag{18.46}$$

18.2.2 Box-Like Potential

In this section, we will obtain the most used position-dependent effective diffusivity, by means of the box-like potential, which can be described as

$$V(z) = 0, \qquad -1 \le z \le 1. \tag{18.47}$$

The calculation of the integrals in Eq. (18.40) is carried out as follows:

$$\int_{-1}^{1} z^2\,\mathrm{e}^{-\beta\cdot 0}\mathrm{d}z = \int_{-1}^{1} z^2\mathrm{d}z = \frac{1}{3}z^3\Big|_{-1}^{1} = \frac{2}{3}, \tag{18.48}$$

and

$$\int_{-1}^{1} \mathrm{e}^{-\beta\cdot 0}\mathrm{d}z = 2. \tag{18.49}$$

Taking their ratio yields

$$\int_{-1}^{1} z^2\,\mathrm{e}^{-\beta\cdot 0}\,\mathrm{d}z \Big/ \int_{-1}^{1} \mathrm{e}^{-\beta\cdot 0}\,\mathrm{d}z = \frac{1}{3}, \tag{18.50}$$

and consequently, $\kappa(x)$ is

$$\kappa(x) = \frac{1}{3}\left[A'(x)\right]^2. \tag{18.51}$$

Finally, for a box-like potential, the effective diffusivity is

$$D(x) = \frac{D_0}{1+\kappa(x)} = \frac{D_0}{1+\frac{1}{3}\left[A'(x)\right]^2}, \tag{18.52}$$

which, written in terms of the channel's width derivative $w'(x) = 2A'(x)$, is

$$D(x) = \frac{D_0}{1+\kappa(x)} = \frac{D_0}{1+\frac{1}{12}w'^2(x)}. \tag{18.53}$$

This is a remarkable result. When the system is confined, the resulting $D(x)$ is independent of the temperature. Its dependence is by means of the confinement's geometrical parameters, so the interactions are ruled by an *entropic potential*. In other words, the boundaries can be effectively described by a temperature-independent potential.

18.3 Zwanzig's Derivation of the FJ Equation in 3D

The derivation for the one-dimensional reduction for a three-dimensional (3D) tube and a two-dimensional (2D) channel follow essentially the same steps. In the 3D derivation, the tube is assumed to have cylindrical symmetry. As in the 2D case, the potential is assumed to have the form $V(r/w(z))$. The differential equation for the evolution of the marginal concentration has the same structure as the modified FJ equation in 2D, Eq. (18.37). The main differences are that, in 3D, to obtain the marginal equation, the integration in the transverse coordinates involves y and z and is given by

$$\rho(x,t) \equiv \int_0^{R(x)} c(x,y,z,t)\,\mathrm{d}y\mathrm{d}z, \tag{18.54}$$

where $R(x)$ is the radius of the tube and its area is $A(x) = 2\pi R(x)^2$ and

$$\mathrm{e}^{-\beta f(x)} = A(x), \tag{18.55}$$

so consequently,

$$\frac{\partial \rho(x,t)}{\partial t} = \frac{\partial}{\partial x}\left\{A(x)\,D(x)\,\frac{\partial}{\partial x}\,\frac{\rho(x,t)}{A(x)}\right\}. \tag{18.56}$$

Using cylindrical coordinates (see Appendix B.2), the center line corresponds to the z axis, and the radial coordinate is r. The position-dependent diffusion coefficient has the same form as in Eq. (18.39), except that now we have to integrate over the cross-sectional area, namely,

$$\kappa(x) = \left[R'(x)\right]^2 \int z^2 \, \mathrm{e}^{-\beta V(z)} \, \mathrm{d}z \Big/ \int \mathrm{e}^{-\beta V(z)} \, \mathrm{d}z, \tag{18.57}$$

where $r(x)$ is the variable tube radius. Performing the integrals, we have

$$\int_0^1 \int_0^{2\pi} r^2 \, \mathrm{e}^{-\beta \cdot 0} r \mathrm{d}r\mathrm{d}\phi = 2\pi \int_0^1 r^3 \mathrm{d}r = \frac{2\pi}{4} r^4 \Big|_0^1 = \frac{\pi}{2}, \tag{18.58}$$

and

$$\int_0^1 \int_0^{2\pi} \mathrm{e}^{-\beta \cdot 0} r \mathrm{d}r\mathrm{d}\phi = \frac{2\pi}{2} r^2 \Big|_0^1 = \pi, \tag{18.59}$$

so consequently,

$$\int_0^1 \int_0^{2\pi} r^2 r \mathrm{d}r\mathrm{d}\phi \Big/ \int_0^1 \int_0^{2\pi} r \mathrm{d}r\mathrm{d}\phi = \frac{1}{2}. \tag{18.60}$$

Substituting this last result into Eq. (18.57), $\kappa(x)$ becomes

$$\kappa(x) = \frac{1}{2} \left[R'(x)\right]^2. \tag{18.61}$$

Finally, for a box-like potential, the effective diffusivity in 3D is

$$D(x) \approx \frac{D_0}{1 + \kappa(x)} = \frac{D_0}{1 + \frac{1}{2} R'^2(x)}. \tag{18.62}$$

Summarizing, in a 3D tube with cylindrical symmetry $w(x)$ is the radius of the tube at x, $R(x)$, and $\mathrm{e}^{-\beta f(x)} = \pi R(x)^2$. Since in a 2D channel $w(x)$ is the half width, $w(x) = 2h(x)$, and $\mathrm{e}^{-\beta f(x)} = h(x)$. For a box-like potential, both dependent-position effective diffusion constants are

$$D(x) \approx \frac{D_0}{1 + \gamma w'(x)^2}, \tag{18.63}$$

where γ is 1/3 for a 2D channel and 1/2 for a 3D tube.

18.4 3D Hyperboloidal Cone

In this section we will compare Zwanzig's theoretical approach to a specific example. Unfortunately, there are very few exactly solved problems that can be used for this test. One of them is the steady-state diffusion through a three-dimensional hyperboloidal cone, shown in Fig. 18.1, using the following boundary conditions: an absorbing boundary is placed on the small exit hole or bottleneck, and at the opposite end of the infinite cone, a constant concentration c_0 is imposed. It is convenient to describe the shape of the tube using oblate spheroidal coordinates (ξ, η, ϕ)[1] (see Fig. 18.2), which are related to cylindrical coordinates (r, z, ϕ) by

$$r^2 = a^2(\xi^2 + 1)(1 - \eta^2), \quad z = a\xi\eta. \tag{18.65}$$

In this coordinate system, η is the angular coordinate, ranging from $[-1, 1]$, ξ is the radial coordinate that goes from $(-\infty, \infty)$, ϕ is the azimuth coordinate ranging from $[0, 2\pi]$, and a is the focal distance. The surface $\eta = 1$ corresponds to the positive z axis, whereas when $\eta = 0$, the surface becomes the x, y plane except for the part that is inside the circle of radius a. The surfaces' ξ constant >0 are flattened spheroids of thickness $2\xi a$ and of radius, at the equator, of $a\sqrt{\xi^2 + 1}$ (see Fig. 18.3a). The surfaces' η constant are hyperboloids of one sheet, asymptotic to the cone of angle $\arccos(\eta)$ with respect to the z axis (see Fig. 18.3b). Semi-planes can be constructed for constant ϕ and varying ξ and η.

The surface of a semi-infinite hyperboloidal cone is made by fixing $\eta = \eta_0$, where η goes from η_0 to 1, varying ϕ from 0 to 2π, and ξ from 0 to ∞. Then, the

[1] Oblate spheroidal coordinates can be defined by the following transformation:

$$\begin{aligned} x &= a\sqrt{1+\xi^2}\sqrt{1-\eta^2}\cos(\phi), \\ y &= a\sqrt{1+\xi^2}\sqrt{1-\eta^2}\sin(\phi) \\ z &= a\xi\eta, \end{aligned}$$

where (x, y, z) correspond to the Cartesian components. The oblate spheroidal coordinate system is related to the spherical system at the limit $a \to 0$. The scale factors for (r, z, ϕ) are

$$\begin{aligned} h_\xi &= a\sqrt{\frac{\xi^2+\eta^2}{1+\xi^2}}, \\ h_\eta &= a\sqrt{\frac{\xi^2+\eta^2}{1-\eta^2}}, \\ h_\phi &= a\sqrt{(1+\xi^2)(1-\eta^2)}. \end{aligned} \tag{18.64}$$

The infinitesimal volume element is $dV = a^3(\xi^2 + \eta^2)\mathrm{d}\xi\mathrm{d}\eta\mathrm{d}\phi$. At constant ξ the infinitesimal area element is $dA = a^2\sqrt{(\xi^2 + \eta^2)(1 - \xi^2)}\mathrm{d}\eta\mathrm{d}\phi$.

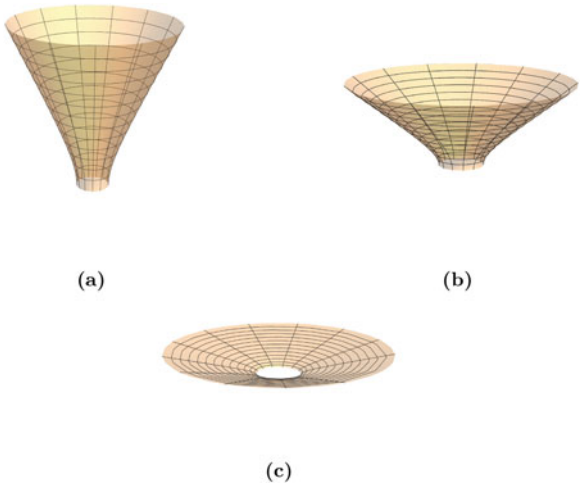

Fig. 18.1 Three-dimensional hyperboloidal cone with cylindrical symmetry. The tubes are obtained when setting $0 < \xi < 5$ and $a = 1$ for three different values of η_0. (**a**) $\eta_0 = 0.9$. (**b**) $\eta_0 = 0.6$. (**c**) $\eta_0 = 0.2$

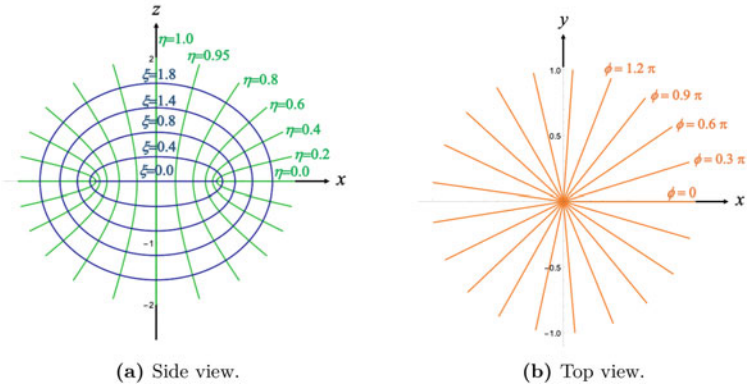

(**a**) Side view. (**b**) Top view.

Fig. 18.2 Oblate spheroidal coordinates (ξ, η, ϕ). (**a**) The curves of constant ξ and η are the blue ellipses and the green half-hyperbolae, respectively. (**b**) The lines of constant ϕ are in orange, which lie over the $x - y$ plane

bottleneck is at $\xi = 0$ and the far end of the tube at $\xi \to \infty$. Then, diffusion takes place into the following region:

$$0 < \xi < \infty, \quad \eta_0 < \eta < 1, \quad 0 < \phi < 2\pi. \tag{18.66}$$

Because of the symmetry, concentration is not dependent on the angle ϕ. Therefore, the steady-state diffusion equation in these coordinates is

$$\nabla^2 c(\xi, \eta) = \frac{1}{a(\xi^2 + \eta^2)} \left\{ \frac{\partial}{\partial \xi} \left(1 + \xi^2\right) \frac{\partial c(\xi, \eta)}{\partial \xi} + \frac{\partial}{\partial \eta} \left(1 - \eta^2\right) \frac{\partial c(\xi, \eta)}{\partial \eta} \right\} = 0. \tag{18.67}$$

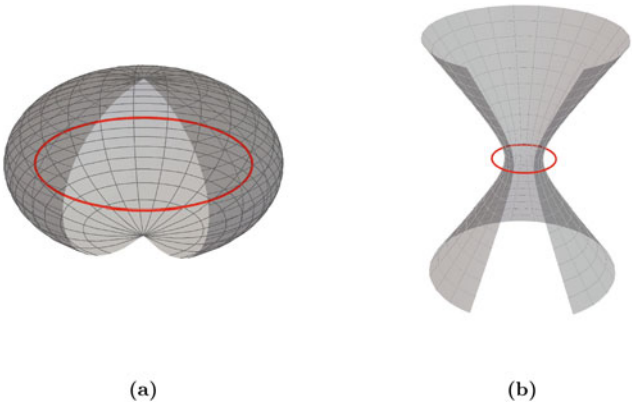

Fig. 18.3 The level surface is an oblate spheroid for ξ constant and varying η and ϕ and a one-sheet hyperboloid for a constant η and varying ξ and ϕ. The red circle shows the focal circle a. (**a**) Oblate spheroid. (**b**) Hyperboloid of one sheet

A solution for this differential equation can be proposed from the observation that the derivative of arctan (ξ) is equal to $(1+\xi^2)^{-1}$, which reduces with the scale factor h_ξ, nullifying the second derivative with respect to ξ in Eq. (18.67). Therefore, a solution is given by

$$c(\xi) = \mathcal{A} \arctan(\xi) + \mathcal{P}, \tag{18.68}$$

where $\mathcal{A}$ and $\mathcal{P}$ are constants, which we will be setting by means of the boundaries conditions. The same result is obtained by integrating Eq. (18.67) if we assume that the concentration only depends on ξ. The differential equation (18.67) was solved previously using the separation of variables method (for further details see Sect. 14.6). Imposing the boundary conditions, $c(\xi = 0, \eta) = 0$ and $c(\xi, \eta) = c_0$ for $\xi \to \infty$, Eq. (18.68) becomes

$$c(\xi) = \frac{2}{\pi} c_0 \arctan(\xi). \tag{18.69}$$

This solution also fulfills the no-flux condition on the surface:

$$\left.\frac{\partial c(\xi)}{\partial \eta}\right|_{\eta=\eta_0} = 0. \tag{18.70}$$

Once we have the steady-state concentration, we can obtain the flux, which in these coordinates is given by

$$\mathbf{J}(\xi,\eta) = -D_0 \nabla c(\xi) = -\frac{D_0}{a}\sqrt{\frac{1+\xi^2}{\xi^2+\eta^2}}\,\frac{\partial c(\xi)}{\partial \xi}\,\hat{\mathbf{e}}_\xi = \frac{2D_0}{\pi a}\sqrt{\frac{1+\xi^2}{\xi^2+\eta^2}}\,\frac{1}{1+\xi^2}\,c_0\,\hat{\mathbf{e}}_\xi, \tag{18.71}$$

where D_0 is the bulk diffusivity. Then, the normal flux through the bottleneck is

$$J(\xi=0,\eta) = \mathbf{J}(\xi,\eta)\Big|_{\xi=0}\cdot(-\hat{\mathbf{e}}_\xi) = D_0\,\frac{2}{\pi a \eta}\,c_0. \tag{18.72}$$

Using this last equation, we can calculate the current flow, I_{ss}, and using this result, we can also calculate the association rate constant. We also need to calculate the surface integral of the flux over the bottleneck, namely,

$$I_{ss} = \int_{\eta_0}^{1}\int_0^{2\pi} D_0\,\frac{2}{\pi a\eta}c_0\,a^2\eta \mathrm{d}\eta \mathrm{d}\phi = 4D_0 a(1-\eta_0)c_0. \tag{18.73}$$

From this last equation, we can see that the association rate constant is

$$\mathrm{k}_{hc} = 4D_0 a(1-\eta_0). \tag{18.74}$$

When $\eta_0 = 0$, the association rate constant for a disk-like absorber on a flat wall, given by Eq. (4.22), is recovered as expected.

Now, by means of Eq. (18.73), which is a simple and exact result, we can test the theoretical approximations obtained by Zwanzig's approach.

To such end, let's calculate the predictions for current flux for the three-dimensional hyperboloidal cone obtained through Zwanzig's 1D reduction. The starting point is the modified Fick-Jacobs equation for a 3D tube, substituting the entropic potential, Eq. (18.16), and the cross-sectional area $A(z)$ leads to

$$\frac{\partial c(z,t)}{\partial t} = \frac{\partial}{\partial z}\left\{A(z)\;D(z)\;\frac{\partial}{\partial z}\left[\frac{\rho(z,t)}{A(z)}\right]\right\}. \tag{18.75}$$

Then, the steady-state flux, J_{ss}, is given by

$$J_{ss} = A(z)\;D(z)\;\frac{\partial}{\partial z}\left[\frac{\rho(z)}{A(z)}\right]. \tag{18.76}$$

Let's rewrite this equation in the following form:

$$\frac{\rho(z)}{A(z)} = J_{ss}\int_0^z \frac{\frac{\partial}{\partial z'}}{D(z'A(z'))}. \tag{18.77}$$

The benefits will be clearly seen below. To be consistent with our 1D reduction, we can approximate $\rho(z)$ from the definition of the marginal concentration,

Eq. (18.4). Because the concentration now only depends on ξ, or z, the integral becomes

$$\rho(z) = c(z) \int_{\eta_0}^{1} \int_{0}^{2\pi} a^2 \eta \mathrm{d}\eta \mathrm{d}\phi = A(z)c(z). \tag{18.78}$$

Using the boundary condition when z goes to infinity, we have that $\rho(z) = A(z)c_0$, and substituting this relation into Eq. (18.77), and taking the limit when z goes to infinity, leads to

$$I_{ss} = J_{ss} = c_0 \int_0^{\infty} \frac{\mathrm{d}z'}{D(z')A(z')}. \tag{18.79}$$

The equality $I_{ss} = J_{ss}$ is because the current flux coincides with the flux in 1D.

Finally, we can test the theoretical approximations by comparing Eq. (18.79) with the exact result given by Eq. (18.74). It is worth noting that even when we calculate the flux for a very distant z, it is the same as that for the absorbing bottleneck, given that, in 1D, the steady-state flux does not depend on the space coordinates, but rather, it is constant, and consequently, the concentration is a linear function. These results come from the continuity equation, Eq. (2.71).

To perform the integral in Eq. (18.79), we first have to find the formula for the cross-sectional area of a hyperboloidal cone, $A(z)$, as well as the derivative of the radius at z to be used in Eq. (18.62). On the surface of the tube, $z = a\xi\eta_0$ or $\xi = z/a\eta_0$. Then, from Eq. (18.65), we have that

$$r(z)^2 = \left(\frac{1}{\eta_0} - 1\right)\left(z^2 + a^2\eta_0^2\right), \tag{18.80}$$

where $A(z) = \pi R(z)^2$. Taking the derivative of $R(z)$ with respect to z, we arrive at the following relation:

$$R'(z) = \frac{\left(\frac{1}{\eta^2} - 1\right) z}{\sqrt{\left(\frac{1}{\eta^2} - 1\right)\left(a^2\eta^2 + z^2\right)}}. \tag{18.81}$$

The effective diffusivity for the FJ approximation is obtained when approximating $D(z) \approx D_0$. Direct substitution of this approximation and the cross-sectional area $A(z)$ into the integral (18.79) leads to

$$I_{ss}^{\mathrm{FJ}} = 2\sqrt{\frac{1}{\eta^2}}\left(1 - \eta^2\right). \tag{18.82}$$

On the other hand, substituting Eq. (18.81) into the effective diffusivity predicted by Zwanzig, Eq. (18.62), becomes

$$D(x) \approx D_{\mathrm{Zw}}(x) = \frac{D_0}{1 + \frac{1}{2}r'(z)^2} = D_0 \left[1 + \frac{\left(\frac{1}{\eta^2} - 1\right) z^2}{2\left(a^2\eta^2 + z^2\right)} \right]^{-1}. \tag{18.83}$$

Substituting $A(z)$ and Eq. (18.83) into Eq. (18.79), we find that the predicted current flux is

$$I_{ss}^{\mathrm{Zw}} = \frac{8\eta\left(1 - \eta^2\right)}{1 + 3\eta^2}. \tag{18.84}$$

Now we will calculate the current flux using the approximation for $D(x)$ given by Eq. (18.35), namely, $D_0\left[1 - \frac{1}{2}R'(x)^2\right]$. Our main intention is to show that under this approximation predictions are very poor, this being the main reason why Zwanzig proposed Eq. (18.62) instead. Under this approximation, we arrive at the following equation:

$$I_{ss}^{\text{Zw-2}} = \frac{8\eta\left(1 - \eta^2\right)}{3\eta^2 + 1}. \tag{18.85}$$

Figure 18.4 shows a comparison of the exact value of the current flux at the bottleneck of the hyperboloidal cone, Eq. (18.73), with the FJ and the modified FJ approach using the two possible approximations for $D(x)$, in the latter case. As we can see, the modified FJ considerably extends the application of the FJ reduction when using Eq. (18.84). On the contrary, very poor results are obtained when using Eqs. (18.82) and (18.85). All of them fail as η_0 decreases, when the tube becomes a flat wall. We can conclude that the modified FJ is effective for treating diffusion

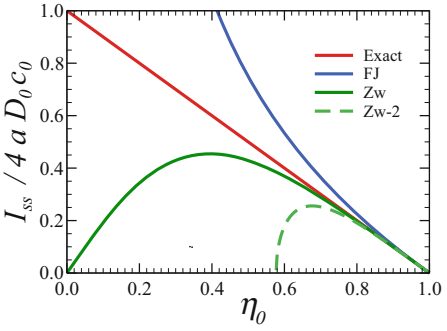

Fig. 18.4 The current flux through the bottleneck of the hyperboloidal cone normalized by $4aD_0c_0$ is plotted against η_0, setting $a = D_0 = 1$ and $0 < \xi < 5$. Comparison of the exact expression for the steady-state current flux given by Eq. (18.73) (solid red line) against the approximation values by FJ, Eq. (18.82), and the modified FJ equation, Eq. (18.84), depicted by the blue and green solid lines, respectively. The result obtained with Eq. (18.85) is represented by the dashed green line

in a tube of varying cross sections when its shape does not change to quickly, *i.e.*, when $| R'(x) | \ll 1$ by means of Eq. (18.83). These criteria are also applicable for the two-dimensional case.

18.5 The Effective Diffusion Coefficient

18.5.1 Exact Formula for the Hyperboloidal Cone

Fortunately, we can go further into the analysis and compare the 1D reduction to an exact value for the position-dependent effective diffusion coefficient, because an exact formula can be obtained for the hyperboloidal cone. To such end, we have to compare the flux obtained by the marginal concentration with a dependent-position effective diffusivity, Eq. (17.24),

$$J(z) = -D(z)A(z)\frac{\partial}{\partial z}\frac{\rho(z)}{A(z)}, \tag{18.86}$$

with the exact expression for the flux given by Eq. (18.74), $J_{ss} = 4D_0 a(1-\eta_0)c_0$. From Eq. (18.86), we see that there are many steps involved in calculating $J(z)$. First we have to calculate $\rho(z)$, divide it over $A(z)$, and take the derivative with respect to (z). Consequently, the first step is to calculate the flux from the marginal concentration, $\rho(z)$. As we know that the concentration is given by Eq. (18.69), $c(\xi) = (2/\pi)c_0 \arctan(\xi)$, we can calculate this marginal concentration using Eq. (18.4), which in oblate coordinates becomes

$$\rho(\xi) = \int_0^{2\pi}\int_{\eta_0}^{1} c(\xi)\, a^2\sqrt{(\xi^2+\eta^2)(1-\xi^2)}\mathrm{d}\eta\mathrm{d}\phi. \tag{18.87}$$

The result of this integral is less complicated to manipulate algebraically if we rewrite it in cylindrical coordinates, namely,

$$\rho(z) = \int_0^{2\pi}\int_0^{R(z)} c(z)\, r\mathrm{d}r\mathrm{d}\phi, \tag{18.88}$$

where $R(z)$ is the radius at a given z. Performing the integral over ϕ, we have 2π. To perform the integral over r, we go from 0 to $R(z)$. In such a case, $2r\,\mathrm{d}r = 2y\,\mathrm{d}y = \mathrm{d}r^2$, then

$$\rho(z) = \pi\int_0^{R(z)} c(z)\,\mathrm{d}r^2\,\mathrm{d}\phi. \tag{18.89}$$

To find a relation between $\mathrm{d}r^2$ and $\mathrm{d}\xi$ at constant z, we have to use the relation between oblate spherical and cylindrical coordinates, Eq. (18.65), and the formula for the radius given by Eq. (18.80), then

$$\frac{\mathrm{d}r^2}{\mathrm{d}\xi} = 2a^2\xi + \frac{2z^2}{\xi^3}\,\mathrm{d}\xi. \tag{18.90}$$

Consequently, Eq. (18.89) can be rewritten as

$$\rho(\xi) = 2c_0 \int_{z/a}^{z/a\eta_0} 2\left(a^2\xi + \frac{z^2}{\xi^3}\right) \arctan(\xi)\,\mathrm{d}\xi. \tag{18.91}$$

This integral can be solved by parts, leading to

$$\rho(\xi) = 2c_0 \left\{ \left[\left(a^2\xi^2 - \frac{z^2}{\xi^2}\right) \arctan(\xi) \right]_{z/a}^{z/a\eta_0} - \int_{z/a}^{z/a\eta_0} \left(a^2\xi^2 - \frac{z^2}{\xi^2}\right) \frac{\mathrm{d}\xi}{\xi^2+1} \right\}. \tag{18.92}$$

After performing the integral on the right-hand side and evaluating the whole expression, we arrive at

$$\rho(z) = 2c_0 \left[\frac{(1-\eta_0^2)\left(a^2\eta_0^2 + z^2\right) \arctan\left(\frac{zx}{a\eta_0}\right)}{\eta_0^2} - \frac{az(1-\eta_0)^2}{\eta_0} \right]. \tag{18.93}$$

Dividing this last expression by $A(z) = \pi R(z)^2$ leads to

$$\frac{\rho(z)}{A(z)} = \frac{2c_0}{\pi} \arctan\left(\frac{z}{a\eta_0}\right) - \frac{2ac_0(1-\eta_0)\eta_0\, z}{\pi(1+\eta_0)\left(a^2\eta_0^2 + z^2\right)}. \tag{18.94}$$

Substituting this last expression into Eq. (18.86) and equating it with Eq. (18.74), we find that

$$4aD(z)\frac{(\eta-1)\left(a^2\eta_0^3 + x^2\right)}{\eta_0\left(a^2\eta_0^2 + x^2\right)}c_0 = 4aD_0(1-\eta_0)c_0. \tag{18.95}$$

Finally, solving for $D(x)$, the exact formula for the position-dependent effective diffusivity for the hyperboloid cone is

$$D(z) = \frac{\eta_0(z^2 + \eta_0^2a^2)}{z^2 + \eta_0^3a^2}D_0. \tag{18.96}$$

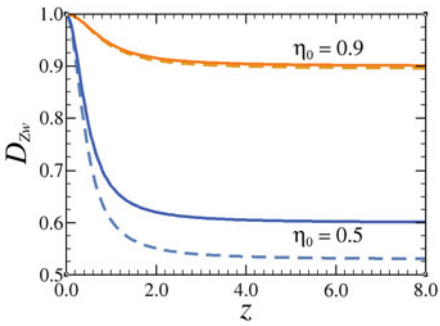

Fig. 18.5 Effective diffusion coefficient $D(z)$, dependent on the longitudinal coordinate z, for the 3D hyperboloidal cone, setting $a = 1$ and $\eta_0 = 0.9$ and $\eta_0 = 0.6$. The solid lines depict the exact function, Eq. (18.96); dashed lines represent the approximation given by Eq. (18.83)

This formula was derived by P. Kalinay and J. Percus, and its limits are when z goes to zero $D(x) = D_0$ and when $z \to \infty$, $D(x) = \eta_0 D_0$.

The effective diffusivities predicted by Eq. (18.96), that is dependent on the longitudinal z-coordinate, are shown in Fig. 18.5 for $\eta_0 = 0.6$ and $\eta_0 = 0.5$ by solid lines, where $a = D_0 = 1$. As we can see, close to the bottleneck, around $z = 0$, the value of the effective diffusivity is D_0, where $D_z = D_0$. This is because the shape of the bottleneck is like a cylindrical tube. Because of its angular symmetry, the diffusion process into a tube is described by one-dimensional. As the bottleneck begins to become a straight cone, a drastic decrease in the coefficient is observed due to the large space that the particles now have to diffuse, which makes their diffusion in the longitudinal axis slower. As $\eta_0 \to 0$ the decay is more abrupt. Finally, the particles that are far away from the bottleneck explore the straight cone and experience a constant diffusion coefficient. The values of this constant is $\eta_0 D_0$. Then, for a cylindrical tube, when $\eta_0 \to 1$, we recover D_0. On the other hand, when $\eta_0 \to 0$, the effective diffusivity goes to 0.

The comparison of Eq. (18.96) formula with the approximation equation obtained by Zwanzig, Eq. (18.83), is shown in Fig. 18.4 for two values of η_0. As we can see, Eq. (18.83) is only accurate for η_0's no smaller than 0.6, as we expected from Fig. 18.5.

It is worth noting that when $\xi \to \infty$, the shape of the hyperboloidal cone becomes a conical tube. In such a case, Eq. (18.96) predicts that the effective diffusion coefficient is constant and given by $D(z) = \eta_0 D_0$. On the other hand, this cone has an angle $\theta = \arccos(\eta_0)$ with respect to the z axis. If the radius of these cones is given by $r(z) = \lambda x + b$, then the slope λ is given by $\lambda = \tan(\theta)$. Consequently,

$$D(z) = \cos(\arctan(\lambda)) D_0 = \frac{D_0}{\sqrt{1+\lambda^2}}. \tag{18.97}$$

The relation on the right-hand side is obtained by using the definitions of the cosine and tangent functions. Applying the same limit to the concentration, Eq. (18.69), the prediction is that, in a conical tube, the concentration is constant and given by c_0 at the steady-state.

18.5.2 Mean Square and Transient Behavior

To help readers gain further insight on the physical meaning of effective diffusion coefficient or effective diffusivity, in this section we will study the mean square displacement of a Brownian point-like particles under confinement.

Free diffusion of unbiased motion is a coarse-grained description that is applicable at sufficiently long times: When the typical displacement of the diffusing particle exceeds a characteristic length scale associated with the heterogeneity of the medium. For example, the description of the motion of water in terms of self-diffusion is applicable at times greater than 100 ps when the average displacement exceeds the average distance between water molecules. In crystalline solids, the description of diffusion works for times when the displacement exceeds the lattice period. On the other hand, diffusion in biological systems frequently occurs in microheterogeneous media where the description in terms of effective free diffusion may become applicable only for times that are comparable to or even longer than the duration of the experiment. The effective diffusion coefficient associated with this coarse-grained description is commonly calculated from the data obtained from mean-square displacements, $\langle \Delta \mathbf{r}^2(t) \rangle$, which are frequently described by the dependency $\langle \Delta \mathbf{r}^2(t) \rangle \propto t^{\alpha}$. For free diffusion, the exponent α is unity and reached before a transient behavior, when $\alpha < 1$ is a fingerprint of anomalous subdiffusion. The fundamental difference between the transient behavior and anomalous subdiffusion is that the exponent α is a function of time in the former case, but a constant in the case of anomalous subdiffusion.

To illustrate the transient behavior until the effective diffusivity is reached, let's consider the hyperboloidal cone with cylindrical symmetry, shown in Fig. 18.1a, which has an absorbing bottleneck, assuming that the particle's initial position is uniformly distributed.

The time dependence of the mean-square displacement obtained by simulations is shown in Fig. 18.6. As we can see from this figure, α goes form unity, for a free particle diffusing, following for a transient behavior, where α depends on time and goes from values less than unity, reaches a minimum, and then goes to unity again (see inset in Fig. 18.6), where the diffusion coefficient can be described by an

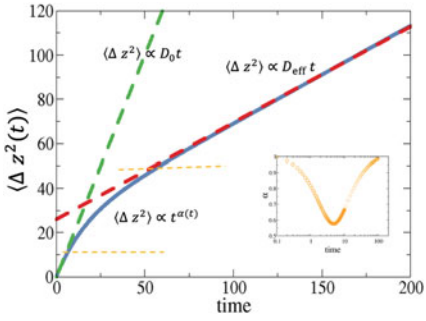

Fig. 18.6 The main square displacement of a Brownian particle along the z axis of a hyperboloidal cone with and absorbing end (blue continues line). The system parameters in dimensionless units: $0 < \xi < 5$, $\eta_0 = 0.8$, $a = 1$, and $D_0 = 1$. The dependence on time of α is shown in the inset

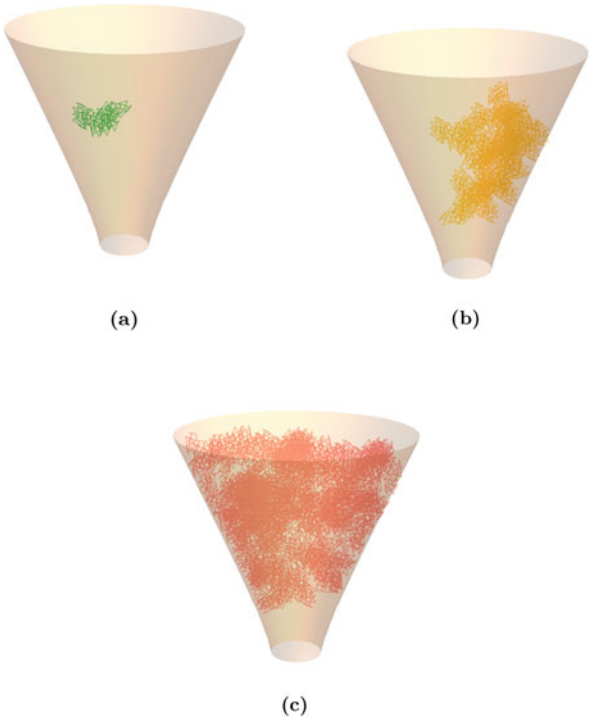

Fig. 18.7 Typical trajectories of a Brownian particle in a hyperboloidal cone setting $\eta_0 = 0.8$. (**a**) Shortly after starting its path the Brownian particle follows free diffusion. (**b**) The Brownian particle begins to realize the presence of dead ends. (**c**) Once the Brownian particles have had enough time to explore the system, the process can be described by means of an effective diffusion coefficient

effective diffusivity coefficient. This description is a fingerprint of diffusion under confinement.

To gain deeper insight, let's take a look at the typical trajectories of a Brownian particle diffusing into our system, shown in Fig. 18.7. Let's assume that our Brownian particle starts its trajectory at the cylinder tube. As we can see from Fig. 18.7a, at first it is not aware of the presence of dead ends. Consequently, its mean square displacement is proportional to t and its diffusivity equals to D_0. As times goes by, the particle begins to realize the presence of the dead ends, but while the particle continues to explore, the mean square displacement is proportional to $t^{\alpha(t)}$ (see Fig. 18.7b). Finally, once the particle has had enough time to equilibrate into the system, as shown in Fig. 18.7c, α is unity again, and the diffusion coefficient value reaches a plateau and can then be represented as an effective diffusion coefficient.

It is worth mentioning that theoretically finding the effective coefficients as function of the position and geometric parameters of the constraints is one of the main tasks when studying diffusion under confinement. An in-depth study of this is included in the following chapters.

18.6 Concluding Remarks

In this chapter, we reviewed the main ideas of Robert Zwanzig to arrive at a more general and rigorous derivation of the Fick-Jacobs equation. The method consists of performing a reduction in the number of coordinates from the two- or three-dimensional Smoluchowski equation to a one-dimensional description. The key point of this derivation is the assumption of equilibration in the transverse direction.

Finally, Zwanzig showed that the range of applicability of the Fick-Jacobs equation can be extended by introducing a position-dependent effective diffusion coefficient, also known as the modified Fick-Jacobs equation. He derived explicit formulas for effective diffusivity by treating the channel width variation rate, $w'(x)$, as a small parameter. It is also worth noting that Zwanzig showed that the modified Fick-Jacobs equation is equivalent to Smoluchowski's equation, if one defines an entropic potential that is proportional to $w(x)/w(0)$.

We also discussed the main properties of the diffusion coefficient's transient behavior as function of time. We find that as t goes from zero to infinity, this time dependence monotonically decreases from D_0 to D_{eff}, where D_0 is the bulk diffusivity and D_{eff} is the effective diffusion coefficient in the presence of confinement. This transient behavior ultimately reaches an effective diffusivity, which is a fingerprint of diffusion under confinement. This effective diffusivity is dependent on geometrical parameters and position.

The most important equations that were obtained in this chapter are listed below:

$$\frac{\partial \rho(x,t)}{\partial t} = \frac{\partial}{\partial x}\left[D(x)\, w(x) \frac{\partial}{\partial x} \frac{\rho(x,t)}{w(x)} \right]$$

(Modified Fick-Jacobs equation in 2D)

$$\frac{\partial \rho(x,t)}{\partial t} = \frac{\partial}{\partial x}\left[D(x)\, A(x) \frac{\partial}{\partial x} \frac{\rho(x,t)}{A(x)} \right]$$

(Modified Fick-Jacobs equation in 3D)

$$D(x)_{\text{Zw}} \approx \frac{D_0}{1 + \frac{1}{12} w'^2(x)}.$$

(2D Zwanzig effective diffusivity)

$$D(x)_{\text{Zw}} \approx \frac{D_0}{1 + \frac{1}{2} R'^2(x)}.$$

(3D Zwanzig effective diffusivity)

$$D(z) = \frac{\eta_0 (z^2 + \eta_0^2 a^2)}{z^2 + \eta_0^3 a^2} D_0.$$

(Effective diffusivity for a hyperboloidal cone)

18.A Mathematical Computations

18.A.1 Derivation of Eq. (18.29)

The first step to arrive at Eq. (18.29) is to take the derivative of $\delta c(x, y, t)$ with respect to time

$$\begin{aligned}\frac{\partial \delta c(x,y,t)}{\partial t} &= \frac{\partial c(x,y,t)}{\partial t} - \frac{\partial}{\partial t}\left[\rho(x,t)\ \vartheta(y|x)\right] \\ &= \frac{\partial c(x,y,t)}{\partial t} - \vartheta(y|x)\ \frac{\partial \rho(x,t)}{\partial t}.\end{aligned} \tag{18.98}$$

Substituting Eqs. (18.1) and (18.22) into this last expression yields

$$\begin{aligned}\frac{\partial \delta c(x,y,t)}{\partial t} &= D_x\ \frac{\partial}{\partial x}\left\{\mathrm{e}^{-\beta U(x,y)}\frac{\partial}{\partial x}\left[\mathrm{e}^{\beta U(x,y)}\ c(x,y,t)\right]\right\} \\ &\quad + D_y\ \frac{\partial}{\partial y}\left\{\mathrm{e}^{-\beta U(x,y)}\frac{\partial}{\partial y}\left[\mathrm{e}^{\beta U(x,y)}\ c(x,y,t)\right]\right\} \\ &\quad - D_x\ \vartheta(y|x)\frac{\partial}{\partial x}\left\{\mathrm{e}^{-\beta f(x)}\frac{\partial}{\partial x}\left[\mathrm{e}^{\beta f(x)}\ \rho(x,t)\right]\right\} \\ &\quad - D_x\ \vartheta(y|x)\frac{\partial}{\partial x}\int \vartheta(y|x)\ \mathrm{e}^{-\beta f(x)}\frac{\partial}{\partial x}\left[\frac{1}{\vartheta(y|x)}\mathrm{e}^{\beta f(x)}\ \delta c(x,y,t)\right]\mathrm{d}y.\end{aligned} \tag{18.99}$$

Recalling that $c(x, y, t) = \delta c(x, y, t) + \rho(x, t)\vartheta(y|x)$, we find

$$\begin{aligned}\frac{\partial \delta c(x,y,t)}{\partial t} &= D_x\ \frac{\partial}{\partial x}\left\{\mathrm{e}^{-\beta U(x,y)}\frac{\partial}{\partial x}\left[\mathrm{e}^{\beta U(x,y)}\ \delta c(x,y,t)\right]\right\} \\ &\quad + D_y\ \frac{\partial}{\partial y}\left\{\mathrm{e}^{-\beta U(x,y)}\frac{\partial}{\partial y}\left[\mathrm{e}^{\beta U(x,y)}\ \delta c(x,y,t)\right]\right\} \\ &\quad + D_x\ \frac{\partial}{\partial x}\left\{\mathrm{e}^{-\beta U(x,y)}\frac{\partial}{\partial x}\left[\mathrm{e}^{\beta U(x,y)}\vartheta(y|x)\ \rho(x,t)\right]\right\} \\ &\quad + D_y\ \frac{\partial}{\partial y}\left\{\mathrm{e}^{-\beta U(x,y)}\frac{\partial}{\partial y}\left\{\mathrm{e}^{\beta U(x,y)}\vartheta(y|x)\ \rho(x,t)\right]\right\} \\ &\quad - D_x\ \vartheta(y|x)\frac{\partial}{\partial x}\left\{\mathrm{e}^{-\beta f(x)}\frac{\partial}{\partial x}\left[\mathrm{e}^{\beta f(x)}\rho(x,t)\right]\right\} \\ &\quad - D_x\ \vartheta(y|x)\frac{\partial}{\partial x}\int \vartheta(y|x)\ \mathrm{e}^{-\beta f(x)}\frac{\partial}{\partial x}\left[\frac{1}{\vartheta(y|x)}\mathrm{e}^{\beta f(x)}\ \delta c(x,y,t)\right]\mathrm{d}y.\end{aligned} \tag{18.100}$$

The first term on the right-hand side can be rewritten as

$$\begin{aligned}\mathcal{P}\delta c(x,y,t) = D_x \frac{\partial}{\partial x}\left\{e^{-\beta U(x,y)}\frac{\partial}{\partial x}\left[e^{\beta U(x,y)}\,\delta c(x,y,t)\right]\right\} \\ + D_y \frac{\partial}{\partial y}\left\{e^{-\beta U(x,y)}\frac{\partial}{\partial y}\left[e^{\beta U(x,y)}\,\delta c(x,y,t)\right]\right\}.\end{aligned} \tag{18.101}$$

In this last expression, we used the so-called Smoluchowski operator, defined by

$$\mathcal{P} \equiv D_x \frac{\partial}{\partial x}\left\{e^{-\beta U(x,y)}\frac{\partial}{\partial x}e^{\beta U(x,y)}\right\} + D_y \frac{\partial}{\partial y}\left\{e^{-\beta U(x,y)}\frac{\partial}{\partial y}e^{\beta U(x,y)}\right\}. \tag{18.102}$$

The substitution of Eq. (18.4) into the second right-hand side term of Eq. (18.100) leads to

$$\begin{aligned}&\frac{\partial}{\partial x}\left\{e^{-\beta U(x,y)}\frac{\partial}{\partial x}\left[e^{\beta U(x,y)}\vartheta(y|x)\,\rho(x,t)\right]\right\} \\ &\quad+\frac{\partial}{\partial y}\left\{e^{-\beta U(x,y)}\frac{\partial}{\partial y}\left[e^{\beta U(x,y)}\vartheta(y|x)\,\rho(x,t)\right]\right\} \\ &=\frac{\partial}{\partial x}\left\{\vartheta(y|x)\,e^{-\beta f(x)}\frac{\partial}{\partial x}\left[\vartheta(y|x)\frac{1}{\vartheta(y|x)}e^{\beta f(x)}\,\rho(x,t)\right]\right\} \\ &\quad+\frac{\partial}{\partial y}\left\{\vartheta(y|x)\,e^{-\beta f(x)}\frac{\partial}{\partial y}\left[\vartheta(y|x)\frac{1}{\vartheta(y|x)}\,e^{\beta f(x)}\rho(x,t)\right]\right\} \\ &=\frac{\partial}{\partial x}\left\{\vartheta(y|x)\,e^{-\beta f(x)}\frac{\partial}{\partial x}\left[e^{\beta f(x)}\,\rho(x,t)\right]\right\} \\ &\quad+\frac{\partial}{\partial y}\left\{\vartheta(y|x)\,e^{-\beta f(x)}\frac{\partial}{\partial y}\left[e^{\beta f(x)}\,\rho(x,t)\right]\right\}.\end{aligned} \tag{18.103}$$

Noting the functional dependency of the exponentials and the function $\rho(x,t)$, one can obtain

$$\frac{\partial}{\partial y}\left\{\vartheta(y|x)\,e^{-\beta f(x)}\frac{\partial}{\partial y}\left[e^{\beta f(x)}\,\rho(x,t)\right]\right\} = 0. \tag{18.104}$$

Consequently, Eq. (18.103) results in

$$\begin{aligned}
&\frac{\partial}{\partial x}\left\{\mathrm{e}^{-\beta U(x,y)}\frac{\partial}{\partial x}\left[\mathrm{e}^{\beta U(x,y)}\ \vartheta(y|x)\ \ \rho(x,t)\right]\right\}\\
&\quad+\frac{\partial}{\partial y}\left\{\mathrm{e}^{-\beta U(x,y)}\frac{\partial}{\partial y}\left[\mathrm{e}^{\beta U(x,y)}\vartheta(y|x)\ \rho(x,t)\right]\right\}\\
&\quad=\frac{\partial}{\partial x}\left\{\vartheta(y|x)\ \mathrm{e}^{-\beta f(x)}\frac{\partial}{\partial x}\left[\mathrm{e}^{\beta f(x)}\ \rho(x,t)\right]\right\}.
\end{aligned}\tag{18.105}$$

Using this last equation, the last right-hand side term of Eq. (18.100), and applying the chain rule for derivatives, one can write

$$\begin{aligned}
&\frac{\partial}{\partial x}\left\{\vartheta(y|x)\ \mathrm{e}^{-\beta f(x)}\frac{\partial}{\partial x}\left[\mathrm{e}^{\beta f(x)}\ \ c(x,t)\ \right]\right\}\\
&\quad=\vartheta(y|x)\frac{\partial}{\partial x}\left\{\mathrm{e}^{-\beta f(x)}\frac{\partial}{\partial x}\left[\mathrm{e}^{\beta f(x)}\ \rho(x,t)\right]\right\}\\
&\qquad+\left[\frac{\partial}{\partial x}\vartheta(y|x)\right]\mathrm{e}^{-\beta f(x)}\frac{\partial}{\partial x}\left[\mathrm{e}^{\beta f(x)}\ \rho(x,t)\right],
\end{aligned}\tag{18.106}$$

or

$$\begin{aligned}
&\left[\frac{\partial}{\partial x}\vartheta(y|x)\right]\mathrm{e}^{-\beta f(x)}\frac{\partial}{\partial x}\left[\mathrm{e}^{\beta f(x)}\ \ \rho(x,t)\ \right]\\
&\quad=\frac{\partial}{\partial x}\left\{\vartheta(y|x)\ \mathrm{e}^{-\beta f(x)}\frac{\partial}{\partial x}\left[\mathrm{e}^{\beta f(x)}\ \rho(x,t)\right]\right\}\\
&\qquad-\vartheta(y|x)\frac{\partial}{\partial x}\left\{\mathrm{e}^{-\beta f(x)}\frac{\partial}{\partial x}\left[\mathrm{e}^{\beta f(x)}\ \rho(x,t)\right]\right\}.
\end{aligned}\tag{18.107}$$

Using this last equation, Eq. (18.100) can be rewritten as

$$\begin{aligned}
\frac{\partial\delta c(x,y,t)}{\partial t}&=\mathcal{P}\delta c(x,y,t)\\
&+D_x\left[\frac{\partial}{\partial x}\vartheta(y|x)\right]\mathrm{e}^{-\beta f(x)}\frac{\partial}{\partial x}\left[\mathrm{e}^{\beta f(x)}\ \rho(x,t)\right]\\
&-D_x\ \vartheta(y|x)\frac{\partial}{\partial x}\left\{\mathrm{e}^{-\beta f(x)}\int\vartheta(y|x)\frac{\partial}{\partial x}\left[\frac{1}{\vartheta(y|x)}\mathrm{e}^{\beta f(x)}\ \delta c(x,y,t)\right]\mathrm{d}y\right\}.
\end{aligned}\tag{18.108}$$

Using the chain rule for derivatives one more time, now applied to the expression inside the integral of the last equation, we arrive at

$$\begin{aligned}
&\frac{\partial}{\partial x}\left[\vartheta(y|x)\frac{\mathrm{e}^{\beta f(x)}}{\vartheta(y|x)}\,\delta p(x,y,t)\right]\\
&\quad=\left[\frac{\partial}{\partial x}\vartheta(y|x)\right]\frac{\mathrm{e}^{\beta f(x)}}{\vartheta(y|x)}\delta c(x,y,t)\\
&\qquad+\vartheta(y|x)\,\mathrm{e}^{-\beta f(x)}\frac{\partial}{\partial x}\left[\frac{1}{\vartheta(y|x)}\mathrm{e}^{\beta f(x)}\,\delta c(x,y,t)\right],
\end{aligned}\tag{18.109}$$

which substituted into Eq. (18.108) can be seen as

$$\begin{aligned}
&\int\vartheta(y|x)\,\mathrm{e}^{-\beta f(x)}\frac{\partial}{\partial x}\left[\frac{1}{\vartheta(y|x)}\,\mathrm{e}^{\beta f(x)}\,\delta c(x,y,t)\right]\mathrm{d}y\\
&\quad=\frac{\partial}{\partial x}\int\vartheta(y|x)\frac{\mathrm{e}^{\beta f(x)}}{\vartheta(y|x)}\,\delta c(x,y,t)\,\mathrm{d}y\\
&\qquad-\int\left[\frac{\partial}{\partial x}\vartheta(y|x)\right]\frac{\mathrm{e}^{\beta f(x)}}{\vartheta(y|x)}\,\delta c(x,y,t)\,\mathrm{d}y.
\end{aligned}\tag{18.110}$$

Using the first term on the right-hand side leads to

$$\begin{aligned}
&\frac{\partial}{\partial x}\int\vartheta(y|x)\frac{\mathrm{e}^{\beta f(x)}}{\vartheta(y|x)}\,\delta c(x,y,t)\,\mathrm{d}y\\
&\quad=\frac{\partial}{\partial x}\left\{\mathrm{e}^{\beta f(x)}\int\delta c(x,y,t)\,\mathrm{d}y\right\}\\
&\quad=\frac{\partial}{\partial x}\left\{\mathrm{e}^{\beta f(x)}\int[c(x,y,t)-\rho(x,t)\,\vartheta(y|x)]\,\mathrm{d}y\right\}\\
&\quad=\frac{\partial}{\partial x}\left\{\mathrm{e}^{\beta f(x)}\left[\int c(x,y,t)\mathrm{d}y-\rho(x,t)\int\vartheta(y|x)\,\mathrm{d}y\right]\right\}\\
&\quad=\frac{\partial}{\partial x}\left\{\mathrm{e}^{\beta f(x)}\left[\rho(x,t)-\rho(x,t)\int\frac{\mathrm{e}^{-\beta U(x,y)}}{\mathrm{e}^{-\beta f(x)}}\,\mathrm{d}y\right]\right\}\\
&\quad=\frac{\partial}{\partial x}\left\{\mathrm{e}^{\beta f(x)}\left[\rho(x,t)-\frac{\rho(x,t)}{\mathrm{e}^{-\beta f(x)}}\int\mathrm{e}^{-\beta U(x,y)}\,\mathrm{d}y\right]\right\}\\
&\quad=\frac{\partial}{\partial x}\left\{\mathrm{e}^{\beta f(x)}\left[\rho(x,t)-\frac{\rho(x,t)}{\mathrm{e}^{-\beta f(x)}}\mathrm{e}^{-\beta f(x)}\right]\right\}\\
&\quad=\frac{\partial}{\partial x}\left\{\mathrm{e}^{\beta f(x)}\left[\rho(x,t)-\rho(x,t)\right]\right\}\\
&\quad=0,
\end{aligned}\tag{18.111}$$

where the result was obtained by means of Eq. (18.4) and Eq. (18.8). Now, if Eqs. (18.111) and (18.110) are substituted into Eq. (18.108), we have that

$$\begin{aligned}\frac{\partial \delta c(x,y,t)}{\partial t} &= \mathscr{P}\delta c(x,y,t) \\ &+ D_x\left[\frac{\partial}{\partial x}\vartheta(y|x)\right]\mathrm{e}^{-\beta f(x)}\frac{\partial}{\partial x}\left[\mathrm{e}^{\beta f(x)}\,\rho(x,t)\right] \\ &+ D_x\,\vartheta(y|x)\frac{\partial}{\partial x}\left\{\mathrm{e}^{-\beta f(x)}\int\left[\frac{\partial}{\partial x}\vartheta(y|x)\right]\frac{\mathrm{e}^{\beta f(x)}}{\vartheta(y|x)}\,\delta c(x,y,t)\,\mathrm{d}y\right\},\end{aligned} \tag{18.112}$$

which reduces to

$$\begin{aligned}\frac{\partial \delta c(x,y,t)}{\partial t} &= \mathscr{P}\delta c(x,y,t) + D_x\left[\frac{\partial}{\partial x}\vartheta(y|x)\right]\mathrm{e}^{-\beta f(x)}\frac{\partial}{\partial x}\left[\mathrm{e}^{\beta f(x)}\,\rho(x,t)\right] \\ &+ D_x\,\vartheta(y|x)\frac{\partial}{\partial x}\int\left[\frac{\partial}{\partial x}\vartheta(y|x)\right]\frac{1}{\vartheta(y|x)}\delta c(x,y,t)\,\mathrm{d}y.\end{aligned} \tag{18.113}$$

Now, we approximate this last result keeping only the first-order terms of $\partial_x \rho$, resulting in

$$\frac{\partial \delta c(x,y,t)}{\partial t} = \mathscr{P}\delta c(x,y,t) + D_x\left[\frac{\partial}{\partial x}\vartheta(y|x)\right]\mathrm{e}^{-\beta f(x)}\frac{\partial}{\partial x}\left[\mathrm{e}^{\beta f(x)}\,\rho(x,t)\right], \tag{18.114}$$

which needs to be operated using the Laplace transform

$$\begin{aligned}\mathcal{L}\left\{\frac{\partial \delta c(x,y,t)}{\partial t}\right\} &= \mathcal{L}\left\{\mathscr{P}\delta c(x,y,t)\right\} \\ &+ D_x\,\mathcal{L}\left\{\left[\frac{\partial}{\partial x}\vartheta(y|x)\right]\mathrm{e}^{-\beta f(x)}\frac{\partial}{\partial x}\left[\mathrm{e}^{\beta f(x)}\,\rho(x,t)\right]\right\},\end{aligned} \tag{18.115}$$

yielding

$$\begin{aligned}s\,\mathcal{L}\left\{\frac{\partial \delta c(x,y,t)}{\partial t}\right\} &- \delta C(x,y,0) \\ &= \mathscr{P}\mathcal{L}\left\{\delta c(x,y,t)\right\} + D_x\left[\frac{\partial}{\partial x}\vartheta(y|x)\right]\mathrm{e}^{-\beta f(x)}\frac{\partial}{\partial x}\left[\mathrm{e}^{\beta f(x)}\,\mathcal{L}\left\{\rho(x,t)\right\}\right],\end{aligned} \tag{18.116}$$

from where we can obtain

$$(s-\mathscr{P})\,\mathcal{L}\{\delta c(x,y,t)\} = D_x\left[\frac{\partial}{\partial x}\vartheta(y|x)\right]\mathrm{e}^{-\beta f(x)}\frac{\partial}{\partial x}\left[\mathrm{e}^{\beta f(x)}\,\mathcal{L}\{\rho(x,t)\}\right]. \tag{18.117}$$

Leaving the explicit Laplace transform on the left side, the equation becomes

$$\mathcal{L}\{\delta c(x,y,t)\} = \frac{D_x}{(s-\mathscr{P})}\left[\frac{\partial}{\partial x}\vartheta(y|x)\right]\mathrm{e}^{-\beta f(x)}\frac{\partial}{\partial x}\left[\mathrm{e}^{\beta f(x)}\,\mathcal{L}\{\rho(x,t)\}\right]. \tag{18.118}$$

Applying the inverse Laplace transform gives

$$\delta c(x,y,t) = \mathcal{L}^{-1}\left\{\frac{D_x}{(s-\mathscr{P})}\left[\frac{\partial}{\partial x}\vartheta(y|x)\right]\mathrm{e}^{-\beta f(x)}\frac{\partial}{\partial x}\left[\mathrm{e}^{\beta f(x)}\,\mathcal{L}\{\rho(x,t)\}\right]\right\}. \tag{18.119}$$

Using the inverse transform given by Eq. (A.65), and the convolution theorem given by Eq. (A.74), we finally arrive at Eq. (18.29), namely,

$$\delta c(x,y,t) = D_x\int_0^t \mathrm{e}^{t'\mathscr{P}}\left[\frac{\partial}{\partial x}\rho(y|x)\right]\mathrm{e}^{-\beta f(x)}\frac{\partial}{\partial x}\left[\mathrm{e}^{\beta f(x)}\,\rho(x,t-t')\right]\mathrm{d}t'. \tag{18.29}$$

18.A.2 Derivation of Eq. (18.39)

To lead into Eq. (18.39), the operator $\mathscr{P}'$ should be rewritten in terms of another operator $\mathcal{Q}$, namely,

$$\mathscr{P}'\vartheta(y|x)f = \vartheta(y|x)\,\mathcal{Q}f, \tag{18.120}$$

so then

$$\kappa(x) = \int\left[\frac{\partial}{\partial x}\vartheta(y|x)\right]\int_0^\infty \frac{1}{\vartheta(y|x)}\mathrm{e}^{t\mathscr{P}'}\left[\frac{\partial}{\partial x}\vartheta(y|x)\right]\mathrm{d}t\;\mathrm{d}y. \tag{18.121}$$

For practicality purposes, we define

$$\psi(y|x) \equiv \int_0^\infty \frac{1}{\vartheta(y|x)}\mathrm{e}^{t\mathscr{P}'}\left[\frac{\partial}{\partial x}\vartheta(y|x)\right]\mathrm{d}t. \tag{18.122}$$

As such, we can see that the operator given by Eq. (18.120) must obey

$$\mathcal{Q}\psi(y|x) = -\frac{\partial}{\partial x}\ln\left[\vartheta(y|x)\right]. \tag{18.123}$$

Moreover,

$$\begin{aligned}\mathcal{Q}\psi(y|x) &= -\frac{\partial}{\partial x}\ln\left[\vartheta(y|x)\right] \\ &= -\frac{1}{\vartheta(y|x)}\frac{\partial}{\partial x}\vartheta(y|x) = \frac{1}{\vartheta(y|x)}\mathcal{P}'\left[\vartheta(y|x)\ \psi(y|x)\right].\end{aligned} \tag{18.124}$$

This last equation can be rewritten as follows:

$$-\frac{\partial}{\partial x}\vartheta(y|x) = \mathcal{P}'\left[\vartheta(y|x)\ \psi(y|x)\right] = \frac{\partial}{\partial y}\left\{\vartheta(y|x)\frac{\partial}{\partial y}\left[\frac{\vartheta(y|x)}{\vartheta(y|x)}\psi(y|x)\right]\right\}, \tag{18.125}$$

then

$$-\frac{\partial}{\partial x}\vartheta(y|x) = \frac{\partial}{\partial y}\left\{\vartheta(y|x)\frac{\partial}{\partial y}\psi(y|x)\right\}. \tag{18.126}$$

Now, Eq. (18.121) is given by

$$\kappa(x) = \int\left[\frac{\partial}{\partial x}\vartheta(y|x)\right]\psi(y|x)\ \mathrm{d}y. \tag{18.127}$$

By choosing the potential wisely, $\kappa(x)$ can be modified to a more practical form, so we propose that

$$U(x, y) = V\left(\frac{y}{h(x)}\right) = V(z), \tag{18.128}$$

where the system boundary $h(x)$ is used as a scale factor for the y-coordinate, namely,

$$z \equiv \frac{y}{h(x)}. \tag{18.129}$$

By defining

$$q \equiv \int \mathrm{e}^{-\beta V(z)}\ \mathrm{d}z, \tag{18.130}$$

and using Eq. (18.9) one more time, we obtain

$$\rho(y|x) = \frac{\mathrm{e}^{-\beta V(z)}}{qh(x)}, \tag{18.131}$$

where

$$\mathrm{e}^{-\beta f(x)} = qh(x). \tag{18.132}$$

Seeing that

$$\frac{\partial z}{\partial y} = \frac{\partial}{\partial y}\left[\frac{y}{h(x)}\right] = \frac{1}{h(x)}, \tag{18.133}$$

$$\frac{\partial z}{\partial x} = \frac{\partial}{\partial x}\left[\frac{y}{h(x)}\right] = y\frac{A'(x)}{A^2(x)}, \tag{18.134}$$

these can be used to write

$$\begin{aligned}\frac{\partial}{\partial y}\vartheta(y|x) &= \frac{\partial}{\partial y}\left[\frac{\mathrm{e}^{-\beta V(z)}}{qh(x)}\right] = \frac{1}{qh(x)}\frac{\partial}{\partial y}\mathrm{e}^{-\beta V(z)} \\ &= \frac{1}{qh(x)}\left[-\beta V'(z)\ \frac{\partial z}{\partial y}\mathrm{e}^{-\beta V(z)}\right] \\ &= -\frac{\beta V'(z)}{qh(x)}\ \mathrm{e}^{-\beta V(z)}\frac{1}{h(x)} = -\beta\frac{V'(z)}{h(x)}\ \vartheta(y|x),\end{aligned} \tag{18.135}$$

and multiplying by y yields

$$y\frac{\partial}{\partial y}\rho(y|x) = -\beta\frac{y}{h(x)}V'(z)\ \vartheta(y|x). \tag{18.136}$$

A similar procedure can be followed for the x-coordinate, namely,

$$\begin{aligned}\frac{\partial}{\partial x}\rho(y|x) &= \frac{\partial}{\partial x}\left[\frac{\mathrm{e}^{-\beta V(z)}}{qh(x)}\right] \\ &= \frac{1}{q}\left\{\mathrm{e}^{-\beta V(z)}\frac{\partial}{\partial x}\left(\frac{1}{h(x)}\right) + \frac{1}{h(x)}\frac{\partial}{\partial x}\left(\mathrm{e}^{-\beta V(z)}\right)\right\} \\ &= \frac{1}{q}\left\{-\mathrm{e}^{-\beta V(z)}\frac{A'(x)}{A^2(x)} + \frac{1}{h(x)}\left[-\beta V'(z)\frac{\partial z}{\partial x}\mathrm{e}^{-\beta V(z)}\right]\right\} \\ &= -\frac{1}{qh(x)}\mathrm{e}^{-\beta V(z)}\left[\frac{A'(x)}{h(x)} + \beta V'(z)y\frac{A'(x)}{A^2(x)}\right] \\ &= -\frac{A'(x)}{h(x)}\vartheta(y|x)\left[1 + \beta V'(z)y\frac{1}{h(x)}\right] \\ &= -\frac{A'(x)}{h(x)}\left[\vartheta(y|x) + y\frac{\partial}{\partial y}\vartheta(y|x)\right],\end{aligned} \tag{18.137}$$

and consequently,

$$\frac{\partial}{\partial x}\vartheta(y|x) = -\frac{A'(x)}{h(x)}\frac{\partial}{\partial y}\left[y\ \vartheta(y|x)\right]. \tag{18.138}$$

Now, Eq. (18.126) can be substituted in this last equation to obtain

$$\frac{\partial}{\partial y}\left\{\vartheta(y|x)\frac{\partial}{\partial y}\psi(y|x)\right\} = \frac{A'(x)}{h(x)}\frac{\partial}{\partial y}\left[y\ \vartheta(y|x)\right], \tag{18.139}$$

which can be integrated in the y-coordinate, leading to

$$\frac{\partial}{\partial y}\psi(y|x) = \frac{A'(x)}{h(x)}y + c_1, \tag{18.140}$$

where c_1 is an integration constant. Substituting Eq. (18.138) into $\kappa(x)$, given by Eq. (18.127), we obtain

$$\begin{aligned}\kappa(x) &= \int\left\{-\frac{A'(x)}{h(x)}\frac{\partial}{\partial y}\left[y\ \vartheta(y|x)\right]\right\}\psi(y|x)\ \mathrm{d}y \\ &= -\frac{A'(x)}{h(x)}\int\psi(y|x)\frac{\partial}{\partial y}\left[y\vartheta(y|x)\right]\ \mathrm{d}y.\end{aligned} \tag{18.141}$$

Integrating by parts leads to

$$\kappa(x) = -\frac{A'(x)}{h(x)}\left\{\left[\psi(y|x)\ y\ \vartheta(y|x)\right]\Big|_a^b - \int y\ \vartheta(y|x)\frac{\partial}{\partial y}\left[\psi(y|x)\right]\ \mathrm{d}y\right\}. \tag{18.142}$$

The first right-hand side term is a constant that is discarded; then Eq. (18.140) is used, yielding

$$\kappa(x) = \frac{A'(x)}{h(x)}\int y\vartheta(y|x)\frac{A'(x)}{h(x)}\ y\ \mathrm{d}y = \left[A'(x)\right]^2\int\frac{y^2}{A^2(x)}\vartheta(y|x)\ \mathrm{d}y. \tag{18.143}$$

Now, using Eqs. (18.131) and (18.129), we arrive at

$$\kappa(x) = \left[A'(x)\right]^2\frac{1}{q}\int z^2\ \frac{\mathrm{e}^{-\beta V(z)}}{h(x)}w\ \mathrm{d}z, \tag{18.144}$$

Finally, using Eq. (18.130) allows us to obtain a useful expression for $\kappa(x)$, Eq. (18.39), namely,

$$\kappa(x) = \left[A'(x)\right]^2\int z^2\ \mathrm{e}^{-\beta V(z)}\ \mathrm{d}z\ \Big/\ \int\mathrm{e}^{-\beta V(z)}\ \mathrm{d}z. \tag{18.39}$$

Further Reading and References

A.M. Berezhkovskii, L. Dagdug, S.M. Bezrukov, Discriminating between anomalous diffusion and transient behavior in microheterogeneous environments. Biophys. J. **106**, L09–L011 (2014). https://www.cell.com/biophysj/fulltext/S0006-3495(13)05802-5

L. Dagdug, A.M. Berezhkovskii, Y.A. Makhnovskii, V.Yu. Zitserman, Transient diffusion in a tube with dead ends. J. Chem. Phys. **127**, 224712 (2007). https://aip.scitation.org/doi/10.1063/1.2805068

M.H. Jacobs, *Diffusion Processes* (Springer, Berlin, 1935)

P. Kalinay, J.K. Percus, Projection of two-dimensional diffusion in a narrow channel onto the longitudinal dimension. Phys. Rev. E **74**, 041203 (2006). https://journals.aps.org/pre/abstract/10.1103/PhysRevE.74.041203

P.M. Morse, H. Feshbach, *Methods of Theoretical Physics* (McGraw-Hill, New York, 1953)

R. Zwanzig, J. Phys. Chem. **96**(10), 3926–3930 (1992). Diffusion past an entropy barrier. https://doi.org/10.1021/j100189a004

Chapter 19
Reguera and Rubi Kinetic Equation

19.1 Introduction

Using the mesoscopic non-equilibrium thermodynamics theory, David Reguera and Miguel Rubi derived a general kinetic equation in the presence of potential barriers. Using this theoretical framework, they studied diffusion under confinement where the presence of boundaries induces an entropy barrier when approaching the exact dynamics by a coarse-grained description. Under this approximation, they derived the modified Fick-Jacobs equation, previously found by Zwanzig, as discussed in the previous chapter. They also proved that this equation can be generalized formulating a scaling law for the position-dependent diffusion coefficient, which depends on the shape of the boundaries. It is worth noting that in their theoretical description, they also included an external energetic term.

This theoretical framework is applicable to a wide variety of systems of different nature, such as protein folding, glassy systems, transport of ions and macromolecules through membranes or channels, motion of polymers subjected to rigid constraints, protein binding kinetics, drug release, nucleation, or polymer crystallization, to mention just a few examples, where the presence of entropic barriers becomes relevant.

This chapter is devoted to the in-depth study of the mesoscopic non-equilibrium thermodynamics theory in the presence of entropic barriers, as well as its application to diffusion under geometrical constraints.

19.2 Entropy Production

We start the derivation of the modified Fick-Jacobs equation using mesoscopic non-equilibrium thermodynamics by considering Gibbs' entropy postulate, which describes deviations of entropy from its equilibrium value, namely,

L. Dagdug et al., *Diffusion Under Confinement*,
https://doi.org/10.1007/978-3-031-46475-1_19

$$S = -k_B \int p(\mathbf{r}, t)\, \ln \frac{p(\mathbf{r}, t)}{p_{\text{eq}}(\mathbf{r})}\, \mathrm{d}\mathbf{r} + S_{eq}, \tag{19.1}$$

where k_B is the Boltzmann constant and $p(\mathbf{r}, t)$ is the probability density. p_{eq} and S_{eq} are the system's equilibrium probability and entropy, respectively. $\mathbf{r}$ represents a phase space point, a set of mesoscopic quantities, such as the position and velocity of a particle, the orientation of a spin, the number of particles of a cluster, or a reaction coordinate. This system obeys the continuity equation, found in Sect. 2.7.1,

$$\frac{\partial p(\mathbf{r}, t)}{\partial t} + \nabla \cdot \mathbf{J}(\mathbf{r}, t) = 0, \tag{2.72}$$

where the flux over the boundaries is null because the system is confined. Then,

$$\boldsymbol{J}(\mathbf{r}, t)\Big|_{h_1} = \mathbf{J}(\mathbf{r}, t)\Big|^{h_2} = 0, \tag{19.2}$$

with h_1 and h_2 being the lower and upper boundaries of the system, respectively. Calculating the time derivative of entropy, Eq. (19.1), and considering the boundary conditions, this yields

$$\frac{\partial S}{\partial t} = k_B \int \left\{ \ln \left[\frac{p(\mathbf{r}, t)}{p_{\text{eq}}(\mathbf{r})} \right] \nabla \cdot \mathbf{J}(\mathbf{r}, t) \right\} \mathrm{d}\mathbf{r}, \tag{19.3}$$

and after integrating by parts, this leads us to

$$\sigma \equiv \frac{\partial S}{\partial t} = -k_B \int \mathbf{J}(\mathbf{r}, t)\, \nabla \left[\ln \frac{p(\mathbf{r}, t)}{p_{\text{eq}}(\mathbf{r})} \right] \mathrm{d}\mathbf{r}, \tag{19.4}$$

that is, the system's *entropy production*.

19.2.1 Continuity Equations

From thermodynamics, we learn that the internal energy density u is given by

$$\mathrm{d}u = T\,\mathrm{d}s + \sum_j \mu_j\, \mathrm{d}N_j + \phi\, \mathrm{d}\rho, \tag{19.5}$$

where we have j different kinds (species) of particles, μ_j are their respective chemical potentials, and ϕ is the electric potential. This can be rewritten in terms of the entropy density as

$$\mathrm{d}s = \frac{1}{T}\,\mathrm{d}u - \frac{1}{T}\sum_j \mu_j\,\mathrm{d}N_j - \frac{\phi}{T}\,\mathrm{d}\rho. \tag{19.6}$$

The coefficients along the differential terms are intensive quantities and can be seen as potential energies. The extensive variables, which are expressed as differential quantities, must be conserved. With this in mind, let us think of a relation between generalized densities ρ_k and their respective generalized potentials, namely,

$$\phi_k = \frac{\partial s}{\partial \rho_k}, \tag{19.7}$$

where the relation takes the form

$$\mathrm{d}s = \sum_k \phi_k\,\mathrm{d}\rho_k, \tag{19.8}$$

and every extensive quantity (generalized density) obeys a continuity equation of the form

$$\frac{\partial \rho_k}{\partial t} + \nabla \cdot \mathbf{J}_k = 0, \tag{19.9}$$

with $\mathbf{J}_k$ being a generalized current density. The entropy is not conserved but follows its own special continuity-like equation, namely,

$$\frac{\partial s}{\partial t} + \nabla \cdot \mathbf{J}_s = \frac{\partial s_i}{\partial t}, \tag{19.10}$$

where the right-hand side is due to the irreversible part of the processes.

19.2.2 Kinetic Coefficients

If we restrict ourselves to the linear regime, the response of a system to an applied force is given by a stationary current, then

$$\mathbf{J}_i = \sum_j L_{ij}\,\nabla\phi_j, \tag{19.11}$$

where L_{ij} are the so-called kinetic coefficients. The Nobel Prize winner, Lars Onsager, showed in 1931 that those coefficients are symmetrical, namely,

$$L_{ij} = L_{ji}, \tag{19.12}$$

which are known as the Onsager reciprocal relations.

19.2.3 Kinetic Equation

Given the production of entropy, Eq. (19.4), together with the relation of the stationary current $\mathbf{J}$, expression (19.11), which is related to its conjugate kinetic coefficient $L(\mathbf{r})$, allows us to write

$$\mathbf{J}(\mathbf{r},t) = -k_B\, L(\mathbf{r})\, \nabla \left[\ln \frac{p(\mathbf{r},t)}{p_{\text{eq}}(\mathbf{r})} \right], \tag{19.13}$$

which, following a continuity equation, gives

$$\frac{\partial p(\mathbf{r},t)}{\partial t} = \nabla \cdot \left\{ D(\mathbf{r})\, p(\mathbf{r},t)\, \nabla \left[\ln \frac{p(\mathbf{r},t)}{p_{\text{eq}}(\mathbf{r})} \right] \right\}, \tag{19.14}$$

where the next definition was used

$$D(\mathbf{r}) \equiv k_B\, \frac{L(\mathbf{r})}{p(\mathbf{r},t)}. \tag{19.15}$$

If $\Delta W(\mathbf{r})$ is the required amount of reversible work needed to change the system's state, then the expression of the Boltzmann factor is

$$p_{\text{eq}}(\mathbf{r}) \sim \exp\left[-\beta \Delta W(\mathbf{r})\right], \tag{19.16}$$

which needs to be replaced in Eq. (19.14) to become

$$\frac{\partial p(\mathbf{r},t)}{\partial t} = \nabla \cdot \left[D(\mathbf{r})\, \nabla p(\mathbf{r},t) + \beta D(\mathbf{r})\, c(\boldsymbol{r},t)\, \nabla \Delta W(\mathbf{r}) \right]. \tag{19.17}$$

The work in this last equality can be substituted using the Helmholtz free energy, namely,

$$W = F = U - TS, \tag{19.18}$$

then,

$$\frac{\partial p(\mathbf{r},t)}{\partial t} = \nabla \cdot \left\{ D(\mathbf{r})\, \nabla p(\mathbf{r},t) + \beta D(\mathbf{r})\, p(\mathbf{r},t)\, \nabla \left[\Delta U(\mathbf{r}) - T \Delta S(\mathbf{r}) \right] \right\}. \tag{19.19}$$

This last equation is a generalization of Eq. (6.16) for entropic and energetic potentials, with a non-constant diffusion coefficient. Moreover, it is a generalized Smoluchowski equation.

19.3 Reduction of the Kinetic Equation

In the last section, we deduced an extension of the diffusion equation that includes not only the contribution of an external energetic potential but also the effects of an entropic potential. Following the spirit of Zwanzig's works, we will take the kinetic expression of Reguera and Rubi (RR) in the practical form of Eq. (19.14) and then apply a dimensional reduction.

This is developed for a two-dimensional confined system, with boundaries that are defined by the function $y = h_i(x)$, with $i = 1, 2$ for the lower and upper walls, respectively. Obeying the described configuration, the spatial coordinates are $\mathbf{r} = (x, y)$, and the probability density is $p(\mathbf{r}, t) \to p(x, y, t)$. Also, the *del* operators will be expanded along the bracketed terms as coordinate-separated partial derivatives, as a result of the dot product (divergence). Then, this particular form of Eq. (19.14) looks like

$$\begin{aligned}\frac{\partial p(x,y,t)}{\partial t} &= \frac{\partial}{\partial x}\left\{D_x\, p(x,y,t)\,\frac{\partial}{\partial x}\left[\ln\frac{p(x,y,t)}{p_{\mathrm{eq}}(x,y)}\right]\right\} \\ &\quad + \frac{\partial}{\partial y}\left\{D_y\, p(x,y,t)\,\frac{\partial}{\partial y}\left[\ln\frac{p(x,y,t)}{p_{\mathrm{eq}}(x,y)}\right]\right\},\end{aligned} \tag{19.20}$$

where the diffusion coefficient was separated into two parts, one for each component, but also, the diffusion coefficients are now considered as constants. The next step is to define a reduced density in the transversal coordinate y, namely,

$$\rho(x,t) \equiv \int_{h_1(x)}^{h_2(x)} p(x,y,t)\,\mathrm{d}y, \tag{19.21}$$

By integrating Eq. (19.20) and using this last equation, we obtain

$$\begin{aligned}\frac{\partial \rho(x,t)}{\partial t} &= D_x \int_{h_1(x)}^{h_2(x)} \frac{\partial}{\partial x}\left\{p(x,y,t)\,\frac{\partial}{\partial x}\left[\ln\frac{p(x,y,t)}{p_{\mathrm{eq}}(x,y)}\right]\right\}\mathrm{d}y \\ &\quad + D_y \int_{h_1(x)}^{h_2(x)} \frac{\partial}{\partial y}\left\{p(x,y,t)\,\frac{\partial}{\partial y}\left[\ln\frac{p(x,y,t)}{p_{\mathrm{eq}}(x,y)}\right]\right\}\mathrm{d}y,\end{aligned} \tag{19.22}$$

where the second integral of the right-hand side is readily solved, this being

$$\begin{aligned}&D_y \int_{h_1(x)}^{h_2(x)} \frac{\partial}{\partial y}\left\{p(x,y,t)\,\frac{\partial}{\partial y}\left[\ln\frac{p(x,y,t)}{p_{\mathrm{eq}}(x,y)}\right]\right\}\mathrm{d}y \\ &= D_y\left\{p(x,y,t)\,\frac{\partial}{\partial y}\left[\ln\frac{p(x,y,t)}{p_{\mathrm{eq}}(x,y)}\right]\right\}\Bigg|^{y=h_2(x)} \\ &\quad - D_y\left\{p(x,y,t)\,\frac{\partial}{\partial y}\left[\ln\frac{p(x,y,t)}{p_{\mathrm{eq}}(x,y)}\right]\right\}\Bigg|_{y=h_1(x)}.\end{aligned} \tag{19.23}$$

The system is confined, which means that there are no-flux conditions on the boundaries, and these can be written by knowing that the derivative of the function describing the wall must be parallel to the flux of the particles, yielding

$$\mathbf{J} \times \mathbf{h}_i'(x) = 0, \tag{19.24}$$

from where we can see that

$$\mathbf{h}_i'(x) = (1, h_i'(x)), \tag{19.25}$$

and

$$\mathbf{J} = (J_x, J_y, 0). \tag{19.26}$$

Now, Eq. (19.24) can be written as

$$\mathbf{J} \times \pm\mathbf{h}_i'(x) = \begin{vmatrix} \hat{\boldsymbol{\imath}} & \hat{\boldsymbol{\jmath}} & \hat{\boldsymbol{k}} \\ J_x & J_y & 0 \\ 1 & h_i'(x) & 0 \end{vmatrix} = \hat{\boldsymbol{k}} \left[\pm h_i'(x)\, J_x - J_y \right] = 0, \tag{19.27}$$

obtaining

$$\pm\, h_i'(x)\, J_x = J_y. \tag{19.28}$$

The last set of equations are the BCs, but we must explicitly specify the components of the flux. These should be obtained from the kinetic equation (19.20) by comparing it with a continuity equation such as Eq. (19.9) or (2.72). Then, we can state that

$$J_x = D_x\, p(x, y, t)\, \frac{\partial}{\partial x} \left[\ln \frac{p(x, y, t)}{p_{\mathrm{eq}}(x, y)} \right], \quad J_y = D_y\, p(x, y, t)\, \frac{\partial}{\partial y} \left[\ln \frac{p(x, y, t)}{p_{\mathrm{eq}}(x, y)} \right], \tag{19.29}$$

which can be substituted into Eq. (19.28) to obtain

$$\begin{aligned} & h_i'(x)\, D_x\, p(x, y, t)\, \frac{\partial}{\partial x} \left[\ln \frac{p(x, y, t)}{p_{\mathrm{eq}}(x, y)} \right] \Bigg|_{y=h_i} \\ & \quad = D_y\, p(x, y, t)\, \frac{\partial}{\partial y} \left[\ln \frac{p(x, y, t)}{p_{\mathrm{eq}}(x, y)} \right] \Bigg|_{y=h_i}, \end{aligned} \tag{19.30}$$

where we must note that the fluxes have to be evaluated over the boundaries. Recalling the calculations made for the right-hand side of Eq. (19.22), which are portrayed in Eq. (19.23), together with the BCs, yields

$$
\begin{aligned}
D_y \int_{h_1(x)}^{h_2(x)} \frac{\partial}{\partial y} \left\{ p(x,y,t) \frac{\partial}{\partial y} \left[\ln \frac{p(x,y,t)}{p_{\text{eq}}(x,y)} \right] \right\} \mathrm{d}y \\
= h_2'(x)\, D_x\, p(x,y,t) \frac{\partial}{\partial x} \left[\ln \frac{p(x,y,t)}{p_{\text{eq}}(x,y)} \right] \Bigg|_{y=h_2} \\
- h_1'(x)\, D_x\, p(x,y,t) \frac{\partial}{\partial x} \left[\ln \frac{p(x,y,t)}{p_{\text{eq}}(x,y)} \right] \Bigg|_{y=h_1}.
\end{aligned}
\tag{19.31}
$$

Determining the first integral on the right-hand side of Eq. (19.22) requires the use of the Leibniz rule for integrals, Eq. (A.9), which is written in Appendix A.3. By these means, we have that

$$
\begin{aligned}
D_x \frac{\partial}{\partial x} \int_{h_1(x)}^{h_2(x)} \frac{\partial}{\partial x} \left\{ p(x,y,t) \frac{\partial}{\partial x} \left[\ln \frac{p(x,y,t)}{p_{\text{eq}}(x,y)} \right] \right\} \mathrm{d}y \\
= D_x \int_{h_1(x)}^{h_2(x)} \frac{\partial}{\partial x} \left\{ p(x,y,t) \frac{\partial}{\partial x} \left[\ln \frac{p(x,y,t)}{p_{\text{eq}}(x,y)} \right] \right\} \mathrm{d}y \\
+ D_x\, h_2'(x)\, p(x,y,t) \frac{\partial}{\partial x} \left[\ln \frac{p(x,y,t)}{p_{\text{eq}}(x,y)} \right] \Bigg|_{y=h_2} \\
- D_x\, h_1'(x)\, p(x,y,t) \frac{\partial}{\partial x} \left[\ln \frac{p(x,y,t)}{p_{\text{eq}}(x,y)} \right] \Bigg|_{y=h_1}.
\end{aligned}
\tag{19.32}
$$

This last equation can be substituted together with Eq. (19.31) back into Eq. (19.22), and after reducing terms, we obtain

$$
\frac{\partial \rho(x,t)}{\partial t} = D_x \frac{\partial}{\partial x} \int_{h_1(x)}^{h_2(x)} p(x,y,t) \frac{\partial}{\partial x} \left[\ln \frac{p(x,y,t)}{p_{\text{eq}}(x,y)} \right] \mathrm{d}y, \tag{19.33}
$$

where the internal derivative can be manipulated, leading us to obtain

$$
\frac{\partial \rho(x,t)}{\partial t} = D_x \frac{\partial}{\partial x} \int_{h_1(x)}^{h_2(x)} p_{\text{eq}}(x,y) \frac{\partial}{\partial x} \left[\frac{p(x,y,t)}{p_{\text{eq}}(x,y)} \right] \mathrm{d}y. \tag{19.34}
$$

This is the reduced kinetic equation for a 2D confined system.

A key component in the construction of the kinetic equation is the Boltzmann factor, which is written as a probability distribution. This is the main reason why we wrote down the calculations in this section in terms of probabilities instead of concentration, as done in previous chapters. Nevertheless, all the results can be written in terms of concentration by using the relation $c(\mathbf{r},t) = Np(\mathbf{r},t)$, where N is the number of particles, as stated in Sect. 4.2. Further steps to get usable results will depend on the precise form of the equilibrium probability.

19.3.1 Reduced Equation for a Gravitational-Like Field

As a specific case, we are studying a confined two-dimensional system under the influence of a gravitational-like field to obtain its reduced kinetic equation. For this system, the Boltzmann factor (19.16) is

$$p_{\mathrm{eq}}(x, y) \sim \mathrm{e}^{-\beta G y}, \tag{19.35}$$

where G is a gravitational-like force pointing downward. Now, a practical definition is made, which is

$$g \equiv \beta G, \tag{19.36}$$

and then, Eq. (19.35) becomes

$$p_{\mathrm{eq}}(x, y) \sim \mathrm{e}^{-g y}. \tag{19.37}$$

Under all these considerations, the equilibrium probability density depends only on the y-coordinate. Also, a proportionality constant k is needed to achieve equality, and its dimensions are L^{-2}, so then

$$p_{\mathrm{eq}}(y) = k\, \mathrm{e}^{-g y}. \tag{19.38}$$

Moreover, the substitution of the last equation into the reduced kinetic Eq. (19.34) yields

$$\frac{\partial \rho(x, t)}{\partial t} = D_x \frac{\partial}{\partial x} \int_{h_1(x)}^{h_2(x)} \frac{\partial p(x, y, t)}{\partial x}\, \mathrm{d}y. \tag{19.39}$$

The same equation will be found later in Chap. 20 starting from the 2D Smoluchowski equation, from which an effective diffusivity coefficient is found using the Kalinay & Percus method.

19.3.1.1 Equilibrium Solution

Only the equilibrium solution is discussed in this chapter. To such end, we consider a relative equilibrium, that is, the diffusivity of the transversal direction, that is *infinitely* fast enough, allowing us to separate the two parts of the probability as independent functions and propose that

$$p_0(x, y, t) = \frac{1}{\mathcal{F}(x)}\, Y(y)\, \rho_0(x, t), \tag{19.40}$$

where $Y(y)$ and $\mathcal{F}(x)$ are functions to be determined to make $p_0(x,t)$ a solution of Eq. (19.39). Plugging the equilibrium solution into Eq. (19.39) gives

$$\frac{\partial \rho_0(x,t)}{\partial t} = D_x \frac{\partial}{\partial x} \int_{h_1(x)}^{h_2(x)} \frac{\partial}{\partial x} \left[\frac{1}{\mathcal{F}(x)} Y(y)\, \rho_0(x,t) \right] \mathrm{d}y, \tag{19.41}$$

where the dependencies are accounted for to obtain

$$\frac{\partial \rho_0(x,t)}{\partial t} = D_x \frac{\partial}{\partial x} \int_{h_1(x)}^{h_2(x)} Y(y)\, \mathrm{d}y\, \frac{\partial}{\partial x} \left[\frac{\rho_0(x,t)}{\mathcal{F}(x)} \right]. \tag{19.42}$$

We also know that the equilibrium solution in Eq. (19.40) must obey the reduced density equation (19.21), so then

$$\rho_0(x,t) = \int_{h_1(x)}^{h_2(x)} \frac{1}{\mathcal{F}(x)} Y(y)\, \rho_0(x,t)\, \mathrm{d}y = \int_{h_1(x)}^{h_2(x)} Y(y)\, \mathrm{d}y\, \frac{\rho_0(x,t)}{\mathcal{F}(x)} \tag{19.43}$$

leading us to

$$\mathcal{F}(x) = \int_{h_1(x)}^{h_2(x)} Y(y)\, \mathrm{d}y, \tag{19.44}$$

which allows us to write

$$\frac{\partial \rho_0(x,t)}{\partial t} = D_x \frac{\partial}{\partial x} \mathcal{F}(x)\, \frac{\partial}{\partial x} \left[\frac{\rho_0(x,t)}{\mathcal{F}(x)} \right], \tag{19.45}$$

which can be recognized as a Fick-Jacobs equation. In Zwanzig's approach, the quantity appearing along the concentration is an exponential of a free-energy term; this is why the proposal for using the Boltzmann factor as the function $Y(y)$ is plausible in this case, namely,

$$Y(y) = \mathrm{e}^{-g\,y}. \tag{19.46}$$

Then, function $\mathcal{F}(x)$ reads

$$\mathcal{F}(x) \equiv \int_{h_1(x)}^{h_2(x)} \mathrm{e}^{-g\,y}\, \mathrm{d}y = \frac{1}{g} \left[e^{-g\,h_1(x)} - e^{-g\,h_2(x)} \right], \tag{19.47}$$

which, for a symmetric channel where $h(x) \equiv h_2(x) = -h_1(x)$, yields

$$\mathcal{F}(x) = \frac{2}{g} \sinh\left[g\, h(x) \right]. \tag{19.48}$$

This precise form of $Y(y)$ needs to be consistent with previous results, *i.e.* $g \to 0$. Subsequently,

$$\mathcal{F}(x) = \int_{h_1(x)}^{h_2(x)} \mathrm{d}y = h_2(x) - h_1(x) = w(x). \tag{19.49}$$

Then, Eq. (17.19) can be immediately recovered. Also, for symmetric channels, we have

$$\mathcal{F}(x) = \int_{-h(x)}^{h(x)} \mathrm{d}y = 2h(x). \tag{19.50}$$

The last couple of equations are analogous to Eq. (18.16) in Zwanzig's frame.

It is important to note that the proposal of the $Y(y)$ function is not a coincidence. The functional form of the Boltzmann factor made us think of the exponential term in Eq. (18.8) where the free-energy function $\ell(x)$ was introduced. Also, the comparison of Eq. (19.45) to the FJ equation obtained using the Zw method suggests that function $Y(y)$ should have the form shown in Eq. (19.46).

The non-equilibrium solution or general solution will be worked out using the so-called projection method developed by Pavol Kalinay and Jerome Percus, which is based on a perturbative series, a technique that is similar to the one used in quantum mechanics approximate methods.

19.3.2 Diffusion Coefficient

The two-dimensional bulk diffusion coefficient is related to the mean squared displacement as

$$D_0 \sim \frac{(\Delta \mathbf{r})^2}{\Delta t} = \frac{(\Delta x)^2}{\Delta t}\left[1 + \left(\frac{\Delta y}{\Delta x}\right)^2\right], \tag{19.51}$$

which also can be seen in Eq. (2.19). If the effective diffusivity contains only information about dispersion along coordinate x, then

$$D(x) \sim \frac{(\Delta x)^2}{\Delta t}, \tag{19.52}$$

where using Eq. (19.51) gives

$$D_0 \sim D(x)\left[1 + \left(\frac{\Delta y}{\Delta x}\right)^2\right], \tag{19.53}$$

or written for the effective diffusivity

$$D(x) \sim D_0 \frac{1}{\left[1 + \left(\frac{\Delta y}{\Delta x}\right)^2\right]}. \tag{19.54}$$

Decreasing the ratio of the increments in both directions so as to allow it to remain finite, this could be interpreted as the derivative of y, namely,

$$\lim_{\substack{\Delta x \to 0 \\ \Delta y \to 0}} \frac{\Delta x}{\Delta y} = \frac{\mathrm{d}y}{\mathrm{d}x} = h'(x), \tag{19.55}$$

which also can be referred to as the derivative of the system's boundary. With this information and a heuristic derivation, Reguera and Rubi proposed what they called a *scaling law* for the effective diffusivity, which features an exponent α to generalize the behavior, that is,

$$D_{RR} = \frac{D_0}{\left[1 + h'(x)^2\right]^{\alpha}}, \tag{19.56}$$

where $\alpha = 1/3$ for two-dimensional systems and $\alpha = 1/2$ for three-dimensional ones.

In recent works, the width of the channel $w(x)$ takes the place of the boundary function $h(x)$ inside the effective diffusion coefficient. As a result, their relation in terms of its derivatives is

$$h'(x) = \frac{1}{2} w'(x), \tag{19.57}$$

and Eq. (19.56) becomes

$$D_{RR} = \frac{D_0}{\left[1 + \frac{1}{4} w'(x)^2\right]^{\alpha}}, \tag{19.58}$$

where if $\alpha = 1/3$ for a two-dimensional system, the formula can be expanded as follows:

$$D_{RR} = \frac{D_0}{\left[1 + \frac{1}{4} w'^2(x)\right]^{1/3}} = 1 - \frac{1}{12} w'(x)^2 + \frac{1}{18} w'(x)^4 - \frac{7}{162} w'(x)^6 + \ldots, \tag{19.59}$$

where Newton's binomial generalized theorem, Eq. (A.42), was used in the form of Eq. (A.45). Also, Zwanzig's formula can be expanded as

$$D_{Zw} = \frac{D_0}{1 + \frac{1}{4}w'^2(x)} = 1 - \frac{1}{4}w'(x)^2 + \frac{1}{16}w'(x)^4 - \frac{1}{64}w'(x)^6 + \ldots. \tag{19.60}$$

Using Eq. (19.60) in Eq. (19.59), we can write

$$D_{RR} = D_{Zw} + \frac{1}{6}w'(x)^2 - \frac{7}{144}w'(x)^4 + \frac{67}{5184}w'(x)^6 + \ldots. \tag{19.61}$$

Then, Zwanzig's result for effective diffusivity is included into the RR proposal.

19.4 Concluding Remarks

Starting with well-established concepts of non-equilibrium thermodynamics, the so-called kinetic equation proposed by Reguera and Rubi was found as in Eq. (6.16). As it turns out, this expression is a generalization of the Smoluchowski equation for when we have not only an entropic but also an energetic potential, and it even includes a non-constant diffusion coefficient.

Then, following the Zwanzig method of dimensional reduction, we calculated Eq. (19.34), and as a first approach to obtain useful information from it, we proposed equilibrium solution for systems that are under the influence of an energetic gravitational-like force field. Moreover, this procedure led us to find a corresponding Fick-Jacobs-like equation, which will be the basis for the development of a general solution in further chapters.

Last but not least, a heuristical 2D and 3D proposal for a new diffusion coefficient was made. It is remarkable that this can not only be reduced to but also even improve the one calculated by Zwanzig.

Further Reading and References

S.R. de Groot, P. Mazur, *Non-Equilibrium Thermodynamics* (Dover Publications, Mineola, 1984)

D. Reguera, J.M. Rubi, Kinetic equations for diffusion in the presence of entropic barriers. Phys. Rev. E **64**, 061106 (2006). https://doi.org/10.1103/PhysRevE.64.061106

Chapter 20
Kalinay and Percus Projection Method

Kalinay and Percus (KP) presented the first systematical treatment of diffusion in quasi-one-dimensional (two-dimensional (2D) and three-dimensional (3D)) narrow channels, with varying cross-section along the longitudinal coordinate. Consequently, only the one-dimensional (1D) probability density or corresponding 1D flux is of interest. In other words, changes along the unconfined direction of the particle's motion last longer in comparison to the transversal direction, for which local equilibration is reached faster. KP proposed a mapping procedure of the diffusion equation onto 1D, eliminating transients (i.e., the quick relaxation processes) in transverse direction, which allows us to derive an expansion of the position-dependent effective diffusion coefficient, $D(x)$. This procedure represents systematical corrections to the Fick-Jacobs (FJ) equation in terms of an expansion parameter $\epsilon = D_x/D_y$. This scaling parameter expresses anisotropy of space with respect to diffusion coefficients in longitudinal (D_x) and transverse (D_y) directions. Using this scaling, the fast transverse modes (transients) are separated from the slow longitudinal ones, and the n-dimensional diffusion equation can be projected out into a Fick-Jacobs-like equation by integrating over the transverse direction. This one-dimensional equation contains an effective longitudinal diffusion coefficient, which depends on the x-coordinate. In this chapter, we will show how to apply the projection method introduced by KP to the case of an asymmetric 2D channel and a symmetric 3D tube. From the results obtained for the 2D asymmetric channel, the reduction to a symmetric channel is calculated.

L. Dagdug et al., *Diffusion Under Confinement*,
https://doi.org/10.1007/978-3-031-46475-1_20

20.1 2D Asymmetric Channel: Projection Method

20.1.1 The Projection Method

The problem under consideration is the study of the time evolution of the concentration of noninteracting point-like Brownian particles without external fields, diffusing into a narrow 2D channel, i.e., where the typical width of the channel is smaller than its length. The channel lies in the XY-plane and is bounded by hard walls described by the two boundary functions: $y = h_1(x)$ and $y = h_2(x)$. We assume that $h_1(x)$ and $h_2(x)$ are arbitrary smooth single-valued functions of x, which are defined in the domain: $\Omega = (-\infty, \infty)$, being $h_2(x) > h_1(x)\ \forall\, x \in \Omega$ (see Fig. 20.1).

The KP projection method is based on introducing an artificial anisotropy of the diffusion coefficient into the diffusion equation. It assumes that the transversal diffusion constant D_y is much faster than the one for the longitudinal direction, D_x, i.e., $D_y \gg D_x$. The ratio between these two bulk constants allows us to introduce the anisotropy and define a small parameter $\epsilon = D_x/D_y$. This results in a recurrence scheme that provides systematical corrections to the FJ equation, encoded in the position-dependent diffusion coefficient.

Following the techniques outlined in Sect. 18.1, we are interested in projecting the 2D diffusion equation:

$$\frac{\partial c(x, y, t)}{\partial t} = D_x \frac{\partial^2 c(x, y, t)}{\partial x^2} + D_y \frac{\partial^2 c(x, y, t)}{\partial y^2}, \tag{20.1}$$

onto the longitudinal dimension as an expansion in ϵ. To such end, we have to define the projected or marginal one-dimensional (1D) density $\rho(x, t)$ as

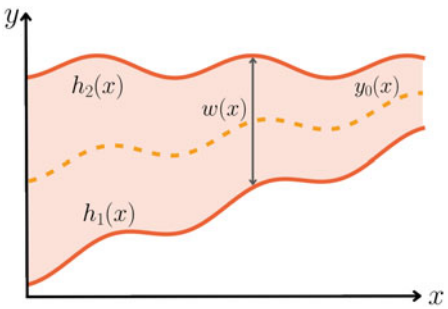

Fig. 20.1 Schematic representation of a 2D narrow asymmetric channel with varying width. The hard walls of the channel are described by the two boundary functions $y = h_1(x)$ and $y = h_2(x)$, where $h_2(x) > y > h_1(x)\,\forall\, x \in \Omega$. On the boundaries, the normal vector of flux density is parallel to the walls. The centerline of the channel is given by $y_0(x) = [h_2(x) + h_1(x)]/2$, and the channel width by $w(x) = h_2(x) - h_1(x)$

$$\rho(x,t) \equiv \int_{h_1(x)}^{h_2(x)} c(x,y,t)\,\mathrm{d}y, \tag{20.2}$$

where the boundaries of the channel are defined within the interval $h_1(x) < y < h_2(x)$. Using Eq. (20.2) and integrating the first term on the right-hand side of Eq. (20.1) by means of the Leibniz integral rule (see Appendix A.3), we have

$$\begin{aligned}
&\int_{h_1(x)}^{h_2(x)} D_x \frac{\partial}{\partial x}\left[\frac{\partial c(x,y,t)}{\partial x}\right]\mathrm{d}y \\
&= D_x\left\{\frac{\partial}{\partial x}\left[\frac{\partial}{\partial x}\int_{h_1(x)}^{h_2(x)} c(x,y,t)\mathrm{d}y + h_1'(x)\,c(x,h_1(x),t) - h_2'(x)\,c(x,h_2(x),t)\right]\right. \\
&\quad \left. + h_1'(x)\frac{\partial c(x,y,t)}{\partial x}\bigg|_{y=h_1(x)} - h_2'(x)\frac{\partial c(x,y,t)}{\partial x}\bigg|_{y=h_2(x)}\right\} \\
&= D_x\left\{\frac{\partial^2 \rho(x,t)}{\partial x^2} + \frac{\partial}{\partial x}\Big[h_1'(x)\,c(x,h_1(x),t) - h_2'(x)\,c(x,h_2(x),t)\Big]\right. \\
&\quad \left. + h_1'(x)\frac{\partial c(x,y,t)}{\partial x}\bigg|_{y=h_1(x)} - h_2'(x)\frac{\partial c(x,y,t)}{\partial x}\bigg|_{y=h_2(x)}\right\}.
\end{aligned} \tag{20.3}$$

Then, we use the fundamental theorem of calculus to integrate the second term, namely,

$$\int_{h_1(x)}^{h_2(x)} D_y \frac{\partial^2 c(x,y,t)}{\partial y^2}\,\mathrm{d}y = D_y \frac{\partial c(x,y,t)}{\partial y}\bigg|_{y=h_1(x)}^{y=h_2(x)}, \tag{20.4}$$

leading to

$$\begin{aligned}
\frac{\partial \rho(x,t)}{\partial t} &= D_x\left\{\frac{\partial^2 \rho(x,y,t)}{\partial x^2} + \frac{\partial}{\partial x}\Big[h_1'(x)\,c(x,h_1(x),t) - h_2'(x)\,c(x,h_2(x),t)\Big]\right. \\
&\quad \left. + h_1'(x)\frac{\partial c(x,y,t)}{\partial x}\bigg|_{y=h_1(x)} - h_2'(x)\frac{\partial c(x,y,t)}{\partial x}\bigg|_{y=h_2(x)}\right\} \\
&\quad + D_y \frac{\partial c(x,y,t)}{\partial y}\bigg|_{y=h_1(x)}^{y=h_2(x)},
\end{aligned} \tag{20.5}$$

where primed quantities denote differentiation with respect to x. Imposing the boundary conditions (BCs) that establish that the flow

$$\mathbf{J}(x, y, t) = -D_x \frac{\partial c(x, y, t)}{\partial x}\,\hat{\mathbf{e}}_x - D_y \frac{\partial c(x, y, t)}{\partial y}\,\hat{\mathbf{e}}_y, \tag{20.6}$$

along the channel walls must be parallel to these walls, the Newmann BCs have to be satisfied, i.e.,

$$\mathbf{h}_i' \times \mathbf{J}(x, y, t) = 0, \tag{20.7}$$

where $\mathbf{h}_i'$ is a tangent vector to the upper ($i = 2$) and lower ($i = 1$) boundaries at x, namely,

$$\mathbf{h}_i' = \hat{\mathbf{e}}_x\, h_i'(x) + \hat{\mathbf{e}}_y. \tag{20.8}$$

Substituting the vectors in Eqs. (20.6) and (20.8) into Eq. (20.7), we arrive at

$$\mathbf{h}_i' \times \mathbf{J}(x, y, t) = \begin{vmatrix} 1 & h_i'(x) \\ -D_x \dfrac{\partial c(x, y, t)}{\partial x} & -D_y \dfrac{\partial c(x, y, t)}{\partial y} \end{vmatrix} \hat{\mathbf{e}}_z = 0, \tag{20.9}$$

and consequently,

$$D_y \left.\frac{\partial c(x, y, t)}{\partial y}\right|_{y=h_i(x)} = D_x\, h_i'(x) \left.\frac{\partial c(x, y, t)}{\partial x}\right|_{y=h_i(x)}, \qquad i = 1, 2. \tag{20.10}$$

Applying these BCs to Eq. (20.5), we obtain the projected 1D diffusion equation:

$$\frac{\partial \rho(x, t)}{\partial t} = D_x \left\{ \frac{\partial^2 \rho(x, t)}{\partial x^2} - \frac{\partial}{\partial x}\Big[h_2'(x)\, c(x, h_2(x), t) - h_1'(x)\, c(x, h_1(x), t) \Big] \right\}. \tag{20.11}$$

Now, we must express the value of the 2D concentration at the upper and lower boundaries, $c(x, h_i(x), t)$, $i = 1, 2$, in terms of the 1D density $\rho(x, t)$. The first approximation is obtained when an infinite transverse diffusion rate is imposed, $D_y \gg D_x$. In other words, when we assume that the system relaxes infinitely fast along the y-axis. This is sometimes called the *equilibrium solution*. Then, from Eq. (20.2) we have

$$c_0(x, y, t) = \frac{\rho(x, t)}{h_2(x) - h_1(x)}, \tag{20.12}$$

where we must recall that the varying width is given by $w(x) = h_2(x) - h_1(x)$. Then,

$$c_0(x, y, t) = \frac{\rho(x, t)}{w(x)}. \tag{20.13}$$

By substituting this last expression into Eq. (20.11), we obtain

$$\frac{\partial \rho(x,t)}{\partial t} = D_x \left\{ \frac{\partial^2 \rho(x,t)}{\partial x^2} - \frac{\partial}{\partial x}\left[\frac{w'(x)}{w(x)} \rho(x,t) \right] \right\}, \tag{20.14}$$

where we set $D_x = D_0$ to recover the FJ equation. Now, we can rewrite this equation as

$$\frac{\partial \rho(x,t)}{\partial t} = D_0 \frac{\partial}{\partial x} w(x) \frac{\partial}{\partial x} \frac{\rho(x,t)}{w(x)}. \tag{20.15}$$

Under the KP theoretical frame, the FJ equation is the zeroth-order approximation of the projected 1D diffusion equation in the parameter ϵ. In the following section, we will outline the procedure to obtain higher-order corrections of the operator.

20.1.2 Recurrence Formula for the Operators $\hat{\sigma}_j(x, y, \partial_x)$

In order to find a general solution to the 2D FJ equation, Eq. (20.1), we can formally write $c(x, y, t)$ as a perturbation series, where the first term, that is, the zeroth-order, must be the previously found approximation, Eq. (20.15).

Furthermore, we propose that the perturbation series in terms of parameter ϵ be

$$c(x, y, t) = \sum_{j=0}^{\infty} \epsilon^j \, \hat{\sigma}_j(x, y, t) \, \frac{\rho(x,t)}{w(x)}. \tag{20.16}$$

It is worth noting that when comparing Eq. (20.16) to Eq. (20.13), we see that $\hat{\sigma}_0(x, y, \partial_x) = 1$. Next, we outline the steps to obtain a recurrence formula for the operators $\hat{\sigma}_j(x, y, \partial_x)$, once we know the zero order. With this procedure, we will be able to obtain high orders on the FJ description, by means of the position-dependent effective coefficient.

To incorporate the operators $\hat{\sigma}_j(x, y, t)$ into the diffusion equation, Eq. (20.1), the first step is to rewrite it as follows:

$$\frac{1}{D_y} \frac{\partial c(x, y, t)}{\partial t} - \frac{D_x}{D_y} \frac{\partial^2 c(x, y, t)}{\partial x^2} = \frac{\partial^2 c(x, y, t)}{\partial y^2}. \tag{20.17}$$

As Eq. (20.16) is the solution of Eq. (20.17) by construction, we substitute the former into the latter, yielding

$$\left(\frac{1}{D_x} \frac{\partial}{\partial t} - \frac{\partial^2}{\partial x^2} \right) \sum_{j=0}^{\infty} \epsilon^{j+1} \, \hat{\sigma}_j(x, y, \partial_x) \frac{\partial}{\partial x} \frac{\rho(x,t)}{w(x)}$$

$$= \sum_{j=0}^{\infty} \epsilon^j \frac{\partial^2}{\partial y^2} \hat{\boldsymbol{\sigma}}_j(x, y, \partial_x) \frac{\partial}{\partial x} \frac{\rho(x,t)}{w(x)}. \tag{20.18}$$

Then, we also substitute Eq. (20.16) into Eq. (20.11), to obtain

$$\frac{\partial \rho(x,t)}{\partial t} = D_x \frac{\partial^2 \rho(x,t)}{\partial x^2} - D_x \frac{\partial}{\partial x} \left\{ \sum_{j=0}^{\infty} \epsilon^j \Big[h_2'(x)\, \hat{\boldsymbol{\sigma}}_j(x, h_2(x), \partial_x) - h_1'(x)\, \hat{\boldsymbol{\sigma}}_j(x, h_1(x), \partial_x) \Big] \right\} \frac{\partial}{\partial x} \frac{\rho(x,t)}{w(x)}, \tag{20.19}$$

which by explicitly expressing the $j = 0$ term, after a small mathematical reorganization, gives

$$\frac{\partial \rho(x,t)}{\partial t} = D_x \frac{\partial}{\partial x} \left\{ w(x) - \sum_{j=1}^{\infty} \epsilon^j \Big[h_2'(x)\, \hat{\boldsymbol{\sigma}}_j(x, h_2(x), \partial_x) - h_1'(x)\, \hat{\boldsymbol{\sigma}}_j(x, h_1(x), \partial_x) \Big] \right\} \frac{\partial}{\partial x} \frac{\rho(x,t)}{w(x)}. \tag{20.20}$$

Now, let us rewrite Eq. (20.17) as

$$\sum_{j=0}^{\infty} \epsilon^j \frac{\partial^2}{\partial y^2} \hat{\boldsymbol{\sigma}}_j(x, y, \partial_x) \frac{\partial}{\partial x} \frac{\rho(x,t)}{w(x)} = \sum_{j=0}^{\infty} \epsilon^{j+1} \left[\frac{\hat{\boldsymbol{\sigma}}_j(x, y, \partial_x)}{D_x} \frac{\partial}{\partial x} \frac{1}{w(x)} \frac{\partial \rho(x,t)}{\partial t} - \frac{\partial^2}{\partial x^2} \hat{\boldsymbol{\sigma}}_j(x, y, \partial_x) \frac{\partial}{\partial x} \frac{\rho(x,t)}{w(x)} \right]. \tag{20.21}$$

By replacing $\partial_t \rho(x,t)$ in Eqs. (20.21) and (20.20), we arrive at

$$\sum_{j=0}^{\infty} \epsilon^j \frac{\partial^2}{\partial y^2} \hat{\boldsymbol{\sigma}}_j(x, y, \partial_x) \frac{\partial}{\partial x} \frac{\rho(x,t)}{w(x)} = \sum_{j=0}^{\infty} \epsilon^{j+1} \left\{ \hat{\boldsymbol{\sigma}}_j(x, y, \partial_x) \frac{\partial}{\partial x} \frac{1}{w(x)} \frac{\partial}{\partial x} \left\{ w(x) - \sum_{k=1}^{\infty} \epsilon^k \Big[h_2'(x)\, \hat{\boldsymbol{\sigma}}_k(x, h_2(x), \partial_x) - h_1'(x)\, \hat{\boldsymbol{\sigma}}_k(x, h_1(x), \partial_x) \Big] \right\} - \frac{\partial^2 \hat{\boldsymbol{\sigma}}_k(x, y, \partial_x)}{\partial x^2} \right\} \frac{\partial}{\partial x} \frac{\rho(x,t)}{w(x)}. \tag{20.22}$$

Expanding the left-hand side and collecting terms proportional to ϵ^j, we have

$$
\begin{aligned}
&\left\{\epsilon^j \frac{\partial^2}{\partial y^2}\hat{\boldsymbol{\sigma}}_j(x,y,\partial_x)\right\}\frac{\partial}{\partial x}\frac{\rho(x,t)}{w(x)} = \left\{\epsilon^j\,\hat{\boldsymbol{\sigma}}_{j-1}(x,y,\partial_x)\frac{\partial}{\partial x}\frac{1}{w(x)}\frac{\partial}{\partial x}w(x)\right.\\
&+\epsilon^{j-1}\,\hat{\boldsymbol{\sigma}}_{j-2}(x,y,\partial_x)\frac{\partial}{\partial x}\frac{1}{w(x)}\frac{\partial}{\partial x}\\
&\times\left[-\epsilon^1\left(h_2'(x)\hat{\boldsymbol{\sigma}}_1(x,h_2(x),\partial_x)-h_1'(x)\,\hat{\boldsymbol{\sigma}}_1(x,h_1(x),\partial_x)\right)\right]\\
&+\epsilon^{j-2}\,\hat{\boldsymbol{\sigma}}_{j-3}(x,y,\partial_x)\frac{\partial}{\partial x}\frac{1}{w(x)}\frac{\partial}{\partial x}\\
&\times\left[-\epsilon^2\left(h_2'(x)\,\hat{\boldsymbol{\sigma}}_2(x,h_2(x),\partial_x)-h_1'(x)\,\hat{\boldsymbol{\sigma}}_2(x,h_1(x),\partial_x)\right)\right]\\
&+\cdots\\
&+\epsilon^2\,\hat{\boldsymbol{\sigma}}_1(x,y,\partial_x)\frac{\partial}{\partial x}\frac{1}{w(x)}\frac{\partial}{\partial x}\\
&\left[-\epsilon^{j-2}\left(h_2'(x)\,\hat{\boldsymbol{\sigma}}_{j-2}(x,h_2(x),\partial_x)-h_1'(x)\,\hat{\boldsymbol{\sigma}}_{j-2}(x,h_1(x),\partial_x)\right)\right]\\
&+\epsilon^1\,\hat{\boldsymbol{\sigma}}_0(x,y,\partial_x)\frac{\partial}{\partial x}\frac{1}{w(x)}\frac{\partial}{\partial x}\\
&\times\left[-\epsilon^{j-1}\left(h_2'(x)\,\hat{\boldsymbol{\sigma}}_{j-1}(x,h_2(x),\partial_x)-h_1'(x)\,\hat{\boldsymbol{\sigma}}_{j-1}(x,h_1(x),\partial_x)\right)\right]\\
&+\quad\cdots\quad\left.-\epsilon^j\frac{\partial^2}{\partial x^2}\hat{\boldsymbol{\sigma}}_{j-1}(x,y,\partial_x)\right\}\frac{\partial}{\partial x}\frac{\rho(x,t)}{w(x)}.
\end{aligned}
\tag{20.23}
$$

Comparing the coefficients at the same order in ϵ, we obtain the recurrence formula for operators $\hat{\boldsymbol{\sigma}}_j(x,y,\partial_x)$:

$$
\begin{aligned}
&\frac{\partial^2}{\partial y^2}\hat{\boldsymbol{\sigma}}_{j+1}(x,y,\partial_x) =\\
&-\sum_{k=1}^{j}\hat{\boldsymbol{\sigma}}_{j-k}(x,y,\partial_x)\frac{\partial}{\partial x}\frac{1}{w(x)}\frac{\partial}{\partial x}\left[h_2'(x)\,\hat{\boldsymbol{\sigma}}_k(x,h_2(x),\partial_x)-h_1'(x)\,\hat{\boldsymbol{\sigma}}_k(x,h_1(x),\partial_x)\right]\\
&+\hat{\boldsymbol{\sigma}}_j(x,y,\partial_x)\frac{\partial}{\partial x}\frac{1}{w(x)}\frac{\partial}{\partial x}w(x)-\frac{\partial^2}{\partial x^2}\hat{\boldsymbol{\sigma}}_j(x,y,\partial_x).
\end{aligned}
\tag{20.24}
$$

Finally, to calculate $\hat{\boldsymbol{\sigma}}_{j+1}(x,y,\partial_x)$ at any order, one has to perform a double integration over y. The integration constants are set to fulfill the BCs, and following the same steps that led us to Eq. (20.10) applied to Eq. (20.19), we obtain

$$h_2'(x)\frac{\partial}{\partial x}\hat{\boldsymbol{\sigma}}_j(x,y,\partial_x)\frac{\partial}{\partial x}\frac{\rho(x,t)}{w(x)}\bigg|_{y=h_2(x)}+h_1'(x)\frac{\partial}{\partial x}\hat{\boldsymbol{\sigma}}_j(x,y,\partial_x)\frac{\partial}{\partial x}\frac{\rho(x,t)}{w(x)}\bigg|_{y=h_1(x)}$$

$$=\frac{\partial}{\partial y}\hat{\boldsymbol{\sigma}}_{j+1}(x,y,\partial_x)\frac{\partial}{\partial x}\frac{\rho(x,t)}{w(x)}\bigg|_{y=h_2(x)}+\frac{\partial}{\partial y}\hat{\boldsymbol{\sigma}}_{j+1}(x,y,\partial_x)\frac{\partial}{\partial x}\frac{\rho(x,t)}{w(x)}\bigg|_{y=h_1(x)}, \tag{20.25}$$

and the normalization condition is

$$\int_{h_1(x)}^{h_2(x)}\hat{\boldsymbol{\sigma}}_j(x,y,\partial_x)\frac{\partial}{\partial x}\frac{\rho(x,t)}{w(x)}\,\mathrm{d}y=0,\qquad j>0. \tag{20.26}$$

The symmetrical case is recovered when $h_1(x)=-h_2(x)$.

20.1.3 First- and Second-Order Corrections

In this section, we will calculate the first two operators $\hat{\boldsymbol{\sigma}}_j(x,y,\partial_x)$, namely, for $j=1,2$, by applying the normalization conditions, Eqs. (20.25) and (20.26). For this procedure, we need to recall that $\hat{\boldsymbol{\sigma}}_0(x,y,\partial_x)\,\partial_x=1$. Now, to obtain the first-order term, we have to set $j=0$ on the left-hand side and $j=1$ on the right-hand side of Eq. (20.18), noting that $\rho_0(x,t)$ does not depend on y, leading to

$$\left(\frac{1}{D_x}\frac{\partial}{\partial t}-\frac{\partial^2}{\partial x^2}\right)\epsilon^1\frac{\rho(x,t)}{w(x)}=\epsilon^1\frac{\partial^2}{\partial y^2}\hat{\boldsymbol{\sigma}}_1(x,y,\partial_x)\frac{\partial}{\partial x}\frac{\rho(x,t)}{w(x)}. \tag{20.27}$$

On the left-hand side of this last equation, we substitute the Fick-Jacobs equation rewritten in the following form:

$$\left(\frac{1}{D_x}\frac{\partial}{\partial t}-\frac{\partial^2}{\partial x^2}\right)\frac{\rho(x,t)}{w(x)}=\frac{w'(x)}{w(x)}\frac{\partial}{\partial x}\left[\frac{\rho(x,t)}{w(x)}\right], \tag{20.28}$$

which allows us to obtain

$$\hat{\boldsymbol{\sigma}}_1(x,y,\partial_x)\frac{\partial}{\partial x}\left[\frac{\rho(x,y)}{w(x)}\right]=\frac{w'(x)}{w(x)}\frac{\partial}{\partial x}\left[\frac{\rho(x,t)}{w(x)}\right]\int\int\mathrm{d}y\,\mathrm{d}y. \tag{20.29}$$

Performing a double integration over y, we arrive at

$$\hat{\boldsymbol{\sigma}}_1(x,y,\partial_x)\frac{\partial}{\partial x}\frac{\rho(x,t)}{w(x)}=\left\{\frac{w'(x)}{w(x)}\frac{\partial}{\partial x}\frac{\rho(x,t)}{w(x)}\right\}\frac{y^2}{2}+\mathcal{A}\,y+\mathcal{B}, \tag{20.30}$$

where $\mathcal{A}$ and $\mathcal{B}$ are the integration constants. Imposing the BCs given by Eq. (20.25), we find that

$$\mathcal{A} = \left[\frac{h_2(x)\,h_1'(x) - h_1(x)\,h_2'(x)}{w(x)}\right]\frac{\partial}{\partial x}\frac{\rho(x,t)}{w(x)}. \tag{20.31}$$

When the normalization condition, Eq. (20.26), is fulfilled, we obtain

$$\begin{aligned}\mathcal{B} = -\frac{1}{w(x)^2}\Bigg\{&\frac{w'(x)}{6}\left[h_2(x)^3 - h_1(x)^3\right]\\ &-\frac{1}{2}\left[h_2(x)^2 - h_1(x)^2\right]\left[h_1(x)\,h_2'(x) - h_2(x)\,h_1'(x)\right]\Bigg\}\frac{\partial}{\partial x}\frac{\rho(x,t)}{w(x)}.\end{aligned} \tag{20.32}$$

Finally, substituting these last two equations into Eq. (20.30), we have the first-order correction operator, namely,

$$\begin{aligned}\hat{\boldsymbol{\sigma}}_1(x,y,\partial x) = \frac{1}{w(x)}\Bigg\{&\left[h_2'(x) - h_1'(x)\right]\frac{y^2}{2} - \left[h_1(x)\,h_2'(x) - h_2(x)\,h_1'(x)\right]y\\ &-\frac{1}{6}\left[h_2(x)^2 + h_2(x)\,h_1(x) + h_1(x)^2\right]\left[h_2'(x) - h_1'(x)\right]\\ &+\frac{1}{2}\left[h_2(x) + h_1(x)\right]\left[h_1(x)\,h_2'(x) - h_2(x)\,h_1'(x)\right]\Bigg\}.\end{aligned} \tag{20.33}$$

An important relation, which we will use later, is found by noting that the expression inside the square brackets in Eq. (20.20) indicates that $\hat{\boldsymbol{\sigma}}_1$ must be evaluated at both the top and bottom boundaries. Therefore, by direct computation, we find that

$$\begin{aligned}&h_2'(x)\,\hat{\boldsymbol{\sigma}}_1(x,h_2(x),\partial x) - h_1'(x)\,\hat{\boldsymbol{\sigma}}_1(x,h_1(x),\partial x)\\ &\quad = \frac{1}{3}w(x)\left[h_2'(x)^2 + h_2'(x)\,h_1'(x) + h_1'(x)^2\right].\end{aligned} \tag{20.34}$$

To obtain the second-order operator, $\hat{\boldsymbol{\sigma}}_2(x,y,t)$, we have to set $j = 1$ on the left-hand side and $j = 2$ on the right-hand side of Eq. (20.18), and make use of Eq. (20.33), leading to

$$\begin{aligned}&\frac{\partial^2}{\partial y^2}\hat{\boldsymbol{\sigma}}_2(x,y,\partial_x)\frac{\partial}{\partial x}\frac{\rho(x,t)}{w(x)}\\ &\quad = \Bigg\{-\frac{1}{w(x)}\frac{\partial}{\partial x}\left[\frac{1}{3}w(x)\left(h_2'(x)^2 + h_2'(x)\,h_1'(x) + h_1'(x)^2\right)\right]\\ &\qquad + \hat{\boldsymbol{\sigma}}_1(x,y,\partial_x)\frac{\partial}{\partial x}\frac{1}{w(x)}\frac{\partial}{\partial x}w(x) - \frac{\partial^2}{\partial x^2}\hat{\boldsymbol{\sigma}}_1(x,y,\partial_x)\Bigg\}\frac{\partial}{\partial x}\frac{\rho(x,t)}{w(x)}.\end{aligned} \tag{20.35}$$

Following the same steps, which allow us to integrate Eq. (20.27), we arrive at

$$h_2'(x)\,\hat{\boldsymbol{\sigma}}_2(x,h_2(x),\partial x) - h_1'(x)\,\hat{\boldsymbol{\sigma}}_2(x,h_1(x),\partial x) - \frac{1}{5}w(x)\left[h_2'(x)^4 + h_2'(x)^3\,h_1'(x) + h_2'(x)^2\,h_1'(x)^2 + h_2'(x)\,h_1'(x)^3 + h_1'(x)^4\right]. \tag{20.36}$$

Finally, substituting Eqs. (20.34) and (20.36) into Eq. (20.11), we arrive at the projected 1D diffusion equation up to the first order on the derivatives of the boundaries, that is,

$$\begin{aligned}\frac{\partial\rho(x,t)}{\partial t} = D_x\,\frac{\partial}{\partial x}\Bigg\{ & w(x) - \frac{\epsilon}{3}w(x)\left[h_2'(x)^2 + h_2'(x)\,h_1'(x) + h_1'(x)^2\right] \\ & + \frac{\epsilon^2}{5}w(x)\Big[h_2'(x)^4 + h_2'(x)^3\,h_1'(x) + h_2'(x)^2\,h_1'(x)^2 \\ & + h_2'(x)\,h_1'(x)^3 + h_1'(x)^4\Big] + \cdots\Bigg\}\,\frac{\partial}{\partial x}\,\frac{\rho(x,t)}{w(x)}.\end{aligned} \tag{20.37}$$

In the following section, we will provide the steps that allow us to link Eq. (20.37) with the position-dependent effective diffusion coefficient.

20.1.4 The Position-Dependent Effective Diffusion Coefficient

By applying KP's projection method, we can systematically obtain higher-order corrections in the evolution of concentration, which are explicitly written in Eq. (20.19) by means of parameter ϵ. Now, our goal is to compare this equation with the modified FJ equation, allowing us to obtain higher-order corrections of the position-dependent effective diffusion coefficient. This procedure is carried out by equating the flows obtained from both equations in the steady state. It is worth mentioning that these quantities are only equal in steady state. To such end, let us write Eq. (20.19) in a compact form, namely,

$$\frac{\partial\rho(x,t)}{\partial x} = D_0\,\frac{\partial}{\partial x}w(x)\Big[1 - \epsilon\,\hat{\boldsymbol{Z}}(x,\partial_x)\Big]\frac{\partial}{\partial x}\,\frac{\rho(x,t)}{w(x)}, \tag{20.38}$$

where $\hat{\boldsymbol{Z}}(x,\partial_x)$ is the operator defined as

$$\hat{\boldsymbol{Z}}(x,\partial_x) = \sum_{k=0}^{\infty}\epsilon^k\,\hat{\boldsymbol{\sigma}}_{k+1}(x,w(x),\partial_x). \tag{20.39}$$

The expression on the right-hand side of Eq. (20.38) can be identified as the flux, yielding

$$J(x,t) = -w(x)\Big[1 - \epsilon\,\hat{\boldsymbol{Z}}(x,\partial_x)\Big]\frac{\partial}{\partial x}\frac{\rho(x,t)}{w(x)}. \tag{20.40}$$

On the other hand, the flux, Eq. (17.19), is given by

$$J(x,t) = -w(x)\,D(x)\frac{\partial}{\partial x}\frac{\rho(x,t)}{w(x)}. \tag{20.41}$$

In the steady state, i.e., $\partial_t \rho(x,t) = 0$, we can compare these last two equations as $J(x,t) \to J$ and identify the relation between $D(x)$ and $1 - \epsilon\,\hat{\boldsymbol{Z}}(x,\partial_x)$.

In order to find $D(x)$ such that the solution of Eq. (20.41) also satisfies Eq. (20.40), we substitute $\partial_x[\rho(x,t)/w(x)]$ from the former equation into the latter, finding that

$$1 = w(x)\Big[1 - \epsilon\,\hat{\boldsymbol{Z}}(x,\partial_x)\Big]\frac{1}{w(x)\,D(x)}. \tag{20.42}$$

This relation enables us to express the series of function $D(x)$ uniquely within a recurrence scheme coming from the mapping procedure. By expanding Eq. (20.42) using the binomial theorem in Appendix A.6.5, we have

$$\frac{1}{D(x)} = w(x)\Big[1 + \epsilon\,\hat{\boldsymbol{Z}}(x,\partial_x) + \epsilon^2\,\hat{\boldsymbol{Z}}(x,\partial_x) + \cdots\Big]\frac{1}{w(x)}. \tag{20.43}$$

When simplifying factors and terms, we find that

$$\frac{1}{D(x)} = \left[1 - \epsilon\,w(x)\,\hat{\boldsymbol{Z}}(x,\partial_x)\frac{1}{w(x)}\right]^{-1}. \tag{20.44}$$

Relaxing the rule that operators act on everything to the right in products and assuming that $\hat{\boldsymbol{Z}}(x,\partial_x)$ acts only on the following $w(x)^{-1}$, we can perform the final inversion, yielding

$$D(x) \simeq 1 - \epsilon w(x)\hat{\boldsymbol{Z}}(x,\partial_x)\frac{1}{w(x)}. \tag{20.45}$$

Making an approximation of Eq. (20.37) by discarding the second- and higher-order derivatives of h_i, $\hat{\boldsymbol{Z}}(x,\partial_x)$, this becomes

$$\begin{aligned}\hat{\boldsymbol{Z}}(x,\partial_x) = {} & \frac{1}{3}\Big[h_2'(x)^2 + h_2'(x)\,h_1'(x) + h_1'(x)^2\Big] \\ & - \frac{\epsilon}{5}\Big[h_2'(x)^4 + h_2'(x)^3\,h_1'(x) + h_2'(x)^2\,h_1'(x)^2 + h_2'(x)\,h_1'(x)^3 + h_1'(x)^4\Big],\end{aligned} \tag{20.46}$$

which, by substituting into Eq. (20.45), gives

$$D(x) \approx 1 - \frac{\epsilon}{3}\left[h_2'(x)^2 + h_2'(x)\,h_1'(x) + h_1'(x)^2\right] + \frac{\epsilon^2}{5}\left[h_2'(x)^4 + h_2'(x)^3\,h_1'(x) + h_2'(x)^2\,h_1'(x)^2 + h_2'(x)\,h_1'(x)^3 + h_1'(x)^4\right] + \cdots . \tag{20.47}$$

Taking the isotropic case, where $\epsilon = 1$, using the relation for the channel width, $w(x) = h_2(x) - h_1(x)$, and the derivative of the midline $y_0'(x) = [h_2'(x) + h_1'(x)]/2$, this series can be rewritten as follows:

$$D(x) \approx 1 - y_0'(x)^2 - \frac{1}{3}\left[\frac{w'(x)}{2}\right]^2 + y_0'(x)^4 + 2y_0'(x)^2\left[\frac{w'(x)}{2}\right]^2 + \frac{1}{5}\left[\frac{w'(x)}{2}\right]^4 - \cdots \tag{20.48}$$

Neglecting the second and higher derivatives of $w(x)$ and $y_0(x)$, the remaining terms that depend only on $w'(x)$ and $y_0\prime(x)$ allow us to express the effective diffusion coefficient as follows:

$$D(x) = D_0 \sum_{n=0}^{\infty} \frac{(-1)^n}{2n+1} \sum_{i=0}^{2n} \left[y_0'(x) + \frac{w'(x)}{2}\right]^i \left[y_0'(x) - \frac{w'(x)}{2}\right]^{2n-i} . \tag{20.49}$$

After performing the internal sum on the right-hand side of this equation, we obtain

$$D(x) = D_0 \sum_{n=0}^{\infty} \frac{(-1)^n}{2n+1} \frac{1}{w'(x)} \left[y_0'(x) + \frac{w'(x)}{2}\right]^{2n+1} - D_0 \sum_{n=0}^{\infty} \frac{(-1)^n}{2n+1} \frac{1}{w'(x)} \left[y_0'(x) - \frac{w'(x)}{2}\right]^{2n+1} . \tag{20.50}$$

Finally, this last expression can be reduced to

$$D(x) \approx D_{\mathrm{DP}}(x) = \left\{ \arctan\left[y_0'(x) + \frac{w'(x)}{2}\right] - \arctan\left[y_0'(x) - \frac{w'(x)}{2}\right] \right\} \frac{D_0}{w'(x)} . \tag{20.51}$$

This equation, known as the *Dagdug-Pineda formula*, is the main result of this chapter and gives a general expression for the position-dependent diffusion coefficient along the slow x-coordinate for an asymmetric 2D channel. This equation generalizes KP's result for 2D symmetric channels. For a symmetric channel that has a straight centerline, $y_0'(x) = 0$, Eq. (20.51) reduces to

$$D(x) \approx D_{\mathrm{KP}}(x) = \frac{\arctan\left[\frac{1}{2}w'(x)\right]}{\frac{1}{2}w'(x)} D_0. \tag{20.52}$$

Additionally, the equation obtained by Bradley is a truncated expansion of Eq. (20.51) when its Taylor series is kept up to the first order in $w'(x)$ and $y_0\prime(x)$, namely,

$$D(x)_{\mathrm{Br}} \approx D_0 \left[1 - y_0'(x)^2 - \frac{1}{12}w'(x)^2\right] \approx \frac{D_0}{1 + y_0'(x)^2 + \frac{1}{12}w'(x)^2}. \tag{20.53}$$

From this last equation, if $y_0 = 0$, the symmetric case is recovered, i.e., Zwanzig's formula. Moreover, when setting a variable midline and $w'(x) = 0$, which represents a channel of constant width along x-axis, we can recover the result for a serpentine channel previously studied by Yariv, Brenner, and Kim, which reads

$$D(x) \approx D_{\mathrm{YBK}}(x) = \frac{D_0}{1 + y_0\prime(x)^2}. \tag{20.54}$$

Equation (20.51) is a general and simple expression that recovers all the well-known approximations for the effective diffusion coefficient for both asymmetric and symmetric 2D channels.

The approximated formulas for position-dependent diffusion coefficients for quasi-one-dimensional channels are summarized in Table 20.1 as they appear in the literature.

20.2 Trapezoidal 2D Channel

In this section, we study the diffusion coefficient of a 2D channel formed by straight walls, where the boundaries are $h_1(x) = m_1 x - b$ and $h_2(x) = m_2 x + b$ (see Fig. 20.2). The midline and channel width are $y_0(x) = \frac{1}{2}(m_1 + m_2)\, x$ and $w(x) = (m_2 - m_1)\, x + 2b$, respectively. Substituting these expressions into Eq. (20.51), we find that

$$D_{\mathrm{eff}} = \frac{\arctan(m_2) - \arctan(m_1)}{m_2 - m_1} D_0. \tag{20.55}$$

Table 20.1 Position-dependent diffusion coefficient formulas

Author	2D channel	3D tube
Jacobs (1935)	D_0	D_0
Zwanzig (1992)	$\dfrac{D_0}{1+\frac{1}{12}w'(x)^2}$	$\dfrac{D_0}{1+\frac{1}{2}R'(x)^2}$
Reguera and Rubi (2001)	$\dfrac{D_0}{\sqrt[3]{1+\frac{1}{4}w'(x)^2}}$	$\dfrac{D_0}{\sqrt{1+R'(x)^2}}$
Yariv et al. (2004)	$\dfrac{D_0}{1+y_0\prime(x)^2}$	
Kalinay and Percus (2006)	$\dfrac{1}{w'(x)}D_0 \arctan\left[\dfrac{1}{2}w'(x)\right]$	$\dfrac{D_0}{\sqrt{1+R'(x)^2}}$
Bradley (2009)	$\dfrac{D_0}{1+\frac{1}{12}w'(x)^2+y_0\prime(x)^2}$	
Berezhkovskii and Szabo (2011)	$\dfrac{D_0}{1+\frac{1}{12}w'(x)^2+y_0\prime(x)^2}$	$\dfrac{D_0}{1+\frac{1}{2}R'(x)^2+\mathbf{r}_0\prime(x)^2}$
Dagdug and Pineda (2012)	$\dfrac{D_0}{w'(x)}\left\{\arctan\left[y_0'(x)+\dfrac{w'(x)}{2}\right]-\arctan\left[y_0'(x)-\dfrac{w'(x)}{2}\right]\right\}$	

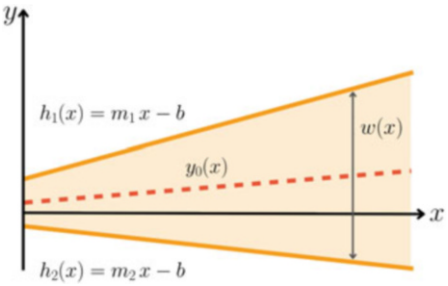

Fig. 20.2 Schematic representation of a 2D conical asymmetric channel with varying width. The walls of the channel are described by the two boundary functions $h_1(x) = m_1x - b$ and $h_2(x) = m_2x + b$. The centerline of the channel is given by $y_0(x) = \frac{1}{2}(m_1 + m_2)x$, and the channel width by $w(x) = (m_2 - m_1)x + 2b$

As a first example, we consider a set of constant-width tilted channels. These are made by setting $m_1 = m_2 = y_0'$, where the channel width is $2b$. Computing the limit when $m_1 = m_2$, or equivalently, when $w'(x) \to 0$, Eq. (20.55) reduces to

$$D(x) \approx D_{\text{eff}} = \frac{D_0}{1+y_0'^2}. \tag{20.56}$$

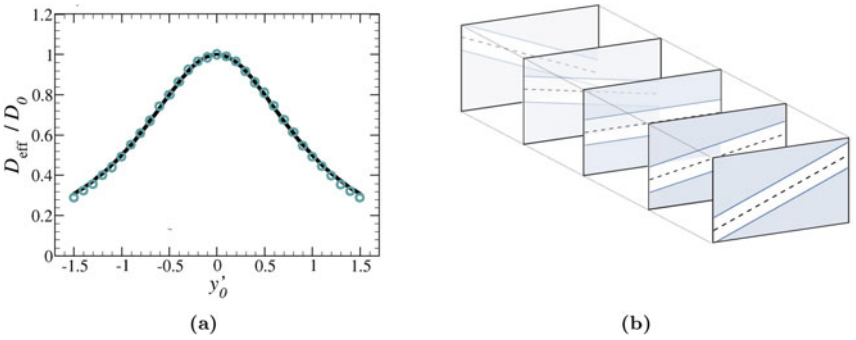

Fig. 20.3 Determination of the effective diffusivity using simulations from the long-time behavior of $\langle \Delta x^2(t) \rangle$, setting $D_0 = 1$ (panel (a)). (**a**) Effective diffusivity found with Brownian dynamics simulations (open circles) and predicted by Eq. (20.56) (solid curve). (**b**) Constant-width title channels with y_0' from -1.5 to 1.5

The effective diffusion coefficient predicted by Eq. (20.56) depends only on the channel slope, as expected. In Fig. 20.3, the circles show the $D_{\rm eff}/D_0$ ratio values from Brownian dynamics simulations, while the continuous line is the prediction made by Eq. (20.56), which is in good agreement with the numerical result over the entire domain. This theoretical description works very well for $w'(x) = 0$.

As a second example, a set of conical channels is constructed by fixing the slope of the lower wall to $m_1 = -1$ and setting the width of the channel to $2b = 1$ at the origin while allowing the slope of the upper wall, m_2, to vary within the range of 0 to 2. In Fig. 20.4, we compare the effective diffusivity predicted by Brownian dynamics simulations and Bradley's formula, Eq. (20.53), and Eq. (20.55). It is worth noting that Eq. (20.55) provides an excellent approximation for the effective diffusivity for $m_2 > 1$, as Eq. (20.53) underestimates the expected values over the full tested range.

In the next section, we will conduct an exhaustive study of the range of applicability of the one-dimensional description in terms of the modified Fick-Jacobs equation.

20.3 First-Passage Time in Conical Channels

As we know, axial diffusion in a two-dimensional (2D) narrow channel of smoothly varying geometry can be approximately described as one-dimensional (1D) diffusion with position-dependent effective diffusivity by means of the modified Fick-Jacobs equation. In addition to the problem of deriving the modified FJ equation, there are questions around the range of applicability of this approximate 1D description and the accuracy of the expressions for effective position-dependent diffusivity. In this section, Brownian dynamics simulations are used to answer these questions, which will help us to clarify the practical utility of the expressions for

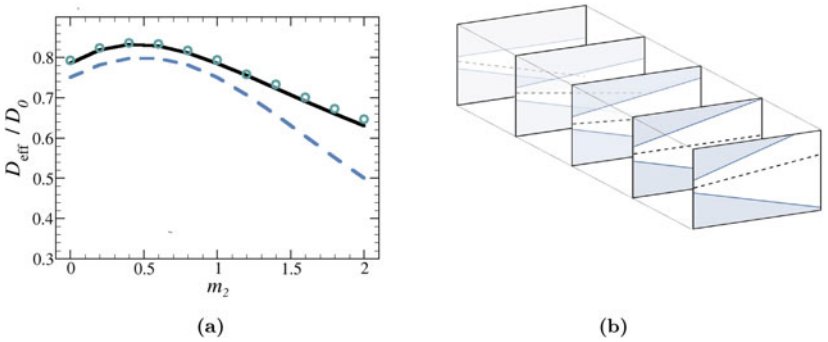

Fig. 20.4 Comparison of different dependencies of the effective diffusivity. The values from simulations were found from the long-time behavior of $\langle \Delta x^2(t) \rangle$, setting $D_0 = 1$. (**a**) Effective diffusion found by Brownian dynamics simulations (open circles), and predicted by Eqs. (20.55) (solid curve) and (20.53) (dashed line). (**b**) Schematic illustration of a 2D channel formed by fixing the slope of the lower wall to $m_1 = -1$ while allowing the slope of the upper wall, m_2, to vary from 0 to 2

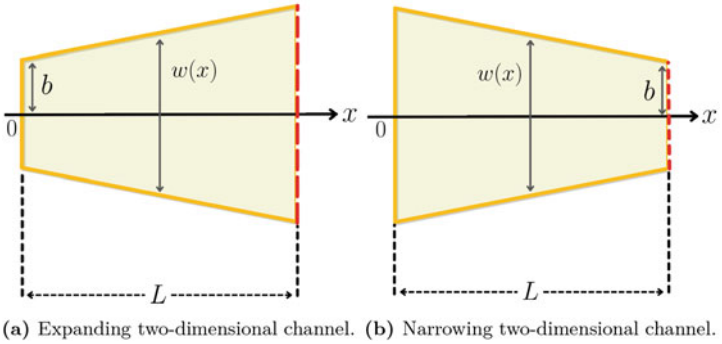

(**a**) Expanding two-dimensional channel. (**b**) Narrowing two-dimensional channel.

Fig. 20.5 Schematic illustration of the expanding (**a**) and narrowing (**b**) two-dimensional channels of length L and variable width $w(x) = 2(b + \lambda x)$ for the expanding channel, and $w(x) = 2[b + \lambda(L - x)]$ for the narrowing channel, where $0 \le x \le L$. In both cases, $w'(x) = 2\lambda$. The particle starts from the reflecting boundary located at $x = 0$ and is trapped by the absorbing boundary at $x = L$ (red dashed lines)

the effective diffusivity for 2D channels proposed by different authors, which are summarized in Table 20.1.

We will study diffusion into narrowing and expanding 2D channels, which are schematically shown in Fig. 20.5. Specifically, we take advantage of the fact that effective diffusivity is a function of the channel's width variation rate, meaning that when this quantity is constant, the effective diffusivity is also a constant. In order to obtain the values for the effective diffusivity from simulations and compare such results with the theoretical formulas, we will focus on the wide-to-narrow ($w \to n$) and narrow-to-wide ($n \to w$) transitions between the two ends of a 2D channel with linear varying width $w'(x)$, straight walls, and length L (see Fig. 20.5). Otherwise

stated, we want to calculate the mean first-passage time (MFPT) when particles start from a reflecting wall at the origin, $x_0 = 0$, and are trapped at the perfectly absorbing end at $x = L$. For the expanding channel, the upper and lower boundaries are given by $h_2(x) = \lambda x + b$ and $h_1(x) = -\lambda x - b = -h_2(x)$, respectively, and consequently $w(x) = 2(b + \lambda x)$ and $w'(x) = 2\lambda$. For the narrowing channel, these are given by $h_2(x) = \lambda(L - x) + b$ and $h_1(x) = -\lambda(L - x) - b = -h_2(x)$, respectively, so then, $w(x) = 2[b + \lambda(L - x)]$ and $w'(x) = 2\lambda$. The reason why we are interested in these transitions will be clear shortly.

Previously, in Chap. 17, we saw that the FJ equation, Eq. (17.19), is equivalent to the Smoluchowski equation when the entropic potential is carefully chosen (see Sect. 17.2). Therefore, $\mathrm{e}^{-\beta U(x)} = w(x)/w_0$, where $w_0 = w(x = 0)$, $\beta = 1/(k_B T)$, with k_B and T denoting the Boltzmann constant and absolute temperature, respectively. Then, for the expanding channel $-\beta U(x) = \ln(1 + \lambda x/b)$ and, for the narrowing channel, $-\beta U(x) = \ln[1 - \lambda x/(b + \lambda L)]$, which shows that in these two transitions, the particles face different entropic barriers.

The theoretical formulas for the effective diffusivity associated with these channels, which follow from the different expressions for $D(x)$, are

$$D(x) \approx D_{\mathrm{FJ}}(x) = D_0 \qquad \text{(Fick-Jacobs)}, \tag{20.57}$$

$$D(x) \approx D_{\mathrm{Zw}}(x) = \frac{1}{1 + \frac{1}{12} w'(x)^2} D_0 = \frac{1}{1 + \frac{1}{3}\lambda^2} D_0 \qquad \text{(Zwanzig)}, \tag{20.58}$$

$$D(x) \approx D_{\mathrm{RR}}(x) = \frac{1}{\left[1 + \frac{1}{4} w'(x)^2\right]^{1/3}} D_0 = \frac{1}{\left[1 + \lambda^2\right]^{1/3}} D_0 \quad \text{(Reguera-Rubi)}, \tag{20.59}$$

$$D(x) \approx D_{\mathrm{KP}}(x) = \frac{\arctan\left[\frac{1}{2} w'(x)\right]}{\frac{1}{2} w'(x)} D_0 = \frac{\arctan \lambda}{\lambda} D_0 \qquad \text{(Kalinay-Percus)}. \tag{20.60}$$

Due to the fact that these formulas depend only on λ, which is a constant, we denote all of them by D_λ.

We can conclude, from our theoretical results in this simple system, that particles face different entropic potential yet diffuse with the same effective diffusivity, for either of these two channels. But how accurate is this statement? The answer to this question will allow us to establish the range of applicability and the accuracy of our description by means of the modified Fick-Jacobs equation.

The calculation of the effective diffusivity from simulations can be carried out by means of the MFPT, $\langle t(x_0)\rangle$, for transitions $w \to n$ and $n \to w$. Our starting point to calculate the MFPT is Eq. (6.38):

$$\frac{\partial}{\partial x_0}\left[D(x_0)\,\mathrm{e}^{-\beta U(x_0)}\,\frac{\partial}{\partial x_0}\langle t(x_0)\rangle\right] = -\mathrm{e}^{-\beta U(x_0)}. \tag{6.38}$$

As previously mentioned, in our case, $\mathrm{e}^{-\beta U(x_0)} = w(x_0)/w_0$ and $D(x_0) = D_\lambda$. Consequently,

$$\frac{D_\lambda}{w(x_0)} \frac{\mathrm{d}}{\mathrm{d}x_0} \left[w(x_0) \frac{\mathrm{d}}{\mathrm{d}x_0} \langle t(x_0) \rangle \right] = -1. \tag{20.61}$$

This equation must be solved together with the following BCs:

$$\left. \frac{\mathrm{d}\langle t(x_0) \rangle}{\mathrm{d}x_0} \right|_{x_0=0} = 0, \tag{20.62}$$

which describes a reflecting wall at $x = 0$, and

$$\langle t(x_0 = L) \rangle = 0, \tag{20.63}$$

which describes a perfectly absorbing end at $x = L$.

Integrating Eq. (20.61) with respect to x_0 gives

$$w(x_0) \frac{\mathrm{d}}{\mathrm{d}x_0} \langle t(x_0) \rangle = -\frac{1}{D_\lambda} \int w(x_0)\, \mathrm{d}x_0 + \mathcal{B}_1, \tag{20.64}$$

where $\mathcal{B}_1$ is an integration constant. Imposing the boundary condition at the starting point, Eq. (20.62), we find that $\mathcal{B}_1 = 0$.

Now, we have to substitute the channel width depending on the transition. If $w(x) = 2(b + \lambda x)$, we have the $n \to w$ transition. Therefore, by using Eq. (20.64) and integrating again, we arrive at

$$\langle t(x_0) \rangle_{n \to w} = -\frac{1}{4D_\lambda} x_0^2 - \frac{b}{2\lambda D_\lambda} x_0 + \frac{b^2}{2\lambda^2 D_\lambda} \ln(b + \lambda x_0) + \mathcal{B}_2, \tag{20.65}$$

where $\mathcal{B}_2$ is a constant, which can be found by means of Eq. (20.63), i.e.,

$$\mathcal{B}_2 = \frac{1}{4D_\lambda} L^2 + \frac{b}{2\lambda D_\lambda} L - \frac{b^2}{2\lambda^2 D_\lambda} \ln(b + \lambda L), \tag{20.66}$$

which by substituting into Eq. (20.65), we obtain

$$\langle t(x_0) \rangle_{n \to w} = \frac{1}{4\lambda^2 D_\lambda} \left\{ \lambda^2 (L^2 - x_0^2) + 2\lambda b - 2b^2 \ln \left[\frac{b + \lambda L}{b + \lambda x_0} \right] \right\}. \tag{20.67}$$

Now, setting $x_0 = 0$,

$$\langle t(x_0) \rangle_{n \to w} = \frac{1}{4\lambda^2 D_\lambda} \left[\lambda L(2b + \lambda L) - 2b^2 \ln \left(1 + \frac{\lambda L}{b} \right) \right]. \tag{20.68}$$

From this last equation, we can see that if the MFPT for the $n \to w$ transition can be obtained either from Brownian dynamics simulations or experimentally. Moreover, we can obtain the effective diffusivity as

$$D_{\lambda}^{n\to w} = \frac{1}{4\lambda^2 \langle t(x_0)\rangle_{n\to w}} \left\{ \lambda L(2b + \lambda L) - 2b^2 \ln\left(1 + \frac{\lambda L}{b}\right)\right\}. \tag{20.69}$$

To obtain D_{λ} for the $w \to n$ transition, we follow the same steps that led us to Eq. (20.69). Using the fact that in this case $w(x) = h_2(x) - h_1(x) = 2\,[b + \lambda(L - x)]$, we arrive at

$$\langle t(x_0)\rangle_{w\to n} = \frac{1}{4\lambda^2 D_{\lambda}} \left\{ -\lambda^2(L^2 - x_0^2) \right.$$
$$\left. -2\lambda b(L - x_0) - 2(b + \lambda L)^2 \ln\left[\frac{b}{(b + \lambda L) - \lambda x_0}\right]\right\}. \tag{20.70}$$

Setting $x_0 = 0$,

$$\langle t(x_0)\rangle_{w\to n} = -\frac{1}{4\lambda^2 D_{\lambda}} \left\{ 2(b + \lambda L)^2 \ln\left(\frac{b}{b + \lambda L}\right) + \lambda L(2b + \lambda L)\right\}. \tag{20.71}$$

Finally, from this equation, we can obtain

$$D_{\lambda}^{w\to n} = -\frac{1}{4\lambda^2 \langle t(x_0)\rangle_{w\to n}} \left\{ 2(b + \lambda L)^2 \ln\left(\frac{b}{b + \lambda L}\right) + \lambda L(2b + \lambda L)\right\}. \tag{20.72}$$

Figure 20.6 shows a comparison of the effective diffusivity values obtained by 2D Brownian dynamics simulations and the theoretical predictions.

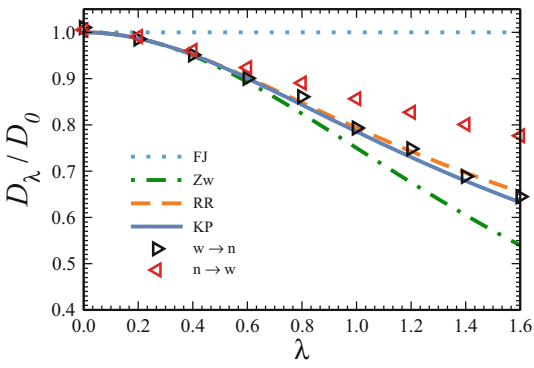

Fig. 20.6 Comparison of different D_{λ} drawn using Eqs. (20.57)–(20.60) (curves) to the values of $D_{\lambda}^{n\to w}$, and $D_{\lambda}^{w\to n}$, obtained from Brownian dynamics simulations (symbols) using Eqs. (20.72) and (20.69). The symbols indicate the simulation results with settings $D_0 = 1$, $L = 20$, and $b = 1$

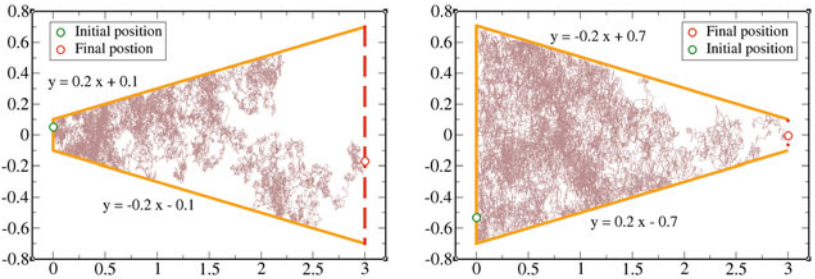

(a) Expanding two-dimensional channel. **(b)** Narrowing two-dimensional channel.

Fig. 20.7 Typical trajectories obtained through Brownian dynamics simulations for Brownian particles diffusing into expanding (**a**) and narrowing (**b**) two-dimensional trapezoidal channels of length $L = 3$ and variable width $w(x) = 2(0.2 + \lambda x)$ for the expanding channel, and $w(x) = 2\,[0.2 + \lambda(3 - x)]$ for the narrowing channel, where $0 \leq x \leq 3$. The particle starts from the reflecting boundary located at $x = 0$ and is trapped by the absorbing boundary at $x = L$ (red dashed lines). The effect of the entropic potential shows that in the expanding channel, the interaction with the walls is weaker than in the narrowing channel

The approximated 1D description in terms of the modified FJ equation is applicable when the effective diffusivities $D_\lambda^{n\to w}$ and $D_\lambda^{w\to n}$ are equal to one another and independent of the channel length. From Fig. 20.6, we can conclude that the first assumption is fulfilled when $w'(x) \leq 1$, and from simulations, we found that the second assumption, when $L \geq 2$, is within 8%. In the domain where the 1D description is applicable, the best approximations for the position-dependent effective diffusivity, entering into the modified FJ equation, are given by the Reguera-Rubi (RR) and Kalinay-Percus (KP) formulas, Eqs. (20.59) and (20.60), respectively.

It is worth noting that the RR and KP formulas work well when particles are going in the $w \to n$ direction and fail when they are going in the opposite, $n \to w$, direction. The physical reason for this is that in the $w \to n$ direction, after many unsuccessful attempts to reach the absorbing end, the particles experience many collisions with the channel walls. Due to these collisions, the particle learns about the entropy potential. The situation is completely different when the particles are going in the $n \to w$ direction in the channel when $\lambda > 1$. In such case, particles do not experience enough collisions with the walls before they reach the absorbing end, which results in an underestimated entropic potential effect, as shown in Fig. 20.7b.

When running simulations to generate the trajectories, we consider an overdamped point-like Brownian particle freely diffusing in a 2D trapezoidal channel. The particle starts from the reflecting boundary located at $x = 0$ and is trapped by the absorbing end at $x = L$. The overdamped dynamics of the particle, in the absence of an external force, is modeled by the overdamped Langevin equation, Eq. (10.83):

$$\frac{\mathrm{d}\mathbf{r}}{\mathrm{d}t} = \sqrt{2D_0\Delta t}\,\eta(t), \tag{10.94}$$

where D_0 is the bulk diffusivity, $\mathbf{r} = (x, y)$, $\xi(t) = (\xi_x(t), \xi_y(t))$ are zero-mean white Gaussian noise with autocorrelation function $\langle \xi_i(t), \xi_j(t') \rangle = \delta_{i,j}\,\delta(t - t')$ where $i, j = x, y$, given by Eqs. (10.19) and (10.20), respectively. When running simulations, we take $D_0 = 1$ and the time step $\Delta t = 10^{-6}$, so that $\sqrt{2D_0\Delta t} \ll 1$. The actual particle position $\mathbf{r}_n$ is given by $\mathbf{r}_n = \mathbf{r}_0 + \mathbf{r}_{ran}$, where $\mathbf{r}_0$ is the former position and $\mathbf{r}_{ran}$ is a vector of pseudorandom numbers generated with a Gaussian distribution ($\mu = 0, \sigma = \sqrt{2D_0\,\Delta t}$). For more details on Brownian dynamics simulations, see Chap. 10.

20.4 3D Tube: Projection Method

20.4.1 The Projection Method

In this section, we extend the Kalinay-Percus one-dimensional (1D) projection method to a quasi-one-dimensional three-dimensional symmetrical tube with a varying cross-section along the longitudinal coordinate (see Fig. 20.8). To such end, we must follow the steps outlined in Sect. 20.1.

The diffusion equation for a symmetrical 3D tube in cylindrical coordinates, where it is assumed that the concentration does not depend on the angle ϕ, is

$$\frac{\partial c(x, r, t)}{\partial t} = D_x \frac{\partial^2 c(x, r, t)}{\partial x^2} + D_r \frac{1}{r}\frac{\partial}{\partial r}\left[r \frac{\partial c(x, r, t)}{\partial r} \right], \tag{20.73}$$

where $c(x, r, t)$ is the concentration of the diffusing particles, the x-coordinate is measured along the tube axis (centerline), and D_x and D_r are the diffusivity constants in the x and radial (r) coordinates in free space. The cross-section of the channel is given by $w(x) = \pi R(x)^2$. Now, we define the projected 1D density ρ as

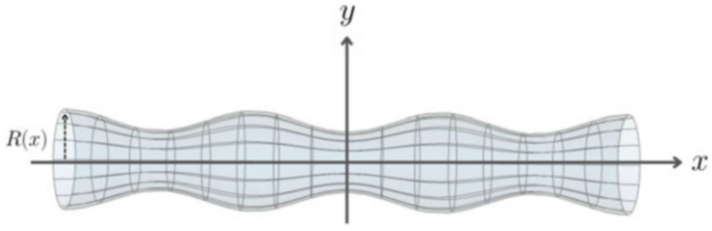

Fig. 20.8 Schematic representation of a 3D narrow symmetric tube with varying width $w(x) = \pi R(x)^2$. Each boundary has a unit normal vector of the flux, which is perpendicular to the surface

$$\rho(x,t) \equiv \int_0^{2\pi} \int_0^{R(x)} c(x,r,t)\, r\, \mathrm{d}r\, \mathrm{d}\phi = 2\pi \int_0^{R(x)} c(x,r,t)\, r\, \mathrm{d}r. \tag{20.74}$$

Using the latter equation, multiplying it by r, and integrating Eq. (20.73) over r yields

$$2\pi \int_0^{R(x)} \frac{\partial c(x,r,t)}{\partial t}\, r\, \mathrm{d}r = 2\pi \int_0^{R(x)} \left\{ D_x \frac{\partial^2 c(x,r,t)}{\partial x^2} + D_r \frac{1}{r} \frac{\partial}{\partial r} \left[r \frac{\partial c(x,r,t)}{\partial r} \right] \right\} r\, \mathrm{d}r. \tag{20.75}$$

Using the Leibniz rule (see Eq. (A.9)) in the first term of the right-hand side of the resulting equation yields

$$\begin{aligned} &\int_0^{R(x)} D_x \frac{\partial}{\partial x} \left[\frac{\partial c(x,r,t)}{\partial x} \right] r\, \mathrm{d}r \\ &= D_x \left\{ \frac{\partial}{\partial x} \int_0^{R(x)} \frac{\partial c(x,r,t)}{\partial x}\, r\, \mathrm{d}r - R'(x) \left[r \frac{\partial c(x,r,t)}{\partial x} \right] \Big|_{r=R(x)} \right\} \\ &= D_x \left\{ \frac{\partial}{\partial x} \left[\frac{\partial}{\partial x} \int_0^{R(x)} c(x,r,t)\, r\, \mathrm{d}r - R(x)\, R'(x)\, c(x,R(x),t) \right] \right. \\ &\quad \left. - R'(x)\, R(x) \frac{\partial c(x,r,t)}{\partial x} \Big|_{r=R(x)} \right\}, \end{aligned} \tag{20.76}$$

and using the fundamental theorem of calculus on the second right-hand side term leads to

$$2\pi \int_0^{R(x)} D_r \frac{1}{r} \frac{\partial}{\partial r} \left[r \frac{\partial c(x,r,t)}{\partial r} \right] r\, \mathrm{d}r = 2\pi D_r \left[r \frac{\partial c(x,r,t)}{\partial r} \right] \Big|_{r=0}^{r=R(x)}, \tag{20.77}$$

we arrive at

$$\begin{aligned} \frac{\partial p(x,t)}{\partial x} &= D_x \left\{ \frac{\partial^2 \rho(x,t)}{\partial x^2} - 2\pi \frac{\partial}{\partial x} \left[R(x)\, R'(x)\, c(x,R(x),t) \right] \right. \\ &\left. - 2\pi R(x)\, R'(x) \frac{\partial c(x,r,t)}{\partial x} \Big|_{r=R(x)} \right\} + 2\pi D_r \left[r \frac{\partial c(x,r,t)}{\partial r} \right] \Big|_{r=0}^{r=R(x)}. \end{aligned} \tag{20.78}$$

Taking advantage of the symmetry of the problem, the equation for the flux can be written as

$$\mathbf{J}(x,r,t) = -D_x \frac{\partial c(x,r,t)}{\partial x}\, \hat{\mathbf{e}}_x - D_r \frac{\partial c(x,r,t)}{\partial r}\, \hat{\mathbf{e}}_r. \tag{20.79}$$

The unit vector normal to the circular wall at $r = R(x)$ is $\hat{\mathbf{n}} = \left[R'(x)\hat{\mathbf{e}}_x - \hat{\mathbf{e}}_r\right]/\sqrt{1 + R'(x)^2}$ and the boundary condition for a perfect reflecting wall is given by $\hat{\mathbf{n}} \cdot \mathbf{J}(x, r, t) = 0$. Therefore, after performing the dot product, we obtain

$$D_r \left.\frac{\partial c(x, r, t)}{\partial r}\right|_{r=R(x)} = D_x\, R'(x) \left.\frac{\partial c(x, r, t)}{\partial x}\right|_{r=R(x)}. \tag{20.80}$$

Imposing (20.80) into (20.78) leads to the projected diffusion equation, which reads

$$\frac{\partial \rho(x, t)}{\partial t} = D_x \left\{ \frac{\partial^2 \rho(x, t)}{\partial x^2} - 2\pi \frac{\partial}{\partial x}\Big[R(x)\, R'(x)\, c(x, R(x), t)\Big]\right\}. \tag{20.81}$$

Recalling that the first approximation comes from imposing an infinite transverse diffusion rate, by assuming that $D_r \gg D_x$, we have

$$c(x, r, t) = \frac{\rho(x, t)}{\pi R(x)^2} = \frac{\rho(x, t)}{w(x)}. \tag{20.82}$$

Be aware that now $w(x)$ is the cross-section area of the tube. By substituting this last equation into Eq. (20.81) and setting $D_x = D_0$, we are led to the FJ equation:

$$\frac{\partial \rho(x, t)}{\partial t} = D_0 \frac{\partial}{\partial x}\left[w(x)\, \frac{\partial}{\partial x} \frac{\rho(x, t)}{w(x)}\right]. \tag{20.83}$$

In the next section, we will find the effective diffusivity using higher-order corrections. The process is very similar to that used in the previous sections.

20.5 Recurrence Formula for Operators $\hat{\boldsymbol{\sigma}}_j(x, r, \partial_x)$

We start by writing the concentration $c(x, y, t)$ as a perturbation series, namely,

$$c(x, r, t) = \sum_{j=0}^{\infty} \epsilon^j\, \hat{\boldsymbol{\sigma}}_j(x, r, \partial_x) \frac{\partial}{\partial x} \frac{\rho(x, t)}{w(x)}, \tag{20.84}$$

where $\hat{\boldsymbol{\sigma}}_j$ are operators acting on their right side and $\epsilon = D_x/D_r$. Setting $j = 0$, the FJ approximation is recovered as expected. Consequently,

$$\hat{\boldsymbol{\sigma}}_0(x, r, t) \frac{\partial}{\partial x} = 1. \tag{20.85}$$

On the one hand, using Eq. (20.84), the diffusion equation (20.73) becomes

$$\left(\frac{1}{D_x}\frac{\partial}{\partial t}-\frac{\partial^2}{\partial x^2}\right)\sum_{j=0}^{\infty}\epsilon^{j+1}\,\hat{\boldsymbol{\sigma}}_j(x,r,\partial_x)\frac{\partial}{\partial x}\frac{\rho(x,t)}{w(x)}$$
$$=\sum_{j=0}^{\infty}\epsilon^j\,\frac{1}{r}\frac{\partial}{\partial r}\left[r\frac{\partial}{\partial r}\hat{\boldsymbol{\sigma}}_j(x,r,\partial_x)\frac{\partial}{\partial x}\frac{\rho(x,t)}{w(x)}\right], \tag{20.86}$$

and on the other hand, the projected diffusion equation, Eq. (20.81), reads

$$\frac{\partial\rho(x,t)}{\partial t}=D_x\left\{\frac{\partial^2\rho(x,t)}{\partial x^2}\right.$$
$$\left.-2\pi\frac{\partial}{\partial x}\left[R(x)\,R'(x)\sum_{j=0}^{\infty}\epsilon^j\,\hat{\boldsymbol{\sigma}}_j(x,R(x),\partial_x)\frac{\partial}{\partial x}\frac{\rho(x,t)}{w(x)}\right]\right\}. \tag{20.87}$$

Because $w'(x)=2\pi R(x)\,R'(x)$, we can rewrite this equation as

$$\frac{\partial\rho(x,t)}{\partial t}=D_x\,\frac{\partial}{\partial x}\left[w(x)-w'(x)\sum_{j=1}^{\infty}\epsilon^j\,\hat{\boldsymbol{\sigma}}_j(x,R(x),\partial_x)\right]\frac{\partial}{\partial x}\frac{\rho(x,t)}{w(x)}. \tag{20.88}$$

Substituting Eq. (20.88) into Eq. (20.86), we arrive at

$$\sum_{j=0}^{\infty}\epsilon^{j+1}\left\{\hat{\boldsymbol{\sigma}}_j(x,r,\partial_x)\frac{\partial}{\partial x}\frac{1}{w(x)}\frac{\partial}{\partial x}\left[w(x)-w'(x)\sum_{k=1}^{\infty}\epsilon^k\,\hat{\boldsymbol{\sigma}}_k(x,R(x),\partial_x)\right]\right.$$
$$\left.-\frac{\partial^2}{\partial x^2}\hat{\boldsymbol{\sigma}}_j(x,r,\partial_x)\right\}\frac{\partial}{\partial x}\frac{\rho(x,t)}{w(x)}=\sum_{j=0}^{\infty}\epsilon^j\,\frac{1}{r}\frac{\partial}{\partial r}\left[r\frac{\partial}{\partial r}\hat{\boldsymbol{\sigma}}_j(x,r,\partial_x)\frac{\partial}{\partial x}\frac{\rho(x,t)}{w(x)}\right]. \tag{20.89}$$

The recurrence formula is obtained by rewriting this last equation using the linear independence of all ϵ powers, namely,

$$\left\{\frac{1}{r}\frac{\partial}{\partial r}\left[r\frac{\partial}{\partial r}\;\hat{\boldsymbol{\sigma}}_{j+1}(x,r,\partial_x)\right]\right\}\frac{\partial}{\partial x}\frac{\rho(x,t)}{w(x)}$$
$$=\left\{-\sum_{k=1}^{j}\hat{\boldsymbol{\sigma}}_{j-k}(x,r,\partial_x)\frac{\partial}{\partial x}\frac{1}{w(x)}\frac{\partial}{\partial x}w'(x)\,\hat{\boldsymbol{\sigma}}_k(x,R(x),\partial_x)\right. \tag{20.90}$$
$$\left.+\hat{\boldsymbol{\sigma}}_j(x,r,\partial_x)\frac{\partial}{\partial x}\frac{1}{w(x)}\frac{\partial w(x)}{\partial x}-\frac{\partial^2}{\partial x^2}\hat{\boldsymbol{\sigma}}_j(x,r,\partial_x)\right\}\frac{\partial}{\partial x}\frac{\rho(x,t)}{w(x)}.$$

Performing a double integration over r, setting the constants in such a way that the boundary conditions $\hat{\mathbf{n}} \cdot \mathbf{J}(x, r = R(x), t) = 0$, and using the normalization condition

$$2\pi \int_0^{R(x)} \hat{\boldsymbol{\sigma}}_j(x, r, \partial_x) \frac{\partial}{\partial x} \frac{\rho(x,t)}{w(x)} r \, \mathrm{d}r = 0, \qquad j > 0, \tag{20.91}$$

we obtain the recurrence formula, that is,

$$\left\{ \epsilon^j \frac{\partial}{\partial r} \hat{\boldsymbol{\sigma}}_j(x, r, \partial_x) \frac{\partial}{\partial x} \frac{\rho(x,t)}{w(x)} \right\} \Bigg|_{r=R(x)} = \left\{ \epsilon^{j+1} w'(x) \frac{\partial}{\partial r} \hat{\boldsymbol{\sigma}}_j(x, r, \partial_x) \frac{\partial}{\partial x} \frac{\rho(x,t)}{w(x)} \right\} \Bigg|_{r=R(x)}. \tag{20.92}$$

20.5.1 First- and Second-Order Corrections

To find the first-order operator $\hat{\boldsymbol{\sigma}}_1(x, r, \partial_x)$, we set $j = 0$ on the left-hand side and $j = 1$ on the right-hand side of Eq. (20.86), yielding

$$\hat{\boldsymbol{\sigma}}_1(x, r, t) \frac{\partial}{\partial x} \frac{\rho(x,t)}{w(x)} = \int \frac{1}{r} \int r \left(\frac{1}{D_x} \frac{\partial}{\partial t} - \frac{\partial^2}{\partial x^2} \right) \hat{\boldsymbol{\sigma}}_0(x, r, \partial_x) \frac{\partial}{\partial x} \frac{\rho(x,t)}{w(x)} \, \mathrm{d}r \, \mathrm{d}r, \tag{20.93}$$

where $\hat{\boldsymbol{\sigma}}_0(x, r, \partial_x) \, \partial_x = 1$. Using the FJ equation, Eq. (20.83), one finds

$$\hat{\boldsymbol{\sigma}}_1(x, r, t) \frac{\partial}{\partial x} \frac{\rho(x,t)}{w(x)} = \int \frac{1}{r} \int r \frac{w'(x)}{w(x)} \frac{\partial}{\partial x} \frac{\rho(x,t)}{w(x)} \, \mathrm{d}r \, \mathrm{d}r. \tag{20.94}$$

Integrating this last equation, we have

$$\hat{\boldsymbol{\sigma}}_1(x, r, t) \frac{\partial}{\partial x} \frac{\rho(x,t)}{w(x)} = \frac{r^2}{4} \frac{w'(x)}{w(x)} \frac{\partial}{\partial x} \frac{\rho(x,t)}{w(x)} + \mathcal{B}_1 \ln r + \mathcal{B}_2. \tag{20.95}$$

where $\mathcal{B}_1$ and $\mathcal{B}_2$ are constants. The first constant is found imposing that the concentration is equal to zero when $r = 0$, and consequently $\mathcal{B}_1 = 0$. The second constant is found from the normalization condition (20.91). Then, Eq. (20.95) is

$$
\begin{aligned}
&2\pi \int_0^{R(x)} \hat{\boldsymbol{\sigma}}_1(x,r,t)\frac{\partial}{\partial x}\frac{\rho(x,t)}{w(x)}\, r\, \mathrm{d}r \\
&\quad = 2\pi \int_0^{R(x)} \left[\frac{r^2}{4}\frac{w'(x)}{w(x)}\frac{\partial}{\partial x}\frac{\rho(x,t)}{w(x)} + \mathcal{B}_2\right] r\, \mathrm{d}r \\
&\quad = 2\pi \left\{ \left[\frac{w'(x)}{w(x)}\frac{\partial}{\partial x}\frac{\rho(x,t)}{w(x)}\right]\frac{r^4}{16} + \mathcal{B}\frac{r^2}{2}\right\}\Bigg|_{r=0}^{r=R(x)} \\
&\quad = 0,
\end{aligned}
\tag{20.96}
$$

where

$$
\mathcal{B}_2 = -\frac{R(x)^2}{8}\left[\frac{w'(x)}{w(x)}\frac{\partial}{\partial x}\frac{\rho(x,t)}{w(x)}\right] = -\frac{R(x)\,R'(x)}{4}\frac{\partial}{\partial x}\frac{\rho(x,t)}{w(x)}. \tag{20.97}
$$

From Eq. (20.96), we find that the first-order operator is

$$
\hat{\boldsymbol{\sigma}}_1(x,r,\partial_x) = \left[\frac{r^2}{2R(x)} - \frac{R(x)}{4}\right] R'(x), \tag{20.98}
$$

which evaluated at the boundary $r = R(x)$, leads to

$$
\hat{\boldsymbol{\sigma}}_1(x,R(x),\partial_x) = \frac{1}{4}\,R(x)\,R'(x). \tag{20.99}
$$

The second-order operator $\hat{\boldsymbol{\sigma}}_2(x,r,\partial_x)$ is obtained from the recurrence relation, Eq. (20.90), setting $j = 1$, once we know the previous order operator, namely,

$$
\begin{aligned}
&\left\{\frac{1}{r}\frac{\partial}{\partial r}\left[r\,\frac{\partial}{\partial r}\hat{\boldsymbol{\sigma}}_2(x,r,\partial_x)\right]\right\}\frac{\partial}{\partial x}\frac{\rho(x,t)}{w(x)} \\
&\quad = \left\{-\frac{1}{w(x)}\frac{\partial}{\partial x}w'(x)\left[\frac{1}{4}\,R(x)\,R'(x)\right]\right. \\
&\quad + \left[\frac{r^2}{2R(x)} - \frac{R(x)}{4}\right]R'(x)\,\frac{\partial}{\partial x}\frac{1}{w(x)}\frac{\partial w(x)}{\partial x} \\
&\quad \left. - \frac{\partial^2}{\partial x^2}\left[\frac{r^2}{2R(x)} - \frac{R(x)}{4}\right]R'(x)\right\}\frac{\partial}{\partial x}\frac{\rho(x,t)}{w(x)},
\end{aligned}
\tag{20.100}
$$

which can be rewritten as

$$
\left\{\frac{1}{r}\frac{\partial}{\partial r}\left[r\,\frac{\partial}{\partial r}\hat{\boldsymbol{\sigma}}_2(x,r,\partial_x)\right]\right\}\frac{\partial}{\partial x}\frac{\rho(x,t)}{w(x)}
$$

$$= \left\{ r^2\, \hat{Q}_1(x, \partial_x) + \hat{Q}_2(x, \partial_x) \right\} \frac{\partial}{\partial x} \frac{\rho(x,t)}{w(x)}, \tag{20.101}$$

where

$$\hat{Q}_1(x, \partial_x) = \frac{R'(x)}{2R(x)} \frac{\partial}{\partial x} \frac{1}{w(x)} \frac{\partial}{\partial x} w(x) - \frac{\partial^2}{\partial x^2} \frac{R'(x)}{2R(x)}, \tag{20.102}$$

and

$$\hat{Q}_2(x, \partial_x) = -\frac{1}{4w(x)} \frac{\partial}{\partial x} w'(x)\, R(x)\, R'(x) - \frac{R(x)\, R'(x)}{4} \frac{\partial}{\partial x} \frac{1}{w(x)} \frac{\partial}{\partial x} w(x) + \frac{\partial^2}{\partial x^2} \frac{R(x)\, R'(x)}{4}. \tag{20.103}$$

After doing some algebra, these auxiliary operators can be rewritten as

$$\hat{Q}_1(x, \partial_x) = \frac{1}{2R(x)^2} \left\{ 2\Big[2R'(x)^2 - R(x)\, R''(x) \Big] \frac{\partial}{\partial x} - R(x)\, R'''(x) + 5R'(x)\, R''(x) - \frac{4R'(x)^3}{R(x)} \right\}, \tag{20.104}$$

and

$$\hat{Q}_2(x, \partial_x) = \frac{1}{4} \left\{ -2\Big[R'(x)^2 - R(x)\, R''(x) \Big] \frac{\partial}{\partial x} + R(x)\, R'''(x) - 3R'(x)\, R''(x) - \frac{2R'(x)^3}{R(x)} \right\}. \tag{20.105}$$

Now, by integrating Eq. (20.100) twice over r and using Eqs. (20.104) and (20.105), we see that

$$\left\{ \hat{\boldsymbol{\sigma}}_2(x, r, \partial_x) \right\} \frac{\partial}{\partial x} \frac{\rho(x,t)}{w(x)} = \left\{ \frac{r^4}{16}\, \hat{Q}_1(x, \partial_x) + \frac{r^2}{4}\, \hat{Q}_2(x, \partial_x) \right\} \frac{\partial}{\partial x} \frac{\rho(x,t)}{w(x)} + \mathcal{B}_1\, \ln r + \mathcal{B}_2, \tag{20.106}$$

where $\mathcal{B}_1$ is zero, just as in the calculation of the previous operator. The constant $\mathcal{B}_2$ is found again from the normalization condition, yielding

$$\mathcal{B}_2 = \left\{ -\frac{R(x)^4}{48}\, \hat{Q}_1(x, \partial_x) - \frac{R(x)^2}{8}\, \hat{Q}_2(x, \partial_x) \right\} \frac{\partial}{\partial x} \frac{\rho(x,t)}{w(x)}. \tag{20.107}$$

If we now use Eq. (20.107) in Eq. (20.106),

$$\hat{\boldsymbol{\sigma}}_2(x, r, \partial_x) = \frac{r^4}{16}\,\hat{Q}_1(x, \partial_x) + \frac{r^2}{4}\,\hat{Q}_2(x, \partial_x) - \frac{R(x)^2}{8}\left[\frac{R(x)^2}{6}\,\hat{Q}_1(x, \partial_x) + \hat{Q}_2(x, \partial_x)\right], \tag{20.108}$$

and when substituting $\hat{Q}_1(x, \partial_x)$ and $\hat{Q}_2(x, \partial_x)$, this leads to

$$\begin{aligned}\hat{\boldsymbol{\sigma}}_2(x, r, \partial_x) = \frac{r^4}{32R(x)^2}\Bigg\{&2\Big[2R'(x)^2 - R(x)\,R''(x)\Big]\frac{\partial}{\partial x} \\ &- R(x)\,R'''(x) + 5R'(x)\,R''(x) - \frac{4R'(x)^3}{R(x)}\Bigg\} \\ &+ \frac{r^2}{16}\Bigg\{-2\Big[R'(x)^2 - R(x)\,R''(x)\Big]\frac{\partial}{\partial x} \\ &+ R(x)\,R'''(x) - 3R'(x)\,R''(x) - \frac{2R'(x)^3}{R(x)}\Bigg\} \\ &- \frac{R(x)^2}{48}\Bigg\{-\Big[R'(x)^2 - 2R(x)\,R''(x)\Big]\frac{\partial}{\partial x} \\ &+ R(x)\,R'''(x) - 2R'(x)\,R''(x) - \frac{5R'(x)^3}{R(x)}\Bigg\},\end{aligned} \tag{20.109}$$

which by evaluating at $r = R(x)$ becomes

$$\begin{aligned}\hat{\boldsymbol{\sigma}}_2(x, R(x), \partial_x) = \frac{R(x)^2}{96}\Bigg\{&2\Big[R'(x)^2 + R(x)\,R''(x)\Big]\frac{\partial}{\partial x} \\ &+ R(x)\,R'''(x) + R'(x)\,R''(x) - \frac{14R'(x)^3}{R(x)}\Bigg\}.\end{aligned} \tag{20.110}$$

The operators for $j > 3$ are obtained in the same way. Each operator $\hat{\boldsymbol{\sigma}}_j(x, r, \partial_x)$ is a polynomial in powers of r^{2k}, $k = 0, 1, \ldots, j$, and the order of its derivatives with respect to x is $j - 1$, with the proof being by mathematical induction. Finally, we substitute the obtained operators evaluated at $r = R(x)$, Eqs. (20.99) and (20.110), in Eq. (20.88), to find the equation for projected diffusion, namely,

$$\begin{aligned}\frac{\partial \rho(x, t)}{\partial t} = D_x\,\frac{\partial}{\partial x}\Bigg\{&w(x) - \frac{\epsilon}{4}\,w'(x)\,R(x)\,R'(x) \\ &- \frac{\epsilon^2}{96}\,w'(x)\,R(x)^2\Big[2\Big(R'(x)^2 + R(x)\,R''(x)\Big)\frac{\partial}{\partial x}\end{aligned}$$

$$+ R(x)\, R'''(x) + R'(x)\, R''(x) - \frac{14R'(x)^3}{R(x)}\Bigg] - \cdots \Bigg\}$$
$$\times \frac{\partial}{\partial x}\frac{\rho(x,t)}{w(x)}. \tag{20.111}$$

Now, our next task is to provide the steps that allow us to link Eq. (20.5.1) with the position-dependent diffusion coefficient.

20.5.2 The Position-Dependent Effective Diffusion Coefficient

In three dimensions, Eq. (20.45) remains the same, but with $w(x) = \pi R(x)^2$, so then,

$$D(x) \approx 1 - \epsilon\, R(x)^2\, \hat{\boldsymbol{Z}}(x, \partial_x)\frac{1}{R(x)^2}, \tag{20.112}$$

where

$$\hat{\boldsymbol{Z}}(x, \partial_x) = \frac{1}{2}R'(x)^2 + \frac{\epsilon}{48}\, R(x)\, R'(x)\Bigg[2\Big(R'(x)^2 + R(x)\, R''(x)\Big)\frac{\partial}{\partial x}$$
$$+ R(x)\, R'''(x) + 7R'(x)\, R''(x) - \frac{18R'(x)^3}{R(x)}\Bigg] + \cdots. \tag{20.113}$$

Substituting this last equation into Eq. (20.112), and after some simplifications, we arrive at

$$D(x) \approx 1 - \frac{\epsilon}{2}\, R'(x)^2$$
$$+ \frac{\epsilon^2}{48}\, R(x)\, R'(x)\Bigg[18\frac{R'(x)^3}{R(x)} + 3R'(x)\, R''(x) - R(x)^2\, R'''(x)\Bigg] + \cdots. \tag{20.114}$$

This equation is the effective diffusion coefficient for a three-dimensional channel of radial symmetry and radius $R(x)$. If the radius of the channel does not change abruptly, that is, $R'(x) < 1$, then Eq. (20.114) can be approximated as

$$D(x) \approx 1 - \frac{\epsilon}{2}\, R'(x)^2 + \frac{3}{8}\,\epsilon^2\, R'(x)^4 - \frac{5}{16}\,\epsilon^3\, R'(x)^6 + \cdots. \tag{20.115}$$

From the recurrence relation between the operators, we find that

$$D(x) = \sum_{n=0}^{\infty} \frac{(2n-1)!!}{(2n)!!} \left[-\epsilon\, w'(x)^2\right]^n, \tag{20.116}$$

which is a convergent series given by

$$D(x) = \frac{1}{\sqrt{1+\epsilon R'(x)^2}}. \tag{20.117}$$

For the isotropic case, we have that $\epsilon = 1$. Consequently,

$$D(x) = \frac{1}{\sqrt{1+R'(x)^2}}, \tag{20.118}$$

which is one of the main results of this chapter. It is worth noting that this equation is the one proposed by RR, and the first two terms of Eq. (20.118) are Zwanzig's approximation. In the following chapters, we will study the range of applicability of Eq. (20.118).

The equations for the position-dependent diffusion coefficients for quasi-one-dimensional channels are summarized in Table 20.1 as they appear in the literature.

The calculation of the effective diffusivity from simulations can be carried out by means of the mean first-passage time (MFPT), $\langle t(x_0)\rangle$, for the $w \to n$ and $n \to w$ transitions, as done previously. Our starting point to calculate the MFPT is Eq. (6.38).

20.6 First Passage in Conical Tubes

In this section, we apply the techniques outlined in Sect. 20.3 to study the range of applicability of the one-dimensional (1D) description of a particle diffusing in a three-dimensional tube in terms of the modified (FJ) equation. Therefore, we will focus on the wide-to-narrow ($w \to n$) and narrow-to-wide ($n \to w$) transitions between the two ends of a tube of varying linear radius, $R'(x) = \lambda$, as shown in Fig. 20.9. For this conical tube, we have that the entropic potential is given by $\mathrm{e}^{-\beta U(x)} = w(x)/w_0$, where $w(x) = \pi R(x)^2$, $w_0 = w(x=0)$, $\beta = 1/(k_B T)$, with k_B and T denoting the Boltzmann constant and absolute temperature, respectively. For the expanding conical tube, we have $R(x) = \lambda x + b$, and consequently, $\beta U(x) = -\ln[(b+\lambda x)/b]^2$. Additionally, for the narrowing tube, we set $R(x) = \lambda(L-x)+b$, yielding to $\beta U(x) = -\ln[(\lambda(L-x)+b)/(\lambda L + b)]^2$.

We start by writing the theoretical formulas for the effective diffusivity for a conical tube with constant width λ, which follow the different expressions for $D(x)$, namely,

$$D(x) \approx D_{\mathrm{FJ}}(x) = D_0 \qquad \text{(Fick-Jacobs)}, \tag{20.119}$$

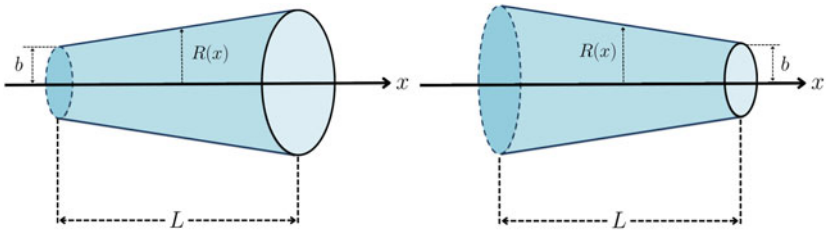

(a) Expanding three-dimensional channel. (b) Narrowing three-dimensional channel.

Fig. 20.9 Schematic representation of expanding (**a**) and narrowing (**b**) tubes of length L with constant radius variation rate, i.e., $R'(x) = \text{constant}$. In both cases, particles starting from the left reflecting boundary are trapped by the right perfect absorbing end

$$D(x) \approx D_{\text{Zw}}(x) = \frac{1}{1 + \frac{1}{2} R'(x)^2} D_0 = \frac{1}{1 + \frac{1}{2}\lambda^2} D_0 \qquad \text{(Zwanzig)}, \tag{20.120}$$

$$D(x) \approx D_{\text{RR}}(x) = \frac{1}{\left[1 + \frac{1}{4} R'(x)^2\right]^{1/2}} D_0 = \frac{1}{\left[1 + \lambda^2\right]^{1/2}} D_0 \quad \text{(Reguera-Rubi)}, \tag{20.121}$$

$$D(x) \approx D_{\text{KP}}(x) = \frac{1}{\left[1 + \frac{1}{4} R'(x)^2\right]^{1/2}} D_0 = \frac{1}{\left[1 + \lambda^2\right]^{1/2}} D_0 \qquad \text{(Kalinay-Percus)}. \tag{20.122}$$

It is worth remembering that the Kalinay-Percus (KP) and Reguera-Rubi (RR) formulas are the same for three dimensions. Because these formulas depend only on λ, we denote all of them by D_λ, as we did before.

To calculate D_λ from simulations, we first have to obtain the mean first-passage time (MFPT), as discussed in Sect. 20.3, given by Eq. (20.61), which has to be solved together with the BCs given by Eqs. (20.62) and (20.63). Something to keep in mind is that the main difference between both dimensions is $w(x)$, which in 3D is the transverse area.

Recalling Eq. (20.61),

$$\frac{D_\lambda}{w(x_0)} \frac{\mathrm{d}}{\mathrm{d}x_0} \left[w(x_0) \frac{\mathrm{d}}{\mathrm{d}x_0} \langle t(x_0) \rangle \right] = -1, \tag{20.61}$$

let us solve it by *quadratures* (see Appendix A.12). Since $\langle t(x_0) \rangle$ at the origin is known, Eq. (20.62), it is best to integrate Eq. (20.61) from 0 to x_0. Before performing the integration, and to avoid confusion with the notation, it is also practical to set $x_0 = x'$ in Eq. (20.62), namely,

$$\int_0^{x_0} \frac{\mathrm{d}}{\mathrm{d}x'}\left[w(x')\frac{\mathrm{d}}{\mathrm{d}x'}\langle t(x')\rangle\right]\mathrm{d}x' = -\int_0^{x_0}\frac{w(x')}{D_\lambda}\,\mathrm{d}x'. \tag{20.123}$$

A first integration gives

$$w(x_0)\frac{\mathrm{d}\langle t(x_0)\rangle}{\mathrm{d}x_0} - w(0)\frac{\mathrm{d}\langle t(x_0)\rangle}{\mathrm{d}x_0}\bigg|_{x_0=0} = -\frac{1}{D_\lambda}\int_0^{x_0} w(x')\,\mathrm{d}x'. \tag{20.124}$$

From the BCs, the flux is null at the origin (see Eq. (20.62)) and the second term of the left-hand side is zero. Again, before integrating, it is practical to set $x_0 = x''$, i.e.,

$$\int_0^{x_0}\frac{\mathrm{d}\langle t(x'')\rangle}{\mathrm{d}x''}\mathrm{d}x'' = -\frac{1}{D_\lambda}\int_0^{x_0}\frac{1}{w(x'')}\left[\int_0^{x''} w(x')\,\mathrm{d}x'\right]\mathrm{d}x''. \tag{20.125}$$

Then, a second integration gives

$$\langle t(x_0)\rangle - \langle t(x_0=0)\rangle = -\frac{1}{D_\lambda}\int_0^{x_0}\frac{1}{w(x'')}\left[\int_0^{x''} w(x')\,\mathrm{d}x'\right]\mathrm{d}x''. \tag{20.126}$$

The integrations are to be carried out in order, first with respect to x' and then with respect to x''. By imposing the absorbing boundary at $x_0 = L$, we find that

$$\langle t(x_0=0)\rangle = \frac{1}{D_\lambda}\int_0^{L}\frac{1}{w(x'')}\left[\int_0^{x''} w(x')\,\mathrm{d}x'\right]\mathrm{d}x''. \tag{20.127}$$

Introducing $\langle t(x_0=0)\rangle$ into Eq. (20.126) yields

$$\begin{aligned}\langle t(x_0)\rangle = {} & \frac{1}{D_\lambda}\int_0^{L}\frac{1}{w(x'')}\left[\int_0^{x''} w(x')\,\mathrm{d}x'\right]\mathrm{d}x'' \\ & - \frac{1}{D_\lambda}\int_0^{x_0}\frac{1}{w(x'')}\left[\int_0^{x''} w(x')\,\mathrm{d}x'\right]\mathrm{d}x''.\end{aligned} \tag{20.128}$$

Recalling definite integral properties and given x_0 lies within the interval $[0, L]$, the limits of the first integral of the right-hand side over x'' can be split into two sums: one integral from 0 to x_0 and another one from x_0 to L. The latter integral cancels out with the second integral of Eq. (20.128), and as a result, the general solution of Eq. (20.61) is

$$\langle t(x_0)\rangle = \frac{1}{D_\lambda}\int_{x_0}^{L}\frac{1}{w(x'')}\left[\int_0^{x''} w(x')\,\mathrm{d}x'\right]\mathrm{d}x''. \tag{20.129}$$

It is worth mentioning that if instead of integrating Eq. (20.124) from 0 to x_0, we had done it from x_0 to L, this result would have been obtained directly. Finally, setting $x_0 = 0$ results in

$$\langle t(0 \to L)\rangle = \frac{1}{D_\lambda}\int_0^L \frac{1}{w(x'')}\left[\int_0^{x''} w(x')\mathrm{d}x'\right]\mathrm{d}x''. \tag{20.130}$$

We can use the latter equation to obtain the MFPT for the $n \to w$ and the $w \to n$ transitions. In the first case, the tube's cross-sectional area is $w(x) = b + \lambda x$. Thus, substituting $w(x)$ into Eq. (20.130) results in

$$\langle t(0 \to L)\rangle = \frac{1}{D_\lambda}\int_0^L \frac{1}{b+\lambda x''}\left[\int_0^{x''} (b+\lambda x')\mathrm{d}x'\right]\mathrm{d}x''. \tag{20.131}$$

Integrating with respect to x' over $[0, x'']$ leads to

$$\langle t(0 \to L)\rangle = \frac{1}{D_\lambda}\int_0^L \frac{1}{b+\lambda x''}\left(bx'' + \frac{\lambda}{2}x''^2\right)\mathrm{d}x'', \tag{20.132}$$

and integrating with respect to x'' over $[0, L]$ finally gives

$$\langle t(x_0)\rangle_{n\to w} = \frac{L^2}{6D_\lambda}\frac{3b+\lambda L}{b+\lambda L}. \tag{20.133}$$

Then, we can obtain the effective diffusivity as

$$D_\lambda^{n\to w} = \frac{L^2}{6\langle t(x_0)\rangle_{n\to w}}\frac{3b+\lambda L}{b+\lambda L}. \tag{20.134}$$

Furthermore, for a narrowing tube, $w(x) = b + \lambda(L - x)$. Introducing this expression into Eq. (20.129) and integrating leads to

$$\langle t(x_0)\rangle_{w\to n} = \frac{L^2}{6D_\lambda}\left(3 + 2\frac{\lambda L}{b}\right). \tag{20.135}$$

Consequently,

$$D_\lambda^{w\to n} = \frac{L^2}{6\langle t(x_0)\rangle_{w\to n}}\left(3 + 2\frac{\lambda L}{b}\right). \tag{20.136}$$

The λ-dependence of the D_λ/D_0 ratio and the theoretical approximations given by Eqs. (20.119)–(20.122) normalized to D_0 are shown in Fig. 20.10. We can see that when the radius variation rate falls within the range of the applicability of the

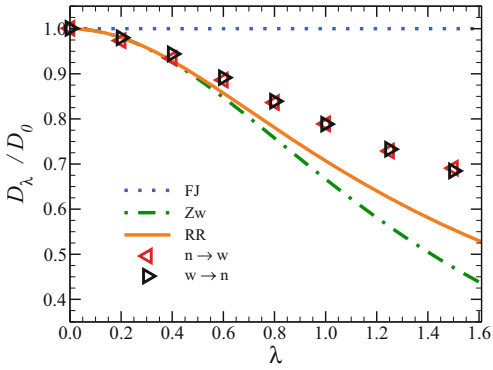

Fig. 20.10 Comparison of different D_λ drawn using Eqs. (20.119)–(20.122) (lines) and the values of $D_\lambda^{n\to w}$ and $D_\lambda^{w\to n}$, obtained from 3D Brownian dynamics simulations (symbols). The symbols give the simulation results for a channel of length $L = 10$

1D description, $\lambda \leq 1$, the predictions of the RR formula are reasonably good. The relative error increases with λ, and at $\lambda = 1$, it is around 10%.

20.7 Position-Dependent Diffusion Coefficient Formulas

The approximated formulas for position-dependent diffusion coefficients in two and three dimensions for quasi-one-dimensional channels are summarized in the following table as they appear in the literature.

20.8 Concluding Remarks

In this chapter, we introduced the projection method, first presented by P. Kalinay and J. K. Percus. We found the enhanced Fick-Jacobs operator in differential form for a quasi-one-dimensional asymmetric two-dimensional channel with a curved midline $y_0(x)$ and varying width $w(x)$ along the longitudinal coordinate, as well as for a three-dimensional symmetric tube. The position-dependent diffusion coefficient is given by Eq. (20.51) for an asymmetric channel and by Eq. (20.118) for a symmetric tube.

The reduction of axial diffusion in two-dimensional channels and three-dimensional tubes to the effective one-dimensional description in terms of the modified Fick-Jacobs equation is applicable when the channel width variation rate, or radius variation rate, does not exceed unity, $\left|w'(x)\right| \leq 1$. This condition is not as restrictive as the one imposed by Zwanzig in deriving the modified Fick-Jacobs equation.

Further Reading and References

M. Berezhkovskii, A. Szabo, Time scale separation leads to position-dependent diffusion along a slow coordinate. J. Chem. Phys. **135**, 074108 (2011). https://aip.scitation.org/doi/10.1063/1.3626215

M. Bradley, Diffusion in a two-dimensional channel with curved midline and varying width: reduction to an effective one-dimensional description. Phys. Rev. E **80**, 061142 (2009). https://journals.aps.org/pre/abstract/10.1103/PhysRevE.80.061142

L. Dagdug, I. Pineda, Projection of two-dimensional diffusion in a curved midline and narrow varying width channel onto the longitudinal dimension. J. Chem. Phys. **137**, 024107 (2012). https://aip.scitation.org/doi/10.1063/1.4733394

M.H. Jacobs, *Diffusion Processes* (Springer, Berlin, 1935)

P. Kalinay, J.K. Percus, Projection of two-dimensional diffusion in a narrow channel onto the longitudinal dimension. J. Chem. Phys. **122**, 204701 (2005). https://aip.scitation.org/doi/10.1063/1.1899150

P. Kalinay, J.K. Percus, Projection of two-dimensional diffusion in a narrow channel onto the longitudinal dimension. Phys. Rev. E **74**, 041203 (2006). https://journals.aps.org/pre/abstract/10.1103/PhysRevE.74.041203

R. Magnus, *Essential Ordinary Differential Equations* (Springer, Berlin, 2023)

Martens, G. Schmid, L. Schimansky-Geier, P. Hänggi, Entropic particle transport: higher-order corrections to the Fick-Jacobs diffusion equation. Phys. Rev. E **83**, 051135 (2011). https://journals.aps.org/pre/abstract/10.1103/PhysRevE.83.051135

Reguera, J.M. Rubi, Kinetic equations for diffusion in the presence of entropic barriers. Phys. Rev. E **64**, 061106 (2001). https://journals.aps.org/pre/abstract/10.1103/PhysRevE.64.061106

E. Yariv, H. Brenner, S. Kim, Curvature-induced dispersion in electro-osmotic serpentine flows. SIAM J. Appl. Math. **64**, 1099 (2004). https://epubs.siam.org/doi/10.1137/S003613990342284X

R. Zwanzig, J. Phys. Chem. **96**(10), 3926–3930 (1992). Diffusion past an entropy barrier. https://doi.org/10.1021/j100189a004

Chapter 21
External Transverse Field: 2D Narrow Channel

In this chapter, we focus on the derivation of a general position-dependent effective diffusion coefficient to describe two-dimensional (2D) diffusion in a narrow and smoothly asymmetric channel of varying width under the influence of a transverse gravitational external field. In order to do so, we employ the projection method by Kalinay and Percus (KP) to project the 2D Smoluchowski equation into an effective one-dimensional generalized Fick-Jacobs equation. Additionally, we show that diffusivity can be described by the interpolation formula proposed by Kalinay, namely, $D_0/(1 + (1/4)w'^2(x))^{-\eta}$, where spatial confinement, asymmetry, and the presence of a constant transverse force can be encoded in parameter η, which is naturally a function of channel width (w), channel centerline, and transverse force. The interpolation formula also simplifies to well-known previous results, e.g., those obtained by Reguera and Rubi.

Then, we study the crossing time statistics of diffusing point particles between the two ends of an expanding and narrowing two-dimensional conical channel subject to a transverse external gravitational field. The theoretical expression for the mean first-passage time (MFPT) for such a system is derived under the assumption that the axial diffusion in a two-dimensional channel of smoothly varying geometry can be approximately described as one-dimensional diffusion in an entropic potential with position-dependent effective diffusivity in terms of the modified Fick-Jacobs equation. We analyze the channel crossing dynamics in terms of the MFPT, combining our analytical results with extensive two-dimensional Brownian dynamics simulations, which allows us to find the range of applicability of the one-dimensional approximation. Ultimately, we find that effective particle diffusivity decreases with increasing amplitude of the external potential. Interestingly, the MFPT for crossing the channel is shown to assume a minimum at finite values of the potential amplitude.

To gain some insight into diffusion under confinement in the presence of an external perpendicular force g, we present representative trajectories of diffusing particles in Fig. 21.1 for both cases: when $g = 0$ and when $g \neq 0$.

L. Dagdug et al., *Diffusion Under Confinement*,
https://doi.org/10.1007/978-3-031-46475-1_21

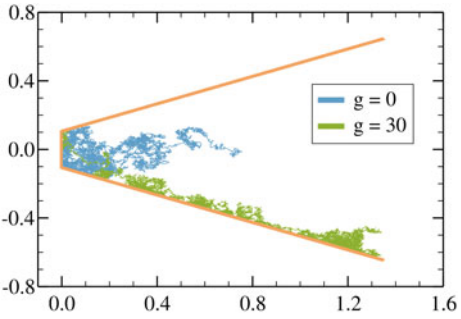

Fig. 21.1 Comparison between trajectories of Brownian particles confined within a two-dimensional channel with hard walls determined by the boundary functions $\pm h(x) = \pm 0.4x \pm 0.1$. The blue line corresponds to the trajectory of a particle subject solely to confinement, while the green line illustrates the trajectory of a diffusing particle influenced by a gravity-like force with a magnitude of $|g| = 30$. For both simulations, we set $D_0 = 1$ and $\Delta t = 1 \times 10^{-5}$. The simulation ended after 10,000 time steps

21.1 Projection of the Smoluchowski Equation

In the case of either a symmetrical or asymmetrical two-dimensional channel, we start by invoking the two-dimensional Smoluchowski equation, i.e.,

$$\frac{\partial c(x,y,t)}{\partial t} = D_x \frac{\partial}{\partial x}\left\{ \mathrm{e}^{-\beta U(x,y)} \frac{\partial}{\partial x}\left[\mathrm{e}^{\beta U(x,y)}\, c(x,y,t) \right] \right\} + D_y \frac{\partial}{\partial y}\left\{ \mathrm{e}^{-\beta U(x,y)} \frac{\partial}{\partial y}\left[\mathrm{e}^{\beta U(x,y)}\, c(x,y,t) \right] \right\}. \tag{18.1}$$

Since the particles are subjected to a gravitational potential, then

$$U(x,y) = Gy. \tag{21.1}$$

A schematic representation of a two-dimensional asymmetric channel is shown in Fig. 21.2.

For the sake of convenience, we define

$$g \equiv G\beta, \tag{21.2}$$

which allows us to write Eq. (18.1) as

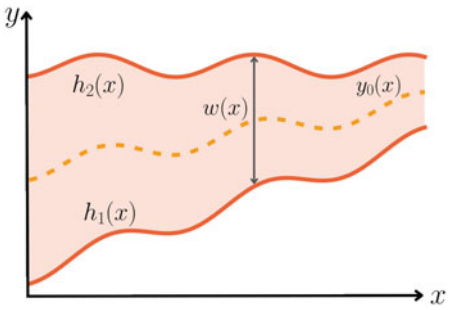

Fig. 21.2 Schematic representation of a two-dimensional asymmetric channel in the presence of a constant transverse force G. The channel has two reflecting walls given by $h_1(x)$ and $h_2(x)$, variable width $w(x) = h_2(x) - h_1(x)$, and curved midline $y_0(x) = [h_1(x) + h_2(x)]/2$

$$\frac{\partial c(x,y,t)}{\partial t} = D_x \frac{\partial}{\partial x}\left\{ \mathrm{e}^{-gy} \frac{\partial}{\partial x}\left[\mathrm{e}^{gy}\, c(x,y,t)\right]\right\} + D_y \frac{\partial}{\partial y}\left\{ \mathrm{e}^{-gy} \frac{\partial}{\partial y}\left[\mathrm{e}^{gy}\, c(x,y,t)\right]\right\}. \tag{21.3}$$

By manipulating the first term on the right-hand side of the latter equation, we obtain

$$\begin{aligned}
\frac{\partial}{\partial x}\left\{ \mathrm{e}^{-gy} \frac{\partial}{\partial x}\left[\mathrm{e}^{gy}\ \ c(x,y,t)\right]\right\} &= \mathrm{e}^{-gy} \frac{\partial}{\partial x}\left\{ \mathrm{e}^{gy} \frac{\partial c(x,y,t)}{\partial x} + c(x,y,t) \frac{\partial \mathrm{e}^{gy}}{\partial x}\right\} \\
&\quad + \left(\frac{\partial \mathrm{e}^{gy}}{\partial x}\right) \frac{\partial}{\partial x}\left[\mathrm{e}^{gy}\, c(x,y,t)\right] \\
&= \mathrm{e}^{-gy} \frac{\partial}{\partial x}\left\{ \mathrm{e}^{gy} \frac{\partial c(x,y,t)}{\partial x}\right\} \\
&= \mathrm{e}^{-gy}\left\{ \mathrm{e}^{gy} \frac{\partial^2 c(x,y,t)}{\partial t^2} + \left[\frac{\partial c(x,y,t)}{\partial x}\right]\left(\frac{\partial \mathrm{e}^{gy}}{\partial x}\right)\right\} \\
&= \frac{\partial^2 c(x,y,t)}{\partial x^2}.
\end{aligned} \tag{21.4}$$

Applying that

$$\frac{\partial}{\partial x}\, \mathrm{e}^{\pm gy} = \frac{\partial}{\partial x}\left(\pm gy\, \mathrm{e}^{\pm gy}\right) = 0, \tag{21.5}$$

we can simplify the Smoluchowski equation to

$$\frac{\partial c(x,y,t)}{\partial t} = D_x \frac{\partial^2 c(x,y,t)}{\partial x^2} + D_y \frac{\partial}{\partial y}\left\{ \mathrm{e}^{-gy} \frac{\partial}{\partial y}\left[\mathrm{e}^{gy}\, c(x,y,t)\right]\right\}. \tag{21.6}$$

Moreover, by using Fick's first law, Eq. (2.73), and the conservation equation given by Eq. (2.71), we identify the flux components for this system, namely,

$$J_x = -D_x \frac{\partial c(x,y,t)}{\partial x}, \tag{21.7}$$

and

$$J_y = -D_y\, \mathrm{e}^{-gy} \frac{\partial}{\partial y}\left[\mathrm{e}^{gy}\, c(x,y,t)\right], \tag{21.8}$$

from which $\mathbf{J} = (J_x, J_y, 0)$ is determined.

The subsequent examination is centered on a system with a two-dimensional symmetric channel, wherein we derive the boundary conditions (BCs) using the flux vector $\mathbf{J}$ and the functions that describe the channel walls. In this context, the channel walls are defined by

$$y = \pm h(x). \tag{21.9}$$

It is worth noting that the presence of perfectly reflecting boundaries implies that the flux through the walls should be null. This condition can be mathematically expressed as follows:

$$\mathbf{J} \times \pm \mathbf{h}'(x) = 0, \tag{21.10}$$

where

$$\pm\, \mathbf{h}(x) = (x, \pm h(x)), \tag{21.11}$$

and consequently,

$$\pm\, \mathbf{h}'(x) = (1, \pm h'(x)), \tag{21.12}$$

where the prime notation indicates a derivative with respect to x. By writing Eq. (21.10) explicitly, we see that

$$\mathbf{J} \times \pm \mathbf{h}'(x) = \begin{vmatrix} \hat{\mathbf{i}} & \hat{\mathbf{j}} & \hat{\mathbf{k}} \\ J_x & J_y & 0 \\ 1 & h'(x) & 0 \end{vmatrix} = \hat{\mathbf{k}}\left[\pm h'(x)\; J_x - J_y \right] = 0, \tag{21.13}$$

leading to

$$\pm\, h'(x)\; J_x = J_y. \tag{21.14}$$

Upon substituting Eqs. (21.7) and (21.8) into Eq. (21.14), we obtain

$$\pm\, h'(x)\; D_x \left.\frac{\partial c(x,y,t)}{\partial x}\right|_{y=\pm h(x)} = D_y\, \mathrm{e}^{-gy}\, \frac{\partial}{\partial y}\left[\mathrm{e}^{gy}\, c(x,y,t)\right]\Big|_{y=\pm h(x)}, \tag{21.15}$$

which constitute the requisite BCs.

21.1.1 The Projection Method

Now, we proceed to Eq. (21.6) in order to obtain a Fick-Jacobs-like equation (see Eq. (18.15)). To such end, we start by defining the projected or marginal one-dimensional (1D) density $\rho(x,t)$ as

$$\rho(x,t) = \int_{-h(x)}^{h(x)} c(x,y,t)\, \mathrm{d}y. \tag{21.16}$$

Then, by integrating Eq. (21.6) with respect to y, we arrive at

$$\frac{\partial \rho(x,t)}{\partial t} = D_x \int_{-h(x)}^{h(x)} \frac{\partial^2 c(x,y,t)}{\partial t^2}\, \mathrm{d}y + D_y\, \mathrm{e}^{-gy}\, \frac{\partial}{\partial y}\left[\mathrm{e}^{gy}\, c(x,y,t)\right]\Big|_{y=-h(x)}^{y=h(x)}. \tag{21.17}$$

The second term on the right-hand side of the latter equation is rearranged to give

$$\begin{aligned} & D_y\, \mathrm{e}^{-gy} \frac{\partial}{\partial y}\left[\mathrm{e}^{gy}\, c(x,y,t)\right]\Big|_{y=-h(x)}^{y=h(x)} \\ & \quad = D_y \left\{ \mathrm{e}^{-gy} \frac{\partial}{\partial y}\left[\mathrm{e}^{gy}\, c(x,y,t)\right]\Big|^{y=h(x)} - \mathrm{e}^{-gy} \frac{\partial}{\partial y}\left[\mathrm{e}^{gy}\, c(x,y,t)\right]\Big|_{y=-h(x)} \right\} \\ & \quad = D_x\, h'(x) \left\{ \left.\frac{\partial c(x,y,t)}{\partial x}\right|^{y=h(x)} + \left.\frac{\partial c(x,y,t)}{\partial x}\right|_{y=-h(x)} \right\}, \end{aligned} \tag{21.18}$$

where we used the BCs in Eq. (21.15) to simplify computations. Subsequently, we integrate the first term of Eq. (21.17) using the Leibniz integral rule, Eq. (A.9), yielding

$$D_x \frac{\partial}{\partial x} \int_{-h(x)}^{h(x)} \frac{\partial c(x,y,t)}{\partial x}\, \mathrm{d}y = D_x \int_{-h(x)}^{h(x)} \frac{\partial^2 c(x,y,t)}{\partial t^2}\, \mathrm{d}y$$

$$+ D_x\, h'(x) \left.\frac{\partial c(x,y,t)}{\partial x}\right|^{y=h(x)} - D_x \left[-h'(x)\right] \left.\frac{\partial c(x,y,t)}{\partial x}\right|_{y=-h(x)}. \tag{21.19}$$

Furthermore,

$$D_x \int_{-h(x)}^{h(x)} \frac{\partial^2 c(x,y,t)}{\partial t^2}\, \mathrm{d}y = D_x \frac{\partial}{\partial x} \int_{-h(x)}^{h(x)} \frac{\partial c(x,y,t)}{\partial x} \mathrm{d}y$$

$$- D_x\, h'(x) \left.\frac{\partial c(x,y,t)}{\partial x}\right|^{y=h(x)} - D_x\, h'(x) \left.\frac{\partial c(x,y,t)}{\partial x}\right|_{y=-h(x)}. \tag{21.20}$$

Thereafter, by inserting Eqs. (21.18) and (21.20) into Eq. (21.17), we ultimately obtain

$$\frac{\partial \rho(x,t)}{\partial t} = D_x \frac{\partial}{\partial x} \int_{-h(x)}^{h(x)} \frac{\partial c(x,y,t)}{\partial x}\, \mathrm{d}y. \tag{21.21}$$

21.1.1.1 Equilibrium Solution

As a first approach, we study the limiting case when $D_y \to \infty$. In such case, the concentration in the transverse direction reaches equilibrium almost instantly. Accordingly, an equilibrium density is proposed to encompass this condition, specifically

$$c_0(x,y,t) = \frac{1}{\mathtt{F}(x)}\, \mathrm{e}^{-gy}\, \rho(x,t), \tag{21.22}$$

where a free energy $\mathtt{F}(x)$ is included as a normalization factor, which is analogous to the free energy used in Zwanzig's approach defined through Eq. (18.8). Furthermore, $\mathtt{F}(x)$ contains information about the system's boundaries and the external energetic potential. More explicitly, we have that

$$\mathtt{F}(x) = \int_{-h(x)}^{h(x)} \mathrm{e}^{-gy}\, \mathrm{d}y = -\frac{1}{g} \mathrm{e}^{-gy} \Big|_{-h(x)}^{h(x)} = \frac{2}{g} \left[\frac{\mathrm{e}^{+gh(x)} - \mathrm{e}^{-gh(x)}}{2}\right], \tag{21.23}$$

resulting in

$$\mathtt{F}(x) = \frac{2}{g}\sinh\left[gh(x)\right]. \tag{21.24}$$

Moreover, the substitution of Eqs. (21.22) and (21.24) into Eq. (21.21) yields

$$\begin{aligned}\frac{\partial\rho(x,t)}{\partial t} &= D_x\,\frac{\partial}{\partial x}\int_{-h(x)}^{h(x)}\frac{\partial}{\partial x}\frac{\mathrm{e}^{-gy}\rho(x,t)}{\mathtt{F}(x)}\,\mathrm{d}y \\ &= D_x\,\frac{\partial}{\partial x}\int_{-h(x)}^{h(x)}\mathrm{e}^{-gy}\,\mathrm{d}y\,\frac{\partial}{\partial x}\frac{\rho(x,t)}{\mathtt{F}(x)},\end{aligned} \tag{21.25}$$

and by using the definition of $\mathtt{F}(x)$, we obtain

$$\frac{\partial\rho(x,t)}{\partial t} = D_x\,\frac{\partial}{\partial x}\left\{\mathtt{F}(x)\frac{\partial}{\partial x}\frac{\rho(x,t)}{\mathtt{F}(x)}\right\}. \tag{21.26}$$

This equation was previously derived in Sect. 19.3.1.1 using Reguera and Rubi's method. Equation (21.26) has the same structure and functional dependence as the Fick-Jacobs equation, i.e., Eq. (17.19). Furthermore, an equivalent equation can be written when there is position-dependent diffusivity, namely,

$$\frac{\partial\rho(x,t)}{\partial t} = \frac{\partial}{\partial x}\left\{D(x)\,\mathtt{F}(x)\frac{\partial}{\partial x}\frac{\rho(x,t)}{\mathtt{F}(x)}\right\}. \tag{21.27}$$

If the gravitational-like external potential is too weak, namely, $g \to 0$, then $\mathtt{F}(x)$ takes the form

$$\mathtt{F}(x) = \int_{-h(x)}^{h(x)}\mathrm{e}^{-gy}\,\mathrm{d}y = \int_{-h(x)}^{h(x)}\mathrm{d}y = 2h(x), \tag{21.28}$$

and the system with a single entropic potential system is recovered. In the absence of an external potential, the normalization function $\mathtt{F}(x)$ becomes the width of the channel.

21.1.1.2 General Solution of $c(x, y, t)$

The reader may note that Eq. (21.22) is not really a solution of the Smoluchowski equation if $D_y \neq \infty$. Nevertheless, given that we have found a solution at equilibrium, we can propose a general solution in terms of a perturbative series, namely,

$$c(x,y,t) = \mathrm{e}^{-gy}\sum_{n=0}^{\infty}\epsilon^n\,\hat{\boldsymbol{\sigma}}_n(x,y,\partial_x)\frac{\rho(x,t)}{\mathtt{F}(x)}, \tag{21.29}$$

where $\epsilon \equiv D_x/D_y$ and ∂_x is used to represent the partial derivative operator $\partial/\partial x$. Then, we explicitly write the first term of the series in Eq. (21.29), that is,

$$c(x, y, t) = \mathrm{e}^{-gy}\ \hat{\boldsymbol{\sigma}}_0(x, y, \partial_x)\frac{\rho(x,t)}{\mathrm{F}(x)} + \mathrm{e}^{-gy}\sum_{n=1}^{\infty}\epsilon^n\ \hat{\boldsymbol{\sigma}}_n(x, y, \partial_x)\frac{\rho(x,t)}{\mathrm{F}(x)}. \tag{21.30}$$

The first term of the series should be equal to the solution at equilibrium; therefore,

$$\hat{\boldsymbol{\sigma}}_0(x, y, \partial_x) = 1, \tag{21.31}$$

leading to

$$c(x, y, t) = \mathrm{e}^{-gy}\ \frac{\rho(x,t)}{\mathrm{F}(x)} + \mathrm{e}^{-gy}\sum_{n=1}^{\infty}\epsilon^n\ \hat{\boldsymbol{\sigma}}_n(x, y, \partial_x)\frac{\rho(x,t)}{\mathrm{F}(x)}. \tag{21.32}$$

Furthermore, the reduced Smoluchowski equation, Eq. (21.21), can be rewritten by means of Eqs. (21.23) and (21.32), yielding

$$\begin{aligned}\frac{\partial\rho(x,t)}{\partial t} &= D_x\,\frac{\partial}{\partial x}\left\{\mathrm{F}(x)\frac{\partial}{\partial x}\frac{\rho(x,t)}{\mathrm{F}(x)}\right\}\\ &+ D_x\,\frac{\partial}{\partial x}\left\{\mathrm{F}(x)\sum_{k=1}^{\infty}\epsilon^k\frac{1}{\mathrm{F}(x)}\int_{-h(x)}^{h(x)}\mathrm{e}^{-gy}\,\frac{\partial}{\partial x}\left[\hat{\boldsymbol{\sigma}}_k(x, y, \partial_x)\,\frac{\rho(x,t)}{\mathrm{F}(x)}\right]\mathrm{d}y\right\}.\end{aligned} \tag{21.33}$$

The last equation suggests the definition of the following operator:

$$\hat{\boldsymbol{Z}}_k(x, \partial_x)\ \partial_x\,\boxed{\cdot} \equiv -\frac{1}{\mathrm{F}(x)}\int_{-h(x)}^{h(x)}\mathrm{e}^{-gy}\frac{\partial}{\partial x}\left[\hat{\boldsymbol{\sigma}}_k(x, y, \partial_x)\,\boxed{\cdot}\right]\,\mathrm{d}y, \tag{21.34}$$

in which $\boxed{\cdot}$ is the placeholder for the function over which the operator is applied. We simplify the notation by writing

$$\hat{\boldsymbol{Z}}_k(x, \partial_x)\ \partial_x\,\boxed{\cdot} \equiv -\frac{1}{\mathrm{F}(x)}\int_{-h(x)}^{h(x)}\mathrm{d}y\ \mathrm{e}^{-gy}\ \frac{\partial}{\partial x}\hat{\boldsymbol{\sigma}}_k(x, y, \partial_x)\ \boxed{\cdot}. \tag{21.35}$$

Moreover, the notation without explicit grouping symbols also applies for $\hat{\boldsymbol{\sigma}}_k(x, y, \partial_x)$ operators. Additionally, it is practical to define

$$\epsilon\hat{\boldsymbol{Z}}(x, \partial_x)\,\boxed{\cdot} \equiv \sum_{k=1}^{\infty}\epsilon^k\ \hat{\boldsymbol{Z}}_k(x, \partial_x)\,\boxed{\cdot}. \tag{21.36}$$

By using the definitions in Eqs. (21.35) and (21.36), Eq. (21.33) simplifies to

$$\frac{\partial \rho(x,t)}{\partial t} = D_x \frac{\partial}{\partial x}\left\{ \mathrm{F}(x)\left[1 - \epsilon \hat{\mathbf{Z}}(x,\partial_x)\right]\frac{\partial}{\partial x}\left[\frac{\rho(x,t)}{\mathrm{F}(x)}\right]\right\}. \tag{21.37}$$

21.1.2 Recurrence Formula for the Operators $\hat{\boldsymbol{\sigma}}_k(x, y, \partial_x)$

Moving forward, we must find a recurrence relation for the operator $\hat{\boldsymbol{\sigma}}_k(x, y, \partial_x)$. Initially, we know that the perturbative series in Eq. (21.29) is a solution of the Smoluchowski equation, Eq. (18.1). Then, substituting the former equation into the latter, we obtain

$$\begin{aligned}
&\left(\frac{1}{D_x}\frac{\partial}{\partial t} - \frac{\partial^2}{\partial x^2} - \frac{1}{\epsilon}\frac{\partial}{\partial y}\mathrm{e}^{-gy}\frac{\partial}{\partial y}\mathrm{e}^{gy}\right)\left[\mathrm{e}^{-gy}\sum_{j=0}^{\infty}\epsilon^j\,\hat{\boldsymbol{\sigma}}_j(x,y,\partial_x)\frac{\rho(x,t)}{\mathrm{F}(x)}\right] \\
&= \sum_{j=0}^{\infty}\epsilon^j\left[\mathrm{e}^{-gy}\left(\frac{1}{D_x}\frac{\partial}{\partial t} - \frac{\partial^2}{\partial x^2}\right) - \frac{1}{\epsilon}\frac{\partial}{\partial y}\mathrm{e}^{-gy}\frac{\partial}{\partial y}\right]\hat{\boldsymbol{\sigma}}_j(x,y,\partial_x)\frac{\rho(x,t)}{\mathrm{F}(x)} = 0,
\end{aligned} \tag{21.38}$$

where the whole equation was divided by D_x. Noting that $\hat{\boldsymbol{\sigma}}_j(x, y, \partial_x)$ does not have a time dependency, we obtain

$$\begin{aligned}
&-\mathrm{e}^{-gy}\sum_{j=0}^{\infty}\epsilon^j\frac{\partial^2}{\partial x^2}\hat{\boldsymbol{\sigma}}_j(x,y,\partial_x)\frac{\rho(x,t)}{\mathrm{F}(x)} - \hat{\boldsymbol{\sigma}}_j(x,y,\partial_x)\frac{1}{D_x}\frac{\partial}{\partial t}\frac{\rho(x,t)}{\mathrm{F}(x)} \\
&= \sum_{j=0}^{\infty}\epsilon^{j-1}\frac{\partial}{\partial y}\mathrm{e}^{-gy}\frac{\partial}{\partial y}\hat{\boldsymbol{\sigma}}_j(x,y,\partial_x)\frac{\rho(x,t)}{\mathrm{F}(x)} \\
&= \sum_{n=-1}^{\infty}\epsilon^{j-1}\frac{\partial}{\partial y}\mathrm{e}^{-gy}\frac{\partial}{\partial y}\hat{\boldsymbol{\sigma}}_{n+1}(x,y,\partial_x)\frac{\rho(x,t)}{\mathrm{F}(x)} \\
&= \epsilon^{-1}\frac{\partial}{\partial y}\mathrm{e}^{-gy}\frac{\partial}{\partial y}\hat{\boldsymbol{\sigma}}_0(x,y,\partial_x)\frac{\rho(x,t)}{\mathrm{F}(x)} \\
&\quad + \sum_{n=0}^{\infty}\epsilon^{j-1}\frac{\partial}{\partial y}\mathrm{e}^{-gy}\frac{\partial}{\partial y}\hat{\boldsymbol{\sigma}}_{n+1}(x,y,\partial_x)\frac{\rho(x,t)}{\mathrm{F}(x)} \\
&= \sum_{n=0}^{\infty}\epsilon^{j-1}\frac{\partial}{\partial y}\mathrm{e}^{-gy}\frac{\partial}{\partial y}\hat{\boldsymbol{\sigma}}_{n+1}(x,y,\partial_x)\frac{\rho(x,t)}{\mathrm{F}(x)},
\end{aligned} \tag{21.39}$$

where we used a subscript change of the form $(j-1) \to n$, the fact $\hat{\boldsymbol{\sigma}}_0(x, y, \partial_x) = 1$, and $\partial_y \left[\rho(x,t)/\mathtt{F}(x)\right] = 0$. This leads to

$$
\begin{aligned}
&- \mathrm{e}^{-gy} \sum_{j=0}^{\infty} \epsilon^j \left\{ \frac{\partial^2}{\partial x^2} \hat{\boldsymbol{\sigma}}_j(x, y, \partial_x) \frac{\rho(x,t)}{\mathtt{F}(x)} - \hat{\boldsymbol{\sigma}}_j(x, y, \partial_x) \frac{1}{D_x} \frac{\partial}{\partial t} \frac{\rho(x,t)}{\mathtt{F}(x)} \right\} \\
&\quad = \sum_{n=0}^{\infty} \epsilon^{j-1} \frac{\partial}{\partial y} \mathrm{e}^{-gy} \frac{\partial}{\partial y} \hat{\boldsymbol{\sigma}}_{n+1}(x, y, \partial_x) \frac{\rho(x,t)}{\mathtt{F}(x)}.
\end{aligned} \tag{21.40}
$$

The second term on the right-hand side can be computed using Eq. (21.37), yielding

$$
\begin{aligned}
&\sum_{j=0}^{\infty} \epsilon^j \, \hat{\boldsymbol{\sigma}}_j(x, y, \partial_x) \frac{1}{D_x} \frac{\partial}{\partial t} \frac{\rho(x,t)}{\mathtt{F}(x)} \\
&\quad = \frac{1}{D_x} \sum_{j=0}^{\infty} \epsilon^j \, \hat{\boldsymbol{\sigma}}_j(x, y, \partial_x) \frac{1}{\mathtt{F}(x)} D_x \frac{\partial}{\partial x} \left\{ \mathtt{F}(x) \frac{\partial}{\partial x} \frac{\rho(x,t)}{\mathtt{F}(x)} \right. \\
&\qquad \left. - D_x \frac{\partial}{\partial x} \mathtt{F}(x) \sum_{k=1}^{\infty} \epsilon^k \, \hat{\boldsymbol{Z}}_k(x, \partial_x) \frac{\partial}{\partial x} \frac{\rho(x,t)}{\mathtt{F}(x)} \right\} \\
&\quad = - \sum_{j=0}^{\infty} \epsilon^j \, \hat{\boldsymbol{\sigma}}_j(x, y, \partial_x) \frac{1}{\mathtt{F}(x)} \frac{\partial}{\partial x} \mathtt{F}(x) \sum_{k=0}^{\infty} \epsilon^k \, \hat{\boldsymbol{Z}}_k(x, \partial_x) \frac{\partial}{\partial x} \frac{\rho(x,t)}{\mathtt{F}(x)},
\end{aligned} \tag{21.41}
$$

where we used that

$$
\frac{\partial}{\partial x} \mathtt{F}(x) \frac{\partial}{\partial x} \frac{\rho(x,t)}{\mathtt{F}(x)} = - \frac{\partial}{\partial x} \mathtt{F}(x) \, \epsilon^0 \, \hat{\boldsymbol{Z}}_0(x, \partial_x) \frac{\partial}{\partial x} \frac{\rho(x,t)}{\mathtt{F}(x)}, \tag{21.42}
$$

with $\epsilon^0 = 1$ and $\hat{\boldsymbol{Z}}_0(x, \partial_x) = -1$. The next step requires the Cauchy product for infinite power series, which mathematical details can be found in Appendix A.6.4. Particularly, we use Eq. (A.41) in Eq. (21.41) to obtain

$$
- \sum_{j=0}^{\infty} \epsilon^j \sum_{k=0}^{\infty} \hat{\boldsymbol{\sigma}}_{j-k}(x, y, \partial_x) \frac{1}{\mathtt{F}(x)} \frac{\partial}{\partial x} \mathtt{F}(x) \, \hat{\boldsymbol{Z}}_k(x, \partial_x) \frac{\partial}{\partial x} \frac{\rho(x,t)}{\mathtt{F}(x)}. \tag{21.43}
$$

After changing the dummy index j by n and substituting the latter equation into Eq. (21.40), we obtain

$$\sum_{n=0}^{\infty}\epsilon^n\left\{\frac{\partial}{\partial y}\mathrm{e}^{-gy}\frac{\partial}{\partial y}\hat{\boldsymbol{\sigma}}_{n+1}(x,y,\partial_x)\frac{\rho(x,t)}{\mathrm{F}(x)}\right.$$
$$+\mathrm{e}^{-gy}\left[\frac{\partial^2}{\partial x^2}\hat{\boldsymbol{\sigma}}_j(x,y,\partial_x)\frac{\rho(x,t)}{\mathrm{F}(x)}\right. \tag{21.44}$$
$$\left.\left.+\sum_{k=0}^{n}\hat{\boldsymbol{\sigma}}_{n-k}(x,y,\partial_x)\frac{1}{\mathrm{F}(x)}\frac{\partial}{\partial x}\mathrm{F}(x)\hat{\boldsymbol{Z}}_k(x,\partial_x)\frac{\partial}{\partial x}\frac{\rho(x,t)}{\mathrm{F}(x)}\right]\right\}=0.$$

Given that every power of ϵ is linearly independent of any other and that Eq. (21.44) is equal to zero, we have that

$$\frac{\partial}{\partial y}\mathrm{e}^{-gy}\frac{\partial}{\partial y}\hat{\boldsymbol{\sigma}}_{n+1}(x,y,\partial_x)\frac{\rho(x,t)}{\mathrm{F}(x)}$$
$$=-\mathrm{e}^{-gy}\left[\frac{\partial^2}{\partial x^2}\hat{\boldsymbol{\sigma}}_n(x,y,\partial_x)\frac{\rho(x,t)}{\mathrm{F}(x)}\right. \tag{21.45}$$
$$\left.+\sum_{k=0}^{n}\hat{\boldsymbol{\sigma}}_{n-k}(x,y,\partial_x)\frac{1}{\mathrm{F}(x)}\frac{\partial}{\partial x}\mathrm{F}(x)\hat{\boldsymbol{Z}}_k(x,\partial_x)\frac{\partial}{\partial x}\frac{\rho(x,t)}{\mathrm{F}(x)}\right].$$

Each side of the latter equation can be considered as an operator acting over $\rho(x,t)/\mathrm{F}(x)$. More accurately, we write such operator as

$$\frac{\partial}{\partial y}\mathrm{e}^{-gy}\frac{\partial}{\partial y}\hat{\boldsymbol{\sigma}}_{n+1}(x,y,\partial_x)=-\mathrm{e}^{-gy}\left[\frac{\partial^2}{\partial x^2}\hat{\boldsymbol{\sigma}}_n(x,y,\partial_x)\right.$$
$$\left.+\sum_{k=0}^{n}\hat{\boldsymbol{\sigma}}_{n-k}(x,y,\partial_x)\frac{1}{\mathrm{F}(x)}\frac{\partial}{\partial x}\mathrm{F}(x)\ \hat{\boldsymbol{Z}}_k(x,\partial_x)\frac{\partial}{\partial x}\right]. \tag{21.46}$$

By observing the subscripts, we conclude that this last equation represents a recurrence relation over $\hat{\boldsymbol{\sigma}}_i(x,y,\partial_x)$.

21.1.2.1 Boundary Conditions

Now, if the perturbative series of Eq. (21.29) is substituted into the BCs in Eq. (21.15), we obtain the following equation:

$$\frac{1}{\epsilon}\mathrm{e}^{-gy}\frac{\partial}{\partial y}\mathrm{e}^{gy}\left[\mathrm{e}^{-gy}\sum_{n=0}^{\infty}\epsilon^n\hat{\boldsymbol{\sigma}}_n(x,y,\partial_x)\right]\Bigg|_{y=\pm h(x)}$$

$$= \pm h'(x) \frac{\partial}{\partial x} \left[\mathrm{e}^{-gy} \sum_{n=0}^{\infty} \epsilon^n \hat{\boldsymbol{\sigma}}_n(x, y, \partial_x) \right] \Bigg|_{y=\pm h(x)}, \tag{21.47}$$

which has been written using operator notation. After performing a few operations, we arrive at

$$\frac{\partial}{\partial y} \sum_{n=0}^{\infty} \epsilon^{n-1} \hat{\boldsymbol{\sigma}}_n(x, y, \partial_x) \Bigg|_{y=\pm h(x)} = \pm h'(x) \frac{\partial}{\partial x} \sum_{n=0}^{\infty} \epsilon^n \hat{\boldsymbol{\sigma}}_n(x, y, \partial_x) \Bigg|_{y=\pm h(x)}. \tag{21.48}$$

By switching the indices of the sums, this is $j = n-1$, then $n = j+1$, we obtain

$$\frac{\partial}{\partial y} \sum_{j=-1}^{\infty} \epsilon^j \hat{\boldsymbol{\sigma}}_n(x, y, \partial_x) \Bigg|_{y=\pm h(x)} = \pm h'(x) \frac{\partial}{\partial x} \sum_{n=0}^{\infty} \epsilon^n \hat{\boldsymbol{\sigma}}_n(x, y, \partial_x) \Bigg|_{y=\pm h(x)}, \tag{21.49}$$

where we again changed the dummy index $j \rightarrow n$. Additionally, the term corresponding to $n = 0$ is explicitly written to obtain

$$\begin{aligned} &\frac{\partial}{\partial y} \epsilon^{-1} \hat{\boldsymbol{\sigma}}_0(x, y, \partial_x) \Big|_{y=\pm h(x)} + \frac{\partial}{\partial y} \sum_{n=0}^{\infty} \epsilon^n \, \hat{\boldsymbol{\sigma}}_{n+1}(x, y, \partial_x) \Big|_{y=\pm h(x)} \\ &\quad = \pm h'(x) \frac{\partial}{\partial x} \sum_{n=0}^{\infty} \epsilon^n \, \hat{\boldsymbol{\sigma}}_n(x, y, \partial_x) \Big|_{y=\pm h(x)}, \end{aligned} \tag{21.50}$$

where the first term on the left-hand side of the latter equation is null since we are computing the derivative of a constant. By recalling the linear independence of each of the ϵ powers, this yields

$$\frac{\partial}{\partial y} \hat{\boldsymbol{\sigma}}_{n+1}(x, y, \partial_x) \Big|_{y=\pm h(x)} = \pm h'(x) \frac{\partial}{\partial x} \hat{\boldsymbol{\sigma}}_n(x, y, \partial_x) \Big|_{y=\pm h(x)}. \tag{21.51}$$

This last equation represents the BCs applied to the operators $\hat{\boldsymbol{\sigma}_n}$.

21.1.3 First-Order Correction

Our next task is to find the first-order correction operator $\hat{\boldsymbol{\sigma}}_1(x, y, \partial_x)$. In order to do that, we need to use the recurrence relation of Eq. (21.46). Therefore, considering that $\hat{\boldsymbol{\sigma}}_0(x, y, \partial_x) = 1$ and $\hat{\mathbf{Z}}_0(x, \partial_x) = -1$, we write

$$\frac{\partial}{\partial y}\mathrm{e}^{-gy}\frac{\partial}{\partial y}\hat{\boldsymbol{\sigma}}_1(x,y,\partial_x) = -\mathrm{e}^{-gy}\left[\frac{\partial^2}{\partial x^2}\hat{\boldsymbol{\sigma}}_0(x,y,\partial_x) + \sum_{k=0}^{0}\hat{\boldsymbol{\sigma}}_{0-k}(x,y,\partial_x)\frac{1}{\mathrm{F}(x)}\frac{\partial}{\partial x}\mathrm{F}(x)\;\hat{\boldsymbol{Z}}_k(x,\partial_x)\frac{\partial}{\partial x}\right]$$

$$= \mathrm{e}^{-gy}\frac{1}{\mathrm{F}(x)}\frac{\partial}{\partial x}\mathrm{F}(x)\frac{\partial}{\partial x}. \tag{21.52}$$

The value of $\mathrm{F}(x)$ is given in Eq. (21.24), that is,

$$\begin{aligned}\frac{\partial}{\partial y}\mathrm{e}^{-gy}\frac{\partial}{\partial y}\hat{\boldsymbol{\sigma}}_1(x,y,\partial_x) &= -\mathrm{e}^{-gy}\frac{2g\;h'(x)\;\cosh[gh(x)]}{\sinh[gh(x)]}\frac{\partial}{\partial x}\\ &= \mathrm{e}^{-gy}\;g\;h'(x)\;\coth[gh(x)]\frac{\partial}{\partial x}.\end{aligned} \tag{21.53}$$

After integrating both sides of the last equation, we arrive at

$$\begin{aligned}\int\left[\frac{\partial}{\partial y}\,\mathrm{e}^{-gy}\frac{\partial}{\partial y}\hat{\boldsymbol{\sigma}}_1(x,y,\partial_x)\right]\mathrm{d}y &= \frac{1}{D_x}\int\mathrm{e}^{-gy}\;g\;h'(x)\;\coth[gh(x)]\frac{\partial}{\partial x}\,\mathrm{d}y\\ &= -\frac{1}{D_x}\mathrm{e}^{-gy}\;h'(x)\;\coth[gh(x)]\frac{\partial}{\partial x} + \hat{\boldsymbol{C}}_1.\end{aligned} \tag{21.54}$$

Furthermore, to find the constant operator $\hat{\boldsymbol{C}}_1$, we use the BCs given in Eq. (21.51), replacing $n = 0$, yielding

$$\frac{\partial}{\partial y}\hat{\boldsymbol{\sigma}}_1(x,y,\partial_x)\bigg|_{y=\pm h(x)} = \pm h'(x)\frac{\partial}{\partial x}\hat{\boldsymbol{\sigma}}_0(x,y,\partial_x)\bigg|_{y=\pm h(x)}, \tag{21.55}$$

which, together with Eq. (21.54), leads to

$$\pm h'(x)\frac{\partial}{\partial x} = -h'(x)\;\coth[gh(x)]\frac{\partial}{\partial x} + \mathrm{e}^{gy}\;\;\hat{\boldsymbol{C}}_1\Big|_{y=\pm h(x)}. \tag{21.56}$$

Furthermore, by evaluating the upper boundary, i.e., $y = h(x)$, we have

$$\hat{\boldsymbol{C}}_1 = h'(x)\;\mathrm{e}^{-gh(x)}\;(1+\coth[gh(x)])\;\frac{\partial}{\partial x}. \tag{21.57}$$

By substituting this last expression into Eq. (21.54), we obtain

$$\begin{aligned}\frac{\partial}{\partial y}\hat{\boldsymbol{\sigma}}_1(x,y,\partial_x) &= -h'(x)\ \coth[gh(x)]\frac{\partial}{\partial x}\\ &\quad + h'(x)\,\mathrm{e}^{-gh(x)}\,\mathrm{e}^{gy}\,\{1+\coth[gh(x)]\}\,\frac{\partial}{\partial x}\\ &= \frac{h'(x)}{\sinh[gh(x)]}\Big\{-\cosh[gh(x)]\\ &\quad +\mathrm{e}^{-gh(x)}\mathrm{e}^{gy}\,(\sinh[gh(x)]+\cosh[gh(x)])\Big\}\,\frac{\partial}{\partial x}\\ &= \frac{h'(x)}{\sinh[gh(x)]}\Big\{-\cosh[gh(x)]+\mathrm{e}^{-gh(x)}\,\mathrm{e}^{gy}\,\mathrm{e}^{gh(x)}\Big\}\,\frac{\partial}{\partial x},\end{aligned} \tag{21.58}$$

where we used Eq. (A.6). Following simplification, we arrive at

$$\frac{\partial}{\partial y}\hat{\boldsymbol{\sigma}}_1(x,y,\partial_x) = \frac{h'(x)}{\sinh[gh(x)]}\left\{\mathrm{e}^{gy}-\cosh[gh(x)]\right\}\frac{\partial}{\partial x}. \tag{21.59}$$

To find the operator $\hat{\boldsymbol{\sigma}}_1(x,y,\partial_x)$, we integrate the latter equation, resulting in

$$\hat{\boldsymbol{\sigma}}_1(x,y,\partial_x) = \frac{h'(x)}{\sinh[gh(x)]}\left\{\frac{1}{g}\mathrm{e}^{gy}-y\cosh[gh(x)]\right\}\frac{\partial}{\partial x}+\hat{\boldsymbol{C}}_0, \tag{21.60}$$

where the constant operator is calculated in Appendix 21.A.1, yielding

$$\hat{\boldsymbol{C}}_0 = \frac{h'(x)}{g}\left\{\frac{\cosh[gh(x)]}{\sinh[gh(x)]}-gh(x)\left(1+\frac{2}{\sinh^2[gh(x)]}\right)\right\}\frac{\partial}{\partial x}. \tag{21.61}$$

Now, $\hat{\boldsymbol{C}}_0$ is substituted into Eq. (21.60), leading to

$$\begin{aligned}&\hat{\boldsymbol{\sigma}}_1(x,y,\partial_x)\\ &\quad = \frac{h'(x)}{g}\left[\frac{\mathrm{e}^{gy}+(1-gy)\cosh[gh(x)]}{\sinh[gh(x)]}-gh(x)\left(1+\frac{2}{\sinh^2[gh(x)]}\right)\right]\frac{\partial}{\partial x}.\end{aligned} \tag{21.62}$$

Then, we compute the correction operator $\hat{\boldsymbol{Z}}_1(x,\partial_x)$ by means of Eq. (21.35) with $k=1$, that is,

$$\hat{\boldsymbol{Z}}_1(x,\partial_x) = -\frac{1}{\mathrm{F}(x)}\int_{-h(x)}^{h(x)}\mathrm{e}^{-gy}\,\frac{\partial}{\partial x}\hat{\boldsymbol{\sigma}}_1(x,y,\partial_x)\,\mathrm{d}y. \tag{21.63}$$

The calculation, which is shown in detail in Appendix 21.A.2, results in

$$\hat{\boldsymbol{Z}}_1(x,\partial_x) = \frac{h'^2(x)}{\sinh^2[gh(x)]}\left\{1+\cosh^2[gh(x)] - 2g\ h(x)\ \coth[gh(x)]\right\}, \tag{21.64}$$

which is the first-order correction operator for the Fick-Jacobs equation.

21.1.3.1 Limiting Case

The results we have found must be consistent at the previously described limit cases. To verify our results, we take $g \to 0$ and expand Eq. (21.64) using a Laurent series in Appendix A.6.1. For the sake of simplicity, we perform a change in variables, i.e., $\alpha \equiv gh(x)$, and keeping terms up to h'^2, we obtain

$$\hat{\boldsymbol{Z}}_1 = \operatorname{csch}^2[\alpha]\left\{1+\cosh^2[\alpha] - 2\alpha\coth[\alpha]\right\} \tag{21.65}$$

$$\approx \frac{2}{\alpha^2} - \frac{1}{3} + \frac{2}{3} - \frac{2}{\alpha^2} \tag{21.66}$$

$$= \frac{1}{3}, \tag{21.67}$$

concluding that

$$\lim_{g\to 0}\hat{\boldsymbol{Z}}_1(x,\partial_x) = \frac{1}{3}h'^2(x). \tag{21.68}$$

The last equation verifies that Eq. (18.51) is recovered, which is Zwanzig's result for a boxlike potential. Moreover, an analogy between these terms is worth pointing out, namely,

$$\kappa(x) \leftrightarrow \hat{\boldsymbol{Z}}_1(x,\partial_x). \tag{21.69}$$

21.1.4 The Position-Dependent Effective Diffusion Coefficient

In order to write the *corrected* effective diffusivity, Eqs. (21.37) and (21.27) must be used together with the expressions for continuity and flux, i.e., Eqs. (2.71) and (2.73), yielding

$$J(x,t) = -D_x\,\mathtt{F}(x)\left[1-\epsilon\hat{\boldsymbol{Z}}(x,\partial_x)\right]\frac{\partial}{\partial x}, \tag{21.70}$$

$$J(x,t) = -\mathtt{F}(x)\,D(x)\frac{\partial}{\partial x}. \tag{21.71}$$

We assume a constant (stationary) flux $J(x,t) = J$ for a long-time regime, enabling us to compare Eqs. (21.70) and (21.71). The combination of these equations leads to

$$1 = D_x\, \mathtt{F}(x) \left[1 - \epsilon\, \hat{\mathbf{Z}}(x, \partial_x)\right] \frac{1}{\mathtt{F}(x)\, D(x)}, \tag{21.72}$$

a relation from which we want to obtain the diffusion coefficient. Thereafter, considering that the term inside the square brackets is an operator, we obtain

$$\left[1 - \epsilon\, \hat{\mathbf{Z}}(x, \partial_x)\right]^{-1} \frac{1}{D_x\, \mathtt{F}(x)} = \frac{1}{\mathtt{F}(x)\, D(x)}, \tag{21.73}$$

which can be expanded using the binomial theorem presented in Appendix A.6.5, yielding

$$\frac{1}{D(x)} = \mathtt{F}(x) \left[1 + \epsilon\, \hat{\mathbf{Z}}(x, \partial_x) + \epsilon^2\, \hat{\mathbf{Z}}(x, \partial_x)^2 + \cdots\right] \frac{1}{D_x\, \mathtt{F}(x)}. \tag{21.74}$$

Further arrangements lead us to

$$\frac{D_x}{D(x)} = \left[1 + \epsilon\, \hat{\mathbf{Z}}(x, \partial_x)\, \frac{1}{\mathtt{F}(x)} + \epsilon^2\, \hat{\mathbf{Z}}(x, \partial_x)^2\, \frac{1}{\mathtt{F}(x)} + \cdots\right], \tag{21.75}$$

or

$$\frac{D_x}{D(x)} = \left[1 - \epsilon\, \mathtt{F}(x)\, \hat{\mathbf{Z}}(x, \partial_x)\, \frac{1}{\mathtt{F}(x)}\right]^{-1}. \tag{21.76}$$

Moreover, we assume that the operator $\hat{\mathbf{Z}}(x, \partial_x)$ acts solely on $\mathtt{F}(x)$. Therefore,

$$\frac{D(x)}{D_x} \simeq \left[1 - \epsilon\, \mathtt{F}(x)\, \hat{\mathbf{Z}}(x, \partial_x)\, \frac{1}{\mathtt{F}(x)}\right]. \tag{21.77}$$

This last expression can be turned into a series-dependent expression by means of Eq. (21.36), namely,

$$\frac{D(x)}{D_x} = 1 - \sum_{k=1}^{\infty} \epsilon^k\, \mathtt{F}(x)\, \hat{\mathbf{Z}}_k(x, \partial_x)\, \frac{1}{\mathtt{F}(x)}. \tag{21.78}$$

This is the procedure for finding the effective diffusion as an ϵ power series. If the first term is explicitly written, together with the use of Eq. (21.64), we find that for an isotropic system ($\epsilon = 1$),

$$\frac{D(x)}{D_0} \approx \frac{D_{Kg}(x)}{D_0} = 1 - \frac{h'^2(x)}{\sinh^2[gh(x)]} \left\{ 1 + \cosh^2[gh(x)] - 2gh(x) \coth[gh(x)] \right\}, \tag{21.79}$$

where D_x is renamed as D_0 to avoid ambiguity. This result includes only the first-order correction operator. In his original work, Kalinay presented an expression that contains terms of the second-order correction. It is worth noting that this was the first attempt to include a transversal force in a two-dimensional system.

21.2 2D Asymmetric Channel: Projection Method

In all computations made in the last section, we considered that the system's boundaries were symmetric, namely, $\pm h(x)$. In this section, we present a generalization to asymmetric boundaries $h_i(x)$ $(i = 1, 2)$, where $h_1(x)$ is the lower boundary and $h_2(x)$ is the upper boundary. The computations are very similar to the procedure used for symmetric channels.

The reader may notice that from Eqs. (21.9) to (21.23), the corresponding equations for the asymmetrical case can be derived simply by making $\pm h(x) \to h_i(x)$. In the case of Eq. (21.17), we need the explicit use of BCs. Nevertheless, we come to find that all contributions become null.

When considering asymmetric boundaries, free energy $\mathtt{F}(x)$ is given by

$$\mathtt{F}(x) = \int_{h_1(x)}^{h_2(x)} \mathrm{e}^{-gy}\, \mathrm{d}y = \frac{1}{g} \left[\mathrm{e}^{-gh_1(x)} - \mathrm{e}^{-gh_2(x)} \right], \tag{21.80}$$

which is a function that leads us to the steady-state solution and to a function that resembles the Fick-Jacobs equation, namely,

$$\frac{\partial}{\partial t} \rho(x,t) = D_x \frac{\partial}{\partial x} \left\{ \mathtt{F}(x) \frac{\partial}{\partial x} \left[\frac{\rho(x,t)}{\mathtt{F}(x)} \right] \right\}. \tag{21.81}$$

For the asymmetric case, we start our analysis from Eq. (21.28), as we will show in the next section.

21.2.1 Recurrence Formula for Operators $\hat{\sigma}_k(x, y, \partial_x)$

21.2.1.1 General Solution

Equation (21.58) is a recurrence relation for operators $\hat{\boldsymbol{\sigma}}_j$. In previous sections, the BCs were not used until $\mathtt{F}(x)$ was explicitly computed. As a first step to find $\hat{\boldsymbol{\sigma}}_1$, we must calculate the derivative of $\mathtt{F}(x)$, namely,

$$\begin{aligned}\frac{\partial}{\partial x}\mathrm{F}(x) &= \frac{\partial}{\partial x}\left\{\frac{1}{g}\left[\mathrm{e}^{-gh_1(x)} - \mathrm{e}^{-gh_2(x)}\right]\right\} \\ &= \frac{1}{g}\left[-gh_1'(x)\,\mathrm{e}^{-gh_1(x)} + gh_2'(x)\,\mathrm{e}^{-gh_2(x)}\right] \\ &= h_2'(x)\,\mathrm{e}^{-gh_2(x)} - h_1'(x)\,\mathrm{e}^{-gh_1(x)}.\end{aligned} \tag{21.82}$$

Substitution into the recurrence relation gives

$$\begin{aligned}&\frac{\partial}{\partial y}\mathrm{e}^{-gy}\frac{\partial}{\partial y}\hat{\boldsymbol{\sigma}}_1(x, y, \partial_x) \\ &= \mathrm{e}^{-gy}\frac{g}{\mathrm{e}^{-gh_1(x)} - \mathrm{e}^{-gh_2(x)}}\left[h_2'(x)\,\mathrm{e}^{-gh_2(x)} - h_1'(x)\,\mathrm{e}^{-gh_1(x)}\right]\frac{\partial}{\partial x}.\end{aligned} \tag{21.83}$$

The complete calculation of operator $\hat{\boldsymbol{\sigma}}_1$ is shown in Appendix 21.A.3, which results in

$$\begin{aligned}\hat{\boldsymbol{\sigma}}_1(x, y, \partial_x) = &\left\{y\,\frac{h_1'(x)\,\mathrm{e}^{-gh_1(x)} - h_2'(x)\,\mathrm{e}^{-gh_2(x)}}{\mathrm{e}^{-gh_1(x)} - \mathrm{e}^{-gh_2(x)}} + h_2'(x)\,\mathrm{e}^{-gh_2(x)}\,\mathrm{e}^{gy}\,\frac{1}{g}\right. \\ &\left.-\frac{h_1'(x)\,\mathrm{e}^{-gh_1(x)} - h_2'(x)\,\mathrm{e}^{-gh_2(x)}}{\mathrm{e}^{-gh_1(x)} - \mathrm{e}^{-gh_2(x)}}\mathrm{e}^{-gh_2(x)}\,\mathrm{e}^{gy}\,\frac{1}{g}\right\}\frac{\partial}{\partial x} \\ &+ \frac{h_2(x) - h_1(x)}{\mathrm{e}^{-gh_2(x)} - \mathrm{e}^{-gh_1(x)}}\left[h_2'(x)\,\mathrm{e}^{-gh_2(x)}\right. \\ &\left.+\frac{h_1'(x)\,\mathrm{e}^{-gh_1(x)} - h_2'(x)\,\mathrm{e}^{-gh_2(x)}}{\mathrm{e}^{-gh_1(x)} - \mathrm{e}^{-gh_2(x)}}\,\mathrm{e}^{-gh_2(x)}\right]\frac{\partial}{\partial x} \\ &+ \frac{h_1'(x)\,\mathrm{e}^{-gh_1(x)} - h_2'(x)\,\mathrm{e}^{-gh_2(x)}}{\left[\mathrm{e}^{-gh_1(x)} - \mathrm{e}^{-gh_2(x)}\right]^2}\left\{h_2'(x)\,\mathrm{e}^{-gh_2(x)}\right. \\ &\left.- h_1'(x)\,\mathrm{e}^{-gh_1(x)} + \frac{1}{g}\left[\mathrm{e}^{-gh_2(x)} - \mathrm{e}^{-gh_1(x)}\right]\right\}\frac{\partial}{\partial x}.\end{aligned} \tag{21.84}$$

21.2.2 First-Order Correction

First, let us define certain pragmatic quantities; all of the following definitions will be a function of x unless otherwise specified. The first one is channel width, namely,

$$w(x) \equiv h_2(x) - h_1(x). \tag{21.85}$$

The next one is the midline, that is,

$$y_0(x) \equiv \frac{1}{2}\left[h_1(x) + h_2(x)\right]. \tag{21.86}$$

Additionally, the boundaries are determined by

$$y_{\pm}(x) \equiv y_0(x) \pm \frac{1}{2}w(x), \tag{21.87}$$

which are equivalent to

$$y_+(x) = h_2(x), \qquad y_-(x) = h_1(x). \tag{21.88}$$

Finally, we define

$$\xi(x) \equiv \frac{1}{2}gw(x). \tag{21.89}$$

As previously established, the derivatives with respect to x will be denoted with a prime. Moreover, we will use some hyperbolic functions to simplify certain terms involving real exponential functions. Considering this, Eq. (21.84) transforms to

$$\begin{aligned}\hat{\boldsymbol{\sigma}}_1(x, y, \partial_x) = \Bigg\{ & y\left[y_0' - \frac{1}{2}w'\coth\xi\right] + \frac{1}{2g}\mathrm{e}^{+gy}\,\mathrm{e}^{-gy_+}w'\left[1+\coth\xi\right] \\ & - \frac{1}{4}ww'\left[2\coth^2\xi - 1\right] + \frac{1}{2}w'y_0\,\coth\xi + \frac{1}{2}wy_0'\,\coth\xi \\ & - y_0\,y_0' - \frac{1}{g}y_0' + \frac{1}{2g}w'\coth\xi\Bigg\}\frac{\partial}{\partial x}.\end{aligned} \tag{21.90}$$

The first-order correction operator is

$$\begin{aligned}\hat{\boldsymbol{Z}}_1(x, \partial_x)\,\partial_x = & \frac{w'^2}{4\sinh^2\left[\frac{1}{2}gw\right]}\left\{1 + \cosh^2\left[\frac{1}{2}gw\right] - gw\,\coth\left[\frac{1}{2}gw\right]\right\}\frac{\partial}{\partial x} \\ & + y_0'\left\{y_0' - w'\coth\left[\frac{1}{2}gw\right] + \frac{1}{2}gww'\mathrm{csch}^2\left[\frac{1}{2}gw\right]\right\}\frac{\partial}{\partial x}.\end{aligned} \tag{21.91}$$

The computations to obtain the latter equation are presented in detail in Appendix 21.A.4.

21.2.3 The Position-Dependent Effective Diffusion Coefficient

In order to find the effective diffusion coefficient, the first-order correction operator, Eq. (21.91), is substituted into Eq. (21.78). When considering an isotropic system ($\epsilon = 1$), this yields

$$D(x) \approx D_{asym-g}(x) = 1 - \frac{w'^2(x)}{4\sinh^2\left[\frac{1}{2}gw\right]}\left\{1+\cosh^2\left[\frac{1}{2}gw\right] - gw\ \coth\left[\frac{1}{2}gw\right]\right\} - y_0'\left\{y_0' - w'\coth\left[\frac{1}{2}gw\right] + \frac{1}{2}gww'\mathrm{csch}^2\left[\frac{1}{2}gw\right]\right\}. \tag{21.92}$$

The second term on the right-hand side of the latter equation, which is multiplied by y_0', contains the asymmetric contribution of the channel to the diffusion of Brownian particles. This term vanishes if the system has symmetric walls instead, as we can see from the derivative of Eq. (21.86). Given that the effective diffusivity was found using Eqs. (21.70) and (21.71) (both obtained from the Smoluchowski equation), the system's potential can be easily found using the free energy or normalization function $\mathtt{F}(x)$, namely,

$$-\beta U(x) = \frac{1}{g}\ln\left[\mathrm{e}^{-gh_1(x)} - \mathrm{e}^{-gh_1(x)}\right]. \tag{21.93}$$

This means that the difference in potential is

$$-\beta U(x) = -\beta\left[U(x) - U(x_0)\right] = \ln\left[\frac{\mathrm{e}^{-gh_1(x)} - \mathrm{e}^{-gh_2(x)}}{\mathrm{e}^{-gh_1(x_0)} - \mathrm{e}^{-gh_2(x_0)}}\right], \tag{21.94}$$

where the reference potential has been defined as $U(x_0) = 0$. The potential function $U(x)$ contains information about the system's boundaries and external forces exerted over the system. In other words, the potential is entropic and energetic.

21.3 Interpolation Formula

The position-dependent diffusion coefficient found by Zwanzig represents the first terms of a series. Inspired by this, Reguera and Rubi came up with the idea that the effective diffusivity should be written as in Eq. (19.56), a suggestion that was followed by Kalinay. This is the so-called interpolation formula, and its generalization considers that an external potential is

$$D(x) \approx D_\alpha(x) = \frac{D_0}{\left[1 + \frac{1}{4}\epsilon w'^2(x)\right]^{\alpha(gw, y_0')}}, \tag{21.95}$$

where α is a function that is dependent on the product gw. The midline derivative of the channel is y_0', while w' is the derivative of the width of the channel. By writing the effective diffusivity in the form of Eq. (21.95) and series-expanding such equation, we obtain the widely known first terms of the effective diffusion coefficient, in addition to further corrections to the original proposal by Fick-Jacobs.

Then, for an asymmetric channel subject to an external transverse field, the exponent for the interpolation formula reads

$$\begin{aligned}\alpha_{Ag}(gw, y_0') = &\frac{1}{\sinh^2\left[\frac{1}{2}gw\right]}\left\{1 + \cosh^2\left[\frac{1}{2}gw\right] - gw\coth\left[\frac{1}{2}gw\right]\right\} \\ &+ 4\frac{y_0'}{w'^2}\left\{y_0' - w'\coth\left[\frac{1}{2}gw\right] + \frac{1}{2}gww'\mathrm{csch}^2\left[\frac{1}{2}gw\right]\right\},\end{aligned} \tag{21.96}$$

which can be substituted into Eq. (21.95), and the resulting series expression. This expansion yields to Eq. (21.92) as the first terms of the series.

21.4 Limiting Cases

21.4.1 Symmetric Channel with a Transverse Force

For a symmetric channel, we have $y_0(x) = 0$, which means that $y_0'(x) = 0$ and $w(x) = 2h(x)$. This means that Eq. (21.92) simplifies to the result that was first reported by Kalinay, also calculated in this chapter (see Eq. (21.79)), which is

$$\frac{D_{Kg}(x)}{D_0} = 1 - \frac{h'^2(x)}{\sinh^2[gh(x)]}\left\{1 + \cosh^2[gh(x)] - 2gh(x)\ \coth[gh(x)]\right\}. \tag{21.79}$$

The last equation allows us to write an α function to use in the interpolation formula, namely,

$$\alpha_{Kg} = \frac{1}{\sinh^2[gh]}\left\{1 + \cosh^2[gh] - 2gh\ \coth[gh]\right\}, \tag{21.97}$$

which clearly replicates the first terms in Eq. (21.79) when substituted into Eq. (21.95).

21.4.2 Dominant g

Assuming that the external gravitational-like potential is too large, we compute the limit $g \to \pm\infty$ of Eq. (21.92). Using the relation of the ξ variable defined in Eq. (21.89), we are able to write

$$g \to \pm\infty \qquad \Rightarrow \qquad \xi = \frac{1}{2} g w \to \pm\infty, \tag{21.98}$$

where we considered that $w(x)$ and $w'(x)$ remain finite. We first compute the following:

$$\begin{aligned}
\lim_{g\to\pm\infty} g w \operatorname{csch}^2\xi &= \lim_{g\to\pm\infty} \frac{g w}{\sinh^2\left[\frac{1}{2} g w\right]} \\
&= \lim_{g\to\pm\infty} \frac{w}{\left[2\frac{1}{2} g\right] \sinh\left[\frac{1}{2} g w\right] \cosh\left[\frac{1}{2} g w\right]} \\
&= \lim_{g\to\pm\infty} \frac{4}{\left[\mathrm{e}^{\xi} - \mathrm{e}^{-\xi}\right]\left[\mathrm{e}^{\xi} + \mathrm{e}^{-\xi}\right]} \\
&= \lim_{g\to\pm\infty} \frac{4}{\mathrm{e}^{2\xi} - \mathrm{e}^{-2\xi}} \\
&= 0,
\end{aligned} \tag{21.99}$$

where we used the L'Hôpital rule. Additionally,

$$\begin{aligned}
\lim_{g\to\pm\infty} \coth^2\xi &= 1, \qquad & \lim_{g\to\pm\infty} \coth\xi &= \pm 1 \\
\lim_{g\to\pm\infty} \coth\xi \operatorname{csch}^2\xi &= 0, \qquad & \lim_{g\to\pm\infty} \operatorname{csch}^2\xi &= 0.
\end{aligned} \tag{21.100}$$

Using these results, the limit of the effective diffusivity is given by

$$\begin{aligned}
\frac{D_{g\to\pm\infty}}{D_0} &= 1 - \frac{w'^2}{4}\left\{\operatorname{csch}^2\xi + \coth^2\xi - g w \coth\xi \operatorname{csch}^2\xi\right\} \\
&\quad - y_0'\left\{y_0' - w' \coth\xi + \frac{1}{2} g w w' \operatorname{csch}^2\xi\right\} \\
&= 1 - \frac{w'^2(x)}{4}\{0 + 1 - 0\} - y_0'\left\{y_0' \mp w' + 0\right\},
\end{aligned} \tag{21.101}$$

leading to

$$\frac{D_{g\to\pm\infty}}{D_0} = 1 - y_0'^2 - \frac{1}{4} w'^2 \pm y_0' w'. \tag{21.102}$$

The sign in $\pm y_0' w'$ is fixed by the direction of the external constant force. Moreover, by rewriting Eq. (21.102) using the boundary functions h_1 y h_2, we arrive at

$$\frac{D_{g\to\pm\infty}}{D_0} = 1 - \frac{1}{2}\left\{h_1'^2 + h_2'^2 \mp \left(h_2'^2 - h_1'^2\right)\right\}, \tag{21.103}$$

or

$$\frac{D_{g\to+\infty}}{D_0} = 1 - h_1'^2, \qquad \frac{D_{T,g\to-\infty}}{D_0} = 1 - h_2'^2, \tag{21.104}$$

which, by following Zwanzig's suggestion, are

$$D_{g\to+\infty} = \frac{D_0}{1+h_1'^2}, \qquad D_{g\to-\infty} = \frac{D_0}{1+h_2'^2}. \tag{21.105}$$

If $g \to \pm\infty$, then $G \to \mp\infty$ (see Eq. (21.2)) due to the fact that G points *d*ownward as depicted in Fig. 21.2. Therefore,

$$D_{G\to-\infty} = \frac{D_0}{1+h_1'^2}, \qquad D_{G\to+\infty} = \frac{D_0}{1+h_2'^2}. \tag{21.106}$$

In other words, when experiencing a very intense external field, the Brownian particle will be *pushed* to one of the walls of the system, forcing it to follow a one-dimensional motion through that boundary of the diffusive channel.

21.4.3 Small Values of g

When $g \ll 1$, the Laurent series of the hyperbolic functions can be used to write $D(x)$, that is,

$$\begin{aligned}
\frac{D_{a,g}(x)}{D_0} &= 1 - \frac{1}{4}\left\{\left[\frac{1}{\xi^2} - \frac{1}{3} + \frac{1}{15}\xi^2 + \mathcal{O}(\xi^4)\right] + \left[\frac{1}{\xi^2} + \frac{2}{3} + \frac{1}{15}\xi^2 + \mathcal{O}(\xi^4)\right]\right. \\
&\quad \left. -2\xi\left[\frac{1}{\xi} + \frac{1}{3}\xi - \frac{1}{45}\xi^3 + \mathcal{O}(\xi^5)\right]\left[\frac{1}{\xi^2} - \frac{1}{3} + \frac{1}{15}\xi^2 + \mathcal{O}(\xi^4)\right]\right\} \\
&\quad - y_0'\left\{y_0' - w'\left[\frac{1}{\xi} + \frac{1}{3}\xi - \frac{1}{45}\xi^3 + \mathcal{O}(\xi^5)\right]\right. \\
&\quad \left. +\xi w'\left[\frac{1}{\xi^2} - \frac{1}{3} + \frac{1}{15}\xi^2 + \mathcal{O}(\xi^4)\right]\right\} \\
&\approx 1 - \frac{1}{4}w'^2\left\{\frac{2}{\xi^2} + \frac{1}{3} + \frac{2}{15}\xi^2 - \frac{2}{15}\xi^2 - \frac{2}{\xi^2}\right\} - y_0'\left\{y_0' - \frac{2}{3}\xi w'\right\} \\
&= 1 - \frac{1}{12}w'^2 - y_0'\left\{y_0' - \frac{2}{3}\xi w'\right\} = \frac{D_a}{D_0},
\end{aligned} \tag{21.107}$$

where the terms of order higher than two in ξ were neglected. It follows that

$$\frac{D_a(x)}{D_0} = 1 - y_0'^2 - \frac{1}{12}w'^2 + \frac{1}{3}gww'y_0', \tag{21.108}$$

or in Zwanzig notation

$$D_a(x) = \frac{D_0}{1 + y_0'^2 + \frac{1}{12}w'^2 - \frac{1}{3}gww'y_0'}. \tag{21.109}$$

The last equation is a generalization of Bradley's equation, Eq. (20.53). Then we can write

$$D_a(x) = D_{Br}(x) + \frac{1}{3}D_0\, gww'y_0'. \tag{21.110}$$

An α function can also be found by using the Laurent series of the hyperbolic functions in Eq. (21.96), leading to

$$\alpha_{Bg} = \frac{1}{3} + 4y_0'^2\frac{1}{w'^2} - \frac{4}{3}gwy_0'\frac{1}{w'}, \tag{21.111}$$

where α_{Bg} is the proposed α function for a modified Bradley equation, which includes the influence of a weak external transverse field. By substituting Eq. (21.111) into Eq. (21.95), the Bradley-like equation for low gravity values, Eq. (21.109), is recovered.

21.4.4 Asymmetric Channel Without an External Field

Once we have found the equations for a weak gravity force, we can extend such results to completely remove the field effect over the system, depicted in Fig. 21.3, that is, $g = 0$. In this case, the substitution of a null g into Eq. (21.111) leads to the Bradley equation, allowing us to write

$$\alpha_{Br} = \frac{1}{3} + 4y_0'^2\frac{1}{w'^2}. \tag{21.112}$$

It is even possible to obtain the Reguera and Rubi diffusion coefficient considering a symmetric channel, that is, $y_0' = 0$. Then, for

$$\alpha_{RR} = \frac{1}{3}, \tag{21.113}$$

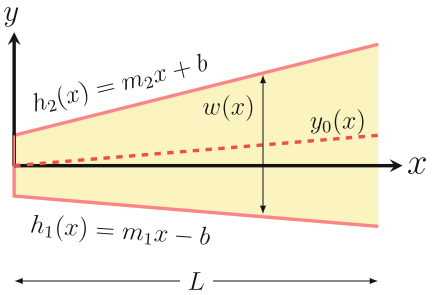

Fig. 21.3 Schematic representation of a two-dimensional variable-width asymmetric channel, $w(x) = h_2(x) - h_1(x)$, with curved midline, $y_0(x) = [h_1(x) + h_2(x)]/2$. The perfectly reflecting channel boundaries are given by $h_1(x)$ and $h_2(x)$

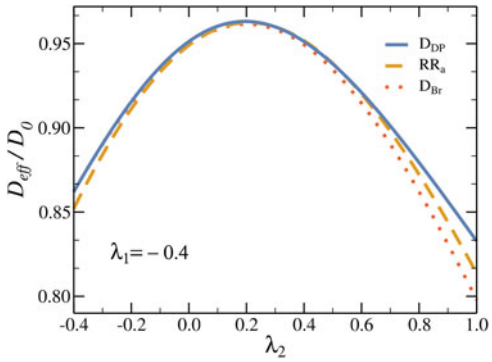

Fig. 21.4 Effective diffusion coefficient predicted by Eqs. (20.51) (blue solid line) and (20.53) (red dotted line) and the set of lines representing Eqs. (21.95), (21.112) denoted by RR_a (orange dashed line). The system consists of a 2D asymmetrical cone channel with perfectly reflecting boundaries given by $h_1(x) = -0.4x - 0.1$ and $h_2(x) = \lambda_2 x + 0.1$

we obtain Eq. (19.56) immediately. Furthermore, by making a series of diffusivity D_{RR}, we obtain the first terms of Zwanzig's results, that is,

$$D_{Zw}(x) = \frac{D_0}{1 + \frac{1}{12}w'^2(x)}. \tag{21.114}$$

We conclude that with the α function proposed in Eq. (21.96), we are able to obtain all previous results when substituting it in Eq. (21.95), as shown in Fig. 21.4. Thus, it is considered a generalization that is able to replicate all previous results under certain conditions.

21.5 First-Passage Times in Conical Channels

In previous sections, we found the effective diffusivities for two-dimensional channels under the influence of external potentials, particularly for a gravitational potential. These results allow us determine the time it takes for diffusing particles to

be absorbed by a perfectly absorbing wall. In simple terms, we calculate the solution to Eq. (6.38), namely,

$$\frac{\partial}{\partial x_0}\left[D(x_0)\ \mathrm{e}^{-\beta U(x_0)}\ \frac{\partial\langle t(x_0)\rangle}{\partial x_0}\right] = -\mathrm{e}^{-\beta U(x_0)}. \tag{6.38}$$

In Chap. 20, the exponential functions contained information about boundaries, which were referred to as the entropic potential. In the present case, the exponential functions contain both entropic and energetic potentials.

21.5.1 Asymmetrical Cone Under the Influence of Gravity

The system studied in the KP chapter exclusively considered the entropic potential, leading to $\mathrm{e}^{-\beta U(x_0)} \to w(x)$. For this system, we need a modification that accounts for the effects of the external potential, leading to the use of $\mathrm{e}^{-\beta U(x_0)} \to \mathtt{F}(x)$, where $\mathtt{F}(x)$ is given by Eq. (21.80), namely,

$$\mathtt{F}(x) = \int_{h_1(x)}^{h_2(x)} \mathrm{e}^{-gy}\ \mathrm{d}y = \frac{1}{g}\left[\mathrm{e}^{-gh_1(x)} - \mathrm{e}^{-gh_2(x)}\right], \tag{21.80}$$

which makes the equation for mean first-passage time (MFPT) be

$$\frac{1}{\mathtt{F}(x_0)}\frac{\mathrm{d}}{\mathrm{d}x_0}\left[D(x_0)\ \mathtt{F}(x_0)\frac{\mathrm{d}\langle t(x_0)\rangle}{\mathrm{d}x_0}\right] = -1. \tag{21.115}$$

After integrating this last equation, we find that

$$D(x_0)\ \mathtt{F}(x_0)\ \frac{\mathrm{d}\langle t(x_0)\rangle}{\mathrm{d}x_0} = -\int \mathtt{F}(x_0)\ \mathrm{d}x_0 + C_1. \tag{21.116}$$

We require an explicit form of an asymmetrical channel's boundaries to obtain a closed form of the free energy, as shown in Fig. 21.5. We make such computation for two different cases: narrow to wide ($n \to w$) and wide to narrow ($w \to n$).

The $n \to w$ boundaries are

$$h_2(x_0) = \lambda x_0 + b, \qquad h_1(x_0) = -\mu\lambda x_0 - b, \tag{21.117}$$

where μ is an asymmetry factor. When $\mu = 1$, then the symmetric case is obtained. First, we substitute the latter relations into Eq. (21.80), yielding

$$\mathtt{F}(x_0) = \frac{1}{g}\left\{\mathrm{e}^{+gb}\ \exp\left[+\mu g\lambda x_0\right] - \mathrm{e}^{-gb}\ \exp\left[-g\lambda x_0\right]\right\}. \tag{21.118}$$

Then, we integrate Eq. (21.116) using the explicit form of $\mathtt{F}(x_0)$, obtaining

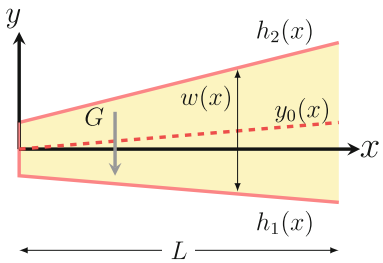

Fig. 21.5 Schematic representation of an asymmetrical cone wherein Brownian particles diffuse from narrow to wide ($n \to w$). The channel starts at $x = 0$ and ends at $x = L$. The width is given by $w(x) = h_2(x) - h_1(x)$, while the midline is defined by $y_0(x) = [h_1(x) + h_2(x)]/2$

$$D(x_0)\ \mathtt{F}(x_0)\ \frac{\mathrm{d}\langle t(x_0)\rangle}{\mathrm{d}x_0} = -\frac{1}{\lambda g^2}\left\{\frac{1}{\mu}\mathrm{e}^{+gb}\ \exp\left[+\mu g\lambda x_0\right] + \mathrm{e}^{-gb}\ \exp\left[-g\lambda x_0\right]\right\} + C_1. \tag{21.119}$$

The integration constant C_1 is obtained from the condition that the wall at $x_0 = 0$ is perfectly reflecting, meaning that

$$\left.\frac{\mathrm{d}\langle t(x_0)\rangle}{\mathrm{d}x_0}\right|_{x_0=0} = 0. \tag{21.120}$$

Therefore,

$$C_1 = \frac{1}{\lambda g^2}\left\{\frac{1}{\mu}\mathrm{e}^{+gb} + \mathrm{e}^{-gb}\right\}. \tag{21.121}$$

Substituting the latter equation into Eq. (21.116) yields

$$D(x_0)\ \mathtt{F}(x_0)\ \frac{\mathrm{d}\langle t(x_0)\rangle}{\mathrm{d}x_0} = -\frac{1}{\lambda g^2}\left\{\frac{1}{\mu}\mathrm{e}^{+gb}\ \exp\left[+\mu g\lambda x_0\right] + \mathrm{e}^{-gb}\ \exp\left[-g\lambda x_0\right]\right\} + \frac{1}{\lambda g^2}\left\{\frac{1}{\mu}\mathrm{e}^{+gb} + \mathrm{e}^{-gb}\right\}, \tag{21.122}$$

which can be written as

$$D(x_0)\ \mathtt{F}(x_0)\ \frac{\mathrm{d}\langle t(x_0)\rangle}{\mathrm{d}x_0} = -\frac{1}{\lambda g^2}\left\{\frac{1}{\mu}\mathrm{e}^{+gb}\ \left(\exp\left[+\mu g\lambda x_0\right] - 1\right) + \mathrm{e}^{-gb}\ \left(\exp\left[-g\lambda x_0\right] - 1\right)\right\}. \tag{21.123}$$

By integrating this last result, considering that the boundaries of the system are $x = 0$ and $x = L$, we obtain

$$\langle t(x_0 = L)\rangle - \langle t(x_0 = 0)\rangle = -\frac{1}{\lambda g^2}\int_0^L \frac{1}{D(x_0)\ \mathrm{F}(x_0)} \times \left\{\frac{1}{\mu}\mathrm{e}^{+gb}\ (\exp[+\mu g\lambda x_0] - 1) + \mathrm{e}^{-gb}\ (\exp[-g\lambda x_0] - 1)\right\}\mathrm{d}x_0. \tag{21.124}$$

Considering a perfectly absorbing wall at $x = L$, then

$$\langle t(L)\rangle = 0. \tag{21.125}$$

Thus, by using this condition, we arrive at

$$\langle t(0 \to L)\rangle \equiv \langle t(x_0 = 0)\rangle = \frac{1}{\lambda g^2}\int_0^L \frac{1}{D(x_0)\ \mathrm{F}(x_0)}\left\{\frac{1}{\mu}\mathrm{e}^{+gb}\ (\exp[+\mu g\lambda x_0] - 1) + \mathrm{e}^{-gb}\ (\exp[-g\lambda x_0] - 1)\right\}\mathrm{d}x_0, \tag{21.126}$$

where the notation $0 \to L$ indicates that the particle starts to diffuse at $x = 0$ and ends at $x = L$. This trajectory is identified as the $n \to w$ case, i.e.,

$$\langle t\rangle_{n\to w} = \langle t(0 \to L)\rangle. \tag{21.127}$$

In previous results, the free energy and the effective diffusivity could be written as a function of the channel's slope without an x_0 dependency. This is the reason why we take them out of the integral as constants. Now, for a system under the influence of an external field, the corresponding D also depends on the width of the channel w, which cannot be considered as constant in terms of x_0. This is the reason to numerically solve the integral to find the MFPT.

The approximate theoretical result of the MFPT for the $n \to w$ configuration is in excellent agreement with the Brownian dynamics simulations, seen in Fig. 21.6. Additionally, a remarkable behavior is observed as the MFPT is not bounded by the limiting case $g \to \infty$. For larger values of the slope λ and intermediate values of g, the MFPT lies under the limiting case. Let us gain some physical insights about the mentioned results. When the force g is large, particles are driven to one of the boundaries, preventing them from exploring the channel in the transversal direction. Therefore, the particles cannot benefit from the entropic force pushing them toward the exit of the channel. In other words, particles cannot exit the channel faster since the force does not allow them to bounce onto the walls. Furthermore, moderated values of the force cause an optimal interplay between that force and the entropic

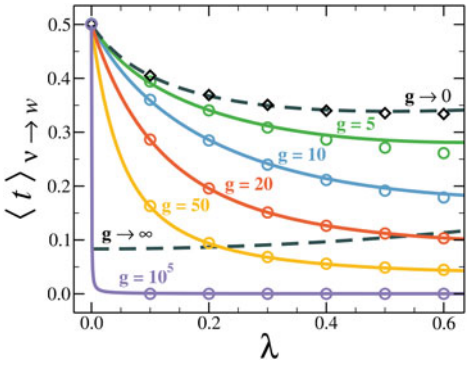

Fig. 21.6 Mean first-passage times for an asymmetrical cone with parameters $L = 1$, $b = 0.1$, $\mu = 0.8$, and different g values. The configuration of the cone is from narrow to wide $(n \to w)$

potential (boundaries), resulting in a beneficial *bouncing* on the walls, thrusting the particle to the exit and consequently decreasing the MFPT.

21.5.1.1 Wide to Narrow

For the case of a $(w \to n)$ channel, the boundaries are

$$h_2(x_0) = -\lambda(x_0 - L) + b, \qquad h_1(x_0) = \mu\lambda(x_0 - L) - b. \tag{21.128}$$

Let us find a solution using quadratures as explained in Sect. 20.6. In this case, the particle starts to diffuse at $x_0 = L$ and will be at x_0 a certain time t. These conditions establish the integration limits of the integrals in the computation of the MFPT. To simplify computations, let us make $x_0 \to x'$, which makes the integral of the MFPT to be

$$\int_L^{x_0} \frac{\mathrm{d}}{\mathrm{d}x'} \left[D(x')\ \mathtt{F}(x')\ \frac{\mathrm{d}\langle t(x')\rangle}{\mathrm{d}x'} \right] \mathrm{d}x' = -\int_L^{x_0} \mathtt{F}(x')\ \mathrm{d}x'. \tag{21.129}$$

The right-hand side of this last equation results in

$$D(x_0)\ \mathtt{F}(x_0)\ \frac{\mathrm{d}\langle t(x_0)\rangle}{\mathrm{d}x_0} - D(L)\ \mathtt{F}(L)\ \left.\frac{\mathrm{d}\langle t(x')\rangle}{\mathrm{d}x'}\right|_{x'=L} = D(x_0)\ \mathtt{F}(x_0)\ \frac{\mathrm{d}\langle t(x_0)\rangle}{\mathrm{d}x_0}, \tag{21.130}$$

where we used $\mathrm{d}\langle t(x')\rangle/\mathrm{d}x\big|_{x0=L} = 0$. We substitute this last result into Eq. 21.129 and then integrate again, namely,

$$\langle t(0)\rangle - \langle t(x_0)\rangle = -\int_{x_0}^{0} \frac{1}{D(x'')\ \mathtt{F}(x'')} \int_L^{x_0} \mathtt{F}(x')\ \mathrm{d}x'\ \mathrm{d}x''. \tag{21.131}$$

The perfectly absorbing wall implies that

$$\langle t(0)\rangle = 0, \tag{21.132}$$

leading us to

$$\langle t(x_0)\rangle = \int_{x_0}^{0} \frac{1}{D(x'')\ \mathtt{F}(x'')} \int_{L}^{x_0} \mathtt{F}(x')\ \mathrm{d}x'\ \mathrm{d}x''. \tag{21.133}$$

The limits of integration of both integrals can be inverted by factorizing a minus sign for each integral, yielding

$$\langle t(x_0)\rangle = \int_{0}^{x_0} \frac{1}{D(x'')\ \mathtt{F}(x'')} \int_{x''}^{L} \mathtt{F}(x')\ \mathrm{d}x'\ \mathrm{d}x''. \tag{21.134}$$

This last equation is

$$\langle t(L\to 0)\rangle \equiv \langle t(x_0 = L)\rangle = \int_{0}^{L} \frac{1}{D(x'')\ \mathtt{F}(x'')} \int_{x''}^{L} \mathtt{F}(x')\ \mathrm{d}x'\ \mathrm{d}x'', \tag{21.135}$$

which is also the case for $w \to n$, so then

$$\langle t\rangle_{w\to n} = \langle t(L\to 0)\rangle. \tag{21.136}$$

Now, the first integral inside Eq. (21.135) can be computed in a straightforward manner by using the explicit form of $\mathtt{F}(x')$, resulting in

$$\begin{aligned}\int_{x''}^{L} \mathtt{F}(x')\ \mathrm{d}x' = -\frac{1}{g^2\lambda} \Bigg\{ &\frac{1}{\alpha} \exp\left[+g\ (b+\alpha\lambda L)\right]\ \exp\left[-g\alpha\lambda x'\right] \\ &- \exp\left[-g\ (b+\lambda L)\right]\ \exp\left[+g\lambda x'\right] \Bigg\}\Bigg|_{x'=x''}^{x'=L}.\end{aligned} \tag{21.137}$$

By substituting this integral into Eq. (21.135) and evaluating at the limits, we arrive at

$$\begin{aligned}\langle t(L\to 0)\rangle = -\frac{1}{g^2\lambda} \int_{0}^{L} &\frac{1}{D(x'')\ \mathtt{F}(x'')} \\ &\times \Bigg\{ \frac{1}{\alpha} \exp\left[+g\ (b+\alpha\lambda L)\right]\ \left(\exp\left[-g\alpha\lambda L\right] - \exp\left[-g\alpha\lambda x''\right]\right) \\ &- \exp\left[-g\ (b+\lambda L)\right]\ \left(\exp\left[+g\lambda L\right] - \exp\left[+g\lambda x''\right]\right) \Bigg\}\ \mathrm{d}x''.\end{aligned} \tag{21.138}$$

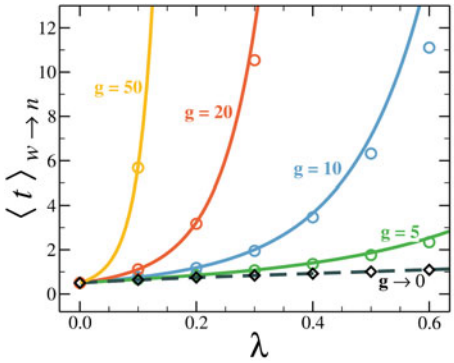

Fig. 21.7 Mean first-passage times for an asymmetrical cone with $L = 1$, $b = 0.1$, and $\mu = 0.8$ for different values of g. The circle markers are the values obtained from Brownian dynamics simulations. The cone has a wide-to-narrow ($w \rightarrow n$) configuration. It is worth noting that the vertical scale is rather different to the one presented in Fig. 21.6 for the $n \rightarrow w$ configuration, which shows times shorter than 0.5. For the present case, the time increases rapidly for almost all λ values

The numerical evaluation of $\langle t \rangle_{w \rightarrow n}$ is shown in Fig. 21.7.

Notably, very good agreement between the theoretical MFPT expression is shown. Some deviations are observed at intermediate boundary slopes and larger g values. Regardless of these derivations, the one-dimensional description can be validated for this channel configuration by noting that the 1D reduction is actually an approximation technique.

21.6 Concluding Remarks

In this chapter, the projection method technique was applied to 2D systems, specifically to symmetrical and asymmetrical channels under the influence of a gravitational-like potential. We obtained the position-dependent diffusion coefficients for those systems. Interestingly, Eq. (21.92) simplifies previous solutions under certain conditions. More specifically, we found that every effective diffusion coefficient in the literature is contained within the first terms of a binomial expansion if the interpolation formula (19.15) and the appropriate exponent are properly selected.

Finally, based on the results of $D(x)$, an equation for the MFPT of a conical 2D channel was obtained. Subsequently, we found the numerical solution of the MFPT and compared such results to the times obtained by means of Brownian dynamics simulations to validate the range of applicability of these equations.

21.A Mathematical Computations

21.A.1 Derivation of Eq. (21.61)

The constant operator $\hat{\boldsymbol{C}}_0$ is obtained by substituting the perturbative series of Eq. (21.29) into Eq. (21.16), that is,

$$\begin{aligned}
\rho(x,t) &= \int_{-h(x)}^{h(x)} \mathrm{e}^{-gy}\, \hat{\boldsymbol{\sigma}}_n(x,y,\partial_x)\,\mathrm{d}y \\
&= \int_{-h(x)}^{h(x)} \mathrm{e}^{-gy} \sum_{n=0}^{\infty} \epsilon^n\, \hat{\boldsymbol{\sigma}}_n(x,y,\partial_x) \frac{\rho(x,t)}{\mathrm{F}(x)}\,\mathrm{d}y \\
&= \int_{-h(x)}^{h(x)} \mathrm{e}^{-gy}\, \epsilon^0 \cancelto{1}{\hat{\boldsymbol{\sigma}}_0(x,y,\partial_x)} \frac{\rho(x,t)}{\mathrm{F}(x)}\,\mathrm{d}y \\
&\quad + \sum_{n=1}^{\infty} \epsilon^n \int_{-h(x)}^{h(x)} \mathrm{e}^{-gy}\, \hat{\boldsymbol{\sigma}}_n(x,y,\partial_x) \frac{\rho(x,t)}{\mathrm{F}(x)}\,\mathrm{d}y \\
&= \cancelto{\mathrm{F}(x)}{\int_{-h(x)}^{h(x)} \mathrm{e}^{-gy}\,\mathrm{d}y}\, \frac{\rho(x,t)}{\mathrm{F}(x)} \\
&\quad + \sum_{n=1}^{\infty} \epsilon^n \int_{-h(x)}^{h(x)} \mathrm{e}^{-gy}\, \hat{\boldsymbol{\sigma}}_n(x,y,\partial_x)\,\mathrm{d}y\, \frac{\rho(x,t)}{\mathrm{F}(x)} \\
&= \rho(x,t) + \sum_{n=1}^{\infty} \epsilon^n \int_{-h(x)}^{h(x)} \mathrm{e}^{-gy}\, \hat{\boldsymbol{\sigma}}_n(x,y,\partial_x)\,\mathrm{d}y\, \frac{\rho(x,t)}{\mathrm{F}(x)},
\end{aligned} \tag{21.139}$$

which means

$$0 = \sum_{n=1}^{\infty} \epsilon^n \int_{-h(x)}^{h(x)} \mathrm{e}^{-gy}\, \hat{\boldsymbol{\sigma}}_n(x,y,\partial_x)\,\mathrm{d}y\, \frac{\rho(x,t)}{\mathrm{F}(x)}. \tag{21.140}$$

Every term inside the series satisfies $\epsilon \neq 0$ and $\rho(x,t)/\mathrm{F}(x) \neq 0$. In other words, we have linear independence between the ϵ powers. Therefore, the equation is satisfied if

$$\int_{-h(x)}^{h(x)} \mathrm{e}^{-gy}\, \hat{\boldsymbol{\sigma}}_n(x,y,\partial_x)\,\mathrm{d}y = 0, \qquad \forall n > 0. \tag{21.141}$$

We proceed to integrate $\hat{\boldsymbol{\sigma}}_1$, namely,

$$\begin{aligned}
&\int_{-h(x)}^{h(x)} \mathrm{e}^{-gy} \left\{ \frac{h'(x)}{\sinh[gh(x)]} \left(\frac{1}{g} \mathrm{e}^{-gy} - y \cosh[gh(x)] \right) \frac{\partial}{\partial x} + \hat{\boldsymbol{C}}_0 \right\} \mathrm{d}y \\
&\quad = \frac{h'(x)}{g \sinh[gh(x)]} 2h(x) \frac{\partial}{\partial x} - \frac{h'(x) \cosh[gh(x)]}{\sinh[gh(x)]} \int_{-h(x)}^{h(x)} y \, \mathrm{e}^{-gy} \, \mathrm{d}y \, \frac{\partial}{\partial x} \\
&\qquad + \hat{\boldsymbol{C}}_0 \int_{-h(x)}^{h(x)} \mathrm{e}^{-gy} \, \mathrm{d}y \\
&\quad = \frac{2h(x) \, h'(x)}{g \sinh[gh(x)]} \frac{\partial}{\partial x} - \frac{h'(x) \cosh[gh(x)]}{\sinh[gh(x)]} \int_{-h(x)}^{h(x)} y \, \mathrm{e}^{-gy} \, \mathrm{d}y \, \frac{\partial}{\partial x} \\
&\qquad + \hat{\boldsymbol{C}}_0 \left[-\frac{1}{g} \mathrm{e}^{-gy} \right] \Bigg|_{-h(x)}^{h(x)} \\
&\quad = 0.
\end{aligned} \tag{21.142}$$

The remaining integral is solved by parts, i.e.,

$$\begin{aligned}
\int_{-h(x)}^{h(x)} y \, \mathrm{e}^{-gy} \, \mathrm{d}y &= - \, y \, \frac{1}{g} \mathrm{e}^{-gy} \Big|_{-h(x)}^{h(x)} + \frac{1}{g} \left[-\frac{1}{g} \mathrm{e}^{-gy} \right] \Bigg|_{-h(x)}^{h(x)} \\
&= -\frac{h(x)}{g} \left[\mathrm{e}^{-gh(x)} + \mathrm{e}^{gh(x)} \right] - \frac{1}{g^2} \left[\mathrm{e}^{-gh(x)} - \mathrm{e}^{gh(x)} \right],
\end{aligned} \tag{21.143}$$

which, after using Eqs. (A.6) and (A.7), simplifies to

$$\int_{-h(x)}^{h(x)} y \, \mathrm{e}^{-gy} \, \mathrm{d}y = -\frac{h(x)}{g} \left\{ 2 \cosh[gh(x)] \right\} + \frac{1}{g^2} \left\{ 2 \sinh[gh(x)] \right\}. \tag{21.144}$$

Upon substitution of the latter equation into Eq. (21.142), we arrive at

$$\begin{aligned}
&\frac{2h(x) \, h'(x)}{g \sinh[gh(x)]} \frac{\partial}{\partial x} + \hat{\boldsymbol{C}}_0 \left\{ 2 \sinh[gh(x)] \right\} \\
&\qquad - \frac{h'(x) \cosh[gh(x)]}{\sinh[gh(x)]} \left\{ -\frac{h(x)}{g} \left(2 \cosh[gh(x)] \right) + \frac{1}{g^2} \left(2 \sinh[gh(x)] \right) \right\} \frac{\partial}{\partial x} \\
&= 0,
\end{aligned} \tag{21.145}$$

which leads us to

$$\begin{aligned}\hat{\boldsymbol{C}}_0 &= \frac{h'(x)}{g}\left\{\frac{\cosh[gh(x)]}{\sinh[gh(x)]} - \frac{h(x)\ g\left(\cosh^2[gh(x)]+1\right)}{\sinh^2[gh(x)]}\right\}\frac{\partial}{\partial x}\\ &= \frac{h'(x)}{g}\left\{\frac{\cosh[gh(x)]}{\sinh[gh(x)]} - gh(x)\left(\frac{1+\sinh^2[gh(x)]+1}{\sinh^2[gh(x)]}\right)\right\}\frac{\partial}{\partial x}.\end{aligned} \tag{21.146}$$

Finally, by rearranging, we find that

$$\hat{\boldsymbol{C}}_0 = \frac{h'(x)}{g}\left\{\frac{\cosh[gh(x)]}{\sinh[gh(x)]} - gh(x)\left(1+\frac{2}{\sinh^2[gh(x)]}\right)\right\}\frac{\partial}{\partial x}. \tag{21.61}$$

21.A.2 Derivation of Eq. (21.64)

In order to obtain the correction operator $\hat{\boldsymbol{Z}}_1(x,\partial_x)$, we make use of Eq. (21.63). The derivative inside the integral is computed first, reading

$$\begin{aligned}&\frac{\partial}{\partial x}\hat{\boldsymbol{\sigma}}_1(x,y,\partial_x)\\ &\quad= \frac{h''(x)}{g}\left\{\frac{\mathrm{e}^{gy}+(1-gy)\ \cosh[gh(x)]}{\sinh[gh(x)]} - gh(x)\left(1+\frac{2}{\sinh^2[gh(x)]}\right)\right\}\\ &\qquad+\frac{h'(x)}{g}\left\{\frac{\sinh[gh(x)]\ \left(gh'(x)\ [1-gy]\ \sinh[gh(x)]\right)}{\sinh^2[gh(x)]}\right.\\ &\qquad-\frac{[\mathrm{e}^{gy}+(1-gy)\ \cosh[gh(x)]]\ gh'(x)\ \cosh[gh(x)]}{\sinh^2[gh(x)]}\\ &\qquad-gh'(x)\left(1+\frac{2}{\sinh^2[gh(x)]}\right)\\ &\qquad\left.-gh(x)\left(-4g\ h'(x)\ \coth[gh(x)]\ \mathrm{csch}^2[gh(x)]\right)\right\}.\end{aligned} \tag{21.147}$$

Then, we multiply this last equation by e^{-gy} and integrate the term containing $h''(x)$ along the y direction, resulting in

$$
\begin{aligned}
I = \frac{1}{\sinh[gh(x)]} \Bigg\{ & \int_{-h(x)}^{h(x)} \mathrm{d}y + \cosh[gh(x)] \int_{-h(x)}^{h(x)} \mathrm{e}^{-gy}\, \mathrm{d}y \\
& - g \cosh[gh(x)] \int_{-h(x)}^{h(x)} y\, \mathrm{e}^{-gy}\, \mathrm{d}y \Bigg\} \\
& - gh(x) \left\{ \int_{-h(x)}^{h(x)} \mathrm{e}^{-gy}\, \mathrm{d}y + \frac{2}{\sinh^2[gh]} \int_{-h(x)}^{h(x)} \mathrm{e}^{-gy}\, \mathrm{d}y \right\},
\end{aligned} \tag{21.148}
$$

which after simplifying the terms yields

$$
\begin{aligned}
I &= \frac{1}{\sinh[gh(x)]} \left\{ 2h(x) + \frac{2}{g} \sinh[gh(x)]\ \cosh[gh(x)] \right. \\
&\quad - g \cosh[gh(x)] \left(-\frac{2h(x)}{g}\ \cosh[gh(x)] + \frac{2}{g^2} \sinh[gh(x)] \right) \Bigg\} \\
&\quad - 2h(x)\ \sinh[gh(x)] \left\{ 1 + \frac{2}{\sinh^2[gh(x)]} \right\} \\
&= \frac{1}{\sinh[gh(x)]} \left\{ 2h(x) + \frac{2}{g} \sinh[gh(x)]\ \cosh[gh(x)] \right. \\
&\quad + 2h(x)\ \cosh^2[gh(x)] - \frac{2}{g} \sinh[gh(x)]\ \cosh[gh(x)] \Bigg\} \\
&\quad - 2h(x)\ \sinh[gh(x)] - \frac{4h(x)}{\sinh[2h(x)]}.
\end{aligned} \tag{21.149}
$$

Then,

$$
\begin{aligned}
I &= \frac{1}{\sinh[gh(x)]} \left\{ 2h(x) \left[1 + \cosh^2[gh(x)] \right] \right\} \\
&\quad - 2h(x) \sinh[gh(x)] - \frac{4h(x)}{\sinh[2h(x)]} \\
&= 2h(x)\ \sinh[gh(x)] + \frac{4h(x)}{\sinh[2h(x)]} - 2h(x)\ \sinh[gh(x)] \\
&\quad - \frac{4h(x)}{\sinh[2h(x)]} \\
&= 0,
\end{aligned} \tag{21.150}
$$

and reducing terms

$$
\begin{aligned}
&\frac{\partial}{\partial x}\hat{\boldsymbol{\sigma}}_1(x, y, \partial_x) \\
&\quad = \frac{h'^2(x)}{\sinh[gh(x)]}\left\{\sinh[gh(x)] - gy\,\sinh[gh(x)] - \mathrm{e}^{gy}\,\coth[gh(x)]\right. \\
&\qquad - \cosh[gh(x)]\,\coth[gh(x)] + gy\,\cosh[gh(x)]\,\coth[gh(x)] \\
&\qquad \left. - \sinh[gh(x)] - 2\mathrm{csch}[gh(x)] + 4g\,h(x)\coth[gh(x)]\,\mathrm{csch}[gh(x)]\right\}.
\end{aligned}
\tag{21.151}
$$

Then, we multiply this last result by e^{-gy} and integrate with respect to y, leading to

$$
\begin{aligned}
I_2 &= \int_{-h(x)}^{h(x)} \mathrm{e}^{-gy}\frac{\partial}{\partial x}\hat{\boldsymbol{\sigma}}_1(x, y, \partial_x)\,\mathrm{d}y \\
&= \{-\cosh[gh(x)]\,\coth[gh(x)] - 2\mathrm{csch}[gh(x)] \\
&\quad + 4g\,h(x)\coth[gh(x)]\,\mathrm{csch}[gh(x)]\}\int_{-h(x)}^{h(x)} \mathrm{e}^{-gy}\,\mathrm{d}y \\
&\quad + g\,\{\cosh[gh(x)]\,\coth[gh(x)] - \sinh[gh(x)]\}\int_{-h(x)}^{h(x)} y\,\mathrm{e}^{-gy}\,\mathrm{d}y \\
&\quad - \coth[gh(x)]\int_{-h(x)}^{h(x)}\mathrm{d}y \\
&= -\frac{2}{g}\cosh^2[gh(x)] - \frac{4}{g} + 8h(x)\,\coth[gh(x)] \\
&\quad + g\,\{\cosh[gh(x)]\,\coth[gh(x)] - \sinh[gh(x)]\} \\
&\qquad \times\left\{\frac{2}{g^2}\sinh[gh(x)] - \frac{2h(x)}{g}\cosh[gh(x)]\right\} \\
&= -\frac{2}{g}\cosh^2[gh(x)] - \frac{4}{g} + 8h(x)\,\coth[gh(x)] \\
&\quad - 2h(x)\,\coth[gh(x)] + \frac{2}{g}\cosh^2[gh(x)] \\
&\quad - 2h(x)\,\cosh[gh(x)]\,\coth[gh(x)] \\
&\quad - \frac{2}{g}\sinh^2[gh(x)] + 2h(x)\,\sinh[gh(x)]\,\cosh[gh(x)] \\
&= 6h(x)\,\coth[gh(x)] - \frac{4}{g} - \frac{2}{g}\sinh^2[gh(x)] \\
&\quad - 2h(x)\,\cosh^2[gh(x)]\,\coth[gh(x)] + 2h(x)\,\sinh[gh(x)]\,\cosh[gh(x)],
\end{aligned}
\tag{21.152}
$$

and by substituting $\mathtt{F}(x)$ into Eq. (21.24), we obtain

$$\begin{aligned}\hat{\boldsymbol{Z}}_1(x,\partial_x) &= -\frac{1}{\mathtt{F}(x)} I_2 \\ &= \frac{h'^2(x)}{\sinh^2[gh(x)]}\Big\{-3g\ h(x)\ \coth[gh(x)] + 2 + \sinh^2[gh(x)] \\ &\quad + gh(x)\ \cosh^2[gh(x)]\coth[gh(x)] - gh(x)\ \sinh[gh(x)]\ \cosh[gh(x)]\Big\} \\ &= \frac{h'^2(x)}{\sinh^2[gh(x)]}\Big\{-3g\ h(x)\ \coth[gh(x)] + 2 + \cosh^2[gh(x)] \\ &\quad - 1 + gh(x)\ \coth[gh(x)]\Big(1 + \sinh^2[gh(x)]\Big) \\ &\quad - gh(x)\ \sinh[gh(x)]\ \cosh[gh(x)]\Big\},\end{aligned} \tag{21.153}$$

finally leading to

$$\hat{\boldsymbol{Z}}_1(x,\partial_x) = \frac{h'^2(x)}{\sinh^2[gh(x)]}\Big\{1 + \cosh^2[gh(x)] - 2g\ h(x)\ \coth[gh(x)]\Big\}. \tag{21.64}$$

21.A.3 Derivation of Eq. (21.84)

We start by integrating Eq. (21.83) along the y direction, namely,

$$\begin{aligned}&\int \frac{\partial}{\partial y}\left[\mathrm{e}^{-gy}\frac{\partial}{\partial y}\hat{\boldsymbol{\sigma}}_1(x,y,\partial_x)\right]\mathrm{d}y \\ &= \int \frac{g\mathrm{e}^{-gy}}{\mathrm{e}^{-gh_1(x)} - \mathrm{e}^{-gh_2(x)}}\left[h_2'(x)\ \mathrm{e}^{-gh_2(x)} - h_1'(x)\ \mathrm{e}^{-gh_1(x)}\right]\frac{\partial}{\partial x}\ \mathrm{d}y,\end{aligned} \tag{21.154}$$

resulting in

$$\mathrm{e}^{-gy}\frac{\partial}{\partial y}\hat{\boldsymbol{\sigma}}_1(x,y,\partial_x) = \frac{h_1'(x)\ \mathrm{e}^{-gh_1(x)} - h_2'(x)\ \mathrm{e}^{-gh_2(x)}}{\mathrm{e}^{-gh_1(x)} - \mathrm{e}^{-gh_2(x)}}\mathrm{e}^{gy}\ \frac{\partial}{\partial x} + \hat{\boldsymbol{C}}_1, \tag{21.155}$$

where $\hat{\boldsymbol{C}}_1$ is a constant integration operator to be determined. We use Eq. (21.51) for the particular case when $n = 0$, yielding

$$\frac{\partial}{\partial y}\hat{\boldsymbol{\sigma}}_1(x,y,\partial_x)\Big|_{y=h_i(x)} = h_i'(x)\ \ \frac{\partial}{\partial x}\hat{\boldsymbol{\sigma}}_0(x,y,\partial_x)\Big|_{y=h_i(x)}, \tag{21.156}$$

and since $\hat{\boldsymbol{\sigma}}_0 = 1$, we obtain

$$h_i'(x)\left.\frac{\partial}{\partial x}\hat{\boldsymbol{\sigma}}_0(x, y, \partial_x)\right|_{y=h_i(x)} = h_i'(x) \Big/ \left.\frac{\partial}{\partial x}\right|_{y=h_i(x)}. \tag{21.157}$$

Now, we see that

$$h_i'(x)\frac{\partial}{\partial x} = \frac{h_1'(x)\,\mathrm{e}^{-gh_1(x)} - h_2'(x)\,\mathrm{e}^{-gh_2(x)}}{\mathrm{e}^{-gh_1(x)} - \mathrm{e}^{-gh_2(x)}}\frac{\partial}{\partial x} + \mathrm{e}^{gy}\,\hat{\boldsymbol{C}}_1\Big|_{y=h_i(x)}. \tag{21.158}$$

By choosing the upper boundary $y = h_2(x)$, the integration constant operator is obtained, that is,

$$\hat{\boldsymbol{C}}_1 = h_2'(x)\,\mathrm{e}^{-gh_2(x)}\frac{\partial}{\partial x} - \frac{h_1'(x)\,\mathrm{e}^{-gh_1(x)} - h_2'(x)\,\mathrm{e}^{-gh_2(x)}}{\mathrm{e}^{-gh_1(x)} - \mathrm{e}^{-gh_2(x)}}\,\mathrm{e}^{-gh_2(x)}\,\frac{\partial}{\partial x}, \tag{21.159}$$

from which, by substitution into Eq. (21.155), we obtain

$$\begin{aligned}\mathrm{e}^{-gy}\,\frac{\partial}{\partial y}\hat{\boldsymbol{\sigma}}_1(x, y, \partial_x) = {} & \frac{h_1'(x)\,\mathrm{e}^{-gh_1(x)} - h_2'(x)\,\mathrm{e}^{-gh_2(x)}}{\mathrm{e}^{-gh_1(x)} - \mathrm{e}^{-gh_2(x)}}\mathrm{e}^{gy}\,\frac{\partial}{\partial x} \\ & + h_2'(x)\,\mathrm{e}^{-gh_2(x)}\frac{\partial}{\partial x} \\ & - \frac{h_1'(x)\,\mathrm{e}^{-gh_1(x)} - h_2'(x)\,\mathrm{e}^{-gh_2(x)}}{\mathrm{e}^{-gh_1(x)} - \mathrm{e}^{-gh_2(x)}}\,\mathrm{e}^{-gh_2(x)}\,\frac{\partial}{\partial x}.\end{aligned} \tag{21.160}$$

Then, the integration yields

$$\begin{aligned}\hat{\boldsymbol{\sigma}}_1(x, y, \partial_x) = {} & \int\left\{\frac{h_1'(x)\,\mathrm{e}^{-gh_1(x)} - h_2'(x)\,\mathrm{e}^{-gh_2(x)}}{\mathrm{e}^{-gh_1(x)} - \mathrm{e}^{-gh_2(x)}} + h_2'(x)\,\mathrm{e}^{-gh_2(x)}\mathrm{e}^{gy}\right. \\ & \left. - \frac{h_1'(x)\,\mathrm{e}^{-gh_1(x)} - h_2'(x)\,\mathrm{e}^{-gh_2(x)}}{\mathrm{e}^{-gh_1(x)} - \mathrm{e}^{-gh_2(x)}}\mathrm{e}^{-gh_2(x)}\,\mathrm{e}^{gy}\right\}\frac{\partial}{\partial x}\partial y \\ = {} & \left\{y\,\frac{h_1'(x)\,\mathrm{e}^{-gh_1(x)} - h_2'(x)\,\mathrm{e}^{-gh_2(x)}}{\mathrm{e}^{-gh_1(x)} - \mathrm{e}^{-gh_2(x)}}\right. \\ & + h_2'(x)\,\mathrm{e}^{-gh_2(x)}\,\mathrm{e}^{gy}\,\frac{1}{g} \\ & \left. - \frac{h_1'(x)\,\mathrm{e}^{-gh_1(x)} - h_2'(x)\,\mathrm{e}^{-gh_2(x)}}{\mathrm{e}^{-gh_1(x)} - \mathrm{e}^{-gh_2(x)}}\,\mathrm{e}^{-gh_2(x)}\,\mathrm{e}^{gy}\,\frac{1}{g}\right\}\frac{\partial}{\partial x} \\ & + \hat{\boldsymbol{C}}_0.\end{aligned} \tag{21.161}$$

We integrate again to find that

$$\begin{aligned}
0 &= \int_{h_1(x)}^{h_2(x)} \mathrm{e}^{-gy}\, \hat{\boldsymbol{\sigma}}_1(x,t,\partial_x)\, \mathrm{d}y \\
&= \hat{\boldsymbol{C}}_0 \int_{h_1(x)}^{h_2(x)} \mathrm{e}^{-gy}\, \mathrm{d}y \\
&\quad - \frac{1}{g}\,[h_2(x) - h_1(x)] \left[h_2'(x)\, \mathrm{e}^{-gh_2(x)} \right. \\
&\quad \left. + \frac{h_1'(x)\, \mathrm{e}^{-gh_1(x)} - h_2'(x)\, \mathrm{e}^{-gh_2(x)}}{\mathrm{e}^{-gh_1(x)} - \mathrm{e}^{-gh_2(x)}}\, \mathrm{e}^{-gh_2(x)} \right] \frac{\partial}{\partial x} \\
&\quad + \frac{h_1'(x)\, \mathrm{e}^{-gh_1(x)} - h_2'(x)\, \mathrm{e}^{-gh_2(x)}}{\mathrm{e}^{-gh_1(x)} - \mathrm{e}^{-gh_2(x)}} \int_{h_1(x)}^{h_2(x)} y\, \mathrm{e}^{-gy}\, \mathrm{d}y\, \frac{\partial}{\partial x},
\end{aligned} \tag{21.162}$$

where we have used Eq. (21.141). After integrating, we find that

$$\begin{aligned}
0 &= \frac{1}{g} \left[\mathrm{e}^{-gh_1(x)} - \mathrm{e}^{-gh_2(x)} \right] \hat{\boldsymbol{C}}_0 + \frac{1}{g}\,[h_2(x) - h_1(x)] \left\{ h_2'(x)\, \mathrm{e}^{-gh_2(x)} \right. \\
&\quad \left. - \frac{h_1'(x)\, \mathrm{e}^{-gh_1(x)} - h_2'(x)\, \mathrm{e}^{-gh_2(x)}}{\mathrm{e}^{-gh_1(x)} - \mathrm{e}^{-gh_2(x)}}\, \mathrm{e}^{-gh_2(x)} \right\} \frac{\partial}{\partial x} \\
&\quad - \frac{h_1'(x)\, \mathrm{e}^{-gh_1(x)} - h_2'(x)\, \mathrm{e}^{-gh_2(x)}}{\mathrm{e}^{-gh_1(x)} - \mathrm{e}^{-gh_2(x)}} \left\{ \frac{1}{g} \left[h_2(x)\, \mathrm{e}^{-gh_2(x)} \right. \right. \\
&\quad \left. \left. - h_1(x)\, \mathrm{e}^{-gh_1(x)} \right] + \frac{1}{g^2} \left[\mathrm{e}^{-gh_2(x)} - \mathrm{e}^{-gh_1(x)} \right] \right\} \frac{\partial}{\partial x}.
\end{aligned} \tag{21.163}$$

Finally, solving for $\hat{\boldsymbol{C}}_0$ takes us to

$$\begin{aligned}
\hat{\boldsymbol{C}}_0 &= \frac{h_2(x) - h_1(x)}{\mathrm{e}^{-gh_2(x)} - \mathrm{e}^{-gh_1(x)}} \left[h_2'(x)\, \mathrm{e}^{-gh_2(x)} \right. \\
&\quad \left. + \frac{h_1'(x)\, \mathrm{e}^{-gh_1(x)} - h_2'(x)\, \mathrm{e}^{-gh_2(x)}}{\mathrm{e}^{-gh_1(x)} - \mathrm{e}^{-gh_2(x)}}\, \mathrm{e}^{-gh_2(x)} \right] \frac{\partial}{\partial x} \\
&\quad + \frac{h_1'(x)\, \mathrm{e}^{-gh_1(x)} - h_2'(x)\, \mathrm{e}^{-gh_2(x)}}{\left[\mathrm{e}^{-gh_1(x)} - \mathrm{e}^{-gh_2(x)} \right]^2} \left\{ h_2'(x)\, \mathrm{e}^{-gh_2(x)} \right. \\
&\quad \left. - h_1'(x)\, \mathrm{e}^{-gh_1(x)} + \frac{1}{g} \left[\mathrm{e}^{-gh_2(x)} - \mathrm{e}^{-gh_1(x)} \right] \right\} \frac{\partial}{\partial x},
\end{aligned} \tag{21.164}$$

which is substituted into Eq. (21.161), namely,

$$\begin{aligned}\hat{\boldsymbol{\sigma}}_1(x,y,\partial_x) = \Bigg\{ & y\,\frac{h_1'(x)\,\mathrm{e}^{-gh_1(x)} - h_2'(x)\,\mathrm{e}^{-gh_2(x)}}{\mathrm{e}^{-gh_1(x)} - \mathrm{e}^{-gh_2(x)}} + h_2'(x)\,\mathrm{e}^{-gh_2(x)}\,\mathrm{e}^{gy}\,\frac{1}{g} \\ & - \frac{h_1'(x)\,\mathrm{e}^{-gh_1(x)} - h_2'(x)\,\mathrm{e}^{-gh_2(x)}}{\mathrm{e}^{-gh_1(x)} - \mathrm{e}^{-gh_2(x)}}\mathrm{e}^{-gh_2(x)}\,\mathrm{e}^{gy}\,\frac{1}{g}\Bigg\}\,\frac{\partial}{\partial x} \\ & + \frac{h_2(x) - h_1(x)}{\mathrm{e}^{-gh_2(x)} - \mathrm{e}^{-gh_1(x)}}\Bigg[h_2'(x)\,\mathrm{e}^{-gh_2(x)} \\ & + \frac{h_1'(x)\,\mathrm{e}^{-gh_1(x)} - h_2'(x)\,\mathrm{e}^{-gh_2(x)}}{\mathrm{e}^{-gh_1(x)} - \mathrm{e}^{-gh_2(x)}}\,\mathrm{e}^{-gh_2(x)}\Bigg]\frac{\partial}{\partial x} \\ & + \frac{h_1'(x)\,\mathrm{e}^{-gh_1(x)} - h_2'(x)\,\mathrm{e}^{-gh_2(x)}}{\left[\mathrm{e}^{-gh_1(x)} - \mathrm{e}^{-gh_2(x)}\right]^2}\Bigg\{h_2'(x)\,\mathrm{e}^{-gh_2(x)} \\ & - h_1'(x)\,\mathrm{e}^{-gh_1(x)} + \frac{1}{g}\left[\mathrm{e}^{-gh_2(x)} - \mathrm{e}^{-gh_1(x)}\right]\Bigg\}\,\frac{\partial}{\partial x}. \end{aligned} \tag{21.84}$$

21.A.4 Derivation of Eq. (21.91)

We start by computing the derivative with respect to x of Eq. (21.90), namely,

$$\begin{aligned}\frac{\partial}{\partial x}\hat{\boldsymbol{\sigma}}_1(x,y,\partial_x) = & \; y\left\{y_0'' - \frac{1}{2}w''\coth\xi + \frac{1}{2}\xi' w'\mathrm{csch}^2\xi\right\} \\ & + \frac{1}{2g}\mathrm{e}^{+gy}\,\mathrm{e}^{-gy_+}\left\{w'' + w''\coth\xi - \xi' w'\mathrm{csch}^2\xi\right\} \\ & - \frac{1}{4}ww'\left\{-4\xi'\coth\xi\;\mathrm{csch}^2\xi\right\} \\ & - \frac{1}{4}\left\{2\coth^2\xi - 1\right\}\left\{ww'' + w'w'\right\} \\ & - y_0'\,y_0' - y_0\,y_0'' + \frac{1}{2g}w''\coth\xi - \frac{1}{2g}\xi' w'\mathrm{csch}^2\xi \\ & + \frac{1}{2}\left[w'y_0' + w''y_0\right]\coth\xi - \frac{1}{2}\xi' w'y_0\,\mathrm{csch}^2\xi \\ & + \frac{1}{2}\left[w'y_0' + wy_0''\right]\coth\xi - \frac{1}{2}\xi' wy_0'\mathrm{csch}^2\xi \\ & + \frac{1}{2g}\mathrm{e}^{+gy}\,\mathrm{e}^{-gy_+}\left[w' + w'\coth\xi\right]\left\{-g\left[y_0' + \frac{1}{2}w'\right]\right\} - \frac{1}{g}y_0'', \end{aligned} \tag{21.165}$$

where the value of Eq. (21.89) is used to obtain

$$\begin{aligned}
&\frac{\partial}{\partial x}\hat{\boldsymbol{\sigma}}_1(x, y, \partial_x) \\
&\quad = y\left\{y_0'' - \frac{1}{2}w''\coth\xi + \frac{1}{4}gw'w'\mathrm{csch}^2\xi\right\} \\
&\qquad + \frac{1}{2g}\mathrm{e}^{+gy}\mathrm{e}^{-gy_+}\left\{w'' + w''\coth\xi - \frac{1}{2}gw'w'\mathrm{csch}^2\xi\right. \\
&\qquad \left. - gw'y_0' - \frac{1}{2}gw'w' - gw'y_0'\coth\xi - \frac{1}{2}gw'w'\coth\xi\right\} \\
&\qquad + \frac{1}{2}gww'w'\coth\xi\ \mathrm{csch}^2\xi + \frac{1}{4}ww'' + \frac{1}{4}w'w' - \frac{1}{2}ww''\coth^2\xi \\
&\qquad - \frac{1}{2}w'w'\coth^2\xi - y_0'\,y_0' - y_0\,y_0'' + \frac{1}{2g}w''\coth\xi - \frac{1}{4}w'w'\mathrm{csch}^2\xi \\
&\qquad + w'y_0'\coth\xi + \frac{1}{2}w''y_0\coth\xi - \frac{1}{4}gw'w'y_0\mathrm{csch}^2\xi + \frac{1}{2}wy_0''\coth\xi \\
&\qquad - \frac{1}{4}gww'y_0'\mathrm{csch}^2\xi - \frac{1}{g}y_0''.
\end{aligned} \tag{21.166}$$

We proceed to compute

$$\frac{1}{\mathtt{F}(x)}\int_{y_-}^{y_+}\mathrm{e}^{-gy}\ \frac{\partial}{\partial x}\hat{\boldsymbol{\sigma}}_1(x, y, \partial_x)\,\mathrm{d}y, \tag{21.167}$$

which is a direct integral. A quick inspection shows that the following three integrals must be solved:

$$\int_{y_-}^{y_+}\mathrm{d}y = y_+ - y_- = w, \tag{21.168}$$

$$\int_{y_-}^{y_+}\mathrm{e}^{-gy}\,\mathrm{d}y = -\frac{1}{g}\left[\mathrm{e}^{-gy_+} - \mathrm{e}^{-gy_-}\right] = \frac{2}{g}\mathrm{e}^{-gy_0}\,\sinh\xi, \tag{21.169}$$

and

$$\int_{y_-}^{y_+} y\,\mathrm{e}^{-gy}\,\mathrm{d}y = \frac{1}{g}\mathrm{e}^{-gy_0}\left[2y_0\sinh\xi - w\cosh\xi\right] + \frac{2}{g^2}\,\mathrm{e}^{-gy_0}\,\sinh\xi. \tag{21.170}$$

Additionally, $1/\mathtt{F}(x)$ can be written using hyperbolic functions, i.e.,

$$\frac{1}{\mathrm{F}(x)} = \frac{1}{2} g \, \mathrm{e}^{+gy_0} \, \mathrm{csch}\xi. \tag{21.171}$$

Then, the integrals mentioned above become

$$\frac{1}{\mathrm{F}(x)} \int_{y_-}^{y_+} \mathrm{d}y = \frac{1}{2} g w \, \mathrm{e}^{+gy_0} \, \mathrm{csch}\xi, \tag{21.172}$$

$$\frac{1}{\mathrm{F}(x)} \int_{y_-}^{y_+} \mathrm{e}^{-gy} \, \mathrm{d}y = 1, \tag{21.173}$$

and

$$\frac{1}{\mathrm{F}(x)} \int_{y_-}^{y_+} y \, \mathrm{e}^{-gy} \, \mathrm{d}y = y_0 - \frac{1}{2} w \, \coth\xi + \frac{1}{g}, \tag{21.174}$$

respectively. The rest of the computation is rather tedious but straightforward, that is,

$$\begin{aligned}
&\frac{1}{\mathrm{F}(x)} \int_{y_-}^{y_+} \mathrm{e}^{-gy} \frac{\partial}{\partial x} \hat{\boldsymbol{\sigma}}_1(x, y, \partial_x) \, \mathrm{d}y \\
&\quad = \left\{ y_0 - \frac{1}{2} w \, \coth\xi + \frac{1}{g} \right\} \left\{ y_0'' - \frac{1}{2} w'' \coth\xi + \frac{1}{4} g w' w' \mathrm{csch}^2\xi \right\} \\
&\qquad + \frac{1}{4} \mathrm{e}^{-gy_+} \, \mathrm{e}^{+gy_0} \, w \mathrm{csch}\xi \left\{ w'' + w'' \coth\xi - \frac{1}{2} g w' w' \mathrm{csch}^2\xi - g w' y_0' \right. \\
&\qquad \left. - \frac{1}{2} g w' w' - g w' y_0' \coth\xi - \frac{1}{2} g w' w' \coth\xi \right\} \\
&\qquad + \frac{1}{2} g w w' w' \coth\xi \, \mathrm{csch}^2\xi \\
&\qquad + \frac{1}{4} w w'' + \frac{1}{4} w' w' - \frac{1}{2} w w'' \coth^2\xi - \frac{1}{2} w' w' \coth^2\xi - y_0' \, y_0' - y_0 \, y_0'' \\
&\qquad + \frac{1}{2g} w'' \coth\xi - \frac{1}{4} w' w' \mathrm{csch}^2\xi + w' y_0' \coth\xi + \frac{1}{2} w'' y_0 \coth\xi \\
&\qquad - \frac{1}{4} g w' w' y_0 \mathrm{csch}^2\xi + \frac{1}{2} w y_0'' \coth\xi - \frac{1}{4} g w w' y_0' \mathrm{csch}^2\xi - \frac{1}{g} y_0'' \\
&\quad = \frac{1}{4} g w w' w' \coth\xi \, \mathrm{csch}^2\xi + \frac{1}{4} g w w' y_0' - \frac{1}{4} g w w' y_0' \coth^2\xi \\
&\qquad + \frac{1}{4} w' w' - \frac{1}{2} w' w' \coth^2\xi - y_0' \, y_0' + w' \, y_0' \coth\xi - \frac{1}{4} g w w' y_0' \mathrm{csch}^2\xi,
\end{aligned} \tag{21.175}$$

where we can use ξ, given by Eq. (21.89), together with Eq. (21.35) for $k = 1$. Ultimately, we find that

$$\hat{\mathbf{Z}}_1(x, \partial_x)\, \partial_x = \frac{w'^2}{4\sinh^2\left[\frac{1}{2}gw\right]} \left\{1 + \cosh^2\left[\frac{1}{2}gw\right] - gw\, \coth\left[\frac{1}{2}gw\right]\right\} \frac{\partial}{\partial x} + y_0' \left\{y_0' - w' \coth\left[\frac{1}{2}gw\right] + \frac{1}{2}gww'\mathrm{csch}^2\left[\frac{1}{2}gw\right]\right\} \frac{\partial}{\partial x}. \tag{21.91}$$

Further Reading and References

P.S. Burada, G. Schmid, Steering the potential barriers: entropic to energetic. Phys. Rev. E **82**, 051128 (2010). https://journals.aps.org/pre/abstract/10.1103/PhysRevE.82.051128

P. Kalinay, Effective one-dimensional description of confined diffusion biased by a transverse gravitational force. Phys. Rev. E **84**, 011118 (2011). https://journals.aps.org/pre/abstract/10.1103/PhysRevE.84.011118

I. Pompa-García, L. Dagdug, Two-dimensional diffusion biased by a transverse gravitational force in an asymmetric channel: reduction to an effective one-dimensional description. Phys. Rev. E **104**, 044118 (2021). https://journals.aps.org/pre/abstract/10.1103/PhysRevE.104.044118

I. Pompa-García, R. Castilla, R. Metzler, L. Dagdug, First-passage times in conical varying-width channels biased by a transverse gravitational force: comparison of analytical and numerical results. Phys. Rev. E **106**, 064137 (2022). https://journals.aps.org/pre/abstract/10.1103/PhysRevE.106.064137

Chapter 22
Periodical Systems

Periodic channels are quite common in both natural and artificial systems. These systems have gained relevance due to the applications they have in a wide range of diffusion phenomena. Zeolites are an interesting example: They are solid nanoporous crystals with well-defined internal structures. They naturally occur as minerals, but they can also be artificially synthesized for specific uses. They contain internal cavities that join together to form chambers and channels. Zeolites facilitate the movement of both neutral and electrically charged particles into the structure. In addition, they can function as filters for particles that are larger in size than the length of the width of these channels. Thanks to these characteristics, zeolites can improve the efficiency of catalytic processes.

Nanopores are another example of systems that can be made up of periodic structures. They are highly confined structures with small openings. The shape of these structures plays an important role in the behavior of the stream of particles that translocate inside them. In some situations, they act as gates that regulate the transport of ions or molecules. Nanopores are found in nature connecting the inside and outside of cells through cell membranes. As mentioned in earlier chapters of this book, they also regulate ionic transport in cells in the presence of electrochemical gradients. Artificial nanopores are used today to characterize the behavior of molecules such as DNA and RNA.

This chapter is devoted to study the diffusion of Brownian particles through long, narrow, periodic channels or tubes. To such end, we have to simplify the effective diffusivity by means of the so-called Lifson-Jackson formula, which in fact, considerably simplifies the problem. This formula is an exact result for the one-dimensional Smoluchowski equation in the presence of a periodic potential and periodic diffusivity. For example, if the formula is applied to a periodic narrow channel, the effective diffusion coefficient is initially dependent on the position and later becomes independent and is reduced to the geometric parameters of the channel. Consequently, the effective diffusion coefficient becomes constant once the geometrical parameters, then, the system can be described by means of the

L. Dagdug et al., *Diffusion Under Confinement*,
https://doi.org/10.1007/978-3-031-46475-1_22

Fick-Jacobs equation, instead of the Fick-Jacobs-Zwanzig equation. We will also present the application of the formula for explicit periodic channels in two and three dimensions, as well as a system formed by cylindrical obstacles.

22.1 Lifson-Jackson Formula

In this section, we will obtain the Lifson-Jackson formula, which is an exact result for the one-dimensional Smoluchowski equation with periodic potential and diffusivity. Let us assume that we have a Brownian particle with initial position x_0, diffusing in a one-dimensional system in the presence of periodic potential and diffusivity of period L, where $U(x) = U(x + L) = U(x - L)$ and $D(x) = D(x + L) = D(x - L)$ (see Fig. 22.1).

The deduction presented here, which differs from the original one proposed by Shneior Lifson and Julius L. Jackson, is rigorous and much simpler. It arises from the observation that once the particle reaches a distance $x_0 + L$ or $x_0 - L$, it comes back to the same situation as when it started. Consequently, it is like considering the mean round-trip time (RT), $\langle t_{RT}(a, b)\rangle$, of a particle diffusing between two reflecting boundaries located at points $a = x_0 - L$ and $b = x_0 + L$. This mean time is the sum of the mean first-passage times (MFPT) between the two points, $\langle t(a \to b)\rangle$ and $\langle t(b \to a)\rangle$. Then, the Lifson-Jackson formula for the effective diffusivity is given by

$$D_{\text{eff}} = \frac{L^2}{\langle t_{RT}(a, b)\rangle}. \tag{22.1}$$

To find the mean RT, we first need to find $\langle t(a \to b)\rangle$ and $\langle t(b \to a)\rangle$. Because of its periodicity, the simplest way to perform this task is calculating the MFPT between a reflecting boundary at a and an absorbing boundary at b and vice versa. These quantities can be obtained by solving Eq. (6.38):

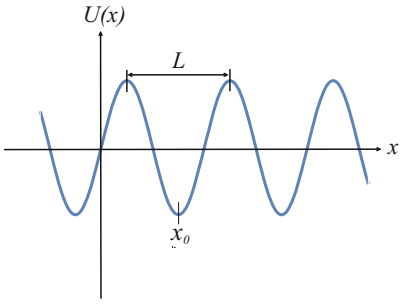

Fig. 22.1 Depiction of the periodic potential $U(x)$ as a function of x, with period L

$$\frac{\mathrm{d}}{\mathrm{d}x_0}\left[D(x_0)\mathrm{e}^{-\beta U(x_0)}\frac{\mathrm{d}}{\mathrm{d}x_0}\langle t(x_0)\rangle\right] = -\mathrm{e}^{-\beta U(x_0)}. \tag{6.38}$$

To such end, we will solve this ordinary differential equation in quadratures.[1] Then, we will apply the boundary conditions to our specific transitions.

After integrating Eq. (6.38) once from a to x_0, we have

$$D(x_0)\,\mathrm{e}^{-\beta U(x_0)}\frac{\mathrm{d}}{\mathrm{d}x_0}\langle t(x_0)\rangle = \mathcal{A} - \int_a^{x_0}\mathrm{e}^{-\beta U(x')}\,\mathrm{d}x'. \tag{22.2}$$

Now, integrating again, the general solution to Eq. (6.38) is

$$\langle t(x_0)\rangle = \mathcal{B} + \mathcal{A}\int_a^{x_0}\frac{\mathrm{e}^{\beta U(x'')}}{D(x'')}\,\mathrm{d}x'' - \int_a^{x_0}\frac{\mathrm{e}^{\beta U(x'')}}{D(x'')}\left(\int_a^{x''}\mathrm{e}^{-\beta U(x')}\,\mathrm{d}x'\right)\mathrm{d}x''. \tag{22.3}$$

This last formula is the general solution of differential equation (6.38) in close quadratures.

The next step is to introduce the boundary conditions to find the transitions. We start by calculating $\langle t(a \to b)\rangle$, for which we need to impose a reflecting boundary at a and an absorbing boundary at b. From the first boundary, we find that $\mathcal{A} = 0$, and from the absorbing boundary, we find that

$$\mathcal{B} = \int_a^{b}\frac{\mathrm{e}^{\beta U(x'')}}{D(x'')}\left(\int_a^{x''}\mathrm{e}^{-\beta U(x')}\,\mathrm{d}x'\right)\mathrm{d}x''. \tag{22.4}$$

Introducing the found values of $\mathcal{A}$ and $\mathcal{B}$ into Eq. (22.3) yields

$$\begin{aligned}\langle t(x_0)\rangle = &\int_a^{b}\frac{\mathrm{e}^{\beta U(x'')}}{D(x'')}\left(\int_a^{x''}\mathrm{e}^{-\beta U(x')}\,\mathrm{d}x'\right)\mathrm{d}x'' \\ &- \int_a^{x_0}\frac{\mathrm{e}^{\beta U(x'')}}{D(x'')}\left(\int_a^{x''}\mathrm{e}^{-\beta U(x')}\,\mathrm{d}x'\right)\mathrm{d}x''.\end{aligned} \tag{22.5}$$

Finally, setting $x_0 = a$, we can write

$$\langle t(a \to b)\rangle = \int_a^{b}\frac{\mathrm{e}^{\beta U(x'')}}{D(x'')}\left(\int_a^{x''}\mathrm{e}^{-\beta U(x')}\,\mathrm{d}x'\right)\mathrm{d}x''. \tag{22.6}$$

[1] This method is presented in Appendix A.12.

Now, in order to calculate $\langle t(a \to b)\rangle$, we need to integrate Eq. (6.38) from x to b and apply the boundary conditions, namely, a reflecting boundary at $x = b$ and an absorbing boundary at $x = a$. Then, after setting $x_0 = b$, the final result is

$$\langle t(b \to a)\rangle = \int_a^b \frac{\mathrm{e}^{\beta U(x'')}}{D(x'')} \left(\int_{x''}^b \mathrm{e}^{-\beta U(x')}\, \mathrm{d}x' \right) \mathrm{d}x''. \tag{22.7}$$

By adding Eqs. (22.6) and (22.7), we find that the mean round-trip time is

$$\begin{aligned} \langle t_{RT}(a,b)\rangle = &\int_a^b \frac{\mathrm{e}^{\beta U(x'')}}{D(x'')} \left(\int_a^{x''} \mathrm{e}^{-\beta U(x')}\, \mathrm{d}x' \right) \mathrm{d}x'' \\ &+ \int_a^b \frac{\mathrm{e}^{\beta U(x'')}}{D(x'')} \left(\int_{x''}^b \mathrm{e}^{-\beta U(x')}\, \mathrm{d}x' \right) \mathrm{d}x''. \end{aligned} \tag{22.8}$$

Now, to simplify this last expression, we need to define the antiderivative of the argument of the integral as

$$F(x) \equiv \int \mathrm{e}^{-\beta U(x)}\, \mathrm{d}x. \tag{22.9}$$

Consequently, by means of the fundamental theorem of calculus, we see that

$$\begin{aligned} \langle t_{RT}(a,b)\rangle = &\int_a^b \frac{\mathrm{e}^{\beta U(x'')}}{D(x'')}\, \mathrm{d}x'' \left[F(x'') - F(a)\right] \\ &+ \int_a^b \frac{\mathrm{e}^{\beta U(x'')}}{D(x'')}\, \mathrm{d}x'' \left[F(b) - F(x'')\right], \end{aligned} \tag{22.10}$$

which ultimately simplifies to

$$\begin{aligned} \langle t_{RT}(a,b)\rangle &= [F(b) - F(a)] \int_a^b \frac{\mathrm{e}^{\beta U(x'')}}{D(x'')}\, \mathrm{d}x'' \\ &= \int_a^b \mathrm{e}^{\beta U(x')}\, \mathrm{d}x' \int_a^b \frac{\mathrm{e}^{\beta U(x'')}}{D(x'')}\, \mathrm{d}x''. \end{aligned} \tag{22.11}$$

Setting $a = x_0$ and $b = x_0 + L$ in this last expression and substituting the result into Eq. (22.1), we finally arrive at the so-called Lifson-Jackson formula:

$$D_{\mathrm{eff}} = \frac{L^2}{\int_{x_0}^{x_0+L} e^{-\beta U(x)}\, \mathrm{d}x \int_{x_0}^{x_0+L} \frac{e^{\beta U(x)}}{D(x)}\, \mathrm{d}x}. \tag{22.12}$$

This equation can be rewritten in a more simplified form by defining

$$\langle f(x)\rangle \equiv \frac{1}{L}\int_{x_0}^{x_0+L} f(x)\,\mathrm{d}x, \tag{22.13}$$

where the angular brackets denote averaging over the period, as

$$D_{\mathrm{eff}} = \frac{1}{\left\langle e^{-\beta U(x)}\right\rangle\left\langle \frac{e^{\beta U(x)}}{D(x)}\right\rangle}. \tag{22.14}$$

In the following section, we will provide some specific examples of the Lifson-Jackson formula applying it to calculate the effective diffusivity of narrow two-dimensional channels and three-dimensional tubes and for diffusion in the presence of obstacles.

22.2 Diffusion into a Periodic Tube Formed by Contacting Spheres

In this section, we will focus on calculating the effective diffusivity in a tube formed by periodic contacting spherical cavities of radius R (see Fig. 22.2), over the entire range of the entropy barrier height, namely, for the whole circular aperture connecting neighboring cavities, a, from 0 to R. To establish the range of applicability of the theoretical predictions, they will be compared to the results obtained by Brownian dynamics simulations.

It is worth noting that when the mean squared displacement of a diffusing particle is much greater than the tube period L, the particle motion can be characterized by an effective diffusivity constant D_{eff}. This D_{eff} is smaller than the particle diffusion D_0, i.e., the diffusivity with no geometrical constraints. Then, we can approximately describe diffusion in a two-dimensional channel or three-dimensional tube of varying width, as one-dimensional diffusion along the channel axis in the presence of entropy potential using the generalized Fick-Jacobs (FJ) equation, Eq. (22.14). This one-dimensional description allows us to find D_{eff} by means of the Lifson-Jackson (LJ) formula. Then, our first task for finding the effective diffusivity of a periodical tube will be to find the entropic potential.

In general, since the entropic potential is given by the logarithm of the area, namely, $U(x) = -k_B T \ln[A(x)/A(0)]$, where $A(0)$ is a constant, then the LJ formula, Eq. (22.14), for narrow tubes or channels is

$$D_{\mathrm{eff}} = \frac{1}{\left\langle \frac{A(x)}{A(0)}\right\rangle\left\langle \frac{1}{D(x)\frac{A(x)}{A(0)}}\right\rangle} = \frac{1}{\left\langle A(x)\right\rangle\left\langle \frac{1}{D(x)A(x)}\right\rangle}. \tag{22.15}$$

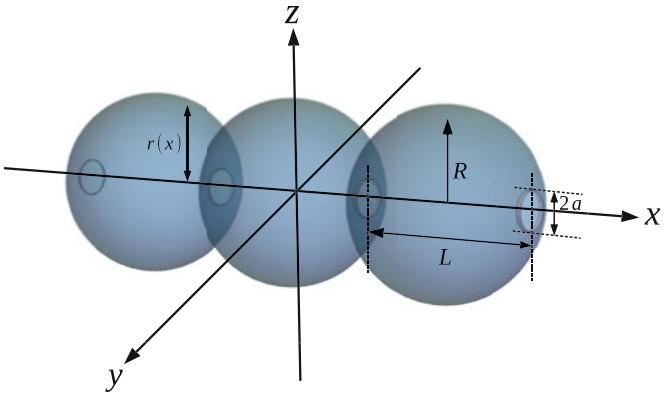

Fig. 22.2 Schematic representation of a periodic sphere with period L, with its height given by $r(x) = \sqrt{R^2 - x^2}$. The radius a of the circular aperture is given by $a = \sqrt{R^2 - (L^2/4)}$. Consequently, if the tube period increases, the circular aperture decreases and vice versa

From this last result, we can conclude that the calculation of D_{eff} reduces averaging of $\left\langle w(x) \right\rangle$ and $\left\langle 1/(D(x)\, w(x)) \right\rangle$. As we can see, the approximation for the position-dependent diffusion coefficient is expressed explicitly in the second integral.

For our specific tube formed by overlapping spheres, the cross-sectional area is given by $A(x) = \pi r(x)^2$, where $r(x) = \sqrt{R^2 - x^2}$ is the height of the sphere. Although this is all the information we need to find the effective diffusivity, it is a good idea to pause for a bit to explicitly calculate the entropic potential and describe its main characteristics. Explicitly, the entropy potential defined by $U(x) = -k_B T \ln A(x)/A(x = 0)$, setting $A(x = 0) = \pi R^2$, is given by

$$U(x) = -k_B T \ln \frac{\pi (R^2 - x^2)}{\pi R^2}. \tag{22.16}$$

We observe that when the tube period increases, the radius a of the circular aperture connecting neighboring cavities decreases as $a = \sqrt{R^2 + (L^2/4)}$, where L is within the domain $[0, 2R]$. As a result, the entropy barrier increases and the ratio D_{eff}/D_0 decreases. Potentials $U(x)$ with high and low entropy barriers are shown in Fig. 22.3.

Now, let's obtain two approximations for the LJ formula: one with a position-independent diffusion coefficient, $D(x) = D_0$, otherwise known as the Fick-Jacobs approximation, and another where the effective diffusivity is approximated by the Reguera-Rubi or Kalinay-Percus formula, Eq. (20.118), namely,

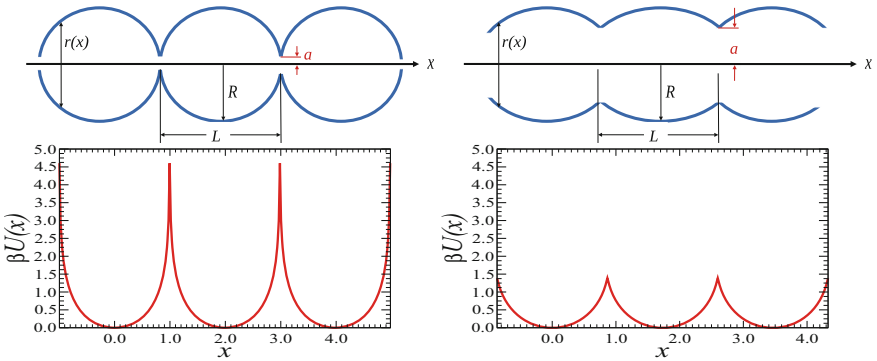

Fig. 22.3 Entropy potential for tubes with $(a/R) = 0.1$ (left panel) and $(a/R) = 0.5$ (right panel). The dimensionless maximum heights of the entropy barriers are $\Delta U/(k_B T) = 2\ln 10 = 4.6051$ (left panel) and $\Delta U/(k_B T) = 2\ln 2 = 1.3862$ (right panel)

$$D(x) \approx D_{\mathrm{RR}} = \frac{D_0}{\sqrt{1 + r'(x)^2}} = \frac{\sqrt{R^2 - x^2}}{R} D_0. \tag{22.17}$$

Consequently, we need to know the channel width, its derivative, and the approximated position-dependent diffusivity, in order to substitute them into the Lifson-Jackson equation, Eq. (22.26). In the first case, when $D(x) = D_0$, we have to calculate the following two integrals:

$$\begin{aligned} \Big\langle A(x) \Big\rangle &= \frac{1}{L} \int_{-L/2}^{L/2} A(x)\, \mathrm{d}x = \frac{1}{L} \int_{-L/2}^{L/2} \pi (R^2 - x^2)\, \mathrm{d}x \\ &= \pi \left(R^2 - \frac{L^2}{12} \right), \end{aligned} \tag{22.18}$$

and

$$\begin{aligned} \left\langle \frac{1}{D_0\, A(x)} \right\rangle &= \frac{1}{D_0\, L} \int_{-L/2}^{L/2} \frac{\mathrm{d}x}{A(x)} = \frac{1}{L D_0} \int_{-L/2}^{L/2} \frac{\mathrm{d}x}{\pi (R^2 - x^2)} \\ &= \frac{2}{\pi L R} \coth^{-1} \left(\frac{2R}{L} \right) = \frac{1}{\pi L R} \left[\ln \left(\frac{L}{2R} + 1 \right) - \ln \left(1 - \frac{L}{2R} \right) \right]. \end{aligned} \tag{22.19}$$

Substituting $L = 2\sqrt{R^2 - a^2}$ into Eqs. (22.18) and (22.18), and the resulting expressions into Eq. (22.15), yields

$$D_{\mathrm{eff}}^{\mathrm{FJ}} = \frac{6\sqrt{1 - (a/R)^2}}{2 + (a/R)^2} \ln \left[\frac{1 - \sqrt{1 - (a/R)^2}}{1 + \sqrt{1 - (a/R)^2}} \right] D_0. \tag{22.20}$$

Now, let's calculate the effective diffusivity by means of the RR approximation for the position-dependent diffusivity. In this case, $\langle w(x)\rangle$ is the same as the one we already calculated and is given by Eq. (22.18). On the other hand, to calculate $\langle 1/(D(x)\,w(x))\rangle$, we need to introduce Eq. (22.17) into this last average, which gives

$$\left\langle \frac{1}{D(x)\,A(x)} \right\rangle = \frac{1}{L}\int_{-L/2}^{L/2} \frac{\mathrm{d}x}{D(x)\,A(x)} = \frac{1}{LD_0}\int_{-L/2}^{L/2} \frac{\mathrm{d}x}{\frac{\sqrt{R^2-x^2}}{R}\,\pi(R^2-x^2)}$$
$$= \frac{R}{\pi L D_0}\int_{-L/2}^{L/2} \frac{\mathrm{d}x}{(R^2-x^2)^{\frac{3}{2}}} = \frac{2}{\pi D_0 R\sqrt{4R^2-L^2}}. \tag{22.21}$$

Since $L = 2\sqrt{R^2-a^2}$, substituting Eqs. (22.18) and (22.21) into Eq. (22.15), leads to

$$D_{\mathrm{eff}}^{\mathrm{RR}} = \frac{3(a/R)}{2+(a/R)^2} D_0. \tag{22.22}$$

Figure 22.4 shows that the results obtained by Brownian dynamics simulations is in good agreement with $D_{\mathrm{eff}}^{\mathrm{FJ}}$ for $a/R > 0.8$. On the other hand, $D_{\mathrm{eff}}^{\mathrm{RR}}$ provides a reasonably good approximation for D_{eff} over the entire size range of the aperture. From these results it becomes clear that we need to introduce the diffusivity's dependence on position to obtain a better description.

Looking to get a better approximation of the effective diffusivity over the entire range of the tube period, an empirical formula for periodic systems was proposed in 2016 by R. Verdel *et al*. To such end, they introduced a dimensionless parameter, γ, given by

$$\gamma = \frac{L/a}{1+(L/a)} = \frac{L}{a+L}, \tag{22.23}$$

which increases from zero to unity as the period increases from zero to infinity. They used this parameter to define the effective diffusivity as

$$D_{\mathrm{eff}}^{\gamma} = D_0 - \gamma(D_0 - D_{\mathrm{eff}}^{\mathrm{LJ}}), \tag{22.24}$$

where $D_{\mathrm{eff}}^{\mathrm{LJ}}$ is the approximated formula obtained by the LJ formula. We can see that Eq. (22.24) decreases from D_0 to D^{LJ} as γ goes from zero to unity. Replacing $D_{\mathrm{eff}}^{\mathrm{LJ}} = D_{\mathrm{eff}}^{\mathrm{RR}}$, given by Eq. (22.22), in Eq. (22.23), the formula obtained is in perfect agreement with the results from simulations, as shown in Fig. 22.4.

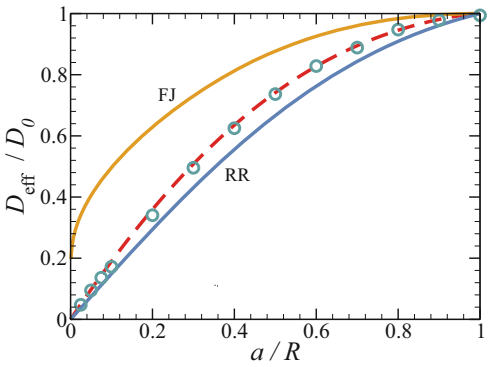

Fig. 22.4 Effective diffusion constants found by Brownian dynamics simulations (open circles) and predicted by Eqs. (22.20), (22.22) (solid curves), and (22.24) (dashed line). Effective diffusivity was determined through simulations for the long-time behavior of $\langle \Delta x^2(t) \rangle$, setting $D_0 = 1$

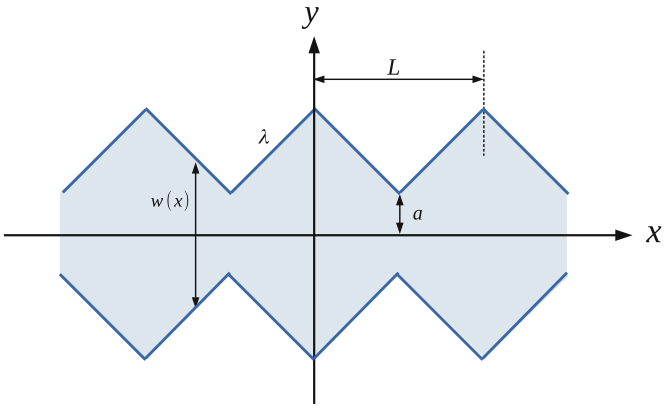

Fig. 22.5 Schematic representation of a linearly corrugated two-dimensional channel of period L, minimum half-width a, wall slope λ, and position-dependent width $w(x)$

22.3 Diffusion in a Periodic Channel with Corrugated Walls

In this section, we calculate the effective diffusivity for a two-dimensional periodic channel with linearly corrugated walls shown in Fig. 22.5. The coordinate system is chosen in a way that its x-axis coincides with the channel centerline. The channel width is a periodic function of x given by

$$\frac{w(x)}{2} = a + \lambda(L/2) - |x|, \tag{22.25}$$

where $|x| \leq L/2$, a and L are the minimum half-width of the channel and its period, respectively, and λ is one half of the absolute value of the width variation rate.

One can approximately describe the diffusion into this channel of varying width as one-dimensional diffusion along the channel axis in the presence of entropy potential. Then, to calculate the effective diffusivity of this channel, we will apply the techniques outlined in Sect. 22.2. Then, for a two-dimensional channel, since

the entropic potential is given by the logarithm of the width, namely, $U(x) = -k_B T \ln[w(x)/w(0)]$, where $w(0)$ is a constant, the Lifson-Jackson equation, Eq. (22.15), becomes

$$D_{\text{eff}} = \frac{1}{\left\langle \frac{w(x)}{w(0)} \right\rangle \left\langle \frac{1}{D(x)\frac{w(x)}{w(0)}} \right\rangle} = \frac{1}{\left\langle w(x) \right\rangle \left\langle \frac{1}{D(x)w(x)} \right\rangle}. \tag{22.26}$$

Then, to calculate the integrals involved in the processes, we need to know the channel width, given by Eq. (22.25), its derivative, and the position-dependent diffusivity. By substituting Eq. (22.25) into the Kalinay-Percus formula, Eq. (20.118), we are led to

$$D(x) \approx \frac{\arctan\left[w'(x)/2\right]}{w'(x)/2} D_0 = \frac{\arctan \lambda}{\lambda} D_0 = D_\lambda. \tag{22.27}$$

Now, we have the information needed to perform the averaging of $\langle w(x) \rangle$ and $\langle 1/(D(x)\, w(x)) \rangle$; hence,

$$\begin{aligned} \left\langle w(x) \right\rangle &= \frac{1}{L} \int_0^L w(x)\, \mathrm{d}x = \frac{1}{L} \int_0^L 2\left[a + \lambda(L/2) - |x|\right] \mathrm{d}x \\ &= 2a + (\lambda - 1)L, \end{aligned} \tag{22.28}$$

and

$$\begin{aligned} \left\langle \frac{1}{D_0\, w(x)} \right\rangle &= \frac{1}{D_\lambda\, L} \int_0^L \frac{\mathrm{d}x}{w(x)} = \frac{1}{L D_\lambda} \int_0^L \frac{\mathrm{d}x}{2\left[a + \lambda(L/2) - |x|\right]} \\ &= \frac{2}{L\, D_\lambda} \left[\ln(2a + \lambda L) - \ln\left[2a + (\lambda - 2)L\right]\right]. \end{aligned} \tag{22.29}$$

Substituting these last equations and Eq. (22.27) into Eq. (22.15), we arrive at

$$D_{\text{eff}}^{\lambda} = \frac{\lambda L/(2a)}{\left[1 + \lambda L/(4a)\right] \ln[1 + \lambda L/(2a)]} \frac{\arctan \lambda}{\lambda} D_0. \tag{22.30}$$

To test the accuracy of this approximate theoretical expression for effective diffusivity and to establish the range of its applicability as a function of the channel period L, we compare it to the values obtained from Brownian dynamics simulations (see Fig. 22.6). The solid curves show the L-dependences of the effective diffusivity and the symbols give the values of D_{eff}/D_0 obtained from simulations, for $\lambda = 0.5$. Comparison shows that the accuracy of the theoretical predictions increases with the channel period and that the theory fails to predict the behavior of the effective diffusivity as $L \to 0$, as if the particles were diffusing in a channel with

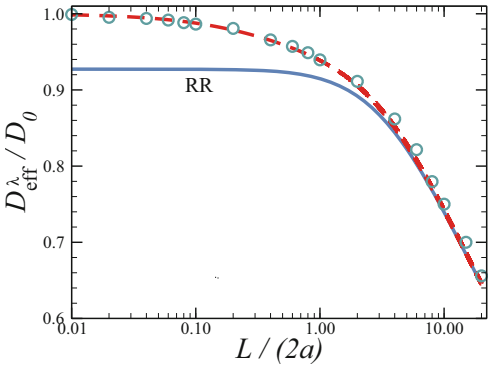

Fig. 22.6 Effective diffusivity normalized to D_0, as a function of the L/a ratio for $\lambda = 0.5$. The solid curve is the theoretically predicted dependence drawn by Eq. (22.30). Symbols are the normalized values of the effective diffusivity obtained from Brownian dynamics simulations. Dashed curve is drawn using Eq. (22.24)

practically flat walls. The reason why the theory fails is because the one-dimensional description in terms of the modified Fick-Jacobs equation is not applicable in this limiting case. To construct an expression that describes the effective diffusivity over the entire range of the channel period, including small L, we can use Eq. (22.24) again.

22.4 Diffusion in the Presence of Cylindrical Obstacles

As discussed in the two preceding sections, the generalized Fick-Jacobs equation is widely used to study diffusion of Brownian particles in three-dimensional tubes and quasi-two-dimensional channels of varying constrained geometry. In this section, we show how this equation can be applied to studying the slowdown of unconstrained diffusion in the presence of obstacles. Particularly, we will study diffusion in the presence of identical cylindrical obstacles arranged in a square lattice. To such end, we consider an equivalent problem of diffusion on a plane containing disks arranged in a square lattice, as shown in Fig. 22.7. A distinctive feature of this geometry is that D_{eff} is identical to the effective diffusion coefficient of the particle in a corresponding two-dimensional channel, two examples of which are shown in Fig. 22.7. Again, one can approximately describe diffusion in this channel of varying width as one-dimensional diffusion along the channel axis in the presence of entropy potential.

Now, following the techniques outlined in Sect. 22.2, we need to know the channel width and its derivative, as well as the position-dependent diffusivity, and substitute them into the Lifson-Jackson equation, Eq. (22.15). From the upper right panel of Fig. 22.7, we can see that because of the symmetry along the channel axis, we only need to take half of the channel to perform the integrals into the LJ formula. In such a case, the channel's width is given by

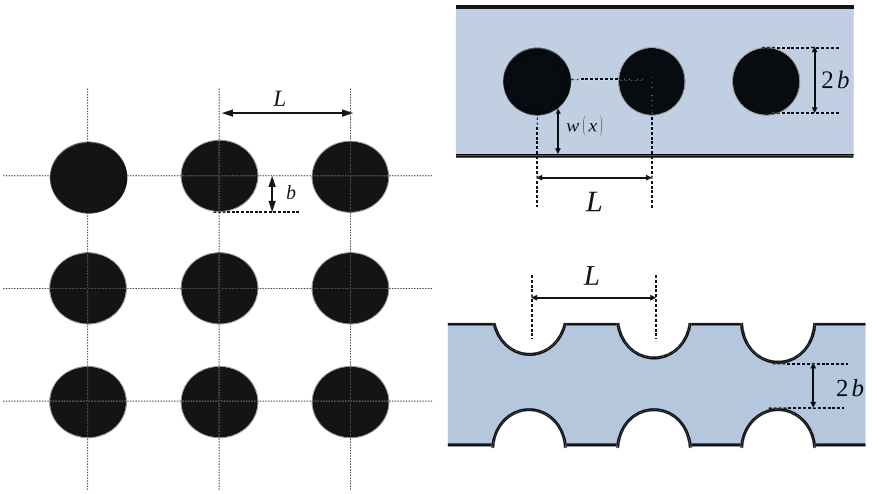

Fig. 22.7 Schematic diagram of a square lattice of perfectly reflecting circular disks (left panel) representing cylindrical obstacles and equivalent two-dimensional channels (right panel)

$$w(x) = \begin{cases} L - 2\sqrt{b^2 - x^2}, & 0 < x < b \\ \\ L, & b < x < L/2 \end{cases} . \tag{22.31}$$

which in compact form can be written as $w(x) = L - 2\sqrt{b^2 - x^2}H(b - |x|)$ for $0 \leq |x| \leq L/2$. The x-coordinate originates at the center of one of the disks and $H(z)$ is the Heaviside step function. Then, $w'(x)$ is given by

$$w'(x) = \begin{cases} \dfrac{2x}{\sqrt{b^2 - x^2}}, & 0 < x < b \\ \\ 0, & b < x < L/2 \end{cases} . \tag{22.32}$$

Now, we will approximate the effective diffusivity by means of the position-dependent diffusivity given by three approximations. In the first case, we will assume $D(x) = D_0$, which is known as the Fick-Jacobs approximation. Then, we will take a couple of position-dependent approximation by means of the Reguera-Rubi and Kalinay-Percus approaches. For the first case, from Eq. (22.26), we need to calculate the following two integrals:

$$\left\langle w(x)\right\rangle = \frac{2}{L}\int_0^{L/2} w(x)\,\mathrm{d}x = \frac{2}{L}\left[\int_0^b (L - 2\sqrt{b^2 - x^2})\mathrm{d}x + \int_b^{L/2} L\,\mathrm{d}x\right]$$
$$= L\left(1 - \frac{\pi b^2}{L^2}\right), \tag{22.33}$$

$$\left\langle \frac{1}{D_0\, w(x)}\right\rangle = \frac{2}{D_0\, L}\int_0^{L/2} \frac{\mathrm{d}x}{w(x)} = \frac{2}{LD_0}\left[\int_0^b \frac{\mathrm{d}x}{L - 2\sqrt{b^2 - x^2}} + \int_b^{L/2} \frac{\mathrm{d}x}{L}\right]$$
$$= \frac{2}{LD_0}\left[\int_0^b \frac{\mathrm{d}x}{L - 2\sqrt{b^2 - x^2}} + \frac{1}{L}\left(\frac{L}{2} - b\right)\right]. \tag{22.34}$$

Now, we will focus on calculating the first integral in Eq. (22.34), but first, we need to make a couple of transformations to solve it. By introducing the change of variable $y = x/b$, this integral becomes

$$\int_0^b \frac{\mathrm{d}x}{L - 2\sqrt{b^2 - x^2}} = \frac{1}{2}\int_0^1 \frac{\mathrm{d}y}{\frac{L}{2b} - \sqrt{1 - y^2}}. \tag{22.35}$$

Furthermore, by introducing a second change of variable, $y = \sin\varphi$, where $dy = \cos\varphi\, d\varphi$, it transforms into

$$\frac{1}{2}\int_0^{\pi/2} \frac{\mathrm{d}\varphi}{\frac{L}{2b} - \cos\varphi}. \tag{22.36}$$

After some algebraic manipulations, we can write this integral as

$$\frac{1}{2}\int_0^{\pi/2}\left(\frac{1}{1 - \frac{2b}{L}\cos\varphi} - 1\right)\mathrm{d}\varphi = \frac{1}{2}\int_0^{\pi/2}\left(\frac{\mathrm{d}\varphi}{1 - \frac{2b}{L}\cos\varphi}\right) - \frac{\pi}{4}. \tag{22.37}$$

The remaining integral can be found in tables,[2] and after a bit of algebra, one finds that

$$\left\langle \frac{1}{w(x)}\right\rangle = \frac{1}{L}\left[\frac{2}{\sqrt{1 - \left(\frac{2b}{L}\right)^2}}\arctan\left(\sqrt{\frac{1 + \frac{2b}{L}}{1 - \frac{2b}{L}}}\right) - \frac{\pi}{2} + 1 - \frac{2b}{L}\right]. \tag{22.38}$$

[2] $\int_0^{\pi/2} \frac{\mathrm{d}\varphi}{1 - A\cos\varphi} = \frac{2}{\sqrt{1 - A^2}}\arctan\left(\sqrt{\frac{1 + A}{1 - A}}\right)$.

Direct substitution of Eqs. (22.33) and (22.38) into Eq. (22.26) yields

$$D_{\text{eff}}^{\text{FJ}} = \frac{D_0}{\left(1 - \frac{\pi}{4}\nu^2\right)\left[\frac{2}{\sqrt{1-\nu^2}}\arctan\left(\sqrt{\frac{1+\nu}{1-\nu}}\right) - \frac{\pi}{2} + 1 - \nu\right]}, \tag{22.39}$$

where $\nu = 2b/L$.

Now, let us calculate the effective diffusivity by means of the RR approximation for the position-dependent diffusivity given by

$$D(x) \approx \begin{cases} \dfrac{D_0}{\left(1 + \frac{1}{4}w'^2(x)\right)^{1/3}}, & 0 < x < b \\ D_0, & b < x < L/2 \end{cases}. \tag{22.40}$$

By substituting the explicit values of the derivative of width, given by Eq. (22.32), we have

$$D_{\text{RR}}(x) = \begin{cases} \dfrac{D_0}{\left(\frac{b^2}{b^2-x^2}\right)^{1/3}}, & 0 < x < b \\ 0, & b < x < L/2 \end{cases}. \tag{22.41}$$

In this case, $\langle w(x)\rangle$ is the same as the one we already calculated and is given by Eq. (22.33). On the other hand, to calculate $\langle 1/(D(x)\,w(x))\rangle$, we need to substitute Eqs. (22.32), (22.40), and (22.41) into it, yielding

$$\begin{aligned} \left\langle \frac{1}{D(x)\,w(x)} \right\rangle &= \frac{2}{L}\int_0^{L/2} \frac{\mathrm{d}x}{D_{\text{RR}}(x)\,w(x)} \\ &= \frac{2}{L}\left[\int_0^b \frac{\mathrm{d}x}{D_{\text{RR}}(x)\,w(x)} + \int_b^{L/2} \frac{\mathrm{d}x}{D_0\,w(x)}\right] \\ &= \frac{2}{L}\left[\int_0^b \frac{\left(\frac{b^2}{b^2-x^2}\right)^{1/3}}{D_0\,(L - 2\sqrt{b^2-x^2})}\mathrm{d}x + \int_b^{L/2} \frac{\mathrm{d}x}{D_0\,L}\right] \\ &= \frac{2}{L\,D_0}\left[b^{2/3}\int_0^b \frac{\mathrm{d}x}{(b^2-x^2)^{1/3}(L - 2\sqrt{b^2-x^2})} + \frac{1}{2}\left(1 - \frac{2b}{L}\right)\right]. \end{aligned} \tag{22.42}$$

Now, let's calculate the remaining integral. To such end, we introduce the following two changes of variable: first $y = x/b$ and then $y = \sin(\varphi)$, as we did previously, so that

$$b^{\frac{2}{3}}\int_0^b \frac{\mathrm{d}x}{(b^2-x^2)^{1/3}(L-2\sqrt{b^2-x^2})} = \frac{1}{2}\int_0^1 \frac{\mathrm{d}y}{(1-y^2)^{1/3}\left(\frac{L}{2b}-\sqrt{1-y^2}\right)}$$
$$= \frac{b}{L}\int_0^{\frac{\pi}{2}} \frac{\cos\varphi\,\mathrm{d}\varphi}{(\cos\varphi)^{\frac{1}{3}}\left(1-\frac{2b}{L}\cos\varphi\right)}. \tag{22.43}$$

This last integral must be solved numerically. Finally, after some algebra and by substituting Eq. (22.43) into Eq. (22.42), we have

$$D_{\mathrm{eff}}^{\mathrm{RR}} = \frac{D_0}{\left(1-\frac{\pi}{4}\nu^2\right)\left[\nu\int_0^{\pi/2}\frac{(\cos\varphi)^{1/3}\,\mathrm{d}\varphi}{(1-\nu\cos\varphi)}+1-\nu\right]}, \tag{22.44}$$

where $\nu = 2b/L$.

Finally, let's proceed to calculate the KP approach. Substituting Eq. (22.32) into the KP approximation

$$D(x) \approx \begin{cases} \dfrac{\arctan\left(\frac{w'^2(x)}{2}\right)}{\frac{w'^2(x)}{2}} D_0, & 0 < x < b \\ D_0, & b < x < L/2 \end{cases}, \tag{22.45}$$

yields

$$D_{\mathrm{KP}}(x) = \begin{cases} \dfrac{x}{\sqrt{b^2-x^2}\,\arctan\left(\frac{x}{\sqrt{b^2-x^2}}\right)} D_0, & 0 < x < b \\ D_0, & b < x < L/2 \end{cases}. \tag{22.46}$$

In this case, $\langle w(x)\rangle$ is the same as in the previous cases and is given by Eq. (22.33). Additionally, to calculate $\langle 1/(D(x)\,w(x))\rangle$, we have to substitute Eqs. (22.32), (22.40), and (22.46) into it, which gives

$$
\begin{aligned}
&\left\langle \frac{1}{D(x)\,w(x)} \right\rangle \\
&\quad = \frac{2}{L}\int_0^{L/2} \frac{\mathrm{d}x}{D_{\mathrm{KP}}(x)\,w(x)} \\
&\quad = \frac{2}{L}\left[\int_0^{b} \frac{\mathrm{d}x}{D_{\mathrm{KP}}(x)\,w(x)} + \int_b^{L/2} \frac{\mathrm{d}x}{D_0\,w(x)}\right] \\
&\quad = \frac{2}{L}\left[\int_0^{b} \frac{\left(\frac{x}{\sqrt{b^2-x^2}}\right)}{D_0\,\arctan\left(\frac{x}{\sqrt{b^2-x^2}}\right)(L-2\sqrt{b^2-x^2})}\mathrm{d}x + \int_b^{L/2} \frac{\mathrm{d}x}{D_0\,L}\right] \\
&\quad = \frac{2}{L\,D_0}\left[\int_0^{b} \frac{\left(\frac{x}{\sqrt{b^2-x^2}}\right)}{\arctan\left(\frac{x}{\sqrt{b^2-x^2}}\right)(L-2\sqrt{b^2-x^2})}\mathrm{d}x + \frac{1}{2}\left(1-\frac{2b}{L}\right)\right].
\end{aligned}
\tag{22.47}
$$

Now, let's calculate the remaining integral. To such end, we introduce the following two changes of variable: first $y = x/b$ and second $y = \sin(\varphi)$, as done previously, so then,

$$
\begin{aligned}
&\int_0^{b} \frac{\left(\frac{x}{\sqrt{b^2-x^2}}\right)}{\arctan\left(\frac{x}{\sqrt{b^2-x^2}}\right)(L-2\sqrt{b^2-x^2})}\mathrm{d}x \\
&\quad = b\int_0^{1} \frac{\frac{y}{\sqrt{1-y^2}}}{\arctan\left(\frac{y}{\sqrt{1-y^2}}\right)\left(L-2b\sqrt{1-y^2}\right)}\mathrm{d}y \\
&\quad = \frac{b}{L}\int_0^{\frac{\pi}{2}} \frac{\sin\varphi\,\mathrm{d}\varphi}{\varphi\left(1-\frac{2b}{L}\cos\varphi\right)}.
\end{aligned}
\tag{22.48}
$$

This last integral must be solved numerically. Finally, after some algebra and by substituting Eq. (22.48) into Eq. (22.47), we have

$$
D_{\mathrm{eff}}^{\mathrm{KP}} = \frac{D_0}{\left(1-\frac{\pi}{4}\nu^2\right)\left[\nu\int_0^{\pi/2}\frac{\sin\varphi\,\mathrm{d}\varphi}{\varphi(1-\nu\cos\varphi)}+1-\nu\right]},
\tag{22.49}
$$

where $\nu = 2b/L$.

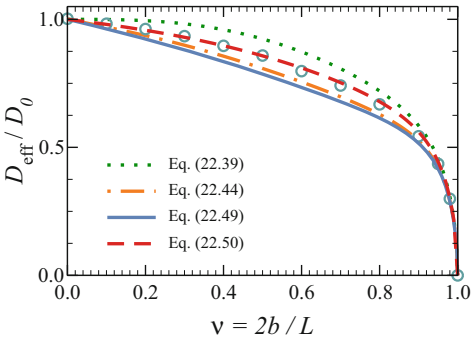

Fig. 22.8 Effective diffusivity normalized to D_0, as a function of the ratio $\nu = 2b/L$. Comparison of the approximate formulas in Eqs. (22.39), (22.44), (22.49), and (22.50) (curves), with the values of the effective diffusion coefficient obtained from Brownian dynamics simulations (symbols)

In Fig. 22.8, we show the ν-dependencies predicted by this equation, which is in good agreement with the simulation results over the entire range. Also shown are the predictions made by Eqs. (22.39) and (22.44).

The expression that describes the effective diffusivity over the entire range of the channel period can be constructed using Eqs. (22.24) and (22.49), namely,

$$D_{\rm eff}^{\gamma} = D_0 - \gamma (D_0 - D_{\rm eff}^{\rm KP}), \tag{22.50}$$

where

$$\gamma = \frac{L}{a+L} = \frac{L}{(L-b)+L} = \frac{1}{2-\nu}. \tag{22.51}$$

It is remarkable to see that when a Brownian particle diffuses in the presence of obstacles, one can use the generalized Fick-Jacobs equation to describe the effect of varying constrained geometry on particle motion. Consequently, this equation can be used to analyze the slowdown of the particle's constrained diffusion due to its interaction with the obstacles.

22.5 Concluding Remarks

In this chapter, we studied the diffusion of Brownian particles through long, narrow, periodic channels. To such end, we need to simplify the effective diffusivity by means of the so-called Lifson-Jackson formula, which considerably simplifies the problem. This formula is an exact result for the one-dimensional Smoluchowski equation in the presence of a periodic potential and periodic diffusivity.

For the reader's convenience, listed below are the most important equations to depict and define diffusion in the presence of periodic potentials.

$$D_{\text{eff}} = \frac{1}{\left\langle e^{-\beta U(x)} \right\rangle \left\langle \dfrac{e^{\beta U(x)}}{D(x)} \right\rangle}, \qquad \text{(Lifson-Jackson equation)}$$

where

$$\langle f(x) \rangle \equiv \frac{1}{L} \int_{x_0}^{x_0+L} f(x)\, \mathrm{d}x. \tag{22.52}$$

$$D_{\text{eff}} = \frac{1}{\left\langle R(x) \right\rangle \left\langle \dfrac{1}{D(x)R(x)} \right\rangle}, \qquad \text{(LJ equation for narrow tubes/channels)}$$

where $R(x)$ represents the transverse area or width of the tubes and channels, respectively.

Further Reading and References

A.M. Berezhkovskii, L. Dagdug, Biased diffusion in periodic potentials: three types of force dependence of effective diffusivity and generalized Lifson-Jackson formula. J. Chem. Phys. **151**, 11102 (2019). https://doi.org/10.1063/1.5120279

L. Dagdug, M.-V. Vazquez, A.M. Berezhkovskii, S.M. Bezrukov, Unbiased diffusion in tubes with corrugated walls. J. Chem. Phys. **133**, 034707 (2010). https://doi.org/10.1063/1.3431756

L. Dagdug, M.-V. Vazquez, A.M. Berezhkovskii, V.Yu. Zitserman, S.M. Bezrukov, Diffusion in the presence of cylindrical obstacles arranged in a square lattice analyzed with generalized Fick-Jacobs equation. J. Chem. Phys. **136**, 204106 (2012). https://doi.org/10.1063/1.4720385

S. Lifson, J.L. Jackson, 3/1.4832035 On the self-diffusion of ions in a polyelectrolyte solution. J. Chem. Phys. **36**, 2410 (1962). https://doi.org/10.1063/1.1732899

I. Pineda, M.-V. Vazquez, A.M. Berezhkovskii, L. Dagdug, Diffusion in periodic two-dimensional channels formed by overlapping circles: comparison of analytical and numerical results. J. Chem. Phys. **135**, 224101 (2011), **133**, 034707 (2010). https://doi.org/10.1063/1.3664179

M.-V. Vazquez, A.M. Berezhkovskii, L. Dagdug, Diffusion in linear porous media with periodic entropy barriers: a tube formed by contacting spheres. J. Chem. Phys. **129**, 046101 (2008). https://doi.org/10.1063/1.2955447

R. Verdel, L. Dagdug, A.M. Berezhkovskii, S.M. Bezrukov, Unbiased diffusion in two-dimensional channels with corrugated walls. J. Chem. Phys. **144**, 084106 (2016). https://doi.org/10.1063/1.4942470

Chapter 23
Active Brownian Particles

Unlike passive Brownian particles, active particles, also known as self-propelled Brownian particles, microswimmers, or nanoswimmers, are capable of taking up energy from their environment and converting it into directed motion. Active particles can be microscopic and nanoscopic in size and have propulsion speeds that are typically up to a fraction of a millimeter per second. Studying these particles provides us with a whole new field of physics and is spearheading the way toward the development of novel strategies for designing smart devices and materials. In recent years, a significant and growing effort has been devoted to exploring their applications in a diverse set of disciplines such as statistical physics, biology, robotics, soft matter, and biomedicine.

Self-propelled Brownian particles include biological organisms (e.g., *spermatozoa* and *E. coli* bacterium) or man-made objects (e.g., Janus rods or spheres[1] and vesicles) that can propel themselves by taking up energy from their environment and converting it into directed motion. They were originally studied to model the swarm behavior of animals at the macroscale. We can find examples to simulate the aggregate motion of flocks of birds, herds of land animals, and schools of fish. Swarming systems give rise to emergent behaviors that occur at many different scales. Some of these behaviors are turning out to be counterintuitive, robust, and universal, i.e., they are independent of the type of animals constituting the swarm. Important progress has recently been made toward the fabrication of artificial active particles, which can self-propel based on different propulsion mechanisms.

[1] Janus particles, which are named after the two-faced Roman god Janus, have two or more distinct sides with different surface features, structures, and compositions. A Janus particle may have one-half of its surface composed of hydrophilic groups and the other half of hydrophobic groups. When added to water, their hydrophobic sides huddle together, protected by the polar side. They locally decompose water into H_2O and O_2 and thus create a local concentration gradient that eventually leads to self-diffusiophoresis.

L. Dagdug et al., *Diffusion Under Confinement*,
https://doi.org/10.1007/978-3-031-46475-1_23

This chapter deals with self-propelled Brownian particles subject to thermal fluctuations confined in a two-dimensional narrow cavity. In such case, both hydrodynamic effects near the walls and particle-particle interactions are neglected. We derive the corresponding Fick-Jacobs-Zwanzig equation for the probability distribution function of the active particle moving inside a narrow asymmetric channel effective swimmer diffusivity.

23.1 Low Reynolds Number

In 1851, George Stokes originally introduced Reynolds number, which is given by the ratio of the forces required to accelerate masses (inertial forces) to the forces required to generate shear (viscous forces). This dimensionless ratio describes the onset of turbulent flow of a fluid within a pipe. Laminar flow occurs at high viscosities (low Reynolds numbers), since turbulent flow occurs at low viscosities (high Reynolds numbers). The Reynolds number of a particle that moves at a velocity v in a fluid is defined by

$$R = \frac{l^2 v^2 \rho}{l v \eta} = \frac{l v \rho}{\eta}, \tag{23.1}$$

where l is the size of the particle (the characteristic linear dimension) and ρ and η are the density and the viscosity of the fluid, respectively.

A classic example to understand the physical meaning of the Reynolds number consists of comparing this value for a bacterium to the Reynolds number for a fish swimming in water. Typically for a bacterium, $v \simeq 10^{-3}\,\mathrm{cm\,s^{-1}}$ and $l \simeq 10^{-4}\,\mathrm{cm}$, since water has a $\rho \simeq 1\,\mathrm{g\,cm^{-3}}$, and $\eta \simeq 10^{-2}\,\mathrm{g\,cm^{-1}\,s^{-1}}$, and by substituting into Eq. (23.1), we find that $R \simeq 10^{-5}$. In contrast, typical values for a fish are $v \simeq 10^{2}\,\mathrm{cm\,s^{-1}}$ and $l \simeq 10\,\mathrm{cm}$, consequently $R \simeq 10^{5}$. As seen from this example, these two values are quite different.

The time and distance that these swimmers can coast before they come to a stop are very useful quantities that can help us to understand the physical consequences of different Reynolds numbers. For a spherical particle swimming in a viscous material, according to Newton's second law, we arrive at the following relation:

$$m\frac{\mathrm{d}v}{\mathrm{d}t} = -6\pi\eta a, \tag{23.2}$$

where m is the mass of the particle, v is the velocity, η is the viscosity of the fluid, and a is the particle radius (derivation of Eq. (23.2) is given in Appendix 23.A). Solving this differential equation results in

$$v(t) = v(0)\,\mathrm{e}^{-t/\tau}, \tag{23.3}$$

where $v(0)$ is the initial velocity of the spherical particle and τ is given by

$$\tau = \frac{m}{6\pi\eta a} = \frac{2a^2\rho}{9\eta}, \tag{23.4}$$

where ρ is the density of the particle. Equation (23.3) can be integrated to obtain the distance coasted, d, by the spherical object before it comes to a halt:

$$d = \int_0^\infty v(t)\,\mathrm{d}t = v(0)\tau = \frac{2a^2\rho}{9\eta}v(0). \tag{23.5}$$

The stopping distance scales up as the initial velocity and square of the particle's radius increase. Consequently, small particles coast much smaller distances than large particles.

Through substitution of typical values for v, a, ρ, and η as done above, we find that the coasting distance of a bacterium is counterintuitively small, around 0.04 Å, and it stops in 1×10^{-7} s! A counterintuitive behavior is observed for low Reynolds numbers. Then, we found that the fish's coasting distance is around 2 m, and it stops in 0.2 s! From these results, we can conclude that the fish propels itself by the acceleration of the water that surrounds it, whereas bacterium uses viscous shear.

It is worth mentioning that the Reynolds number is found to be very useful through an analysis of the Navier-Stokes equation: a partial differential equation that describes the motion of viscous fluids. This equation for an incompressible fluid is

$$-\nabla p + \eta\nabla^2\mathbf{v} = \rho\frac{\partial\mathbf{v}}{\partial t} + \rho(\mathbf{v}\cdot\nabla)\mathbf{v}. \tag{23.6}$$

From Eq. (23.1), we can see that for low Reynolds numbers, the right-hand side of the Navier-Stokes equation, the inertial terms, can be neglected at reasonably long-time scales (>0.001 s), and time makes no difference. The reversibility of the pressure when the direction is changed implies reversibility of the flow.

Finally, we can conclude that low-Reynolds-number hydrodynamics are at the heart of the ability of bacterium to generate propulsion at the micrometer scale.

23.2 Rotational Diffusion: Debye's Problem

Consider a spherical particle of radius a immersed in a molecular fluid, constrained to rotating only about a fixed axis through its center that is perpendicular to a unit vector $\hat{\mathbf{e}}_u$. By choosing x- and y-axes on the plane in which $\hat{\mathbf{e}}_u$ moves, we can represent its configuration by a single angle φ (see Fig. 23.1).

Fluid molecule collisions with the sphere will generate a fluctuating torque on the sphere. On the other hand, if we try to rotate the sphere by means of an externally

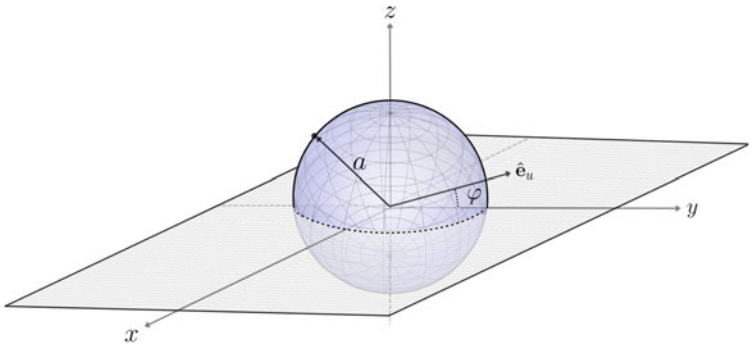

Fig. 23.1 Schematic representation of a spherical particle of radius a constrained to rotating on the xy-plane

applied torque, there will be a systematic drag resistance to rotation proportional to the angular velocity. Then, the Langevin-like equation for the angular momentum L about the rotation axis (z-axis) is given by

$$\frac{\mathrm{d}L(t)}{\mathrm{d}t} = I\frac{\mathrm{d}^2\varphi(t)}{\mathrm{d}t^2} = -\zeta\frac{\mathrm{d}\varphi(t)}{\mathrm{d}t} + T_B(t), \tag{23.7}$$

where I is the moment of inertia about the rotation axis, ζ is a rotational friction coefficient, and T_B is a fluctuating Brownian torque. The effect of the fluctuating torque can be summarized by giving its first and second moments as time averages over an infinitesimal time interval:

$$\langle T_B(t)\rangle = 0, \quad \langle T_B(t)\ T_B(t')\rangle = \Gamma(t-t'). \tag{23.8}$$

The random torque exhibits no time correlation between impacts in any distinct time intervals dt and dt', but has a characteristic strength factor Γ that does not change over time, which strength factor is a measure of the strength of the fluctuating torque.

We can find the mean of the squared angular velocity, $\mathrm{d}\varphi/\mathrm{d}t = \omega$, using the delta correlation. Then, integrating Eq. (23.7) as in the translational case leads to the relation:

$$\langle\omega^2(t)\rangle = \langle\omega^2(0)\rangle\mathrm{e}^{-2\zeta t/I} + \frac{\Gamma}{2I\zeta}\left(1-\mathrm{e}^{-2\zeta t/I}\right). \tag{23.9}$$

At long times, the mean squared angular velocity tends to a constant value given by

$$\lim_{t\to\infty}\langle\omega^2(t)\rangle = \frac{\Gamma}{2I\zeta}. \tag{23.10}$$

If we use the equilibrium equipartition theorem, $\langle \frac{1}{2} I \omega^2 \rangle = \frac{1}{2} k_B T$, we find the fluctuation-dissipation relation:

$$\Gamma = 2\zeta k_B T. \tag{23.11}$$

On the slow time scale, the angular displacement is

$$\langle (\varphi(t) - \varphi(0))^2 \rangle = \frac{2k_B T}{\zeta} t = 2D_\Omega t, \tag{23.12}$$

with a rotational diffusion coefficient:

$$D_\Omega \equiv \frac{k_B T}{\zeta}. \tag{23.13}$$

It is worth noting that physically, angles φ and $\varphi + 2\pi$ are identical. Consequently, the result is identical to that for translational diffusion only in a mathematical sense. For a sphere of uniform density ρ and radius a, $\zeta = 8\pi\rho a^3$, and the rotational diffusion coefficient is

$$D_\Omega = \frac{k_B T}{8\pi\rho a^3}. \tag{23.14}$$

On the other hand, the translational diffusion constant for a spherical particle, denoted here by D_B to clearly differentiate it from its rotational counterpart, is

$$D_B = \frac{k_B T}{6\pi\eta a}. \tag{23.15}$$

A brief inspection of the above equation reveals that while the translational diffusion of a particle scales with its linear dimension, its rotational diffusion scales with its volume. For example, since water has a $\rho \simeq 1\,\mathrm{g\,cm^{-3}}$ and $\eta \simeq 10^{-2}\,\mathrm{g\,cm^{-1}\,s^{-1}}$, for a particle with $a = 1\mu\mathrm{m}$ in water, $D_B \simeq 0.2\,\mu\mathrm{m^2\,s^{-1}}$ and $D_\Omega \simeq 0.17\,\mathrm{rad^2\,s^{-1}}$, while for a particle ten times smaller, $a = 100\,\mathrm{nm}$, $D_B \simeq 2\,\mu\mathrm{m^2\,s^{-1}}$ is one order of magnitude larger, but $D_\Omega \simeq 170\,\mathrm{rad^2\,s^{-1}}$ is three orders of magnitude larger.

The evolution equation for the probability density $p(\varphi, t)$ for finding the particle with velocity $\mathbf{u}$ at angle φ at time t, i.e., the corresponding Smoluchowski equation, is given by the rotational diffusion equation:

$$\frac{\partial p(\varphi, t)}{\partial t} = D_\Omega \frac{\partial^2 p(\varphi, t)}{\partial \varphi^2}. \tag{23.16}$$

This equation can be deduced by following the same steps used in Sect. 2.2.

23.3 Fick-Jacobs-Zwanzig Equation for Active Brownian Particles

In this section, we will study the effect of confinement in two-dimensional narrow cavities for diffusing spherical active particles of radius a. The upper and lower boundaries of the system are defined by $A_1(x)$ and $A_2(x)$, where $A_2(x) > y > A_1(x)$. Consequently, the channel width is given by $w(x) = A_2(x) - A_1(x)$. Both the hydrodynamic effects near the walls and particle-particle interactions are neglected. The self-propelling particle has a swimming velocity, $U_s(t) = U_s(t)\hat{\mathbf{e}}(t)$, where $e(t) = [e_1(t), e_2(t)]$ is the instantaneous unit vector in the direction of swimming with the origin at its center. For rotational collisions between active particles and walls, we assume a frictionless wall that does not affect the particle's orientation. For the case of translation reflections, we assume a mirror reflective wall, as we did in the previous chapters.

Our main goals are to derive the Fick-Jacobs-Zwanzig equation and obtain the effective diffusivity, which are the key results of this chapter. To such end, we use the diffusion equation to calculate the translation, Eq. (6.50), and the Fokker-Planck equation, Eq. (23.16), to describe the evolution equation for the propagator, $p(x, y, \varphi, t)$, of an active particle, namely,

$$\frac{\partial p(x,y,\varphi,t)}{\partial t} + U_s\,\hat{\mathbf{e}}(t)\cdot\nabla p(\mathbf{r},t|\mathbf{r}_0) = D_B\,\nabla^2 p(x,y,\varphi,t) + D_\Omega \frac{\partial^2 p(x,y,\varphi,t)}{\partial\varphi^2}, \tag{23.17}$$

where $p(x, y, \varphi, t)$ represents the probability of locating the particle at position (x, y) and orientation φ at time t. Our first goal is to show how to extend the projection method introduced by Kalinay and Percus to Eq. (23.17) onto the longitudinal dimension, as an expansion in parameter $\lambda = D_x/D_y$, for an asymmetrical channel. To such end, we have to define the projected one-dimensional density $p(x, y, \varphi, t)$ as

$$\mathcal{G}(x,\varphi,t) = \int_{A_1(x)}^{A_2(x)} p(x,y,\varphi,t)\,\mathrm{d}y. \tag{23.18}$$

For the sake of brevity, from now on, we will omit the dependence of $A_1(x)$, $A_2(x)$, $p(x, y, \varphi, t)$, and $\mathcal{G}(x, \varphi, t)$. Using Eq. (23.18) and integrating the diffusion equation (23.17) over y, valuing the upper and lower limits, we arrive at

$$\begin{aligned}\frac{\partial\mathcal{G}}{\partial t} + U_s\,e_1\left[\frac{\partial\mathcal{G}}{\partial x} + \frac{\mathrm{d}A_1}{\mathrm{d}x}p\bigg|_{y=A_1}\right] - U_s\,e_1\frac{\mathrm{d}A_2}{\mathrm{d}x}p\bigg|_{y=A_2} + U_s\,e_2\,p\big|_{y=A_1}^{y=A_2} \\ = D_B\frac{\partial^2\mathcal{G}}{\partial x^2} + D_B\,\frac{\partial p}{\partial y}\bigg|_{y=A_1}^{y=A_2} + D_\Omega\frac{\partial^2\mathcal{G}}{\partial\varphi^2} - D_B\frac{\partial}{\partial x}\left(\frac{\mathrm{d}A_2}{\mathrm{d}x}p\bigg|_{A_2} - \frac{\mathrm{d}A_1}{\mathrm{d}x}p\bigg|_{y=A_1}\right)\end{aligned}$$

$$+ D_B \left.\frac{\partial p}{\partial x}\right|_{y=A_1} \frac{\mathrm{d}A_1}{\mathrm{d}x} - D_B \left.\frac{\partial p}{\partial x}\right|_{y=A_2} \frac{\mathrm{d}A_2}{\mathrm{d}x}. \tag{23.19}$$

On the boundaries, the vector of the current density must be parallel to the walls. Consequently, the translational and rotational fluxes, i.e., $\mathbf{J}^t = -D_B \nabla p + U_s(t)\,\mathbf{e}(t)\,p$ and $\mathbf{J}^R = -D_\Omega(\partial p/\partial\varphi)\,\widehat{\varphi}$, respectively, must satisfy

$$\widehat{v}_u \times \mathbf{J}^t = \mathbf{0}, \quad \widehat{v}_l \times \mathbf{J}^t = \mathbf{0}, \tag{23.20}$$

where $\widehat{v}_u = \left[\mathbf{i} + A_2'(x)\mathbf{j}\right]/\sqrt{1 + A_2'(x)^2}$ is the upper unit tangent vector to $y = A_2(x)$, and $\widehat{v}_l = \left[\mathbf{i} + A_1'(x)\mathbf{j}\right]/\sqrt{1 + A_1'(x)^2}$ is the lower unit tangent vector to $y = A_1(x)$. Here the prime denotes the derivative with respect to x. Subtracting the flux given in Eq. (23.20) results in

$$\begin{aligned} &D_B \left.\frac{\partial p}{\partial y}\right|_{y=A_1}^{y=A_2} + D_B\, A_1' \left.\frac{\partial p}{\partial x}\right|_{y=A_1} - D_B\, A_2' \left.\frac{\partial p}{\partial x}\right|_{y=A_2} \\ &\quad = U_s\, e_2\, p\big|_{y=A_1}^{y=A_2} + U_s\, e_1 \left[A_1' p\big|_{y=A_1} - A_2' p\big|_{y=A_2}\right]. \end{aligned} \tag{23.21}$$

Later, after imposing an infinite transverse diffusion rate, from Eq. (23.18) we have that

$$\begin{aligned} p(x, A_2(x), \varphi, t) &\simeq p(x, A_1(x), \varphi, t) \\ &= \frac{\mathcal{G}(x, \varphi, t)}{A_2(x) - A_1(x)}. \end{aligned} \tag{23.22}$$

Finally, inserting Eq. (23.21) into Eq. (23.19), and using Eq. (23.22), we see that

$$\frac{\partial \mathcal{G}}{\partial t} = D_B \frac{\partial}{\partial x}\left[w(x)\frac{\partial}{\partial x}\left(\frac{\mathcal{G}}{w(x)}\right)\right] + D_\Omega \frac{\partial^2 \mathcal{G}}{\partial \varphi^2} - U_s\, e_1 \frac{\partial \mathcal{G}}{\partial x}, \tag{23.23}$$

which is the Fick-Jacobs equation for a confined active particle swimming inside an asymmetric channel, and in KP's scheme, it is the zeroth order of the projected 1D diffusion equation in the parameter λ. It is worth noting that, if $w(x)$ is constant, we recover the one-dimensional diffusion problem of an active particle performing translational and rotational Brownian motion.

23.4 Effective Diffusivity for Active Brownian Particles

In this section, we will focus on obtaining the effective diffusion considering both confinement and that the Brownian particles are active. For an active particle

swimming at constant speed $U_s(t) = U$ without constraints, the then one-dimensional diffusivity is given by[2]

$$D_B + \frac{U^2}{2D_\Omega}. \tag{23.24}$$

Regarding effective diffusion that is position-dependent, we propose the following ansatz: The active particle is affected by the presence of walls in the same manner as passive particles are. Consequently, $D_0 = D_B + U^2/(2D_\Omega)$. Using this expression in one of the position-dependent effective diffusivity coefficients, in the Reguera-Rubi approximation, Eq. (20.118), for example, we arrive at

$$D_{ap}(x) = \frac{D_B + U^2/(2D_\Omega)}{\left[1 + (1/4)w'(x)^2\right]^{1/3}}. \tag{23.25}$$

In order to verify the ansatz, in the next section, we will apply Eq. (23.25) to a corrugated periodical channel and compare the theoretical result with Brownian dynamics simulations.

23.5 Corrugated Periodical Channel

To find the effective diffusivity for a corrugated periodical channel (see Fig. 22.2), we need to use the Lifson-Jackson equation, Eq. (22.26),

$$D_{\text{eff}} = \frac{1}{\left\langle \frac{w(x)}{w(0)} \right\rangle \left\langle \frac{1}{D(x)\frac{w(x)}{w(0)}} \right\rangle} = \frac{1}{\left\langle w(x) \right\rangle \left\langle \frac{1}{D(x)w(x)} \right\rangle}, \tag{22.26}$$

and follow the method outlined in Sect. 22.3.

To calculate the integrals involved in the processes, we need to know the channel width, given by Eq. (22.25), its derivative, and the position-dependent diffusivity, given by Eq. (23.25), which for this specific channel is constant and given by

$$D_{\lambda ap} = \frac{D_B + U^2/(2D_\Omega)}{\left(1 + \lambda^2\right)^{1/3}}. \tag{23.26}$$

Now, we have the information needed to perform the averaging appearing in Eq. (22.26), namely, $\langle w(x) \rangle$ and $\langle 1/(D(x)\, w(x)) \rangle$. Averaging over channel width

[2] The deduction of this formula is out of the scope of this book. Readers interested in learning the details are referred to the original article by P. S. Lovely and F. W. Dahlquist.

was performed in Sect. 22.3, arriving at the following result:

$$\Big\langle w(x)\Big\rangle = 2a + (\lambda - 1)L. \tag{22.28}$$

On the other hand, the second averaging in this case is given by

$$\left\langle \frac{1}{D_0\, w(x)} \right\rangle = \frac{1}{D_{\lambda ap}\, L} \int_0^L \frac{\mathrm{d}x}{w(x)} = \frac{1}{L D_{\lambda ap}} \int_0^L \frac{\mathrm{d}x}{2(a + \lambda(L/2) - |x|)}$$
$$= \frac{2}{L\, D_{\lambda ap}} \left[\ln(2a + \lambda L) - \ln(2a + (\lambda - 2)L)\right]. \tag{23.27}$$

Substituting these last equations and Eq. (22.27) into Eq. (22.15), we arrive at

$$D_{\mathrm{eff}}^{\lambda ap} = \left[\frac{D_B + U^2/(2D_\Omega)}{\left(1+\lambda^2\right)^{1/3}}\right] \frac{2\lambda \frac{2L}{a}}{\left[2 + \lambda \frac{2L}{a}\right] \ln\left(1 + \lambda \frac{2L}{a}\right)}, \tag{23.28}$$

which is the effective diffusion formula for an active confined particle.

To test the accuracy of this approximate theoretical expression for the effective diffusivity and to establish the range of its applicability as a function of the channel period L, we compare it to the values obtained from Brownian dynamics simulations.

In simulations, we consider a spherical swimmer of radius $a = 1$ μm, immersed in water at $T = 300$ K, swimming at speed $U_s(t) = U = 1$ μm/s, inside two different corrugated periodical channels with slopes $\lambda = 0.5$ and $\lambda = 1$, and period $L = 20$ μm. The results are shown in Fig. 23.2. From this figure, we can observe there is excellent agreement between theory and simulations almost over

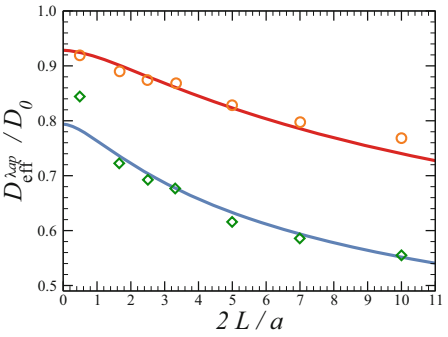

Fig. 23.2 Effective diffusion coefficient $D_{\mathrm{eff}}^{\lambda ap}$, [Eq. (23.28)], for two corrugated periodical channels with $\lambda = 0.5$ and $\lambda = 1$, normalized by $D_0 = D_B + U^2/(2D_\Omega)$ (non-confined active diffusion), plotted as a function of $2L/b$ (solid lines). Brownian simulation results are shown as open circles and diamonds, for $\lambda = 0.5$ and $\lambda = 1$, respectively, with period $L = 20$ μm

the entire range, except for smaller L/b, when the theory fails. It is worth noting that excellent agreement between theory and numerical experiments is observed at moderate swimming velocities of the order of 1 μm/s. For higher swimming velocities, the theory predicts a larger effective diffusion coefficient compared to the one obtained in simulations.

23.6 Concluding Remarks

In this chapter, we study Brownian active particles under confinement by means of the Fick-Jacobs approach. As part of the description, we derive an approximation formula for position-dependent diffusivity, which seems to work very well for low velocities when compared with Brownian dynamics simulations. Another conclusion is that particles with large Reynolds numbers propel themselves by the acceleration of the liquid that surrounds them, while particles with small Reynolds numbers use viscous shear.

For the reader's convenience, listed below are the most important equations to depict active particles into a two-dimensional channel:

$$R = \frac{lv\rho}{\eta}. \qquad \text{(Reynolds number)}$$

$$D_\Omega = \frac{k_B T}{8\pi\rho a^3}. \qquad \text{(Rotational diffusion coefficient for a sphere)}$$

$$D_B = \frac{k_B T}{6\pi\eta a}. \qquad \text{(Translational diffusion coefficient for a sphere)}$$

$$\frac{\partial \mathcal{G}}{\partial t} = D_B \frac{\partial}{\partial x}\left[w(x)\frac{\partial}{\partial x}\left(\frac{\mathcal{G}}{w(x)}\right)\right] + D_\Omega \frac{\partial^2 \mathcal{G}}{\partial \varphi^2} - U_s\, e_1 \frac{\partial \mathcal{G}}{\partial x}$$

(Fick-Jacobs equation for an active particle)

$$D_0 = D_B + \frac{U^2}{2D_\Omega}. \qquad \text{(Diffusivity for an active particle)}$$

23.A Translational and Rotational Friction Coefficients

In this appendix, we derive the translational and rotational friction coefficients for a sphere. Firstly, we compute the local fluid velocity $\mathbf{v}$ by means of an auxiliary

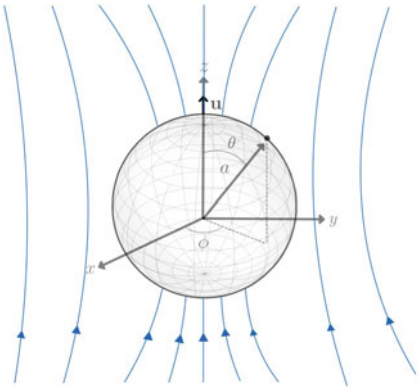

Fig. 23.3 Schematic representation of the Stokes problem: a moving sphere of radius a in an incompressible viscous fluid. We indicate the direction of the current lines for the translation of a sphere in viscous fluid with black arrows. The velocity $\mathbf{u}$ is parallel to the z-axis

vectorial function $\mathbf{A}$. Secondly, we use $\mathbf{v}$ to determine the pressure p, and thirdly we use p to find the force associated with the problem. To such end, we consider the problem of a Stokes flow caused by a moving sphere of radius a in an incompressible viscous fluid (see Fig. 23.3). We start with the Navier-Stokes equation, which is Newton's equation of motion for a viscous fluid per unit volume. Such equation, in its convective form, is given by

$$\rho\left(\frac{\partial}{\partial t}+\mathbf{v}\cdot\boldsymbol{\nabla}\cdot\right)\mathbf{v}=-\nabla p+\eta\nabla^2\mathbf{v}+\mathbf{g}, \tag{23.29}$$

where ρ is the mass density, $\mathbf{v}(\mathbf{r},t)$ the local fluid velocity, p the pressure, η the viscous coefficient, and $\mathbf{g}$ the body acceleration. The ratio of the nonlinear inertial term, $\rho\mathbf{u}\cdot\nabla\mathbf{v}$, to the viscous dissipation term, $\eta\nabla^2\mathbf{v}$, is the so-called Reynolds number, given by Eq. (23.1). At low Reynolds numbers, $R\ll 1$, the flow is dominated by viscosity and the inertial term vanishes. Moreover, in the steady state, the partial derivative of the local fluid is neglected, and the Navier-Stokes equation, in the absence of acceleration, is simplified to the Stokes equation, namely,

$$\nabla p=\eta\nabla^2\mathbf{v}. \tag{23.30}$$

On taking the curl of the latter equation and applying the fact that $\boldsymbol{\nabla}\times(\boldsymbol{\nabla}\phi)=0$ for any scalar field ϕ twice-differentiable (differenciability class C^2), together with $\boldsymbol{\nabla}\times(\nabla^2\mathbf{v})=\nabla^2(\boldsymbol{\nabla}\times\mathbf{v})$, we find

$$\nabla^2(\boldsymbol{\nabla}\times\mathbf{v})=0. \tag{23.31}$$

The problem of a sphere moving in a viscous fluid is equivalent to the flow through a fixed sphere, where the fluid is given a constant velocity $\mathbf{u}$ at infinity. In order to find the Stokes formula, we will use spherical coordinates[3] considering

[3] See Appendix B, Sect. B.3, for further details on spherical coordinates.

that there is no privileged direction other than the direction of velocity $\mathbf{v}$. Given the symmetry of the problem, the velocity $\mathbf{v}$ has to be contained within the plane passing through the Z-axis. Additionally, $\mathbf{v}$ must remain unchanged as we pivot around such axis in the $\hat{\mathbf{e}}_k$ direction. These requirements imply that $\mathbf{v}$ is subject to the following conditions:

$$\frac{\partial v_r}{\partial \phi} = 0, \qquad \frac{\partial v_\theta}{\partial \phi} = 0, \qquad v_\phi = 0, \tag{23.32}$$

meaning that v_r and v_θ are functions of r and θ only. Furthermore, $\mathbf{u} = u\cos\theta\,\hat{\mathbf{e}}_r - u\sin\theta\,\hat{\mathbf{e}}_\theta$. Then,

$$\boldsymbol{\nabla}\cdot(\mathbf{v}-\mathbf{u}) = 0, \tag{23.33}$$

which is an extension of the equation of continuity, namely, $\boldsymbol{\nabla}\cdot(\mathbf{v}-\mathbf{u}) = \boldsymbol{\nabla}\cdot\mathbf{v} = 0$. Therefore, $\mathbf{v}-\mathbf{u}$ can be expressed as

$$\mathbf{v}-\mathbf{u} = \boldsymbol{\nabla}\times\mathbf{A}. \tag{23.34}$$

Let $\mathbf{A}$ be $\mathbf{A} = \boldsymbol{\nabla} f \times \mathbf{u}$, where $f = f(r)$ is a scalar function of r. Then, the velocity can be written as

$$\mathbf{v} = \mathbf{u} + \boldsymbol{\nabla}\times(\boldsymbol{\nabla} f(r)\times\mathbf{u}), \tag{23.35}$$

or

$$\mathbf{v} = \mathbf{u} + \boldsymbol{\nabla}\times\boldsymbol{\nabla}\times(f\mathbf{u}), \tag{23.36}$$

if we consider $\mathbf{u}$ as a constant vector. Now, by taking the curl of the latter equation, and comparing it to Eq. (23.31), we obtain

$$\nabla^2\nabla^2[(\boldsymbol{\nabla} f)\times\mathbf{u}] = 0. \tag{23.37}$$

This last equation is satisfied if

$$\nabla^2\nabla^2(\boldsymbol{\nabla} f) = 0. \tag{23.38}$$

Direct integration of Eq. (23.38) yields[4]

$$\nabla^2\nabla^2 f = \frac{1}{r^2}\frac{\mathrm{d}}{\mathrm{d}r}\left(r^2\frac{\mathrm{d}}{\mathrm{d}r}\right)\nabla^2 f = 0, \tag{23.39}$$

[4] Since the velocity must vanish at infinity, the constant of the first integration is automatically zero.

the solution of which is

$$\nabla^2 f = \frac{2A}{r} + C, \tag{23.40}$$

where A and C are constants, yet C is set to zero without any loss of generality, allowing us to compose a final ordinary differential equation for f, namely,

$$\frac{\mathrm{d}}{\mathrm{d}r}\left[r^2\left(\frac{\mathrm{d}}{\mathrm{d}r}f\right)\right] = 2Ar. \tag{23.41}$$

The solution is directly found, yielding

$$f(r) = Ar + \frac{B}{r}. \tag{23.42}$$

Substituting Eq. (23.42) into Eq. (23.36) leads to

$$\mathbf{v} = \mathbf{u} + \boldsymbol{\nabla} \times \boldsymbol{\nabla} \times \left[\left(Ar + \frac{B}{r}\right)\mathbf{u}\right]. \tag{23.43}$$

Using Eq. (B.16), we obtain

$$\begin{aligned}\boldsymbol{\nabla} \times (f\mathbf{u}) &= \frac{1}{r}\left\{\frac{\partial}{\partial r}\left[-\left(Ar^2 + B\right)u\sin\theta\right] - \frac{\partial}{\partial\theta}\left[\left(Ar + \frac{B}{r}\right)u\cos\theta\right]\right\}\hat{\mathbf{e}}_\phi \\ &= \left(-A + \frac{B}{r^2}\right)u\sin\theta\,\hat{\mathbf{e}}_\phi.\end{aligned} \tag{23.44}$$

Therefore, $\boldsymbol{\nabla} \times \boldsymbol{\nabla} \times (f\mathbf{u})$ is

$$\begin{aligned}\boldsymbol{\nabla} \times \boldsymbol{\nabla} \times (f\mathbf{u}) &= -\frac{A}{r}\left(u\cos\theta\hat{\mathbf{e}}_r + \mathbf{u}\right) + \frac{B}{r^3}\left(3u\cos\theta\hat{\mathbf{e}}_r - \mathbf{u}\right) \\ &= -\frac{A}{r}[(\mathbf{u}\cdot\hat{\mathbf{e}}_r)\hat{\mathbf{e}}_r + \mathbf{u}] + \frac{B}{r^3}\left[3(\mathbf{u}\cdot\hat{\mathbf{e}}_r)\hat{\mathbf{e}}_r - \mathbf{u}\right],\end{aligned} \tag{23.45}$$

where we used that $\mathbf{u}\cdot\hat{\mathbf{e}}_r = (u\cos\theta\hat{\mathbf{e}}_r - u\sin\theta\hat{\mathbf{e}}_\theta)\cdot\hat{\mathbf{e}}_r = u\cos\theta$. Constants A and B are computed by imposing the boundary condition at the surface of the sphere $\mathbf{v}(r = a) = 0$, i.e.,

$$\mathbf{v} = -A\frac{\mathbf{u} + (\mathbf{u}\cdot\hat{\mathbf{e}}_r)\hat{\mathbf{e}}_r}{a} + B\frac{3(\mathbf{u}\cdot\hat{\mathbf{e}}_r)\hat{\mathbf{e}}_r - \mathbf{u}}{a^3} + \mathbf{u} = 0. \tag{23.46}$$

When rearranging this last equation, we obtain

$$\mathbf{u}\left(-\frac{A}{a}-\frac{B}{a^3}+1\right)+(\mathbf{u}\cdot\hat{\mathbf{e}}_r)\,\hat{\mathbf{e}}_r\left(-\frac{A}{a}+\frac{3B}{a^3}\right)=0, \tag{23.47}$$

a relation that is satisfied if both scalar factors are zero, giving a linear system of equations:

$$-\frac{A}{a}-\frac{B}{a^3}+1=0 \quad \text{and} \quad -\frac{A}{a}+\frac{3B}{a^3}=0, \tag{23.48}$$

with solutions $A = 3a/4$ and $B = a^3/4$. Consequently, substituting all components of the local velocity in spherical coordinates, together with constants A and B, we find

$$\begin{aligned} v_r &= u\cos\theta\left(1-\frac{3a}{2r}+\frac{a^3}{2r^3}\right)\hat{\mathbf{e}}_r, \\ v_\theta &= -u\sin\theta\left(1-\frac{3a}{4r}-\frac{a^3}{4r^3}\right)\hat{\mathbf{e}}_\theta, \end{aligned} \tag{23.49}$$

as well as

$$f(r)=\frac{3ar}{4}+\frac{a^3}{4r}. \tag{23.50}$$

Once we have Eqs. (23.49) and (23.50), we can calculate the pressure by using Eq. (23.30), namely,

$$\boldsymbol{\nabla} p=\eta\nabla^2\mathbf{v}=\eta\nabla^2[\boldsymbol{\nabla}\times\boldsymbol{\nabla}\times(f\mathbf{u})]. \tag{23.51}$$

Since both ∇^2 and $\boldsymbol{\nabla}\cdot$ are scalar operators, $\boldsymbol{\nabla}\times(\boldsymbol{\nabla}\times\mathbf{V})=\boldsymbol{\nabla}(\boldsymbol{\nabla}\cdot\mathbf{V})-\nabla^2\mathbf{V}$ for any vector $\mathbf{V}$, and given that $\nabla^2\nabla^2 f=0$ (see Eq. (23.38)), we can assure that

$$\boldsymbol{\nabla} p=\eta\boldsymbol{\nabla}\left\{\nabla^2[\boldsymbol{\nabla}\cdot(f\mathbf{u})]\right\}, \tag{23.52}$$

from which we find the following equation:

$$p=p_0+\eta\mathbf{u}\cdot\boldsymbol{\nabla}(\nabla^2 f), \tag{23.53}$$

where p_0 is the pressure far away from the sphere. For the sake of simplicity, we first compute $\nabla^2 f$ using the simplified version of f, i.e., in terms of A and B. With the use of Eq. (B.17), we obtain

$$\nabla^2 f=\frac{1}{r^2}\frac{\partial}{\partial r}\left[r^2\frac{\partial}{\partial r}\left(Ar+\frac{B}{r}\right)\right]=\frac{2A}{r}. \tag{23.54}$$

Now, the gradient of a scalar function $g = g(r, \theta, \phi)$ in spherical coordinates is given by (see Eq. (B.14))

$$\nabla g = \frac{\partial g}{\partial r}\hat{\mathbf{e}}_r + \frac{1}{r}\frac{\partial g}{\partial \theta}\hat{\mathbf{e}}_\theta + \frac{1}{r\sin\theta}\frac{\partial g}{\partial \phi}\hat{\mathbf{e}}_\phi, \tag{23.55}$$

then,

$$\mathbf{u}\cdot\nabla = u\cos\theta\frac{\partial}{\partial r} - \frac{u\sin\theta}{r}\frac{\partial}{\partial\theta}, \tag{23.56}$$

$$\eta\mathbf{u}\cdot\nabla(\nabla^2 f) = u\,\eta\cos\theta\frac{\partial}{\partial r}\left(\frac{2a}{r}\right) = -\frac{2au\eta}{r^2}\cos\theta. \tag{23.57}$$

Substituting into Eq. (23.53) finally leads to

$$p = p_0 - \frac{3au\eta}{2r^2}(\mathbf{u}\cdot\hat{\mathbf{e}}_r). \tag{23.58}$$

The force $\mathbf{F}$ acting on a unit surface area is given by

$$\mathbf{F} = -\sigma_{ik}n_k = pn_i - \sigma'_{ik}n_k, \tag{23.59}$$

with σ_{ik} being the stress tensor and σ'_{ik} the viscous stress tensor. In a process of inertial friction in an incompressible fluid, σ_{ik} is

$$\sigma_{ik} = -p\,\delta_{ik} + \eta\left(\frac{\partial v_i}{\partial x_k} + \frac{\partial v_k}{\partial x_i}\right), \tag{23.60}$$

where δ_{ik} is the Kronecker delta. In spherical coordinates, the normal and tangential components of the viscous stress tensor are

$$\sigma'_{rr} = 2\eta\frac{\partial v_r}{\partial r} \quad \text{and} \quad \sigma'_{r\theta} = \eta\left(\frac{1}{r}\frac{\partial v_r}{\partial\theta} + \frac{\partial v_\theta}{\partial r} - \frac{v_\theta}{r}\right), \tag{23.61}$$

which are simplified when substituting v_r and v_θ as in Eq. (23.49), and evaluated at the surface, namely,[5]

$$\sigma'_{rr} = 0 \qquad \sigma'_{r\theta} = -\frac{3u\eta}{2a}\sin\theta. \tag{23.63}$$

[5] The reader should be able to verify that, for an arbitrary radius r,

$$\sigma'_{rr} = \frac{3u\eta\cos\theta a}{r^2}\left[1 - \left(\frac{a}{r^2}\right)^2\right], \quad \text{and} \quad \sigma'_{r\theta} = -\frac{3u\eta\sin\theta}{2r^4}a^3. \tag{23.62}$$

As we can see, **F** has to be in the **u** direction. Thus, the projection of the total force (Eq. (23.59) integrated over the surface of the sphere leads to the magnitude of the Stokes force, i.e.,

$$F_z = \oint (-p\cos\theta + \sigma'_{rr}\cos\theta - \sigma'_{r\theta}\sin\theta)\,\mathrm{d}S. \tag{23.64}$$

Substituting Eqs. (23.58) and (23.63) evaluated at the surface into the latter equation yields

$$\begin{aligned} F_{zs} &= \oint \left[-\left(p_0 - \frac{3u\eta}{2a}\cos\theta\right)\cos\theta + \left(\frac{3u\eta}{2a}\sin\theta\right)\sin\theta \right] \mathrm{d}S \\ &= -\oint p_0\cos\theta\,\mathrm{d}S + \frac{3\eta}{2a}\oint \mathrm{d}S. \end{aligned} \tag{23.65}$$

Therefore,

$$F_z = -\int_0^{2\pi}\int_0^{\pi} p_0 a^2\cos\theta\sin\theta\,\mathrm{d}\theta\,\mathrm{d}\phi + \frac{3\eta}{2a}\int_0^{2\pi}\int_0^{\pi} a^2\sin\theta\,\mathrm{d}\theta\,\mathrm{d}\phi. \tag{23.66}$$

The first term of the latter equation is zero, since $\sin\theta$ and $\cos\theta$ are orthogonal functions. The second term in F_z is the solid angle in spherical coordinates. Thus,

$$F_z = 6\pi\eta a u. \tag{23.67}$$

As mentioned earlier, the problem of a moving sphere in a viscous fluid is the exact same problem as that of a fluid passing through a fixed sphere. For that reason, the reader may find the Stokes force in the literature either as in Eq. (23.67) or as

$$F_z = -6\pi\eta a u. \tag{23.68}$$

The difference remains in the direction of velocity **u**. The velocity distribution for the moving sphere problem (the problem we solved here) is obtained from the fixed sphere problem by subtracting **u** from **v**, as done in Eq. (23.34).

Further Reading and References

C. Bechinger, R. Di Leonardo, H. Löwen, Ch. Reichhardt, G. Volpe, G. Volpe, Active particles in complex and crowded environments. Rev. Mod. Phys. **88**, 045006 (2016). https://journals.aps.org/rmp/abstract/10.1103/RevModPhys.88.045006

H.C. Berg, *Random Walks in Biology* (Princeton University Press, Princeton, 1983)

H.C. Berg, *E. coli* in Motion (Springer, Berlin, 2004)

P.S. Lovely, F.W. Dahlquist, Statistical measures of bacterial motility and chemotaxis. J. Theor. Biol. **50**, 477 (1975). https://www.sciencedirect.com/science/article/abs/pii/0022519375900946?via%3Dihub

E.M. Purcell, Life at low Reynolds number. Am. J. Phys. **45**, 3 (1977). https://aapt.scitation.org/doi/10.1119/1.10903

M. Sandoval, L. Dagdug, Effective diffusion of confined active Brownian swimmers. Phys. Rev. E **90**, 062711 (2014). https://journals.aps.org/pre/abstract/10.1103/PhysRevE.90.062711

Chapter 24
Diffusion in Narrow Channels Embedded on Curved Manifolds

The emergence of the concept of *membrane fluidity* motivated the study of diffusion on curved manifolds of molecular components in biological membranes. The plasma membrane is composed of several different kinds of lipids and a great diversity of proteins, spatially and temporally organized as a requirement for the membrane's biological function. In fact, the two-dimensional diffusion coefficients of both lipids and proteins are at least two orders of magnitude lower than those of typical globular proteins.

The diffusion processes of molecules in cell membranes can also be hindered by the presence of impermeable lateral heterogeneities, patches, rafts, microdomains, holes, and tubular networks. Proteins that are anchors in membranes provide an example in which spatially restricted diffusion is important. Moreover, analysis of experimental data has revealed that, in some cases, diffusion proceeds at a different rate than conventional diffusion on the plane. As such, lateral diffusion of membrane components will resemble the problem of particles in a confined embedded channel on a curved surface.

Inspired by two-dimensional diffusion across the cell membrane, this chapter extends the generalization of the Kalinay-Percus projection method for asymmetric channels introduced in Chap. 20. To such end, we will project the anisotropic two-dimensional diffusion equation on a curved manifold into an effective one-dimensional generalized Fick-Jacobs equation that is modified according to the curvature of the surface. To have a complete description of this reduction, we also derive a general position-dependent effective diffusion coefficient and analyze a collection of systems having major symmetries.

For readers who are not familiar with differential geometry, we strongly recommend reading Appendix C before reading the last two chapters of this book.

L. Dagdug et al., *Diffusion Under Confinement*,
https://doi.org/10.1007/978-3-031-46475-1_24

24.1 Transformation of Differential Operators

The Brownian motion of particles in curved manifolds provides interesting insights on the diffusion process. The development of the theory describing this phenomena requires a detailed understanding of small particles moving throughout bounded domains in at least a two-dimensional system. Notwithstanding, in a number of interest, the transport of mass takes place along a privileged direction, such as in narrow channels or domains, which serve as an advantageous representation of an array of biological systems occurring on a curved surface in both nature and technology. The presence of such biological machinery extends from ion translocation through biological channels embedded in cell membranes, nanoscaled channels, and carbon nanotubes to artificial pores in thin solid films. As such, it naturally follows to characterize the problem in one effective direction, or more precisely, to conceive this problem as a quasi-one-dimensional problem by introducing a reduced or marginal concentration $\rho(x,t)$ (see Eq. (20.2)). The reduction of the diffusion equation to the effective one-dimensional problem has been studied in flat Euclidean spaces (for further examples, see Chaps. 18, 20, and 21). Intending to obtain the one-dimensional reduction of the diffusion equation together with the position-dependent diffusivity on curved manifolds, we analyze the covariant form of the diffusion equation by first considering a slightly more general equation, the Fokker-Planck equation, Eq. (2.12).

The N-dimensional Fokker-Planck equation can be written as follows:

$$\frac{\partial p(\mathbf{x},t)}{\partial t} = \left[-\frac{\partial}{\partial x_i}\zeta_i(\mathbf{x},t) + \frac{\partial^2}{\partial x_i \partial x_j} D_{ij}(\mathbf{x},t) \right] p(\mathbf{x},t), \tag{24.1}$$

where the propagator $p(\mathbf{x},t)$ now depends on N variables $\mathbf{x} = \{x_1, x_2, x_3, \cdots, x_N\}$, while $\zeta_i(\mathbf{x},t) = (\zeta_1(\mathbf{x},t), \cdots, \zeta_N(\mathbf{x},t))$ is the drift vector and D_{ij} the diffusion tensor. Let's say that we want to use other N variables $\mathbf{x}' = \{x_1', x_2', x_3, \cdots, x_N\}$ to express the Fokker-Planck equation, so that

$$x_i' = x_i'(x_1, x_2, x_3, \cdots, x_N, t), \tag{24.2}$$

for $i = 1, 2, 3, \cdots, N$, meaning that each variable x_i' is a function of the N non-primed variables, x_i, and time t.[1] This defines a *transformation of variables*, something that is commonly used in classical mechanics and dynamical systems. Physically, the probability of finding a particle in a volume element $\mathrm{d}^N x$ and its corresponding transformation $\mathrm{d}^N x'$ remains the same, namely,

[1] This relation could be inverted to find

$$x_i = x_i(x_1', x_2', x_3', \cdots, x_N', t), \qquad i = 1, 2, 3, \cdots, N. \tag{24.3}$$

$$p(\mathbf{x},t)\mathrm{d}^N x = p'(\mathbf{x}',t)\mathrm{d}^N x', \tag{24.4}$$

allowing us to find the probability density $p'(\mathbf{x}',t)$ in terms of $p(\mathbf{x},t)$ through the Jacobian J, which is given by

$$J = \frac{\partial(x_1,x_2,x_3,\cdots,x_N)}{\partial(x_1',x_2',x_3',\cdots,x_N')} = \epsilon_{i_1 i_2 i_3\cdots i_N}\frac{\partial x_i}{\partial x_1'}\frac{\partial x_2}{\partial x_{i_2}'}\frac{\partial x_3}{\partial x_{i_3}'}\cdots\frac{\partial x_N}{\partial x_{i_N}'}, \tag{24.5}$$

where $\epsilon_{i_1 i_2 i_3\cdots i_N}$ is the Levi-Civita symbol. Since $J = 1/J'$, the probability densities satisfy the equation

$$p'(\mathbf{x}',t) = \frac{p(\mathbf{x},t)}{J'} = Jp(\mathbf{x},t). \tag{24.6}$$

The next step is to find the derivative of the Jacobian and use the result to compute new differential operators. Given that that[2]

$$\frac{\partial x_i'}{\partial x_j}\frac{\partial x_j}{\partial x_k'} = \delta_{ik}, \tag{24.8}$$

with δ_{ik} being the Kronecker delta, the j,kth cofactor c^{jk} of an element $a_{ji} = \partial x_i'/\partial x_j$ of the Jacobian J' reads

$$c^{jk} = J'\frac{\partial x_j}{\partial x_k'}. \tag{24.9}$$

Furthermore, by invoking the *Laplace expansion* of a determinant,[3] we can assure that

[2] This is easily shown noting that, by direct partial differentiation, we have

$$\frac{\partial x_i'}{\partial x_j}\frac{\partial x_j}{\partial x_k'} = \frac{\partial x_i'}{\partial x_l'}. \tag{24.7}$$

Considering that both x_i' and x_j' are independent coordinates, the variation of x_i' with respect to x_j' must be zero if they are different, or one if they coincide.

[3] The Laplace expansion of a determinant provides an alternative method to calculate determinants: Considering a square matrix $B = (b_{ij})$ with $(b_{i1}, b_{i2}, b_{i3}, \cdots, b_{iN})$ a typical row, we can expand the determinant $\det(B)$ as a function of $b_{i1}, b_{i2}, b_{i3}, \cdots, b_{iN}$, yielding

$$\begin{aligned}\delta_{ij}\det B &= b_{i1}c^{j1} + b_{i2}c^{j2} + b_{i3}c^{j3} + \cdots + b_{iN}c^{jN}\\ &= b_{1i}c^{1j} + b_{2i}c^{2j} + b_{3i}c^{3j} + \cdots + b_{Ni}c^{Nj}.\end{aligned} \tag{24.10}$$

$$c^{jk} = \frac{\partial J'}{\partial a_{jk}}, \tag{24.11}$$

thus,

$$c^{jk} = \frac{\partial J'}{\partial a_{jk}} = J' \frac{\partial x_j}{\partial x'_k}. \tag{24.12}$$

Now, using the chain rule, together with Eqs. (24.6), (24.12), and $\partial J'/\partial x_i = \left[\partial J'/\partial a_{jk}\right]\left[\partial a_{jk}/\partial x_i\right]$, we find

$$-\frac{1}{J}\frac{\partial J}{\partial x_i} = \frac{\partial}{\partial x'_k}\frac{\partial}{\partial x'_k} x_i \text{ and } -\frac{1}{J}\left(\frac{\partial J}{\partial t}\right)_{\mathbf{x}} = \frac{\partial}{\partial x'_k}\left(\frac{\partial x'_k}{t}\right)_{\mathbf{x}}, \tag{24.13}$$

where the subscript $\mathbf{x}$ indicates partial derivative at constant $\mathbf{x}$. Additionally, we can compute the differential operator $\partial/\partial x_i$ similarly, namely,

$$\frac{\partial}{\partial x_i} = \frac{\partial}{\partial x'_k}\frac{\partial x'_k}{\partial x_i} + \frac{1}{J}\frac{\partial J}{\partial x_i}, \tag{24.14}$$

Using the chain rule once more, we obtain

$$\frac{\partial}{\partial x_i} = \frac{1}{J}\frac{\partial}{\partial x'_k}\frac{\partial x'_k}{\partial x_i} J. \tag{24.15}$$

Applying this last equation twice, we ultimately find

$$\frac{\partial^2}{\partial x_i x_j} = \frac{1}{J}\frac{\partial^2}{\partial x'_k \partial x'_r}\frac{\partial x'_k}{\partial x_i}\frac{\partial x'_r}{\partial x_j} J - \frac{1}{J}\frac{\partial}{\partial x'_k}\frac{\partial^2 x'_k}{\partial x_i \partial x_j} J. \tag{24.16}$$

The components of the time derivative,

$$\left(\frac{\partial}{\partial t}\right)_{\mathbf{x}} = \left(\frac{\partial}{\partial t}\right)_{\mathbf{x}'} + \left(\frac{\partial x'_k}{\partial t}\right)_{\mathbf{x}}\frac{\partial}{\partial x'_k}, \tag{24.17}$$

are carried out similarly, yielding

$$\left(\frac{\partial}{\partial t}\right)_{\mathbf{x}} = \frac{1}{J}\left(\frac{\partial}{\partial t}\right)_{\mathbf{x}'} J + \frac{1}{J}\frac{\partial}{\partial x'_k}\left(\frac{\partial x'_k}{\partial t}\right)_{\mathbf{x}} J. \tag{24.18}$$

Substituting Eqs. (24.15), (24.16), and (24.18) into Eq. (24.1), leads to

$$\left[\frac{1}{J}\left(\frac{\partial}{\partial t}\right)_{\mathbf{x}'} J + \frac{1}{J}\frac{\partial}{\partial x_k'}\left(\frac{\partial x_k'}{\partial t}\right)_{\mathbf{x}}\right] p(\mathbf{x},t) = -\frac{1}{J}\frac{\partial}{\partial x_k'}\frac{\partial x_k'}{\partial x_i} J\ \zeta_i(\mathbf{x},t)p(\mathbf{x},t)$$

$$+\frac{1}{J}\frac{\partial^2}{\partial x_k'\partial x_t'}\frac{\partial x_k'}{\partial x_i}\frac{\partial x_t'}{\partial x_j} J\ D_{ij}(\mathbf{x},t)p(\mathbf{x},t)$$

$$-\frac{1}{J}\frac{\partial}{\partial x_k'}\frac{\partial^2 x_k'}{\partial x_i\partial x_j} J\ D_{ij}(\mathbf{x},t)p(\mathbf{x},t). \tag{24.19}$$

By implementing Eq. (24.6) into this last equation and rearranging the terms, we obtain

$$\left(\frac{\partial p'(\mathbf{x}',t)}{\partial t}\right)_{\mathbf{x}'} = -\frac{\partial}{\partial x_k'}\left[\left(\frac{\partial x_k'}{\partial t}\right)_{\mathbf{x}} + \frac{\partial x_k'}{\partial x_i}\zeta_i(\mathbf{x},t) + \frac{\partial^2 x_k'}{\partial x_i\partial x_j}D_{ij}(\mathbf{x},t)\right] p'(\mathbf{x}',t)$$

$$+\frac{\partial^2}{\partial x_k'\partial x_r'}\frac{\partial x_k'}{\partial x_i}\frac{\partial x_r'}{\partial x_j}D_{ij}(\mathbf{x},t)p'(\mathbf{x}',t), \tag{24.20}$$

which by making

$$D_{kr}' = \frac{\partial x_k'}{\partial x_i}\frac{\partial x_r'}{\partial x_j}D_{ij}(\mathbf{x},t), \tag{24.21}$$

$$\boldsymbol{\zeta}_k' = \left(\frac{\partial x_k'}{\partial t}\right)_{\mathbf{x}} + \frac{\partial x_k'}{\partial x_i}\zeta_i(\mathbf{x},t) + \frac{\partial x_k'}{\partial x_i x_j}D_{ij}(\mathbf{x},t), \tag{24.22}$$

we can finally write the Fokker-Planck equation with the new variables $\mathbf{x}'$, i.e.,

$$\left(\frac{\partial p'(\mathbf{x}',t)}{\partial t}\right)_{\mathbf{x}'} = \left(-\frac{\partial}{\partial x_k'}\boldsymbol{\zeta}_k' + \frac{\partial^2}{\partial x_k'\partial x_r'}D_{kr}'\right) p'(\mathbf{x}',t). \tag{24.23}$$

From this last relation, we can obtain the diffusion equation in the absence of drift by setting $\boldsymbol{\zeta}_k'$ equal to zero, namely,

$$\left(\frac{\partial p'(\mathbf{x}',t)}{\partial t}\right)_{\mathbf{x}'} = \frac{\partial^2}{\partial x_k'\partial x_r'}D_{kr}'p'(\mathbf{x}',t). \tag{24.24}$$

In the following section, we will introduce the elements required to write the covariant form of the diffusion equation.

24.2 Covariant Form of the Diffusion Equation

Consider a proper coordinate transformation independent of time, namely,[4]

$$x_i' = x'^i(x^1, x^2, x^3, \cdots, x^N), \tag{24.25}$$

$$x^i = x^i(x'^1, x'^2, x'^3, \cdots, x^N), \tag{24.26}$$

provided that it is continuous and can be inverted. This is equivalent to saying that the Jacobian J in finite and different from zero. Under this statement, the differential of the coordinates obeys the linear transformation law:

$$\mathrm{d}x'^i = \frac{\partial x'^i}{\partial x^j}\mathrm{d}x^j, \tag{24.27}$$

or,

$$\mathrm{d}\mathbf{x}' = \boldsymbol{\epsilon}_j \mathrm{d}x^j, \tag{24.28}$$

with $\boldsymbol{\epsilon}_j = \left(\frac{\partial x'^j}{\partial x^1}, \frac{\partial x'^j}{\partial x^2}, \frac{\partial x'^j}{\partial x^3}, \cdots, \frac{\partial x'^j}{\partial x^N}\right)$, i.e., a prototype of the contravariant surface vector. In addition, we say that A'^i is a contravariant surface vector if, in the coordinate system $\mathbf{x}'$, its components are given by

$$A'^i = \frac{\partial x'^i}{\partial x^j}A^j, \tag{24.29}$$

while covariant surface vectors transform according to

$$A_i' = \frac{\partial x^j}{\partial x'^i}A_j. \tag{24.30}$$

Similarly, for any (scalar) function $f = f(\mathbf{x})$ defined in the domain, its partial derivatives transform as follows:

$$\frac{\partial f}{\partial x'^i} = \frac{\partial x^j}{\partial x'^i}\frac{\partial f}{\partial x^j}, \tag{24.31}$$

which defines the gradient, giving a covariant vector. Moreover, a scalar is not changed by a coordinate transformation, that is, $f' = f$.

The transformation of the diffusion tensor $\bar{D}^{ij} = D_{ij}$, a tensor of rank 2 having two contravariant indices, giving a purely contravariant tensor, reads

[4] The new coordinates are in general nonlinear functions of the old coordinates, such as spherical coordinates (see Appendix B).

$$\bar{D}'^{kr} = \frac{\partial x'^k}{\partial x_i}\frac{\partial x'^r}{\partial x_j}\bar{D}^{ij}, \tag{24.32}$$

as anticipated by Eq. (24.21).

We now need the probability density, since $p'(\mathbf{x}', t)\,\mathrm{d}^N x'$ is a dimensionless invariant number and must transform as a scalar does. Given that $p(\mathbf{x}, t)$ cannot be used as a scalar, we need something that is analogous to this quantity to continue with the covariant description. Let us follow the classical approach by making

$$\bar{p}(\mathbf{x}, t) \equiv \sqrt{\mathrm{Det}}\; p(\mathbf{x}, t), \tag{24.33}$$

with $\mathrm{Det} \equiv \det(\bar{D}^{ij})$, on the condition that the determinant of the diffusion matrix is real, and not negative or null. By looking at Eq. (24.32), we conclude that[5]

$$\mathrm{Det}' = \frac{\mathrm{Det}}{J^2}, \tag{24.35}$$

meaning that $\bar{p}(\mathbf{x}, t)$ is in fact a scalar. In addition, we implement the covariant divergence:

$$\bar{V}^i_{;i} \equiv \mathrm{Det}\frac{\partial}{\partial x^i}\frac{\bar{V}^i}{\mathrm{Det}} \tag{24.36}$$

and the covariant gradient of a scalar f:

$$f_{;i} = \frac{\partial f}{\partial x^i}, \tag{24.37}$$

where $\bar{V}^i$ is the contravariant probability flux (for the flat Euclidean diffusion with drift system, see Eq. (6.1) and its simplification to that of the diffusion equation in Eq. (2.73)), which in this case is given by

$$\bar{V}^i = -\bar{D}^{ij}\frac{\partial \bar{p}(\mathbf{x}, t)}{\partial x^j}. \tag{24.38}$$

Then, by using Eqs. (24.33), (24.36)–(24.38), we find

$$\begin{aligned}\frac{\partial \bar{p}(\mathbf{x}, t)}{\partial t} &= -\bar{V}^i_{;i}\left[\bar{D}^{ij}\frac{\partial \bar{p}(\mathbf{x}, t)}{\partial x^i}\right]_; \\ &= \sqrt{\mathrm{Det}}\frac{\partial}{\partial x^i}\frac{1}{\sqrt{\mathrm{Det}}}\bar{D}^{ij}\frac{\partial \bar{p}(\mathbf{x}, t)}{\partial x^j},\end{aligned} \tag{24.39}$$

[5] Note that for square matrices of equal size A and B, the product AB fulfills the following relation:

$$\det(AB) = \det(A)\det(B). \tag{24.34}$$

which is the covariant form of the diffusion equation. Furthermore, the diffusion matrix $\bar{D}^{ij}$ is associated with the contravariant metric tensor g^{ij}, namely,

$$g^{ij} = \bar{D}^{ij}, \tag{24.40}$$

and therefore, the covariant metric tensor g_{ij} is the inverse of the diffusion matrix:

$$g_{ij} = (D^{-1})_{ij}, \tag{24.41}$$

a relation that, when using Eq. (24.34), leads to $\sqrt{\text{Det}} = \sqrt{g}$, with $g = \det(g_{ij})$. In other words, on a curved surface, diffusion will always be inherently anisotropic.

The main reason for writing a manifestly covariant diffusion equation is that, as presumed, all relations expressing physical assets should be manifestly covariant, since all physical properties should be independent of any coordinates. Afterward, we write Eq. (24.39) for a two-dimensional system and use the Kalinay-Percus projection method to obtain the quasi-one-dimensional problem.

24.3 2D Asymmetric Channel in Curved Surfaces: Projection Method

24.3.1 Fick-Jacobs Equation on Curved Surfaces

Consider the manifestly covariant form of the diffusion equation in the two-dimensional coordinate system $\mathbf{x} = \{\xi, \eta\}$. In the anisotropic case, the diffusion matrix can be arranged as the following diffusion tensor:

$$D^i_j = \begin{pmatrix} D_\xi & 0 \\ 0 & D_\eta \end{pmatrix}, \tag{24.42}$$

while the metric tensor is defined as

$$g_{ij} = \begin{pmatrix} g_1(\xi) & 0 \\ 0 & g_2(\xi) \end{pmatrix}, \qquad g^{ij} = \begin{pmatrix} g_1^{-1}(\xi) & 0 \\ 0 & g_2^{-1}(\xi) \end{pmatrix}. \tag{24.43}$$

Moreover, let us introduce the anisotropy into the diffusion constant by $D_\xi \neq D_\eta$. Note that when writing the last two equations, we have implicitly chosen $x_1 = \xi$ as the privileged direction for the diffusion process and imposed $x_2 = \eta$ as the fast equilibrium in the transverse direction. Then, we are able to write Eq. (24.39) using Eqs. (24.33) and (24.41) as follows:

$$\frac{\partial \bar{p}(\xi, \eta, t)}{\partial t} = \frac{1}{\sqrt{g}} \frac{\partial}{\partial x^i} \sqrt{g} D^i_j g^{jk} \frac{\partial \bar{p}(\xi, \eta, t)}{\partial x^k}, \tag{24.44}$$

where x_i are the local coordinates on the surface. More specifically, the diffusion equation on the curved two-dimensional surface, in local coordinates, is the isotropic diffusion. The diffusion tensor is proportional to the identity $D^i_j = D\delta^i_j$, denoting that the corresponding diffusion equation is obtained by substituting the Laplacian operator in Eq. (2.13) for the Laplace-Beltrami operator, i.e., $\nabla^2_g = \frac{1}{\sqrt{g}}\partial_i\left(\sqrt{g}g^{ij}\partial_j\right)$:

$$\frac{\partial \bar{p}(\xi,\eta,t)}{\partial t} = \frac{D_\xi}{\sqrt{g_1 g_2}}\frac{\partial}{\partial \xi}\left[\sqrt{\frac{g_2}{g_1}}\frac{\partial}{\partial \xi}\bar{p}(\xi,\eta,t)\right] + \frac{D_\eta}{\sqrt{g_1 g_2}}\sqrt{\frac{g_1}{g_2}}\frac{\partial^2}{\partial \eta^2}\bar{p}(\xi,\eta,t). \tag{24.45}$$

Once we have managed to write Eq. (24.45), the goal is to derive the position-dependent diffusion coefficient for narrow asymmetric channels embedded on a curved manifold by means of the mapping procedure presented in Chap. 20. We will refer to Chap. 20 for certain mathematical steps, since most of the computations are quite similar to those performed previously.

Due to the reasons outlined above, η is the variable to be integrated to obtain the marginal probability distribution $\rho(\xi,t)$, namely,

$$\rho(\xi,t) = \int_{h_1(\xi)}^{h_2(\xi)} \bar{p}(\xi,\eta,t)\,\mathrm{d}\eta, \tag{24.46}$$

where $h_1(\xi)$ and $h_2(\xi)$ are the lower and upper boundaries of the channel, i.e., $h_2(\xi) > \eta > h_1(x)$. Using the Leibniz integral rule, Eq. (A.9), we obtain (see Eq. (20.5))

$$\begin{aligned}\frac{\partial \rho(\xi,t)}{\partial t} = \frac{D_\xi}{\sqrt{g_1 g_2}}\Bigg\{ & \frac{\partial}{\partial \xi}\sqrt{\frac{g_2}{g_1}}\rho(\xi,t) \\ & - \frac{\partial}{\partial \xi}\sqrt{\frac{g_2}{g_1}}\left[h_2'(\xi)\,\bar{p}(\xi,h_2(\xi),t) - h_1'(\xi)\,\bar{p}(\xi,h_1(\xi),t)\right] \\ & - \left[h_2'(\xi)\sqrt{\frac{g_2}{g_1}}\frac{\partial \bar{p}(\xi,\eta,t)}{\partial t}\bigg|_{h_2(\xi)} - h_1'(\xi)\sqrt{\frac{g_2}{g1}}\frac{\partial \bar{p}(\xi,\eta,t)}{\partial \xi}\bigg|_{h_1(\xi)}\right]\Bigg\} \\ & + \frac{D_\eta}{g_2}\frac{\partial^2 \bar{p}(\xi,\eta,t)}{\partial \eta}\bigg|_{h_1(\xi)}^{h_2(\xi)}.\end{aligned} \tag{24.47}$$

Now, we obtain the boundary conditions (BCs) from the flux components in a manifold, which are determined by (see Eq. (24.38))

$$J^i = -D_j^{\xi} \frac{1}{g_1} \frac{\partial \bar{p}(\xi, \eta, t)}{\partial \xi} - D_{\eta}^{i} \frac{1}{g_2} \frac{\partial \bar{p}(\xi, \eta, t)}{\partial \eta}. \tag{24.48}$$

Following the same process, we used to obtain Eq. (25.14), we find

$$\frac{D_\eta}{g_2} \frac{\partial \bar{p}(\xi, \eta, t)}{\partial \eta}\bigg|_{h_n(\xi)} = \frac{D_\xi h_n'(\xi)}{g_1} \frac{\partial \bar{p}(\xi, \eta, t)}{\partial \xi}\bigg|_{h_n(\xi)}, \qquad n = 1, 2, \tag{24.49}$$

where the $\hat{v}_n$ unit vector tangent to the upper ($n = 2$) and lower ($n = 1$) boundaries is now given by

$$\hat{v}_n = \frac{\hat{\xi}^i + h_n'(\xi)\hat{\eta}^i}{\sqrt{1 + h_n'(\xi)^2}}. \tag{24.50}$$

By inserting Eq. (24.49) into Eq. (24.47), we are led to

$$\begin{aligned} \frac{\partial \rho(\xi, t)}{\partial t} = \frac{D_\xi}{\sqrt{g_1 g_2}} \Bigg\{ \frac{\partial}{\partial \xi} \left[\sqrt{\frac{g_2}{g1}} \frac{\partial}{\partial \xi} \rho(\xi, t) \right] \\ - \frac{\partial}{\partial \xi} \sqrt{\frac{g_2}{g_1}} \left[h_2'(\xi)\, \bar{p}(\xi, h_2(\xi), t) - h_1'(\xi)\, \bar{p}(\xi, h_1(\xi), t) \right] \Bigg\}. \end{aligned} \tag{24.51}$$

The first approximation is obtained when we provide an infinite transverse diffusion rate, an artificial anisotropy, assuming that $D_\eta \gg D_\xi$. From Eq. (24.46), we see that

$$\bar{p}(\xi, \eta, t) = \frac{\rho(\xi, t)}{h_2(\xi) - h_1(\xi)}. \tag{24.52}$$

This allows us to simplify Eq. (24.51), yielding the Fick-Jacobs-like equation on a symmetric curved surface, namely,

$$\frac{\partial \rho(\xi, t)}{\partial t} = \frac{D_\xi}{\sqrt{g_1 g_2}} \frac{\partial}{\partial \xi} \left[\sqrt{\frac{g_2}{g_1}} w(\xi) \frac{\partial}{\partial \xi} \frac{\rho(\xi, t)}{w(\xi)} \right], \tag{24.53}$$

where we used $w(\xi) \equiv h_2(\xi) - h_1(\xi)$ as the function of the channel's width. Note the similarity between the latter equation and Eq. (20.15). In the rest of the chapter, we will focus on obtaining the recurrence formula for operators $\hat{\sigma}_j(\xi, \eta, \partial_\xi)$.

24.3.2 Recurrence Formula for Operators $\hat{\sigma}_j(\xi, \eta, \partial_\xi)$

Kalinay and Percus suggested an operator procedure to map the solutions of Eq. (24.53) into the space of solutions to the original two-dimensional problem.

The intention of this section is to obtain the corrections of the Fick-Jacobs-like equation on curved surfaces, Eq. (24.53). Using the same approach as the one shown in Sect. 20.1, we define the parameter of anisotropy as the ratio of the two diffusion coefficients, i.e., $\epsilon = D_\xi/D_\eta$, and construct $\bar{p}(\xi,\eta,t)$ as a perturbation series, namely,

$$\bar{p}(\xi,\eta,t) = \sum_{j=0}^{\infty} \epsilon^j \boldsymbol{\sigma}_j(\xi,\eta,t), \tag{24.54}$$

where $\boldsymbol{\sigma}(\xi,\eta,t)$ will have the form of some operators acting on $\rho(\xi,t)$ in order to make Eq. (24.51) self-consistent:

$$\boldsymbol{\sigma}_j(\xi,\eta,t) = \hat{\boldsymbol{\sigma}}_j(\xi,\eta,\partial_\xi)\frac{\partial}{\partial\xi}\frac{\rho(\xi,t)}{w(\xi)}. \tag{24.55}$$

The first operator $j = 0$ is simply $\hat{\boldsymbol{\sigma}}_0(\xi,\eta,\partial_\xi)\frac{\partial}{\partial\xi} = 1$. Using Eq. (24.54), Eq. (24.53) translates to

$$\begin{aligned}\frac{\partial\rho(\xi,t)}{\partial t} = \frac{D_\xi}{\sqrt{g_1 g_2}}\frac{\partial}{\partial\xi}\sqrt{\frac{g_1}{g_2}}\Bigg\{w(\xi) - \sum_{j=1}^{\infty}\epsilon^j\Big[h_2'(\xi)\,\hat{\boldsymbol{\sigma}}_j(\xi,h_2(\xi),\partial_\xi)\\ - h_1'(\xi)\,\hat{\boldsymbol{\sigma}}_j(\xi,h_1(\xi),\partial_\xi)\Big]\Bigg\}\frac{\partial}{\partial\xi}\frac{\rho(\xi,t)}{w(\xi)}.\end{aligned} \tag{24.56}$$

With the present methods, we are able to find the recurrence relation for operators $\hat{\boldsymbol{\sigma}}(\xi,\eta,\partial_\xi)$. To do this, we use Eqs. (24.54) and (24.55) to rewrite (24.45) and then substitute $\partial\rho(\xi,t)/\partial t$ as seen in Eq. (24.56), yielding

$$\begin{aligned}\frac{1}{g_2}\frac{\partial^2}{\partial\eta^2}\hat{\boldsymbol{\sigma}}_{j+1}(\xi,\eta,\partial_\xi) = &-\sum_{k=1}^{j}\hat{\boldsymbol{\sigma}}_{j-k}(\xi,\eta,\partial_\xi)\frac{\partial}{\partial\xi}\frac{1}{\sqrt{g_1 g_2}w(x)}\frac{\partial}{\partial\xi}\sqrt{\frac{g_2}{g_1}}\\ &\times\Big[h_2'(\xi)\,\hat{\boldsymbol{\sigma}}_k(\xi,h_2(\xi),\partial_\xi) - h_1'(\xi)\,\hat{\boldsymbol{\sigma}}_k(\xi,h_2(\xi),\partial_\xi)\Big]\\ &+\hat{\boldsymbol{\sigma}}_j(\xi,\eta,\partial_\xi)\frac{\partial}{\partial\xi}\frac{1}{\sqrt{g_1 g_2}w(\xi)}\frac{\partial}{\partial\xi}\sqrt{\frac{g_2}{g_1}}w(\xi)\\ &-\frac{1}{\sqrt{g_1 g_2}}\frac{\partial}{\partial\xi}\sqrt{\frac{g_2}{g_1}}\frac{\partial}{\partial\xi}\hat{\boldsymbol{\sigma}}_j(\xi,\eta,\partial_\xi).\end{aligned} \tag{24.57}$$

A double integration over η will allow us to calculate $\hat{\boldsymbol{\sigma}}_{j+1}(\xi, \eta, \partial_\xi)$ at any order. The first integration constant is set to fulfill the boundary condition (BC) in Eq. (24.49), while the second integration constant provides a normalization condition, yielding

$$\int_{h_1(\xi)}^{h_2(\xi)} \hat{\boldsymbol{\sigma}}_j(\xi, \eta, t) \frac{\partial}{\partial \xi} \frac{\rho(\xi, t)}{w(\xi)} \, \mathrm{d}\eta = 0, \qquad j > 0. \tag{24.58}$$

The reader should be aware of the similarity between Eqs. (20.20) and (24.56) and Eqs. (20.24) and (24.57). More generally, each of the steps carried out in Chap. 20, and therefore those in Sect. 20.1.3, can be implemented in this case where diffusion occurs on a curved manifold. We show the first operator of this recurrence scheme:

$$\begin{aligned} \hat{\boldsymbol{\sigma}}_1(\xi, \eta, \partial_\xi) = \frac{g_2}{g_1 w(\xi)} \Bigg\{ \Big[y_0'(\xi) - \eta \Big] \Big[h_1(\xi) h_2'(\xi) - h_2 h_1'(\xi) \Big] \\ + \frac{w'(\xi)}{2} \left[\eta^2 - \frac{1}{3} \Big(h_1^2 + h_1(\xi) h_2(\xi) + h_2^2(\xi) \Big) \right] \Bigg\}, \end{aligned} \tag{24.59}$$

where the midline derivative is defined as $y_0'(\xi) = [h_2'(\xi) + h_1'(\xi)]/2$. Note that we can obtain Eq. (24.59) simply by multiplying the ratio of the components of the metric tensor g_2/g_1 times Eq. (20.33). This means that the effect of diffusing on a curved surface translates to a scaling in the Euclidean flat corrections of the propagator obtained in Chap. 20. In the following section, we provide the steps to determine the position-dependent diffusion coefficient.

24.3.3 The Position-Dependent Effective Diffusion Coefficient

Let us write Eq. (24.56) as follows:

$$\frac{\partial \rho(\xi, t)}{\partial t} = D_0 \frac{\partial}{\partial \xi} w(\xi) [1 - \epsilon \hat{\mathbf{Z}}(\xi, \partial_\xi)] \frac{\partial}{\partial \xi} \frac{\rho(\xi, t)}{w(\xi)}, \tag{24.60}$$

where $\hat{\mathbf{Z}}$ is an operator. In the steady state, there is no difference between using this operator and the diffusion coefficient $D(\xi)$. Therefore, both equations represent the same physical phenomena, i.e., a 1D mass conservation law, enabling us to write the flux as

$$J = -w(\xi) D(\xi) \frac{\partial}{\partial \xi} \frac{\rho(\xi)}{w(\xi)}, \tag{24.61}$$

as well as

$$J = -w(\xi)\left[1 - \epsilon\hat{\mathbf{Z}}(\xi, \partial_\xi)\right]\frac{\partial}{\partial\xi}\frac{\rho(\xi)}{w(\xi)}. \tag{24.62}$$

In order to find $D(\xi)$, we combine these last two equations, finding that

$$1 = w(\xi)\left[1 - \epsilon\hat{\mathbf{Z}}(\xi, \partial_{xi})\right]\frac{1}{w(\xi)D(\xi)}, \tag{24.63}$$

which, as it turns out, has the exact same structure of Eq. (20.42). Thus, we can be certain that, on a curved surface, we will obtain

$$D(\xi) \simeq 1 - \epsilon w(\xi)\hat{\mathbf{Z}}(\xi, \partial_\xi)\frac{1}{w(\xi)}, \tag{24.64}$$

as we did in the flat Euclidean space.

The first-order correction is obtained by setting $D_\xi = D_0$, together with $\epsilon = 1$, in the use of Eq. (24.60), yielding

$$\begin{aligned} D_\xi &= D_0\left[1 - \left(\sqrt{\frac{g_2}{g_1}}y_0'(\xi)\right)^2 - \frac{1}{3}\left(\sqrt{\frac{g_2}{g_1}}\frac{w'(\xi)}{2}\right)^2\right] \\ &\simeq \frac{D_0}{1 + \left(\sqrt{\frac{g_2}{g_1}}y_0'(\xi)\right)^2 + \frac{1}{3}\left(\sqrt{\frac{g_2}{g_1}}\frac{w'(\xi)}{2}\right)^2}, \end{aligned} \tag{24.65}$$

which is analogous to Bradley's result (see Table 20.1). The effective diffusion coefficient up to the second order reads

$$\begin{aligned} D(\xi) = D_0\Bigg[1 &- \left(\sqrt{\frac{g_2}{g_1}}y_0'(\xi)\right)^2 - \frac{1}{3}\left(\sqrt{\frac{g_2}{g_1}}\frac{w'(\xi)}{2}\right)^2 + \left(\sqrt{\frac{g_2}{g_1}}y_0'(\xi)\right)^4 \\ &+ 2\left(\sqrt{\frac{g_2}{g_1}}y_0'(\xi)\right)^2\left(\sqrt{\frac{g_2}{g_1}}\frac{w'(\xi)}{2}\right)^2 + \frac{1}{5}\left(\sqrt{\frac{g_2}{g_1}}\frac{w'(\xi)}{2}\right)^4 - \cdots\Bigg]. \end{aligned} \tag{24.66}$$

By neglecting the second and higher derivatives of $w(\xi)$ and $y_0(\xi)$, we arrive at

$$D(\xi) = D_0\sum_{n=0}^{\infty}\frac{(-1)^n}{2n+1}\sum_{i=0}^{2n}\left[\sqrt{\frac{g_2}{g_1}}\left(y_0'(\xi) + \frac{w'(\xi)}{2}\right)\right]^i\left[\sqrt{\frac{g_2}{g_1}}\left(y_0'(\xi) - \frac{w'(\xi)}{2}\right)\right]^{2n-i}. \tag{24.67}$$

The last expression can be reduced to

$$D(\xi) = \frac{D_0}{w'(\xi)}\sqrt{\frac{g_2}{g_1}}\left\{\arctan\left[\sqrt{\frac{g_2}{g_1}}\left(y_0'(\xi) + \frac{w'(\xi)}{2}\right)\right]\right.$$
$$\left. - \arctan\left[\sqrt{\frac{g_2}{g_1}}\left(y_0'(\xi) - \frac{w'(\xi)}{2}\right)\right]\right\}. \tag{24.68}$$

This last equation is the main result of the study of diffusion in narrow channels embedded on curved manifolds. Moreover, by making $g_2 = g_1$, Eq. (20.51) is recovered, meaning that Eq. (24.68) is a general expression for the effective diffusion coefficient along the slow coordinate ξ. It recovers all the well-known approximations for the effective diffusion coefficient for both symmetric and asymmetric 2D channels, either in a flat Euclidean space or in a curved manifold.

24.4 Narrow Channels on Curved Manifolds

In this section, we study the effective diffusion coefficient for a narrow channel embedded on different curved surfaces, specifically on a cylinder, a sphere, and a torus. As previously outlined in the introduction, surfaces of this kind play a significant role in physical and biophysical systems. To such end, we need to determine the width $w(\xi)$ and the midline $y_0(\xi)$ functions for the chosen channel, with ξ being the longitudinal coordinate across the surface. This process is carried out using the components of the metric, namely, g_1 and g_2.

Generally, the metric tensor is determined by

$$g_{ij} = \sum_{kl} \delta_{kl} \frac{\partial x^k}{\partial q'^i} \frac{\partial x^l}{\partial x'^j} = \sum_k \frac{\partial x^k}{\partial x'^i} \frac{\partial x^k}{\partial x'^j}, \tag{24.69}$$

or, in its matrix form, by

$$g = J^T J. \tag{24.70}$$

The notation J^T indicates that we have to take the transpose of the Jacobian matrix. For instance, the Euclidean metric tensor is written as

$$g = \begin{pmatrix} 1 & 0 \\ 0 & 1 \end{pmatrix}. \tag{24.71}$$

However, due to the physical reasons, we are interested in the *induced metric*. The induced metric will allow us to define distances on a surface (submanifold) that is embedded in a higher-dimensional space (manifold), a task that is accomplished by restricting the original metric to the tangent space of the surface. The induced metric

is computed as follows:

$$g_{ij}^{\text{induced}} = \sum_k \mathbf{e}_{\mathbf{t}i} \cdot \mathbf{e}_{\mathbf{t}j}, \tag{24.72}$$

where the tangent vectors to the surface are given by

$$\mathbf{e}_{\mathbf{t}i} = \frac{\partial x^k}{\partial x'^i} \text{ and } \mathbf{e}_{\mathbf{t}j} = \frac{\partial x^k}{\partial x'^j}. \tag{24.73}$$

The components of the induced metric, g_{ij}^{induced}, will be the required input in Eq. (24.68) to find a closed form of the effective diffusion coefficient $D(\xi)$. Additionally, along the computation of the induced metric, we will rely on the fact that, assuming orthogonal tangent vectors in the off-diagonal components, $g_{ij}^{\text{induced}} = 0$ for $i \neq j$, meaning that we only have to calculate the diagonal components of the tensor. These specifications fit perfectly for the curved surfaces discussed in this chapter.

Initially, it is essential to establish a parametric relation between x^i and x'^i to characterize the surface (from flat Euclidean coordinates x^i to curved coordinates x'^i, in this practical case).

Let us consider a cylinder with constant radius r having a narrow channel oriented along the angular variable θ.[6] The connection of Cartesian coordinates (x, y, z) and cylindrical coordinates (r, θ, z) is given by (see Appendix B, Sect. B.2)

$$x = r\,\cos\theta, \qquad y = r\,\sin\theta, \qquad z = z, \tag{24.75}$$

where the parametric variables will be (θ, z) with $0 \leq \theta \leq 2\pi$ and $-\infty < z < \infty$. Thus, by using Eq. (24.72) together with Eq. (24.73), we obtain

$$\begin{aligned} g_{11} = g_1 &= \left(\frac{\partial x}{\partial \theta}\right)^2 + \left(\frac{\partial y}{\partial \theta}\right)^2 + \left(\frac{\partial z}{\partial \theta}\right)^2 \\ &= (-r\sin\phi)^2 + (r\cos\theta)^2 + 0 = r^2 \end{aligned} \tag{24.76}$$

[6] In principle, we can orient the channel along the z-axis, as well as around the cylinder, yielding different results for Eq. (24.68) (the factor $\sqrt{g_i/g_j}$ is set, with $i = 1$ and $j = 2$, depending on the orientation of the channel). Nonetheless, the reader should be able to verify that, for a cylinder oriented along the z-axis having a narrow channel of varying width formed by straight walls defined as

$$\theta_1(z) = m_1\frac{z}{r} - \theta_0, \text{ and } \theta_2(z) = m_2\frac{z}{r} + \theta_0, \tag{24.74}$$

the resulting $D(z)$ is likewise defined by Eq. (24.85).

and

$$g_{22} = g_2 = \left(\frac{\partial x}{\partial z}\right)^2 + \left(\frac{\partial y}{\partial z}\right)^2 + \left(\frac{\partial z}{\partial z}\right)^2 = 1 \tag{24.77}$$

yielding

$$g_{\text{cyl}} = \begin{pmatrix} r^2 & 0 \\ 0 & 1 \end{pmatrix}. \tag{24.78}$$

An identical procedure is implemented for spheres and tori. In the case of a sphere of constant radius r having a narrow channel oriented in the θ-direction, where the parameterized coordinates are (θ, ϕ), with $0 \leq \theta \leq \pi$ and $0 \leq \phi \leq 2\pi$, we have (see Appendix B, Sect. B.3)

$$x = r\sin\theta\cos\phi, \qquad y = r\sin\theta\sin\phi, \qquad z = r\cos\theta. \tag{24.79}$$

Therefore, the induced metric is

$$g_{11} = g_1 = (r\cos\theta\cos\phi)^2 + (r\cos\theta\sin\phi)^2 + (-r\sin\theta)^2 = r^2 \tag{24.80}$$

and

$$g_{22} = g_2 = (-r\sin\theta\sin\phi)^2 + (r\sin\theta\cos\phi)^2 = r^2\sin^2\theta, \tag{24.81}$$

leading to

$$g_{\text{sph}} = \begin{pmatrix} r^2 & 0 \\ 0 & r^2\sin^2\theta \end{pmatrix} \tag{24.82}$$

Finally, a torus of radii a and b (with $a > b$) is parameterized as

$$x = (a + b\cos\theta)\cos\phi, \qquad y = (a + b\cos\theta)\sin\phi, \qquad z = b\sin\theta, \tag{24.83}$$

where, again, (θ, ϕ) are the surface parameters both ranging from 0 to 2π, while θ is chosen as the privileged direction. Thus,

$$g_{\text{torus}} = \begin{pmatrix} b^2 & 0 \\ 0 & (a + b\cos\theta)^2. \end{pmatrix} \tag{24.84}$$

Equations (24.78), (24.82), and (24.84) will be used in the following sections, where we compute the diffusion coefficient for special systems.

24.4.1 Cylindrical Surface

In the case of a cylindrical surface, the induced metric is given by Eq. (24.78). If we focus on a channel of varying width formed by straight walls defined by $f_1(\theta) = m_1 r\theta - z_0$ and $f_2(\theta) = m_2 r\theta + z_0$, then, by direct computation, the position-dependent diffusion coefficient is

$$D_{\text{cyl}}(\theta) = \frac{\arctan(m_2) - \arctan(m_1)}{m_2 - m_1} D_0, \tag{24.85}$$

which is the same result obtained for the flat surface case, Eq. (20.55). This is because the metric components are constants with zero curvature.

24.4.2 Spherical Surface

In this section, we examine the effective diffusion on the surface of a sphere, which its induced metric being given by Eq. (24.82). Each value of r is considered fixed and only θ varies. We consider both the symmetrical and asymmetrical conical channels. In the case of a symmetric channel, the upper boundary is given by $f_2(\theta) = r(m\theta + \phi_0)$, while the lower boundary is $f_2(\theta) = -f_1(\theta)$, leading to

$$D_{\text{sph}}(\theta) = \frac{\arctan(rm \sin\theta)}{rm \sin\theta} D_0, \tag{24.86}$$

where, in comparison with flat Euclidean geometry, we have additional dependence on both r and θ. In Fig. 24.1, we show a schematic representation of this system together with representative plots of the effective diffusion coefficient, as a function of the angular variable for different values of the radius. The dependence on θ of the diffusion coefficient increases as the effective diffusion decreases. This behavior is also observed for large radii. Moreover, for large radii, the flat surface solution is recovered, whereas for small angles, the boundaries have no influence on the dynamics of the particles, yielding to free diffusion.

For the asymmetrical simple conical channel, we set $f_1(\theta) = r(m_1\theta - \phi_0)$ and $f_2(\theta) = r(m_2\theta + \phi_0)$ (see Fig. 24.2 for a graphic representation of the channel). Therefore,

$$D_{\text{sph}}(\theta) = \frac{\arctan(rm_1 \sin\theta) - \arctan(rm_2 \sin\theta)}{r(m_1 - m_2)\sin\theta} D_0. \tag{24.87}$$

Representative plots of the latter equation are shown in Fig. 24.3, where we kept constant the upper slope m_2 while varying the lower slope m_1. The typical behavior of the flat surface is recovered when r is large enough.

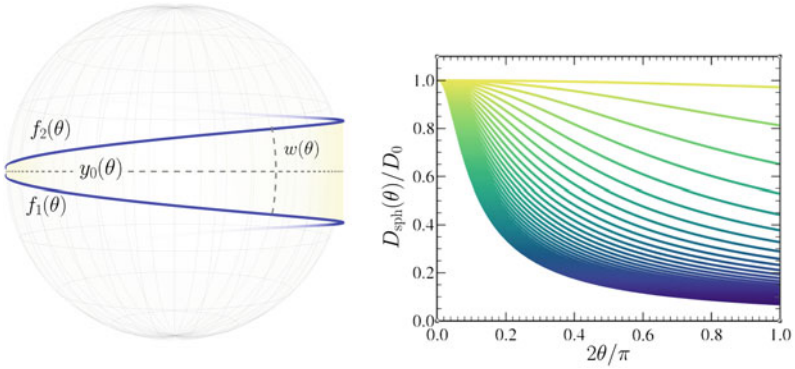

Fig. 24.1 On the left-hand side, we see an schematic representation of the system, a symmetric channel with straight walls, $f_1(\theta)$ and $f_2(\theta)$, and midline $y_0(\theta)$ embedded in a spherical surface, i.e., a *conical channel*. The dependence of the angular coordinate θ can be seen in the varying width $w(\theta)$ of the channel. On the right-hand side, we present the diffusion coefficient as a function of $2\theta/\pi$. The yellow color is for small radii, changing to blue as the radius increases

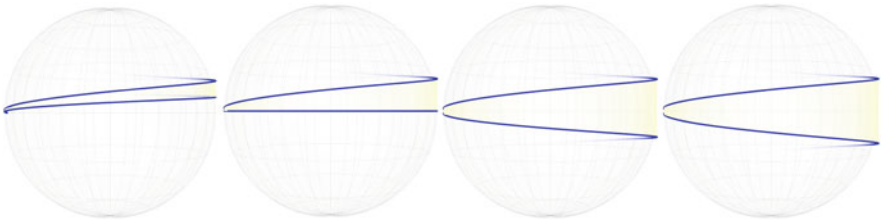

Fig. 24.2 Schematic representation on an asymmetric channel with straight walls, i.e., $f_1 = r(m_1\theta - \phi_0)$ and $f_2(\theta) = r(m_2\theta\phi_0)$, embedded in a spherical surface. In this case, the upper boundary is held constant at a fixed m_2, whereas the lower boundary gradually increases its slope m_1

24.4.3 Torus Surface

A torus is a surface of revolution generated by rotating a circle in three-dimensional space about an axis that does not intersect the circle. The corresponding metric of this system is given by Eq. (24.84). Furthermore, the torus' curvature depends on the corresponding angle θ and is given by

$$K = \frac{\cos\theta}{b(a + b\cos\theta)}. \tag{24.88}$$

Additionally, Eq. (24.84) allows us to write the ratio $\sqrt{g_1(\theta)/g_2(\theta)}$ as

$$\sqrt{\frac{g_1(\theta)}{g_2(\theta)}} = \frac{1}{a/b + \cos\theta}. \tag{24.89}$$

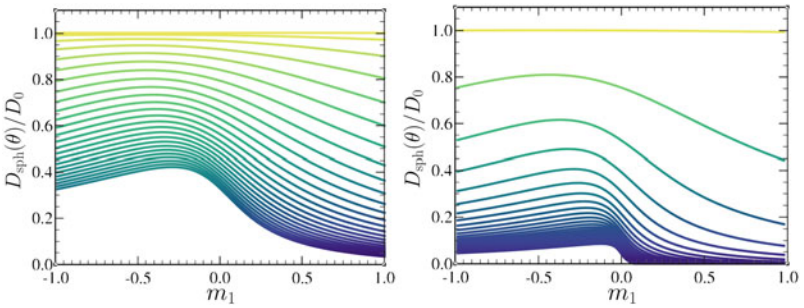

Fig. 24.3 Characteristic plots of the diffusion coefficient in Eq. (24.87), where the increase in radius is shown with the change in color from yellow to blue. The slope of the upper boundary is set at $m_2 = 1$ and the slope of the lower boundary varies from $-1 \leq m_1 \leq 1$. The left-hand side plot is showing the effective diffusion coefficient at $\theta = \pi/20$, i.e., in close proximity to the beginning of the channel. In contrast, the right-hand side graph exhibits its behavior at $\theta = \pi/2$

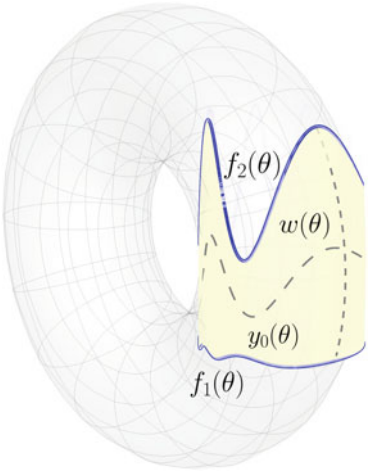

Fig. 24.4 Schematic representation of an asymmetric channel embedded in a torus. The walls are given by the boundary functions $f_1(\theta)$ and $f_2(\theta)$m and determine the width and midline functions, $w(\theta)$ and $y_0(\theta)$, respectively

In Fig. 24.4, we show a schematic representation of an asymmetric channel embedded in a torus.

With regard to a simple asymmetrical conical channel made up of two straight lines, $\phi_2 = m_2\theta - \phi_0$ and $\phi_1 = m_1\theta + \phi_0$, and inserting the latter equation, together with the width and midline functions into Eq. (24.68), we arrive at

$$D_{\rm torus}(\theta) = \frac{D_0}{m_1 - m_2}\frac{1}{a/b + \cos\theta}\left\{\arctan\left[m_1\left(\frac{a}{b} + \cos\theta\right)\right] - \arctan\left[m_2\left(\frac{a}{b} + \cos\theta\right)\right]\right\}. \tag{24.90}$$

In Fig. 24.5, we show a schematic representation of this system together with characteristic plots of the effective diffusion coefficient, where we keep constant

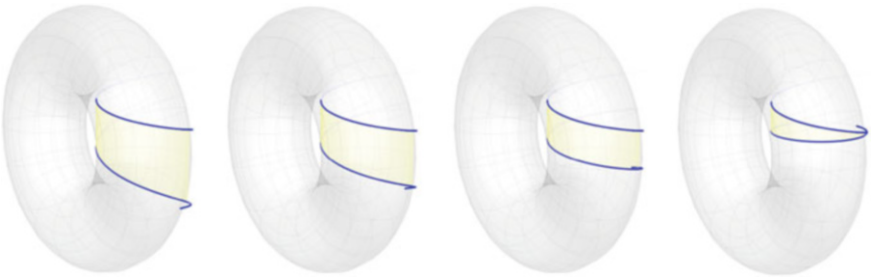

Fig. 24.5 Schematic representation of an asymmetric channel with straight walls, i.e., $\phi(\theta) = m_2\theta - \phi_0$ and $\phi_1 = m_1\theta + \phi_0$, embedded in a torus. In this case, the upper boundary is held constant at a fixed m_2, whereas the lower boundary gradually increases its slope m_1

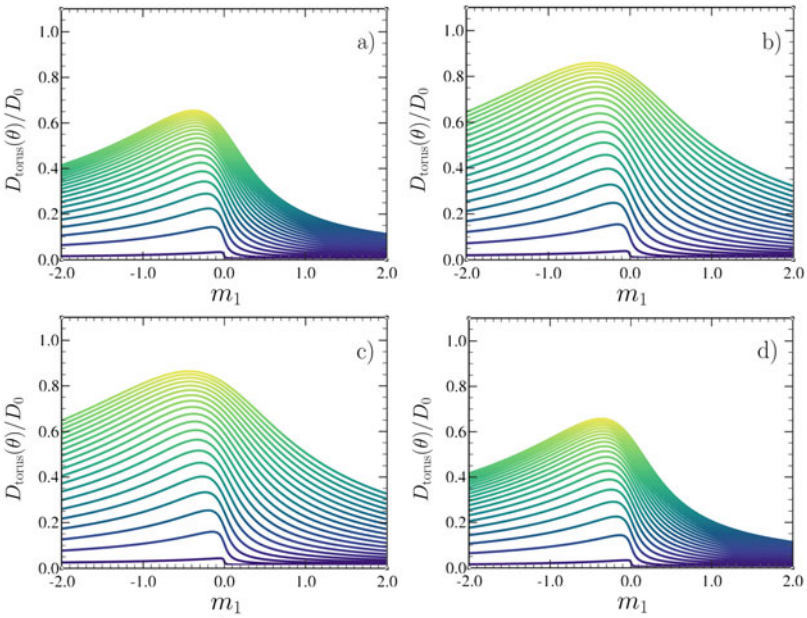

Fig. 24.6 Characteristic plots of the diffusion coefficient given by Eq. (24.90), where the increase in radius is shown with the change in color from yellow to blue. The slope of the upper boundary is set at $m_2 = 1$ and the slope of the lower boundary varies from $-2 \leq m_1 \geq 2$. The effective diffusion coefficient is plotted at (**a**) $\theta \approx 0$, (**b**) $\theta = \pi/2$, (**c**) $\theta = \pi$, and (**d**) $\theta = 3\pi/2$. From (**a**) to (**b**), the diffusion coefficient grows and continues growing until (**c**). Subsequently, it starts to decrease again to $\theta = 2\pi$, or equivalently to $\theta = 0$. In all cases, we keep the radius fixed at $a = 1$, while the small radius b takes values in the range $0.01 \leq b \leq 1$

the upper slope m_2 while varying the lower slope, i.e., m_1, demonstrating that the diffusion coefficient increases as the radius increases as shown in Fig. 24.6. Equation (24.90) can be written in terms of the curvature, noting that

$$\sqrt{\frac{g_1(\theta)}{g_2(\theta)}} = \frac{b}{a}(1 - b^2K), \tag{24.91}$$

is equivalent to Eq. (24.89). Therefore, Eq. (24.90) becomes

$$D_{\text{torus}} = \frac{D_0 b(1 - b^2K)}{a(m_1 - m_2)} \left\{ \arctan\left[\frac{a}{b(1 - b^2K)} m_1 \right] - \arctan\left[\frac{a}{b(1 - b^2K)} m_2 \right] \right\}. \tag{24.92}$$

This last equation provides us with insights into how the curvature of the manifold changes the dynamics of the system. More specifically, it shows how it influences the effective diffusion in the confined geometry, i.e., as the curvature varies, the effective diffusion coefficient changes.

24.5 Mean First-Passage Time

In Chap. 6, we derived the evolution equation for the moments of mean first-passage time (MFPT) in the presence of a force field by means of the backward Smoluchowski operator, Eq. (6.28), and relations obtained in Chap. 2, ultimately yielding

$$\frac{\partial}{\partial x_0}\left[D(x_0) \mathrm{e}^{-\beta U(x_0)} \frac{\partial}{\partial x_0} \langle t(x_0) \rangle \right] = -\mathrm{e}^{-\beta U(x_0)}, \tag{6.38}$$

which, by introducing the entropic potential $U(x)$ as defined in Eq. (17.21), becomes

$$\frac{1}{w(x_0)} \frac{\partial}{\partial x_0} D(x_0) w(x_0) \frac{\partial}{\partial x_0} \langle t(x_0) \rangle = -1. \tag{24.93}$$

This last result is extended in a straightforward manner for narrow channels embedded in manifolds as

$$\frac{1}{\sqrt{g_1 g_2} w(x_0)} \frac{\partial}{\partial x_0} D(x_0) w(x_0) \frac{\partial}{\partial x_0} \langle t(x_0) \rangle = -1. \tag{24.94}$$

24.5.1 Mean First-Passage Time on a Cylinder

As a simple example, we compute the MFPT for an asymmetric narrow channel embedded in a cylinder surface of constant radius r made by straight walls given by $z_1(\theta) = m_1 r\theta - z_0$ and $z_2(\theta) = m_2 r\theta + z_0$, with $z_2(\theta) > z_1(\theta)\ \forall\, \theta \in [0, \theta_L]$. The corresponding BCs of this system are

$$\frac{\mathrm{d}}{\mathrm{d}\theta_0}\left\langle t(\theta_0)\right\rangle\Big|_{\theta_0} = 0, \text{ and } \left\langle t(\theta_0)\right\rangle\Big|_{\theta_0} = \theta_L, \tag{24.95}$$

i.e., we have a reflecting boundary at $\theta_0 = 0$ and an absorbing target at $\theta_0 = \theta_L$. In this given situation, the backward equation reads

$$\frac{1}{r w(\theta_0)}\frac{\partial}{\partial\theta_0} w(\theta_0) D(\theta_0)\frac{\partial}{\partial\theta_0}\left\langle t(\theta_0)\right\rangle . \tag{24.96}$$

Using Eq. (24.85) and setting the initial position of the particles at the origin $\theta_0 = 0$, the solution to the latter equation is found directly, obtaining

$$\left\langle t(\theta_0 = 0)\right\rangle = \frac{1}{4D(\theta_0 = 0)\gamma^2 r}\left\{\gamma^2 r^2\theta_L^2 + 4z_0\gamma r\theta_L + 8\gamma^2\log\left[\frac{2h}{2h + r\theta_L\gamma}\right]\right\}, \tag{24.97}$$

with $\gamma = m_2 - m_1$. The difference between the flat Euclidean case and the last equation is the radius of the cylinder, meaning that the metric components of the surface play an important role in the structure of the MFPT if the channels are embedded in a manifold.

24.6 Concluding Remarks

In this chapter, we used the Kalinay and Percus projection method for a two-dimensional narrow asymmetrical channel with varying width $w(\xi)$ and a non-straight midline $y_0(\xi)$, embedded in a symmetric curved manifold. Along this procedure, we introduced the corresponding Fick-Jacobs-like equation, Eq. (24.53), from which we found the recurrence formula for $\hat{\boldsymbol{\sigma}}_j$ operators, and ultimately, the position-dependent effective diffusion coefficient to the first order in the metric determinant, Eq. (24.68), which is a general expression that contains all the previous results of the flat Euclidean space as particular cases (see Eq. (20.51)).

Then, we brought forward an asymmetric channel embedded on three different curved surfaces, i.e., a cylinder, a sphere, and a torus. For each of the systems, we computed the diffusivity and analyzed its behavior when varying the geometrical properties of either the walls of the channel or the surface itself.

Finally, we showed that by using backward equations, we can study the mean first-passage time (MFPT) for asymmetric channels embedded in curved surface. In addition, we calculated the MFPT when a channel is embedded in a cylindrical surface, where the effect of the metric elements is clear (see Eq. (24.97)). Equations (24.68) and (24.94) are the main results of this chapter and listed below for the reader's convenience.

(Position-dependent diffusion coefficient)

$$D(\xi) = \frac{D_0}{w'(\xi)}\sqrt{\frac{g_2}{g_1}}\left\{\arctan\left[\sqrt{\frac{g_2}{g_1}}\left(y_0'(\xi) + \frac{w'(\xi)}{2}\right)\right]\right.$$
$$\left. - \arctan\left[\sqrt{\frac{g_2}{g_1}}\left(y_0'(\xi) - \frac{w'(\xi)}{2}\right)\right]\right\}. \tag{24.98}$$

$$\frac{1}{\sqrt{g_1 g_2}\, w(x_0)}\frac{\partial}{\partial x_0} D(x_0) w(x_0) \frac{\partial}{\partial x_0}\langle t(x_0)\rangle = -1. \qquad \text{(Mean first-passage time)}$$

Further Reading and References

P. Castro-Villareal, Brownian motion meets Riemann curvature. J. Stat. Mech. **P08006** (2010). https://doi.org/10.1088/1742-5468/2010/08/P08006

R. Graham, Covariant formulation of non-equilibrium statistical thermodynamics. Z Physik B **26**, 397–405 (1977). https://doi.org/10.1007/BF01570750

I. Pineda, G. Chacón-Acosta, L. Dagdug, Diffusion coefficients for two-dimensional narrow asymmetric channels embedded on flat and curved surfaces. Eur. Phys. J. Spec. Top. **223**, 3045–3062 (2014). https://doi.org/10.1140/epjst/e2014-02318-4

E. Poisson, *A Relativist's Toolkit* (Cambridge University Press, Cambridge, 2004)

H. Risken, *The Fokker-Planck Equation: Methods of Solution and Applications* (Springer, Berlin, 1996)

L. Susskind, A. Cabannes, *General Relativity: The Theoretical Minimum* (Basic Books, New York City, 2023)

L. Susskind, A. Friedman, *Special Relativity and Classical Field Theory: The Theoretical Minimum* (Basic Books, New York City, 2017)

N.G. van Kampen, Brownian motion in a manifold. J. Stat. Phys. **44**, 1–54 (1985). https://doi.org/10.1007/BF01010902

Chapter 25
Representation of a Channel as a Tubular Manifold: Frenet-Serret Moving Frame

In this chapter, we will apply the Kalinay-Percus (KP) projection method to narrow channels and tubes where the coordinate frame is placed at the axis curve of the tube or channel, using the Frenet-Serret moving frame as the coordinate system to study the diffusion of bounded Brownian point-like particles. This covariant description for the diffusion equation maps the shape of a general channel in two dimensions or a tube in three dimensions, in a straight tube or channel seen in a non-Cartesian space. In other words, this description mimics traveling within a moving frame that travels through the midline and that allows us to constantly keep the perspective of being confined by a straight channel or tube. Significant contributions of this method include the possibility of extending the study of geometrical confinement to variable cross-section as well as the possibility of considering more general parametric curves to describe the channel or tube axis. Moreover, the zeroth order of this theoretical frame is capable of reproducing the first order of the KP approach.

The method consists of writing the covariant anisotropic diffusion equation in tubular coordinates, namely, (s, θ, ρ) (see Fig. 25.1), and projecting it along the tube's axis, eliminating the transverse degrees of freedom due to fast equilibration. The resulting equation for marginal concentration is rewritten as a generalized Fick-Jacobs-Zwanzig-like equation, from which one can identify the effective diffusion coefficient, namely,

$$\frac{\partial \mathrm{p}(s,t)}{\partial t} = \frac{\partial}{\partial s}\left[D(s)\mathcal{A}(s)\frac{\partial}{\partial s}\left(\frac{\mathrm{p}(s,t)}{\mathcal{A}(s)}\right)\right],$$

where the marginal concentration $\mathrm{p}(s,t)$ in terms of the arclength s of the mid-curve is obtained by integrating the concentration $c(s,\theta,\rho,t)$ over transversal coordinates, θ and ρ, which parameterize the closed curve in the orthogonal planes. The cross-sectional area $A(s)$ can be calculated by integrating the determinant of the tubular metric $\Delta(s,\theta,\rho)$ over $\theta \in [0, 2\pi]$ and $\rho \in [0, 1]$. The position-dependent

L. Dagdug et al., *Diffusion Under Confinement*,
https://doi.org/10.1007/978-3-031-46475-1_25

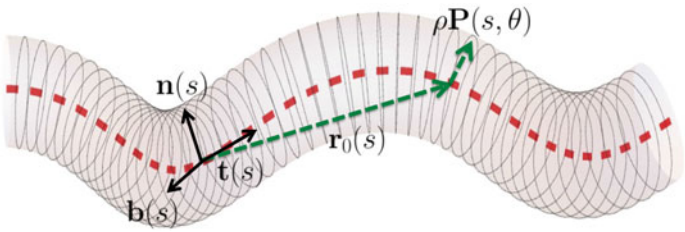

Fig. 25.1 Schematic representation of tube parametrization for a circular tube. A curve representing the tubular axis (red dashed line) is surrounded by a set of circles that represent the tube's boundary, which lie at the planes' normal to the curve's tangent direction. The tube is constructed considering a continuous set of such circles centered around $\mathbf{r}(s)$. At any point along s, we can define the moving orthonormal frame, namely, the Frenet-Serret trihedron. This theoretical representation can be pictured as a ride on a roller coaster through a tube, where the rail is the axis of the tube

diffusion coefficient $D(s)$ considerably extends the validity of the FJ equation, which is recovered when $D(s) = D_0$.

In this chapter, we will give a very general introduction to the theoretical framework used to describe the diffusion processes for two-dimensional asymmetric varying-width channels and for three-dimensional curved midline tubes formed by straight walls. For more details, readers are referred to the references cited at the end of the chapter.

25.1 Fick's Laws in General Coordinates

In this section, we will present the geometrical properties of diffusion in any coordinate system, such as Fick's laws and the reflecting boundary condition. Consider that diffusion processes are confined by a three-dimensional (3D) tube represented by a subset of space $\mathbb{R}^3$. Then, the line element can be written using the Cartesian metric g as $dl^2 = g(d\mathbf{r}, d\mathbf{r}) = g_{ab} dX^a dX^b$, where dX^a is the displacement in direction $a = 1, 2, 3$, corresponding to (x, y, z), and g_{ab} are the components of the metric tensor g in Euclidean coordinates, where

$$g_{ab} = \text{diag}(1, 1, 1), \tag{25.1}$$

and $X^1 = X$, $X^2 = Y$, $X^3 = Z$. Using Eq. (25.1), the metric is obtained through the following transformation:

$$g_{\mu\nu} = g_{ab} \frac{\partial X^a}{\partial x^\mu} \frac{\partial X^b}{\partial x^\nu}, \tag{25.2}$$

where $\mu, \nu = 1, 2, 3$ refer to the tubular coordinates, denoted in covariant language as $s = x^1$, $\theta = x^2$ and $\rho = x^3$. In summary, Greek indices take the values $\{1, 2, 3\}$, where, in our case, x^μ corresponds to the tubular coordinates (s, θ, ρ), respectively.

The corresponding Christoffel symbols can be obtained through the coordinate transformation, namely,

$$\Gamma^{\mu}_{\nu\sigma} = \Gamma^{a}_{bc} \frac{\partial x^\mu}{\partial X^a} \frac{\partial X^b}{\partial x^\nu} \frac{\partial X^c}{\partial x^\sigma} + \frac{\partial x^\mu}{\partial X^a} \frac{\partial^2 X^a}{\partial x^\nu \, \partial x^\sigma}. \tag{25.3}$$

Clearly, for the Euclidean metric, the first term vanishes because all Γ^{a}_{bc} are identically zero. To compute Eq. (25.3), one needs the inverse transformation, given by

$$\frac{\partial x^\mu}{\partial X^a} = \frac{\epsilon_{abc} \epsilon^{\mu\nu\sigma}}{2\Delta(x)} \frac{\partial X^b}{\partial x^\nu} \frac{\partial X^c}{\partial x^\sigma}, \tag{25.4}$$

where ϵ_{abc} and $\epsilon^{\mu\nu\sigma}$ are the 3D Levi-Civita symbols, such that $\epsilon_{123} = \epsilon^{123} = +1$. The function $\Delta(x)$ is the Jacobian of the transformation, in our case, from Cartesian to tubular coordinates. Due to the Euclidean metric, this coincides with the determinant of the metric $\det G_{\mu\nu}$ in tubular coordinates, namely,

$$\Delta(x) = \frac{1}{3!} \epsilon^{\mu\nu\sigma} \, \epsilon_{abc} \frac{\partial X^a}{\partial x^\mu} \frac{\partial X^b}{\partial x^\nu} \frac{\partial X^c}{\partial x^\sigma}. \tag{25.5}$$

Then, the expression for Christoffel connections is

$$\Gamma^{\mu}_{\nu\sigma} = \frac{1}{2\Delta(x)} \, \epsilon_{abc} \, \epsilon^{\mu\eta\lambda} \frac{\partial X^b}{\partial x^\eta} \frac{\partial X^c}{\partial x^\lambda} \frac{\partial^2 X^a}{\partial x^\nu \, \partial x^\sigma}, \tag{25.6}$$

which is used in the definition of the covariant derivative:

$$\nabla_\mu = \partial_\mu + \Gamma^{(\cdot)}_{\mu(\cdot)}. \tag{25.7}$$

The corresponding diffusion tensor components can be obtained using Eq. (25.4):

$$D^{\mu\nu} = D^{ab} \frac{\partial x^\mu}{\partial X^a} \frac{\partial x^\nu}{\partial X^b}, \tag{25.8}$$

which are useful for calculating other quantities, such as the flux.

Now, let us write the diffusion equation in tubular coordinates. To such end, we consider that the particle concentration $c(\mathbf{r}, t)$ and flux $\mathbf{J}(\mathbf{r}, t)$ must satisfy the continuity equation, Eq. (2.72):

$$\frac{\partial c}{\partial t} + \nabla \cdot \mathbf{J} = 0, \tag{2.72}$$

where c is assumed to be an invariant scalar field under coordinate transformations. Now, the term $\nabla \cdot \mathbf{J}$ is the contraction of the covariant derivative ∇ and the flux field $\mathbf{J}$, given through the metric g. Then, the flux is defined as follows:

$$\mathbf{J} = -D(\nabla C), \tag{25.9}$$

It is worth noting that, in this last equation, D is the diffusion tensor, whose Euclidean components are $D^{ab} = \text{diag}\,(D^x, D^y, D^z)$. Equations (2.72) and (25.9) are Fick's laws in general coordinates, and in terms of their components, they become

$$J^{\mu} = -D^{\mu\nu}\,\partial_{\nu} C, \tag{25.10}$$

and

$$\partial_t C = (\partial_{\mu} D^{\mu\nu})\partial_{\nu} C + D^{\mu\nu}\partial^2_{\mu\nu} C + \Gamma^{\mu}_{\mu\nu} D^{\nu\sigma}\,\partial_{\sigma} C, \tag{25.11}$$

respectively. $D^{\mu\nu}$ are the diffusion tensor components in general coordinates that can be obtained from D^{ab} through the corresponding transformation, and $\Gamma^{\mu}_{\mu\nu}$ are the Christoffel symbols.

The derivatives are taken with respect to the transformation from coordinates X^a to any set of well-behaved coordinates x^{μ}, and Δ is the determinant of the metric given by Eq. (25.5). Now, introducing these geometrical quantities, the diffusion equation (25.11) reads

$$\partial_t C = \partial_{\mu}[D^{\mu\nu}\partial_{\nu} C] + \frac{1}{\Delta}(\partial_{\mu}\Delta) D^{\mu\nu}\partial_{\nu} C, \tag{25.12}$$

and by multiplying both sides by Δ, it results in

$$\Delta\partial_t C = \partial_{\mu}\left[\Delta D^{\mu\nu}\partial_{\nu} C\right]. \tag{25.13}$$

Let's conclude this section by determining the boundary conditions (BCs) in tubular coordinates as defined by a reflecting boundary. Assuming that the flux component perpendicular to the channel wall is equal to zero at the boundary, ρ_0, we have that

$$J^{\rho}|_{\rho=\rho_0} = -D^{\rho\mu}\partial_{\mu} C|_{\rho=\rho_0} = 0. \tag{25.14}$$

This last expression will be used to obtain the diffusion effective coefficient for narrow tubes.

25.2 Representation of a Channel as a Tubular Manifold

A tube with no self-intersections, and therefore, not knotted, can be constructed through a vector $\mathbf{r}_0(s)$, which represents the axis of the tube. As the parameter s varies, the endpoint of this vector moves along the axis, which is a curve in the space. In Cartesian coordinates,

$$\vec{r}_0(s) = X(s)\hat{\mathbf{e}}_i + Y(s)\hat{\mathbf{e}}_j + Z(s)\hat{\mathbf{e}}_k, \tag{25.15}$$

where $X(s)$, $Y(s)$, and $Z(s)$ are the parametric equations of the curve. Along this curve, we can define the Frenet-Serret basis, $(\mathbf{t}(s), \mathbf{n}(s), \mathbf{b}(s))$. The unit tangent vector $\mathbf{t}$ is given by

$$\mathbf{t} = \frac{1}{l(s)}\frac{d\mathbf{r}_0}{ds}, \tag{25.16}$$

the principal normal vector, $\mathbf{n}$, by

$$\mathbf{n} \equiv \frac{\mathbf{t}'}{||\mathbf{t}'||} = \frac{\mathbf{t} \times (\mathbf{r}_0'' \times \mathbf{r}_0')}{||\mathbf{r}_0'' \times \mathbf{r}_0'||}, \tag{25.17}$$

and the binormal (product of tangent and normal) vector $\vec{b}$, by

$$\mathbf{b} \equiv \mathbf{t} \times \mathbf{n} = \frac{\mathbf{r}_0' \times \mathbf{r}_0''}{||\mathbf{r}_0' \times \mathbf{r}_0''||}, \tag{25.18}$$

where primes denote differentiation with respect to the curve parameter s, and $l(s) = \sqrt{X'^2(s) + Y'^2(s) + Z'^2(s)}$ is the arclength function of the curve. The three mutually perpendicular unit vectors form a right-handed triad (see Fig. 25.1).

Using the normal vectors $\mathbf{n}(s)$ and $\mathbf{b}(s)$, we can define the normal plane where the tube's cross-section lies. The tube's boundaries can be defined with a closed curve $\mathbf{P}$ in this $nb-$plane, and described in polar coordinates (R, θ), which depend on s, namely,

$$\mathbf{P}(s, \theta) = R(s, \theta)\, \cos\theta\, \mathbf{n}(s) + R(s, \theta)\, \sin\theta\, \mathbf{b}(s). \tag{25.19}$$

Consequently, any point on the surface of the channel, where $\mathbf{r}_0$ is the tube's axis, can be written as $\mathbf{r}_0 + \mathbf{P}(s, \theta)$.

In order to foliate the space inside the tube, we can introduce a parameter $\rho \in [0, \rho_0]$, and points on the surface and within the tube are given by

$$\mathbf{r}_c(s, \theta, \rho) = \mathbf{r}_0(s) + \rho\mathbf{P}(s, \theta). \tag{25.20}$$

On the other hand, the function $R(s,\theta)$ can be written as

$$R(s,\theta) = \sqrt{a(s)}\,\tilde{R}(\theta), \tag{25.21}$$

where $a(s)$ characterizes changes in surface area and $\tilde{R}(\theta)$ the shape of the closed curve at the *nb*-plane. Consequently, the cross-sectional area of the tube is given by

$$A_c(s) = \frac{|a(s)|}{2}\int_0^{2\pi} \tilde{R}^2(\theta)\,d\theta. \tag{25.22}$$

Finally, let us insert Eqs. (25.16)–(25.18) into Eqs. (25.20) and (25.21), in order to obtain the Cartesian components of points inside the tube $\mathbf{r}_c(s,\theta,\rho)$:

$$X_c = X(s) + \frac{\rho\sqrt{a(s)}\,\tilde{R}(\theta)}{\rho_0\,||\vec{r}_0'' \times \vec{r}_0'||}\left\{\frac{\left[X''(Y'^2+Z'^2) - Y''X'Y' - Z''X'Z'\right]}{l(s)}\cos\theta + \left(Z''Y' - Y''Z'\right)\sin\theta\right\}, \tag{25.23}$$

$$Y_c = Y(s) + \frac{\rho\sqrt{a(s)}\,\tilde{R}(\theta)}{\rho_0\,||\vec{r}_0'' \times \vec{r}_0'||}\left\{\frac{\left[-X''X'Y' + Y''(X'^2+Z'^2) - Z''Y'Z'\right]}{l(s)}\cos\theta + \left(X''Z' - Z''X'\right)\sin\theta\right\}, \tag{25.24}$$

$$Z_c = Z(s) + \frac{\rho\sqrt{a(s)}\,\tilde{R}(\theta)}{\rho_0\,||\vec{r}_0'' \times \vec{r}_0'||}\left\{\frac{\left[-X''X'Z' - Y''Y'Z' + Z''(X'^2+Y'^2)\right]}{l(s)}\cos\theta + \left(Y''X' - X''Y'\right)\sin\theta\right\}. \tag{25.25}$$

Expressions (25.23)–(25.25) depict the relation between the Cartesian coordinates and (s,θ,ρ), which become our new coordinates. It is worth noting that the components of $\mathbf{r}_c$ have a linear dependence on ρ. The tube's surface, given by $\rho = \rho_0$, facilitates the reduction of the diffusion equation on (s,θ,ρ).

We will outline the steps needed to arrive at Fick's law equation in tubular coordinates in the section that follows.

25.3 Generalized Fick-Jacobs-Like Equation: 3D Frenet-Serret Moving Frame

Now, we will project the diffusion Eq. (25.13) on the tube's axis $\vec{r}_0$ to perform a one-dimensional reduction following the procedure, introduced by P. Kalinay and J.

Percus, previously outlined in Chap. 20. This projection is performed by integrating over the tube radius $\rho \in [0, \rho_0]$ and the angular coordinate $\theta \in [0, 2\pi)$. The integral on ρ, expanding the sum in μ, is given by

$$\int_0^{\rho_0} d\rho\, \Delta \partial_t c = \partial_s \int_0^{\rho_0} d\rho\, \Delta D^{s\nu} \partial_\nu c + \int_0^{\rho_0} d\rho\, \partial_\rho \Delta D^{\rho\nu} \partial_\nu c + \partial_\theta \int_0^{\rho_0} d\rho\, \Delta D^{\theta\nu} \partial_\nu c, \tag{25.26}$$

where ∂_t is the time partial derivative. Integrating the second term on the right-hand side, we obtain $\Delta D^{\rho\nu} \partial_\nu C|_{\rho=\rho_0}$ and $\Delta D^{\rho\nu} \partial_\nu C|_{\rho=0}$. The first relation vanishes due to the boundary condition, Eq. (25.14). The second is proportional to $\Delta(s, \theta, \rho = 0)$, which is zero, since the determinant is null at $\rho = 0$.

Now, integrating this equation with respect to θ for a closed curve on the $nb-$plane leads to

$$\int_0^{2\pi} \int_0^{\rho_0} d\theta d\rho\, \Delta \partial_t c = \partial_s \int_0^{2\pi} \int_0^{\rho_0} d\theta d\rho\, \Delta D^{s\nu} \partial_\nu c + \int_0^{2\pi} d\theta\, \partial_\theta \int_0^{\rho_0} d\rho\, \Delta D^{\theta\nu} \partial_\nu c. \tag{25.27}$$

Now, integrating the second term on the right-hand side with respect to θ, this last equation can be rewritten in terms of flux components, which gives

$$-\int d\rho\, \left(\Delta(s, 2\pi, \rho) J^\theta|_{\theta=2\pi} - \Delta(s, 0, \rho) J^\theta|_{\theta=0} \right). \tag{25.28}$$

Because the determinant Δ depends on the angle through $\tilde{R}(\theta)$ and because $\tilde{R}(0) = \tilde{R}(2\pi)$ for closed curves, then $\Delta(s, 0, \rho) = \Delta(s, 2\pi, \rho)$, the determinant can be factorized, and Eq. (25.28) results in the difference between fluxes. On the other hand, we can also consider that the angular component of the flux is periodic $J^\theta|_{\theta=0} = J^\theta|_{\theta=2\pi}$, so this term also vanishes.

By defining the marginal concentration (see Eq. (18.4)) as

$$\mathrm{p}(s) \equiv \int_0^{2\pi} \int_0^{\rho_0} c \Delta\, d\rho\, d\theta, \tag{25.29}$$

Eq. (25.27) becomes

$$\partial_t \mathrm{p} = \partial_s \iint d\theta\, d\rho\, \Delta \left[D^{ss} \partial_s c + D^{s\theta} \partial_\theta c + D^{s\rho} \partial_\rho c \right]. \tag{25.30}$$

Now, this equation can be rewritten to obtain a generalized Fick-Jacobs-like equation as follows:

$$\partial_t \mathrm{p} = \partial_s \left[D(s) A(s) \partial_s \left(\frac{\mathrm{p}}{A(s)} \right) \right], \tag{25.31}$$

where the cross-sectional area of the tube associated with the corresponding entropic potential is given by

$$A(s) = \int_0^{2\pi} \int_0^{\rho_0} \Delta \, d\rho \, d\theta, = \int_0^{2\pi} d\theta \left(\frac{1}{2} \alpha(s) \tilde{R}^2(\theta) + \frac{1}{3} \tilde{R}^3(\theta) \beta(s) \cos\theta \right), \tag{25.32}$$

where α and β are certain functions of s that can be associated with geometrical properties of the curve. Comparing (25.30) with (25.31), we find that the diffusion coefficient is given by

$$D(s) = \frac{\iint d\theta \, d\rho \, \Delta \left[D^{ss} \partial_s c + D^{s\theta} \partial_\theta c + D^{s\rho} \partial_\rho c \right]}{A(s) \, \partial_s \left[\frac{1}{A(s)} \iint \Delta \, c \, d\theta \, d\rho \right]}. \tag{25.33}$$

It is worth noting that this expression depends on $\partial_\theta c$, $\partial_\rho c$, and $\partial_s c$. To express these quantities as functions of $\partial_s c$, we can use the transversal flow components, given by

$$J^\theta = -D^{\theta s} \partial_s c - D^{\theta\theta} \partial_\theta c - D^{\theta\rho} \partial_\rho c, \tag{25.34}$$

$$J^\rho = -D^{\rho s} \partial_s c - D^{\rho\theta} \partial_\theta c - D^{\rho\rho} \partial_\rho c. \tag{25.35}$$

Solving this system of equations for $\partial_\theta c$ and $\partial_\rho c$ results in

$$\partial_\theta c = \frac{D^{\theta\rho} J^\rho - D^{\rho\rho} J^\theta + (D^{\theta\rho} D^{\rho s} - D^{\rho\rho} D^{\theta s}) \partial_s C}{D^{\rho\rho} D^{\theta\theta} - D^{\theta\rho} D^{\rho\theta}}, \tag{25.36}$$

$$\partial_\rho c = \frac{D^{\theta\theta} J^\rho - D^{\rho\theta} J^\theta + (D^{\theta\theta} D^{\rho s} - D^{\rho\theta} D^{\theta s}) \partial_s C}{D^{\rho\theta} D^{\theta\rho} - D^{\theta\theta} D^{\rho\rho}}. \tag{25.37}$$

Substituting these expressions into Eq. (25.33) gives

$$D(s) = \frac{\mathcal{F}(s) + \iint d\theta \, d\rho \, \Delta \left(D^{ss} + \frac{D^{s\theta} D^{\theta\rho} D^{\rho s} - D^{s\theta} D^{\rho\rho} D^{\theta s} - D^{s\rho} D^{\theta\theta} D^{\rho s} + D^{s\rho} D^{\rho\theta} D^{\theta s}}{D^{\theta\theta} D^{\rho\rho} - D^{\rho\theta} D^{\theta\rho}} \right) \partial_s C}{A(s) \, \partial_s \left[\frac{1}{A(s)} \iint \Delta \, C \, d\theta \, d\rho \right]}, \tag{25.38}$$

where

$$\mathcal{F}(s) = \iint d\theta d\rho \Delta \frac{\left(D^{s\theta} D^{\theta\rho} - D^{s\rho} D^{\theta\theta} \right) J^\rho + \left(D^{s\rho} D^{\rho\theta} - D^{s\theta} D^{\rho\rho} \right) J^\theta}{D^{\rho\rho} D^{\theta\theta} - D^{\theta\rho} D^{\rho\theta}}. \tag{25.39}$$

Equation (25.39) can be simplified by applying additional approximations. For channels with a circular cross-section or boundary, we can assume that $c(s,\theta,\rho) \approx c(s)$ for stationary flow. Consequently, even though J^{ρ} may have nonzero projections over the entire range of integration, we assume that these deviations are negligible. Due to this symmetry, the concentration dependencies are canceled out, $D^{s\theta} = D^{\theta s} = 0$, and $J^{\theta} = 0$. With these considerations, Eq. (25.39) can be neglected and Eq. (25.38) is simplified as follows:

$$D(s) = \frac{\iint d\theta\, d\rho\, \Delta \left(D^{ss} + \dfrac{D^{s\theta} D^{\theta\rho} D^{\rho s} - D^{s\theta} D^{\rho\rho} D^{\theta s} - D^{s\rho} D^{\theta\theta} D^{\rho s} + D^{s\rho} D^{\rho\theta} D^{\theta s}}{D^{\theta\theta} D^{\rho\rho} - D^{\rho\theta} D^{\theta\rho}} \right)}{A(s)\, \partial_s \left[\frac{1}{A(s)} \iint \Delta\, d\theta\, d\rho \right]}. \tag{25.40}$$

By means of Eqs. (25.31) and (25.40), we have a theoretical framework that gives the projected Fick-Jacobs-like equation in 3D, as well as its effective diffusion.

Summarizing, in order to obtain the position-dependent effective diffusivity for an asymmetric channel or tube, one has to follow these steps: (1) define the centerline of the tube of interest, (2) find the Frenet-Serret basis, and (3) calculate the determinant and the components of the diffusion tensor.

25.4 Straight Tube with Circular-Shaped Cross-Section

In this section, we will calculate the effective diffusion coefficient for a straight tube with circular-shaped cross-section. To such end, we need to calculate the explicit expressions involved in the transformation of tubes with a straight axis and circular-shaped cross-sections into tubular coordinates, as depicted in the last paragraph of the preceding section.

The normal and binormal vectors are not uniquely specified in this particular case. For simplicity, we propose writing the straight axis line as a limiting case of a curve by the parameter K. Let us consider the parametric space curve $\vec{r}_0(s;K) = (s, KY(s), KZ(s))$, where $Y(s)$ and $Z(s)$ are functions of the tube's axis parameter and K is an additional variable that is set equal to zero when $\vec{r}_0$ is a straight line. For plane curves, we additionally consider $Y(s) = 0$ and $Z''(s) > 0$. Under such conditions and setting $K \to 0$, the Frenet-Serret trihedron reduces to

$$\mathbf{t} \to \hat{\mathbf{e}}_i, \quad \mathbf{n} \to \hat{\mathbf{e}}_k, \quad \mathbf{b} \to -\hat{\mathbf{e}}_j. \tag{25.41}$$

Now, according to Eqs. (25.23)–(25.25), the Cartesian components of points into the tube are given by

$$X_c = s, \quad Y_c = \frac{\rho\sqrt{a(s)}}{\rho_0} \sin\theta, \quad Z_c = \frac{\rho\sqrt{a(s)}}{\rho_0} \cos\theta. \tag{25.42}$$

To write Eqs. (25.5)–(25.8) in tubular coordinates, we need to evaluate the derivatives of the transformation (25.42), namely,

$$\frac{\partial X_c}{\partial s} = 1, \quad \frac{\partial X_c}{\partial \theta} = \frac{\partial X_c}{\partial \rho} = 0,$$

$$\frac{\partial Y_c}{\partial s} = -\frac{\rho a'(s)}{2\rho_0\sqrt{a(s)}}\sin\theta, \quad \frac{\partial Z_c}{\partial s} = \frac{\rho a'(s)}{2\rho_0\sqrt{a(s)}}\cos\theta,$$

$$\frac{\partial Y_c}{\partial \theta} = -\frac{\rho\sqrt{a(s)}}{\rho_0}\cos\theta, \quad \frac{\partial Z_c}{\partial \theta} = -\frac{\rho\sqrt{a(s)}}{\rho_0}\sin\theta,$$

$$\frac{\partial Y_c}{\partial \rho} = -\frac{\sqrt{a(s)}}{\rho_0}\sin\theta, \quad \frac{\partial Z_c}{\partial \rho} = \frac{\sqrt{a(s)}}{\rho_0}\cos\theta. \tag{25.43}$$

These relations and Eq. (25.5) allow us to calculate the determinant for our particular case:

$$\Delta(x) = -\frac{\rho}{\rho_0^2}a. \tag{25.44}$$

It is worth noting that the determinant is proportional to ρ, so consequently $\Delta(s, \theta, \rho = 0) = 0$.

From (25.8), we find that the tubular components of the diffusion tensor are given by

$$D^{ss} = \left(\frac{\partial s}{\partial X_c}\right)^2 D^x + \left(\frac{\partial s}{\partial Y_c}\right)^2 D^y + \left(\frac{\partial s}{\partial Z_c}\right)^2 D^z,$$

$$D^{s\theta} = D^{\theta s} = \frac{\partial s}{\partial X_c}\frac{\partial \theta}{\partial X_c}D^x + \frac{\partial s}{\partial Y_c}\frac{\partial \theta}{\partial Y_c}D^y + \frac{\partial s}{\partial Z_c}\frac{\partial \theta}{\partial Z_c}D^z,$$

$$D^{s\rho} = D^{\rho s} = \frac{\partial s}{\partial X_c}\frac{\partial \rho}{\partial X_c}D^x + \frac{\partial s}{\partial Y_c}\frac{\partial \rho}{\partial Y_c}D^y + \frac{\partial s}{\partial Z_c}\frac{\partial \rho}{\partial Z_c}D^z,$$

$$D^{\theta\theta} = \left(\frac{\partial \theta}{\partial X_c}\right)^2 D^x + \left(\frac{\partial \theta}{\partial Y_c}\right)^2 D^y + \left(\frac{\partial \theta}{\partial Z_c}\right)^2 D^z,$$

$$D^{\theta\rho} = D^{\rho\theta} = \frac{\partial \theta}{\partial X_c}\frac{\partial \rho}{\partial X_c}D^x + \frac{\partial \theta}{\partial Y_c}\frac{\partial \rho}{\partial Y_c}D^y + \frac{\partial \theta}{\partial Z_c}\frac{\partial \rho}{\partial Z_c}D^z,$$

$$D^{\rho\rho} = \left(\frac{\partial \rho}{\partial X_c}\right)^2 D^x + \left(\frac{\partial \rho}{\partial Y_c}\right)^2 D^y + \left(\frac{\partial \rho}{\partial Z_c}\right)^2 D^z. \tag{25.45}$$

Explicitly, using Eqs. (25.43), we find that

$$D^{ss} = D^X \frac{a^2\rho^2}{\Delta^2\rho_0^4}, \quad D^{s\theta} = D^{\theta s} = 0,$$

$$D^{\rho s} = D^{s\rho} = -D^X \frac{a\, a'\rho^3}{2\Delta^2\rho_0^4},$$

$$D^{\theta\theta} = \frac{a}{\Delta^2\rho_0^2}\left(D^Y \cos^2\theta + D^Z \sin^2\theta\right),$$

$$D^{\theta\rho} = D^{\rho\theta} = \frac{a}{\Delta^2\rho_0^2}\left(D^Y - D^Z\right)\rho\cos\theta\ \sin\theta,$$

$$D^{\rho\rho} = D^X \frac{a'^2\rho^4}{4\Delta^2\rho_0^4} + \frac{a\rho^2}{\Delta^2\rho_0^2}\left(D^Z \cos^2\theta + D^Y \sin^2\theta\right). \tag{25.46}$$

Given the factorization in Eq. (25.21), the circular shape can be depicted by setting the function $\tilde{R}(\theta) = 1$. For such a case, the components (25.23)–(25.25) and all the geometric quantities are significantly reduced, especially the functions $-\alpha(s) = a(s) = R(s)^2$ and $\beta(s) = 0$. Consequently, the determinant and the cross-sectional area have the following expressions:

$$\Delta = -\frac{\rho}{\rho_0^2}a(s), \tag{25.47}$$

and

$$A(s) = -\pi a(s) = -\pi R^2(s). \tag{25.48}$$

Given the geometry and using these last expressions, now the corresponding transversal flux (25.35) is given by

$$J^\rho = -D^{\rho s}\partial_s c(s). \tag{25.49}$$

By imposing the BCs in Eq. (25.49), we have

$$J^\rho|_{\rho=\rho_0} = \frac{D^X\rho_0\, a'}{2a}\partial_s c(s) = 0. \tag{25.50}$$

Because the equilibrium concentration does not depend on the transversal coordinates, the denominator of Eq. (25.40) becomes proportional to $A(s)\partial_s c(s)$. As a consequence, the term $\partial_s c(s)$ is removed from Eq. (25.40). Considering the

components of the diffusion tensor given by Eq. (25.4) and setting $D^X = D_0$, we finally find that effective diffusion coefficient is

$$D(x) = D_0 \frac{\ln\left(1 + R'(x)^2\right)}{R'(x)^2}, \tag{25.51}$$

where we set $D^Y = D^Z$ and $D^X/D^Y = D^X/D^Z = 1$ for the isotropic medium. This coefficient explicitly depends on $R'(x)^2$. In fact, the first two terms of the series expansion of Eqs. (25.51) reproduce Zwanzig's formula, Eq. (18.62). For values of R' up to 1, the difference between Eq. (25.51) and Rubi-Reguera's formula, Eq. (20.118), is less than 4%. And under the range of applicability, $R' << 1$, they are practically identical.

Finally, it is worth mentioning that Eq. (25.50) gives us the condition of validity of our model at this order, namely,

$$\frac{a'}{2a} = \frac{R'(s)}{R(s)} \ll 1. \tag{25.52}$$

25.5 Tilted Straight Tube with Circular-Shaped Cross-Section

Now, we will show how to obtain the effective diffusivity of a straight tube with a circular-shaped cross-section when it is tilted, a simple extension of the result obtained in the preceding section. What is interesting is that the new property does not appear in Eq. (25.51) in a trivial way. As previously mentioned, we first need to define the centerline of the tube of interest. Next, we need to find the Frenet-Serret basis. Then, using these values, we need to calculate the determinant and all the components of the diffusion tensor. The above data is inserted into Eq. (25.40), giving us the diffusion coefficient. Let us consider the parametric space curve, $\mathbf{r}(t) = (0, s, r_0' s)$, for a curved midline tube with constant slope r_0'. Then, the Frenet-Serret basis is given by the unit tangent vector $\mathbf{t}$:

$$\mathbf{t} = \frac{1}{\sqrt{1 + r_0'^2}}(0, 1, r_0'), \tag{25.53}$$

the binormal vector:

$$\mathbf{b} = \left(1/\sqrt{1 + r_0'^2}\right)(1, 0, 0), \tag{25.54}$$

and the principal normal vector:

$$\mathbf{n} = \frac{1}{\sqrt{1 + r_0'^2}}(0, -r_0', 1). \tag{25.55}$$

In terms of the Frenet-Serret basis, we can now write out the parametric equation as follows:

$$\mathbf{r}(s, \rho, \theta) = \rho\sqrt{a(s)}\left(\sin\theta, s - \frac{r_0'\cos\theta}{\sqrt{1 + r_0'^2}}, r_0' s + \frac{\cos\theta}{\sqrt{1 + r_0'^2}}\right). \tag{25.56}$$

Now, setting $R(\theta) = 1$ for a closed circular tube, the determinant is given by

$$\triangle = -\rho\sqrt{1 + r_0'^2}a(s). \tag{25.57}$$

This last relation allows us to calculate the terms of the diffusion tensor, $D^{\mu\nu}$, and therefore, Eq. (25.40). When integrating over θ and ρ, for this specific case, we have

$$D(x) = D_0 \frac{\ln\left(1 + \frac{R'(x)^2}{1 + r_0'^2}\right)}{R'(x)^2}. \tag{25.58}$$

Note that the effect of the curved midline simply appeared in the logarithm argument. By setting $r_0' = 0$, we recover Eq. (25.51), as expected.

25.6 Generalized Fick-Jacobs-Like Equation: 2D Frenet-Serret Moving Frame

Once the 3D case has been resolved, it is not difficult to expand our theoretical framework to describe particles diffusing into a two-dimensional (2D) narrow channel. To determine the Frenet-Serret moving frame in 2D, we only need to define the tangent vector and the principal normal. Let us take points of $\mathbb{R}^2$ in Cartesian coordinates and a centerline given by a well-behaved curve $\vec{r}_0(s, \rho) = (s, y_0(s))$, with $y_0'(x)$ being the centerline of the channel. Then, points on the surface and within a channel (see Fig. 25.2) are given by

$$\vec{r}_c(s, \rho) = \vec{r}_0(s) + \frac{\rho a(s)}{\rho_0}\rho a(s)\hat{\mathbf{e}}_n. \tag{25.59}$$

The Cartesian components of points inside the channel are given by

$$X_c(s, \rho) = s - \frac{a(s)\rho}{l\rho_0}y_0'(s) \tag{25.60}$$

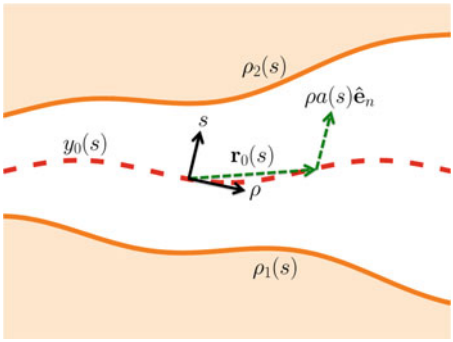

Fig. 25.2 Schematic representation of an asymmetric 2D channel of varying width formed by walls defined by $\rho_1(s)$, $\rho_2(s)$, and the centerline $y_0(s)$. The channel is constructed considering a continuous set of perpendicular lines to the normal unit vector centered around $\vec{r}(s)$. For each value of s, it is possible to define the moving orthonormal frame through the normal and unit tangent vectors

and

$$Y_c(s,\rho) = y_0(s) + \frac{a(s)\rho}{l\rho_0}, \tag{25.61}$$

where $l = \sqrt{1+y_0'^2}$ and $\rho \in [-\rho_1, \rho_2]$. Then,

$$\frac{\partial X_c(s,\rho)}{\partial \rho} = -\frac{a(s)}{l\rho_0} y_0'(s) \tag{25.62}$$

and

$$\frac{\partial Y_c(s,\rho)}{\partial \rho} = \frac{a(s)}{l\rho_0}. \tag{25.63}$$

The width of the channel is given by $w = |\vec{r}_c(s,\rho_0) - \vec{r}_c(s,-\rho_0)| = \int_{-\rho_0}^{\rho_0} \Delta d\rho = 2a(s)$, and the determinant by

$$\Delta = \frac{\partial X_c}{\partial s}\frac{\partial Y_c}{\partial \rho} - \frac{\partial Y_c}{\partial s}\frac{\partial X_c}{\partial \rho} = -\frac{la(s)\rho}{\rho_0}\left(1 - \frac{\rho a(s) y_0''(s)}{l^3\rho_0}\right). \tag{25.64}$$

Using Eq. (25.8), the components of the diffusion tensor have the following expressions:

$$D^{ss} = \frac{1}{\Delta^2}\left[D^x\left(\frac{\partial Y_c}{\partial \rho}\right)^2 + D^y\left(\frac{\partial X_c}{\partial \rho}\right)^2\right] = \frac{1}{\Delta^2}\left(D^X Y_\rho^2 + D^Y X_\rho^2\right), \tag{25.65}$$

$$D^{s\rho} = D^{\rho s} = -\frac{1}{\Delta^2}\left[D^x\left(\frac{\partial Y_c}{\partial \rho}\frac{\partial Y_c}{\partial s}\right)^2 + D^y\left(\frac{\partial X_c}{\partial \rho}\frac{\partial X_c}{\partial s}\right)^2\right] = -\frac{1}{\Delta^2}\left(D^X Y_\rho Y_s + D^Y X_\rho X_s\right), \tag{25.66}$$

$$D^{\rho\rho} = \frac{1}{\Delta^2}\left[D^x\left(\frac{\partial Y_c}{\partial s}\right)^2 + D^y\left(\frac{\partial X_c}{\partial s}\right)^2\right] = \frac{1}{\Delta^2}\left(D^X Y_s^2 + D^Y X_s^2\right). \tag{25.67}$$

Following the same steps as in Sect. 25.3, we have to project the diffusion equation in general coordinates, Eq. (25.13), namely,

$$\int_{-\rho_0}^{\rho_0} d\rho\, \Delta \partial_t c = \partial_s \int_{-\rho_0}^{\rho_0} d\rho\, \Delta D^{sv}\partial_v c + \int_{-\rho_0}^{\rho_0} d\rho\, \partial_\rho \Delta D^{\rho v}\partial_v c.$$

Introducing the BCs, Eq. (25.14), this last equation becomes

$$\partial_t \mathrm{p} = \partial_s\left[D(s)w(s)\partial_s\left(\frac{\mathrm{p}}{w(s)}\right)\right], \tag{25.68}$$

where the marginal concentration is defined as

$$\mathrm{p}(s) \equiv \int_{-\rho_0}^{\rho_0} c\Delta\, d\rho. \tag{25.69}$$

Finally, using $c(s, \theta, \rho) \approx c(s)$, and $J^\rho = 0$, $D(s)$ is given by

$$D(s) = \frac{\int_{-\rho_0}^{\rho_0} d\rho \Delta\left(\frac{D^{ss}D^{\rho\rho} - D^{s\rho}D^{\rho s}}{D^{\rho\rho}}\right)}{w(s)}. \tag{25.70}$$

This last expression allows us to calculate the position-dependent effective diffusivity in two dimensions, once the channel of interest is parameterized.

25.7 Diffusivity Coefficient for an Asymmetric and Curved Midline Channel

For an asymmetric 2D channel, the centerline is given by the well-behaved curve $\vec{r}_0(s, \rho) = (s, y_0(s))$, where y_0 is the channel midline. Now, we have to substitute our parameterization into Eq. (25.64), as shown in the previous section. Once we know the determinant, we can calculate the numerator of Eq. (25.70), which depends explicitly on the determinant times the elements of the diffusion tensor:

$$\Delta\left(\frac{D^{ss}D^{\rho\rho}-D^{s\rho}D^{\rho s}}{D^{\rho\rho}}\right)=\frac{D^{x}D^{y}}{\Delta^{2}}. \tag{25.71}$$

We can now substitute this last expression into Eq. (25.70), and because we are interested in an asymmetric channel, we need to integrate from $\rho_1(s)$ to $\rho_2(s)$, the lower and upper walls of the channel, where $\rho_1(s) > y_0 > \rho_2(s)$. Finally for this specific case, we find

$$D(x)=\frac{\arctan\left(y_0'(x)+\frac{1}{2}w'(x)\right)}{w'(x)}-\frac{\arctan\left(y_0'(x)-\frac{1}{2}w'(x)\right)}{w'(x)}. \tag{25.72}$$

This equation is the same expression obtained by Dagdug and Pineda, Eq. (20.51).

25.8 Concluding Remarks

In this chapter, we present a theoretical framework to study the problem of diffusion where the reference frame is placed at the axis of the tube or channel, depending on the number of dimensions. It has the advantage of allowing us to consider more general parametric curves to describe the tube or channel axis and boundaries. These elements, along with dimensionality, provide a great deal of flexibility to adapt this theory to more diverse kinds of confinements.

Further Reading and References

Y. Chávez, G. Chacón-Acosta, L. Dagdug, Effects of curved midline and varying width on the description of the effective diffusivity of Brownian particles. J. Phys. Condens. Matter **30**, 194001 (2018). https://doi.org/10.1088/1361-648X/aaba0d

Y. Chávez, G. Chacón-Acosta, L. Dagdug, Unbiased diffusion of Brownian particles in a helical tube. J. Chem. Phys. **148**, 214106 (2018). https://doi.org/10.1063/1.5030892

L. Dagdug, A.A. García-Chung, G. Chacón-Acosta, On the description of Brownian particles in confinement on a non-Cartesian coordinates basis. J. Chem. Phys. **145**, 074105 (2016). https://doi.org/10.1063/1.4960652

A.A. García-Chung, G. Chacón-Acosta, L. Dagdug, On the covariant description of diffusion in two-dimensional confined environments. J. Chem. Phys. **142**, 064105 (2015). https://doi.org/10.1063/1.4907553

Appendix A
Mathematical Requirements

A.1 Useful Trigonometric Identities

Here is a short list of trigonometric identities:

$$\sin(x)^2 + \cos(x)^2 = 1 \tag{A.1}$$

$$\sin(x) = \frac{e^{ix} - e^{-ix}}{2i}. \tag{A.2}$$

$$\cos(x) = \frac{e^{ix} + e^{-ix}}{2}. \tag{A.3}$$

$$e^{ix} = \cos(x) + i\ \sin(x) \tag{A.4}$$

$$e^{-ix} = \cos(x) - i\ \sin(x) \tag{A.5}$$

A.2 Hyperbolic Function Relations

A basic list of relations between hyperbolic functions is given below:

$$\cosh(x) + \operatorname{senh}(x) = e^{x}. \tag{A.6}$$

L. Dagdug et al., *Diffusion Under Confinement*,
https://doi.org/10.1007/978-3-031-46475-1

$$\cosh(x) - \operatorname{senh}(x) = \mathrm{e}^{-x}. \tag{A.7}$$

$$\cosh^2(x) - \operatorname{senh}^2(x) = 1. \tag{A.8}$$

A.3 Leibniz Rule for Integrals

The Leibniz integral rule provides a formula for differentiation with respect to x of a definite integral with respect to t of a function $f = f(x,t)$ whose limits are functions of the differential variable x:

$$\frac{\mathrm{d}}{\mathrm{d}x}\left(\int_{a(x)}^{b(x)} f(x,t)\,\mathrm{d}t\right) = \int_{a(x)}^{b(x)} \frac{\partial f(x,t)}{\partial x}\,\mathrm{d}t + f(x,b(x))\cdot b'(x) - f(x,a(t))\cdot a'(x), \tag{A.9}$$

where the primes denote differentiation with respect to x.

A.4 Table of Integrals

$$\int_0^\infty x^n\,\mathrm{e}^{-\mu x}\,\mathrm{d}x = n!\,\mu^{-n-1}. \tag{A.10}$$

$$\int x\,\mathrm{e}^{-x^2}\,\mathrm{d}x = -\frac{1}{2}\,\mathrm{e}^{-x^2}. \tag{A.11}$$

$$\int_0^\infty \mathrm{e}^{-ax^2}\cos(bx)\,\mathrm{d}x = \frac{\sqrt{\pi}}{2\sqrt{a}}\mathrm{e}^{-\frac{b^2}{4a}}. \tag{A.12}$$

$$\int_0^\infty \exp\left(-ax^2 - \frac{b}{x^2}\right)\mathrm{d}x = \frac{1}{2}\sqrt{\frac{\pi}{a}}\exp\left(-2\sqrt{ab}\right) \tag{A.13}$$

A.5 Gaussian Integral and the Feynman Rule

The Gaussian integral is given by

$$\int_{-\infty}^{\infty} \mathrm{e}^{-\lambda x^2}\, \mathrm{d}x = \sqrt{\frac{\pi}{\lambda}}. \tag{A.14}$$

By differentiating with respect to the λ parameter, we can obtain higher-order Gaussian integrals, a procedure that leads to the so-called Feynman rule:

$$(-1)^n \int_{-\infty}^{\infty} x^{2n}\, \mathrm{e}^{-\lambda x^2}\, \mathrm{d}x = \frac{\mathrm{d}^n}{\mathrm{d}\lambda^n}\sqrt{\frac{\pi}{\lambda}}. \tag{A.15}$$

When working with Gaussian integrals, it is sometimes practical to know the following general result:

$$\int_{-\infty}^{\infty} x^n\, \mathrm{e}^{-\lambda x^2}\, \mathrm{d}x = \frac{1+(-1)^n}{2}\lambda^{-\frac{1+n}{2}}\, \Gamma\left(\frac{1+n}{2}\right). \tag{A.16}$$

A.6 Series and Products

A.6.1 Taylor Series

Taylor series are the sum representations of analytical functions expressed in terms of the function's derivatives. Typically, every function is a sum of infinite and convergent terms. In order to expand a function in a Taylor series around a point a, the function has to be class C^∞ (i.e., infinitely differentiable or smooth). The Taylor expansion of function $f(x)$ around a is

$$f(x) = \sum_{n=0}^{\infty} \frac{f^{(n)}(a)}{n!}(x-a)^n. \tag{A.17}$$

When the expansion is around $a = 0$, the Taylor series is also called a Maclaurin series, specifically

$$f(x) = \sum_{n=0}^{\infty} \frac{f^{(n)}(0)}{n!}x^n. \tag{A.18}$$

A brief list of Taylor and Maclaurin series expansions is presented below:

$$\mathrm{e}^x = \sum_{n=0}^{\infty} \frac{x^n}{n!}. \tag{A.19}$$

$$\ln(1+x) = \sum_{n=1}^{\infty} (-1)^{n+1} \, \frac{x^n}{n}. \tag{A.20}$$

$$\ln(1-x) = -\sum_{n=1}^{\infty} \frac{x^n}{n}. \tag{A.21}$$

$$\mathrm{erf}(x) = \frac{2}{\sqrt{\pi}} \sum_{n=0}^{\infty} \frac{(-1)^n \, x^{2n+1}}{n! \, (2n+1)} = \frac{2}{\sqrt{\pi}} \left(x - \frac{x^3}{3} + \frac{x^5}{10} - \frac{x^7}{42} + \cdots \right). \tag{A.22}$$

A.6.1.1 Series of Hyperbolic Functions

$$\mathrm{csch}\, x = \sum_{n=0}^{\infty} \frac{2(1-2^{2n-1}) \, B_{2n} \, x^{2n-1}}{(2n)!} = \frac{1}{x} - \frac{x}{6} + \cdots, \qquad 0 < |x| < \pi. \tag{A.23}$$

$$\mathrm{csch}^2\, x = \left[\sum_{n=0}^{\infty} \frac{2(1-2^{2n-1}) \, B_{2n} \, x^{2n-1}}{(2n)!} \right]^2 = \frac{1}{x^2} - \frac{1}{3} + \frac{x^2}{15} + \cdots, \qquad 0 < |x| < \pi. \tag{A.24}$$

$$\coth x = \sum_{n=0}^{\infty} \frac{2^{2n} \, B_{2n} \, x^{2n-1}}{(2n)!} = \frac{1}{x} + \frac{x}{3} + \cdots, \qquad 0 < |x| < \pi. \tag{A.25}$$

$$\coth^2 x = \left[\sum_{n=0}^{\infty} \frac{2^{2n} \, B_{2n} \, x^{2n-1}}{(2n)!} \right]^2 = -\frac{1}{x^2} + \frac{2}{3} + \frac{x^2}{15} + \cdots, \qquad 0 < |x| < \pi. \tag{A.26}$$

$$-2x\coth x\ \operatorname{csch}^2 x = \frac{2}{x^2} + \frac{2x^2}{15} + \cdots . \tag{A.27}$$

A.6.2 Euler Formula to Fourier Series Coefficients

Assuming that a function with period p can be written as a trigonometric series,

$$f(x) = \frac{a_0}{2} + \sum_{n=1}^{\infty} [a_n\ \cos(nt) + b_n\ \sin(nt)]\,, \tag{A.28}$$

we could find the Fourier sine and cosine series. The Fourier sine of $f(x)$ series of the function $f(x)$ is

$$f(x) = \sum_{n=1}^{\infty} b_n \sin\left(\frac{n\pi x}{p}\right) \qquad \text{with} \qquad b_n = \frac{2}{p}\int_0^p f(x)\sin\left(\frac{n\pi x}{p}\right) \mathrm{d}x, \tag{A.29}$$

and the Fourier cosine series of $f(x)$ is given by

$$f(x) = \frac{a_0}{2} + \sum_{n=1}^{\infty} a_n\ \cos\left(\frac{n\pi x}{p}\right), \tag{A.30}$$

with

$$a_0 = \frac{2}{p}\int_0^p f(x)\ \mathrm{d}x \qquad \text{and} \qquad a_n = \frac{2}{p}\int_0^p f(x)\ \cos\left(\frac{n\pi x}{p}\right) \mathrm{d}x. \tag{A.31}$$

A.6.3 Table of Series

$$\sum_{k=1}^{\infty} \frac{\sin(2k-1)\,x}{2k-1} = \frac{\pi}{4}\ \operatorname{sgn}(x). \tag{A.32}$$

$$\sum_{k=1}^{\infty} \frac{(-1)^{k-1}\ \sin(kx)}{k} = \frac{x}{2}. \tag{A.33}$$

$$\sum_{k=1}^{\infty} \frac{\sin(kx)}{k} = \frac{\pi - x}{2}. \tag{A.34}$$

$$\sum_{k=1}^{\infty} \frac{\sin(k\,x)}{k^3} = \frac{\pi^2 x}{6} - \frac{\pi x^2}{4} + \frac{x^3}{12}. \tag{A.35}$$

$$\sum_{k=1}^{\infty} (-1)^{k-1} \frac{\cos(k\,x)}{k^2} = \frac{\pi^2}{12} - \frac{x^2}{4}. \tag{A.36}$$

$$\sum_{k=1}^{\infty} (2k-1)^{-2(2n+1)} = \left[1 - 2^{-2(n+1)}\right] \zeta[2(n+1)]. \tag{A.37}$$

$$\sum_{k=1}^{\infty} \frac{\cos[(2n-1)\,\pi]}{(2k-1)^2} = -\frac{\pi^2}{8}. \tag{A.38}$$

A.6.4 Cauchy Product for Power Series

The Cauchy product for power series is given in terms of a discrete convolution. Let two infinite series be

$$\sum_{i=0}^{\infty} a_i\, x^i, \qquad \sum_{j=0}^{\infty} b_j\, x^j, \tag{A.39}$$

where its coefficients are complex numbers, that is,

$$\{a_i\}, \qquad \{b_j\}. \tag{A.40}$$

Then, the product of the series in Eq. (A.39) is

$$\left(\sum_{i=0}^{\infty} a_i\, x^i\right)\left(\sum_{j=0}^{\infty} b_j\, x^j\right) = \sum_{k=0}^{\infty} \sum_{l=0}^{k} a_l\, b_{k-l}\, x^k. \tag{A.41}$$

A.6.5 Generalized Binomial Theorem

Also known as Newton's generalized binomial theorem, this theorem shows us how to write a binomial expansion as a series (sum). Let us take $r \in \mathcal{R}$ and $|x| < |y|$; therefore,

$$(x+y)^r = \sum_{k=0}^{\infty} {}^rC_k \, x^k \, y^{r-k}, \tag{A.42}$$

where the ${}^rC_k$ are the combinations of r in k, or the generalized binomial coefficients, that is,

$${}^rC_k = \frac{r(r-1)\cdots(r-k+1)}{k(k-1)\cdots 1}, \tag{A.43}$$

where $k \in \mathcal{N}$. Then, for the specific case of $r = -1/3$, the binomial expansion reads

$$(1+x)^{-\frac{1}{3}} = \sum_{k=0}^{\infty} {}^{\frac{1}{3}}C_k \, x^k \, 1^{\frac{1}{3}-k}, \tag{A.44}$$

and after explicitly writing out certain terms, it becomes

$$\begin{aligned}(1+x)^{-1/3} &= 1 + \frac{-\frac{1}{3}}{1!}\,x^1 + \frac{-\frac{4}{9}}{2!}\,x^2 + \frac{-\frac{27}{28}}{3!}\,x^3 + \cdots \\ &= 1 - \frac{1}{3}\,x + \frac{2}{9}\,x^2 - \frac{14}{81}\,x^3 + \cdots,\end{aligned} \tag{A.45}$$

where in order for this series expansion to be valid, $|x| < 1$.

A.7 Fourier Transform

One of the most useful integral transforms is the Fourier transform. The definition of this operator is

$$\mathcal{F}\{f(x)\} = f(k) = \int_{-\infty}^{\infty} f(x)\, \mathrm{e}^{ikx}\, \mathrm{d}x, \tag{A.46}$$

where $\mathcal{F}\{f(x)\}$ and $f(k)$ are the notations to indicate that $f(x)$ is being transformed.

If we wish to transform two variables, we should write

$$f(u,v) = \int_{-\infty}^{\infty}\int_{-\infty}^{\infty} f(x,y)\, \mathrm{e}^{i(ux+vy)}\, \mathrm{d}x\, \mathrm{d}y. \tag{A.47}$$

Once our problem has been solved in the Fourier space, we need to go back to the original state coordinate system by using the inverse Fourier transform:

$$f(x) = \frac{1}{2\pi}\int_{-\infty}^{\infty} f(k)\, \mathrm{e}^{-ikx}\, \mathrm{d}k. \tag{A.48}$$

There is a useful representation of the Dirac delta function using the Fourier transform, i.e.,

$$\delta(x - x_0) = \int_{-\infty}^{\infty} \mathrm{e}^{ik(x-x_0)}\, \mathrm{d}k. \tag{A.49}$$

A.7.1 Table of Transforms

$$\mathcal{F}\{x\ g(x)\} = -i\ \frac{\mathrm{d}\mathcal{F}\{g(x)\}}{\mathrm{d}k}. \tag{A.50}$$

$$f(k) = e^{-ak^2+bik}, \qquad f(x) = \frac{1}{2\sqrt{\pi a}} e^{-\frac{(x-b)^2}{4a}}. \tag{A.51}$$

$$\mathcal{F}\left\{\frac{\mathrm{d}g(x)}{\mathrm{d}x}\right\} = -ik\ \mathcal{F}\{g(x)\}, \qquad \mathcal{F}\left\{\frac{\mathrm{d}^2 g(x)}{\mathrm{d}x^2}\right\} = -k^2\ \mathcal{F}\{g(x)\}. \tag{A.52}$$

A.8 Laplace Transform

The Laplace transform of a function $f(t)$ is defined as

$$\mathcal{L}\{f(t)\} = f(s) = \int_0^{\infty} f(t)\, \mathrm{e}^{-st}\, \mathrm{d}t, \tag{A.53}$$

where the function's transformation is shown in the dependence of the function, for instance, $f(s)$ instead of $f(x)$. Unlike the Fourier transform, the Laplace integral does not have a unique inverse structure for a given function $f(s)$. In order to invert its effects, we must always make use of complex analysis with the Bromwich

integral, sometimes called the Fourier-Mellin integral:

$$f(t) = \mathcal{L}^{-1}\{f(s)\} = \frac{1}{2\pi i} \lim_{T\to\infty} \int_{\gamma - iT}^{\gamma + iT} \mathrm{e}^{st}\ f(s)\ \mathrm{d}s, \tag{A.54}$$

where γ is such a number that the path of integration is the region of convergence of $f(s)$, whereas the derivatives in time transform as

$$\mathcal{L}\left\{\frac{\mathrm{d}f(t)}{\mathrm{d}t}\right\} = \int_0^\infty \mathrm{e}^{-st} \left[\frac{\mathrm{d}f(t)}{\mathrm{d}t}\right] \mathrm{d}t = s\ \mathcal{L}\{f(t)\} - f(0), \tag{A.55}$$

leading to the general result:

$$\mathcal{L}\{f^n\} = s^n\ \Lambda\{f(t)\} - s^{n-1}\ f(+0) - \cdots - f^{n-1}(+0), \tag{A.56}$$

in which the zero needs to be approached from the positive side.

The derivatives of transforms of the form $f(s)$ can be computed as follows:

$$\frac{\partial^n f(s)}{\partial s} = \int_0^\infty \mathrm{e}^{-st}(-t)^n f(t)\ \mathrm{d}t = \mathcal{L}\left\{(-t)^n f(t)\right\}, \tag{A.57}$$

A.8.1 Change of Laplace Variable

In certain problems, where we have a function $f(s)$, it is practical to change the original Laplace variable s for a function $z(s)$ to facilitate the computation of the inverse Laplace transform of $f(s)$. Consider an arbitrary function $f(t)$. We already know that the direct and inverse Laplace transforms in the Laplace variable s are given by Eqs. (A.53) and (A.54), respectively. Additionally, we introduce the direct and inverse Laplace transforms in the arbitrary function $z(s)$, namely,

$$f(z(s)) = \mathcal{L}_{z(s)}\{f(t)\} = \int_0^\infty \mathrm{e}^{-z(s)t} f(t)\ \mathrm{d}t, \tag{A.58}$$

and

$$f(t) = \mathcal{L}^{-1}_{z(t)} f(z(s)) = \frac{1}{2\pi i} \lim_{T\to\infty} \int_{\gamma - iT}^{\gamma + iT} \mathrm{e}^{z(s)t} f(z(s))\ \mathrm{d}z(s). \tag{A.59}$$

Equations (A.58) and (A.59) represent a formal substitution of s by $z(s)$ in the original operators $\mathcal{L}$ and $\mathcal{L}^{-1}$. Therefore, all properties and previous results obtained for the ordinary Laplace transforms can be used for $\mathcal{L}_{z(s)}$ and $\mathcal{L}^{-1}_{z(t)}$. Moreover, if in the original Laplace transform we replace the variable s for an arbitrary function $z(s)$ under the transformation

$$f(s) = f(s(z)) = f^*(z(s)), \tag{A.60}$$

the relation between $f(t)$ and $f^*(t)$ is given by[1]

$$f(t) = \int_0^\infty f^*(\tau)\phi(t,\tau)\,\mathrm{d}\tau, \tag{A.62}$$

with

$$\phi(t,\tau) = \mathcal{L}^{-1}\left\{\mathrm{e}^{-z(s)\tau}\right\}. \tag{A.63}$$

A brief table of a few useful transformations and their inverse transformation is provided in the next section.

A.8.2 Table of Transforms

$$f(s) = \frac{1}{s}, \qquad f(t) = 1. \tag{A.64}$$

$$f(s) = \frac{1}{s-\alpha}, \qquad f(t) = \mathrm{e}^{\alpha t}. \tag{A.65}$$

$$f(s) = \frac{1}{\sqrt{s}}, \qquad f(t) = \frac{1}{\sqrt{\pi t}}. \tag{A.66}$$

$$f(s) = \frac{1}{s^2(\alpha s+\beta)}, \qquad f(t) = \frac{\alpha(\mathrm{e}^{-t\beta/\alpha}-1)+t\beta}{\beta^2}. \tag{A.67}$$

[1] To verify this claim, we should Laplace transform Eq. (A.62), i.e.,

$$f(s) = \mathcal{L}\left\{\int_0^\infty f^*(\tau)\phi(t,\tau)\,\mathrm{d}\tau\right\} = \int_0^\infty f^*(\tau)\mathcal{L}\left\{\mathcal{L}^{-1}\left[\mathrm{e}^{-z(s)\tau}\right]\right\}\mathrm{d}\tau$$

$$= \int_0^\infty \mathrm{e}^{-z(s)\tau} f^*(\tau)\,\mathrm{d}\tau = \mathcal{L}_{z(s)}\left\{f^*(\tau)\right\} = f^*(z(s)). \tag{A.61}$$

$$f(s) = \frac{1}{s(\alpha s + \beta)}, \qquad f(t) = \frac{1 - \mathrm{e}^{-t\beta/\alpha}}{\beta}. \tag{A.68}$$

$$f(s) = e^{-\sqrt{s}\alpha}, \qquad f(t) = \frac{\alpha\, \mathrm{e}^{-\alpha^2/4t}}{2\sqrt{\pi t^3}}. \tag{A.69}$$

$$f(s) = \frac{\mathrm{e}^{-\alpha\sqrt{s}}}{\sqrt{s}}, \qquad f(t) = \frac{\mathrm{e}^{-\frac{\alpha^2}{4t}}}{\sqrt{\pi t}}. \tag{A.70}$$

$$f(s) = \frac{\mathrm{e}^{-2a\sqrt{s}}}{s}, \qquad f(t) = \operatorname{erfc}\left(\frac{a}{\sqrt{t}}\right). \tag{A.71}$$

$$f(s) = \frac{1 - e^{-\sqrt{\frac{4s}{\beta}}\alpha}}{s}, \qquad f(t) = \operatorname{erf}\left(\frac{\alpha}{\sqrt{\beta t}}\right). \tag{A.72}$$

A.9 Convolution of Functions

A mathematical definition of convolution is

$$(f \star g)(t) \equiv \int_{-\infty}^{\infty} f(\tau)\, g(t - \tau)\, \mathrm{d}\tau, \tag{A.73}$$

that is, a functional operator between two functions. The result is a third function where the shape of one function is modified by the other function.

A.9.1 Convolution Theorem

If a convolution under a Fourier transform is given, then

$$\mathcal{F}\{(f \star g)(t)\} = \mathcal{F}\left\{\int_{-\infty}^{\infty} f(\tau)\, g(t - \tau)\, \mathrm{d}\tau\right\} = f(k)\, \tilde{g}(k), \tag{A.74}$$

that is, the product of the transformed functions.

A.10 Special Functions

A.10.1 Gamma Function

The gamma function appears quite often in physical and mathematical problems such as in the computation of probabilities in statistical mechanics (i.e., the propagator $p(x, t|x_0)$ in the diffusion equation). The first definition made by Euler in terms of a limit is

$$\Gamma(z) = \lim_{n\to\infty} \frac{1 \cdot 2 \cdot 3 \cdots n}{z(z+1)(z+2)\cdots(z+n)}\, n^z, \qquad z \neq 0, -1, -2, -3, \ldots, \tag{A.75}$$

and defined by the Euler integral, it takes the following form:

$$\Gamma(z) = \int_0^\infty t^{z-1}\, \mathrm{e}^{-t}\, \mathrm{d}t. \tag{A.76}$$

The basic functional relation of the gamma function is rather a function of $z + 1$, leading to

$$\Gamma(z+1) = z\Gamma(z) = z! = \prod(z). \tag{A.77}$$

Probably, the best known value of the gamma function is that of a non-integer argument:

$$\Gamma\left(\frac{1}{2}\right) = \sqrt{\pi}, \tag{A.78}$$

which can be generalized for non-integer values, namely,

$$\Gamma\left(\frac{1}{2} - n\right) = \frac{(-4)^n\, n!}{(2n)!}\sqrt{\pi} = \frac{\sqrt{\pi}}{\binom{-1/2}{n} n!}, \tag{A.79}$$

$$\Gamma\left(\frac{1}{2} + n\right) = \frac{(2n!)}{4^n\, n!}\sqrt{\pi} = \binom{n - 1/2}{n}\, n!\, \sqrt{\pi}. \tag{A.80}$$

A.10.2 Error Functions

The error and complementary error integrals are

$$\mathrm{erf}(x) = \frac{2}{\sqrt{\pi}} \int_0^x \mathrm{e}^{-t^2}\, \mathrm{d}t, \qquad \mathrm{erfc}(x) = \frac{2}{\sqrt{\pi}} \int_x^\infty \mathrm{e}^{-t^2}\, \mathrm{d}t. \tag{A.81}$$

A pair of equations that have the following properties:

$$\operatorname{erf}(-x) = -\operatorname{erf}(x), \qquad \operatorname{erf}(0) = 0, \qquad \operatorname{erf}(\infty) = 1, \tag{A.82}$$

and

$$\operatorname{erfc}(-x) = 2 - \operatorname{erfc}(x), \qquad \operatorname{erfc}(0) = 1, \qquad \operatorname{erfc}(\infty) = 0, \tag{A.83}$$

respectively.

Moreover, a quick proof of the relation between the erf function and the complementary error function can be done when separating the limits of the integral in a practical manner, namely,

$$\frac{2}{\pi}\int_x^\infty \mathrm{e}^{-t^2}\,\mathrm{d}t = \frac{2}{\sqrt{\pi}}\int_0^\infty \mathrm{e}^{-t^2}\,\mathrm{d}t - \frac{2}{\sqrt{\pi}}\int_0^x \mathrm{e}^{t^2}\,\mathrm{d}t. \tag{A.84}$$

Therefore,

$$\frac{2}{\sqrt{\pi}}\int_x^\infty \mathrm{e}^{-t^2}\,\mathrm{d}t = 1 - \operatorname{erf}(x) = \operatorname{erfc}(x). \tag{A.85}$$

In addition to the properties mentioned above, it is also useful to know the derivative and integral of the error function. The derivative can be easily obtained by its definition and the fundamental theorem of calculus, leading to

$$\frac{\mathrm{d}}{\mathrm{d}x}\operatorname{erf}(x) = \frac{2}{\sqrt{\pi}}\,\mathrm{e}^{-x^2}, \qquad \frac{\mathrm{d}}{\mathrm{d}x}\operatorname{erfc}(x) = -\frac{2}{\sqrt{\pi}}\,\mathrm{e}^{-x^2}. \tag{A.86}$$

Higher-order derivatives are given by

$$\frac{\mathrm{d}^{(k)}}{\mathrm{d}x^{(k)}}\operatorname{erf}(x) = \frac{2(-1)^{k-1}}{\sqrt{\pi}}\,H_{k-1}(x)\,\mathrm{e}^{-x^2} = \frac{2}{\sqrt{\pi}}\frac{\mathrm{d}^{(k-1)}}{\mathrm{d}x^{(k-1)}}\left(\mathrm{e}^{-x^2}\right), \tag{A.87}$$

where H represents the Hermite polynomials.

An antiderivative of the error function is obtainable by integration by parts:

$$\int \operatorname{erf}(x)\,\mathrm{d}x = \frac{2}{\sqrt{\pi}}\int\left[\int_0^x \mathrm{e}^{-t^2}\,\mathrm{d}t\right]\mathrm{d}x = \frac{2}{\sqrt{\pi}}\left[x\int_0^x \mathrm{e}^{-t^2}\,\mathrm{d}t - \int x\,\mathrm{e}^{-x^2}\,\mathrm{d}x\right], \tag{A.88}$$

and by using Eqs. (A.11) and (A.81), one finds

$$\int \operatorname{erf}(x)\,\mathrm{d}x = x\,\operatorname{erf}(x) + \frac{1}{\sqrt{2}}\,\mathrm{e}^{-x^2}. \tag{A.89}$$

A.10.3 Dirac Delta Function (Distribution)

The Dirac delta function[2] (or distribution) is defined by its properties. It can be visualized as a very sharp narrow pulse. The formal properties of the δ-function are

$$\delta(x) = 0, \qquad x \neq 0, \tag{A.90}$$

which is generalized to

$$\delta(x - x_0) = 0, \qquad x \neq x_0, \tag{A.91}$$

and

$$f(a) = \int_{-\infty}^{\infty} f(x)\, \delta(x - a)\, \mathrm{d}x, \tag{A.92}$$

where $f(x)$ is any smooth function inasmuch as the integration includes the point $x = a$, as otherwise the integral equals zero. The latter equation yields to[3]

$$\int_{-\infty}^{\infty} \delta(x)\mathrm{d}x = 1. \tag{A.95}$$

It follows that the Dirac delta function must be even in x, meaning that

$$\delta(-x) = \delta(x). \tag{A.96}$$

Using integration by parts, one can also define the derivative of the Dirac delta function as follows:

$$\int_{-\infty}^{\infty} f(x)\, \delta'(x - a)\, \mathrm{d}x = -\int_{-\infty}^{\infty} f'(x)\, \delta(x - a)\, \mathrm{d}x = -f'(a). \tag{A.97}$$

[2] Even though it is not really a function, in the usual sense of what being a function means, it represents a special notation for the limit of a sequence of functions, i.e., a distribution.

[3] The result that can be also written as

$$\int_{-a}^{b} \delta(x)\, \mathrm{d}x = 1, \qquad \text{for all } a, b > 0. \tag{A.93}$$

Thus,

$$\int \delta(x - a)\, \mathrm{d}x = 1. \tag{A.94}$$

The δ-function can be represented in terms of any basis of real and orthogonal functions, as long as the orthogonality relations are satisfied by such functions, namely,

$$\int_a^b \phi_m(x)\, \phi_n(x)\, \mathrm{d}x = \delta_{mn}. \tag{A.98}$$

Therefore,

$$\delta(x-a) = \sum_{n=0}^{\infty} \phi_n(x)\, \phi_n'(x). \tag{A.99}$$

Evidently, coefficients $\phi_n(a)$ are functions of the variable a. If Eq. (A.99) is multiplied by $\phi_n'(x)$ and integrated over the domain, Eq. (A.96) is proven.

Another useful side of the Dirac delta function is its integral representation. The Fourier transform leads to the identification of[4]

$$\delta(x-a) = \frac{1}{\pi} \int_{-\infty}^{\infty} \exp[ik(a-x)]\, \mathrm{d}k. \tag{A.100}$$

A.10.4 Heaviside Function

The Heaviside function, sometimes called the step function, is defined by parts as follows:[5]

$$H(x) = \begin{cases} 1, & x > 0 \\ 0, & x \leq 0. \end{cases} \tag{A.102}$$

The Dirac delta function is the derivative of the Heaviside function:

$$\delta(x) = \frac{\mathrm{d}H(x)}{\mathrm{d}x}, \tag{A.103}$$

[4] The constant factor in Eq. (A.100) may differ from application and theoretical interest.

[5] Or as an indicator function,

$$H(x) := \mathbf{1}_{x>0}. \tag{A.101}$$

while the ramp function[6] is an antiderivative of the Heaviside step function:

$$\int_{-\infty}^{x} H(x')\,\mathrm{d}x' = x\ H(x). \tag{A.105}$$

A.10.5 Riemann Zeta Function

The Riemann zeta function, sometimes called Euler-Riemann zeta function, is a function for complex variables in the form of $s = \sigma + it$, defined as follows:

$$\zeta(s) = \sum_{n=1}^{\infty} \frac{1}{n_s} = \int_0^{\infty} \frac{x^{s-1}}{\mathrm{e}^{x-1}}\,\mathrm{d}x. \tag{A.106}$$

Above and beyond that, Euler succeeded in proving the identity:

$$\sum_{n=1}^{\infty} \frac{1}{n^s} = \prod_{p,\ \text{prime}} \frac{1}{1-p^{-s}}, \tag{A.107}$$

where on the right-hand side, the product extends over all prime numbers p, leading to the so-called Euler products.

The zeta function satisfies the functional equation:

$$\zeta(s) = 2^s\ \pi^{s-1}\ \sin\Big(\frac{\pi s}{2}\Big)\Gamma(1-s)\ \zeta(1-s). \tag{A.108}$$

A brief list of specific values of the ζ-function is given below:

$$\zeta(2n) = \frac{(-1)^{n+1}\ B_{2n}(2\pi)^{2n}}{2(2n)!}, \tag{A.109}$$

in which B_{2n} is the $2n$-th Bernoulli number:

$$\zeta(-n) = (-1)^n\ \frac{B_{n+1}}{n+1} \text{ for } n \geq 0. \tag{A.110}$$

On the other hand, by analytic continuation, we have the following results:

[6] The ramp function is the unary real function defined as

$$R(x) = \begin{cases} x, & x \geq 0 \\ 0, & x < 0. \end{cases} \tag{A.104}$$

$$\zeta(-1) = -\frac{1}{12}. \tag{A.111}$$

$$\zeta(0) = -\frac{1}{2}. \tag{A.112}$$

$$\zeta(1) = 1 + \frac{1}{2} + \frac{1}{3} + \cdots \tag{A.113}$$

$$\zeta(2) = 1 + \frac{1}{2^2} + \frac{1}{3^2} + \cdots = \frac{\pi^2}{6}. \tag{A.114}$$

A.10.6 The Sign Function

The sign function returns the sign of a real number. It is defined as follows:

$$\operatorname{sgn}(x) = \frac{\mathrm{d}}{\mathrm{d}x}|x| = \begin{cases} -1 & x < 0, \\ 0 & x = 0 \\ 1 & x > 0. \end{cases} \tag{A.115}$$

An alternative representation of such function is

$$\operatorname{sgn} = -1 + 2\int_{-\infty}^{x} \delta(z)\,\mathrm{d}z. \tag{A.116}$$

A.11 Bessel Differential Equation

The linear second-order ordinary differential equation

$$x^2\frac{\mathrm{d}^2y}{\mathrm{d}x^2} + x\frac{\mathrm{d}y}{\mathrm{d}x} + (x^2 - \nu^2)y = 0, \tag{A.117}$$

is called the Bessel equation. The number ν is the order of the Bessel equation. This differential equation is named after Friedrich Wilhelm Bessel, a German mathematician and astronomer who studied it in detail and demonstrated that its solutions can be expressed using a special class of functions known as cylinder functions or Bessel functions. Assuming that ν is non-integer and positive, the general solution of the Bessel equation can be written as

$$y(x) = \mathcal{A} J_\nu(x) + \mathcal{B} J_{-\nu}(x), \tag{A.118}$$

where $\mathcal{A}$ and $\mathcal{B}$ are arbitrary constants and J_ν and $J_{-\nu}$ are Bessel functions of the first kind. These Bessel function can be represented by a series:

$$J_\nu(x) = \sum_{z=0}^{\infty} \frac{(-1)^z}{\Gamma(z+1)\,\Gamma(z+\nu+1)} \left(\frac{x}{2}\right)^{2z+\nu}, \tag{A.119}$$

and

$$J_{-\nu}(x) = \sum_{z=0}^{\infty} \frac{(-1)^z}{\Gamma(z+1)\,\Gamma(z-\nu+1)} \left(\frac{x}{2}\right)^{2z-\nu}, \tag{A.120}$$

respectively.

If ν is an integer, the Bessel functions become dependent on each other: $J_{-\nu}(x) = (-1)^\nu J_\nu(x)$. In this case, the general solution is given by

$$y(x) = \mathcal{A} J_\nu(x) + \mathcal{B} Y_\nu(x), \tag{A.121}$$

where $\mathcal{A}$ and $\mathcal{B}$ are arbitrary constants, and Y_ν is the Bessel function of the second kind, which can be expressed in terms of the Bessel functions of the first kind, namely,

$$Y_\nu(x) = \frac{J_\nu(x)\cos(\pi\nu) - J_{-\nu}(x)}{\sin(\pi\nu)}. \tag{A.122}$$

The modified Bessel equation is obtained replacing x for ix in the Bessel equation, becoming

$$x^2 \frac{\mathrm{d}^2 y}{\mathrm{d}x^2} + x \frac{\mathrm{d}y'}{\mathrm{d}x} - (x^2 - \nu^2) y = 0. \tag{A.123}$$

The general solution of this equation is given by

$$y(x) = \mathcal{A} J_\nu(-ix) + \mathcal{B} Y_\nu(-ix) = \mathcal{C} I_\nu(x) + \mathcal{D} K_\nu(x), \tag{A.124}$$

where $\mathcal{A}$, $\mathcal{B}$, $\mathcal{C}$, and $\mathcal{D}$ are arbitrary constants and I_ν and K_ν are the modified Bessel functions of the first and second kind. These functions can be represented as

$$I_\nu(x) = i^\nu J_\nu(ix) = \sum_{z=0}^{\infty} \frac{1}{z!\,\Gamma(z+\nu+1)} \left(\frac{x}{2}\right)^{2z+\nu}, \tag{A.125}$$

and

$$K_\nu(x) = \frac{\pi}{2}\frac{I_{-\nu}(x) - I_\nu(x)}{\sin(\pi\nu)}, \tag{A.126}$$

respectively.

The general solution of the differential equation

$$x^2\frac{\mathrm{d}^2y}{\mathrm{d}x^2} + x\frac{\mathrm{d}y}{\mathrm{d}x} - (a^2x^2 + \nu^2)y = 0, \tag{A.127}$$

is given by

$$y(x) = \mathcal{A}J_\nu(ax) + \mathcal{B}Y_\nu(ax), \tag{A.128}$$

where $\mathcal{A}$ and $\mathcal{B}$ are arbitrary constants.

To express a solution of the diffusion equation when it depends on the radial coordinate in a compact form, it is convenient to define the following function:

$$Q^{(i)}_{\alpha,\beta}(w,z) \equiv I_\alpha(w)K_\beta(z) + (-1)^i I_\beta(z)K_\alpha(w). \tag{A.129}$$

A.11.1 Recurrence Formulas: Derivatives

$$\frac{\mathrm{d}}{\mathrm{d}x}\left[x^\nu J_\nu(x)\right] = x^\nu J_{\nu-1}(x). \tag{A.130}$$

$$\frac{\mathrm{d}}{\mathrm{d}x}\left[x^{-\nu} J_\nu(x)\right] = -x^{-\nu} J_{\nu+1}(x). \tag{A.131}$$

$$\frac{\mathrm{d}}{\mathrm{d}x}\left[x^\nu Y_\nu(x)\right] = x^\nu Y_{\nu-1}(x). \tag{A.132}$$

$$\frac{\mathrm{d}}{\mathrm{d}x}\left[x^{-\nu} Y_\nu(x)\right] = -x^{-\nu} Y_{\nu+1}(x). \tag{A.133}$$

$$\frac{\mathrm{d}}{\mathrm{d}x}\left[x^\nu I_\nu(x)\right] = x^\nu I_{\nu-1}(x). \tag{A.134}$$

$$\frac{\mathrm{d}}{\mathrm{d}x}\left[x^{-\nu}I_{\nu}(x)\right] = x^{-\nu}I_{\nu+1}(x). \tag{A.135}$$

$$\frac{\mathrm{d}}{\mathrm{d}x}\left[x^{\nu}K_{\nu}(x)\right] = -x^{\nu}K_{\nu-1}(x). \tag{A.136}$$

$$\frac{\mathrm{d}}{\mathrm{d}x}\left[x^{-\nu}K_{\nu}(x)\right] = -x^{-\nu}K_{\nu+1}(x). \tag{A.137}$$

$$\frac{\mathrm{d}}{\mathrm{d}x}\left[x^{\nu}Q^{(1)}_{\alpha,\alpha}(a,x)\right] = -x^{\nu}Q^{(2)}_{\alpha,\alpha-1}(a,x). \tag{A.138}$$

$$\frac{\mathrm{d}}{\mathrm{d}x}\left[x^{\nu}Q^{(1)}_{\alpha,\alpha}(x,a)\right] = x^{\nu}Q^{(2)}_{\alpha,\alpha-1}(a,x). \tag{A.139}$$

$$\frac{\mathrm{d}}{\mathrm{d}x}\left[x^{\nu}Q^{(2)}_{\alpha,\alpha-1}(x,a)\right] = -x^{\nu}Q^{(1)}_{\alpha-1,\alpha-1}(a,x). \tag{A.140}$$

A.12 Solution of Differential Equations by Quadratures

It is said that a differential equation is solved in quadratures if its general solution is expressed in terms of one or more integrals. The name *quadrature* originates from geometry, where quadrature means finding an area, a task overtaken in modern mathematics by integration. There is no known method to solve the general n-th order linear differential equation by quadratures if $n \geq 2$, only special cases, such as equations with constant coefficients. For example, consider the following ordinary differential equation (EDO):

$$\frac{\mathrm{d}y(x)}{\mathrm{d}x} = f(x), \tag{A.141}$$

where $y(a)$ is known. Then, to express the solution of this ODE in terms of an integral, we must integrate both sides from a to x (to avoid confusion with notation, first we have to set $x = x'$ in Eq. (A.141)), resulting in

$$y(x) - y(a) = \int_a^x f(x')\,\mathrm{d}x'. \tag{A.142}$$

Finally, the general solution in quadratures is given by

$$y(x) = y(a) + \int_a^x f(x')\,\mathrm{d}x'. \tag{A.143}$$

Moreover, if x lies within the interval $[a, b]$, and using the properties of the definite integrals, we can write Eq. (A.142) as

$$y(x) = y(a) + \int_a^b f(x')\,\mathrm{d}x' - \int_x^b f(x')\,\mathrm{d}x', \tag{A.144}$$

or

$$y(x) = y(a) + \int_a^b H(x - x')\, f(x')\,\mathrm{d}x', \tag{A.145}$$

where $H(x)$ is the Heaviside function or discontinuous step function, the definition of which is given by Eq. (A.101). This function subtracts the over-value of the integral from x to b.

Now, we can consider a second-order differential equation, that is,

$$\frac{\mathrm{d}^2 y(x)}{\mathrm{d}x^2} = f(x), \tag{A.146}$$

and we need two conditions to obtain a solution. In this case, we will consider

$$y(a) = y_a, \qquad y'(a) = y'_a. \tag{A.147}$$

By integrating Eq. (A.146), we obtain

$$\frac{\mathrm{d}y(x)}{\mathrm{d}x} = y'_a + \int_a^x f(x')\,\mathrm{d}x', \tag{A.148}$$

and performing a second integration yields

$$y(x) = y_a + y'_a\,(x - a) + \int_a^x \int_a^{x''} f(x')\,\mathrm{d}x'\,\mathrm{d}x''. \tag{A.149}$$

The (dummy) variables of integration are x' and x'', and both integrals have a as starting point. This allows us to represent the region of integration in the $x'\,x''$-plane, where the intersection (a, a) is shown on the lower left corner as a kind of origin (see Fig. A.1). The corresponding region of integration for expression (A.149) is the intersection of the lines generated by the integration limits, which corresponds to the upper triangle in the figure.

Furthermore, the same region can also be obtained if the integration order is inverted, meaning that the integration with respect to x'' will be carried out first, and then we will perform the integration with respect to the x' variable. This is often

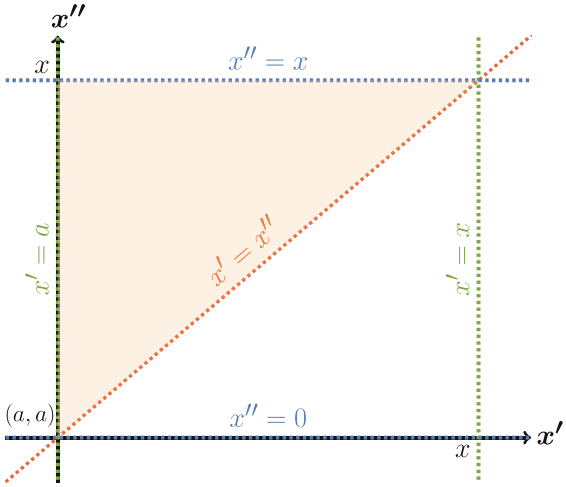

Fig. A.1 The order of integration of Eq. (A.149) can be switched if the integration region defined by its limits is the same. The region in the $x'\,x''$-plane is defined (visually) by drawing straight lines: From the inner integral, we draw two vertical lines (dashed green), one at $x' = a$ and the other at $x' = x''$. Then we draw two horizontal lines (dashed blue) at $x'' = a$ and $x = x$. The integration limits also define an equality, $x'' = x'$, that is represented on the plane by a dashed red straight tilted line. The region formed by the intersection is the upper triangle filled in orange, but the same region can be obtained if the integration is carried out looking first at the horizontal lines $x'' = x'$ and $x'' = x$, and then the vertical ones at $x' = a$ and $x' = x$. This last step allows us to write Eq. (A.149) as Eq. (A.151)

convenient and simplifies the calculations. Now, the limits need to be changed. From the figure, we can ascertain that the new form for Eq. (A.149) is

$$y(x) = y_a + y'_a\,(x - a) + \int_a^x f(x') \int_{x'}^x \mathrm{d}x''\,\mathrm{d}x', \tag{A.150}$$

which can be integrated to finally obtain

$$y(x) = y_a + y'_a\,(x - a) + \int_a^x (x - x')\,f(x')\,\mathrm{d}x'. \tag{A.151}$$

This last equation is solved in quadratures as its solution is expressed in terms of an integral.

Appendix B
Vector Analysis of Differential Operators

The math involved in the computation of different features of the theory of diffusion under confinement requires the knowledge of differential operators in various coordinates. This appendix is intended to be a shortcut in the description of differential operators, as well as a brief reminder on how a specific coordinate system is arranged. Even though there are at least 11 coordinate systems where vector analysis can be performed, the discussion in this section is limited to rectangular (Cartesian) coordinates, circular cylindrical coordinates, and spherical polar coordinates.

B.1 Rectangular (Cartesian) Coordinates

Rectangular (or Cartesian) coordinates are defined by a set of three lines perpendicular to one another (see Fig. B.1). Each line eventually becomes a number line. Every position within the system is fully determined by specifying its components along all axes. Then one reads (x, y, z) as the position.

The Cartesian representation of the gradient $\boldsymbol{\nabla}$, divergence $\boldsymbol{\nabla}\cdot$, and Laplacian ∇^2 acting on a function $f = f(x, y, z)$ or vector $\mathbf{u} = (u_x, u_y, u_z)$ are given below

$$\boldsymbol{\nabla} f = \frac{\partial f}{\partial x}\hat{\mathbf{e}}_i + \frac{\partial f}{\partial y}\hat{\mathbf{e}}_j + \frac{\partial f}{\partial z}\hat{\mathbf{e}}_k. \tag{B.1}$$

$$\boldsymbol{\nabla}\cdot\mathbf{u} = \frac{\partial u_x}{\partial x} + \frac{\partial u_y}{\partial y} + \frac{\partial u_z}{\partial x}. \tag{B.2}$$

L. Dagdug et al., *Diffusion Under Confinement*,
https://doi.org/10.1007/978-3-031-46475-1

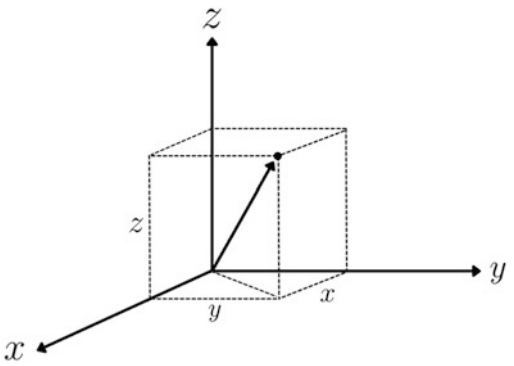

Fig. B.1 Three-dimensional rectangular (Cartesian) coordinate system with origin O and axis lines x, y and z, oriented as depicted in the figure. A specific location is represented by a point with coordinates $P(x, y, z)$

$$\nabla \times \mathbf{u} = \left(\frac{\partial u_z}{\partial y} - \frac{\partial u_y}{\partial z}\right)\hat{\mathbf{e}}_i + \left(\frac{\partial u_x}{\partial z} - \frac{\partial u_z}{\partial x}\right)\hat{\mathbf{e}}_j + \left(\frac{\partial u_y}{\partial x} - \frac{\partial u_x}{\partial y}\right)\hat{\mathbf{e}}_k. \tag{B.3}$$

$$\nabla^2 f = \frac{\partial^2 f}{\partial x^2} + \frac{\partial^2 f}{\partial y^2} + \frac{\partial^2 f}{\partial z^2}. \tag{B.4}$$

B.2 Circular Cylindrical Coordinates

In this case, the three curvilinear coordinates are labeled as (r, ϕ, z), whose unitary vectors are also orthogonal. From Fig. B.2 one can verify that $r\cos\phi$ and $r\sin\phi$ are the projections along the x- and y-axes, respectively, while z stands for the height.

The gradient ∇, divergence $\nabla\cdot$, and Laplacian ∇^2 acting on a function $f = f(r, \phi, z)$ or vector $\mathbf{u} = (r, \phi, z)$ are

$$\nabla f = \frac{\partial f}{\partial r}\hat{\mathbf{e}}_r + \frac{1}{r}\frac{\partial f}{\partial \phi}\hat{\mathbf{e}}_\phi + \frac{\partial f}{\partial z}\hat{\mathbf{e}}_k. \tag{B.5}$$

$$\nabla \cdot \mathbf{u} = \frac{1}{r}\frac{\partial (r\, u_r)}{\partial r} + \frac{1}{r}\frac{\partial u_\phi}{\partial \phi} + \frac{\partial u_z}{\partial z}. \tag{B.6}$$

$$\nabla \times \mathbf{u} = \left(\frac{1}{r}\frac{\partial u_z}{\partial \phi} - \frac{\partial u_\phi}{\partial z}\right)\hat{\mathbf{e}}_r + \left(\frac{\partial u_r}{\partial z} - \frac{\partial u_z}{\partial r}\right)\hat{\mathbf{e}}_\phi + \frac{1}{r}\left[\frac{\partial (r\, u_\phi)}{\partial r} - \frac{\partial u_r}{\partial \phi}\right]\hat{\mathbf{e}}_k. \tag{B.7}$$

$$\nabla^2 f = \frac{1}{r}\frac{\partial}{\partial r}\left(r\frac{\partial f}{\partial r}\right) + \frac{1}{r^2}\frac{\partial^2 f}{\partial \phi^2} + \frac{\partial^2 f}{\partial z^2}. \tag{B.8}$$

For which we identify

$$x = r\cos\phi, \qquad y = r\sin\phi, \qquad z = z, \tag{B.9}$$

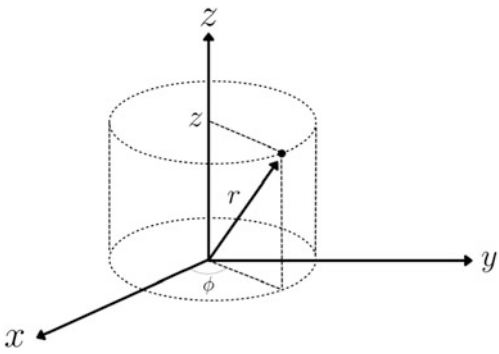

Fig. B.2 Three-dimensional circular cylindrical coordinate system together with their equivalent Cartesian projections. A specific location is represented by a point with coordinates $P(r, \phi, z)$

in addition to

$$r = \sqrt{x^2 + y^2}, \qquad \phi = \arctan\left(\frac{y}{x}\right). \tag{B.10}$$

The relations between unit vectors in Cartesian coordinates and unit vectors in circular cylindrical coordinates are

$$\begin{aligned} \hat{\mathbf{e}}_x &= \cos\phi\hat{\mathbf{e}}_r - \sin\phi\hat{\mathbf{e}}_\phi, \quad \hat{\mathbf{e}}_r = \cos\phi\hat{\mathbf{e}}_x + \sin\phi\hat{\mathbf{e}}_y, \\ \hat{\mathbf{e}}_y &= \sin\phi\hat{\mathbf{e}}_r + \cos\phi\hat{\mathbf{e}}_\phi, \quad \hat{\mathbf{e}}_\phi = -\sin\phi\hat{\mathbf{e}}_x + \cos\phi\hat{\mathbf{e}}_y, \\ \hat{\mathbf{e}}_k &= \hat{\mathbf{e}}_k. \end{aligned} \tag{B.11}$$

B.3 Spherical Coordinates

The spherical polar coordinate system is constructed as shown in Fig. B.3, where r is the radial distance of a particular point from the origin, θ is the angle with respect to the polar axis, and ϕ corresponds to the angle of rotation from the initial meridian plane.

From the figure, one can see that

$$x = r\sin\theta\cos\phi, \qquad y = r\sin\theta\sin\phi, \qquad z = r\cos\theta, \tag{B.12}$$

along with

$$r = \sqrt{x^2 + y^2 + z^2}, \qquad \phi = \arctan\left(\frac{y}{x}\right) \text{ and } \theta = \arctan\left(\frac{\sqrt{x^2 + y^2}}{z^2}\right). \tag{B.13}$$

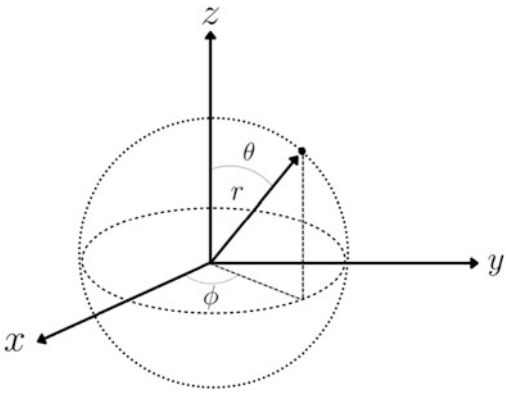

Fig. B.3 Three-dimensional spherical polar coordinates' system together with their equivalent Cartesian projections. A specific location is represented by a point with coordinates $P(r, \theta, \phi)$

The gradient $\boldsymbol{\nabla}$, divergence $\boldsymbol{\nabla}\cdot$, and Laplacian ∇^2 acting on a function $f(r, \theta, \phi)$ or vector $\mathbf{u} = (r, \theta, \phi)$ are

$$\boldsymbol{\nabla} f = \frac{\partial f}{\partial r}\hat{\mathbf{e}}_r + \frac{1}{r}\frac{\partial f}{\partial \theta}\hat{\mathbf{e}}_\theta + \frac{1}{r\sin\theta}\frac{\partial f}{\partial \phi}\hat{\mathbf{e}}_\phi. \tag{B.14}$$

$$\boldsymbol{\nabla}\cdot\mathbf{u} = \frac{1}{r^2}\frac{\partial (r^2 u_r)}{\partial r} + \frac{1}{r\,\sin\theta}\frac{\partial (\sin\theta\, u_\theta)}{\partial \theta} + \frac{1}{r\,\sin\theta}\frac{\partial u_\phi}{\partial \phi}. \tag{B.15}$$

$$\begin{aligned}\boldsymbol{\nabla}\times\mathbf{u} = {} & \frac{1}{\sin\theta}\left[\frac{\partial}{\partial\theta}(\sin\theta\, u_\phi) - \frac{\partial u_\theta}{\partial\phi}\right]\hat{\mathbf{e}}_r + \frac{1}{r}\left[\frac{1}{\sin\theta}\frac{\partial u_r}{\partial\phi} - \frac{\partial}{\partial r}(r\, u_\phi)\right]\hat{\mathbf{e}}_\theta \\ & + \frac{1}{r}\left[\frac{\partial}{\partial r}(r\, v_\theta) - \frac{\partial u_r}{\partial\theta}\right]\hat{\mathbf{e}}_\phi.\end{aligned} \tag{B.16}$$

$$\nabla^2 f = \frac{1}{r^2}\frac{\partial}{\partial r}\left(r^2\frac{\partial f}{\partial r}\right) + \frac{1}{r^2\sin\theta}\frac{\partial}{\partial\theta}\left(\sin\theta\frac{\partial f}{\partial\theta}\right) + \frac{1}{r^2\sin^2\theta}\frac{\partial^2 f}{\partial\phi^2}. \tag{B.17}$$

The relations between unit vectors in Cartesian coordinates and unit vectors in spherical coordinates are

$$\begin{aligned}
\hat{\mathbf{e}}_x &= \sin\theta\cos\phi\hat{\mathbf{e}}_r + \cos\theta\cos\phi\hat{\mathbf{e}}_\theta - \sin\phi\hat{\mathbf{e}}_\phi,\\
\hat{\mathbf{e}}_r &= \sin\theta\cos\phi\hat{\mathbf{e}}_x + \sin\theta\sin\phi\hat{\mathbf{e}}_y + \cos\theta\hat{\mathbf{e}}_k,\\
\hat{\mathbf{e}}_y &= \sin\theta\sin\phi\hat{\mathbf{e}}_r + \cos\theta\sin\phi\hat{\mathbf{e}}_\theta + \cos\phi\hat{\mathbf{e}}_\phi,\\
\hat{\mathbf{e}}_\theta &= \cos\theta\cos\phi\hat{\mathbf{e}}_x + \cos\theta\sin\phi\hat{\mathbf{e}}_y - \sin\theta\hat{\mathbf{e}}_k,\\
\hat{\mathbf{e}}_k &= \cos\theta\hat{\mathbf{e}}_r - \sin\theta\hat{\mathbf{e}}_\theta,\\
\hat{\mathbf{e}}_\phi &= -\sin\phi\hat{\mathbf{e}}_x + \cos\phi\hat{\mathbf{e}}_y.
\end{aligned} \tag{B.18}$$

Appendix C
Differential Geometry in a Nutshell

Differential geometry is a mathematical discipline that studies the geometry of smooth shapes and smooth spaces, also referred to as smooth manifolds. It makes use of the techniques of differential calculus, integral calculus, linear algebra, and multilinear algebra. We use the concept of a *manifold* to mathematically describe curved spaces, defined as a topological space that is modeled closely on Euclidean space locally but may vary widely in its overall properties, in simple terms, a smoothly curved space that is locally flat. Therefore, in a small enough neighborhood, Euclidean geometry applies. The line, for instance, is a one-dimensional manifold since each point on it can be described by a single coordinate.

If a manifold is differentiable and has a symmetric tensor, it is known as a *Riemannian manifold* and has a line element

$$\mathrm{d}l^2 = g_{ij}\mathrm{d}x^i\mathrm{d}x^j, \tag{C.1}$$

where g_{ij} is the *metric*, dx^i and dx^j are the *coordinate differentials*, and the *Einstein summation convention* is used, i.e., when the same index appears twice in the same term, the term is implicitly summed over all possible values for that index, and no summation sign is needed. It is worth noting that the metric determines the coefficients of the line element. For example, the three-dimensional Euclidean line element in Cartesian coordinates is given by

$$\mathrm{d}l^2 = \mathrm{d}x^2 + \mathrm{d}y^2 + \mathrm{d}z^2. \tag{C.2}$$

In such a case, the Euclidean metric results in

$$g_{ij} = \begin{pmatrix} 1 & 0 & 0 \\ 0 & 1 & 0 \\ 0 & 0 & 1 \end{pmatrix}. \tag{C.3}$$

L. Dagdug et al., *Diffusion Under Confinement*,
https://doi.org/10.1007/978-3-031-46475-1

The metric has an inverse that is written with raised indices defined as

$$g_{ik}g^{kj} = \delta_i^j, \tag{C.4}$$

where δ_i^j is the *Kronecker delta function* defined as follows:

$$\delta_i^j = \begin{cases} 1, & \text{for } i = j \\ 0, & \text{for } i \neq j. \end{cases} \tag{C.5}$$

Now, let us find the line element and metric for Euclidean two-dimensional space using polar coordinates. The polar angle θ and radius r are defined in terms of the Cartesian coordinates as $x = r\cos\theta$ and $y = r\sin\theta$. Then,

$$\mathrm{d}x = \cos\theta\,\mathrm{d}r - r\sin\theta\,\mathrm{d}\theta, \tag{C.6}$$

and

$$\mathrm{d}y = \sin\theta\,\mathrm{d}r + r\cos\theta\,\mathrm{d}\theta. \tag{C.7}$$

Substituting these two equations into (C.2) leads to

$$\mathrm{d}l^2 = \mathrm{d}r^2 + r^2\,\mathrm{d}\theta^2, \tag{C.8}$$

resulting in the following metric tensor:

$$g_{ij} = \begin{pmatrix} 1 & 0 \\ 0 & r^2 \end{pmatrix}. \tag{C.9}$$

The inverse is found by observing that

$$g^{rr}g_{rr} = 1 \quad \Rightarrow g^{rr} = 1, \tag{C.10}$$

and that

$$g^{\theta\theta}g_{\theta\theta} =^{\theta\theta} r^r \quad \Rightarrow g^{\theta\theta} = \frac{1}{r^r}, \tag{C.11}$$

consequently,

$$g^{ij} = \begin{pmatrix} 1 & 0 \\ 0 & \dfrac{1}{r^2} \end{pmatrix}. \tag{C.12}$$

By definition, the relation between metric tensor and its inverse, in terms of components, is defined as follows: $g_{\alpha\gamma}g^{\gamma\beta} = \delta^{\alpha}_{\beta}$

$$\delta^{\alpha}_{\beta} \equiv \frac{\partial x^{\alpha}}{\partial x^{\beta}}, \tag{C.13}$$

where the partial derivative is either 1, if $\alpha = \beta$, or 0 otherwise.

Scalars, *contravariant vectors*, *covariant vectors* or *one-forms*, and *tensors* are four examples of objects that live on a manifold. To be more specific, scalars, contravariant vectors, and covariant vectors are all different types of tensors. The transformation properties of the components of tensors in general are basis-independent, which means that if a tensor equation is true in one coordinate system, it is true in all coordinate systems.

We commonly describe a vector by the number of basis vectors that must be added to form it. However, there is another method to express a vector in terms of basis vectors. This is accomplished by taking the vector's dot product with each of the basis vectors: Assume that in the first scenario, we double the length of each of the basis vectors. As a result, the components decrease by double. On the contrary, decreasing the length of the basis vectors causes the vector's components to increase by the same amount. Because these two values change in reverse order, we refer to them as the vector's contravariant components. Form the same reason, contravariant components are specified using superscripts, opposite of basis vectors which are specified with subscripts. A contravariant vector, $\mathbf{V} = V^{\alpha}\mathbf{e}_{\alpha}$, can be expanded into a linear combination of its components and *coordinate basis*, for example, in three dimensions:

$$\mathbf{V} = V^{1}\mathbf{e}_{1} + V^{2}\mathbf{e}_{2} + V^{3}\mathbf{e}_{3}. \tag{C.14}$$

However, if we describe the vector in terms of its dot product with each of the basis vectors, then doubling the length of the basis vectors will double its related dot product. As a result, increasing the length of the basis vector increases the dot product. On the contrary, as the length of the basis vectors reduces, so does the dot product. Because both quantities vary in the same way, we refer to them as covariant components to describe the vector.

The covariant vectors are always denoted by a lower index and its components are given by the dot product of $\mathbf{V}$ with the basis vector $\mathbf{e}_{\alpha}$, namely,

$$V_{\alpha} = \mathbf{V} \cdot \mathbf{e}^{\alpha}. \tag{C.15}$$

Generally speaking, any system of quantities, which is transformed according to the transformation law

$$V'^{\alpha} = \frac{\partial x'^{\alpha}}{\partial x^{\beta}} V^{\beta}, \tag{C.16}$$

is called contravariant vector, where V^β are the components of the contravariant vector expressed in the original x^β coordinate system and V'^α are the components of the same contravariant vector expressed in the new x'^α coordinate system. The partial derivative term represents a transformation matrix, which describes the relationship between the old and new coordinate systems.

Any system of quantities, which is transformed according to the transformation law

$$V'_\alpha = \frac{\partial x^\beta}{\partial x'^\alpha} V_\beta, \tag{C.17}$$

is called covariant vector or one-form, where V_β are the components of the covariant vector expressed in the original x^β coordinate system and V'_α are the components of the same covariant vector expressed in the new x'^α coordinate system.

A contravariant vector is a tangent vector to a parameterized curve, since a covariant vector is the gradient of a scalar field. If this parametric curve is, for example, the world line of a particle moving through spacetime, the four-velocity is a contravariant vector given by

$$U^\mu = \frac{\mathrm{d}x^\mu}{\mathrm{d}\tau} = \left(\frac{\mathrm{d}t}{\mathrm{d}\tau}, \frac{\mathrm{d}x}{\mathrm{d}\tau}, \frac{\mathrm{d}y}{\mathrm{d}\tau}, \frac{\mathrm{d}z}{\mathrm{d}\tau}\right), \tag{C.18}$$

where the four-velocity is defined as the rate of change of the particle's four-position (t, x, y, z) with respect to the proper time τ.

Now, consider a scalar field ϕ function of x^β (β=0,1,2,3). Then, its gradient components are given by

$$\frac{\partial \phi}{\partial x^\beta} = \left(\frac{\partial \phi}{\partial x^0}, \frac{\partial \phi}{\partial x^1}, \frac{\partial \phi}{\partial x^2}, \frac{\partial \phi}{\partial x^3}\right). \tag{C.19}$$

Each partial derivative is a component of the covariant vector.

Generally speaking, when differentiating a tensor, we have to take into account the derivatives of the basis vectors. Consider a contravariant vector V^α. Then, using the product rule,

$$\frac{\partial \tilde{V}^\alpha}{\partial x^\beta} = \frac{\partial V^\alpha}{\partial x^\beta}\mathbf{e}_\alpha + V^\alpha \frac{\partial \mathbf{e}_\alpha}{\partial x^\beta}. \tag{C.20}$$

The *Christoffel symbols* or *connection coefficients* $\Gamma^\gamma_{\alpha\beta}$ are given by

$$\frac{\partial \mathbf{e}_\alpha}{\partial x^\beta} = \Gamma^\gamma_{\alpha\beta}\mathbf{e}_\gamma, \tag{C.21}$$

and represent the rate of change of components V^α with respect to x^β. In an n-dimensional Riemannian manifold, there are n^3 different Christoffel symbols.

To calculate the Christoffel symbols of the two-dimensional Euclidean space using polar coordinates, let us consider the transformation rule (C.16):

$$\mathbf{e}'_\alpha = \frac{\partial x^\beta}{\partial x'^\alpha}\mathbf{e}_\beta. \tag{C.22}$$

Therefore,

$$\mathbf{e}_r = \frac{\partial x}{\partial r}\,\mathbf{e}_x + \frac{\partial y}{\partial r}\,\mathbf{e}_y = \cos\theta\,\mathbf{e}_x + \sin\theta\,\mathbf{e}_y, \tag{C.23}$$

and

$$\mathbf{e}_\theta = \frac{\partial x}{\partial \theta}\,\mathbf{e}_x + \frac{\partial y}{\partial \theta}\,\mathbf{e}_y = -r\sin\theta\,\mathbf{e}_x - r\cos\theta\,\mathbf{e}_y. \tag{C.24}$$

Then, the derivatives are given by

$$\frac{\partial \mathbf{e}_r}{\partial r} = 0, \tag{C.25}$$

$$\frac{\partial \mathbf{e}_r}{\partial \theta} = -\sin\theta\,\mathbf{e}_x + \cos\theta\,\mathbf{e}_y, \tag{C.26}$$

$$\frac{\partial \mathbf{e}_r}{\partial \theta} = \frac{\partial \mathbf{e}_\theta}{\partial r} = \frac{1}{r}\,\mathbf{e}_\theta, \tag{C.27}$$

$$\frac{\partial \mathbf{e}_\theta}{\partial r} = -\sin\theta\,\mathbf{e}_x + \cos\theta\,\mathbf{e}_y. \tag{C.28}$$

$$\frac{\partial \mathbf{e}_\theta}{\partial \theta} = -r\cos\theta\,\mathbf{e}_x - r\sin\theta\,\mathbf{e}_y, \tag{C.29}$$

and

$$\frac{\partial \mathbf{e}_\theta}{\partial \theta} = -r\,\mathbf{e}_r. \tag{C.30}$$

From these last relations, the Christoffel symbols finally become

$$\Gamma^\theta_{r\theta} = \Gamma^\theta_{\theta r} = \frac{1}{r}, \quad \Gamma^r_{\theta\theta} = -r, \quad \Gamma^r_{r\theta} = \Gamma^r_{\theta r} = \Gamma^r_{rr} = \Gamma^\theta_{rr} = \Gamma^\theta_{\theta\theta} = 0. \tag{C.31}$$

A tensor is a function that maps contravariant and covariant vectors to a real number. Tensors are classified according to their rank or type. The rank is given by the number of indices, and the type (n, m) is given by the n number of upper indices and m number of lower indices. For example, the type $(0, 0)$ is a scalar, the type

(1, 0) is a contravariant vector, and the type (0, 1) is a covariant vector or one-form. These two tensors can be multiplied to form a rank-2 tensor, namely,

$$T^{\alpha}_{\beta} = V^{\alpha} W_{\beta}. \tag{C.32}$$

For example, the Kronecker delta δ^{α}_{β} is a rank-2 tensor that transforms as

$$\delta'^{\alpha}_{\beta} = \frac{\partial x'^{\alpha}}{\partial x^{\mu}} \frac{\partial x^{\nu}}{\partial x'^{\beta}} \delta^{\mu}_{\nu}. \tag{C.33}$$

Lastly, we should mention the meaning of *contraction*, one of the rules of tensor algebra. By summing over identical upper and lower indices, a tensor can be contracted. For example, $T_{\beta} = A_{\alpha\beta} B^{\alpha}$, where the upper and lower α indices are summed over.

Index

L. Dagdug et al., *Diffusion Under Confinement*,
https://doi.org/10.1007/978-3-031-46475-1